NASA TECHNICAL MEMORANDUM

NASA TM X-73,170

NASA TM X-73,170

TWELFTH ANNUAL CONFERENCE ON MANUAL CONTROL

Coordinated Science Laboratory
University of Illinois
Urbana, Illinois 61801

and

Ames Research Center
Moffett Field, California 94035

May 1976

1 Report No.	2 Government Accession No	3 Recipient's Catalog No
NASA TM X-73,170		

4 Title and Subtitle	5 Report Date
TWELFTH ANNUAL CONFERENCE ON MANUAL CONTROL	6 Performing Organization Code

7 Author(s)	8 Performing Organization Report No
	A-6762
9 Performing Organization Name and Address	10 Work Unit No
Coordinated Science Laboratory, University of Illinois, Urbana, IL 61801, and Ames Research Center, NASA, Moffett Field, CA 94035	505-09-33
	11 Contract or Grant No
12 Sponsoring Agency Name and Address	13 Type of Report and Period Covered
National Aeronautics and Space Administration Washington, D. C. 20546	Technical Memorandum
	14. Sponsoring Agency Code

15. Supplementary Notes

Proceedings of a meeting held at Coordinated Science Laboratory, University of Illinois, Urbana, Illinois, May 25-27, 1976.

16 Abstract

This volume contains a compilation of written versions of papers presented at the Twelfth Annual Conference on Manual Control in a meeting held at the Coordinated Science Laboratory, University of Illinois, May 25-27, 1976. Eleven main topics were discussed during this three-day conference. These were covered in sessions on Multi-task Decision Making, Attention Allocation and Workload Measurement, Displays and Controls, Nonvisual Displays, Tracking and other Psychomotor Tasks, Automobile Driving, Handling Qualities and Pilot Ratings, Remote Manipulation, System Identification, Control Models, and Motion and Visual Cues. Sixty-five papers are included with presentations on results of analytical studies to develop and evaluate human operator models for a range of control task, vehicle dynamics and display situations; results of tests of physiological control systems and applications to medical problems; and on results of simulator and flight tests to determine display, control and dynamics effects on operator performance and workload for aircraft, automobile, and remote control systems.

17. Key Words (Suggested by Author(s))	18. Distribution Statement
Manual control, Physiological control, Man-machine systems, Displays, Vehicle handling qualities, Operator performance, Flight management systems, Simulation	Unlimited STAR Category - 54

19. Security Classif. (of this report)	20. Security Classif. (of this page)	21. No. of Pages	22. Price*
Unclassified	Unclassified	1020	$25.25

*For sale by the National Technical Information Service, Springfield, Virginia 22161

FOREWORD

This volume contains the proceedings of the Twelfth Annual Conference on Manual Control held at the Coordinated Science Laboratory of the University of Illinois at Urbana-Champaign from May 25 to 27, 1976. This report contains complete manuscripts of most of the papers presented at the meeting.

This was the twelfth in a series of conferences dating back to December 1964. These earlier meetings and their proceedings are listed below:

First Annual NASA-University Conference on Manual Control, The University of Michigan, December 1964. (Proceedings not printed.)

Second Annual NASA-University Conference on Manual Control, MIT, February 28 to March 2, 1966, NASA SP-128.

Third Annual NASA-University Conference on Manual Control, University of Southern California, March 1-3, 1967, NASA SP-144.

Fourth Annual NASA-University Conference on Manual Control, The University of Michigan, March 21-23, 1968, NASA SP-192.

Fifth Annual NASA-University Conference on Manual Control, MIT, March 27-29, 1969, NASA SP-215.

Sixth Annual Conference on Manual Control, Wright-Patterson AFB, April 7-9, 1970.

Seventh Annual Conference on Manual Control, University of Southern California, June 2-4, 1971, NASA SP-281.

Eighth Annual Conference on Manual Control, University of Michigan, Ann Arbor, Michigan, May 17-19, 1972.

Ninth Annual Conference on Manual Control, Massachusetts Institute of Technology, May 23-25, 1973.

Tenth Annual Conference on Manual Control, Wright-Patterson AFB, April 9-11, 1974.

Eleventh Annual Conference on Manual Control, NASA-Ames Research Center, May 21-23, 1975, NASA, TM X-62,464.

CONFERENCE CHAIRMAN

William B. Rouse
University of Illinois

PROGRAM COMMITTEE

Renwick E. Curry
Massachusetts Institute of Technology

Rudolph G. Mortimer
University of Illinois

Richard W. Pew
Bolt Beranek and Newman

Thomas B. Sheridan
Massachusetts Institute of Technology

Robert C. Williges
University of Illinois

PUBLICATION COMMITTEE

Melvin Sadoff
NASA - Ames Research Center

Thomas E. Wempe
NASA - Ames Research Center

CONTENTS

Session I. MULTI-TASK DECISION MAKING

Chairman: R. W. Allen

Page

1. Review of the Symposium on Monitoring Behavior and Supervisory Control (Berchtesgaden, F. R. Germany, March 8-12, 1976) *by T. B. Sheridan* 3

2. Human Control and Monitoring - Models and Experiments, *by P. H. Wewerinke*. 14

3. An Experimental Situation for Study of Pilot Interaction With Automated Airborne Decision Making Systems, *by W. B. Rouse, Y-Y. Chu, and R. S. Walden*. 39

4. An Experimental Situation for Study of Human Decision Making in Multi-Process Monitoring, *by W. B. Rouse and J. S. Greenstein* . . 45

5. The Psychophysics of Random Processes, *by R. E. Curry and T. Govindaraj* 50

Session II. ATTENTION ALLOCATION AND WORKLOAD MEASUREMENT

Chairman: R. G. Mortimer

6. A Novel Approach to the Cross-Adaptive Auxiliary Task, *by A. R. Ephrath*. 63

7. Is There An Optimum Workload in Manual Control, *by W. L. Verplank* . 72

8. Task Interference in Multi-Axis Aircraft Stabilization, *by E. D. Onstott*. 80

9. Results of a Display Design Technique Applied to VTOL Aircraft, *by W. C. Hoffman, R. E. Curry, D. L. Kleinman* (This paper was presented but not received for inclusion in the proceedings.)

10. Telling a Computer How a Human Has Allocated His Attention Between Control and Monitoring Tasks, *by K. D. Enstrom and W. B. Rouse*. . 104

11. The Use of Event-Related Potentials in the Enhancement of System Performance, *by C. D. Wickens, J. Isreal, G. McCarty, D. Gopher, and E. Donchin*. 124

12. Pupillometric Measurement of Cognitive Workload, *by J. Beatty* . . . 135

Session III. DISPLAYS AND CONTROLS

Chairmen: R. W. Allen

13. Left-Brain/Right-Brain and Symbolic/Analogic Human Operator Output Compatibility, *by W. L. Verplank* 147

14. A Regression Approach to Generate Aircraft Predictor Information, *by P. D. Gallaher, R. A. Hunt, and R. C. Williges*. . 156

15. Introduction to a Coordinated Cockpit Display Concept, *by D. L. Baty* 166

16. Implications of a Mixture of Aircraft With and Without Traffic Situation Displays for Air Traffic Management, *by J. Kreifeldt, L. Parkin, P. Rothschild, and T. Wempe*. 179

17. Investigating the Use of a Moving Map Display and a Horizontal Situation Indicator in Simulated Powered-Lift Short-Haul Operations, *by W. F. Clement*. 201

18. Air-to-Ground Visual Display System, *by D. L. Kugel and R. V. Gressang*. 225

19. In-Flight Simulation Study of Decoupled Longitudinal Controls for the Approach and Landing of a STOL Airplane, *by E. Seckel and B. Feinreich*. 244

20. High Acceleration Cockpit Displays and Controls, *by J. A. Townsend and N. J. Kropewnicki* 271

Session IV. NONVISUAL DISPLAYS

Chairman: W. H. Levison

21. Design of an English Language Data Base Question-Answering System, *by D. L. Waltz*. 283

22. Effects of Linguistic Redundancy on Pilot's Comprehension of Synthesized Speech, *by C. A. Simpson*. 294

23. Effects of Linguistic Redundancy on Synthesized Cockpit Warning Message Comprehension and Concurrent Time Estimation, *by S. G. Hart and C. A. Simpson* 309

24. Tactual Commands for Pilot Flare Training, *by R. D. Gilson, and R. W. Ventola* 322

25. Two-Dimensional Compensatory Tracking With Tactile Displays, *by H. P. Schmid, G. A. Bekey, and J. B. Reswick* 332

26. A Simulator Study of Helicopter Pilot Workload Reduction Using a Tactile Display, *by R. S. Dunn, R. D. Gilson, and P. Sun.* . . . 355

27. Control Augmentation and Workload Reduction by Kinesthetic Information From the Manipulator, *by S. J. Merhav and O. Ben Ya'acov.* 361

Session V. TRACKING AND OTHER PSYCHOMOTOR TASKS

Chairman: D. L. Baty

28. Time Optimal Control of an Undamped Harmonic Oscillator: Evidence for Biases and Schemata, *by R. J. Jagacinski, M. W. Burke, and D. P. Miller* 383

29. Continuous Compensatory Audio Manual Tracking, *by R. G. Costello.* . 406

30. Eye Tracking: Horizontal vs. Vertical, *by J. Hornseth, G. Stanley, J. Porterfield, and P. Carson* 422

31. Head Tracking: A Fatigue Study, *by J. Hornseth, G. Stanley, and P. Carson* 430

32. A Comparison of In-Flight and Ground-Based Pitch Attitude Tracking Experiments, *by M. F. C. van Gool and H. A. Mooij.* . . . 443

33. Effects of Headgear and Visual Angle on Head Rotation Spectral Characteristics, *by D. K. Shirachi, D. L. Monk, and J. H. Black, Jr.* 455

34. Human Engineering Laboratory Helicopter Observer Performance Studies, *by J. A. Barnes.* 469

35. Interaction Between Warning Signal and Fore-Period in Simple Foot Reaction Time, *by N. S. Nataraj and J. M. Howard* 477

Session VI. AUTOMOBILE DRIVING

Chairman: G. A. Bekey

36. A Simulator for Driving Research, *by R. G. Mortimer and R. L. Adkins.* 493

37. Alcohol Effects on Performance of Driver Decision-Making Tasks in a Laboratory Simulation, *by R. W. Allen, S. H. Schwartz, and D. T. McRuer*
(This paper was presented but not received for inclusion in the proceedings.)

38. Expected Value Analysis of Driver Decision Making Under Alcohol, *by S. H. Schwartz and R. W. Allen*
(This paper was presented but not received for inclusion in the proceedings.)

39. Spectral Analysis of the Driver-Vehicle System in Car Following, *by R. Herman, R. Rothery, and R. Rule*
(This paper was presented but not received for inclusion in the proceedings.)

Session VII. HANDLING QUALITIES AND PILOT RATINGS

Chairman: S. J. Merhav

40. A Statistical Approach to the Analysis of the Pilot Behavior on Multiloop Systems, *by N. Goto* 501

41. Application of a Model-Based Flight Director Design Technique to a Helicopter Hover Task, *by R. A. Hess*
(This paper was presented but not received for inclusion in the proceedings.)

42. A Method for Generating Numerical Pilot Opinion Ratings Using the Optimal Pilot Model, *by R. A.Hess*
(This paper was presented but not received for inclusion in the proceedings.)

43. Ride Quality Sensitivity to SAS Control Law and to Handling Quality Variations, *by P. A. Roberts, D. K. Schmidt, and R. L. Swaim* 528

44. A Unified Theory for Pilot Opinion Rating, *by R. H. Smith* 542

45. Longitudinal Flying Qualities in the Landing Approach, *by W. W. Rickard*. 559

46. Worth Assessments of Approach to Landing, *by R. E. Curry*. 585

Session VIII. REMOTE MANIPULATION

Chairman: T. B. Sheridan

47. **A Computer-Controlled Machining and Manipulating Device,** *by T. C. Woo and J. M. Paul* 595

48. **Mechanical Design and Computer Configuration in the Computer-Aided Manipulator Control Problem,** *by P. Coiffet, J. Vertur, and E. Dombre* 607

49. **A Preliminary Evaluation of Manual Control Tasks Associated With the Space Shuttle Remote Manipulator System,** *by L. Reid* 624

50. Modeling a Manipulation Task of Variable Difficulty, *by J. W. Hill and S. J. Matthews* 639

51. A Comparison of Master-Slave and Rate Control in the Presence of a Transmission Time Delay, *by G. P. Starr* 661

Session IX. SYSTEM IDENTIFICATION

Chairman: L. Reid

52. A Comparison of Techniques for Identifying Human Operator Dynamics Utilizing Time Series Analysis, *by K. Tanaka, N. Goto, and K. Washizu* 673

53. System Identification via a Microcomputer, *by R. Mekel and A. Singh* 694

54. PID (Proportional Integral Derivative) Modeling Techniques Applied to Studies of Motion and Peripheral Display Effects on Human Operator Performance, *by D. W. Repperger and A. M. Junker* 703

55. Sensitivity Analysis of Motion and Peripheral Display Effects on Tracking Performance, *by D. W. Repperger and A. M. Junker* 719

Session X CONTROL MODELS

Chairman: S. Baron

56. Low Visibility Landing Simulation Experiments, *by R. V. Gressang, J. J. Pollard, and D. L. Kugel* 733

57. The Application of Pilot Modeling to the Study of Low Visibility Landing, *by W. W. Harrington* 748

58. Stability of the Pilot-Aircraft System in Maneuvering Flight, *by J. R. Broussard and R. F. Stengel* 778

59. Analysis of a Manned Anti-Aircraft Artillery (AAA) System Using a Proportional-Integral-Derivative (P-I-D) Structure Optimal Control Gunner Model, *by A. V. Phatak and K. M. Kessler* 795

60. Analysis of Controls and Displays for a Terminal Controlled Vehicle (Abstract), *by W. H. Levison and S. Baron* 819

61. A Model of the EMG-Torque-Movement Relationships for Knee Extension, *by E. Dombre, G. A. Bekey, and J. Perry* 820

62. A Model of the Reflex Arc and Analysis of the Behavior of the Peripheral Receptors During Clonus, *by J. E. Dollman, A. M. Iannone, and L. T. Andrews* 836

Session XI. MOTION AND VISUAL CUES

Chairman: R. C. Williges

63. A Pilot Model With Visual and Motion Cues, *by R. E. Curry, L. R. Young, W. C. Hoffman, and D. L. Kugel* 851

64. The Evaluation of Peripheral Display Units in a Fixed Base Simulator, *by L. Reid and A. J. Fraser*. 855

65. Roll Axis Tracking Improvement Resulting From Peripheral Vision Motion Cues, *by T. E. Moriarty, A. M. Junker, and D. R. Price* . . 868

66. Comparative Effects of Motion and Peripheral Displays on Roll Axis Tracking, *by A. M. Junker*
(This paper was presented but not received for inclusion in the proceedings.)

67. Use of Motion Cues in Steady-State Tracking, *by W. H. Levison* . . . 895

68. The Influence of Loss of Visual Cues on Pilot Performance During the Final Approach and Landing Phase of a Remotely Piloted Vehicle Mission, *by J. C. Howard*. 918

69. Simulation of Conventional Aircraft Approach and Landing: The Effect of Withholding Motion or Instrument Cues, *by R. V. Gressang* 932

70. Effects of Differing Motion System Drives on Simulation of Approach and Landing, *by J. J. Pollard*. 941

71. Thresholds of Motion and Perception Measured in a Flight Simulator, *by R. J. A. W. Hosman and J. C. van der Vaart*. 956

72. Biomechanical Response and Manual Tracking Performance in Sinusoidal, Sum-of-Sines, and Random Vibration Environments, *by W. H. Levison*. 985

SESSION I

MULTI-TASK DECISION MAKING

Chairman: R. W. Allen

REVIEW OF THE SYMPOSIUM ON MONITORING BEHAVIOR AND SUPERVISORY CONTROL

(BERCHTESGADEN, F.R. GERMANY, MARCH 8-12, 1976)*

by Thomas B. Sheridan

Massachusetts Institute of Technology
Cambridge, Ma. 02139

SUMMARY

The motivation for this meeting was the fact that the role of the human operator in manned systems is changing from that of a continuous in-the-loop controller to that of a monitor and supervisor. The rapid development of the computer is the primary force which is causing this change, especially the fact of marked decrease in cost and size, along with associated new and more sophisticated developments in software and display technology.

To deal with these issues, over 100 participants from fifteen countries assembled during 8-12 March, 1976, at Berchtesgaden, F.R. Germany, in the Bavarian Alps. Thirty-five papers were presented in three categories: vehicle control (aircraft, automobiles and urban mass transit, ships); process control (industrial manufacture, nuclear reactors); and general models of monitoring and supervisory control.

Intensive workshop discussions involving all the participants were held throughout the symposium to define better the human operator's role changes, the concommitant changes that are necessary (new priorities) in research, the associated problems in implementation, and required new interdisciplinary and institutional arrangements.

INTRODUCTION:
THE NATURE OF SUPERVISORY CONTROL

Figure 1 characterizes the trend in controlling complex systems. Figure 1a represents control of a modern aircraft, where at the lowest level of control and on a short time scale, thrust, pitch, roll and yaw are stabilized relative to gust disturbances and reference commands coming from guidance logic. At a next level, the vehicle's course is controlled relative to prevailing winds and reference commands from the navigation logic. Finally, the navigation process can be automated, in part, by ground-based as well as on-board computers. At each level in the multi-loop control heirarchy the

* Dr. Gunnar Johannsen of Forschungsinstitut für Anthropotechnik, Meckenheim, Germany, was Co-director along with the author. The meeting was sponsored by the Special Programmes Panel on Human Factors, Scientific Affairs Div., NATO, and by the Federal Republic of Germany. The papers and workshop reports will soon be available from Plenum Press in a book entitled Monitoring Behavior and Supervisory Control.

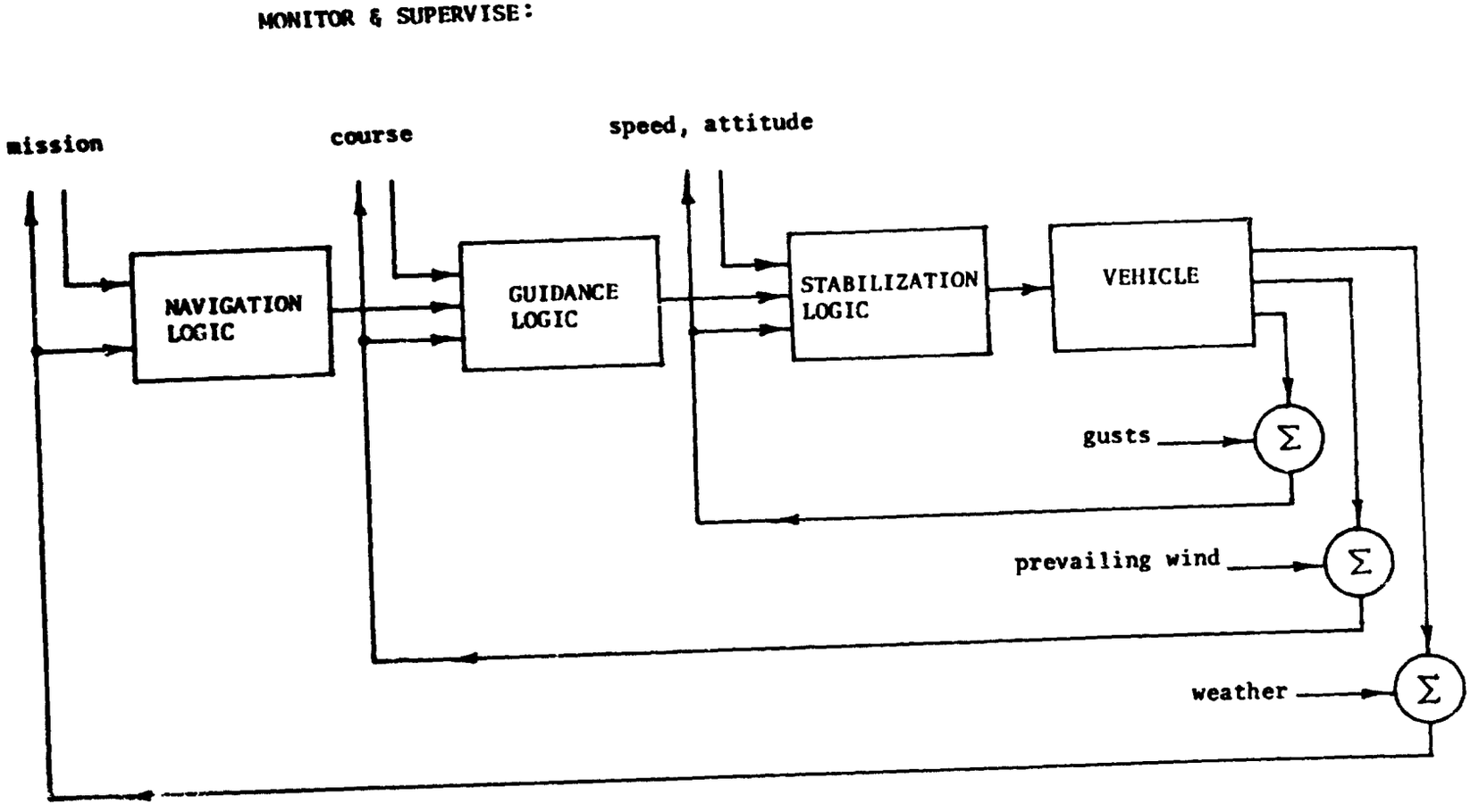

Figure 1a. Supervisory Control of Aircraft

human operator can make inputs. At the lowest level he can provide continuous stick-pedal commands to the inner loop (and does, of course, during critical take-off and landing maneuvers). At the middle level he can provide intermittent course changes by resetting course relative to a computer-navigation base. At the highest level he can modify the flight plan or mission in major ways, in conjunction with persons on the ground and/or other aircraft. At each higher level the nature of his control is different, responses becoming more intermittent (longer time between responses) and involving more monitoring and more interaction with computers and with other persons.

Actually it was probably in spacecraft where the multi-level control first was implemented to any degree of sophistication and where one might say we first saw "supervisory control". It is rather arbitrary to set the number of levels in the control heirarchy at three (except that the conjunction of the three words "navigation", "guidance" and "stabilization" has come into common use in the aerospace industry). In the Apollo spacecraft one can list many more levels of control for some functions, especially if one considers nested control loops in computer software, layers of backup or abort modes, etc.

Turning to a different kind of system, the chemical plant, one finds a similar heirarchy or nesting of control loops, with successively longer time constants, successively less continuous real-time automatic control, and successively more human interaction with higher level control. Figure 1b suggests three levels of control associated with: "valve control" to regulate instant-by-instant temperature and pressure; "mixing logic" to effect longer term mixing procedures; and "plant management" to control the major steps of producing the given product.

A third example (Figure 1c) is found with the industrial robot, as used for manipulating and assembling discrete parts on the production line. At the lowest level conventional servomechanisms control instantaneous forces and positions of the actuators for each degree of freedom. At a middle level a computer decides what sequences of positions and forces for the component degrees of freedom to command in order to achieve certain elementary manipulations ("therbligs")which are programmed from above, like: reach, grasp, insert, release, etc. The highest level the control system coordinates is the robot's accomplishment of various tasks in conjunction with the production line, special parts feeders, other robots or human workers, etc. Again, most of the human effort is in monitoring and supervising at the highest control level,though in case of emergencies or for maintenance or repair the human operator may intervene into automatic loops and apply direct control to lower levels.

Figure 2 illustrates supervisory control from the viewpoint of the human operator. He observes displays which may present pictorial, graphic, or alphanumeric information. In the near future he may also listen to computer-generated speech information. He operates hand controls which may be of the symbolic type (keyboard) or analogic type (joystick, light pen). In the near future he may speak in specialized code and be recognized by computer.

The characterization in Figure 2 shows a "local" control loop in which the human operator can test his plans and programs before committing them to action. This is analogous to the way the chief executive uses planning

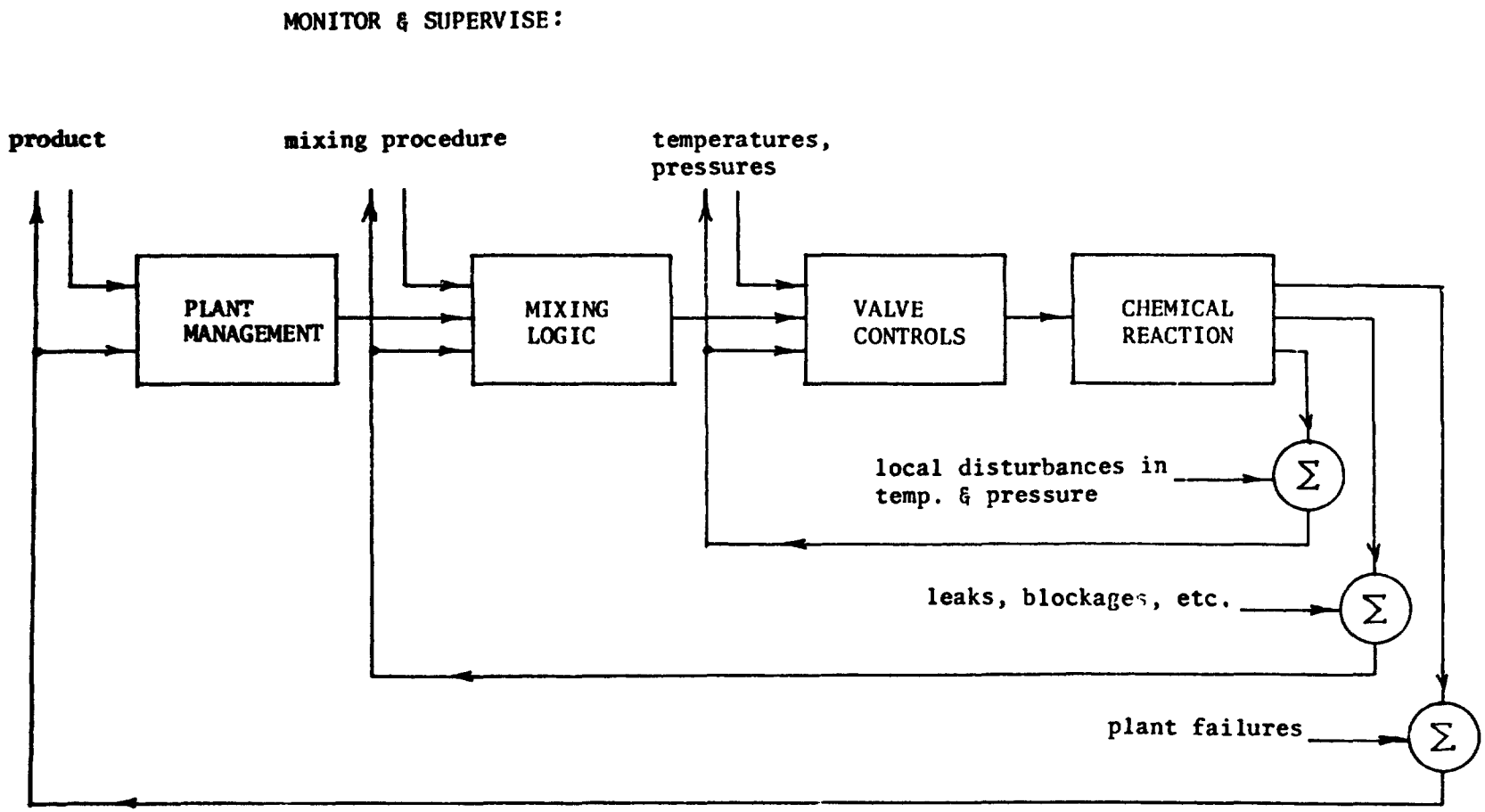

Figure 1b. Supervisory Control of Chemical Plant

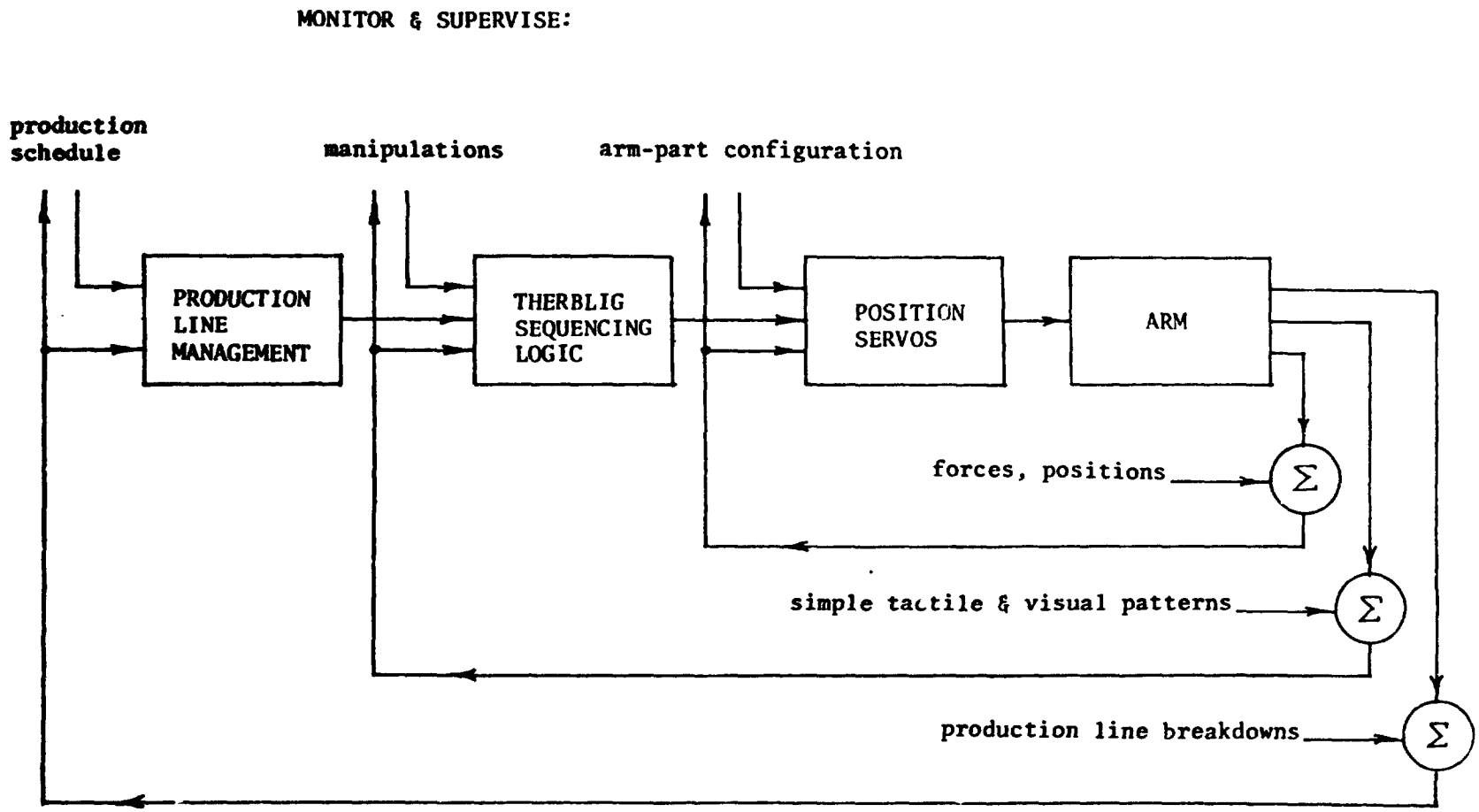

Figure 1c. Supervisory Control of Industrial Robot

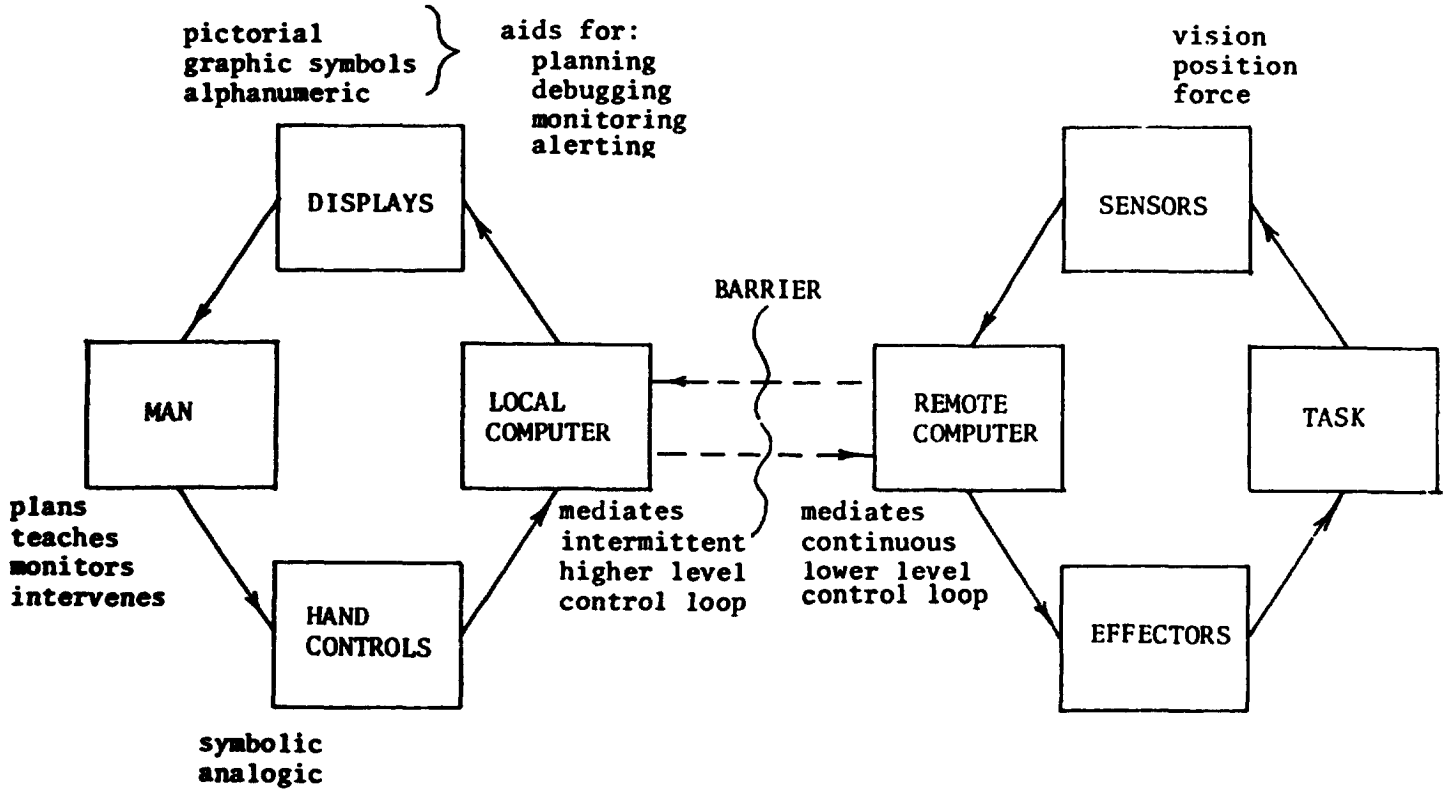

Figure 2. Paradigm of Supervisory Control

staff in the managerial heirarchy of any large organization. After both plans and communications (teaching or programming in this case) have been worked out, the chief executive orders his line organization into action (via the supervisory link in Figure 2). He then monitors what happens as his subordinates (in this case the "remote" control loop, with its own sensors, delegated decision-making powers, and capability to effect its own actions) take over, reassuming control in emergency or when his instructions have been executed.

EMPHASES AND POINTS OF CONSENSUS

The following, in the opinion of the author, constitute the major highlights, emphases of the papers presented at the Symposium, and points of consensus which emerged from the workshops. The reader is referred to the full papers and workshop reports, forthcoming from Plenum Press.

Multiplicity of Interfaces

Understanding monitoring behavior and supervisory control requires observation and analysis at a multiplicity of system interfaces. Figure 3 (after E. Edwards of the University of Loughborough, England) is a convenient way of portraying these interfaces: the conventional man-machine interface between a human operator ("liveware") and the hardware; a linguistic interface between him and the software; a physiological interface between him and the environment; and a social interface between him and other persons in the system. Edwards called this the "SHELL" model for obvious reasons.

Use of Simulators

The papers and workshops affirmed the increasing use of simulators in complex man and computer-controlled systems. A first reason is that, because of the rich electronic intercommunication of component subsystems in simulators and the availability of computers intrinsic to the system, it is relatively easy to do measurements, data storage, data correlation, and even on-line modeling of human behavior. A second reason for simulation is that it is the best way (perhaps the only viable way) to provide human operators exposure to low probability events - which is one of the major reasons that human operators are included in such systems.

Workload

There was a great deal of discussion about human operator workload. Four alternative definitions of workload were evident. A first definition is in terms of what the task demands are for "satisfactory performance" (required reduction in uncertainty, positioning speed or accuracy, forces required, etc.). A second is in terms of the level of effort or difficulty as perceived (subjectively) by the operator. A third is in terms of what the

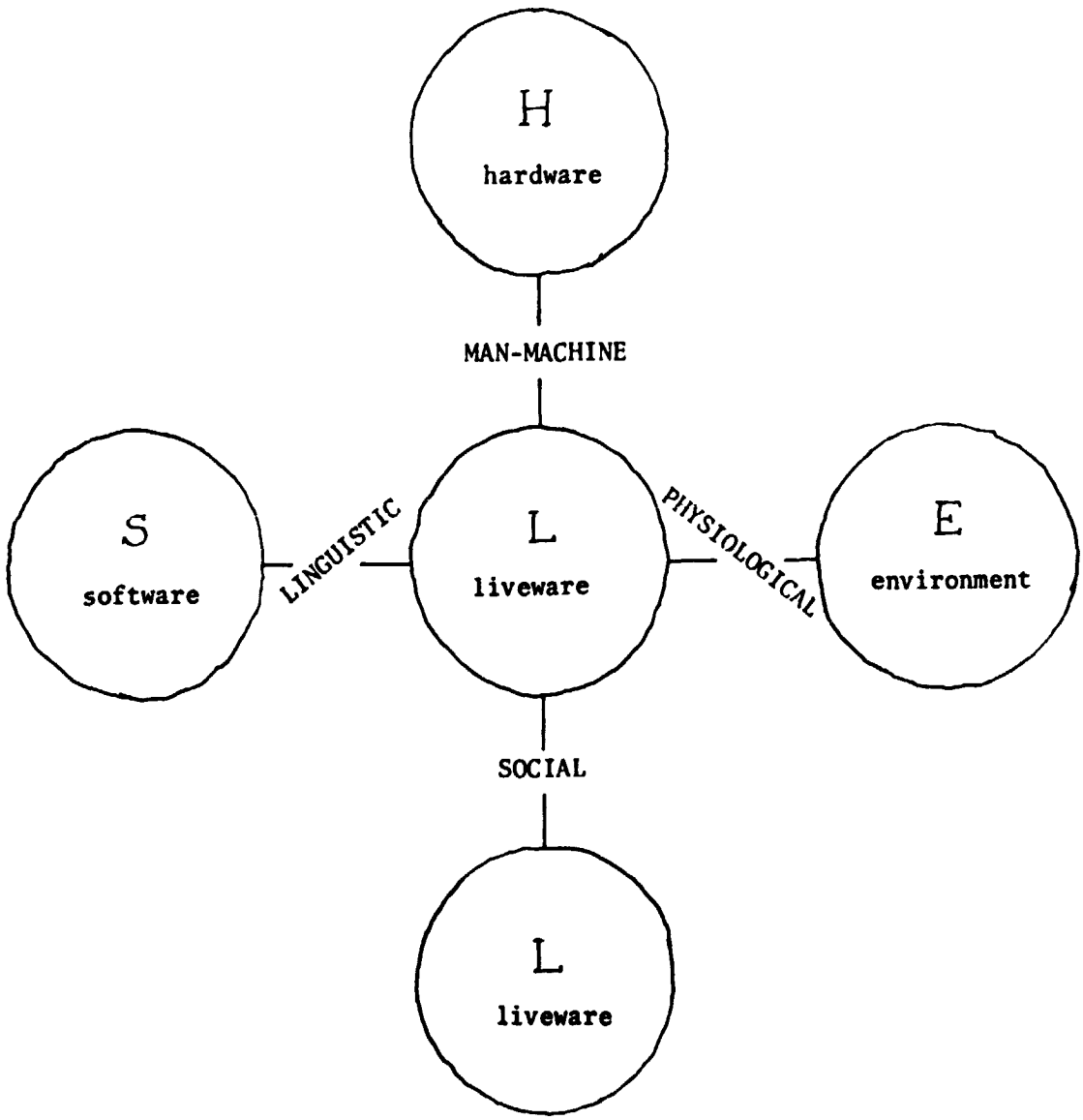

Figure 3. SHELL Model of Interfaces

operator actually accomplishes, or some objective measure of his decision success, speed, accuracy, or force. A fourth is in terms of risk or actual detriment to his health or future capabilities. The common technique of defining workload as the negative of "spare capacity" (objective performance on a "side task") would fit the third category. The greatest problems in workload analysis seemed to be in finding operational definitions which are common across a variety of tasks.

Internal Models of External Systems

Keen interest in "internal modeling" was evident. The internal model is as old as the ancients: the notion is that somehow the brain has an internal representation of structures in the external world - of which it can ask"what would happen if ... " and get reasonable answers. In more recent years, "plant-model" controllers and Kalman filters have become useful tools in control, and human operator modelers have hypothesized that people make use of such internal models too - at least that is a convenient normative base from which to model. For example, the well-known "Kleinman-Baron-Levison optimal control model" of the human operator includes a Kalman predictor as an internal model, and so do recent failure-detection models of Curry and Gai.

When considering man-computer cooperation in supervisory control systems, the problem arises whether the human operator needs an internal model not only of the process or vehicle to be controlled but also of the decision-making processes which involve the computer serving as a lower-level controller. Such a consideration elicited further concern by some Symposium participants that the computer needs not only an internal model of the process to do its control job, but must also have some model of what the human is likely or able to do in order that it can decide when to relinquish control to the human or take back control. More is said of this man-computer responsibility problem later.

Representation of Goals and Performance Criteria

Closely associated with the "internal models" discussions were those of performance criteria, objective functions, cost functions, payoff functions, tradeoff functions (and other terms, all of which mean the specification of what is good and what is bad for a particular system).

It is not easy for the experimenter to communicate to an experimental subject a precise performance criterion or objective function, nor can a human operator in an actual system explain precisely what function of relevant variables he is seeking to maximize. Attempts to communicate such functional relationships in mathematical form almost always fail because most people simply don't understand their own behavior in such terms. Thus the experimenter or the analyst of actual system behavior must <u>infer</u> the performance criterion actually being used - either from observation of actual system behavior or from a battery of subjective judgments which the subject says he would make if confronted with given particular situations.

If inference of performance criterion is made from subjective judgments,

there are several techniques which are under active development. One of these is "multidimensional scaling" - a technique developed at Bell Telephone Laboratories and based upon subjective judgment of dissimilarity between multi-dimensional stimuli. By least-squares regression it yields "principal axes" of difference between stimuli. A second technique is "multi-attribute utility", developed by Raiffa, Keeney and others, and based on indifference judgments of utility (or worth) with respect to lotteries. It yields multi-dimensional cardinal scales of utility. A third technique called "interpretive structural modeling" was developed by Warfield and his colleagues at Battelle Institute, and is appropriate where transitive orderings can be made among stimuli. A fourth technique called "policy capturing" makes use of direct worth assessment . And so on. All of these techniques have interactive computer procedures to accompany them.

Tradeoffs in System Strategy

The Symposium also dealt with what might be called "system strategy tradeoffs" - questions of management philosophy regarding overall strategy for making the system work best.

Perhaps two such tradeoffs are most important. The first is the question of relative power of the human operator vs. the computer over one another. Who monitors whom? Should the human operator always have the upper hand, the final word? Or should system designers endow the computer with the capability to overrule erratic and detrimental decisions of the operator? To what extent should man and computer be working in parallel, independently and in relative ignorance of what the other is intending? Or is it preferable that man and computer cooperate in close harmony, each being continually updated on what the other is doing and intending? These questions were in no way resolved. But the need for further research was evident.

A second "strategy tradeoff" is between acquiring enough data to be confident of action vs. acting with anticipation. This is a somewhat older problem of cybernetics, and does have a quantitative solution provided the event states are well defined, and all the appropriate prior and contingent probabilities of these events are known, as well as the costs/benefits of possible outcomes.

Tradeoffs in Modeling

Questions of modeling philosophy were of particular interest because, as systems become more complex and the role of the human operator becomes more "supervisory" and thus less amenable to definition, modeling becomes more difficult.

These questions might, again, be posed in terms of trading relations:

a) Mathematical models of man-machine systems are complex and incomprehensible to many people to begin with, and lately are becoming more so. Yet the more traditional verbal model of classical behavioral and social science is often ambiguous and not seen as particularly useful in doing an engineering job. Is there a practical compromise between mathematical complexity and verbal ambiguity?

b) Controlled experiments require a constraint and distortion of reality,

and the experimental subject knows this. Thus validity of his behavior is questioned. Reality, on the other hand, is chaotic. How to trade between the unreality of experimental control and the chaos of reality?

c) A common criticism of man-machine systems and technological "progress" generally is that the people involved are more and more forced to behave like (and be modeled like) machines. Should that trend continue? Or should there be a counter-trend to enable human operators to behave and be modeled as fully free, creative, social, emotional people?

d) As engineering areas have matured there have been efforts to standardize certain models, definitions, measures, etc. across the professional community. Should no standardization be introduced in this field, is it impossible or premature, or should some standardization efforts be pursued?

e) Man-machine modelers have been criticized as being "mechanistic", "logical-positivist", "behaviorist", and therefore presumably out of date, especially as we move toward supervisory control. The opposite might be a "gestalt", "holistic" approach. E.R.F.W. Crossman has used the term "polyvalent craftsman" to characterize the human supervisor. Can modeling in such terms be useful, and what compromises are appropriate?

Ethical Implications

There is much talk these days of making individuals, companies, and nations more "productive". Mostly, it seems, "productivity" is considered in functional terms - speed, reliability, etc. At the Symposium there was great concern, especially among the Scandanavian delegates, about productivity in human terms - job satisfaction- and whether work is meaningful.

What changes is the computer making with respect to job satisfaction, not only as regards employment statistics and training requirements? We are warned that the computer and associated automation may be making the human worker spatially more remote from actually handling the product, and temporally less synchronized with the rhythms of traditional work. The worker may perceive that he has less and less direct effect on the product, is more and more specialized, and has less and less understanding of the production process generally.

The rumblings in this problem area seemed a bit more significant than I remember them to have been in previous meetings.

HUMAN CONTROL AND MONITORING-MODELS AND EXPERIMENTS

By P.H. Wewerinke

National Aerospace Laboratory (NLR)

SUMMARY

This paper deals with the results of a theoretical and experimental program concerning human monitoring behavior. Apart from monitoring an automatic approach, combined monitoring and manual flight director control was studied to determine the interference between subtasks. Also simultaneously monitoring and auditory tracking was included.

The results demonstrate that the multivariable monitor model adequately describes human behavior in the aforementioned tasks. Furthermore, a multivariable workload model is developed. Computed workload is shown to agree excellently with subjective ratings.

INTRODUCTION

With increasing complexity and automation of aerospace vehicles the human operator's role shifts from controller to supervisor. This necessitates the proper tools for describing these manned vehicle systems. Apart from controlling the system (to which situation considerable modeling effort has been devoted), the pilot often has to fulfil other crucial functions, such as monitoring the automatic system, making decisions, detecting system failures, etc. The insight in this higher mental functioning is still rather incomplete although several attempts have been made to investigate and model signal- and failure detection behavior.

The object of this study was to describe human monitoring behavior and to determine how it is affected by performing other tasks (interference). For this, a model for monitoring multivariable systems has been developed which can be considered as an extension of the research of Levison et al (Ref. 4). Essentially, it is a cascade combination of the subjective expected utility model (Refs. 2 and 3) and the state estimation submodel of the optimal control model.

The model has been tested against experimental results of a fixed base simulator program, dealing with monitoring the automatic approach of a DC-8. Also combined monitoring and manual flight director control (using the optimal

control model) was investigated to determine the interference between several subtasks using the task interference model given in reference 5. For the same reason, the monitor tasks were combined with an auditory tracking task.

In section 2 the human operator models involved will be briefly reviewed. Section 3 contains a discussion of the experimental program and a comparison of the predicted and measured results. In section 4 pilot workload is analyzed and a multivariable workload model is developed in accordance with the task interference model fractional workload model suggested in reference 5.

HUMAN OPERATOR MODELS

This section summarizes the mathematical models which are used to predict and analyze the results of the experimental program discussed in the next section. The models deal with human control-, monitor- and decision making behavior as well as their mutual interference.

Human control behavior is described by the optimal control model (OCM) developed by Kleinman and Baron (Ref. 1). This model consists of a perceptual model indicating how the "displayed" variables are related to the "perceived" variables, and a response model. The latter model describes how the internal representation of the task environment results in the actual control input(s).

Human decision making behavior is described by the perceptual model, however now in a cascade combination with the subjective expected utility model (Refs. 2-4). This model, reflecting how "perceived" information results in an optimal (binary) decision strategy, will be briefly discussed in the next chapter.

Interference between several tasks is accounted for by the task interference model developed and partly validated by Levison et al (Refs. 4 and 5). This model plays a major role in the present study not only to predict the interference between the pertinent control- and decision making tasks but also to formulate the fractional and total workload involved in performing the tasks. For this reason the task interference model is briefly discussed in chapter 2.2.

Human operator workload is expressed in terms of the fractional attention corresponding with each subtask (Ref. 5). One objective of the present study was to extend and validate this model in order to predict human operator workload corresponding with multivariable control- and decision making tasks.

Decision making model

Perceptual model

Decision making is assumed to be based on the internal representation of the state of the world, $\hat{x}$. This internal model of the system state, x, is based on the "perceived" variables, y_p according to

$$y_p(t) = y(t-\tau) + v_y(t-\tau) \qquad (1)$$

where y represents the "displayed" variables, τ is a lumped "equivalent" perceptual time delay, and v_y is a vector of independent, white, Gaussian observation noises. The autocovariance of each noise component appears to vary proportionally with mean-squared signal level and may be represented as

$$V_{y_i}(t) = \tau P_{y_i} E\left\{ y_i^2(t) \right\} \qquad (2)$$

where P_{y_i} is the "noise/signal" ratio corresponding with the fractional attention paid to variable y_i (see chapter 2.2).

Denoting the covariance of the difference between the instantaneous value of the state vector and the estimate of it ($e(t) = x(t) - \hat{x}(t)$) by Σ, the pair $(\hat{x}, \Sigma)$ constitutes a sufficient statistic to test hypotheses about x, based on the data y_p.

Subjective expected utility model

It is assumed that the human's decision strategy is reflected by the following stages (Refs. 2-4).

- formulate (N) possible hypotheses, H_j
- assess probabilities of all hypotheses based on the available information y_p, $P(H_j/y_p)$
- determine (M) possible decisions, D_i
- assign the utilities to each hypothesis/decision combination U_{ij}
- determine the maximum utility-decision D^* according to $D_i = D^*$ for $E = E_{max}$, where

$$E\left\{U/D_i\right\} = \sum_{j=1}^{N} U_{ij} P(H_j/y_p) \qquad (3)$$

Many decision making situations involve binary decisions (the choice between two hypotheses, e.g., the probability of a successful landing is large enough or not). Both the following analysis and experimental program deal with this class of decision tasks.

Now, let the mutually exclusive hypotheses H_0 and H_1 correspond to the events that $x \in R$ and $x \notin R$, respectively, where R is defined as some region (or window) in the state space. Using eq. (3) the human's decision is therefore given by

$$D = D_1 \text{ if } \frac{P(H_1/y_p)}{P(H_0/y_p)} > \frac{U_{00}-U_{10}}{U_{11}-U_{01}} \equiv \frac{U_0}{U_1}$$
$$D = D_0 \text{ otherwise} \tag{4}$$

In the following the target region R is given by a multidimensional "window"; then for H_0 can be written

$$H_0 : x_{TL_i} < x_i < x_{TU_i} \quad \text{for all } i,\ i=1,\ldots,n \tag{5}$$

where x_{TL_i} and x_{TU_i} represent the lower and upper target boundary, respectively. Computation of eq. (4) requires the posterior probability of hypothesis H_0

$$P(H_0/y_p) = \int_{x_{TL_1}}^{x_{TU_1}} \cdots \int_{x_{TL_n}}^{x_{TU_n}} p(x/y_p)\, dx_1 \ldots dx_n \tag{6}$$

where $p(x/y_p)$ is (assumed to be) Gaussian with mean $\hat{x}$ (maximum likelihood estimate) and covariance Σ. For the computation of various measures of decision performance it is convenient to define the human's decision space DS using eq. (4)

$$\frac{P(H_1/y_p)}{P(H_0/y_p)} = \frac{U_0}{U_1} \tag{7}$$

or

$$P(H_0/y_p) = \frac{U_1}{U_0+U_1} \tag{8}$$

Combining eqs. (6) and (8) yields

$$\int_{x_{TL_1}}^{x_{TU_1}} \cdots \int_{x_{TL_n}}^{x_{TU_n}} p(\delta, \Sigma)\, dx_1 \cdots dx_n = \frac{U_1}{U_0+U_1} \qquad (9)$$

where $p(\delta,\Sigma)$ represents the normal probability density function with mean δ (representing the elements of DS) and covariance Σ. Now the probability that decision D_0 is made can be computed according to

$$P(D_0) = P(\hat{x} \in DS) \qquad (10)$$

The probability of wrongly deciding D_0 is given by

$$P(H_1,D_0) = P(x \notin R, \hat{x} \in DS) \qquad (11)$$

Alternatively, the probability of wrongly deciding D_1 can be computed according to

$$P(H_0,D_1) = P(x \in R, \hat{x} \notin DS) \qquad (12)$$

Foregoing theoretical decision making measures will be compared with the corresponding measures obtained in the experimental program discussed in section 3.

Task interference model

Task interference is modeled in terms of the following relationship between fraction of attention, f_i, paid to subtask (indicator) i, and the corresponding human's internal noise/signal ratio, P_i

$$P_i = P_{o_i}/f_i \qquad (13)$$

where P_{o_i} is the ratio corresponding to single-task performance ("full attention"). Furthermore, it is assumed that the amount of information-processing capacity is determined by the demand of the subtasks and not by the amount of subtasks to perform. In formula

$$\sum_{i=1}^{M} f_i = 1 \qquad (14)$$

This model developed by Levison et al, has been partly validated for some multivariable control situations (Ref. 5) and dual decision making tasks (Ref. 4). In the present study the model will be tested in multivariable

hypotheses-situations, and in combined control and decision making tasks (both interacting and non-interacting).

In reference 5 the concept of fractional attention, is related to fractional workload. Based on this suggestion a multivariable workload model (both for control and decision making situations) will be presented and compared with experimental data (subjective ratings). The model will be discussed in section 4, because it has not been used to predict the experimental results.

EXPERIMENTS

Experimental set-up

In order to investigate monitoring behavior for various task situations, the following single-task configurations were examined in the experimental program (figure 1)

- monitoring the fast/slow- and the glideslope indicator during an automatic approach of a DC-8 (indicated by M2).
- monitoring the fast/slow-, the glideslope- and the localizer indicator (M3).
- manual (flight director) approach (only longitudinally) of a DC-8 (C).
- auditory presented unstable first order tracking task with a time constant of 1 sec (A).

Also combinations of these tasks were included to validate the aforementioned task interference model for both control and monitoring tasks. Combining the longitudinal control task and the two monitoring tasks results in "two" interacting tasks, or put another way, the prior probabilities of the monitor tasks depend on the human control behavior. The combinations of the monitor tasks and the auditory tracking task were included to study the interference between the monitor tasks and non-interacting (side-) tasks (e.g., radio-communication, procedural tasks, etc). So, the resulting combined task configurations are M2C, M3C, M2A and M3A.

Single-task configurations

Referring to figure 1, the decision making tasks were intended to represent the pilot's task of deciding whether or not he is within the "landing

window". Each indicator was displayed along with two reference indicators showing the "target" or region of acceptable deviations. The subject depressed a response button whenever he decided hypothesis H_1 to be true (one or more indicators outside their region of acceptance).

The longitudinal control task was a manual approach tracking task (without the time varying aspect involved in an actual approach and landing task) using a flight director (FD in figure 1). The flight director design, autopilot characteristics and turbulence levels are derived from reference 6.

The first order instability task was presented auditory. The display characteristics were such that the perceived tone (pitch) was linearly related to the system output (Ref. 7). No external driving noise was included, so the subject's task was to minimize his remnant by manipulating an isometric side-arm controller.

Measures, subjects and procedure

For the decision making tasks the measures discussed in section 2 were taken. Tracking performance was measured in terms of the relevant variance-scores (ILS-deviations, flight director deviations, speed deviations, stick activity, and audio display-deviation). Furthermore, pilot workload was measured in terms of subjective ratings on the scales presented in table 1. In case of the dual task configurations, an overall impression of the total task difficulty was given.

Four general aviation pilots participated in the experiment. The subjects were provided with about fifty training trials totally (six on each of the eight configurations) corresponding with a relatively stable level of performance. In the formal experiment each configuration was presented four times per subject. The duration of the trials was five minutes and the order of presentation of the trials per subject was random.
In the combined control- and decision making task the subjects were instructed to perform the control task as well as possible and to spend their "reserve capacity" on the decision making task.

Theoretical and experimental results

Since space does not permit an extensive presentation of the experimental results*, only the principal results will be discussed corresponding with the model predictions.

* These will be contained in a later report.

Single-indicator tasks

In order to obtain noise/signal ratios corresponding to monitor single-display indicators ("full attention") a base-line experiment was conducted to "calibrate" the displays. Three subjects performed each of the three single-indicator decision making tasks two times. The measured decision making scores are shown in table 2. Two model parameters were varied to match the corresponding scores: the observation noise level associated with the displayed variable and the utility ratio U_1/U_0. The perceptual time delay, τ, was kept constant (0.20 sec). The resulting model scores are also given in table 2. Although the subjects were instructed to weigh "miss"-errors and "false alarm"-errors equally and to minimize the total decision error, P_e, they were apparently somewhat reluctantly in deciding "in" (U_1/U_0=1.75). Based on this result U_1/U_0=1.5 was used for the subsequent model predictions. The resulting observation noise levels* reflect display phenomena and/or "indifference" thresholds. These values were assumed to be the ratios corresponding to "full attention" (P_{o_i}).

Using eq. (13) the actual noise/signal ratio could be determined given the fraction of attention, f_i, paid to indicator i for the multivariable decision making (and control) tasks.

Multivariable decision tasks

Decision scores were predicted for the M2- and M3-tasks assuming an equal division of attention among the display indicators. A comparison of measured and predicted scores (Table 3) reveals an excellent agreement between all corresponding scores. The effect of the ratio U_1/U_0 on the decision making scores is shown in figure 2. As expected the probability of deciding "in" as well as the joint probabilities are relatively sensitive to this ratio; however, the total decision error, P_e, increases only slightly when U_1/U_0 varies from 1 to 1.5**.

Decision making and non-interacting control

Next the combined auditory tracking and decision making tasks are considered. The following procedure was used.

---

* Observation noise levels corresponding with indicator position are modified because of the non-zero references (Ref. 4).

** The assumed value of 1.5 turned out to be rather close to the actually "measured" ratio. Pilot's comments clarified why this ratio was larger than one: after being out the "window" they wanted to be "sure" before deciding "in" again.

The noise levels of the single audio task were determined by matching the model scores to the measured ones using figure 3; these values correspond to "full attention". The same was done for the audio tasks when performed in combination with the decision tasks. The corresponding fractions of attention (f_A) were used to predict the attention paid to the decision tasks ($1-f_A$). The resulting decision scores are given in table 3. Comparing these scores with the measured errors shows that the model predicts a larger interference than actually measured (about ten percent too large for both M2(A) and M3(A)). Matching the measured decision scores using figures 4 and 5 containing the theoretical curves of decision error versus fraction of attention results in an actual fraction of attention paid to M2(A) of 0.7 and to M3(A) of 0.73.

The explanation for the smaller interference is, of course, the fact that the decision task involves visual information and that the control task is presented auditory. So, we see that the interference between visual and aural information is less than between two visual tasks. It is particularly interesting to note that the amount of interference for the combined M2(A) task is just the same as for the M3(A) task: the total amount of information processing capacity is for both configurations 1.2. Based on these results it is concluded that the task interference model has to be adjusted for multi-modality tasks. For combined visual and auditory tasks the total amount of information processing capacity is tentatively hypothesized to be 1.2 (instead of 1 (2) for full (no) interference).

Decision making and interacting control

The third set of configurations was included to determine the extent to which the task interference model would hold for simultaneous control and decision making when control behavior affects the (a priori) decision making statistics. For this reason the aforementioned split-axis manual approach and monitor task was investigated. The basic assumption in modeling this situation was that control behavior was based on the perception of the flight director and decision making on the basis of the perceived monitor indicators (u, d and y). In other words, it was assumed that two separate internal models were used.

The same procedure was followed as before. The single control task (C) was modeled by matching the model scores to the measured ones. The resulting correspondance (shown in table 4) is obtained for a noise ratio of -18.7 dB. By varying only the observation noise ratio the control tasks when performed in combination with the decision tasks (C(M2) and C(M3)) were matched. The result is also contained in table 4. The corresponding fractions of attention (f_c), shown in figure 6, were used to predict the attention paid to the decision tasks ($1-f_c$). The resulting decision scores are given in table 3. Comparing these with the measured errors shows an excellent agreement for the M3(C) task, however, the predicted errors for the M2(C) task are considerably larger (20 %) than the measured errors. For this reason the measured decision scores were matched using figure 7. The resulting scores (given in

table 3) correspond with a fraction of attention which is about 0.1 smaller than the predicted fraction (based on the interference model).

It is concluded from the foregoing results that the total information processing capacity is relatively constant (1.0 for the M3(C) task and 0.9 for the M2(C) task). However, an interesting refinement to the model will be discussed in the next section incorporating the aspect of pilot workload.

PILOT WORKLOAD

In accordance with the task interference model and the fractional workload model suggested in reference 5, a multi-task workload model is proposed in this section and compared with measured workload (subjective ratings).

Assuming the workload corresponding with performing a single task (indicator), W_o, the fractional workload when performing this task in combination with other tasks is

$$W_i = W_o F(f_i) \tag{15}$$

where $F(f_i)$ represents the functional relationship between the fraction of attention dedicated to the subtask i and the corresponding fractional workload. The total workload involved in performing M tasks is given by

$$W_t = \sum_{i=1}^{M} W_i \tag{16}$$

implicitly assuming that the function F is such that W_i is expressed in units along an interval scale.

Subjective ratings were used which were obtained on the adjectival "demand-scale" shown in table 1 (Ref. 8). This scale is assumed to be an interval scale. Assuming a logarithmic relationship between f_i and W_i results in $F(f_i) = \text{Log } cf_i$ where c is an empirical constant corresponding to the zero of the interval scale. A value of c = 10.5 results in computed total workload values surprisingly close to the measured workload ratings. This is shown in table 5 and plotted in figure 8*.

Returning to configuration M2(C) one can see that the computed workload based on the predicted fraction of attention on the monitor task is larger than the measured workload. This is in accordance with the predicted performance which was superior to the measured decision error. Using the "matched"

* During the single-indicator experiment no workload data were obtained. Therefore, W_{o_u}, etc. were assumed to be equal and estimated by matching the M2 configuration. The result was a rating of 3.1.

fraction of attention results in a predicted workload very close to the value actually measured (see table 5 and figure 8). So, the only question is why the predicted performance-workload trade-off differs from the measured one.

In figure 9 the theoretical curves of decision error versus fraction of attention are shown for both M2(C) and M3(C). For the matched M2(C) task the performance versus workload trade-off, $\Delta P_e / \Delta W = .12$. This is close to the value for the M3(C) configurations (.11). So, the suggestion is that the subjects were not motivated enough to spend their "full" capacity because the pay-off was insufficient. More experimentation will be needed to establish this capacity/pay-off relationship. However, this can be considered as a (useful) refinement to the models which have been shown to describe encouragingly the control and decision making tasks studied in this program, both in terms of performance and workload.

REFERENCES

1. Kleinman, D.L. and Baron, S.: Manned Vehicle System Analysis by Means of Modern Control Theory. NASA CR-1753, June 1971.

2. Edwards, W. et al: "Emerging Technologies for Making Decisions", in New Directions in Psychology II. Holt, Rinehart and Winston, New York, 1965.

3. Edwards, W. and Tversky, A. (Ed.): Decision Making. Penguin Modern Psychology UPS 8, 1967.

4. Levison, W.H. and Tanner, R.B.: A Control-Theory Model for Human Decision Making. NASA CR-1953, December 1971.

5. Levison, W.H. et al: Studies of Multivariable Manual Control Systems: A Model for Task Interference. NASA CR-1746, May 1971.

6. Graham, D. et al: Investigation of Measuring System Requirements for Instrument Low Visibility Approach. AFFDL-TR-70-102, February 1971.

7. Wewerinke, P.H.: A Simulator Experiment to Investigate a Lateral Rate Field Display. NLR TR 74093, June 1974.

8. McDonnell, J.D.: Pilot Rating Techniques for the Estimation and Evaluation of Handling Qualities. AFFDL-TR-68-76, December 1968.

TABLE 1: RATING SCALES

Name:

Task:

Using the scale below, indicate the degree of effort you spend on performing the task

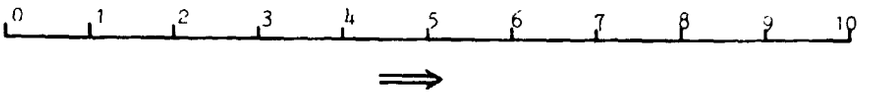

increasing effort

Rating scale for Controllability/observability and Precision

0
1 — Extremely easy to control/monitor with excellent precision
2
3 — Very easy to control/monitor with good precision
4
5 — Easy to control/monitor with fair precision
6
7 — Controllable/observable with somewhat inadequate precision
7 — Controllable/observable, but only very imprecisely
8 — Difficult to control/monitor
8 — Very difficult to control/monitor
9 — Nearly uncontrollable/unobservable
10 ☐ Uncontrollable/unobservable
☐ Not applicable

Rating Scale for Demands on Pilot

0
1
2 — Completely undemanding, very relaxed and comfortable
3
4 — Largely undemanding relaxed
5
6 — Mildly demanding of pilot attention, skill, or effort
7 — Demanding of pilot attention, skill, or effort
8 — Very demanding of pilot attention, skill, or effort
9 — Completely demanding of pilot attention, skill, or effort
Nearly uncontrollable/unobservable
10 ☐ Uncontrollable/unobservable
☐ Not applicable

DISPLAY INDICATOR	PROBABILITY	$P(H_0)$	$P(D_0)$	$P(H_1,D_0)$	$P(H_0,D_1)$	P_e	OBSERV. NOISE (dB)	
							$P_{\dot{y}}$	P_y
u	MEASURED	.70	.68	.02	.04	.06		
	MODEL	.70	.68	.02	.04	.06	-15.	-18.8
d	MEASURED	.82	.79	.02	.04	.06		
	MODEL	.82	.80	.02	.04	.06	-13.	-15.5
y	MEASURED	.75	.73	.03	.04	.07		
	MODEL	.75	.73	.03	.04	.07	-13.	-15.5

AVERAGES OF THREE SUBJECTS, 2 RUNS PER SUBJECT, $U_1/U_0 = 1.75$

TABLE 2: COMPARISON OF MEASURED AND MODEL PROBABILITIES FOR THE SINGLE-INDICATOR TASKS

CONF.	PROBABILITY	$P(H_0)$	$P(D_0)$	$P(H_1, D_0)$	$P(H_0, D_1)$	P_e
M2	MEASURED	.56	.53	.050	.079	.129
	MODEL	.56	.52	.048	.082	.130
M2(A)	MEASURED	.56	.53	.057	.086	.144
	MODEL PREDICTED	.56	.52	.061	.098	.158
	MODEL MATCHED	.56	.52	.053	.089	.142
M2(C)	MEASURED	.47	.43	.088	.116	.204
	MODEL PREDICTED	.47	.41	.057	.110	.167
	MODEL MATCHED	.47	.41	.069	.132	.201
M3	MEASURED	.47	.44	.060	.088	.148
	MODEL	.47	.42	.053	.097	.150
M3(A)	MEASURED	.47	.43	.065	.096	.161
	MODEL PREDICTED	.47	.42	.067	.117	.183
	MODEL MATCHED	.46	.42	060	.101	.161
M3(C)	MEASURED	.36	.32	.086	.115	.201
	MODEL	.36	.31	.072	.128	.201

AVERAGES OF 4 SUBJECTS, 4 RUNS PER SUBJECT

TABLE 3: COMPARISON OF PREDICTED AND MEASURED MONITOR PERFORMANCE

CONF.	SCORE	σ_u FT/SEC	σ_d FT	σ_{FD} DEG.DISPLAY	σ_{δ_e} DEG.
C	MEASURED	3.5	15.7	3.5	2.0
	MODEL	3.4	15.7	3.7	1.9
C(M2)	MEASURED	3.7	17.0	4.0	2.3
	MODEL	3.6	17.0	4.2	2.0
C(M3)	MEASURED	3.7	18.4	4.3	2.2
	MODEL	3.7	18.3	4.5	2.1

AVERAGES OF 4 SUBJECTS, 4 RUNS PER SUBJECT

TABLE 4: LONGITUDINAL CONTROL TASK - COMPARISON OF MEASURED AND MODEL SCORES

CONF.	SUBTASK	W_o	f_i	$F(f_i)$	W_i	W_t	MEASURED WORKLOAD
M2	M_u	3.1	.50	.72	2.2	4.4	4.4
	M_d	3.1	.50	.72	2.2		
M2A	A	3.4	.50	.72	2.4	5.6	5.7
	M2	4.4	.50	.72	3.2		
M2C	C	5.8	.43	.66	3.8	7.2	6.7
	M2	4.4	.57	.78	3.4		
	C	5.8	.43	.66	3.8	6.8	
	M2	4.4	.46	.68	3.0		
M3	M2	4.4	.67	.85	3.7	5.4	5.4
	M_y	3.1	.33	.54	1.7		
M3A	A	3.4	.46	.68	2.3	6.4	6.5
	M3	5.4	.54	.75	4.1		
M3C	C	5.8	.25	.42	2.4	7.3	7.5
	M3	5.4	.75	.90	4.9		

TABLE 5: COMPARISON OF COMPUTED AND MEASURED WORKLOAD

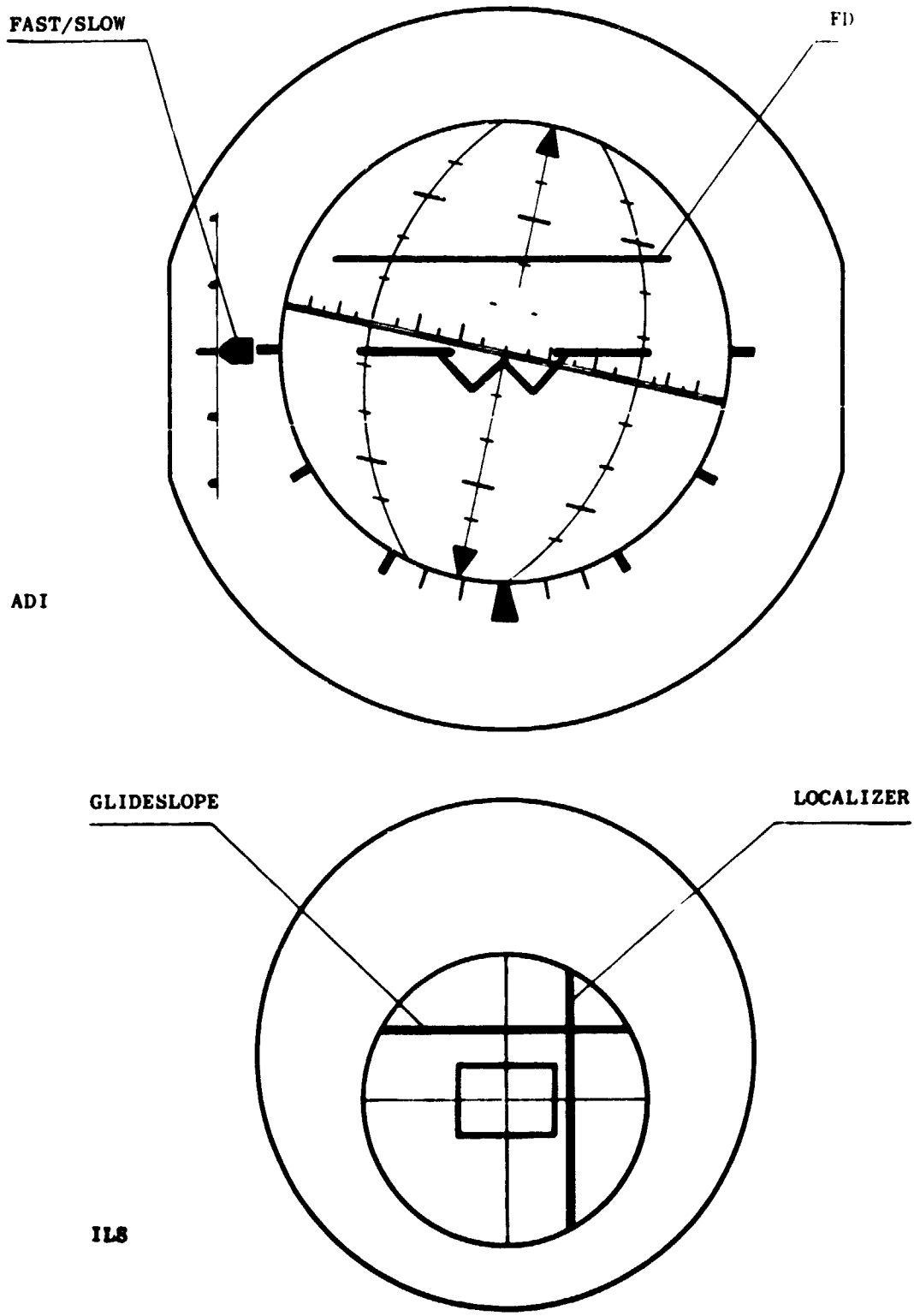

FIG. 1: DISPLAY FORMAT

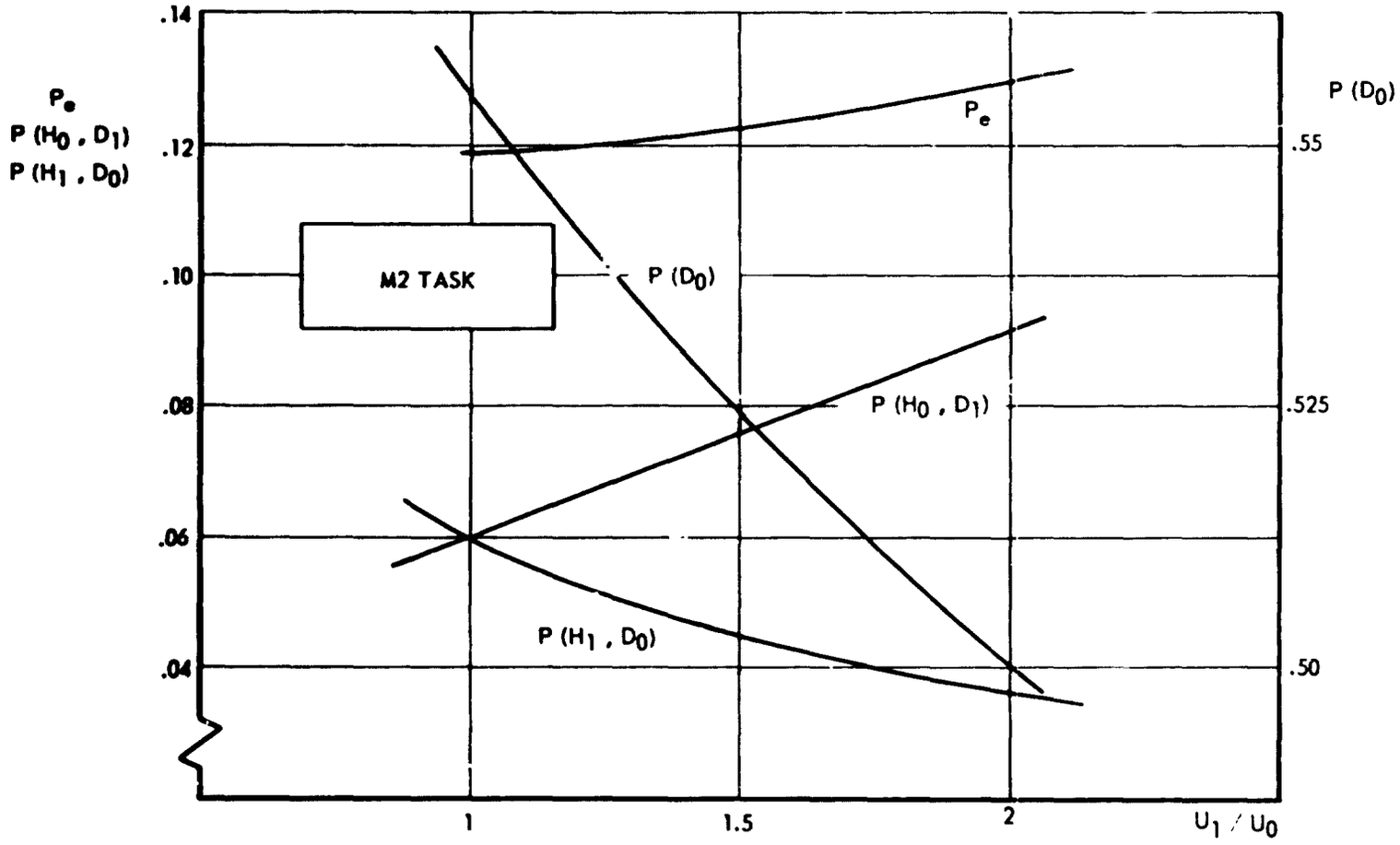

FIG. 2: THE EFFECT OF UTILITIES ON THE MONITOR PERFORMANCE MEASURES

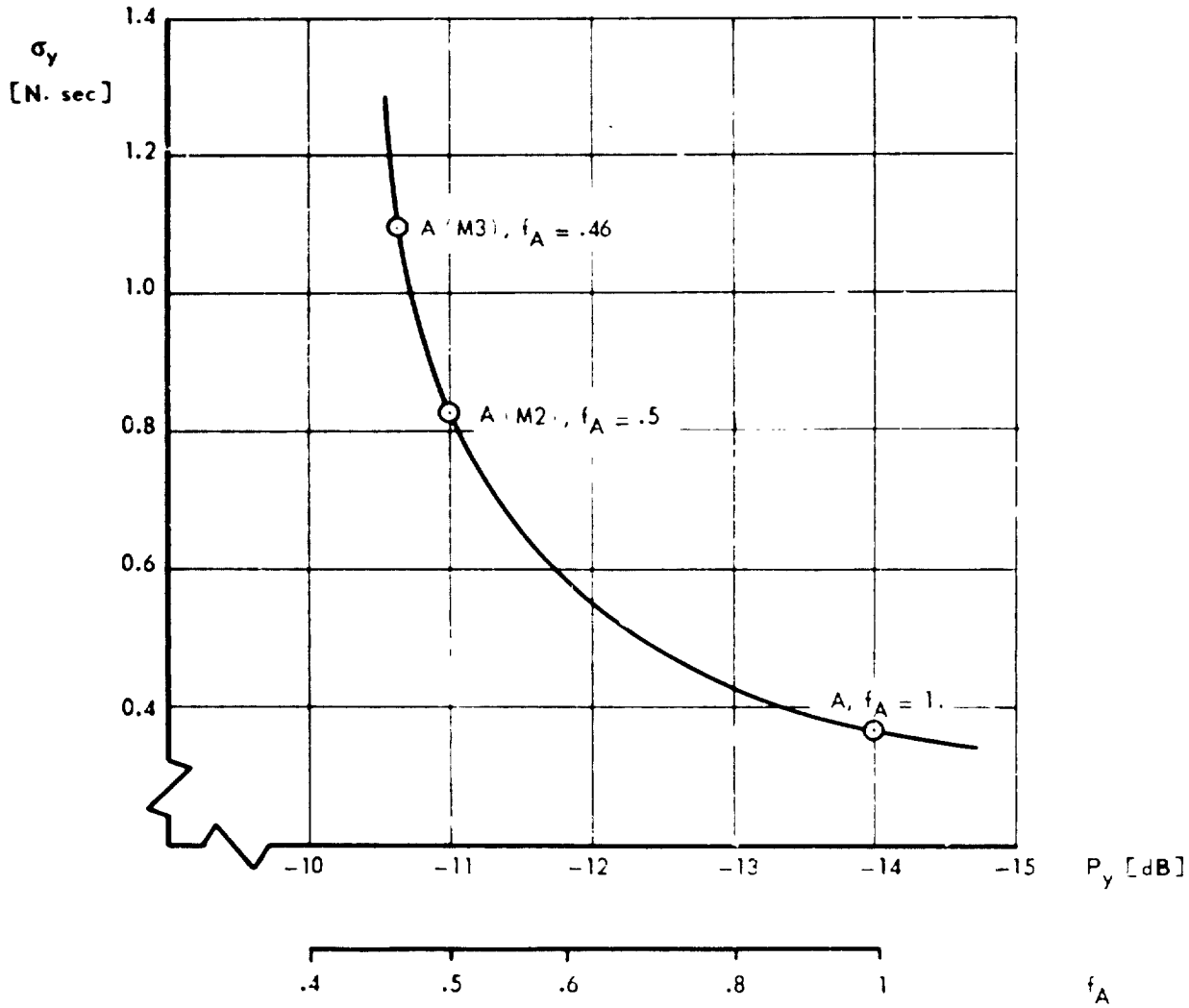

FIG. 3: AUDITORY TRACKING TASK - PERFORMANCE VERSUS FRACTION OF ATTENTION

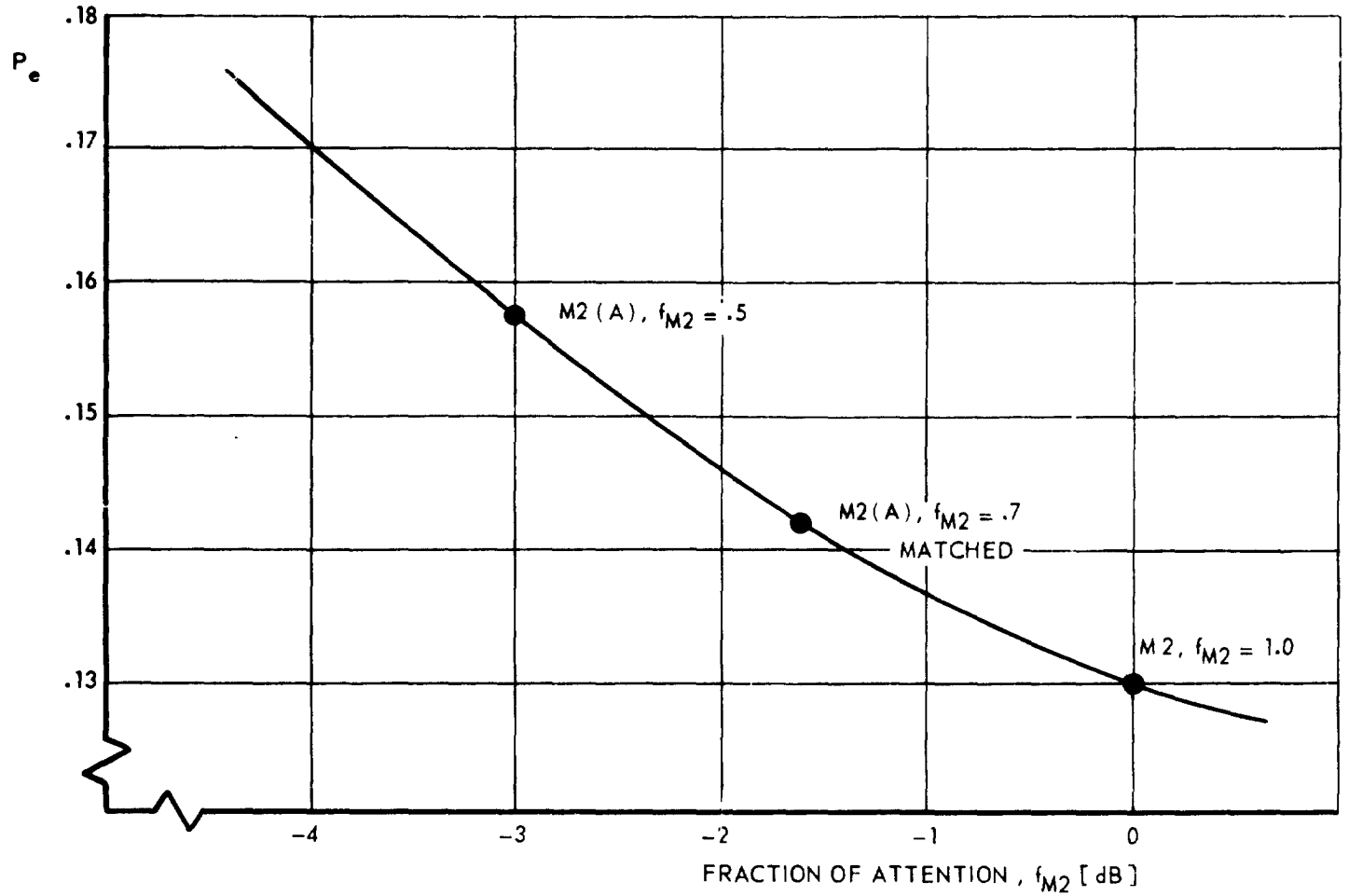

FIG. 4: MONITOR TASK, M2 - PERFORMANCE VERSUS FRACTION OF ATTENTION

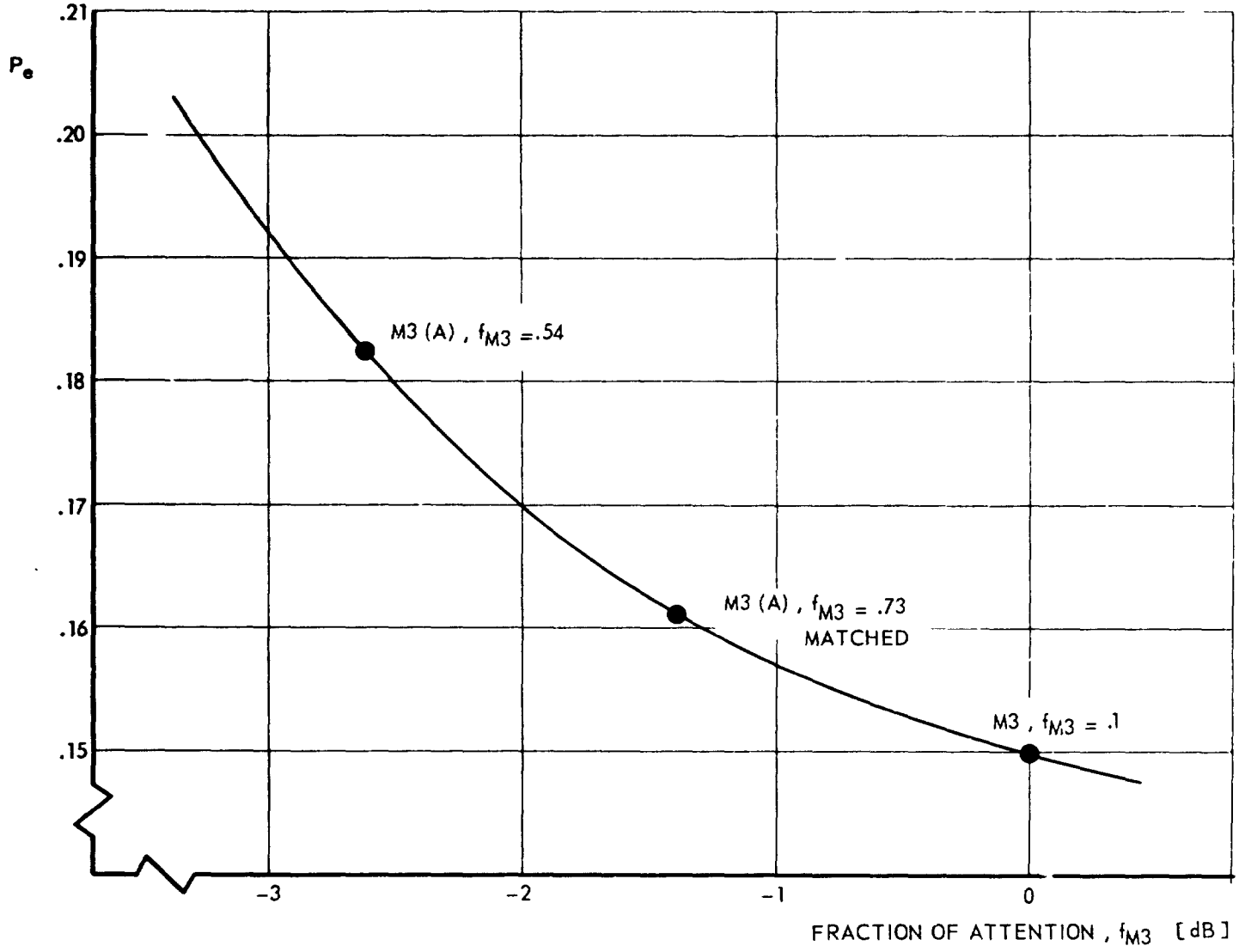

FIG. 5: MONITOR TASK, M3 - PERFORMANCE VERSUS FRACTION OF ATTENTION

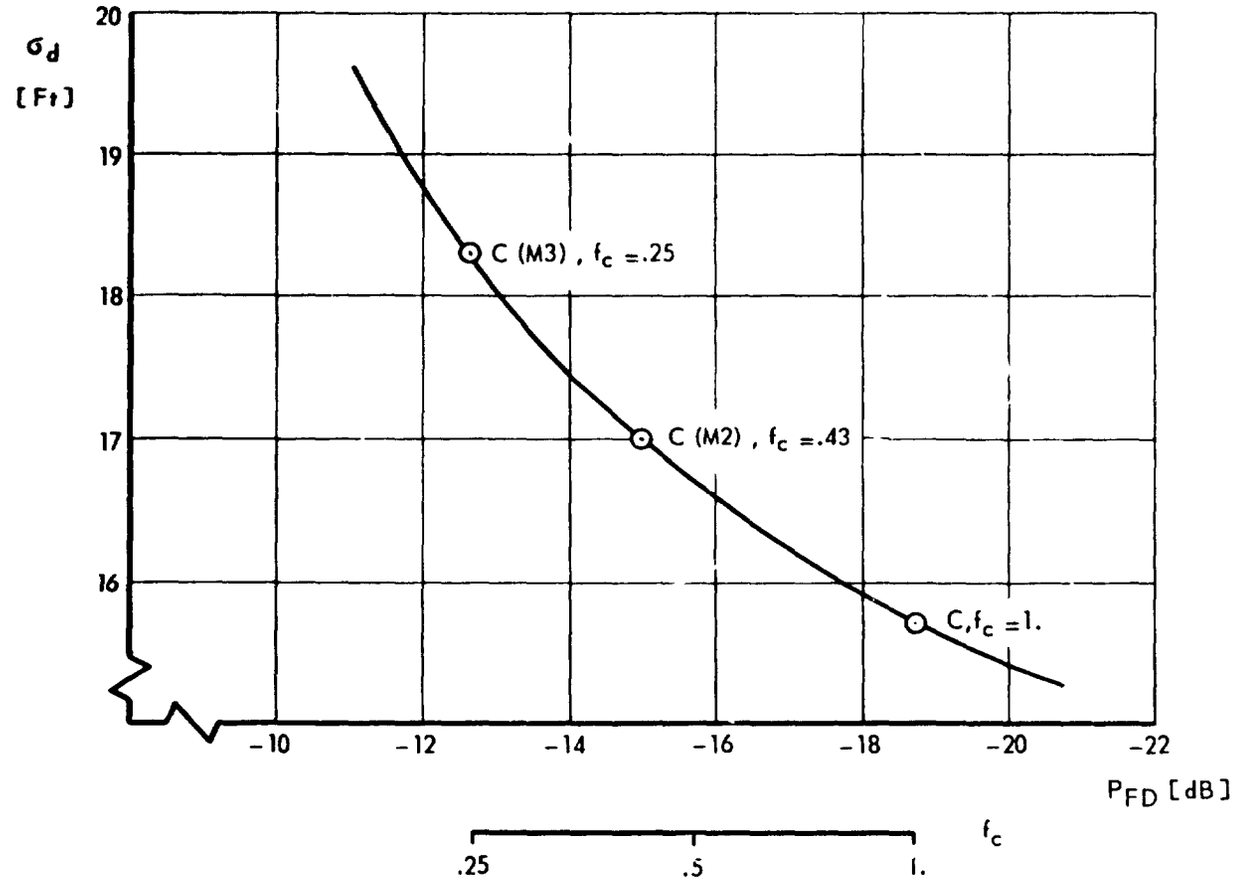

FIG. 6: LONGITUDINAL CONTROL TASK - PERFORMANCE VERSUS FRACTION OF ATTENTION

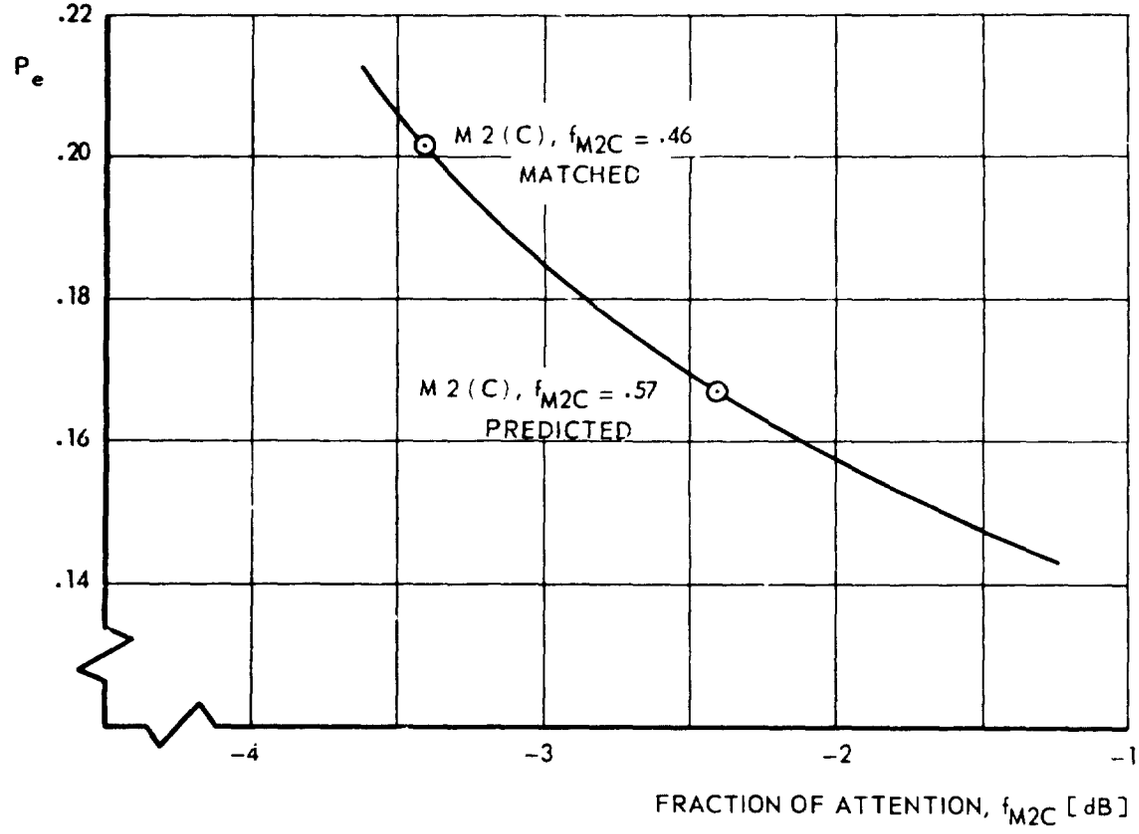

FIG. 7: MONITOR TASK, M2(C) - PERFORMANCE VERSUS FRACTION OF ATTENTION

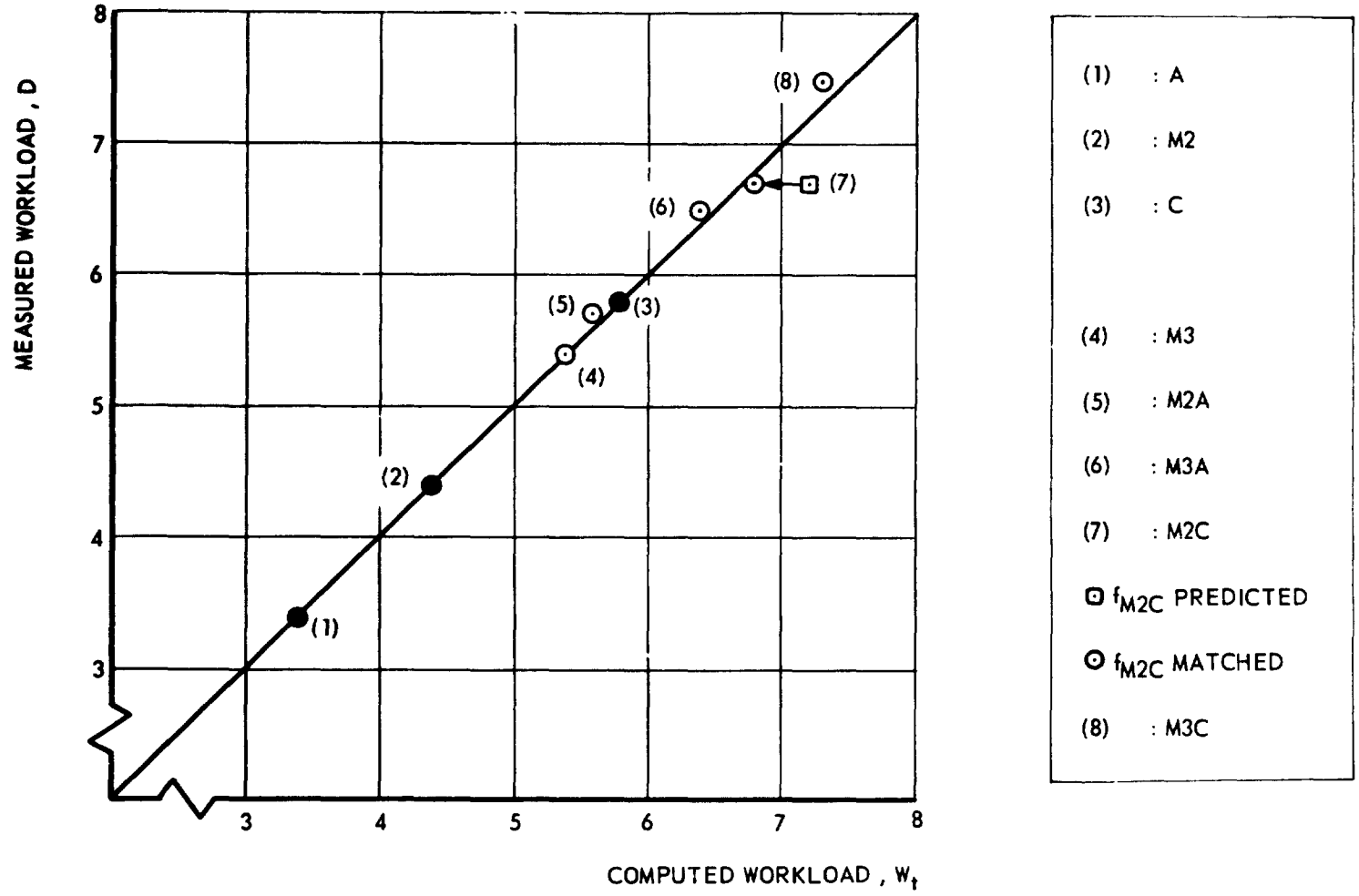

FIG. 8: COMPARISON OF MEASURED AND COMPUTED WORKLOAD

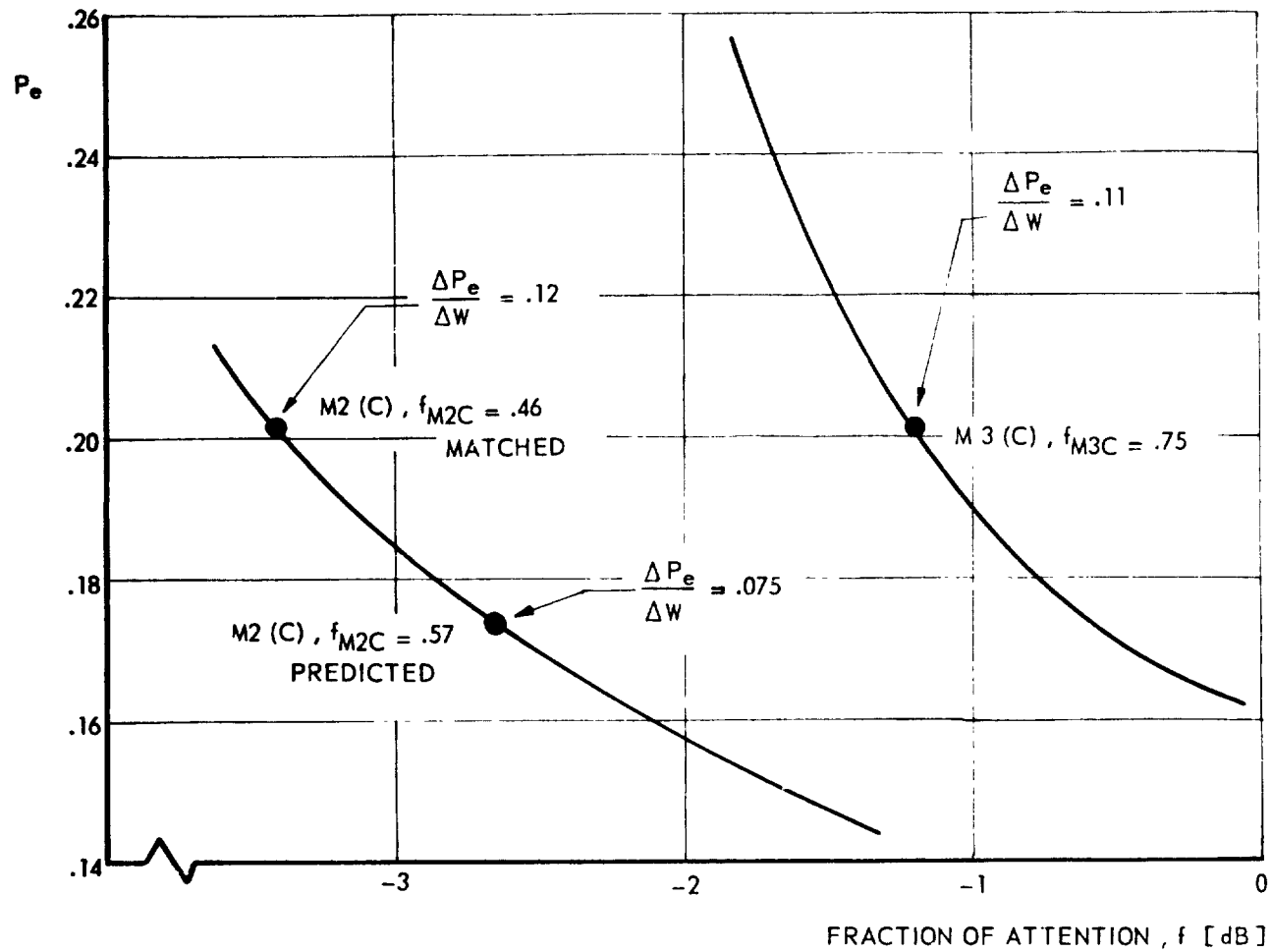

FIG. 9: MONITOR TASKS, MC - PERFORMANCE VERSUS ATTENTION AND WORKLOAD

AN EXPERIMENTAL SITUATION FOR STUDY OF PILOT INTERACTION WITH AUTOMATED AIRBORNE DECISION MAKING SYSTEMS*

By William B. Rouse, Yee-Yeen Chu, and Rex S. Walden

University of Illinois
Urbana, Illinois 61801

SUMMARY

This paper describes an experimental situation which allows varying degrees of automation in a set of control and monitoring tasks. The control tasks involve flying a map display at specified altitude and speed. The monitoring tasks involve detection of events in N dynamic processes each of which has an associated display. Events evoke actions which involve a checklist-like tree search. Computer aid, with adjustable reliability, is available for both the control and monitoring tasks. A series of experiments which are to be performed in this experimental situation are described.

INTRODUCTION

Several factors are leading to the consideration of automated decision making systems for aircraft operations. Aircraft are becoming more sophisticated and complicated while greater precision and performance is being required of the pilot. The pilot simply does not have the time to do everything well. At the same time, computers are becoming smaller, faster, and cheaper. Thus, computer-aided decision making is (or will be) both desirable and feasible.

However, it is unlikely that the computer will completely replace the pilot. In failed or unusual situations, the pilot will be called upon to manually perform tasks normally allocated to the computer. Also, the pilot will serve as an executive or manager providing goals to the computer, monitoring overall performance, and occasionally preempting inappropriate decisions by the computer.

The problem area addressed by the project discussed in this paper is the interaction between a human pilot and a computer with decision making responsibility. The goal of the research is to enhance cooperation between the two decision makers by understanding and then avoiding possible modes of competition between them.

* Supported by the National Aeronautics and Space Administration under NASA - Ames Grant NSG-2119.

To be more specific, we are concerned with multi-task situations and the issues of primary interest include:

1. Allocation of responsibility between human and computer.
2. Resolution of conflicts between human and computer.
3. Human confidence in the computer system.

Considering allocation of decision making responsibility, we have proposed that responsibilities not be strictly assigned to each decision maker [1,2]. Instead, allocation should adapt to the state of the aircraft and the state of the pilot. Both pilot and computer would have responsibility for all or most decision making tasks with responsibility at any particular instant being assigned to the decision maker most able at that moment to perform the task. Simple concepts from queueing theory indicate that such a procedure for allocation of responsibility would improve the utilization of system (aircraft plus pilot) resources and thereby improve system performance. This approach would allow the pilot to retain a coherent role in the sense of having overall responsibility for the whole aircraft while the computer would enable the pilot to avoid having to continually exercise all of these responsibilities.

The most significant disadvantage of adaptive allocation is the possibility of conflict between the two decision makers. Without sufficient information about each other's actions, the pilot and computer might compete to perform tasks. This would degrade system performance (and perhaps be disastrous) and possibly cause adaptive allocation to be an unattractive approach. Theoretical and experimental approaches are being employed to assess the costs of conflict and devise methods of avoiding conflicts.

Of course, the success of any adaptive decision making system will depend on the pilot's confidence in the system. Within our experiments, we plan to study the pilot's decisions concerning mode of use of the computer system and his ability to detect when the decision making system has failed.

THEORETICAL FORMULATION

To investigate the feasibility of adaptively allocating decision making responsibility between human and computer, a mathematical model of multi-task decision making was developed and several simulation experiments were performed [3]. The goal of this effort was determination of the effects of several system variables including number of tasks, mean time between arrivals of action-evoking events, human-computer speed mismatch, probability of computer error, probability of human error, and the level of feedback between human and computer.

The model is based on queueing theory concepts. Multi-task decision making is described in terms of events and actions. The decision maker's

task is to detect action-evoking events and to decide whether or not any particular task warrants his full attention. The model assumes the human to employ a quasi-optimal decision making strategy for scanning displays and allocating attention. However, the results of our simulation studies are probably not very sensitive to the particular strategy employed, mainly because we were most interested in gross effects.

The theoretical formulation has given us valuable insights to problems associated with the design of an adaptive decision making system. However, before we can use this formulation to evaluate potential designs, a better understanding of human decision making in multi-task situations is needed.

AN EXPERIMENTAL SITUATION

We have developed the following experimental situation with two goals in mind. First, we wanted a situation of enough generality to allow several experiments to be performed without substantial changes in the software and/or hardware. Second, we wanted to be consistent with the simulations being developed at NASA Ames Research Center [4].

Figure 1 illustrates the CRT display observed by the pilot. The display is a Hewlett Packard 1310 while the computer generating the display is a PDP-11/40 augmented by special purpose equipment for refreshing the display. The pilot's task is to fly the Boeing 707 dynamics along the map while maintaining specified altitude and air speed. His flight instruments are displayed beside the map. The pilot has aileron, elevator, and thrust controls.

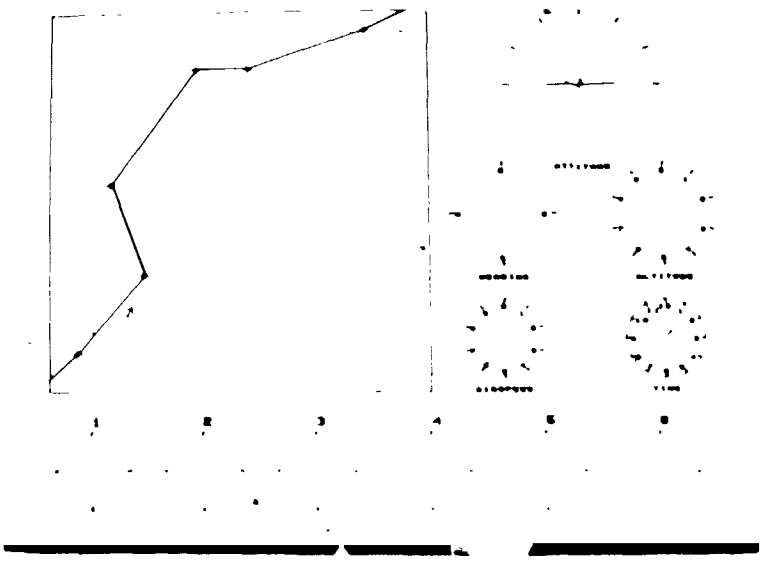

Figure 1: The Experimental Situation

The instruments below the map represent the numerous aircraft subsystems (e.g., electrical, hydraulic, etc.) which the pilot monitors for possible action-evoking events. Each of the subsystem instruments represents a linear dynamic process driven by non-zero mean white noise input. An event is defined as the removal of the input, which causes the state of the process to asymptotically approach zero (pointer down).

Upon detecting an event to which he wishes to respond, the pilot selects that subsystem via a 4 x 3 keyboard. The display shown in Figure 2 then appears. This represents the first level of a checklist-like tree associated with the subsystem of interest. He searches for a branch labeled with a zero and selects that branch with his keyboard. If the tree has more levels, the next level is then displayed. After completing the last level of the tree, the action is complete and the display shown in Figure 1 returns.

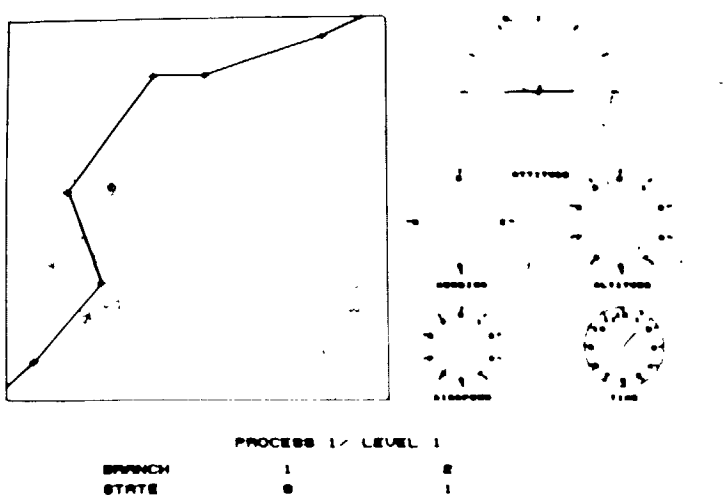

Figure 2: Display When Pilot Has Reacted to an Action-Evoking Event

Within this experimental situation, we can vary the complexity of the map, the availability of autopilot, the number of subsystems, the distribution of arrivals of events among tasks, and many other aircraft and subsystem parameters.

EXPERIMENTS PLANNED

Two sets of experiments are planned using the above experimental situation. The first set will address the question: How is pilot decision making (in terms of response times, errors, and computer usage) affected by task complexity, autopilot, and non-adaptive computer aiding?

At this point, the following scenario is envisioned. Subjects will fly 50 minutes enroute (simple map) and there will be little subsystem activity (few events). Then, they will fly 10 minutes in a landing situation (complex map) where there will be considerable subsystem activity. Experimental measurements will include:

1. Response time to subsystem events,
2. Probabilities of error,
   a. False alarm
   b. Missed event
   c. Incorrect action
3. Course errors,
4. Control actions.

For the first experiment, each subject will perform three trials where the experimental variable of interest will be:

1. No autopilot,
2. Reliable autopilot,
3. Unreliable autopilot.

Reliable autopilot refers to one with a low probability of malfunction while unreliable refers to one with a high probability of malfunction. An autopilot malfunction is characterized by the aircraft maintaining its current bearing and air speed and thereby eventually deviating from the desired path. Once a malfunction occurs, a subject's task is to take over control of the aircraft, return it to the appropriate course, and re-engage the autopilot (which never fails irreparably).

The second experiment of this first set of experiments will employ the same scenario and consider pilot interaction with a decision making system designed to aid him in detecting subsystem events and acting appropriately. This system will be non-adaptive and designed on the basis of results obtained from the first experiment. The computer aid will have two modes of operation (other than "off"):

1. Detection only,
2. Detection and action.

It will also have an internal adjustment whereby its probability of successful decision making can be changed. When initialized, this probability will be high enough to be a significant aid to the pilot. However, if a malfunction occurs, the probability will decrease to the point of making

the computer aid a hinderance. The subject's task will be to detect this occurrence and reset the adjustment via a simple pushbutton. The computer aid will have two levels of reliability which will be characterized in a manner similar to the autopilot, probably using the same numerics to standardize subjects' perception of reliability.

The empirical results obtained from this first set of experiments will be combined with the theoretical formulation discussed above and employed in the design of an adaptive decision making system. Besides the queueing theory formulation, we are also considering control theory as a methodology with which to design an adaptive system. Another issue of special importance to an adaptive system is the measurement of both aircraft and pilot states. Several alternative approaches are being considered. The adaptive system that results from our investigations will be experimentally evaluated using the situation discussed in this paper.

CONCLUSIONS

It appears inevitable that aircraft will become increasingly automated. However, it also appears unlikely that the pilot will disappear from the cockpit. Instead the pilot and computer will have to cooperate in managing the aircraft. This paper has discussed an experimental situation that is being used to theoretically and experimentally determine how cooperation between these two decision makers can be enhanced.

REFERENCES

1. W. B. Rouse, "Human Interaction With an Intelligent Computer in Multi-Task Situations", Proceedings of the Eleventh Annual Conference on Manual Control, NASA Ames Research Center, May 1975, pp. 130-143.

2. W. B. Rouse, "Adaptive Allocation of Decision Making Responsibility Between Supervisor and Computer", Proceedings of the International Symposium on Monitoring Behavior and Supervisory Control, Berchtesgaden, F. R. Germany, March 1976.

3. W. B. Rouse, "Human-Computer Interaction in Multi-Task Situations", Submitted for publication.

4. E. Palmer, "Pilot's Manual for the 4D Area Navigation and Autopilot Systems in the Flight Management Project Cockpit Simulation", NASA Ames Research Center, NASA TM X-73, 100, October 1975.

AN EXPERIMENTAL SITUATION FOR STUDY OF HUMAN DECISION MAKING IN MULTI-PROCESS MONITORING*

by William B. Rouse and Joel S. Greenstein

University of Illinois
Urbana, Illinois 61801

SUMMARY

This paper describes an experimental situation which has been developed to enable study of the human's decision strategy and performance when monitoring multiple dynamic processes. The decision maker's goal is to detect dynamic and/or statistical changes in any of the processes and take appropriate action to return the process to an acceptable mode of behavior. This situation is somewhat analogous to industrial monitoring and air traffic control. A series of planned experiments is discussed whose results are to be employed in the design of a computer-aided process monitoring system where the computer learns how to detect changes by "watching" the human perform the task.

INTRODUCTION

Quite frequently, a human must simultaneously monitor several dynamic processes. His task is to detect action-evoking events and implement the appropriate actions. As the number of processes increases and/or as the frequency of action-evoking events increases, the human becomes overloaded and overall system performance decreases.

The goal of the project discussed in this paper is the design of a computer-aided process monitoring system. Three important issues in the design of such a system are:

1. Allocation of decision making responsibility,
2. Resolution of conflicts between decision makers,
3. Human confidence in the computer system.

Theoretical studies [1,2,3] have led us to suggest that allocation of responsibility should be dynamic (i.e., situation dependent) with particular decision making tasks being assigned to the decision maker who, at the moment, has the time to devote to the task. This approach can yield significant performance benefits if conflicts between decision makers can be avoided.

---

* Supported by the Joint Services Electronics Program (U.S. Army, U.S. Navy, and U.S. Air Force) under Contract DAAB-07-72-C-0259.

Instead of resolving conflicts, it would be preferable to avoid them. An approach to accomplishing this involves giving the computer a model of human behavior so that the computer may infer the state of the human within the overall system. To develop an understanding of human decision making in the simultaneous monitoring of several dynamic processes, we have designed an experimental situation. This situation will be employed both in the development of models of human decision making and for evaluation of potential systems for computer-aided process monitoring.

AN EXPERIMENTAL SITUATION

Figure 1 illustrates the display observed by the subject. The display is generated on a Tektronix 4010 display terminal by a time-shared DEC-System 10 computer and depicts the measured values of the outputs of nine processes over the past 100 sampling intervals. The subject's task is to monitor the processes, via the display, for the occurrence of abnormal events. The processes normally have identical second order system characteristics with zero-mean Gaussian white noise inputs of identical variance. The displayed measurements of the process outputs are corrupted by additive zero-mean Gaussian white noise sequences which normally have identical variance. Abnormal events might be represented by changes in the dynamics of a process, changes in the process input, or an increase in measurement noise variance.

After scanning the nine process histories, the subject is given an opportunity to key in the numbers of processes in which he has decided an abnormal event has occurred. He also enters his estimate of the time at which the event occurred. Upon completion of his responses he is given feedback regarding the actual states of the processes he has keyed in ("1" indicates the normal state, "0" indicates an abnormal state). The display is then erased, any abnormal processes detected by the subject are returned to the normal state, and a new display depicting the process histories advanced in time is generated as illustrated in Figure 2.

Within this experimental situation we can vary the number and type of different events, the frequency of occurrence of events, the distribution of events over processes, and the amount of time the process histories are advanced each iteration. The format in which the subject reports event occurrences and receives feedback can also be varied.

EXPERIMENTS PLANNED

Two sets of experiments are planned that will employ the above experimental situation. The first set will investigate human decision making in event detection and attention allocation. In the second set of experiments, computer-aided process monitoring will be studied.

Within the first set of experiments, one experiment is currently underway while another will soon begin. The first experiment is aimed at

understanding the human's event detection behavior. Subjects are allowed to respond to as many events as they think have occurred. Their false alarms are subtracted from their hits and then, the remainder is divided by a measure of their delay in responding (event waiting time). The resulting measure is their score which they are instructed to maximize.

To model human decision making in this task, we are employing signal detection theory and discriminant analysis. Our goal is to develop a model that will be of real time use to a computer as it attempts to assess the state of the decision maker.

The experiment that is soon to begin emphasizes event detection and attention allocation. In this experiment, subjects will only be allowed to respond to one event per iteration. Thus, they must tradeoff uncertainty and costs to reach a decision. We have developed a queueing theory model of this task and will compare it to the human's decision making performance in this experiment.

The second set of experiments will consider computer-aided process monitoring. We envision that the computer will employ the detection and attention allocation models noted above to assess the state of the decision maker. The computer will then be able to adapt to both the state of the task and the state of the human.

CONCLUSIONS

Many human tasks can be abstracted as the simultaneous monitoring of multiple dynamic processes. Computer aiding may allow the human to monitor an increased number of processes and also to monitor more effectively. The research discussed in this paper is aimed at designing and evaluating a computer-aided process monitoring system along the lines of that proposed in reference 3.

REFERENCES

1. Rouse, W. B.: Human Interaction With an Intelligent Computer in Multi-Task Situations. Proceedings of the Eleventh Annual Conference on Manual Control, NASA Ames Research Center, May 1975, pp. 130-143.

2. Rouse, W. B.: Adaptive Allocation of Decision Making Responsibility Between Supervisor and Computer. Proceedings of the International Symposium on Monitoring Behavior and Supervisory Control, Berchtesgaden, Germany, March 1976.

3. Rouse, W. B.: Human-Computer Interaction in Multi-Task Situations. Submitted for publication.

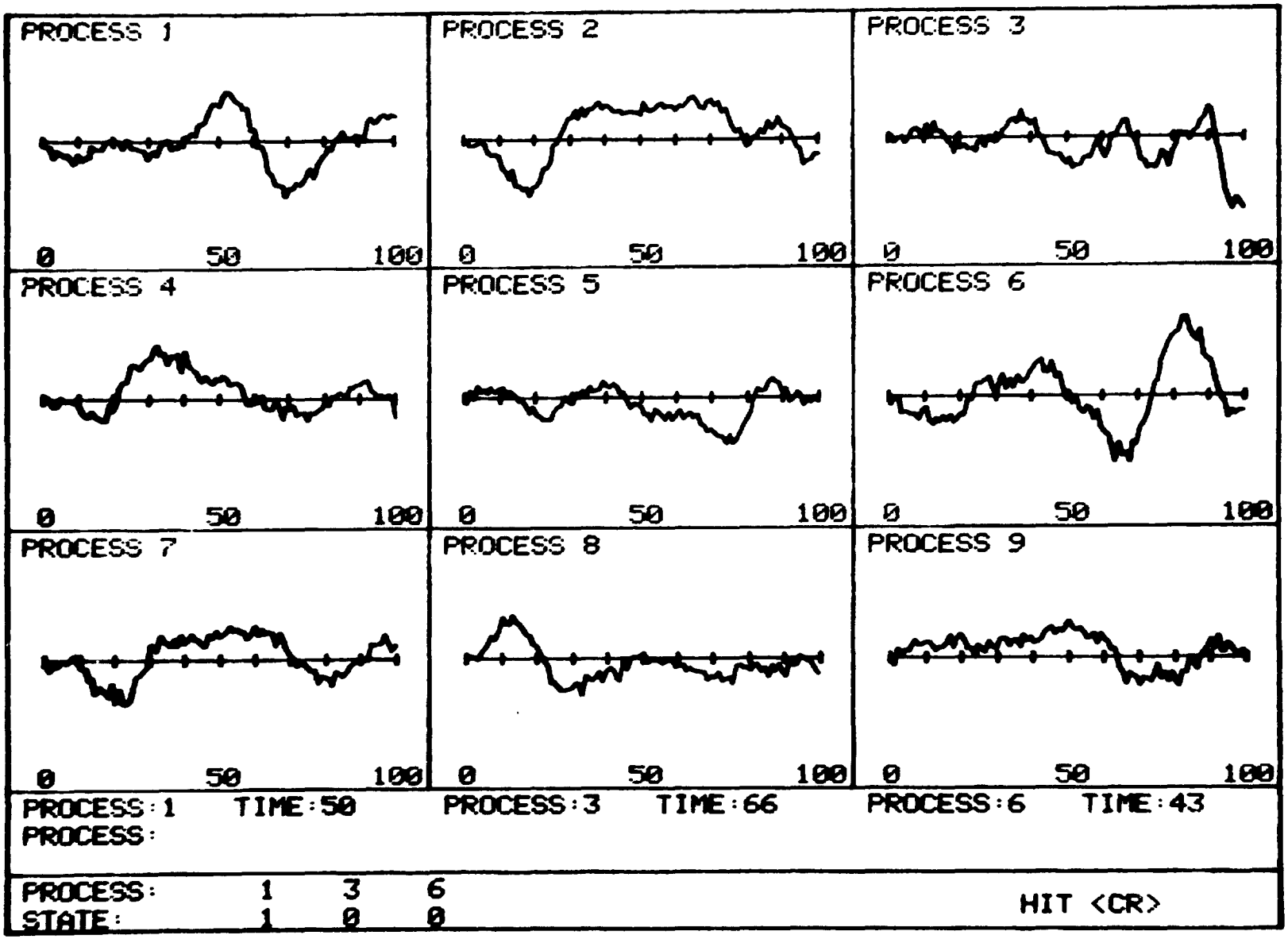

Figure 1: The Experimental Situation

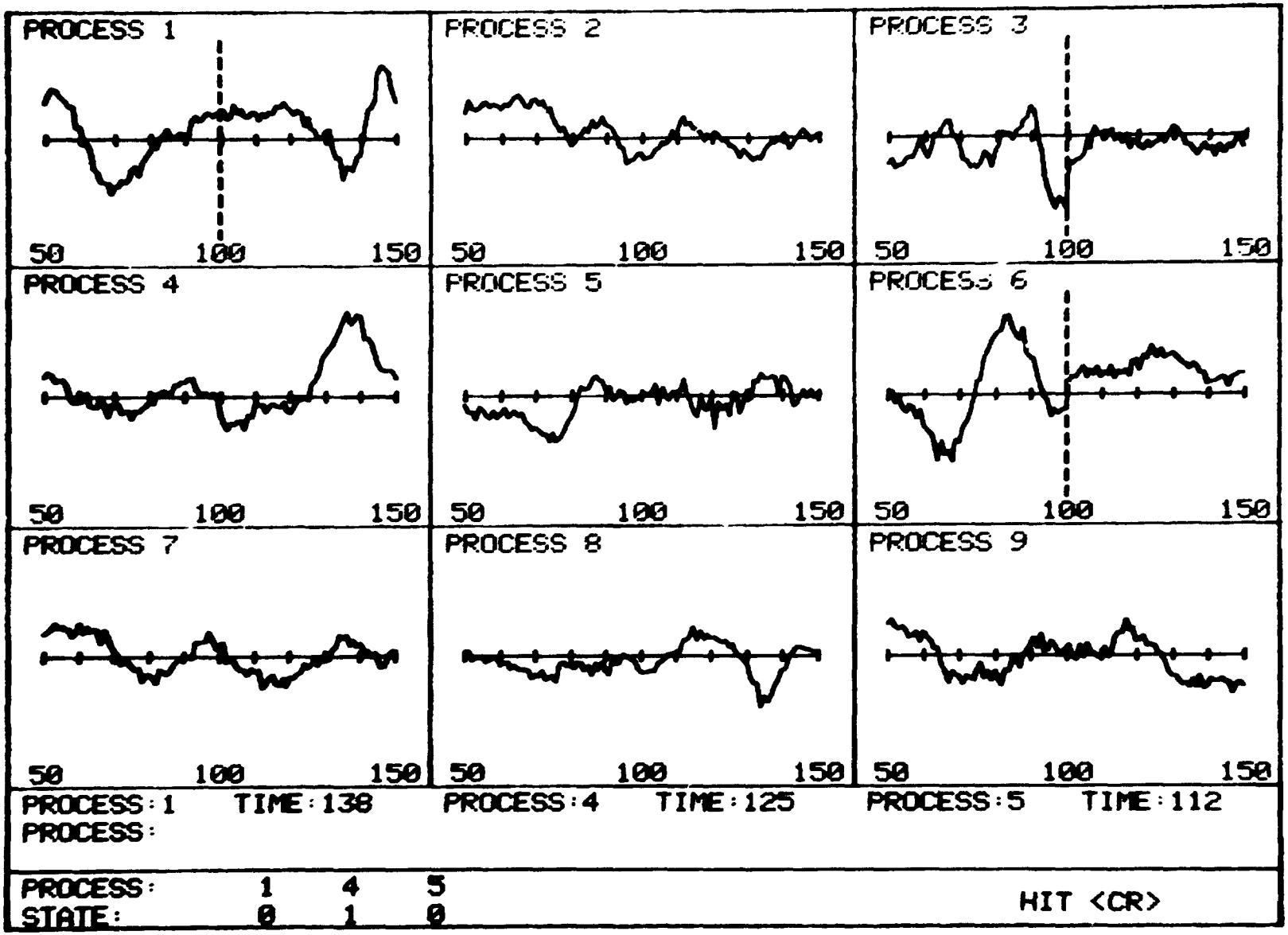

Figure 2: An Updated Display

THE PSYCHOPHYSICS OF RANDOM PROCESSES

Renwick E. Curry and T. Govindaraj

Man-Vehicle Laboratory
Massachusetts Institute of Technology
Cambridge, Mass. 02139

ABSTRACT

One of the major functions of the human monitor is to detect failures in systems under observation. For systems which display continuous-time variables, this is equivalent to determining when the statistical parameters of the random process have changed. This paper reports on some preliminary experiments to determine the threshold values for changes in the variance, bandwidth, and damping ratio of a second order random process. The detection time appears to be summarized by the change in the standard deviation of the velocity of the display.

INTRODUCTION

Human monitoring and supervisory control has become a research topic of increasing interest due to the advances in lower cost automation (Sheridan and Johansen, 1976). One aspect of human monitoring is that of failure detection, and some results and models have been proposed for modelling the human's ability to detect changes the mean of random process (Gai and Curry, 1976). However, there are many other parameters of a random process which are subject to change (Anyakora and Lees, 1972), examples of which are changes in variance, bandwidth, and damping ratio. In a recent review (Curry and Gai, 1976) we were unable to uncover data on the ability of the human to detect changes in these parameters. Thus we performed a set of experiments to determine the preliminary threshold values for changes in these random process parameters, i.e., to determine some of the basic psychophysical constants of random processes. These data when complete will be valuable in designing more extensive experiments, and will also be useful in modelling efforts and in obtaining performance estimates for the human in failure detection tasks.

EXPERIMENT

Overview

This experiment was conducted to determine the thresholds for various parameters of a stochastic process. The process is the output of a second order shaping filter with transfer function

$$\frac{K}{(s/\omega_n)^2 + 2(\zeta/\omega_n)s + 1}$$

and zero mean white noise input. The output was displayed by the vertical displacement of a horizontal line on an oscilloscope screen. After the steady state was reached, one of the parameters of the filter was either increased or decreased (frequency, ω_n, damping, ζ, or the gain, K (for noise power and hence the output variance)): the observer was expected to detect the "failure," or change. All the relevant parameters and the detection time were recorded for each trial.

Equipment

A PDP-11/10 digital computer and TR48 analog computer were used for the experiments. The uniformly distributed zero mean white noise was generated digitally and was passed through a second order (digital) shaping filter. The analog computer was then used to smooth the output for display on an oscilloscope screen. The smoothing filter pole was far away from the shaping filter natural frequency, but sufficiently low to eliminate any discrete jumps when the high frequency content of the process was increased. The subject was seated about 2½ feet in front of the oscilloscope screen. The display was scaled to such that that the screen height was equal to 6σ of the process. Graticule marks provided the reference. The subject had two switches (for responding increase and decrease) to indicate his decision when the change was detected. These switches were continuously read before each update of the output of the process every 1/30 of a second.

Procedure

Sixteen graduate students participated in two sessions lasting approximately 40 minutes each. Each session consisted of three series of trials in which one of the three parameters was changed from its nominal value. Only one of the four nominal random processes was used in each session; the four nominals were obtained by the factorial combination of $T(=2\pi/\omega_n) = 1., 3$ and $\zeta = .2, .707$.

At the start of the familiarization phase, the normal or nominal mode was shown to the subject for two minutes. After this normal mode presentation, large failures were shown to familiarize the subject with the nature of the change. The change occured randomly between 7 and 12 seconds after the start of the trial. Five practice trials were normally sufficient to allow the subject to become familiar with the changes. If the procedure was not clear at this stage the five initial trials were repeated.

Before the beginning of the experiment the subject was told of the stopping criterion, i.e., that the objective was to determine the minimum detectable change in the parameter value. He was instructed to press the switch as soon as he was certain about his decision. Correct detections were acknowledged by the printing of a single character on the teletype which was audible to the subject. When an error was made, the nature of the error was printed on the teleptype and the experimenter informed the subject about the error. Three types of error were possible: if a change was 'detected' before one really occured it was labelled a false alarm; if change was judged as a decrease while it was actually an increase (or vice versa), or if the change was not detected within the time limit, it was labelled as a missed alarm. During any trial, the failed mode continued for 30 seconds after the beginning of the failure; if a decision had not been made by this time, the motion stopped at zero and a period of 5 seconds was given to decide. If a decision was not made after this, it was considered a missed alarm. The experiment continued until he made three or more errors in the most recent six trials.

After each trial, a blanking period of three seconds was given before starting the next trial. From one trial to the next, the parameter change could be either an increase or a decrease according to the following relation

$$\left(\frac{P}{P_N}\right) = \exp \{ \ln R \times S\}$$

P_N - Nominal value of the parameter

P - Changed or failed value

R - Ratio for initial change ($R = 10$)

S - Stimulus ($S = \pm .8, \pm .6, \pm .4, \pm .2, \pm 0.16, \pm 0.12, \pm 0.04, \pm 0.03, \pm 0.02, \pm 0.01, \pm 0.008, \pm 0.006, \pm 0.004, \pm 0.002, \pm 0.0015, \pm 0.0001, \pm 0.0005$)

To avoid guessing by the subject, the decrease in magnitude, Δs, was taken for two steps, resulting in a set of four stimuli (S_1, S_2, $-S_1$, $-S_2$). The stimulus was chosen at random for presentation among these four until all the four were exhausted. Then the next set of four was similarly chosen and presented. The subject was told only that the magnitude of change would be decreasing in such a way that it would become progressively harder to detect its change. Initially, the changes were rather large, $S = \pm .8$ or 0.6 etc.

RESULTS

Figures 1, 2, and 3 show plots of detection time as a function of the ratio of the parameter change (on a logarithmic scale) for variance, bandwidth (period), and damping ratio. For later analysis we have plotted detection times for changes in variance and bandwidth as a function of the change in the standard deviation of the observed random process. The curves shown in Figures 4 and 5 are least squares fit to the detection time data.

Threshold values were obtained using a maximum likelihood estimate for the observed probabilities of correct responses assuming a high-threshold model for detection. The likelihood function for the observed responses is

given by

$$\ell = \prod_i P(C|S_i)^{n_{c_i}} P(W|S_i)^{n_{w_i}}$$

where $P(C|S_i)$ = Probability correct, stimulus S_i

$P(W|S_i) = 1 - P(C|S_i)$

n_{c_i} = number correct, stimulus S_i

n_{w_i} = number wrong, stimulus S_i

The expression for probability of being correct for the high-threshold-theory model is

$$P(C|S_i) = P(C|D)P(D) + P(C|\overline{D})P(\overline{D})$$

where $P(C|D) = 1$

$P(C|\overline{D}) = \frac{1}{2}$ (guessing factor)

$$P(D) = \Phi\left[\frac{\Delta_i - \mu}{\sigma}\right]$$

$D \Rightarrow$ in detection state, $\overline{D} \Rightarrow$ in nondetection state

where Δ_i is the stimulus level, μ is the threshold value and σ is the standard deviation. We found that using $\Delta_i = \log S_i$ gave an appropriate Gaussian form for the stimulus values. (This may be due to the somewhat limited number of responses at each stimulus level, at the most eight).

The calculated thresholds are shown in Table 1 for the four nominal and random processes. The fit of this threshold model to the data was not particularly good because of the small number of samples available, so that these values must be considered extremely preliminary. This is due to the small number of subjects and the measurement technique which we employed to obtain a rapid determination of threshold. Our subsequent experiments will use more conventional psychophysical techniques.

DISCUSSION

The subjects had no difficulty distinguishing between increases and decreases in bandwidth and variance, i.e., all subjects would agree that an "increase" had occurred when so indicated by the experimenter. The same was not true for changes in damping ratio, which is reflected in the wide variation of detection times as shown in Figure 3. We finally arrived at a procedure of never explaining that it was an "increase" or "decrease," but just told the subjects, during the familiarization phase, that they were about to see a change of one sign or the other; we let the subjects determine whether it should be considered an "increase" or "decrease."

Examination of Figure 1 and 2 also indicates that there is an asymmetry in detection times for increase and decreases in variance and bandwidth. A

heuristic explanation for the asymmetry of detection times for changes in variance is suggested by the "exceedance limits" hypothesis. The subjects learn what values are "rarely exceeded" which correspond to (say) 2 σ levels. The first time that the display exceeds this level is an indication that tne variance has increased, and thus an increase of variance is indicated by the subject. On the other hand, when the variance is decreased, it takes the subject more cycles of the random process to determine that the display is not coming as close to the exceedance limit as it had before.

This asymmetry seems somewhat surprising if one considers the stimulus as a change in RMS velocity, because it can be shown that for the random processes considered here, the standard deviation of display velocity is

$$\sigma_x^{\bullet} = \omega_n \sigma_x$$

If the concept of a Weber fraction holds, then we have

$$\frac{\Delta\sigma_x^{\bullet}}{\sigma_x^{\bullet}} = \frac{\Delta\omega_n}{\omega_n} = \frac{\Delta\sigma_x}{\sigma_x}$$

which would not imply any asymmetry in detection times. Such a model would seem appropriate since Brown (1960) has shown that the relative velocity threshold is approximately one-tenth of the absolute velocity. On the other hand, Figures 4 and 5 show that the detection times are reasonably well described by the change in absolute RMS velocity, rather than its relative value (a possibility suggested by Capt. R. Gressang).

As an alternative to the velocity effects, a normative approach to detect the changes in parameters would be to examine the residuals of the Kalman filter designed for the nominal process. If the Kalman filter is operating on the random process for which it was designed, the residuals will be white noise. Any deviation of the residuals from the white noise situation indicates a change has taken place. We have derived the equations for this increment to the residual auto-correlation function (Curry and Gai, 1976) and show in Figure 6 some typical changes to the autocorrelation function for changes in frequency and damping ratio. (In addition to the autocorrelation function shown, the Kalman filter residual has a white-noise component, i.e., an impulse at $\tau = 0$ in Figure 6.) Figure 6 shows that an increase in bandwidth yields a much larger autocorrelation component than does a decrease in bandwidth of even greater magnitude (measured on a logarithmic scale). Thus it seems as though the normative Kalman filter model for failure detection may be a reasonable basis for a descriptive model of human failure detection for these parameter changes, as well as the change in mean of a random process.

REFERENCES

1. Anyakora, S. and Lees, F.: Detection of Instrument Malfunctions by the Process Operator, *Chem Eng*, 1972.

2. Brown, R.H.: Weber Ratio for Visual Discrimination of Velocity, *Science, 131*, 1809-1810, 1960.

3. Curry, R. and Gai, E.: Detection of Random Process Failures by Human Monitors, in Sheridan and Johansen (see below), 1976.

4. Anyakora, S. and Lees, F.: Detection of Instrument Malfunctions by the Process Operator, *Chem Eng*, 1972.

5. Sheridan, T. and Johansen, G.: Monitoring Behavior and Supervisory Control, London: Plenum, 1976.

THRESHOLDS

Nominal	$T^+/T°$	$T^-/T°$	$\sigma x^+/\sigma x°$	$\sigma x^-/\sigma x°$
$T = 1, \quad \zeta = 0.2$	1.1549	0.9326	1.1610	0.8097
$T = 1, \quad \zeta = 0.707$	1.3072	0.9165	1.2655	0.7406
$T = 3, \quad \zeta = 0.2$	1.2167	0.9009	1.3917	0.8710
$T = 3, \quad \zeta = 0.707$	1.2070	0.9517	1.1299	0.7227

Table 1: Calculated Thresholds for Period and Standard Deviation Changes

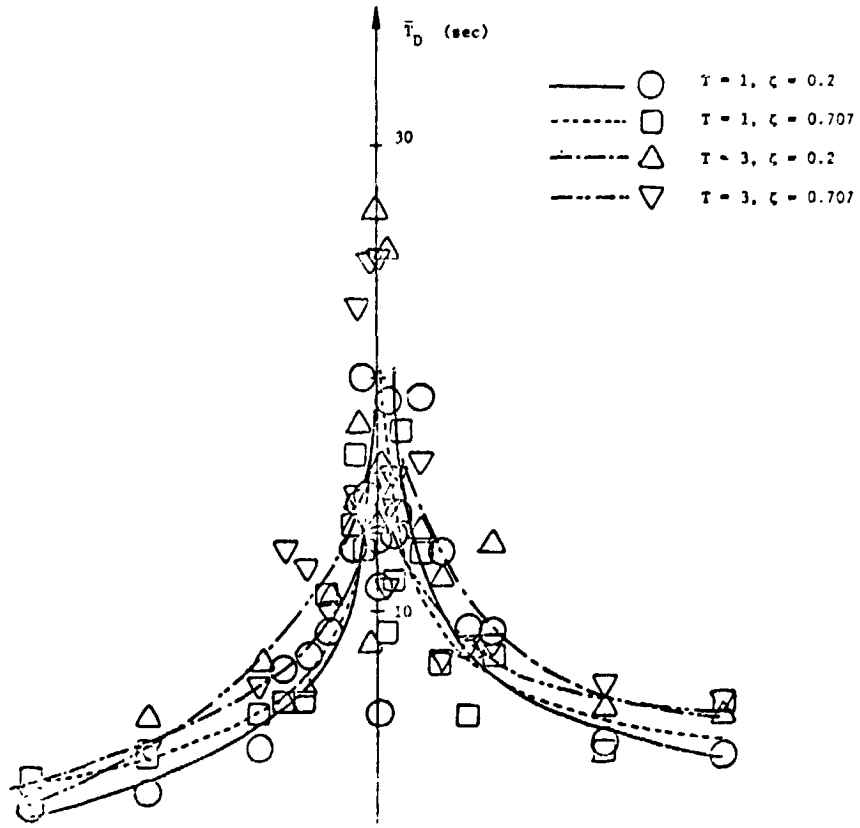

Figure 1: Detection time vs. period change

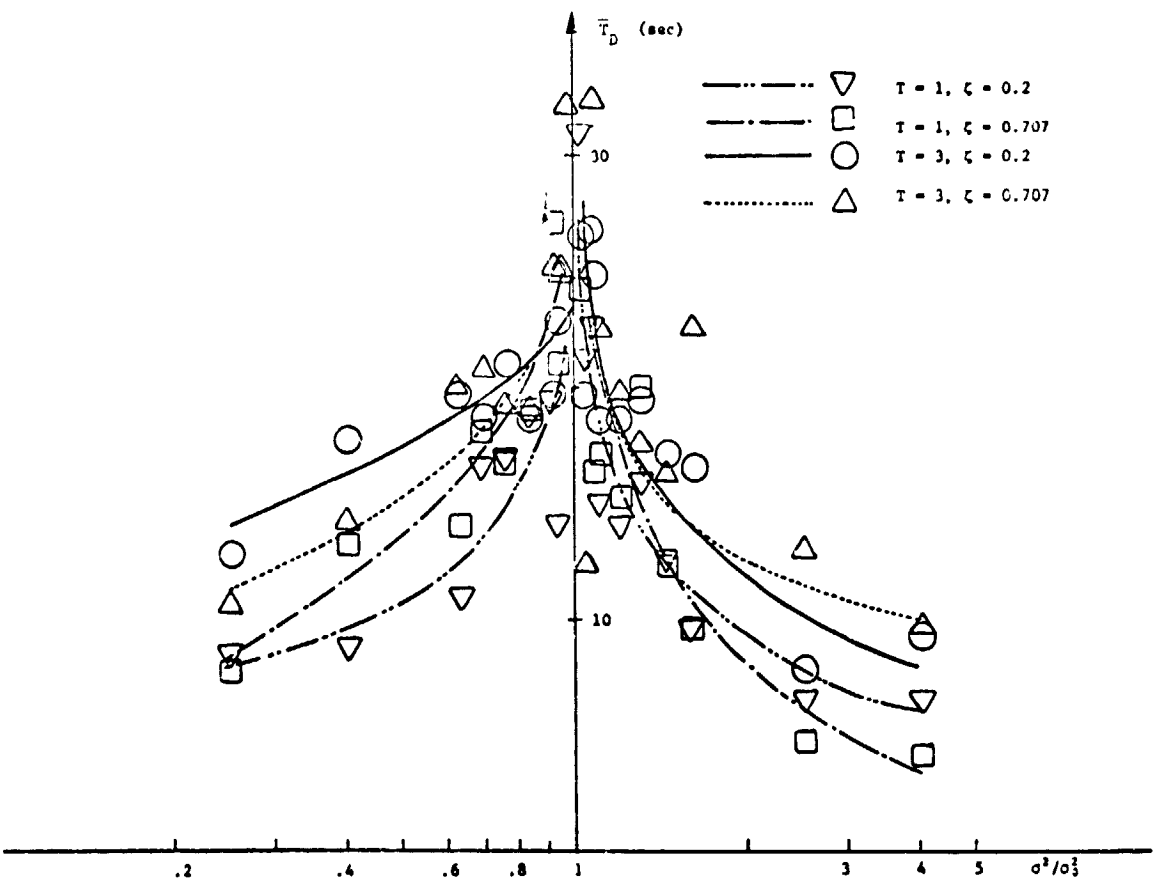

Figure 2: Detection time vs. variance change

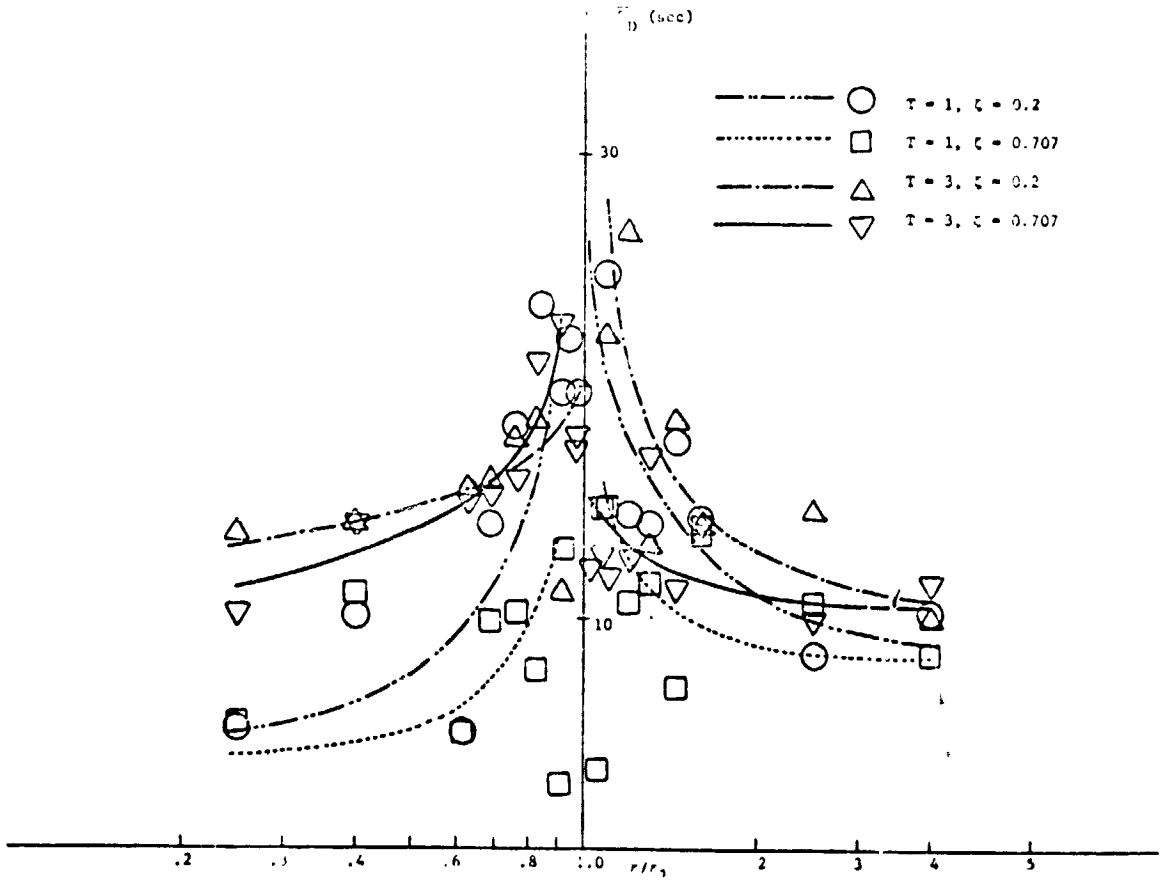

Figure 3: Detection time vs. damping ratio

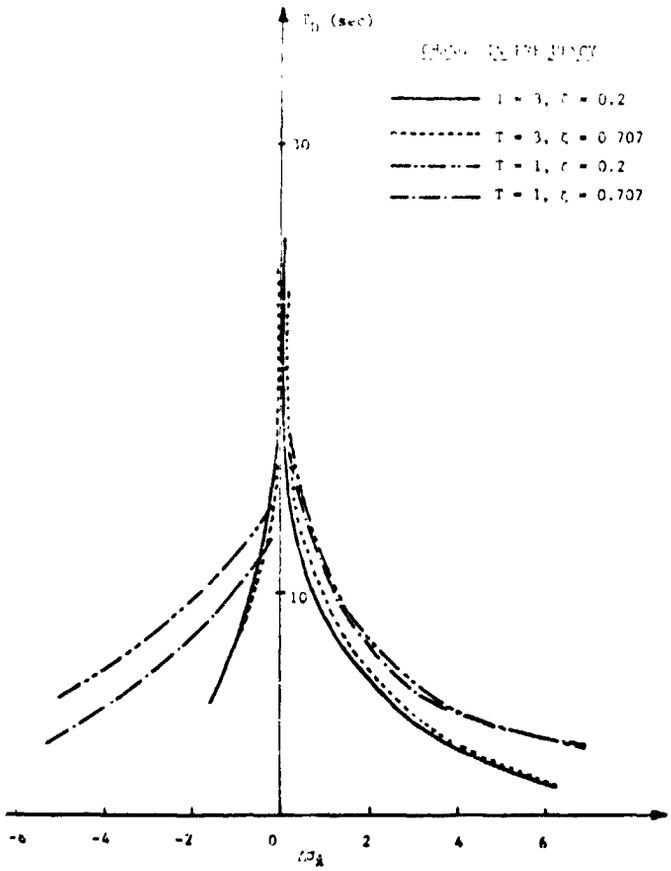

Figure 4: Least squares detection time for natural frequency changes vs. RMS velocity change

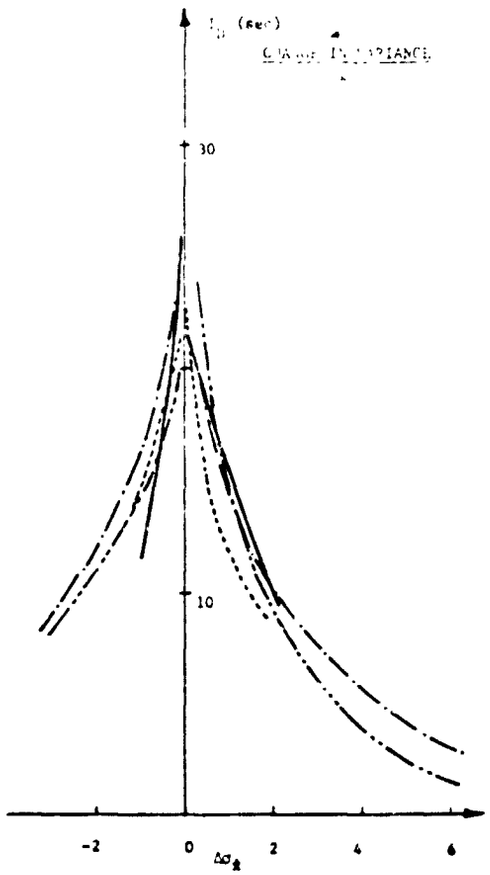

Figure 5: Least squares detection time for variance change vs. RMS velocity change

SESSION II

ATTENTION ALLOCATION AND WORKLOAD MEASUREMENT

Chairman: R. G. Mortimer

A NOVEL APPROACH TO THE CROSS-ADAPTIVE AUXILIARY TASK

By Arye R. Ephrath

National Research Council Associate
NASA Ames Research Center

INTRODUCTION

The technique of the adaptive task was first introduced by Birmingham (1959) and since used by various investigators in operator-performance studies (Kelley, 1962; Birmingham et al., 1962; Hudson, 1964; Kelley, 1970). Under this now-classic adaptive (or self-adjusting) scheme, the task's difficulty is modulated in real time by the operator's performance score: as the operator performs more skillfully, his task becomes more difficult. This technique found useful applications in a number of areas, such as measuring operator skill, personnel selection and training, and manual-control system design (cf. Kelley et al., 1965).

The cross-adaptive loading task technique is a modification of the self-adjusting task scheme and allows the investigator to keep the operator's performance on the primary task constant (Figure 1): the operator's primary task performance is monitored continuously and compared to a predetermined desired level; primary task performance which is better than the standard effects an increase in the difficulty not of the primary task but of a concomitant loading task, thus keeping the primary task performance constant by varying the operator's overall workload.

For the purpose of this research, however, it was considered desirable to keep the overall workload constant at a predetermined level and to study the resulting performance in a primary piloting task. Consequently, a measuring (non-loading) side task was used, and it was placed in the feedback path. This concomitant task continuously measured the operator's workload level and deviation of this measure from the preset standard, properly filtered, modulated the noise content (and hence, the difficulty) of the primary piloting task (Figure 2).

THE PRIMARY TASK

The investigation utilized a fixed-base ground simulator which was configured as the cockpit of a deHaviland CC-115 Buffalo. The primary task consisted of flying a straight, 220° localizer course while descending a 2° glide slope in zero-visibility conditions. In performing this task the subjects relied on the conventional flight instruments - airspeed, attitude, vertical speed and glideslope-deviation indicators, an altimeter, and an electronic horizontal-situation-display.

Simulated wind gusts were introduced to modulate the difficulty of this task. The gusts, both horizontal and vertical, were modelled as filtered noise of constant bandwidth and variable amplitude. This type of disturbance had been shown (Ephrath, 1975b) to affect the pilot's workload and hence, the task's difficulty.

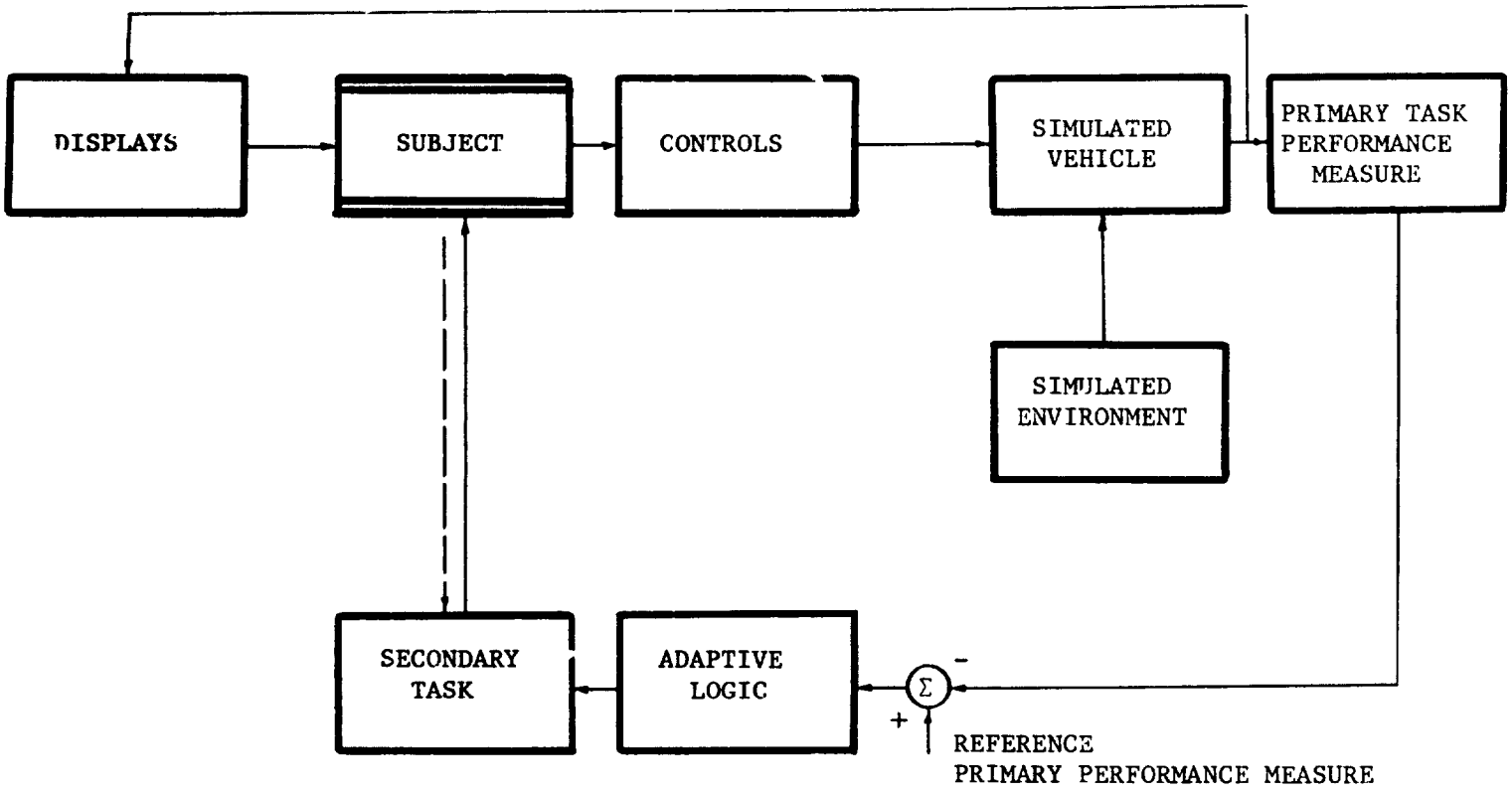

Figure 1. Conventional Cross-Adaptive Secondary Task

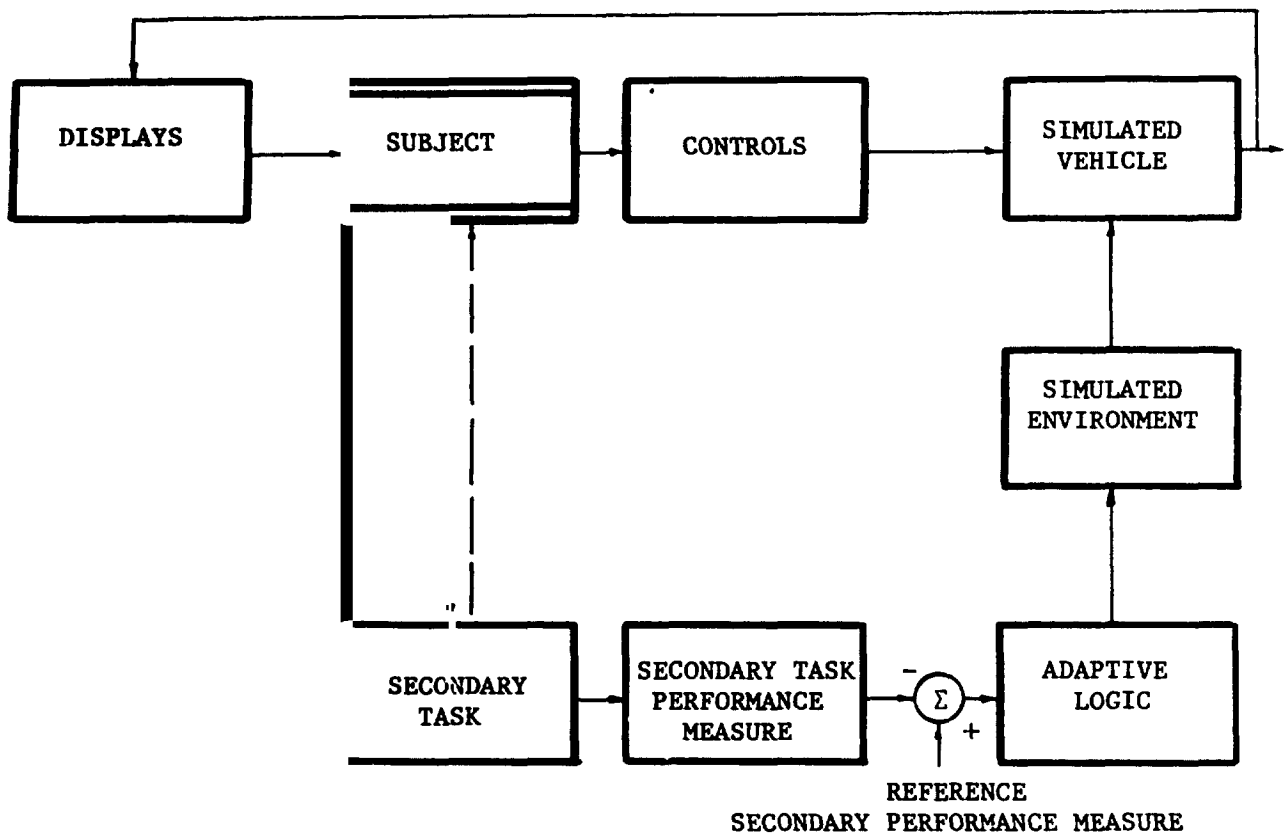

Figure 2. Novel Cross-Adaptive Secondary Task

THE AUXILIARY TASK

The auxiliary task in this study was meant to measure the subjects' instantaneous workload without introducing any significant loading of its own. It consisted of identifying, and responding to, two small red lights which were mounted above the instrument panel (see Figure 3). One or the other of these lights illuminated at random intervals, uniformly distributed between 0.5 and 5.0 seconds, and stayed on for two seconds; the subject's task was to extinguish the illuminated light by moving a toggle switch in the proper direction - up for the top light, down for the bottom light.

The lights were located 75° to the right of the center of the flight instruments. Their intensity was very low and was adjusted individually for each subject via a variable resistance to ensure that the subject would not be able to detect the lights in his peripheral vision. Consequently, the subjects could not perform both the primary and the auxiliary task simultaneously and had to switch continually between the two taks.

The subjects were instructed to regard the piloting task as their major responsibility and to respond to the lights only if they felt that they could do so without sacrificing their piloting performance. Therefore, good auxiliary task performance was assumed to imply ease of the primary piloting task (because if the subject was faced with a difficult piloting task, he could not afford to switch regularly to the low-priority auxiliary task and, consequently, would often fail to respond to an illuminated light), and vice versa.

Each time the subject extinguished an illuminated light a "$MISS_i = 0$" was counted and the subject's response time RT_i was recorded. In the absence of a correct response the light stayed on for two seconds; a "$MISS_i = 1$" was counted and a response-time of two seconds was recorded. A pseudo-instantaneous workload index was updated after the presentation of each light, utilizing the data of the subject's response to the last two stimuli:

$$WLX_i = \frac{78.0(RT_{i-1} + RT_i) + 125.2(MISS_{i-1} + MISS_i)}{5.624}$$

which resulted in a workload-index value between 0 and 100. A measuring auxiliary task of this type has been shown (Ephrath, 1975a and 1975b) to cause minimal loading of the subject; the particular numerical coefficients chosen maximize the sensitivity of this workload measure (Spyker et al., 1971).

This workload index was compared with the desired workload level; the error signal was then integrated (to eliminate steady-state position error),

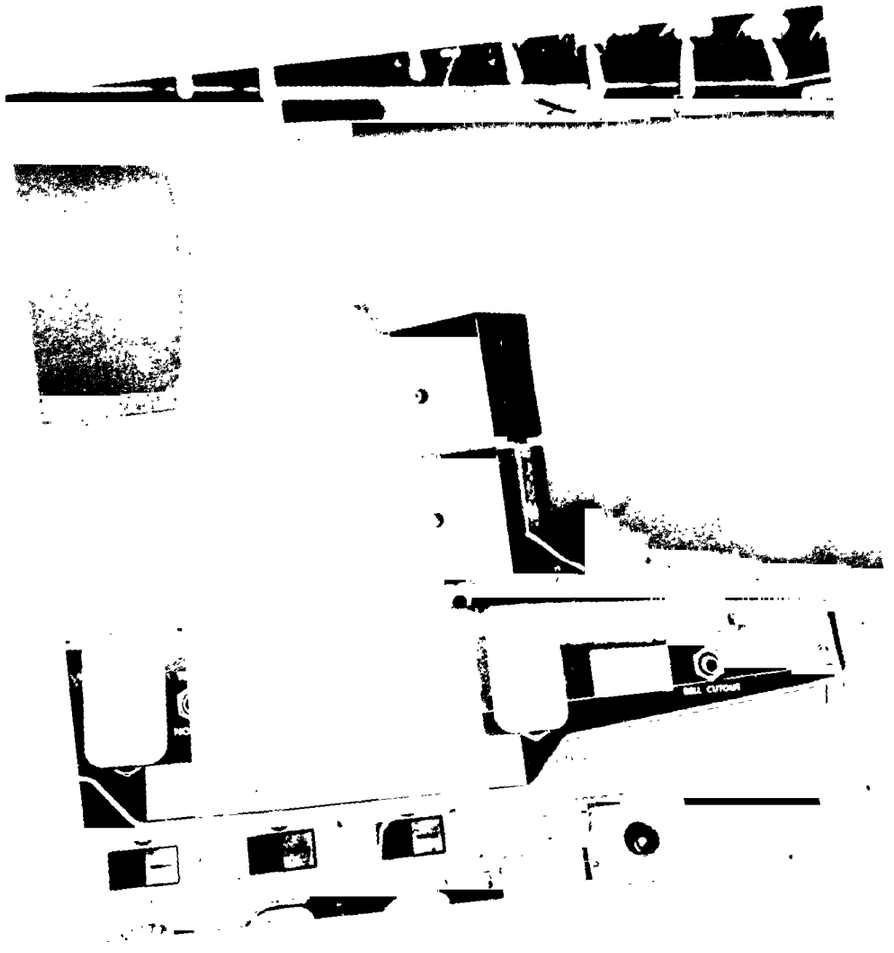

Figure 3. Side-Task Stimulus Lights

limited (to eliminate excessive gusts and to improve stability) and used to modulate the amplitude of the simulated gust disturbance (Figure 4).

RESULTS AND DISCUSSION

Each of the professional airline pilots who served as subjects flew 18 simulated approaches in the course of the formal experiment. We were aware of the fact that they might suspect a causal relationship between their performance on the light-cancelling auxiliary task and the accompanying changes in the strength of the gusts. To minimize this possibility, a value of $K_1 = 0.5$ was chosen for the integrator gain (Figure 4). This value effected a noticeable change in the gusts' strength in approximately ten seconds when the warning lights were completely ignored (implying a workload index of 100); the time lag was short enough to keep the scheme sensitive to changes in measured workload, yet apparently it was also sufficiently long to mask the correlation between gusts' strength and auxiliary-task performance: not only didn't any of our subjects detect the correlation, but neither did the colleagues who served as preliminary subjects and who might have known better or the programmers who wrote the software (without being aware of its purpose) and who had spent countless hours flying and debugging the simulator.

Workload data of a typical experimental run are shown in Figure 5. The workload index was computed from a point 46 seconds after the start of the simulated approach and is seen to oscillate around the approximate reference value WLX_{ref}. At the point indicated by the arrow a simulated guidance malfunction occurred (lateral flight director decoupled from the localizer) and the subject's workload index is seen to rise as he devoted more attention to the primary flying task. The mean workload index in this particular run was 63.6, compared to a desired (reference) workload index of 65.0. At the present time, the data of a total of 108 experimental runs is being processed for more thorough analysis.

CONCLUSIONS

This paper presents a scheme for modulating the difficulty of a primary manual-control task by means of an auxiliary task feedback. The method may find useful applications in operator workload research, in part-task simulation studies and in personnel training.

In our work, primary task difficulty was controlled by modulating the noise content of the forcing function, and our results suggest that a stable workload level may be achieved by proper selection of the subsidiary task to be used and by proper design of the adaptive logic. Other methods of controlling the primary task's dififculty - such as changing d splay and control gains or varying an unstable mode - may perhaps also be used; the latter of these has recently been implemented in a system evaluation study (Clement, 1976), apparently with good results.

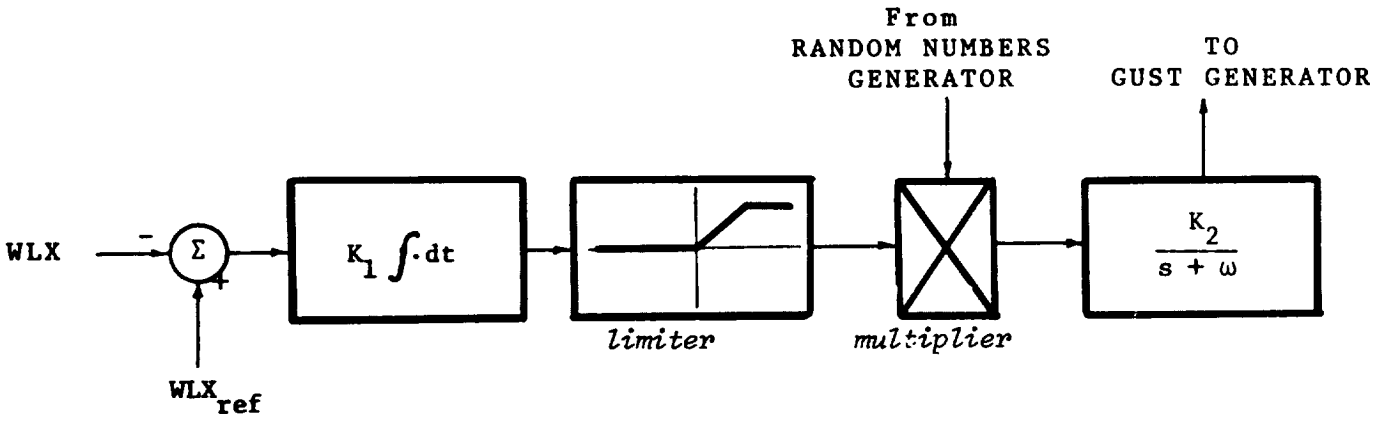

Figure 4. Adaptive Logic

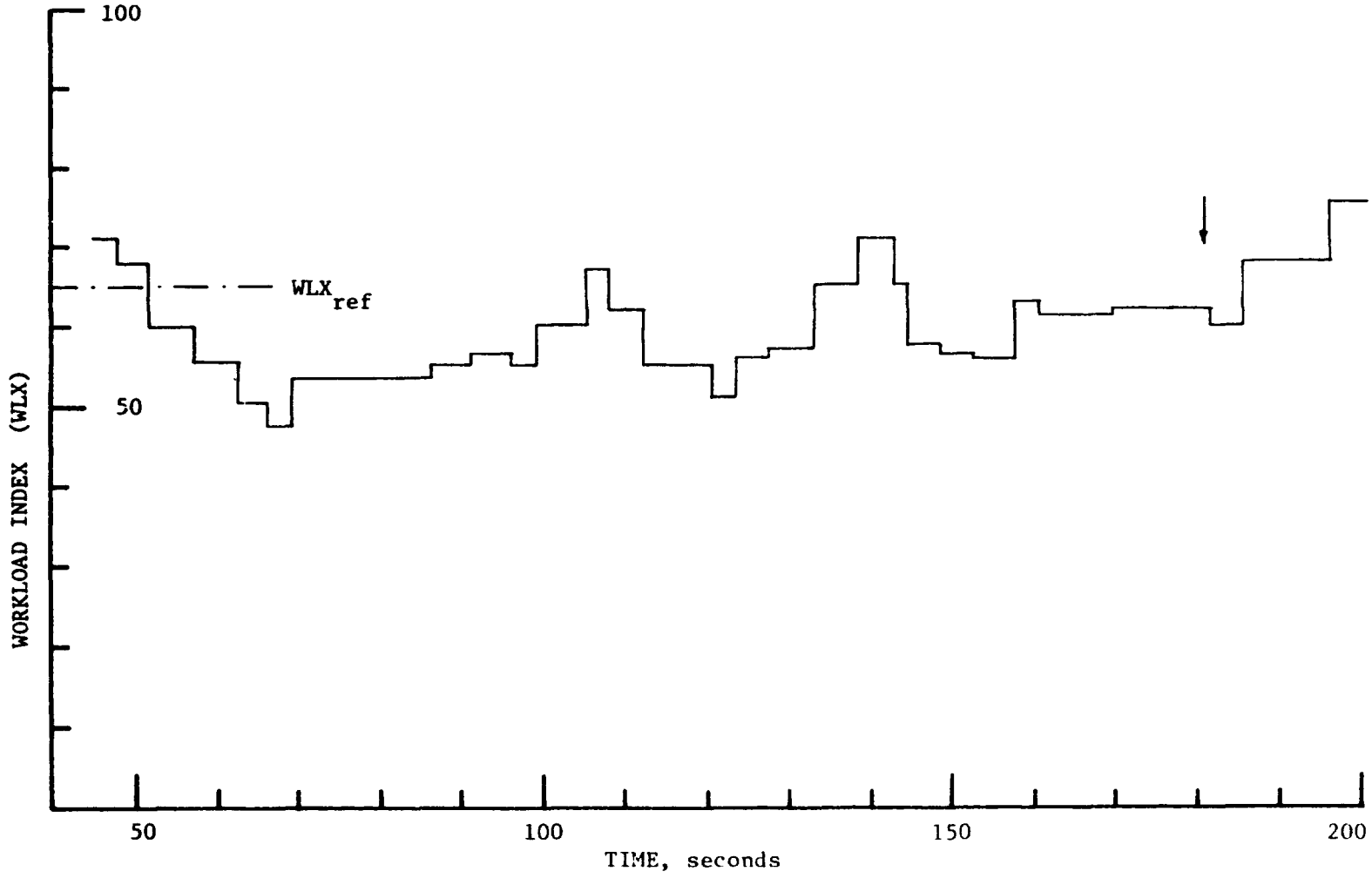

Figure 5.

Finally, this study raised, quite coincidentally, an interesting question about human perception of the correlation between control inputs and the output, its dependence on the dynamics of the plant and the effects of the associated time lags. While this question is basic to the study of human performance in manual control tasks in areas such as system identification, adaptation and fault detection, it has never been addressed explicitly, to our knowledge.

REFERENCES

1. Birmingham, H.P.: The Instantaneous Measurement of Human Operator Bandwidth. USNRL paper presented at 8th Annual Manual Control Conference, 1959.

2. Birmingham, H.P.; Chernikoff, R.; and Ziegler, P.N.: The Design and Use of Equalization Teaching Machines. IRE International Congress on Human Factors in Electronics, 1962.

3. Clement, W.F.: Investigating the Use of a Moving Map Display and a Horizontal Situation Indicator in Simulated Powered-Lift Short-Haul Operations. This conference.

4. Ephrath, A.R.: Detection of System Failures in Multi-Axes Tasks. Eleventh Annual Conference on Manual Control, 1975a.

5. Ephrath, A.R.: Pilot Performance in Zero-Visbility Precision Approach. NASA CR-137759, 1975b.

6. Hudson, E M.: An Adaptive Tracking Simulator. IRE International Congress on Human Factors in Electronics, 1962.

7. Kelley, C.R.: Self-Adjusting Vehicle Simulators. IRE International Congress on Human Factors in Electronics, 1962.

8. Kelley, C.R.; Mitchell, M.B.; and Strudwick, P.H.: The MOL Tracking Task. Preliminary Technical Report, Dunlap and Associates, Inc., 1965.

9. Kelley, C.R.; and Kelley, E.J.: A Manual for Adaptive Techniques. Final Report, Dunlap and Associates, Inc., 1970.

10. Spyker, D.A. et al.: Development of Techniques for Measuring Pilot Workload. NASA CR-1888, 1971.

IS THERE AN OPTIMUM WORK-LOAD IN MANUAL CONTROL?

By William L. Verplank

Massachusetts Institute of Technology

SUMMARY

Experiments on a closed-circuit-television driving simulator were designed to answer the question: is there an optimum work-load that (a) sustains performance in long-term driving and (b) facilitates transitions to new tasks or emergencies? The results affirm (a) with reservations but not (b). A second experiment is planned and a new measure for work-load proposed.

BACKGROUND

Automation or semi-automation in advanced manual control systems suggests the question: Is it possible for tasks to be too easy? Most human factors engineering has been aimed at reducing work-load, but can we go too far? Is there an optimum work-load and what is the appropriate measure? The concept of arousal and the evidence of vigilance and warm-up decrements suggest the search for such a work-load measure.

AN EXPERIMENT

The task was steering a closed-circuit-television driving simulator (reference 1). The subjects were instructed to follow as closely as possible a marked circular course. Three levels of task difficulty were provided by adding different amounts of disturbance to the input of the steering servo. This task corresponds roughly to driving in wind gusts. The experiment is illustrated in Figure 1. A marker in the center of the bottom of the screen was to be lined up on the dotted center-line of the "road".

The three conditions were: A: no disturbance, B: a moderate disturbance consisting of a sum of seven sine-waves with the lower frequencies predominating, and C: a difficult disturbance consisting of a sum of the same seven sine-waves with the higher frequencies more dominant. The speed of the car was held constant throughout the experiment.

Each experimental session consisted of 14 laps (approximately 12 minutes) at one condition, followed by 2 laps of condition C, 14 laps at a second condition followed by 2 laps of condition C, and 14 laps of the third condition followed by 2 laps of C. The subjects were familiarized with each of the three conditions prior to the experiment, and during each session were warned over an intercom, approximately 5 seconds before each change in condition, what

This is an informal paper presented at:
12th Annual Conference on Manual Control
University of Illinois, 25-27 May, 1976.

the new condition was going to be. The change in conditions always occurred at the same point on the track. The whole session lasted approximately 45 minutes. Data were recorded for three subjects over two or three sessions each, with the conditions presented in a different order each time. (See Figures 2-a through g for the orders.)

Each session provided data on the six areas of interest: prolonged performance under three conditions, and adaptation to condition C after these three different conditions.

Instrumentation

Both speed-control for the vehicle and generation of the disturbance were provided by a PDP-8 computer (10 samples/second). The lateral position of the car on the track was recorded on a chart recorder. It was from this record of position error that performance scores were calculated.

Data

The absolute value of the position error was read from the chart by eye at 32 equally spaced intervals for each two-revolution block of data. Thus, if the standard deviation of error in individual measurements from the chart were 10% (with no average bias) then the two-lap average absolute position error is good to approximately 3%. These two-lap average absolute position errors are plotted versus time in Figures 2-a through 2-g. The units are centimeters, measured at the display (T.V.). Each lap took 51.2 seconds, so the two-lap averages represent 102.4 seconds of data.

RESULTS

Hypothesis I: Long-term Performance

To test the hypothesis that performance will deteriorate with time, the difference in averages at the beginning and end of each condition were calculated. Each condition lasted for seven blocks. Figure 3 shows the change in average error from the first 3 blocks to the last 3 blocks for each condition (i.e. the first five minutes versus the last five minutes in a 12 minute run). Lines connect the data points produced in the same experimental session.

There is no significant decrement in performance for conditions A or B, but there is for condition C ($t=5.9$, $df=6$, $p < .005$). These data only support half of hypothesis I, that moderate is better than difficult. Hypothesis I suggests that, as the task gets easier (condition A), there will be a tendency for a vigilance-type decrement. Either condition A was not monotonous enough, or the run (12 minutes) not long enough, or for this particular driving simulation there is no such thing as an optimum task difficulty.

There does appear to be some difference however between conditions A and

B, as they relate to long-term performance. As shown in Figure 3 there is more spread in the changes for A than for B. That is, under condition B, average performance did not change over the run, but in condition A, it did. On some sessions it deteriorated over the run, and on some, it improved. This suggested that if stability of performance is important, condition B may well be superior to condition A.

This was examined by computing the standard deviation of the two-lap averages for each 12 minute. run. The normalized standard deviation is shown in Figure 4. Here is one measure that shows the moderate condition B as better than the easy condition A (paired $t=4.8$, $df=6$, $p < .005$). There is less variability in performance over the 12 minute run. However, the difference between conditions B and C disappears.

Thus, given the present data, it cannot be shown that a task of moderate difficulty is superior in long-term performance to both easier and more difficult tasks. It is, however, superior in certain ways. The moderate task B did not show a performance decrement over time, whereas the difficult task C did. The moderate task B showed less relative variability than did the easier task A.

Hypothesis II: Adaptation

Figure 5 shows error scores on condition C immediately following the extended run of either condition A, B or C. The two-lap error score is broken down into ¼-lap scores. Figure 5-a shows the score for the first ¼-lap (12.8 seconds). Figure 5-b averages the score for the first ¼-lap with that for the second (average for first 25.6 seconds). Similarly 5-c and 5-d are averages of all the performance up to the specified points.

Hypothesis II would suggest that initial performance on the new task would differ with different preparatory conditions, and that upon "adaptation" to the same new task, performance would equalize. Just the opposite appears to be the case. The preparatory conditions cannot be distinguished on the first ¼-lap score - only on the entire two-lap averages (5-d).

It is difficult to draw conclusions from the data because of the large inter-subject variability. In the two-lap averages, the only significant difference is for subjects JK and JM, between conditions B and C (paired within sessions) ($t=5.16$, $df=4$, $p < .01$). An alternative to Hypothesis II is proposed to explain this difference, and depends on a detail of the experimental procedure.

The experiment compared performance in adapting to condition C following an extended run of either A, B or C. If the "adaptation block" was followed by the extended run of C, this "adaptation" block was counted as the first block in that extended run. For "adaptation" following condition C, the block examined was simply the last block in the extended run. This may explain the similarity between Figures 5-d and 3, at least as far as condition C is concerned. Figure 3 shows the difference between the beginning and end of the extended run. For condition C, it shows a significant decrement in performance.

Similarly, Figure 5-d shows the averages at the beginning of a run (C following A or B) and at the end of a run (C following C).

There are two reasons then that the data do not support Hypothesis II. First, if it is truly a process of adaptation, the difference in performance should be greatest at the beginning of the new condition. The only significant difference is in the direction predicted by Hypothesis II (C worse than B), but it is not at the beginning, showing up only in the two-lap average. Second, this difference can be accounted for by an alternative to Hypothesis II. Another possibility is that a different measure of the "preconditioning" work-load could explain the differences in adaptation.

SUMMARY

Two hypotheses were proposed relating the concept of arousal and the evidence of vigilance and warm-up decrements to automobile driving. There should be an optimum work-load that sustains performance on long tasks, and facilitates transition to new tasks.

A simulation of automobile driving under three levels of difficulty showed a moderate disturbance caused less decrement than a difficult disturbance and less variability than no disturbance. No condition was superior at facilitating transitions.

The present evidence is not very strong support for the concept of an optimum work-load. Performance decrements in the "under-load" condition probably cannot be expected over such short runs. A second experiment with longer runs is proposed. The question of what constitutes optimality is also open.

Finally, the measure of work-load ought to include a kind of "self-loading" or "operator-induced work-load", especially in the case where there is no external disturbance and the operator is "tracking his own noise". The second experiment and a new measure of work-load will be reported in a forthcoming Ph.D. thesis [2].

REFERENCES

1. Rudy, R.P. and Willis, G. Monitoring and Control of an Automobile Simulator Using a Real-time Digital Computer. M.I.T. Engineering Projects Laboratory Report, DSR 79728-2, 1969.

2. Verplank, W.L. Sources and Effects of Uncertainty in Sustained Manual Control. Ph.D. Thesis, Mechanical Engineering Department, M.I.T. (in progress).

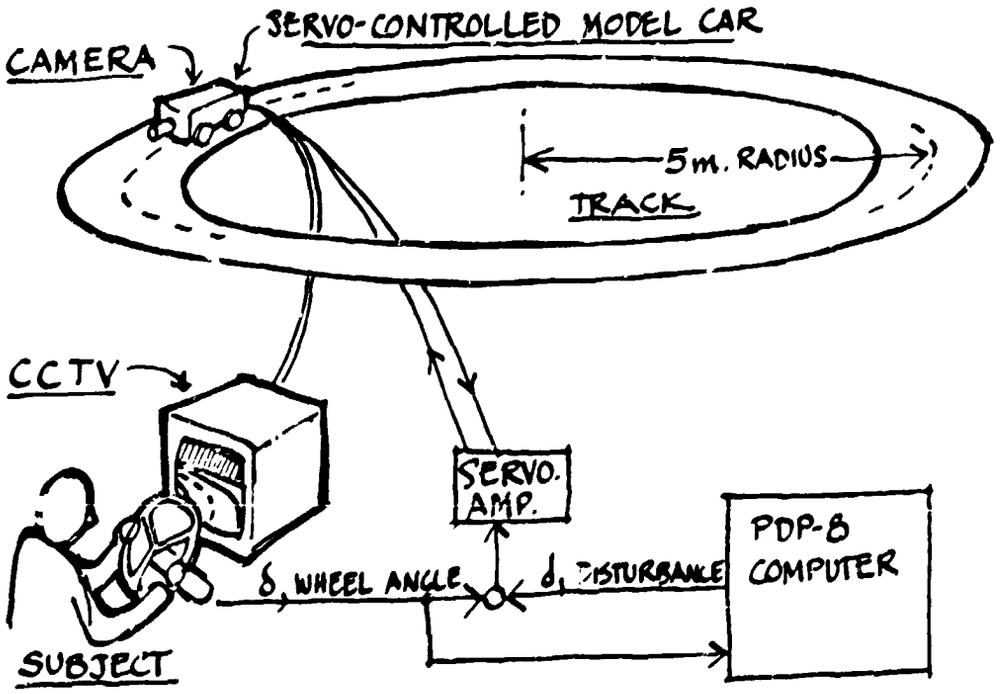

Figure 1. The M.I.T. C.C.T.V. Driving Simulator.

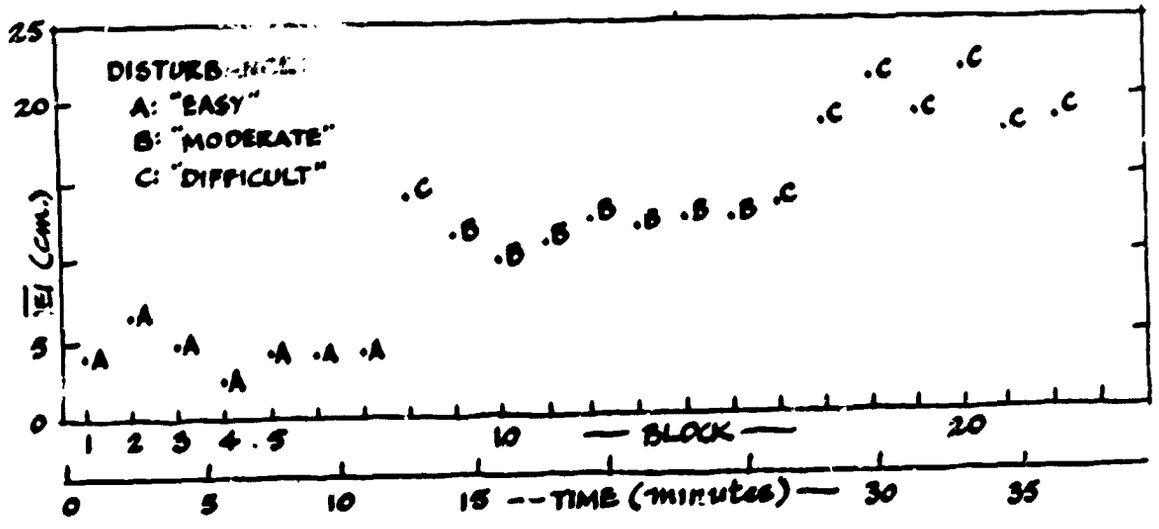

Figure 2a. Average Absolute Error by Two-lap Blocks.
Subject: JM, Session 1.

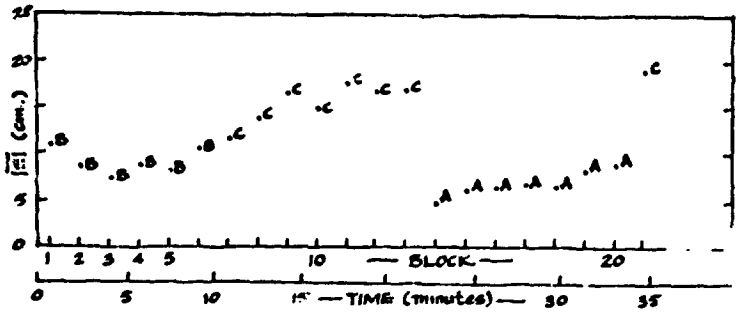

Figure 2b. Error by Blocks. Subject: JM, Session 2.

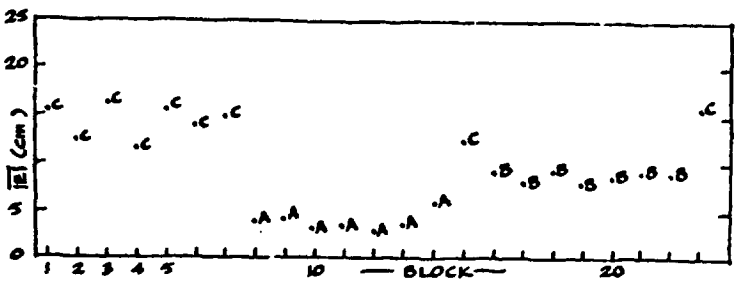

Figure 2c. Error by Blocks. Subject: JM, Session 3.

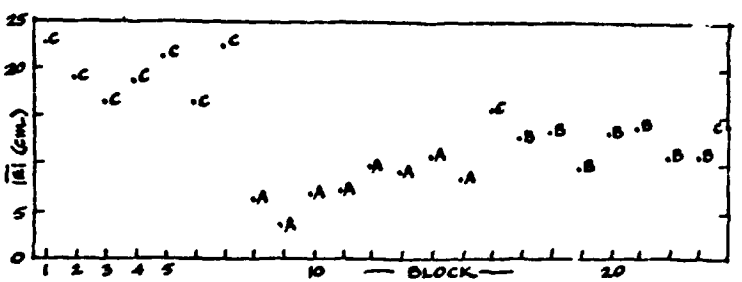

Figure 2d. Error by Blocks. Subject: JK, Session 2.

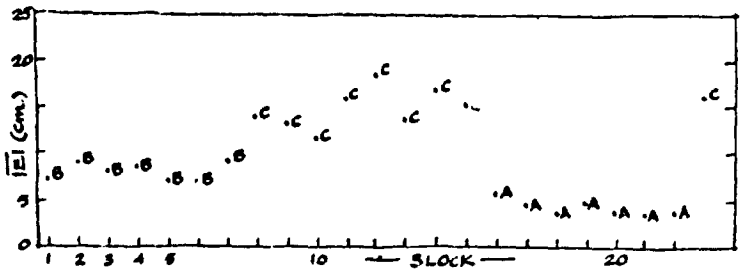

Figure 2e. Error by Blocks. Subject: JK, Session 3.

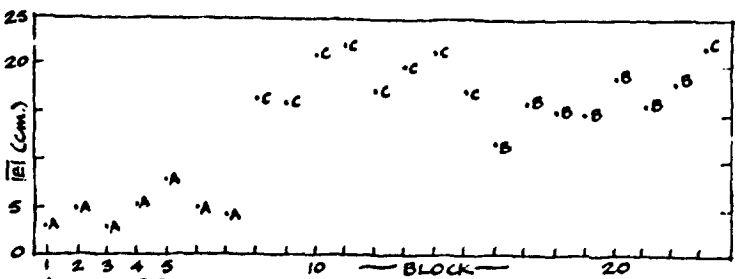

Figure 2f. Error by Blocks. Subject: WR, Session 9.

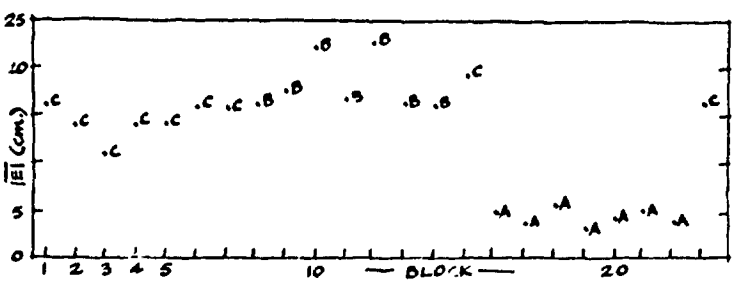

Figure 2g. Error by Blocks. Subject: WR, Session 10.

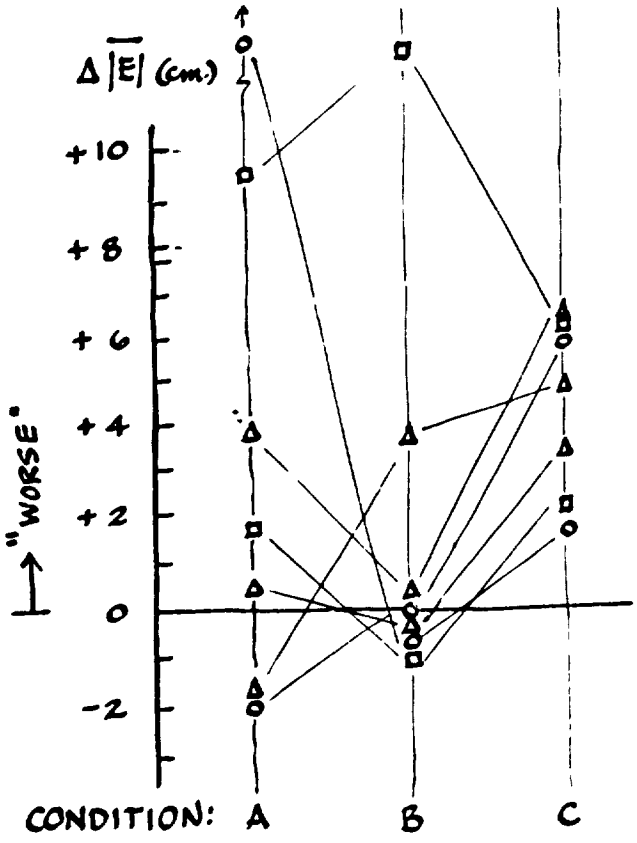

Figure 3. Change in Average Absolute Error From First- to Second-Half of 12 minute Run.

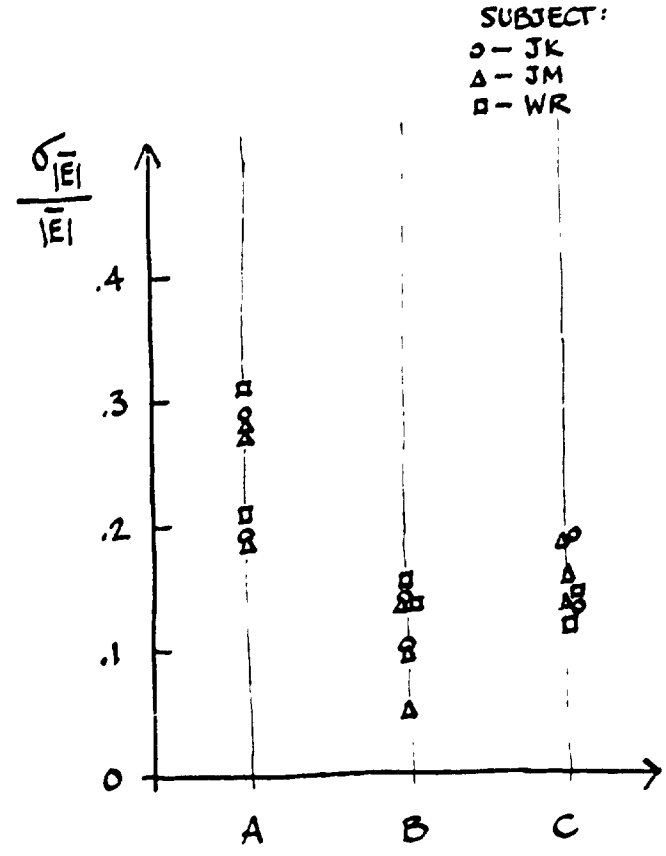

Figure 4. Relative Standard Deviation of (2-minute) Average Absolute Errors

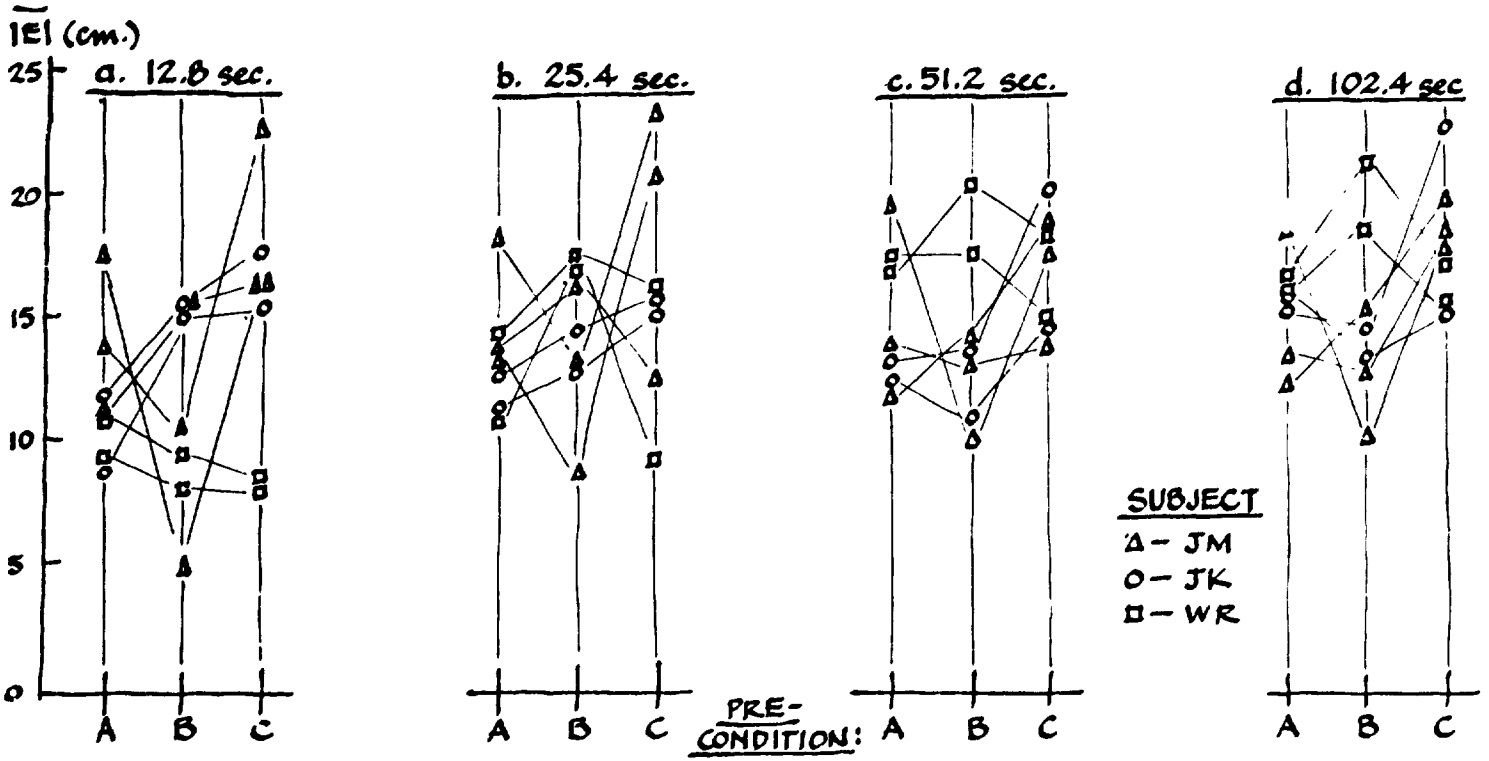

Figure 5. Average Absolute Error on Condition C Following A, B or C.

TASK INTERFERENCE IN MULTI-AXIS AIRCRAFT STABILIZATION

By Edward D. Onstott

Controls Research

Northrop Corporation
Aircraft Division
Hawthorne, California

ABSTRACT

A time domain attention allocating multi-axis pilot model has been used to examine task interference effects in a two-axis attitude stabilization task in turbulence. Configurations from a matrix of uncoupled lateral and longitudinal F-5 dynamics were analyzed to determine the influence of each axis on the control performance of the other. The analysis showed that an inappropriate choice of longitudinal dynamics would deteriorate the roll stabilization with no change in the lateral dynamics or pilot model. Furthermore, the influence of roll versus pitch angle display scalings were analyzed by hypothesizing that the task urgencies used to allocate attention in the pilot model should be weighted by the scaling factors. A fixed base simulation verified the model, the resonant task interference, and the scaling hypothesis; further validation through manned simulation was performed using a complete nonlinear YF-17 aircraft model and the Northrop Large Amplitude Simulator.

INTRODUCTION

Failure to match the dynamics of the pilot and the aircraft in an optimum way may result in not achieving the best performance of both. The result of such dynamic mismatch is greater pilot workload, less accurate weapon delivery, riskier approach and landing, and increased development cost deriving from overdesign in an attempt to achieve better pilot acceptance. Furthermore, the lack of precise methods for analytically evaluating the dynamic pilot-aircraft interface in the preliminary design phase may lead to extensive and unnecessary flight simulation. The analytic ability to recognize and correct significant control shortcomings as well as to identify potential improvements is important at a time when basic design concepts can be freely adapted to new requirements.

This analytical requirement has been partially met for decades by the use of mathematical models of human pilot dynamics. These techniques have been successfully employed in the development of simple low authority control systems where greatly simplified representations of the aircraft and the pilot could be tolerated, References 1-3. However, the advent of advanced tactical aircraft with the availability of high authority, high order control concepts and the associated demands for superior piloted performance requires pilot model aircraft analysis technology that is considerably more general.

In order to meet the current requirements of flying qualities prediction and evaluation, Northrop has evolved a flying qualities analysis procedure including complete generality of the nonlinear aerodynamics and control system. Digital simulation has been adopted as an over-all context for the dynamic representation and computation. With the availability of point-by-point generation of the flight history, pilot models can be developed that take into account not only the statistical features exploited by describing function or optimal control methods, but specific dynamic and decision processes as well. Northrop has validated this digital simulation approach to time domain decision models which generate the characteristics of multi-axis piloted flight, References 4 and 5. In addition to the increased system generality, an important consequence has been the discovery of multi-axis task interference effects that have never before been identified or analytically computed. The objective of this paper is to present these results.

ATTENTION ALLOCATION AND THE MULTI-AXIS HUMAN CONTROLLER

A great deal is known about the dynamics of the human pilot performing continuous linear single axis tasks. Much work has gone into developing models that match the amplitude and phase characteristics of the pilot's output at the controller, and many aspects of the internal structure of the human have been analyzed. These "ultra-precise" models are of use in solving many human factors problems about the interface between pilot and controller, but for the basic objective of determining the total system dynamics, it is usually sufficient to employ simple models that consist of gain K_p, lead T_L, time delay τ, and possible lag T_I:

$$Y_p = K_p \frac{\left(T_L s + 1\right)}{\left(T_I s + 1\right)} e^{-\tau s} \qquad (1)$$

The more exact pilot models can certainly be employed, but for most purposes the above simple model gives good statistical results.

There have been three main approaches previously taken in attempts to extend single-axis model theory to multi-axis tasks. All of these recognize that the human must operate as a time shared device when faced with difficult control tasks on several independent axes. This shifting attention allocation degrades the performance of each axis from what the pilot would achieve in continuous control. As might be expected, these three approaches are 1) decrease the model gain from the optimum for continuous control, 2) increase the time delay to account for the periods of inattention, and 3) inject filtered noise to imitate the spectral content of the shifting pilot control.

The insufficiency with these approaches is this: the human pilot is quite discriminating about when he will abandon the control of one task to take over the control of another. This leads to a pilot sampling criterion that is functionally dependent on the total system variables. In no way can this be regarded as a purely random, or a regular sampling. Thus a multi-axis pilot model must contain an algorithm that determines when attention shifting takes place, and the model must be computed in a way that preserves this information. Recently, Northrop developed a multi-axis pilot model which does just that, the urgency function model.

By using the method of digital simulation, the exact functional criterion, by which a pilot decides his control, can be directly computed without the gross distortions of linearization. The development of the form of these urgency criteria has now advanced to the point where they can be determined from 1) the system dynamics, 2) the task, and 3) the appropriate human factor information about the pilot.

Let x_i be the state variables of one axis, x, of a two axis task, and let the other axis, y, be represented by y_i. Then the attention allocation criterion for the x axis is satisfied identically with the inequality

$$U_x(x_i) \geq U_y(y_i) \tag{2}$$

where U_x and U_y are the urgency functions of the x and the y tasks. These functions are always nonlinear in the state variables, but fall into several precise classes. Some of these classes have been well explored, and a tabulation of the urgency functions for attitude stabilization is included below.

The multi-axis urgency function model thus consists of simple linear dynamics, equation (1), along with the control criterion of (2). Whichever axis has the larger urgency function gets the corrective control attention. The adjustment of the linear coefficients can usually be obtained by an easy search starting with the optimum single axis coefficients. Almost always, the optimum multi-axis coefficients differ significantly from these values, especially in multiloop control on the two axes.

TWO-AXIS ATTITUDE STABILIZATION IN TURBULENCE

It is natural to inquire about applications of the Northrop urgency model to representative tactical fighter dynamics. Since attitude stabilization in the presence of low-level turbulence is an almost ever-present requirement of any Class IV mission, this task was selected for both analytical and experimental study using degraded F-5 aircraft models. The primary objective was to verify the time-sharing of the human pilot, the appropriateness of the urgency function attention allocation algorithm, and the statistical accuracy of the predictions. In order to control the number of parameters involved in optimizing the model, display and controller effects were minimized in the flight simulation. This involved using a large CRT display so that display motions were amplified enough to eliminate visual threshold effects. Recently a general study of this problem, including visual threshold effects, has been completed using the general YF-17 aircraft model. The results of this problem are also discussed.

The simulation display consisted of an illuminated dot against a dimly illuminated grid. Vertical displacement of the dot represented pitch angle, and lateral displacement bank angle as shown in Figure 1.

The actual scaling of the dot displacement was achieved experimentally by going to the most sensitive scope setting which would accommodate all dot excursions. These scalings, μ and α, had units of degrees per centimeter of dot deflection, and provision was made to simulate at various values of μ to α ratios. As this μ/α ratio

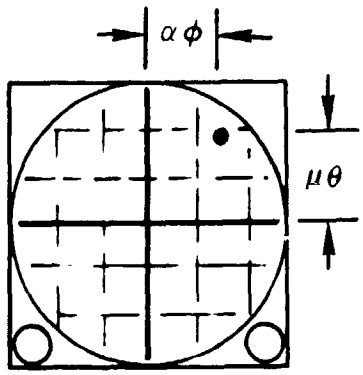

FIGURE 1. TWO-AXIS FLIGHT SIMULATION DISPLAY

increased from zero (continuous lateral tracking only), the pilot was forced to pay greater and greater attention to the longitudinal task. One of the most interesting hypotheses tested was the manner in which this took place. In all flight simulation tests the pilot was instructed to minimize the rms distance of the dot from the center of the display. This is called the radial error, denoted by $r(\phi, \theta)$, and is given by

$$r(\phi, \theta) = \sqrt{(\alpha\phi)^2 + (\mu\theta)^2} \tag{3}$$

In this way the μ/α ratio greatly influences the objective urgency, and the hypothesis tested is that the objective urgency as determined by the μ/α ratio scales exactly as the ratios of the urgency functions of the multi-axis pilot model U_P and U_R; that is,

$$\mu/\alpha = U_P/U_R \tag{4}$$

Limitations in display resolution allowed only the range of values shown in Figure 2.

μ	α	Task
0	1	Continuous Lateral Only
8	1	Two axis, $\mu/\alpha = 8$
16	1	Two axis, $\mu/\alpha = 16$
1	0	Continuous Longitudinal Only

FIGURE 2. URGENCY RATIOS TESTED

It should also be remarked that the aircraft dynamics and data reduction of the flight simulation were digitally generated. A frame time of 0.05 second was used, and the turbulence was generated using a digital random noise source with a 0.15 kHz bandwidth, thus assuring independence of the two gust time histories produced by the digital filters. The equations of motion and all dynamic computations were programmed exactly as in the analytical digital simulation model described below. It should be noted that the method is in no way restricted to linearized equations of motion. In the YF-17 study general nonlinear six-degree-of-freedom equations were used with no change in the pilot model or its use. Three degrees of freedom were mechanized laterally, while the u equation was not required longitudinally, thus giving five degrees of freedom in all. The equations of motion are shown in Figure 3.

$$\dot{w} = \frac{1}{1 - z_{\dot{w}}}\left(u_o + z_q\right) q + z_{\delta e}\, \delta e + z_w\left(w - \delta_{gw}\right) \tag{5}$$

$$\dot{q} = M_{\dot{w}}\, \dot{w} + M_q\, q + M_{\delta e}\, \delta e + M_w\left(w - \delta_{gw}\right) \tag{6}$$

$$\theta = q \tag{7}$$

$$\dot{r} = N'_r\, r + N'_p\, p + N'_{\delta a}\, \delta a + N'_{\delta r}\, \delta r + N'_\beta\left(\beta + \beta_{g\beta}\right) \tag{8}$$

$$\dot{\beta} = y^*_p\, p - r(1 - y^*_r) + \frac{g\phi}{u_o} + y^*_{\delta a}\, \delta a + y^*_{\delta r}\, \delta r + y_v\left(\beta + \delta_{g\beta}\right) \tag{9}$$

$$\dot{p} = L'_p\, p + L'_r\, r + L'_{\delta a}\, \delta a + L'_{\delta r}\, \delta r + L'_\beta\left(\beta + \delta_{g\beta}\right) \tag{10}$$

$$\dot{\phi} = p \tag{11}$$

FIGURE 3. EQUATIONS OF MOTION

The augmentation of each configuration was included in the stability derivatives, since washout is not required for a zero mean small perturbation attitude stabilization task.

The task proved difficult to fly, and about 10 hours were required for asymptotic training. Data were collected for test periods of 30 seconds, and simulation sessions were held to two hours maximum with frequent rest periods. In addition to the digital data reduction of tracking statistics, strip chart recordings were collected for each configuration and each μ/α ratio tested. In order to provide a variety of F-5 configurations, three longitudinal and two lateral sets of dynamics were selected and combined in a matrix of six configurations, designated as shown in Figure 4.

The turbulence simulation used Dryden spectra obtained by filtering Gaussian white noise as described in Mil-F-8785B, where an air speed of 718 fps and an altitude of 1750 feet were used. In order to diminish the effects of drift, a 40-db/decade high-pass prefilter was used on the random number noise source, with the break point set at 0.3 radian. The hand controller was mounted on the side of a chair and had light breakout and gradient forces; both the sensitivity and the polarity were selected by the subjects.

		Lateral	
		A	B
Longitudinal	1	1A	1B
	2	2A	2B
	3	3A	3B

FIGURE 4. F-5 CONFIGURATION DESIGNATION

Analytically, this problem was studied by means of digital simulation. This system model includes the six-degree-of-freedom linear or nonlinear airframe equations of motion, turbulence and command tracking generation, linear pilot model gain, lead, lag and delay, urgency function switching algorithms, pilot remnant, pilot inadvertent crossfeed, rms statistics, histograms of control episodes, and urgency function delay.

Since the turbulence provided a large disturbance to the system, it was not necessary to model remnant and inadvertent crossfeed. The commands to the system are simply $\phi = 0$ and $\theta = 0$.

In order to validate the model as a predictive method, the prediction algorithm should be understood. The various constants and functional forms are identical to those used in the earlier validation examples (Reference 4). The model takes the following form for two-axis multiloop attitude control:

1. Assume a linear model on each axis with a gain, lead (for Class IV aircraft, 0.5 sec), and delay of 0.3 sec (this includes neuromuscular lag which can be modeled separately if desired).

2. Assume continuous control in single-axis tasks, split control in multi-axis tasks. For a two-axis task, the pilot model will switch from one axis to the other based on testing the urgency functions:

$$\text{P axis controlled if and only if } U_P > U_R$$

3. The urgency functions take the form

$$U_P = \left| \alpha \left| \phi_e \right| + \beta \frac{\phi_e}{\left| \phi_e \right|} \dot{\phi}_e \right| \tag{12}$$

$$U_R = \left| \mu \left| \theta_e \right| + \nu \frac{\theta_e}{\left| \theta_e \right|} \dot{\theta}_e \right|$$

where β is equal to zero in single loop multi-axis tasks (this is the case in the two-axis turbulence problem).

4. The quantity α and its counterpart μ on the other axis are determined by the display. (This is the hypothesis mentioned above: that subjective and objective urgency must agree.)

5. Given the above, the model is optimized in the following manner:

   a. Optimize each pilot model gain for a continuous single-axis task.

   b. Use these gains to optimize the radial error r (ϕ, θ)

$$r(\phi, \theta) = \sqrt{(\alpha\phi_e)^2 + (\mu\theta_e)^2} \tag{13}$$

   by perturbing β and its counterpart ν.

   c. The gains should again be checked since it often occurs that optimum multi-axis gains are somewhat lower than single-axis optimum gains.

6. With this procedure complete, the model can be exercised to produce time histories of all dynamic quantities, all statistics of mean, rms, control episode periods, dwell fractions, and other parameters which serve as predictions of the performance of an asymptotically trained human controller for any system disturbance to be modeled such as pilot perception threshold, turbulence, or commands, both continuous and discrete, Gaussian and non-Gaussian.

For the two-axis attitude stabilization task in turbulence, the above algorithm simply requires optimizing two quantities (the pilot model gains) in the separate continuous single axis tasks. Hence

$$\begin{aligned} &\text{Longitudinal Urgency:} \quad U_P = \mu|\theta| \\ &\text{Lateral Urgency:} \quad\quad U_R = \alpha|\phi| \end{aligned} \tag{14}$$

Before examining the quantitative agreement of the model with the flight simulation, certain qualitative similarities with the data will be discussed. Although there has been a wide and rapidly growing recognition that the human pilot behaves as a time sharing device, the sharp division between lateral and longitudinal control has not often been directly exhibited. Two types of examples will be shown. The first illustration is a trace taken during the simulation of lateral versus longitudinal stick deflection, Figure 5. Notice that nearly all stick motion is parallel to either the lateral or the longitudinal control axes. Also note that these traces show that the pilot spent most of his time performing lateral corrections (which is consistent with the dwell fractions computed for this μ/α ratio of 8/1, approximately 0.75 lateral control). The second and most telling illustration of the pilot's switching from one control axis to the other is shown in Figure 6. Here the actual strip chart record is reproduced for a twenty-second sample of the two-axis task. The control episodes have been marked with a step function showing the pilot's apparent control shifting. If the reader will follow the entire record starting at time zero, the left hand side, he can compare the alternation of the control as indicated. Furthermore, if the ϕ and θ time series are compared, it is clear why control shifting takes place when it does.

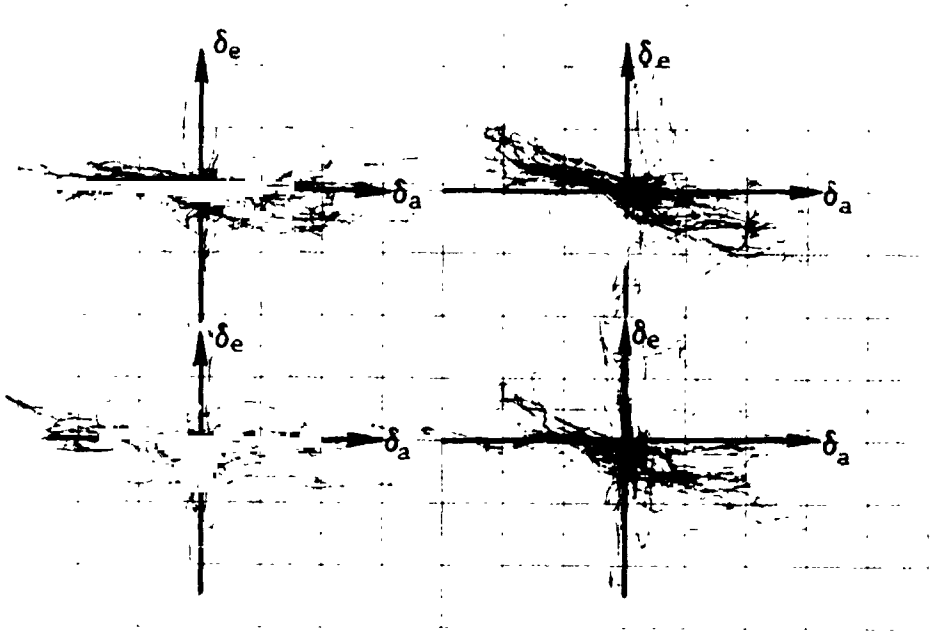

FIGURE 5. LONGITUDINAL VERSUS LATERAL STICK DEFLECTION

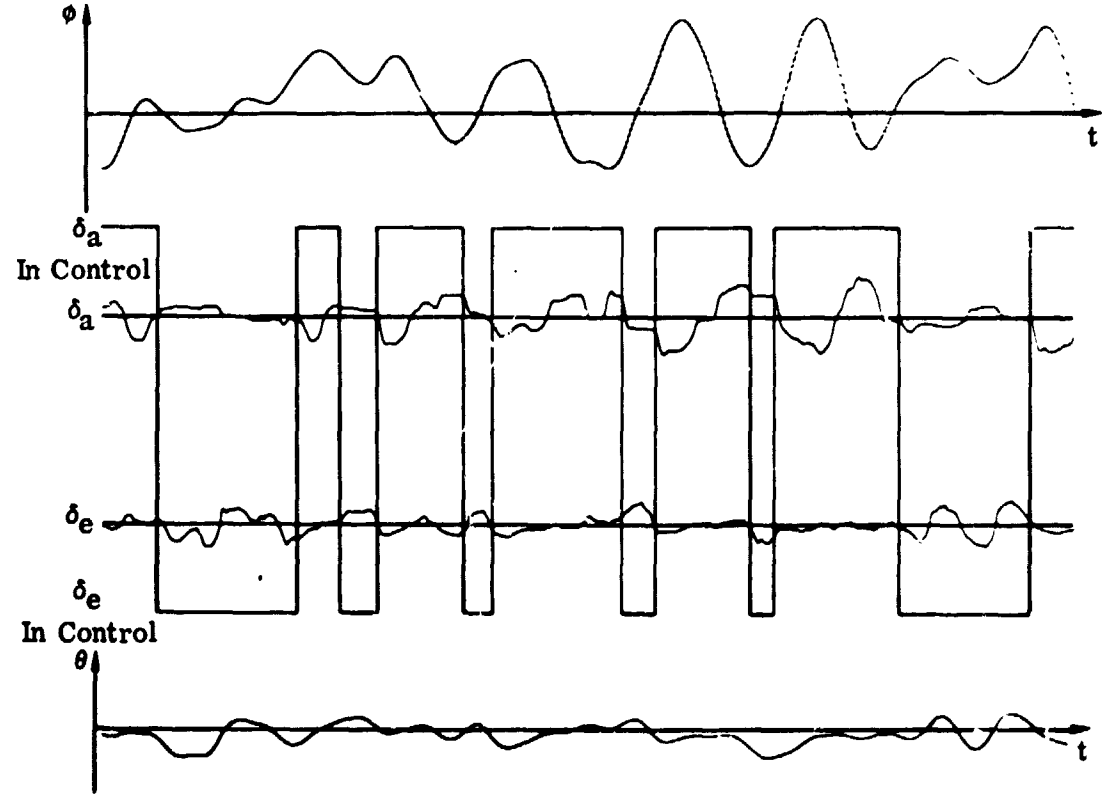

FIGURE 6. CONTROL SHIFTING EPISODES IDENTIFIED FROM SIMULATOR DATA

The most interesting comparisons are, of course, with the quantitative measures of the tracking performance. In the following data presentation, all tracking errors have been normalized to gust levels of 10 ft/sec. This turbulence level is approximately that used in both the analysis and the simulation, but statistical fluctuations produce variations in the actual turbulence level for any given data run, in both the model and the flight simulation.

The first data to be considered are an overall comparison of tracking error predictions and the simulation data. Figure 7 shows a plot of longitudinal θ simulation data versus model predictions. The simulator data are averaged from the 30-second tests for continuous, $\mu/\alpha = 8$, and $\mu/\alpha = 16$ tasks, while the model data were obtained from time histories spanning 1000 seconds. Figure 8 gives a similar comparison for the lateral ϕ data. The agreement here is slightly less good for the $\mu/\alpha = 16$ cases owing to experimental display constraints; at this urgency ratio, the dot motions sometimes went off the display. In particular, note the extremely accurate predictions for the single-axis task (squares). Since the pilot was instructed to minimize the rms distance of the dot from the center of the display, it is of value to compare the radial error data. This is shown for the two-axis data in Figure 9. It should be remarked upon that this agreement between model predictions and simulation data for a two-axis task rivals currently reported results in many single axis studies.

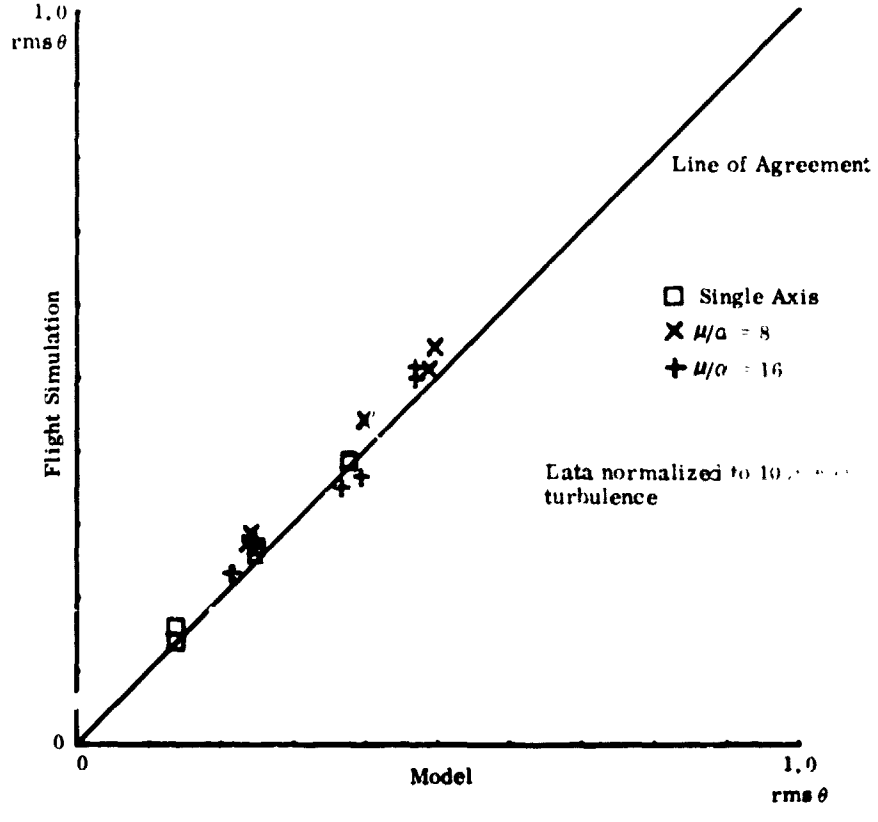

FIGURE 7. MODEL VERSUS FLIGHT SIMULATION DATA FOR ALL LONGITUDINAL TASKS

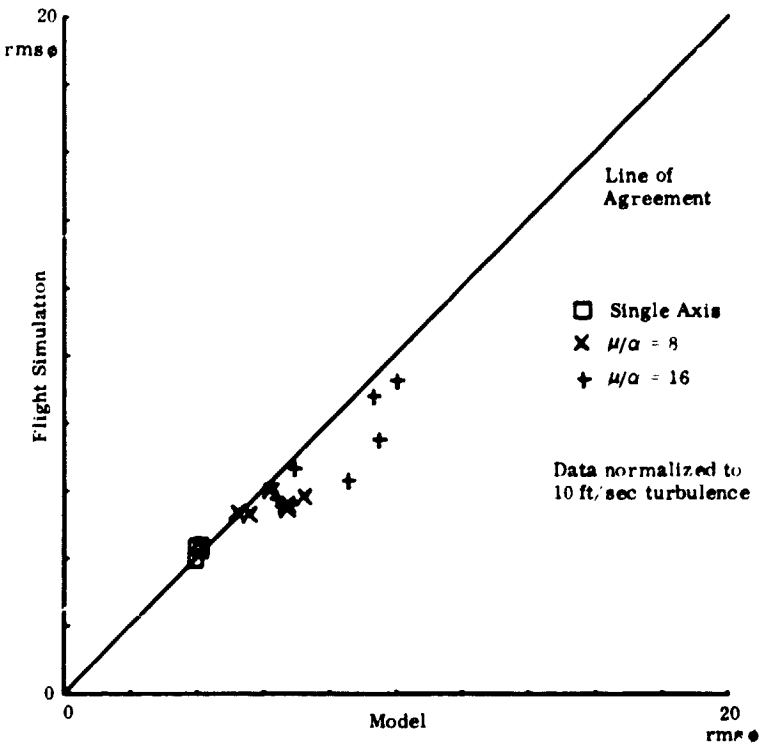

FIGURE 8. MODEL VERSUS FLIGHT SIMULATION DATA FOR ALL LATERAL TASKS

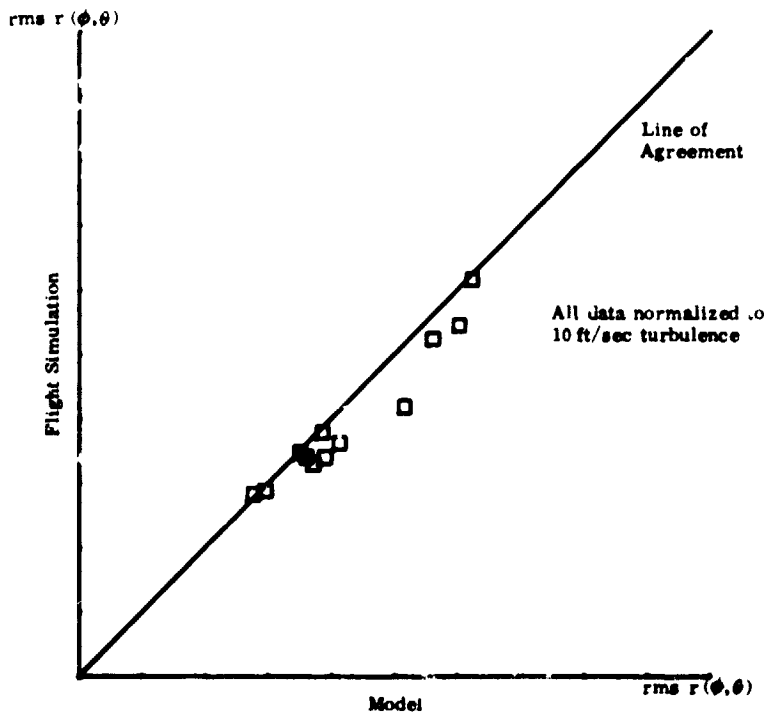

FIGURE 9. RADIAL ERROR OF MODEL VERSUS FLIGHT SIMULATION FOR TWO-AXIS ATTITUDE STABILIZATION

It is useful to examine the individual configurations. A particular type of diagram was evolved that portrays the two axis and the urgency ratio effects. An explanatory example is given in Figure 10. The vertical axis is lateral tracking error, and the horizontal axis is longitudinal tracking error. In order to see how a particular μ/α ratio compares with the open-loop aircraft response and with the continuous single-axis tracking performance, these values have been drawn as lines of constant-tracking error on the diagram as, for example, the line labeled "open loop ϕ." Thus the two-axis performance would be expected to fall somewhere in the rectangle bounded by these lines. For an urgency ratio of zero, i.e., continuous lateral tracking, the model prediction is the lower right-hand corner of the rectangle. The predictions for ratios of 8 and 16 are shown and labeled with the μ/α ratio. The averaged model data are also shown and labeled.

By referring back to the matrix of lateral and longitudinal dynamics, Figure 4, it is possible to see to what extent lateral and longitudinal dynamics interfere with each other through the pilot. The most striking example, and this is one of the most significant findings of the study, is furnished by a comparison of 1B and 3B, Figures 11 and 12. Both of the configurations have the same lateral dynamics, B, but differ longitudinally. A comparison of the data shows that in 3B, the two-axis control stays within the rectangle for urgency ratios of 8 and 16. However, in 1B the different longitudinal dynamics result in deteriorated tracking at a ratio of 8, and grossly deteriorated tracking at 16. The result of this is that task interference and dynamic matching are important aspects of two-axis handling qualities that are seen to exist experimentally, and are subjects that can be accurately predicted and evaluated by the two-axis urgency function pilot model.

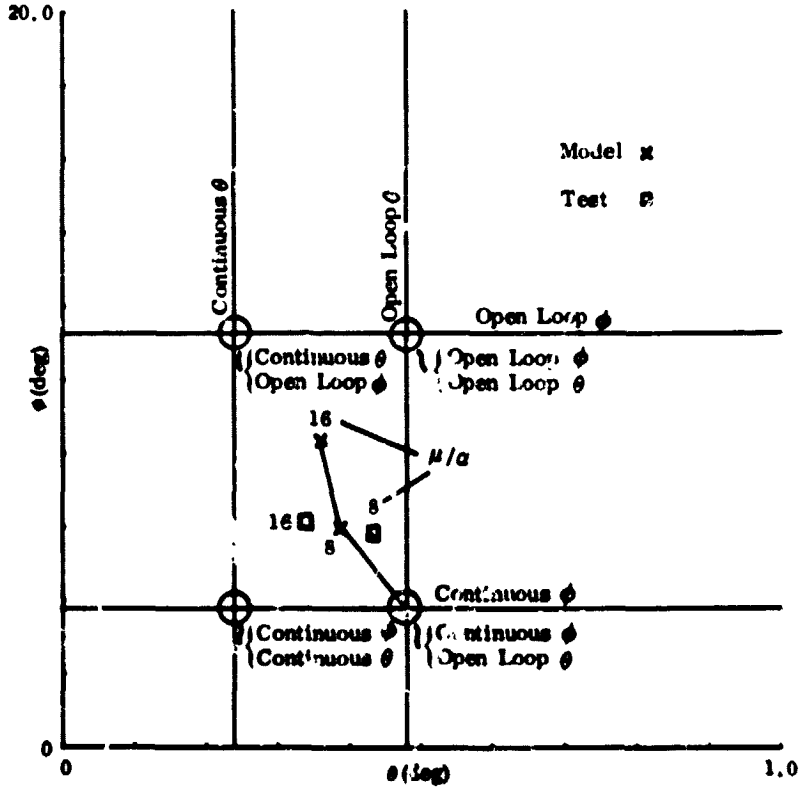

FIGURE 10. HOW TO READ TWO-AXIS DATA PLATES (EXAMPLE)

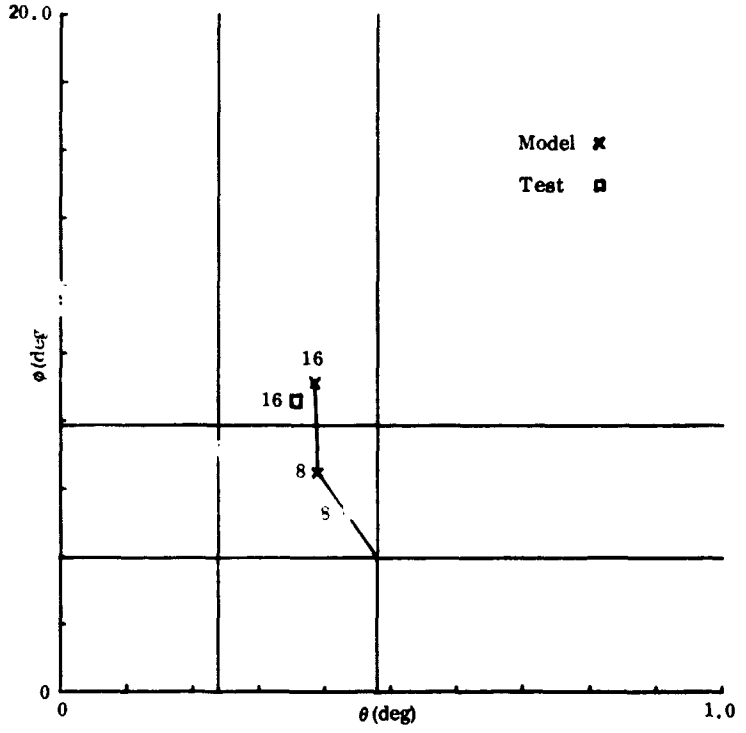

FIGURE 11. MODEL AND TEST DATA FOR F-5 1B

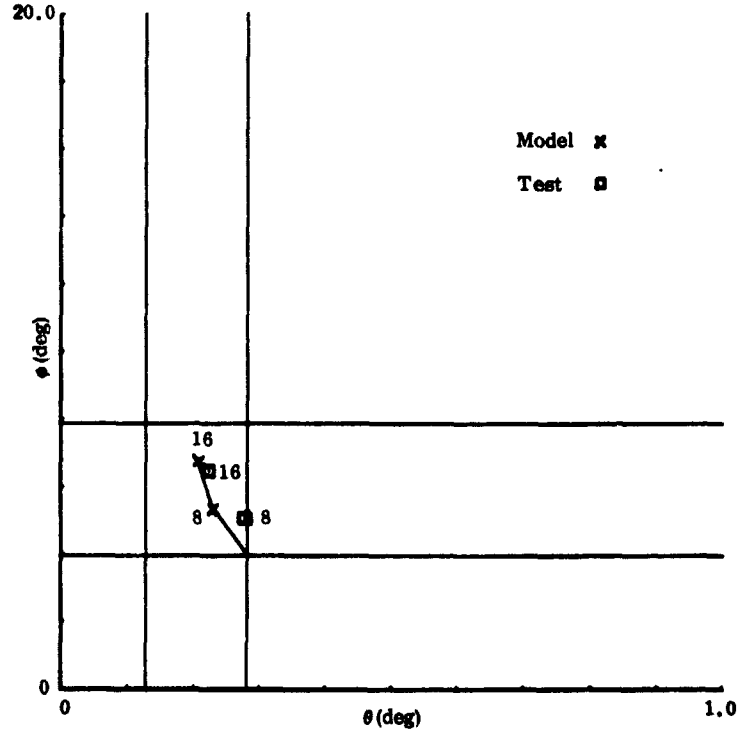

FIGURE 12. MODEL AND TEST DATA FOR F-5 3B

A further point to observe is that even in the configurations where the lateral tracking error is diminished in the $\mu/\alpha = 16$ tasks, the data still fall along the lines of model predictions regarded as interpolations of the urgency ratios. This indicates that when the display limit forced additional attention to the lateral task, the pilot simply shifted his subjective urgency, i.e., his actual weighting of ϕ and θ, thus displacing the data along the urgency interpolation curves. In the other cases where the display limit was not encountered, the data fall close to the curves. This indicates two things: First, the pilot's subjective urgency and the objective urgency of the actual display gains closely agree; second, the greatest source of model prediction inaccuracy is a failure of these two urgencies precisely to match up owing to experimental constraints not modeled in this example.

There is one further statistical comparison that has quite important consequences to aircraft design and air safety, namely, the variation in tracking error as shown in the performance data dispersion of the 30-second simulations. The following Figures 13 and 14 show these 30-second data for two-axis flight simulation data as well as 30-second model data for a comparable number of flights. The significant feature of two-axis handling qualities that these figures exhibit is the propensity of certain configurations to large excursions and tracking error, while others appear more uniform. This demonstrates a varying sensitivity to fluctuations in the effective turbulence power spectrum and probability density during the finite duration flight histories. Here, the model and the flight simulation show a large dispersion, with many flights performing much worse laterally than open-loop response. These

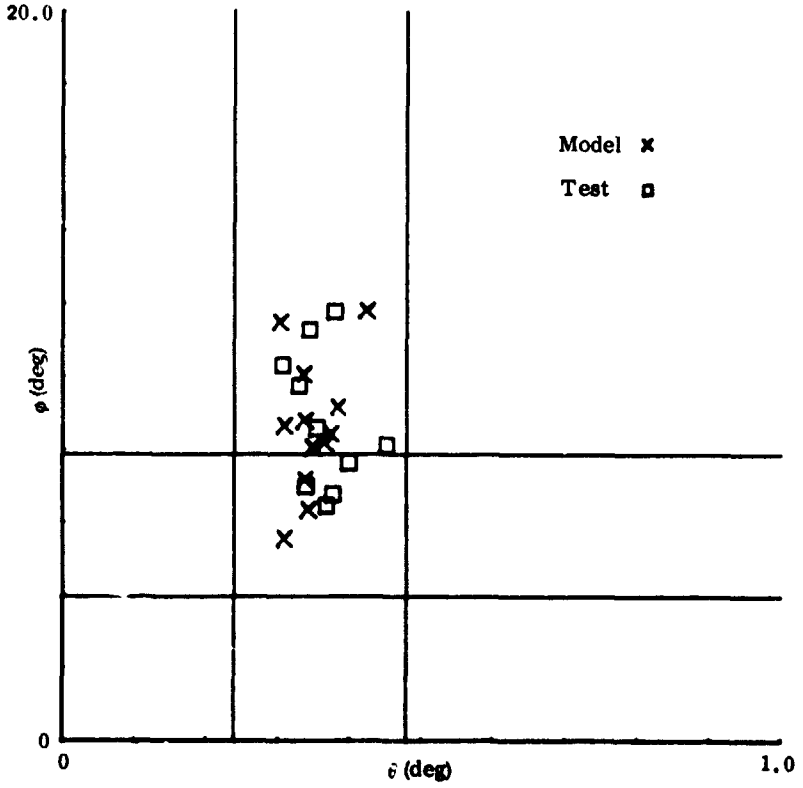

FIGURE 13. MODEL AND SIMULATION DATA DISPERSION FOR 30 SEC FLIGHTS F-5 1B $\mu/\alpha = 16$

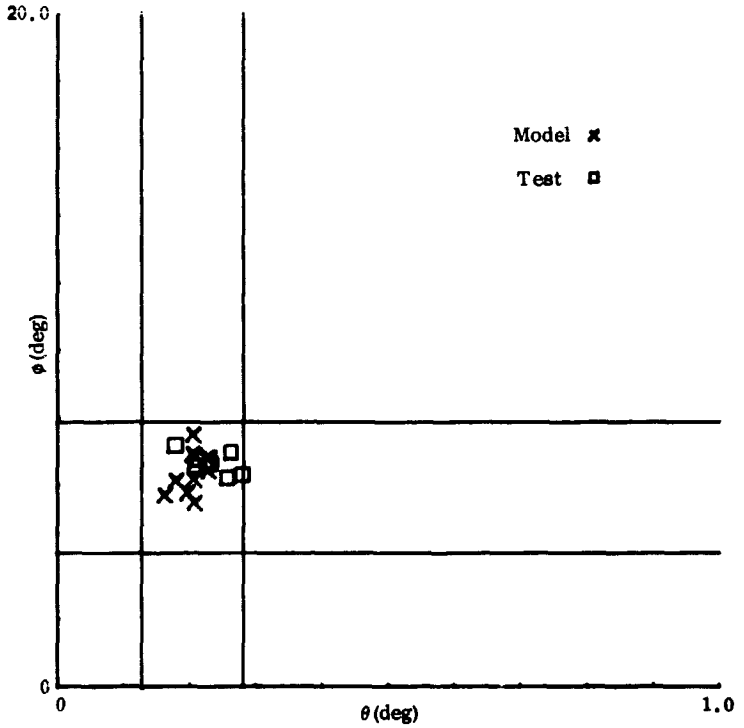

FIGURE 14. MODEL AND SIMULATION DATA DISPERSION FOR 30 SEC FLIGHTS F-5 3B μ/α = 16

effects indicate that not only do certain combinations of lateral and longitudinal dynamics lead to deteriorated tracking errors, but to a large scatter in the performance as well. The actual attitude excursion encountered in examples such as 1B could, in an actual flight, be severe enough to lead to loss of control. This effect is totally due to the two-axis time sharing of the human controller, since such sensitivity is not observed in the continuous single-axis data, or in other configurations involving the lateral or longitudinal dynamics that together produce these examples. Considering 1B further, Figure 15 shows the model time history of 225 seconds lateral tracking error for continuous single-axis tracking and for two-axis tracking with an urgency ratio of 16. In the continuous case, there is a total absence of large excursions, while in the two-axis history large fluctuations occur in local tracking performance as well as numerous severe sudden excursions.

TWO-AXIS ATTITUDE STABILIZATION OF THE YF-17 IN TURBULENCE

In April 1975, the Northrop multi-axis pilot model was further validated through flight simulation of the YF-17 using the fully general aircraft model on the Northrop LAS/WAVS flight simulator. There were three objectives of this study:

- Demonstrate the generality of the Northrop pilot-aircraft model
- Validate the model for external visual flying
- Evaluate the importance of modeling visual deadbands.

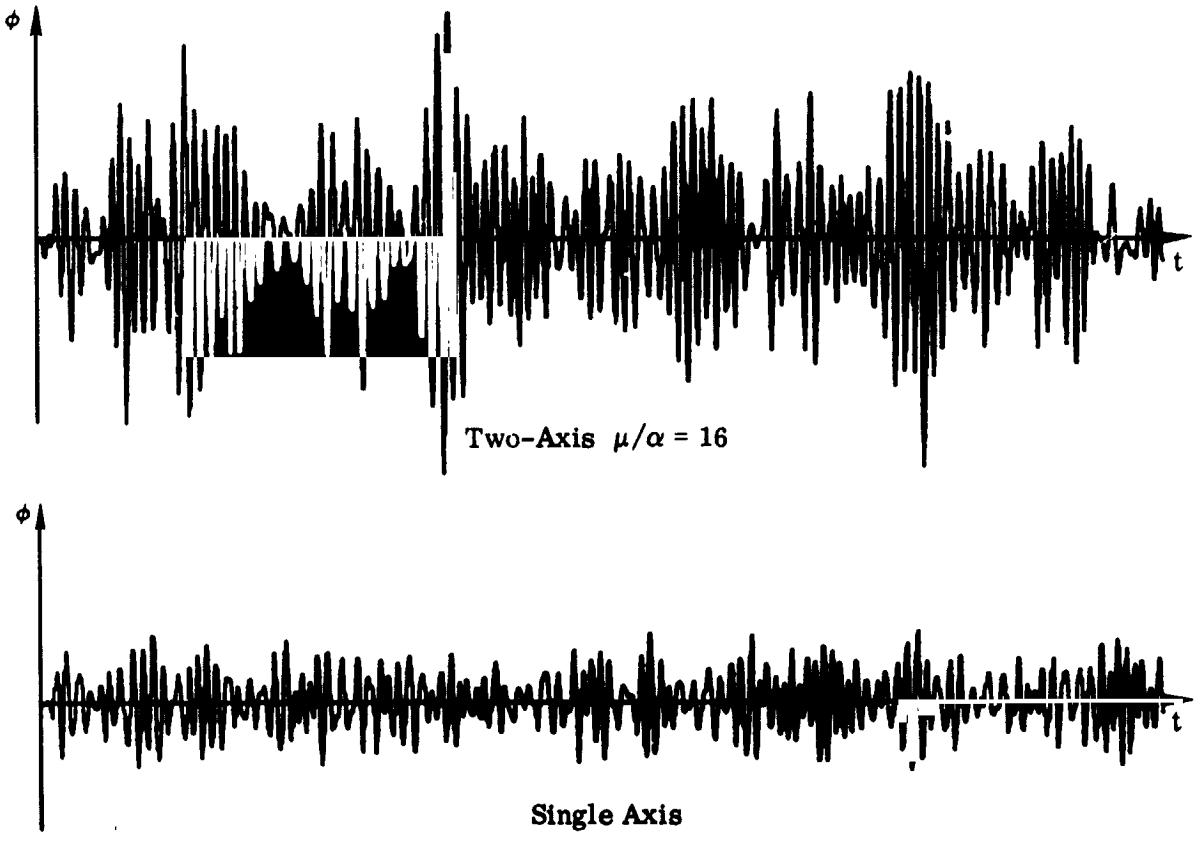

FIGURE 15. LATERAL TIME HISTORIES FOR SINGLE AND TWO-AXIS TURBULENCE TRACKING OF B LATERAL DYNAMICS

The aircraft model included all nonlinear aerodynamics terms and parametric table look-ups as well as the nonlinear control system including automatic flap setting. The cockpit was used with no change from the YF-17 configuration, including stick gradients and all functioning instruments. Dryden turbulence was generated for lateral v and longitudinal w gusts, and stabilization flights were of thirty-second duration.

In order to incorporate visual deadband in a realistic manner, the wide-angle visual-system earth-sky projector projected a horizon of mountainous terrain. By having the pilot (a former U.S. Navy test pilot) attempt to hold zero roll angle, the presence of visual deadband could be both demonstrated and measured from the strip chart recordings. This deadband then was mechanized into the pilot model as an inequality test, not as injected white noise. In this way, the model of the deadband preserved the dynamic characteristics of the actual flight simulation as well as led to the correct statistics.

The model of the piloted YF-17 was exercised by inserting the pilot model into the simulator computers, a small modification. Flights simulations were completed for single- and two-axis tasks at six flight conditions as shown in Figure 16.

ALTITUDE	5K	10K	30K	40K	60K
MACH					
0.4	X		X		
0.8	X			X	
0.9					X
1.1		X			

FIGURE 16. YF-17 FLIGHT CONDITIONS STUDIED

Plots of model versus flight simulation for the single-axis tasks are given in Figures 17 and 18, where the lateral model data have been completed using the deadband, 3 degrees. The data for the two-axis tasks are shown in Figures 19 and 20. The close agreement of these data between the model and the flight simulation validates the model, including the visual deadband. Computations of the model without the deadband agree poorly for the flight conditions of high dynamic pressure where the

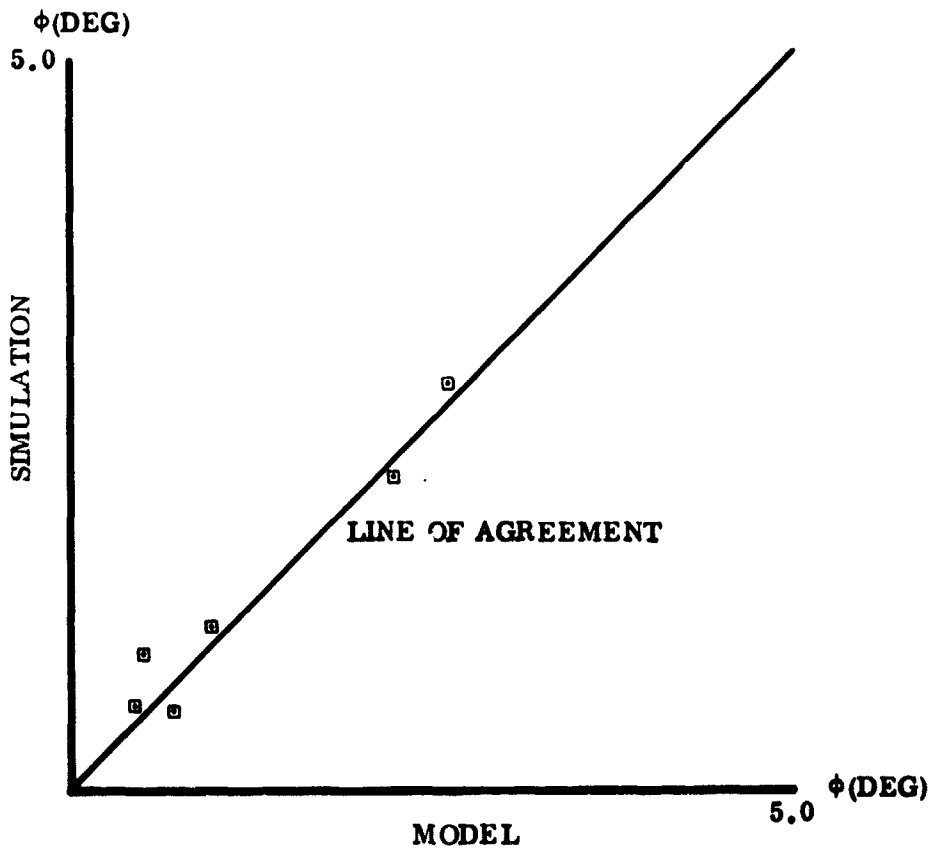

FIGURE 17. LATERAL TURBULENCE TRACKING OF THE YF-17 SINGLE AXIS

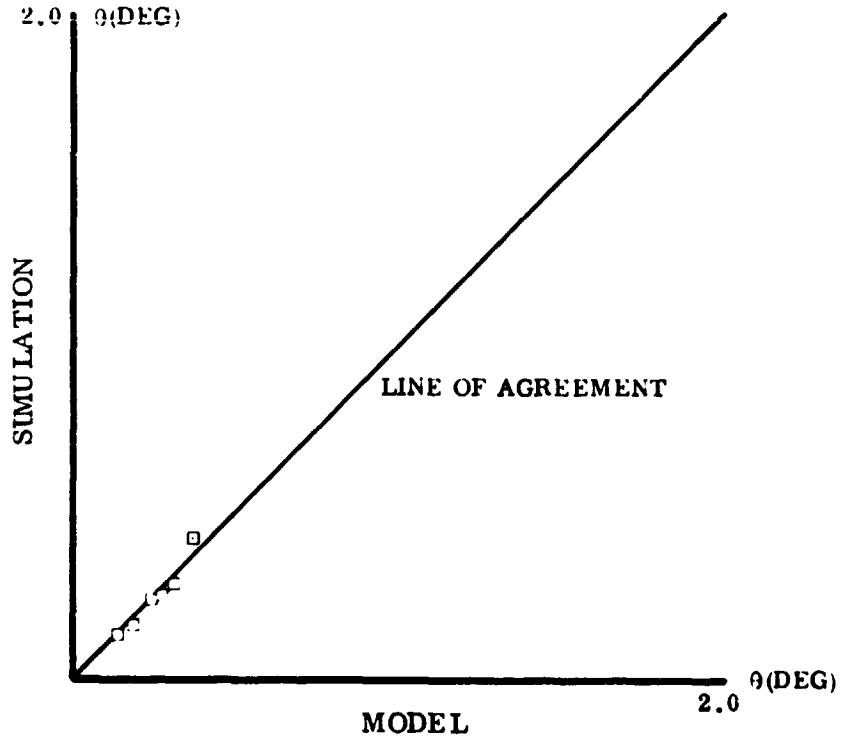

FIGURE 18. LONGITUDINAL TURBULENCE TRACKING OF THE YF-17 SINGLE-AXIS

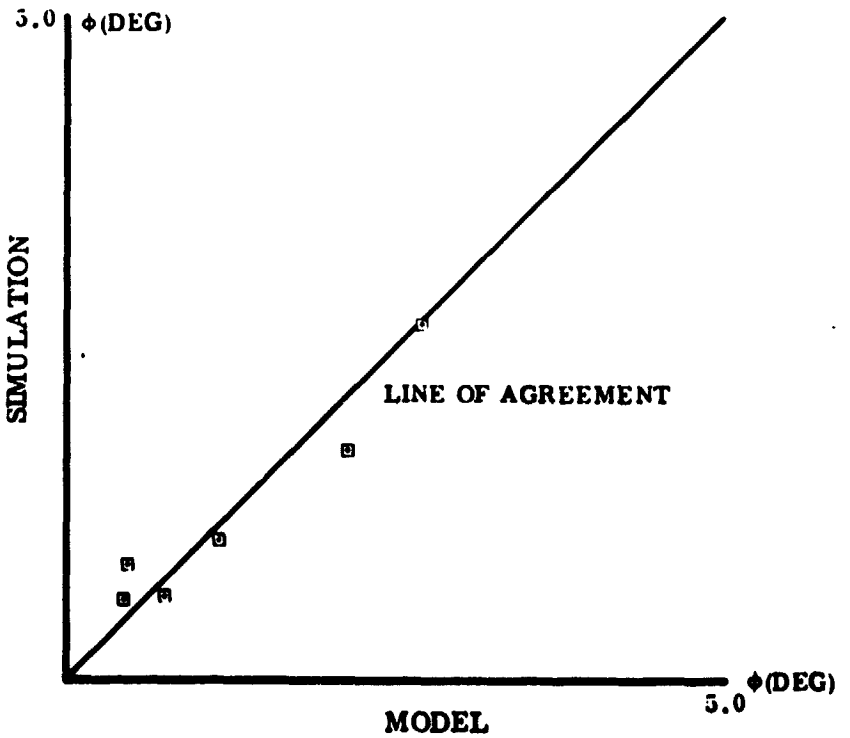

FIGURE 19. LATERAL TURBULENCE TRACKING OF THE YF-17 TWO-AXIS

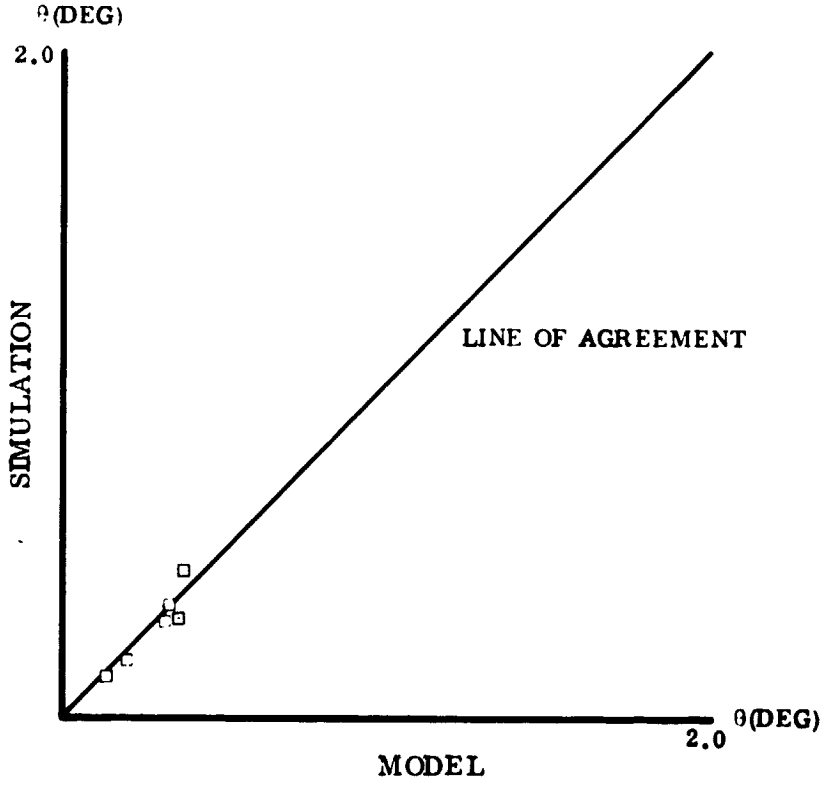

FIGURE 20. LONGITUDINAL TURBULENCE TRACKING OF THE YF-17 TWO-AXIS

turbulence disturbances are low, being roughly one-fifth to one-quarter of the deadband model values. The effects of dispersion between the data of the thirty-second flight identified in the study of the F-5 in turbulence also show in the flight conditions of the YF-17 at low dynamic pressure. The data from the individual flights are presented for the six flight conditions in Figures 21 through 26.

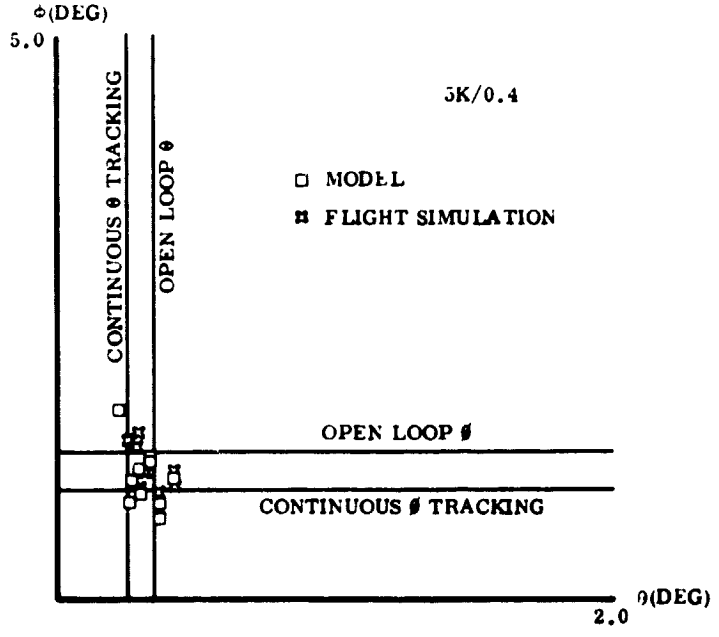

FIGURE 21. TWO-AXIS TRACKING DATA FOR 5,000 FT AT MACH 0.4

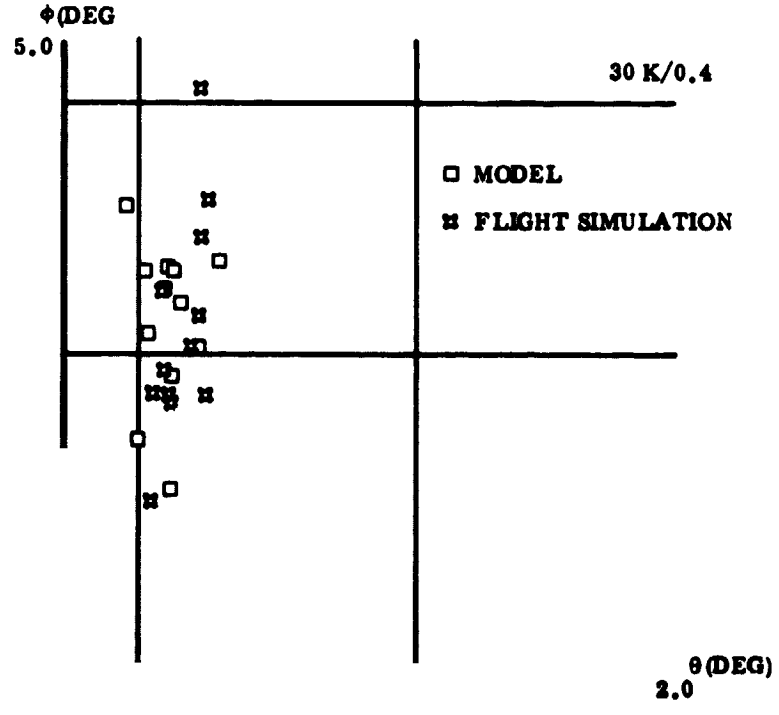

FIGURE 22. TWO-AXIS TRACKING DATA FOR 30,000 FT AT MACH 0.4

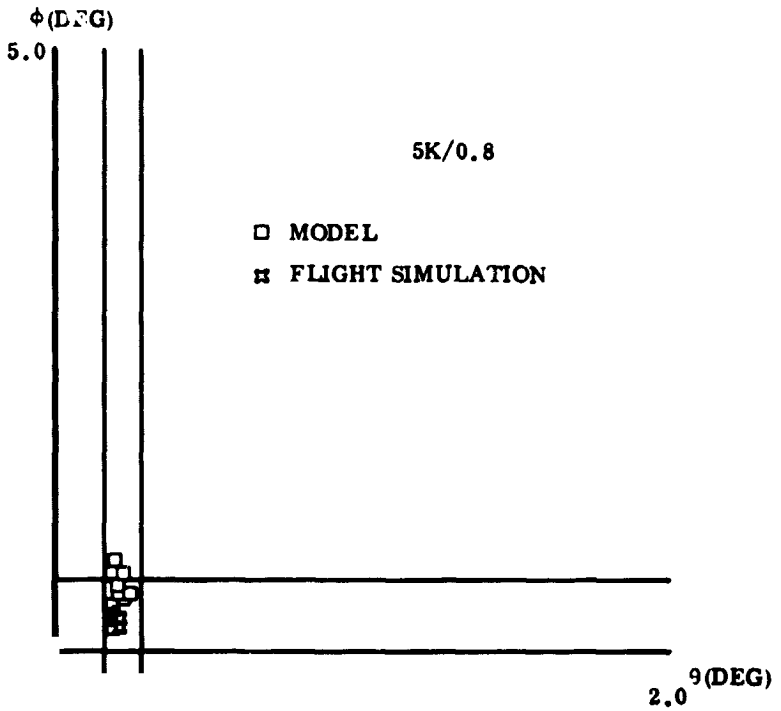

FIGURE 23. TWO-AXIS TRACKING DATA FOR 5,000 FT AT MACH 0.8

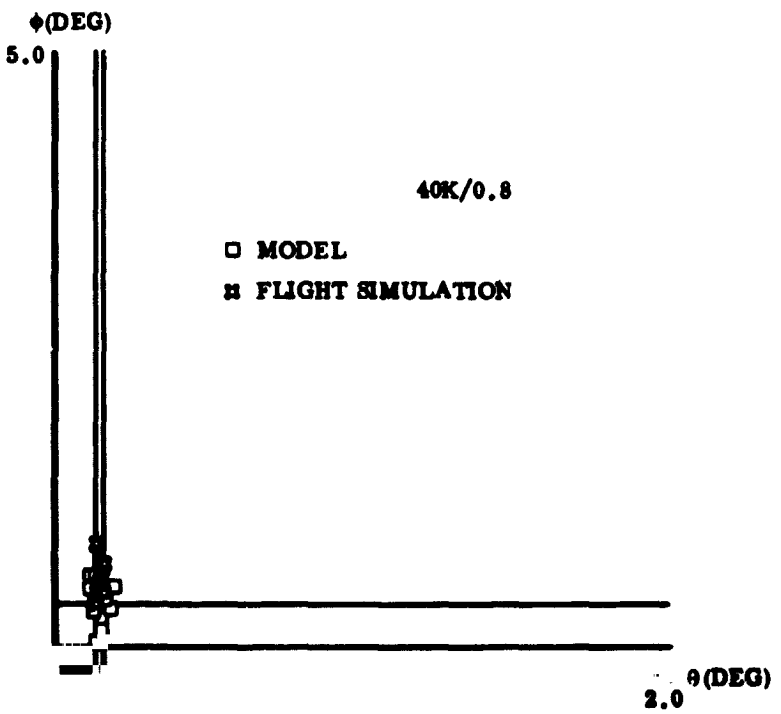

FIGURE 24. TWO-AXIS TRACKING DATA FOR 40,000 FT AT MACH 0.8

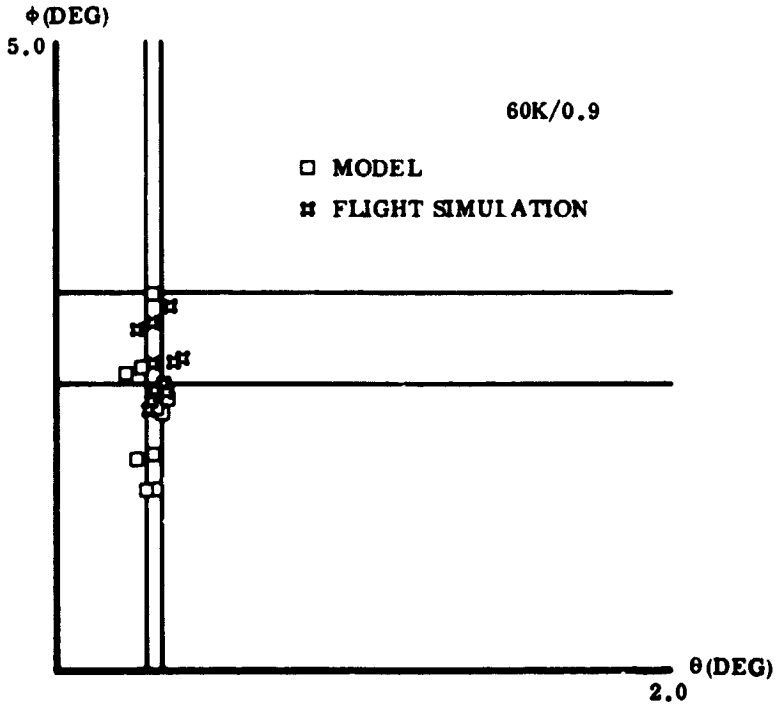

FIGURE 25. TWO-AXIS TRACKING DATA FOR 60,000 FT AT MACH 0.9

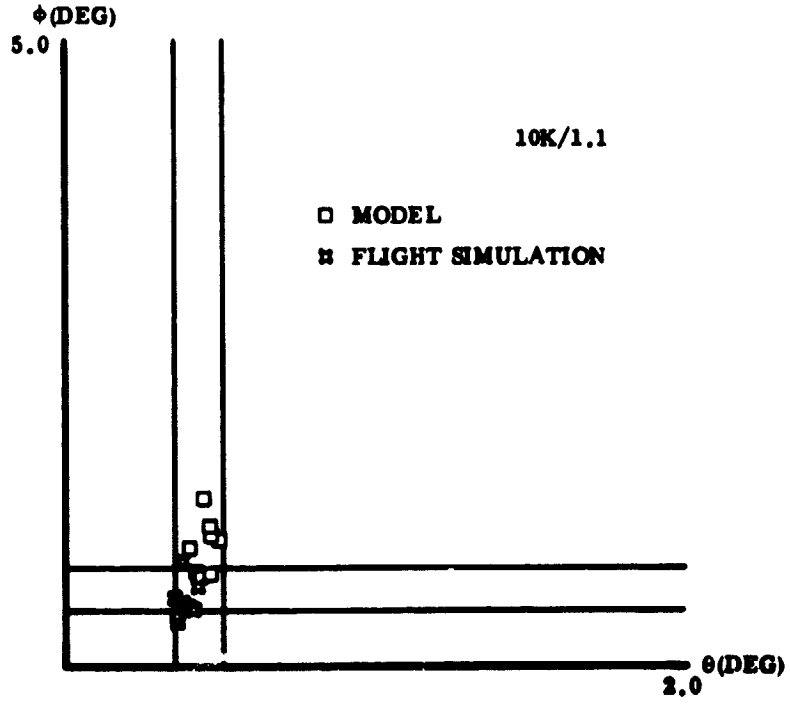

FIGURE 26. TWO-AXIS TRACKING DATA FOR 10,000 FT AT MACH 1.1

APPLICATIONS

Since these methods of digital simulation and multi-axis pilot models allow large scale maneuvers to be studied as the closed loop nonlinear and time-varying problems that they are, there are a large number of applications which can be undertaken. Northrop is currently working on several major examples, and further work will include the following problem areas.

Weapon Delivery

Both air-to-air and air-to-ground problems can be studied. In dive bombing, for example, the analysis includes target acquisition, roll-in, acquisition of the glide slope, tracking using the weapon sight, intense but briefly unstable attitude rate stabilization prior to weapon release, and pull up. The entire maneuver can be digitally "flown" many times in the presence of the realistic environment of low level turbulence and pilot induced system noise, and the statistics of impact error produced.

Landing Approach

The aerodynamics of landing approach are not well represented by constant coefficient linear uncoupled dynamics. Furthermore, the landing task in the presence of low level turbulence make the use of the exact nonlinear models of the problem necessary. Much has been learned from linear methods about the form of the control strategy that the pilot must use, and the study of the behavior of the multi-axis pilot model can utilize this information to produce a comprehensive analysis of the entire maneuver.

Coordination of Analysis and Flight Simulation

The multi-axis pilot model technologies developed at Northrop will not replace piloted flight simulation, but in fact can be used to greatly improve its efficiency. Not only will consistent analytical and experimental results give greater credibility to both, but the ability to screen away needless experiments by analysis will also improve the overall efficiency of aircraft evaluation and design.

Loss of Control at High Angles of Attack

Once aerodynamic descriptions of this flight condition are determined, the nonlinear and time-varying modeling capabilities of the Northrop methods can be immediately applied. The multi-axis pilot models required will be similar to the ones developed for attitude stabilization. As an example, consider Figure 27. This is the time history of one axis of a two-axis attitude stabilization problem. The system remained well-behaved for 120 seconds at which time task interference effects coupled through the pilot model caused a sudden divergence of the system in .3 seconds.

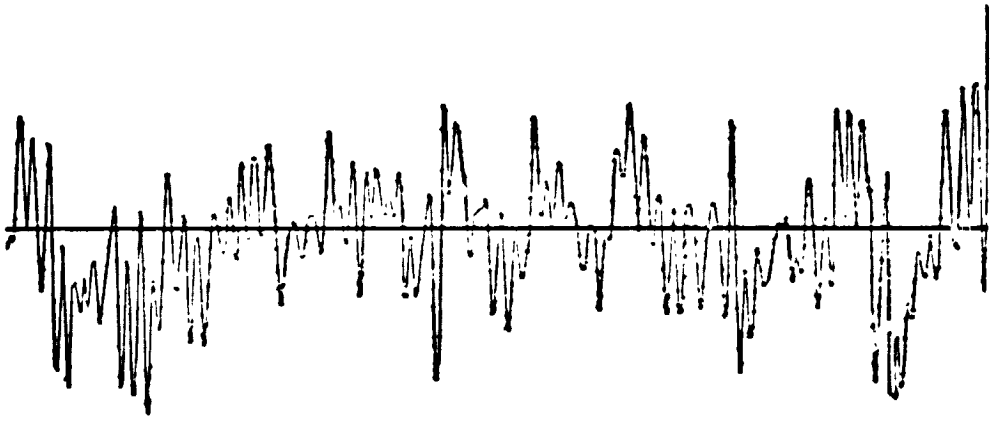

FIGURE 27. SUDDEN LOSS OF CONTROL IN A TWO-AXIS TASK

FUTURE RESEARCH

Apart from continuing work in the areas of the applications discussed above, Northrop is pursuing further development of the basic methods of dynamically modeling human factor pilot model components. The current work addresses the items indicated in Figure 28, which is regarded as the complete pilot model.

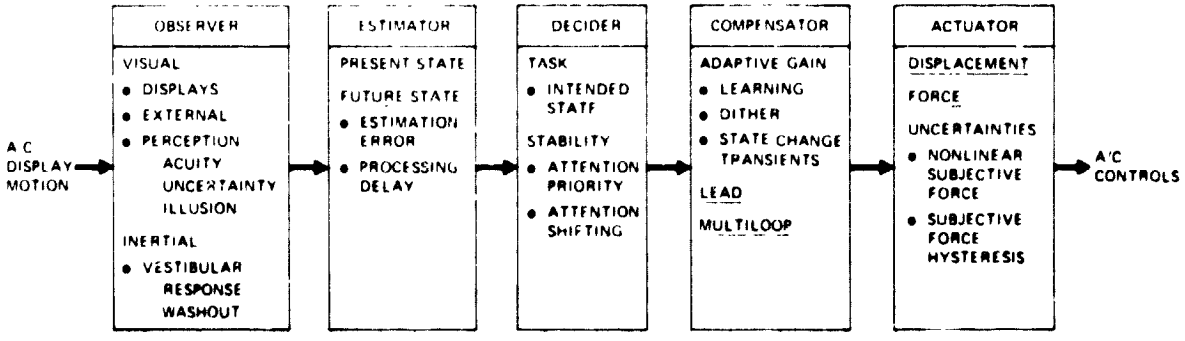

FIGURE 28. TOTAL PILOT MODEL

These five areas of observation, estimation, decision, compensation, and actuation all contribute significantly to the total pilot-aircraft interface. Since only the compensation block lends itself to linear analysis, describing function and optimal control approaches to pilot modeling have been mainly confined to this area. The other functions have been traditionally relegated to a lumped method of degrading the model performance to emulate deteriorated tracking scores through the injection of noise to the model's output. The Northrop time domain pilot model, on the other hand, allows all relevant nonlinearities and time dependent functions of the pilot to be directly represented. The further development of decision algorithms to model attention shifting behavior is currently being performed for several combinations of multi-axis dynamics. Estimation and observation include both the evaluation of

perception position and rate uncertainties and thresholds. Adaptive algorithms to represent the gain optimizing capability of the pilot are also under investigation.

CONCLUDING REMARKS

A comprehensive context for flying qualities prediction and evaluation has been evolved in order to achieve sufficient generality of both pilot and aircraft. Based on the methods of digital simulation, the central part of t[illegible] technology is the development of multi-axis time domain pilot models which include not only the features of dynamical compensation and human factors data relating to human observation and estimation, but decision and evaluation capability as well.

In order to validate the decision models for attitude stabilization in turbulence, analytical and experimental research was completed using fixed and moving base flight simulation of F-5 and YF-17 aircraft. The pilot-vehicle system model was adjusted by optimization either before, or independent from the corresponding flight simulation. In this way, the predictive capability of the method was demonstrated. The time domain statistics predicted by the model closely matc[illegible]d the experimental data including the episodic control shifting characteristics of the multi-axis human controller. Moreover, an important new aspect of multi-axis flying qualities, cross-task resonance, was identified and reproduced analytically.

As a result of this validation study, the importance as well as the practicality of the basic methodology has been demonstrated. General applications are now possible, and basic research into the decision models for piloted control tasks will include weapon delivery, loss of control at high angles of attack, approach and landing, and dynamic pilot-aircraft interface matching of the longitudinal with the lateral-directional dynamics of the aircraft.

REFERENCES

1. Onstott, E. D., and Salmon, E. P., Airplane Flying Qualities in Turbulence, AFFDL-TR-70-143 Air Force Flight Dynamics Laboratory, Wright-Patterson Air Force Base, Ohio, Feb. 1971.

2. Onstott, E. D. et al, Prediction and Evaluation of Flying Qualities in Turbulence, AFFDL-TR-71-162 Air Force Flight Dynamics Laboratory, Wright-Patterson Air Force Base, Ohio, Feb. 1972.

3. Onstott, E. D., Prediction and Evaluation of Flying Qualities in Turbulence, AFFDL-TR-72-92, Proceedings of the Eighth Annual Conference on Manual Control.

4. Onstott, E. D., Multi-Axis Pilot-Vehicle Dynamics, Proceedings of the Tenth Annual Conference on Manual Control, AFIT/AFFDL, April 1974.

5. Onstott, E. D., Validation of the Northrop Multi-Axis Pilot Model, Northrop Report NOR 75-61, March 1975.

TELLING A COMPUTER HOW A HUMAN HAS ALLOCATED HIS ATTENTION BETWEEN CONTROL AND MONITORING TASKS*

Kenneth D. Enstrom
John Deere and Company
Moline, Illinois 61265

William B. Rouse
University of Illinois
Urbana, Illinois 61801

SUMMARY

The computer's knowledge of how the human has allocated his attention is posed as an important issue in the design of human-computer systems where the two decision makers have overlapping responsibilities. It is argued that it is inappropriate to require the human to continually tell the computer how he has allocated his attention. Instead, a computer algorithm employing fading-memory system identification and linear discriminant analysis is proposed for real time detection of human shifts of attention in a control and monitoring situation. Experimental results are presented that validate the usefulness of the method.

INTRODUCTION

While many processes can be completely automated and thus, no longer require a human as part of the system, there is a large class of processes where only partial automation is possible and require that the human remain part of the system. Thus, a human-computer system is formed. One of the most important issues in the design of human-computer decision making systems is the allocation of decision making responsibility [1]. In many cases, where the human and computer have overlapping abilities, it seems desirable for them to have overlapping responsibilities [2]. Thus, allocation of decision making responsibility becomes situation dependent in that a particular task is assigned to the decision maker who, at the moment, has the time to allocate to the task in question. The main shortcoming of this approach is the possibility of conflicts in the sense that the two decision makers lose track of what each other is doing which results in their competing to perform tasks. Such competition can have disastrous effects on performance [3].

An intuitive solution to this problem is to have each decision maker tell each other of their actions. This may be reasonable from the computer's point of view, but such a dialogue might significantly increase the human's workload and subvert the main reason for utilizing the computer. Thus, we need some method for determining what the human is doing without continually asking him.

* Supported by the U. S. Air Force Systems Command under Contract F33615-73-C-1238.

This paper considers this problem in the context of a control and monitoring situation. As an example, in an aircraft, the pilot's control task is maintaining attitude, altitude, heading and speed while his monitoring task involves maintaining his knowledge of the state of his numerous subsystems (i.e., electric, hydraulic, etc.). Assuming a computer system was available for aiding the pilot in detecting and perhaps correcting changes in subsystem states, then the computer would require a knowledge of the pilot's perception of sub-system states. Otherwise, they might individually initiate actions that would jointly be counterproductive or perhaps disastrous.

We could easily develop other examples for various human-vehicle systems. However, we will jump immediately to the essence of the problem. The basic question is: How can the computer determine that the human has allocated to his monitoring task a portion of his attention in excess of what is needed merely to scan the monitoring situation?

This paper proposes a method for real time detection of how the human has allocated his attention. The method utilizes a fading-memory system identifier in conjunction with a linear discriminant function to detect changes in the dynamics of the control situation that indicate a shift in the human's allocation of attention in excess of what is expected with normal scanning. We will now proceed to discuss the method in detail and consider experimental results that validate the usefulness of the method. The interested reader can find more detail in Enstrom's thesis [4].

APPROACH

Considerable research has been devoted to the study of manual control systems and the identification of the human's dynamics (i.e., transfer function or state model) in control situations [5,6]. We require a method that can operate in real time on a digital computer and successfully identify time-variations in system parameters. A fading-memory least-squares identification algorithm was chosen.

The human plus controlled process were modeled as a discrete linear system using

$$X(k + 1) = \Phi X(k) + \Gamma U(K), \tag{1}$$

$$Z(k + 1) = H X(k + 1). \tag{2}$$

where X is an n state vector, U is a p input vector, Φ is an n X n state transition matrix, Γ is an n X p disturbance transition matrix, and H is an m x n matrix. Following Lee [7], these two equations may be transformed into a canonical form, and then, assuming a single-input, single-output system, into a difference equation of the following form.

$$Z(k) = \sum_{i=1}^{n} - a_i Z(k - i) + b_i U(k - i) \tag{3}$$

In matrix notation, this equation becomes

$$Z(k) = S(k - 1)'\phi \tag{4}$$

where $S(k - 1)' = [Z(k - n) \ldots Z(k - 1)\ U(k - n) \ldots U(k - 1)]$ and $\phi = [-a_n \ldots -a_1\ b_n \ldots b_1]$. By minimizing the squared model estimation error, the model parameter vector $\hat{\phi}$ is iteratively estimated using

$$\hat{\phi}(k + 1) = \hat{\phi}(k) + D(k)[Z(k + 1) - S(k)'\hat{\phi}(k)] \tag{5}$$

where

$$D(k) = P(k)\ S(k)[S(k)'P(k)\ S(k) + 1]^{-1} \tag{6}$$

$$P(k) = P(k - 1) - D(k - 1)\ S(k - 1)'\ P(k - 1) \tag{7}$$

Initially $\hat{\phi}(0) = 0$ while P(0) is usually set equal to an arbitrarily large disgonal matrix.

In order to assure unbiased estimates, the method requires that $\hat{\phi}$ be updated only after every n inputs, where n is the order of the difference equation model. (This avoids biases due to correlated residuals). A further modification reflecting this requirement produces the following set of equations.

$$\hat{\phi}[(k + 1)n] = \hat{\phi}\ (kn) + D(kn)[Z(kn + 1) - S(kn)'\ \hat{\phi}\ (kn)], \tag{8}$$

where

$$D(kn) = P(kn)\ S(kn)[S(kn)'\ P(kn)\ S(kn) + 1]^{-1}, \tag{9}$$

$$P(kn) = P[k(n - 1)] - D[k(n - 1)]\ S[k(n - 1)]'\ P[k(n - 1)]. \tag{10}$$

The application of these equations will identify single-input, single-output time invariant systems. However, the method must be modified if systems with time-varying parameters are to be identified.

A slight modification of derivations by Mendel [8] and Morrison [9] allows the identification error vector at time j, E(j), to be multiplied

by a weighting vector at time j, W(j), so that the new squared error term to be minimized is $[W(j)' E(j)]' [W(j)' E(j)]$. The vector W(j) is formulated from the relationship

$$W(j) = \left[\frac{1}{\rho \, W(j-1)}\right] \tag{11}$$

where ρ is always less than or equal to 1.0. By making ρ less than 1.0, recent errors have a greater influence than old errors in the formulation of new model parameters. Errors are forgotten as the weighting coefficients asymptotically approach zero. Applying these concepts, the final algorithm equations are

$$\hat{\phi}[(k+1)n] = \hat{\phi}(kn) + D(kn)[Z(kn+1) - S(kn)' \hat{\phi}(kn)], \tag{12}$$

where

$$D(kn) = P(kn)\, S(kn)[S(kn)' P(kn)\, S(kn) + \rho^{2n}]^{-1} \tag{13}$$

$$P(kn) = \frac{1}{\rho^{2n}}\left[P[k(n-1)] - D[k(n-1)]\, S[k(n-1)]' P[k(n-1)]\right]. \tag{14}$$

Throughout the remainder of this paper, the term ρ^{2n} will be referred to as the memory coefficient.

Given that we can adaptively identify the dynamics of the human plus controlled process, we need a method of determining when the dynamics reflect shifts of attention. The method chosen was linear discriminant analysis [10].

Assume that we have events that fall into two classes and that for each event j, we have m measurements denoted by y_{ij}, i = 1, 2, ..., m. Then the class to which a particular event belongs can be determined using

$$c_j = \alpha + \beta_1 y_{1j} + \beta_2 y_{2j} + \ldots + \beta_m y_{mj} \tag{15}$$

where $c_j = 1$ denotes membership in class 1 while $c_j = 2$ denotes membership in class 2. If we know the classes to which ℓ events belong, then the c_j, j = 1, 2, ..., ℓ are determined and β_i, i = 1, 2, ..., m can be determined if $\ell \geq m$.

First, the measurements are normalized using

$$\tilde{y}_{ij} = y_{ij} - \frac{1}{\ell_1 + \ell_2} \sum_{\delta=1}^{\ell} y_{i\delta} \tag{16}$$

$$\tilde{c}_j = c_j - \frac{1}{\ell_1 + \ell_2} \sum_{\delta=1}^{\ell} c_\delta \tag{17}$$

where ℓ_i is the number of events which belong to class i. Next a set of simultaneous linear equations are formed

$$\begin{bmatrix} \tilde{y}_{11} & \tilde{y}_{21} & \cdots & \tilde{y}_{m1} \\ \tilde{y}_{12} & \tilde{y}_{22} & & \\ \vdots & & & \\ \tilde{y}_{1\ell} & \cdots & & \tilde{y}_{m\ell} \end{bmatrix} \begin{bmatrix} \beta_1 \\ \beta_2 \\ \vdots \\ \beta_m \end{bmatrix} = \begin{bmatrix} \tilde{c}_1 \\ \tilde{c}_2 \\ \vdots \\ \tilde{c}_\ell \end{bmatrix} \tag{18}$$

or, more compactly,

$$\tilde{Y}\,\beta = \tilde{C} \,. \tag{19}$$

The least-squares solution is the familiar

$$\hat{\beta} = (\tilde{Y}'\,\tilde{Y})^{-1}\,\tilde{Y}'\,\tilde{C} \,. \tag{20}$$

Tatsuoka discusses issues such as whether or not two classes are significantly different and the determination of the probability of class membership. The interested reader is referred to reference 10.

The above identification/discrimination methodology is proposed for determining how the human has allocated his attention. The following discussion of experiments will detail the specifics of the method's implementation.

EXPERIMENTS

Three experiments were designed to test the proposed identification/discrimination method. While the first experiment tested the scheme's general ability to detect extreme changes in subject tracking dynamics, the

conditions of the second experiment were chosen to represent more realistic situations and test the method over a range of dynamic systems. The last experiment was closely controlled to provide data from a group of well-trained subjects.

An identical testing setup was used in all of the three experiments. A one-dimensional pursuit tracking task was displayed in the vertical direction on a CRT. (See Figure 1). The CRT was a Hewlett Packard model 1310A, with a screen size of 38.1 X 27.9 cm. A PDP-11 was coupled with a custom built graphics display unit to drive the CRT display. A two axis displacement joystick from Measurement Systems Inc. (model 521) provided the means for controller input. Later, when side tasks were added to the tracking task, the subjects' answers were entered via a keyboard unit from an Infoton Vistar II terminal. To simplify the operation of the keyboard, the unneeded keys were covered and the carriage return button, which was used to signal the completion of data entry, was extended for easy location. (See Figure 2.) All of the tracking tests were five minutes in length.

The displayed input symbol was a square of size 0.68 cm per side, and the output symbol was a cross of similar size. (See Figure 3.) The subject was instructed to move the joystick so as to match the cross's position as closely as possible to that of the moving square. The input path was generated by passing gaussian white noise through a second order filter. A sampled-data second order filter (Δt = 0.10 sec), with a gain of 1.0, natural frequency of 1.0 radian per second, and a damping ratio of 0.5 produced an input path (filter output) with a standard deviation of 447 screen units. The screen coordinates in the vertical direction were -2047 to + 2047. The same input path was used for all tests and the square's position was always updated at a rate of ten times per second.

The joystick range was plus and minus 30 degrees from the vertical position with the full range of the joystick matching the full range of the screen coordinates. The joystick gain was 68.2 screen units per degree; that is a one degree movement in the joystick resulted in an input change of 68.2 screen units. Two stable and two unstable control dynamics were selected for use in the experiments. (See Table 1.) The joystick was of negligible mass and was originally operated without spring resistance. The update frequency for the cross was 10 times per second for experiments one and two but was changed to 20 times per second for experiment three. Also, a light resistance spring was added to the joystick and controller gain was increased from 1.0 to 2.0 for experiment three.

In the first experiment, one subject was tested with two different controller dynamics. Both tests consisted of alternate periods of normal tracking and periods of no tracking, where the joystick location was kept stationary. In the first test, the subject used a type 2 controller (see Table 1), to track for 60 seconds intervals, with dead times between these periods of 10, 20, and 30 seconds. The second test was performed with a type 1 controller. After a 60 second period of continuous tracking, the remainder of the five minute trial consisted of alternate periods of 30 seconds tracking and 5 seconds of dead time.

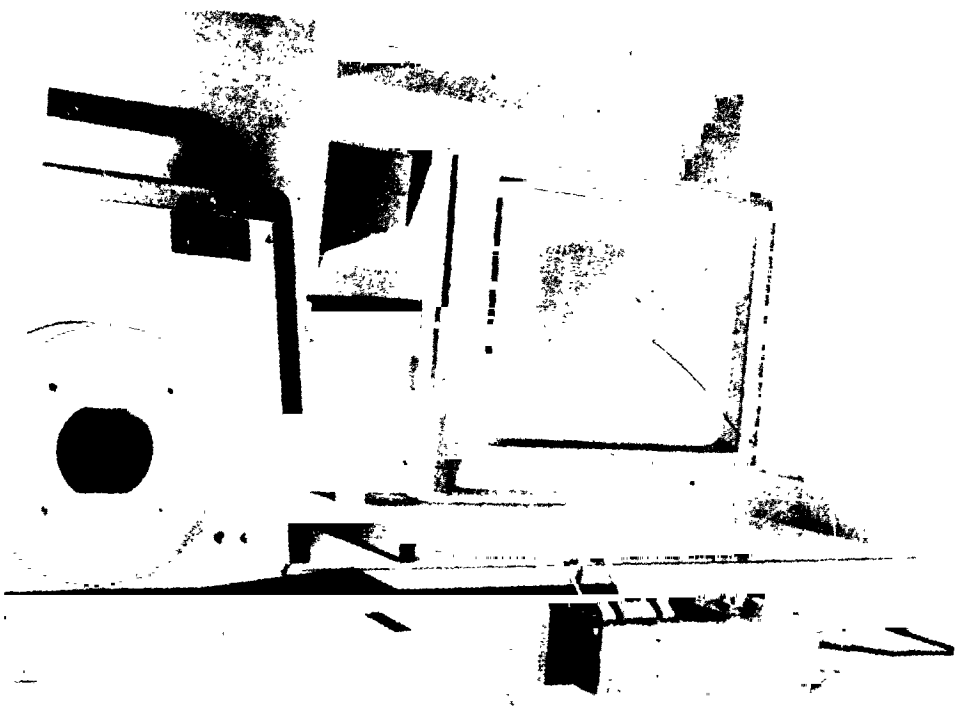

Figure 1. The experimental setup.

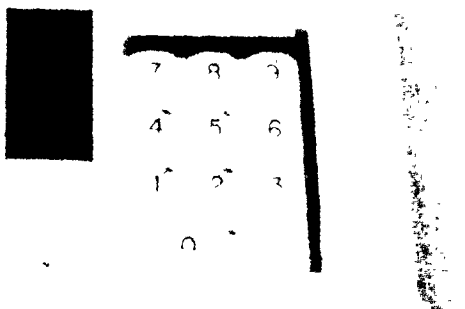

Figure 2. The keyboard used for arithmetic sidetasks.

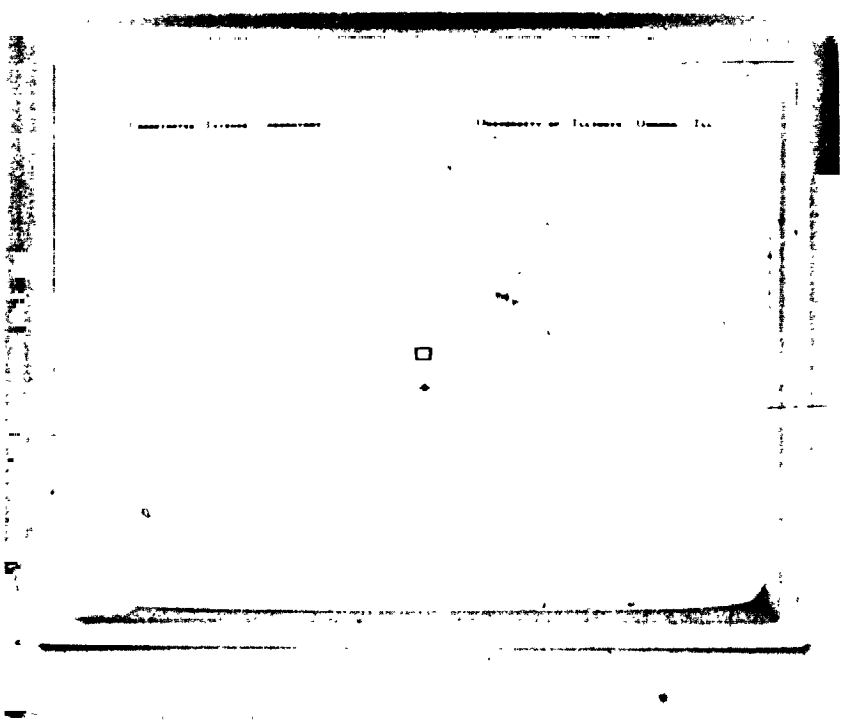

Figure 3. The tracking situation.

TABLE 1

INPUT CONTROL DYNAMICS

	System	Parameters	Sampling Period	Joystick
Type 1	$\frac{K}{(s/\omega_n)^2 + [(2\zeta s/\omega_n) + 1]}$	K=1 ω_n=7.8 ζ=.371	Δt=0.1	No Spring
Type 2	$\frac{K}{(s/\omega_n)^2 + [(2\zeta s/\omega_n) + 1]}$	K=1 ω_n=1.60 ζ=.371	Δt=0.1	No Spring
Type 3	$\frac{K}{s - 0.5}$	K = 1	Δt=0.1	No Spring
Type 4	$\frac{K}{s - 0.5}$	K = 2	Δt=0.05	Spring

After testing the identification scheme with these extremely large changes in subject control dynamics, a more realistic side task replaced the dead times. An arithmetic problem requiring the multiplication of two numbers was chosen as the secondary task. The subject's answer to the problem was entered on the specially designed keyboard (see Figure 2). To minimize the physical activity associated with the side tasks, the data entries were made without removing eye contact from the CRT screen. Each subject was trained on the keyboard to insure familiarity with its operation before any side task tests. All of the subjects tested were right handed and each controlled the joystick with his right hand and operated the keyboard with his left.

The side task was introduced to the subject by displaying it on the CRT tracking screen. (See Figure 4.) When the side task appeared, the subject had been instructed to compute the answer and enter it on the keyboard at a self-paced rate that would eliminate mistakes. The multiplication problem was displayed until the return key was hit, signalling completion of the data entry. To prevent unreasonably long reaction times or neglect of the main tracking task, subjects were scored on both RMS tracking error and the average reaction time to complete the real side tasks. Peer pressure due to the posting of results appeared to serve as ample subject motivation. To control the difficulty of the side tasks, each multiplication included a two digit number and a one digit number; forming a three digit product less than 250.

The scanning required to detect and interpret a side task would require a short attention shift before mathematical calculations were begun. To determine if the scanning effect resulted in significant changes in the control dynamics, "artificial" side tasks were also used. An artificial side task differed from a real side task by using a "K" rather than an "X" for the multiplication sign. (See Figure 5.) The artificial side tasks would still require visual scanning, but would not necessitate mental attention after the text was recognized as a false command. These tasks were automatically erased after being displayed for five seconds. Three actual side tasks were included in each five minute test - always at times 2, 3, and 4 minutes. Since the subjects of the third experiment were only exposed to two side task runs, it is unlikely that the timing of the tasks would have been anticipated by the subjects. Twelve artificial side tasks were randomly distributed throughout the five minute tracking period, with one restriction: artificial side tasks would always follow real side tasks by a sufficient amount of time to guarantee completion of the real task before the introduction of an artificial one. See Table 2 for a summary of the side task times, types and screen locations.

In the second experiment, two subjects were tested with three sets of control dynamics. For each dynamic type, both subjects were run with and without side tasks. The normal tracking task was run first to familiarize the subject with the system dynamics and allow him to devise a satisfactory operating strategy. Then, within a fifteen minute period, a second test was run with the same control dynamics and the predetermined side tasks. Side tasks with different arithmetic problems were used on successive tests.

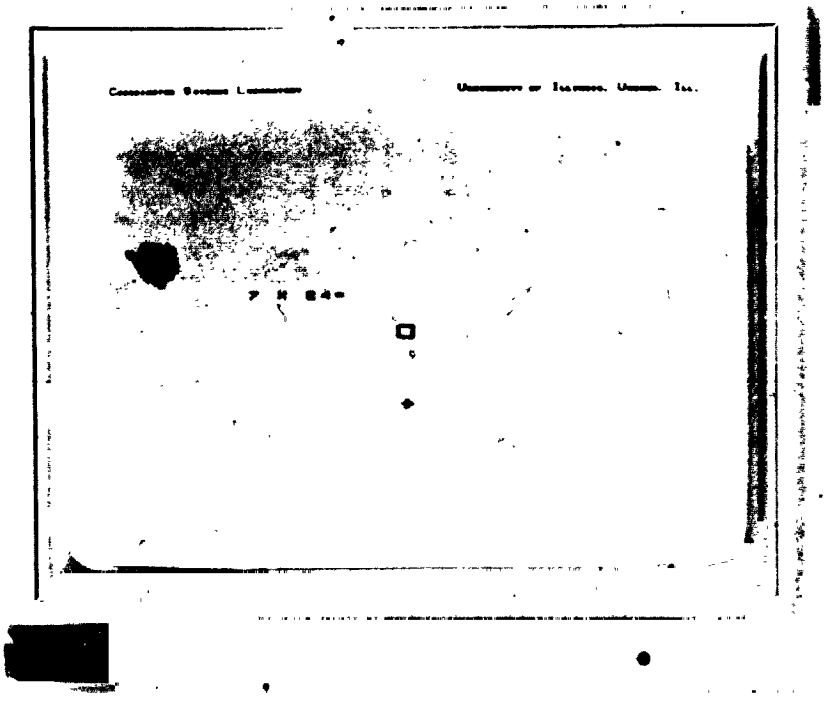

Figure 4. Tracking with a real sidetask.

Figure 5. Tracking with an artificial sidetask.

TABLE 2

SIDE TASK INFORMATION

		Number	Type	Position X	Position Y
5					
	4.720	15	K	2200	1500
	4.444	14	K	700	1800
4	4.000	13	X	3000	300
	3.860	12	K	3100	3500
	3.750	11	K	1200	700
	3.470	10	K	2300	2500
3	3.000	9	X	1000	2200
	2.720	8	K	100	1800
	2.500	7	K	3000	1500
2	2.000	6	X	2100	2800
	1.720	5	K	1000	1500
	1.250	4	K	3000	2000
1					
	0.805	3	K	50	50
	0.416	2	K	500	3000
	0.278	1	K	2200	500
0					

Four subjects were carefully trained on control type 4 for the last experiment. Four practice trials of straight tracking were spaced within a three day period. After the fourth trial, the subjects were tested again with side tasks. The initial reactions to the side tasks were more drastic than anticipated. Several side task errors occurred, while one subject lost control of the output cross, causing the coordinates of the cross to exceed the boundaries of the CRT display area. For this reason, these side task trials were duplicated on the following day with different arithmetic problems. Subject number three was run a third time, due to an error resulting in loss of tracking data.

RESULTS

The raw data collected from each experimental trial consisted of the input and output signals for the tracking tasks and, when side tasks were included in the trial, start and completion times for each task.

Results of the first experiment proved that the identification/discrimination method was capable of adapting to unrealistically large changes in the control system. The two data sets were analyzed using a second order difference equation model and a range of memory coefficients. Substantial changes occurred in the model's four parameters directly corresponding to the dead periods of joystick control. An identification memory coefficient of 0.96 produced model parameter changes that were easily detected by visual inspection of time plots of the parameter values. Since the conditions of this experiment were oversimplified, further analysis was not pursued.

The remaining discussion of side task detection will be divided into two areas. First, the parameters of the identification scheme (i.e., model order and memory coefficient) will be discussed. Then, the application of the linear discriminant function will be considered. The tracking and side task data from experiment two is the basis of these discussions. Finally, we will discuss the results when the data from the third experiment was processed according to the findings from experiment two.

The difference equation model order, which was arbitrarily set to two for experiment one, was studied by forming control models of orders one thru five for the six non-side task tracking data sets from experiment two. The outputs from these models were compared to the real output values to determine an RMS fitting error. The identification model memory coefficient was set to 1.0 for this analysis since side tasks were not used, producing fairly constant system parameters. As expected, the fitting error decreased with increasing model order. Trade-offs between accuracy and feasibility for use in real time applications resulted in a compromise selection of a second order model.

To adaptively identify time-varying system parameters, a memory coefficient less than 1.0 was required. As the coefficient was decreased,

changes in the system would affect this identification scheme quicker. However, noise and inaccuracies would also increase with smaller memory coefficients. Thus, a tradeoff was necessary between identification response time and the accuracy of the results. To determine a suitable memory coefficient, the RMS fitting error was determined for side task data runs from experiment two with memory coefficients of 1.00, 0.95, 0.90, 0.80, and 0.70. The fitting error decreased as the memory coefficient was reduced and then started to increase with a coefficient of 0.70. A value of 0.90 was selected since memory coefficients less than 0.90 produced eratic parameter values - even for non-side-task tracking periods.

Now that a second order model and a memory coefficient of 0.90 have been established, the use of discriminant analysis to detect control system changes will be discussed. A reasonable first choice of discriminant measures was the four parameters of the model, (i.e., the four coefficients of the second-order difference equation). If changes in these parameters were linearly related to side task attention shifts, the discriminant function would be able to detect the side task periods. Visual examination of the parameter vs. time plots indicated that absolute changes in the parameter values did not always correlate well with the side task times. A measure representing the relative changes of the parameters was proposed to correspond more consistently to the side task periods. A long term average of each parameter was calculated and, by comparing the current parameter value to the long term reference value, relative changes were measured. By summing the relative changes over short periods of time, four more discriminant measures were formed. A final measure was added to the group of eight properties by forming an average of the squared tracking errors.

Now we will consider the effects of some of the variables associated with the detection scheme. Such variables include the window size used in the formation of the long term parameter reference values, the relative measure window size, and the a priori probability associated with each classification type. Then, we will consider the scheme's ability to use a single set of sample class measurements to analyze trial data runs within subjects and across dynamics - and within dynamics and across subjects. The scheme's performance with fewer discriminant measures is also of interest.

We have not attempted to determine the optimal settings for the identification/discrimination scheme. Instead, our efforts were aimed at showing some overall trends and characteristics associated with the side task detection algorithm. In many cases when the effect of a single variable was analyzed, the effects of all other variables were assumed to be independent.

Long term reference window sizes of 10.0, 20.0, 25.0, and 30.0 seconds were considered. Fixing the probability of a side task event at 0.05 and a relative measure window size of 6.0 seconds, we found that a reference window size of 25.0 seconds was the only value that detected every side task, and resulted only in false alarms that could be related to artificial

side tasks.

Relative window sizes of 4.0, 6.0, 8.0, 12.0 and 20.0 seconds were considered. Although the results did not show any one window size to be consistently superior to the others, a window size of 8.0 seconds normally produced side task detections with a greater degree of certainty than the others.

The discriminant function requires an initial probability guess for the likelihood of an event being from one of the two classes. As the probability estimate of an event's occurrence is decreased, the discriminant function will predict a lesser number of events for that particular class. Data from experiment two was analyzed using probabilities of a side task event equal to 0.50, 0.10, 0.05, and 0.01. We found that a probability of 0.05 resulted only in false side task detections that were possibly related to an artificial side task, and the one real side task detection that was missed was also missed with values of 0.10 and 0.01.

Until this point, the discriminant function learning samples were formed from the same data file that was to be analyzed. Possibly the similarity among subjects and/or dynamics was great enough to permit the use of one set of discriminant function coefficients in the analysis of different experimental trials. Because experiment two used only two subjects, but three different controller dynamics, this data will be analyzed across the dynamics, but within each subject. Individual learning samples were summed together making one large learning file. The results of these tests are shown in Table 3. Overall, the detection algorithm did not work very well across the different dynamics used in this investigation. However, note that in both subject sets the controller type 2 run was identified far better than the rest. Possibly the discriminant function for this control system was near the average of all three.

Nine measures were used with the discriminant function to take full advantage of as many measures as seemed reasonable. The number of measurements required to make detections was considered by analyzing the same sets of data with a decreasing number of measures. In each reduction, the poorest remaining indicator was dropped. The average order of importance of the measures from experiment two were as follows:

Order of Importance	Measure Number	Description
1	7	Relative Change of Measure No. 3
2	6	Relative Change of Measure No. 2
3	3	Input Value 0.2 Seconds Ago
4	8	Relative Change of Measure No. 4
5	5	Relative Change of Measure No. 1
6	2	Out Value 0.2 Seconds Ago
7	4	Input Value 0.1 Seconds Ago
8	1	Output Value 0.1 Seconds Ago
9	9	Tracking Error Squared

TABLE 3

RESULTS OF USING SAME DISCRIMINANT FUNCTION
ACROSS DYNAMICS, WITHIN SUBJECTS

Subject Number	Controller Type	Number of 2 Second Intervals Detected During Side Task No.			Number of 2 Second Intervals Falsely Detected	
		1	2	3	Total	R.A.S.T.*
1	1	3	0	0	0	0
1	2	6	1	6	0	0
1	3	0	0	1	0	0
2	1	0	2	3	0	0
2	2	6	8	4	0	0
2	3	0	0	0	0	0

*Number related to artificial aide task

TABLE 4

EFFECT OF REDUCING THE NUMBER OF DISCRIMINANT FUNCTION PROPERTIES

Subject Number	1			1			1			2			2			2		
Controller Type	1			2			3			1			2			3		
Number of Properties	Number of Two Second Intervals Detected During Side Task Number																	
	1	2	3	1	2	3	1	2	3	1	2	3	1	2	3	1	2	3
9	6	2	0	6	4	8	4	4	5	4	8	3	4	7	5	8	0	5
8	0	0	0	3	1	4	4	5	5	5	8	3	5	6	5	9	0	4
7	0	0	0	3	1	4	4	5	5	4	8	2	5	6	5	9	0	4
6	0	0	0	3	1	4	3	4	3	5	8	2	5	6	5	8	1	4
5	0	0	0	4	0	4	4	4	3	4	8	2	5	6	4	8	1	3
4	0	0	0	5	0	2	0	0	3	4	8	2	5	6	3	3	0	3
3	0	0	0	5	0	1	3	0	3	8	7	0	1	2	1	-	-	-
2	0	0	0	0	0	0	3	0	3	8	6	0	0	2	1	-	-	-
1	0	0	0	0	0	0	3	0	3	8	6	0	0	2	0	-	-	-

Three important points should be noted about the order of the above property list. First, the relative measure of each property was always a better indicator than the absolute property measure. Note also that of the first five important properties, four of them were relative measures. Secondly, the error squared term which was initially thought to be a good indicator was the poorest. This result was not too surprising after reviewing the circumstances. The error is not only a function of the subject's output position, but also a function of the input position of which the subject has no control. The final point is that the most important variable was the relative change of the measure related to the input value of 0.2 seconds ago. Since the normal reaction time delay for a human controller is in this range, we might conjecture that the subject's time delay is affected during shifts of attention. The results of reducing the number of discriminant function measures appear in Table 4. Of the six data sets tested, four of them were still successfully processed using only five properties. Note that the other two data sets contained side tasks that were not detected with the total nine properties.

Now data from the third experiment will be analyzed using the algorithm parameters (i.e., model order, memory coefficient, window sizes, etc.) determined from the data of the second experiment. Summarizing these parameters, the final side task detection algorithm identified four parameters of a second order difference equation model using a fading-memory identification method with a memory coefficient of 0.90. The four model parameters plus a relative measure of each parameter's changes plus a tracking error squared measure were utilized by a linear discriminant function which was "trained" with sample data from each of the two classifications.

The general results of experiment three are shown in Table 5. Note that every real side task was detected, and all other side task predictions were possibly related to artificial side tasks. Thus, the results of experiment two appear to be applicable to at least some additional control systems with different subjects and different controller types.

The data from experiment three was also used to consider the side task detection algorithm's ability to process data across subjects within the same dynamics using a single learning classification sample group. These results appear in Table 6. The method seems to work reasonably well for different subjects using the same dynamics. Notice that only one real side task was not detected, and the only false detections were again related to artificial side tasks. This is somewhat surprising because, the four subjects did not have similar tracking skills - one was much better, while one was consistently poorer.

Finally, the algorithm's ability to operate in real time was examined. Using a DEC-10 computer, 3.917 cpu seconds were required to initialize variables and read in the raw tracking data from a five minute trial. The time required to form the eight measurements (the squared error term was not used), and make predictions with predetermined discriminant coefficients was 6.333 cpu seconds. Real time use appears to be highly supported, since only about ten cpu seconds were used to process a total of five

TABLE 5

GENERAL RESULTS OF EXPERIMENT 3

Subject Number	Controller Type	Number of 2 Second Intervals Detected During Side Task No.			Number of 2 Second Intervals Falsely Detected	
		1	2	3	Total	R.A.S.T*
3	4	6	5	6	0	0
4	4	6	4	10	2	2
5	4	6	4	3	2	2
6	4	5	11	8	0	0

*Number related to artificial side task

TABLE 6

RESULTS OF USING SAME DISCRIMINANT FUNCTION

FOR ALL SUBJECTS IN EXPERIMENT THREE

Subject Number	Controller Type	Number of 2 Second Intervals Detected During Side Task No.			Number of 2 Second Intervals Falsely Detected	
		1	2	3	Total	R.A.S.T*
3	4	6	3	5	3	3
4	4	4	0	9	0	0
5	4	6	4	2	3	3
6	4	5	7	5	0	0

*Number related to artificial side task

minutes of tracking data. Assuming a PDP-11 to be five to ten times slower than a DEC-10, a PDP-11 or other similar sized computer could also be used for real time application of the detection algorithm.

CONCLUSIONS

If a human and computer are to successfully interact in situations where they have overlapping responsibilities, they need to know what each other is doing. However, it is unreasonable to require the human to continually inform the computer of his actions. A method is needed for the computer to detect what the human is doing.

This paper has considered human-computer interaction in control and monitoring situations and proposed a method utilizing a fading-memory system identifier and linear discriminant analysis that allows real time prediction of how the human has allocated his attention between the control and monitoring tasks. Experimental results have validated the usefulness of the method.

To actually implement the method in, for example, an aircraft or spacecraft, further research is needed to develop heuristics for handling problems such as periods when the human completely stops tracking. Multi-class discriminant analysis and perhaps some nonlinear method might be appropriate to this problem.

The proposed method may also be useful as a research tool for those investigating motor skills or attention allocation. Such research would be of use in interpreting the outputs of multi-class discriminant analyses.

To conclude, we have posed what is a very real problem in the design of human-computer systems. Our solution, in the context of control and monitoring situations, appears feasible in a real time setting, but requires more development work before actual implementation.

REFERENCES

1. W. B. Rouse, "Design of Man-Computer Interfaces for On-Line Interactive Systems," Proceedings of the IEEE, Special Issue on Interactive Computer Systems, Vol. 63, No. 6, pp. 847-857, June 1975.

2. W. B. Rouse, "Adaptive Allocation of Decision Making Responsibilities Between Supervisor and Computer," Proceedings of the International Symposium on Monitoring Behavior and Supervisory Control, Berchtesgaden, Germany, March 1976.

3. W. B. Rouse, "Human Interaction with an Intelligent Computer in Multi-Task Situations," Proceedings of the Eleventh Annual Conference on Manual Control, NASA Ames Research Center, pp. 130-143, May 1975.

4. K. D. Enstrom, "Real-Time Adaptive Modeling of the Human Controller with Application to Man-Computer Interaction," MSIE Thesis, University of Illinois at Urbana-Champaign, 1976.

5. D. McRuer and D. H. Weir, "Theory of Manual Vehicular Controls," IEEE Transactions on Man-Machine Systems, Vol. MMS-10, No. 4, pp. 257-291, 1969.

6. T. B. Sheridan and W. R. Ferrell, Man Machine Systems, Cambridge, Mass.: MIT Press, 1974.

7. R. C. K. Lee, Optimal Estimation, Identification, and Control, Cambridge, Mass.: MIT Press, 1964.

8. J. M. Mendel, Discrete Techniques of Parameter Estimation, New York: Marcel Dekker, 1973.

9. N. Morrison, Introduction to Sequential Smoothing and Prediction, New York: McGraw-Hill, 1969.

10. M. M. Tatsuoka, Multivariate Analysis, New York: Wiley, 1971.

THE USE OF EVENT-RELATED-POTENTIALS IN THE ENHANCEMENT OF SYSTEM PERFORMANCE*

By Christopher Wickens, Jack Isreal, Gregory McCarthy, Daniel Gopher and Emanuel Donchin

Cognitive Psychophysiology Laboratory
Department of Psychology

and Aviation Research Laboratory

University of Illinois

ABSTRACT

Advancing computer technology has facilitated the implementation of on-line adaptive man-machine systems. In these systems, computer decisions based on information concerning the state of the operator can affect the nature of the man-machine interaction. Some limitations of performance measures as sources to provide information to the computer are presented, and it is argued that these limitations are particularly restrictive when the information concerns selective attention in a monitoring task, or the assessment of residual attention. It is suggested that psychophysiological measures such as the event related cortical potential (ERP) may be utilized to bypass these limitations. The characteristics of the ERP and experimental demonstrations of its sensitivity to attentional manipulations are described and a program of relevant research is then outlined. This includes a description of a pilot investigation of the relationship between the ERP to auditory probe stimuli and the workload demands of a two dimensional tracking task.

PSYCHOPHYSIOLOGICAL MEASURES IN THE ADAPTIVE MAN-MACHINE SYSTEM

The remarkable developments in mini- and micro-computers is transforming the design of man-machine systems. The computer industry is producing smaller, faster and more economical computers. It is, therefore, increasingly easier to incorporate computers as control components in man-machine systems with striking effects on the flexibility of the systems. Most notable is the increasing prevalence of adaptive systems. In these the computer can affect the nature of the man-machine interaction by implementing, dynamically, an optimizing algorithm. System behavior can be adjusted to the continually changing states of the operator, the environment and to the

*This research is sponsored by the Cybernetic Technology Office of ARPA monitored by ONR thru Contract number N-000-14-76-C-0002, (Principal Investigator, E. Donchin).

interaction between the two. This flexibility depends on an exchange of information between the operator and the machine. Within the framework of a computer based system it is possible to conceive of novel channels of communication to supplement conventional display and control interfaces. This report describes a program, which is one of several Biocybernetic programs supported by ARPA's Cybernetic Technology Office, which seeks to develop such a communication channel utilizing information which can be derived from brain-waves.

The environment for which we developed these channels is exemplified by the hypothetical high performance aircraft with on-board computer facilities represented in Figure 1. The conventional Display, Pilot, Control and Plant components are supplemented by various performance aids which can be implemented or adjusted on-line. These may consist of the addition or removal of predictive display information, an alteration of the Control or Plant dynamics along various axes or perhaps the assumption of control of certain tasks normally performed by the operator. In order that these adaptive decisions be made intelligently by the on-board aiding center, a managing computer or Decision Center shown in Figure 1 must be well informed. The information it requires includes obviously characteristics of the mission, the status of other aircraft, vehicular disturbances and ground controlled inputs. Additionally, it would be extremely useful to the Decision Center to have estimates of two important aspects of the operator's attentional state: what information he is processing or ignoring at any time (selective attention), and his overall level of workload or involvement with on-going tasks. Operator workload in this sense is often conceptualized as a variable that is reciprocally related to the amount of residual attention available to deal with unexpected environmental contingencies (1).

Various performance measures are traditionally used to index attention and workload. These have been found to provide adequate indices of both aspects of the attentional state. For example, in a multi-display selective attention task, the allocation of attention between sources of discrete stimuli has been revealed by response latency (2, 3) or accuracy (4). Attention allocation to continuous tasks has been successfully identified through changes in tracking gain (2, 4), information transmitted (4), time delay (5), holds in the tracking output (6, 7), remnant or observation noise (8, 9), or by more complex coefficients of a linear discrete time series model (10).

Operator workload or residual attention has often been measured by the "secondary task loading" technique (11). The operator is presumed to possess some limited quantity of processing resources which can be distributed among various tasks. As a primary task is made more difficult--its workload demand increased--a greater quantity of the limited resource is required to maintain criterion performance, and conversely a lesser amount remains to perform the secondary task. As a consequence, secondary task performance decreases, serving as an index of primary task difficulty. Such techniques have proven reliable in comparing different display or control configurations (12), or in validating subjective estimates of control task difficulty (13).

While performance measures do serve adequately as indices of selective attention, their use is necessarily restricted to tasks in which overt

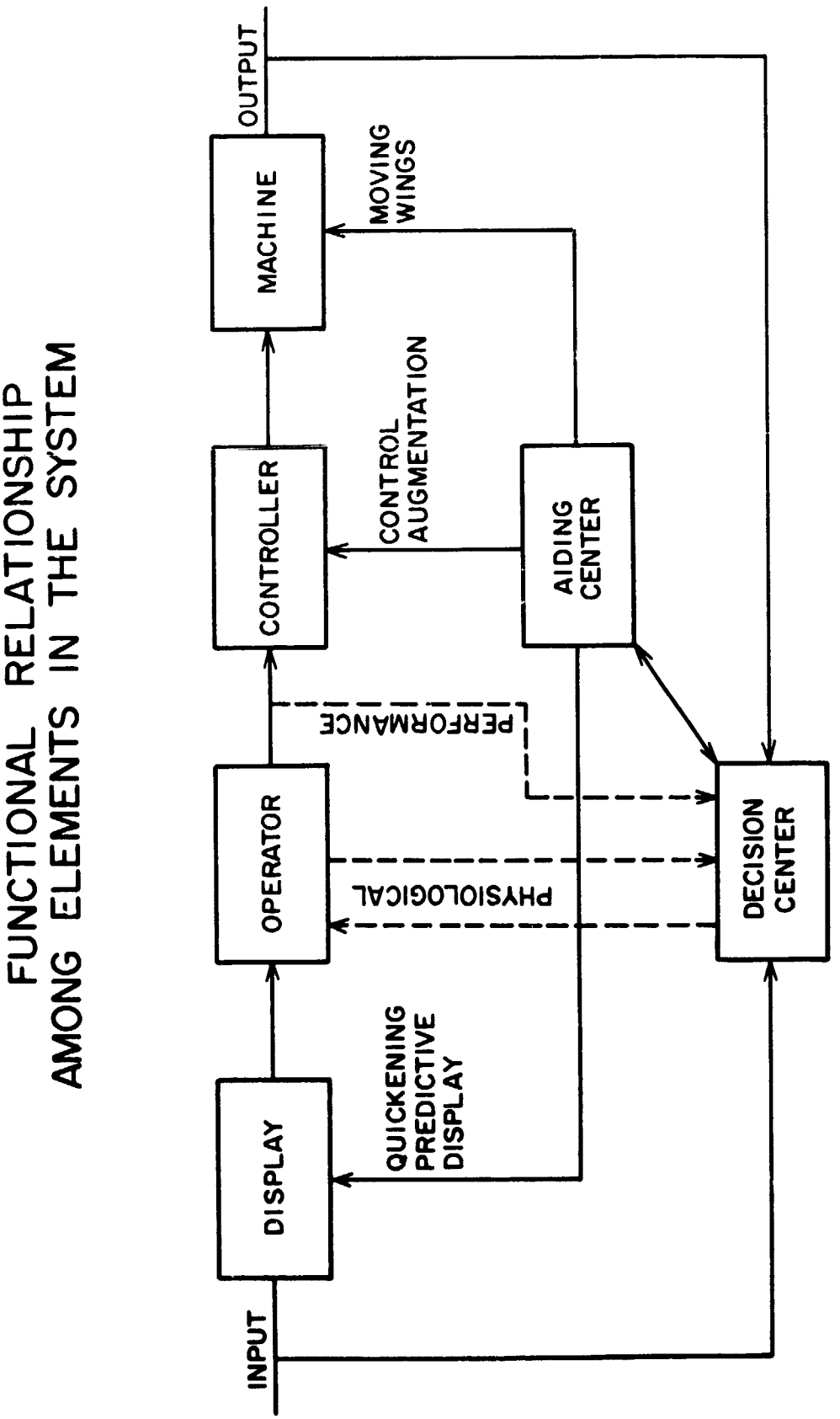
FUNCTIONAL RELATIONSHIP
AMONG ELEMENTS IN THE SYSTEM
OUTPUT
MACHINE
MOVING
WINGS
CONTROLLER
CONTROL
AUGMENTATION
AIDING
CENTER
PERFORMANCE
OPERATOR
PHYSIOLOGICAL
DECISION
CENTER
DISPLAY
QUICKENING
PREDICTIVE
DISPLAY
INPUT

Figure 1

responses are produced. Thus they are inappropriate for a class of tasks that are becoming critically important in modern system control: passive monitoring during which few overt responses are emitted by the operator. To assess the allocation of attention during a monitoring task, periodic probe events must be inserted in the environment and an overt (detection) response to the probes required. Such probes are of necessity disruptive to ongoing performance. The difficulties encountered by an on-line assessment of workload through secondary task loading are more severe. The secondary task performance may well disrupt performance on the primary task with possibly critical consequences. It may also "saturate" the residual attention that it was designed to assess.

Even in situations where the above restrictions are not encountered, (for example divided attention between two information transmission tasks), a further limitation upon the usefulness of performance measures is presented by the inherent response variability which precludes reliable estimates of attention-sensitive parameters from a single observation. Thus assessment of any or all of the performance measures described above must involve a number of behavioral observations taken over time, a requirement which further limits the usefulness of these measures in closing an on-line adaptive loop such as that shown in Figure 1.

The shortcomings of performance measures point to an urgent need for additional sources of information which can either supplement or, as in the monitoring and workload-measurement situations described above, replace the performance measures in providing information to the Decision Center. It is for this reason that we have initiated an investigation to determine if psychophysiological measures can serve as indices of human information processing characteristics. Psychophysiological measures have two important properties that counteract the drawbacks of performance variables pointed out above. (These advantages are, of course, purchased at the cost of increased complexity in measurement. The cost effectiveness of these procedures is a matter for future research and will not be discussed here.) It is reasonable to assume that the inherent random noise sources which perturb, or contribute to the variability of psychophysiological measures are relatively uncorrelated with the sources of performance variability. Assuming an independence of the noise sources, the information provided jointly by both signals in any given observation period should be of greater reliability than the information provided by either source alone. In other words the time required for a Decision Center to obtain an estimate of the subject's internal state at a given level of reliability will be reduced when estimates are based upon joint measures.

The second advantageous feature of psychophysiological measures is that, with proper instrumentation, they may be assessed in a manner that is less disruptive to ongoing performance than the monitoring "probes" or the secondary tasks discussed above. One example of the potential usefulness of such measures has been provided by another Biocybernetics project in which Beatty (14) has demonstrated the utility of pupil diameter as a measure of the operator's cognitive processing load. Our own efforts focus on the scalp recorded event-related-potential (ERP) as a source which may provide useful information concerning the operators cognitive state.

THE EVENT-RELATED-POTENTIAL

The ERP is a transient voltage change in the brain which is elicited by any discrete event, and which may be recorded by surface electrodes attached to the scalp. Superimposed on the ongoing EEG, the ERP extends for at least 500 msec. and is characterized by a series of distinct positive and negative-going peaks with characteristic latencies following the stimulus (15, 16). The amplitude of the different peaks appears to be sensitive to physical and informational characteristics of the stimulus. The multivariate nature of the ERP provided by the separate peaks reinforces its potential value in providing considerable information to an on-board computer.

Although normally the ERP to a single stimulus is masked by the ongoing EEG voltage, rendering it difficult to identify from a visual record, multitrial averaging techniques can serve to cancel the noise contribution and provide an estimated ERP associated with an event. Alternatively, and of critical importance for on-line assessment of behavior, a wide variety of techniques are being developed and implemented as a part of this project which will enable successful identification and classification of the characteristics of an ERP on a single trial (17, 18). Such techniques include frequency domain filtering of EEG activity, iterative time domain adjustment to reveal peaks (19) or application of linear discriminant analysis (20).

Although the success of ERPs as indicants of attention in a complex cockpit-like environment has not been established, there is nevertheless strong experimental evidence that components of the waveform are sensitive to attentional manipulations. Thus for example, Donchin and Cohen (21) have found that the amplitude of the late positive peak of the waveform (P300) reflects the allocation of attention to each of the elements in a two element visual display. This finding has been replicated in the auditory modality (22, 23). Earlier components of the waveform have also been found to be enhanced by focussed attention (24, 25). Clearly then, the evoked potential does reflect all-or-none discrete shifts in attention as defined by the relevance or non-relevance of an information source.

There is much less validation in the literature of the ability of the ERP measures to distinguish between levels of workload or attention on a continuous or graded basis in a manner which has been established with performance variables (e.g., 2, 5). In a study in which ERPs were recorded to stimuli in a two-channel signal detection task, LaFayette, Dinand and Gentil (26) were able to observe changes in the early positive and negative components of the ERP as the stimuli were made more or less relevant by instructional manipulations. In a second study, they found reliable changes in the early components of the ERP to detected tones as the workload of a secondary cognitive reasoning task was manipulated.

PRELIMINARY EXPERIMENTATION

We are currently investigating the capability of ERP measures to reflect the subject's information processing characteristics in an environment that simulates more closely the control and monitoring tasks confronted by the pilot. Our basic experimental approach is to record ERPs to probe auditory or visual stimuli. These probes are either irrelevant to the tasks performed (and may therefore be ignored by the subjects), or require only a minimum amount of cognitive processing, thus avoiding any disruption of primary task performance. In a selective attention/monitoring paradigm, the probe stimulus may occur along one of the relevant channels, displays or information sources to determine if the elicited ERP will reflect the extent to which that source is being processed. The stimulus attribute of the probe will however be different from the attributes of the channel that is relevant to the monitoring task. That is, if the subject is monitoring a visual channel for a spatially defined event, the probe will involve an intensity change. Alternatively, in a divided attention processing task, the ERP-eliciting stimuli can be the same stimuli as those that are processed and responded to in the performance of the tasks. Finally, in a workload manipulation paradigm, the probes are presented along channels that are totally irrelevant to the primary task performed, in order to determine if the elicited ERP's will reflect the residual attention available from that task as its workload is manipulated.

We have investigated ERP's and residual attention in a pilot experiment in which six subjects performed a two-dimensional pursuit tracking task with dynamics of the form

$$Y = \frac{K_1 + K_2 S}{S^2}$$

on both axes. Twelve 3-minute practice trials were first presented to bring the subjects to a stable level of performance via adaptive techniques with forcing function cutoff frequency employed as the adaptive variable.

ERP's were next recorded in two workload manipulation sessions. The probes consisted of a Bernoulli series of rare and frequent tones differing in pitch. The two sessions differed from each other according to whether the probe stimuli were ignored or processed. "Processing" involved maintaining an internal count of the number of rare stimuli that occurred during a trial (see Figure 2).

Within each session, workload was manipulated by two different methods (Figure 3). First, the forcing function bandwidth was increased and decreased by 30% from the asymptotic level, achieved by each subject in the adaptive practice session. This generated 3 different levels of objective task difficulty. Then, based upon the performance of each subject in the intermediate and high bandwidth conditions (moderate and large error respectively), two target diameters were selected, equal in value to the RMS error measured for each subject in those two conditions. A third, larger diameter was also selected of proportionately greater size. In this

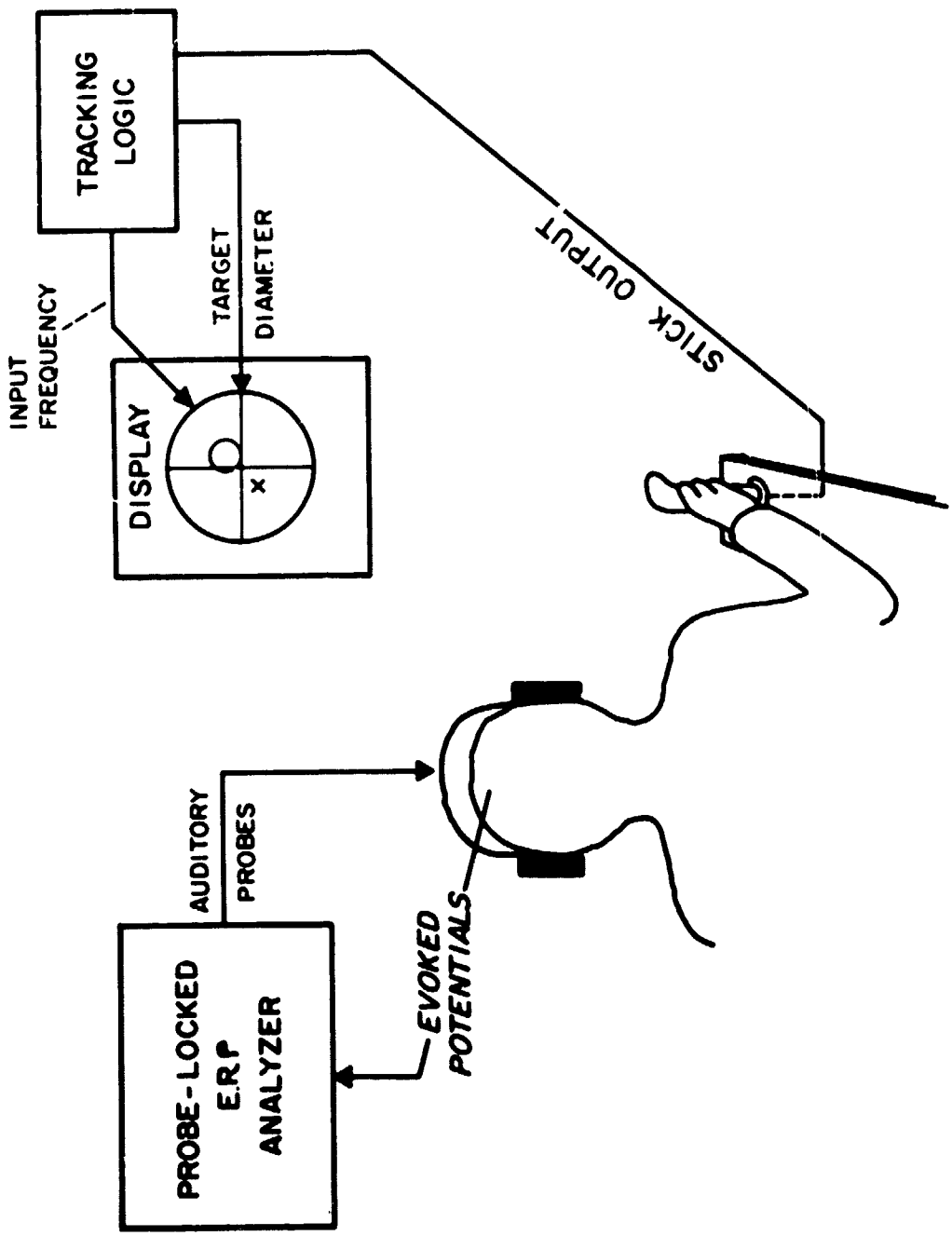
TRACKING LOGIC
INPUT FREQUENCY
TARGET DIAMETER
DISPLAY
STICK OUTPUT
AUDITORY PROBES
EVOKED POTENTIALS
PROBE-LOCKED E.R.P. ANALYZER

Figure 2

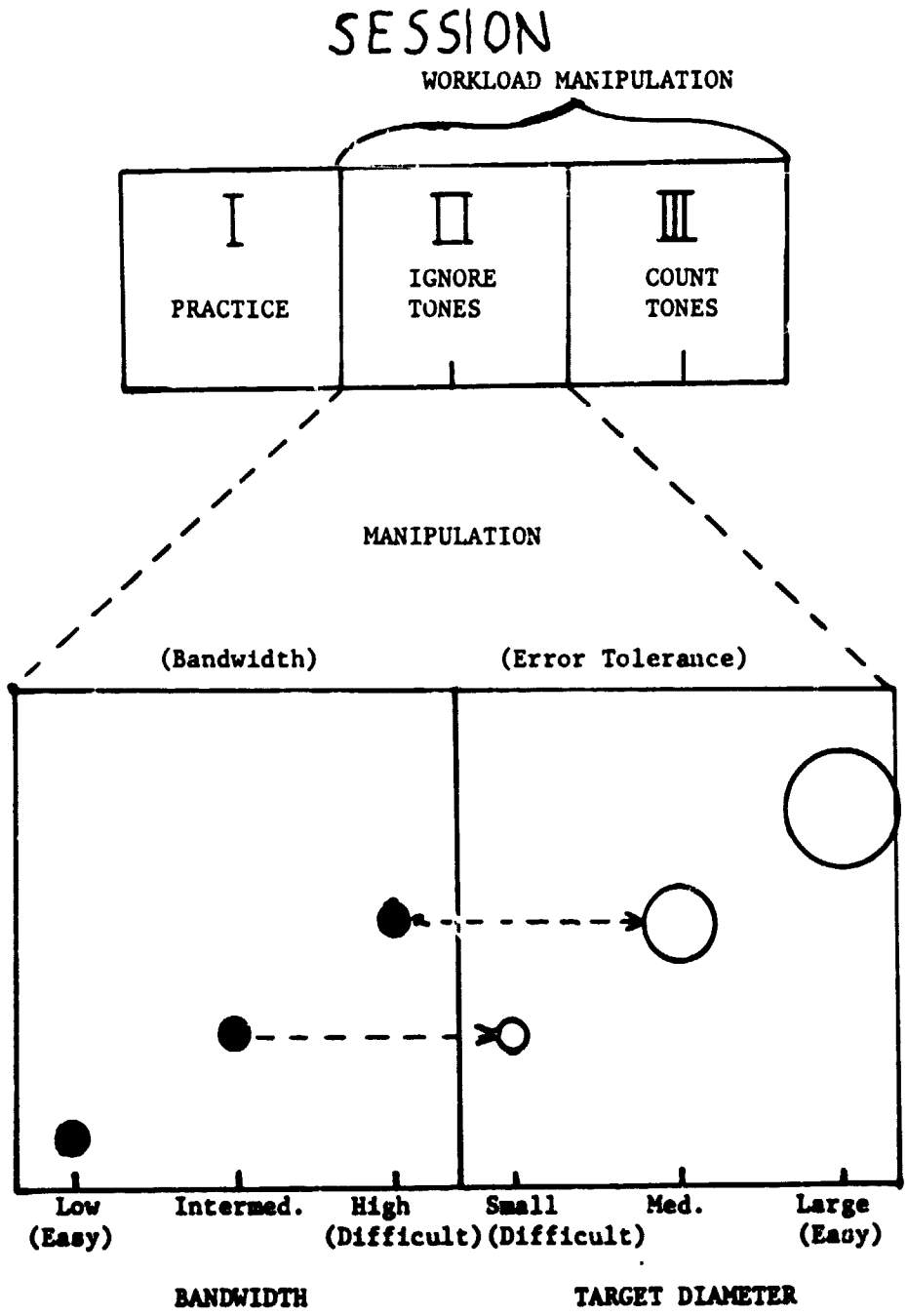

Figure 3
Experimental Design

manner the manipulation of target diameter, or required error tolerance was "calibrated" for each subject according to his sensitivity to the bandwidth manipulations, the object of this calibration being to obtain equivalent manipulations of subjective performance demands across all subjects. Tracking under the three target sizes was performed at the constant intermediate bandwidth level. It was therefore assumed that progressively more residual attention would be made available from the tracking task as the error tolerance (and obtained error) was increased.

The two particular workload manipulations employed may be placed in context by assuming that the attentional demands or subjective difficulty of a task is a joint function of its objective difficulty (e.g., task characteristics such as input bandwidth or dynamics), and the performance level required (in the present case, specified by the target diameter). What we have done then is to manipulate each of these dimensions of difficulty separately, while holding the other constant.

The logic of the tracking task, probe signal presentation and ERP recording was controlled by a PDP 11/40 computer (27). ERP's recorded from 3 electrode sites were amplified and were displayed on-line via a GT-44 graphics display terminal. The data was also recorded on digital tape for later off-line analysis and plotting by a Harris computer.

The preliminary data thus far collected has indicated that stable ERP waveforms can in fact be elicited by probes under the high levels of primary task workload required in the experiment. At this writing the data are being analyzed and it is already clear that there is a substantial degree of individual differences in the shape and temporal characteristics of the waveforms. These may well be related to different strategies that subjects adopt in performing their assigned tasks, and these strategies will be investigated through future analysis of the tracking data in the time and frequency domain. It appears however that there is some consistency within the waveforms of a given subject. In this case the between-subject variability presents no serious difficulty and may well prove useful in assessing individual differences in performance. In a sense, calibrating an ERP analyzer to the physiological response characteristics of an individual operator imposes no greater engineering demands than custom designing the helmet or flight suit to his anthropometric characteristics.

At this point, the state of our research is too preliminary to draw firm conclusions concerning the effects of attentional manipulations upon the event-related-potentials. However, given the projected importance of nondisruptive measures, and the established sensitivity of such measures to certain attentional variations in the laboratory, we are sufficiently encouraged to pursue the direction of experimentation outlined above.

REFERENCES

1. Kahneman, D. Attention and Effort. New York: Prentice Hall, 1973.

2. Gopher, D., & Wickens, C. Strategies and attention allocation in dual-task performance. Proceedings 11th Annual Conference on Manual

Control. NASA TMX-62, 464. Washington, D.C.: U.S. Government Printing Office, 1976.

3. Ephrath, A. Detection of system failures in multi-axis tasks. Proceedings 11th Annual Conference on Manual Control. NASA TMX-62, 464. Washington, D.C.: U.S. Government Printing Office, 1976.

4. Baty, D. L. Human transinformation rates during one-to-four axis tracking. Proceedings 7th Annual Conference on Manual Control. NASA, SP-281. Washington, D.C.: U.S. Government Printing Office, 1972.

5. Jex, H. Two applications of a critical-instability task to secondary work load research. IEEE Transactions on Human Factors in Electronics, 1967, HFE-8, 279-282.

6. Onstott, C. D. Task interference in multi-axis aircraft stabilization. Proceedings 12th Annual Conference on Manual Control. Urbana, Illinois, May, 1976.

7. Cliffe, R. C. The effects of attention sharing in a dynamic dual-task environment. Proceedings 7th Annual Conference on Manual Control. NASA SP-281. Washington, D.C.: U.S. Government Printing Office, 1972.

8. Levison, W. H., Elkind, J. I., & Ward, S. L. Studies of Multivariate Manual Control Systems: A Model for Task Interference (NASA CR-1746) Bolt Beranek & Newman, May 1971.

9. Wickens, C. D. The effects of divided attention on information processing in manual tracking. Journal of Experimental Psychology: Human Perception and Performance, 1976, 2, 1-13.

10. Engstrom, K. D., & Rouse, W. B. Telling a computer how a human has allocated his attention between control and monitoring tasks. Proceedings 12th Annual Conference on Manual Control. Urbana, Illinois, May, 1976.

11. Rolfe, J. M. The secondary task as a measure of mental load. In W. T. Singleton, R. S. Easterby, and D. E. Whitfield (Eds.), Measurement of Man at Work. London: Taylor & Francis, 1971.

12. Krauss, E. F., & Roscoe, S. N. Reorganization of airplane manual control flight dynamics. In W. B. Knowles, M. S. Sanders & F. A. Muckler (Eds.), Proceedings 16th Annual Meeting of the Human Factors Society. Santa Monica, California: October, 1972.

13. Clement, W., McRuer, D., & Klein, R. Application of New Pilot Workload Measure to Manual Control Display Design. System Technology, Inc. Paper No. 133, April 1973.

14. Beatty, J. Pupilometric measurement of cognitive workload in complex man/machine systems. Proceedings 12th Annual Conference on Manual Control. Urbana, Illinois, May 1976.

15. Donchin, E. Brain electrical correlates of pattern recognition. In G. F. Inbar (Ed.), Signal Analysis and Pattern Recognition in Biomedical Engineering. New York: John Wiley, 1975. Pp. 199-218.

16. Regan, D. Evoked Potentials in Psychology, Sensory Physiology and Clinical Medicine. London: Chapman and Hall, Ltd., 1972.

17. Donchin, E., & Herning, R. I. A simulation study of the efficacy of stepwise discriminant analysis in the detection and comparison of event related potentials. Electroencephalography and Clinical Neurophysiology, 1975, 38, 51-68.

18. Squires, K. C., & Donchin, E. Beyond averaging: The use of discriminant functions to recognize event related potentials elicited by single auditory stimuli. Electroencephalography and Clinical Neurophysiology, 1976, In press.

19. Woody, C. D. Characterization of an adaptive filter for the analysis of variable latency neuro-electric signals. Medical and Biological Engineering, 1967, 5, 539-553.

20. Donchin, E. Discriminant analysis in averaged evoked response studies: The study of single trial data. Electroencephalography and Clinical Neurophysiology, 1969, 27, 311-314.

21. Donchin, E., & Cohen, L. Average evoked potentials and intramodality selective attention. Electroencephalography and Clinical Neurophysiology, 1967, 22, 537-546.

22. Smith, D. B., Donchin, E., Cohen, L., & Starr, A. Auditory averaged evoked potentials in man during selective binaural listening. Electroencephalography and Clinical Neurophysiology, 1970, 28, 146-152.

23. Squires, K., Donchin, E., McCarthy, G., & Herning, R. On the influence of task relevance and stimulus probability on ERP components. Electroencephalography and Clinical Neurophysiology, 1976, In press.

24. Schwent, V., & Hillyard, S. A. Auditory evoked potentials during multi-channel selective listening role of pitch and localization cues. Electroencephalography and Clinical Neurophysiology, 1975, 38, 131-138.

25. Wilkinson, R. T., & Lee, M. V. Auditory evoked potentials and selective attention. Electroencephalography and Clinical Neurophysiology, 1972, 33, 411-418.

26. LaFayette, Dinand & Gentil. Average evoked potentials in relation to attitude, mental load, and intelligence. In W. T. Singleton, R. S. Easterby, and D. E. Whitfield (Eds.), Measurement of Man at Work. London: Taylor & Francis, 1971.

27. Donchin, E., & Heffley, E. Minicomputers in the signal-averaging laboratory. American Psychologist, 1975, 30, 299-312.

PUPILLOMETRIC MEASUREMENT OF COGNITIVE WORKLOAD

By Jackson Beatty

Department of Psychology
University of California at Los Angeles

SUMMARY

The momentary workload that is imposed by a cognitive task upon the limited capacity human information-processing system appears to be accurately reflected in the momentary level of central nervous system activation. The utility of pupillometric methods of workload assessment is evaluated and several lines of experimental evidence relating activation and cognitive function are reviewed.

INTRODUCTION

Information processing tasks differ in the extent and duration of the demands that they place upon the limited capacity of the human nervous system to handle information. For most tasks, processing demands are not constant, but vary from moment to moment in response to changes in the functional organization of the task. These demands may be thought to represent the cognitive workload associated with the task, a time-varying function of the demand for limited resources.

Given the assumption that cognitive capacity is fixed (reference 1), the momentary demands of any single processing function for capacity may be estimated by determining the amount of residual capacity that may be allocated to another processing task that is assigned a secondary priority (reference 2). Secondary-task measurement of cognitive workload is of major importance in the study of both cognitive capacity and the resource demands of particular processes, but both technical (reference 2) and theoretical (reference 3) difficulties preclude the utilization of secondary-task procedures in many situations. For this reason the more convenient method of subjective estimation of cognitive workload is still commonly employed (reference 4) despite serious questions as to both the reliability and validity of such rating procedures.

A third approach to the problem of measuring momentary cognitive workload stems from the observation that momentary workload is directly reflected in the mo-

mentary level of central nervous system (CNS) activation (references 5 and 6). Of the various indicators of activation, pupillometric measurement techniques (references 7, 8 and 9) appear to be most sensitive and reliable (reference 10).

The present paper examines several lines of evidence suggesting that pupillometric measures of activation serve as a reliable indicator of cognitive workload in perception, memory, decision and complex problem solving. An extension of this experimental method to the study of problems of workload optimization in complex man/machine systems is then considered.

PERCEPTUAL PROCESSES

Perceptual processes appear to proceed quite effortlessly and place rather little demand upon the limited capacity of the human information-processing system (5). Thus Wickens (reference 11) was unable to observe a secondary task decrement when a sensory signal-detection task was imposed as the primary task in an experiment investigating the distribution of processing capacity. The workload involved in the detection of weak signals is quite small.

In this context, it is of interest to note that small but reliable pupillary dilations accompany the detection of both visual and acoustic signals at near-threshold intensities. Hakerem and Sutton (reference 12) examined the pupillary movements that accompany the perception of weak visual stimuli and were able to show a dilation for signals that were detected which was absent for signals that were missed. More recently Beatty and Wagoner (reference 13) provided a pupillometric analysis of activation in the detection of weak acoustic signals using a rating-scale response procedure (see reference 14). Using unmarked observation intervals, no pupillary dilations were observed in the absence of a signal regardless of the outcome of the observer's decision. In the presence of a signal, a dilation of the pupil appeared in the interval between signal delivery and response cue onset. The magnitude of this dilation varied monotonically with the observer's rated probability that a signal had been presented.

These data raise the interesting possibility that pupillometric methods may provide a more sensitive measure of cognitive load than do conventional secondary-task measurement techniques. Thus the small pupillary dilations observed during perceptual processing may be indexing brain workload levels that are not of sufficient magnitude to be detected by secondary task interference methods.

DECISION PROCESSES

Even simple decision processes appear to impose some workload on the cognitive system as indicated by pupillometric measures of activation. For example, Simpson and Hale (reference 15) measured pupillary diameter in two groups of subjects who were required to move a lever to one of four positions. In the decision group, subjects were told at the beginning of each trial that either of two directions was permissible (e.g., front or left). Seven seconds later a response cue was presented and the subject initiated one of the two movements. In the no-decision control group, subjects were instructed exactly as to the desired movement on each trial (e.g., front). Pupillary dilation in the post-instruction pre-response period was larger and more prolonged for those subjects who had to choose between two movements before responding.

Substantially larger pupillary dilations are observed to accompany more difficult decision processes. In an experiment reported by Kahneman and Beatty (reference 16), listeners were required to determine whether a comparison tone was of higher or lower pitch than the standard. Clear pupillary dilation occurred in the 4-second decision period between presentation of the comparison tone and the response cue. The amplitude of this dilation varied as a direct function of decision difficulty, the difference in frequency between the standard (850 Hz) and comparison tones. This relation is shown in figure 1, which presents both the amplitude of dilation in the decision period and the percent decision errors as a function of the frequency of the comparison tone. These dilations were highly reliable and did not habituate over the experimental session. Pupillary dilations during decision appear to vary as a function of cognitive workload, as inferred from task parameters and performance data.

MEMORY PROCESSES

The idea that human information-processing capacity is limited arose directly from the study of the limitations of human short-term or working memory (reference 17). Our capacity for unrelated items is on the order of seven or eight, with some adjustment being made for the difficulty of the to-be-remembered units. If pupillary movements reflect CNS activation shifts as a function of cognitive workload, then these relations should be clearly revealed in the pupillometric investigation of memory processes.

Kahneman and Beatty (reference 18) provided a demonstration that the momen-

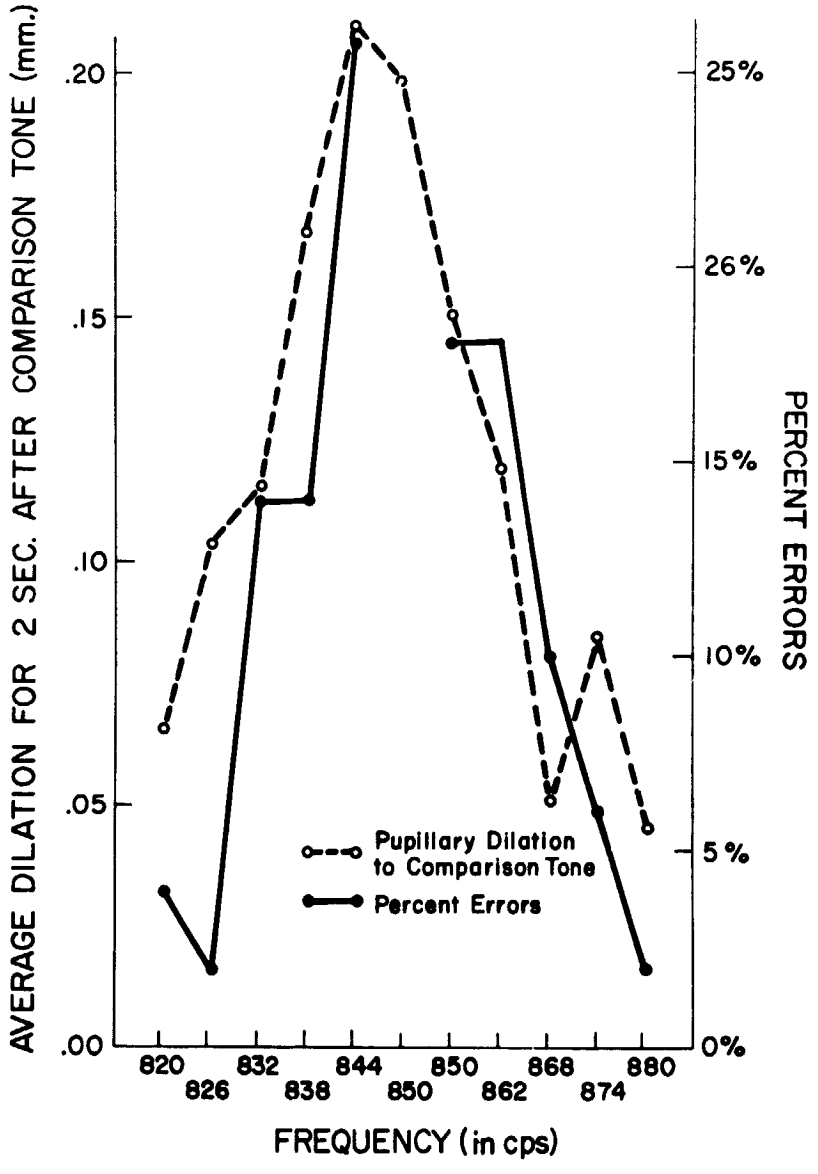

Figure 1. Average pupillary dilation during the decision period and percent errors as a function of the frequency of the comparison tone. The frequency of the standard was 850 cps. (From Kahneman & Beatty, 1967)

tary load placed upon the cognitive system by a memory task is reflected in pupillary diameter. In a series of experiments on short-term serial memory using paced recall, students were required to listen to strings of from one to seven items and, after a 2 second pause, repeat the string at the rate of one item per second. For strings of digits, pupillary diameter increased as each item of the input string was heard and decreased as each item of the output string was spoken. Thus pupillary diameter at the pause between input and output varied as a monotonic function of the number of items held in memory. These pupillary functions are shown in figure 2A.

Workload in a memory task depends not only upon the number of items to be remembered, but also upon the difficulty of each of the items themselves. Thus, as fewer unrelated words may be reliably recalled than unrelated digits, the load imposed by each word upon the cognitive system is presumed to be greater. Figure 2B presents the results of a serial memory experiment involving strings of four digits or four words. For the simple recall conditions, it is apparent that the slope of the pupillary function is greater for the more difficult word strings than for the easier digit strings. That these pupillary response functions are sensitive to processing parameters is evident from the large dilations observed under the condition labelled "transformation," in which the subject was required to respond to the string of 4 digits with another string obtained by adding 1 to each digit of the input string. This transformation task is the most difficult of all memory tasks studied, as indicated by the error data, and it consistently was accompanied by larger pupillary movements indicating CNS activation.

Behavioral data supporting the contention that the demands upon limited information-processing capacity increase during the rising phase of the pupillary response function as items are entered into working memory and decrease during the falling phase of that function as items are successively recalled from memory, is provided by an experiment in which residual capacity was measured using secondary-task measurement. Kahneman, Beatty, and Pollack (reference 19) reported that the pattern of interference with a secondary perceptual-detection task exactly paralleled the pupillary-activation curve obtained for the serial memory transformation task alone. For serial memory tasks, changes in cognitive workload appear to be reflected in the momentary level of CNS activation, as indexed by pupillometric measurement.

COMPLEX PROBLEM SOLVING

Pupillary dilations accompanying complex problem solving appear to be related directly to the difficulty of such processing, although behavioral assessments of workload have not yet appeared for these types of cognitive tasks. For example, Hess

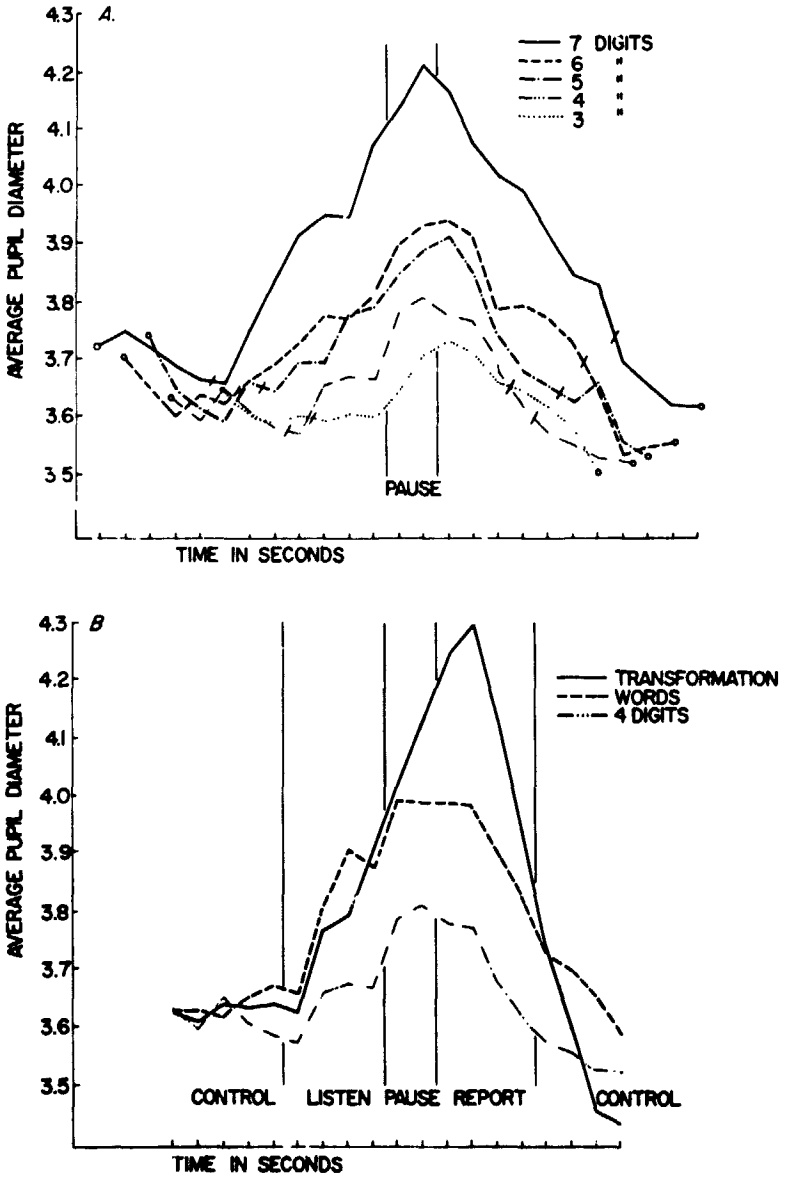

Figure 2. **Upper graph: Average pupillary diameter during presentation and recall of strings of 3 to 7 digits, superimposed about the two second pause between presentation and recall. Slashes indicate the beginning and the end of the memory task. Lower graph: Pupillary diameter during presentation and recall of four digits, words and a digit transformation task.** (From Kahneman & Beatty, 1966)

and Polt (8) examined pupillary movements as multiplication problems were solved mentally. Pupillary diameter increased during the period preceding solution, and the magnitude of dilation was related to presumed problem difficulty. Payne, Parry, and Harasymiw (reference 20) also report a monotonic relation between mean pupillary diameter and problem difficulty, but note that this relationship is markedly nonlinear with respect to difficulty scales based upon percent correct solution, time to solution or subjective rating of difficulty. Pupillary diameter in mental multiplication appears to peak rapidly as a function of difficulty, with more difficult problems requiring more time until solution is reached. This suggests that cognitive capacity is quite fully taxed in complex mental arithmetic problems so that the workload per unit time remains relatively constant as problem difficulty is increased over moderate levels. but that the total time to solution is increased.

Other types of complex problem solving tasks show similar relationships between pupillary dilation and problem difficulty. For example, Bradshaw (reference 21) has reported that larger pupillary dilations accompany the solving of more difficult anagrams, and that these dilations are maintained until solution is reached.

IMPLICATIONS FOR WORKLOAD EVALUATION IN MAN/MACHINE SYSTEMS

Traditional interference and subjective-rating methods of workload evaluation have been employed in the design of complex man/machine interfaces, but neither is without its own particular limitations. Pupillometric methods of workload estimation provide a third alternative that in certain situations might be preferable to either of the more traditional measurements.

One problem for which pupillometric assessment procedures appear to be well-suited is that of display evaluation. Pupillometric methods permit reliable measurement of the small cognitive workloads associated with the processing of sensory information that may not be detectable by interference methods. One project underway in our laboratories examines the effects of display readability on the pupillary dilations accompanying information acquisition. A second experiment is concerned with pupillometrically measuring cognitive workload involved in processing computer-generated speech at various levels of intelligibility.

The most intriguing possibility is that the measurement of central nervous system activation associated with cognitive function might provide a common metric for the comparison of workload in tasks that differ substantially in their functional characteristics. Underlying this possibility is the idea that CNS activation is the limited general resource that is allocated among cognitive processes demanding capacity. If this is the case, then it may be possible to directly compare perceptual, memory,

symbol manipulation and response processes in terms of activation requirements. At present, however, we may only conclude that the pupillometric measures of activation are useful in measuring cognitive load for a range of cognitive processes. No evidence concerning the comparability of measurements made across diverse processes has yet appeared.

REFERENCES

1. Broadbent, D. E.: Perception and Communication. London: Pergamon Press, 1958.
2. Kerr, B.: Processing Demands During Mental Operations. Memory & Cognition, 1973, 1, 401-412.
3. Norman, D. A.; and Bobrow, D. G.: On Data-limited and Resource-limited Processes. Cognitive Psychology, 1975, 7, 44-64.
4. McCormick, E. J.: Human Factors Engineering. (3rd ed.). New York: McGraw-Hill, 1970.
5. Kahneman, D.: Attention and Effort. Englewood Cliffs, New Jersey: Prentice-Hall, 1973.
6. Pribram, K. H.; and McGuinness, D.: Arousal, Activation, and Effort in the Control of Attention. Psychological Review, 1975, 82, 116-149.
7. Loewenfeld, I. E.: Mechanisms of Reflex Dilations of the Pupil, Historical and Experimental Analysis. Documenta Ophthalmologica, 1958, 12, 185-448.
8. Hess, E. H.; and Polt, J. H.: Pupil Size in Relation to Mental Activity During Simple Problem Solving. Science, 1964, 143, 1190-1192.
9. Goldwater, B. C.: Psychological Significance of Pupillary Movements. Psychological Bulletin, 1972, 77, 340-355.
10. Kahneman, D.; Tursky, B.; Shapiro, D.; and Crider, A.: Pupillary, Heart Rate and Skin Resistance Changes During a Mental Task. Journal of Experimental Psychology, 1969, 79, 164-167.
11. Wickens, C. D.: The Effect of Time Sharing on the Performance of Information Processing Tasks: A Feedback Control Analysis. Technical Report No. 51. Human Performance Center, The University of Michigan, 1974.
12. Hakerem, G.; and Sutton, S.: Pupillary Response at Visual Threshold. Nature, 1966, 212, 485.
13. Beatty, J.; and Wagoner, B. L.: Pupillary Measurement of Sensory and Decision Processes in an Acoustic Signal-detection Task. Paper presented at the meeting of the Psychonomic Society, Denver, Colorado, 1975.
14. Green, D. M.; and Swets, J. A.: Signal Detection Theory and Psychophysics. New York: Wiley, 1966.
15. Simpson, H. M.; and Hale, S. M.: Pupillary Changes During a Decision-Making Task. Perceptual and Motor Skills, 1969, 29, 495-498.
16. Kahneman, D.; and Beatty, J.: Pupillary Responses in a Pitch Discrimination Task. Perception and Psychophysics, 1967, 2, 101-105.

17. Miller, G. A.: The Magical Number Seven, Plus or Minus Two. Psychological Review, 1956, 63, 81-97.
18. Kahneman, D.; and Beatty, J.: Pupil Diameter and Load on Memory. Science, 1966, 154, 1583-1585.
19. Kahneman, D.; Beatty, J.; and Pollack, E.: Perceptual Deficit During a Mental Task. Science, 1967, 157, 218-219.
20. Payne, D. T.; Parry, M. E.; and Harasymiw, S. J.: Percentage of Pupillary Dilation as a Measure of Item Difficulty. Perception and Psychophysics, 1968, 4, 139-143.
21. Bradshaw, J. L.: Pupil Size and Problem Solving. Quarterly Journal of Experimental Psychology, 1968, 20, 116-122.

SESSION III

DISPLAYS AND CONTROLS

Chairman: R. W. Allen

LEFT-BRAIN/RIGHT-BRAIN AND SYMBOLIC/ANALOGIC HUMAN OPERATOR OUTPUT COMPATIBILITY

by William L. Verplank

Massachusetts Institute of Technology

SUMMARY

This paper introduces the terms symbolic (e.g., buttons, keyboards) and analogic (e.g., joysticks, light pens) to describe the range of devices for interaction between human operator (h.o.) and computer. With increasing automation, there is a tendency for man-machine communication to become increasingly symbolic. There is a danger that the interface will constrain both the communication and the thinking of the human operator. To remain natural and flexible most systems should allow for simultaneous access over a range from symbolic to analogic. This duality is suggestive of long-recognized duality in human thought and some recent evidence from split-brain patients.

COMPUTER-AIDED MANIPULATION

The structure and capability of any h.o.-computer system is strongly constrained by the form of the h.o.-machine interface. I considered that interface as the first concern in designing a system for supervisory control of remote manipulation [1]. The supervisory control concept was first suggested by Ferrell [2], and Ferrell and Sheridan [3], as a means for overcoming the difficulty of remote manipulation with transmission delay. (See figure 1.)

The Subroutine Approach

The particular form of supervisory control considered was that of providing the manipulator with the capability of an increasing repertoire of subroutines or subtasks. For example, John Hill's "ARM" program at Stanford Research Institute [4] has a "GROPE" subroutine that lowers the jaw around a block using a touch sensor on each finger (figure 2). This subroutine would be part of a larger task, such as collecting blocks. Some parts of the task would be under human- others under computer-control. These can be organized in a task hierarchy as shown in figure 3. Barber [5] wrote a special language for supervisory control. One of the difficulties, however, was that commands could only be given through the teletype. Programming simple motions was time-consuming and laborious.

This is an informal paper presented at:
12th Annual Conference on Manual Control
University of Illinois, 25-27 May, 1976.

Command Hardware

If the h.o. is to communicate arm positions directly, the most appropriate form of command might be "master-slave"-like control with a brace or replica. On the other hand, there may be occasion for the h.o. to indicate a direction, and the computer to modify the path, to avoid obstacles or simply to stop when it touches something. This seems the most elementary form of supervisory control, and would be quite useful with degraded or delayed feedback from a remote manipulator. The brace seems less appropriate at this level, for one thing, because there can no longer be always a one-to-one correspondence between the master and slave which requires re-setting the correspondence every time control is transferred from computer to h.o. At this level, some form of joystick providing rate-control seems more appropriate. G. Starr [6] is doing a detailed study of rate control; supervisory control is a potential application.

At a higher level, any frequently used subroutine could be called by the h.o. pushing a button or flipping a switch (e.g., "STOP IF YOU TOUCH", or "GROPE"). Strings of subroutines, or new programs would be more appropriately input through a special purpose or standard keyboard. Voice seems an appropriate command mode also, especially because it can be combined with others; for example, "SLOW" might lower the gains on a rate control; "EASY" might adjust the servo to produce compliance; "CAREFUL" might increase the sensitivity of touch or proximity sensors.

Symbolic and Analogic

One way to describe this range of command modes is as running from analogic (brace, joystick) to symbolic (button, keyboard, voice) along a continuum of abstraction. It seems important to provide a range of command modes in order that the system be accessible at different levels, possibly at two levels simultaneously. For example: "move in this direction" (ANALOGIC), "but stop if you touch something" (SYMBOLIC).

This division of control or command hardware into symbolic and analogic suggests the parallel between computer-aided manipulation (C.A.M.) and computer-aided design (C.A.D.) (figure 4). In both cases it seems most appropriate to use both symbolic and analogic controls perhaps simultaneously.

VISUAL THINKING

My teaching experience in the Design Division at Stanford University has made me more aware of the importance of this distinction between symbolic and analogic modes and their relationship to thinking. Robert McKim [7] has developed a drawing and design course that focuses on rapid visualization (freehand sketching) and the process of design. The philosophy of the course (and what makes it so popular) is that productive thinking of all sorts requires fluency in not only analytical, verbal modes (on which most education is

focused) but also in the sensory, visual modes (in which our education is severely lacking).

What is visual thinking? To give you an experience in what visual thinking is, here is a problem to solve from McKim's book:

> "Painted Cube: Shut your eyes. Think of a wooden cube such as a child's block. It is painted. Now imagine that you take two parallel and vertical cuts through the cube, dividing it into equal thirds. Now take two additional vertical cuts, at 90° to the first ones, dividing the cube into equal ninths. Finally, take two parallel and horizontal cuts through the cube, dividing it into 27 cubes. Now, how many of these small cubes are painted on three sides? On two sides? On one side? How many cubes are unpainted?"

Most people report quite clear use of some form of visual imagery in counting the cubes. A symbolic, mathematical approach would be cumbersome and inappropriate. One of the unique features of the Visual Thinking course is "experiential exercises for the mind's eye". Mental manipulation of mind's-eye imagery improves with practice.

Two Modes of Thinking

There has long been a distinction made between ways of thinking and great lists can be made of the dichotomies that seem to correlate. My own list is given in figure 5. Of importance to problem solving, what has been referred to as "creative" thinking is the ability to move freely from one mode to the other. The "creative insight" often comes through visual or sensory imagery. There are numerous accounts of this process, the most recent is by T.H. Krueger [8].

Split-Brain Studies

Recent clinical evidence on split-brain human patients (with hemispheres separated to relieve epilepsy) has revived interest in the differing roles of the right and left sides of the brain [9,10,11]. The left hemisphere (which controls the right hand) is usually dominant and controls speech. The right brain is associated more with sensory and spatial thinking. Whether or not the dichotomy strictly holds (both hemispheres have some language ability; vision occurs on both sides), the notion of a dual brain is a powerful metaphor for reminding us that there are distinctly different modes of knowing and thinking.

ANALOGIC PART PROGRAMMING

David Gossard, at M.I.T., has recently applied this notion of the

symbolic and analogic modes to preparing programs for numerically controlled machine tools [12]. Conventionally, a highly trained programmer prepares a program in a symbolic language (e.g., APT) directly from the drawings of the part (figure 6a). This program is compiled to produce an ideal tool-path (cutter location or C/L data) which must be verified. A post-processor computes the commands necessary to making the particular machine tool follow that path. Gossard's system (figure 6b) uses computer graphics with a picture of the work-piece, tool and clamps. The programmer uses knobs (analogic) and keyboard (symbolic) to move the tool through the appropriate paths. The computer can record and play back, straighten out, or interpret symbolically (e.g., circle) paths put in anaologically by the operator. The computer then outputs the C/L data directly.

Gossard's experience with both part programmers and machinists untrained in part-programming points up the advantages of using computer inputs compatible with thinking modes. In three hours the machinists were able to produce part programs equivalent to what they would have needed three months' training to write. Even the trained programmers preferred the analogic mode. One of the unexpected advantages commented on by the users was the ability to instantly see and to avoid problems of interference between tool and clamps. The programming of complicated spatial motions and relationships is a process that clearly benefits from the ability to use both analogic and symbolic command modes.

CONCLUSION

With increasing automation, there is a tendency for man-machine communication to become increasingly symbolic. This is natural and efficient since complete processes can be commanded by simple names or labels. There is, however, the danger that the interface will constrain the thinking of the human operator to symbolic modes. The human operator also has special abilities in visual-spatial thinking. To allow both modes of thinking, the man-machine interface should provide for simultaneous access over a range of control from symbolic to analogic.

REFERENCES

1. Verplank, W.L.: Symbolic and Analogic Command Hardware for Computer-Aided Manipulation. M.S. Thesis, Massachusetts Institute of Technology, 1967.

2. Ferrell, W.R.: Remote Manipulation with Transmission Delay. Ph.D. Thesis, Massachusetts Institute of Technology, 1964.

3. Ferrell, W.R. and Sheridan, T.B.: Supervisory Control of Remote Manipulation, NEREM Record, IEEE Catalogue No. F-70, 1966 (also in: IEEE Spectrum, Vol. 4, No. 10, pp.81-88, October 1967).

4. Hill, J.W. and Sword, A.J.: "Study to Design and Develop Improved Remote Manipulator Systems, NASA Contractor Report CR 2238, Stanford Research Institute, April 1973.

5. Barber, D.J.: MANTRAN: A Symbolic Language for Supervisory Control of an Intelligent Remote Manipulator. M.S. Thesis, Massachusetts Institute of Technology, 1966.

6. Starr, G.: A Comparison of Master-Slave and Rate Control in the Presence of a Transmission Time Delay. 12th Annual Conference on Manual Control, 1976.

7. McKim, R.H.: Experiences in Visual Thinking. Belmont, California, Wadsworth Publishing Co., 1972.

8. Krueger, T.H.: Visual Imagery in Problem Solving and Scientific Creativity. Connecticut, Seal Press, 1976.

9. Gazziniga, M.S.: The Split Brain in Man, Scientific American, Vol. 217, No. 2, pp.24-29 (August 1967) (reprinted in [11]).

10. Bogen, J.E.: The Other Side of the Brain: An Appositional Mind, Bulletin of the Los Angeles Neurological Societies, Vol. 34, No. 3, pp.135-167, July 1969 (reprinted in [11]).

11. Ornstein, R.E. (Ed.): The Nature of Consciousness. San Francisco, W.H. Freeman and Co., 1973.

12. Gossard, D.C.: Analogic Part Programming with Interactive Graphics. Ph.D. Thesis, Massachusetts Institute of Technology, 1975.

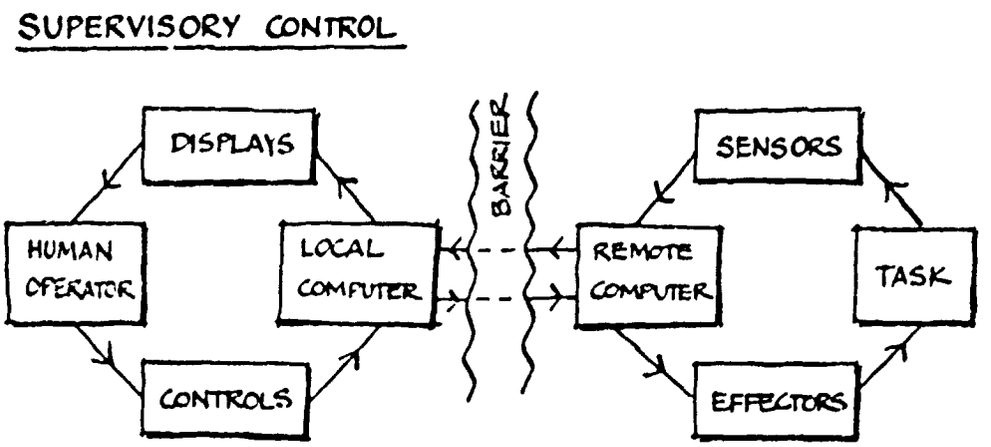

Figure 1. The supervisory control concept for remote manipulation was introduced by Ferrell and Sheridan [2,3].

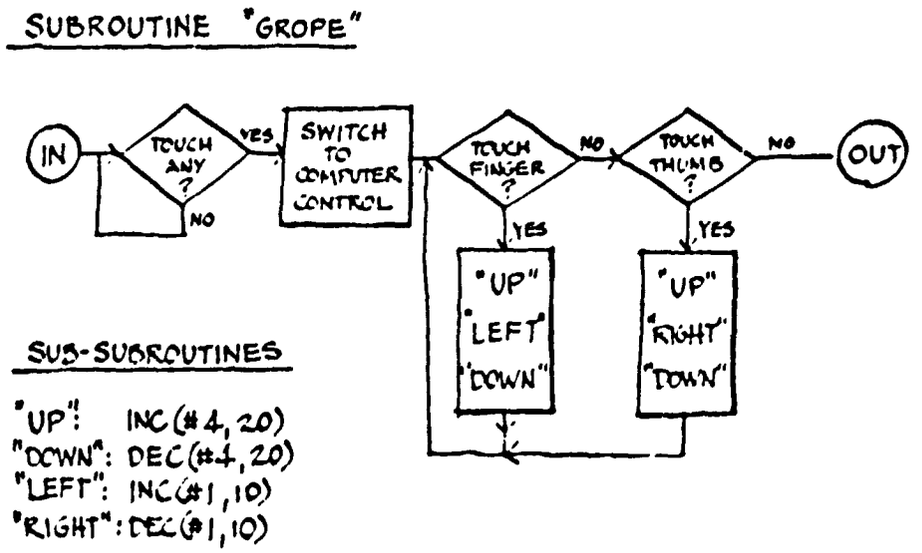

Figure 2. Subroutine "GROPE" uses touch sensors on finger and thumb to center and lower the jaw around an object.

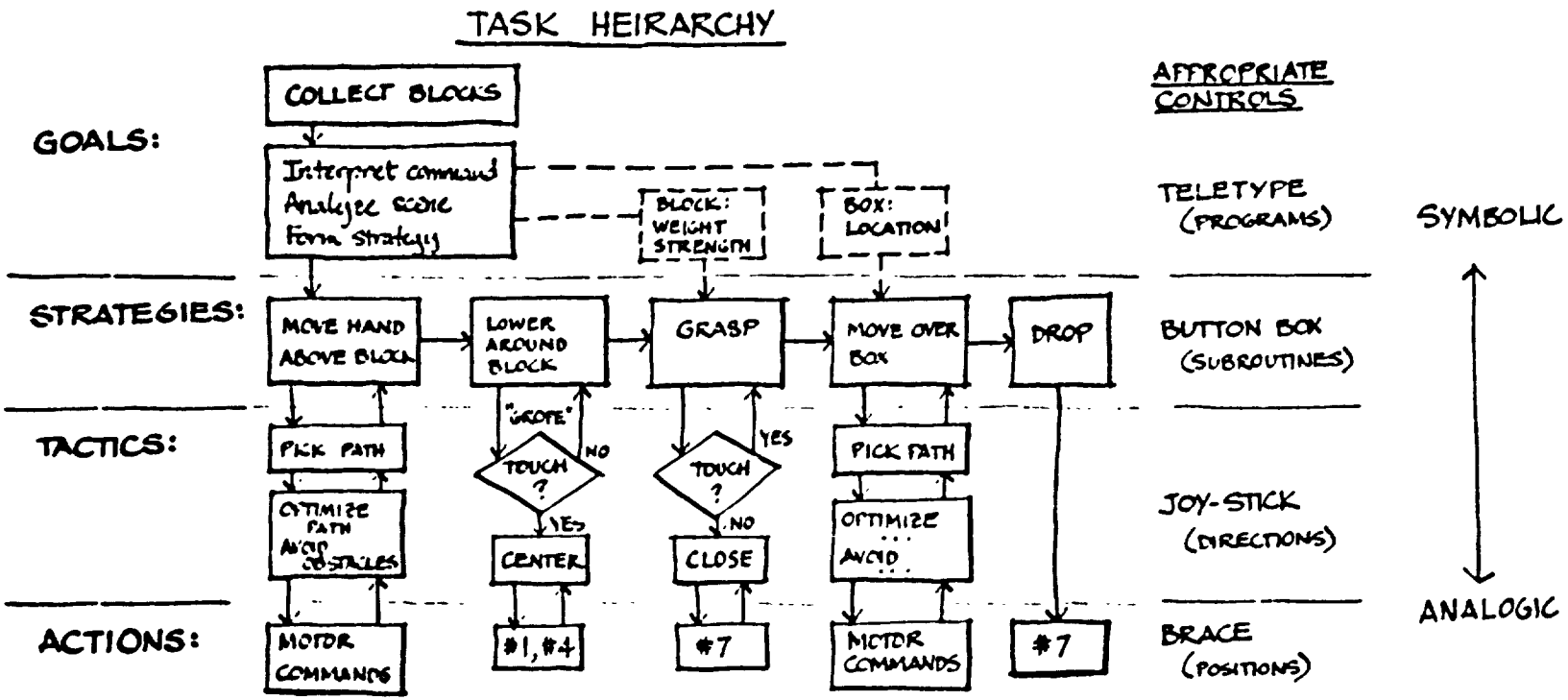

Figure 3. A task hierarchy for picking up blocks shows the interaction of h.o. and computer on a variety of levels. The command hardware appropriate at different levels is shown on the right.

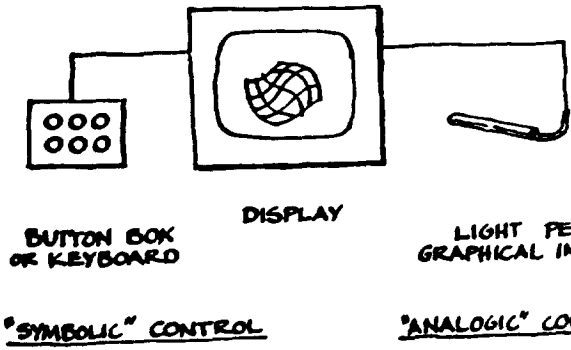

4a. Command Structure for Computer-aided Design (C.A.D.)

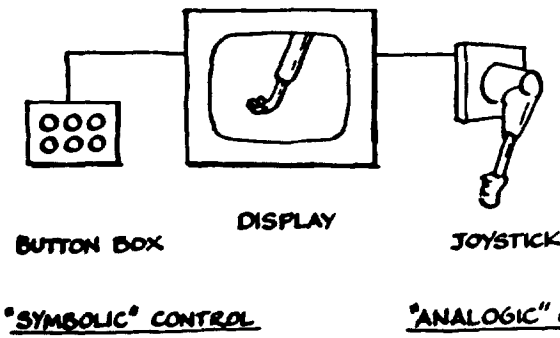

4b. Proposed Command Hardware for Computer-aided Manipulation (C.A.M.)

Figure 4. Comparison of C.A.D. and C.A.M.

RIGHT BRAIN	LEFT BRAIN
ANALOGIC	SYMBOLIC
VISUAL	VERBAL
CONCRETE	ABSTRACT
SYNTHETIC	ANALYTICAL
ARTISTIC	SCIENTIFIC
GEOMETRICAL	LOGICAL
UNCONSCIOUS	CONSCIOUS
INTUITIVE	RATIONAL
METAPHORICAL	LITERAL
APPOSITIONAL	PROPOSITIONAL
SINISTER	ADROIT
LEFT HAND	RIGHT HAND

Figure 5. The dichotomies of thinking modes are associated with each other and the hemispheres of the brain.

Figure 6a. Conventional part programming for numerically controlled (N/C) machine tools requires a part programmer trained in a highly symbolic computer language.

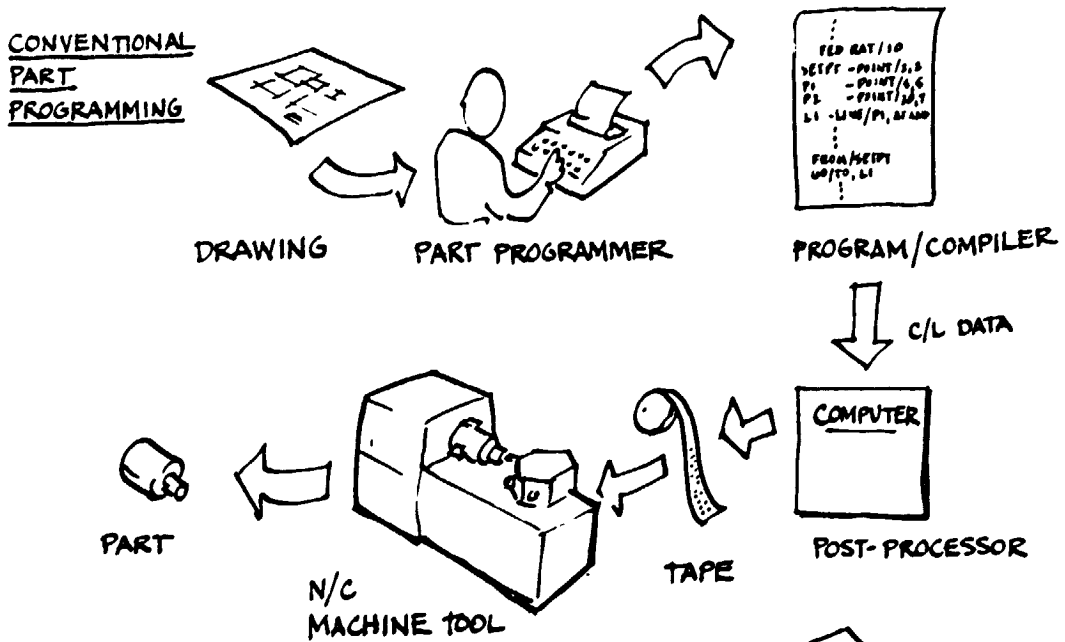

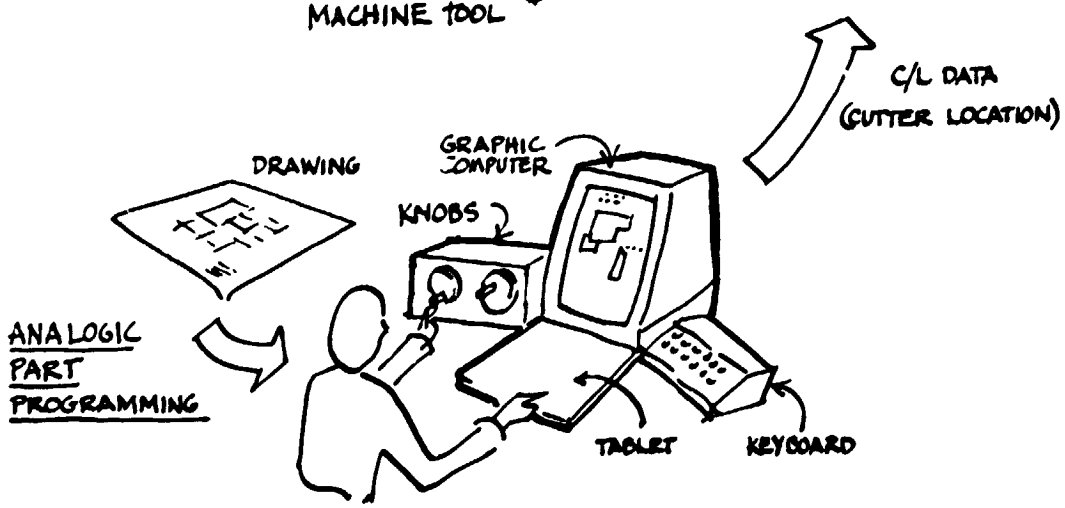

Figure 6b. Analogic Part Programming [12] uses computer displays and analogic (knobs) and symbolic (keyboard) modes for more efficient programming (less training, better programs). There appears to be better compatibility between thinking modes and human operator output (right-brain vs. left-brain and spatial vs. linguistic and analogic vs. symbolic).

A REGRESSION APPROACH TO GENERATE AIRCRAFT PREDICTOR INFORMATION

By Paul D. Gallaher, Roger A. Hunt, and Robert C. Williges

University of Illinois at Urbana-Champaign

SUMMARY

A predictor display shows the human operator future consequences of his immediate control inputs. A contact analog aircraft display is described in which an airplane-like predictor symbol depicts future airplane position and orientation. The standard method for obtaining the predictor information is to use a complete, fast-time model of the controlled vehicle. An alternative approach is presented in this paper in which least-squares, first-order, linear approximations for each of the six degrees of freedom of aircraft motion were calculated. Thirteen variables representing changes in positions and rate of change of positions were selected as parameters for the prediction equations. Separate sets of equations were determined for 7, 14, and 21 seconds prediction times and continuous, 1, and 3 seconds control neutralization assumption times. The advantages and disadvantages of this regression approach are discussed.

INTRODUCTION

Predictor displays provide the operator of manually controlled systems with information about the future state of the variable being controlled. Often this information can be generated by an analog of the system to be controlled, operating repetitively in an accelerated time scale. Ideally, to generate a predictor model using such a fast-time model, the model should be a duplicate of the original plant. For example, to put a predictor display in an aircraft trainer which uses an analog computer for all flight equations and dynamics, a second analog computer just like the first with speeded-up time constants could be used. Such complexity in using an accurate fast-time model imposes a penalty of cost, computer weight, and power requirements. In fact, Kelly (1) pointed out that it may not be necessary to have the complete accuracy of a fast-time model.

Bernotat (2) used a Taylor series expansion rather than the fast-time model approach, and found that even inaccurate predictions gave improved performance over no prediction in the control of a third-order undamped system following a step input. Kelley (3) found the same effect, but he also found that the useful prediction span decreased with model accuracy while learning times for effective manual control were increased. A comprehensive study of simplified models for an automatic predictive control system for aircraft landing in two dimensional sideways looking displays was conducted by Chestnut, Sollecito, and Troutman (4). They pointed out that the model may

be of either the analog or digital form, but they felt the digital approach offers more accuracy and flexibility. They also indicated that the time constants and gains of the model can be in error by two to one without excessive loss in performance.

The main effect of an inaccurate model is closely related to the predictor span. The magnitude of the errors in an inaccurate predictor can be determined analytically or experimentally if the plant can be observed directly or simulated accurately for comparison with a less accurate fast-time model. Errors farther into the future are usually compensated for by the fact that accuracy requirements on short predictions usually are greater than for long predictions. Predictor displays can also overcome the problem of accuracy when they are continuously updated. If updating is inaccurate or infrequent, the fast-time model must be that much more accurate.

This paper presents a least-squares, regression approach for determining first-order, linear approximations of accurate fast-time models used in predictor displays. Such a procedure would eliminate the need for an operational fast-time model while still providing a great deal of predictive accuracy. The accuracy of this regression approach for generating these predictor symbols is evaluated both at various prediction times and at various control input durations.

METHOD

Task

For the purpose of demonstrating the use of a regression approach to generate predictor information, an application incorporating predictor information in an aircraft system during an approach to landing was used. Because of the complexity and sluggishness of the aircraft system in the landing phase, manual performance depends heavily on the anticipatory abilities of the pilot. Under such circumstances, predictive displays might be very useful. Smith, Pence, Queen, and Wulfeck (5) demonstrated that the predictor display did improve performance in an approach to landing on an aircraft carrier. It even facilitated learning to such an extent that mean performance on transfer trials using a predictor was considerably higher than that of a control condition without the predictor.

The specific approach to landing task in this study was generated for a Singer-Link General Aviation Trainer (GAT-2) which simulates general, light, twin-engine aircraft. The predictor symbology was incorporated into a versatile computer-generated dynamic flight display developed by Artwick (6) and was part of an integrated, vertical situation display stylized in Figure 1. In addition to the situational information of runway outline, centerline, touchdown zone, and grid-line ground texture cues, three glide-slope indicators in the form of telephone-pole-shaped symbols and three discrete, airplane-like predictor symbols are shown on the display. The

predictor symbols represent the position of the aircraft at three particular future points in time (7, 14, and 21 seconds as used in this study) given a specified control input by the pilot.

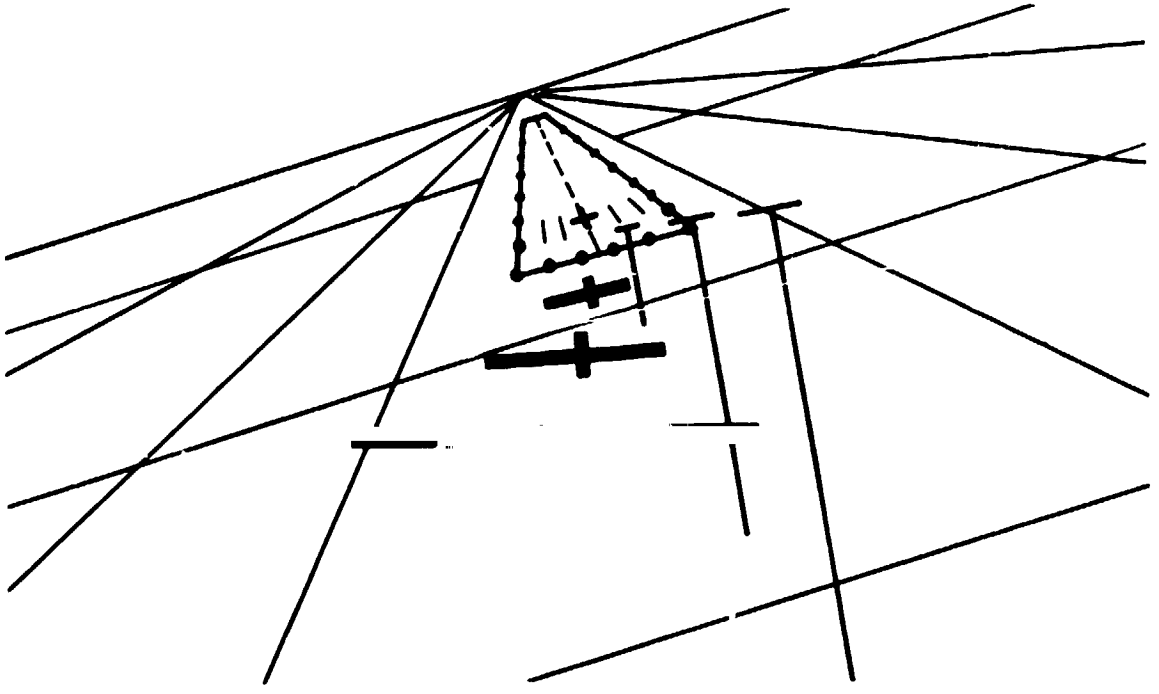

Figure 1. Stylized representation of an integrated vertical situation display showing three aircraft-like predictor symbols.

Regression Procedure

To generate the predictor symbols shown in Figure 1, one must specify the changes in the six degrees of freedom of aircraft motion as listed in Table 1. Each of these six degrees of freedom are determined by the specific flight dynamics of the aircraft. These dynamics are specified in terms of complex, higher-order differential equations which represent position, change in position, and rate of change of position as shown in Table 2. (These values are all accessible as millivolts in the GAT-2 analog computer.)

Rather than use the complete set of complex flight equations, a first-order linear approximation may suffice particularly in the limited range of variables encountered in a final approach to landing situation. A standard, least-squares, multiple linear regression analysis (Tatsuoka, 7) can be used to estimate a raw-score, linear approximation of the general form,

$$Y = \beta_o + \beta_1 X_1 + \ldots + \beta_m X_m \qquad (1)$$

TABLE 1

Changes in Six Degrees of Freedom of Aircraft Motion Required to Specify Aircraft Predictor Symbology

Degrees of Freedom
Change in Bank ($\Delta\theta_B$)
Change in Yaw ($\Delta\theta_Y$)
Change in Pitch ($\Delta\theta_P$)
Change in Lateral Position (Δ_X)
Change in Vertical Position (Δ_Y)
Change in Longitudinal Position (Δ_Z)

TABLE 2

Initial Variables Used to Predict Changes in Six Degrees of Freedom of Aircraft Motion

Predictor Variables
Aileron Position (α)
Rudder Position (ρ)
Elevator Position (ε)
Throttle Position (τ)
Bank Angle (θ_B)
Yaw Angle (θ_Y)
Pitch Angle (θ_P)
Cosine Bank ($\cos\theta_B$)
Rate of Roll ($\dot{\theta}_B$)
Rate of Pitch ($\dot{\theta}_P$)
Rate of Yaw ($\dot{\theta}_Y$)
Rate of Climb (R/C)
Velocity (v)

where Y represents the dependent variable, X_1 through X_m the independent variables, and β_o through β_m the partial regression coefficients. Specifically, the general form of the Equation 1 for the predictor symbology case is,

$$\begin{aligned}\Delta \text{ degree of freedom} = {} & \beta_o + \beta_1 \alpha + \beta_2 \rho + \beta_3 \varepsilon + \beta_4 \theta_B \\ & + \beta_5 \theta_Y + \beta_6 \theta_P + \beta_7 \cos \theta_B + \beta_8 \dot{\theta}_B \\ & + \beta_9 \dot{\theta}_P + \beta_{10} \dot{\theta}_Y + \beta_{11} R/C \end{aligned} \quad (2)$$

where Y is replaced by the particular change in degree of freedom of interest the X's are replaced by selected variables in Table 2, and the β's represent the raw-score, partial regression weights which are empirically determined.

All the independent variables except velocity and throttle can take on both positive and negative values. Velocity and throttle are always zero or some positive value, so their contribution to the predictor equation would always be positive. Furthermore, velocity and throttle changes should amplify the effects produced by control surface position and airplane position changes. Consequently, the independent variables of aileron, rudder, and elevator position as well as the current bank, yaw, and pitch angles shown in Equation 2 are multiplied by the velocity and throttle values of the GAT-2. The remaining four variables in Equation 2 already contain velocity and throttle information, because they are rates of change in position.

Data Collection Procedure

Of the thirteen independent variables shown in Table 2, only the changes in position of the three control surfaces (rudder, aileron, and elevator position) and the throttle position can be directly affected by the pilot. The remaining nine variables are non-linear, interacting functions of these as well as outside disturbances. For each of the four variables under direct pilot control, three levels of change in millivolts (zero, one positive, and one negative) were directly manipulated by the experimenter to obtain the necessary data for generating the regression equations. A one-third replication of the factorial combination of these four variables was observed twice resulting in 54 data collection flights. The remaining nine variables were considered to be approximately random and were not manipulated through experimenter control.

During each of these 54 data collection cycles the GAT-2 was flown in an approach to landing configuration. The landing gear was down and the proper airspeed, flap setting, manifold pressure, etc. was maintained. When the GAT-2 was flown by the pilot to the proper landing configuration, the Raytheon 704 computer maintained the control surfaces at the appropriate level, recorded the initial values of all thirteen independent variables shown in Table 2, and measured the changes in the six degrees of freedom of motion (dependent variables) after 7, 14, and 21 seconds. These latter values provided the three prediction times represented by the successive discrete predictor symbols shown in Figure 1.

To simulate the four designated control surface positions over different flights, the Raytheon 704 computer was used. The analog signals from the GAT-2 representing control surface positions were intercepted prior to their use in the GAT-2 analog computer flight equations. An analog-to-digital converter made these signals available in the form of a 12-bit word. Thus, 0 to 10 volts was converted to 0 to 2048 binary. The software routines then generated changes in these signals as dictated by the one-third replicate of the factorial design. These new signals were sent through the digital-to-analog converter and into the GAT-2 computer to maintain precisely a given set of control movements.

As shown in Table 3, the factorial design of this study also allowed for the calculation of six prediction equations for each of three control assumption times at the 7, 14, and 21 second prediction times. The length of time these control surface changes were maintained prior to neutralization determined the control assumption times. When the control changes were maintained continuously over the 21 second prediction span, this produced the continuous or on-line predictor model (Warner 8). If the control changes were not maintained throughout the data collection phase, an off-line predictor model is used. Two off-line models using control assumption times of 1 and 3 seconds were also investigated in this study. A different set of 54 approaches to landing were required for each control assumption time. Consequently, a total of 162 approaches were measured.

TABLE 3

Factorial Design of Control Assumptions and Prediction Times Used to Generate the Six Regression Equations Predicting the Degrees of Freedom of Motion of the Predictor Symbol

Control Assumptions (Seconds)	Prediction Times (Seconds)		
	7	14	21
Continuous (21)	(6 Regression Equations)	(6 Regression Equations)	(6 Regression Equations)
1	(6 Regression Equations)	(6 Regression Equations)	(6 Regression Equations)
3	(6 Regression Equations)	(6 Regression Equations)	(6 Regression Equations)

RESULTS

A multiple, linear regression analysis was conducted on all 11 independent variables shown in Equation 2 for each dependent variable to determine the appropriate partial-regression coefficient values. Table 3 shows that there were six equations for each predictor time and the associated control assumptions. These six equations determined the changes in the six degrees of freedom of motion for a particular predictor symbol. Because each

prediction equation required a separate regression analysis, a total of 54 regression equations were solved.

For example, Table 4 shows the general form of the six prediction equations needed to represent the airplane predictor symbol at seven seconds in the future for a three second control assumption time. Although this regression analysis was conducted on all 11 of the independent variables shown in Equation 2, only the statistically significant ($p < .05$) predictors are shown in Table 4. Similar sets of prediction equations were derived for the other treatment conditions summarized in Table 3. In each case, however, the specific set of statistically reliable partial-regression weights varied somewhat.

TABLE 4

Prediction Equations with Significant ($p < .05$) Independent Variables Used to Determine Changes in the Six Degrees of Freedom of Aircraft Motion for Seven-Second Prediction Span and Three-Second Neutralization Assumption.

$$\Delta\theta_\beta = \beta_o + \beta_1 \alpha + \beta_2 \rho + \beta_3 \theta_B + \beta_4 \dot{\theta}_B + \beta_5 \dot{\theta}_Y + \beta_6 \dot{\theta}_P$$

$$\Delta\theta_Y = \beta_o + \beta_1 \alpha + \beta_2 \theta_B + \beta_3 \dot{\theta}_B + \beta_4 \dot{\theta}_Y + \beta_5 \dot{\theta}_P$$

$$\Delta\theta_P = \beta_o + \beta_1 \varepsilon + \beta_2 \theta_B + \beta_3 \theta_Y + \beta_4 \theta_P + \beta_5 \dot{\theta}_P + \beta_6 \, R/C$$

$$\Delta X = \beta_o + \beta_1 \alpha + \beta_2 \rho + \beta_3 \theta_B + \beta_4 \theta_Y + \beta_5 \dot{\theta}_B + \beta_6 \dot{\theta}_Y + \beta_7 \dot{\theta}_P$$

$$\Delta Y = \beta_o + \beta_1 \alpha + \beta_2 \varepsilon + \beta_3 \cos \theta_B + \beta_4 \dot{\theta}_B + \beta_5 \dot{\theta}_P + \beta_6 \, R/C$$

$$\Delta Z = \beta_o + \beta_1 \alpha + \beta_2 \varepsilon + \beta_3 \cos \theta_B + \beta_4 \dot{\theta}_B + \beta_5 \dot{\theta}_P + \beta_6 \, R/C$$

One convenient way of assessing the goodness of fit of each of these regression equations is to calculate the multiple correlation coefficient. The square of this value represents the percent of variance accounted for by the regression equation. Table 5 summarizes the multiple correlation coefficients for each of the 54 prediction equations of this study. (For example, the multiple correlation coefficients for the six prediction equations presented in Table 4 are .96, .98, .84, .94, .79, and .85, respectively.) Note that the change in altitude (Y) is the degree of freedom of aircraft motion which resulted in the lowest multiple correlation coefficients. Generally, the one-second control assumption time and the seven-second prediction time also produced regression equations with lower predictive accuracy.

TABLE 5

Multiple Correlation Coefficients for Each Predictor Equation

Prediction Times	Bank	Yaw	Pitch	X	Y	Z
Continuous (21 Second) Control Assumption						
7	.98	.95	.97	.87	.78	.77
14	.98	.98	.98	.95	.85	.94
21	.99	.98	.97	.97	.92	.96
1 Second Control Assumption						
7	.96	.96	.87	.88	.66	.66
14	.97	.95	.94	.92	.71	.61
21	.97	.91	.94	.93	.75	.64
3 Second Control Assumption						
7	.96	.98	.84	.94	.79	.85
14	.98	.98	.91	.98	.83	.92
21	.98	.98	.95	.98	.85	.92

DISCUSSION

The overall consistently high multiple correlation coefficients obtained in this study indicate that the regression approach yields very accurate prediction equations and is a viable alternative to using the complete, fast-time model. The lower multiple correlation coefficients for the one-second control assumption is probably reflective of the fact that a one-second control input is simply too brief to account for any significant movement of the GAT-2 over the prediction interval. Likewise, the lower predictive power of the 7 second prediction times as compared to 14 and 21 seconds merely shows that the GAT-2 dynamics are such that the simulator has not completed a response to the control force inputs. The longer prediction times represent a more complete simulator response.

A simplification of this approach for application to actual aircraft would be to remove the variables representing rates of change of motion which are not normally available. Undoubtedly, this simplification would

reduce the predictive accuracy of the regression equations, because rate parameters provided significant weightings in the prediction equations. From a behavioral point of view, however, these less precise equations may not affect the pilot's performance in flying the aircraft. Additional research is needed to determine the role of predictor symbol accuracy in determining operator control inputs before the allowable degree of predictor simplification can be specified.

This approach to generating predictor symbology offers the advantages of ease of implementation, low cost, and conformity to a digitally-generated display. In fact, this method may be better than an accurate, fast-time model in the sense that time lags are no longer proportional to prediction span because of increased computations being required further into the future. Furthermore, the prediction span need not be compromised by repetition rate, updating frequency, or computing power available because any discrete prediction is as easy to make as any other.

It should be remembered that the specific prediction equations of this study pertain only to the control dynamics of the GAT-2 at the three prediction times and control assumption times varied. In other words, the regression equations are always specific to the device from which the data are collected. The approach and procedure for generating these regression equations, however, are general and can be applied to generating predictor symbology for any specific device. Obviously, there probably are situations in which a multiple linear regression may not provide an adequate representation of the true underlying system dynamics. In such instances a regression approach is still appropriate, because it can be easily extended to higher-order, polynomial regression representations of these complex functions.

ACKNOWLEDGMENTS

Contractual support for this research was provided by the Engineering Psychology Program, Office of Naval Research, Contract Number N00014-76-C-0081. Mr. Gerald Malecki, Assistant Director of Engineering Psychology Programs, was the technical monitor of this program.

REFERENCES

1. Kelly, C. R. Developing and testing the effectiveness of the predictor instrument. Santa Monica, Calif.: Dunlap and Associates, Inc., Technical Report 252-60-1, March 1960.

2. Bernotat, R. Das prinzip der voranzeige und seine anwendung in der flugführung. Zeitschrift für Flugwissenschaften, 1965, 13, 373-377.

3. Kelley, C.R. Further research cn the predictor instrument. Santa Monica Calif.: Dunlap and Associates, Inc., Technical Report 252-60-2, December 1960.

4. Chestnut, H., Sollecito, W. E. and Troutman, P. H. Predictive control system application. Transaction of AIEEE, 1961, 55, 128-139.

5. Smith, R. L., Pence, G. G., Queen, J. E., Wulfeck, J. W. Effect of a predictor instrument on learning to land a simulated jet trainer. Inglewood, Calif.: Dunlap and Associates, Inc., August, 1974.

6. Artwick, B. A. A versatile computer-generated dynamic flight display. Savoy, Ill.: University of Illinois at Urbana-Champaign, Institute of Aviation, Aviation Research Laboratory, Technical Report ARL-76-5/ONR-76-1, May 1976.

7. Tatsuoka, M. M. The general linear model. Institute for Personality and Ability Testing, Champaign, Ill., 1975.

8. Warner, J. A. A fundamental study of predictive display systems, NASA CR-1274, Technical Report, 1969.

INTRODUCTION TO A C)RDINATED COCKPIT DISPLAY CONCEPT

By D. L. Baty

Ames Research Center, NASA
Moffett Field, California 94035

ABSTRACT

The aircraft instrument panel has evolved as an ever growing collection of subsystem indicators. Although human factors design has reduced the difficulty in interpreting the displayed parameters, it has not resulted in a quickly and accurately assimilated body of information. Some efforts have been made to integrate displays from the pilot's viewpoint as evidenced by electronic attitude director indicators and cathode ray tube (CRT) map displays. However, with these displays, full advantage has not yet been taken of the potential of current computer and display device technology. This paper describes an initial three-display configuration, based on a rationale developed earlier, that is designed to present flight status information. Primary emphasis is on the factors that contribute to efficient perception and integration of the pilot's total spatial situation. The display system consists of three orthogonal views containing both qualitative and quantitative information presented on three 17.7 × 17.7 cm (7 × 7 in.) beam-penetration color CRTs. Therefore, the displays will show different views of the same information. In addition, to increase the visual separation of the information elements, the colors red, green, and yellow are used to depict, respectively, the control, performance, and navigation categories of flight instrumentation. As a result the displays are coordinated in information and color; therefore, the name Coordinated Cockpit Display (CCD).

INTRODUCTION

The Man-Machine Integration Branch, Flight Management Program at NASA-Ames Research Center is committed to study and research of pilot procedures and pilot-systems interfaces that will be required for aircraft operating within the National Airspace System of the 1980-1990s (ref. 1). The study of pilot information and display requirements is an integral part of this program. These requirements are generated by many complex systems ranging in scope from the overall National Airspace System to individual on-board avionics systems. If the pilot is to cope efficiently with all relevant information, careful thought must be given to the method of its presentation. In a separate report (ref. 2) several system and perceptual problems were discussed and the rationale for an initial display set was evolved. Three general design goals resulted from that discussion:

1. Div·rce the display configuration from individual subsystems.

2. Display information to the pilot in such a manner that he always uses the same displays regardless of the role he is actively taking.

3. Provide pictorial representations of the aircraft situation with quantitative information appropriately related to the picture.

Based on these concepts the first prototype system was designed as described in this report. The display system is a set of three, beam-penetration color cathode-ray tubes (CRTs). Since one of three orthogonal projections of the aircraft situation will appear on each CRT, the displays will show different views of the same information. The color feature is included primarily to obtain visual separation of information elements, but additional advantage is taken of this capability by differentiating control, performance, and navigation information on the three displays with red, green, and yellow, respectively. Therefore, the displays are coordinated in information and color, and the name Coordinated Cockpit Display (CCD) was chosen to emphasize this feature of the system. Changes in internal detail, but not in overall concept, can be expected in subsequent displays.

GENERAL FEATURES OF THE CCD

The three-display configuration described here is based on three orthogonal projections of the aircraft situation: (1) perpendicular to the pilot's forward line-of-sight; (2) parallel to the ground; and (3) perpendicular to the other two. Figure 1 illustrates the relationships.

The first display is most closely related to the pilot's view out the front window and is perpendicular to the earth. For the CCD system this is called the Vertical Situation Display (VSD) (fig. 1). Because the frame of reference moves in response to aircraft attitude the first CRT presentations of this type were called Electronic Attitude Director Indicators (EADI) and that designation has remained (ref. 3). This reference to attitude is too restrictive and the term vertical situation display is currently more descriptive of the broader function visualized for this display.

The second display represents the horizontal situation and is thus called the Horizontal Situation Display (HSD). This plane is parallel to the earth's surface and is the plane in which maps are commonly drawn.

The display that will show the pilot's situation in a plane perpendicular to the earth and parallel to the pilot's forward line of sight is called the Side Vertical Situation Display (SVSD). In the past, very little attention has been given to this view of the flight situation. In addition to other features to be described, this pictorial view will be ideal for explicitly showing the altitude situation, and should make it easy f r the pilot to maintain altitude awareness.

The combination of these three displays unambiguously shows the total flight situation. Each display explicitly represents two dimensions in space

and shares one of those two dimensions with each of the other two displays. For example, the display elements to be shown on the SVSD will represent up/down and fore/aft situation information; the up/down dimension is also one of the VSD dimensions, and the fore/aft dimension is one of the HSD dimensions. Therefore, each of the three displays is capable of showing different views of the same information; for example, a waypoint in space with a line joining the aircraft with the waypoint. By constructing these different views of selected information the displays are tied together, or coordinated, in terms of information content. The display elements are also to be color coded according to three (perhaps four) classes of function that will be the same on all three displays.

As prime instruments, the three CRTs will be mounted in the center of the aircraft instrument panel with the display surfaces perpendicular to the pilot's line-of-sight. This is not ideal since the pilot will have to mentally rotate coordinates to correspond with the real world. However, the alternatives of positioning the scope faces parallel to the planes they represent, either at the instrument panel or closer to the pilot, present major practical difficulties. To keep this mental rotation task as simple as possible the three displays will be positioned as shown in figure 2. This is the relationship that results if the three planes depicted in figure 1 were folded outward as if they were three sides of a box.

Color Coding

As already mentioned in the Introduction, color will be used as part of this display system, primarily to obtain visual separation of the information elements. The usefulness of different colors to separate display elements is well demonstrated by current mechanical flight directors. Because monochrome CRTs lack color separation, they become visually cluttered by even a few elements. Shape, intensity, and line coding do little to relieve the problem. The beam-penetration CRTs to be used with the initial display system can generate three basic colors: red, green and yellow. (Other intermediate colors, such as orange, can also be generated, but red, green, and yellow are the most easily discriminable.) Rather than arbitrarily assigning a color to each display element, a search was made for some consistent color assignment scheme that would also fulfill the visual separation requirement. An instrument classification scheme used by the Air Force provides three categories to match the three basic colors.

Air Force Manual 51-37 divides flight instruments into three categories: control, performance, and navigation instruments (ref. 4). Loosely defined, the control instruments indicate first response to control inputs such as aircraft attitude and engine power; the performance instruments indicate the effects of changes in the control parameters, such as pitch changes resulting in altitude and airspeed changes; and the navigation instruments indicate aircraft position relative to ground references. These three categories can also be referred to as inner, middle, and outer loop control.

The colors red, green, and yellow have been assigned to control, performance, and navigation information, respectively. (This is probably not critical

from a perceptual standpoint.) Red was chosen for control information for three reasons: (1) pilot response to control requirements must be relatively quick and red is traditionally associated with a requirement for immediate action; (2) there are fewer elements of control information than is the case for performance and navigation so less demand to "look at red"; and (3) because red elements will probably require two beam tracings to attain the desired brightness level, assigning fewer elements to red will save computer time. The present green and yellow assignments were given because early color drawings of potential displays were aesthetically more pleasing to the writer.

Research Hardware

The lines and dots that make up the display elements are generated by an Evans and Sutherland LDS-2, modified to drive beam-penetration color CRTs. Each color CRT measures 17.7 × 17.7 cm (7 × 7 in.). An SEL-840 computer interfaces with the LDS-2 to generate aircraft dynamics, navigation and guidance equations, and performance recording.

FEATURES OF THE INDIVIDUAL CCD DISPLAYS

The CCD concept as outlined so far is quite simple. However, when the amount of specific information that could go on each display is considered, along with the different possible forms that could be given to each piece of information, it is clear that the implementation of CCD could become complex. In the following description of the individual CCD displays, only one form of selected information is described. It is to be understood that changes will be made to accommodate the requirements of specific experiments, and the purpose of these experiments will be to seek better forms of the displays.

Vertical Situation Display

The Vertical Situation Display is the primary display for aircraft attitude. Since everything is referenced to the direction of flight, the center of the display can easily become overly cluttered with aircraft symbol, horizon line, pitch marks, runway symbol and other aiming points. For this reason everything that might logically go on this display cannot be accommodated at the same time. One configuration of the VSD is shown in figure 3. Element color assignments given in the text below are summarized in Table 1.

This method of showing the attitude situation is fairly standard. The combination of aircraft symbol (fixed), horizon line, and roll angle marker show a 10° left bank and zero degree pitch angle. These elements will all be shown in red.

The ground plane is differentiated from the skyplane by a perspective dot pattern. The rate of downward motion could be programmed to be a function of forward velocity and/or altitude and may be studied at a later time. It is believed, however, that the most important function of these dots is the

ground-plane/skyplane differentiation (ref. 5) and secondarily the general streamer effect (ref. 6). Altitude and velocity coding would encounter range problems; for example, the dots would be so far apart close to the ground that the visual illusion of the ground plane would be lost. The ground plane dots will be yellow.

The performance information that will have to be read most precisely during critical maneuvers surrounds the central attitude display. The altitude position reading on the right has a natural up/down relationship on this display. Also the heading readout at the top of the display has a natural right/left relationship. Airspeed has no natural position correspondence so the standard population stereotype, reading upward for larger values, was adopted (ref. 7). Heading, altitude, and airspeed are each read as a combination moving tape and digital readout, taking advantage of the best features of both. Digital readouts can be read more quickly and accurately than an analogue readout, but are poor for rate judgments. A moving tape provides rate and lead information. In operation, the moving tape numbers are blanked from the digital readout box so that the visual effect is that of the tape moving behind the box. For this simulation there will be provision for choosing either moving tape or digital readout separately before beginning a flight.

The rate of change of heading and altitude, more commonly known as turn rate and instantaneous vertical speed indication (IVSI), respectively, are displayed adjacent to the appropriate moving tape. Turn rate is normally shown in terms of a standard 3°/sec turn (although for STOL aircraft this will probably need modification). In like manner the IVSI will be scaled for one or two standard sink and climb rates. If needed, a speed command or error bug will run along the airspeed tape. All these elements on left, top, and right of the VSD will be green.

Two pieces of information, flight path angle (FPA) and potential flight path angle (PFPA), have been combined into one symbol so that the relationship between the two pieces of information cannot be lost among other symbols on the display. In figure 3, the point between the two tips of the FPA marker is the actual direction of aircraft flight at a given moment. This point is also called the aiming point and a line extending from the aircraft toward this point is called the velocity vector. This symbol can be used to show flight path angle relative to the horizon or to any spatially located point such as a 3-D waypoint, runway threshold, or another aircraft. Flight path can be computed relative to the ground or relative to the air mass. At present there are arguments pro and con for each of these frames of reference. First emphasis will be on pilot interpretation problems with different simulated weather conditions. Green is the color from the inner tips of the symbol to the pivot or bending point.

The PFPA is referenced to the FPA. When the PFPA is level with the FPA, the acceleration along the aircraft flight path is equal to zero, therefore speed is constant. If PFPA is above FPA, the acceleration is positive and the speed will increase; if PFPA is below the FPA, acceleration is negative and the speed will decrease. These two indicators make the effect of changes in throttle setting, flaps, landing gear, etc., immediately apparent to the pilot. As an illustration of the use of these two display elements consider the

example shown in figure 3. The potential flight path is shown as being 8° below current flight path. Without a power change, a continuation of the flight path shown will lead to a reduction in airspeed. The pilot can use the information to increase throttle until the potential flight path reads the same value as for flight path, thereby maintaining current flight path and airspeed. Or, continuing with the example in figure 3, the pilot can maintain current airspeed without changing thrust by pitching down until the flight path matches the potential flight path. Because potential flight path is a directly controlled variable, the "flat" portion of the symbol is in red.

Not shown in figure 3, but planned for evaluation are waypoint guidance, runway and touchdown point, and a method for showing a 3-D perspective of desired flight path; for example, tunnel or channel display (ref. 8).

Side Vertical Situation Display

The Side Vertical Situation Display clearly and unambiguously relates present aircraft altitude to future altitude requirements (fig. 4). The aircraft symbol (red) remains fixed at the altitude digital readout box (green). This accomplishes two purposes: (1) the aircraft altitude reference is explicitly established and (2) a required second altimeter is provided. The altitude on the VSD is from radar and the altitude on the SVSD is barometric. The operation of the moving tape/digital readout is the same as described for the VSD. To enhance terrain altitude awareness, significant terrain features (yellow) can be shown referenced to the moving tape. Logic will have to be provided to change these features as a function of lateral displacement from desired ground track.

Flight path angle (green) and potential flight path angle (red) are accurately read against an expanded angle scale (3:1 in fig. 4). The vertical relationships are the same as previously explained for the VSD. The aircraft symbol rotates about its midpoint to indicate aircraft attitude.

An IVSI digital readout (green) in the upper left corner supplies absolute vertical speed information, supplementing the analogue readout on the VSD. An arrow appearing above or below the box reinforces the sign information regarding up or down velocity of the aircraft. There is a ±50 ft/min dead band about zero ft/min so that the arrow is not continually flipping over when the aircraft is flying straight and level. In keeping with the philosophy of relating quantitative information to qualitative information this vertical speed information should be closely related to the flight path angle or the aircraft symbol. Initial attempts to do so resulted in excessive clutter and loss of other information. As with all items on these displays its final form is yet undetermined.

A segmented line (yellow), moving toward the aircraft symbol, indicates the desired vertical track. Relevant tags are shown at waypoints, marker beacons, etc. Vertical and horizontal scaling must be compatible with the flight path angle scaling.

Horizontal Situation Display

The Horizontal Situation Display (fig. 5) relates the aircraft (red) to its geographic position. This may be shown as aircraft position relative to a desired course line, navigation aids, waypoints, runways, or prominent geographic features, all of which would be shown in yellow.

The horizontal projection of the velocity vector or flight path (called a trend vector by Boeing), the range altitude symbol, and ground speed and windspeed vectors would be green. The range altitude symbol shows the point at which the next waypoint altitude will be reached if the present vertical component of the velocity vector is maintained.

If this display is to be used for manual control the lateral track error can be expanded by some factor and shown by a bar parallel to the aircraft, as if a portion of the guide line had been cut out and expanded.

Sufficient work has been done to show the utility of a predictor on the HSD (refs. 9, 10) so that an evaluation of a predictor (not shown in fig. 5) will be part of this work. (This may eventually include evaluation of predictors on the VSD and SVSD as well.) Also not shown, but candidates for HSD presentation, are time slot information for 4-D navigation and symbols showing other aircraft for traffic situation information (refs. 11, 12).

Coordinated Cockpit Display Evaluation

The goal of the CCD concept is to present flight information explicitly in its situational context. The advantages and disadvantages of this approach remain to be studied. In the first simulator study, pilots will manually fly a complex, decelerating landing approach with go-around at 200 ft before touchdown. Using this task, pilot performance will be compared when using the CCD or standard instruments. Pilots will be interviewed for opinions, comments, suggested changes, and additions or deletions.

As display ideas evolve it is expected that various configurations of the CCD will be compared so that new ideas on display content and form can be evaluated. In a parallel effort the CCD will also be integrated into a full mission simulation and evaluated in the larger context of complex navigation with an air traffic control system.

REFERENCES

1. Wempe, Thomas E.: Flight Management-Pilot Procedures and System Interfaces for the 1980-1990's. AIAA Paper No. 74-1297, Nov. 1974.

2. Baty, Daniel L.: Rationale and Description of a Coordinated Cockpit Display (CCD) for Aircraft Flight Management. NASA TM in process.

3. Warner, John D.: Advanced Controls and Displays for Future Commercial Aircraft Operations. AIAA Paper No. 70-938, July 1970.

4. Air Force Manual 51-37, *Instrument Flying*, Dept. of the Air Force, Washington D.C., 15 Nov. 1960.

5. Lincoln, R.; Palmer, E.; and Wempe, T.: Effects of Pictorial Display Configuration on the Frequency of Control Reversals during Aircraft Landing Approaches. NASA TM X-62,191, Oct. 1972.

6. Gibson, J. J.: *The Perception of the Visual World.* The Riverside Press, 1950.

7. McCormick, Ernest J.: *Human Factors Engineering.* McGraw-Hill, 1964.

8. Wilckens, V.: Improvements in Pilot/Aircraft-Integration by Advanced Contact Analog Displays. Proceedings of the Ninth Annual Conference on Manual Control, May 23-25, 1973, M.I.T., Cambridge, Mass., pp. 175-192.

9. Kreifeldt, J. G.; and Wempe, T.: Pilot Performance During a Simulated Standard Instrument Procedure Turn With and Without a Predictor Display. NASA TM X-62,201, Jan. 1973.

10. Baty, D. L.: Evaluating a CRT Map Predictor for Airborne Use. IEEE Trans., Syst., Man, Cybern (in press).

11. Technology Review, "What Role for a Traffic Situation Display?" Jan. 1975, p. 25.

12. Kreifeldt, J.; and Wempe, T.: Human Decision Making in Future ATC Systems: Comparative Studies in Distributed Traffic Management. Presented at the 1974 International Conference of the IEEE Systems, Man and Cybernetics Society, Dallas, Texas, Oct. 1974.

TABLE 1.- Display Element Color Assignments

Display elements	Red	Green	Yellow
VSD			
Horizon line and pitch marks	X		
Aircraft symbol	X		
Roll angle	X		
Ground plane dots			X
Altitude tape and digital readout		X	
Airspeed tape and digital readout		X	
Heading tape and digital readout		X	
Turn rate		X	
IVSI		X	
Flight path (FPA)		X	
Potential flight path (PFPA)	X		
Waypoint guidance (not shown)			X
Runway (not shown)			X
Tunnel or channel (not shown)			X
SVSD			
Aircraft symbol	X		
Altitude tape and digital readout		X	
Terrain features (not shown)			X
Flight path (FPA)		X	
Potential flight path (PFPA)	X		
Angle scale		X	
IVSI		X	
Desired vertical track			X
Waypoints, beacons, etc.			X
HSD			
Aircraft symbol	X		
Flight path		X	
Range altitude		X	
Ground/windspeed vectors		X	
Desired course line			X
Expanded error bar			X
Navigation aid			X
Waypoint			X
Runway			X
Obstructions			X

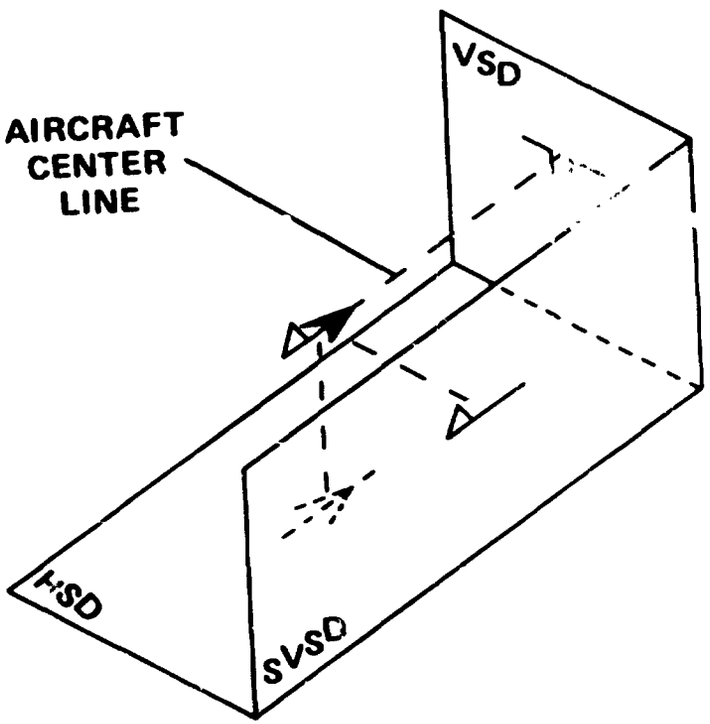

Fig. 1. Three orthogonal planes of aircraft situation.

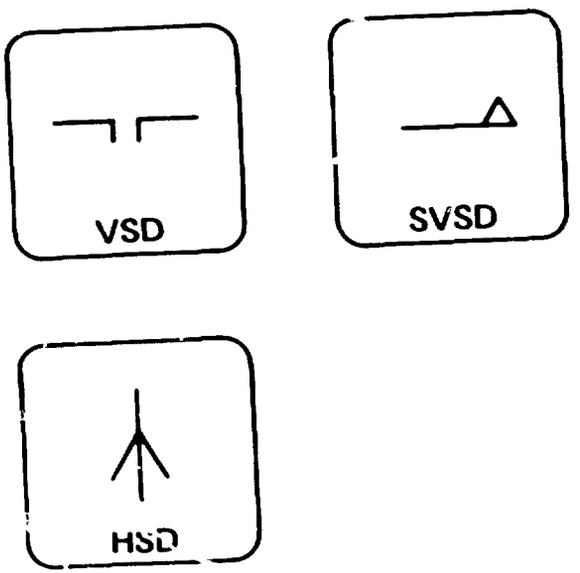

Fig. 2. Position of three displays in aircraft instrument panel.

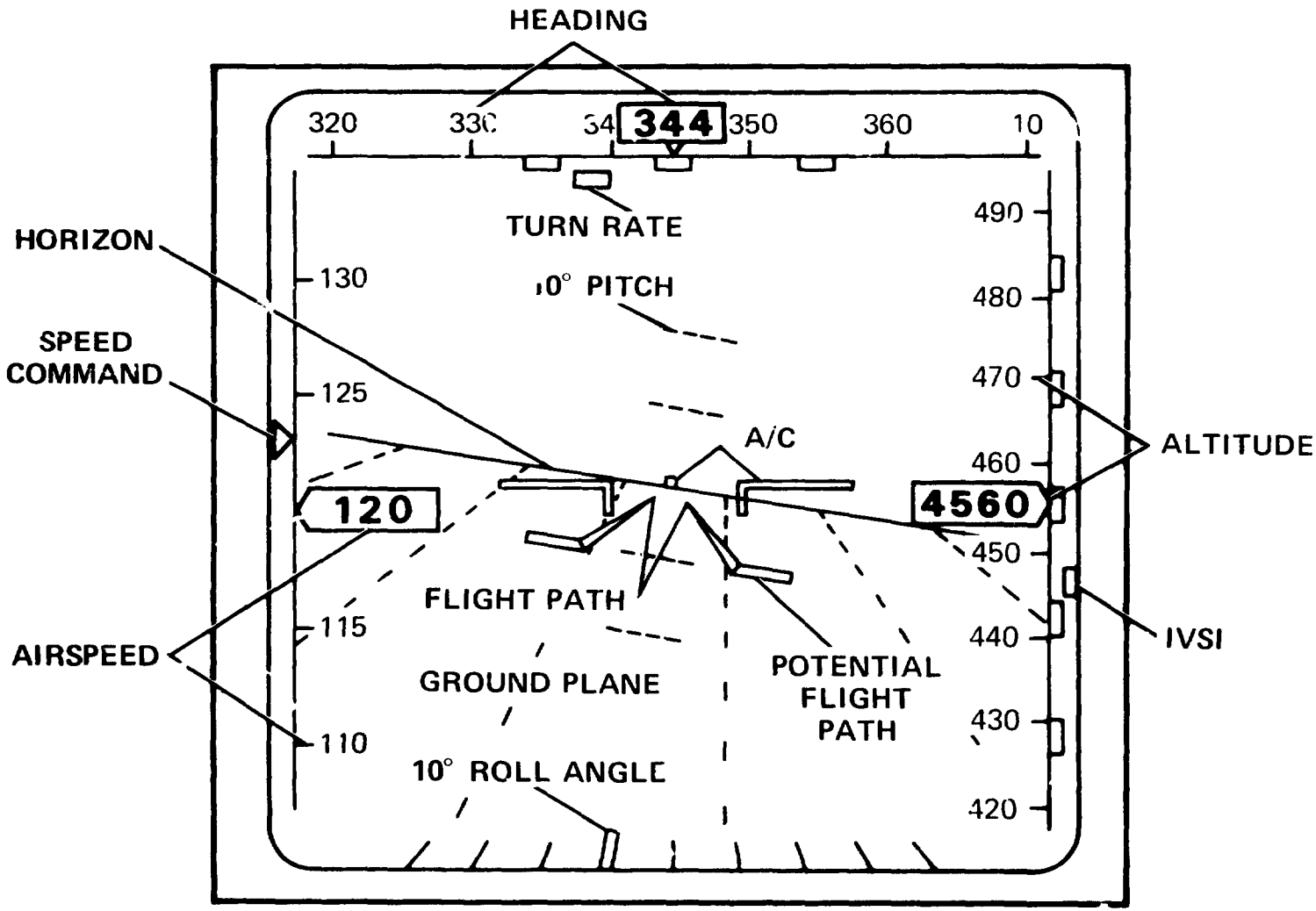

Fig. 3. Vertical situation display.

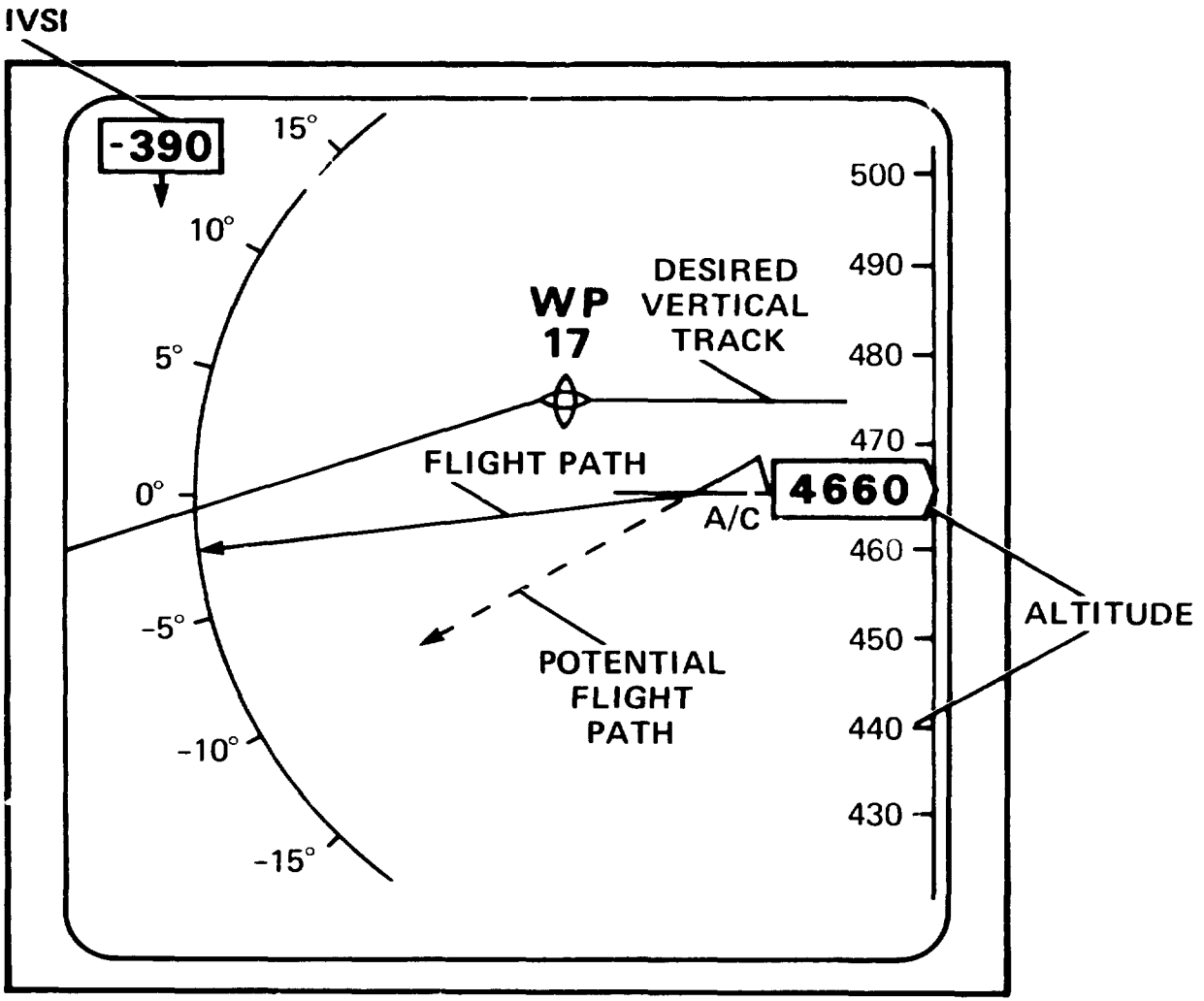

Fig. 4. Side vertical situation display.

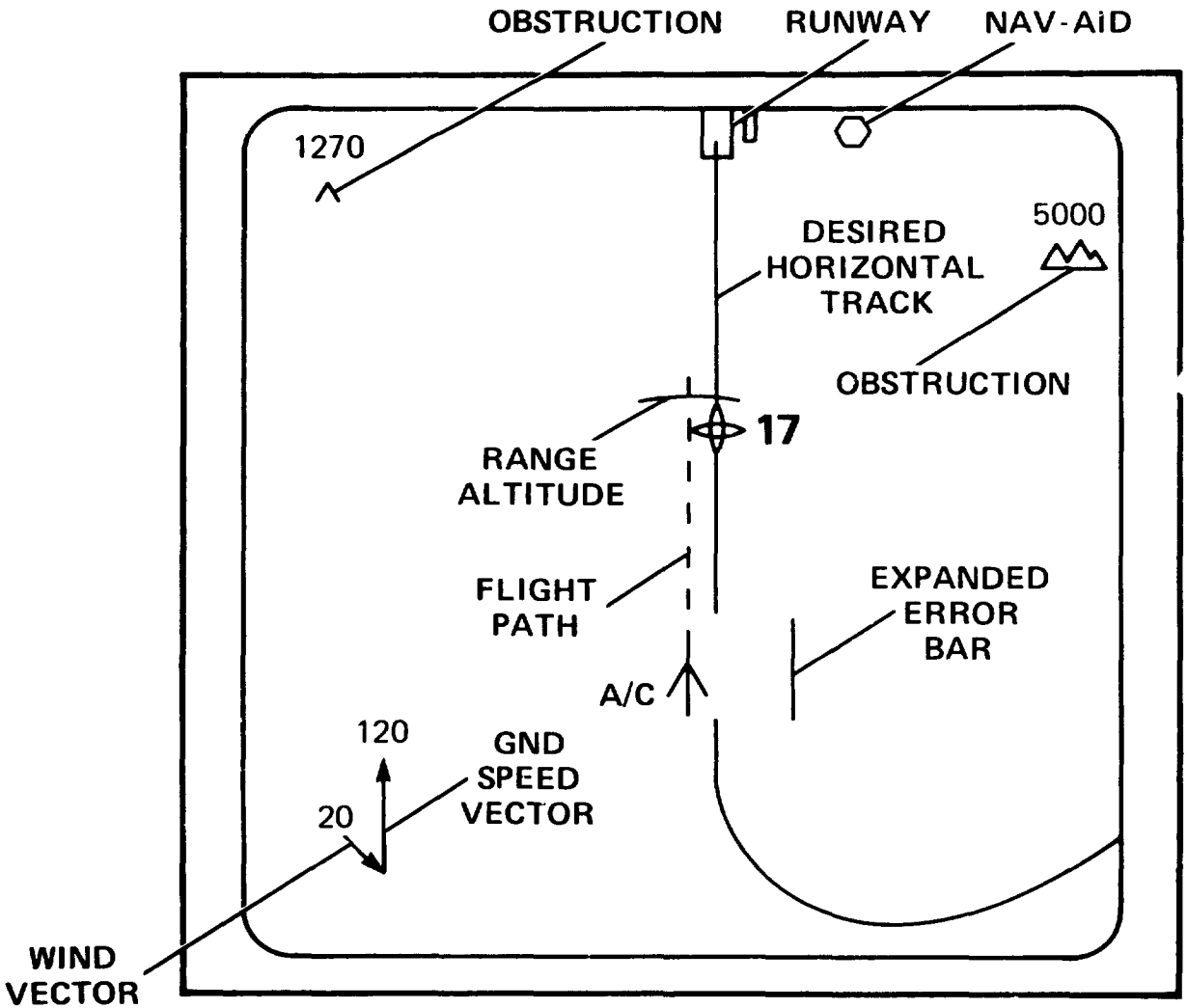

Fig. 5. Horizontal situation display.

IMPLICATIONS OF A MIXTURE OF AIRCRAFT WITH AND WITHOUT TRAFFIC SITUATION DISPLAYS FOR AIR TRAFFIC MANAGEMENT

J. Kreifeldt; L. Parkin; P. Rothschild
Department of Engineering Design
Tufts University, Medford, MA 02155

T. Wempe: Man-Machine Integration Branch
NASA-Ames Research Center
Moffett Field, CA 94035

Presented at the 12th Annual Conference on
Manual Control, 1976

SUMMARY

A mixture of aircraft (A/C) with and without traffic situation displays (TSD) was simulated to ascertain its effects or distributed air traffic management in the terminal area.

A particular type of distributed air traffic management (sequencing) was used as determined from previous experiments with the nonTSD aircraft being vectored. This mixed condition consisting of one A/C simulator without a TSD and two with TSD was compared to a baseline vectoring condition in which all 3 simulator A/C lacked TSD.

The three simulator A/C and four or five computer simulated A/C were embedded in a terminal area traffic problem with as much realism as possible. All A/C were considered to be STOLcraft.

Analyses were made of flight performance measures, verbal communications and subjective evaluations by the professional pilots and controllers who served as subjects.

The analyses favor the TSD equipped A/C and the distributed mode of management permitted by this cockpit capability. However there are indications that an A/C without a TSD in a TSD environment may require or receive considerably more controller attention and pilot disfavor than when it is in an all vectored environment. This may imply that TSD and nonTSD A/C should be segregated and controlled accordingly.

INTRODUCTION

A number of experiments and reports (1, 2, 3) have now documented the considerable potential that Traffic Situation Displays (TSD) in the cockpit hold for increasing the safety, orderliness and expeditiousness of terminal area air traffic management without increasing pilot or controller workloads. The controller's verbal workload in fact can be considerably reduced[4] by a type of distributed management in which the TSD A/C are issued sequence orders only which they then achieve via their TSD without need for any vectoring as in VFR (Visual Flight Rules.)

However, the experiments to date have not treated the very reasonable possibility of a mixed traffic display environment in which some A/C have TSD capability and others do not. This situation could arise by failure of the TSD in an A/C. It could also arise through the more common possibility that not all A/C will have TSD due to cost or other evolutionary factors thus producing a mix of A/C on a traffic information basis. Just as a mix of A/C speed types poses special management problems and techniques it might also be supposed that a mix of A/C information types might have its own impacts on efficient management.

In order to investigate the effects of a mixed TSD environment, an experiment was performed at NASA-ARC utilizing the Air Traffic Control simulation facilities and programs developed in the Man-Machine Integration Branch. This facility permits studying the group interactive aspects and performance of terminal area traffic management based on exploitation of the 360° view of surrounding traffic made available in the cockpit by a Traffic Situation Display.

A previous study[1] showed that distributed management of 3 A/C equipped with TSD was not only possible but also generally superior in a number of respects to the ground centralized vectoring method of control. In particular, a form of distributed management termed sequencing appeared superior to an alternative form of distributed management. In the sequencing mode, the controller issued only sequence order to each TSD equipped A/C leaving them to achieve this order in VFR fashion thus vastly reducing controller verbal workload without any substantial increase in the pilots' workloads. Therefore for this study, the sequencing mode of distributed management was used for the TSD equipped A/C. All non TSD A/C were vectored.

Two basic conditions were simulated in the present experiment. Vectoring as a condition was characterized by all three simulators lacking traffic information and thus requiring vectors. Nonvectoring was identified with the mixed information condition in which two of the simulators had TSD but the remaining one did not. In a sense, the mix could be viewed as an independent variable along a continuum with the

ratio possibly determining the best form of traffic management. The mixed ("nonvectoring") condition was thus a simultan ous VFR-IFR environment.

The two basic conditions (vectoring, nonvectoring) were compared and within the nonvectoring (mixed) condition, the two specific management techniques (Sequencing, Vectoring) were further compared. Comparisons were based on flight performance measures, verbal communications and subjective evaluations obtained after each run and after the experiment. Three groups of three pilots and two controllers per group were used to test for group specific differences in the results. All subjects were practicing professionals.

METHOD

1. Task

The basic task is referenced to the map shown in Figure 1.

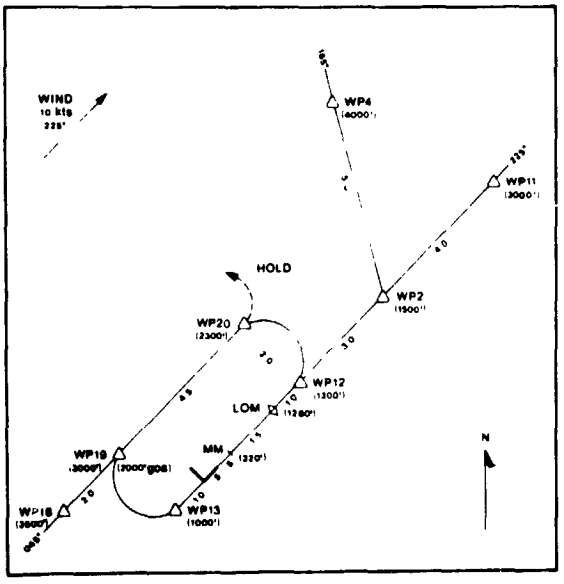

Figure 1. Ground Projection of the Task Layout. Distances are given in Nautical Miles. A STOL Terminal Area is simulated.

The Locations of the Outer Marker (LOM) and Middle Marker (MM) were appropriate for a STOL airport. There were three approaches to the airfield and a go-around (goa) route to be used in case of a missed approach.

Suggested altitudes are given at each waypoint (WP) for traffic purposes although once past WP 12, the altitudes shown are appropriate for a 6° STOL approach which all craft were required to execute.

Computer generated A/C were introduced at WP 11 every two minutes on the average with a 5 second standard deviation. Once introduced, each A/C followed a standard altitude and speed profile appropriate for its type. The controllers could modify only the speed of these craft through keyboard input. Controllers could "hold" the computer A/C at WP 11 and subsequently resume their introduction through appropriate keyboard commands.

The piloted simulator A/C were initially introduced anywhere between or on the 045° and 165° approaches to the terminal area with appropriate headings and speeds. Pilots had aileron, elevator and throttle control of their craft.

The basic task required that the 3 simulator craft be inserted between the computer A/C (scheduled to cross WP 12 every two minutes with some variation.) A basic rule limited spacing to a minimum of 1nm or 60 second between A/C crossing the middle marker. (A fuller description of the problem and subject instructions is given in reference 5.)

Two management conditions for accomplishing this task were compared. In the first condition (vectoring) all 3 A/C were without TSD. Each pilot saw the map of Figure 1 and his own A/C position on it. Because no visual traffic information was available to the pilots they had to be vectored. In the second condition (nonvectoring), two of the three simulators had full 360° visual traffic information while the third remained as in the first condition with the map and only his own position shown on it. Thus two of these A/C (with TSD) could operate in the sequencing mode while the third A/C (without TSD) required vectoring. A common voice circuit was used between all pilots and controllers. Each pilot had a vertical situation display identical to that used in previous studies and a description may be found in Reference 2. A 30 second path predictor was always present on own A/C only.

The basic objective of this study was to determine the impact such a heterogeneous mixture of A/C with and without traffic information would have on terminal area traffic management when compared with a baseline vectoring condition.

2. Measures

Three types of measures were obtained in this experiment. Objective (flight performance) measures of variables such as aileron, elevator and throttle activity in the simulators; final airspeed, heading, glideslope, etc., errors, pitch and roll rates and others: verbal measures based on

tape recordings of the pilots and controller exchanges: and subjective measures obtained from questionnaires completed after each run and after the total experiment.

The experiment was replicated on three separate groups of three pilots and two controllers per group. Three runs of each of the two experimental conditions were obtained from each group. A run lasted 20 to 25 minutes and each group received approximately 4 hours of practice under both conditions. Practice and test runs were made on separate days. All 15 subjects were current airline pilots or air traffic controllers from the San Francisco-Oakland region.

To reiterate, in the Vectoring condition, no A/C had a TSD and thus all A/C required vectoring. In the Nonvectoring condition, the two A/C with traffic displays received sequence order information only from the controller and were left to achieve that order via their TSD and any verbal communication necessary between the pilots. The single A/C without a TSD had to be vectored by the controller among the A/C flying "VFR." Thus the nonvectoring condition had both VFR (TSD equipped A/C) and IFR (nonTSD equipped A/C) traffic.

RESULTS

The results are highlighted here with more detailed analyses to be found in reference 5. Results are presented according to the three types of measures.

1. Objective Measures

   A. Comparisons

A battery of seventeen objective performance measures was recorded on each of the 3 piloted simulated aircraft. These variables are not statistically independent of each other. However, an assessment of the number of independent components present in the battery will depend, to some extent, on the results of the present analyses. Application of principal components and factor analytic-procedures are therefore postponed to a later report.[5] Sixteen of the variables may be thought of as belonging to four general groups as follows:

Group 1 - Landing Accuracy
- FAE: final airspeed error
- FGE: final glideslope error
- FHE: final heading error
- FLE: final lateral error

Group 2 - Manual Workload
- AA: aileron activity
- EA: elevator activity
- TM: throttle movements
- TM/DT: throttle movements per unit of flight time

Group 3 - Expedience/Economy
- HPL: horizontal path length
- DT : duration of flight
- STM: speed total maneuvering
- ICT: intercrossing time

Group 4 - Passenger Comfort
- RRA: roll rms acceleration
- PRA: pitch rms acceleration
- TAC: throttle average change
- STM/DT: speed total man. per unit of flight time

All measures in the Landing Accuracy group were made as the aircraft passed the middle marker (MM on Figure 1) during the final approach.

In the second group, the aileron and elevator activities are rms values of these controls during the simulated flight. Throttle movements (TM) which resulted in speed changes of five knots or more were counted for this variable. The variable TM/DT is the throttle movement count divided by the duration of the flight.

The third group of output variables includes the total length of the aircraft ground track (HPL) and the time duration of the simulated flight (DT). These two variables are highly correlated. Speed total maneuvering (STM) is the sum of all speed changes during the flight. Intercrossing time (ICT) is the time interval between a given aircraft following the one ahead of it across the middle marker on the final approach. (Subjects were instructed to maintain an intercrossing time as close to sixty seconds as possible.) The lowest mean ICT for any of the ATC management schemes was in excess of the sixty second guideline.

The final group of output variables describes the aircraft motion as it may affect passenger comfort. The first two variables are the rms values of roll and pitch accelerations. The average throttle change (TAC) was computed using only throttle changes which would result in speeds in excess of five knots and, therefore, reflects the more gross and perceptible speed changes. The speed total maneuvering was divided by the flight duration to give the last variable in this group, STM/DT.

For each of these sixteen variables, the lowest value is also the most preferred value. A seventeenth output variable is the average speed of the aircraft (AVSPD). There is no obvious optimal value for average speed and since there was no significant difference in this variable among the several ATC management schemes, it was not included in the summary of results to follow.

An a priori summary of the objective performance results is presented in Figure 2, showing four ATC management categories. The first category, vectoring, includes 44 completed flights. The cockpits of simulators were equipped with displays showing the position of that aircraft only in relation to the map. The next three categories involve nonvectoring condition flights. The first of these included 35 completed flights in which the simulators were equipped with traffic situation displays showing the positions of all airborne aircraft

to the pilots. The second of the nonvectoring categories included the 16 vectored flights of simulators with no TSD's. Experimental runs in the nonvectoring condition were heterogeneous since simulators with and without TSD's were in the air at the same time in a ratio of about 2:1. The last category of the nonvectored condition flights included all 51 flights of the two previous categories (both with and without TSD's.) This category reflects the overall performance of the two to one mix of TSD and non TSD aircraft for comparison with the totally vectored condition flights.

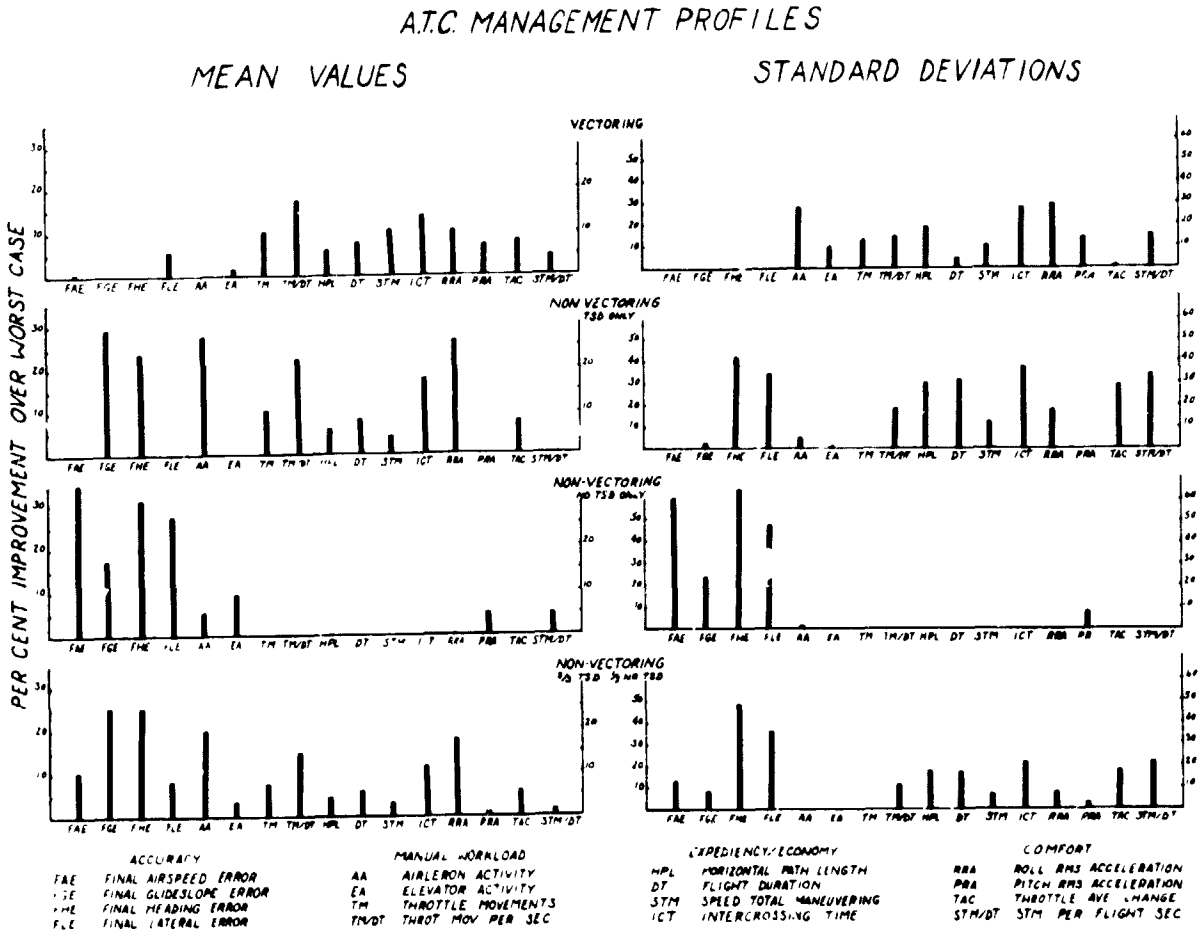

Figure 2 A Relative Comparison of the Means and Standard Deviations of the 16 Objective Measures for Four Types of Flights. Percentages shown are Relative to the lowest Value which is not shown.

When a flight involved a missed approach or "go around", the data describing the portion of the flight after the aircraft passed the middle marker for the first time is not included in the results and analysis. This data was omitted since the high throttle, aileron, and elevator activities and consequent aircraft accelerations associated with recovering from the missed approach tended to produce markedly bimodal distributions for these variables.

The profiles of Figure 2 compare the mean values and standard deviations of the first sixteen output variables. The ATC management category which produced the highest mean or standard deviation for a given variable is taken as the worst case for that variable. The vertical bars indicate the per cent improvement achieved by the given management schemes over the worst case for that variable. For instance, nonvectored TSD's produced the worst results for the mean value of final airspeed error. The vectored flights produced results which were .5 per cent better (lower). Nonvectored condition flights without TSD's (i.e. vectored A/C in the mixed condition) achieved a 35 per cent improvement over the TSD flights on this variable and the combined result for all nonvectored condition flights was about 10 per cent better than the TSD category alone.

Figure 2 shows that the vectoring condition produces poor results in the final error measures both with respect to mean values and standard deviations. Vectoring also resulted in consistent but poor performance with respect to aileron activity. However, the remainder of the manual workload measures, as well as the expediency/economy measures and passenger comfort measures constituted improvements over the respective worst cases. The nonvectored TSD flights produced poor results in final airspeed and final lateral errors, although glideslope and heading errors were low. This category produced the best results with respect to aileron activity and consequent roll acceleration while requiring the greatest amount of elevator activity and pitch acceleration. All other performance measures seem to follow the vectoring profile. The nonvectoring condition runs without TSD's (i.e. vectored flights in the mixed condition) outperformed all other categories on the final error measures. However, this category produced the worst results for almost all other measures.

Figure 3 shows a set of pair-wise comparisons of the various ATC management categories for aiding in comparing flights on the 16 measures. The first comparison contrasts vectoring with the combined nonvectoring category (i.e., no distinction for TSD, nonTSD.) Nonvectoring appears to outperform vectoring in the final error measures while the reverse is true for all but two of the other measures. The aileron activity favored nonvectoring and was the only measure significant at the .01 level. Comparison of the standard deviations on these two categories showed nonvectoring to produce more consistent results in the final error measures. F tests showed the heading and lateral errors to be significantly more consistent (at the 0.1 level) for nonvectoring. The variance in aileron activity and roll acceleration was significantly lower (at the .05 level) for the vectoring flights however.

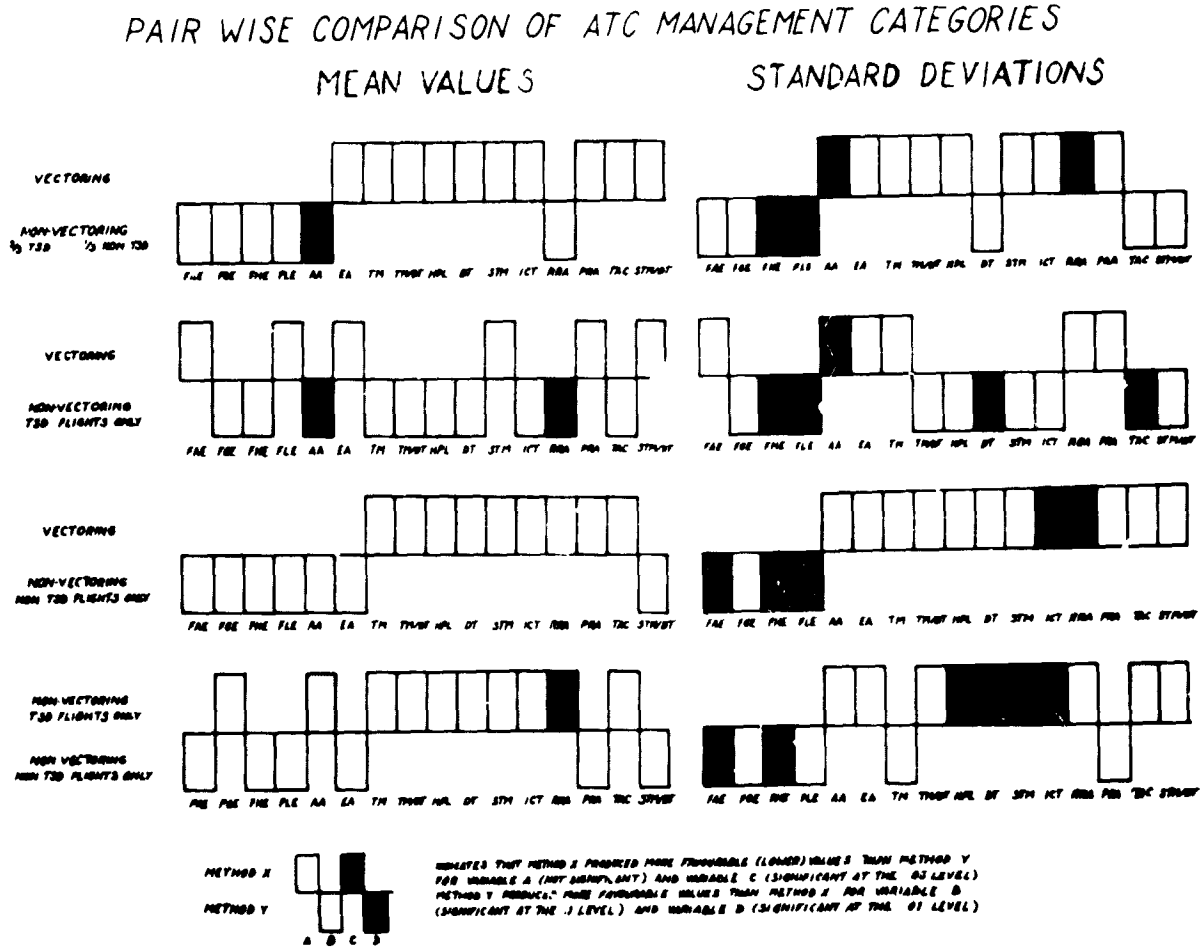

Figure 3 Means and Standard Deviations of the 16 Objective Measures Compared for the Four Types of Flights on a Pair-Wise Basis. The Favoring Direction of a Measure is Indicated. Levels of Statistical Significance are Shown.

Comparison of the vectoring and nonvectoring (TSD) flights generally favored the latter category. The nonvectored flights had significantly lower aileron activity and consequent roll acceleration. The variances of FHE, FLE, DT, TAC, and STM/DT was significantly less for the nonvectored TSD flights while the variance for aileron activity significantly favored the vectored aircraft.

Comparison of vectoring condition flights with the nonvectoring condition non TSD (i.e. vectored) flights showed the latter to perform better with respect to final error measures and aileron and elevator activity, while vectoring was favored on most other measures. No comparison of mean values between these categories was significant. The nonTSD vectored flights in the nonvectoring condition produced less variance in all of the final error measures and three out of four of these comparisons were significant beyond the .01 level. Vectoring condition flights produced lower variances in all other measures although only aileron activity, roll acceleration and intercrossing time were significantly lower.

Finally, the nonvectored TSD flights are compared with the nonTSD (vectored) flights in the nonvectoring condition. The only significant differences in mean values show TSD flights to be superior with respect to aileron activity and roll acceleration. The nonTSD flights have lower variances in all of the final error measures (two out of four were significant) while the TSD flights had significantly lower variances in all of the expedience/economy measures. The variance in throttle average change also favored the TSD flights.

A brief summary comparing the conditions on the relative favorableness of each measure (mean and standard diviation) shows the following:

0 Vectoring condition superior to nonvectoring condition overall.
Vectoring showed more favorable biases than nonvectoring although the most significant differences favored nonvectoring as did the final error measures. Intercrossing times favored vectoring.

0 TSD nonvectoring superior to vectoring.
The truly nonvectored flights (those with TSD) compared to the flights in the vectoring condition showed more favorable biases (10-to-6 for both means and standard deviations) including intercrossing times. In addition, the 7 significant differences all favored the TSD flights.

0 Vectoring condition superior to vectored nonTSD.
The flights in the vectoring condition showed more favorable biases than the vectored flights (noTSD) in the nonvectoring condition, most noticeably in the standard deviations (12-to-4) although again the most significant differences favored the nonvectoring nonTSD flights as did the final errors. Intercrossing times favored the vectoring condition although not significantly.

0 TSD nonvectoring superior to vectored nonTSD.
Within the nonvectoring condition, the TSD (nonvectored) flights showed more favorable biases than the nonTSD (vectored) flights including intercrossing time. However the final errors were smaller and more consistent for the nonTSD.

Thus, based solely on objective measures, the TSD (nonvectored) flights were superior to vectored flights whether or not all the flights in the condition were vectored or just those flights lacking a TSD. On the other hand those flights that were vectored in the mixed (nonvectoring condition were somewhat better on final errors.

B. Multidimensional Analyses

A series of multivariate analyses of variance (MANOVA) and discriminant analyses were performed on the data using the ATC management schemes as the independent or grouping variable. Thus, there were three

groups vectored condition flights, nonvectored condition flights with TSD's, and nonvectored condition flights without TSD's. The purpose of these analyses was to determine if there were significant differences among the 3 groups in terms of the entire set, or a smaller subset, of the output measures. If such differences are present, as a priori analysis implies, discriminant variates should express these differences in a readily interpretable fashion.

The first step in the analysis was to break down the total variance in the measurement battery of seventeen variables into a partition of variance which contained differences among the three groups and a partition which included variation within the groups. The hypothesis H_1, equal within dispersion (variance-covariance) matrixes for the three groups, was then tested using an F-distributed transformation of Box's M statistic[6]. This hypothesis was retained thus validating application of the MANOVA procedure. An F-distributed transformation of Wilk's Lambda statistic[6] was then used to test the hypothesis, H_2, that the column vectors of mean values on the members of the measurement battery were the same for all three groups. It was found that this hypothesis could be rejected with a probability of false rejection less than 0.1.

Inspection of univariate F ratios for the individual measurement variables enabled evaluation of the discriminating power of the various variables. Two of the less useful variables were eliminated to produce a smaller subset of 14 variables and both hypothesis were retested for the smaller measurement battery. Hypothesis H_1 was again retained and hypothesis H_2 was rejected with a smaller probability of false rejection. The number of variables was selectively and finally reduced in ensuing analyses to 8.

The eight member battery included the variables HPL, STM, AA, RRA, FGE, FAE, DT, and ICT and enabled rejection of H_2 with a probability of false rejection at less than 0.01. The discriminant analysis performed on this battery produced two statistically orthogonal components of the battery, both of which provide significant discrimination among the groups. The difference among the three group means on the first component was significant beyond the 0.005 level. This component is defined in terms of the standardized scores of the eight variables and is given in standardized form by the following equation:

$$D_1 = .067\ HPL - .338\ STM + .592\ AA + .372\ RRA - .323\ FAE + .377\ FGE + .320\ DT + .397\ ICT \quad (1)$$

The level of significance of differences among group means on the second component was between 0.05 and 0.02. This component is given by the following equation:

$$D_2 = -.025\ HPL + .491\ STM - 1.299\ AA + 1.132\ RRA - .221\ FAE + .109\ FGE + .307\ DT + .481\ ICT \quad (2)$$

The structure matrix for these components was computed using the total (before partitioning) variance in the test battery. This structure matrix, as well as the communalities achieved by the structure and the univariate F ratios computed in the MANOVA are presented below.

Variable	Structure		Communalities	Univariate F Ratios
	1	2		
HPL	.173	.246	.091	.72
STM	-.056	.312	.101	.70
AA	.09	-.324	.608	6.56
RRA	.602	.129	.379	4.06
FAE	-.147	-.270	.095	.72
FGE	.231	-.226	.04	.89
DT	.217	.298	.36	1.10
ICT	.307	.334	.206	1.176

The elements of the structure matrix are product moment correlations between the variable (row) and the discriminant component (column). The square of an element is, therefore, the proportion of total variance in the variable that is used by the component. The communalities for the variables are the sums of squares across the rows of the structure and are, therefore, the proportions of total variance in the variable that are utilized in the discriminant space defined by the two components. The univariate F ratios and communalities both indicate similar orders of importance for the variables in this measurement battery. The aileron activity is the most important differentiator of the group. The other variables are RRA, ICT, DT, FGE, STM, FAE and HPL in descending order of importance.

The mean group scores on the two discriminant components are plotted in Figure 4. Each group mean is at the center of an eclipse and the ellipses define regions of the discriminant space containing about 67% of their respective populations. The vectors emanating from the origin of the space are projections of the measurement vectors on the discriminant plane indicating their directions of increase in the discriminant space, while their lengths indicate their relative importances as discriminators of the groups.

DISCRIMINANT PLANE

EIGHT VARIABLE CASE

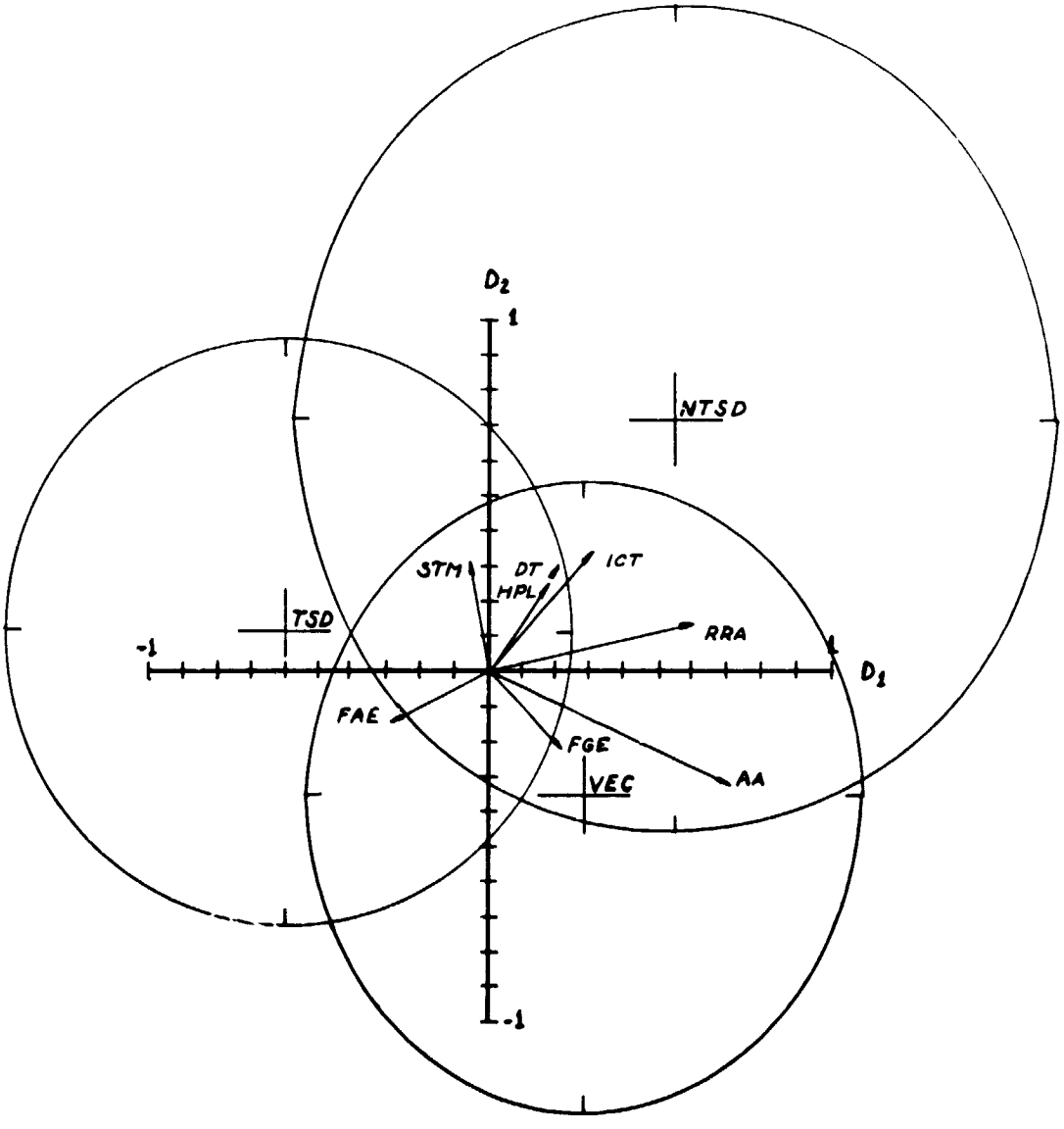

Figure 4 Discriminant Analyses of the Three Different Types of Flight. NTSD Indicates the IFR Flights in the Mixed IFR-VFR Environment. The Figure Shows a Clear Significant Difference Between these Flights. Eight Discriminatory Variables are Shown.

The MANOVA and discriminant analyses have established that the level of significance for differences in the smaller subset of eight variables is beyond the 0.01 level. At this point it would be appropriate and informative to perform a principal components analysis and factor analysis on the data to determine the number of independent components of variance present in the seventeen output variables and to find a rotation of the components which is maximally interpretable. Since the MANOVA showed significant differences among the groups, these further analyses must be performed on a correlation matrix obtained from the pooled within groups dispersion matrix. Use of this within groups partition of variance will eliminate the differences between groups and give a more accurate view of the inter-relationships among the individual variables. This analyses is being performed.

C. Conclusions from Objective Analyses

Therefore based on the above analyses, it appears that the flights that merged and made approaches from sequence order information only (i.e. via TSD) achieved distinctly different and better individual and system performances than vectored flights. On the other hand and perhaps somewhat counterintuitively, those flights that were vectored in a mix of vectored and nonvectored ones were also distinctly different from flights in which all were vectored. This perhaps indicates that controllers found it more difficult to vector A/C in a nonhomogeneous mix than when all were vectored even though the A/C "workload" judged by vectored A/C numerosity was 1/3 lower in the mixed condition than in the all vector condition.

2. Verbal Measures

The verbal communications during each run were tape recorded and later transcribed to hard copy for further analysis of the verbal workload for both vectoring and nonvectoring flight simulations. As before, the traffic situation display flights and those flights without traffic situation displays are compared, and more specifically the flights with TSD are compared to flights with the vectoring condition and to vectored flights within the nonvectoring condition. (Vectored pilots flying in the nonvectoring condition will be referred to as pilots without a TSD.)

A. Word Rates and Word Counts

Running cummulative word rates (averaged over successive 60 second intervals) are shown for pilots, controllers and the total group in Figure 5a, 5b, 5c.

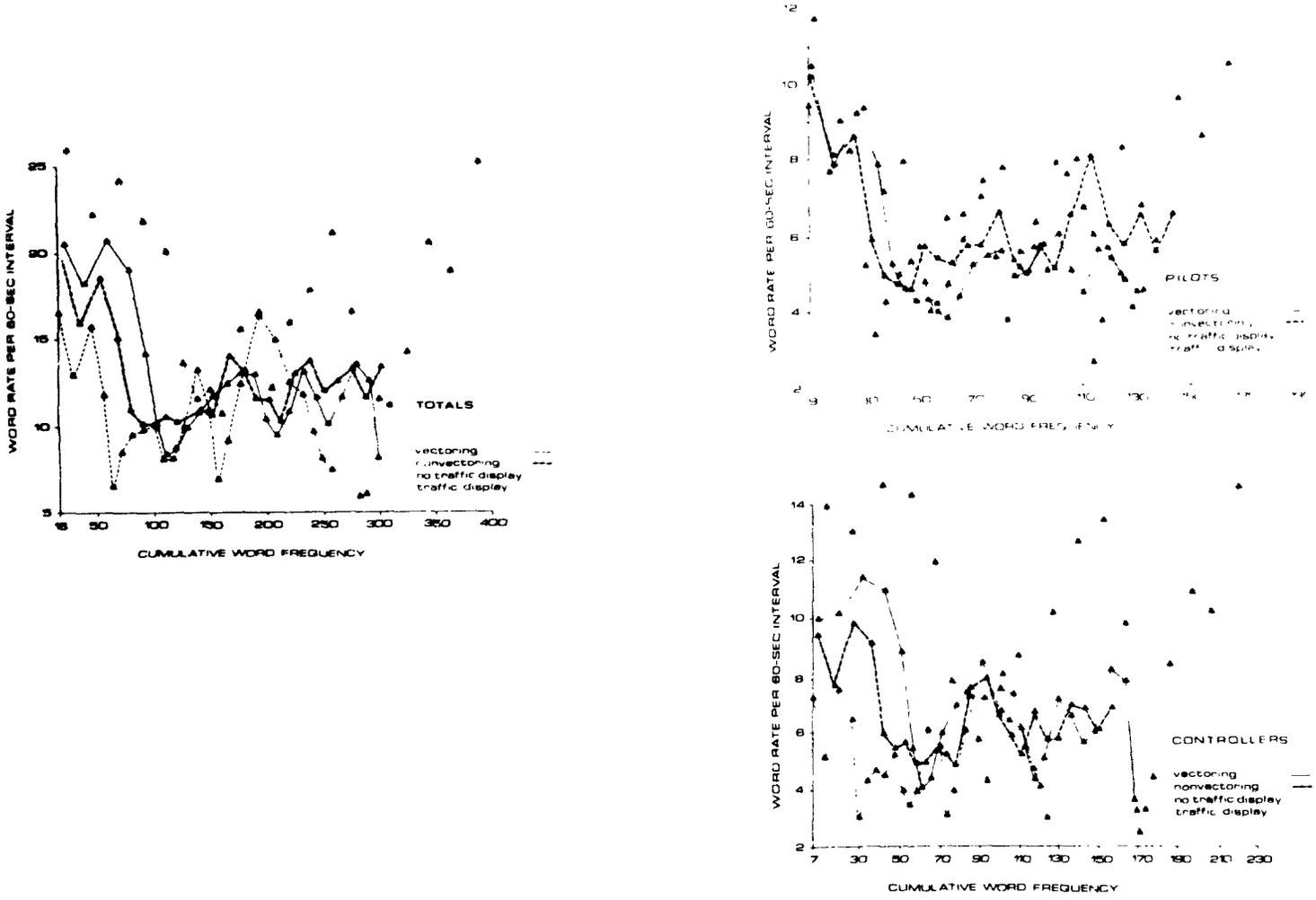

Figure 5 The Word Rates and Cumulative Word Counts for Pilots, Controllers and Both at 60 Second Intervals. The Low Verbal Workload with TSD Flights is Apparent.

In these figures, rates are plotted against the running cummulative word count permitting both to be compared. Comparisons must be made at equal numbers of plot points (60 sec. intervals). One immediate feature of the graphs shows a high initial word rate which decreases sharply followed by a subsequent increase from which point the rate continues to decrease for several minutes. While the exact behavior is no doubt task specific this same general behavior was observed in a previous experiment.[7]

Figure 5a which combines the total pilot and controller communication presents a fair comparison of the conditions. Vectoring and nonvectoring conditions had the same total word count (300) although the initial rates were lower for nonvectoring. However, where the two types of flights (TSD, NTSD) within nonvectoring are compared a large difference is apparent. Both the initial word rate and final word count were about 75% greater for the NTSD flights than for the TSD ones. This type of finding is completely consistent with previous experiments. An interesting and somewhat unexpected finding is that the word rate for the vectored flights in the nonvectoring condition (i.e. nonTSD) was considerably higher even than for flights in the vectoring condition. This phenomenom was observed for each of the three groups individually so that it appears to be fairly robust.

When just the pilot communication is looked at in Figure 5b, the differences between these 4 conditions are not as marked although again the NTSD flights had a higher initial word rate and final word count than either of the other 3 conditions. TSD (nonvectored) flights had the lowest initial word rates.

Figure 5c shows that the effects of the four conditions were most pronounced for the controllers' communication with the same general findings holding as before. The nonvectored flight (TSD) had lowest verbal workload in terms of initial word rate and total word count while the vectored flight in the nonvectoring condition (NTSD) had the highest word rate and total word count.

The group consistency effect is shown visually in figure 6 as a means of suggesting the robustness of the previous findings. Figure 6 plots the normalized differences in total word counts for each comparison. The controller groups were quite consistent across the comparisons with somewhat less consistent results for the 5 pilot groups.

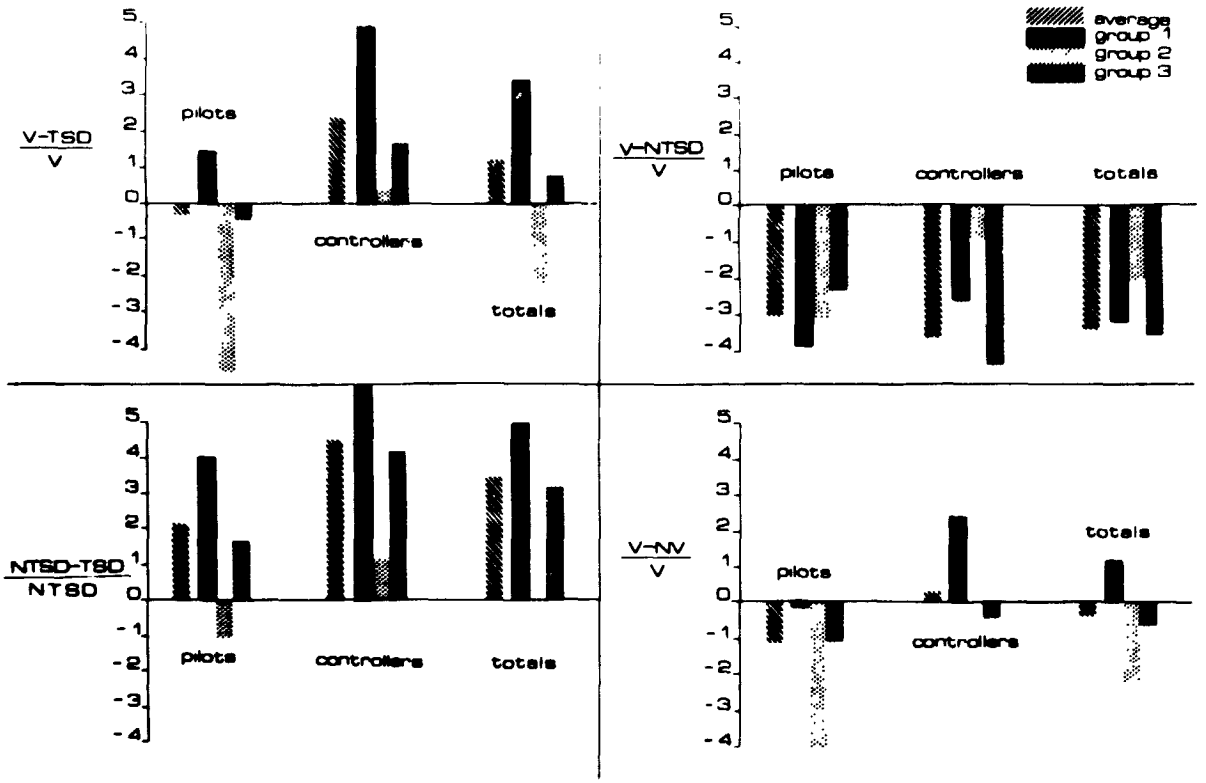

Figure 6 Pair Wise Comparison of Total Word Counts in Each Flight Type for the Three Groups.

B. Content Analyses

Content analyses are being performed on the verbal data. The results to data show that the pilots with TSD's spent significantly less time discussing direction and heading than under either of the two vectoring situations. And not too surprisingly, controllers communicating with the nonvectored flights (TSD) made fewer references to speeds than when communicating with the vectored flights.

C. Conclusions Based on Verbal Analyses

The verbal workload for controllers is considerably reduced in both word rate and total words by taking advantage of the pilots' TSD capability. Pilots with TSD have essentially the same work rate and total word count as when they are in an "all vector" environment. Thus the lower controller verbal workload in the sequencing condition is not reflected in a higher verbal workload for the pilot. This finding is essentially the same as in a previous experiment.(1)

The effect of a mixed traffic information environment however is surprising. The verbal workloads for both controllers and pilots being

vectored in the mixed control environment was markedly higher than when the environment was not so mixed. This may be caused by an increased difficulty in vectoring A/C around in a space also being used in a "VFR" mode by other pilots. It might also simply reflect the increased time the controller has when some of the A/C do not need vectoring causing him to increase his communication with the remaining A/C. Analyses to determine the pertinence of this increased communication is being pursued.

In practice, this finding might suggest a necessity to segregate TSD and NonTSD equipped A/C handling each group separately on a "VFR", "IFR" basis.

3. Subjective Measures

A. Questionnaire Results

Subjects filled out evaluation sheets after each run and a final questionnaire at the conclusion of all of their runs. Figure 7 summarizes some of the averaged results obtained. Subjects were asked to indicate their assessments by placing tic-marks on an ungraduated line. Thus placement of a mark indicates not only relative ordering but strength of the assessment as well.

The overall preference for the two main conditions is shown by System Evaluation on the final questionnaire. As in a previous experiment,[1] controllers preferred vectoring to nonvectoring while pilots preferred the nonvectoring (i.e. mixed) environment even through they had experienced both TSD flights and nonTSD flights (in which they were vectored). The strengths of the two choices were essentially identical for pilots and controllers.

The pilots also felt that the nonvectoring condition was safer than vectoring although again controllers had the reverse opinion. However, a more detailed analysis obtained after each run shows that controllers felt the nonvectoring condition to be slightly safer than vectoring. The pilots judged the TSD (nonvectored) flights as most safe and the vectored flights in the nonvectoring environment (NT) as least safe, even compared to being vectored in an all vector environment.

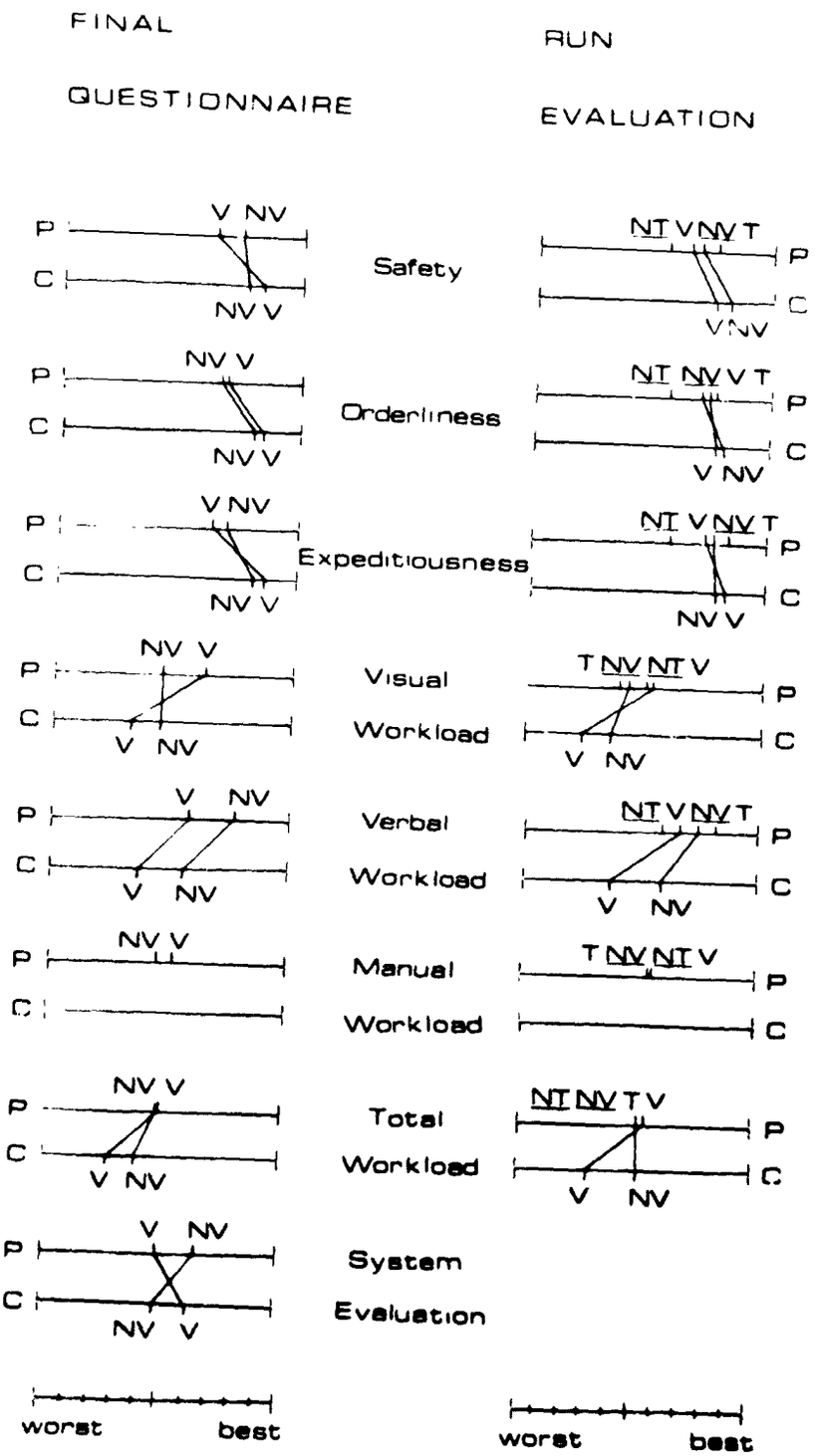

Figure 7 Pilot and Controller Averaged Responses to Questions After each Run and After the Experiment. The Final Questionnaire Compares the Two Basic Conditions. The Run Evaluation Separates TSD (T) from NonTSD (NT) Flights in the NV Condition.

In fact, pilots rated the vectored flights in a mixed environment (NT) lowest on the three primary FAA Criteria of Safety, Orderliness and expeditiousness. The fact that NTSD received lowest marks on these subjective evaluations, on the verbal measures (subjective and objective) and on many of the objective measures is a very strong finding.

Pilots felt the total workload to be essentially the same regardless of the condition (V, NV) or the type of flight made within the NV condition. Controllers quite clearly ranked the vectoring condition as having a higher (worst) verbal and total workload whether assessed after each run or in retrospect at the end of the experiment. Pilots and controllers also clearly assessed the vectoring condition as requiring a higher verbal workload.

B. Conclusions from Subjective Measures

A fairly consistent theme is that even though pilots preferred the nonvectoring condition to vectoring on the whole, they least liked being vectored in an environment where others were flying VFR. Pilots quite consistently preferred flying VFR (even in the mixed condition) to being vectored. Controllers, acknowledged that the nonvectoring condition as a whole had a lower workload and did not necessarily express any large difference between the two conditions on the three primary FAA criteria. However, in an encompassing evaluation, controllers preferred to operate in the wholly vectoring environment.

The above remarks are quite in keeping with a previous experiment particularly as to pilot-controller system preferences. Pilots want to fly VFR after a sequence order is established and controllers want a strong ground centralized system regardless of the workload decrease possible in a distributed management mode of control.

CONCLUSIONS

The conclusions offered are based on the objective, verbal and subjective analyses presented aboved. In considering the reality of an environment in which some A/C have TSD while others don't, it should be remembered that this situation was predicated on two possibilities, the first could be the failure of an onboard TSD in a homogeneous TSD environment while the second follows the simple realization that such a mixed environment could be quite natural based on the cost of TSD equipment.

The analyses support the primary conclusion that the mixed environment simulated can be managed effectively on a distributed management basis in which those A/C with TSD are given initial sequence orderings and then fly "VFR" while the I/C without TSD are vectored and speed controlled.

Since this mixed condition as a whole produced results at least as good as the all vectoring one (and in many cases better) it does not appear that a TSD failure on the insertion of nonTSD equipped A/C into TSD traffic has any real disruptive effect. (Of course neither one of these possibilities is necessarily advocated.)

The TSD equipped A/C operating under distributed management (controllers issue sequence, pilots fly "VFR") achieved generally better results than when they were vectored. For example, verbal communication workload was considerably lower, intercrossing spacing was closer to the desired valve with less variability, etc., and this mode of control had clear pilot acceptance.

However, the nonTSD equipped A/C in the mixed environment required more verbal communication than in an all-vector environment, generally achieved lowest performance scores and was least well accepted by pilots even though from the pilots' point of view he was vectored as in the all-vector condition. This may indicate a lack of assurance by the pilot on being IFR in a VFR-IFR environment without knowledge of where other traffic is. From the controller's viewpoint, the increased verbal communication to the nonTSD A/C in the mixed environment may reflect some increased difficulty in vectoring an A/C among others flying VFR.

In the context of the present experiment, spatially segregating the TSD from the nonTSD A/C and using distributed management for TSD and vectoring for nonTSD should form the basis for a considerably better overall system than either a mixed or all-vector one.

The generally better results with distributed management for TSD in comparison to vectoring is fully in keeping with previous experiments at Ames Research Center.

ACKNOWLEDGEMENT

Funds for the support of this work have been allocated by the NASA-Ames Research Center, Moffett Field, California. under Interchange No. NCA2-OR785-501.

This support is very gratefully acknowledged as is the outstanding programming support provided by Mr. Ronald Schmeckley of PMI.

REFERENCES

1. Kreifeldt, J.G., Wempe, T.E., "Human Decision Making in Future ATC Systems - Comparative Studies in Distributed Traffic Management." Proc. IEEE International Conference on Systems, Man and Cybernetics, Dallas, Texas, October 2-4, 1974.

2. Kreifeldt, J.G., Wempe, T.E., "Future Terminal Air Traffic Management Concepts." Proc. 10th Annual Conference on Manual Control AEIT. AFFDL. April 9-11, 1974.

3. Connelly, M., "The Role of the Airborne Traffic Situation Display in Future ATC Systems." IEEE Transactions on Communications, May 1973.

4. Kreifeldt, J.G., Pardo, B., Wempe, T.E., Huff, E., "Verbal Workload in Distributed Air Traffic Management." Proc. 11th Annual Conference on Manual Control. NASA TMX-62,464, May 1975.

5. Kreifeldt, J.G., Parkin, L., Rothschild, P., The Effects of Heterogeneous Traffic Information Displays on Distributed Air Traffic Management - Final Report. NCA2-OR785-501. In preparation.

6. Cooley, W., Lohnes, P., Multivariate Data Analysis. John Wiley and Sons, 1971.

7. Pardo, B.G., Effects on Verbal Communication and Task Variables of Different Air Traffic Control Configurations. Unpublished Master's Thesis, San Jose State University, San Jose, CA 1974.

INVESTIGATING THE USE OF A MOVING MAP DISPLAY AND A HORIZONTAL SITUATION INDICATOR IN SIMULATED POWERED-LIFT SHORT-HAUL OPERATIONS*

By Warren F. Clement

Systems Technology, Inc., Hawthorne, California

SUMMARY

The purpose of this research-in-progress is to investigate the use which pilots make of a moving map display from enroute through the terminal area and including the approach and go-around flight phases. Various features of each of the primary STOLAND† displays, the electronic moving map Multifunction Display (MFD), Horizontal Situation Indicator (HSI), and Electronic Attitude Director Indicator (EADI), are used in the three phases of flight mentioned above when the STOLAND system is operated in each of three ways: a) flown in the fully automatic mode with the pilot(s) in a monitoring role; b) flown manually using flight director guidance to reduce workload and task requirements in an acceptable level; or c) flown manually using raw instrument situation data. Eye-point-of-regard and workload measurements, coupled with task performance measurements, pilot opinion ratings, and pilot comments are presented. The experimental program was designed to determine the pilots' use of the MFD in conjunction with the other displays. The measurements, ratings, and comments provide an indication of the utility of the MFD as a supplement to the HSI for improving flight safety in following curved courses and holding patterns.

INTRODUCTION

This research is designed to provide for a systematic comparison of an electronic Multifunction Display (MFD) and an electromechanical Horizontal Situation Indicator (HSI) in conjunction with other instruments (EASI, altimeter, airspeed indicator, etc.) in the NASA/Ames Research Center STOLAND digital avionics system for guidance and control of powered-lift short-haul aircraft. This research forms one part of the joint DOT/NASA STOL Operating Systems Experiments Program.

---

*This paper is based on work done for the Aircraft Guidance and Navigation Branch, Flight Systems Research Division, Ames Research Center, under Contract NAS2-8973.

†A versatile digital navigation, guidance, and control system developed by Ames Research Center for conducting experiments with advanced STOL aircraft.

The objective of the joint DOT/NASA STOL Operating System Experiments Program is to provide data to aid the design of terminal area guidance, navigation and control systems and the definition of operational procedures for powered-lift and light wing loading short-haul aircraft under IFR. As a first step in this program experimental digital automatic and flight director guidance and control systems have been developed for the NASA Augmentor Wing powered-lift short-haul aircraft by Sperry Flight Systems (under NASA contract). This system, called STOLAND, is based on the application of current CTOL system techniques and displays to the experimental short-haul aircraft (Ref. 1).

Two of the primary displays used in the system are an Electronic Attitude Director Indicator (EADI) and a standard Horizontal Situation Indicator (HSI). In addition, this digital system has a computer driven, cathode ray display called the Multifunction Display, or MFD, which displays the aircraft position and predicted motion on a moving map of the area. Also displayed are other status data including heading, altitude, raw navaid data and reference flight paths. Annotated illustrations of each of the primary displays are shown in Figs. 1-3, and a view of the pilot's instrument panel in the STOLAND simulator used for this investigation is shown in Fig. 4.

This paper presents a preliminary review of some of the comparative measurements and pilot opinions from a flight simulation in February and March 1976. The experimental program for comparing the MFD and HSI within the context of the whole cockpit will be summarized first. Then, after presenting some of the key results, we shall recapitulate our tentative findings in the concluding section of this paper.

EXPERIMENTAL PROGRAM

The experimental investigation was conducted on the NASA/Ames fixed-base STOLAND simulation facility. This facility includes: a) a fully instrumented cockpit; b) a six-degree-of-freedom C-8A Augmentor Wing Jet STOL Research Aircraft/environment/navigation simulation program implemented on an EAI 8400 digital computer; and c) a complete STOLAND digital avionics system.

If the display content has been suited to the task, the display format and symbology will usually be crucial only if the pilot is at a saturated level of workload in a realistic flight simulation or in actual flight. Consequently, we attempted to emphasize the realistic air route navigation, guidance and control environment for short-haul aircraft in preparing the experimental design summarized in Table 1. Three classes of independent variables are shown in the table. The level of pilot involvement in guidance and control tasks is divided between two independent classes, one of which we have called "technique," i.e., either manual or automatic, and the other of which we have called "the level of display," i.e., either situation (raw data only) or flight director and situation on the EADI with the HSI and MFD the obvious independent display variables for comparison.

The flight phases of interest in this experiment were fourfold: a) enroute within 56 km (30 nm) of Crows Landing, ALF, Colusa County, California; b) the

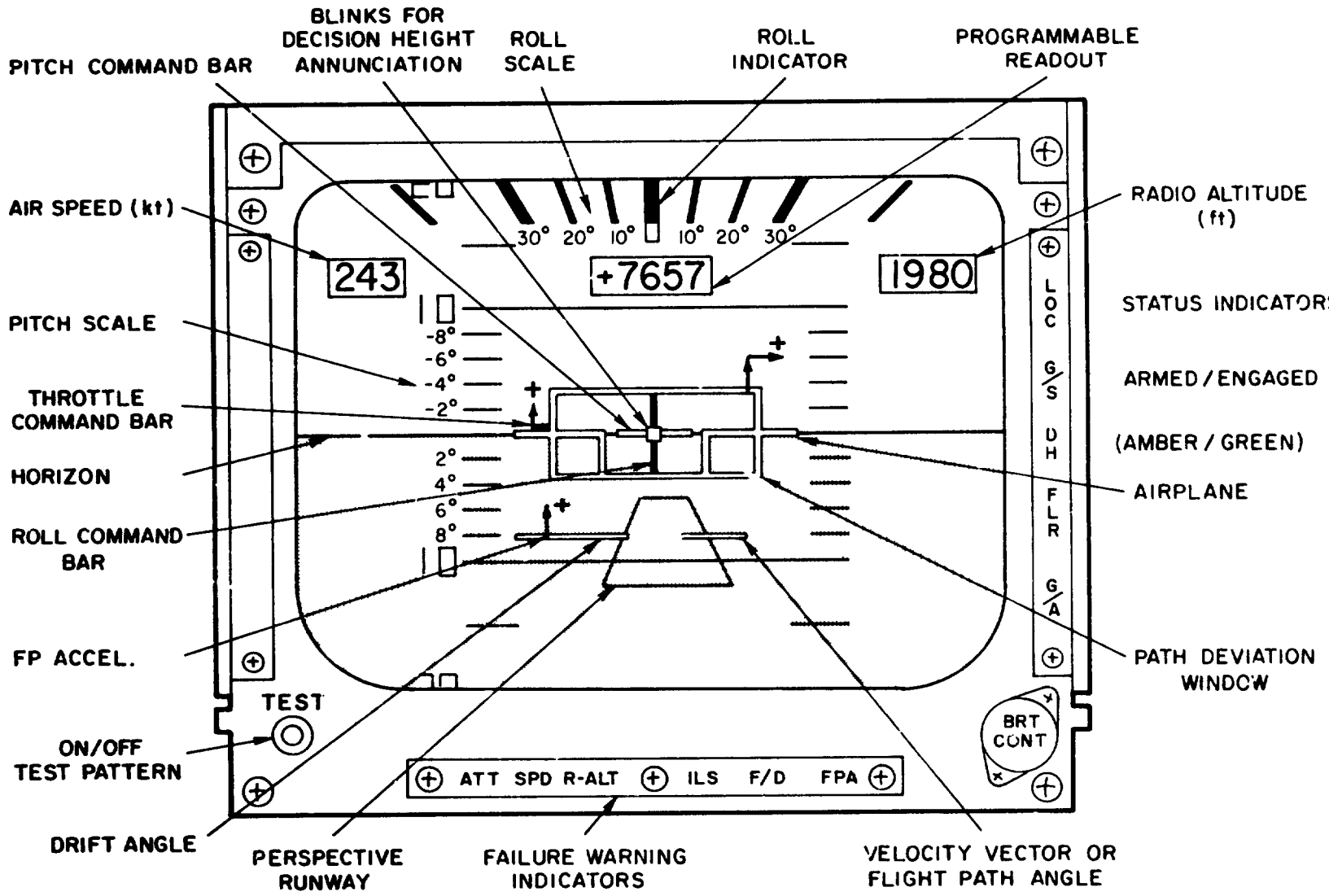

Figure 1. Electronic Attitude Director Indicator (EADI)

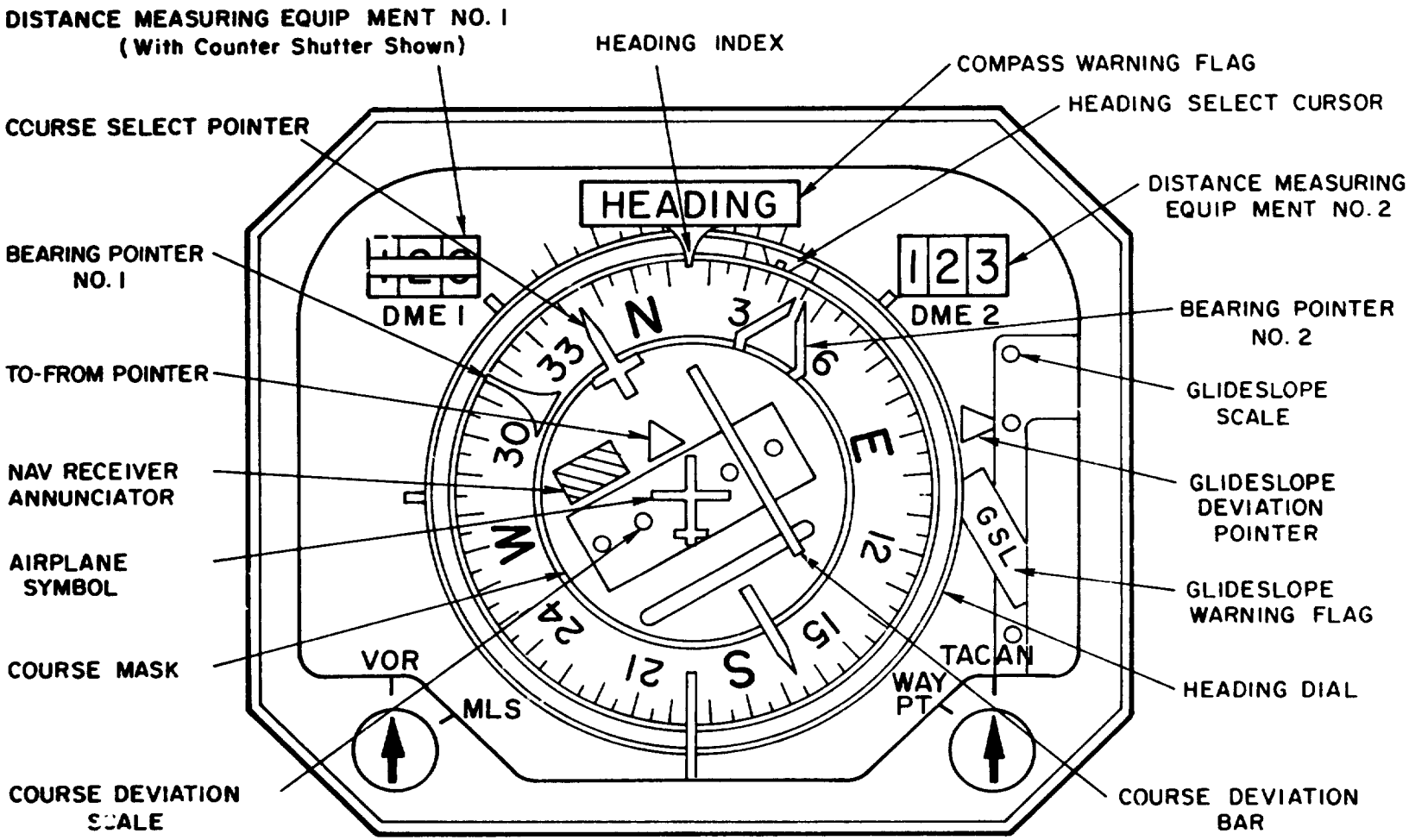

Figure 2. Horizontal Situation Indicator (HSI)

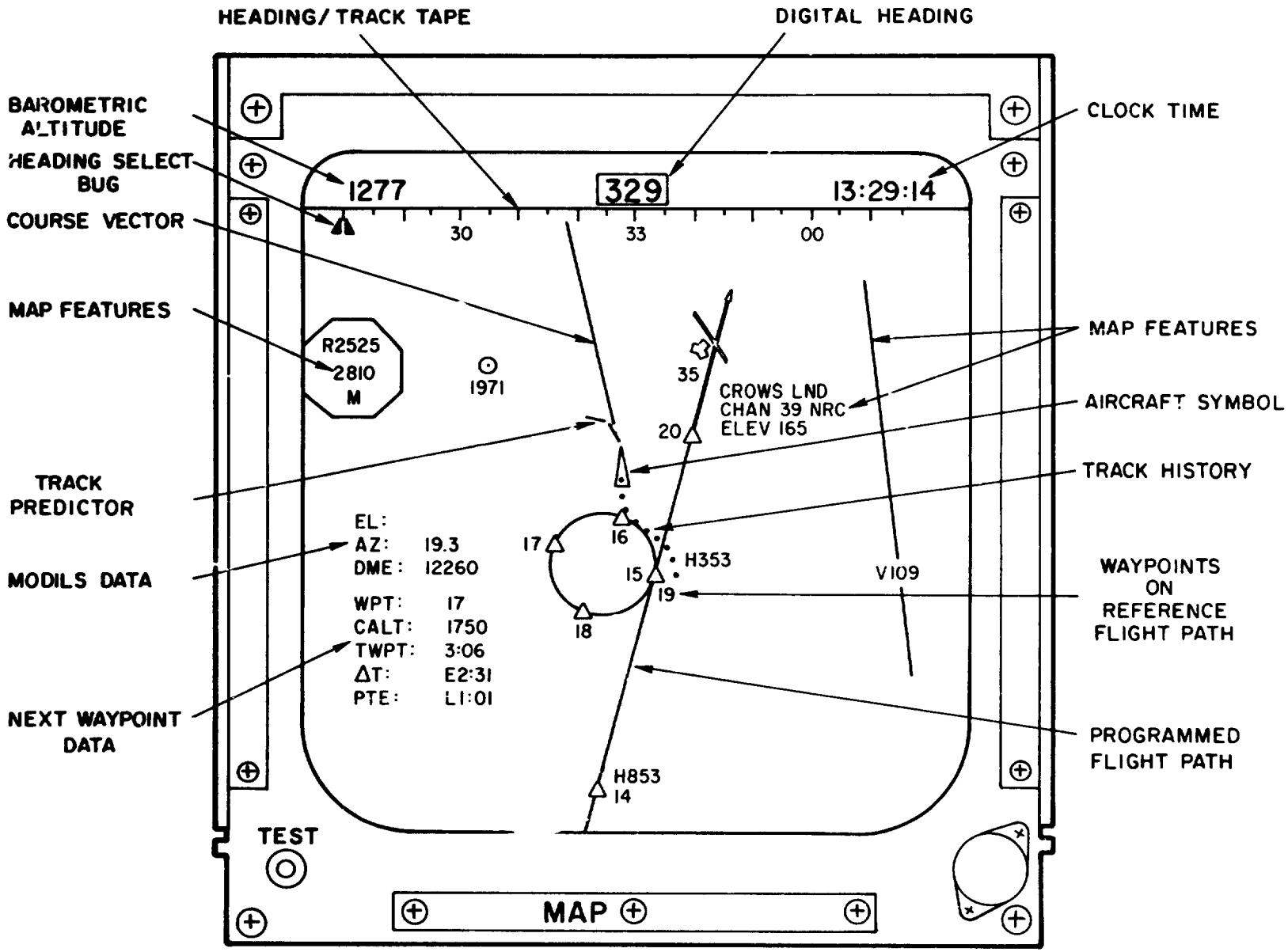

Figure 3. Multifunction Display (MFD)

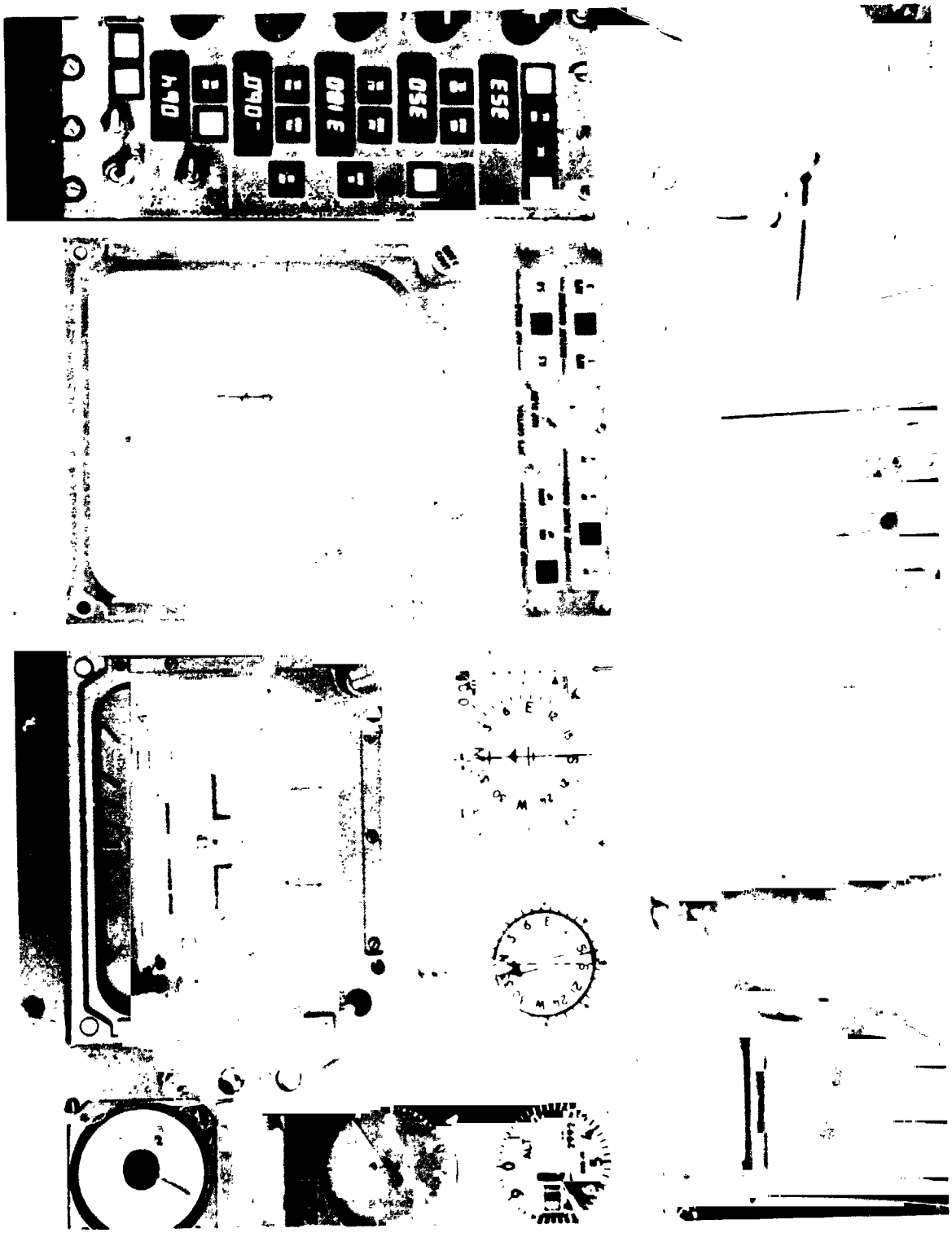

Figure 4. STOLAND Simulator Instrument Panel

TABLE 1. SUMMARY OF EXPERIMENTAL DESIGN

PILOTING TECHNIQUE	NAVIGATION AND CONTROL WORKLOAD	LEVEL OF DISPLAY				
		SITUATION (RAW DATA)		FLIGHT DIRECTOR AND SITUATION ON EADI		
		HSI	MFD	HSI	MFD	BOTH HSI AND MFD
Manual	Tracking a STAR sequence	✓XSCC* Highest Workload	✓ XSCC*	✓	✓	✓ EPR†
	Select different radio navaids enroute for STOLAND and maintain geographic orientation	✓	✓	✓	✓	✓ EPR†
Automatic	Tracking a STAR sequence				Lowest Workload	

10 cells × 2 replications × 5 pilots = 100 runs

*XSCC ≡ Measurement of excess control capacity with cross-coupled secondary control task

†EPR ≡ Measurement of eye-point-of-regard

Dependent Variables (i.e., Measurements

a. Flight plan performance errors:
   - Airspeed error with respect to commanded flight profile
   - Lateral distance error with respect to commanded course
   - Altitude or glide slope displacement error
   - Elapsed time between waypoints in flight plan

b. Other aircraft motion and control variables (e.g., pitch and roll attitudes, pitch and roll rates, heading, turn rate, airspeed, inertial velocity, angles of attack and sideslip, course and path angles [or ground and vertical velocities], translational accelerations]

c. Eye-point-of-regard in azimuth and elevation

d. Subjective display ratings (e.g., controllability-and-precision, status utility, clutter, attentional demand)

e. Excess control capacity

f. Caution advisory response latency (from a light-cancelling task designed to measure the pilot's simple reaction time)

terminal area itself; c) the landing approach; and d) the go-around involving a holding pattern after a missed approach. We included the four flight phases within a class of independent variables representing the level of pilot involvement in air navigation tasks, i.e., whether the pilot is just following a standard terminal arrival route (STAR) assigned initially by a controller or whether the pilot is additionally involved in reselecting radio navaids enroute for STOLAND, both during arrival and after executing a missed approach.

While using the automatic mode of STOLAND during initial training sessions, we discovered that automatic operation is so devoid of pilot workload that a critical comparison of the HSI and MFD cannot be made, because the pilot is not even saturated with monitoring tasks. Therefore, we refocused the experimental design on only the manual piloting technique and deferred investigation of the automatic technique.

We have indicated in Table 1 the cells in the experimental design which were most relevant by check marks. We have also indicated the cells which involved the highest and lowest workloads and the two cells which were most amenable to eye-point-of-regard comparison.

Pilot workload is high to begin with when flying the C-8A Augmentor Wing manually with combinations of powered and aerodynamic lift. Since the several STAR's involved holding patterns and curved paths as well as straight segments, reliance on the HSI (and EADI) without the MFD placed the highest workload demand on the pilot, because he had to keep track of his position mentally with the aid of his enroute and terminal area charts as he progressed along the assigned STAR, reselected radio navaids, and executed missed approaches, go-arounds and holding patterns.

Since the pilot will scan to and fixate on instruments which display redundant information, there is a danger in presenting both the HSI and MFD when the pilot is required to fly with only raw situation data. Having both horizontal displays may actually increase his scanning workload unnaturally when he is already saturated or oversaturated. Therefore, we covered the horizontal display which was not being evaluated in eight cells of Table 1, because the pilot will scan to instruments which display no information or which are temporarily inactive, if given the opportunity. However, both the HSI and MFD were uncovered and presented to the pilot simultaneously in the two cells in the extreme right column of Table 1 when the pilot was using the flight director and situation on the EADI to fly manually. We expected that any outstanding bias in the partitioning of the eye-point-of-regard distribution between the HSI and MFD might afford a measure of pilot preference for or confidence in monitoring the horizontal situation.

The displacement "window" on the EADI was deleted when runs were made to test the HSI alone, since the HSI presents lateral and vertical deviation anyway. The displacement scaling of one "half-window" on the EADI was consistent with the displacement scaling of one dot on the HSI, viz., 381 m (1250 ft) laterally and 30.48 m (100 ft) vertically.

In this connection, we should emphasize that the content of the MFD and HSI are not strictly equivalent, because no waypoint numbers appear on the HSI

and no heading scale appears on the MFD, if the pilot elects the north-up orientation. Furthermore, the format of the altitude presentation on the MFD is purely numerical, and is more unsuitable for tracking than even the counter-pointer altimeter, let alone the vertical deviation indicator (VDI) on the HSI. However, it is as unconventional for the pilots to use the VDI anywhere except on the glide slope as it is to use the displacement "window" on the EADI. Therefore, we may, insofar as the tracking control aspects of this experiment are concerned, be comparing the EADI (supported by the MFD) with the HSI (supported by the EADI without displacement information). Notwithstanding, insofar as the geographic orientation aspects of the experiment are concerned, we are comparing the HSI [supported by an area navigation (RNAV) chart and approach plate] with the MFD, which presents a horizontal moving map of the same RNAV and approach chart.

Heading was provided on the EADI's programmable display during the experiment. We recommended to each pilot that the MFD be used in the course- or heading-up orientation for consistency with the HSI and because the heading tape on the MFD appears only when the course- or heading-up orientation is selected. However, the RMI was always available to present a compass rose when the HSI was covered in the event that a pilot elected to keep the MFD north-up because he experienced disorientation with the revolving map display in turns. The choice of map scale on the MFD was left to the pilot; however, he was instructed that the STAR waypoint numbers would appear only if the 1.5 or 0.5 mn/in. scales were selected.

A steady wind speed of 20 kt from the east or west as required by the flight plan to produce a prevailing tailwind enroute was used throughout the experiment to increase workload, and the wind velocity dispersion was between 3 and 4 ft/sec.

Also listed in Table 1 is the minimum number of 100 runs required for two replications of 10 cells counterbalanced for order effects with 5 pilots. (Over 160 runs were made.) Pilots 1 and 6 are research pilots; Pilots 3 and 4 are commercial airline pilots; Pilot 5 is a general aviation instrument instructor and engineering pilot; and Pilot 2 remained on reserve for this experiment and did not have to participate.

Below the table of independent variables and cells there appears a list summarizing the dependent variables, that is, the measurements which we made. All measurements are self-evident except perhaps "excess control capacity" which is proportional to the value of the spiral divergence required to load the pilot to the point of saturation with control tasks while satisfying primary task performance with respect to a norm or error criterion. Excess control capacity is measured by increasing the spiral divergence until a stationary value is reached by the cross-coupled adaptive regulator of the divergence in balance with the performance error criterion. The regulated average or stationary value of the spiral divergence may be normalized by its critical limit of controllability for each pilot to form a fraction which represents his excess control capacity with respect to the primary task (Ref. 2). To the pilot flying the aircraft the increased spiral divergence seems like a malfunction in lateral stability augmentation, so the measurement can be made while the flight simulation retains high face validity.

Four simple pilot rating scales for use in research on and evaluation of manual control displays were derived and used in the pilot experiments reported in Ref. 3 and were well-suited to the present investigation. The scales shown later in Table 6 are of interval-scale quality and will permit averaging and other standard parametric statistical analyses. The use of four trait categories (task controllability and precision, status utility, clutter, and attentional demand) helped to separate subjective identification of these often confounded effects. Rating forms for the HSI and MFD were filled out by each pilot in the cockpit at the conclusion of a simulated flight.

RESULTS OF THE EXPERIMENT

Although we shall continue to label the displays being compared as "HSI" and "MFD" for conciseness in presenting the results where one or the other horizontal display was uncovered, the reader should clearly understand that "HSI" means "HSI, EADI (without the displacement window) and other instruments" and that "MFD" means "EADI, MFD and other instruments." By design, the HSI and MFD are being compared within the context of the whole STOLAND display and control arrangement in the simulator cockpit.

We shall now turn to present the several forms of comparative results of the experiment under the following subordinate topical headings:

- Blunders
- Tracking errors
- Excess control capacity
- Excess monitoring capacity
- Pilot opinion ratings
- Eye-point-of-regard

Blunders

About 160 simulated flights, each lasting from 10 to 25 minutes in time, were conducted among four standard terminal arrival routes (STAR's). The most dramatic results are the 20 "blunders" partitioned in Tables 2 and 3. Table 2 partitions the 9 blunders which occurred in the first phase of the experiment in February while the pilots were primarily tracking STAR's as reference flight paths. Table 3 partitions the remaining 11 blunders which occurred during terminal area and enroute flight with emphasis on geographic orientation (as well as tracking) in the second phase of the experiment in March involving missed approaches, go-arounds and holding patterns with three different radio navaids. The types of blunders identified include loss of geographic orientation, loss of altitude awareness, and loss of roll attitude control as well as several others.

Five blunders involved the HSI and 4 the MFD, while tracking reference flight paths exclusively (Table 2). However, 8 blunders involved the HSI, 2 the MFD, and 1 both displays, during terminal area and enroute flight with emphasis on geographic orientation (Table 3). The flight director was (or should have been) in use during 11 of the 20 runs wherein blunders occurred. Since 7 of these 11 blunders were also associated with the HSI in Table 3, the combination of using the HSI for orientation with the flight director for tracking while selecting different radio navaids for guidance seemed to conspire to produce the most blunders. There were no blunders involving the MFD and flight director in Table 3 and only three in Table 2. Therefore, we would conclude

TABLE 2

DISTRIBUTION OF BLUNDERS WHILE TRACKING REFERENCE FLIGHT PATHS

BLUNDERS	RAW DATA		FLIGHT DIRECTOR	
	HSI	MFD	HSI	MFD
Loss of geographic orientation	2	None	None	None
Loss of altitude awareness	1	None	None	1
Loss of roll attitude control	1	1	None	2
Other crashes	1 GPIP[a]	None	None	None

[a]Glide path intercept point

TABLE 3

DISTRIBUTIONS OF BLUNDERS DURING TERMINAL AREA AND ENROUTE FLIGHT WITH EMPHASIS ON GEOGRAPHIC ORIENTATION

BLUNDERS	RAW DATA		FLIGHT DIRECTOR[b]	BOTH HSI AND MFD WITH FD
	HSI	MFD	HSI	
Loss of geographic orientation	None	None	3	None
Loss of altitude awareness	None	2 (Crash and missed capture)	1	None
Loss of roll attitude control	None	None	2	1
"Copilot error"	None	None	1	None
Experimenter's error	1	None	None	None

[b]There were none with MFD and Flight Director.

on the basis of the blunder distribution alone from the simulation that the MFD seems to offer a worthwhile improvement in safety, since 13 of 20 blunders involved runs wherein the MFD was not available to the pilot

Tracking Errors

The least dramatic results are to be found among the flight plan tracking errors in three dimensions (lateral and vertical displacement and airspeed) and the related variations in aircraft motions. As one would expect, the flight director provided for more precise tracking of the assigned altitude and the glide slope than otherwise. However, there was no consistent evidence of differences between tracking errors with the HSI versus the MFD even with only raw data. Yet, as we mentioned in beginning the discussion of results, the "MFD" implies the use of the integrated EADI as the tracking display, and occasionally better altitude-keeping performance appeared with the "MFD" than with the "HSI."

Excess Control Capacity

The measurement of excess control capacity was provided by the average cross-coupled adaptive spiral divergence in selected runs with either the HSI or the MFD. The null hypothesis of equality between mean values of excess control capacity within comparable pairs of waypoint groups with either display arrangement was tested for significant differences. The results of these tests are listed in Table 4 by pilot and flight plan. The column heading "neither"

TABLE 4

NUMBER OF COMPARABLE PAIRS OF WAYPOINT GROUPS FOR WHICH ONE OR THE OTHER DISPLAY ARRANGEMENT EXHIBITED SIGNIFICANTLY GREATER AVERAGE EXCESS CONTROL CAPACITY AT THE 0.05 LEVEL[a]

PILOT	FLIGHT PLAN	HSI/EADI	NEITHER	EADI/MFD
1	2	1	4	1
3	2	3	4	1
3	3	1	1	4
4	2	5	1	6
5	2	1	1	4
Totals		11	11	16

[a]The null hypothesis is "neither." The probability of rejecting the null hypothesis when it is true is 0.05. Behrens', Scheffe's, and Tukey's tests produced consistent results.

identifies the number of comparable pairs of waypoint groups for which the null hypothesis was accepted. The probability of rejecting the null hypothesis when it is true is 0.05. Behrens', Scheffe's, and Tukey's tests produced consistent results under the ergodic hypothesis, because the number of samples available within each waypoint group was on the order of several hundred or more.

The column headings "HSI" or "MFD" identify the numbers of comparable pairs of waypoint groups for which the null hypothesis was rejected, i.e., for which one or the other display arrangement exhibited significantly greater average excess control capacity at the 0.05 level. The totals show that the null hypothesis was rejected for 27 of 38 pairs at the 0.05 level. Of these 27 pairs, the "MFD" exhibited greater average excess control capacity for 16, and the "HSI" greater for 11 pairs. In the individual case of Pilot 3 tracking Flight Plan 2 involving only a curved approach, the partition is in favor of the "HSI," a result which was consistent with that pilot's own appraisal of that flight plan. However, the partition for Pilot 3 with Flight Plan 3, involving a missed approach and holding pattern is in favor of the MFD.

Excess Monitoring Capacity

The measurement of excess monitoring capacity was inversely proportional to the average caution advisory response time. The null hypothesis of equality between mean response times within comparable pairs of runs with either display arrangement was tested for significant differences after a correction for the skewness of the response time distribution was made. The results of these tests are listed in Table 5 by pilot. The column heading "neither" identifies

TABLE 5

NUMBER OF COMPARABLE PAIRS OF RUNS FOR WHICH ONE OR THE OTHER DISPLAY ARRANGEMENT EXHIBITED SIGNIFICANTLY GREATER AVERAGE EXCESS MONITORING CAPACITY AT THE 0.05 LEVEL[a]

PILOT	HSI/EADI	NEITHER	EADI/MFD
1	1	4	1
3	0	7	2
4	0	9	2
5	1	4	1
6	1	1	4
Totals	3	25	10

[a]The null hypothesis is "neither." The probability of rejecting the null hypothesis when it is true is 0.05. Behrens', Scheffe's, and Tukey's tests produced consistent results.

the number of comparable pairs of runs for which the null hypothesis was accepted. The probability of rejecting the null hypothesis when it is true is 0.05. Again Behrens', Scheffe's, and Tukey's tests produced consistent results, because there were usually at least eleven samples in the ensemble for each run. The column headings "HSI" or "MFD" identify the numbers of comparable pairs of runs for which the null hypothesis was rejected, i.e., for which one or the other display arrangement exhibited significantly greater average excess monitoring capacity at the 0.05 level. The totals show that the null hypothesis was rejected for 13 of 38 pairs at the 0.05 level. Of these 13 pairs, the "MFD" exhibited greater average excess control capacity for 10, and the "HSI" greater for 3 pairs.

Pilot Opinion Ratings

Tables 6a and 6b present summaries of the subjective opinion ratings of the HSI and MFD by each of Pilots 1, 3, 4, and 6 during the second phase of the experiment in March emphasizing geographic orientation as well as tracking. A comparison of Tables 6a and 6b shows a slightly less favorable central tendency in the ratings of the task controllability and precision when using the HSI, whereas the ratings are more uniformly distributed over four descriptive phrases when using the MFD. Ratings of task controllability and precision with the flight director in use are uniformly distributed over four descriptive phrases when using either the HSI or MFD. Comparison of the ratings for utility of status information between the HSI and MFD shows more favorable ratings for the MFD and a markedly unfavorably skewed distribution of ratings for the HSI which exhibits a mode beside the descriptive phrases: (S4) "inadequate number of states...." Comparison of the ratings for clutter shows few differences in the tendency of both groups of ratings to centralize beside the descriptive phrase: (K3) "some clutter." Only one rating of the MFD was more unfavorable than K3. Comparison of the ratings for display attentional workload shows a more favorable central tendency beside the descriptive phrase: (D3) "mildly demanding" for the MFD, whereas the distribution of ratings for the HSI is unfavorably skewed with a mode beside the descriptive phrase: (D4) "quite demanding."

During the tracking of reference flight paths in the first phase of the experiment in February, slightly different central tendencies in some of the ratings by Pilots 3, 4, and 5 were observed. For example, the ratings for utility of status information on the HSI were bimodally distributed between (S2) "many of desired states presented" and (S4) "inadequate number of states." The rationale was apparent from the accompanying commentary, viz., that the HSI is quite adequate for tracking rectilinear courses whether inclined or not, whereas the HSI is deficient for tracking curved courses in the presence of wind. Ratings of the utility of status information on the MFD were skewed favorably with a mode beside S2. A few more "quite cluttered" (K4) ratings of the MFD were received, although the central tendency on both HSI and MFD remained beside K3. Ratings of attentional workload while tracking with either HSI or MFD were centered on (S4) "quite demanding," although relatively more (D5) "completely demanding" ratings of the HSI were given.

TABLE 6a

SUMMARY OF 3 RATINGS OF HSI BY EACH OF PILOTS 1, 3, 4, 6 DURING SECOND PHASE OF EXPERIMENT EMPHASIZING GEOGRAPHIC ORIENTATION

PILOT OPINION RATING SCALES

RATING SCALE FOR UTILITY OF STATUS INFORMATION

CRITERIA	DESCRIPTIVE PHRASE	RATING	
Usefulness[a] of the information supplied, on the specified display unit, on the vehicle status — especially the relevant flight path vector states, such as: altitude, speed, heading attitude, path error, etc.	All desired states presented with adequate resolution and readability	S1	
	Many of desired states presented, with a few deficiencies in scaling, resolution, or readability	S2	///
	Some desired states presented, and/or some problems with scaling, resolution, or readability	S3	///
	Inadequate number of states, or serious deficiencies in scaling, resolution, or readability	S4	//////
	No direct status information or unusable	S5	

[a]Useful with respect to the mission phase, task criteria, and operator's sense of vehicle safety.

RATING SCALE FOR CLUTTER

CRITERIA	DESCRIPTIVE PHRASE	RATING	
Degree of subjective symbol-background clutter on specified display unit	Completely uncluttered — e.g., only one pair of elements	K1	
	Mostly uncluttered — no confusing or distracting elements	K2	///
	Some clutter — multiple elements competing for attention	K3	//////////
	Quite cluttered — difficult to keep track of desired quantities among competitors	K4	
	Completely cluttered — nearly impossible to tell desired elements or quantities due to competing elements	K5	

RATING SCALE FOR TASK CONTROLLABILITY AND PRECISION

CATEGORY		DESCRIPTIVE PHRASE	RATING	
CONTROLLABLE	PRECISE			
Yes	Yes	Very easy to control, with good precision	C1	
		Easy to control, with fair precision	C2	ⓕ *
	No	Controllable, with inadequate precision	C3	ⓓⓓⓓⓓⓓ
		Marginally controllable	C4	ⓓⓓⓓ
No		Uncontrollable	C5	

* Controllable with difficulty or high workload, but fair precision * C2.5 ⓓⓕ

RATING SCALE FOR DISPLAY ATTENTIONAL WORKLOAD

CRITERIA	DESCRIPTIVE PHRASE	RATING	
Demands on the operator attention, skill, or effort	Completely undemanding and relaxed	D1	
	Mostly undemanding	D2	/
	Mildly demanding	D3	//
	Quite demanding	D4	/////
	Completely demanding	D5	////

ⓓ = Raw data. ⓕ = Flight director and situation.

TABLE 6b

SUMMARY OF 3 RATINGS OF MFD BY EACH OF PILOTS 1, 3, 4, 6 DURING SECOND PHASE OF EXPERIMENT EMPHASIZING GEOGRAPHIC ORIENTATION

PILOT OPINION RATING SCALES

RATING SCALE FOR UTILITY OF STATUS INFORMATION

CRITERIA	DESCRIPTIVE PHRASE	RATING	
Usefulness* of the information supplied, on the specified display unit, on the vehicle status — especially the relevant flight path vector states, such as: altitude, speed, heading attitude, path error, etc.	All desired states presented with adequate resolution and readability	S1	
	Many of desired states presented, with a few deficiencies in scaling, resolution, or readability	S2	ⓅⓅⓅⓅⓅ
	Some desired states presented, and/or some problems with scaling, resolution, or readability	S3	ⓅⓅⓅⓅⓅⓅⓅ
	Inadequate number of states, or serious deficiencies in scaling, resolution, or readability	S4	
	No direct status information or unusable	S5	

*Useful with respect to the mission phase, task criteria, and operator's sense of vehicle safety.

RATING SCALE FOR CLUTTER

CRITERIA	DESCRIPTIVE PHRASE	RATING	
Degree of subjective symbol-background clutter on specified display unit	Completely uncluttered — e.g., only one pair of elements	K1	
	Mostly uncluttered — no confusing or distracting elements	K2	Ⓟⓟ
	Some clutter — multiple element competing for attention	K3	ⓅⓅⓅⓅⓅⓅⓅⓅⓅ
	Quite cluttered — difficult to keep track of desired quantities among competitors	K4	Ⓟ
	Completely cluttered — nearly impossible to tell desired elements or quantities due to competing elements	K5	

RATING SCALE FOR TASK CONTROLLABILITY AND PRECISION

CATEGORY		DESCRIPTIVE PHRASE	RATING	
CONTROLLABLE	PRECISE			
Yes	Yes	Very easy to control, with good precision	C1	
		Easy to control, with fair precision	C2	ⓈⓄⓇ
				*
	No	Controllable, with inadequate precision	C3	ⓈⓄⓇ
		Marginally controllable	C4	ⓈⓄⓇ
No		Uncontrollable	C5	

* Controllable with difficulty or high workload, but fair precision * C2.5 ⓈⓄⓇ

RATING SCALE FOR DISPLAY ATTENTIONAL WORKLOAD

CRITERIA	DESCRIPTIVE PHRASE	RATING	
Demands on the operator attention, skill, or effort	Completely undemanding and relaxed	D1	
	Mostly undemanding	D2	Ⓟ
	Mildly demanding	D3	ⓅⓅⓅⓅⓅⓅⓅ
	Quite demanding	D4	ⓅⓅ
	Completely demanding	D5	ⓅⓅ

Ⓡ = Raw data. Ⓢ = Flight director and situation.

Eye-Point-of-Regard (EPR)

This experiment has resulted in the acquisition of our largest archive of high quality data to date with the STI Eye-Point-of-Regard System Model EPR-2. However, it will be possible to review only a small sample of the EPR data here. The EPR data acquisition was confined to runs wherein both HSI and MFD (as well as all other active displays and controls in the cockpit) were available to the pilot in accord with the experimental plan in Table 1. The reduced data to be presented are from the go-around phase of four runs by two pilots. Figures 5-8 show EPR dwell fractions, look fractions, and transition link fractions for the pilots using either (a) only raw situation data or (b) the flight director with situation data during the go-around phase to a holding fix following a missed approach.

The dwell fraction is merely the relative dwell time-weighted look fraction, and the look fraction is simply the relative number of fixations on each instrument or display. The look fraction represents the ensemble probability of fixation and the dwell fraction, the temporal probability of fixation. The bi-directional link fraction is the relative number of scan transitions in both directions between each pair of instruments or displays. In rare cases, transitions occurred in only one direction noted by an arrow. The sums of each type of fraction may not equal exactly unity, because of round-off errors in the listed values.

Comparison of Figs. 5 and 6 shows that Pilot 3 used the HSI more when the flight director was off and the MFD more when the flight director was on. This is exemplified by all three types of fractions. Pilot 3 was consistent in this dichotomy. There are probably two underlying reasons:

a. When using raw situation data, it may be easier to close the heading control loop with the more familiar HSI, and

b. When using the flight director on the EADI, it may be easier to monitor the aircraft's heading and geographic position simultaneously using the moving map display on the MFD.

Direct crosschecks between the HSI and the MFD, although rare, do appear in one direction from the HSI to the MFD in the results in Figs. 5 and 7 with only raw data.

Pilot 1 (Figs. 7 and 8) used the HSI hardly at all during the go-around phase to a holding fix with raw data and not at all during the go-around with the flight director. The absence of any transitions to the altimeter in Fig. 8 may be because barometric altitude was available on the MFD, although we have not yet analyzed subsidiary transitions within the face of the MFD.

Pilot 1, a research pilot, was much more familiar with the EADI and MFD than Pilot 3, a commercial airline pilot. The familiarity and confidence of Pilot 1 in using the MFD is evident in comparing his eye-point-of-regard distribution with that for Pilot 3, in spite of the extensive training time provided for the commercial pilots who participated in the experiment.

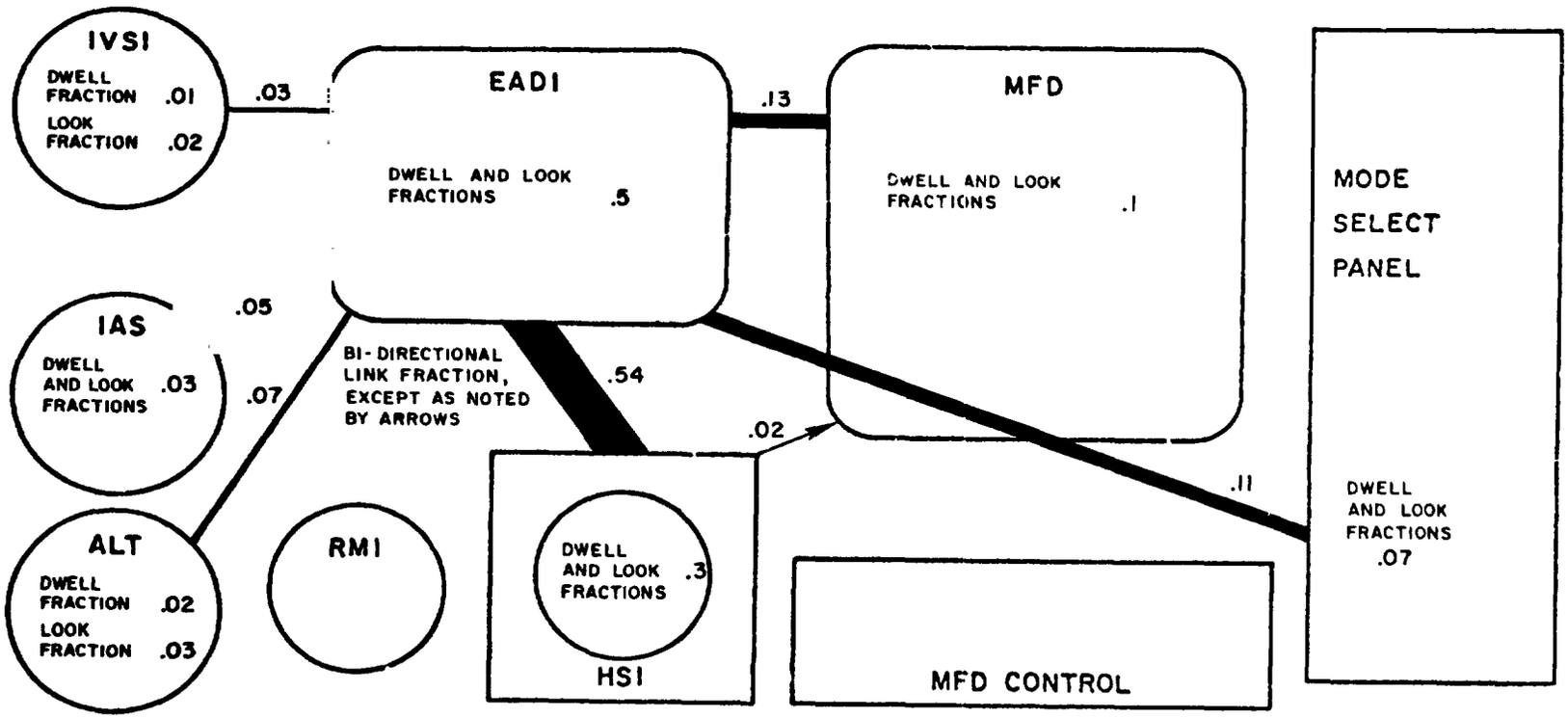

Figure 5. Eye-Point-of-Regard Dwell Fractions, Look Fractions, and Transition Link Fractions Averaged for Pilot 3 Using Raw Data During the Go-Around Phase to a Holding Fix Following a Missed Approach (Waypoints 22-25 of Run 148 with Flight Plan 3)

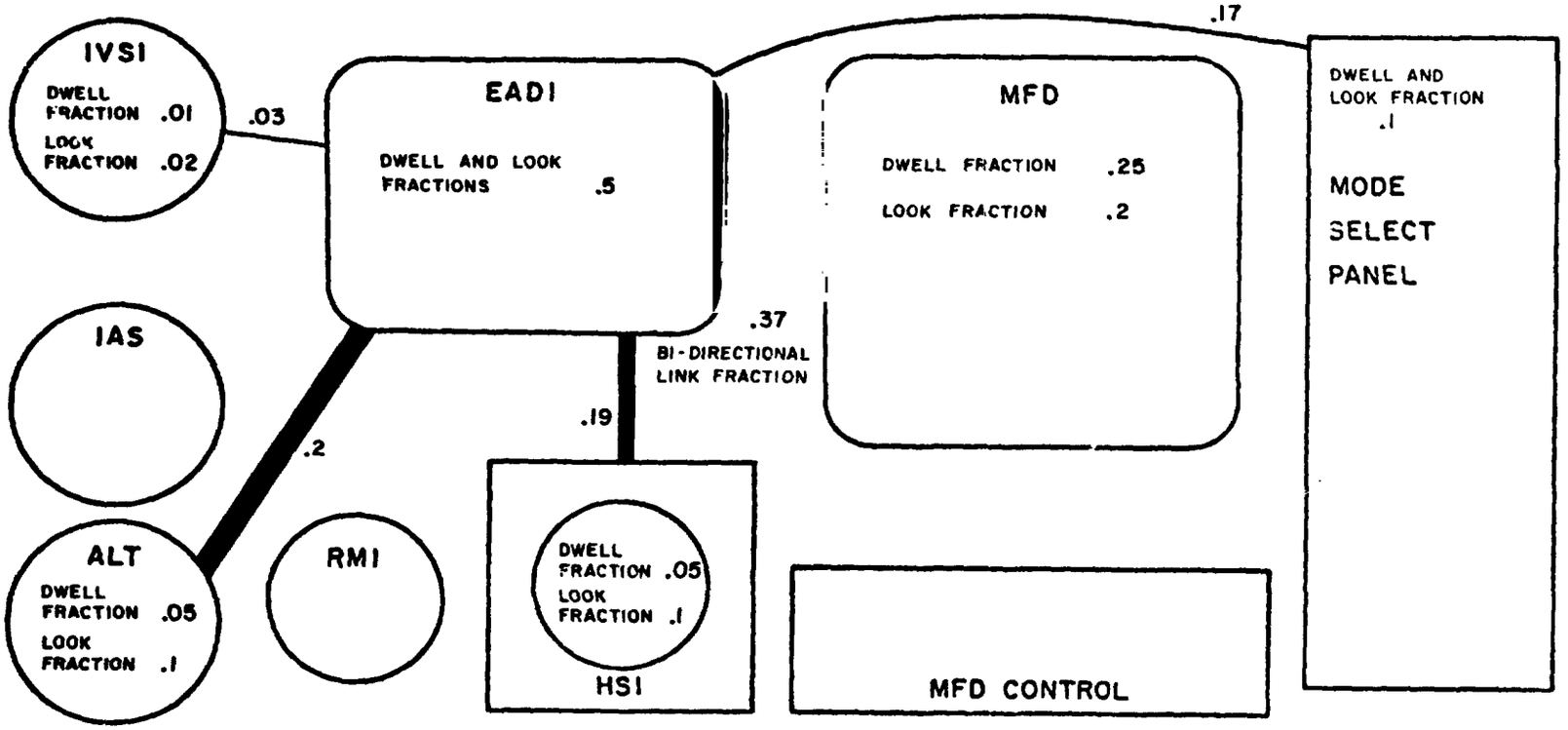

Figure 6. Eye-Point-of-Regard Dwell Fractions, Look Fractions, and Transition Link Fractions Averaged for Pilot 3 Using the Flight Director During the Go-Around Phase to a Holding Fix Following a Missed Approach (Waypoints 22-25 of Run 149 with Flight Plan 3)

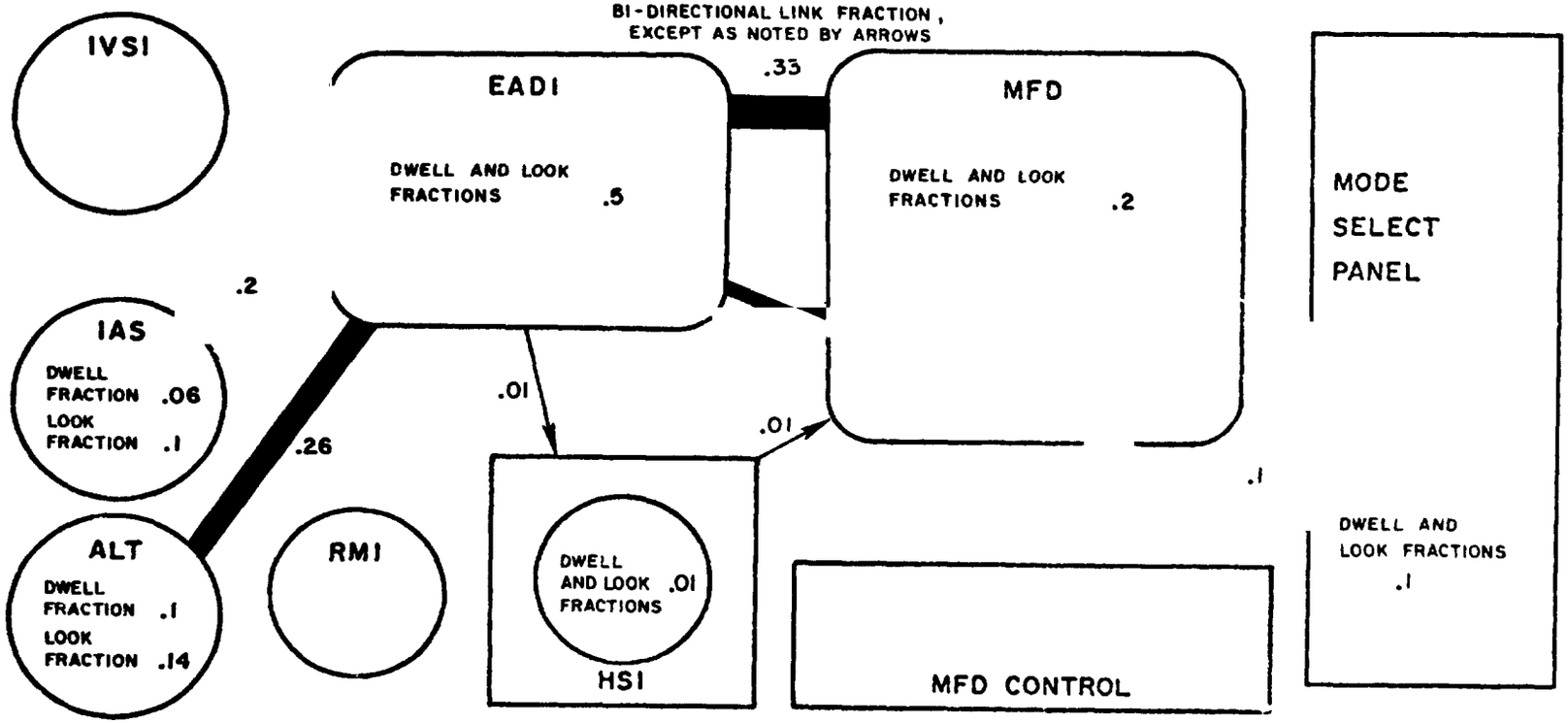

Figure 7. Eye-Point-of-Regard Dwell Fractions, Look Fractions, and Transition Link Fractions Averaged for Pilot 1 Using Raw Data During the Go-Around Phase to a Holding Fix Following a Missed Approach (Waypoints 22-25 of Run 154 with Flight Plan 3)

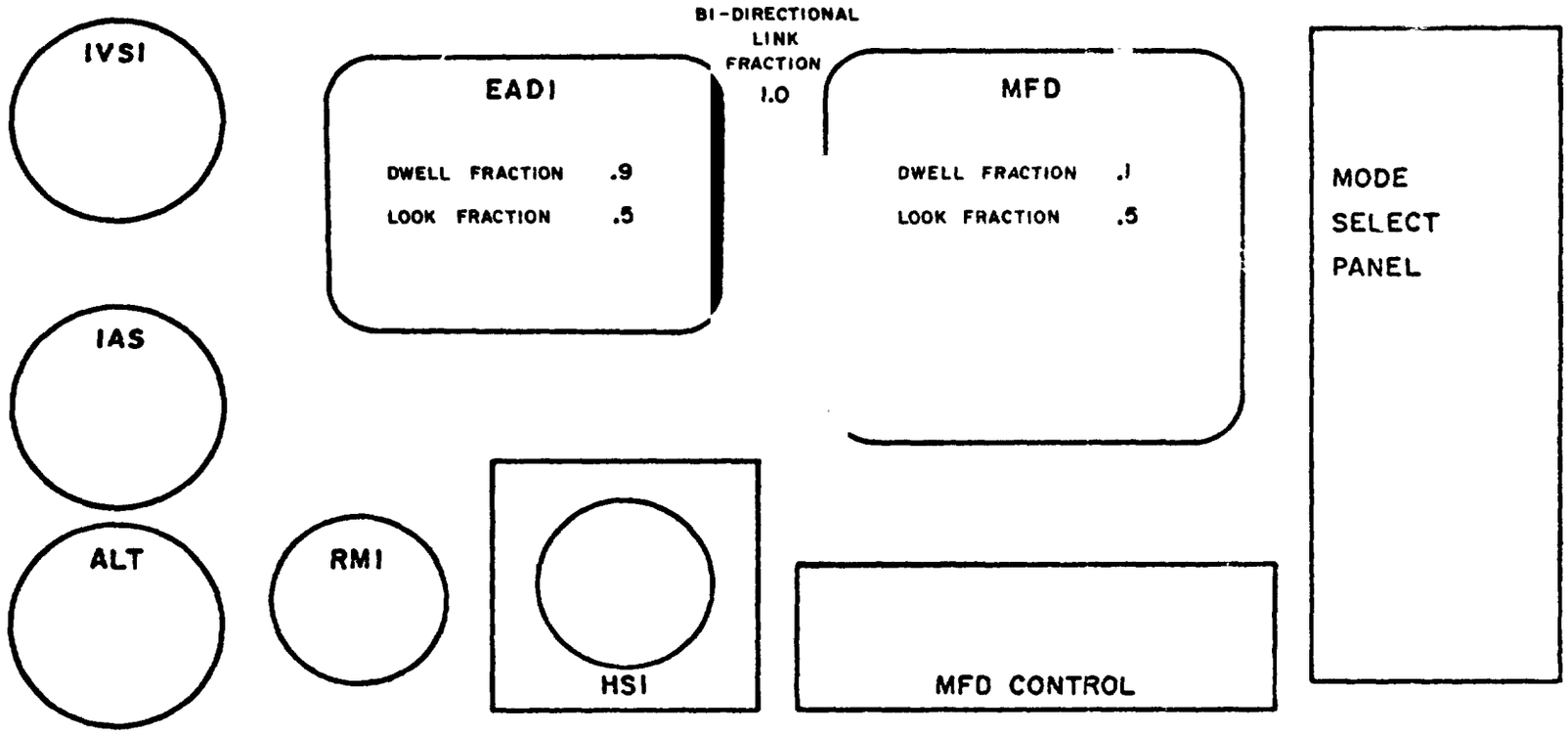

Figure 8. Eye-Point-of-Regard Dwell Fractions, Look Fractions, and Transition Link Fractions Averaged for Pilot 1 Using the Flight Director During the Go-Around Phase to a Holding Fix Following a Missed Approach (Waypoints 22-25 of Run 155 with Flight Plan 3)

Although we must conclude this brief preview of results, we shall, in the summary which follows, provide a concise overview of some of the other trends in the eye-point-of-regard distributions.

SUMMARY OF RESULTS AND CONCLUDING REMARKS

On the basis of the blunder distribution alone from the simulation, the MFD seems to offer a worthwhile improvement in safety, since 13 of 20 blunders among 160 runs involved runs wherein the MFD was not available to the pilot. Six involved runs with the MFD, but not the HSI, and only one involved a run with both.

The flight director provides for more precise tracking of the assigned altitude and the glide slope than otherwise. However, there is no consistent evidence of differences between tracking errors with the HSI versus the MFD among the five practiced pilots who participated in the simulation, although there are instances where altitude-keeping was more precise with the MFD when using only situation data.

The null hypothesis of equality between average excess control capacity within comparable pairs of flight plan waypoint groups using either the HSI or the MFD arrangement was tested for significant differences. The results show that the null hypothesis was rejected for 27 of 38 pairs of comparable waypoint groups at the 0.05 level, where 0.05 is the probability of rejecting the null hypothesis when it is true. Of these 27 rejected pairs, the MFD exhibited greater average excess control capacity for 15, and the HSI greater for 11 pairs.

The null hypothesis of equality between average excess monitoring capacity within comparable pairs of runs using either the HSI or the MFD arrangement was tested for significant differences. The results show that the null hypothesis was rejected for 13 of 38 pairs of comparable runs at the 0.05 level. Of these 13 rejected pairs, the MFD exhibited greater average excess monitoring capacity for 10, and the HSI greater for 3 pairs.

The pilots provided subjective ratings of (a) task controllability and precision, (b) utility of status information, (c) symbol-background clutter on the display, and (d) display attentional workload, each on five-point descriptive scales. Summarized comparisons of all ratings for the MFD and the HSI in each category follow.

Task Controllability and Precision. There is a slightly less favorable central tendency to rate the HSI "controllable, with inadequate precision," in tracking curved paths in the presence of wind, whereas the ratings favor the MFD as "controllable, with fair precision." Ratings with the flight director in use are uniformly distributed over four descriptive phrases from "easily" to "marginally" controllable and exhibit no central tendency with either HSI or MFD.

Utility of Status Information. The MFD received more favorable ratings than the HSI. Ratings of the usefulness of information supplied covered

the three adjectives "adequate":"some":"inadequate" in the ratios 4:3:0 for the MFD and 4:2:5 for the HSI. The bimodality of ratings for the HSI is believed to be associated with the favorable view of the HSI for tracking rectilinear flight paths and the unfavorable view of the HSI for maintaining geographic orientation while tracking curved paths in the presence of wind.

Clutter. Ratings of both the HSI and MFD as having "some clutter" predominate, but there is a slight tendency to rate the MFD less favorably.

Display Attentional Workload. Ratings of the MFD show a central tendency between "mildly" and "quite demanding," whereas ratings of the HSI exhibit a less favorably skewed mode between "quite" and "completely demanding."

The reduced eye-point-of regard (EPR) data for 8 runs among Pilots 1, 3, and 4 reveal that, with few exceptions, there are relatively more looks at and longer fixation dwells on the MFD than the HSI when using raw situation data and especially when using the flight director. This finding is consistent with the respective comments by Pilots 1 and 4 and tends to confirm an expressed preference by Pilot 1 for the MFD in curved path tracking and in negotiating holding patterns. While not definitive in the case of Pilot 4 because of the single flight plan, the EPR data from two runs also suggest a preference by Pilot 4 for the MFD in curved path tracking. In the case of Pilot 3 the EPR data suggest an equitable distribution of looks and dwells between the HSI and MFD throughout the approach with the flight director, but a preference for the MFD during the missed approach, go-around, and throughout the holding pattern in Flight Plan 3. In the case of Pilot 3 using raw data, the EPR measurements offer little basis for inferring a preference between the HSI and MFD, because both horizontal displays are scanned, in turn, from the EADI fairly consistently throughout Flight Plan 3, except during the straight final approach where the HSI receives relatively more looks. Direct crosschecking between the HSI and the MFD is rare, but such scan transitions are predominantly unidirectional from HSI to MFD by Pilots 1, 3, and 4 when using raw situation data.

All of the pilots provided a great number of helpful supporting comments in the course of the experiment. There was a consensus among the pilot comments which acknowledged the excellence of the HSI for tracking rectilinear inclined courses, yet recognized the superiority of the MFD for maintaining confidence in geographical orientation while tracking curved approach courses and establishing holding patterns in the presence of wind. The summary comment by one of the pilots provides a decisive conclusion: "If the MFD in operational aircraft could be shared with the weather display...between the pilot a moving map display might be provided at no extra cost in panel space. The HSI bearings, DME, and deviations would seem to be an essential backup, even for a moving map. I would...want both HSI and MFD, if the MFD could be shared with the weather radar display....The HSI improves my confidence in the moving map on the MFD."

REFERENCES

1. Neuman, F.; Watson, D. M.; and Bradbury, P.: Operational Description of an Experimental Digital Avionics System for STOL Airplanes. NASA TM X-62,448, December 1975.

2. Clement, W. F.; McRuer, D. T.; and Klein, R. H.: Systematic Manual Control Display Design. Proceedings of the 13th AGARD Guidance and Control Symposium on Guidance and Control Displays. AGARD CP-96, February 1972, pp. 6-1 to 6-10.

3. Clement, W. F.; Allen, R. W.; and Graham, D.: Pilot Experiments for a Theory of Integrated Display Format. JANAIR Report 711107, October 1971 (also TR-183-2, Systems Technology, Inc.).

AIR-TO-GROUND VISUAL DISPLAY SYSTEM

Daniel L. Kugel
Randall V. Gressang, Capt, USAF
Air Force Flight Dynamics Laboratory
Wright-Patterson AFB, Ohio

ABSTRACT

The ability to simulate realistic air-to-ground tactical missions is very important in the evaluation of prototype fighter aircraft, testing of new Air Force weapon systems, and the training of pilots for high performance aircraft. Most aerospace simulators however do not have this capability. The Air Force Flight Dynamics Laboratory at Wright-Patterson AFB, Ohio has recently developed, in a joint effort with the Northrop Corporation, a Large Amplitude Multi-mode Aerospace Research Simulator (LAMARS). The use of this simulator for air-to-ground tactical mission simulation is discussed. The utilization of a state-of-the-art helmet sight system and its role in the development of a head slaved visual display system is explained; the major subsystems are described, with principle emphasis placed on the visual display system, terrain model, and helmet sight system. Engineering data gathered to evaluate this area of interest (AOI) display is included, along with details of the drive logic and a summary of pilot comments evaluating the ability of the visual display system to provide the necessary requirements to perform the air-to-ground mission.

I. INTRODUCTION

The LAMARS engineering simulator is currently in operation at the AF Flight Dynamics Laboratory. This high performance simulator will serve as one of the major engineering tools in the new ground-based simulation facility, the Flight Control Development Laboratory. This facility is the focal point for coordinated studies encompassing pilot/vehicle studies, ground based and in-flight simulation as applied to flight dynamic research, prototype evaluation and weapon system development. The LAMARS will be used in support of programs covering advanced development, system development and integration, and simulation support.

The combination of wide angle visual cues and large amplitude motion cues that the simulator gives to the pilot provides an environment which will evoke proper pilot response characteristics for a large number of mission conditions and pilot control tasks. Knowledge of how a pilot will react to various conditions is required during preliminary design and preflight evaluation of military aircraft designs. Such prior knowledge will identify possible trade-offs between aircraft performance, stability and control, and maneuverability. The engineering flight simulator gives the Air Force pilot the

unique opportunity to significantly influence the design of a flight vehicle long before the final configuration is determined.

Though not its principle mission, the Flight Control Division of the AF Flight Dynamics Laboratory has the engineering knowledge and first hand hardware experience to help make determinations of simulator criteria and requirements. Recently, the Simulator System Program Office of the Aeronautical Systems Division, Wright-Patterson AFB began work on testing present Air Force simulators for the purpose of developing visual requirements for air-to-ground mission simulators. This study was to determine both qualitatively and quantitatively the cues which could be generated visually by the LAMARS simulator at the AF Flight Dynamics Laboratory, Wright-Patterson AFB, Dayton, Ohio, the Advanced Simulator for Undergraduate Pilot Training (ASUPT) at Williams AFB, Chandler, Arizona, and the Simulator for Air-to-Air Combat (SAAC) at Luke AFB, Glendale, Arizona. By evaluating these three methods of visual projection one can better determine which methods will best provide the needed visual cues to perform the air-to-ground tactical mission.

It should be noted that this program was conducted to show what present Air Force simulators could provide in the way of air-to-ground visual cues. The intent was not to update these simulators with the most current hardware available but to use what hardware was in the simulators at the time, note any limitations which could be eliminated or improved by recent hardware developments and substantiate these comments with engineering data. It should also be pointed out that the LAMAR simulator was designed primarily for air-to-air combat mission evaluations and handling quality studies. This simulator is not a training simulator but an engineering design and evaluation tool obtained primarily for handling qualities evaluation and air-to-air combat studies.

II. DESCRIPTION OF THE MAJOR SIMULATOR SUBSYSTEMS

Visual Display System

The visual display system of the LAMARS consists of a 20-foot diameter spherical projection screen fixed to the cockpit. Within the sphere are two projectors which display the visual information to the pilot (Figure 1). One projector mounted above and to the rear of the cockpit projects the high resolution detailed terrain image while the other projector, located above and slightly to the rear of the target projector, referred to as the sky/earth projector, projects a passive blue sky, green earth horizon display throughout the entire sphere.

As was mentioned previously, the pilot is at the center of the spherical screen, which helps eliminate distortion of the projected images. As a result, the target projector and the sky-earth projector are off center and the projectors themselves have been specially designed to compensate for this effect. The target projector has a docus servo which moves the cathode-ray tube (CRT) in and out with respect to the projection lens. By knowing the

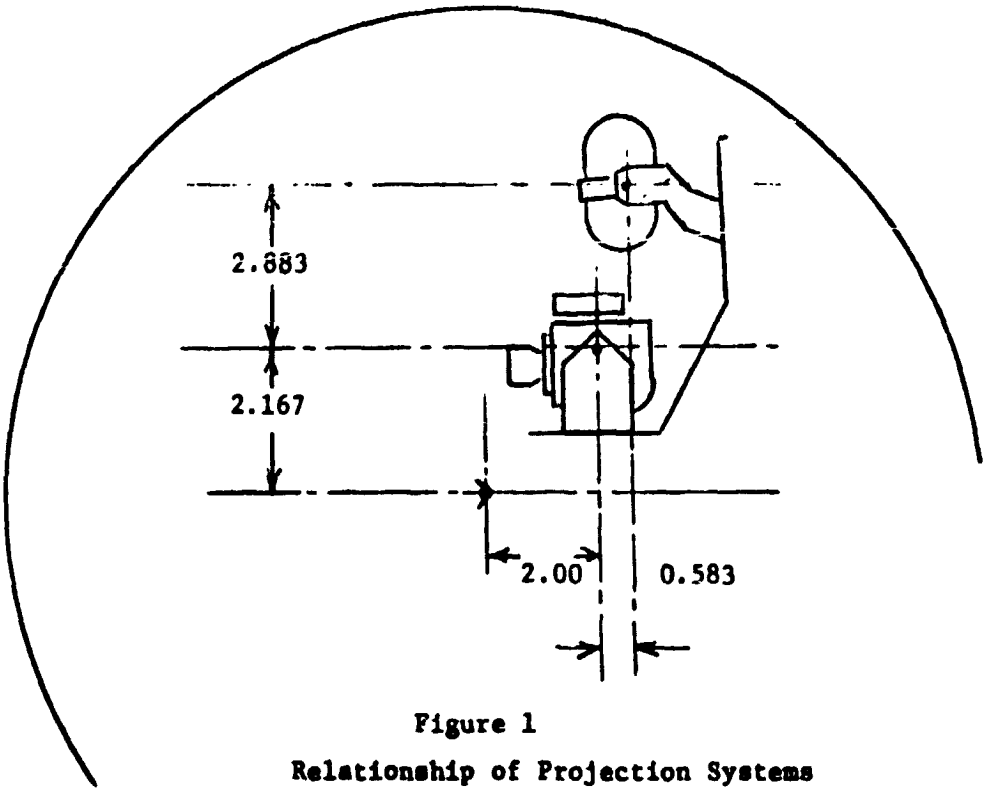

Figure 1

Relationship of Projection Systems

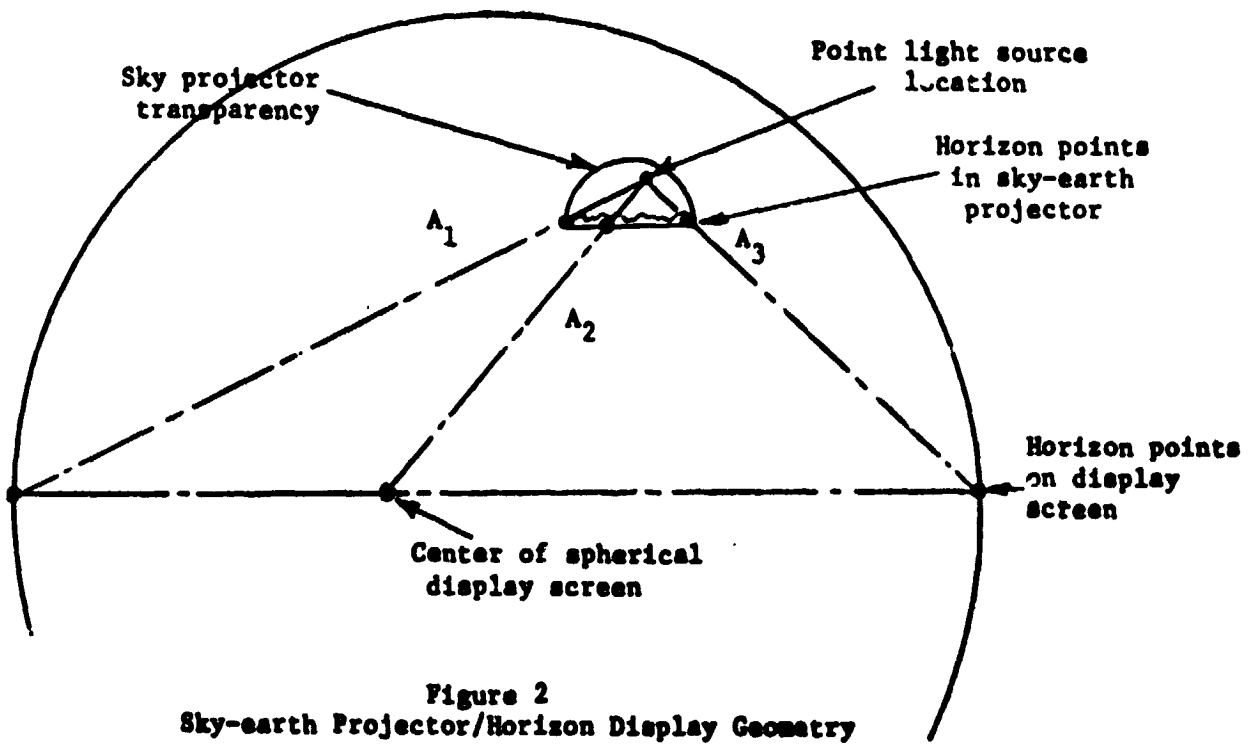

Figure 2

Sky-earth Projector/Horizon Display Geometry

position of the projector with respect to the center of the sphere and also the azimuth and elevation of the projector, the "throw distance" or focal length from the projector to the screen can be calculated and used to drive the focus servo. The target projector also has a "keystone" correction provision in its raster control circuitry to compensate for the varying angles at which the projected image impinges on the surface of the screen. The sky/earth projector has a mechanism inside the twin hemispherical transparent domes which can position the point light source of the "sky" lamp and "earth" lamp, to the proper x, y, and z coordinates within the transparency so that the projected horizon line is always correctly oriented on the screen without distortion. This is demonstrated in Figure 2.

Terrain Model/Computer Image Generation

The image which is presented to the pilot is generated by a large scale model of a typical terrain area. This three dimensional full color terrain model has its own gantry supported, optical probe equipped television camera positioned by precision servo drive systems commanded by computer signals. These computer signals are a result of the aircraft orientation and provide properly oriented visual cues to the pilot. Also, computer generated images (CGI) can be programmed and superimposed over the terrain image to provide moving targets, Forward Air Controller (FAC) aircraft, computer generated heads-up displays, etc; however, their utility using a television display system is questionable (see Appendix I). The resultant video picture is transmitted to the cathode-ray tube of the target projector and is projected onto the spherical screen. The sky/earth horizon display and the horizon in the video picture are synchronized by superposition of the terrain image and sky/earth image on the dome. This provides a 60° diagonal forward field-of-view displaying high resolution terrain imagery and also a wide field of view horizon display to produce the necessary peripheral cues needed to help the pilot in judging sink rate, roll position, roll rates, etc.

Projection Capability

The requirement for a 60° diagonal area-of-interest projection beam which can be positioned anywhere within the field-of-view of the pilot arose from the desire to have a diaplay capability which could provide the visual requirements for such tasks as air-to-ground weapon delivery, terrain following/avoidance, and take off/landing work. The resulting display capability represents a compromise between a full field of view terrain image and what was believed to be a realistic achievement based on a thorough review of existing hardware.

The requirement of a large field of view results from the new aircraft designs, which to properly simulate, require an unlimited view in both azimuth and elevation. The LAMARS simulator was able to achieve a 266° field of view in azimuth and a 108° field of view in elevation. These values were not quite as large as was desired (280° in azimuth, 150° in elevation) but represent the largest field of view possible, limited only by the cockpit

gimbal system and the projector system mounting configuration.

III. THE AIR TO GROUND WEAPONS DELIVERY TASK

In performing an air-to-ground task in the LAMARS there are three methods in which to display the high resolution terrain image. The first, and most basic is to fix the 60° area of interest to the x-axis of the aircraft. In doing this, the rectangular AOI will remain fixed in the front window of the cockpit. The picture within the field of view will change solely as a result of the aircraft orientation. This provides a forward fixed scene but does not permit the pilot to perform his typical roll maneuver when attacking a ground target since the target at that point will be out of the area of interest. Secondly, it does not utilize the large field-of-view capability of the spherical projection screen.

The second approach would be to fix the visual scene to a specific target. This would permit the 60° diagonal terrain image to appear anywhere in the dome based on the relative positions of the aircraft and the target. For example, if the pilot was flying into the target the terrain image would be directly in front of the pilot. If the pilot flew by the target the terrain image would move off to the side and on back to the rear of the dome and finally disappear from view. This is certainly more realistic than the first case but does not permit the pilot to do terrain following and target search since he knows that if he keeps the terrain image directly in front of him he will eventually fly directly over the target. To help eliminate the problems associated with the above methods, an area-of-interest, head-slaved visual display system was developed.

Head Slaved Visual System

To develop a head-slaved visual system, one must first be able to monitor the pilot's head position. This should be done in a manner which is completely unobtrusive to the pilot. Once the head position is known and calibrated with respect to a fixed reference point in the cockpit then drive logic and its associated software can be developed.

The hardware used in this experiment was a state-of-the-art helmet sight system. Sensor surveying units were rigidly fixed to the cockpit and aimed in the direction of the pilot's head. These units emit fan-like beams of infrared light rotating at a constant velocity. The infrared beams sweep over a reference photo sensor and two pairs of helmet mounted photo sensors, one pair on each side of the helmet. The time intervals between the pulses from the helmet photo sensors and the reference pulse are a measure of the pilot's head orientation relative to the body axis of the aircraft. The outputs of the photo sensors are transmitted to the helmet sight computer where the angular computations are performed and converted into azimuth and elevation information. The accuracy of the system is one-half degree CEP.

As was shown before, the target projector and the pilot's head are at

different locations within the sphere. As a result, to point the center of the image projected by the target projector to intercept the point directly in front of the pilot's head, a geometrical transformation is required.

At the same time, it requires that the distance from the target projector lens to the sphere be calculated to drive the focus servo. Because the target projector probe is not as responsive as the angular position servos of the visual probe, the angles of the head are then recalculated using a similar geometric transformation and the position feedback signals from the target projector. The calculated head position and the aircraft position are combined to form a resultant drive signal to the visual probe servos. The probe servos are lead compensated to provide better response. This arrangement permits the pilot to look about within the sphere and view a correctly oriented visual segment.

Other software has also been added to help make the visual image seen by the pilot more realistic. One of these is a dead zone filter which is used to help eliminate small amplitude, high frequency head movements from placing jitter into the system. The dead zone requires that the pilot move his head some predetermined delta value before the target projector repositions itself. This allows the pilot to slowly scan the terrain image without constantly repositioning the projector. It also acts to keep out high frequency noise which could result from calculation errors in the digital machine.

IV. EVALUATION TEST PLAN

The LAMARS air-to-ground visual system was evaluated by six pilots from the Tactical Air Command, Aeronautical Systems Division and the Navy. These pilots were currently rated in various high performance aircraft and were highly experienced in the air-to-ground task.

Each pilot flew the device for a total of eight one-hour sorties. The pilots performed the following weapon deliveries:

1. 10° skip bomb
2. 15° low angle bomb
3. 15° low angle strafe
4. 20° low angle dive bomb
5. 30° high angle strafe
6. 30° dive bomb
7. 45° dive bomb

At weapon release the following data was recorded:

1. aircraft position, velocity, angles, angular velocities

2. weapon miss distance (bomb) or mean impact point (gun)

A number of tactical targets were used during the sorties.

1. range target
2. gravel pit
3. suspension bridge
4. dam pumphouse
5. railroad overpass
6. small house
7. runway lights
8. highway intersection
9. oil tank
10. SAM site
11. parked aircraft
12. bulldozer
13. airport terminal

The aircraft could deliver either a MK82 bomb or deliver gunfire with a 30mm gun.

A pilot questionnaire was used to gather information on:

1. opinion of weapon delivery performance
2. ease of target acquisition
3. comments on AOI display
4. comments on simulation realism
5. other pertinent comments

The following numerical data was computed for each pilot/target/delivery conditions:

1. mean along track miss distance
2. standard deviation, along track miss distance
3. mean cross track miss distance
4. standard deviation, cross track miss distance
5. correlation coefficient, along track and cross track miss distance
6. median radial error
7. maximum miss distance

8. minimum miss distance

9. the number of hits long, short, left, and right of target.

Engineering tests were also conducted on the LAMARS visual system itself. These tests included

1. System Static Resolution/Modulation Transfer Function
2. Image Generator Static Resolution/Modulation Transfer Function
3. Display Static Resolution/Modulation Transfer Function
4. Image Generator Dynamic Resolution/Modulation Transfer Function
5. Display Brightness
6. Display Grayscale
7. Display Contrast
8. Display Shading
9. System Brightness
10. System Grayscale
11. System Contrast
12. System Shading
13. System Geometric Distortion
14. AOI Field-of-View
15. AOI Dynamic Envelope Size
16. AOI Edge Transition Quality
17. Target Image Location Dynamic Lag
18. System Rate Accuracy
19. System Design Data

V. PILOT EVALUATION RESULTS

The pilots were debriefed at the end of each 60 minute sortie and were asked to evaluate the task with respect to the LAMARS head-slaved visual system. The following comments and their cause were noted as being common comments of all pilots.

Attributes

1. Diversified Scene Content - The model board type of image generation is unique in its ability to produce high quality scene detail. The detail has good texture and is significantly more detailed than computer generated imagery.

2. Smooth Projection Surface - The spherical dome does not have discrete display surfaces as do CRT type displays. Because of this the scene can transition throughout the 266° x 108° viewing area with smooth continuity.

3. Head Slaved AOI is Promising - The pilots all felt that the head slaved area-of-interest display was the best of the three projection methods within the LAMARS but felt it was presently limited due to other hardware shortcomings presently found in the rigid model visual system.

Limitations

1. AOI Too Small - The rigid model visual system presently is limited to a 60° diagonal area of interest (48° wise by 36° high). This is inadequate for many tactical maneuvers. For example, to attack a ground target or to turn from base leg to final during landing requires a minimum of 90° field of view. A navigational land mark is used to guide the aircraft and when the target or runway appears over the left wing a turn or roll maneuver is executed. With a 48° wide area of interest, the target and navigational aid are not within the same visual segment. In the head slave mode, the pilot can command the probe/target projector to pick up the visual cues he needs to perform the task. The pilot, however, is now placed in a situation where he is performing unrealistic head movements which degrades his performance. A minimum of 120° diagonal (96° wide by 72° high) area of interest is required to perform a realistic tactical maneuver using a head slaved visual system.

2. 47° Pitch Restriction Too Small - The AFFDL rigid model visual system has a 47° down pitch hardware limit on the visual probe. When this limit is exceeded the visual segment is obscured by a pseudo-cloud cover. In high angle tactical maneuvers, since the head and aircraft now command the probes pitch position, these limits can be easily exceeded. It is quite distracting and unnatural to lose the target near weapon release. An unlimited pitch axis on the probe is an "off-the-shelf" modification which can be easily performed on the AFFDL system.

3. Uncertain Scoring Accuracy - Scoring accuracy using head-slaving is presently uncertain because it was not possible to calibrate it prior to pilot evaluation. Weapon delivery data, at first look, appears to indicate that there is a dynamic lag using head slaving which could cause impact errors on the order of several hundred feet given the approach speeds and dive angles used in this simulation.

4. Horizon Mismatch - The sky/earth horizon display did not always match the horizon display from the rigid model terrain board image. The reason for this is that the two were driven from separate loops, one was programmed for flat earth (terrain board image) while the other was for spherical earth (sky/earth display) and the sky-plate used by the probe to prevent viewing the probe/gantry in the mirrors can displace the apparent horizon location at high altitude or near the mirrors surrounding the board. Further programming improvements will alleviate this problem.

The pilots in general found the combination of the small field-of-view and the pitch restriction on the probe produced unrealistic piloting conditions. They did feel that if these two problems were alleviated/eliminated, a viable air-to-ground display could result.

VI. ACKNOWLEDGEMENTS

Obviously, to conduct a program of this complexity, many people must be involved. The general concepts described in this paper and the software equations were developed by the authors. These equations, however, were in Fortran IV and had to be rewritten in machine language for implementation on the LAMAR simulator. Mr. William J. Waldron, who is responsible for the operation and programming of the LAMARS, spent considerable time with much personal involvement in getting the head slaved visual system operational. Appreciation must be given to Mr. Waldron for his effort in this project and also to Mr. James A. Eicher, who was responsible for tying in the visual system.

REFERENCES

1. Haas, R.L., H.E. Hotz, and G.R. Mills. "The Large Amplitude Multi-Mode Aerospace Research (LAMAR) Simulator". AIAA Paper No. 73-922, AIAA Visual and Motion Simulator Conference, Palo Alto, California. Sept 10-12, 1973.

2. Gressang, R.V., D. Kugel, W. Waldron, J. Eicher. "Drive Signals for Positioning an Area of Interest Visual Display". AFFDL TM 63-13-FGD, February 1976.

3. Kugel, Daniel L. and R.V. Gressang. "Air-to-Ground Visual Display System". Proceedings, AIAA Visual and Motion Simulation Conference, Dayton, Ohio, 26-28 April 1976.

APPENDIX I

TELEVISION DISPLAY RESOLUTION

When a television display is used, one must keep in mind that each visual picture is obtained from a series of raster lines painted by a cathode ray gun. The more lines a display is able to paint across the face of the screen, the more accurate will be the resulting picture. Using a typical 60° field of view probe and a television display whose resolution is 700 effective lines, one can determine at what distance a target of known dimensions will be able to be recognized.

If N = number of effective resolved lines across the sensor's FOV

M = number of lines across the target for identification/recognition

L = maximum dimension of target

S = slant range

then using

$$\text{probe FOV required} = \frac{2N}{M} \tan^{-1} \frac{L}{2S} \qquad \text{(I-1)}$$

if 8 lines are required for recognition of a moving target whose maximum dimension is 30 feet, the effective resolution of the display is 700 lines, and the probe FOV is 60°, then

$$S = \frac{L}{2 \tan \{ \text{probe } \frac{\text{FOV} \cdot M}{2N} \}} \qquad \text{(I-2)}$$

$S \simeq 2500$ ft ~ 1/2 mile.

It is obvious that in unlimited visibility, a 30 ft aircraft can be seen for several miles. Using the same information as above, a 30 ft airplane at two miles would be painted by less than two scan lines resulting in only a single dot on the screen.

APPENDIX II

SOFTWARE EQUATIONS

The block diagram for the head slaved visual system is shown in Figure 3. In this appendix, the important software equations are described.

A. Head to Target Projector Transformation

Azimuth

$$\psi^* = 180.0 - \psi_H$$

$$R_\psi^2 = [10.0]^2 + [2.0]^2 - 2(10.0)(2.0) \cos \psi^*$$

Therefore

$$R_\psi = [104.0 - 40.0 \cos (180.0 - \psi_H)]^{1/2} \qquad \text{(II-A-1)}$$

LAMARS HEAD-SLAVED VISUAL SYSTEM

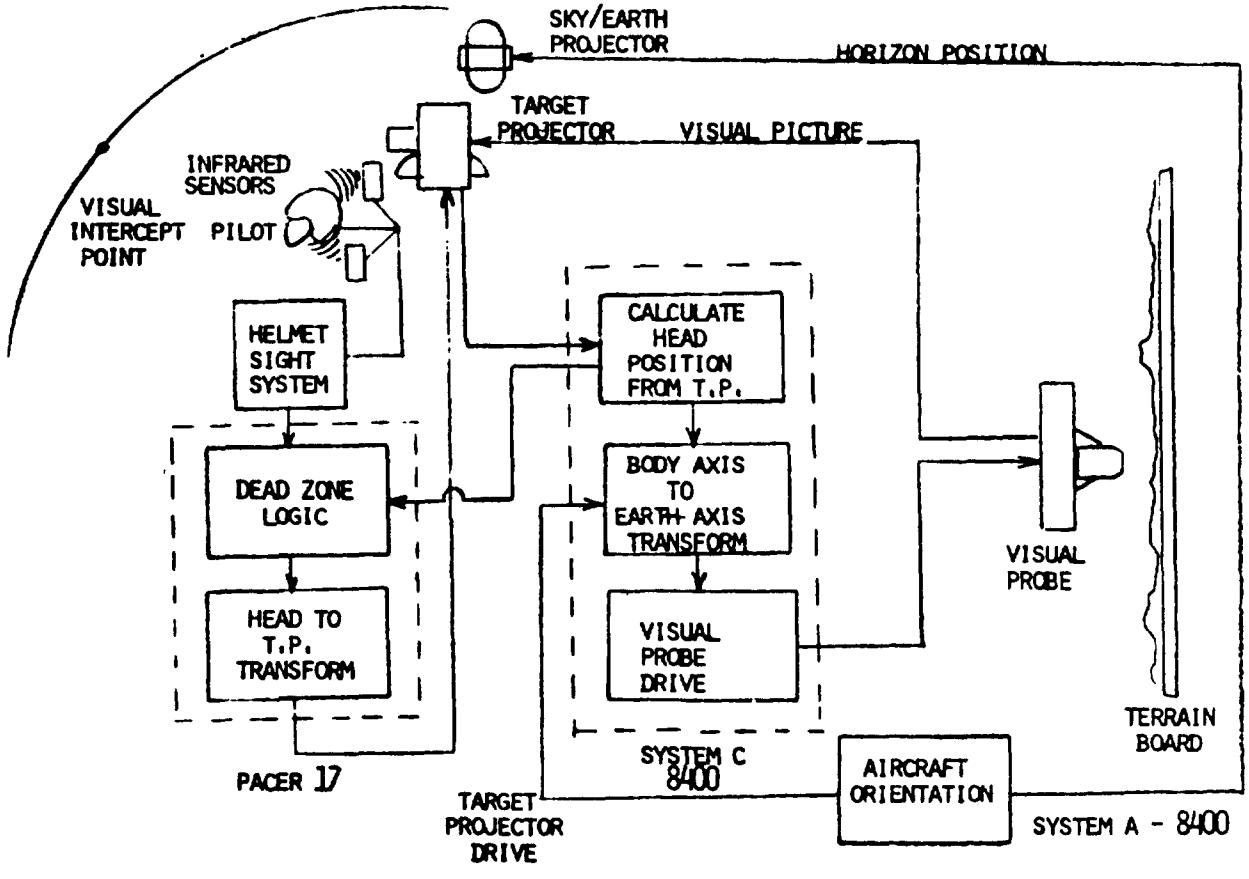

Figure 3

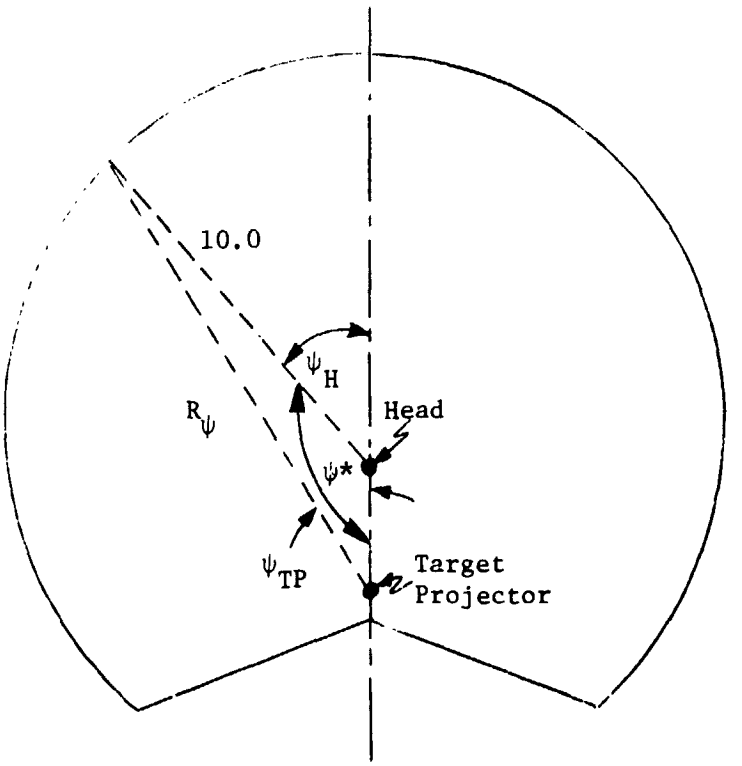

Figure 4

Also,

$$\psi_{TP} = \cos^{-1}\left[\frac{(2.0)^2 + R_\psi^2 - (10.0)^2}{2(2.0)R_\psi}\right]$$

which reduces to

$$\psi_{TP} = \cos^{-1}\left[\frac{R_\psi^2 - 96.0}{4.0R_\psi}\right] \qquad \text{(II-A-2)}$$

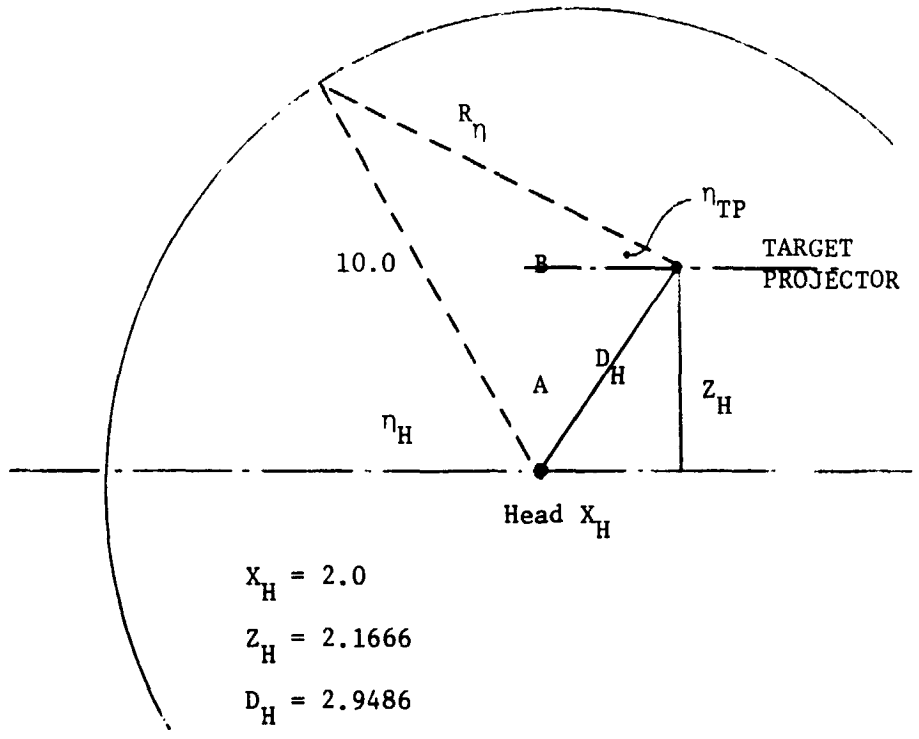

Figure 5

Then

$$\eta_H + A + 47.29° = 180°$$

or

$$A = 132.71 - \eta_H$$

$$R_\eta^2 = [10.0]^2 + [2.9486]^2 - 2[10.0][2.9486] \cos A$$

$$R_\eta = [108.6944 - 58.9727 \cos (132.71 - \eta_H)]^{1/2} \qquad \text{(II-A-3)}$$

Also

$$-\eta_{TP} + B + 42.71 = 90°$$

or

$$\eta_{TP} = B - 47.29°$$

$$B = \cos^{-1}\left[\frac{R_\eta^2 + (2.9486)^2 - (10.0)^2}{2(2.9486)R_\eta}\right]$$

which reduces to

$$B = \cos^{-1}\left[\frac{R_\eta^2 - 91.3055}{5.8973R_\eta}\right]$$

and

$$\eta_{TP} = \cos^{-1}\left[\frac{R_\eta^2 - 91.3055}{5.8973R_\eta}\right] - 47.29° \qquad \text{(II-A-4)}$$

Using the body axis coordinates, x, y, z, then the location of the head with respect to the target projector is

$$x_H = 2.0$$

$$y_H = 0.0$$

$$z_H = -2.1666$$

The components of the vector from the head to the screen can be given by

$$x_p = R \cos \psi_H \cos \eta_H \qquad \text{(II-A-5)}$$

$$y_p = R \sin \psi_H \cos \eta_H \qquad \text{(II-A-6)}$$

$$z_p = R \sin \eta_H \qquad \text{(II-A-7)}$$

The throw distance to the screen is then

$$R_f = [(x_H+x_p)^2 + (y_H+y_p)^2 + (z_H+z_p)^2]^{1/2} \qquad \text{(II-A-8)}$$

B. Calculated Head Angles from Target Projector Feedbacks

To determine the calculated head angles based on the position feedback signals from the target projector, ψ_{TP} and η_{TP} are replaced with $\psi_{TP_{FB}}$

and $\eta_{TP_{FB}}$ respectively, in equations II-A-1 through II-A-4.

The results are

$$R_{\psi_{CAL}} = 2.0 \cos \psi_{TP_{FB}} + 0.5[392.0+8.0 \cos \psi_{TP_{FB}}]^{1/2} \qquad \text{(II-B-1)}$$

$$\psi_{H_{CAL}} = \cos^{-1}\left[\frac{R^2_{\psi_{CAL}} - 104.0}{40.0}\right] \qquad \text{(II-B-2)}$$

$$R_{\eta_{CAL}} = 2.9486 \cos (\eta_{TP_{FB}} + 47.29°) + 0.5\{17.39[1+\cos(2\eta_{TF_{FB}} + 94.58°)] + 365.22\}^{1/2} \qquad \text{(II-B-3)}$$

$$\eta_{H_{CAL}} = 132.71 - \cos^{-1}\left[\frac{108.6944 - R^2_{CAL}}{58.9727}\right] \qquad \text{(II-B-4)}$$

C. Axis Transformations

Given a set of earth fixed axes, tangent to the surface of the earth, z axis down, and the aircraft Euler angles (body axis, ϕ, θ, ψ) and the head angles with respect to the body axis (η_H, ψ_H, $\phi_H = 0$), the various axis transformation matrices are desired. The transformation matrix, C_E^B, from earth axis to body axis is given in terms of the aircraft Euler angles, ϕ, θ, ψ by

$$C_E^B = \begin{bmatrix} c\phi c\psi & c\theta s\psi & -s\theta \\ s\phi s\theta c\psi - c\phi s\psi & s\phi s\theta s\psi + c\phi c\psi & s\phi c\theta \\ c\phi s\theta c\psi + s\phi s\psi & c\phi s\theta s\psi - s\phi c\psi & c\phi c\theta \end{bmatrix} \qquad \text{(II-C-1)}$$

where c denotes cosine and s denotes sine. The transformation matrix, C_B^H, from body axis to head axis, is given by

$$C_B^H = \begin{bmatrix} c\eta_H c\psi_H & c\eta_H s\psi_H & -s\eta_H \\ -s\psi_H & c\psi_H & 0 \\ s\eta_H c\psi_H & s\eta_H s\psi_H & c\eta_H \end{bmatrix} \qquad \text{(II-C-2)}$$

where ψ_H is the head azimuth and η_H is the head elevation (Euler angles) relating head to body axes. For our purposes ϕ_H (head roll) is not measured and is identically equal to zero.

The transformation from earth to head is then calculated using

$$C_E^H = C_B^H \, C_E^B \qquad \text{(II-C-3)}$$

$$= \begin{bmatrix} c\theta_{EQ}c\psi_{EQ} & c\theta_{EQ}s\psi_{EQ} & -s\theta_{EQ} \\ (s\phi_{EQ}s\theta_{EQ}c\psi_{EQ} - c\phi_{EQ}s\psi_{EQ}) & (s\phi_{EQ}s\theta_{EQ}s\psi_{EQ} + c\phi_{EQ}c\psi_{EQ}) & s\phi_{EQ}c\theta_{EQ} \\ (c\phi_{EQ}s\theta_{EQ}c\psi_{EQ} + s\phi_{EQ}s\psi_{EQ}) & (c\phi_{EQ}s\theta_{EQ}s\psi_{EQ} - s\phi_{EQ}c\psi_{EQ}) & c\phi_{EQ}c\theta_{EQ} \end{bmatrix} \qquad \text{(II-C-4)}$$

where

$$\theta_{EQ} = \sin^{-1}\left[c\eta_H c\psi_H s\theta - c\eta_H s\psi_H s\phi c\theta + s\eta_H c\phi c\theta\right] \qquad \text{(II-C-5)}$$

$$\phi_{EQ} = \tan^{-1}\left[\frac{s\psi_H s\theta + c\psi_H s\phi c\theta}{-2\eta_H c\psi_H s\theta + s\eta_H s\psi_H s\phi s\theta + c\eta_H c\psi c\theta}\right] \qquad \text{(II-C-6)}$$

$$\psi_{EQ} = \tan^{-1}\left[\frac{(c\eta_H c\psi_H c\theta c\psi + c\eta_H s\psi_H s\phi s\theta s\psi) + (c\eta_H s\psi_H c\phi c\psi - s\eta_H c\phi s\theta s\psi + s\eta_H s\phi s\psi)}{(c\eta_H c\psi_H c\theta c\psi + c\eta_H s\psi_H s\phi s\theta c\psi) + (-c\eta_H s\psi_H c\phi s\psi - s\eta_H c\phi s\theta c\psi - s\eta_H s\phi s\psi)}\right]$$

(II-C-7)

D. Dead Zone Logic

This is a nonlinear filter realized by two logic tests which allows the target projector to be moved only by head position. Random small amplitude noise is filtered out permitting a smooth projector response. The position and rates of the head can be calculated using the following equations.

$$\text{Elevation position limit} = \text{ABS}(\eta_H(\text{new}) - \eta_H(\text{old})) \qquad \text{(II-D-1)}$$

$$\text{Azimuth position limit} = \text{ABS}(\psi_H(\text{new}) - \psi_H(\text{old})) \qquad \text{(II-D-2)}$$

$$\text{Elevation rate limit} = \text{ABS}(\eta_H(\text{new}) - \eta_{H_{CAL}}(\text{old})) \qquad \text{(II-D-3)}$$

$$\text{Azimuth position limit} = \text{ABS}(\psi_H(\text{new}) - \psi_{H_{CAL}}(\text{old})) \qquad \text{(II-D-4)}$$

Using a 25 sample/second update rate, the required position and rate limits can be calculated. As long as the pilot does not exceed either the position or rate limits, then the target projector will remain fixed. As soon as either the rate limit or the position limit is exceeded, the target projector will move to a new position based on the commands from the head sensing unit. This allows for small head motions to be made and not affect the target projector and also helps eliminate noise on the signals from driving the target projector.

E. Visual Probe Drive Equations

The visual probe is also required to be slaved to the pilot's head (line of sight). The visual probe orientation is determined by the transformation matrix from earth axis to head axis, where

C_E^H, θ_{EQ}, ϕ_{EQ} and ψ_{EQ} are calculated as in section C.

The probe compensation required was based on the target projector transfer function of

$$H(s) = \frac{K}{s^2+2(.7)(25)\ s+(25)^2}$$

The probe was compensated to have a transfer function of

$$H(s) = \frac{K(s+55)}{s^2+2(.7)(25)s+(25)^2}$$

with the compensated probe having a 6% overshoot and a 6 ms lag. The compensation was performed in the digital computer, using the equation

$$\text{DRIVE} = \frac{(\text{ANGLE}_i - \text{ANGLE}_{i-1})}{\Delta T} * \frac{1}{55} + \text{ANGLE}_i.$$

The angles were nondimensionalized and ΔT was about 16 ms.

IN-FLIGHT SIMULATION STUDY OF DECOUPLED LONGITUDINAL CONTROLS FOR THE APPROACH AND LANDING OF A STOL AIRPLANE[1]

By Edward Seckel and Benjamin Feinreich

Princeton University

SUMMARY

A simulation study of a powered lift STOL transport having decoupled longitudinal controls for the approach and landing flight phases has been conducted on the Princeton Navion in-flight simulator. In the decoupled control concept, the natural interacting airplane responses (combined pitch attitude, speed, and flight path angle changes for fore and aft stick motion, for example) are suppressed, and the pilot operates a separate control lever for each variable.

In this study, fore and aft control column motion produced changes in flight path angle without changing attitude or speed; the throttle commanded speed changes independent of attitude or flight path angle; and the pitch trim wheel allowed independent pitch attitude changes.

Landings were made out of various typical STOL straight and segmented approaches using ILS and precision optical guidance. The flying qualities were judged to be very favorable, although a short period of adjustment to the unconventional constant-attitude, constant-speed flare was required. The precise control over flight path resulted in small touchdown point dispersion along with consistently low sink rates.

SYMBOLS

C_L lift coefficient

C_{L_∞} lift coefficient out of ground effect

$d\gamma/du$ change of flight path with speed, thrust constant, deg/kt

[1] This study was performed for NASA, Langley Research Center, under Contract NAS1-13502.

g acceleration due to gravity, m/sec^2, ft/sec^2

h altitude, m, ft

$\dot{h}$ vertical velocity, m/sec, ft/sec

M_u pitch acceleration derivative due to speed, $\frac{1}{I_y}\frac{\partial M}{\partial u}$, rad/sec^2 per m/sec, rad/sec^2 per ft/sec

M_{u_c} pitch acceleration derivative due to forward speed command input, $\frac{1}{I_y}\frac{\partial M}{\partial u_c}$, rad/sec^2 per m/sec, rad/sec^2 per ft/sec

M_α pitch acceleration derivative due to angle of attack, $\frac{1}{I_y}\frac{\partial M}{\partial \alpha}$, rad/sec^2 per rad

$M_{\dot{\alpha}}$ pitch acceleration derivative due to rate of change of angle of attack, $\frac{1}{I_y}\frac{\partial M}{\partial \dot{\alpha}}$, rad/sec^2 per rad/sec

M_γ pitch acceleration derivative due to flight path angle, (used when the equations of motion are written in u, γ, θ, rather than the more common u, α, θ; for unaugmented airplane $M_\gamma = -M_\alpha$), $\frac{1}{I_y}\frac{\partial M}{\partial \gamma}$, rad/sec^2 per rad

$M_{\dot{\gamma}}$ pitch acceleration derivative due to rate of change of flight path angle, $\frac{1}{I_y}\frac{\partial M}{\partial \dot{\gamma}}$, rad/sec^2 per rad/sec

M_{γ_c} pitch acceleration derivative due to flight path command input, $\frac{1}{I_y}\frac{\partial M}{\partial \gamma_c}$, rad/sec^2 per rad

M_θ pitch acceleration derivative due to pitch attitude, $\frac{1}{I_y}\frac{\partial M}{\partial \theta}$, rad/sec^2 per rad

M_{θ_c} pitch acceleration derivative due to pitch command input, $\frac{1}{I_y}\frac{\partial M}{\partial \theta_c}$, rad/sec^2 per rad/sec

$M_{\dot{\theta}}$ pitch rate damping, $\frac{1}{I_y} \frac{\partial M}{\partial \dot{\theta}}$, rad/sec^2 per rad/sec

p_g roll rate equivalent of linearly spanwise distributed vertical gust velocity component, rad/sec, deg/sec

q pitch rate, rad/sec, deg/sec

s Laplace transform variable

S wing reference area, m^2, ft^2

T thrust, N, lb

u airspeed perturbation, m/sec, ft/sec

u_g fore and aft gust velocity component, m/sec, ft/sec

v_g side gust component, m/sec, ft/sec

V_o trim airspeed, knots, m/sec, ft/sec

w vertical speed perturbation, m/sec, ft/sec

w_g vertical gust velocity component, m/sec, ft/sec

X_u longitudinal acceleration derivative due to forward speed, $\frac{1}{m} \frac{\partial X}{\partial u}$, 1/sec

X_{uc} longitudinal acceleration derivative due to forward speed command, $\frac{1}{m} \frac{\partial X}{\partial u_c}$, 1/sec

X_α longitudinal acceleration derivative due to angle of attack, $\frac{1}{m} \frac{\partial X}{\partial \alpha}$, m/sec^2 per rad, ft/sec^2 per rad

X_γ longitudinal acceleration derivative due to flight path angle, $\frac{1}{m} \frac{\partial X}{\partial \gamma}$, m/sec^2 per rad, ft/sec^2 per rad

X_{γ_c} longitudinal acceleration derivative due to flight path command input, $\frac{1}{m}\frac{\partial X}{\partial \gamma_c}$, m/sec^2 per rad, ft/sec^2 per rad

X_θ longitudinal acceleration derivative due to pitch attitude $\frac{1}{m}\frac{\partial X}{\partial \theta}$, m/sec^2 per rad, ft/sec^2 per rad

X_{θ_c} longitudinal acceleration derivative due to pitch attitude command input, $\frac{1}{m}\frac{\partial X}{\partial \theta_c}$, m/sec^2 per rad, ft/sec^2 per rad

Z_u vertical acceleration derivative due to forward speed, $\frac{1}{m}\frac{\partial Z}{\partial u}$, 1/sec

Z_{uc} vertical acceleration derivative due to forward speed command input, $\frac{1}{m}\frac{\partial Z}{\partial u_c}$, 1/sec

Z_w vertical acceleration derivative due to vertical speed, $\frac{1}{m}\frac{\partial Z}{\partial w}$ ($\equiv Z_\alpha / V_o$), 1/sec

Z_α vertical acceleration derivative due to angle of attack, $\frac{1}{m}\frac{\partial Z}{\partial \alpha}$, m/sec^2 per rad, ft/sec^2 per rad

Z_γ vertical acceleration derivative due to flight path angle, $\frac{1}{m}\frac{\partial Z}{\partial \gamma}$, m/sec^2 per rad, ft/sec^2 per rad

Z_{γ_c} vertical acceleration derivative due to flight path angle command input, $\frac{1}{m}\frac{\partial Z}{\partial \gamma_c}$, m/sec^2 per rad, ft/sec^2 per rad

Z_θ vertical acceleration derivative due to pitch attitude, $\frac{1}{m}\frac{\partial Z}{\partial \theta}$, m/sec^2 per rad, ft/sec^2 per rad

Z_{θ_c} vertical acceleration derivative due to pitch command input, $\frac{1}{m}\frac{\partial Z}{\partial \theta_c}$, m/sec^2 per rad, ft/sec^2 per rad

α angle of attack, rad, deg

γ flight path angle, rad, deg

γ_c flight path angle command, rad, deg

$\Delta(\ )$ perturbation from trim condition

δ_c fore and aft control column deflection, cm, in.

δ_f flap deflection, rad, deg

δ_{sp} spoiler deflection, cm, in.

δ_t horizontal tail deflection, rad, deg

δ_{th} throttle deflection, cm, in.

θ pitch attitude, rad, deg

$\dot{\theta}$ pitch rate, $\frac{d\theta}{dt}$, rad/sec, deg/sec

θ_c pitch command, rad, deg

INTRODUCTION

Piloting Problems of STOL Airplanes

The approach and landing is probably the most demanding task performed by the pilot of a transport airplane. It is even more so with an STOL aircraft that is landed out of a steeper glide slope with a higher accuracy requirement on touchdown dispersion. The problem is further complicated in the case of powered lift machines by their poor handling qualities in approach and landing. A stability augmentation system (SAS) is usually necessary to provide acceptable flying qualities. However, some deficiencies, mainly in the longitudinal plane, exist even with the stability augmentation. The most important problem is a poor flight path angle response to attitude changes which makes it difficult to use pitch attitude for precision control of the flight path. In the powered lift airplane a sizable flight path angle response is associated with the throttle, but if jet engines are the power plants, there is a time lag between the throttle movement and the change in engine thrust. This time lag creates problems in attempting to use the throttle as a precision flight path control. The inadequacy of either the control column or the throttle alone in the control of flight path angle necessitates the use of both. Typically all three flight variables,

flight path angle, forward speed, and pitch attitude change in response to control column displacement, and flight path and speed respond to throttle movement. Consequently, the pilot has to coordinate action on both levers in order to control the three coupled variables. All this results in the deficient flying qualities. Adverse ground effect and turbulence cause a substantial increase in pilot workload.

The above observations are substantiated by Reference 1 in which a fixed base simulator study that has been conducted by NASA Langley Research Center (LRC) is described. The purpose of this study was to determine the flight characteristics during the approach and landing of a representative STOL transport airplane having a high wing and equipped with an external-flow jet flap in combination with four high-bypass-ratio fan-jet engines (see Figure 1). Conventional stability augmentation systems (SAS) have been applied to obtain satisfactory handling qualities.

The Concept of Decoupling

Decoupled longitudinal controls have been suggested in Reference 2 in an attempt to improve the handling qualities of the airplane treated in Reference 1. The essence of this concept is to make each one of the three flight variables respond only to one cockpit control. In this study, the column was chosen to affect flight path angle and not to change speed or attitude. The throttle handle was chosen to control speed without affecting flight path or attitude, and a pitch-trim thumb wheel controlled attitude without changing flight path angle or speed. Provided that the quality and authority of each of the flight variable responses to their appropriate cockpit levers are adequate, the pilot can use one lever to control one flight variable.

In landing such a decoupled STOL airplane, speed and pitch attitude are stabilized early in the approach and the pilot does not have to concern himself with their active control any more. He can concentrate on controlling flight path angle by using the column only. With the excellent flight path response to column that was provided, this resulted in a very significant improvement of flying qualities which is especially pronounced in the presence of adverse ground effect and turbulence.

The price that has to be paid for this improvement is an unconventional and complex flight control system that in the configuration suggested in Reference 2, employed four feedback variables (u, α, θ, q) and four active control elements: throttle, symmetric spoiler, flap, and horizontal tail.

Ground Simulator Study of Decoupled Controls

A fixed base, ground simulator study of decoupled controls for the externally blown flap (EBF) STOL in the approach and landing was the subject of Reference 2. An improvement in flying qualities of the longitudinally decoupled airplane in comparison to the conventionally augmented one was reported. Visual cues in the simulator were obtained by a closed circuit television system. However, the use of this system for image generation caused difficulties in sensing altitude and altitude rate resulting in higher sink rates at touchdown and higher touchdown point dispersion along the runway than would be expected in real flight.

The same control concept has been tested on a moving base simulator (Reference 3) which increased the realism of the simulation by providing motion cues. However, a closed circuit television generated image of the same type that had been used on the fixed base simulator, was also used on the moving base simulator. Another deficiency of the moving base simulator resulted from the wash-out circuits needed to prevent position, velocity, and acceleration limiting.

In-flight Simulation Study of Decoupled Controls

This paper summarizes an in-flight simulation study of the longitudinal decoupled controls for the same airplane that was the subject of References 1, 2, and 3. This study which was conducted on Princeton's in-flight simulator, was motivated by the positive results obtained in the ground simulators. The more realistic environment of the in-flight simulator with its real-world visual cues and its full unlimited motion (for the STOL approach and landing problem) produces an investigation tool that is superior to ground simulators.

Decoupled lateral controls were also introduced and tested in the ground simulators; however, the advantages offered over conventional SAS were not as significant as in the case of longitudinal decoupling; therefore, the in-flight investigation included only the latter.

A more detailed account of the in-flight study may be found in Reference 4.

DESCRIPTION OF THE EXPERIMENT

The In-flight Simulator

The in-flight simulator is shown in Figure 2. It is a "fly-by-wire" airplane with adjustable stability and control characteristics. In this test program they were adjusted to match the characteristics of an EBF STOL transport in an approach and landing configuration having decoupled longitudinal controls in some experiments and conventional SAS in others.

Tested Configurations

Five control configurations were tested in this program. Three of them were variations of decoupled controls:

- Steady State Decoupled (SSD)
- Completely Decoupled (CD)
- "Recoupled" (REC)

Two configurations were variations of conventional augmentation:

- Stability Augmentation System (SAS)
- Improved Stability Augmentation System (ISAS)

Following are the descriptions of those configurations and their characteristics.

Steady State Decoupled (SSD) Configuration - The decoupled longitudinal control scheme, described in Reference 2, was the main subject of this study. In this design, steady state, rather than complete decoupling was implemented. The term "steady state decoupling" means that whereas only one of the three flight variables (airspeed, flight path angle, or pitch attitude) exhibits a steady state change in response to the appropriate cockpit control lever, the other two variables may undergo transient variations.

The Navion in-flight simulator control assignments for this configuration were: column to control flight path angle with a beep trimmer on the left horn to trim γ; throttle to control forward speed; pitch thumbwheel to control pitch attitude. The controls were mechanized such that the changes in the flight variables were proportional to control displacements from their trim positions. A constant $\pm 2^{o}$/sec γ rate was associated with the beep trimmer.

The schematic structure of the decoupling control system that was employed in Reference 2 is shown in Figure 3.

This system may be represented by the following equations:

$$\begin{bmatrix} s-X_u & -X_\gamma & -X_\theta \\ Z_u/V_o & (s+Z_\gamma/V_o) & Z_\theta/V_o \\ -M_u & -(M_{\dot\gamma}s+M_\gamma) & (s^2-M_{\dot\theta}s-M_\theta) \end{bmatrix} \begin{bmatrix} \Delta u \\ \Delta\gamma \\ \Delta\theta \end{bmatrix} = \begin{bmatrix} X_{uc} & X_{\gamma c} & \\ -Z_{uc}/V_o & -Z_{\gamma c}/V_o & -Z_{\theta c}/V_o \\ M_{uc} & M_{\gamma c} & \end{bmatrix} \begin{bmatrix} \Delta u_c \\ \Delta\gamma_c \\ \Delta\theta_c \end{bmatrix} \quad (1)$$

The terms in the left hand side (lhs) matrix are made of airframe stability derivatives, augmented by feedbacks of the F matrix. The right hand side matrix is determined by the G matrix. The airplane can be made steady state decoupled by choosing G such that the rhs of equations (1) equals the lhs with s = 0. The lhs matrix determines the airplane's response dynamics; therefore, the F matrix may be used to obtain desired dynamics of the responses of the three variables to their controls, as well as to minimize coupling transients.

Analog computer traces showing the responses of the steady state decoupled (SSD) EBF STOL of Reference 2 are shown in Figure 4. It can be seen that this configuration has a minimal amount of transient coupling. The responses of the three variables to their controls are rapid and very well behaved. This situation was achieved by highly augmenting all stability derivatives with respect to the basic airframe values. High augmentation increases turbulence sensitivity. This will be discussed further in following sections.

Completely Decoupled (CD) Configuration - Transient, as well as steady state decoupling, results from the following set of equations:

$$\begin{bmatrix} (s - X_u) & 0 & 0 \\ 0 & (s + Z_\gamma/V_o) & 0 \\ 0 & 0 & (s^2 - M_{\dot\theta}s - M_\theta) \end{bmatrix} \begin{bmatrix} \Delta u \\ \Delta\gamma \\ \Delta\theta \end{bmatrix} = \begin{bmatrix} -X_u & 0 & 0 \\ 0 & Z_\gamma/V_o & 0 \\ 0 & 0 & -M_\theta \end{bmatrix} \begin{bmatrix} \Delta u_c \\ \Delta\gamma_c \\ \Delta\theta_c \end{bmatrix} \quad (2)$$

In this configuration, feedbacks are used to null off-diagonal terms in the lhs matrix and, again, a prefilter, G, is used to obtain a diagonal right hand side matrix.

Unaugmented Navion derivatives were used in the left hand matrix diagonal with the exception of $M_{\dot{\theta}}$ which was augmented by a factor of about two to improve pitch damping.

Analog computer responses to step inputs of this completely decoupled configuration are shown in Figure 5. As expected, they do not exhibit any coupling transients; also, all three responses are noticeably slower than those of the SSD configuration (Figure 4). The responses could have been made faster by augmenting the Navion derivatives in the diagonal of the left hand side matrix. However, this was not done as the responses were judged to be quite adequate and, therefore, there was no reason to bear the penalty of increased turbulence sensitivity associated with augmented stability derivatives.

"Recoupled" Controls (REC) - This configuration was identical to the completely decoupled (CD) one with one difference: pitch attitude response to control column was restored, such that column displacement caused a change in pitch attitude that was of equal magnitude and in the same direction as the flight path angle change produced by the control column in the completely decoupled configuration. The reason for including this configuration in the study was that attitude changes might provide the pilot with a good visual cue to predict variations in flight path angle. It was felt that the elimination of this cue in the constant attitude landings with the decoupled configurations might present some piloting problems and that they might be alleviated by recoupling pitch attitude to flight path angle as they are coupled in conventional aircraft.

EBF STOL with Conventional Stability Augmentation System (SAS) - This configuration was the subject STOL aircraft with its conventional SAS as tested in a previous flight simulation program that has been carried out at Princeton (Reference 5). The SAS included pitch attitude and pitch rate feedbacks to the horizontal tail to provide a pitch attitude command/hold system. Speed feedback to the flap and symmetric spoilers was incorporated in the system to enhance speed stability.

Improved SAS (ISAS) Configuration - A modified SAS configuration was evaluated in order to explore the possibility of improving handling qualities of the SAS airplane with a control system that is not as complex as the decoupling system. The modifications of the SAS were the following:

- Lift response to angle of attack, Z_{α}, augmentation was incorporated.
- The speed stability parameter, $d\gamma/du$, was changed from zero to a small negative value.

- The thrust response lag was reduced (implying throttle to spoilers or flaps interconnect).
- The thrust control sensitivity, $Z\delta_{th}$, was increased.

Figure 6 shows a comparison of the SAS and ISAS configurations. The major advantage of the ISAS is an improved flight path response to control column input, having a faster rise time and settling down at a positive steady state value rather than going back to zero as in the SAS case. The Z_α augmentation is the main contributor to this improvement. The rise time of the flight path response to throttle was also shortened in the ISAS, mainly by the reduction of the thrust lag.

Simulation of Turbulence - Three components of turbulence were simulated in this program: fore and aft, u_g; vertical, w_g; and spanwise gradient, p_g. Turbulence signals that had been prerecorded on a magnetic tape were channeled into Navion controls to produce simulated turbulence-induced accelerations. The magnitudes of the accelerations were proportional to the appropriate stability derivatives of each configuration. Augmented, rather than bare airframe, stability derivatives were used in calculating turbulence sensitivity, as it was assumed that aerodynamic sensors were used in the feedback loops.

Lateral Directional Dynamics - Lateral directional dynamics that are typical for the subject airplane were employed in this program with all the various longitudinal configurations.

Adverse Ground Effect - A lift loss of $\Delta C_L/C_L \doteq -0.1$ was simulated. No moment or drag changes were included.

Test Procedure and Conditions

The test pattern that was used is shown in Figure 7. The approaches were either straight-in with 6° or 4° glide slope angles, or segmented with an initial 9° or 6° angle transitioning into a final 4° segment. The normal approach speed was 70 kts. The outer part of the approach was simulated IFR using a TALAR (Tactical Landing Approach Radar) MLS (Microwave Landing System) unit. At an altitude of 61 m (200 ft) the pilot transitioned to VFR, using optical glide slope light bars for guidance. The task required touching down within a 61 m (200 ft) long marked area on the runway with a rate of sink as low as possible.

Evaluation was mainly based on pilot rating using the familiar Cooper Harper scale adopted from Reference 6. Landing performance in terms of

touchdown distance and rate of sink was also measured. Most of the evaluations were flown by two Princeton University pilots.

RESULTS AND DISCUSSION

The Decoupled Configurations Compared to the STOL Airplane With Conventional SAS

General Aspects of Landing the Decoupled Airplanes - The steady state decoupled (SSD) STOL airplane turned out to be very well-behaved. The approach-and-landing was performed at a constant pitch attitude, and speed was constant at 70 kts. In calm air, speed and pitch attitude stayed at their selected trimmed values without any pilot intervention so that he had to control only flight path. Flight path response was judged to be very favorable in terms of quickness and authority.

A short period of adjustment was required for one of the pilots to accept the visual aspects of the constant attitude flare. The lack of aircraft rotation made this pilot underestimate the amount of flight path angle change associated with column deflection. This caused him to overflare. An overflare with the decoupled airplane resulted in a substantial touchdown overshoot since it maintained a parallel to the runway or slightly ascending flight path, and a constant speed unlike a conventional airplane that would lose speed and eventually settle down under similar circumstances. The decoupled airplane, following an overflare, had to be brought down by releasing pressure from the column. However, after a short learning period, this pilot was able to acquire the proper technique that resulted in a consistently precise touchdown at the middle of the prescribed zone, with a very low sink-rate and with a very small work load. The other Princeton pilot, having more experience with unconventional configurations, did not need even the short adjustment period. It turned out that the visual and normal acceleration cues that are available in a constant attitude flare, are quite adequate, enabling the pilot to land the airplane with remarkable precision.

Both pilots gave this configuration a Cooper rating of 2.0 for a 4^{o} approach with no turbulence. This applies to the instrument part of the approach to the visual part, and to the flare-and-landing.

The completely decoupled (CD) configuration, in calm air, received ratings practically identical to those for the steady state decoupled (SSD) STOL, as might be predicted considering the similarity of the time responses of the two configurations.

Some quotations from pilot commentary about the decoupled configurations under no-turbulence conditions follow:

> Pilot A: "This configuration, in the ideal no-wind, no-turbulence conditions tested, is very good. The airplane is controlled very easily on the glide slope where speed is maintained automatically and the pilot has to control γ only."
>
> Pilot B: "Airplane can be landed smoothly and accurately; still, it is different from a conventional airplane in the fact that a normal airplane in the case of an overflare will eventually lose some speed and touchdown. In this airplane an overflare results in no touchdown unless pressure is released from yoke."

A flight path to column control sensitivity of $\Delta\gamma/\Delta\delta_c = 1.0$ deg/cm (2.7 deg/inch) was found to be a good value for the approach, and for a flare out of a 4^o approach. A 35% higher value was preferred by the pilots for flying in simulated turbulence or landing out of a 6^o approach.

The capability to trim out forces on the glide slope was considered an important feature of the decoupled system. A flight path trim rate of $\dot{\gamma}_{TRIM} = \pm 2^o$/sec was found to be convenient. The trimmer was used quite extensively to make corrections on the approach.

6^o Approach - No degradation in pilot rating was associated with the steeper, 6^o, final segment of the approach. The pilots felt that the responsive control they had over flight path minimized the increase in work load that might have been associated with a higher rate of sink.

Ground Effect - Ground effect variations of $-0.1 < \Delta C_L/C_{L_\infty} < +0.20$ were tested and found to have no significant impact on landing the decoupled configurations. The pilots felt that with the tight flight path control that could be applied, they had no problem in counteracting the ground effect "suckdown." In contrast to these results, in the case of the STOL with conventional SAS, adverse ground effect contributed to piloting difficulties and accentuated other airplane deficiencies, as reported in Reference 5.

Figure 8 shows a landing time history for the steady state decoupled configuration for a 6^o approach with no turbulence. It is very clear that the flare was performed by the column only. The pilot did not touch the throttle (or rather speed handle) throughout the flare. He made a small θ adjustment prior to flare initiation. Speed and attitude are essentially constant and $\Delta\delta_c$, $\Delta\gamma$, and $\dot{h}$ change smoothly from flare initiation to touchdown at $h = 0$.

Segmented Approaches - $6^{\circ}/4^{\circ}$ and $9^{\circ}/4^{\circ}$ approaches have been performed and have not been found to present any piloting difficulties with the decoupled configurations. The pilots felt that the task was quite easy to perform. The flight path trimmer was the main controller used by the pilots in turning the two segment corner. In calm air almost no control column motion was used and the corner was turned on trimmer only.

Aborted Approaches - Aborted approaches were tested with the decoupled configurations on several runs. The go-around technique for these airplanes was simply to pull on the column in order to command an up flight path angle. This indeed was very easy to do and presented no handling problem, and was rated at 2.0; however, the simulator climb performance was very limited in this maneuver. The Navion in this respect was probably not an accurate simulation of the STOL; however, the climb performance of the STOL is also very limited in the landing configuration, and therefore the simulation was not unrealistic. A rate of climb of 1.52 m/sec (300 ft/min) could be established, and the pilots considered it acceptable.

STOL with Conventional SAS - The STOL with conventional SAS was clearly a more difficult machine to control. It was described by the pilots as sloppy and sluggish and they had to work harder to obtain touchdown performance similar to that of the decoupled configurations. Landing it required the coordinated use of both column and throttle because neither alone provided adequate flight path control. The response of $\dot{\gamma}$ to column contained a transient due to the presence of γ_w, but no steady state as $d\gamma/dv$ was zero. The transient was not big enough to permit using the column as the sole controller in the flare. The throttle, on the other hand, did produce steady state changes in γ, but because of the lag that was associated with it, the pilots could not use it for the rapid fine lift modulations that were required in the flare.

A landing time history for the SAS configuration at a 4° approach with no turbulence but with the nominal ground effect ($\Delta C_{L_{max}} = 0.1\, C_{L_{\alpha}}$) is shown in Figure 9. The extensive use of the throttle is in obvious contrast to the situation in the decoupled airplane. A throttle advance about 8 seconds prior to touchdown is employed in order to obtain the desired steady state change in γ.

Figure 10 provides a comparison of pilot ratings assigned to the completely decoupled (CD) configuration and to the SAS airplane. (CD and SSD have the same ratings in the absence of turbulence.) With no turbulence the SAS is seen to be rated 3.0 for the approach, which is one unit worse than the CD configuration. For the landing, the SAS is rated 4.0, or two units worse than the decoupled airplane.

The improved SAS (ISAS) configuration is seen in Figure 10 to be rated significantly better than the airplane with the conventional SAS. With no turbulence it is rated only 0.5 units below the CD configuration for the approach and 0.75 units for the landing. The ISAS was found to be better than the SAS because of its improved flight path response to column and to throttle. However, the pilots still elected to use both hands in coordination while flying this airplane. They could rely more on the control column and less on the throttle in flaring the airplane, but they still did not have sufficient confidence to use a single control. This explains the slightly worse rating of the ISAS with respect to the decoupled configuration.

The Effects of Turbulence - Turbulence was simulated in this program as described in the Tested Configurations section. In the steady state decoupled configuration (SSD), as was indicated before, highly augmented stability derivatives were employed in order to achieve fast responses to pilot controls, and minimal coupling transients. Since it was assumed that aerodynamic, rather than inertial, sensors were used for augmentation, simulated turbulence disturbances were proportional to the augmented stability derivatives, rather than to those of the bare airframe. This resulted in an excessive sensitivity to turbulence of the SSD configuration that was beyond the control capability of the simulator. Therefore, this configuration had to be tested at a lower level of simulated turbulence (about one-fourth) than the other configurations. Using the same ground rules, the CD configuration was much less sensitive as its off diagonal stability derivatives were nulled (through the use of feedbacks), and all of its derivatives were lower than those of the SSD. This made it possible to test the CD configuration with the same amount of turbulence in which the conventionally augmented (SAS) STOL was tested; therefore, the CD, rather than SSD was used in comparing the effects of turbulence on the decoupled versus SAS configurations.

The main problem incurred by turbulence with all tested configurations, was heave upsets. Increased pilot effort was required to counter those upsets, depending on their magnitude and on the effectiveness of the available flight path control. Speed disturbances were also caused by turbulence; however, since they were mostly of low magnitude and frequency higher than available with speed control, the pilots chose to accept those disturbances rather than try to fight them.

Figure 11 provides a comparison of landing the decoupled configurations with and without turbulence. The turbulence related heave motions can be seen on the $\Delta\gamma$ trace, and the increased pilot activity is very obvious in the control column trace.

The effect of turbulence on pilot ratings of the various configurations can be seen in Figure 10. The CD in landing is seen to be degraded by turbulence from a rating of 2.0 to 3.0 which is still a good position in the Cooper scale. The SAS is degraded from 4.0 to 5.5 which is not too good, as a rating higher than 6.5 puts an airplane under the "major deficiencies" label. The ISAS in landing with turbulence is rated at 4.0, which is not quite as good as the decoupled airplane, but it is significantly better than the SAS.

It should be emphasized that a high sensitivity to turbulence is not inherent in the steady state decoupling concept. The particular configuration that was tested in this study turned out to be that way since, as discussed previously, the best possible transient response was sought in the design, whereas turbulence sensitivity was not taken into account. Turbulence sensitivity is an important factor affecting aircraft handling qualities and it should be taken into account in the design of an augmentation system. Turbulence sensitivity may be reduced by:

- Avoiding highly augmented stability derivatives if aerodynamic sensors are to be used.
- Using inertial sensors.
- Filtering.

Indeed, the turbulence sensitivity of the SSD configuration has been reduced in the moving base simulator study of Reference 3.

Landing Performance

Figure 12 compares the landing performance obtained with the decoupled airplane to the performance of the conventionally augmented STOL. The data used in this figure included runs with turbulence and without it. The median touchdown point of both configurations is seen to be very close to the center of the touchdown zone (0 in the figure). The spread is very small for the decoupled airplane and somewhat bigger for the SAS. The median rate of sink of the decoupled control scheme is a very good deal less than 0.3 m/sec (1 fps), and its spread is very small. The median rate of sink of the SAS is significantly higher, at 0.6 m/sec (2 fps), but still acceptable. The SAS rate of sink spread is markedly higher than the results with the decoupled configuration.

Figure 13 shows a comparison of results obtained with the decoupled airplanes in the in-flight simulation versus the ground simulator studies of References 2 and 3. It is very obvious that the in-flight results are much

better than those of both fixed base and moving base ground simulators. Going from fixed base to moving base ground simulator, seems to improve noticeably the rate of sink performance, but hardly affects touchdown distance results.

The Recoupled Configuration

The recoupled configuration was derived from the completely decoupled one by restoring pitch attitude response to control column, equal to the flight path angle change, as described in the Tested Configurations section. This was done in an attempt to evaluate the role of pitch attitude as a cue that might help the pilot in judging flight path changes. This configuration was introduced into the program after the pilots had flown the decoupled airplanes extensively. The surprising result was that the pilots found the recoupled control scheme to be somewhat less desirable than the decoupled one. The first reaction of both pilots to landing the recoupled airplane was to rate it by 0.5 unit worse than the decoupled case. After some more experience had been gained, one of the pilots thought that the recoupled configuration might be equivalent to the decoupled one, whereas the other pilot retained his opinion that recoupling caused some degradation of flying qualities.

Pilot commentary: "No advantage over the decoupled airplane. ILS tracking: attitude coupling neither helps nor hurts. Visual tracking: don't get much help out of attitude change. Get information from [the glide slope] lights. There is a problem for close-in down-gamma correction; I don't like the nose going down in response to a down-gamma command. Flare and touchdown: very much like a normal airplane. Nose up and down motion interferes with good prediction of the touchdown point. The ability to judge sink rate close-in is not improved by the theta coupling."

To conclude, the results of the tests indicate that coupling attitude to flight path does not provide any advantage over the decoupled situation. This suggests that the perceptions obtained by the pilot from the visual and motion cues that are available in a constant attitude landing, are clearly adequate for the task and no additional improvement is obtained by using pitch attitude changes.

Deceleration Prior to Touchdown

It was felt that it might be advantageous for the powered lift STOL airplane to approach at a speed that is somewhat higher than the touchdown speed, as this might improve handling qualities, and performance for a

possible aborted approach. This, of course, necessitates a speed reduction prior to touchdown. Runs in which the pilots were requested to fly the approach at 75 kts and touchdown at 70 kts were incorporated in the flight program in order to evaluate the effect of the deceleration maneuver on piloting with the various configurations. Speed reduction was performed with the decoupled configurations by simply pulling back on the speed command lever (throttle). In the ISAS configuration, a simulated autopilot speed command dial was employed, and in the SAS, coordinated control column and throttle movements had to be used in slowing the airplane down. The pilots were requested to reduce speed below breakthrough altitude, but no precise point was specified. It turned out that an increment in workload was caused by the deceleration in all cases. The amount of this increment depended on how well the approach was going prior to the deceleration, and on the configuration. With the decoupled configurations deceleration was easy and could be done in coincidence with the flare. The ISAS and SAS configurations required an ever increasing effort. The increased difficulty in performing the deceleration was offset by the pilots' choice to slow the harder configurations down at a higher altitude.

Further details on this subject are given in Reference 4.

CONCLUSIONS

Three variations of decoupled longitudinal control configurations and two variations of conventionally augmented longitudinal control configurations for an EBF STOL airplane in the approach and landing flight phases were studied through in-flight simulation. The conclusions of this study follow:

1. The decoupled longitudinal controls that were tested produced very favorable flying qualities in the approach and landing. This resulted in small touchdown dispersions along with consistently low sink rates.

2. Adverse ground effect did not cause any piloting problems with the decoupled airplane as it could be easily countered by control actions.

3. Segmented approaches, in which an initial 9° glide slope segment was followed by a shallower 4° or 6° final segment, were easy to perform with the decoupled airplane. Turning the corner between segments was found to be an easy task. No significant degradation was associated with using a 6° rather than a 4° final glide slope.

4. No significant differences in flying qualities were found between the steady state and completely decoupled control concepts. This conclusion would seemingly apply for any steady state decoupling scheme in which transients were kept sufficiently small and of short duration.

5. The extreme turbulence sensitivity of the steady state decoupled control scheme that was tested in this study, resulted from the use of high feedback gains along with aerodynamic sensors as sources of feedback signals. High sensitivity to turbulence is not inherent in the steady state decoupling concept. It may be reduced by either using inertial sensors, or by avoidance of high gains in feedback paths. Sensitivity to turbulence must be considered in the design of such a control system.

6. The completely decoupled configuration which, under the assumptions adopted in this study, had a low sensitivity to turbulence produced in simulated turbulence a very significant improvement in flying qualities with respect to the conventional SAS that was tested.

7. The recoupled configuration in which pitch attitude changed along with flight path, but which was otherwise decoupled, did not result in any improvement of flying qualities with respect to the decoupled configurations. This suggests that the perceptions obtained by the pilot from the visual and motion cues that are available in a constant attitude landing, are clearly adequate for the task and no additional improvement is obtained by using pitch attitude changes.

8. The conventionally augmented airplane that was tested had significantly poorer handling qualities than the decoupled configurations, especially for landing in turbulence and with adverse ground effect. The piloting problems of this airplane resulted mainly from its low lift response to angle of attack, the lag associated with the throttle response, and the resulting necessity to use coordinated control column and throttle action in controlling flight path.

9. Modifying the conventional SAS by increasing lift response to angle of attack, Z_α, changing $d\gamma/du$ from zero to a small negative value, increasing thrust control sensitivity, Z_{δ_t}, and reducing thrust response lag, yielded a significant improvement in pilot rating, but the overall level of handling was judged to be not as good as for the decoupled configurations.

REFERENCES

1. Grantham, W. D., Nguyen, L. T., Patton, J. M., Jr., Deal, P. L., Champine, R. A., and Carter, C. R.: Fixed-Base Simulator Study of an Externally Blown Flap STOL Transport Airplane During Approach and Landing. NASA TN D-6898, October 1972.

2. Miller, G. K., Jr., Deal, P. L., and Champine, R. A.: Fixed Base Simulation Study of Decoupled Controls During Approach and Landing of a STOL Transport Airplane. NASA TN D-7363, February 1974.

3. Miller, G. K., Jr. and Deal, P. L.: Moving-Base Visual Simulation Study of Decoupled Controls During Approach and Landing of a STOL Transport Aircraft. NASA TN D-7790, January 1975.

4. Feinreich, B.: In-Flight Simulation Study of Decoupled Longitudinal Controls for the Approach and Landing of a STOL Aircraft. NASA CR-2710, to be published summer 1976.

5. Ellis, D. R.: An In-Flight Simulation of Approach and Landing of a STOL Transport with Adverse Ground Effect. Princeton University Report No. 1267, December 1975.

6. Harper, R. P., Jr. and Cooper, G. E.: The Use of Pilot Rating in the Evaluation of Aircraft Handling Qualities. NASA TN D-5153, April 1969.

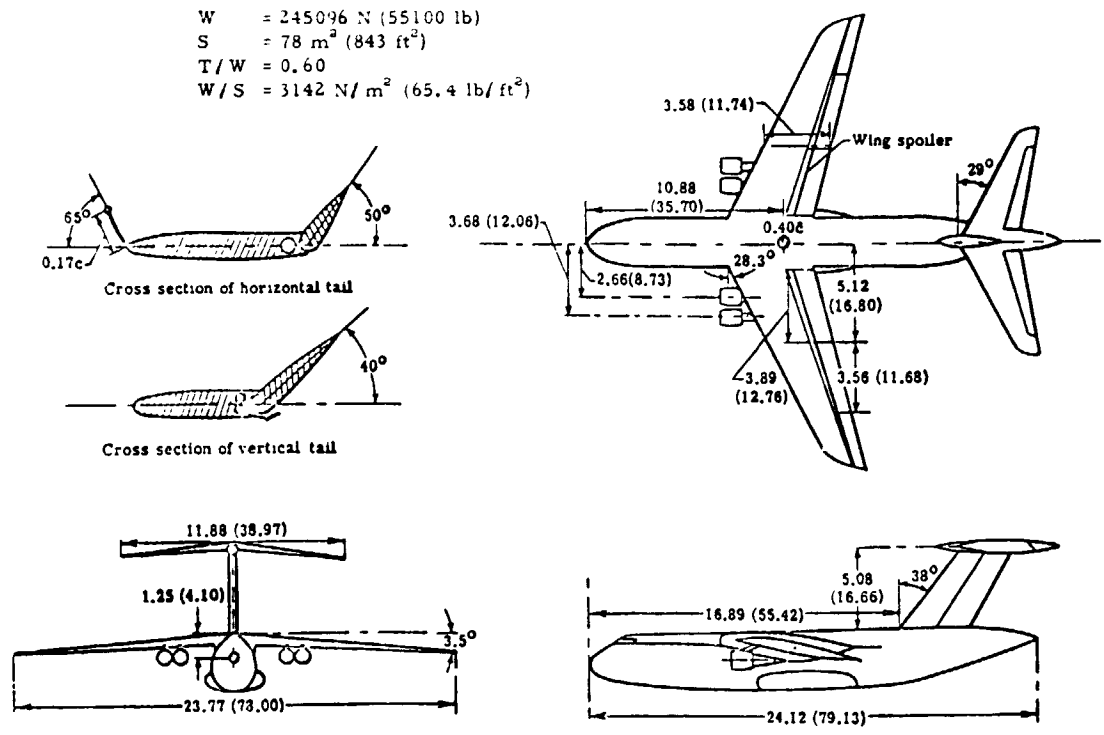

Figure 1. Three-View Drawing of Simulated Airplane (All Linear Dimensions are in Meters (ft))

Figure 2. The Princeton In-Flight Simulator

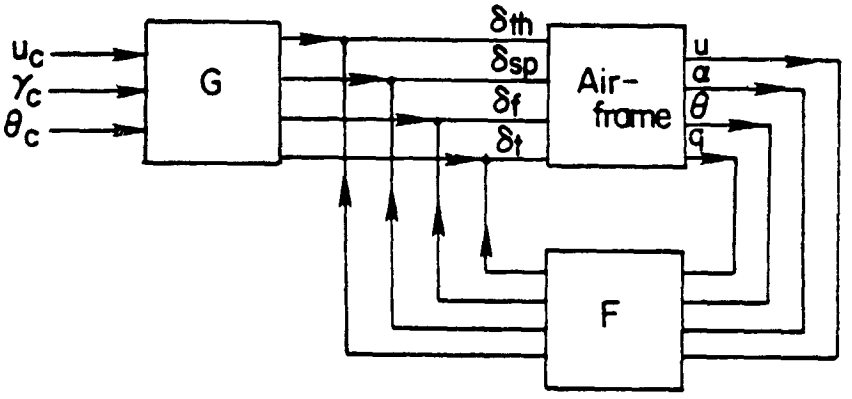

Figure 3. Schematic Block Diagram of the Steady State Decoupling System

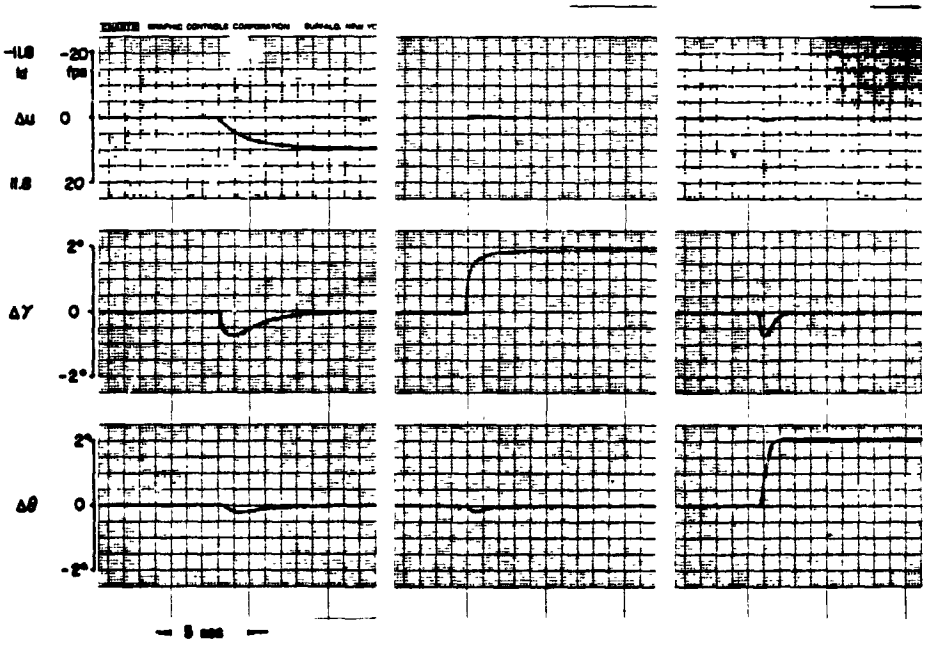

Figure 4. Analog Computer Generated Responses of the Steady State Decoupled Configuration to Step Inputs

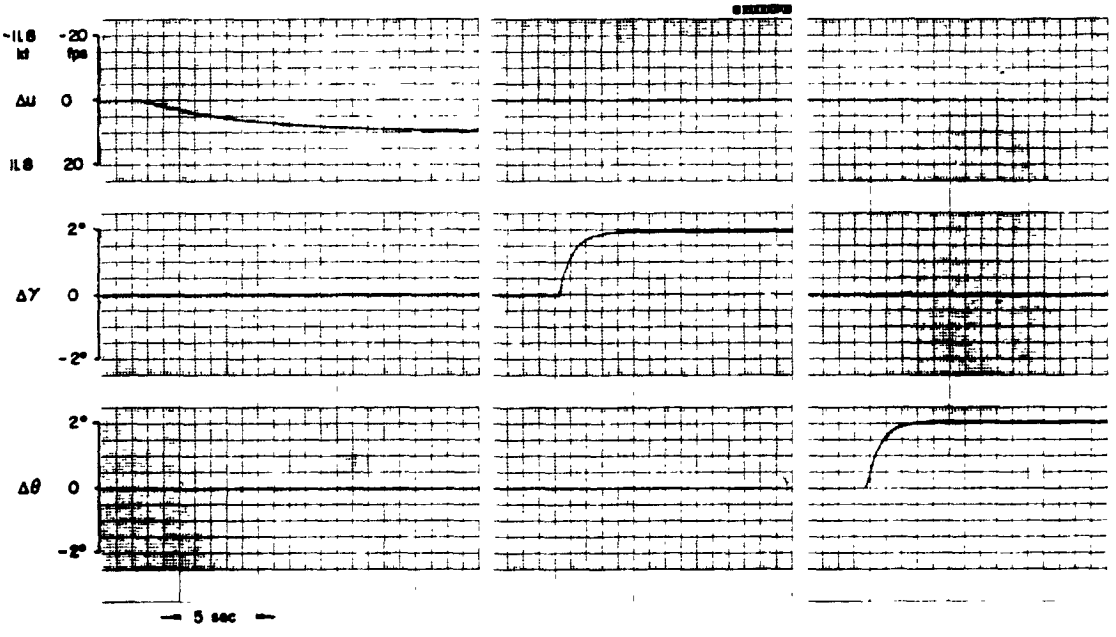

Figure 5. Analog Computer Generated Responses of the Completely Decoupled Configuration to Step Inputs

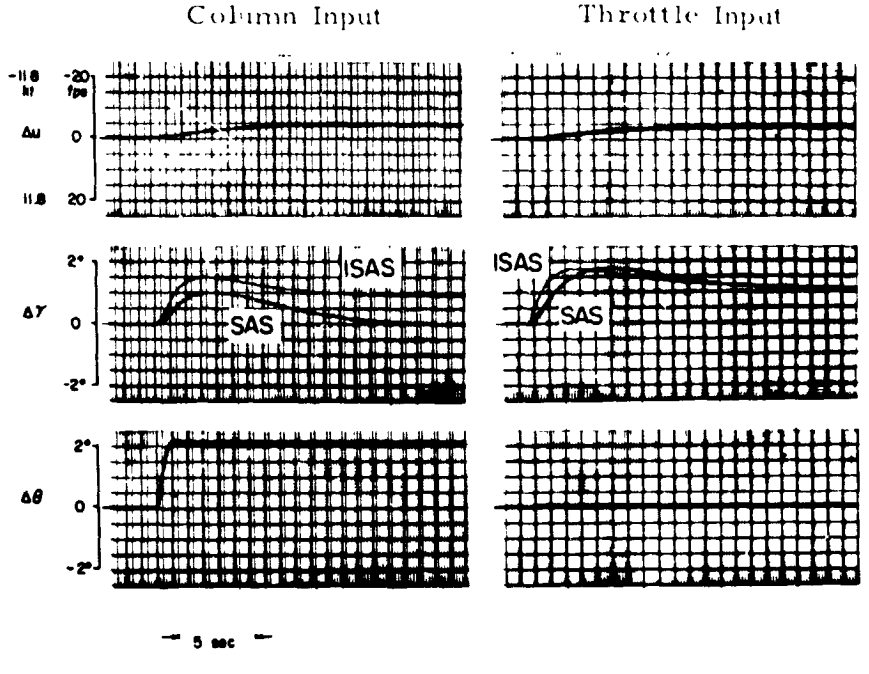

Figure 6. Analog Computer Traces of the SAS and ISAS Configurations' Responses to Step Inputs

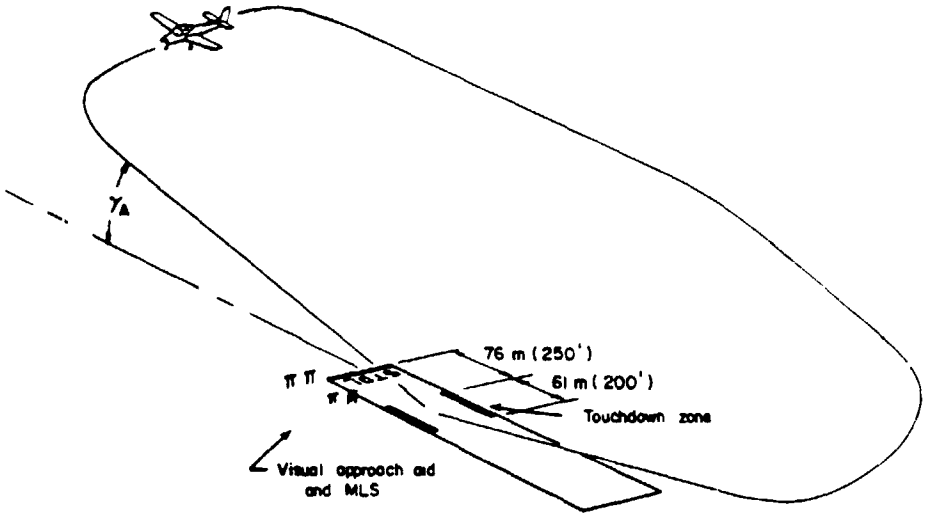

Figure 7. Simulated STOL Runway and Flight Pattern

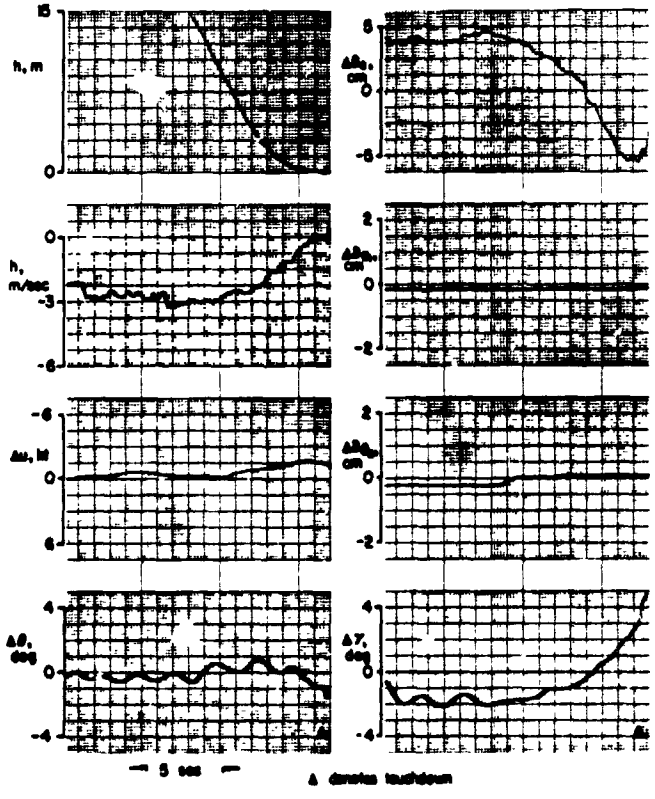

Figure 8. Landing Time History of the Steady State Decoupled Configuration. 6° Approach; Adverse Ground Effect, No Turbulence.

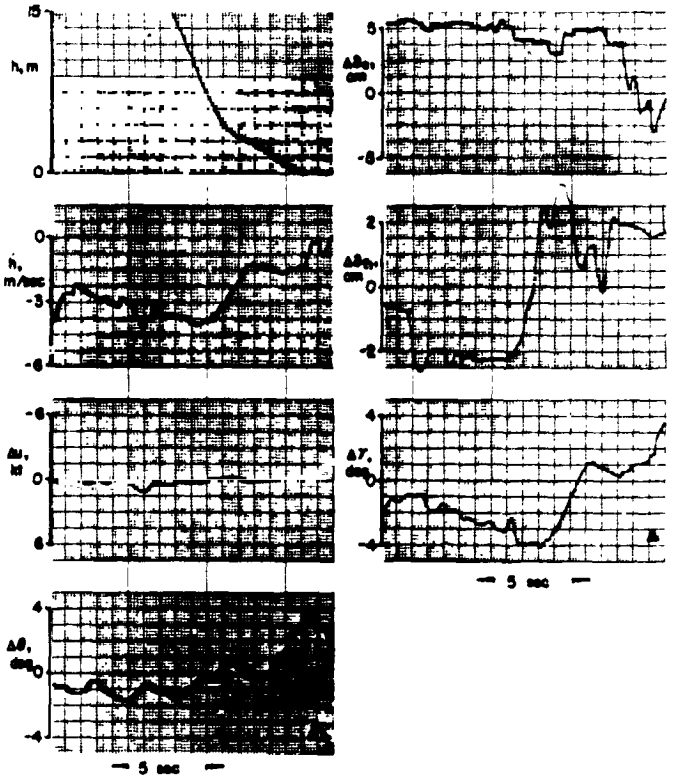

Figure 9. Landing Time History of the SAS Configuration. 4° Approach; Adverse Ground Effect; No Turbulence.

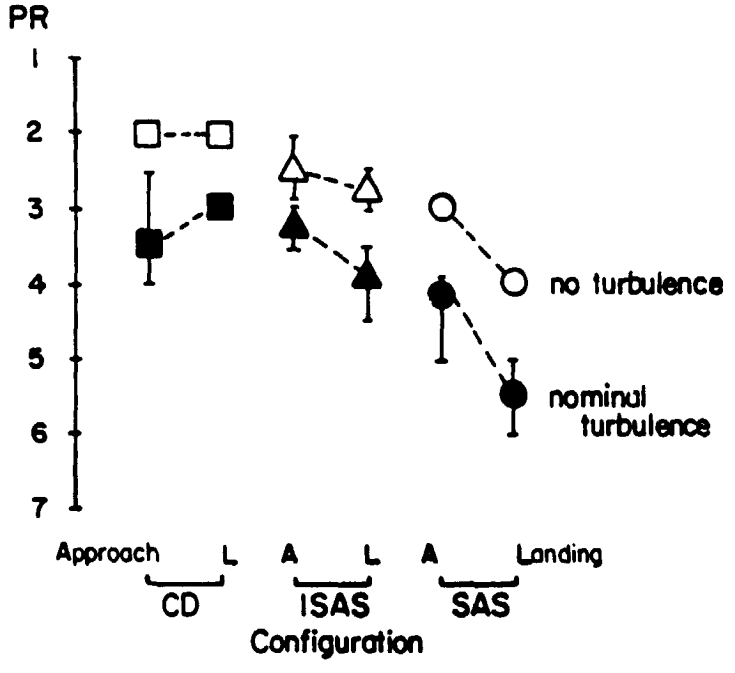

Figure 10. Pilot Ratings for the Approach and Landing of the CD, ISAS, and SAS Configurations

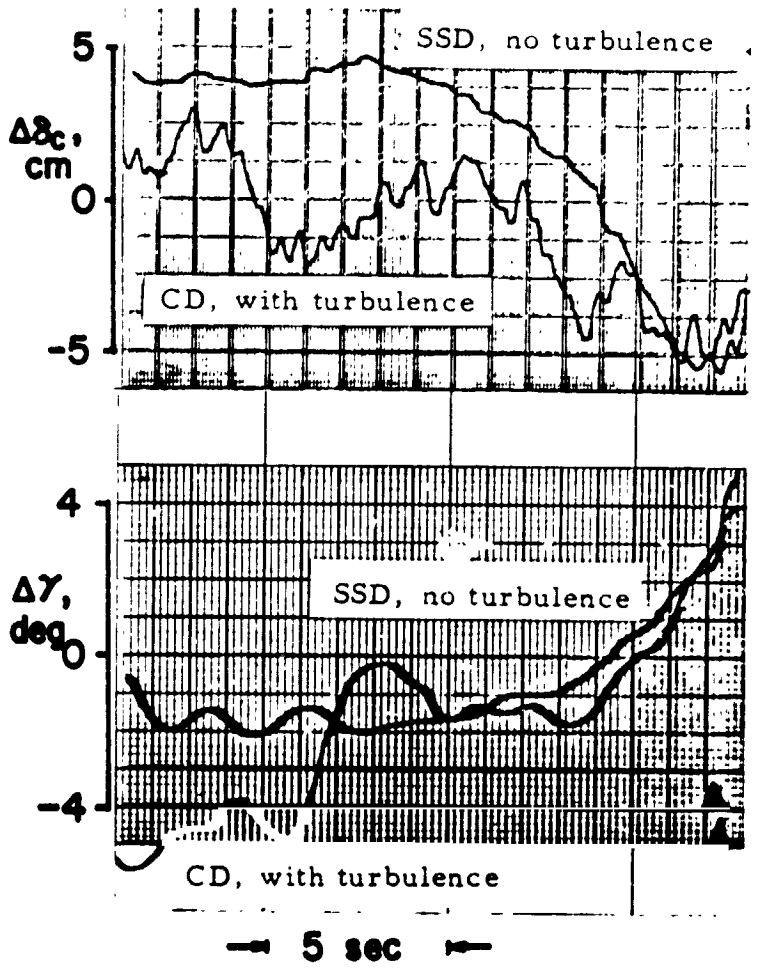

Figure 11. Superimposed Landing Time Histories of CD Configuration with Turbulence, and the SSD with No Turbulence

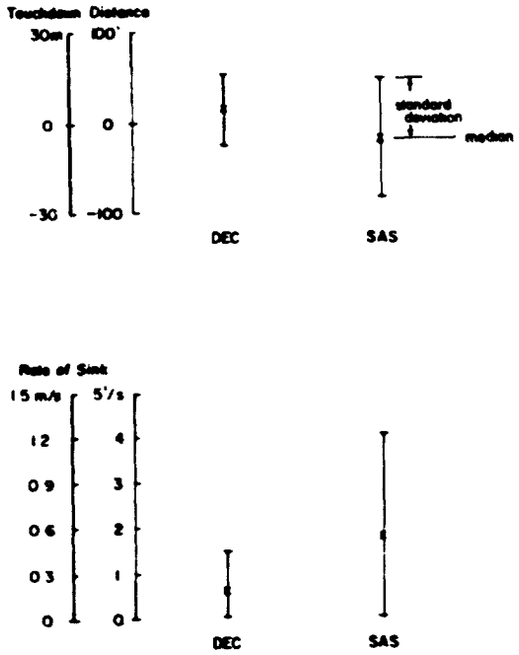

Figure 12. Landing Performance Results

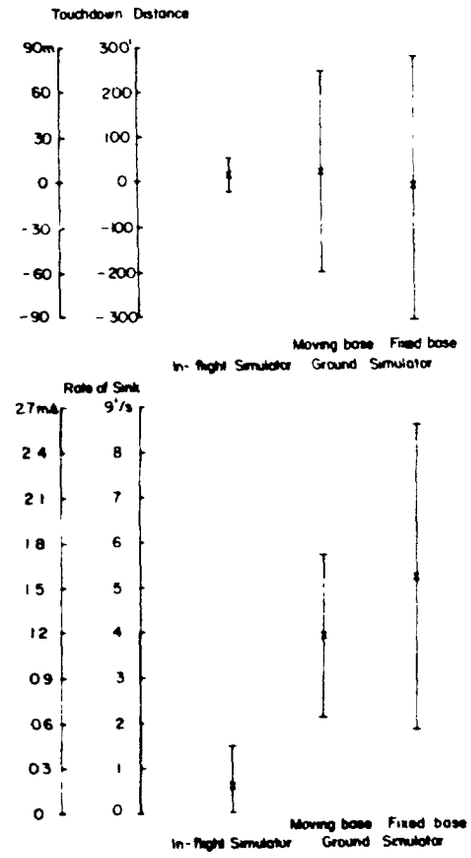

Figure 13. Landing Performance of the Decoupled Airplane Flight vs Ground Simulators

HIGH ACCELERATION COCKPIT DISPLAYS AND CONTROLS

By James A. Townsend and Norbert J. Kropewnicki

Air Force Flight Dynamics Laboratory

SUMMARY

Modern fighter maneuverability has outstripped the pilot's physical capability to perform in air-to-air combat. The objective of the Air Force High Acceleration Cockpit program is to provide pilots with increased physiological protection during sustained and repeated high G air-to-air combat maneuvers. A major breakthrough in useful combat maneuverability can be achieved by providing the pilot with an advanced cockpit design incorporating an articulating pilot seat which allows the pilot to reposition himself for high energy, high G maneuvering. Controls, displays, ejection seat, restraining system, seat supinating/reclining actuation system, and other man-machine interfaces are included in the cockpit design.

This paper describes the High Acceleration Cockpit (HAC) Program in general with emphasis on the fighter cockpit design relationships, including side-stick and throttle characteristics and the design of displays to retain total mission capabilities of the aircraft. Results of pilot evaluations of complete mockups and highlights of other work to date are presented.

INTRODUCTION

A new concept in the field of fighter aircraft crew station design and control display technology has emerged in the form of the High Acceleration Cockpit, commonly referred to as the HAC cockpit. This concept has been developed since 1970 and is just now in the threshold of a full scale evaluation in a TF-15 fighter aircraft. The latest complete step to date in the development of this concept is the HAC Applications Study - the basis of this paper.

BACKGROUND

The beginning of the development activity in HAC was founded on the growing appreciation of the fact that new fighter designs were outgrowing the human pilot's capabilities in sustained high-G (3 to 7) turns

repeated several times in an air combat engagement. Not only were the pilot's maximum G tolerances going to be good over too short a time span compared to the airplane's continuous high G maneuvering capability, but the fatigue effect of repetitive exposures would dramatically reduce post-G tracking accuracy and ability to fly several combat missions a day in a wartime scenario.

The HAC concept, that of repositioning the pilot transverse to the load vector is intended to significantly increase his G tolerance, reduce his workload and fatigue, and improve his cognitive capability.

Figure 1 illustrates the effect of HAC seat back angle on increasing the useable ACM envelope.

Figure 2 illustrates the principle of the HAC seating concept, which provides a reduction in the height of the hydrostatic column between eye and heart by allowing the G forces to act transversely. Blood pressure at eye level can be maintained and blood pooling in the lower extremities can be reduced with a consequent lowering of heart rate.

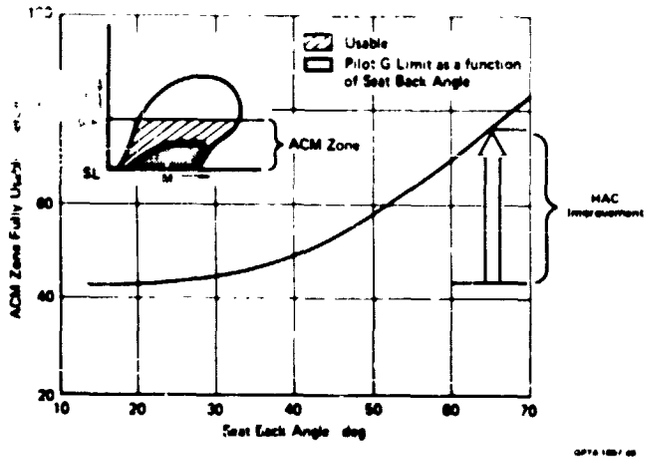

Figure 1
Usable ACM Envelope Expansion
For Continuous Sustained Maneuvering
on a Routine Basis

Centrifuge tests conducted at Wright-Patterson AFB, (AMRL) and Brooks AFB, (AMD/SAM) (Ref. 1) have demonstrated that the HAC concept provides significant improvement in pilot cognitive functioning and physiological condition in the 3 to 10 G range when the seat back angle is rotated above 45 degrees and up to 65 degrees. A 2 to 3 G improvement in normal G tolerance has been shown with substantial increase in tracking performance and comfort at all G levels during combat type maneuvers

Background studies in the last two years have also included two manned air combat simulations at McDonnell Aircraft Company's dome simulator. Manned simulation involved subjects from Tactical Air Command. Results indicated a distinct and consistent combat advantage for the HAC equipped "aircraft" and a reduction in overall high G exposure because of the early advantage attained over the non-HAC equipped adversary. (Ref. 2).

Indications from the latest of these simulations based on one-on-one encounters comparing a HAC-equipped 10.5 G fighter with a non-HAC equipped 7.5 G fighter of otherwise similar design against a common threat aircraft include:

a. 20% more first offensive opportunities for HAC A/C (Engagements converted to first kill).

b. 20% reduction in threat a/c first conversion capability.

c. 50% increase in cumulative missile hits in the first 40 seconds of the encounter.

d. 200% increase in cumulative bullet hits in the first 40 seconds of encounter.

e. 80% increase in kill ratio in the first 40 seconds of encounter.

f. 75% reduction in load limit exposure of HAC fighter versus non-HAC fighter.

g. Average G level reduced from 3.5 G for non-HAC a/c to 3.3 G for HAC a/c.

h. Improved tracking

i. Improved vision

j. Reduced pilot workload-physical and cockpit operations.

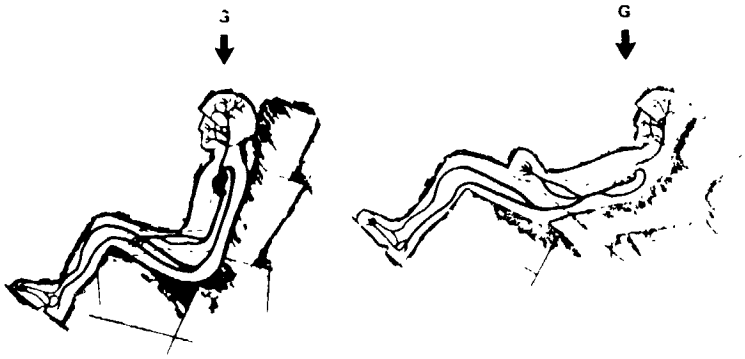

Figure 2

THE APPLICATIONS MOCK-UP STUDY

Our mock-up or design aid study consisted of the following major elements (Ref. 3):

a. Construction of a full scale cockpit mock-up of the single seat version of the F-15.

b. Modification of a conventional ejection seat to include the HAC reclining/lifting capability (positioning system).

c. The effect of the pilot positioning system on the pilot's ability to accomplish his mission tasks.

d. Flight controller (side arm) and throttle integration and evaluation for the range of seat positions.

e. Evaluation of control/display concepts designed to provide accessibility and visibility from all seat positions.

f. Test Plan preparation and static evaluation of candidate cockpit configurations by six operational fighter pilots.

Figure 3 depicts the HAC concept in the full scale mock-up design aid. The standard ejection seat and launch rails are in the normal upright position. The HAC articulating seat liner can be raised to the reclined and lifted position at the pilot's option when he needs load factor protection. The cockpit was designed so that while flying

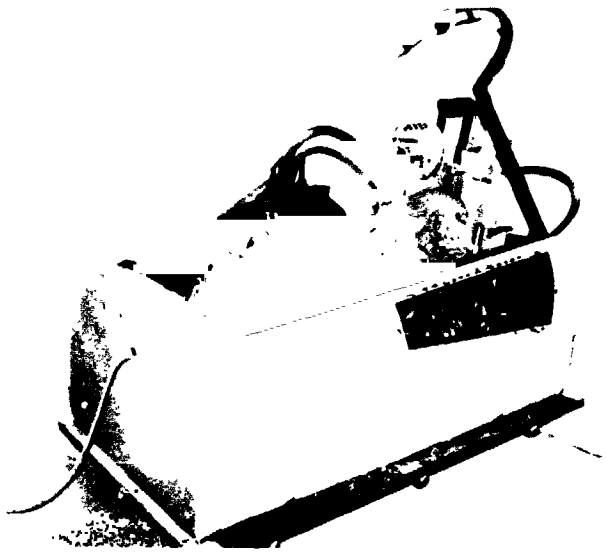

Upright

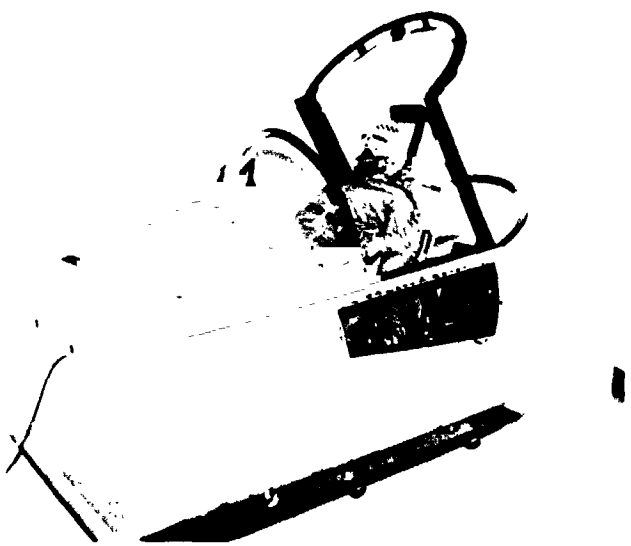

Reclined

Figure 3.- HAC F-15 Cockpit Mock-up

hard maneuvers he retains outside-the-cockpit vision, can see necessary inside-the-cockpit displays, and can reach the required controls and switches. He is provided with side arm controller and low-throw rudder pedals both of which are manually adjustable for the range of 5th to the 95th percentile pilots. Partial automatic adjustment with seat articulation is also provided.

EVALUATION OF THE DESIGN AID

The pilot evaluators were subjected to a series of tests including anthropometric measures, vision envelopes, task performance times and eye and head movements.

Pilot tasks during each simulated mission phase received subjective comments. The crew also ranked individual cockpit items, priority of use, and design location by a "Paired Comparison" technique. Pilot comments were obtained with regard to: control and display design, grouping and location, seat adjustment, back angle, body support, restraint, escape system, and external and internal vision. Two over-all display and control arrangements were presented and evaluated: Configuration A, Figure 4, and Configuration B, Figure 5. The first represented off-the-shelf components suitable for use in a near term flight test evaluation, and the second a concept depicting an advanced HAC cockpit using technology compatible with the 1980/85 time frame. This latter version, Configuration B, maintained a control/display capability equivalent to the baseline F-15 aircraft.

Considerable effort was expended and several iterations were made in finalizing the design and conducting the evaluation of the primary flight and propulsion controls, side arm and throttle (Figure 6). A previous study had also investigated this area and evaluated other controller locations (Ref 4).

The pilot subjects felt that the concept was good and would provide a very real advantage in the combat area. The HAC seat with minor improvements was considered as satisfactory for follow-on testing in an in-flight program. Pilot tasks, visibility and reach, and controls and displays were judged acceptable for an actual aircraft installation and evaluation. Actual production application if decided upon would require Configuration B, as the near term Configuration A was considered compromised for full mission compatibility.

Areas of concern were mainly those which require in-flight evaluation. Control capability with the sidearm controller will require close attention, since precise tracking is required in the fighter mission. High fidelity simulation will be used for this component prior to flight tests. Further effort is also required in design and ground tests to obtain a flightworthy ejection seat design with its articulating mechanism prior to flight.

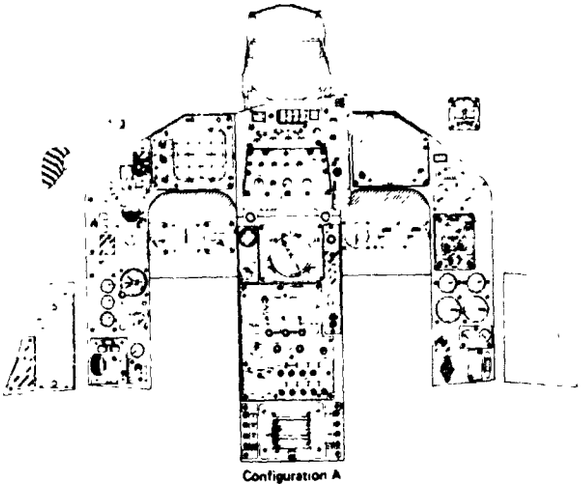

Figure 4

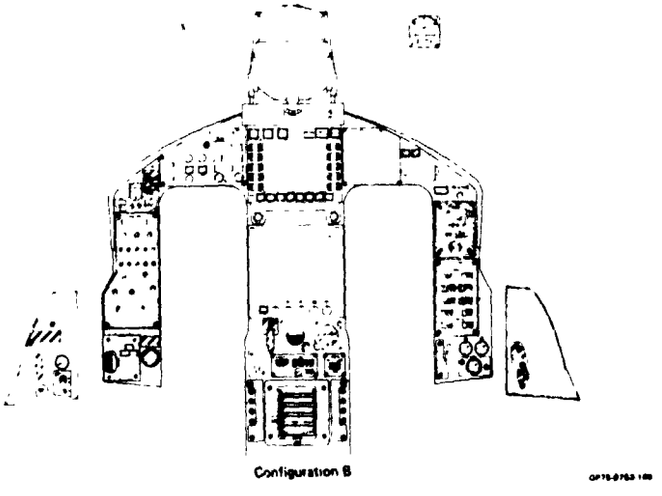

Figure 5

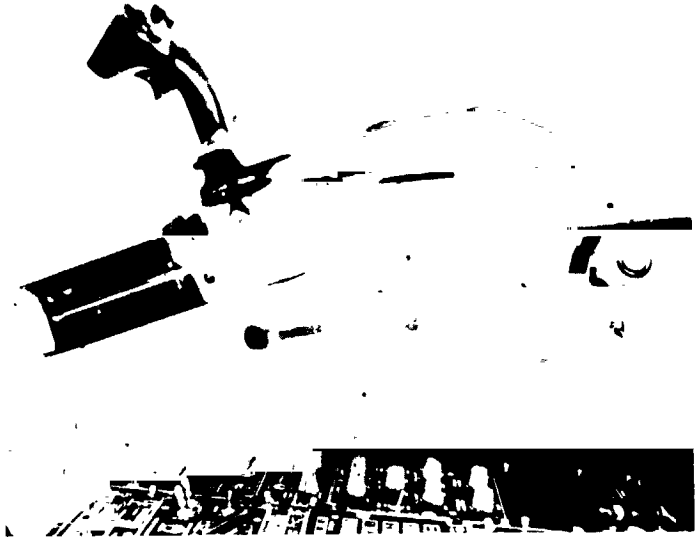

Side Arm Controller

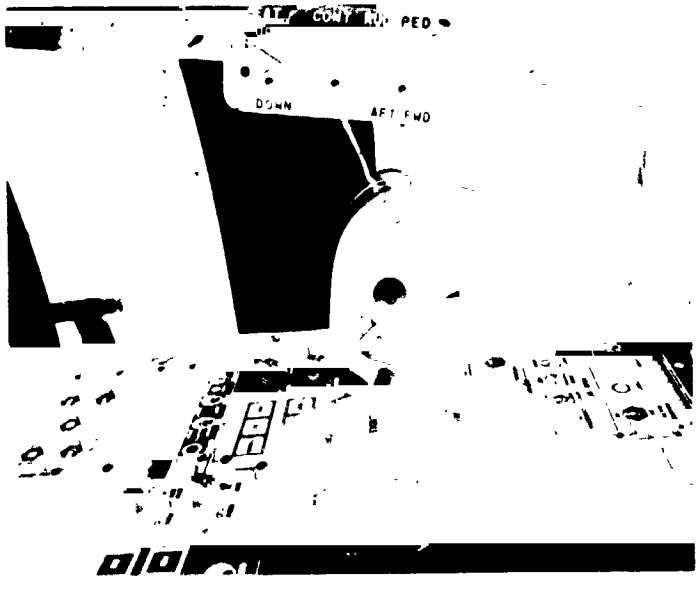

Throttle

Figure 6

A basic issue emerging from the evaluation pointed out a requirement to develop multi-sensor displays for integration into the cockpit if the HAC concept is ever to become a production system. The need for these displays is a result of the reduced main instrument panel area due to the interference of the pilot's legs in the reclined position. Several programs, independent of HAC, dealing with such displays are currently in the development phase at Wright-Patterson AF Base. An example is the Multimode Matrix Display (MMM), which is a short depth, light weight, low power level device using Light Emitting Diodes (LED) to display primarily alpha-numerics.

FUTURE PLANS

The next plateau in the overall High Acceleration Cockpit program is the design, fabrication, and flight test of the cockpit in a TF-15 aircraft. This phase is about to commence in the form of an Advanced Development Program (ADP). The flight test will include basic tracking maneuvers at various G levels and seat back angles, simulated combat with an adversary aircraft, and demonstration flights for interested service and industry personnel. The ADP contract, with McDonnell Aircraft Company, will require 30 months. Flight tests will be run during the last half of 1978.

REFERENCES

1. Burns, J. W.: A Re-evaluation of a Tilt-Backseat as a Means of Increasing Acceleration Tolerance. USAF SAM/VNB, 1974, Brooks AFB, Texas.

2. Sinnett, J. M., Prouhet, E. P., et al: High Acceleration Cockpit Simulator Evaluation. AMRL-TR-75-123, 1976, in draft.

3. Mattes, R. E., et al: High Acceleration Cockpit Applications Study. AFFDL-TR-75-139, 1976, Volumes I to IV.

4. Mattes, R. E., Asiala, C. F.; High Acceleration Cockpit Controller Locations. AFFDL-TR-74-48, 1974, Volume I - Program Summary.

SESSION IV
NONVISUAL DISPLAYS

Chairman: W. H. Levison

DESIGN OF AN ENGLISH LANGUAGE DATA BASE QUESTION-ANSWERING SYSTEM

By David L. Waltz

University of Illinois
Coordinated Science Laboratory and
Department of Electrical Engineering
Urbana, Illinois 61801

SUMMARY

A question-answering system, PLANES, has been written to allow a casual user to obtain information from a large data base by typing natural English questions to the system. This paper discusses design goals, gives examples of PLANES' operation, and discusses helpful factors and design difficulties in the PLANES world.

INTRODUCTION

A prime obstacle for non-technical people who wish to use computers has been the need to either learn a special language for communicating with the machine or communicate via an intermediary. We feel that the time is ripe for computers to be equipped for natural language systems which can be used by persons who are not trained in any special computer language. In order for such systems to be of value to a casual user, the systems must tolerate simple errors, must embody a degree of "common sense," must have a relatively large and complete vocabulary for the subject matter to be treated, must accept a wide range of grammatical constructions, and of course must be capable of providing the information and computations requested by the user.

We are developing such a system called PLANES (for Programmed LANguage-Based Enquiry System) at the University of Illinois Coordinated Science Laboratory (see reference 1). PLANES includes an English language front end with the ability to understand and explicitly answer a user's requests and to carry on clarifying dialogues with him, as well as the ability to answer vague or poorly defined questions. We are also building a library of associated programs which includes functions for recognizing patterns within the data base and for alerting a user when certain patterns of data occur which are of interest to him. This work is being carried out using a subset of the U.S. Navy 3-M data base of aircraft maintenance and flight data, although the ideas can be directly applied to other record-based data bases, both military and non-military.

THE GOAL OF PLANES

Our main goal is to allow a non-programmer to obtain information from a large data base with no prior training or experience. A system to realize this goal (1) must be able to understand to a substantial degree a user's natural language and (2) must be able to help guide and educate the user to formulate requests in a form that the system can understand (see reference 2).

Subgoals of PLANES

We have formulated a number of subgoals which we feel are important for realizing our main goal:

(1) The system must accept a user's "natural" English input, possibly including complex syntactic constructions, abbreviations, pronoun reference, and ellipsis (i.e. omission of one or more words that can be obviously understood in context).

(2) The system must provide explicit answers to questions, and not merely retrieve a file which somewhere contains the answer. The system should phrase its answer in a clear manner, including units or dimensions of numerical answers and a description of the answer values. Whenever possible, graphical output is desirable.

(3) The system must be tolerant of minor errors, e.g. spelling and grammatical errors; it should suggest corrections for user approval whenever possible, and should in general be able to continue processing of the corrected request without requiring a complete retyping of the request.

(4) The system should use clarifying dialogues for several purposes:

(a) to feed back its understanding of the user's request, so that the user can feel confident that the system has understood his request.

(b) to ask the user pointed questions about portions of a request which it does not understand, in the hope of evoking a paraphrase it can understand.

(c) to add new words, phrases and sentences to the system's knowledge base.

(d) to provide appropriate HELP file information in the event of user errors or direct requests for help.

(e) to provide information about the system's capabilities, abbreviations it knows, general contents of the data base, and other such information to help orient a new user.

(5) Such a system should be convenient to use:

(a) it should be interactive and on-line,

(b) it should operate rapidly. One minute seems to us to be a critical length of time: if one in general gets responses in less than a minute, one retains a level of involvement and interest in the interactive process; past a minute, interest begins to wane, and boredom or impatience sets in.

(c) the system should require a minimum of typing; abbreviations and ellipsis should be routinely handled.

(6) The system should be relatively easy to extend, both within its own world, and to new data bases and domains of discourse.

It is unlikely that any design can simultaneously satisfy all these subgoals in an optimum manner. In fact, in PLANES we have chosen a solution which is not particularly easy to extend, either within our world or to another world. In addition, in our current implementation we have not included mechanisms for satisfying all the clarifying dialogue subgoals. In particular, the system now fails totally if it does not recognize any one of the phrases in a sentence. Unlike the problems of extending the system, this subgoal can be realized within our model relatively easily. We have achieved considerable success on all other subgoals, though our current system (as of May 1976) will answer probably no more than 25% of the questions phrased by a novice user.

EXAMPLES OF PLANES' OPERATION

All examples in this section are taken from actual transcripts of PLANES' operation. Figure 1 is a complete transcript of the operation of the current planes system on a single question. Note that the paraphrase and answer are expressed in a form which is not as intelligible as an English form would be. We intend to soon augment the system to provide English paraphrase and answer forms.

Figure 2 shows an extended session, with all but the question and answer suppressed. Figure 2 illustrates the ability of the system to handle ellipsis (i.e. information omitted which is to be understood in context).

Figure 3 shows PLANES' ability to provide answers in a graphical form. NORHRS stands for "Not Operationally Ready HouRS"; ACTDATE stands for "ACTion DATE"; 2001 is the first day of the year 1972.

Figure 4 shows a short dialogue. PLANES first asks for time period information necessary for performing its data base search. It then detects a misspelling and suggests two plausible corrections to the user. Once the user selects the appropriate correction by typing "2", the system is able to continue processing without requiring further typing.

```
Please enter your question.....
     HOW MANY FLIGHTS HOURS DID PLANE 0003 LOG IN JAN 73

parsing......
 {cpu time was 1.74 seconds, real time was 5.95 seconds.
I have understood your request as:
     (COUNT TIME
            (NET NIL)
            (FLY (PLANE (PRONOUN NIL)
                        (TYPE PLANE)
                        (BUSER 3.)
                        (PLNEG NIL)
                        (PLDAM NIL)
                        (PLMAI NIL))
                 NIL)
            (TIME (DATE (MONTH (1. 0. 0.))
                        (DAY NIL) (YEAR 73.)) NIL))

Interpreting.....
 {cpu time was 0.29 seconds, real time was 3.71 seconds.

I have interpreted your request as follows:
     (FIND  ALL
            ((V 0))
            ((SUM (V TOTHRS)))
            (AND (EQU (V ACTDATE) 301.)  (EQU  (V BUSER) 3.))
            NIL)

Evaluating.....
 {cpu time was 6.29 seconds, real time was 16.9 seconds.

        ((SUM TOTHRS) = 33.)
```

Figure 1. Complete transcript of PLANES' answer to a user query

)) How many flights did the A7 with tail number 003 make in January, 1973?

((SUM TOTFLTS) = 17.)

)) How many flights did plane 003 make in Feb. 73?

((SUM TOTFLTS) = 1.)

)) During April?

((SUM TOTFLTS) = 8.)

)) March?

((SUM TOTFLTS) = 13.)

)) All of 1973?

((SUM TOTFLTS) = 39.)

Figure 2. Partial transcript of dialogue showing PLANES' handling of ellipsis

)) plot how much maintenance occurred to plane 2 between Jan. 1 and Jan. 12, '72.

Evaluating.....
{cpu time was 29.32 seconds, real time was 38.11 seconds.

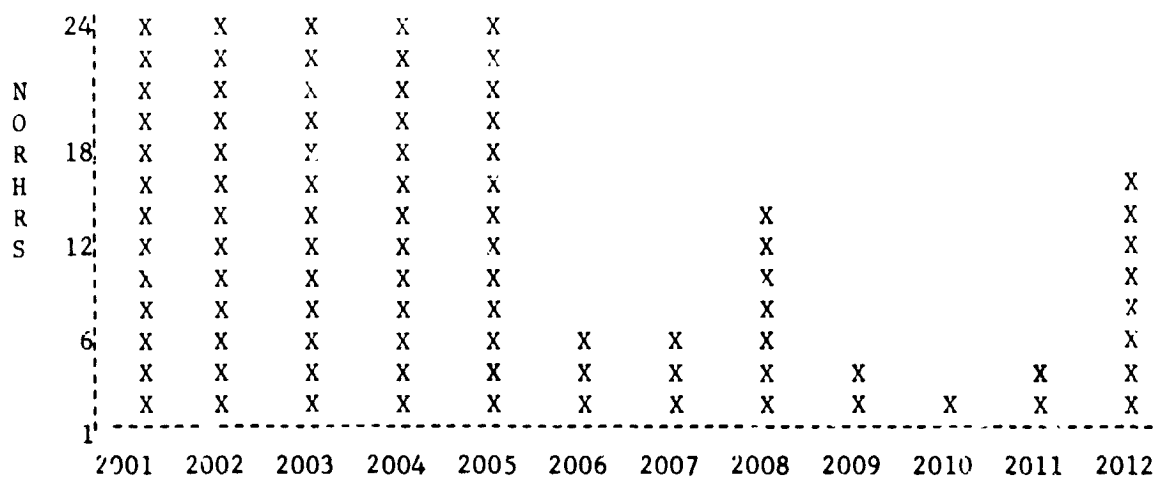

MIN = 1.0 AVERAGE = 14.0 MAX = 24.0

Figure 3. PLANE ' graphical presentation of an answer

)) which Skyhawks logged less than 10 hours

PLEASE ENTER A SPECIFIC TIME PERIOD:

)) between Jan. 1 and Jule 1 '73.

I DON'T KNOW THE MEANING OF JULE
PERHAPS IT'S MISSPELLED?
PLEASE ENTER A NUMBER CORRESPONDING TO ONE OF THE FOLLOWING:

1. JUNE
2. JULY
3. NONE OF THE ABOVE

)) 2.

OK

⟨Answers question⟩

Figure 4. Example of PLANES' dialogue and spelling correction abilities

C-4

Figure 5 shows PLANES' ability to answer general questions about its contents.

THE PLANES WORLD

In this section I describe the general environment in which the language understanding programs operate. This environment includes the data base, the user, and the user's range of queries.

The PLANES Data Base

We have obtained a data base from the Navy 3-M Data Base for Aircraft, Mechanicsburg, PA., consisting of complete records of aircraft maintenance and flight information for 48 A7 and F4 aircraft, extending over a period of two years. Each time a plane is serviced, a record is made including such information as the time and duration of the maintenance, who performed it, what action was taken, which parts were used, the manufacturers of these parts, whether or not the service was scheduled or unscheduled, and so on. Records on the number of flights and the number of hours in the air are also kept for each plane. There are roughly forty different record formats which occur in the data base, each containing between ten and twenty separate fields, where each field encodes information like the date of the action, type of aircraft, serial number of the aircraft, type of malfunction, component serviced, the work station performing maintenance and so on.

The 48 aircraft in our data base are divided into three groups:

(1) 24 planes which crashed or sustained major damage in accidents involving mechanical failures;

(2) 12 planes with bad maintenance records; and

(3) 12 planes with good maintenance records.

"Good" and "bad" records were judged by comparing the ratio of the number of NOR (Not Operationally Ready) hours to the number of flight hours. A high ratio represents a bad record while a low ratio corresponds to a good record.

In addition, we have summaries of maintenance and flight data for all F4 and A7 aircraft for the same two year period, so that we can have some basis for classifying events as "normal" or "unusual."

The PLANES data base contains on the order of 10^8 bits, and occupies about one third of a DEC RP04 disc pack in compressed form. This data base, while quite large, represents only a fraction of the entire 3-M data base, which now contains on the order of 10^{11} bits (10 years' complete

```
Please enter your question.....
  >> What types of aircraft are there.

parsing......


THE FOLLOWING PLANES WILL BE RECOGNIZED BY THE SEMANTIC NET:

        (1) A3
        (2) A7
        (3) F4
        (4) F11
        (5) CHEROKEE
        (6) PHANTOM
        (7) SKYHAWK

   The above planes may be further specified by giving the
   "tail number" (i.e. BUSER, BUNO, Bureau Serial Number, etc.)
   along with the name of the series.

{cpu time was 2.59 seconds, real time was 5.75 seconds.
```

Figure 5. PLANES' ability to answer questions about its contents.

data on all U.S. Navy aircraft, plus summaries).

Helpful Factors in the PLANES World

A number of factors contribute to making our problem much easier to solve than the general problem of understanding unconstrained natural language.

(1) Lack of ambiguity - Relatively few words and virtually no sentences in the PLANES world are ambiguous. The only ambiguous words we have been able to find are "wing" (meaning "a squadron" or "part of a plane") and "flight" (meaning "a flying event" or an adjective, as in "flight computer" or "flight director"). This means that if PLANES can find any interpretation at all for a request, it is in all likelihood to correct interpretation.

(2) Small vocabulary - Our current system has about 1100 words. We estimate that 2000 words will cover 90% or more of all requests made by users with at least a little prior experience with PLANES.

(3) Only two modes - PLANES is always either answering a question from the data base or attempting to help a user express his request in a form PLANES can understand. In general the system need not deal with declarative sentences.

(4) People do not type complex sentences - The increasing likelihood of making typing errors in lengthy requests, the increasing likelihood that long requests will baffle a program in some aspect, and general laziness all contribute to keeping input requests short and simple in construction. Reference 3 describes an experiment in which non-programmers thought that they were communicating with an intelligent program, when in fact they were interacting with another person who would respond appropriately to any input. It was found that 10 simple sentence types covered 78% of all input requests, and that another 10 would handle all but 10% of the requests.

(5) Less than 100% answer rate is acceptable - We feel that a 90% answer rate without rephrasing would be adequate to keep a user's interest and provide a practical and useful system. It is possible that even a lower rate might be acceptable.

(6) We have a good idea of what potential users would like to know - The Navy has made a study of all the requests made to 3-M data base during a one month period, and the frequency with which various requests were made. We thus had a good idea about where to concentrate our initial efforts, and the order in which to proceed.

Not-So-Helpful Factors in The PLANES World

(1) The System must contain a great deal of specialized knowledge -

one of our major realizations has been that a small number of general rules cannot suffice to "translate" natural English requests into data base queries. Consider the sentences:

(S1) "Which A7 has the worst maintenance record?

(S2) "Find any common factors of plane numbers 37 and 78."

Clearly the system must contain special programs to compile a "maintenance record", and special knowledge to judge its "goodness"; the system must know that having the same digit as the fourth element of their serial numbers does not constitute a "common factor", but that similar event sequences are important.

(2) Each request may be expressed in a great many different ways. Clearly, if users are encouraged to sit at a console with little or no prior training or instruction, and if the system is expected to understand enough of a user's input to keep his interest and perform useful actions from the beginning, then the system must be able to make some sense of a large number of types of queries, and a wide range of syntactic constructions.

CONCLUSION

This paper has presented only a brief discussion of some design issues and examples of the performance of a natural language front end for a large data base. Many issues remain, both in the man/machine interface and in the underlying understanding mechanisms, but it is clear that we can now think of the design of such systems in engineering terms - such systems are no longer in the realm of science fiction.

Readers interested in more details of implementation and operation can consult reference 3; a technical report describing the system much more completely will be available in August 1976.

REFERENCES

1. Waltz, D. L. "Natural Language Access to a Large Data Base," Naval Research Reviews, Vol. XXIX, No. 1, Jan. 1976, pp. 11-25. (Also reprinted in Computers and People, Vol. 25, No. 4, April 1976.)

2. Codd, E. F. "Seven Steps to Rendezvous with the Casual User," Proc. IFIP TC-2 Working Conf. on Data Base Management Systems, Cargese, Corsica, April 1974, North-Holland Publ. Co., Amsterdam.

3. Malhotra, A. "Knowledge-Based English Language Systems for Management Support: An Analysis of Requirements," Advance Papers of the 4th Intl. Joint Conf. on Artificial Intelligence, Tbilisi, USSR, 1976, pp. 842-7.

EFFECTS OF LINGUISTIC REDUNDANCY ON PILOT'S COMPREHENSION OF SYNTHESIZED SPEECH

Carol A. Simpson*

Ames Research Center, NASA, Moffett Field, California

SUMMARY

Previous research indicates that pilots' familiarity with aircraft phraseology results in high intelligibility for synthesized speech cockpit messages presented as short sentences - 95 percent articulation (percent correct) for unknown messages heard once (ref. 1). In the present study, the contribution of the sentence context to intelligibility was tested using two levels of linguistic redundancy: (1) two key words in isolation, for example, "*cargo fire*," versus (2) the same two key words in a short sentence context, for example, "You have *cargo* compartment *fire*."

In the first phase, airline pilots listened to unfamiliar messages that differed in linguistic redundancy, and that were presented in a background of continuous weather broadcast at seven signal-to-noise ratios (S/N) ranging from -8 dB to +8 dB. Pilot performance was assessed by the accuracy of comprehension for the two key words in each message and the response times measured from the end of each message to the pilot's signal of comprehension. In the second phase, pilots first studied a list of the same messages while listening to them and were then given recognition tests with and without competing weather broadcast at S/N of 0 dB.

Analysis of the data showed that monosyllabic key words in two-word format were significantly harder to understand than the same key words heard in short sentences. Key words in sentences were approximately 20 percent more intelligible than key words presented alone and response times to sentences were approximately 1 sec shorter than response times to two-word messages across all S/N conditions. For polysyllabic key words, the differences in intelligibility and response times for the two levels of linguistic redundancy were smaller but in the same direction.

It was concluded that synthesized speech messages for the cockpit should be worded in the form of short sentences or phrases, such as "The *fuel* pressure is *low*," instead of in abbreviated key word format, such as "*fuel low*." This design principle is especially important when the key words are monosyllabic.

*National Research Council Associate

INTRODUCTION

Miller, Heise, and Lichten (ref. 2) presented convincing evidence that words in a sentence context are more intelligible than the same words in isolation. Their finding applies to speech heard without the benefit of any particular real-world context. The authors also found that as the number of possible alternative interpretations decreased, due to the context of the situation or to knowledge of the message set, message intelligibility increased. These findings could be extended to predict that listeners familiar with a particular situation, such as flying an aircraft, and familiar with a particular type of well-learned phraseology, such as Air Traffic Control (ATC) phraseology and cockpit terminology, would exhibit, for messages pertaining to the flight situation, little or no intelligibility differences between words presented in isolation and words presented in sentences. It has been found in a previous study (ref. 1) that pilots do indeed have an advantage over nonpilots in understanding flight phraseology. The messages in that study were short ATC clearances and cockpit warnings and advisories. For both human and synthesized speech, pilots familiar with the type of phraseology, but not the particular message set, understood the cockpit messages better than did a control group of nonpilot police patrolmen, even though both groups were equally able to understand messages relating to commonly experienced events for both human and synthesized speech.

The wording of cockpit voice communications - including voice warnings - must be chosen such that the messages are understood accurately, rapidly, with few repetitions, and with as little demand on pilot mental workload and attention as possible. The present study was designed to determine whether the influence of familiarity with flight phraseology would be so strong as to outweigh the advantage that the sentence context was found to have in the Miller, Heise, and Lichten study (ref. 2) where the listeners were airline pilots presented with synthesized speech cockpit warnings. If short sentences, with their additional linguistic redundancy, fulfilled the requirements listed above better than did the key-word-only messages, then the longer, sentence-length format would be preferable for cockpit voice warnings.

A solution to this question is crucial for the following reasons. Brevity has been highly valued for speech communications in the cockpit because it is believed to reduce the length of the comprehension period. It does reduce the probability of temporal overlap with other auditory events. Also, brevity of wording conforms to the style of current cockpit communications with ATC and inside the cockpit for checklists and crew conversations. Finally, for warnings presented in digitized speech, each additional word represents additional cost in terms of dollars and additional read-only-memory. A corresponding additional hardware and memory cost for extra words for synthesized speech is not a problem since additional words are obtained via software modifications and memory increments on the order of only 100 bits per spoken word. The human factors "cost" for using brevity in cockpit voice warnings may be low intelligibility and high demands on pilot attention for comprehension.

EXPERIMENTAL DESIGN

For a comparison of the effectiveness of key-word-only messages to sentence-length messages, airline pilots listened to both types of message wording with and without competing weather broadcast. The study was divided into two phases. For Phase 1, the pilots were given no familiarization with the message set before testing and received no feedback on successive trials. For Phase 2, using the same messages, pilots first obtained familiarization with the warnings by listening to them while reading them from a printed list. Then the pilots were tested for their ability to recognize the warnings with and without competing weather broadcast.

Subjects

Sixteen airline pilots participated in Phase 1. Seven of them returned 6 months later for Phase 2, along with an eighth pilot who had participated in earlier voice warning research using the same speech synthesizer. The pilots' ages ranged from 31 to 44 years. They were paid for their participation.

Test Materials

Sixteen two-word warnings relating to airline transport operations were composed. Eight messages contained monosyllabic words and eight contained polysyllabic words. For each two-word warning, an appropriate sentence-length message was constructed that contained the same two key words presented in the same order as in the two-word version. Both versions of the messages are presented in table 1.

TABLE 1.- COCKPIT WARNING MESSAGES AND MESSAGE DURATIONS IN SECONDS.

MONOSYLLABIC WORDS	DURATION	MONOSYLLABIC WORDS IN SENTENCES	DURATION
1 FUEL LOW	0 56	1 THE FUEL PRESSURE IS LOW	1 68
2 GEAR DOWN	52	2 THE LANDING GEAR IS DOWN	1 75
3 CHECK FLAPS	66	3 CHECK YOUR FLAPS SETTING	1 90
4 BRAKES FAILED	68	4 THE WHEEL BRAKES HAVE FAILED	1 21
5 MAIN DOOR	50	5 THE MAIN DOOR IS NOT LOCKED	1 28
6 BOOST PUMP	54	6 THE FUEL BOOST PUMP IS OUT	1 30
7 OIL HOT	57	7 THE OIL TEMPERATURE IS HOT	1 50
8 ICE VALVES	47	8 THE WING ANTI ICE VALVES ARE INOPERATIVE	2 19
MEAN	57	MEAN	1 62

POLYSYLLABIC WORDS	DURATION	POLYSYLLABIC WORDS IN SENTENCES	DURATION
1 AUTOPILOT DISENGAGED	0 98	1 THE AUTOPILOT IS DISENGAGED	1 36
2 DME MALFUNCTIONING	1 52	2 YOUR DME IS MALFUNCTIONING	2 15
3 CABIN PRESSURE	61	3 THE CABIN PRESSURE IS LOW	1 66
4 SPOILERS INOPERATIVE	1 18	4 YOUR SPOILERS ARE INOPERATIVE	2 23
5. TERRAIN CLOSURE	86	5. YOU HAVE RAPID TERRAIN CLOSURE	2 18
6 CARGO FIRE	74	6 YOU HAVE CARGO COMPARTMENT FIRE	2 42
7 WINDOW OVERHEATED	86	7 THE COCKPIT WINDOW IS OVERHEATED	1.81
8. HYDRAULIC FAILURE	1.06	8 YOU HAVE HYDRAULIC SYSTEM FAILURE	1.86
MEAN	96	MEAN	1 93

The warnings were synthesized on a VOTRAX VS-6 speech synthesizer[1] using identical phoneme coding for the key words in their two-word and in their sentence-length versions. This coding ensured that the key words were pronounced identically in both types of message wording. A tape of the messages can be obtained from the author.

Continuous weather broadcast, used as background "noise", was recorded from a local weather station operated by the National Weather Service. This recording was then edited to eliminate pauses in the speech.

Testing Environment

Pilots were tested individually while sitting in a sound-treated booth. The warning messages and the weather broadcast were individually adjusted for desired peak sound pressure level (SPL)[2] and fed through an audio mixer. The summed output of the mixer was amplified and presented to the pilots binaurally via Koss ESP-9 electrostatic headphones. The pilots sat at a table which contained a reaponse box with a button for signaling message comprehension (used in Phase 1) and a push-to-talk microphone for message readback (used in Phase 2). A PDP-12 computer was programmed to deliver the weather broadcast and the warnings and to record response times.

Experimental Conditions

Phase 1- For Phase 1, the pilots had no prior experience with the message set. Each pilot was assigned a message set containing eight two-word warnings and eight sentence-length warnings. Pilots were alternately assigned to one of two groups. Group 1 pilots were given two-word *mono*syllabic warnings and sentence-length warnings containing *poly*syllabic words. Group 2 pilots heard two-word *poly*syllabic warnings and sentence-length warnings containing *mono*-syllabic key words. In this way, each pilot was tested on all 16 pairs of key words but no pilot received the same key-word pairs in both the two-word and the sentence-length versions. For a baseline comparison of the ability of the two groups to understand the speech produced by the synthesizer, all the pilots were given a pre-test consisting of 16 unfamiliar short ATC clearances and a post-test containing 16 unfamiliar cockpit advisories, without competing weather broadcast.

Each pilot was given repeated trials on his entire message set of eight two-word and eight sentence-length warnings at seven levels of increasing signal-to-weather broadcast (S/W) and peak SPL ratios of -8, -5, -3, 0, +3, +5, and +8 dB. The weather broadcast was held constant at 60 dB SPL, and the SPL of the warnings was varied from 52 dB to 68 dB to obtain the desired S/W. For the eighth and final trial, the 16 warning messages were presented at 60 dB SPL without weather broadcast. The experimental conditions for Phase 1 are shown in Table 2.

---

[1]Invented by Richard T. Gagnon and manufactured by Vocal Interface Division of Federal Screw Works, Troy, Michigan.

[2]Referenced to 0.0002 dyne/cm^2.

TABLE 2.- EXPERIMENTAL CONDITIONS FOR PHASE 1.

	8 TWO WORD WARNINGS	8 SENTENCE WARNINGS
GROUP 1 8 AIRLINE PILOTS	MONOSYLLABIC KEY WORDS	POLYSYLLABIC KEY WORDS IN SENTENCES
GROUP 2 8 AIRLINE PILOTS	POLYSYLLABIC KEY WORDS	MONOSYLLABIC KEY WORDS IN SENTENCES

LISTENING CONDITIONS

WARNING SPL (dB)	52	55	57	60	63	65	68	60
WEATHER SPL (dB)	60	60	60	60	60	60	60	
S/N	8	5	3	0	3	5	8	40
TRIAL No	1	2	3	4	5	6	7	8

SOUND PRESSURE LEVELS IN DECIBELS RE .0002 dyne/cm^2

The order of presentation of the two-word messages and the sentence-length messages was balanced across pilots so that half the pilots in each group heard sentences before the two-word format for all trials and the remainder heard two-word format before sentences. The messages were presented to each pilot in a different random order for each trial. As they arrived for testing, pilots were assigned alternately to either the sentences-first order or to the words-first order.

For trials 1 through 7, continuous weather broadcast occurred throughout each trial. For each SPL, warning messages were presented one at a time at 40-sec intervals. Pilots responded by pressing a button labeled "Understand" as soon as they believed they understood each message. They then wrote the message on a prepared answer sheet. If they did not understand a message, they were instructed to think about it for a while and then press the button and either write their best guess or the word "no." Response times from the end of each message to the pilot's "Understand" button depression were recorded. The procedure for the eighth and final trial and for the pre- and post-tests was the same except that no competing weather broadcast was used and the SPL for all messages was 60 dB.

Phase 2- The same messages used in Phase 1 were also used in Phase 2. Four pilots were assigned to the *mono*syllabic two-word messages and the *poly*-syllabic sentence-length messages. The other four pilots heard the *poly*-syllabic two-word messages and the *mono*syllabic sentence-length messages. Assignment of pilots to message sets was such that the seven pilots originally in Phase 1 heard the opposite message set in Phase 2 than they had heard in Phase 1. As in Phase 1, the order of words-first versus sentences-first was balanced across pilots. Each pilot was given a different presentation order in each of three listening conditions. The first listening condition was a familiarization session. While looking at a printed message list, the pilot heard each message presented twice in succession. Next, he received a recognition test in which the messages were presented only once at 12-sec intervals in a different order and with no competing weather broadcast. The pilot responded by keying a microphone and reading back each message as rapidly as possible, then writing it down on an answer sheet. Finally, he was tested on the same messages presented in a third order and embedded in weather broadcast at a S/W of 0 dB. Again, the pilot responded by keying a microphone and then reading back and writing down the message. The weather broadcast and warning message were delivered concurrently with the weather leading the onset of the warning by approximately 950 msec and continuing until the end of the warning. An interval of 40 sec was used to reduce the changes that the pilots would be prepared for successive presentations. All messages and the weather broadcast

TABLE 3.- EXPERIMENTAL CONDITIONS FOR PHASE 2.

	8 TWO WORD WARNINGS	8 SENTENCE WARNINGS
4 AIRLINE PILOTS	MONOSYLLABIC WORDS	POLYSYLLABIC WORDS IN SENTENCES
4 AIRLINE PILOTS	POLYSYLLABIC WORDS	MONOSYLLABIC WORDS IN SENTENCES

LISTENING CONDITIONS

	LISTEN TO WARNINGS WHILE READING LIST	RECOGNIZE WARNINGS WITHOUT WEATHER	RECOGNIZE WARNINGS DURING WEATHER S/N
WARNING SPL dB	50	50	50
WEATHER SPL dB			50
TRIAL No	1	2	3

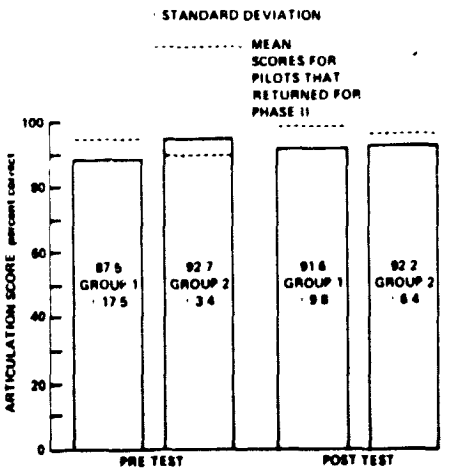

Figure 1.- Mean articulation scores (percent correct) for the two Pilot Groups for synthesized speech Pre- and Post-tests. N = 8 pilots per group.

TABLE 4.- COMPARISON OF RESPONSE TIMES FOR PRE- AND POST-TEST MESSAGES FOR PILOT GROUPS 1 AND 2.

	PRE TEST	POST TEST
GROUP 1 8 AIRLINE PILOTS	3.51 sec 2.37 sec	1.67 sec 0.89 sec
GROUP 2 8 AIRLINE PILOTS	1.66 sec 0.58 sec	1.31 sec 0.85 sec

were delivered at approximately 50 dB SPL. Table 3 shows the experimental conditions for Phase 2.

RESULTS

Group Differences

Wilcoxon's Sum of Ranks for the Pre-test ($R = 68$, $n_1 = 8$, $n_2 = 8$, $p > 0.10$) and the Post-test ($R = 68$, $n_1 = 8$, $n_2 = 8$, $p > 0.10$) indicated that the two groups of pilots were not significantly different in their ability to understand the synthesizer. Means and standard deviations for the two groups for pre- and post-test articulation scores (percent correct) are shown in Figure 1. However, the two groups were significantly different ($t = 2.27$, $df = 14$, $p < 0.05$) in average response times to the pre-test messages. They were not significantly different ($t = 1.16$, $df = 14$, $p > 0.10$) in average response times for the post-test messages. Table 4 shows the means and standard deviations in response time for the two groups for the pre- and post-test. Because of the initial response time difference between the two groups, which may have continued for an indeterminable number of trials on the test messages, the response time data was normalized using individual subjects' means and standard deviations across message type so that between-group comparisons could be made for the same key-word pairs presented in isolation and in sentence context.

Presentation Order

Analysis using Wilcoxon's Sum of Ranks determined that presentation of sentences or words first had no significant effect on the articulation scores for words ($R = 59.5$, $n_1 = 8$, $n_2 = 8$, $p > 0.10$) or for sentences ($R = 68$, $n_1 = 8$, $n_2 = 8$, $p > 0.10$). Similarly, there were no significant presentation

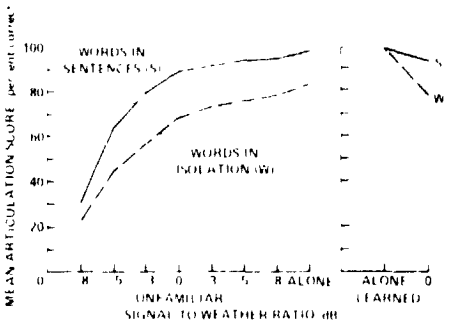

Figure 2.- Mean articulation scores for key monosyllabic words in unfamiliar synthesized speech cockpit warnings with and without a sentence context, heard in background of continuous weather broadcast for repeated trials at increasing signal-to-"noise" ratios (Phase 1) and for the same messages with and without competing weather broadcast after prior learning of the message set (Phase 2).

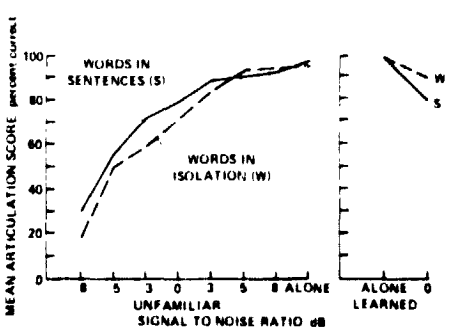

Figure 3.- Mean articulation scores for key polysyllabic words in unfamiliar synthesized speech cockpit warnings with and without a sentence context, heard in background of continuous weather broadcast for repeated trials at increasing signal-to-"noise" ratios (Phase 1) and for the same messages with and without competing weather broadcast after prior learning of the message set (Phase 2).

order effects on response times to words ($R = 52$, $n_1 = 8$, $n_2 = 8$, $p > 0.10$) or for response times to sentences ($R = 58$, $n_1 = 8$, $n_2 = 8$, $p > 0.10$).

Articulation Score

Articulation scores are the percent of key words correctly identified for each message wording type.

Monosyllabic words- Figure 2 shows a between-groups comparison of articulation scores for monosyllabic key words in the two-word and sentence-length versions. The eight trials at increasing S/W for Phase 1 are on the right, and the two testing trials of Phase 2 are on the left. The higher mean articulation scores indicated that for unfamiliar messages, the key words in a sentence context were significantly more intelligible than the same key words presented alone across all S/W conditions, significance being determined by Wilcoxon's Signed Ranks Test ($R = 0$, no. of pairs (n_p) = 8, $p < 0.01$). In Phase 2, when pilots were given prior familiarization with the message set and tested for recognition of the "learned" messages, all pilots scored 100 percent articulation for all messages of both types of wording when no competing weather broadcast was present. With weather broadcast present, mean articulation for words presented alone dropped to 78 percent, but only dropped to 94 percent when the same words were presented in a sentence context. This difference, however, did not reach significance as measured by Wilcoxon's Signed Ranks Test ($R = 2.5$, $n_p = 6$, $p > 0.10$). Only six pairs were used because the difference scores within two of the pairs were zero.

Polysyllabic words- The mean articulation scores for unfamiliar polysyllabic words with and without sentence context in Phase 1 are similar to those for the monosyllabic words at S/W of +3 dB and lower, as shown on the left side of figure 3. Across all S/W conditions, however, the

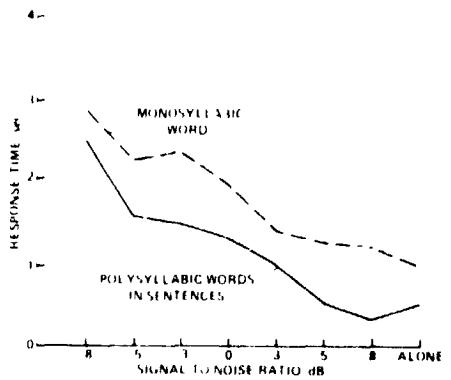

Figure 4.- Response times for Pilot Group 1 for cockpit warnings: Monosyllabic words alone and Polysyllabic words in sentences presented for repeated trials at increasing signal-to-weather ratios. Response times measured from end of warning to pilot's "Understand" signal (Phase 1).

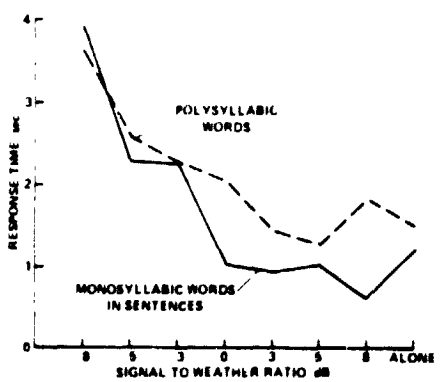

Figure 5.- Response times for Pilot Group 2 for cockpit warnings: Polysyllabic words alone and Monosyllabic words in sentences presented for repeated trials at increasing signal-to-weather ratios. Response times measured from end of warning to pilot's "Understand" signal (Phase 1).

addition of a sentence context did not significantly improve ($R = 3$, $n_p = 8$, $p > 0.10$) intelligibility for polysyllabic key words in initially unfamiliar messages. For previously learned warnings (Phase 2), articulation scores were again 100 percent for both types of wording presented with no competing weather broadcast. When weather broadcast was presented at S/W of 0 dB, articulation scores for words presented alone dropped to 92 percent and articulation for words in sentences dropped to 81 percent. The difference between articulation scores for words alone and in a sentence context was again not significant ($R = 4.5$, $n_p = 6$, $p > 0.10$).

Response Times

The response-time data closely paralleled the intelligibility data in Phase 1. The response times were measured from the end of each message to the time when the pilot pressed the "Understand" button and began his response, regardless of accuracy. For Pilot Group 1 (fig. 4) and Pilot Group 2 (fig. 5), the mean response time for the sentence-length messages was significantly shorter (Group 1: $R = 0$, $n_p = 7$, $p < 0.05$; Group 2: $R = 3$, $n_p = 8$, $p < 0.05$) than the mean response time for the two-word messages. For Group 1, response time data was available for only 7 of the 8 pilots since one pilot misunderstood the instructions and pressed the "Understand" button after he finished his responses.

Included in the response time data are several types of responses:

1) incorrect response,
2) "unable" response,
3) message correct for the first time,
4) message correct on a previous trial and correct again on the current trial.

It would be reasonable to expect differences in response times as a function of the type of response the pilot made. Therefore, mean

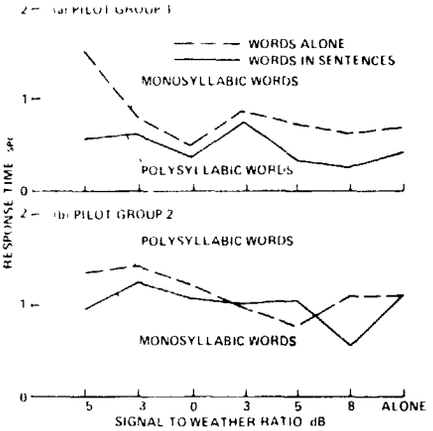

Figure 6.- Response times for cockpit warnings recognized correctly and recognized correctly on previous trial for repeated trials at increasing signal-to-weather ratios (Phase 1).

response times were calculated only for responses of type 4, that is, for messages which a given pilot had understood correctly and had also understood correctly on the previous trial at a lower S/W. The assumption was that for the small message set used in this study, once a pilot correctly understood a particular warning, he was likely to remember it during the next trial and so facilitate the recognition process. The response time to such "previously understood and now familiar" messages should allow a valid comparison between words presented in isolation and those presented in a sentence context, for familiar messages. In general, the response times to the familiar, correctly recognized warnings were shorter for both Pilot Groups (figs. 6(a) and 6(b)) than were the response times to all messages regardless of accuracy (figs. 4 and 5).

Because of group differences in mean response times, each pilot's response times were normalized. The resulting z-scores were then used for between-group comparisons of the effects of sentence context on monosyllabic (fig. 7) and polysyllabic (fig. 8) words. In each case, the response times for each S/W were significantly longer (Monosyllabic words: $R = 0$, $n_p = 8$, $p < 0.01$; Polysyllabic words: $R = 0$, $n_p = 8$, $p < 0.01$) for the two-word messages than for the sentence-length messages. The size of the response time difference diminished slightly for the polysyllabic words at positive S/W conditions, but the difference occurred at all S/W conditions for both mono- and polysyllabic words.

Four-way Comparison of Message Types

In addition to the major comparisons of articulation scores and response times for the mono- and polysyllabic words with and without a sentence context,

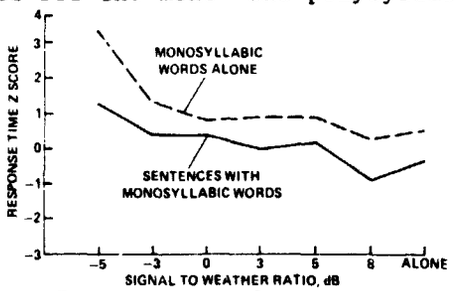

Figure 7.- Z-scores for response times for "familiar" cockpit warnings containing monosyllabic words, with and without sentence context, presented for repeated trials at increasing signal-to-weather ratios (Phase 1).

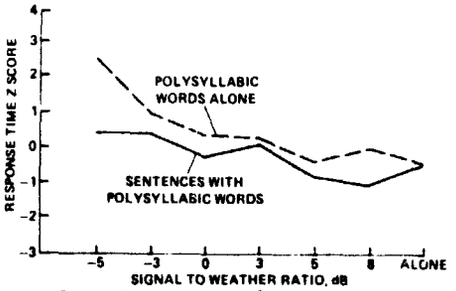

Figure 8.- Z-scores for response times for "familiar" cockpit warnings containing polysyllabic words, with and without sentence context, presented for repeated trials at increasing signal-to-weather ratios (Phase 1).

it is interesting to note that pilot performance for monosyllabic words presented alone (MW) is poorer than performance for the other three presentation types: monosyllabic words in sentences (MS), polysyllabic words alone (PW), and polysyllabic words in sentences (PS). Peak intelligibility for MW was only 84 percent compared to 98 percent for MS (fig. 2) and 95 percent and 97 percent for PW and PS, respectively (fig. 3). Similarly, the z-scores for response times to familiar messages for the last trial are well above the mean for MW (+0.46) and below the mean for MS (-0.37) (fig. 7), PW (-0.56), and PS (-0.58) (fig. 8). These data indicate that response times to the monosyllabic words presented alone were consistently longer than response times to polysyllabic words presented alone and both mo- - and polysyllabic words presented in sentences.

DISCUSSION

The reader is cautioned against an interpretation of intelligibility and response time as a direct function of S/W, because this function is confounded with learning. The experimental paradigm used in this study makes use of the modified method of limits, also known as the ascending method of limits (ref. 3). It is recommended for obtaining only the *relative* thresholds for some variable, such as S/N ratio, for two or more classes of stimuli which are to be identified by the subject without prior knowledge of the total set of response alternatives. By presenting repeated trials on alternating lists of the different classes of stimuli at increasing intensities, durations, or S/N ratios, the relative thresholds for the different classes of stimuli under equal conditions of number of previous trials can be obtained while minimizing the effects of subject familiarity with the individual stimuli. If anything, the effects of increasing familiarity with the message set would be expected at higher levels of S/W to reduce the chances of significant intelligibility and response-time differences between the two levels of linguistic redundancy for message wording.

Nevertheless, intelligibility scores are higher and reaction times are shorter for synthesized-speech cockpit warnings presented as short sentences than they are for warnings presented in a briefer two key-word format. For listeners who are experienced with cockpit phraseology, this relationship is true across a wide range of S/W broadcast ratios. The advantage of the sentence context is larger for monosyllabic words than for polysyllabic words in that for polysyllabic words the facilitating effect of the added linguistic redundancy decreases or perhaps disappears at S/W of +3 dB or higher. Familiarity with individual messages decreases reaction time and increases intelligibility but does not override the facilitating effect of the sentence context for recognition and response times. Monosyllabic words alone produce consistently poorer performance in terms of lower intelligibility and longer response times than do polysyllabic words alone and both monosyllabic and polysyllabic words in sentences. This performance relationships is consistent with Howe's research (ref. 4), in which longer words were found to be more intelligible than shorter words, presumably because of their phonetic redundancy - there are far more restrictions on allowable sequences of sounds that "make sense" when additional syllables are included.

It would seem, then, that the additional linguistic redundancy provided by the sentence context, and to a lesser degree by the additional syllables in the polysyllabic words, helps pilots process synthesized warning messages more accurately and more quickly than when the two-word format is used. This conclusion is further supported by a subsequent study, also presented at the 12th Annual Conference on Manual Control (ref. 5) and using time estimation as a secondary task, in which it was found that the more redundant sentences required less attention for processing. It was also found that *total* listening time - measured from the beginning of the warning with the warnings repeated until the pilot cancelled the message to signal that he understood - was shorter for sentences than for two-word messages, because the pilots allowed the two-word warnings to repeat more times than the sentence-length warnings. This difference occurred despite a ratio of sentence to two-word warning-message duration 2.3 to 1. The operational implications of this finding are strengthened by the fact that the actual duration of any sentence warnings synthesized for use in the cockpit would be slightly shorter than the durations used in this study. The durations of the key words in this study were made identical for the words-alone and the words-in-sentences versions of the warnings so as to present identical acoustic stimuli for both conditions of linguistic redundancy. In human speech, the pronunciation of all but the final words in sentences and phrases is actually shorter than when the words are pronounced in isolation (ref. 6). Additionally, the shortening of the key words in the sentences would improve timing rhythm of the sentence pronunciation, which would be expected to result in still higher sentence intelligibility because of the perceptual importance of proper timing relationships among the segments of sentences (ref. 7).

If the increased recognition accuracy and decreased response time for the sentences versus the two-word warnings is taken as an indicator of less cognitive effort for processing the sentences, then it is possible that under extremely high workload conditions in the cockpit, sentence messages would be understood more reliably by conveying the warning more accurately and rapidly; possibly with only a single repetition.

This suggestion is supported by judgments from the eight pilots who participated in Phase 2. They were asked to judge the difficulty of learning and recognizing the two types of message wording in the experimental situation and to give their preferences for warning-message wording in the cockpit. While most of the pilots found both types of wording equally easy to learn and to recognize in the absence of competing speech, five of the eight thought that the sentences were easier to recognize during simultaneous weather broadcast, and six of the eight would prefer the sentence-type wording over the two-word format for cockpit warnings (table 5). Their reasons for this preference were obtained in response to an open-ended question, "Why do you think the _____ were easier than the _____?" The reasons the pilots gave for preferring sentences to two-word messages fell into three general categories:

1) Extra words in the sentence help you figure out the words you missed.

2) The first words of the sentence get your attention and cue you in to the particular voice that is talking so that you are listening for the critical words.

TABLE 5.- AIRLINE PILOT PREFERENCES FOR COCKPIT WARNING MESSAGE WORDING: TWO KEY WORDS VS A SENTENCE (PHASE 2).

		TWO WORD FORMAT EASIER	SENTENCE FORMAT EASIER	NO DIFFERENCE	N
SITUATION	MESSAGE LEARNING	2	0	6	8
SITUATION	RECOGNITION WITH NO COMPETING WX	1	2	5	8
SITUATION	RECOGNITION DURING COMPETING WX	0	5	3	8
LISTENING	PREFERENCE IN COCKPIT	2*	6	0	8

*THE TWO PILOTS WHO PREFERRED THE TWO WORD FORMAT FOR USE IN THE COCKPIT THOUGHT THE LONGER MESSAGES WOULD DISTRACT THEM FROM OTHER FLIGHT TASKS BOTH FOUND THE FORMAT WARNING + KEY WORD + KEY WORD

TABLE 6.- AIRLINE PILOT RESPONSES TO A PROPOSED COCKPIT VOICE-WARNING SYSTEM (PHASE 2).

REPLACE ALL CURRENT AURAL WARNINGS WITH VOICE

AUTOMATIC VOLUME CONTROL (AVC) TO MAINTAIN CONSTANT S/N RATIO

PRIMARY DELIVERY VIA HEADSETS AT LEVEL EQUAL TO INDIVIDUAL PILOT SELECTED COMMUNICATIONS AUDIO LEVEL

BACK UP DELIVERY VIA SPEAKER USING AVC TO MAINTAIN CONSTANT SIGNAL TO COCKPIT NOISE LEVEL

PILOT PREFERENCE

YES		NO		N
ELIMINATE ALL BELLS, HORNS, CLACKERS, BUZZERS	KEEP FIRE BELL ONLY	VOICE OK FOR SOME WARNINGS	NO VOICE	
No OF PILOTS 4	3	1	0	8

TABLE 7.- AIRLINE PILOT PREFERENCES FOR REPETITION OF COCKPIT VOICE WARNINGS (PHASE 2).

SHOULD VOICE WARNINGS BE REPEATED?

YES	NO	N
8	0	8

NUMBER OF REPEATS FOR COCKPIT VOICE WARNINGS

CRITICALITY OF WARNING SITUATION	1	2 OR 3	UNTIL CANCELLED OR PROBLEM CORRECTED	UNTIL PROBLEM CORRECTED - NOT CANCELLABLE	N
CRITICAL	0	1	7	(1) LANDING GEAR AND FLAPS ONLY	8
NON-CRITICAL	0	4	4	0	8

3) The longer pattern of the sentence with extra words between the critical ones gives you more time to understand the words.

The two pilots who preferred two-word warnings expressed a preference for brevity of verbal communications. One thought that the sentences, being longer, would distract his attention more from his flight tasks (but see ref. 5). Both these pilots, however, thought that a warning message format would be acceptable if it consisted of an alerting word such as "warning" followed by a sequence of key words.

These eight pilots generally favored the concept of cockpit voice warnings. Table 6 shows their responses to a question proposing that voice warnings replace *all* current aural warnings but with the provision that the voice warnings be presented at a comfortable listening level adjusted to individual pilot preference and with back-up via speaker and automatic adjustment of voice warning volume relative to the changing cockpit noise level. Seven of the eight pilots favored voice for all current aural warning situations. Three of the seven wanted to keep the fire bell and have the voice announce the engine number. The eighth pilot said that voice would be acceptable for some warnings.

Table 7 deals with warning repetition and cancellation. All eight pilots thought that the warnings should be repeated more than once. Preferences for the number of repeats and type of cancellation depended to some extent on the criticality of the warnings. For critical warnings seven of the

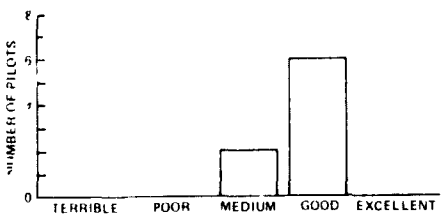

Figure 9.- Airline pilot ratings of clarity of pronunciation of synthesized-speech cockpit warnings after learning message set and recognizing warnings with and without competing weather broadcast (Phase 2).

TABLE 8.- AIRLINE PILOT ACCEPTABILITY OF SYNTHESIZED SPEECH AND DIGITIZED SPEECH FOR COCKPIT VOICE WARNINGS (PHASE 2).

	YES	NO	N
WOULD WANT THIS VOICE IN OWN COCKPIT	7	1	8
WOULD WANT GPWS TYPE VOICE IN OWN COCKPIT	8	0	8

DOTTED LINES INDICATE PREFERENCES OF THE 7 PILOTS WHO RETURNED SIX MONTHS LATER FOR TESTING ON THE SAME MESSAGES WITH PRIOR FAMILIARIZATION WITH MESSAGE SET

Figure 10.- Airline pilot ratings of pronunciation clarity of initially unfamiliar synthesized-speech cockpit warnings heard at increasing signal-to-weather broadcast sound pressure level ratios (Phase 1).

eight pilots thought that the warnings should be repeated until either a crew member cancelled them or the situation was corrected, whichever happened first. One of these seven made an exception to this for the landing gear and flaps warning, stating that at low altitudes above the ground, he would not want to be able to cancel this warning until the problem was corrected.

For noncritical warnings, the pilots were divided in opinion with four preferring two or three repeats with automatic cut-off and the other four preferring to have the warnings repeated until cancelled either by a crew member or by correction of the problem.

These pilots judged the clarity of pronunciation of the messages produced on this synthesizer as generally good, and seven of the eight said that they would find this particular voice acceptable in their cockpit (fig. 9 and table 8). All eight pilots judged the voice quality of the Ground Proximity Warning System (GPWS) - representing digitized speech - acceptable but thought that the current GPWS voice is too loud. It is interesting to compare the responses of these pilots to their responses after the earlier testing in the unfamiliar message condition of Phase 1. Figure 10 shows the voice clarity ratings of the 16 pilots in the Unfamiliar Message Set condition. As a group, they tended to rate this synthesizer as having medium clarity of pronunciation, and half the group said they were "bothered by the voice quality." The dotted lines show the responses of the seven pilots who returned six months later for retesting on the same messages under the familiar condition. They were representative of the larger group, as evidenced by their medium ranking of pronunciation and divided opinion regarding voice quality. Several factors may have combined to cause them to change their rating of the pronunciation and to be willing to have this particular voice

in their own cockpit, such as familiarity with the particular messages and experience listening to the synthesizer voice.

CONCLUDING REMARKS

Advantages seemingly may be gained from carefully designed cockpit voice warnings. One design principle that should be followed in order to ensure the effectiveness of this mode of presenting warning information to pilots is to include sufficient linguistic redundancy in the message wording to ensure rapid and accurate comprehension. The context provided by a short sentence has been found to improve accuracy and decrease response times to cockpit warnings, particularly when the key words in the warning are monosyllabic. This effect is significant despite a strong facilitating effect of pilots' familiarity with flight phraseology. Further research will be directed at assessing the facilitating effects of the different types of linguisitic redundancy - semantic and syntactic - and the alerting and "accent"-cueing effect of an initial low information word provided by the sentence context. These effects will be studied under simulated flight conditions with varying levels of pilot attention workload.

REFERENCES

1. Simpson, C. A.: Occupational Experience with a Specific Phraseology: Group Differences in Intelligibility for Synthesized and Human Speech. Abstract in the Journal of the Acoustical Society of America, vol. 58, Suppl. 1, 1975, p. 57. Paper presented at the 90th Meeting of the Acoustical Society of America, San Francisco, Nov. 5, 1975 and available from the author.

2. Miller, G. A.; Heise, G. A.; and Lichten, W.: The Intelligibility of Speech as a Function of the Context of the Test Materials. Journal of Experimental Psychology, vol. 41, 1951, pp. 329-335.

3. Dember, W. N.: The Psychology of Perception. Holt, New York, 1960, pp. 60-65.

4. Howes, D. H.: On the Relation Between the Intelligibility and Frequency of Occurrence of English Words. Journal of the Acoustical Society of America, vol. 29, 1957, pp. 296-305.

5. Hart, S. G.; and Simpson, C. A.: Effects of Linguistic Redundancy on Synthesized Cockpit Warning Message Comprehension and Concurrent Time Estimation. Paper presented at the 12th Annual Conference on Manual Control, Coordinated Science Laboratory, University of Illinois at Urbana-Champaign, May 25-27, 1976. To be published in the Conference Proceedings as a NASA TMX (in press).

6. Klatt, D. H.: Vowel Lengthening is Syntactically Determined in a Connected Discourse. Journal of Phonetics, vol. 3, 1975, pp. 129-140.

7. Dooling, D. J.: Rhythm and Syntax in Sentence Perception. Journal of Verbal Learning and Verbal Behavior, vol. 13, 1974, pp. 255-264.

EFFECTS OF LINGUISTIC REDUNDANCY ON SYNTHESIZED COCKPIT WARNING MESSAGE COMPREHENSION AND CONCURRENT TIME ESTIMATION

Sandra G. Hart*
University of California, Berkeley, California

Carol A. Simpson**
Ames Research Center, NASA, Moffett Field, California

SUMMARY

The relative amounts of attention required to comprehend and recognize two types of speech messages that differed in linguistic redundancy were evaluated with two concurrent time estimation tasks. Two-word and sentence-length synthesized-speech cockpit warning messages were presented to 12 commercial airline pilots with and without competing weather broadcast. The pilots had two tasks: a) to read back and write down the warning messages and b) to give two types of time estimates. It was found that the intelligibility of messages presented in a redundant sentence-length format was higher, and that listening time and number of repetitions was less, during the Familiarization Phase. Sentences were also more intelligible than two-word messages when presented in a background of competing weather broadcast for recognition. Differences in verbal estimates of session length and in the length of 10-sec estimates produced by pilots indicated that messages presented in a sentence format required less attention for comprehension than did two-word messages.

INTRODUCTION

It might be expected that the many different concurrent tasks performed in flight would demand varying amounts of attention and mental workload, even though such variation might not be reflected in pilot performance on the primary flying task. Two types of time estimation tasks have been used as quantitative measures of such concurrent task processing requirements: a) verbal estimation in which the length of an interval of time that has been experienced is estimated in minutes or seconds and b) time production in

---

*This author's research was supported by NASA Grant NGL 05-046-002 to the San Jose State University Foundation.

**This author's research was supported by a post-doctoral fellowship from the National Research Council.

which the duration of an interval of time that is specified verbally is estimated by reproducing it operationally. Hart (ref. 1) and Hart and McPherson (ref. 2) reported that the length of time productions made during compensatory tracking and simulated flight, and the length of verbal estimates made of intervals filled with tracking, covaried with the difficulty of the manual control tasks. It was suggested that the length of verbal produced time estimates reflected the attention demands of concurrent activity. In the present study, similar time estimation tasks were used to assess the attention required for two speech processing tasks: a) comprehending unfamiliar two-word and sentence-length synthesized-speech cockpit warnings (Familiarization Phase), and b) recognizing these messages once they were familiar (Recognition Phase).

It has been previously reported that words presented in a sentence context are more intelligible than the same words in isolation, by virtue of the increased redundancy (refs. 3, 4). Linguistic redundancy refers to a reduction in the number of interpretations which can be assigned to the segments of an utterance due to semantic, syntactic, and phonological constraints such as those provided by a sentence frame. Since the results of Simpson's research (ref. 3) showed increased intelligibility and decreased response time as the redundancy in synthesized cockpit warnings was increased, it seemed reasonable to assume that the attention required of pilots to comprehend messages initially and recognize them once they were familiar would be inversely related to redundancy. The present study was designed to assess by means of verbal and produced time estimates, the attention required to comprehend and recognize warnings presented in either two-word or sentence formats. The operational motivation for this study was to examine the possibility that increased linguistic redundancy would reduce the attention required for pilots to process synthesized-speech warning messages in the cockpit. If warnings could be worded so as to reduce the attention required for their comprehension, this could leave more attention available for flying the airplane and taking proper corrective actions. This savings in attention would be especially important in emergency situations, where higher-than-normal attention demands exist.

It was predicted that less redundant two-word warnings would require longer listening time and more repetitions for initial comprehension and that they would be less intelligible than messages presented in a sentence format during both the Familiarization and Recognition Phases. If attention demands vary inversely with redundancy, as predicted, pilots should increasingly underestimate the passage of time as message redundancy is progressively decreased. (Underestimation occurs when concurrent activity momentarily diverts attention from timekeeping so clock time passes relatively unnoticed.) Increasing underestimation of time will in turn result in progressively shorter verbal estimates and longer produced durations.

TASK AND PROCEDURE

Subjects

Twelve commercial airline pilots, ranging in age from 35 to 45 years, served as paid participants in the present study.

Test Materials

The intelligibility of 16 monosyllabic and polysyllabic two-word synthesized-speech warning messages was assessed by computing the percentage of words correctly identified in a pilot study. Eight messages were then assigned to each of two message sets so that the average intelligibility of the sets was approximately equal. Sixteen sentence-length warning messages were then constructed from each of the sixteen two-word messages. As shown in table 1, each sentence-length warning contained the same two words in the same order as in its corresponding two-word version.

TABLE 1.— COCKPIT WARNING MESSAGES AND THEIR DURATION IN SECONDS

	TWO-WORD FORMAT	DURATION (Sec)	SENTENCE FORMAT	DURATION (Sec)
GROUP 1 PILOTS	FUEL LOW	.55	YOU HAVE HYDRAULIC SYSTEM FAILURE.	1.89
	CABIN PRESSURE	.61	THE FUEL BOOST PUMP IS OUT.	1.39
	GEAR DOWN	.52	THE COCKPIT WINDOW IS OVERHEATED.	1.51
	DME MALFUNCTIONING	1.52	THE WHEEL BRAKES HAVE FAILED.	1.21
	CHECK FLAPS	.66	THE AUTOPILOT 'S DISENGAGED.	1.36
	SPOILERS INOPERATIVE	1.18	THE OIL TEMPERATURE IS HOT.	1.59
	TERRAIN CLOSURE	.86	THE WING ANTI-ICE VALVES ARE INOPERATIVE.	2.19
	CARGO FIRE	.74	THE MAIN DOOR IS NOT LOCKED.	1.28
	MEAN DURATION	.83	MEAN DURATION	1.56

	TWO-WORD FORMAT	DURATION (Sec)	SENTENCE FORMAT	DURATION (Sec)
GROUP 2 PILOTS	HYDRAULIC FAILURE	1.05	THE FUEL PRESSURE IS LOW.	1.13
	BOOST PUMPS	.54	THE CABIN PRESSURE IS LOW.	1.13
	WINDOW OVERHEATED	.65	THE LANDING GEAR IS DOWN.	1.20
	BRAKES FAILED	.68	YOUR DME IS MALFUNCTIONING.	1.60
	AUTOPILOT DISENGAGED	.98	CHECK YOUR FLAPS SETTING.	1.35
	OIL HOT	.57	YOUR SPOILERS ARE INOPERATIVE.	1.68
	ICE VALVES	.47	YOU HAVE RAPID TERRAIN CLOSURE.	1.63
	MAIN DOOR	.59	YOU HAVE CARGO COMPARTMENT FIRE.	1.87
	MEAN DURATION	.69	MEAN DURATION	1.45

The warnings were synthesized on a VOTRAX VS-6 speech synthesizer using identical phoneme coding for the key works in both the two-word and sentence-length message formats. A PDP-12 computer delivered the messages and recorded the response times.

The background noise used in the Recognition Phase was continuous weather broadcast recorded from a local station operated by the National Weather Service and edited to eliminate pauses. The ratio of warning-message signal peak sound pressure level (SPL) to weather-broadcast noise SPL was +3 dB.

Procedure

Each pilot was tested individually in a sound-attenuated booth. The warning messages and weather broadcast were presented to the pilots binaurally through Koss earphones, Model ESP-9. Pilots were asked to initiate message readback by keying a hand-held microphone. Subsequent to verbal readback, pilots were asked to write down on a prepared answer sheet as much as they had understood of the message. Message readback via keyed microphone was used to provide pilots with a response mode similar to that which they normally use for responding to spoken messages in the cockpit. It was also expected that vocalization would result in shorter response times than would be obtained using written responses. However, for intelligibility scoring, a written record of the pilot's response was required so as to eliminate possible experimenter bias in listening to recorded spoken responses.

Pilots made verbal time estimates during the Familiarization Phase by writing their estimate of elapsed time on the answer sheet. They produced 10-sec intervals during the Recognition Phase by pressing one button to begin their estimate when cued to do so by a pre-recorded message and a second button to terminate their production when they believed that 10 sec had elapsed.

Half of the pilots were randomly assigned to each of two test groups. The six pilots in one group received the first set of eight two-word messages and the eight sentence-length messages constructed from the second set of two-word warnings. Conversely, the second group of six pilots received the second set of two-word warnings and the sentence-length messages constructed from the first set of two-word warnings. The messages given to each group and their durations can be seen in table 1.

All twelve pilots were given three familiarization runs for each of eight two-word messages and each of eight sentence-length messages. After a 30-min break, pilots were given one recognition run in which each message was presented one time only in a background of continuous weather broadcast. The order of presentation of the two-word and sentence-length warning message sets was balanced across subjects so that three pilots in each group heard sentences before two-word messages during all the test runs. The other three pilots in each group heard the two-word versions first, and then the sentence-length versions. The eight two-word and eight sentence-length messages within the two sets were presented in a different random order for each pilot.

Familiarization phase— During the Familiarization Phase, pilots heard each of the 16 warning messages for their group at least 3, but not more than 30, times to give them an opportunity to understand and become familiar with as many messages as possible. The eight two-word and eight sentence-length messages were all presented on each of three familiarization runs without competing weather broadcast. Within a familiarization run, each message was repeated after 950 msec intervals until the pilot keyed his microphone and read back the message. After 10 repetitions of any 1 message, its presentation was automatically terminated under the assumption that the pilot was not going to understand it on that run. Following verbal message readback, pilots wrote down whatever they had understood of each message on a prepared answer sheet. They were also asked to estimate the amount of time that they had spent listening to that particular message. The response time, which is the interval between the beginning of the first message repetition and the time when the pilot keyed his microphone, was recorded and used to calculate the number of message repeats and the ratio of estimated to actual time. Pilots were given no feedback on message comprehension or time estimation accuracy. This procedure generated the following data: a) response latency, b) number of message repeats, c) verbal time estimate, and d) pilots' written versions of the warning.

Recognition phase— During the Recognition Phase, pilots were asked to produce eight 10-sec intervals during which no other activity occurred (baseline) and then sixteen 10-sec intervals during which one of the eight two-word or eight sentence-length messages that had been presented during the Familiarization Phase was repeated one time only with a background of continuous weather broadcast. It was assumed that the majority of the messages had been comprehended during the Familiarization Phase and that for these familiar messages, the Recognition Phase of the experiment involved only simple recognition.

A pre-recorded message cued pilots when to begin each 10-sec production. By pressing one button, pilots initiated their production and the onset of the background weather broadcast. Approximately 2 sec later, 1 of the 16 warning messages was presented imbedded in the weather broadcast. Following warning-message presentation, which lasted no longer than 2.20 sec (table 1), the weather broadcast continued until pilots pressed a second button to terminate their 10-sec production. Then, they were asked to key their microphone and as quickly as possible, read back and then write down the warning message. This procedure generated the following data: a) length of time productions, b) pilots' written versions of the warning, and c) the length of time pilots waited after the end of their production to begin message readback (response latency).

RESULTS

Familiarization Phase

Overall performance change across runs— Intelligibility, as measured by the percentage of words correctly identified, increased significantly ($F = 5.12$; $df = 2,20$; $p < .025$) across the three familiarization runs (fig. 1(a)). The total time spent listening to each message (fig. 1(b)) decreased significantly ($F = 15.50$; $df = 2,20$; $p < .001$) across runs. The number of times that messages were repeated (fig. 1(d)) also decreased significantly ($F = 12.81$; $df = 2,20$; $p < .001$) across runs. The ratio of overall verbal estimate length to actual time spent listening to messages (fig. 1(c)) increased nonsignificantly ($F = 2.77$; $df = 2,20$; $p > .10$) across runs.

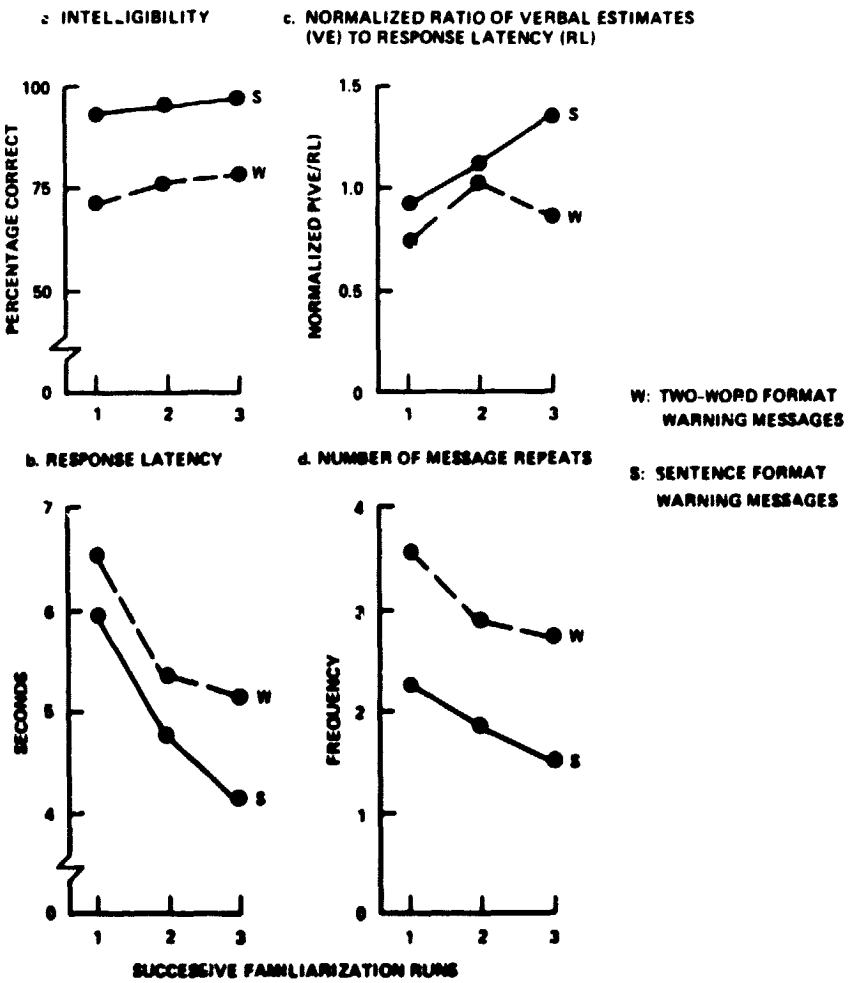

Figure 1.— Performance during the familiarization runs

Two-word versus sentence-length format— Warning messages presented in a two-word format were significantly ($F = 13.39$; $df = 1, 10$; $p < .005$) less intelligible than those presented in a sentence format for all runs (fig. 1(a)). Note that there were more words to be remembered in the sentence-length messages than the two-word messages. Even so, the sentence-length messages were more intelligible as a further consequence of the added linguistic redundancy.

Pilots allowed the two-word messages to repeat (fig. 1(d)) significantly ($F = 15.32$; $df = 1, 10$; $p < .005$) more often (at least one more time, on the average) than sentence-length messages. The time spent listening to two-word messages (fig. 1(b)) was also consistently longer than that spent listening to sentence-length messages even though each sentence-length message lasted longer than its corresponding two-word message. This difference was not statistically significant ($F = 2.06$; $df = 1, 10$; $p > .10$) because of a Pilot Group X Message Format interaction ($F = 7.09$; $df = 1, 10$; $p < .025$).

Verbal estimates of the length of time spent listening to two-word warnings were consistently shorter than the amount of time that had actually passed, whereas verbal estimates of intervals filled with messages presented in a sentence format were close to, or slightly longer than, elapsed clock time (fig. 1(c)). This difference in verbally estimated duration as a funtion of message format was statistically significant ($F = 25.79$; $df = 1,10$; $p < .001$).

Influence of key word intelligibility— The 16 pairs of key words were rank ordered on the basis of intelligibility scores across familiarization runs, and then divided into quartiles that represented increasing intelligibility. As can be seen in figure 2(a), there was a large difference in intelligibility scores for two-word messages. Less intelligible two-word messages were repeated more often (fig. 2(b)) and were associated with the shortest verbal estimates (fig. 2(c)). These same key words, when presented in a sentence, were consistently more intelligible (fig. 2(a)). The facilitation provided by a sentence format was particularly great for the messages that were the least intelligible when presented in a two-word format. Sentences were repeated less often (fig. 2(b)) and sentences were associated with verbal estimates that most closely approximated the amount of time that had actually elapsed, for all quartiles of key word intelligibility (fig. 2(c)). The differences between two-word and sentence formats for all three measures (intelligibility, number of repetitions, and verbal estimate duration) were statisfically significant ($p < .002$) in each case, as measured by Wilcoxon's signed ranks test for differences between 16 pairs of means.

Influence of message duration— Intelligibility was not correlated with simple message length. For example, the two-word message "DME Malfunctioning" was the longest two-word warning (1.5 sec), yet it was the least intelligible message when presented in a two-word format. The message "Your DME is Malfunctioning" was, by contrast, one of the most intelligible messages by virtue of the additional words "your" and "is" in the sentence context.

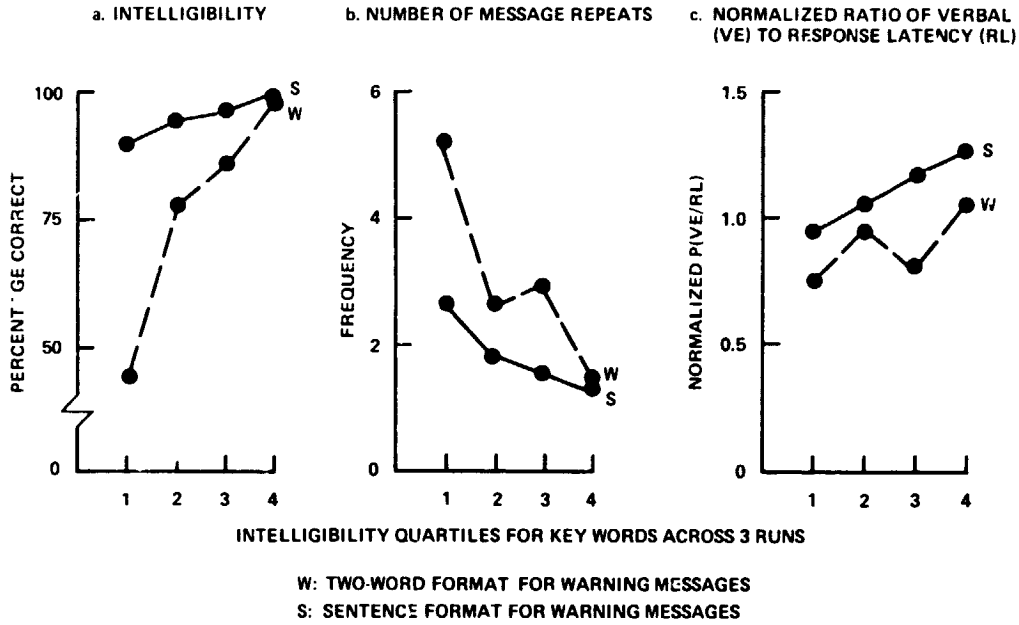

Figure 2.— Comparison of two-word versus sentence format for intelligibility quartiles (based on key word intelligibility for 3 familiarization runs)

Recognition Phase

During the one recognition run, the intelligibility scores were higher than they were during the three familiarization runs, even though each of the 16 messages was presented only once and with competing weather broadcast. Two-word message intelligibility increased from 76 percent to 82 percent and sentence intelligibility increased from 95 percent to 96 percent between the last familiarization run and the one recognition run.

Two-word versus sentence-length format— As before, sentences were more intelligible than two word messages (fig. 3(a)). Pilots also began sentence readback more quickly than two-word message readback (fig. 3(b)). Overall, produced durations lasted 12.55 sec, and were nearly identical for intervals filled with two-word and sentence-length messages (fig. 3(c)). This represents an increase of 2.5 sec in production length over the length of baseline productions made with no warning meassage presentation.

Influence of message familiarity— Several of the messages had not yet been completely understood at the end of the Familiarization Phase so 26 percent of the messages were still unfamiliar at the beginning of the Recognition Phase. This phenomenon occurred more often for two-word than sentence-length messages (fig. 4(a)). For messages that were still unfamiliar, response latencies were 1.0 sec slower (fig. 4(b)) and produced durations were 2.0 sec longer (fig. 4(c)) than were response latencies and produced durations for messages that had already been understood and were simply recognized. The length of produced durations that had been filled with unfamiliar two-word messages was 1.5 sec longer than the length of productions filled with

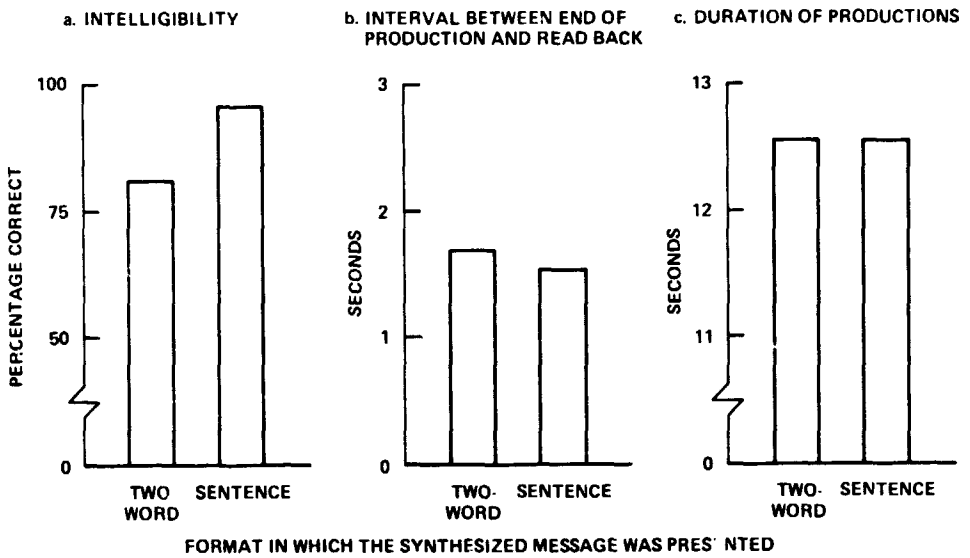

Figure 3.— Performance during the recognition phase

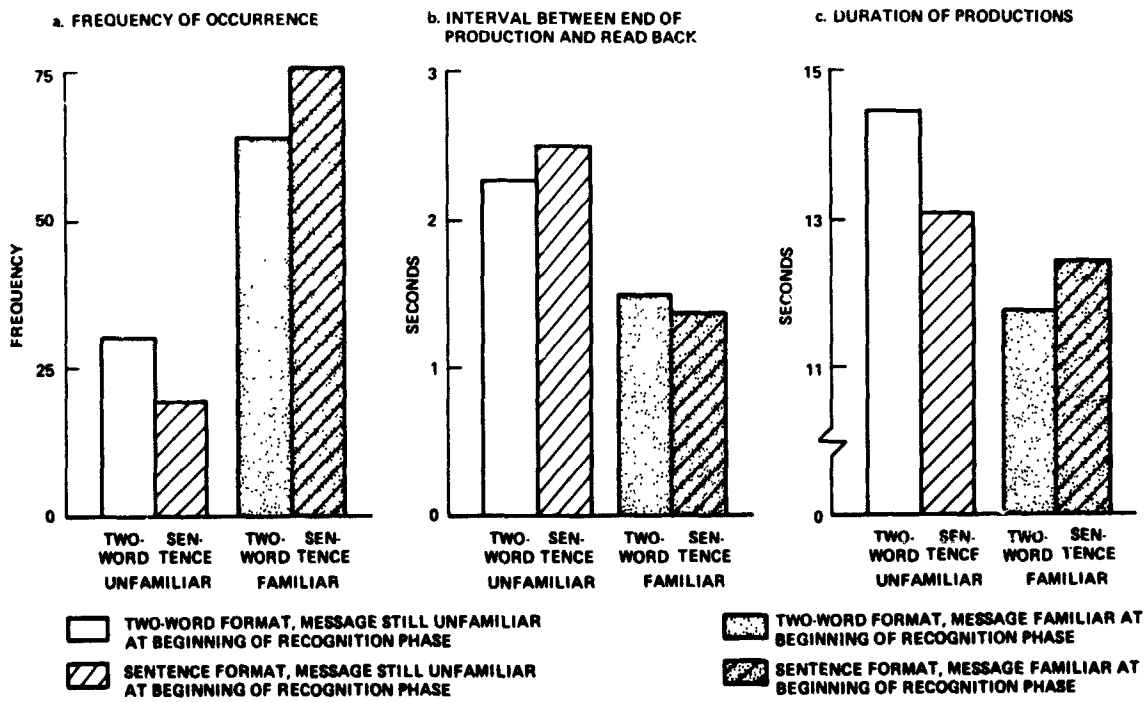

Figure 4.— Performance during the recognition phase as a function of warning message familiarity

unfamiliar sentence-length messages. For familiar messages, however, produced durations filled with two-word messages were slightly shorter (0.5 sec) than productions filled with sentences.

Influence of Number of Syllables

In order to compare the results of the present study to results by Simpson (ref. 3), the influence that the number of syllables had on intelligibility was also determined for both the Familiarization and Recognition Phases. While polysyllabic words were not necessarily longer in duration than monosyllabic words, the former were more intelligible, again suggesting that linguistic redundancy, rather than simple duration, was the most important factor in intelligibility. These results confirm the results of Simpson's research (ref. 3). During familiarization runs, both monosyllabic and

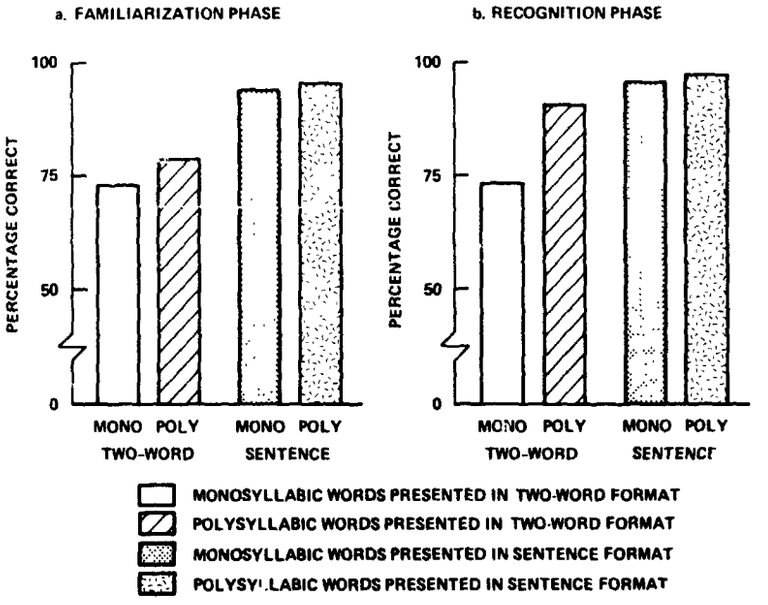

Figure 5.— The influence of monosyllabic and polysyllabic words on intelligibility as a function of message format

polysyllabic two-word warnings were less intelligible than the same monosyllabic and polysyllabic messages presented in sentences (fig. 5(a)). During recognition, with competing weather broadcast, polysyllabic words increased two-word message intelligibility to 91 percent. However, there was no corresponding gain in intelligibility for monosyllabic words (fig. 5(b)).

DISCUSSION

The results of the current research confirm and expand the research reported by Simpson (ref. 3) with respect to the facilitating influence of linguistic redundancy on initial comprehension and subsequent recognition. Warning messages presented in a sentence format were consistently more intelligible, required fewer repetitions and less listening time than two-word messages during familiarization, and were more easily recognized and read back more quickly during recognition.

Variation in the length of verbal time estimates and productions was used to assess the attention required to process messages differing in linguistic redundancy. It has been suggested that active verbal time estimation requires attention (ref. 1). If attention is diverted from timekeeping by concurrent activity, clock time continues whereas subjective timekeeping does not. This disparity results in an underestimation of elapsed time so that verbal estimates of the duration of an interval are too short. As expected, verbal estimates of the duration of intervals filled with less redundant, less intelligible, two-word messages were consistently shorter and less accurate than those of intervals filled with sentence-length messages during familiarization. These very short verbal estimates indicate that comprehending two-word messages may require more attention than comprehending similar messages presented in sentences.

It was further suggested (refs. 1, 2) that active time production also requires attention. If concurrent activity momentarily diverts attention from timekeeping, the amount of time that has passed may be underestimated causing subjects to wait too long to terminate their productions. This results in produced durations that are too long. In the present study, presenting weather broadcast and warning messages while the time production was in progress was associated with an increase of 2.5 sec in the average length of productions as compared to baseline. Produced durations filled with two-word messages were generally equivalent in length to those filled with sentences. This occurred even though sentence-length messages had the potential for greater distraction from timekeeping, simply because they lasted longer. If the foregoing hypothesis is correct, it appears that the linguistic redundancy provided by the sentence format not only facilitated understanding but did not require additional attention.

It is also interesting to note that produced durations filled with messages that had not yet been learned at the beginning of the recognition phase were 2.0 sec longer than those filled with previously learned messages that required only simple recognition. We infer that this length difference is a consequence of the additional attention required to comprehend a message that had not yet been learned as compared to the relatively simple task of recognizing a previously learned message. This difference in produced durations was particularly great for two-word messages which appear to be less intelligible and so require more attention when unfamiliar than when familiar.

Sentence-length warnings appear to require less attention to comprehend initially than two-word messages. The former were associated with productions that were 1.5 sec shorter than those for intervals filled with two-word messages. However, sentences that had been previously learned had longer production times than did two-word messages that were familiar. Once a familiar message had been recognized, pilots had to hold it in memory during the remainder of the production. Distraction from time estimation most likely varied as a function of the number of items held momentarily in memory. If pilots attended to the passage of time only at the end of each mental repetition of the recognized message, the sentences, being longer units, resulted in less frequent attention to time, and thereby longer productions, than did the two-word warnings.

CONCLUDING REMARKS

From these, as well as previously reported results, it appears that verbal and produced time estimates may provide a useful index of the attention demands of concurrent activity. Factors associated with the intelligibility of synthesized warning messages, such as redundancy and familiarity, presumably influenced the attention required to process them. The length of verbal estimates and produced durations provided an indirect measure of the amount of attention required by messages differing in intelligibility.

The results of this research, and of that reported by Simpson (ref. 3), have demonstrated the facilitating influence of linguistic redundancy, such as that provided by a sentence format, on cockpit-warning comprehension and recognition. Even though sentences last longer and contain more words to be remembered than do two-word messages, the former require fewer repetitions, less time, and less attention to comprehend initially and are read back more quickly and accurately once they are familiar.

REFERENCES

1. Hart, S. G.: Time Estimation as a Secondary Task to Measure Workload. Proceedings of the 11th Annual Conference on Manual Control. NASA TM X-62,464, Ames Research Center, Moffett Field, California, 1975.

2. Hart, S. G., and McPherson, D.: Airline Pilot Time Estimation During Concurrent Activity Including Simulated Flight. Paper presented at the 47th Annual Meeting of the Aerospace Medical Association, Bal Harbour, Florida, May, 1976.

3. Simpson, C. A.: Effects of Linguistic Redundancy on Pilot's Comprehension of Synthesized Speech. Paper presented at the 12th Annual Conference on Manual Control, Champaign, Illinois, May, 1976.

4. Miller, G. A.; Heise, G. A.; and Lichten, W.: The Intelligibility of Speech as a Function of the Context of the Test Materials. *Journal of Experimental Psychology*, vol. 41, 1951, pp. 329-335.

TACTUAL COMMANDS FOR PILOT FLARE TRAINING*

Richard D. Gilson and Ronald W. Ventola

Departments of Aviation, Psychology
and Electrical Engineering

The Ohio State University
Columbus, Ohio

INTRODUCTION

The problem of aircraft control during approach and landing operations deserves strong attention, as evidenced by aircraft accident statistics. Approximately one-half of all aircraft accidents occur during such operations despite their contributing only a brief portion of the total flight time. (1)

A primary cause is the heavy demand placed on a pilot--especially the division of visual attention required to control the flight path and airspeed. During the approach to landing, information pertaining to the flight path is primarily obtained from visual cues outside the cockpit, while pitch information is obtained via a panel-mounted airspeed display.

In addition, just prior to touchdown, the pilot's visual attention is progressively drawn towards runway-specific cues allowing little, if any use of instrument panel information.

It is hypothesized then, that the use of a non-visual display would allow:

(a) An alleviation of this unwanted division of visual attention, and
(b) the opportunity of presenting accurate pitch-command information during the roundout (or flare) just prior to touchdown.

* The efforts reported here were sponsored by the National Aeronautics and Space Administration (NASA), Contract No. NAS 2-8954.

this should be especially benefitial to a novice pilot - who lacks the experience to use relevant visual, inertial, and aural cues. This should result in the following benefits:

(1) His task should be simplified
(2) His performance should be improved and
(3) His learning of the appropriate visual cues from outside the cockpit should be enhanced.

Previous work by Fenton, Gilson and others (2, 3, 4 & 5) has shown an effective and practically implemented non-visual display for automobile, aircraft, and helicopter controls. Based on their findings, the use of a kinesthetic-tactual display appears to be a natural way of overcoming the unwanted division of visual attention during flight, while also avoiding any further division of auditory attention.

In the present study, information pertaining to the aerodynamic state of an aircraft was continuously presented via a kinesthetic-tactual display during takeoffs and landings. Figure 1 depicts the desired control information during an approach and landing. The tactual display is programmed to present critical-pitch directives from the beginning of takeoff roll through the approach and flare-to-landing. The reference input is the desired angle-of-attack (AOA) which is, of course, related to the desired approach airspeed. Whenever the aircraft is higher than 50 feet above the ground the desired angle-of-attack is held constant. Below 50 feet the desired AOA is an increasing inverse function of height, so that the aircraft is near stall at liftoff and at touchdown.

Figure 2 shows the control loop. The feedback signal is the measured AOA. The display input is the difference between the measured and reference (or desired) AOA--thus, a compensatory tactual "pitch director."

The tactual display was built into the head of a conventional aircraft control yoke. The display itself, photographed in Figure 3 consisted of a moveable section of the control grip. This is shown as protruding from the forward part of the grip and recessed into the aft part. This protrusion corresponds to an unwanted increase in angle-of-attack, and a pilot responds by moving the yoke forward so as to decrease this angle and return the display to its neutral or flush position. Next, in Figure 4 is a view of the display protruding "backward" which requires an aft corrective motion of the control yoke. In essence, the pilot

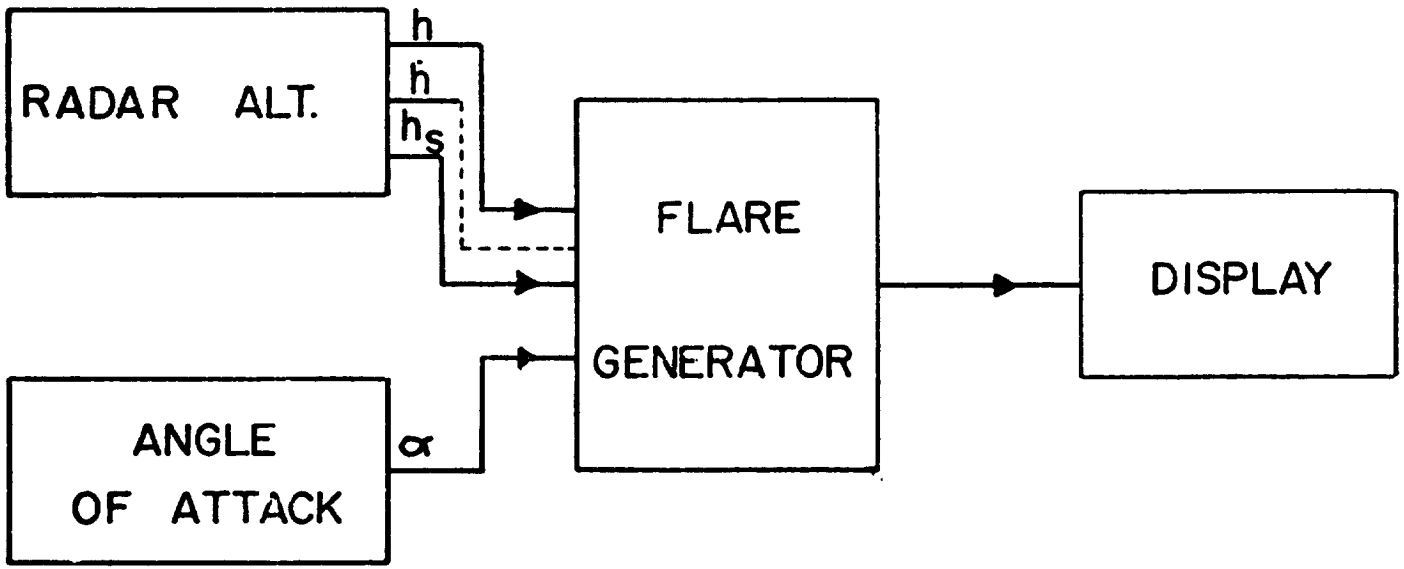

h = Absolute Altitude
ḣ = Verticle Velocity
h_s = Flare Altitude set
α = Angle of Attack

Figure 1. Desired Control Information

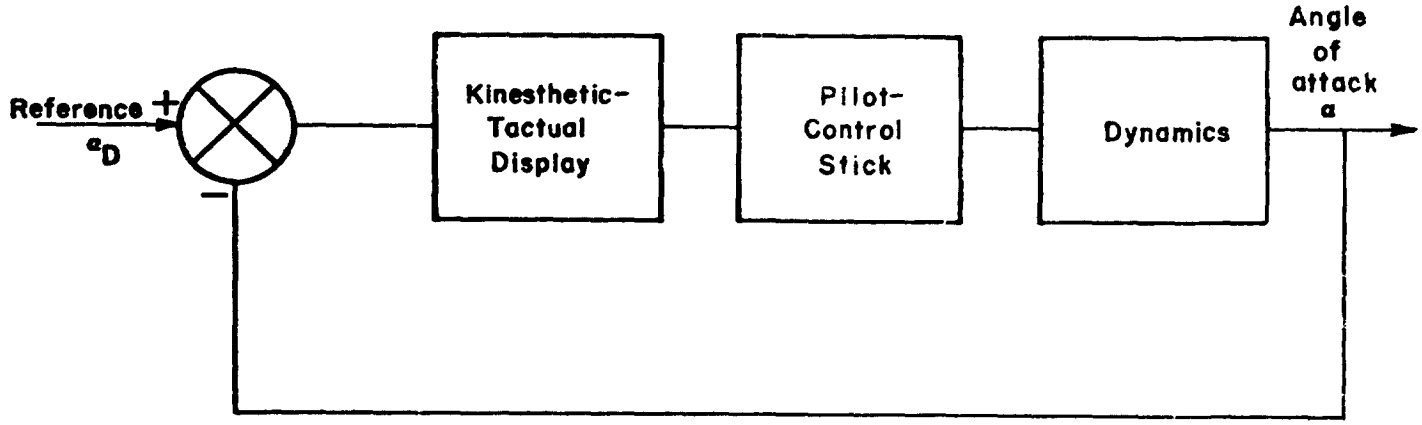

Fig. 2 Control loop for angle-of-attack

Figure 3 Kinesthetic-tactual display protruding forward

Figure 4 Kinesthetic-tactual display protruding rearward

follows the display commands to reduce errors to zero.

PROCEDURE

The experimental inflight study considered novice pilot performance while flying approaches to landing. Initially, each of 12 novice pilots received flight instruction with a standard, 3-hour primary training syllabus designed to teach them fundamentals of aircraft control (but without allowing practice of landings.) At the completion of this Preliminary Training, the subjects were evaluated on a standard series of test maneuvers designed to equally match subjects, by performance, into two groups.

The first experimental phase then commenced, wherein the subjects flew four one-hour test periods of six takeoffs and landings. One group, designated the airspeed group, received only the conventional visual display of airspeed. The other, the tactual group, received only the tactual displayed information.

The second experimental phase then followed, consisting of two one-hour test periods, wherein the display conditions were reversed; that is, the airspeed trained group now flew with the tactual display, while the tactually trained group received visual airspeed information only. In all the experimental phases, performance was analyzed during the final approach and landing from approximately 1½ miles out to touchdown. Performance measures included: the number of instructor pilot (a) verbal assists, (b) assisted landings and (c) actual takeovers during landing (where safety of flight was involved). Touchdown performance measures consisted of: (a) lateral deviations from runway centerline, (b) longitudinal touchdown position measured from the fixed distance marker and (c) sink rate or "g" loading at touchdown. Other performance measures recorded but not as yet analyzed include, angle of attack, flight controls positions, runway lineup, and glide path errors during the final approach.

RESULTS AND DISCUSSION

Preliminary data are shown in Figures 5 and 6. Figure 5 depicts the total number of unassisted landings performed by

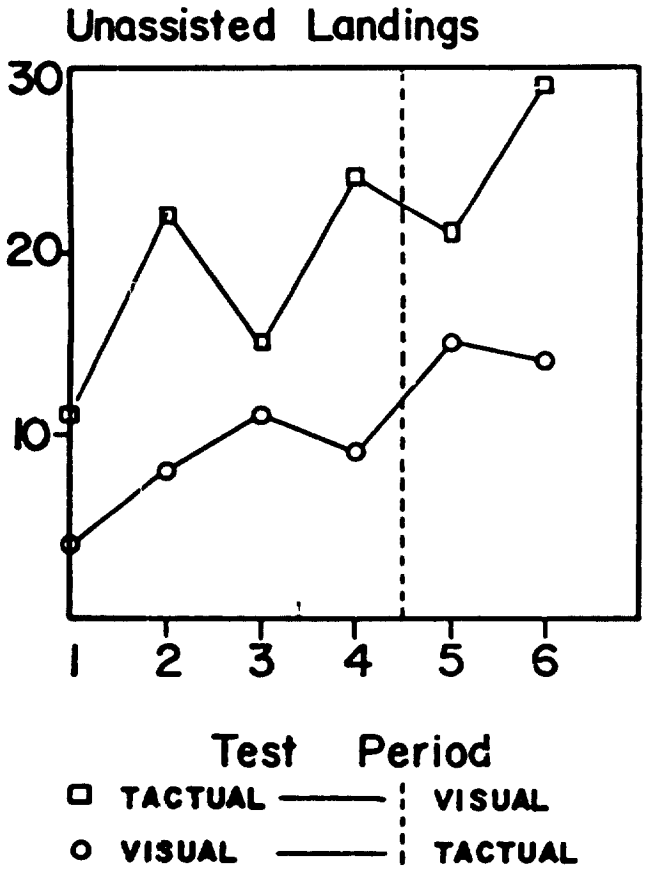

Figure 5.
Total number of
Unassisted Landings
36 possible/group/period

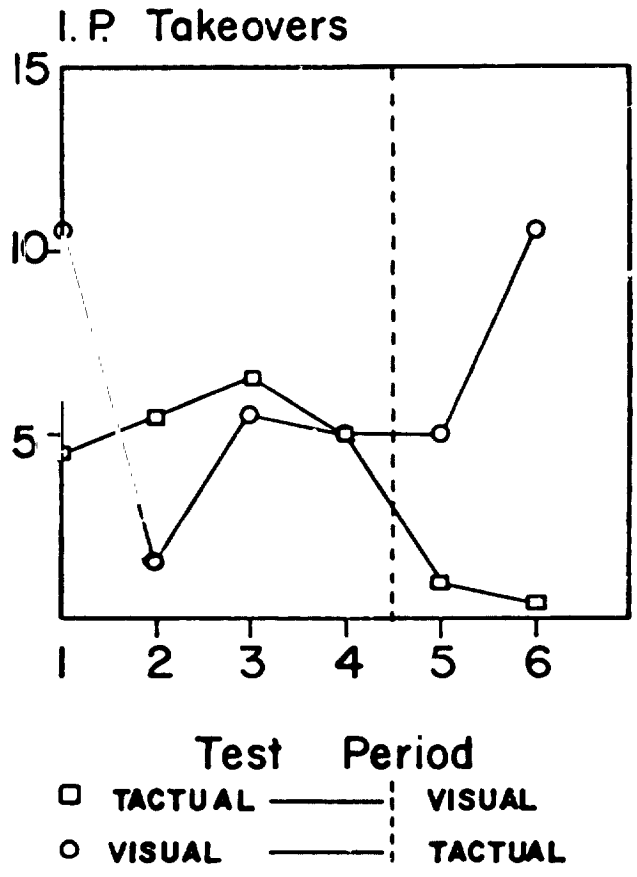

Figure 6.
Total number of
Instructor-pilot takeovers
36 possible/group/period

subject groups per test period. Unassisted landings were those expected not to exceed three "g's" at touchdown. With 6 landings per hour and 6 subjects per group, a total of 36 landings per test period were possible. The group initially trained with the tactual display significantly ($p<.01$) out-performed the airspeed group not only in the first four periods but subsequently when they were transferred to fly with the visual airspeed indicator only.

This suggests that the group initially trained with the tactual display was facilitated in their flares-to-landing by following the display (50% unassisted landings), and that they had learned enough to subsequently perform quite well (almost 70% unassisted landings) with the conventional airspeed display only. The latter rejected an initial hypothesis that a "crutch-like dependency on the display might develop when this group was transferred to the visual-only condition. On the other hand, the group first trained with the airspeed display performed like typical flight students with approximately 22% unassisted landings during the first four periods. What was remarkable, however, was that the airspeed group did not significantly improve when they were transferred to the tactual display--there were only 40% unassisted landings in the last test periods (5 & 6) compared to 50% unassisted landings in the initial training periods for the tactual group.

The reason for this lack in improvement is suggested in Figure 6--summarizing the number of instructor takeovers. An analysis of variance for the takeover restuls shows a significant interaction effect of group by test period ($p<.05$).

It is apparent that when the airspeed group was transferred to use the tactual display (shown by test periods 5 & 6) there was a dramatic increase in the number of takeovers. These data indicate that some apparent conflict occurred when the airspeed group was transferred to the use of the tactual display. This conflict may occur for the airspeed group because their initial strategy, in utilizing the available visual cues, developed largely by trial and error. Such strategies most likely differed from the approach commanded by the tactual display. Conversely, the group initially trained with the tactual display was forced to use and observe the desired flare-to-landing strategy. Thus, when this tactual group was transferred to use the visual airspeed display, they relied on what they had learned before rather than trial and error.

Among the other performance measures, no significant differences were found in either the number of verbal assists given by the instructor-pilot, or in the vertical velocity or "g" loading, just at touchdown for unassisted landings. This suggests that no apparent biases were introduced by the instructor-pilot.

CONCLUSIONS

There are several directions of future research that are envisioned at this time.

(1) For pilot training purposes, tactual commands may benefit a student's understanding of the interactions between aircraft attitude, speed and power by means of a tight control loop and the display's natural stimulus-response compatibility.

(2) For more basic studies, cognative, perceptual, and motor learning may be investigated by employing appropriate tactual feedback to differentially augment visual or tactual display-control relationships. Such studies are currently being initiated in a flight simulator with a computer graphics display of the landing environment.

(3) For practical aircraft control, kinesthetic-tactual displays incorporated within the appropriate control levers could allow for zero-zero landings. For example, during an instrument approach, a power command could be located in the throttle lever and a lineup command could be incorporated in a multiaxis control yoke. Indeed, the tactual pitch commands currently allow an ILS approach to touchdown if the cross-pointer indicator is utilized.

In summary, the exploration of the efficacy of tactual displays in the aircraft environment has only begun and many, perhaps significant, improvements may be made in both the safety and precise control of aircraft.

REFERENCES

(1) National Transportation Safety Board, Annual Review of U.S. General Aviation Accidents Occuring in Calender Year 1969.

(2) Rule, R.G., and Fenton, R.E. On the Effects of State Information on Driver-Vehicle Performance in Car Following, IEEE Transactions SMC, No. 5, November 1972, pp.630-637.

(3) Gilson, R.D. and Fenton, R.F. Kinesthetic-tactual information presentations -- Inflight studies. IEEE Transactions SMC, No. 6, November 1974, pp. 531-535.

(4) Gilson, R.D. and Fenton, R.F. Development of a Concept for a Stall-Deterrent Device for Small Airplanes, Federal Aviation Administration, Report No. FAA RD-75-53 June 1975 NTIS Springfield,VA

(5) Dunn, R.S. and Gilson, R.D. A Simulation Study of Helicopter Pilot Workload Reduction Using a Tactile Display. (See These Proceedings).

TWO-DIMENSIONAL COMPENSATORY TRACKING WITH TACTILE DISPLAYS*

By H. P. Schmid
General Dynamics Pomona Division, Ph.D. Fellow
University of Southern California

G. A. Bekey
Department of Electrical Engineering
University of Southern California,
and Rancho Los Amigos Hospital

J. B. Reswick
Rehabilitation Engineering Center,
Rancho Los Amigos Hospital and
University of Southern California

SUMMARY

Compensatory tracking experiments in one and two axes using tactile displays are described. The electro-tactile inputs to the operator are located circumferentially about the waist region utilizing four electrodes. The error signal, applied to the operator through the electrodes, is an amplitude modulated 100 Hz pulse train with a fixed pulse width of 40 μsec. The dynamic range of the display between sensation threshold and pain is one order of magnitude. The operator's output is isometric muscle force applied to a two degree of freedom joystick. Describing functions for both one and two-dimensional tracking with low frequency pseudo-random noise inputs are presented. The results indicate that tactile tracking with this particular display in one- and two-dimensions is indeed practical. Coherence analysis of the two-dimensional tracking task indicates that, for the low frequency forcing function utilized, no significant linear cross-coupling exists in the operator model. Therefore, a two-dimensional task can be considered to be two independent one-dimensional tasks. A comparison of the tracking ability of traumatic paraplegics with that of normal individuals allows the conclusion that there are no essential differences between these groups.

INTRODUCTION

Paraplegics with spinal cord lesions at or above L3 have a great deal of difficulty in ambulating. One of their major problems is the lack of motor control over knee and hip joints. Poliomyelitis paraplegics, whose condition is due to a virus which selectively attacks motor fibers, have their sensory ability remaining intact, which allows them to perceive the position and velocity of their paralyzed limbs. This perception of position and motion is called proprioception. In contrast, traumatic

* Supported in part by the Rehabilitation Services Administration, DHEW under grant number RD-23-P-55442.

paraplegics with a spinal cord lesion due to a traumatic injury usually have neither muscular control nor proprioception of the affected limbs. The poliomyelitis paraplegic with no hip control can functionally walk in long leg braces with forearm crutches, whereas the traumatic paraplegic chooses to utilize a wheelchair. The lack of proprioception in the legs and hips is the only difference between these individuals. Based on this fact, it has been hypothesized that the provision of synthetic sensory feedback of body posture information from the affected areas will help the traumatic paraplegic to maintain a better static vertical posture. The maintenance of static posture is a prerequisite for stable, possibly electrically stimulated, gait.

Out of the three commonly used channels of communication, which are visual, auditory and tactile, the latter was chosen to be the mode of information display for the sensory feedback. The visual channel is utilized extensively during walking, mostly for path choice in obstacle avoidance and for the admiration of scenery. Although the auditory channel is less utilized in a walking task, it can be most easily jammed or overloaded by inputs such as horns, sirens, etc. For both visual and auditory displays the problem of providing a cosmetically acceptable mechanization presents great difficulty. For the tactile channel, especially when the display is located in the waist region, the problems of interference and cosmetic acceptability are greatly diminished.

A number of tactile tracking studies have been reported; their approach and results are summarized in Reference 1. The displays for these studies were mainly vibratory. They were applied at diverse body locations such as on the thumbs, fingernails, hands, arms, forehead and chest. All studies concluded that tactile tracking is possible, but with generally poorer performance as compared with visual displays. More recently, Reference 2 reports experiments with tactile displays for aircraft control. In this study, electrotactile and vibratory displays were utilized. Better consistency and pilot acceptance were attained with the vibratory display. The displays were multi-electrode or vibrator type arranged in + or H fashion on the chest and abdomen of the pilot. The problems with all previous studies are that they do not provide an easy mode of presenting body posture information to the subject wearing the display. The models presented also were not analyzed for cross-coupling components and do not provide a model of the human tracking an input whose power spectrum resembles static posture sway. Humans standing erect control small oscillatory movements about the normal upright position; this deviation is called sway. It has been measured and its power spectral content has been reported in Reference 3.

The basic objectives of this study are (1) to show the feasibility of tracking a forcing function, having a power spectral density (PSD) similar to standing sway in humans, utilizing an electro tactile display of four electrodes located about the waist, (2) to model the human operator tracking this forcing function in one- and two-dimensional compensatory tasks, (3) to investigate the cross coupling terms in the human operator model in order to determine their relative importance and (4) to compare the tracking ability of normals to that of paraplegics.

EXPERIMENTAL DESIGN

The simple tactile compensatory tracking task considered in this experiment is shown in Figure 1. The subject in the loop has the task of minimizing the error displayed to him. A pseudo-random binary sequence generator, appropriately filtered, provides the forcing function c to be tracked. The subject's force response r, a function of his voluntary muscle force transformed by the isometric joystick manipulator, is subtracted from c to provide a measure of the tracking error ϵ. The tactile display signal generator produces negative constant current pulses at a frequency of 100 Hz with a duration of 40 μsec and an amplitude directly proportional to the error. The tactile display consists of an elastic belt, four (4) electrodes and the associated wiring shown in Figure 2. The placement of the electrodes about the waist region is shown in Figure 3. Details of the surface electrode can be seen in Figure 4. These electrodes are constructed from silver according to the findings in Reference 4 and are of the concentric type. The center circular region is the active area supplying the negative current. It is isolated from the rectangular ground plane by a small teflon spacer.

The dynamic range of the display is one order of magnitude between the threshold of sensation and the threshold of pain. This range is indicated in the strength duration curves presented in Figure 5. There the current stimulus amplitude for sensation and pain threshold is plotted for a number of pulse durations. The duration of 40 μsec was chosen since it provides a reasonable dynamic range without requiring unduly large voltages. The electrodes are applied to the skin after a small amount of electrode gel is applied. The electrodes in this configuration present a dynamic impedance of approximately 2-4K ohms. The minimum level of stimulation throughout the experiments was adjusted to the threshold of sensation in order to eliminate the dead zone inherent in this display configuration.

The two-dimensional tracking system is shown in Figure 6, in block diagram form. The pseudo-random noise generator is a 17 stage digital shift-register with a modulo-2 adder in the feedback path. Design details may be found in Reference 5. An original sequence S_1 and a delayed version S_2 can be generated through utilization of additional modulo-2 adders. For this particular design, utilizing a clock rate of 30 Hz, the duration of the sequence is 72.8 minutes. The delayed sequence is shifted by 36.4 minutes providing two independent signals. Each of these sequences are filtered by identical filters labeled A/P (anterior/posterior) and Lat. (lateral) sway filter. The output of each summing junction, representing the tracking errors ϵ, is amplified, separated into positive and negative components, synchronously sampled, converted to stimulus current and finally applied to the subject via the electrodes. The tactile display gain (TDG) was set at five for all experiments presented and is included in the models. This gain setting minimizes the tracking error; that is, lower and higher gains tend to increase the tracking error score as measured by the performance monitor (PM). The performance monitor calculates the integral of the absolute value of the tracking error, which is displayed on a meter for on-line performance evaluation. The isometric force response measured by

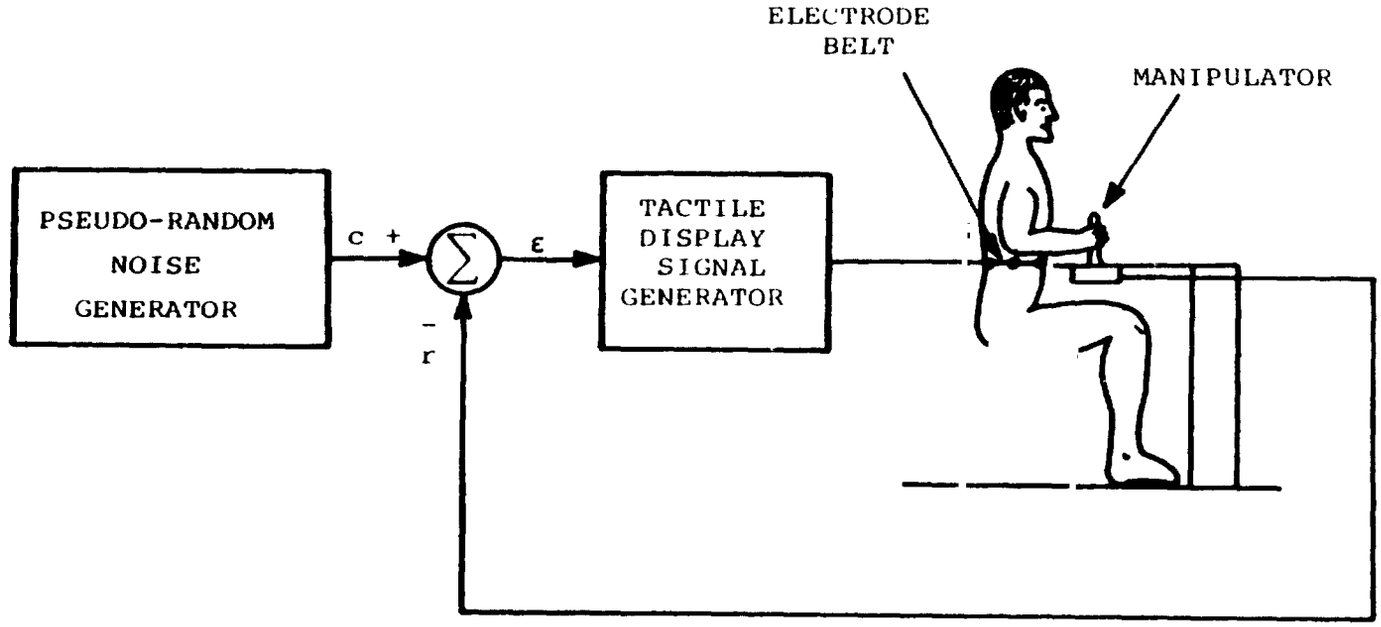

FIGURE 1. Tactile Compensatory Tracking Task

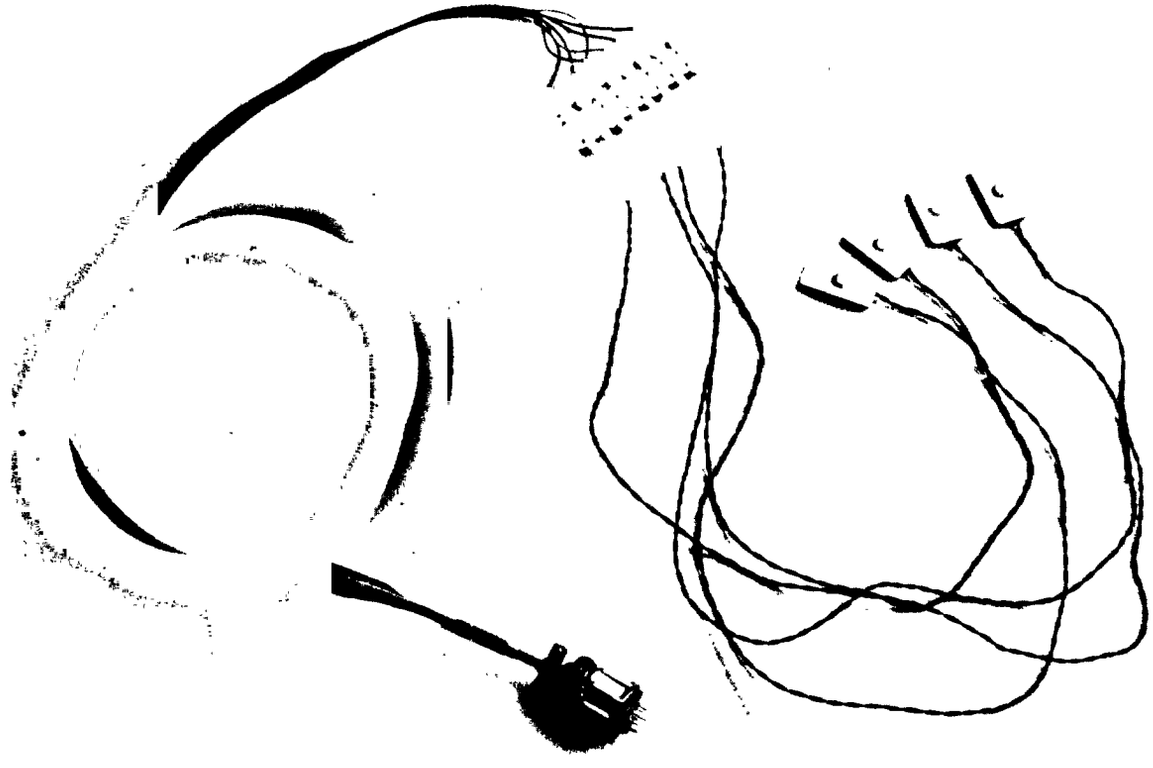

FIGURE 2. Tactile Display (Electrode Belt).

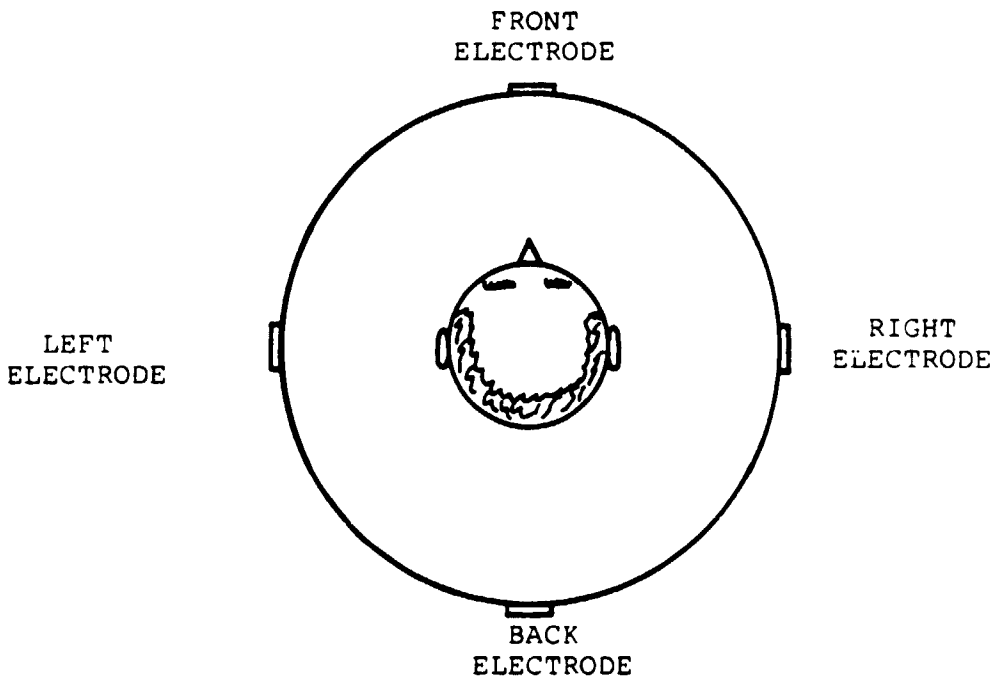

FIGURE 3. Electrode Placement

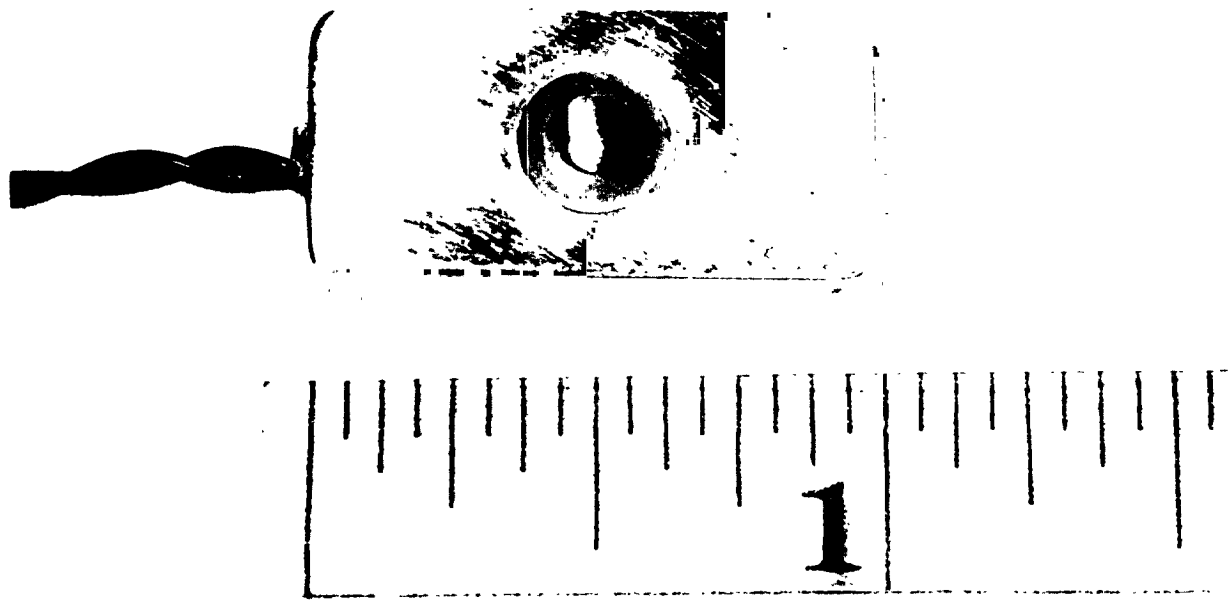

FIGURE 4. Surface Electrode

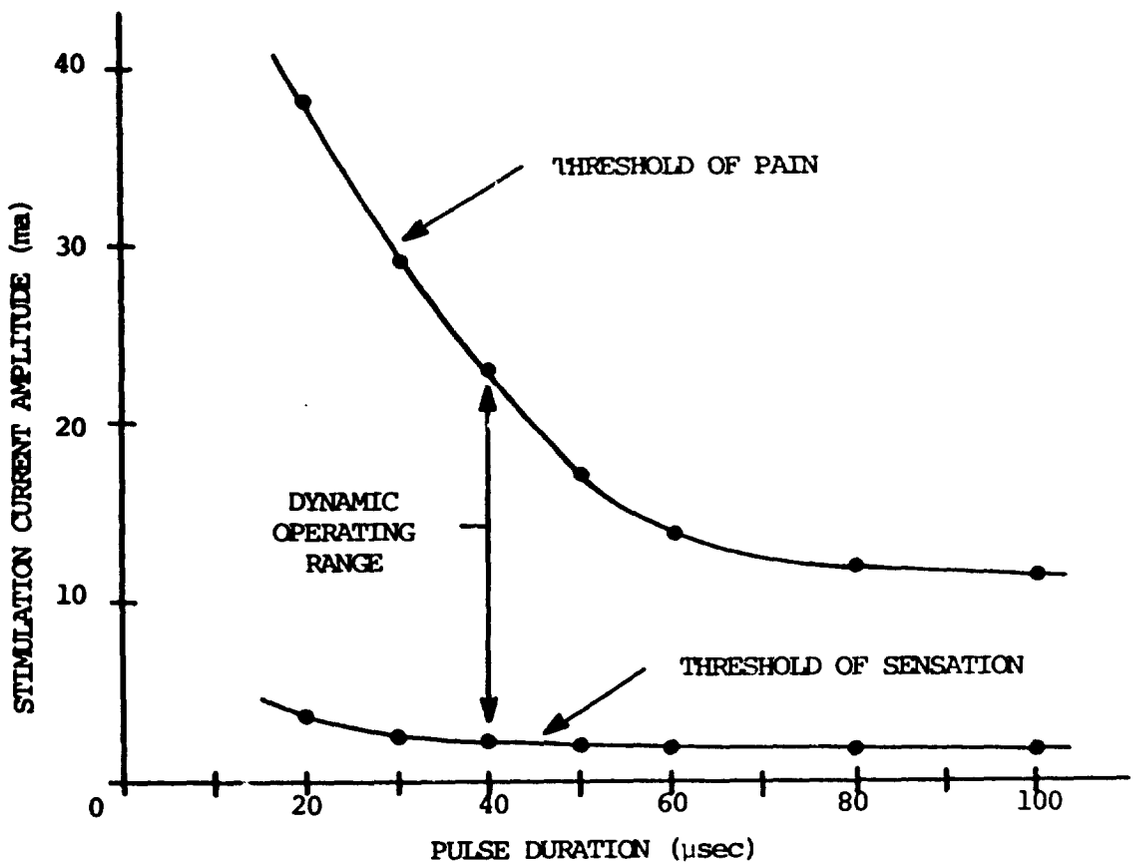

FIGURE 5. Strength Duration Curve Indicating Dynamic Range of Display

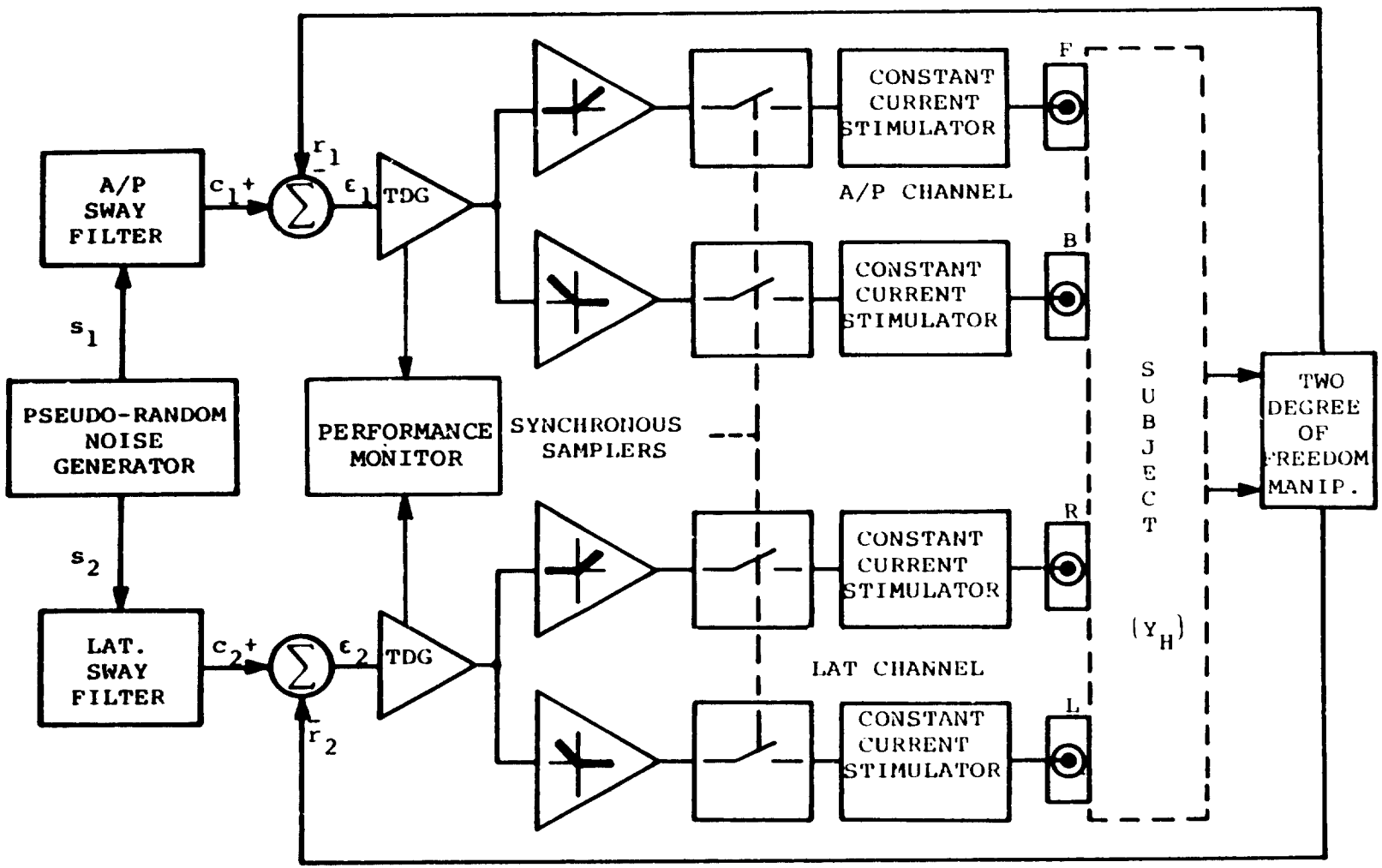

FIGURE 6. Tracking System Block Diagram

the two degree of freedom manipulator (joystick) is fed back to the summing junction.

The physical configuration of the tracking system hardware is shown in Figure 7 and contains all the elements described above.

One paraplegic and three normal subjects have been tested in two one-dimensional and one two-dimensional compensatory tracking task. The one-dimensional tasks are (1) tracking in the anterior/posterior plane and (2) tracking in the lateral plane. The two-dimensional task is the combination of these individual tracking tasks.

For each experiment the forcing functions (c_1 and c_2), the tracking error (ϵ_1 and ϵ_2), the force response (r_1 and r_2), and a 100 Hz trigger signal synchronous with the stimulation rate are recorded on analog tape. The analog data is later digitized at the 100 Hz rate and finally analyzed at a 10 Hz rate. Proper precautions are taken to reduce aliasing due to sampling by appropriately filtering the data at each step of the operation.

The time history of the recorded signals for a typical tracking run are shown in Figure 8. The similarity between the forcing function and the force response are obvious. The tracking error is plotted on an expanded scale.

ANALYSIS

Quasilinear describing functions, based on spectral analysis, are utilized to represent the human operator model in this tactile compensatory tracking task. The model for the human operator in a single axis task is shown in Figure 9. Models of this form have been extensively discussed in the literature on human operators, such as Reference 6. The open loop describing function for the human operator (Reference 6) is found to be

$$Y_H(j\omega) = \frac{S_{cr}(j\omega)}{S_{c\epsilon}(j\omega)} \quad , \tag{1}$$

where $S_{cr}(j\omega)$ and $S_{c\epsilon}(j\omega)$ are the input-output and input-error cross-power spectral densities.

Estimates of the cross-power spectral densities are obtained by a method of averaging modified periodograms as described in Reference 7. In this procedure the time domain data is sectioned into M overlapping segments of length N. The overlap here has been chosen to be N/2 in order to minimize the variance of the spectral estimate for the total available data length. Each data section is tapered in some fashion; the Hamming Window was chosen to perform this function. The Fourier Transform, defined as

$$X_k = \sum_{n=0}^{N-1} x_n w_n e^{-j\frac{2\pi nk}{N}} \quad k=0, 1, \ldots, N-1 \tag{2}$$

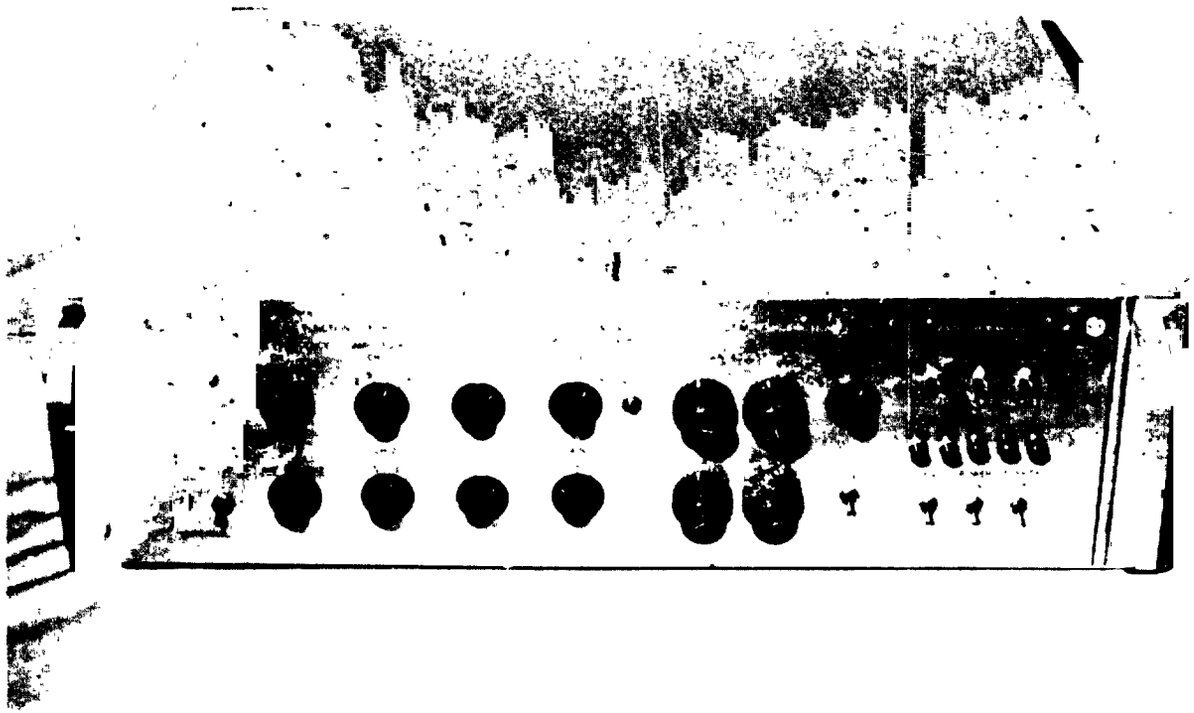

FIGURE 7. Tracking System Hardware

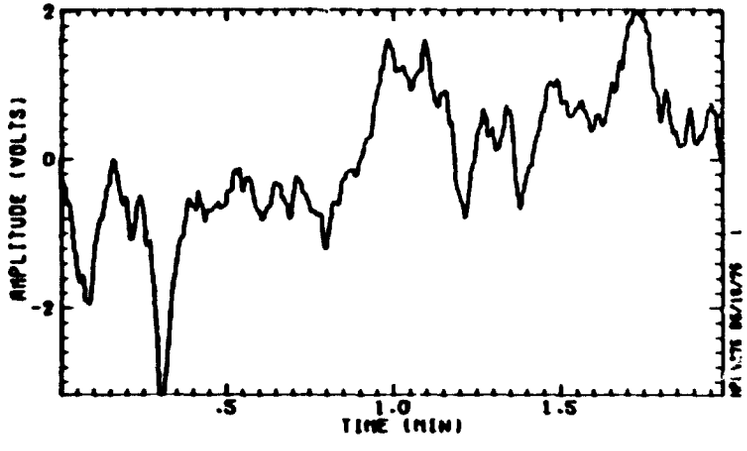

LAT FORCING FUNCTION C2(T),FC=.1HZ

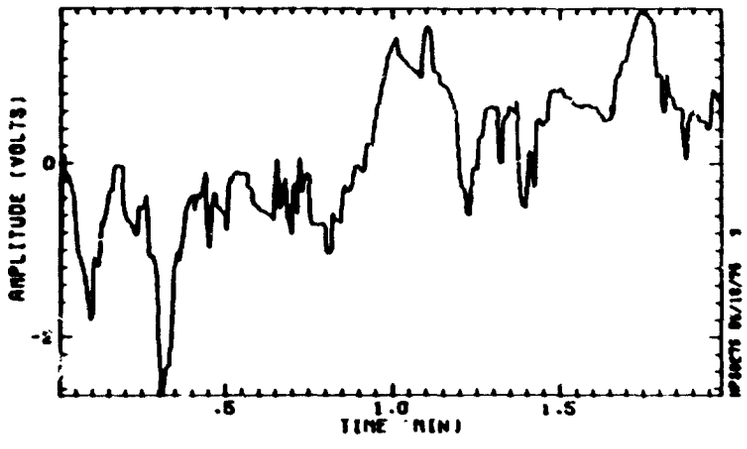

SINGLE CH. LAT FORCE RESPONSE R2(T) , SUBJECT PV

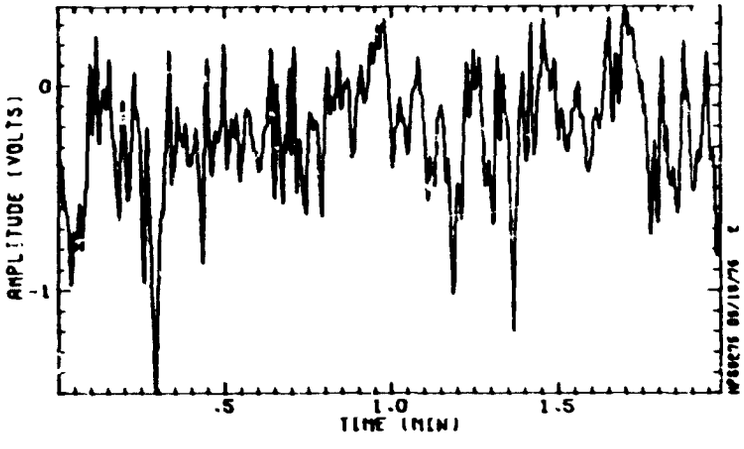

SINGLE CH. LAT TRACKING ERROR E2(T) , SUBJECT PV

FIGURE 8. Typical Tracking Signal Time History

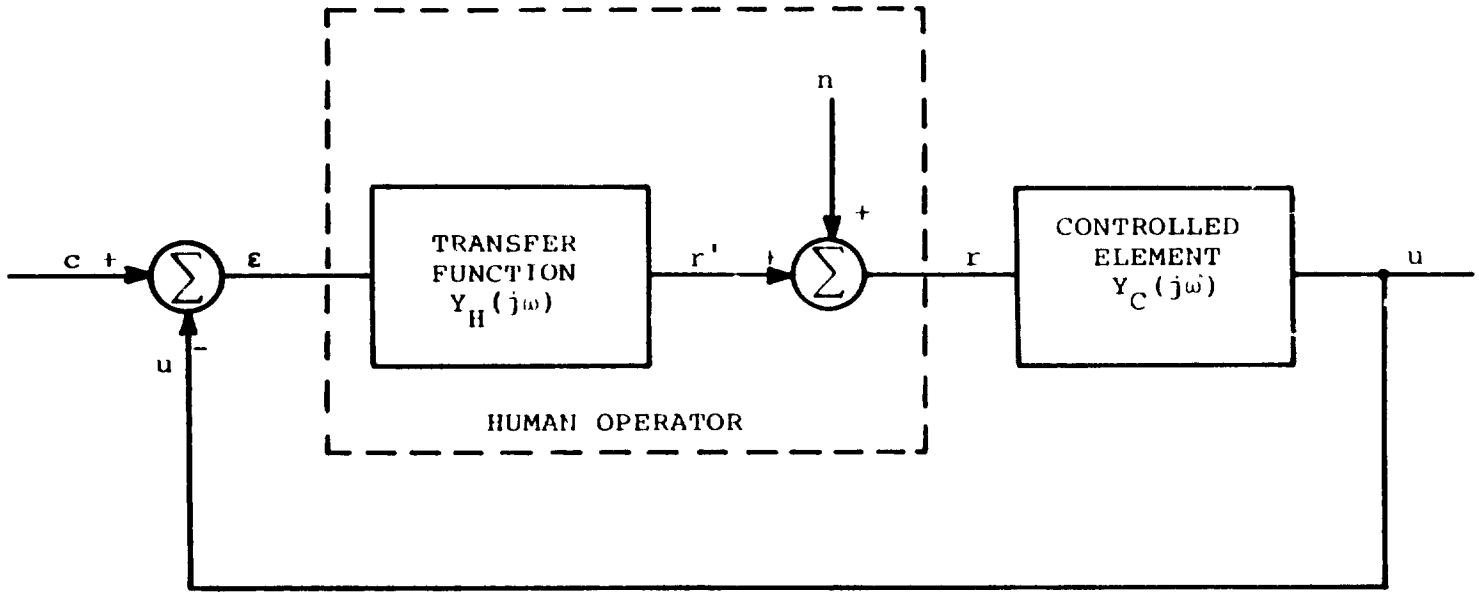

FIGURE 9. Single Axis Compensatory Tracking Task

is calculated for each windowed section utilizing a standard FFT algorithm. The modified periodogram

$$I_m(\omega_k) = \frac{\Delta t}{NU} \left| X_k \right|^2 \qquad m=1,\ldots, M \tag{3}$$

is formed, where U is a function of the total energy in the window and Δt is the time between samples. The estimate of the Spectral Density is then obtained by averaging the modified periodograms according to the equation

$$S_{xx}(\omega) = \frac{1}{M} \sum_{m=1}^{M} I_m(\omega_k) \quad . \tag{4}$$

Cross-power spectral density estimates are obtained by following the same procedure, except in this case the modified periodogram is defined as

$$I_m(\omega_k) = \frac{\Delta t}{NU} \left| X_k^* Y_k \right| , \tag{5}$$

where X and Y are the Fourier transforms of the two signals under consideration and the asterisk indicates the complex conjugate.

For this particular analysis, ten sections of 1024 points overlapped by 512 points were used. Under these conditions it can be shown, Reference 7, that the variance of the spectral estimate is given by

$$\text{Var} \left\{ S_{xx}(\omega_k) \right\} = \frac{\left| S_{xx}(\omega_k) \right|^2}{9.104} \quad . \tag{6}$$

Utilizing this technique to estimate the PSD of the forcing function gives the results presented in Figure 10. The time domain signal C1 is shown in the top portion of the figure and the estimate of its PSD (GC1C1) is shown in the lower portion of the figure.

In order to investigate the cross coupling in the human operator for the two dimensional tracking task, the closed loop cross-coupled model shown in Figure 11 is utilized. Ordinary, partial and multiple coherence functions can be calculated as described in Reference 7. For notational convenience the frequency dependence of all terms in the following equations has been dropped. The ordinary coherence between input c_1 and output r_1 is given by

$$\rho^2_{c_1 r_1} = \frac{\left| S_{c_1 r_1} \right|^2}{S_{c_1 c_1} S_{r_1 r_1}} \quad . \tag{7}$$

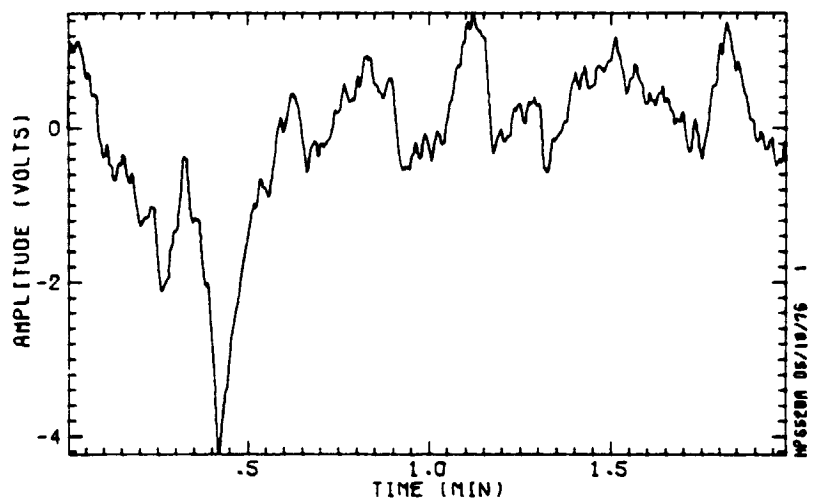

A/P FORCING FUNCTION C1(T),FC=.1HZ

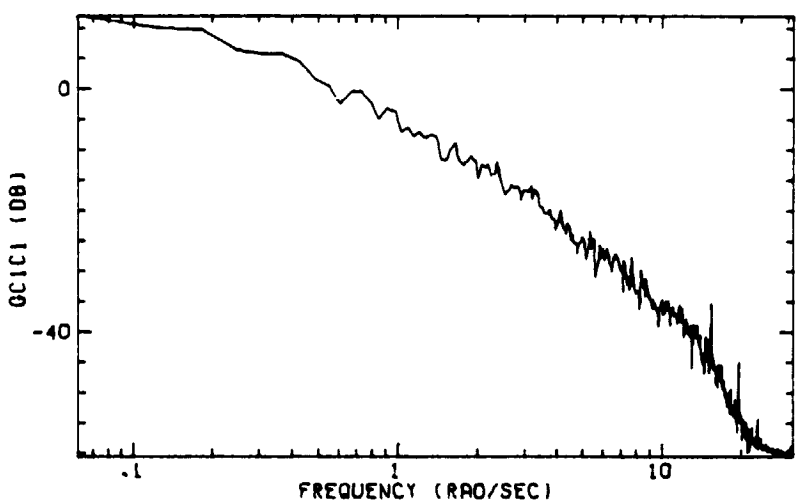

PSD OF A/P FORCING FUNCTION C1(T),FC=.1HZ

FIGURE 10

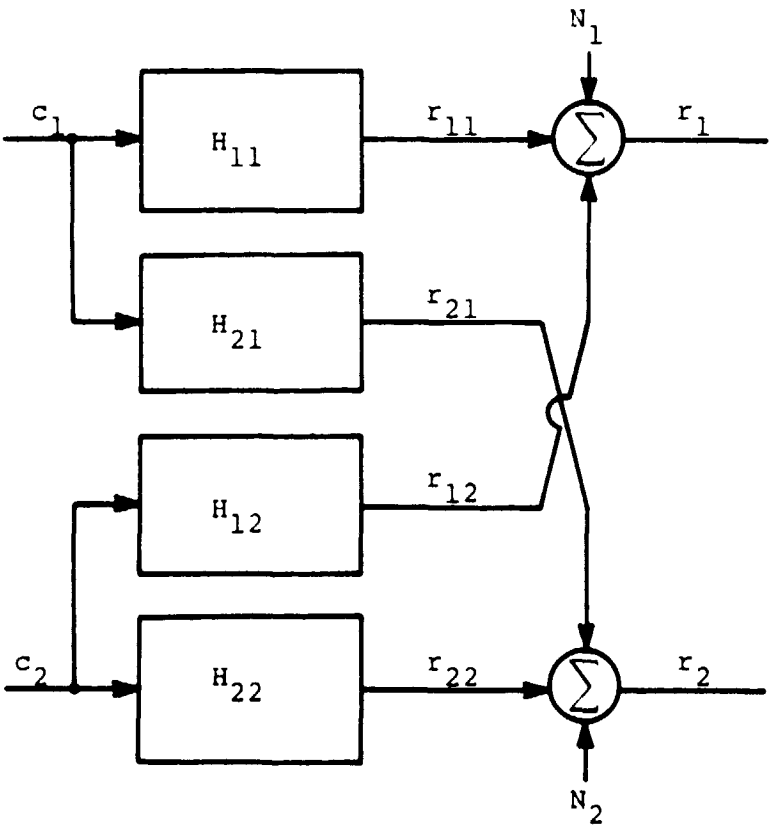

FIGURE 11. Closed Loop Cross-Coupled Model

This function describes the portion of the power contained in the output r_1 which is attributable to c_1 passed through a linear system H_{11}. The ordinary coherence for H_{22} is obtained by changing all the subscripts from one (1) to two (2).

The partial coherence between input c_2 and output r_1 is given by

$$\rho^2_{c_2r_1 \cdot c_1} = \frac{\left| S_{c_1c_1} S_{c_2r_1} - S^*_{c_1c_2} S_{c_1r_1} \right|^2}{S^2_{c_1c_1} S_{c_2c_2} S_{r_1r_1} \left[1-\rho^2_{c_1c_2} \right] \left[1-\rho^2_{c_1r_1} \right]} \quad . \tag{8}$$

This function describes the portion of the power contained in the output r_1 which is attributable to c_2 passed through a linear system H_{12}, with all effects of c_1 removed.

The multiple coherence function

$$\rho^2_{r_1 \cdot c} = 1 - \left[1-\rho^2_{c_1r_1} \right] \left[1-\rho^2_{c_2r_1 \cdot c_1} \right] \tag{9}$$

describes the portion of the output power attributable to both inputs via linear systems. For equations 8 and 9, the coherence functions for the other input can be determined, as it was for equation 7, by interchanging the numerical subscripts.

The remnant, that is the remaining output power which is not explained by the linear system, may be found from

$$G_{NN} = (1-\rho^2)\, G_{rr} \quad , \tag{10}$$

where G_{NN} is the remnant power. When the coherence (ρ^2) is large, that is as it approaches 1, the remnant power can be seen to approach 0.

RESULTS

The results of a typical anterior/posterior tracking experiment are shown in Figure 12. The magnitude of the describing function YH1 is given in the top left of the figure. The phase of YH1 is given in the lower left of the figure and the coherence function for this task is presented at the right. The vertical bars indicate the 95 percent confidence intervals for the estimates of magnitude and phase. The phantom curve is a visual fit to the estimated magnitude and phase. The equation of this model is

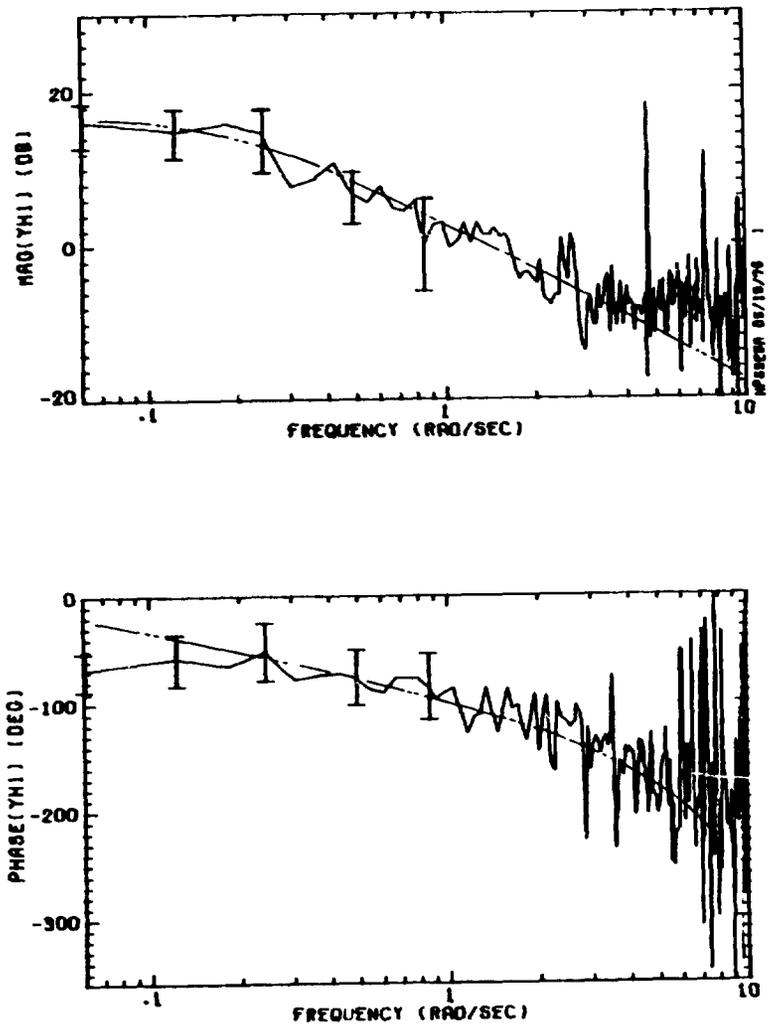

SINGLE CHANNEL TRACKING TASK , A/P PLANE
YH1 DESCRIBING FUNCTION , SUBJECT PV

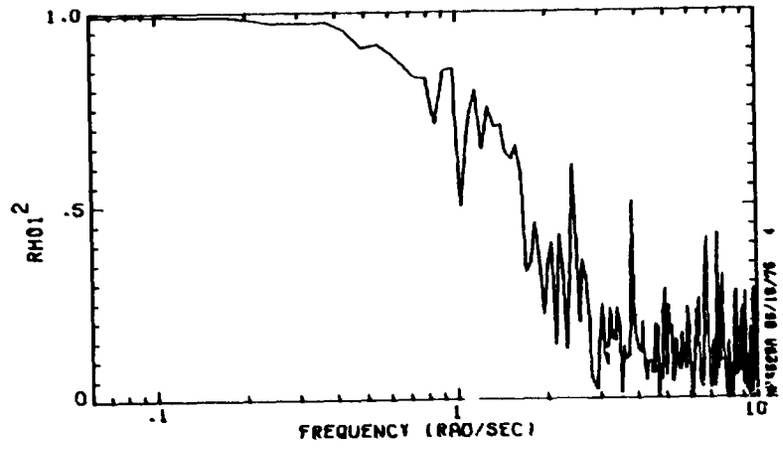

SINGLE CH. A/P COHERENCE FUNCTION , SUBJECT PV

FIGURE 12. Typical Results of One-Dimensional Analysis

$$Y_{H1}(s) = \frac{6.31e^{-0.29s}}{5s + 1} \qquad (11)$$

The coherence function indicates that a linear model describes most of the output power to a frequency just beyond 1 radian per second for this particular task. The main difference between this model and those obtained from visual tracking tasks is the delay time. For tactile tracking, delay times of 250 to 300 msec have been found where delay times of 100 to 150 msec are reported for visual tracking.

The results of the coherence function analysis for the two-dimensional task are shown in Figures 13 and 14. The results for the Anterior/Posterior (A/P) output (Figure 13) indicate that the ordinary and multiple coherence functions are almost identical. This is due to the extremely low coherence of the A/P output with the Lateral input as shown in the partial coherence function on the right side of the figure. This lack of coherence leads to the conclusion that there is no linear system which can explain the A/P output power from the Lateral input. Figure 14 presents the same results for the Lateral output. Again the contribution of the cross-coupling term in explaining the Lateral output is not significant. This analysis shows that, for the task considered here, the subject is capable of uncoupling the two-dimensional task into two one-dimensional tasks. Therefore, it suffices to model the subject in a two-dimensional tracking task by using two one-dimensional models as shown in Figure 9, represented by an equation of the form given in equation 11.

The parameters of equation 11 will vary as a function of task dimensionality. This can be seen by comparing the open loop describing function magnitude for one- and two-dimensional tactile tracking (see Figure 15). The describing function bandwidth is reduced when the complexity of the task is increased. In addition to that change, the time delay associated with two-dimensional tactile tracking is approximately twice that of one-dimensional tactile tracking, or 500 msec.

Tracking tests accomplished with an L3 paraplegic indicate that his ability to track the signal is as good as that of normals.

CONCLUSIONS

The feasibility of tracking with a tactile display using electrocutaneous stimulation at the waist has been demonstrated in one- and two-dimensions. Quasilinear models have been fitted to the data. The cross-coupling terms in the model are negligible; hence, for the range of frequencies used as forcing functions in this study, the subjects are capable of decoupling a two-axis tracking task into two independent single axis tasks. Paraplegics seem to be able to track with this type of display as efficiently as normal individuals.

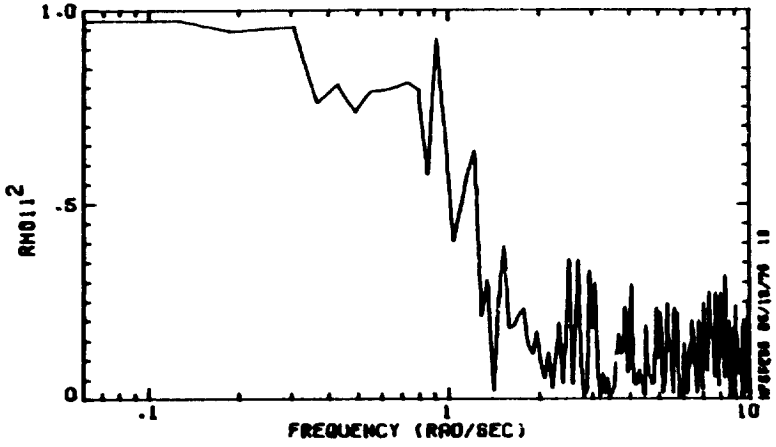

DUAL CH. AP ORD. COHERENCE FUNCTION , SUBJECT PV

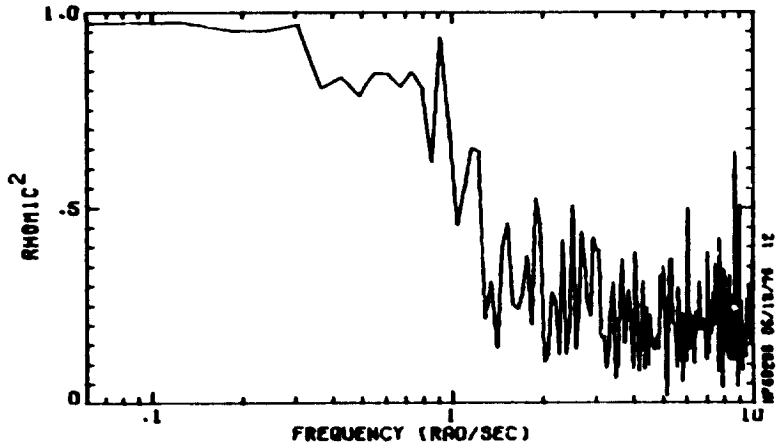

DUAL CH. MULT. COHERENCE FUNCTION , SUBJECT PV

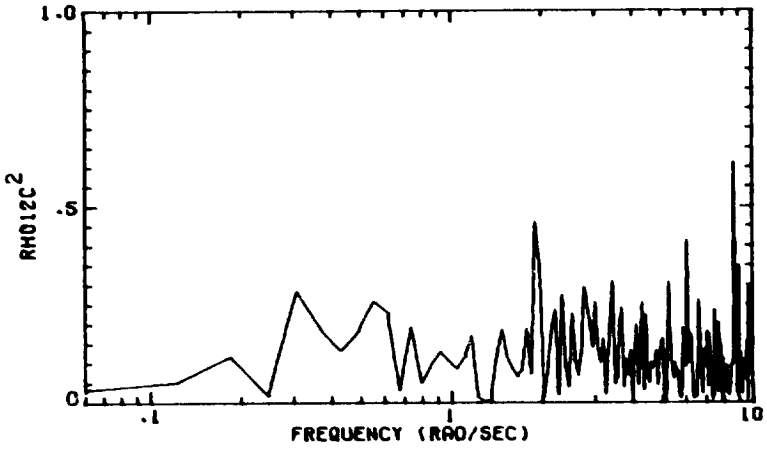

DUAL CH. AP/L PART. COHERENCE FUNCTION , SUBJECT PV

FIGURE 13. Results of Anterior/Posterior Coherence Function Analysis

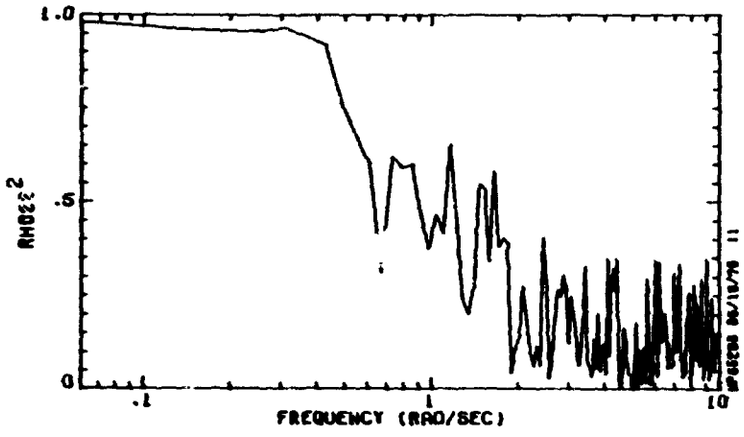

DUAL CH. LAT. ORD. COHERENCE FUNCTION , SUBJECT PV

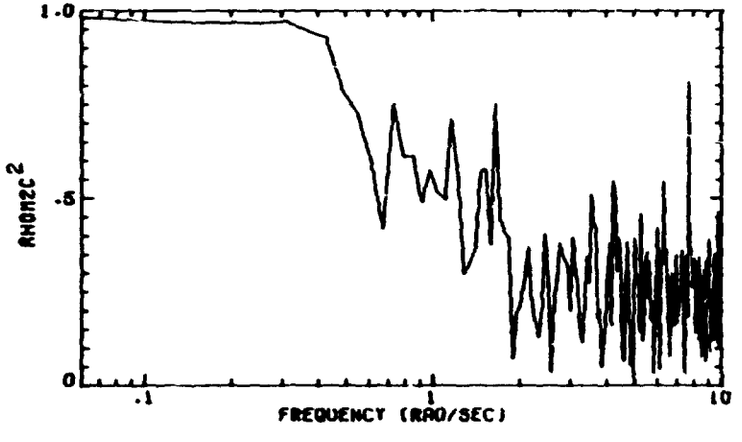

DUAL CH. MULT. COHERENCE FUNCTION , SUBJECT PV

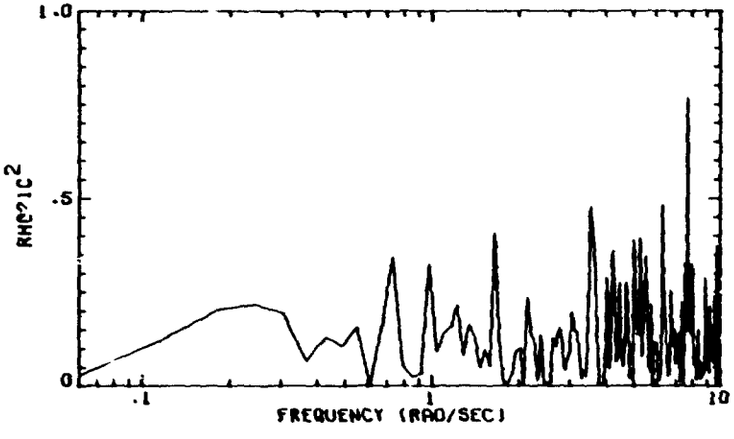

DUAL CH. L/AP PART. COHERENCE FUNCTION , SUBJECT PV

FIGURE 14. Results of Lateral Coherence Function Analysis

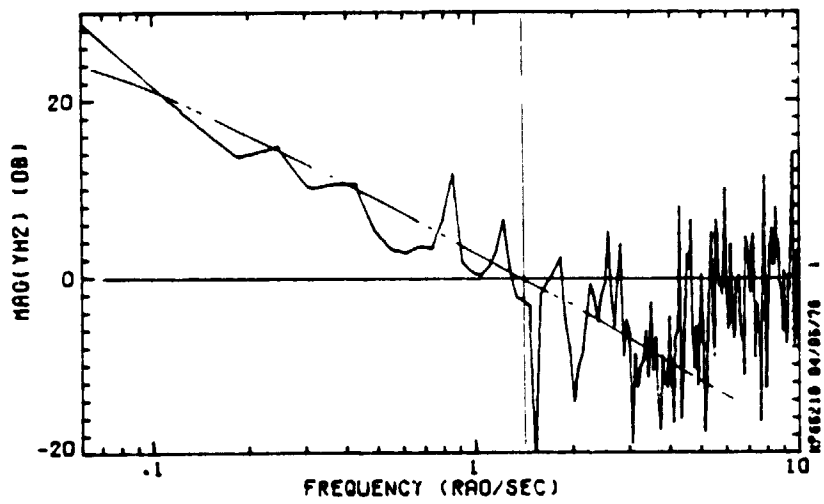

SINGLE CHANNEL TRACKING TASK . LAT PLANE
YH2 DESCRIBING FUNCTION . SUBJECT DT

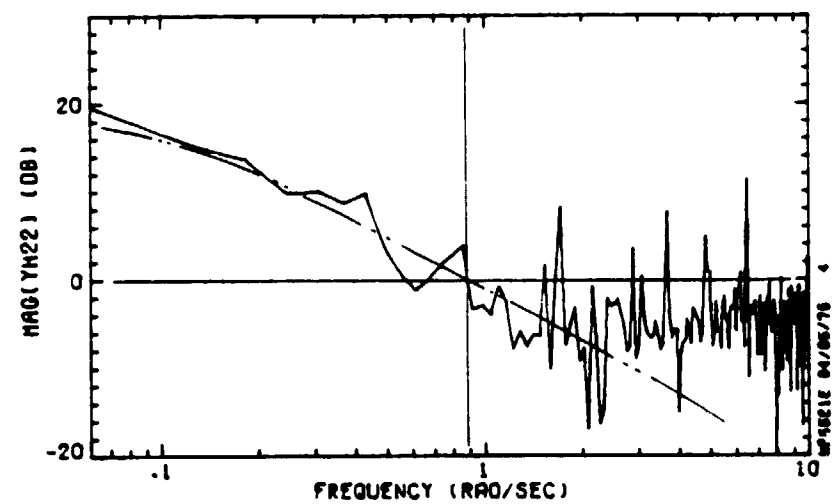

DUAL CHANNEL TRACKING TASK . LATERAL PLANE
YH22 DESCRIBING FUNCTION . SUBJECT DT

FIGURE 15

REFERENCES

1. Hill, J. W., "A describing Function Analysis of Tracking Performance Using Two Tactile Displays", IEEE Trans. on Man-Machine Systems, Vol. MMS-11, No. 1, pp. 92-101, March 1970.

2. Ross, D., Sauneman, R., Levinson, W., Tanner, R. and Triggs, T., "Tactile Display for Aircraft Control", Final Technical Report, Contract N00014-73-C-0031, August 1973.

3. Bensel, C. K., Dzendolet, E., "Power Spectral Density Analysis of the Standing Sway of Males", Perception and Psychophysics, Vol. 4, pp. 285-288, 1968.

4. Saunders, F. A., "Electrocutaneous Displays" in Geldard, F. A. (Ed), Conference on Vibrotactile Communication, Austin, Texas: The Psychonomic Society, 1974.

5. Hampton, R. L. T., "A Hybrid Analog-Digital Pseudo-Random Noise Generator", Proc. Spring JCC Vol. 25, pp. 287-301, 1964.

6. McRuer, D. T. and Krendel, E. S., "The Human Operator as a Servo System Element", Journal of the Franklin Institute, Vol. 267, No. 5, pp. 1-49, 1959.

7. Welch, P. D., "The Use of Fast Fourier Transform for the Estimation of Power Spectra: A Method Based on Time Averaging Over Short, Modified Periodograms", IEEE Trans. on Audio and Electroacoustics, Vol. AU-15, No. 2, pp. 70-73, June 1967.

8. Bendat, J. S. and Piersol, A. G., Random Data: Analysis and Measurement Procedures, Wiley-Interscience, 1971.

A SIMULATOR STUDY OF HELICOPTER PILOT WORKLOAD REDUCTION USING A TACTILE DISPLAY

An informal report presented to the
Twelfth Annual Conference on Manual Control

By Richard S. Dunn, Richard D. Gilson, Pershing Sun

Mission performance in current tactical Army helicopter operations is significantly limited by high visual workload. Aircrew tasks in low level or terrain flight demand continuous outside visual reference to fly, navigate, and perform mission functions. In nap-of-the-earth or contour flight, the airspace is a ground-defined environment in which operators strive for masking cover, speed and accurate navigation. This kind of visual contact flight leaves no time for scanning display devices in the cockpit. These considerations have generated interest in a simple tactile display concept which may form the basis of an effective information display strategy for Army helicopter cockpits.

This is a brief report of a limited simulation experiment intended to test the feasibility of a tactile display. It had two objectives: to determine whether the adaptive measurement procedure developed by Dr. Pershing Sun at the Avionics Laboratory (Reference 1) could be used to evaluate novel display devices in tactical operations; and to determine whether a tactile display could provide useful reductions in visual workload in tactical helicopter operations.

The laboratory prototype single channel tactile display used for these tests has been described in previous reports to this conference (Reference 2) and is shown in figure 1.

Figure 1. Tactile Display Prototype

The piston moves in both directions to cue a 2-way tracking control movement. It is a compensatory display in use; the operator tracks the output to obtain a centered or flush piston. Tests were conducted at the US Army Electronics Command's Avionics Laboratory, Fort Monmouth, New Jersey using the fixed base helicopter simulator, the Tactical Avionics System Simulator (TASS). The device was installed on the collective lever to provide altitude or power commands as shown in figure 2.

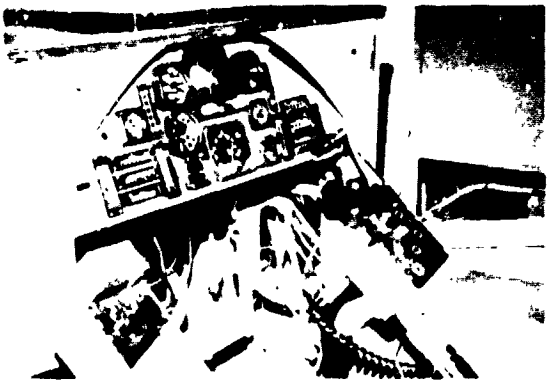

Figure 2. TASS Cockpit with Tactile Display on Collective Control

Two separate tests were performed. The first task was a steep ILS approach with a deceleration phase in the last 400 feet of altitude. The math model for this task represented a UH-1 helicopter. Here, tactile cueing was compared with the normal glide slope command in a four cue electromechanical flight director. A unique adaptive scoring procedure was employed as the dependent variable. Dr. Sun has described this procedure in detail at previous meetings. Briefly, the handling qualities of the vehicle are slowly degraded by the introduction of a pure time delay in the cycle roll control. The amount of time delay is increased adaptively until a primary task performance measurement circuit indicates that the equally weighted sum of errors in vertical, lateral, speed, and heading (the four commands of the flight director) are at a criterion value. This procedure has the disadvantage of altering the vehicle handling qualities, but the advantage that every subject gives the same level of system performance. He flies just at the acceptable error criterion. In this adaptive measurement, primary task performance alters primary task difficulty until the criterion is reached. The amount of time delay present after reaching criterion is taken as an indicator of workload for the combined display-control-task combination. After practice, five qualified helicopter pilots each made five ILS approaches with the standard visual cue on the flight director and five approaches with the tactile display. Typical results are shown in figure 3.

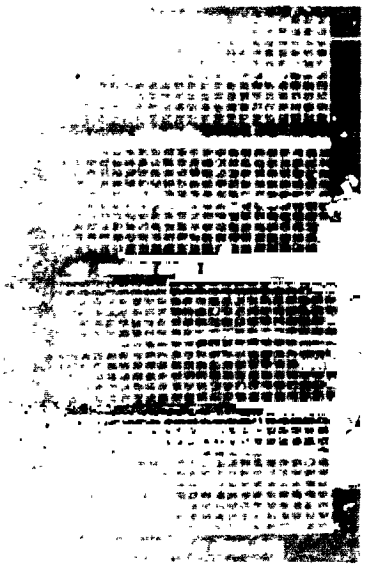

Figure 3. Tracking Command and Time Delay Results

The two tracings on top show the glide slope error (or command) signal; first visual tracking, and below it tactile tracking. Time delay achieved is taken after the build up period, the first 90 seconds, has elapsed. All subjects on all trials showed a greater time delay when using the tactile display. Over all subjects and trials, the increase in time delay using the tactile display averaged 38%. This along with the higher frequency of response to altitude seen in the tracings for the collective command support the hypothesis that visual workload relief is present and is effective at enhancing system performance.

But visual scanning in a flight director is not clearly an example of the kind of visual workload present in tactical helicopter operations. To get closer to the operational environment of interest a second, basically different, simulation was made.

For this task a visual scene was employed, generated by a 300 to 1 scale moving-belt terrain model. The display was a small black and white TV without collimated viewing. The task required hovering over a point at an assigned heading. Changes in altitude were commanded to simulate a tactical bob-up maneuver. The helicopter math model employed represented an OH-6 scout helicopter.

Command information shown in Figure 4 was superimposed over the video display. It was the Integrated Trajectory Error Display operating in the hover display mode (Reference 3). It provides both attitude and position cues which can be employed for hover position tasks. The cross

is a movable indicator of desired ground position. The circle is a fixed ownship position indicator. The line displays velocity, both magnitude and direction, while the small bug is an acceleration cue. For these tests, the left hand vertical band displayed absolute altitude with a collective command on the left inner scale. The heading command was provided by the indicator at the center bottom of the display.

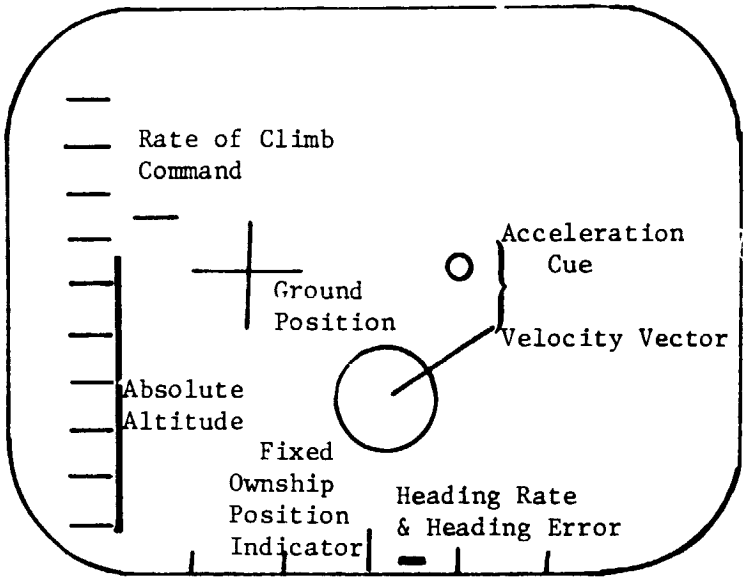

Figure 4. Integrated Trajectory Error Display - Command Information

The task required hovering in position while holding an assigned heading, and altitude. After one minute a maximum performance climb was required to a new altitude with subsequent holding at the new level. This was followed by descent to the original altitude. The change was from 25 feet to 125 feet and back. Auditory warning signals were presented to alert the pilot to upcoming altitude changes.

To estimate the effect of the tactile display on visual workload a visual secondary task was employed as the dependent variable. As before, the adaptive circuits computed primary task performance and provided a weighted sum of error scores. But the output was not used to alter the vehicle handling qualities and no time delays were applied. Instead, the adaptive measurement procedure was used to alter the difficulty of a secondary task by turning the task on and off.

The task involved cancelling lights and was similar to a secondary visual task employed by Kelley and Wargo (Reference 4). Two lamps were mounted in the peripheral field of view so that it was clear when one came on, but a shift in gaze away from the main display was required to determine which one. Lights were illuminated randomly one half second after the previous response. Cancelling required operation of the appropriate left or right rocker switch on the cyclic grip. These were stan-

dard Army intercom or radio push-to-talk switches. When the primary task scoring circuits showed performance within the error criteria, the secondary task was activated. When performance exceeded the criteria, the secondary task was deleted Thus, the situation represented cross-adaptive control of secondary task difficulty by measurement of primary task performance. As might be expected, the basic flight task proved to be very difficult with the narrow field of view visual display and no motion cues.

Only three subjects obtained sufficient practice in the time available to perform the task reliably without loss of control. It is important to note, however, that the cross-adaptive procedure resulted in stable system performance at or near the error criteria for all these subjects. Each one performed the task six times with the visual cue and six times with the tactile display.

Here the results also favored the tactile display. Overall, the trials with the tactile cue resulted in activation of the secondary task about the same amount of time or slightly longer, but with more than 15 percent more correct light cancellation responses when using the tactile display. This supports the hypothesis of equal system performance with an increase in visual workload reserve.

Unfortunately, scheduling for both the experimenters and the TASS facility prevented testing of enough subjects to solidify these findings. They must therefore be classed as preliminary and only suggestive. But they are encouraging and support the contention that the tactile display concept can produce useful reductions in helicopter pilot visual workload -- useful in the sense that the workload reductions can free visual attention for other productive tasks.

This research was jointly sponsored by the US Army Air Mobility Research and Development Laboratory and the Avionics Laboratory of US Army Electronics Command; and aided by participation of personnel from the Research Foundation of Ohio State University.

REFERENCES

1. Dukes, T.A.; and Sun P.: A Performance Measure for Manual Control Systems. Proceedings of the Seventh Annual Conference on Manual Control, June 1971, 257-263.

2. Gilson, R.; and Fenton, R.E.: A Tactual Pilot Aid for the Approach-and-Landing Task. Proceedings of the Eighth Annual Conference on Manual Control, May 1972.

3. Dukes, T.A.: An Integrated Display for Trajectory Control of Helicopters and VTOL Aircraft. Proceedings of the Sixth Annual Conference on Manual Control, April 1970, 133-145.

4. Kelley, C.R.; and Wargo, M.J.: Cross-Adaptive Operator Loading Tasks. Human Factors, 1967, 9(5), 395-404.

CONTROL AUGMENTATION AND WORKLOAD REDUCTION BY KINESTHETIC INFORMATION FROM THE MANIPULATOR

S.J. Merhav and O. Ben Ya'acov

Department of Aeronautical Engineering,
Technion - Israel Institute of Technology,
Haifa, Israel

SUMMARY

This paper is concerned with control augmentation and workload reduction by means of kinesthetic information provided by the manipulator. The control stick is loaded by a torque motor and the system is so interconnected that it presents complete kinesthetic input and output information from the controlled plant. Thus, the control task involves the same kinesthetic cues and the low workload as in nonintermediary handling of objects. It is demonstrated that within 20 rad/sec, which is the effective bandwidth in manual control, the method is realizable for a large variety of plants which may be unstable and time varying. Tracking and regulating tests demonstrate that very substantial improvements in accuracy and reduction in workload are obtained in comparison with ordinary isotonic, isomorphic or isometric manipulators. A test for the fixed set point regulation task involving a second order plant reveals that the control force law involved is strikingly similar to that of a linear regulator with an energy constraint obeying a quadratic performance criterion. The corresponding theoretical closed loop transfer function is in agreement with known linear models of the manual neuro-muscular system.

INTRODUCTION

With the advent of high performance aircraft, attention has focused on display augmentation and control augmentation systems (CAS). This paper is concerned with a special form of CAS, in which complete kinesthetic information is provided by the manipulator. Conventional manipulators are essentially passive linear transducers which translate manual commands into electrical input signals. In accordance with control theoretic man-vehicle models, e.g., McRuer et al [1], Kleinman et al [2], the generation of these manual commands require state estimation and optimum weighting which are executed by the functions of visual perception and cerebral data processing of the central nervous system. This explains the considerable workload generally experienced in the manual control of dynamical systems. Several studies in recent years attempted to reveal whether, and to what extent isotonic, isomorphic, isometric, inertia loaded, or other passive manipulators affect tracking and regulation performance [3, 4].

Since the muscle spindles and Golgi tendons in the manual neuromotor system provide position velocity and force measurements [5], different combinations of neuromotor loop closures should be involved in the operation of various types of passive manipulators. Recent laboratory open-loop tracking tests [6] have indeed revealed significantly different motor noise levels indicating such differences. They become, however, insignificant in closed loop tracking tasks as a result of the overriding supervisory visual loop closure. The dominant factors which determine performance and stress remain plant dynamics and system inputs, since the operations of state estimation and optimal weighting [2] are essentially the same with all types of passive manipulators. An interesting attempt to overcome this shortcoming of passive manipulators is due to Herzog [7] (1969), who studied the effect of a "matched manipulator". It ideally consists of a plant inverse operator at the input of the controlled plant. Thus, the human operator is always presented with a zero order system. Torque loading proportional to the plant input was applied to the manipulator so that an illusion of "natural feel" was provided. Significant improvement in tracking accuracies was reported [7] even when the manipulator match was not perfect. Two major shortcomings in this concept, have apparently prevented its emergence from the laboratory stage: 1) Inadequacy for systems with large parameter variations, as present in high performance aircraft. 2) Absence of response to external disturbances. Thus no advantage over passive manipulators exists in this important respect. Other investigations with similar techniques for the control of unstable systems were reported by Noggle [8] (1969) and more recently a tactile display of angle of attack was reported by Gilson et al [9] (1974), in particular when much attention was required in the visual channel.

The encouraging results obtained by these previous researchers were motivating factors in the work presented in this paper. Its specific objectives, however, are:

1) The method should improve control performance and reduce work-load for a large variety of dynamical systems and the design should not require adjustment of parameters for different systems.

2) The design should be realizable for time varying, high order stable or unstable plants.

3) The system should provide complete kinesthetic cues including the effect of external disturbances.

4) Comparative evaluations with conventional manipulators should consider both accuracy and workload.

These goals have been reached and the results have been experimentally demonstrated by means of a specially constructed single axis torque-motor-loaded manipulator suitably integrated into the control loop.

2. BASIC MANIPULATOR MODELS

Figs. 1a-1c schematically describe the interconnections of basic manipulators with the man-machine system, and their corresponding kinesthetic feedback paths. The diagrams suggest that the commanded scalar control u_c consists of a contribution u_c^v from the central nervous system which comprises visual perception and cerebral processing and a contribution u_c^N from the manual neuromuscular center associated with the cerebellum. In the sequel it is shown that the type of manipulator determines whether the visual-cerebral or the manual neuromotor center carries the main burden in the control task. A desired goal is clearly to achieve the latter. A control theoretic approach suggests that in either case, estimates $\hat{\underline{x}}$ and $\hat{u}$ of the system state $\underline{x}$ and control force u are available so that an optimal weighting matrix $\underline{l}$ can be set in accordance with a suitable performance criterion. Fig. 1a represents the situation of the nonintermediary handling of an object (natural feel). In this case the system output y equals the manual deflection σ. T_i, the torque exerted by the muscle output equals the reaction torque T_0 and is identical to the plant control input u. The muscle spindles G_{sp} measure position $x = x_1$ velocity $\dot{x} = x_2$ from y [1, 5]. The Golgi tendons [1] G_k measure T_i or u. These signals, corrupted by their corresponding measurement noises V_p and V_k yield the estimates $\hat{\underline{x}}_N$ and $\hat{u}_N$. Thus, the optimal setting of $\underline{l}_N$ is possible

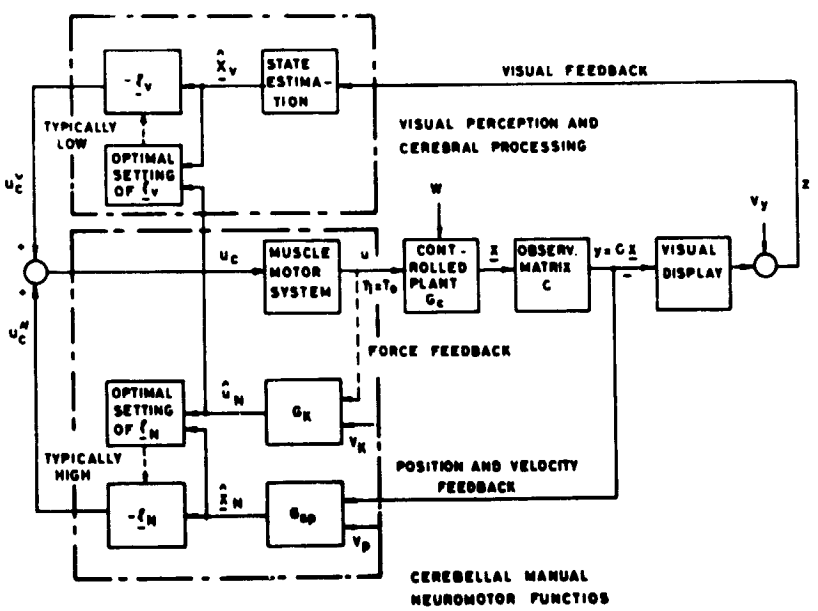

FIGURE 1a. Schematic description of the manual control system in ordinary nonintermediary handling tasks.

and $u_c^N = -\underline{l}_N \underline{\hat{x}}_N$ is a substantial contribution to the control signal u_c. Consequently the contribution of the visual center $u_c^v = -\underline{l}_v \underline{\hat{x}}_v$ will be comparatively small. This explains the small workload involved in nonintermediary handling of objects and the relative ease of manual operations in darkness or with closed eyes. Only in operations which require extreme precision (as the threading of a needle) the main burden is on the visual channel since a large $\underline{l}_v$ is required to suppress the effect of V_k and V_p. This is possible since $\overline{V}_y$ is very small by comparison.

Fig. 1b describes the man-machine system with a conventional isomorphic manipulator. The kinesthetic information path is now disconnected from the plant output y. e, the manipulator deflection is proportional to u. Since $T_0 = T_i = ku$ (k - spring constant), G_k and G_p both provide measures of u only. Since $\underline{\hat{x}}_N$ is not present, the setting of $\underline{l}_N$ must be zero so that $u_c^N = 0$. Consequently, the central nervous system must take the entire control task load and the optimal setting of $\underline{l}_v$ is consequently high. The lack of kinesthetic information from the system output thus explains the considerable workload which prevails with all types of passive manipulators, isotonic ($k = 0$), isomorphic ($k \neq 0$) and isometric ($k = \infty$). Only in the special case of a zero order plant, $y \propto e$, so that G_p provides information proportional to $\underline{\hat{x}}$ and the setting of $\underline{l}_N$ is high. This explains the small work load experienced in the control of zero order systems.

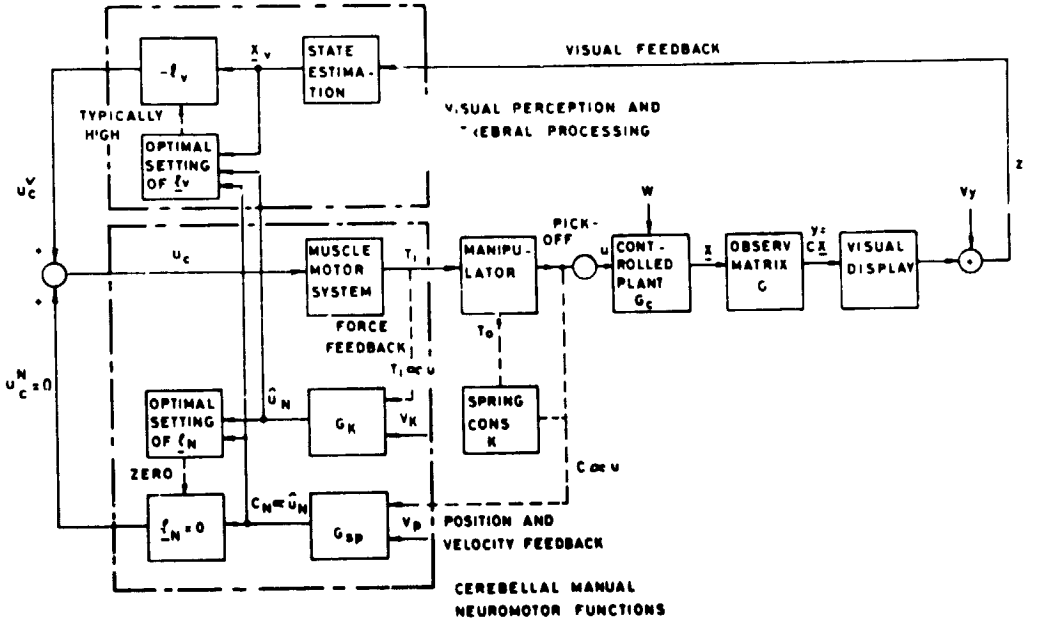

FIGURE 1b. Schematic description of the manual control system with a passive isomorphic manipulator.

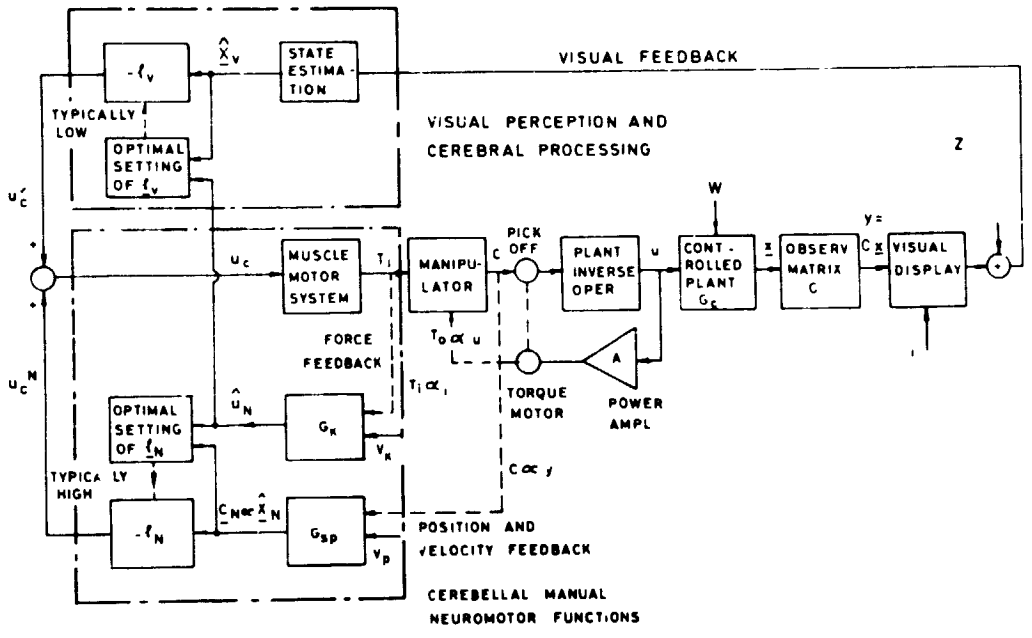

FIGURE 1c. Schematic description of the manual control system with a "matched manipulator" according to Herzog [7].

Fig. 1c represents the idea of kinesthetic feedback by a "matched" manipulator according to Herzog [7]. The manipulator output signal is fed into an inverse plant operator. Thus, ideally y is proportional to c and effectively the system acts like the zero order system mentioned above. In addition, however, $T_0 = AHu$ (A - amplifier gain, H - torque motor constant) provides a measure of the actual control effort and the situation of "natural feel" as described in Fig. 1a, in principle, reestablished. However, since the kinesthetic information path is actually disconnected from y, the system cannot react to external disturbances w. Thus, in this important aspect - the method has no advantage over conventional passive manipulators. Another limitation is the impossibility of maintaining the match of the inverse operator if $G_c(s)$ undergoes substantial parameter variations. Moreover, the method is inadequate for unstable plants.

In the following section it is shown how complete kinesthetic input and output information can be provided and that the method involved can be implemented for a large variety of stable and unstable plants which may undergo large parameter variations.

3. REALIZATION OF MANIPULATOR SYSTEM WITH COMPLETE KINESTHETIC INFORMATION

Let $G_c(s)$ denote the plant dynamics. Instead of an inverse operator $G_c^{-1}(s)$ in tandem as indicated in Fig. 1c, the inverse operation can be approximated by placing $G_c(s)$ in the feedback path of a high gain amplifier K as shown in Fig. 2. N_1 and N_2 are compensation networks to ensure stability of the corresponding feedback loops. The plant input u is amplified by the power amplifier A driving the torque motor which is mechanically linked to the manipulator and the pick-off. Since $G_c(s)\ U(s) = Y(s)$ and $[Y_c(s)-Y(s)]KN_1(s) = U(s)$, it follows that:

$$\frac{Y(s)}{Y_c(s)} = \frac{K}{K + \dfrac{1}{N_1(s)G_c(s)}} \tag{1}$$

If it is possible to maintain the condition

$$K >> 1/N_1(s)G_c(s) \tag{2}$$

up to the frequency of $\omega \approx 20$ rad/sec, which is the effective bandwidth in

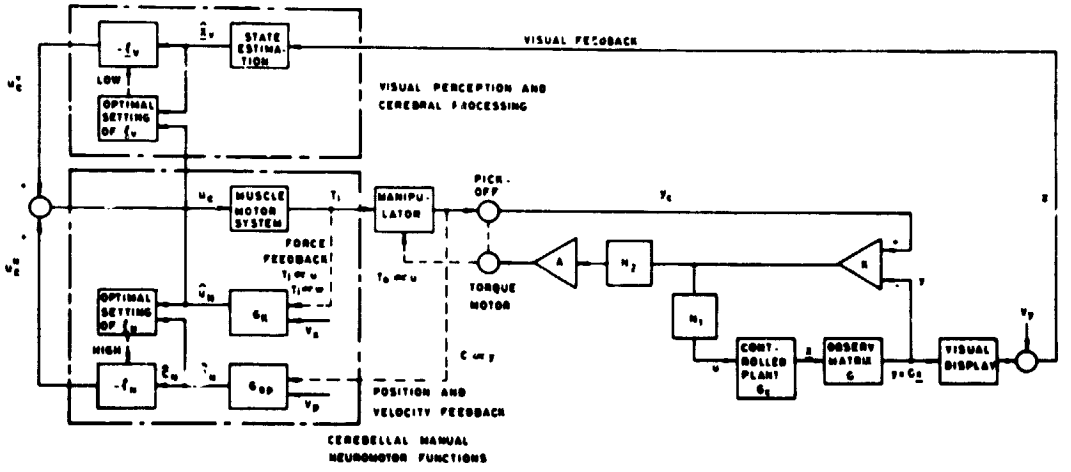

FIGURE 2. Realization of manual control system with complete kinesthetic information.

manual control, then from (1) one has:

$$Y(s) \simeq Y_c(s) \tag{3}$$

Since $y_c \propto e$ (Fig. 2), it follows that the kinesthetic feedback path from e is equivalent to that from y in Fig. 1c. Since $N_2(s)$ is in practice a wide band network, it follows that $T_0 \propto u$ in the relevant frequency band, and it is equivalent to the direct reaction torque T_0 in Fig. 1c. In view of (2), equality (3) is insensitive to wide parameter variations in $G_c(s)$ and if $N_1(s)$ is suitably designed, (3) holds for an unstable $G_c(s)$ as well.

It is easily verified that the reaction to the external disturbances $W(s)$ is satisfactorily provided by the system shown in Fig. 2:

$$Y(s) = G_c(s)\ [U(s) - W(s)] \tag{4}$$

$$U(s) = KN_1(s)\ [Y_c(s) - Y(s)] \tag{5}$$

Thus,

$$Y(s) = \frac{KN_1(s)G_c(s)}{1+KN_1(s)G_c(s)}\ Y_c(s) - \frac{G_c(s)}{1+KN_1(s)G_c(s)}\ W(s) \tag{6}$$

In view of (2) and since $N_1(s) \approx 1$ in the effective frequency band,

$$Y(s) \approx Y_c(s) - \frac{W(s)}{K} \tag{7}$$

Thus, due to the large gain K, if $y_c = 0$, the response to the disturbance is effectively eliminated. The torque required to maintain $Y_c(s) \equiv 0$ is determined by substituting (6) into (5), and deriving $U(s)$:

$$U(s) = KN_1(s)\ \frac{G_c(s)}{1+KN_1G_c(s)}\ W(s) \approx W(s) \tag{8}$$

Thus,

$$T_i(s) = AHU(s) \approx AHW(s) \tag{9}$$

The value of A must be so adjusted that for a typical disturbance level of $W(s)$, $T_i(s)$ should not cause muscular fatigue.

From the foregoing it follows that the system shown in Fig. 2 provides complete kinesthetic information in equivalence to Fig. 1a. It fulfills all the requirements regarding:

- Wide variations of plant parameters
- Unstable systems
- External disturbances

It now remains to show that the condition in (2) which underlies the validity

of the concept described, can indeed be guaranteed by practically realizable networks $N_1(s)$ and $N_2(s)$.

4. CONTROL LOOP DESIGN

The initial design of the control loop was carried out for $G_c(s) = 1/s^2$. This system is on the verge of instability. The networks $N_1(s)$ and $N_2(s)$ were then checked for other stable and unstable forms of $G_c(s)$. The detailed block diagram of the manipulator feedback loop is shown in Fig. 3. The brushless torque motor develops a maximum torque of 12 Kg-cm which is stepped up by a factor of 4 by means of an antibacklash gear. The transfer function of the torque motor is:

$$\frac{C(s)}{e_m(s)} = \frac{2145}{s(s+5.5)(s+167)} \tag{10}$$

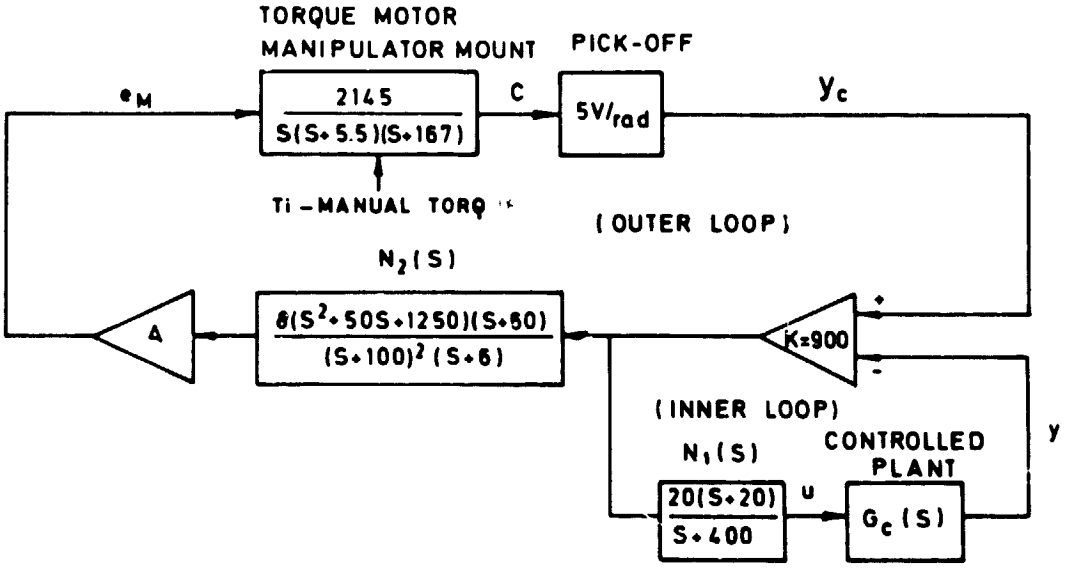

FIGURE 3. Block diagram of manipulator feedback loops.

The root locus of the inner loop involving $G_c(s)$, K and $N_1(s)$ is shown in Fig. 4. The complex zeros in $N_2(s)$ (Fig. 3) are intended to arrest the complex pole pair arising in the inner loop. The lag-lead network $(s+60)/(s+6)$ is introduced to increase the D.C. gain of the loop without impairing its dynamic performance within the 20 rad/sec band. The root locus of the complete

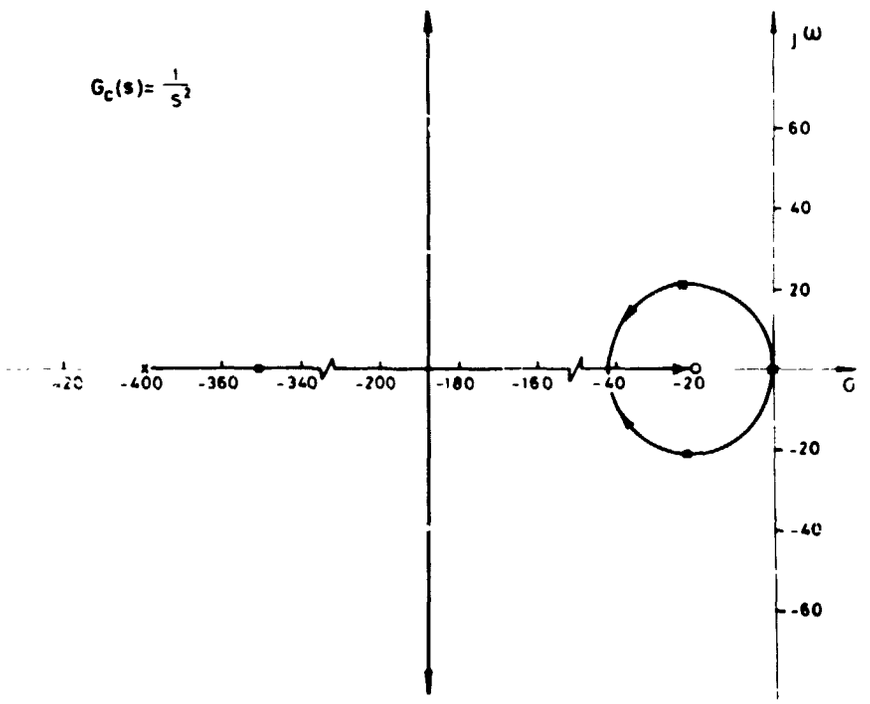

FIGURE 4. Root locus of inner loop, $G_c(s) = 1/s^2$.

manipulator system of Fig. 3 is shown in Fig. 5. Since all the closed loop poles are either compensated by neighboring zeros or are outside the 20 rad 20 rad/sec bandwidth, the required proportionality $c \propto y$ is effectively implemented. On replacing $G_c(s)$ by $1/s$, $1/s(s-1)$, $1/(s^2+0.66s+10)$ while retaining the same values for K, $N_1(s)$ and $N_2(s)$ as in Fig. 3, it was found that the closed loop pole locations vary only slightly so that $c \propto y$ is guaranteed. The gain yielded a control force of $\sim\pm 2.5$ Kg for $c = \pm 20°$. The complete manipulator is depicted in Fig. 6. It should be noted that though $c \propto y$ for different plants $G_c(s)$, large differences exist in the corresponding reaction torques T_0. For a given command output $Y_c(s)$, and since $Y(s) \approx Y_c(s)$, T_0 is given by

$$T_0(s) \simeq \frac{Y_c(s)}{G_c(s)} AH = uAH \tag{11}$$

This display of u, characteristic of each $G_c(s)$ is essential in the ability of the human operator to execute optimal or near optimal control inputs. This is demonstrated in the next section.

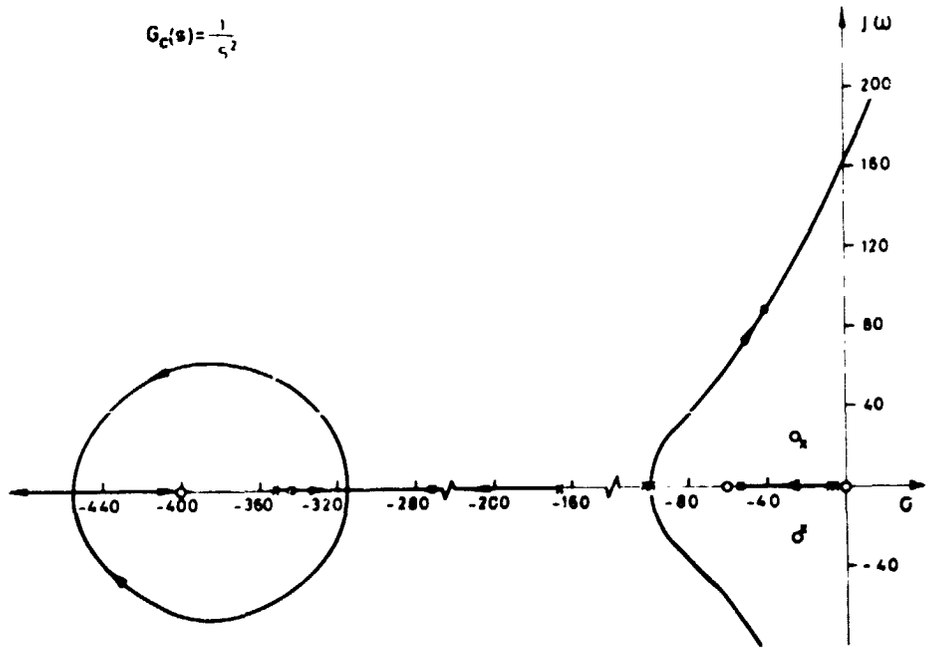

FIGURE 5. Root locus of complete manipulator feedback system, $G_c(s) = 1/s^2$.

FIGURE 6. Torque motor loaded kinesthetic manipulator .

5. OPTIMAL CONTROL IN A SECOND ORDER PLANT

The control objective is to eliminate an initial deflection y_0 in minimum time, subject to constraints on the control effort u. The controlled plant was $G_c(s) = k/s^2$. A recorded sample of the time history of four such transient responses obtained in laboratory tests and the corresponding control inputs $u(t)$ are shown in Fig. 7. The results demonstrate the remarkable closeness between y and y_c and its excellent dynamic response. This, and the typical shape of the control time history $u(t)$, indicate that a linear control law is actually implemented by the human operator. This hypothesis was tested by the optimal solution of the corresponding analytical model as follows:

The state space representation of $G_c(s)$ is:

$$\dot{\underline{x}}(t) = A\underline{x}(t) + Bu(t) \tag{12}$$

The system matrix is 2×2, $x_1 = x$ and $x_2 = \dot{x}$. The controlled variable is

$$y(t) = C\underline{x}(t) \tag{13}$$

$$C(1,0) \quad ; \quad B = (0,k)^T \quad ; \quad A = \begin{pmatrix} 0 & 1 \\ 0 & 0 \end{pmatrix} \tag{14}$$

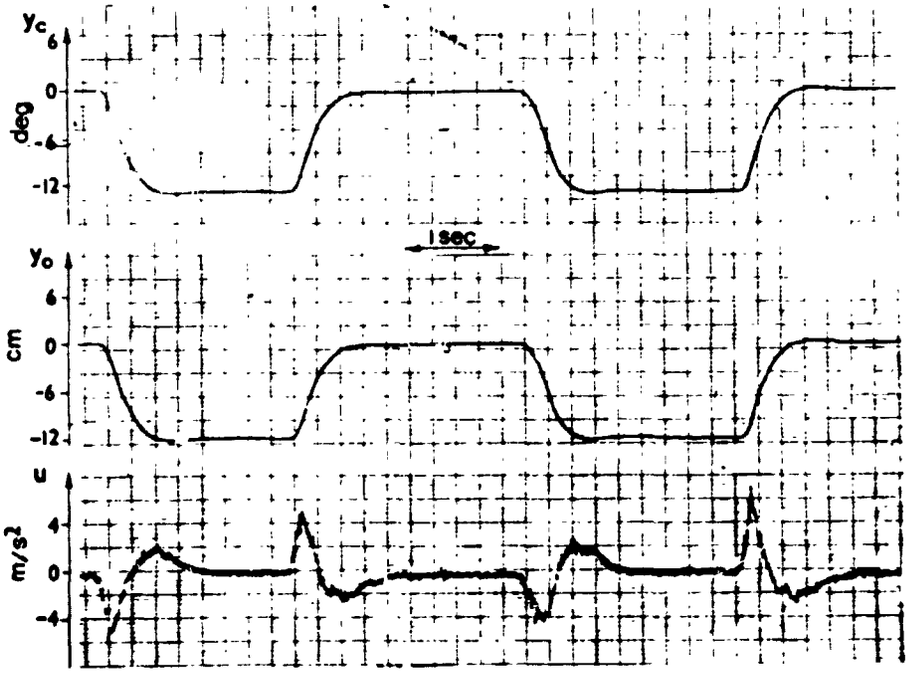

FIGURE 7. Time history of transient responses of a fixed set-point regulation task for $G_c(s) = 1/s^2$.

The performance criterion which is assumed to underly the control policy is the minimization of:

$$J = \int_0^\infty [y^2(t) + \rho u^2(t)]\, dt \tag{15}$$

$\rho \geq 0$ is the weight on the control effort.

In accordance with Fig. 1c, the observed variable is:

$$z(t) = C\underline{x}(t) + V_y(t) \tag{16}$$

where $V_y(t)$ represents white observation noise.

Let $\underline{\hat{x}} = (\hat{x}_1, \hat{x}_2)^T$ be the reconstructed state vector provided by a full state observer. The optimal control law is then given by:

$$u(t) = -\underline{l}\,\underline{\hat{x}}(t) \tag{17}$$

where $\underline{l} = (1/\rho)\, B^T P$ and P is the solution of the 2×2 Ricatti equation $C^T C - PBB^T P + A^T P + PA = 0$.

The result is:

$$\underline{l} = \left(\frac{1}{\sqrt{\rho}} \;,\; \sqrt{\frac{2}{\sqrt{\rho}k}}\right)^T \tag{18}$$

The full state observer is of the form:

$$\dot{\underline{\hat{x}}}(t) = A\underline{x}(t) + Bu(t) + K[y(t) - C\underline{\hat{x}}(t)] \tag{19}$$

where $y(t) = Cx(t)$, and $K = (k_1, k_2)^T$.

Defining $\underline{e}(t) \triangleq \underline{x}(t) - \underline{\hat{x}}(t)$, the resulting augmented differential equation interconnecting $\underline{x}(t)$ and $\underline{\hat{x}}(t)$ for the closed loop system [10] is given by

$$\begin{bmatrix} \dot{\underline{x}}(t) \\ \dot{\underline{e}}(t) \end{bmatrix} = \begin{bmatrix} A-B\underline{l} & -B\underline{l} \\ 0 & A-KC \end{bmatrix} \begin{bmatrix} \underline{x}(t) \\ \underline{e}(t) \end{bmatrix} \tag{20}$$

The characteristic values can be shown to be those of $A-B\underline{l}$ (regulator poles) and those of $A-KC$ (observer poles).

The characteristic equation of the observer is of the form $s^2 + k_1 s + k_2 = 0$. Given $k = 160$ and choosing $k_1 = \sqrt{2k_2}$, substituting (14) into (20), the numerical solution of $(\underline{x},\underline{e})^T$ for the initial conditions $(x_0, e_0)^T = (x_1(0), 0, e_1(0), e_2(0))^T = (x_1(0), 0, x_1(0), 0)^T$ yields the best fit to Fig. 7 for the parameters $\rho = 64$, $k_1 = 25$ and $k_2 = 312$. The plot of the computed optimal $u(t)$ for these parameter values is shown in Fig. 8. It is

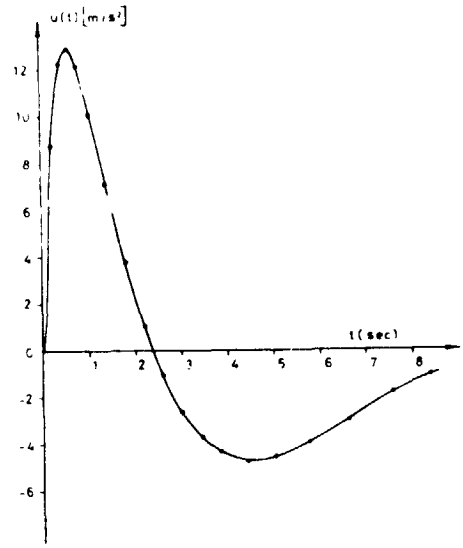

FIGURE 8. Computed optimal control force $u(t)$ for the fixed set point regulating task.

$\rho = 64 \quad k = 160, \quad k_1 = 25, \quad k_2 = 312.$

easily verified that the closed loop transfer function $H_c(s)$ relating $y(s)$ to $u(s)$ is given by:

$$H_c(s) = \frac{\frac{k}{\sqrt{\rho}}}{s^2 + \sqrt{\frac{2k}{\sqrt{\rho}}}\, s + \frac{k}{\sqrt{\rho}}} \tag{21}$$

It follows therefore that with torque feedback the human operator strongly resembles a linear optimal regulator with observation noise, subject to a quadratic performance criterion with an energy constraint (15).

It is also of interest to compare the closed loop transfer function of (20) with the neuromuscular limb-manipulator model according to McRuer et al [15]. From this model it follows that the closed loop transfer function for a purely inertially loaded manipulator, (equivalent to our example $G_c(s) = k/s^2$), the closed loop transfer function $C(s)/U_c(s)$ (Fig. 1c) is:

$$\frac{C(s)}{U_c(s)} \simeq \frac{\frac{K_{sp}\, C_f}{M}}{s^2 + \frac{B_m}{M}\, s + \frac{K_{sp}\, C_f}{M}} \tag{22}$$

where:

K_{sp} - Muscle spindle gain factor

$C_f = \partial P/\partial f$, f neuromotor firing rate, P muscle tension

M - Combined limb-manipulator mass

B_m - $\partial p/\partial v$, muscle damping factor, V - velocity.

Since $T_0 = AHu$ and since $U(s) = Y(s)s^2/k$, it follows that $T_0(s) = AH/ks^2Y(s)$. Thus, AH/k is equivalent to a mass M. With the given torque motor gain settings, $M \simeq 0.3$ Kg. Since $c \propto y$, it is justified to compare (22) to $H_c(s)$ in (21). It is significant that they are of the same form.

The corresponding coefficients are:

$$\sqrt{\frac{2k}{\sqrt{\rho}}} = \frac{B_m}{M} \tag{23}$$

$$\frac{k}{\sqrt{\rho}} = \frac{K_{sp}\, C_f}{M} \tag{24}$$

The parameters B_m and C_f can vary widely [5]. Thus, for different values of M, the neuromuscular system has sufficient freedom to maintain the optimal parameter values dictated by the left hand sides of (23), (24). This is due to the independent control of B_m and C_f. By comparison, the measured and computed values of $u(t)$, it was found that $B_m = 1.9$ Kg sec/cm, which is in the region of values reported in the literature.

6. PERFORMANCE EVALUATION METHOD

From Sections 2 and 5 it follows that a major advantage of kinesthetic information must be workload reduction since the strenuous task of state estimation and optimal weighting by the visual perception and mental processing is nearly eliminated. In order to evaluate the method, two requirements had to be met:

1. The evaluation should be on a comparative basis.
2. It should involve workload measures.

Consequently all performance tests were carried out so that every type of $G_c(s)$ was tested both for the kinesthetic manipulator mode and the

conventional isomorphic manipulator mode. In practice, in order to keep all other factors unchanged, the same manipulator was switched into the system in either the isomorphic or the kinesthetic mode.

The specific requirements of the evaluation method were:

- It should provide an objective measure for the control task effort for any type of manipulator or controlled plant.
- The evaluation method should present a control task which is similar to that encountered in flight practice.
- The operator should not be able to influence the outcome by adopting "clever strategies."

In all tests the primary task was tracking and/or regulating $G_c(s)$ for a stationary random input or disturbance band limited to ~1 rad/sec. The control test was single axis and in the vertical plane.

In order to meet the foregoing requirements a secondary task method was developed and adopted in the evaluation. A general block diagram is given in Fig. 9. The method consists of reading out (to permit supervision) of two-digit random numbers displayed outside the foveal field of the primary task display. The random numbers change at a increasing rate $\lambda(t) = Bt$, where B is a constant. During the initial 20 seconds, the operator concentrates on the

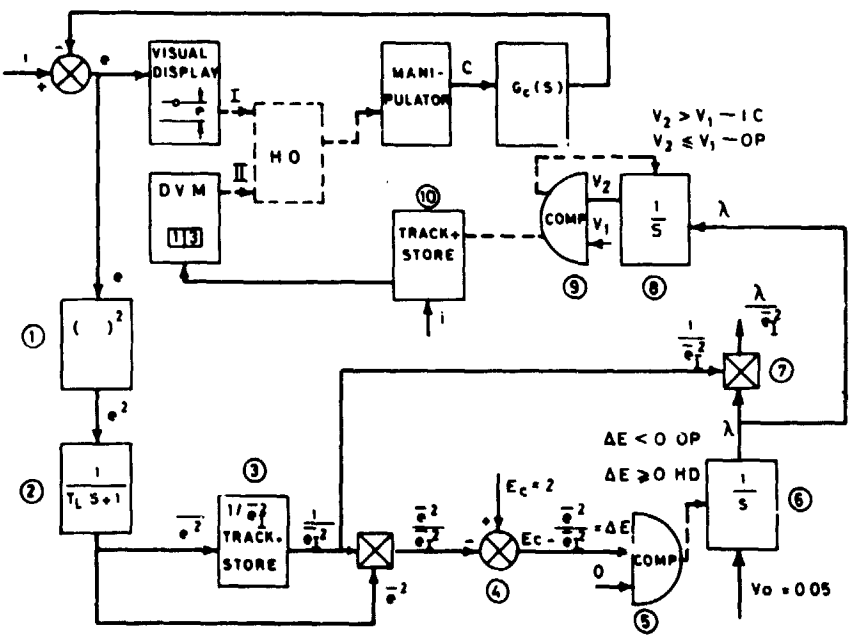

FIGURE 9. Block diagram of the secondary task evaluation system.

primary task only and the initial mean squared error $\overline{e_I^2}$ is determined. Thereafter the secondary task is activated. The operator has to control the primary task but simultaneously read out the random numbers the subsequent error variance $\overline{e^2}$ is normalized to $\overline{e_I^2}$ as in Jex [11]. Due to the workload of the secondary task $\overline{e^2}/\overline{e_I^2}$ gradually increases. When some predetermined level E_c is reached, the system automatically stops at $\lambda = \lambda_c$. The performance measure was chosen as $\lambda_c/\overline{e_I^2}$. A comparatively easy task will have a small $\overline{e_I^2}$ and a large λ_c and vice versa. Thus, a large value of $\lambda_c/\overline{e_I^2}$ indicates a system with good handling qualities. It easily verified that the method meets all three requirements listed above. In particular, the operator has no choice of "clever" strategies. For example, if he chooses initially to devote less attention to the primary task in order to reach a higher λ_c, his initial $\overline{e_I^2}$ will tend to be larger so that $\lambda_c/\overline{e_I^2}$ tends to remain constant. The noise generator output i provides both the primary task input and the random numbers to the secondary task display. Preliminary tests of the evaluation method with several subjects demonstrated that $\lambda_c/\overline{e_I^2}$ is significantly and consistently different for different types of $G_c(s)$ like $1/s$, $1/s^2$, $1/s(s-1)$. The method was therefore adopted for the comparative evaluation of the kinesthetic manipulator.

7. EXPERIMENTS AND RESULTS

The tracking and regulation experiments were carried out by a group of five students with no flying experience. They were selected from a larger group after undergoing preliminary screening tests of reaction time and tracking ability.

The experimental equipment used was:

- EAI-580 hybrid analog computer which was also used for the realization of the compensation networks $N_1(s)$ and $N_2(s)$ and gain K.
- HP H01-3722 noise generator for input, disturbance and secondary task signals.
- HP 1310A CRT display with a 30×40 cm screen.
- The single axis manipulator is loaded by medium power brushless torque motor and the pick off is linear low torque potentiometer.
- The power amplifier A has 200W output and a voltage gain amplification range of 10÷110.

The input i is obtained from a 1.5 Hz rectangular spectrum filtered by a single lag filter $1/(s+1)$. The disturbances w are obtained from the same source but after a delay τ to avoid correlation with i.

The first series of tests were tracking tasks with $i \neq 0$, $w \equiv 0$ for $G_c(s) = 1/(s^2+0.66s+10)$, $G_c(s) = 1/s^2$, $G_c(s) = 1/s(s-1)$. The duration of each test was approximately 2 min, depending on the instant $\overline{e^2}/\overline{e_I^2} = E_c$.

A typical set of results of 10 tests for subject I is shown in Fig. 10.

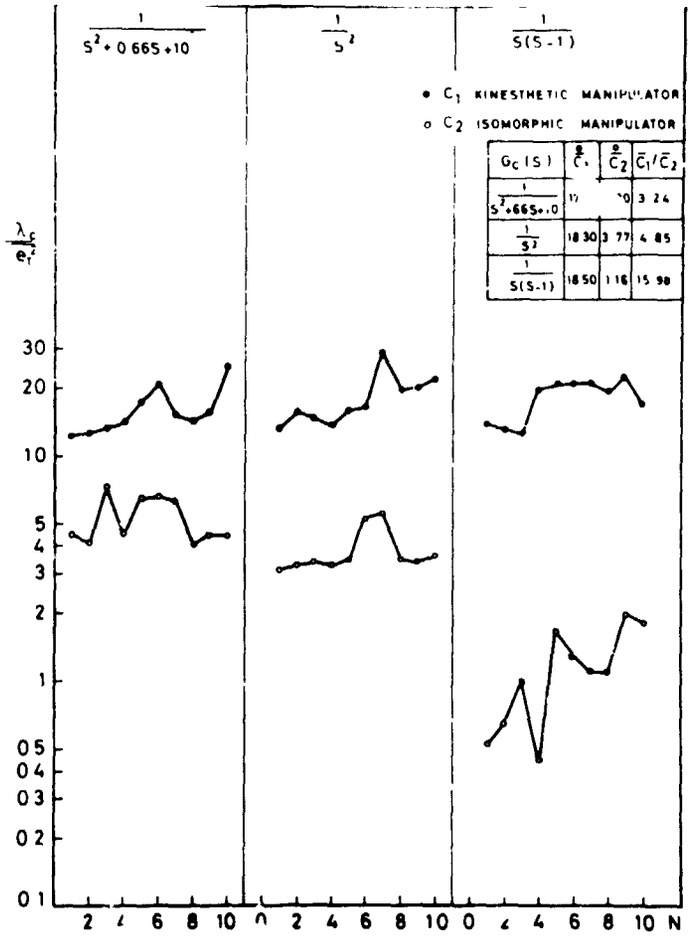

FIGURE 10. Results of tracking experiments - Subject I.

The results of other subjects were quite similar. The following conclusions can be drawn:

1. For the isomorphic manipulator the performance measure $\lambda_c/\overline{e_I^2}$ is significantly lower, the harder the control task. This demonstrates the increasing work-load associated with difficult control tasks due to the load on the visual channel and mental processing. It also indicates the potential of the evaluation method in workload measurements, and task rating. A certain tendency of learning can be noticed for $1/s^2$ and $1/s(s\text{-}1)$. It was also present in the results of the other subjects.

2. For the kinesthetic manipulator, $\lambda_c/\overline{e_I^2}$ is practically the same for all types of $G_c(s)$, and it is considerably higher. This demonstrates the unloading of the visual channel by the provision of complete kinesthetic information paths. It is significant that even an unstable system yields the same performance measure.

The second series of tests were regulating tasks with $i \equiv 0$ and $w \not\equiv 0$. In this case the control task with the kinesthetic manipulator reduced to holding the manipulator in a "stick fixed" position against the jerks induced by $w(t)$. The visual feedback path was only required for occasional monitoring. Consequently $\lambda_c/\overline{e_I^2}$ was extremely high.

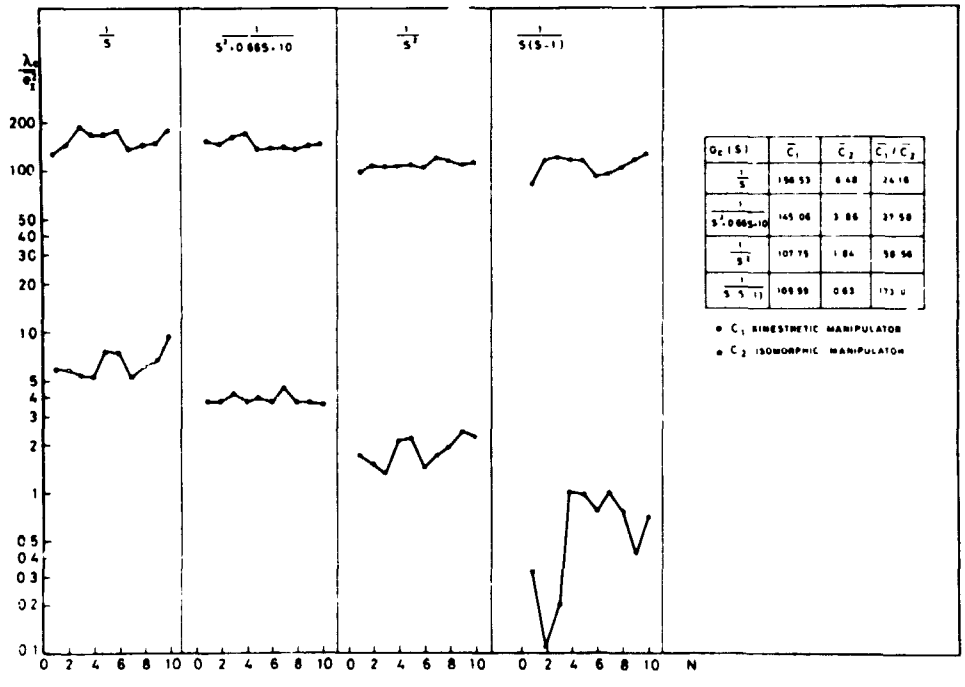

FIGURE 11. Results of combined tracking and regulating experiments - Subject I.

The third series of tests was a combined tracking and regulation, i.e., $i \neq 0$, $w \neq 0$. This is a typical situation in practical control tasks. The results are, as expected, intermediate between th first and second series of tests. The results for subject I are shown in Fig. 11 for $G_c(s) = 1/s$; $1/(s^2+0.66s+10)$; $1/s^2$; $1/s(s-1)$. The results for the other subjects again were very similar. In all tests $\overline{e_I^2}$ with the kinesthetic manipulator was between 3÷10 times smaller than with the isomorphic manipulator, depending on the type of $G_c(s)$. The main observations are:

1. The performance measure $\lambda_c/\overline{e_I^2}$ deteriorates gradually by an order of magnitude from $1/s$ to $1/s(s-1)$ in a consistent manner. It is also considerably lower than for the pure tracking task shown in Fig. 10.

2. The performance measure $\lambda_c/\overline{e_I^2}$ for the kinesthetic manipulator deteriorates only by ~50% from $1/s$ to $1/s(s-1)$ and is higher by 170 as compared with the isomorphic manipulator.

3. The secondary task method and the criterion $\lambda_c/\overline{e_I^2}$ provide a consistent and sensitive yardstick for performance evaluation.

8. CONCLUSIONS

The kinesthetic information paths in manual control have been shown to play a vital role in workload reduction and that in the case of high order or unstable plants, this role may be decisive in stabilizing the system. It has also been shown that by the technique described in Sec. 3 it is possible to essentially close the same kinesthetic feedback paths that exist in the natural nonintermediary handling of objects. These loop closures provide the required state estimates for implementing near optimal control without loading the visual channel and mental processes. Comparative test demonstrates the superiority of the method both in precision and workload reduction.

9. REFERENCES

1. **McRuer, D.T. et al**, *New Approaches to Human-Pilot/Vehicle Dynamic Analysis*, AFFDL-TR-67-150, (1968).
2. **Kleinman, D.L. et al**, "An Optimal Control Model of Human Response, Part I: Theory and Validation," *Automatica*, Vol. 6, pp. 357-369, (1970).
3. **McRuer, D.T., and Magdaleno, R.E.**, *Human Pilot Dynamics with Various Manipulators*, AFFDL-TR-66-138, (1966).
4. **Kraiss, K.F.**, "Can Proprioceptive Cues Unload the Human Operator," *6th An. Conference on Manual Control*, (1970).
5. **McRuer, D.T. et al**, "A Neuromuscular Actuation System Model," *IEEE Transactions on Man Machine Systems*, Vol. MMS-9, No. 3, Sept. (1968), pp.61-71.
6. **Ben Ja'acov, O.**, *Torque Feedback in Manual Control of Aircraft*, M.Sc. Thesis, Dept. of Aeronautical Engineering, Technion, May 1975.
7. **Herzog, H.J.**, *Proprioceptive Cues and Their Influence on Operator Performance in Manual Control*, NASA CR-1248 (1969).
8. **Noggle, P.L.**, *Manual Control of Unstable Vehicles Using Kinesthetic Cues*, MIT Report, MV-69-4 (1969).
9. **Gilson, R.D., et al**, "Kinesthetic Tactual Information Presentation-Inflight Studies," *IEEE Trans. on SMC*, Vol. 4, pp. 531-536 (1974).
10. **Kwakernaak, H., and Sivan, R.**, *Linear Optimal Control Systems*, Wiley, Interscience (1972).
11. **Jex, H.R., et al**, "Development of the Dual Axis and Crosscoupled Critical Tasks, *8th Ann. Conference on Manual Control*, May 1972.

SESSION V

TRACKING AND OTHER PSYCHOMOTOR TASKS

Chairman: D. L. Baty

TIME OPTIMAL CONTROL OF AN UNDAMPED HARMONIC OSCILLATOR: EVIDENCE FOR BIASES AND SCHEMATA[1]

By Richard J. Jagacinski, Michael W. Burke, and Dwight P. Miller

The Ohio State University

SUMMARY

Choosing the appropriate environmental conditions for executing a given response is argued to be a task basic to many kinds of skilled performance. As an example of this skill, three experiments investigated how human subjects solve the problem of bringing an undamped harmonic oscillator to rest as quickly as possible by means of bang-bang control. Comparison with the optimal control theory solution to this problem suggests that subjects have difficulty in using acceleration information in both learning the form of the optimal switching pattern and also in executing their learned switching patterns when the harmonic oscillator is speeded up. Excellent transfer by several subjects in situations involving system positions and velocities not previously encountered constitutes evidence for stimulus recognition schemata underlying their performance.

INTRODUCTION

The optimal control patterns derived from optimal control theory can be used as a reference for examining the actual control patterns used by human subjects. Several control problems which have been investigated from this viewpoint have involved first order unstable systems (refs. 1, 2, 3, 4), pure inertia systems (refs. 5, 6, 7, 8, 9), and undamped harmonic oscillators (ref. 9). The present set of experiments investigates how human subjects solve the problem of bringing an undamped harmonic oscillator to rest as quickly as possible when they are limited to applying a rightward or leftward force of fixed magnitude.

A second aspect of these experiments is to investigate the level of generality of the subjects' control patterns by means of various transfer tasks. The term schema has been used in various ways in psychology to refer to a generalized response generating capability that is not limited to stimulus situations previously encountered. Adams (ref. 10) and Schmidt (ref. 11) have recently reviewed three uses of the term schema corresponding

[1]The present work was supported by grants from the Graduate School and from the College of Social and Behavioral Science of The Ohio State University.

to motor recall schema, motor recognition schema, and stimulus recognition schema. While there have been numerous studies supporting the notion of a stimulus recognition schema for various types of static visual forms (e.g., refs. 12, 13), the present authors are unaware of any previous experiments relating this concept to motor behavior or the control of dynamic systems. Motor theorists have tended to concentrate on the concepts of motor recall schema and motor recognition schema, which refer respectively to the capability of producing or recognizing movement patterns not previously experienced. However, a generalized ability for choosing the appropriate conditions in a dynamic environment for executing a given response would also appear to be an important aspect of many kinds of skilled performance. For example, a baseball player who has reached the limits of the outfield fence and who must leap to catch the baseball has to choose an appropriate point in the ball's trajectory to begin his response. Jumping either too early or too late may result in his missing the ball. Similarly, a rifleman attempting to hit a distant target on a windy day will introduce a certain amount of compensation into his aim for wind velocity, indicated by the state of specific visual cues such as the motion of tall grasses. He will wait for the instant when the wind velocity is appropriate for that precise amount of compensation before pulling the trigger. Both of these situations involve recognizing special conditions of a dynamic environment and the notion of a stimulus recognition schema is appropriate for describing this kind of generalized skill.

An experimental strategy for demonstrating the existence of a schema using a within subject design is to show that over the course of an experiment a subject learns a new response pattern, and that he exhibits this learned pattern when he is transferred to a new situation in which he has no previous practice. The present experiments will involve a variety of transfer tasks to explore the applicability of the concept of a schema to controlling a dynamic system. The subject's responses in these tasks will be limited, however, to simple button pressings, thus making the selection of the appropriate environmental conditions more critical. Because evidence for motor recall schema and motor recognition schema must necessarily involve production or recognition respectively of new movements, any evidence for schemata in the present experiments will be interpreted as stimulus recognition schemata. These experiments will also attempt to determine the implications of the subject's transfer behavior for a process model of performance.

TIME OPTIMAL CONTROL OF AN UNDAMPED HARMONIC OSCILLATOR

The present set of experiments investigates one particular control problem -- bringing an undamped harmonic oscillator to rest as quickly as possible by the application of a leftward or rightward force of fixed magnitude. The problem is analogous to bringing an oscillating pendulum to rest by means of two magnets which can exert either a constant rightward or leftward force on the pendulum. The optimal switching locus for bringing the pendulum-like system to rest at the origin as quickly as possible is shown in figure 1. The locus consists of a string of dashed semicircular ar

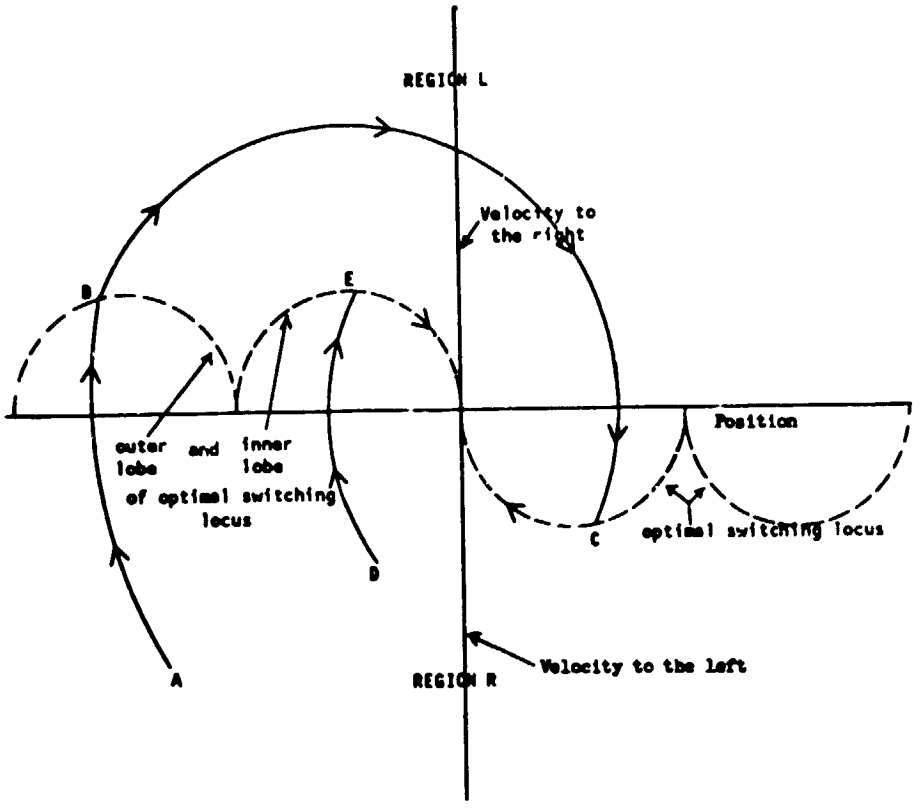

Figure 1. Optimal switching locus (—— ——) for bringing the system to rest at the origin as quickly as possible.

(ref. 14) that divides the phase plane into two regions, R and L. When the system has a position and velocity corresponding to Region R, a rightward force should be applied. In Region L, the leftward force should be applied. Two examples of the optimal switching strategy (A-B-C-Origin and D-E-Origin) are shown in figure 1.

Miller (ref. 9) instructed subjects as to the optimal switching strategy and measured their asymptotic performance using five different displays. Even when the optimal switching curve was available on a phase plane display, subjects experienced some difficulty in this control task. They tended to be least consistent in switches occurring near the cusp region between the inner and outer lobes and also tended to switch a little late along the outer lobe. These difficulties were considerably magnified with the least aided display, a single dimensional display of system position. Subjects' switches with this display tended to be both late and highly variable in the cusp region and out into the outer lobe. Miller was unable to account for this pattern of errors in terms of the subjects' psychophysical and reaction time limitations, and suggested that more research is necessary to clarify how subjects plan their responses in controlling such a system. The present experiments pursue this problem by investigating how subjects using a single

dimensional display learn to stop an undamped harmonic oscillato when they are given no prior instructions as to the optimal switching strategy.

EXPERIMENT 1

The first experiment examined subjects' performance with initial values of position and velocity that corresponded to optimal switching performance along the inner lobe in figure 1.

Method

Apparatus. The undamped harmonic oscillator system was simulated on an EAI Pace TR-48 analog computer, and system position was displayed as a 1/8-inch (.32-cm) diameter white dot moving horizontally across a 14-inch (35.56-cm) video monitor. The target region was represented by a 1/8-inch (.32-cm) wide mark in the middle of the television monitor. Above the monitor a pair of adjacent arrows pointing in opposite directions away from the center of the field alternately lighted, indicating whether a leftward or rightward force was being applied to the system. Subjects controlled the direction of the applied force with their right middle and index fingers by means of two pushbuttons. Momentarily depressing the left button caused the left arrow to light, produced a 500-Hz 110-msec tone over the earphones worn by the subject, and caused a leftward force to be applied to the pendulum-like system. The leftward force persisted until the right button was momentarily depressed. The right button functioned similarly.

Subjects. Four male, right-handed Ohio State University students participated in all four experiments.

Design. Each subject received 80 trials per session for 8 sessions. Each session lasted approximately 1 hour. The 80 trials consisted of four randomized blocks of the 20 initial conditions represented as black dots in figure 2. The undamped harmonic oscillator corresponded to the differential equation

$$(1/\underline{w}^2)\ \ddot{\underline{x}} + \underline{x} = \underline{\mu} \qquad (1)$$

where $\underline{x}$ is system position reltive to its natural resting position in inches, $\ddot{\underline{x}}$ is system acceleration in inch/sec^2, $\underline{w}$ = .4 rad/sec, and $\underline{\mu}$ = $\pm$ 1.75 inch (4.45 cm), depending on whether the right or left button was last depressed. At the beginningof each trial the system had one of the 20 initial conditions pictured in figure 2 and the rightward force was applied to the system. Optimal performance for bringing the system to rest at the origin as quickly as possible consisted of appyling a leftward force when the system intersected the inner switching lobe (figure 1). If a subject behaved in this manner, the time between the beginning of a trial to the optimal switch would range from 840 to 3,040 msec over the 20 initial conditions.

The system was considered to be at rest and on target when system velocity was less than 1/8 inch/sec (.32 cm/sec) and the system was within 1/16

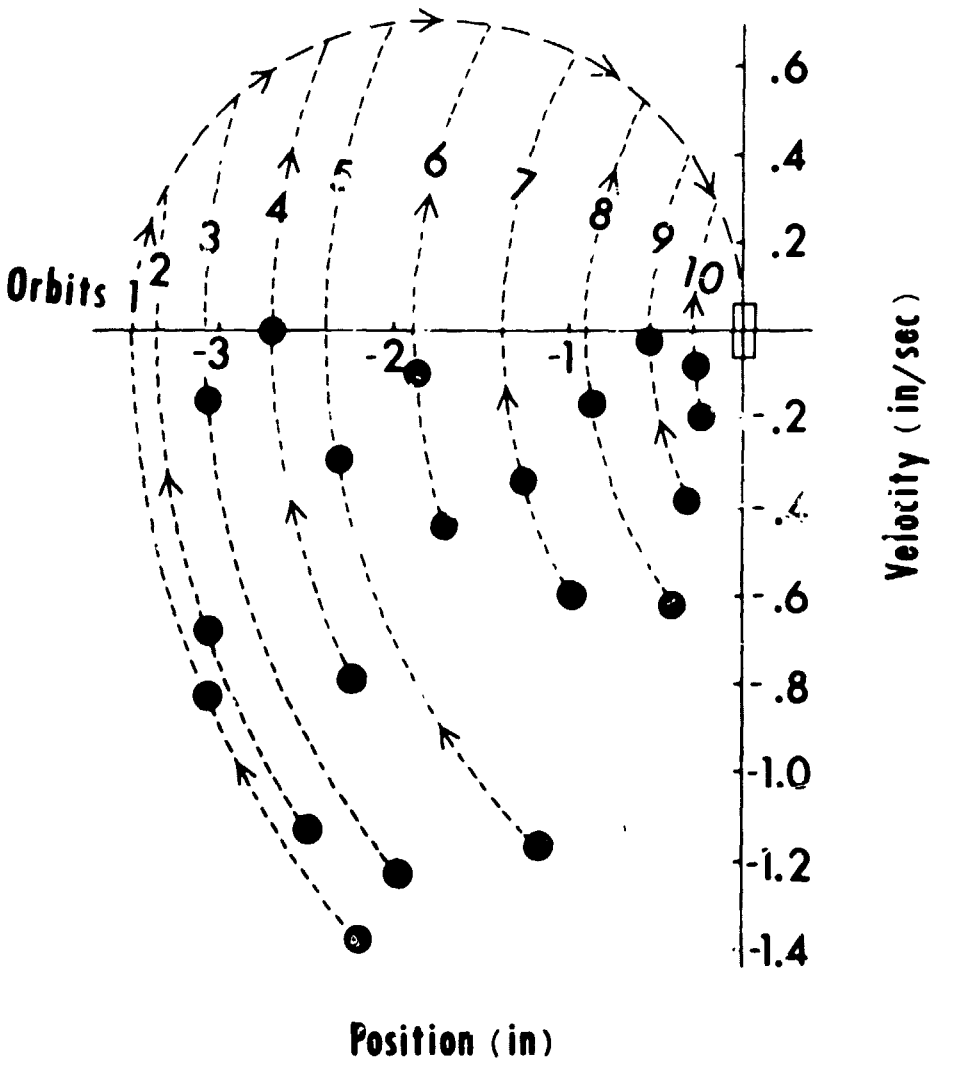

Figure 2. Initial positions and velocities for Experiments 1 and 3.

inch (.16 cm) of the center of the video monitor. Subjects were paid a base salary of $0.75 per session, and an additional amount per trial contingent on their performance. They received 4 cents per trial if they brought the system to rest on target as quickly as an ideal subject whose switching locus corresponded to the inner lobe in figure 1. For less than optimal performance, payoffs decreased linearly to zero as the time to bring the system to rest increased to 4 seconds longer than optimal performance.[2]

[2]Technically, the optimal switching locus is slightly different from the inner lobe shown in figure 1 because the effective target in the phase plane is a small rectangle about the origin rather than a single point at the origin. However, for the purposes of this experiment, the optimal switching locus for the point target was used to define optimal performance.

Procedure. Subjects were told that the dot represented a vehicle which would have a rightward force applied to it at the beginning of each trial. Their task was to stop the vehicle at the target region as quickly as possible by applying a leftward force at the appropriate instant. If the dot overshot or undershot the target, then the subjects were to apply rightward and leftward forces until the dot finally slowed to criterion over the 1/8-inch (.32-cm) target region. The dot then disappeared from the screen, and the trial was over. Immediately after each trial, subjects were told how much they had earned for that trial to the nearest 1/10 cent. If at any time the dot exceeded the bounds of the 14-inch (35.56-cm) viewing window, the trial immediately ended and the subjects received zero payoff.

The data for each trial consisted of the position and velocity when the subject executed his first three switches for each trial, the elapsed time for the first two switches, and the total elapsed time for the trial.

Results

Median switching points were calculated for subjects' first switches with each of the 20 initial conditions. The medians were calculated in terms of elapsed time along a given orbit in the phase plane. In figure 3 the upper and the lower medians for each of the 10 orbits have been connected with straight lines to indicate the average switching patterns for two of the four subjects. The optimal switching pattern for a point target is indicated by the dashed semicircle.

One qualitative property of the optimal switching pattern is that it is a line through the phase plane. In other words, the two initial conditions lying along each orbit in figure 2 have the same optimal switching point. The width of the subjects' switching loci in figure 3 indicate how closely their performance approximated a line through the phase plane. All subjects markedly reduced their intra-orbit inconsistency over the first several days of practice (e.g., compare A-1 and B-1 with A-3 and B-3). However, Subjects B and E then exhibited increased inconsistency in the five orbits farthest from the target (e.g., see B-8). A 1% level multiple F_{max} ratio test (ref. 15) revealed that the increase in variance was statistically significant for Subject B (F_{max} (7, 5) = 67.92), but not for Subject E (F_{max} (5, 5) = 8.59).

If a subject's intra-orbit inconsistency is relatively small, one may then meaningfully compare the shape of his switching locus with the optimal locus. All four subjects achieved roughly monotonic switching loci with the root mean square difference between intra-orbit medians less than 200 msec (e.g., A-3, and B-3). However, the large intra-orbit variance exhibited by Subjects B and E late in practice was judged too large to warrant any more detailed analysis of the shapes of their switching loci. Further analyses were only conducted for Subjects A and C. Comparisons of the switching times on Days 2 and 3 with Days 7 and 8 revealed that by Days 7 and 8 both Subjects A and C switched significantly earlier on the outer orbits (1-5) and significantly later on the inner orbits (6-10). To test whether the shapes of the switching loci for Subjects A and C were non-monotonic in the phase

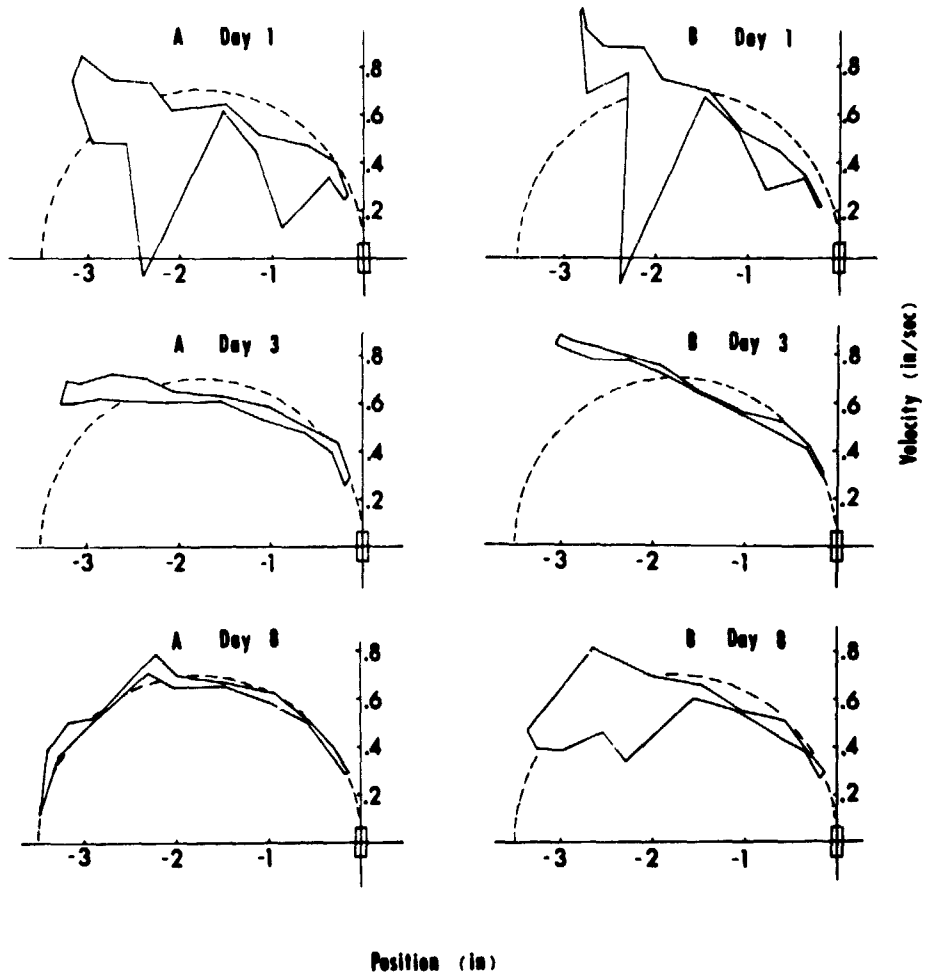

Figure 3. Median first switches in Experiment 1 for Subjects A and B.

plane, the switching velocity at the two middle orbits (5 and 6) was compared with the switching velocity at the outermost orbits (1 and 2) and at the innermost orbits (9 and 10). On Days 2 and 3, these two subjects had not achieved a non-monotonic switching pattern in that the switching velocity for the two outermost orbits was not significantly less than the switching velocity in the middle orbits. However, by Days 7 and 8 Subjects A and C did have a significantly lower switching velocity in the two outermost orbits.

One final measure of how closely these two subjects approximated optimal performance is the root mean square deviation from the dashed semi-circular locus shown in figure 2. This statistic equalled 114 msec for

Subject A and 160 msec for Subject C on Days 7 and 8, and both differences were significant at the .05 level.

Discussion

In order to interpret the manner in which the subjects' switching patterns changed over the 8 days of this experiment, it is useful to ask, "What must the subjects learn about the system in order to approximate the optimal control solution?" By trial and error subjects could arrive at a set of paired associations between the 20 initial conditions and the 20 corresponding switching points necessary to stop at the target without undershooting or overshooting. Each of the initial conditions is uniquely specified by a combination of position and velocity cues, and the switching points could be specified in terms of position, velocity, and/or elapsed time cues. As suggested by Preyss and Meiry (ref. 8), overshooting the target would cause the subjects to revise the switching point for a given initial condition to occur sooner, and undershooting would result in a similar revision in the opposite direction, assuming that subjects are attempting to stop in the target region with a single switch. According to this model of learning behavior, one might expect an initially random-looking phase plane switching pattern to converge in a relatively uniform manner toward the optimal control solution. This simple model seems inadequate because of the extremely slow and non-uniform manner in which subjects did approach the optimal control solution after a more rapid initial convergence toward a monotonic switching pattern. The monotonic switching loci suggest that subjects are relying on control patterns that are appropriate for stopping a freely moving vehicle, but inappropriate for a pendulum-like system. More specifically, one typical property of braking systems for moving vehicles is that if one is traveling on a smooth level surface, stopping distance is an increasing function of the vehicle's velocity, but does not depend on its location. This property does not hold for the harmonic oscillator. As indicated in equation 1, when the leftward force is applied to the system, the net braking force is an additive combination of the constant leftward force and the system's pendulum-like tendency to move rightward toward its natural equilibrium at the center of the target.

Assuming an initial bias toward characterizing the task as an ordinary vehicular braking task, one might expect the subjects' transition to a more veridical characterization of the system's dynamic properties to cover three stages of learning. In Stage 1 early in practice subjects assume that the braking force is not a function of position, and their switching velocity increases with distance from the target. Such behavior would be analogous to the manner in which car drivers traveling at higher velocities typically begin to apply the brakes farther from the intersection in order to stop in time. In Stage 2, subjects begin to realize that the braking force decreases with distance from the target and begin to apply the leftward force at correspondingly lower velocities. A switching pattern in which switching velocity continually increases with distance from the target is also consistent with this stage. If the subjects believe that the braking force actually decreases to zero for longer distances from the target, then they

should adjust their switching patterns so that the switching velocity becomes a constant for distances farthest from the target. Subjects cannot be in Stage 1 if they exhibit this switching pattern (e.g., figure 3, A-3), which represents the maximum downward adjustment possible in Stage 2. In Stage 3, subjects not only realize that the braking force decreases with distance from the target, but also realize that for longer distances from the target the system accelerates even though the leftward force is applied. This increasing acceleration with distance from the target requires the subjects to curve their phase plane switching patterns downward.

Within each of these three stages it is plausible that subjects might adjust their switching loci in accordance with the simple learning model previously mentioned. The stages place different limitations on how far such adjustment can proceed. Unless subjects reach Stage 3, they cannot produce a nonmonotonic switching locus. According to this interpretation, the slowness of subjects to approach the optimal control pattern can be attributed to their difficulty in making the two qualitative transitions to Stages 2 and 3. Subjects A and C showed clear evidence of reaching Stage 3 (e.g., figure 3, A-8). Whether Subjects B and E also reached Stage 3 is uncertain. Statistical tests of monotonicity were not performed for these latter two subjects due to the large intra-orbit variance they exhibited. The increase in intra-orbit variance shown by Subject B is still unexplained in this model.

The three stage theory just outlined deals with qualitative aspects of the phase plane switching patterns, namely their monotonicity. Further interpretation is possible if one assumes that subjects have non-veridical internal representations of the pendulum-like system, and that at any point in time subjects are attempting to behave optimally with respect to those non-veridical models. Assuming that subjects try to reach the origin without overshooting or undershooting, the pattern of switches must all lie on what the subjects believe to be a single trajectory to the target. One may therefore interpret the phase plane switching loci as trajectories of the subjects' internal models. An additional, but not very restrictive assumption is that the subjects' internal models do have unique trajectories that reach the origin when a constant force is applied. Under this interpretation the phase plane loci can be used to generate analytic representations of the subjects' internal models (R.A. Miller, personal communication). The detailed calculations and the problems of uniqueness of these analytic representations will not be pursued in the present paper.

EXPERIMENT 2

The second experiment extended the range of initial conditions so that on some trials it was necessary to use two switches in order to stop the system in the target area (see the outer lobe in figure 1). One aim of this experimental manipulation was to investigate how closely the subjects' first switch patterns would approximate the double lobe pattern of optimal performance for a point target. A second aim was to seek evidence for schemata by testing whether the observed switching patterns would transfer to new initial

positions and velocities. If subjects simply learn a set of paired associations between the initial conditions and corresponding switching points, then they should not be able to perform this transfer task.

Method

The same four subjects used in Experiment 1 received 8 days of practice with the 20 initial conditions represented as black dots in figure 4. The

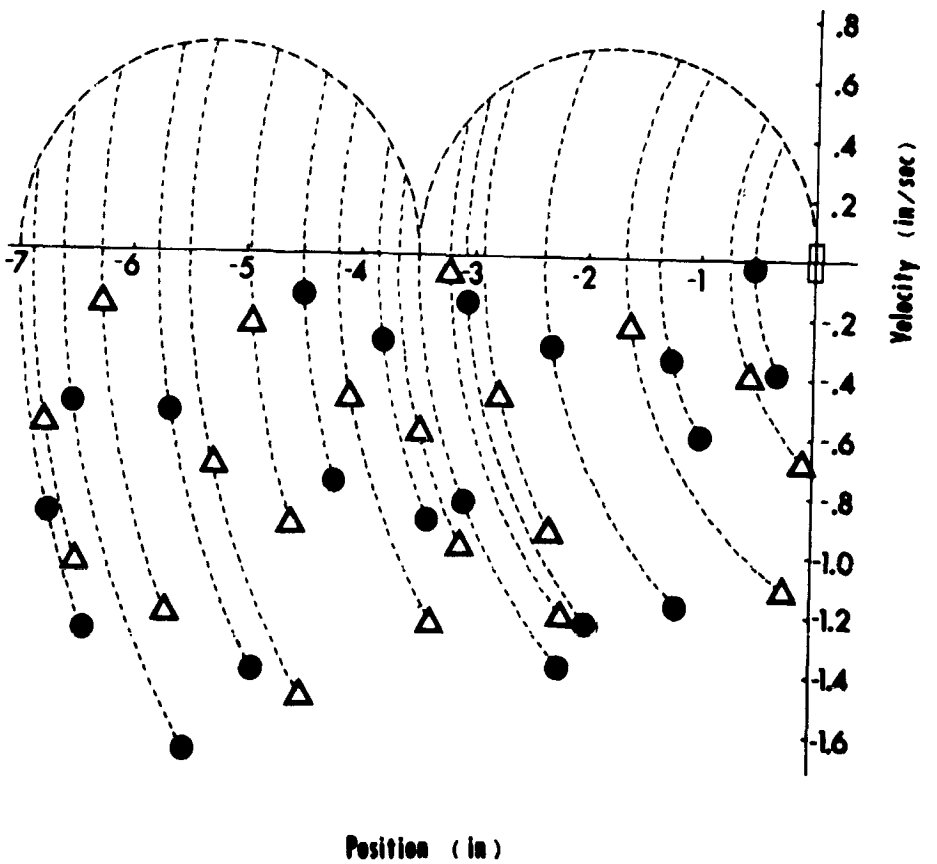

Figure 4. Well-practiced initial positions and velocities (●) and new initial positions and velocities (Δ) for the transfer test in Experiment 2.

10 initial conditions requiring only a single switch were identical to 10 of the initial conditions used in Experiment 1. Subjects were instructed that the range of starting positions would be extended, but that otherwise the system would be the same. Following Day 8 there were scheduling delays of 56, 54 and 11 days for Subjects A, B and C respectively. Each of these three subjects was therefore given 1 extra day of practice upon his return to the

experiment. All four subjects were then given 1 day of performance with the well-practiced initial conditions, 1 day of performance with 20 new initial conditions which are represented as triangles in figure 4, and a final day of performance with the well-practiced initial conditions. Subjects were not told that there had been any procedural change on the day with the new initial conditions.

Results

The median switch point was calculated for each initial condition as in the previous experiment. The means of each intra-orbit pair of medians have been connected with straight lines in figure 5 for the day with the new initial conditions (————————) and for the preceding (-------) and following (—··—··) days using the well-practiced initial conditions.

To assure the subjects' performance on the new initial conditions cannot be attributed to previous practice on these very orbits, it was necessary to ascertain that second and third switches in Experiments 1 and 2 did not occur along these "new" orbits. Available records indicated that such switches were rare in the region of the outermost eight new orbits, and subsequent analysis was restricted to this region.

For each subject an F test was performed at the .05 level to determine whether there was a significant increase in intra-orbit variance with the new initial conditions. None of the F tests was significant. In order to test whether the switching pattern for the new initial conditions differed from the patterns on the preceding and following days, a polynomial was fit via multiple regression to the median switching points with the new initial conditions and a second polynomial was fit to the data for the preceding and following days. An F test was then performed to compare the sum of the residuals from these two polynomials with the residual when the data from all 3 days were fit by a single polynomial of the same degree. Only the reduction in residual for Subject B, $F\ (2, 40) = 4.17$, $p < .05$, was significant at the .05 level.

Two types of analyses were similarly conducted to test whether the performance of Subjects A, C and E with the new initial conditions differed from their performance on the outer seven orbits on the first 2 days of Experiment 2. First, an F test was performed for each subject at the .05 level to test whether the intra-orbit variance was larger at the beginning of Experiment 2. Subject C, $F\ (14, 8) = 2.29$, $p < .001$, did exhibit significantly larger intra-orbit variance at the beginning of Experiment 2; however, Subjects A and E did not. Polynomial regression analyses revealed that the shape of Subject A's switching pattern early in Experiment 2 was significantly different from the pattern for the new initial conditions; however, Subject E did not exhibit any significant difference.

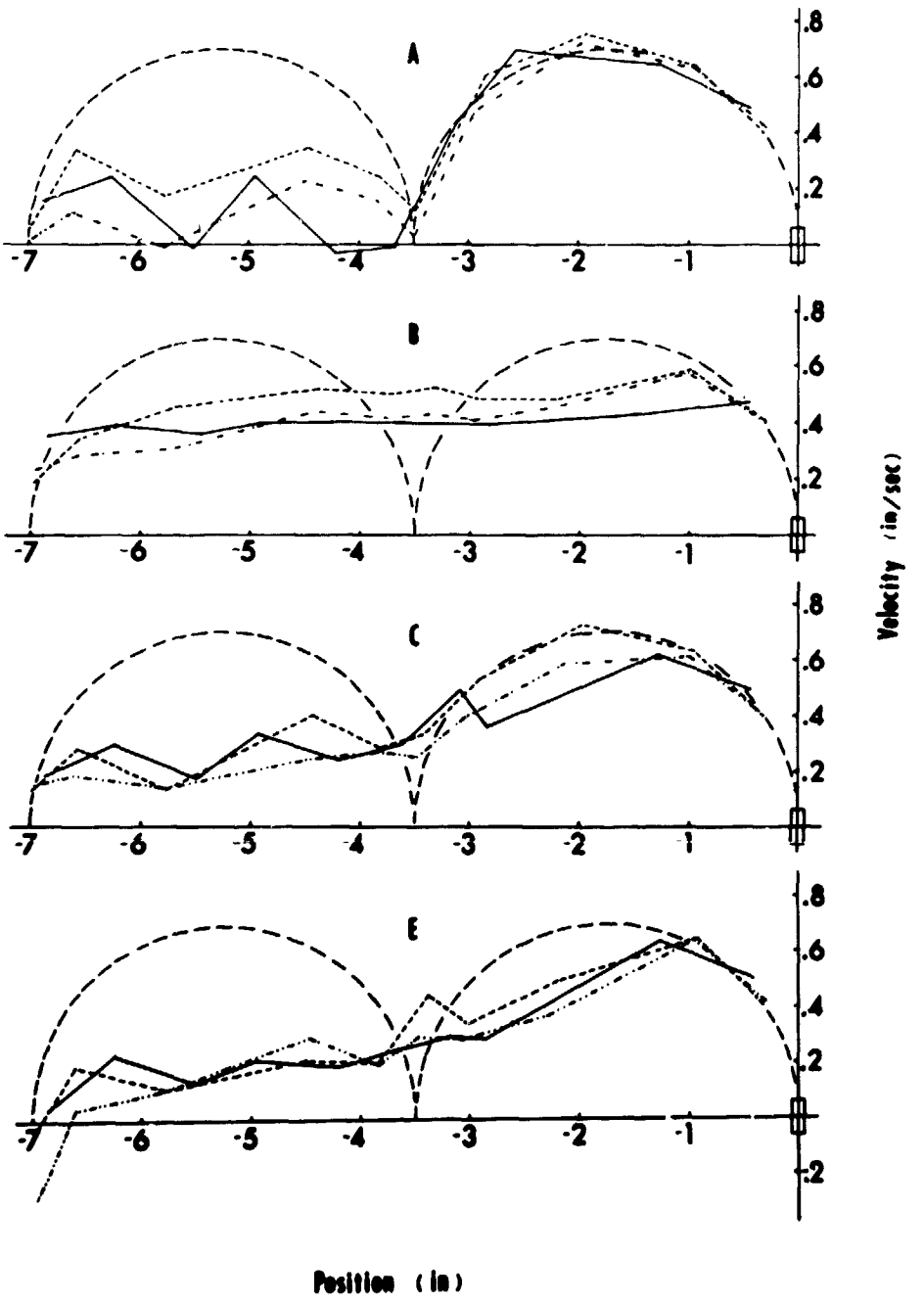

Figure 5. Means of median first switches for Subjects A, B, C, and E in Experiment 2 for well-practiced initial conditions (- - - and -·-·-·) and new initial conditions (————).

Discussion

That none of the four subjects' switching loci resembled the double lobe optimal solution is perhaps not very surprising if one considers the difficulty involved in discovering such a solution by trial and error. The inner optimal lobe is part of a trajectory of the system through the phase plane, and subjects could have approached the optimal solution in this region by adjusting their switching points so as to eliminate undershoot or overshoot of the target. In contrast, the outer optimal lobe is not part of a trajectory, and subjects will overshoot the target for trials starting in this region of the phase plane no matter when their first switch occurs. The outer optimal lobe is not even the switching locus that minimizes overshoot of the target. A second reason for difficulty is that the total time to reach the target is not very sensitive to deviations from the outer optimal lobe. Engineers implementing automated switching devices typically take advantage of this fact by substituting a zero velocity switching locus in place of the outer optimal lobe. Such a locus is easier to construct and does not increase the total time to reach the target by more than 5% (ref. 16). In the present experiment it would probably be difficult for subjects to detect a 5% difference between optimal and sub-optimal loci because of variation in their second switch performance.

Within the accuracy of experimental measurement, Subjects A, C and E exhibited the same switching pattern for the new initial conditions as for the well-practiced initial conditions. Secondly, for Subjects A and C this pattern was significantly different from the switching pattern exhibited at the beginning of Experiment 2. Finally, records of previous performance indicate that these two subjects had negligible practice along the new orbits prior to the transfer task. Together these statements constitute evidence for the existence of schemata underlying the performance of Subjects A and C. While Subject E did show excellent transfer to the new initial conditions, this subject did not exhibit a significant change in switching pattern with practice. Therefore, this subject's performance does not constitute evidence for a schema. Subject B's performance also does not meet the strict criterion previously specified for the existence of a schema.

In order to further delineate the nature of the schemata implied by the performance of Subjects A and C, it is necessary to discuss alternative process models for behavior in this experiment. In the present task, the detailed time course of the button pressing responses was not measured; however, a simple, unvarying movement pattern would be sufficient to perform well. The concepts of motor recall schema and motor recognition schema, which respectively involve production and recognition of new movements, therefore need not be invoked for these experiments. What is necessary is that subjects know when to execute the button pressing response as the harmonic oscillator passes through states not previously observed. Stimulus recognition schema is an appropriate concept for describing this skill.

A more detailed question concerns what aspect of the subjects' performance is encoded in the recognition schema. Does the schema encode states of the oscillator system at which the subject should initiate the button pressing response, or does the schema encode states of the oscillator system at which

the actual depression of the switch should be completed? If the button pressing response could be executed instantaneously, this distinction would be meaningless. However, assuming at least a 200 msec reaction time in the subjects' execution of such a response, the distinction is important for this task. Unfortunately, the data in the present experiment do not distinguish between these two possibilities. These data do imply that subjects have learned a skill which is not specific either to the positions and velocities at the beginnings of trials or to particular orbits. However, subjects could perform the transfer task if they had learned a generalized locus of system states for either response initiation or for completing the switch depression. The basic difference between these two kinds of recognition schema is that the latter assumes subjects can predict when the system is one reaction time away from the switch completion locus. To distinguish between the two possible kinds of schemata, it is necessary to use a transfer task that necessitates the prediction capability postulated by the response completion schema. Such a test is provided by using a speeded simulation of the harmonic oscillator system.

EXPERIMENT 3

In order for subjects to achieve perfect transfer of a switching pattern with a speeded simulation of the oscillator system, three conditions must obtain. First, they must encode the switch completion locus rather than the switch initiation locus. Because the simulation is speeded, the oscillatory system will move through a larger fraction of its phase plane orbit during the subjects' reaction time. The locus of response initiation necessary to achieve the same switching locus will therefore be pushed farther back from the switch completion locus. Ability to make this necessary compensation is evidence for the use of a response completion locus. Secondly, subjects must be able to time scale their representation of the response completion locus if they use time or velocity cues to encode this locus. For example, assume subjects encode the locus at the accustomed speed as F_c ($\underline{t}$, $\underline{x}$, $\underline{v}$), where $\underline{t}$ is elapsed time, $\underline{x}$ is system position, and $\underline{v}$ is system velocity. If the speeded simulation is twice as fast as the accustomed speed, the subjects' new locus should be F_c ($\frac{1}{2}\underline{t}$, $\underline{x}$, $2\underline{v}$). Elapsed time cues must be halved, position cues need not be changed, and velocity cues must be doubled, because the speeded simulation covers the same distances as before with twice the velocity and in half the elapsed time. Thirdly, subjects' ability to predict when the system is one reaction time away from F_c must be of such quality as not to deteriorate significantly in its predictive accuracy when applied over a relatively longer fraction of the phase plane orbit. For example, a simple constant velocity extrapolation of the system's motion might provide adequate predictive accuracy when the simulation is slow, because the fraction of the phase plane orbit covered in one reaction time is small, and the system undergoes relatively little acceleration over the prediction interval. This approximation may break down, however, with a speeded simulation. In summary, perfect transfer with a speeded simulation will be evidence that all three of these necessary conditions obtain. Less than perfect transfer will be evidence that at least one of these conditions does not obtain.

At a more general level of description, this experiment also provides a further test of the subjects' ability to transfer to a new situation.

Perfect transfer would provide additional support for stimulus recognition schemata.

Method

The same four subjectsused in the first two experiments were given 1 day of practice with the initial conditions used in Experiment 1. Subjects were then given another day at the accustomed speed, 2 days with the simulation running twice as fast as usual, and a final day at the accustomed speed. On the first day with the fast simulation, subjects were told that the system had been speeded up, but that nothing else was changed.

Results

The first switch data for the day immediately preceding and the day immediately following the speeded simulation were analyzed to determine how closely subjects approached the optimal switching locus. To test for a non-monotonic switching pattern, the average switching velocity in the middle two orbits (5 and 6) was compared with the average switching velocity in the innermost and outermost pairs of orbits. Subjects A, C and E all exhibited a non-monotonic pattern. However, for Subject B the switching velocities for the middle and outermost orbits were not significantly different (figure 6).

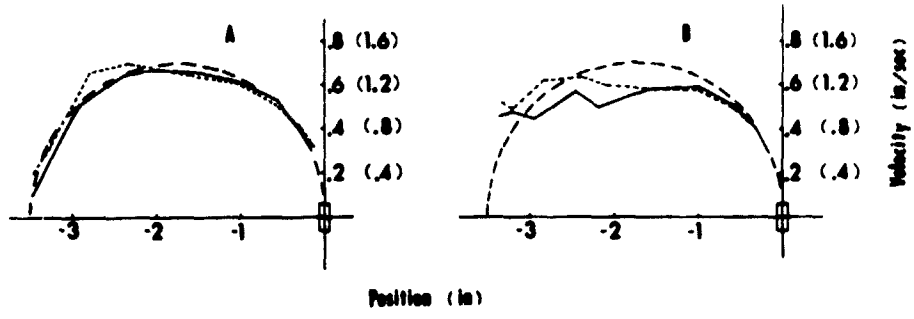

Figure 6. Means of median first switches for Subjects A and B in Experiment 3 with the speeded simulation (----) and the simulation at the accustomed speed (————). The ordinate values in parentheses refer to performance with the speeded simulation.

A second analysis compared the first switch data on the two speeded simulation days with the immediately preceding and the immediately following day at regular speed. In order to facilitate comparison, switching times on the two speeded days were all multiplied by a factor of 2 for the following analyses. F tests were conducted for each subject to determine whether

intra-orbit variance on the five outer orbits (1-5) and the five inner orbits (6-10) increased with the speeded system. For the outer orbits, Subject E exhibited a large increase in intra-orbit variance, F (10,10) = 9.10, p <.001, and Subject C exhibited a smaller increase, F (10,10) = 2.97, that approached significance at the .05 level. No other statistically significant increases were detected.

In order to test whether a change in the shape of the switching locus had occurred with the speeded system, separate analyses of variance were performed on the outer five and inner five orbits for Subjects A, B and C, but only for the inner orbits for Subject E, because of the large increase in variance he exhibited on the outer orbits on the speeded days. As shown in

Table 1

Mean Differences Between Non-speeded and 2 x Speeded

Switching Times in Experiment 3

	Outer orbits (1-5) (msec)		Inner orbits (6-10) (msec)	
Subjects	Obtained difference	Difference necessary for significance, p <.05	Obtained difference	Diff. necessary for significance p < .05
A	106*	±86	-6	±60
B	119*	±107	-15	±25
C	77*	±55	42	±57
E	--	--	21	±115

*p < .05

Table 1, Subjects A, B and C all switched significantly later in the outer orbits with the speeded simulation. None of the four subjects exhibited a significant difference in the inner orbits. In order to indicate the sensitivity of these contrasts, the mean differences between speeded and non-speeded switching times necessary to achieve statistical significance at the .05 level have been listed in Table 1. The power of the contrasts for detecting differences as large as these is about .56; the power for detecting differences twice as large is about .97.

Given that subjects did show excellent transfer for the inner orbits, it becomes important to test whether this switching pattern was learned over the course of the experiment. Accordingly, F tests were conducted to test

whether the intra-orbit variance on the 2 days with the speeded system was significantly less than intra-orbit variance on the first 2 days of Experiment 1 for these five orbits. Subjects A, F (10,10) = 26.35, $p < .001$, Subject C, F (10,10) = 6.65, $p < .01$, and Subject E, F (10,10) = 12.15, $p < .001$, all exhibited significantly higher intra-orbit variance on Days 1 and 2 of Experiment 1. Only Subject B, did not exhibit a significantly higher variance and this subject also exhibited no significant change in his mean switching times with practice.

Discussion

Subjects A, C and E all exhibited non-monotonic phase plane loci; however Subject B did not. In terms of the three stage model described in Experiment 1, Subjects A, C and E reached Stage 3, but Subject B only reached Stage 2. In other words, in adjusting his switching locus Subject B still did not take into account the system's increasing acceleration for orbits farthest from the target. This subject's failure to converge on the optimal solution after such prolonged practice lends further credence to the three stage model as a necessary elaboration of the simple learning model.

The perfect transfer exhibited by Subjects A, C and E in the inner orbits constitutes evidence for the existence of schemata. The transfer was to a new situation not previously practiced; within the limits of experimental measurement the pattern was identical to the pattern exhibited on the immediately preceding and following days at the usual speed; and the pattern of behavior was different from the behavior exhibited by the subjects at the very beginning of practice in Experiment 1. These results imply that over the course of the experiments Subjects A, C and E learned a general response generating strategy, which may be called a schema. Although one cannot conclude that Subject B learned his switching pattern in the inner orbits over the course of these experiments, his transfer behavior did exhibit the same general pattern as Subjects A and C. In the following discussion of possible underlying process models the construct F_c should therefore be called a response completion locus rather than schema for Subject B. However, for ease in exposition, this point will not be constantly reiterated.

The perfect transfer exhibited in the inner five orbits is consistent with the assumptions that subjects used a stimulus recognition schema for switch completion, that they were able to time scale this locus if it involved time and velocity cues, and that their ability to extrapolate the system's motion pattern was relatively accurate. If subjects used a response initiation schema and appropriately time scaled any time and velocity cues, the measured switching locus with the speeded simulation would be shifted upward by one-half the duration of the subjects' reaction time. Assuming a reaction time of at least 200 msec, the shift would amount to at least 100 msec in real time, and at least 200 msec on the doubled time scale used for comparing the two simulations. In fact, no statistically significant shift was observed in the inner orbits, and the power for detecting a 200 msec shift was approximately .94 for Subject E and considerably greater than .99 for Subjects A, B and C.

The hypothesis that subjects used a response initiation schema must therefore be rejected unless one additionally assumes that subjects used velocity cues and failed to time scale them sufficiently. Failure to time scale would lead to initiating the response at a lower velocity and would move the measured switching locus downward in the phase plane, reducing the prediction of a full 200 msec shift. A similar explanation would also need to be invoked to account for the considerably less than 200 msec shift observed in the outer five orbits for Subjects A, B and C. The large increase in intra-orbit variance in the outer orbits for Subject E does not fit this description, and suggests that the decision of when to switch is based on different information for the two initial conditions within each orbit. In this regard Subject E's behavior appears to differ in a more fundamental manner from normative switching behavior than the performance of the other three subjects and will not be included in the discussion that follows.

While it is not possible to rigorously rule out the above response initiation schema hypothesis on the basis of the present data, the assertion of nearly equal, but opposite effects to account for the excellent transfer in the inner orbits is not very plausible. A second explanation of the data for Subjects A, B and C is that they did use a response completion schema, but failed to sufficiently time scale the locus in the region of the outer five orbits. Failure to time scale elapsed time cues by a factor of one-half would result in subjects' switching at too long an elapsed time, and hence the observed switching locus for the speeded system would be shifted upward. The excellent transfer in the inner orbits would then be attributed to the subjects' using position and/or velocity cues to specify the switching locus in that region of the phase plane.

In evaluating the plausibility of this explanation it is important to note that subjects must estimate elapsed time relative to some easily identified starting point. The only two likely starting points in the present task are the beginning of the trial and the point at which the system reverses direction from left to right. The beginning of the trial cannot be the starting point, or subjects would not have been able to exhibit the excellent transfer observed in Experiment 2. The point at which the system reverses direction is also implausible. Subjects having to wait for this event before starting their prediction process could not exhibit switching times less than one reaction time after the system reversed direction. However, for the orbits farthest from the target Subjects A and C exhibited switching times less than 200 msec. Without a likely starting point for estimating elapsed time, this second explanation also appears implausible.

A third explanation of the upward shift for Subjects A, B and C is that in using a response completion schema their ability to predict the motion of the system over the duration of one reaction time was relatively accurate for the inner orbits, but not for the outer orbits. the outer orbits, the motion of the system more nearly approximated a constant acceleration in the period immediately prior to the observed switching loci. Rosenbaum (ref. 17) has reported correlational data indicating subjects can extrapolate constantly accelerated motion to a fixed reference point with considerable accuracy. There are, however, a number of other studies in which subjects have had

considerable difficulty in extrapolating accelerated motion in manual tracking tasks (refs. 18, 19, 20) and in predicting collision with a second object moving at constant velocity (ref. 21). In these latter experiments, subjects tended to underestimate or ignore the increase in velocity of an accelerated motion. In the present experiment, this kind of bias would lead to subjects initiating their switching response too late and overshooting the desired switching locus in agreement with the observed data. This bias would have much less effect in the inner orbits because of the lower level of acceleration in these orbits.

While it is not possible to rigorously exclude any of the above three explanations on the basis of the present data, the third explanation does lend itself as the most plausible alternative both because of its agreement with previous studies showing difficulty in extrapolating accelerated motion and because this explanation does not have to postulate any different kind of information processing for the inner and outer orbits. One special case of a process model fitting this third explanation is a model used by Miller (ref. 9). He assumed that subjects specify the switch completion locus in terms of position cues and use a constant velocity extrapolation of the system's motion over a 200 msec reaction time. For each of the four subjects in the present experiment, this model predicts an upward shift of the speeded switching locus on the inner five orbits of approximately 50 msec on the doubled time scale used to compare performance on the two simulations. The probability of failing to reject the null hypothesis for at least one of the four subjects given a true shift of this magnitude is approximately .005, which suggests that this model should be rejected. The probability value is so low primarily due to the data of Subject B.

A model assuming constant acceleration extrapolation predicts shifts of less than 6 msec on the doubled time scale for both the inner and outer orbits, even with an assumed reaction time as long as 350 msec. This model can also be rejected by the present data. One cannot, however, reject the possibility that subjects made some, though insufficient, use of acceleration information. This latter kind of model can approximate the present data more accurately than Miller's model by assuming some usage of acceleration extrapolation and a reaction time longer than 200 msec.

CONCLUDING REMARKS

One aspect of these experiments was to compare subjects' switching patterns with optimal switching behavior. The optimal control theory solution to stopping the harmonic oscillator was not used in a direct way to generate a process model for the human controller as has been done by Kleinman, Baron, and Levison (ref. 22) for tasks involving continuous correction of random disturbances. Rather, the optimal control solution was used as a reference for examining qualitative aspects of the subjects' performance such as intra-orbit switching variance and the monotonicity of the switching locus. The Kleinman, Baron, and Levison model assumes that the human controller has a veridical representation of the system he is attempting to control, and when necessary the criterion function that the subject is assumed to be optimizing

is adjusted away from nominal values in order to match the model to subjects' behavior. In the present experiments it has been assumed that subjects are always attempting to minimize time, and that deviations from optimal performance can be attributed to a non-veridical characterization of the pendulum-like system. The plausibility of this interpretation would be enhanced if incorporating evidence for non-veridical internal models into the more detailed process models of continuous tracking behavior led to superior prediction of subjects' performance in those tasks.

According to the three stage learning model described in Experiment 1, the subjects' difficulty in approaching the optimal control solution is attributable to their not taking into account the system's tendency to accelerate toward its natural equilibrium position at the center of the target. However, even after Subjects A and C overcame this difficulty, their lack of perfect transfer on the outer orbits with the speeded simulation has been attributed to insufficient use of acceleration cues in predicting the system's motion over the duration of their reaction times. These results are not surprising in that only ordinal knowledge of the increasing acceleration of the system with distance from the target is necessary to permit subjects to curve their switching loci downward. In contrast, more than ordinal knowledge of acceleration is necessary for appropriate short-term prediction of the system's motion to permit perfect transfer with the speeded simulation. The data for Subject B are surprising, however, because this subject showed the most evidence of using acceleration information for short-term prediction in the inner orbits, but did not take the system's acceleration into account in the shape of his switching locus.

Another aspect of these experiments was their support for the existence of schemata. Subjects' ability to exhibit the same switching locus with new initial conditions not previously encountered and with the speeded simulation are evidence that a generalized skill was learned. The three different types of transfer tasks used in these experiments occurred at different points in practice and tested different segments of the overall first switch pattern. By combining some of these transfer tests, future research may begin to ask more specific questions about developmental aspects of the skill involved in controlling a dynamic system.

In their schema theories of motor skills, both Pew (ref. 23) and Schmidt (ref. 11) have treated the conditions of the external environment and the performer's musculature as inputs which determine the choice of an appropriate motor response. However, the converse relationship is also quite plausible for many skills -- namely, that the range of possible reponses determines the performer's choice of internal and external environmental conditions for beginning a response. In the present experiments it has been assumed that subjects had only a single possible motor response, a stereotyped button press, and the choice of external environmental conditions for response initiation was therefore the only choice available to them. In more complex skills involving a variety of possible responses, both kinds of choices are probably involved. For example, the skilled tennis player described by Bartlett (ref. 24) may possess the versatility to begin his stroke over an entire range of possible conditions of the ball, the racket, and his muscula-

ture and be capable of altering the form of his stroke accordingly. However, to at least some extent, he has the ability to choose the internal and external environmental conditions for his stroke by appropriately positioning himself and waiting for a particular point in the ball's trajectory. The form of the stroke he wishes to execute will determine his choice of environmental conditions, as well as vice versa. The conception of a motor recall schema as emphasized by motor theorists is appropriate for describing a generalized ability to choose the form of the response given the environmental conditions. The conception of stimulus recognition schema as emphasized in the present experiments is appropriate for describing a generalized ability to choose the environmental conditions given the desired form of the response. An issue that any general theory of skilled performance must ultimately address is how these two aspects of choice are related in situations where neither the form of the response nor the environmental conditions are fixed.

REFERENCES

1. Ray, H. W.: The application of dynamic programming to the study of multistage decision processes in the individual. Unpublished Doctoral Dissertation, The Ohio State University, 1963.

2. Rapoport, A.: A study of human control in a stochastic multistage decision task. Behavioral Science, 1966, 11, 18-32.

3. Rapoport, A.: A study of a multistage decision making task with an unknown duration. Human Factors, 1966, 8, 54-61.

4. Rapoport, A.: Dynamic programming models for multistage decision-making tasks. Journal of Mathematical Psychology, 1967, 4, 48-71.

5. Pew, R. W.: A model of human controller performance in a relay control system. Proceedings of the Fifth National Symposium on Human Factors in Electronics, San Diego, California, May, 1964, 241-251.

6. Pew, R. W.: Performance of human operators in a three-state relay control system with velocity-augmented displays. IEEE Transactions on Human Factors in Electronics, 1966, HFE-7, 77-83.

7. Pew, R. W.: Acquisition of hierarchical control over the temporal organization of a skill. Journal of Experimental Psychology, 1966, 71, 764-771.

8. Preyss, A. E., and Meiry, J. L.: Stochastic modeling of human learning behavior. IEEE Transactions on Man-Machine Systems, 1968, MMS-9, 36-46.

9. Miller, D. C.: Behavioral sources of suboptimal human performance in discrete control tasks. Massachusetts Institute of Technology, Engineering Projects Laboratory Technical Report, No. DSR 70283-9, January, 1969.

10. Adams, J. A.: Issues for a closed-loop theory of motor learning. In G. E. Stelmach (Ed.), Motor control: Issues and trends. New York: Academic Press, 1976.

11. Schmidt, R. A.: A schema theory of discrete motor skill learning. Psychological Review, 1975, 82, 225-260.

12. Attneave, F.: Transfer of experience with a class-schema to identification-learning of patterns and shapes. Journal of Experimental Psychology, 1957, 54, 81-88.

13. Posner, M. I., and Keele, S. W.: On the genesis of abstract ideas. Journal of Experimental Psychology, 1968, 77, 353-363.

14. Athans, M., and Falb, P. L.: Optimal control. New York: McGraw-Hill, 1966.

15. David, H. A.: The ranking of variances in normal populations. Journal of the American Statistical Association, 1956, 51, 621-626.

16. Knudsen, H.: Maximum effort control for an oscillatory element. Unpublished M.S. Thesis, University of California, Berkeley, 1960. As cited in M. Athans & P. L. Falb, Optimal control. New York: McGraw-Hill, 1966, 587.

17. Rosenbaum, D. A.: Perception and extrapolation of velocity and acceleration. Journal of Experimental Psychology: Human Perception and Performance, 1975, 1, 395-403.

18. Gottsdanker, R. M.: The accuracy of prediction motion. Journal of Experimental Psychology, 1952, 43, 26-36.

19. Gottsdanker, R. M.: Prediction-motion with and without vision. American Journal of Psychology, 1952, 65, 533-543.

20. Gottsdanker, R. M.: A further study of prediction-motion. American Journal of Psychology, 1955, 68, 432-437.

21. Runeson, S.: Visual prediction of collision with natural and nonnatural motion functions. Perception and Psychophysics, 1975, 18, 261-266.

22. Kleinman, D. L., Baron, S., and Levison, W. H.: A control theoretic approach to manned-vehicle systems analysis. IEEE Transactions on Automatic Control, 1971, AC-16, 824-832.

23. Pew, R. W.: Human perceptual motor performance. In B. Kantowitz (Ed.), Human information processing: Tutorials in performance and cognition. New Jersey: Lawrence Erlbaum, 1974, 1-39.

24. Bartlett, F. C.: Remembering. Cambridge, England: University Press. 1932.

CONTINUOUS COMPENSATORY AUDIO MANUAL TRACKING

Richard Gray Costello

The Cooper Union For The Advancement Of Science And Art
Electrical Engineering Department
Cooper Square
New York, N.Y. 10003

SUMMARY

For the purpose of this investigation, continuous compensatory audio manual tracking is defined as the set of circumstances under which a human operator manipulates a manual control in response to a continuous audio input or command signal; and attempts to null out any changes in the audio command by generating appropriate manual responses.

The investigation was prompted by several recreational glider pilots, who commonly employ a device called an audio variometer to adjust their flight path. The audio variometer is a sensitive differentiating altimeter, which produces an audio output proportional to the glider's rate of climb (or rate of sink, as the case may be). If the glider is climbing, the pitch of the audio tone output climbs, if the glider is falling, the audio pitch falls. The glider pilot is thus able to adjust his control tactics in response to the audio tone output, and use his eyes for enjoying the scenery.

An analog computer, a voltage controlled oscillator, and a side arm controller were employed to simulate a single axis continuous compensatory audio manual trucking task. A student built digital interface sampled four channels of real time simulation data, for later analysis by a dedicated NOVA 1200 mini computer.

The rather limited results indicated a corner frequency for this task in the region of 1/10 hz., well below the corner frequency for visual manual tracking tasks. It was observed that those subjects who had had some musical training produced consistently better audio-manual tracking results, when compared to subjects who had had no musical training.

INTRODUCTION

Intermittent control of a human operator system, utilizing an audio feedback link, has been with mankind for a surprising long period of time. An eighteenth century helmsman piloting a sailing vessel through fog used his ears to select a course in response to bells, foghorns, and perhaps the sound of breaking waves. A mule skinner, backing his rig, with its team of twenty mules into a borax loading station, responded to yelled audio commands. Under such circumstances, where both decision and system time constants easily exceeded one second, audio control worked and still works admirably.

In more recent times, intermittent audio control is used in an expanding variety of applications. Audio warning systems, which call for one or more human operator actions in response to a bell, whistle, woop, or siren, are seen everywhere - from the controversial atomic reactor scramming controls to the surly sounding automobile ignition on buzzer. Recently, electronically generated voice commands have been investigated and then applied as a possibly improved audio feedback control link. Simpson and Williams (6) investigated such an audio control link in the context of aircraft collision avoidance; specifically they discussed the ground proximity warning system which is now being installed in commercial airlines, and which electronically yells "Whoop, Whoop - Pull up! Pull up!" Here again, a discrete action or set of actions is required in response to the audio signal, and the audio systems appear to work admirably.

Vinje, who wrote his Ph.D. thesis on audio compensatory tracking, has written several papers dealing with aural compensatory tracking. His 1972 paper, co-authored with Pitkin (9), enumerates several early investigations of a pilot's ability to control an aircraft in response to audio control signals; including DeFlorez's (1) 1936 paper dealing with "True blind flight", Forbes et al.'s (2) 1957 description of the "Flybar" experiments, (Flybar = Flying by auditory reference), and Katz, et al.'s (3) 1966 paper concerning "***Acoustic displays*** in a simulated aerospace vehicle".

Conversely, when continuous manual responses are required of an operator in response to an audio control input, the quality of system performance reported in the literature is somewhat vague. A small to fair amount of experimental work can be found in the literature, primarily dealing with flying an airplane blind under instrument flight rules (IFR), with a primary flight display instrument, such as a pitch, roll, or yaw display replaced by some sort of audio whistle, chirp, buzz or other continuously variable aural display.

1972 was a good year for audio manual tracking papers. Mirchandani (4) discussed, "An Auditory Display in a Dual-Axis Tracking Task", based upon his MIT Master's thesis of 1971. Mirchandani suggested that "supplementary auditory displays in existing systems, such as, in airplanes (especially helicoptors and VTOL) *** could improve the performance of the operators and make the systems more efficient". Vinje wrote his second paper of 1972 (8) on audio displays for IFR Hover Control, and presented the results at almost the exact same time that Mirchandani suggested the application.

Vinje concluded that, "*** pilots could control an aurally displayed function and another visually displayed function better that if the two functions were both presented visually and separately displayed".

That is, Vinje concluded that audio tracking could be superior to visual tracking, when more than one display had to be simultaneously tracked.

This is directly opposed to the conclusion reached three years later,

in 1975, by Uhlemann and Geiser (7), when they reported on "Multivariable Manual Control with Simultaneous Visual and Auditory Presentation of Information". Uhlemann and Geiser specifically state that "*** visual displays are indispensable". Furthermore, if visual displays are widely separated, by, say 70 degrees of arc, so that the pilot must turn his head to watch various displays, then, in this case, auditory support of the visual display can help - but - "the auditory support should be attached to the least important control system". This is exactly opposite to Vinje's 1972 conclusion, that "An audio display was most effective when it presented a signal which was important to the pilot, e.g., a nonredundant signal which changed rapidly and which was directly related to a controlled variable".

Clearly, uniform agreement on the value of auditory control does not presently exist.

Furthermore, agreement on the most suitable type of audio display does not exist either. Vinje found the best display to be continuously varying tones from 330 to 4300 hz., interrupted near the zero error point, and presented to either the left or the right ear as the operator's input function switched sign. Vinje's audio display is illustrated in Figure 1. Uhlemann and Geiser found the best display to be a constant frequency 800 hz. tone, of varying amplitude or volume, presented to either the left or the right ear as the operator's input functions switched sign. Uhlemann and Geiser's audio display is illustrated in Figure 2.

To the best of my knowledge, none of these experimentally investigated audio-control systems has seen the light of day to day use. Intermittent or discrete audio-manual control systems do not exist in quantity. Continuous audio-manual control systems do not exist in quantity.

However, at least one continuous audio-manual control system does commercially exist and is used with same degree of regularity.

This investigation was prompted by several recreational glider pilots, who commonly employ a device called an audio variometer to adjust their flight path. The audio variometer is a sensitive differentiating altimeter, which produces an audio output proportional to the glider's rate of climb (or rate of sink, as the case may be). If the glider is climbing, the pitch of the audio tone output climbs, if the glider is falling, the audio pitch falls. The glider pilot is thus able to adjust his control tactics in response to the audio tone output, and use his eyes for enjoying the scenery. Figure 3 displays the response of such an audio variometer.

AUDIO VARIOMETERS

Several types of Audio Variometers are marketed by the firm of GRAHAM THOMSON LTS.,* who kindly supplied the information concerning variometers that is presented here. A most significant point concerns the establishment of a set point or zero point, when continuous audio tones are employed to convey information which varies both in magnitude and in polarity, or

algebraic sign.

Consider the tone assignments, shown in Figure 4, which were used for one experiment concerning a model for a "Zero-Reader" Speed Director and Variometer (A Compensatory Tracking System).

A relatively high audio frequency of 3000 hz. as shown in Figure 4 represented the maximum positive error in the flight vector allowed, and a relatively low audio frequency of 333 hz. represented the maximum negative error allowed. The geometric midpoint frequency of 1000 hz. represented the set point ot zero error. For compensatory tracking, the human operator or pilot wishes to keep the error at zero. For the audio case illustrated in Figure 4, this means keeping the audio tone at the zero set point of 1000 hz. Zero error does not correspond to zero sound or zero frequency, but rather to some intermediate frequency. Without a sense of perfect audio pitch, keeping a frequency reference in mind is extraordinarily difficult, if not impossible. Hence, another audio tactic is almost invariably employed to distinguish positive errors from negative errors, and to indicate zero or tolerably small errors.

The commercial "Cambridge Triple-Range Variometer with Speed Director and Mark II Audio" uses an interrupted tone for positive rate of climb errors and a continuous whistle tone for negative rate of climb errors. This is illustrated in Figure 5.

Note that the audio information is identically displayed to both ears. Glider pilots do not usually wear earphones, which essentially precludes switching the tracking signal from the right ear to the left ear as the signal changes sign. Thus, the audio display modes favored by Vinje or Uhlemann and Geiser are not used in this particular application of audio manual tracking to the control of a glider.

Several glider pilots with thousands of hours of experience were interviewed, and two of them claimed that the audio variometer was a big improvement over the visual variometer. A third stated that he liked it at first, but later stopped using it entirely, because the whistle got on his nerves. The two pilots who held favorable opinions concerning the effectiveness and usefulness of the audio variometer also mentioned that they often disconnected or turned down the audio output in order to hear the rush of the wind, or just plain silence.

This application of audio manual tracking by glider pilots was the first and only such application the author has knowledge of. Commercial airline pilots, NASA researchers, and every control expert that was questioned agreed that actual applications of audio-manual tracking were as rare as a quiet politician in an election year - that is, there were not any applications at all, aside from the glider system.

*Graham Thomson Ltd., 3200 Airport Avenue
Santa Monica, California 90405 (213) 398-4714

EXPERIMENTAL APPARATUS

The investigation consisted of a simulation, flown by students who, with only one exception, had no musical training. The basically simple experimental set-up is depicted by the block diagram of Figure 6. The TR-20 analog computer generated the single sine wave input signal, and formed the system error in response to the input signal and the system dynamics modeled by the analog computer. The results presented later on deal only with the case of unity controlled dynamics, although other higher order dynamics were investigated. A NOVA model 1200 digital computer sampled the system input signal (sine and cosine components), the operator's input signal (which was the system error), and the operator's output signal (which was the system output for unity dynamics). Sampling was performed ten times a second, and the analog information was digitized, and stored on a magnetic disk file for later data analysis. Figure 7 displays the major digital components utilized.

The simulation was run as part of a special projects electrical engineering course taught at the Cooper Union in N.Y.C. One group of students designed and built the multiplexer, another group built the analog to digital converter and the requisite computer interface, another group built the digital to analog converter and computer interface, and the last group built the voltage controlled oscillator and amplifier, which produced the actual audio output signal. After much trial and an astounding amount of error, the entire instrument package was pronounced up and running all in its own bright blue relay rack. Funding was obtained from the field, stream and sponge department, with the exception of a $200 hard cash IEEE research prize won by the supervising student group that performed the actual experiment.

RESULTS

The results of the audio-manual glider pilot tracking simulation are bothersome. The results appear to indicate that audio-manual tracking is decidedly inferior to visual manual tracking - even though some glider pilots claim otherwise.

To allow for a ready comparison of results, the three minute tracking runs were performed by the same subject three different ways. The subject performed via audio tracking alone, via visual tracking alone, and via audio plus visual tracking.

The order of runs was reversed, to see if this made any difference. It did not. Several different audio diaplays were used. Some were clearly inferior, some were clearly superior. Head phones were superior to a loudspeaker, even with no ear switching - apparently the phones cut our extraneous audio noise. A pure variable tone signal with no absolute zero reference was cleary inferior. See Figure 8. The best audio tracking signal found in these experiments is shown in Figure 9. The signal consists of a continuously variable tone of constant amplitude, to which is

added a constant center frequency tone, corresponding to a zero error. When the tracking tone equals or is nearly equal to the center frequency reference tone, beats are heard. The beats grow lower in frequency as the error is nulled out, from either error polarity. Zero error yields zero beat, an extremely easy to perceive condition. Large errors produce tones of either high or low frequency, which clearly give polarity information.

Without such polarity information, sign reversals are common - the operator does not know which way to move his stick. An example of polarity reversal is shown in the recordings of Figure 10, for the case of audio-manual tracking with no zero tone reference. Figure 11 shows the operator's response for the case of compensatory visual manual tracking, using an oscilloscope display. It is effectively identical to Figure 12, which shows the operator's response for the case of compensatory audio-visual-manual tracking, with a zero beat reference tone. In both these cases, the data indicate an approximate magnitude corner frequency of approximately 0.4 hz. When the very best data for the compensatory audio-manual tracking task with a zero beat reference tone is examined, the approximate magnitude corner frequency is found to be slightly less than .2 hz, or almost an octave lower than the visual case. Note that these frequencies are all significantly lower than the figures generally reported for trained operators performing tracking experiments.

CONCLUSIONS

This data indicates that visual tracking performance enjoys a bandwidth advantage nearly double that for audio-manual tracking, for the idealistically simple case of unity dynamics and a single axis tracking task, with sinusoidal inputs. It is interesting to note that the single students who had had musical training learned far faster than the other students, and consistently outscored them in minimizing total mean square error.

In conclusion, it may be worthwhile to speculate upon how a glider pilot actually utilizes his audio variometer. It is the author's opinion that the glider pilot does not continuously track the audio signal, but rather uses it in an intermittant fashion, to provide directional goals for his flight path, which he controls via visual tracking of the horizon and other visual cues. That is, it is conjectured that the glider pilot actually uses visual information for the second by second fine control of his glider, and uses the audio variometer to provide relatively long term information concerning his overall performance (is he going up? or down?) which he then uses to alter his flight strategy, in a long term fashion.

REFERENCES

1. DeFlorez, L., "True Blind Flight", Journal of The Aeronautical Sciences, Vol. 3, March 1936, pp. 168-170.

2. Forbes, T.W., Garner, W.R., and Howard, J.G., "Flying by Auditory Reference ("FLYBAR")" Applied Experimental Psychology - Human Factors in Engineering Design, Chapanis, A., Ed., New York, N.Y., John Wiley & Sons, 1957, Ch. 9.

3. Katz, D., et al., "Experimental Study of Acoustic Displays of Flight Parameters in a Simulated Aerospace Vehicle", NASA Technical Report, CR-509, July 1966.

4. Mirchandani, Pitu, B., "An Auditory Display in a Dual-Axis Tracking-Task", IEEE Transactions on Systems, Man, and Cybernetics, Vol. SMC-2, No. 3, July 1972, pp. 375-380.

5. Pitkin, Edward T., and Vinje, Edward W., "Comparison of Human Operator Critical Tracking Task Performance with Aural and Visual Displays". IEEE Transactions on Systems, Man, and Cybernetics, March 1973, pp. 184-187.

6. Simpson, C.A., and Williams, D.H., "Human Factors Research Problems in Electronic Voice Warning System Design", Eleventh Annual Conference on Manual Control, Ames Research Center, Moffett Field, California, NASA TM X-62, 464, May 1975, pp. 94-106.

7. Uhlemann, Hartmut, and Geiser, George, "Multivariable Manual Control with Simulataneous Visual and Auditory Presentation of Information", Eleventh Annual Conference on Manual Control, Ames Research Center, Moffett Field, California, NASA TM X-62, 464, May 1975, pp. 3-18.

8. Vinje, E. Wayne, "Flight Simulator Evaluation of Audio Displays For IFR Hover Control", Proceedings of the Eigth Annual Conference on Manual Control, held at the University of Michigan, AFFDL-TR-72-92, May 1972, pp. 625-649.

9. Vinje, Edward W. and Pitkin, Edward T., "Human Operator Dynamics for Aural Compensatory Tracking", IEEE Transactions on Systems, Man, and Cybernetics, Vol. SCM-2, No. 4, Sept. 1972, pp. 504-512.

Figure 1 - Pilot's Input Signal, Varying Tone, From Vinje (8)

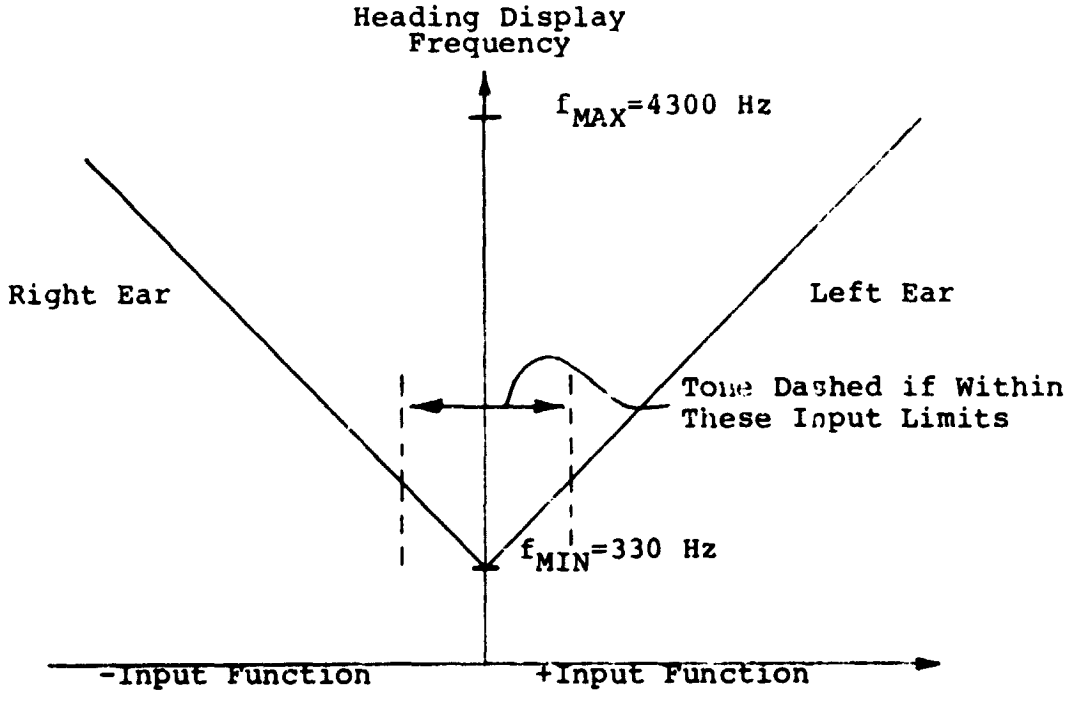

Figure 2 - Pilot's Input Signal, Varying Volume,
From Uhlemann and Geiser (7)

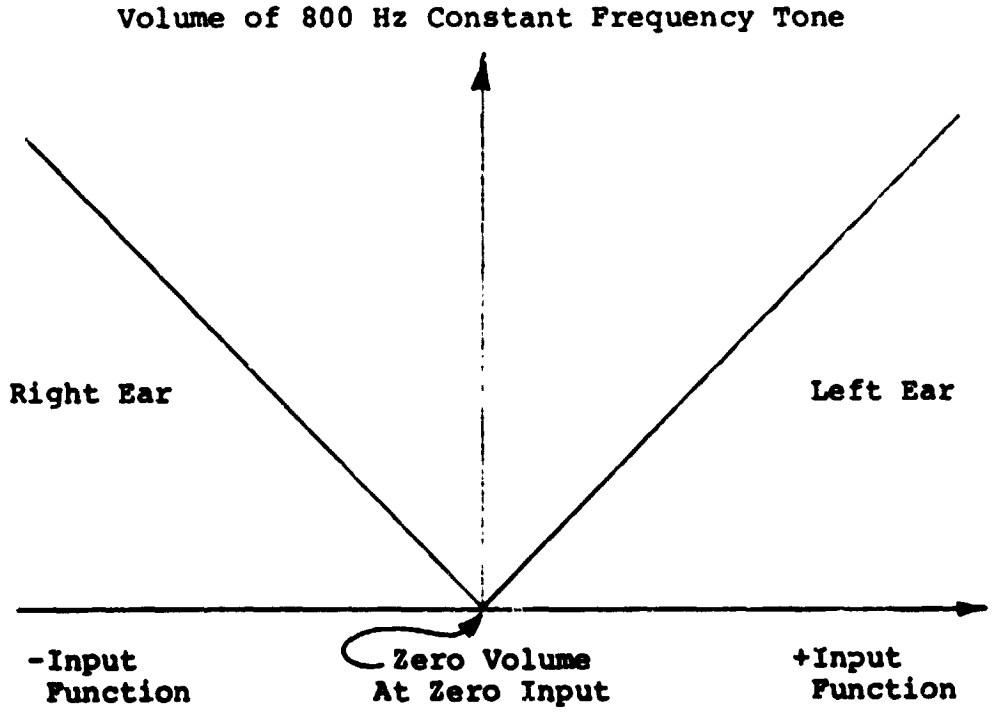

Figure 3 - Response Of The PIEP Audio Unit For Variometers

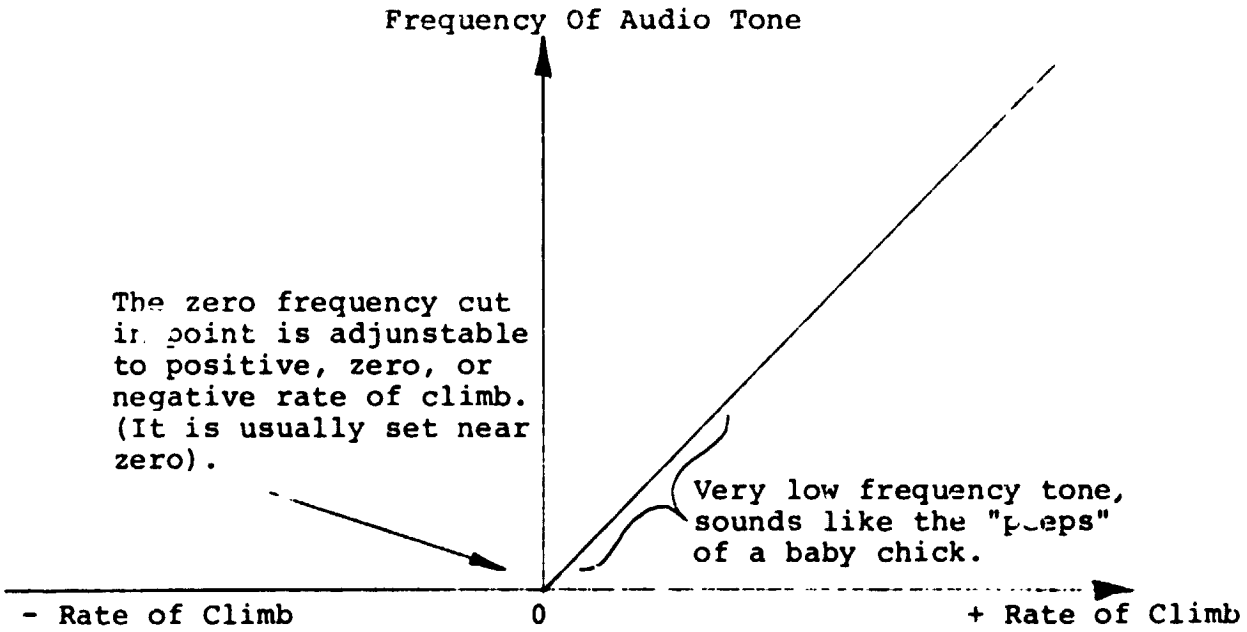

Figure 4 - Continuous Audio Pitch Versus Flight Vector Error For A Model Of A "Zero-Reader" Speed Director And Variometer (Compensatory Tracking System)

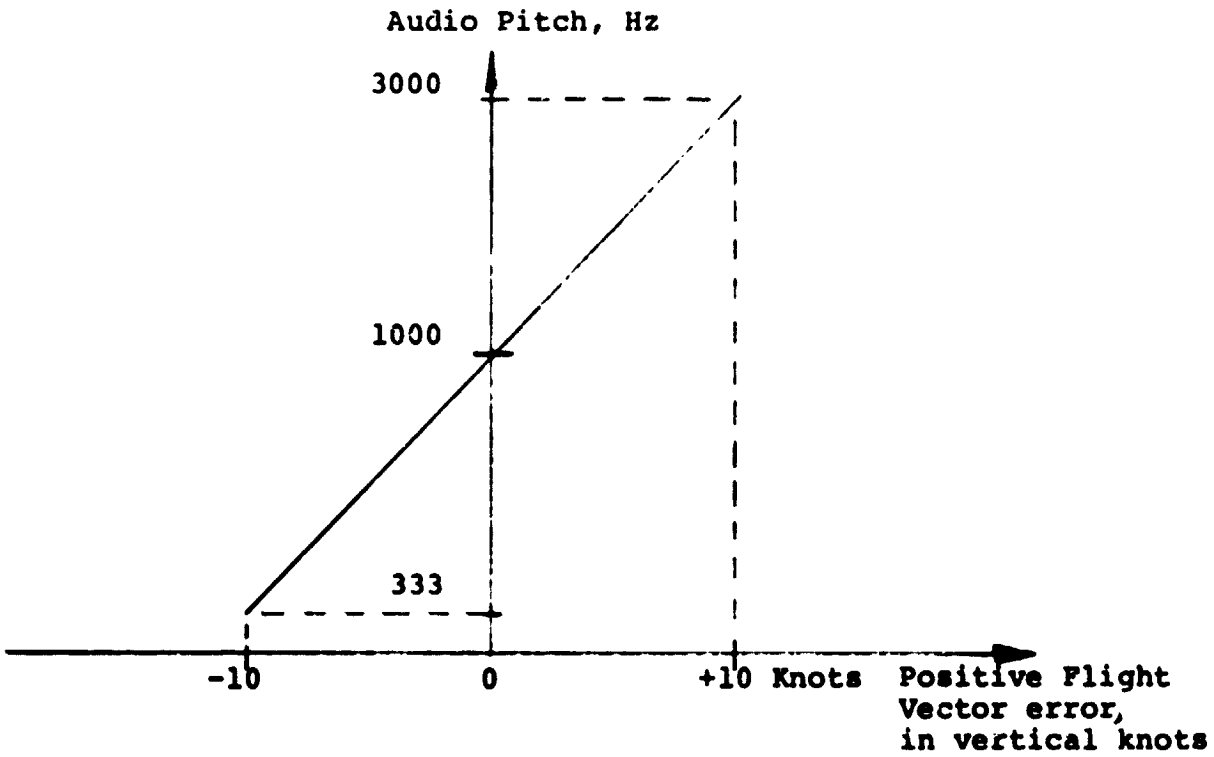

Figure 5 - Audio Output Of The Cambridge Triple-Range Variometer With Speed Director And Mark II Audio Unit

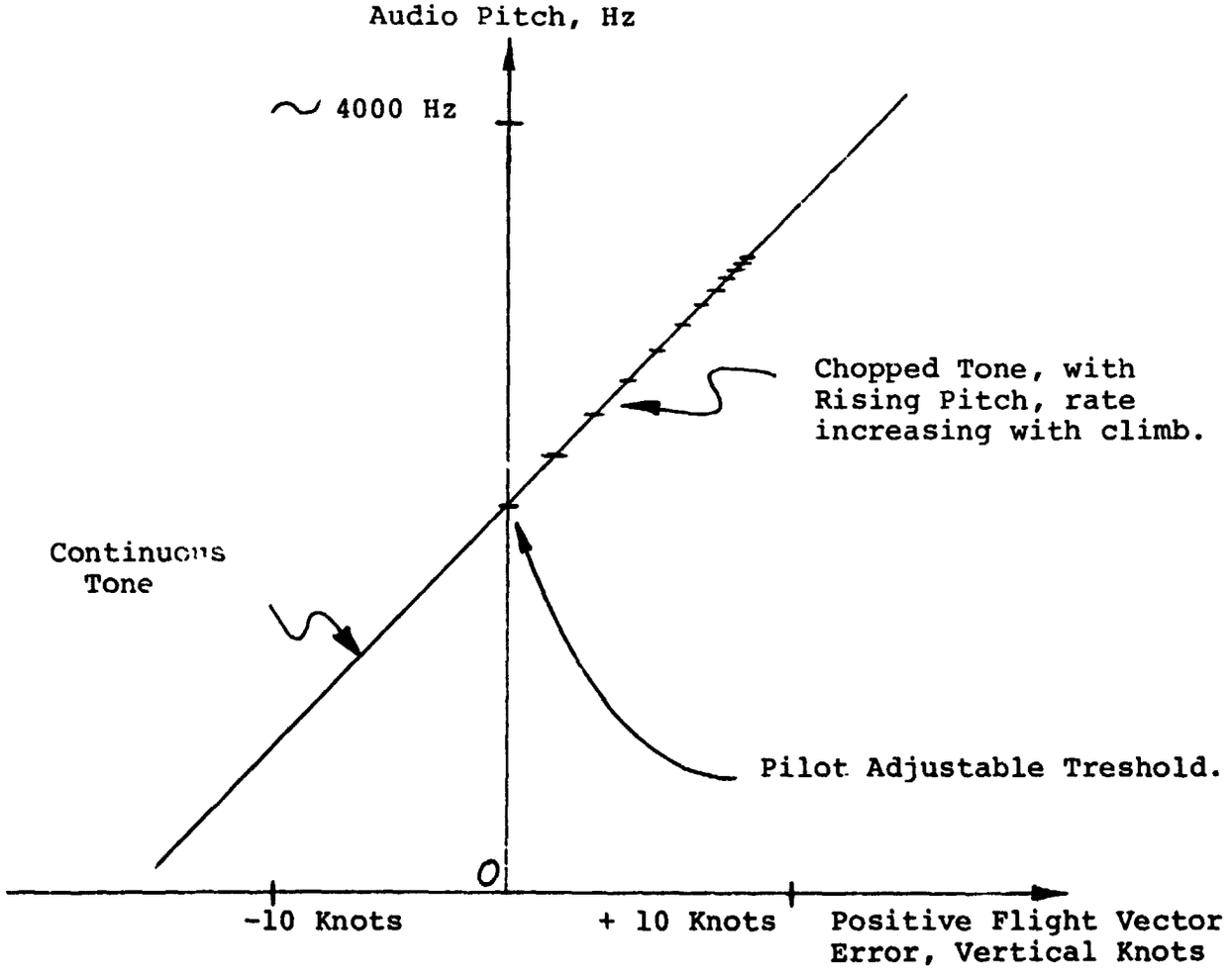

Figure 6

ANALOG SIMULATION SEGMENT OF THE
COMPENSATORY AUDIO-MANUAL TRACKING EXPERIMENT

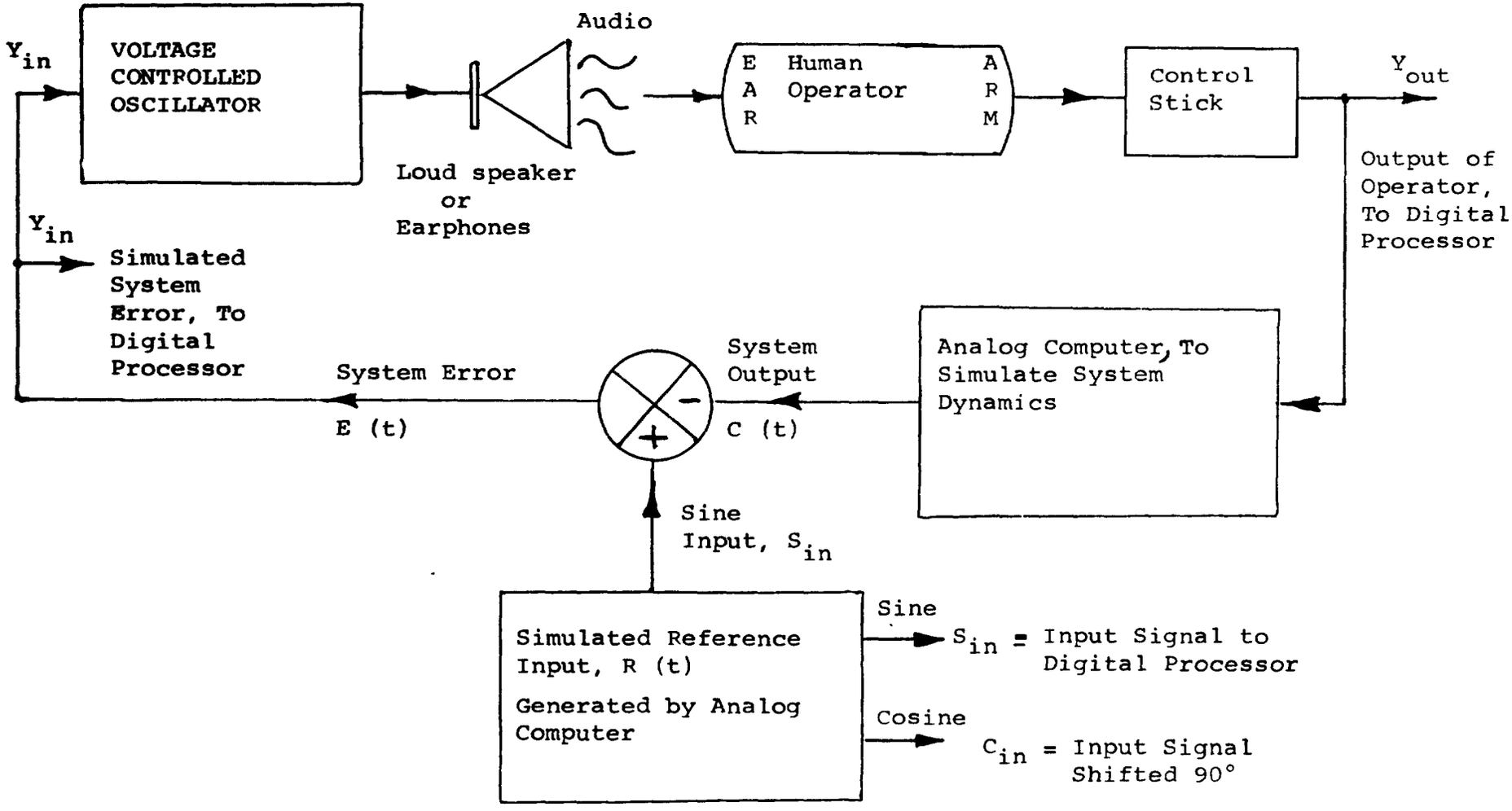

Figure 7 DIGITAL DATA PROCESSING SEGMENT OF THE AUDIO-MANUAL TRACKING EXPERIMENT

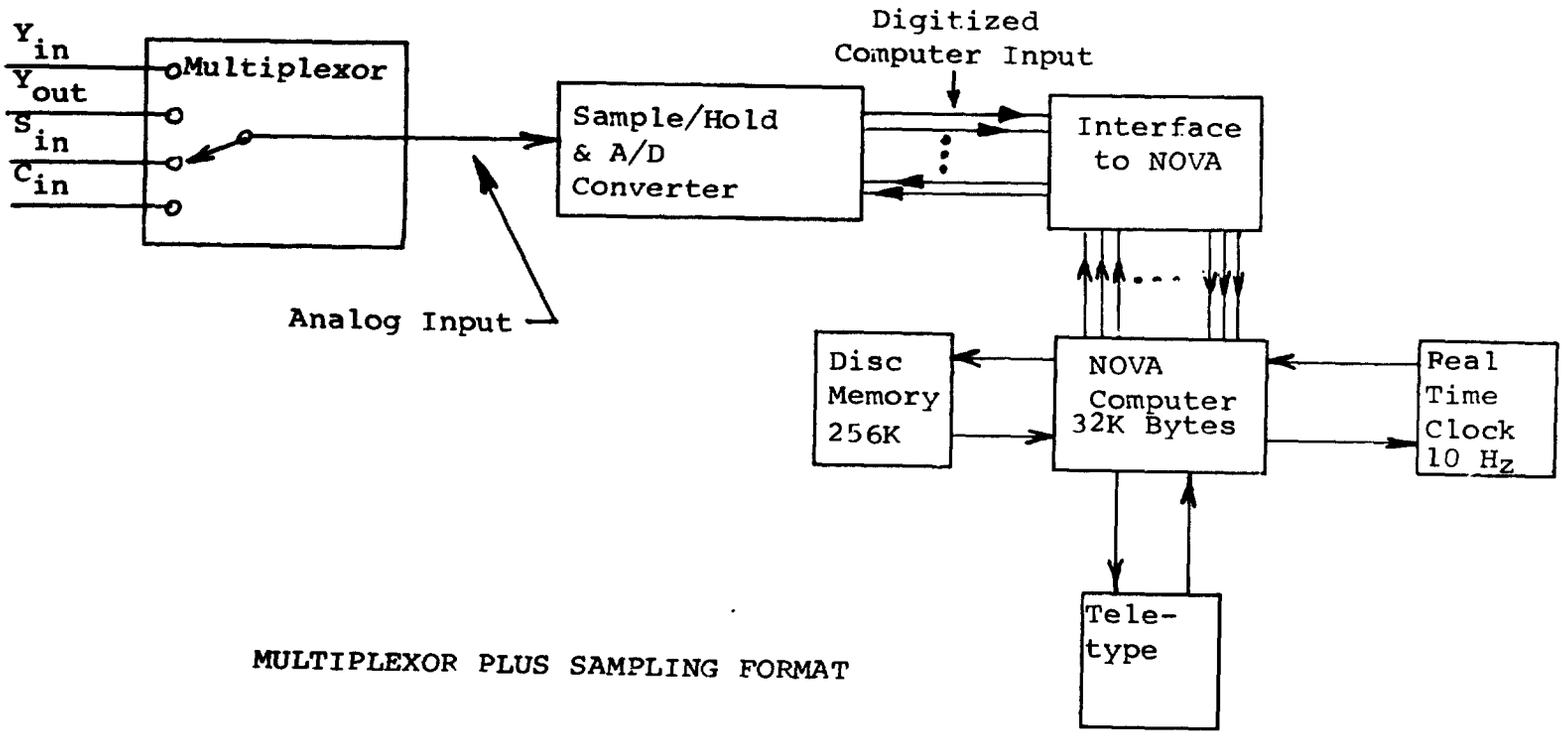

MULTIPLEXOR PLUS SAMPLING FORMAT

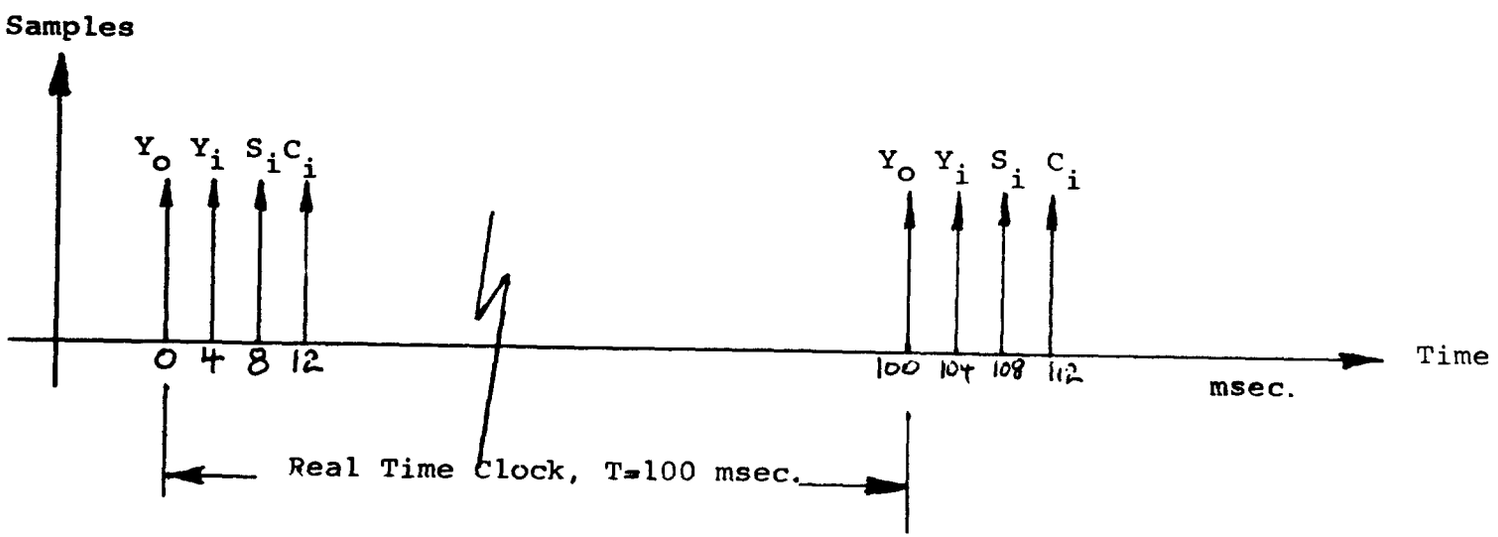

Figure 8_a - Compensatory Audio Manual Tracking Performance With No Zero Reference Tone

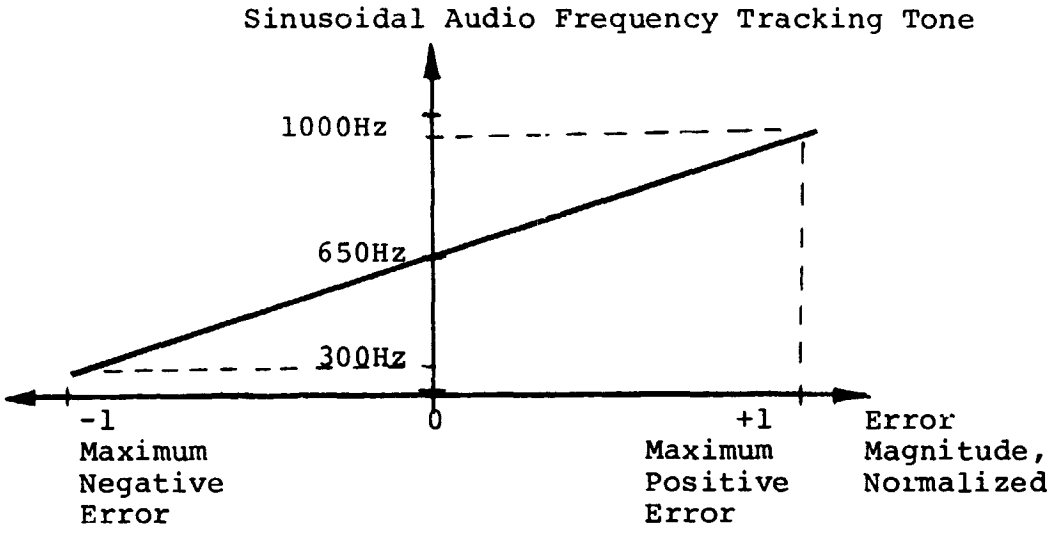

Figure 8_b - Normalized Operator's Response to Single Sinusoidal Inputs (average of 10 runs)

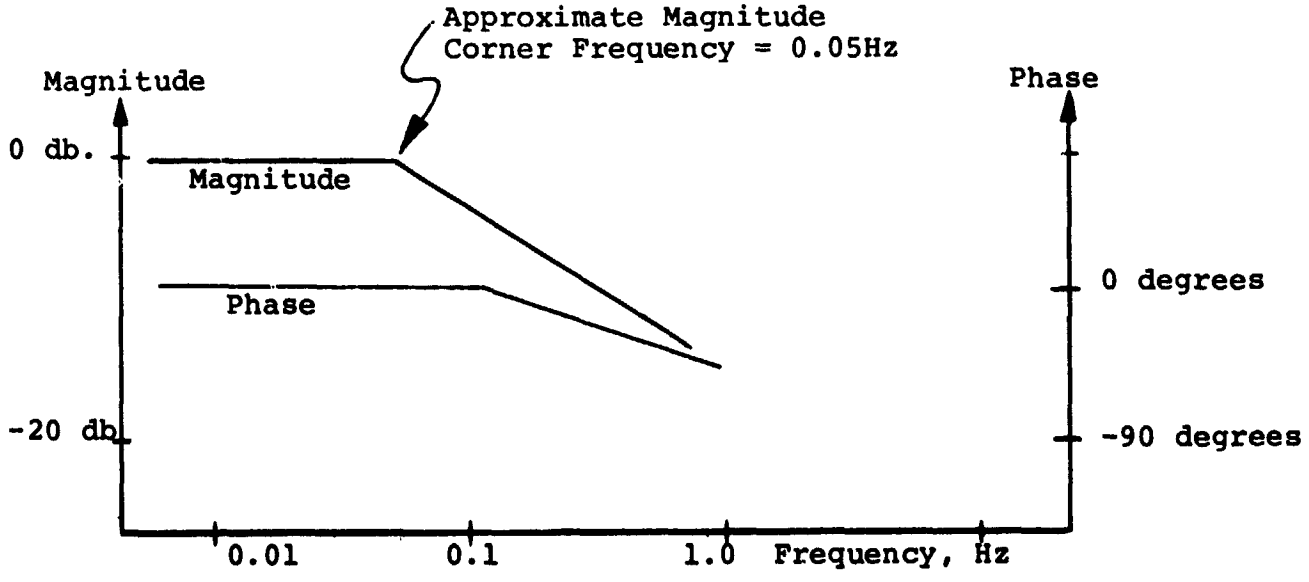

Figure 9_a - Compensatory Audio-Manual Tracking With A Zero Beat Reference Tone

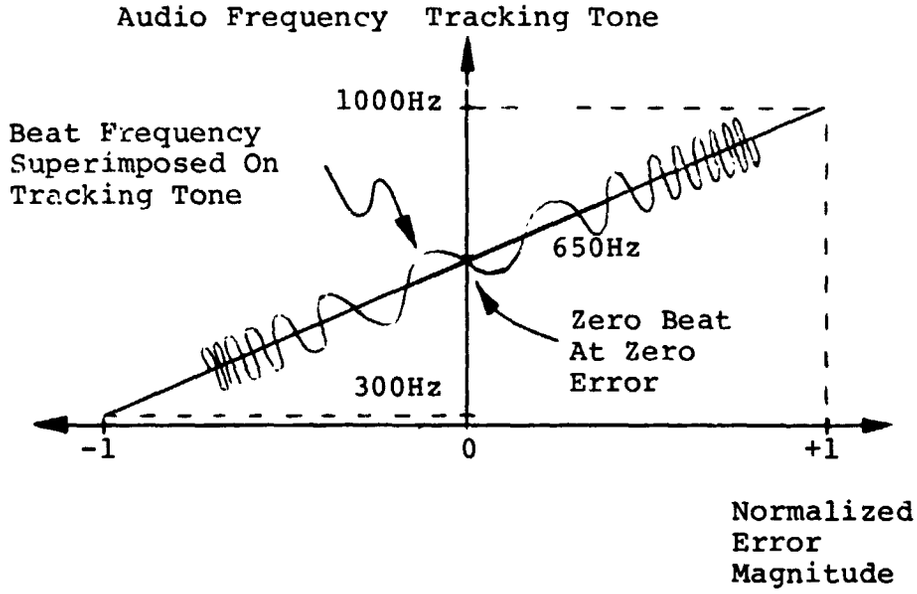

Figure 9_b - Operator's Performance For Compensatory Audio-Manual Tracking With A Zero Beat Reference Tone

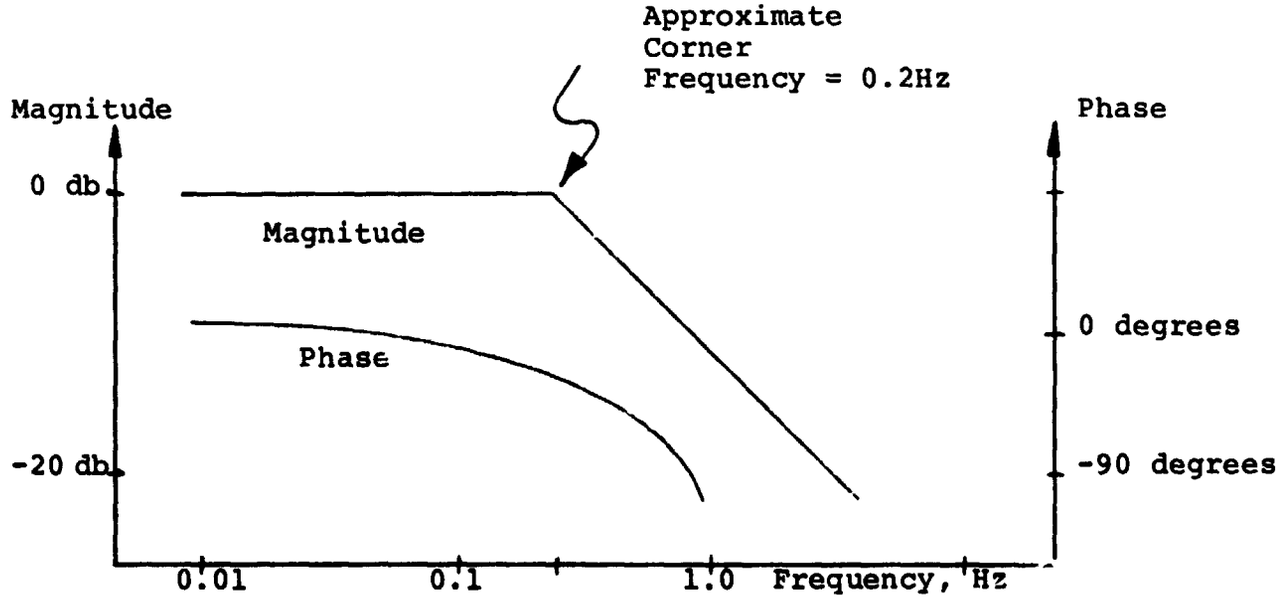

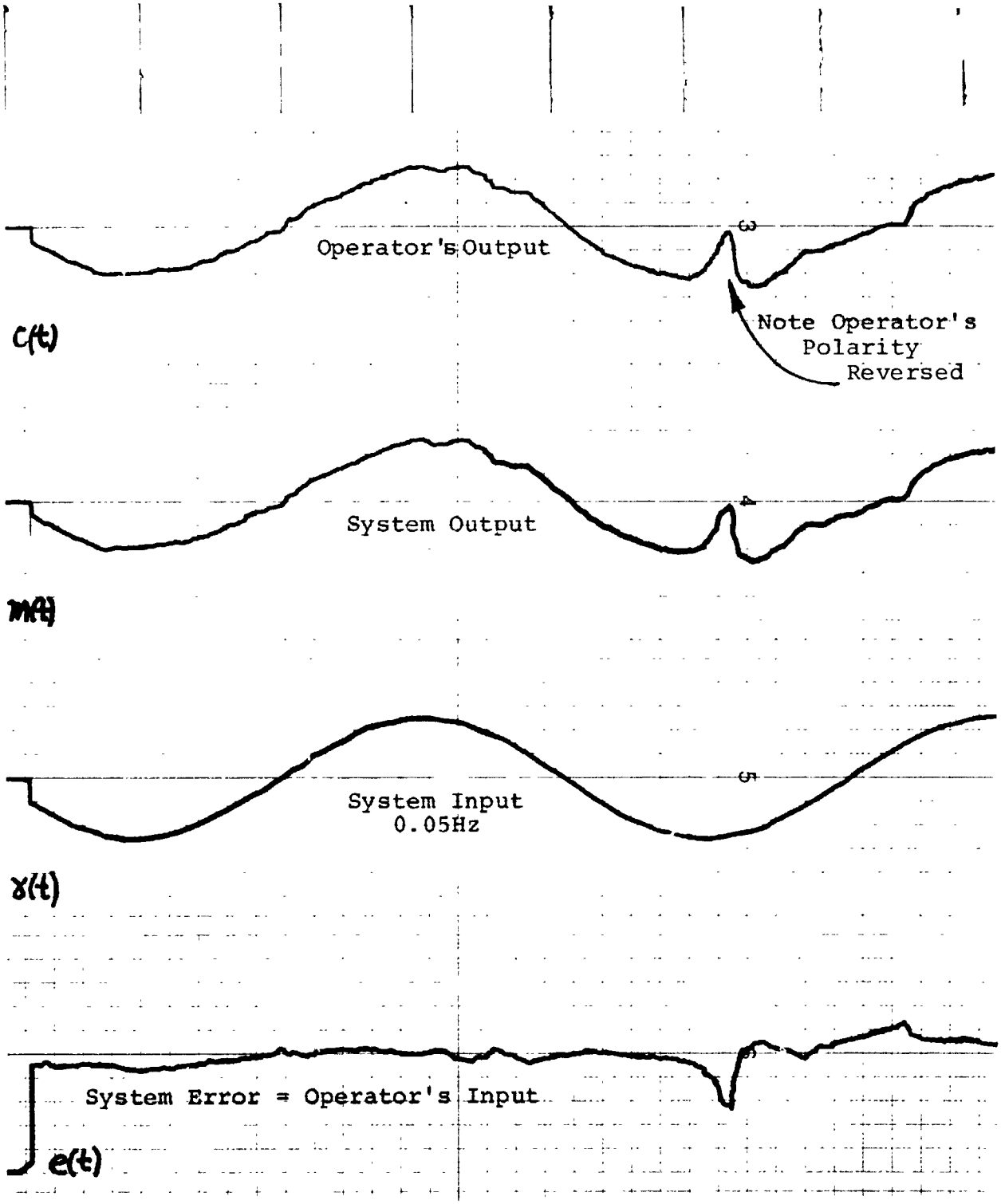

Figure 10 - Analog Outputs Recorded From An Audio-Manual Tracking Simulation Utilizing A Pure Tone Signal With No Zero Reference Tone. (As shown in Figure 4)

Figure 11 - Compensatory Visual Manual Tracking Performance, Oscilloscope Display, 10 runs of 3 minutes

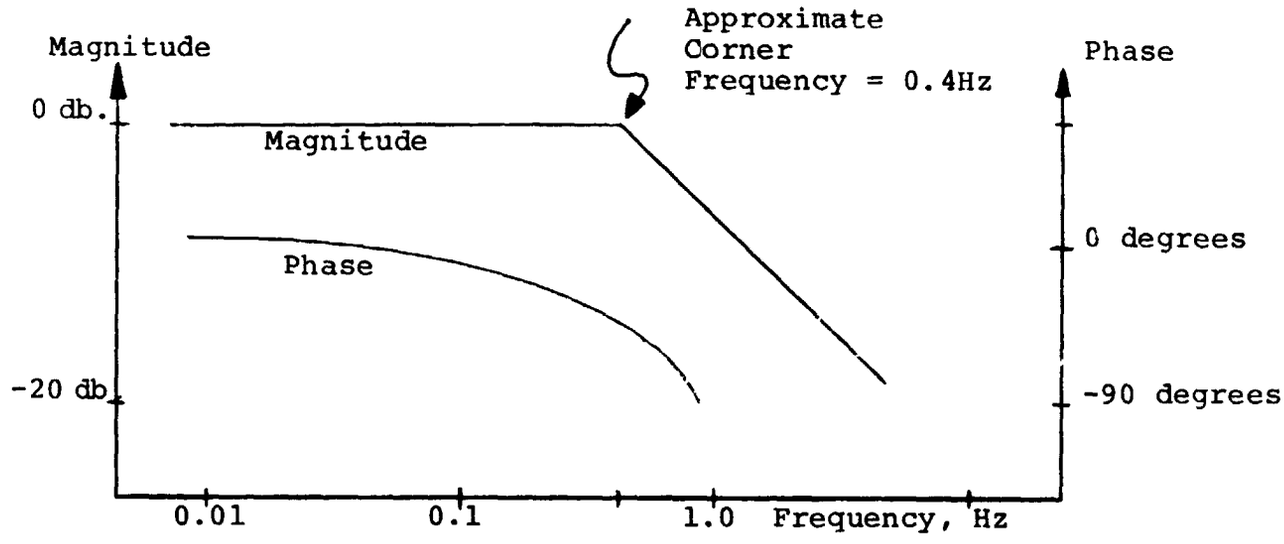

Figure 12 - Compensatory Audio-Visual Manual Tracking Performance, With A Zero Beat Frequency Reference Tone, And Oscilloscope Display.

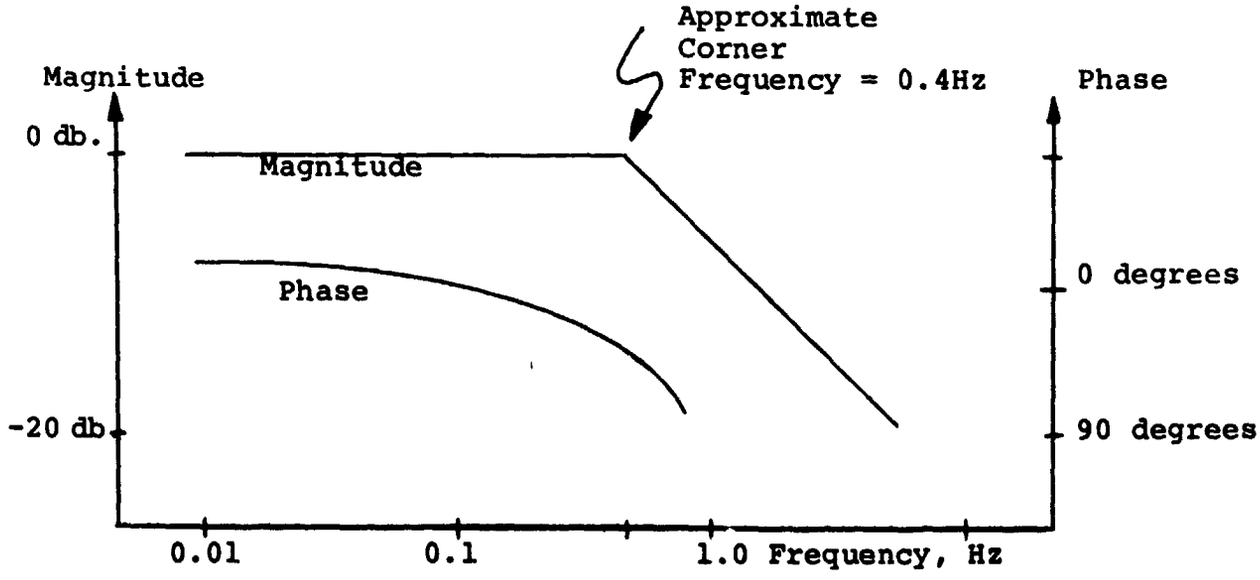

EYE TRACKING: HORIZONTAL VS. VERTICAL

By John Hornseth, Gary Stanley, James Porterfiel
Crew Station Integration Branch
Human Engineering Division
6570 Aerospace Medical Research Laboratory
Wright-Patterson AFB, Ohio 45433

Paul Carson
University of Dayton Research Institute
300 College Park Avenue
Dayton, Ohio 45409

SUMMARY

The Honeywell Remote Oculometer was used to obtain eye pursuit tracking data on eight subjects. A three-minute recording of Gaussian noise, bandwidth limited to 1.5 Hz served as the forcing function. A galvo-laser system rear projected the forcing function onto a vertical viewing screen as a spot of light randomly moving in one dimension (horizontally or vertically) with a maximum excursion of $\pm 5^{\circ}$ visual angle as viewed by the subject. Each subject tracked the forcing function twice vertically and twice horizontally in a balanced design. Frequency analysis of the data showed: (1) coherence values were essentially the same for both horizontal and vertical eye tracking, (2) average vertical gain (.70) was significantly higher than average horizontal gain (.62) with both showing no drop with frequency, and (3) phase was essentially the same for both vertical and horizontal eye tracking, was linearly correlated (-.99) with frequency, and could be represented as a transport delay of .125 seconds.

INTRODUCTION

Stated similarities, or differences, between horizontal and vertical eye tracking capabilities, in smooth pursuit tracking, are based upon meager experimental evidence. This study was designed to obtain substantial eye tracking data on eight subjects. Of specific interest were possible differences in coherence, gain, and phase.

APPARATUS

A three-minute recording of a Hewlett-Packard 3722A Noise Generator, set at infinite sequence length and at 0.0 to 1.5 Hz Gaussian Noise Bandwidth, served as the forcing function. An optical projection system consisting of a low power laser and a pair of galvo-mirrors rear projected the forcing function onto a cloth screen in the form of a 1/2" diameter spot of red light

randomly moving in one dimension, either horizontally or vertically, about a center spot marked on the screen. The maximum excursion of the forcing function was $\pm 5°$ visual angle, as viewed by the subject. The $\pm 5°$ visual angle positions were also marked on the screen and, along with the center spot, served as calibration points for both the forcing function and the subject's eye movement response. The subject tracked the forcing function from a position on the opposite side of the screen from the optical projection system and equidistant from the screen.

The subject's eye line-of-sight was computed using the AMRL Honeywell Remote Oculometer. For a complete description of the Oculometer see reference 1. Calibration of the Oculometer prior to each tracking run was accomplished by using a second optical projection system positioned adjacent to the forcing function optical projection system. The Oculometer-driven laser spot was turned off during the tracking run.

Five channels of a seven channel 1/2-inch Ampex 300 instrumentation tape recorder were used to record: (1) time code, (2) forcing function on horizontal runs, (3) forcing function on vertical runs, (4) horizontal eye movements, and (5) vertical eye movements.

PROCEDURE

Eight male students from the University of Dayton were tested using an ABBA order of presenting the horizontal and vertical tracking runs. Four subjects were given the horizontal run first and four subjects were given the vertical run first in a balanced design. After seating the subject, the operation of Oculometer was checked and calibrated. The subject was instructed to sit in a natural, comfortable position. The only constraint placed upon the subject was the instruction to refrain from making large head movements. The subject was not given any practice trials. The subject was instructed to follow (pursue) the moving spot of light with his eyes as the spot moved horizontally (or vertically) on the screen. The subjects were screened for uncorrected 20/20 vision. Between runs subjects were given a short rest while the forcing function tape was rewound to its starting position and the equipment calibration was checked.

RESULTS

Frequency analyses of the tracking sessions for the eight subjects were accomplished by the Dynamics Technology Applications Branch (AFDL/FBG) at Wright-Patterson Air Force Base. For each run the power spectral density of the forcing function, the power spectral density of the eye response output, the cross power spectral density, the cross correlation, the coherence, and the transfer functions in gain and phase were computed. Only the statistical analyses of these data are presented in this report. Development of a de-

scriptive model representing subjects' performances will be accomplished at a later date.

The data for the two horizontal runs and for the two vertical runs for each subject were averaged for each of fifteen frequency points between 0 and 1.5 Hz. Analyses of variance were performed on these averaged data to obtain the horizontal and vertical comparisons presented in this report.

An 8 x 2 x 15 analysis of variance was performed on the coherence, gain, and phase data. The results of these analyses are presented in Tables I, II, and III for coherence, gain, and phase respectively. Plots of coherence by frequency, gain by frequency, and phase by frequency were obtained by averaging the data across subjects for each axis (Figures 1, 2, and 3).

The analysis of variance of the coherence data (Table I) shows no significant difference between horizontal and vertical coherence. In addition, there was no significant interaction between axes and frequency. However, the effect of frequency on coherence was significant and can be observed in Figure 1.

Vertical gain was significantly higher than horizontal gain (Table II and Figure 2). Vertical gain, averaged across subjects and frequency, was .70 and average horizontal gain was .62. No interaction between axis and frequency was present as can be observed in Figure 2.

No significant difference between horizontal phase and vertical phase was observed (Table III and Figure 3) although a small, but significant, interaction between axis and frequency was found. The increase of phase lag with frequency was highly significant. The regression of phase and frequency for both axes is plotted in Figure 4. Both horizontal and vertical phase showed a high linear correlation (-.99) with frequency. The slopes of the regression lines, -71.13 for the horizontal data and -66.85 for the vertical data, represent transport delays of .131 seconds and .119 seconds for horizontal and vertical eye tracking respectively. (The transport delay of 1/15 sec introduced by the Oculometer was subtracted before computing these values.)

DISCUSSION

The major finding of this study was the significantly higher vertical gain as compared with the horizontal gain. This result confirms the observation made last year by Shirachi and Black (Reference 2). However, two of the eight subjects tested showed slightly higher horizontal than vertical gains. Further study is planned to examine the range of these individual differences (emphasized by Huddleston in Reference 3) and the persistence of this observed horizontal-vertical gain difference with training.

Figure 3 does not appear to reflect the significant, but small, interaction between axes and frequency observed in the analysis of variance of the phase data (Table III). However, the difference in slopes of the regression lines shown in Figure 4 does reflect this interaction.

CONCLUDING REMARKS

In this study comparing horizontal and vertical eye tracking performance, vertical gain was found to be significantly higher than horizontal gain. No differences were found in coherence or in phase.

REFERENCES

1. Merchant, John; Morrissette, Richard; and Porterfied, James L: Remote Measurement of Eye Direction Allowing Subject Motion over one Cubic Foot of Space. IEEE Transactions in Biomedical Engineering, Vol. BME-21 No. 4, July 1974.

2. Shirachi, D.K.; and Black, J.H., Jr.: Head-Eye Tracking in Two-Dimensional Pursuit Tasks. Eleventh Annual Conference on Manual Control, NASA TM X-62, 464, 1975.

3. Huddleston, H.F.: Oculometer Pursuit of Vertical Sinusoidal Targets. Nature, Vol. 222, May 10, 1969.

TABLE I

ANOVA for Coherence

Source	Error Term	df	Mean Square	F
Axis (A)	AxS	1	0.0814	0.5458
Frequency (F)	FxS	14	0.0923	13.0216*
Subject (S)		7	0.4214	
AxS		7	0.1492	
FxS		98	0.0071	
AxF	AxFxS	14	0.0044	0.9451

* $p < .001$

TABLE II

ANOVA for Gain

Source	Error Term	df	Mean Square	F
Axis (A)	AxS	1	0.3810	6.6652*
Frequency (F)	FxS	14	0.0325	3.8734**
Subject (S)		7	0.2967	
AxS		7	0.0572	
FxS		98	0.0084	
AxF	AxFxS	14	0.0064	1.7109
AxFxS		98	0.0038	

* $p < .05$
** $p < .001$

TABLE III

ANOVA for Phase

Source	Error Term	df	Mean Square	F
Axis (A)	AxS	1	22.26	0.0980
Frequency (F)	FxS	14	13010.20	145.7360**
Subject (S)		7	1409.12	
AxS		7	227.21	
FxS		98	89.27	
AxF	AxFxS	14	60.57	1.8996*
AxFxS		98	31.88	

* $p < .05$
** $p < .001$

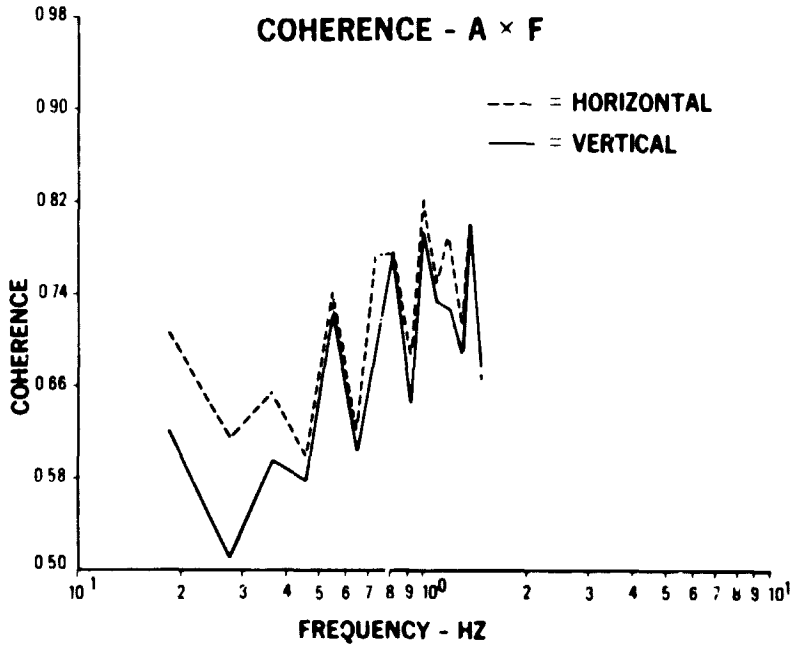

Figure 1. Horizontal and Vertical Conerence as a Function of Frequency.

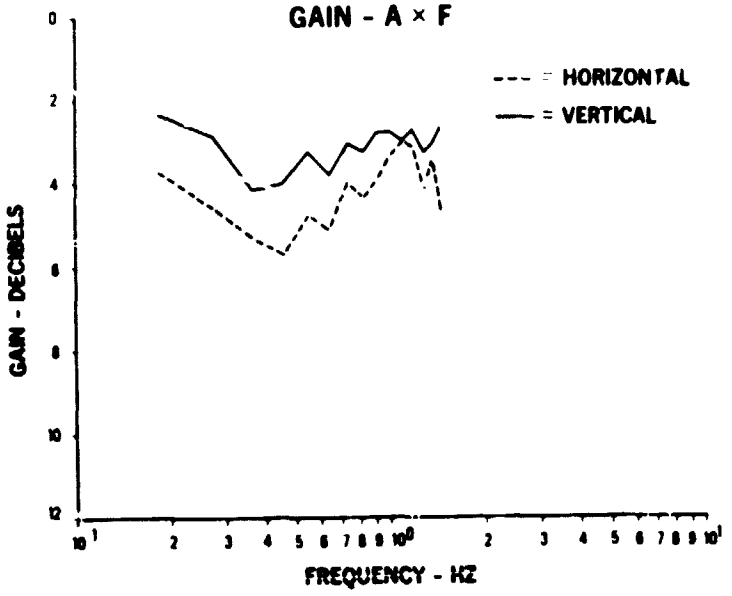

Figure 2. Horizontal and Vertical Gain as a Function of Frequency.

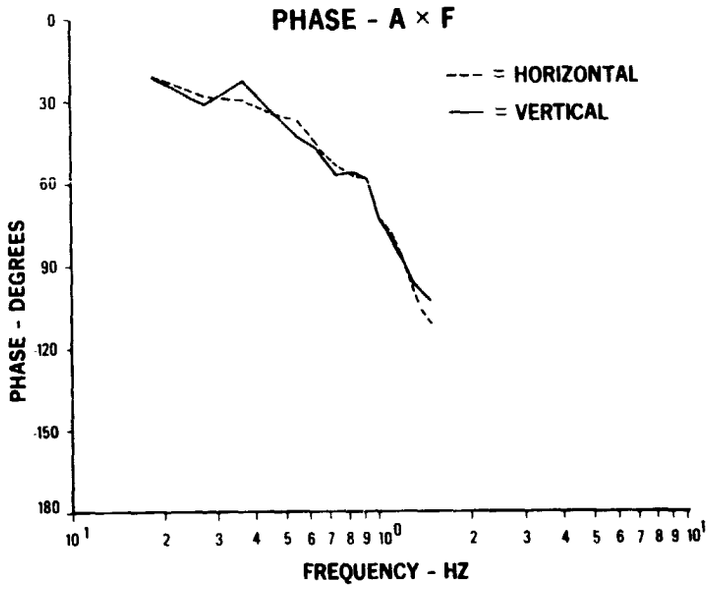

Figure 3. Horizontal and Vertical Phase as a Function of Frequency.

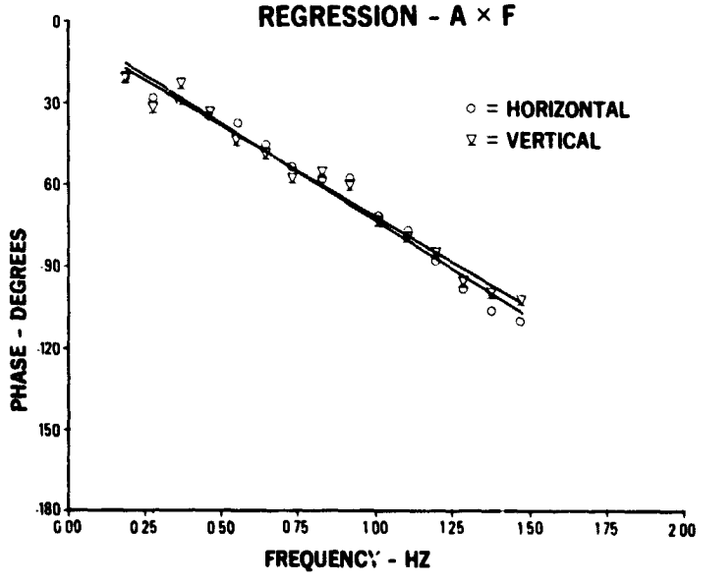

Figure 4. The Regression Between Frequency and Phase for Horizontal and Vertical Data.

HEAD TRACKING: A FATIGUE STUDY

By John Hornseth and Gary Stanley
Crew Station Integration Branch
Human Engineering Division
6570 Aerospace Medical Research Laboratory
Wright-Patterson AFB, Ohio 45433

Paul Carson
University of Dayton Research Institute
300 College Park Avenue
Dayton, Ohio 45409

SUMMARY

A Helmet-Mounted Sight was used to obtain two dimensional head pursuit tracking data on eight subjects. For each dimension, Gaussian noise, bandwidth limited to 0.5 Hz or 1.5 Hz, was alternately recorded (for four minutes and 2.5 minutes respectively) five times to obtain a 32.5 minute continuous forcing function. A galvo-laser system projected the forcing function as a (target) spot randomly moving in two-dimensions with a maximum excursion of $\pm 10°$ visual angle. The follower spot (computed head position) was projected by a second galvo-laser system. Frequency analysis of the beginning and final tracking periods for the 0.5 Hz tracking data revealed: (1) no change in horizontal or vertical coherence with trials; (2) a significant reduction in gain from trial 1 to trial 5; (3) a significant increase in phase lag from trial 1 to trial 5; (4) significant differences between horizontal and vertical tracking dimensions in coherence and phase lag; and (5) several significant higher order interactions involving trials, axes, and frequency. Coherence analysis of the 1.5 Hz tracking data revealed a breakdown in linear tracking performance.

INTRODUCTION

This study was conducted to determine whether extended continuous pursuit tracking in two-dimensions with a helmet-mounted sight would produce significant changes in tracking performance. Of specific interest were possible changes which might occur in coherence, gain, and phase.

APPARATUS

Gaussian noise was recorded for 32-1/2 minutes independently on two channels of an instrumentation tape recorder. The bandwidth of the noise generator was alternately set at .5 Hz, for four minutes, and then at 1.5 Hz, for 2-1/2 minutes, five times to make up a 32-1/2 minute, two-dimension-

al, forcing function consisting of a sequence of slow and fast tracking sessions.

An optical projection system consisting of a low-power laser and a pair of mirror galvanometers rear projected the forcing function onto a cloth screen in the form of a target spot of red light randomly moving in two dimensions about a center point on the screen. The maximum excursion of the forcing function in both X and Y dimensions was $\pm 10°$ visual angle, as viewed by the subject. Lower left and upper right 10° visual angle positions marked on the screen served as calibration points for both the forcing function and subject's line-of-sight, as computed by the helmet-mounted sight. The Honeywell Helmet-Mounted Sight (HMS) used in this study is described in Reference 1. The output of the HMS was used to drive a second optical projection system which produced the follower spot of light controlled by the subject. The subject tracked the target laser beam from a position on the opposite side of the screen from the optical projection system and equidistant from the screen.

Five channels of a second instrumentation tape recorder were used to record: (1) time code generator signal, (2) horizontal forcing function, (3) vertical forcing function, (4) horizontal (azimuth) head tracking response, and (5) vertical (elevation) head tracking response.

PROCEDURE

Eight male students from the University of Dayton served as subjects for this study. After seating the subject and adjusting the helmet as snugly and comfortably as possible to his head, the HMS was boresighted and calibrated for proper alignment and gain settings. The subject then tracked the forcing function (target spot) with his follower spot continuously for 32-1/2 minutes. Subjects received no practice trials prior to the experimental session. The helmet visor and reticle were up and out of sight during the tracking run.

RESULTS

Frequency analyses of the first and fifth slow-fast tracking sessions for the eight subjects of this study were performed by the Dynamics Technology Applications Branch (AFDL/FBG) at W-PAFB. Only a statistical treatment of the data is presented in this report. Development of a descriptive model representing subjects' performance will be accomplished at a later date.

Slow (.5 Hz) Tracking Data

The analysis of variance (Table I) of the coherence data for the first and fifth slow (.5 Hz) tracking runs showed no significant overall change in

coherence with extended tracking. However, the presence of significant higher order interactions indicates that changes did occur at specific frequencies (observable in Figure 1) and for specific axis by frequency combinations. The analysis also shows that while horizontal coherence was significantly greater than vertical coherence, this difference was also specific to certain frequencies (observable in Figure 2) and for certain frequency by trial combinations.

A significant reduction in gain from Trial 1 to Trial 5 was noted (Table II, Figure 3). However, a significant interaction between trials and frequency was present (observable in Figure 3). No overall difference between horizontal and vertical gain was found, but a significant interaction between axes and frequency was observed, as can be seen in Figure 4.

A significant increase in phase lag from Trial 1 to Trial 5 was observed with no interaction effect between trial and frequency (Table III and Figure 5). Vertical phase lag was found to be significantly greater than horizontal phase lag but a significant interaction between axes and frequency was present as can be seen in Figure 6. Linear regression plots of phase lag with frequency are shown in Figure 7, comparing Trial 1 and Trial 5, and in Figure 8, comparing horizontal and vertical axes. The coefficient of correlation for these regression lines are between -.98 and -.99. The slopes of the regression lines shown in Figure 7 for Trial 1 and Trial 5 are essentially the same and represent a transport delay of .176 seconds. The slopes of the regression lines shown in Figure 8 represent transport delays of .123 seconds for the horizontal axis and .232 seconds for the vertical axis. (A transport delay of 1/30 second introduced by the helmet-mounted sight was subtracted before computing these values.)

Fast (1.5 Hz) Tracking Data

Coherence values for the 1.5 Hz tracking runs averaged well below .5. Consequently the analysis of the gain and phase data was not considered appropriate. An analysis of variance of the coherence data was carried out (Table IV). The analysis reveals no significant trial effect, but a significant interaction between trial and frequency (Figure 9). Horizontal coherence was significantly higher than vertical coherence. However, a significant interaction between axes and frequency was also present (Figure 10).

DISCUSSION

The coherences observed for the fast tracking runs were surprisingly low. It is believed that the chief reason for these low coherence values was the subject's lack of experience in head tracking. A study to examine the effect of practice in head tracking upon subject's coherence scores, as a function of forcing function bandwidth, is planned. Further study is also needed to determine whether the significant interactions between trials and frequency and between axes and frequency, as observed in the coherence

analyses of both the slow and fast tracking sessions, are meaningful. For the slow tracking coherence data, the interaction effects do not appear to be large enough to be practically significant. For the fast tracking coherence data, the reduced vertical coherence, as compared with the horizontal coherence, at the higher frequencies (Figure 10) may be meaningful in terms of helmet mass. However, it is more difficult to account for the reduction in coherence at low frequencies on Trial 5 as compared to Trial 1 as seen in Figure 9.

The significant trial by frequency and axis by frequency interactions present in the analysis of variance of slow tracking gain (observable in Figures 3 and 4) do not appear to be of sufficient magnitude to be meaningful. Although it was anticipated that trials (fatigue) would have more of an effect upon the vertical axis gain than upon the horizontal axis gain, it is interesting to note that the trial (fatigue) effect is similar for both the horizontal and vertical axes.

As anticipated, the significant axis by frequency interaction found in analyzing phase angle data showed (Figure 6) that vertical phase was larger than horizontal phase at the higher frequencies. However, this effect was not enhanced by trials (fatigue) as was expected (i.e., the trial by axis by frequency interaction was not significant). Of final interest is the observation that trials (fatigue) did not affect subject's transport delay (as represented by the slopes of the regression lines) but instead affected the Y intercepts (see Figure 7) which presumably represents an increase in the operation of some sort of non-linear dead zone by the subject. Further study is needed to establish the significance of this observation.

CONCLUDING REMARKS

Extended continuous pursuit tracking, in two dimensions, with a helmet-mounted sight does produce significant changes in tracking performance. The results of this study showed that 32-1/2 minutes of continuous tracking produced a significant reduction in gain and a significant increase in phase.

REFERENCES

1. Ferrin, F.J.: "F4 Visual Target Acquisition System," Proceedings of A Symposium on Visually Coupled Systems: Development and Application, sponsored by Aerospace Medical Division, Brooks Air Force Base, Texas and 6570th Aerospace Medical Research Laboratory, Wright-Patterson AFB, Ohio. AMD-TR-73-1, September 1973, pp. 15-32. AD 916572.

TABLE I

ANOVA for Slow Coherence

Source	Error Term	df	Mean Square	F
Axis (A)	AxS	1	0.0684	10.6386*
Trial (T)	TxS	1	0.3766	5.2078
Frequency (F)	FxS	8	0.0226	11.4054***
Subject (S)		7	0.2008	
AxS		7	0.0064	
TxS		7	0.0723	
AxT	AxTxS	1	0.0066	1.6285
FxS		56	0.0020	
AxF	AxFxS	8	0.0054	2.9605**
TxF	TxFxS	8	0.0079	2.5036*
AxTxS		7	0.0041	
AxFxS		56	0.0018	
TxFxS		56	0.0032	
AxTxF	AxTxFxS	8	0.0094	4.6307***
AxTxFxS		56	0.0020	

* $p < .05$
** $p < .01$
*** $p < .001$

TABLE II

ANOVA for Slow Gain

Source	Error Term	df	Mean Square	F
Axis (A)	AxS	1	0.1753	0.5626
Trial (T)	TxS	1	1.6763	9.1965*
Frequency (F)	FxS	8	0.3962	26.7230***
Subject (S)		7	0.1868	
AxS		7	0.3116	
TxS		7	0.1823	
AxT	AxTxS	1	0.0446	1.5769
FxS		56	0.0148	
AxF	AxFxS	8	0.0225	3.3025**
TxF	TxFxS	8	0.0301	2.4085*
AxTxS		7	0.0282	
AxFxS		56	0.0068	
TxFxS		56	0.0125	
AxTxF	AxTxFxS	8	0.0049	0.9502
AxTxFxS		56	0.0052	

* $p < .05$
** $p < .005$
*** $p < .001$

TABLE III

ANOVA for Slow Phase

Source	Error Term	df	Mean Square	F
Axis (A)	AxS	1	5597.5	35.6682**
Trial (T)	TxS	1	2056.6	5.8132*
Frequency (F)	FxS	8	5670.7	64.3181**
Subject (S)		7	1277.9	
AxS		7	156.9	
TxS		7	353.8	
AxT	AxTxS	1	21.5	1.0928
FxS		56	88.2	
AxF	AxFxS	8	397.8	9.2252**
TxF	TxFxS	8	18.5	0.6683
AxTxS		7	19.6	
AxFxS		56	43.1	
TxFxS		56	27.6	
AxTxF	AxTxFxS	8	33.6	1.1698
AxTxFxS		56	28.8	

* $p < .05$
** $p < .001$

TABLE IV

ANOVA for Fast Coherence

Source	Error Term	df	Mean Square	F
Axis (A)	AxS	1	0.5696	7.8571*
Trial (T)	TxS	1	1.1553	3.6152
Frequency (F)	FxS	15	0.0429	2.7184**
Subject (S)		7	1.3447	
AxS		7	0.0725	
TxS		7	0.3196	
AxT	AxTxS	1	0.0181	1.2516
FxS		105	0.0158	
AxF	AxFxS	15	0.0613	5.4819***
TxF	TxFxS	15	0.0352	2.5506**
AxTxS		7	0.0145	
AxFxS		105	0.0112	
TxFxS		105	0.0138	
AxTxF	AxTxFxS	15	0.0351	2.8318**
AxTxFxS		105	0.0124	

* $p < .05$
** $p < .005$
*** $p < .001$

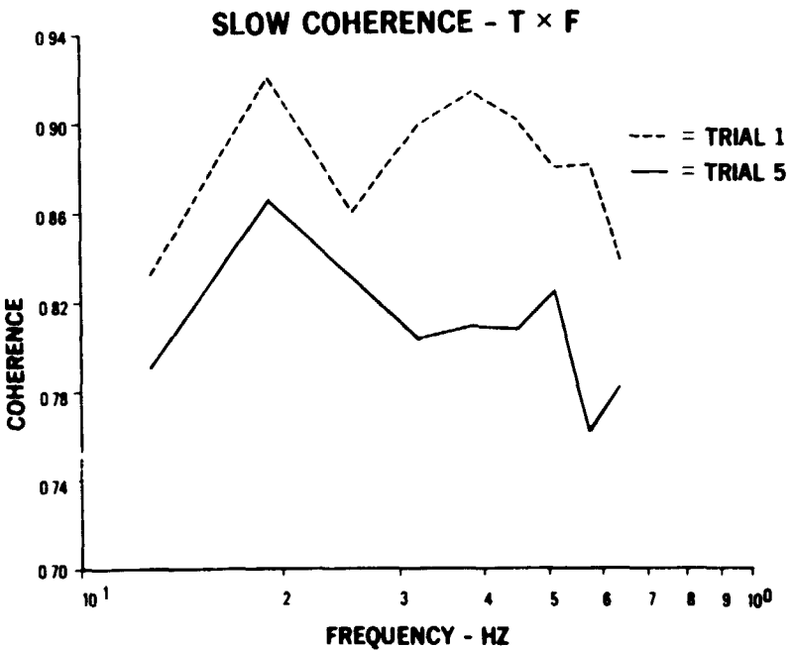

Figure 1. Coherence as a Function of Frequency for Trial 1 and Trial 5: Slow (.5 Hz) Tracking Data.

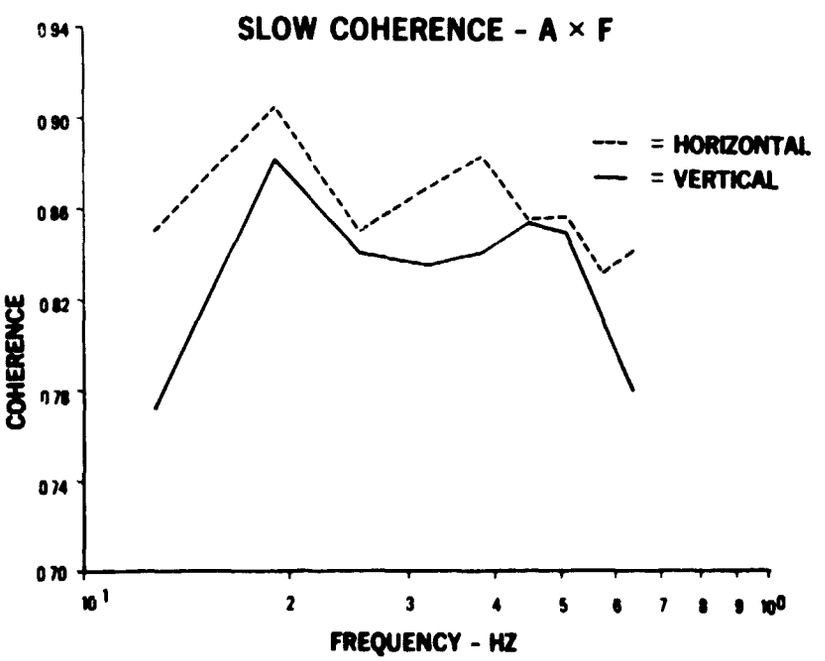

Figure 2. Coherence as a Function of Frequency for Horizontal and Vertical Tracking Dimensions: Slow (.5 Hz) Tracking Data.

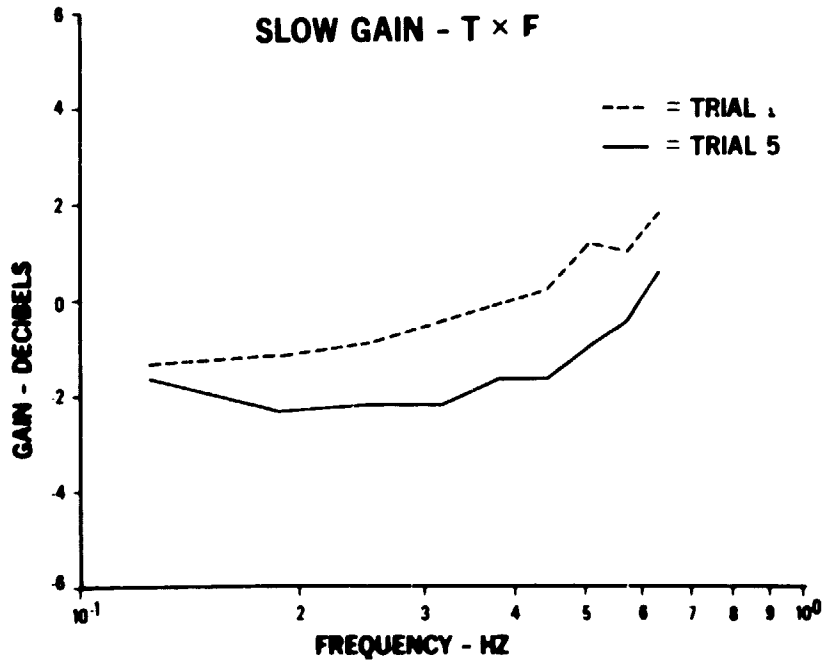

Figure 3. Gain as a Function of Frequency for Trial 1 and Trial 5: Slow (.5 Hz) Tracking Data.

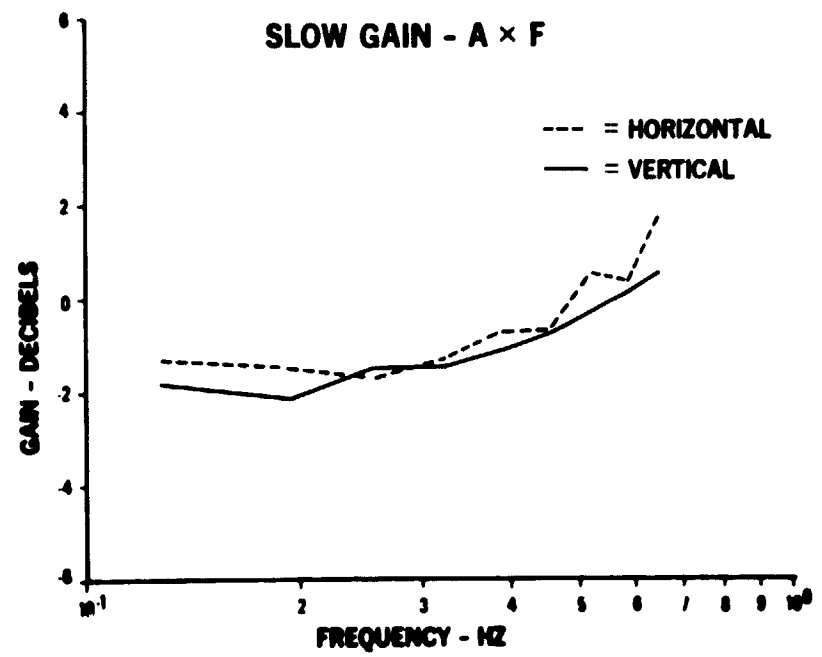

Figure 4. Gain as a Function of Frequency for Horizontal and Vertical Tracking Dimensions: Slow (.5 Hz) Tracking Data.

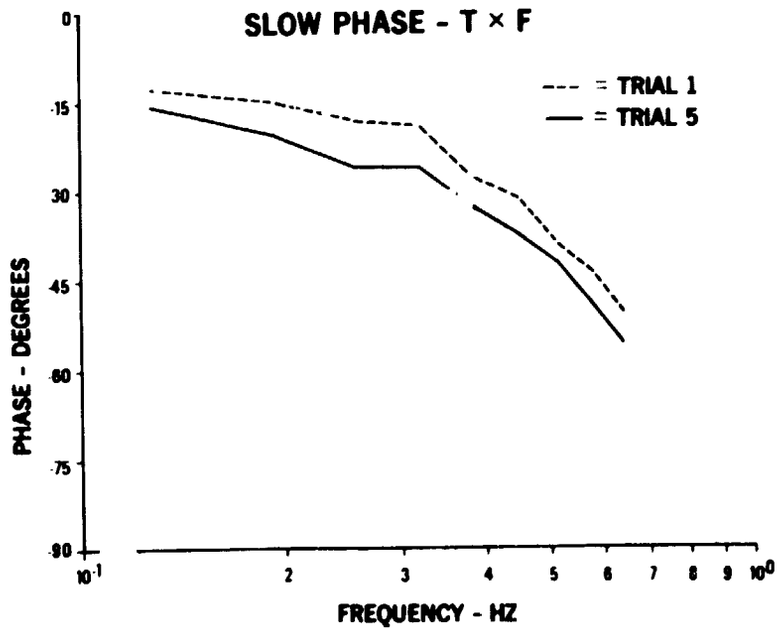

Figure 5. Phase as a Function of Frequency for Trial 1 and Trial 5: Slow (.5 Hz) Tracking Data.

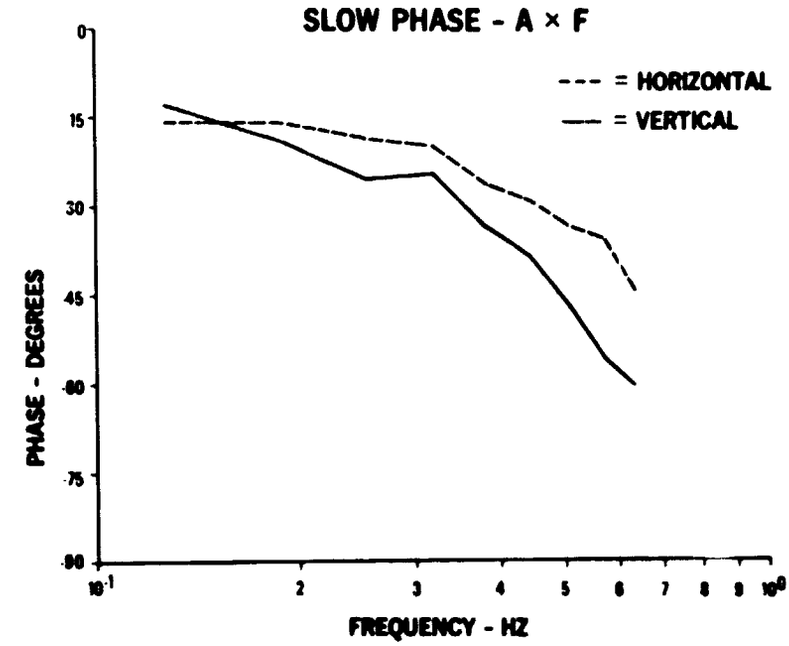

Figure 6. Phase as a Function of Frequency for Horizontal and Vertical Tracking Dimensions: Slow (.5 Hz) Tracking Data.

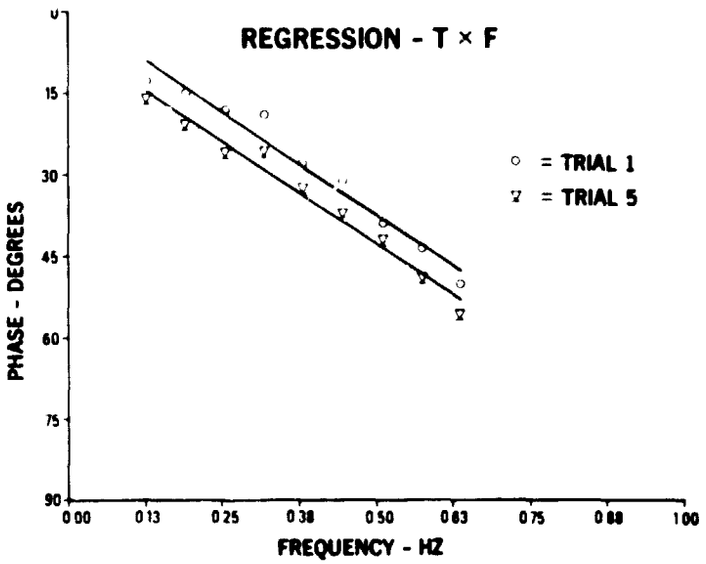

Figure 7. Regression Between Phase and Frequency for Trial 1 and Trial 5: Slow (.5 Hz) Tracking Data.

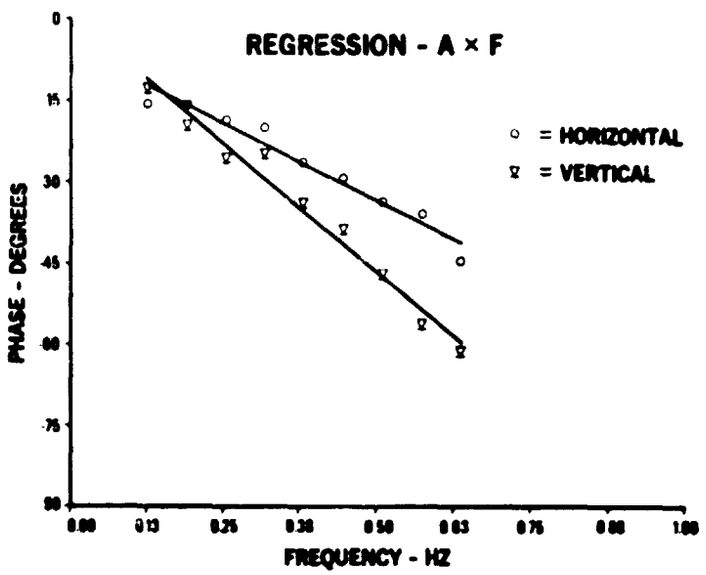

Figure 8. Regression Between Phase and Frequency for Horizontal and Vertical Tracking Dimensions: Slow (.5 Hz) Tracking Data.

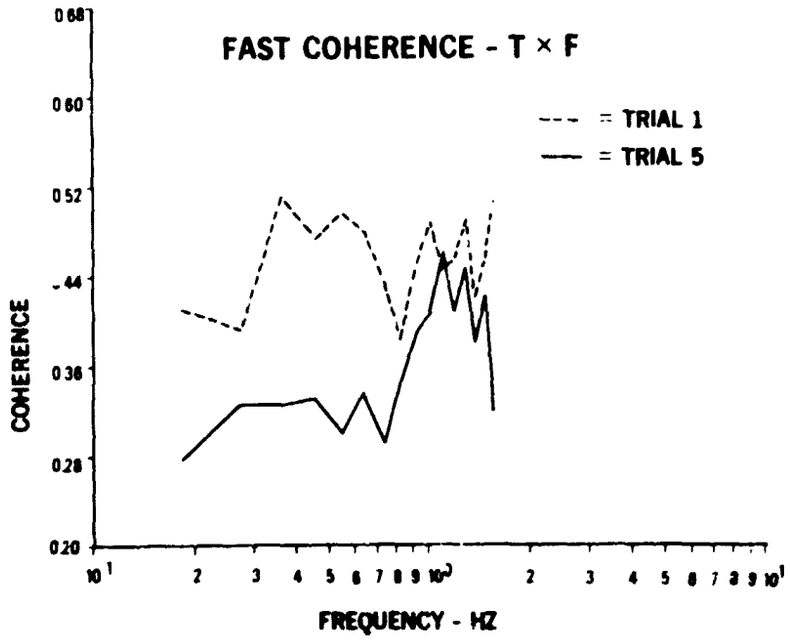

Figure 9. Coherence as a Function of Frequency for Trial 1 and Trial 5: Fast (1.5 Hz) Tracking Data.

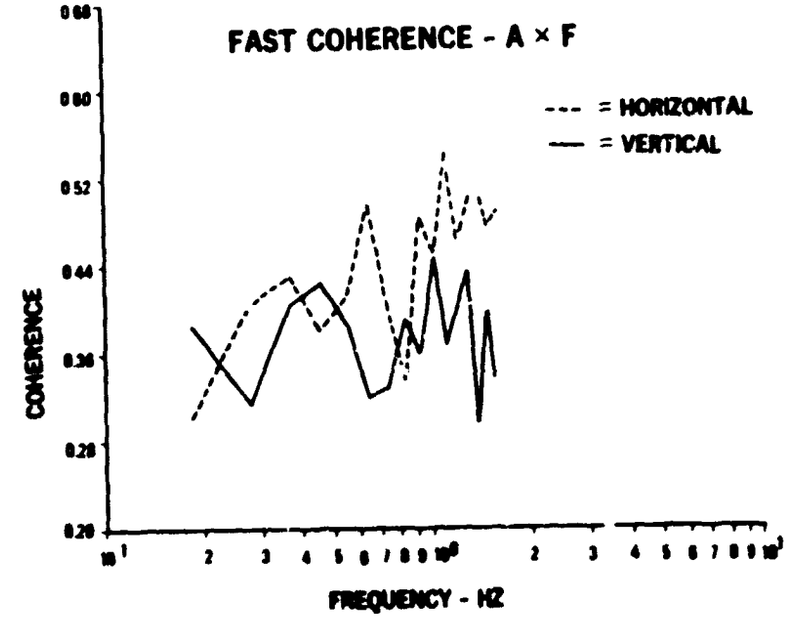

Figure 10. Coherence as a Function of Frequency for Horizontal and Vertical Tracking Dimensions: Fast (1.5 Hz) Tracking Data.

A COMPARISON OF IN-FLIGHT AND GROUND-BASED PITCH ATTITUDE TRACKING EXPERIMENTS

by M.F.C. van Gool and H.A. Mooij

National Aerospace Laboratory NLR

SUMMARY

Servo-analysis, applying mathematical models of human pilot behaviour, is an efficient approach to broaden the understanding of the "match" between the characteristics of the flight control system-aircraft combination, the human pilot and the displays. Quasi-linear models can be used in this type of analysis.

The influence of motion on the human pilot characteristics in command-type pitch attitude tracking experiments is investigated in flight and in a moving-base flight simulator (also used fixed-base).

The results are compared with results of similar investigations published in the literature.

INTRODUCTION

Research directed at the development of criteria for good handling qualities of aircraft under manual control has been in the past and will be in the future an important on-going activity. The emergence of new techniques in aircraft design and the associated changes in operational use forms the most important reason for these activities. Recent emphasis on CCV/FBW (Control Configured Vehicle/Fly-By-Wire) technology to be applied in production type aircraft emphasizes the need for development of adequate handling quality criteria.

Handling quality criteria formulated in the form of "specifications" or "regulations" are in many cases not directly applicable to aircraft with the electrical, closed-loop, primary flight control systems as they are proposed in contemporary design studies.

Servo-analysis, applying mathematical models of human pilot control behaviour, is an efficient approach to broaden the understanding of the "match" between the characteristics of the flight control system/aircraft combination, the human pilot and the displays and can therefore be used in the formulation of handling quality criteria.

Quasi-linear models can be used in this type of analysis. Available quasi-linear models have been developed for certain simple piloting control tasks such as single-loop compensatory tracking, using data which

have been mainly obtained under laboratory-type experimental conditions. It is considered valuable to be able to validate the applicability of these models for particular circumstances such as handling qualities investigations using flight simulators. Following such a validation, servo-analysis studies can be carried out to predict stability and performance of the pilot-aircraft system for a wide range of dynamical configurations in the flight simulator. In addition, if knowledge on the relation between the pilot's control behaviour in flight simulators and in-flight is available, the prediction can be extended to the in-flight situation.

A discussion of the correlation of in-flight and ground-based measured pilot transfer characteristics based on results obtained during three experiments will be presented.

HUMAN OPERATOR DYNAMICS IN CLOSED-LOOP CONTROL SYSTEMS

Because many piloting problems involve principally one axis and because experimental analysis of the multiloop control situation is very complex, most of the research effort reported in the literature up to now has been related to the investigation of single-loop compensatory control systems. In such control situations, the pilot, characterized by the describing function Y_p, driving the controlled element, characterized by its transfer function Y_c, pays his attention to one control task having a visual stimulus which shows the "error" between command input and system output.

A helpful concept for describing the relation between the human pilot and the controlled element transfer characteristics in single-loop compensatory control systems is the "crossover model" as formulated by McRuer and others (Refs. 1 and 2).

Based on the observations of compensatory control systems covering a wide range of dynamic properties of the controlled element, the open-loop transfer function $Y_p\ Y_c$ can be represented by a single two-parameter model in the frequency range where $|Y_p\ Y_c| = 1$.

The model has the following form:

$$Y_p(j\omega)\ Y_c(j\omega) = \frac{\omega_c e^{-j\omega\tau_e}}{j\omega}$$

where ω_c = crossover frequency
τ_e = effective time delay

Up to now the majority of accurate describing functions have been determined only on the ground (and mostly from fixed-base experiments). The set of experiments, described in this paper covers in-flight as well as moving-base flight simulator and fixed-base flight simulator environments.

The dynamic characteristics of the controlled element (flight control system/aircraft combination) and the operational environment were the principal experimental variables during the investigations, listed below:

- Experiment I The controlled element was a pitch attitude controller with

pitch-rate-command/attitude-hold properties and selectable dynamic characteristics.
The experiments were carried out in flight with a Beechcraft Queen Air aircraft fitted with a model-following flight control system. The general expression for the transfer function of the controlled element is:

$$\frac{\theta}{\delta_s} = \frac{K_\theta(s+1/\tau_\theta)}{s(s^2+2\zeta_\theta\omega_\theta s+\omega_\theta^2)}$$

$1/\tau_\theta$, ω_θ and K_θ were selectable over a wide range while ζ_θ was maintained close to 0.7 in all cases.
The variable dynamics were mechanized according to the so-called Prefilter Model Following principle as described in reference 3.

- Experiment II The dynamics of the flight control system/aircraft combination were identical to those used in Experiment I, but the experiments were carried out in the moving-base flight simulator of the Department of Aeronautics and Space Engineering of the Delft University of Technology which was also used fixed-base.
- Experiment III The controlled element again was of the pitch-rate-command/attitude-hold type, although this characteristic was not obtained through model-following but was inherent to a pitch attitude controller designed around a simulated jet transport aircraft having neutral static stability as described in reference 4.

  In one configuration Direct Lift Control (DLC) "augmentation" was provided for improving manoeuvring. Lift modulation was commanded directly by stick displacement through a wash-out filter. These experiments were carried out in the same flight simulator used in Experiment II.

This paper presents only a small part of the result of these experiments. More controlled elements than presented here have been evaluated. Furthermore remnant data, measured for all controlled elements, are not presented in this paper. However these results are presented in the complete report on these experiments, reference 5.

For Experiment I and II a comparison of the tracking results for one of the controlled elements (C-3) in different environments (in-flight, moving-base and fixed-base simulator) will be presented to demonstrate the effect of motion on human tracking behaviour. For Experiment III a comparison of the tracking results for two controlled elements having identical pitch attitude characteristics, but differing due to direct lift control augmentation (B-4 with, and A-1 without DLC), will be presented to demonstrate the effect of DLC-heave motion. The transfer functions of these controlled elements are presented in figure 1.

PILOT DESCRIBING FUNCTIONS AND MATHEMATICAL MODELS

Experiment I and II

The forcing function, injected into the display was a sum of 10 sinusoids with a cut-off frequency of 1.5 rad/sec. (4 sinusoids were used as low

amplitude high-frequency shelf). The average pilot describing functions for three environmental conditions are presented in figure 2.

In accordance with the crossover model a large amount of pilot lead has been generated. This can be demonstrated by the parameters of a 4-parameter pilot model that has been fitted to the describing functions:

$$Y_p = K_p \frac{\tau_L j\omega+1}{\tau_I j\omega+1} e^{-j\omega\tau_e}$$

K_p = gain
τ_L = lead time constant
τ_I = lag time constant
τ_e = effective time delay

With a fitting procedure that emphasizes a good fit in the neighbourhood of crossover frequency, the following average results are obtained:

	$K_p(\frac{\text{deg stick}}{\text{cm display}})$	τ_I(sec)	τ_L(sec)	τ_e(sec)
In-Flight (2 pilots, 5 runs each)	0.5	0.1	8.0	0.26
Moving-Base (4 pilots, 5 runs each)	0.5	0.1	7.0	0.31
Fixed-Base (2 pilots, 5 runs each)	1.6	0.1	2.2	0.30

Fixed-base results are different from results with motion. With motion higher lead time constants and lower steady state gains are obtained.

Experiment III

The forcing function consisted of a sum of sinusoids forming a spectrum with a first-order roll-off shape with a cut-off frequency of 1 rad/sec (again augmented with a low-amplitude high-frequency shelf). The average pilot describing functions for the configurations with and without direct lift control are presented in figure 3.

The parameters of the 4-parameter pilot model, obtained in the same way as for Experiment I and II, are as follows.

	$K_p(\frac{\text{deg stick}}{\text{cm display}})$	τ_I(sec)	τ_L(sec)	τ_e(sec)
With DLC (4 pilots, 5 runs each)	13.4	0.6	1.2	0.32
Without DLC (2 pilots, 5 runs each)	17.8	0.3	0.8	0.35

It is observed that with additional translational motion due to DLC, the gain decreases and the lead time constant increases

Pilot-aircraft performance

Loop bandwidth and stability as expressed in crossover frequency and phase margin and the performance measures Score ($= 1 - \frac{\sigma_e^2}{\sigma_i^2}$), and relative remnant, ($\rho^2_{a_e} = \frac{\sigma^2_{e_i}}{\sigma^2_e}$), related to the pilot's input, are as follows.

	ω_c	φ_m	Score	$\rho^2_{a_e}$
Exp. I In-Flight	1.7	35	0.34	0.66
Exp. II Moving-Base	2.0	31	0.55	0.74
Exp. II Fixed-Base	2.0	16	0.48	0.66
Exp. III Moving-Base with DLC	1.4	54	0.81	0.86
Exp. III Moving-Base without DLC	1.8	44	0.84	0.82

With respect to Experiments I and II it can be observed that in-flight the crossover frequency is lower, the phase margin is higher and the Score is lower than moving-base.

With respect to Experiment II, it is observed that moving-base the phase margin, Score and the relative remnant are higher than fixed-base.

With respect to Experiment III it can be observed that for the controlled element with DLC the crossover frequency is lower and the phase margin is higher than for the controlled element without DLC.

INFLUENCE OF MOTION

In the evaluation of the influence of motion on the outcome of the experiments it has to be kept in mind that command-type tracking has been carried out in which the displayed error signal is not congruent with the actual pitching motion and in which a frequency dependent relation exists between pitch and heave motion.

In general, sensing of angular motion, usually associated with the "semicircular canals" can be characterized as a second-order response to angular acceleration (Ref. 6). It is believed that a threshold is incorporated in this mechanism which has a value of 0.5 deg/sec^2. The dynamics of the second-order system are such that from 0.2 to 10 rad/sec, angular motion perception is proportional to angular rate. For prolonged turning the "subjective" signal

washes out. The treshold value for angular rate based on this number is 2.6 deg/sec for the pitch axis (Ref. 2)

Sensing of linear motion is ordinarily associated with the "utricles" which are sensitive to the total applied force (Because the utricles do not respond only to inertial accelerations but to the total applied force, they have to be considered specific force indicators).

For the discussion here, the inputs to the utricles will be referred to as accelerations. The model for linear motion sensing presented by the author of reference 6 can be characterized as that of a second-order system responding to linear acceleration. Because it is estimated that the two first-order break-points are located at frequencies of 0.1 and 1.5 rad/sec, the subjective perception of acceleration over the frequency range of interest is accompanied by large phase lags. It is believed that also in this case a threshold is present which has a value of 0.1 m/sec^2 (Ref. 6) for the vertical axis.

Possibly the mentioned threshold values are even higher in tracking experiments, because the pilot experiences both visual and motion inputs, as opposed to the experimerts described in reference 6 were the subject concentrated solely on the task of detection motion.

To be able to estimate the amount of motion during the experiments, the level of motion in each of the three experiments has been computed. Root mean square (r.m.s.) values of pitch rate and vertical acceleration are as follows

	r.m.s. pitch rate (deg/sec)	r.m.s. vertical acceleration (m/sec^2)
Exp. I In-Flight	1.0	1.24
Exp. II Moving-base	1.1	0.08
Exp. III with DLC	1.9	0.08
Exp. III without DLC	2.1	0.05
Threshold of perception suggested	2.6	0.1

For Experiments I and II the r.m.s. values of pitch rate have been below the threshold of perception. The difference between Experiment I and II with respect to motion was the r.m.s. value of vertical acceleration which has been well above the perception threshold for Experiment I and of the same magnitude as the perception threshold for Experiment II.

For Experiment III the r.m.s. of pitch rate was somewhat below the perception threshold. With respect to the r.m.s. value of vertical acceleration an increase of 50 % is observed for the experiment with DLC as compared to the experiment without DLC. Assuming that during an appreciable part of the time a level of motion equal to twice the r.m.s. value existed, the vertical acceleration with DLC has been above the perception threshold.

Turning to the literature it is observed that most tracking investigations including rotational motion have been performed with distu-bance-type

forcing functions, thus having rotational motion congruent to the displayed error signal; this type of investigations are described in references 7 to 11.

Although not directly applicable to the test described in this study it is remarked in reference 11 that previous work by R.S. Shirley (Sc.D. Thesis, M.I.T., 1968) has shown that addition of congruent motion (disturbance tracking) in a single-axis tracking task is beneficial if the lead information that the motion supplies is not redundant and can be used to maintain better control of the system. Another way of saying this is that the merits of motion are dependent on task difficulty in single-axis control tasks. However, it should be observed that the improved performance for Exp. II moving-base as compared to fixed base shows the same trend.

Stapleford, Peters and Alex (Ref.12, 1969) state that their studies indicated that motion cues will be used except when tracking a random-appearing command input with a compensatory display. Due to the fact that with a command input the visual system will only sense the difference between the input and the vehicle motion, while the vestibular system senses the actual vehicle motion there is a "conflict" between the two modalities involved. The authors of reference 12 conclude that when this conflict exists, the pilots apparently ignores the motion inputs.

A study on the effect of rotational motion using a large amplitude command-type forcing function is reported by Junker and Replogle (Ref. 13, 1975). The authors conclude from their investigations that, "the human operator will make use of large amplitude motion information when controlling a moving platform with dynamics of the general form K/s^2". A controlled element with K/s^2 characteristics discussed in the present paper is Controlled Element C-3, although the level of rotational motion was small.

No literature with respect to translational motion in command tracking could be located. Although not directly applicable to the tests described in this study it is considered interesting to mention that Ringland and Stapleford (Ref. 14, 1973) state that among others the following conclusions can be drawn from the work they performed with respect to disturbance tracking:

- Low level linear acceleration cues can be effectively used by pilots to improve performance in tracking tasks
- Performance improvements with linear motion cues are highly subject dependent.

CONCLUSIONS

Command-type tracking experiments have been carried out with a pitch-rate-command/attitude-hold flight control system controlled by side stick with and without motion.

The results of the experiments give reason to believe that the effect of rotational motion during the experiments resulted in an increase in system stability as well as in improved performance for a controlled element requiring low-frequency lead generation. This is observed for an experiment during which the simulator motion level was lower than the commonly

accepted threshold of human motion perception. This result is in accordance with an observation made by Junker and Replogle (1975) for large amplitude motion.

Translational motion existing during the tracking tasks (aircraft dynamics) lowered the values of crossover frequency and Score and thus degraded the pilot-aircraft performance in the pitch tracking tasks as compared to the performance obtained fixed-base.

REFERENCES

1. McRuer, D.T.; Graham, D.; Krendel, E.S. and Reisener, Jr. W.: Human Pilot Dynamics in Compensatory Systems: Theory, Models and Forcing Functions Variations. AFFDL TR-65-15 1965.

2. McRuer, D.T. and Krendel E.S.: Mathematical Models of Human Pilot Behaviour. AGARDograph No. 188 1974.

3. Mooij, H.A.: Flight Experience with an Experimental Electrical Pitch-Rate-Command/Attitude-Hold Flight Control System. AGARD-CP-137 1974.

4. Mooij, H.A.: Handling Quality Criteria Development for Transport Aircraft with Fly-by-Wire Flight Control Systems. NLR TR 74141 U 1975.

5. Gool, M.F.C. van and Mooij, H.A.: Human Pilot Describing Function, Remnant and Associated Information for Pitch Attitude Control: Results from In-Flight and Ground-Based Tracking Experiments. NLR TR 75062 U 1975.

6. Peters, R.A.: Dynamics of the Vestibular System and their Relation to Motion Perception, Spatial Disorientation and Illusions. NASA CR-1309 1969.

7. Guercio, J.C. and Wall, R.L.: Congruent and Spurions Motion in the Learning and Performance of a Compensatory Tracking Task. Human Factors, 14(3) 1972.

8. Bergeron, H.P. and Adams, J.J.: Measured Transfer Functions of Pilots during Two-Axis Tasks with Motion. NASA TN D-2177 1964.

9. Ringland, R.F.; Stapleford, R.L. and Magdaleno, R.E.: Motion Effects on an IFR Hovering Task-Analytical Predictions and Experimental Results. NASA CR-1933 1971.

10. Ringland, R.F. and Stapleford, R.L.: Experimental Measurements of Motion Cue Effects on STOL Approach Tasks. NASA CR-114458 1972.

11. Bergeron, H.P.; Adams, J.J. and Hurt, G.J.: The Effects of Motion Cues and Motion Scaling on One- and Two-Axis Compensatory Control Tasks. NASA TN D-6110 1971.

12. Stapleford, R.L.; Peters, R.A. and Alex, F.R.: Experiments and a Model for Pilot Dynamics with Visual and Motion Inputs. NASA CR-1325 1969.

13. Junker, A.M. and Replogle, C.R.: Motion Effects on the Human Operator in a Roll Axis Tracking Task. Aviation, Space and Environmental Medicine. June, 1975.

14. Ringland, R.F. and Stapleford, R.L.: Pilot Describing Function Measurements for Combined Visual and Linear Acceleration Cues. Proceedings of the Eight Annual Conference on Manual Control, AFFDL-TR-72-92. (1973).

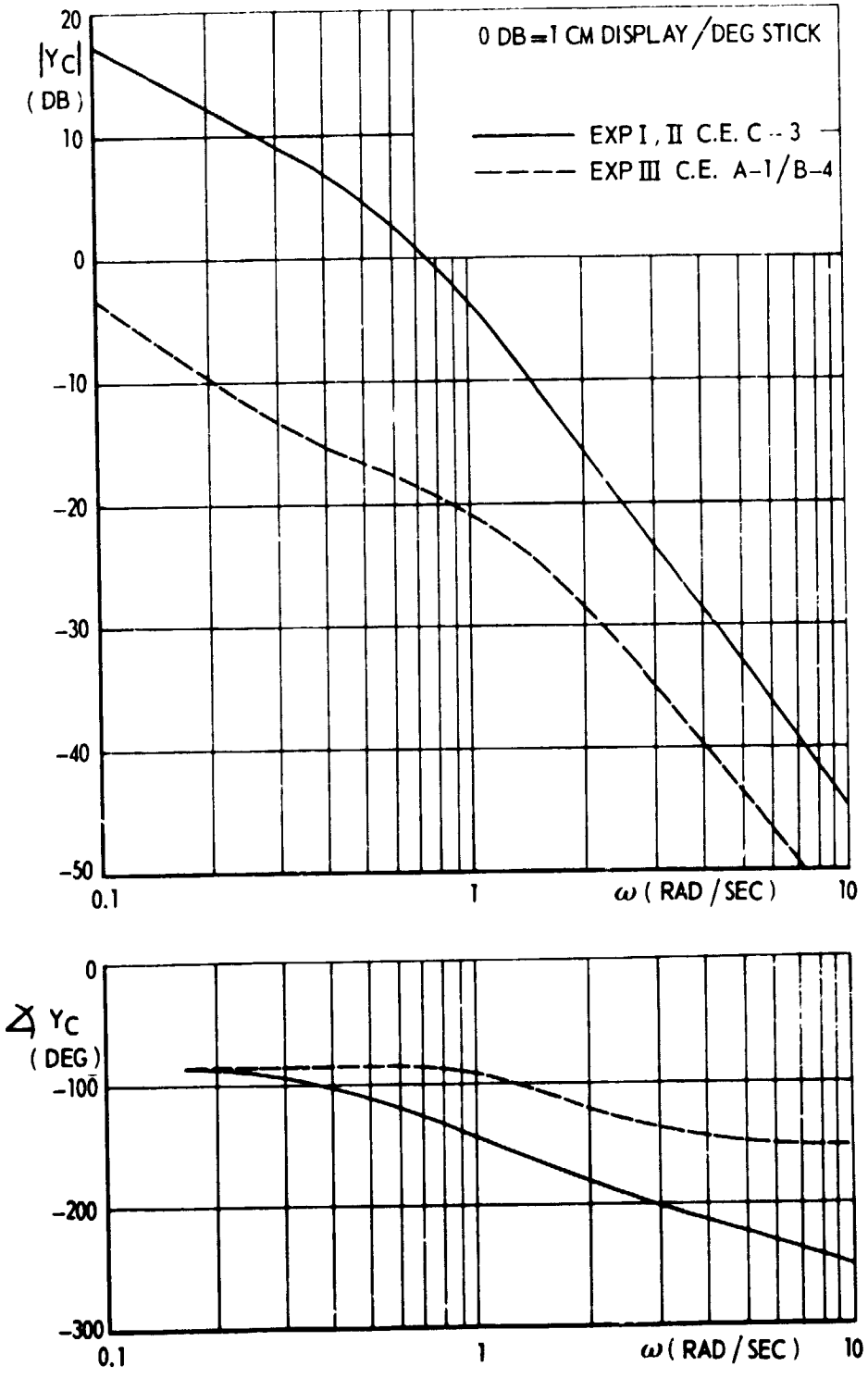

CONTROLLED ELEMENT DYNAMICS

Fig. 1

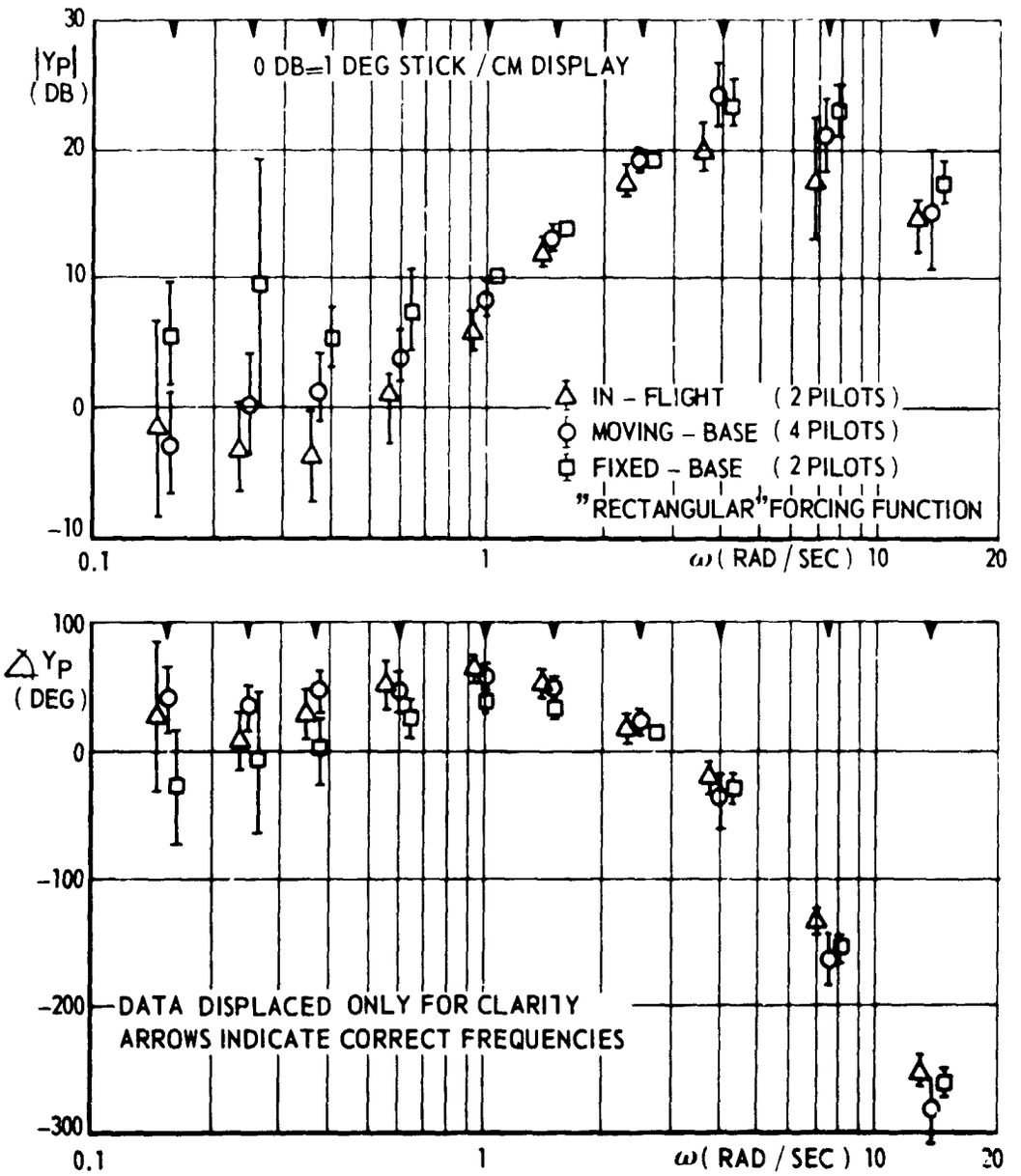

PILOT DESCRIBING FUNCTION FOR EXPERIMENT I AND II

Fig. 2

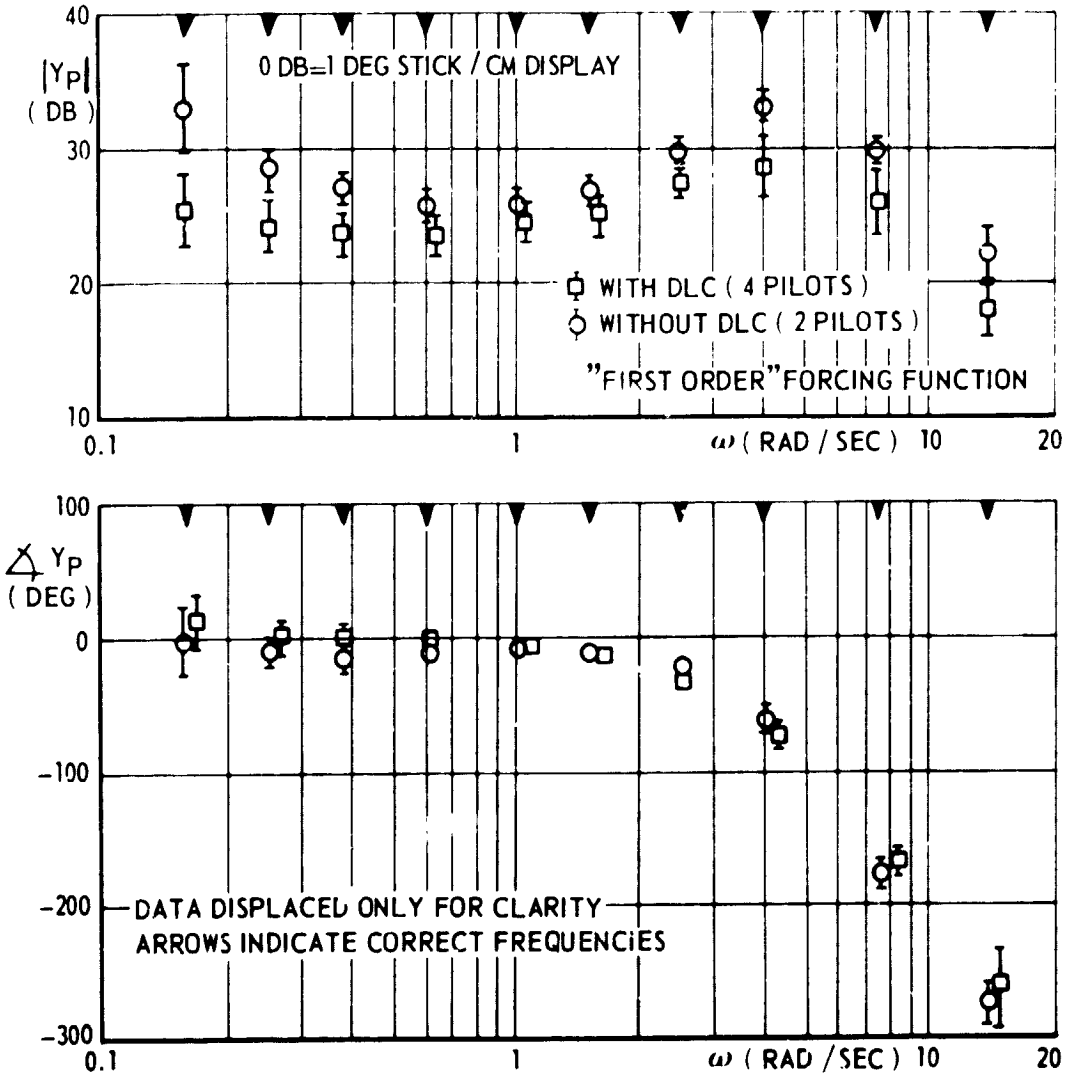

PILOT DESCRIBING FUNCTION FOR EXPERIMENT III

Fig. 3

EFFECTS OF HEADGEAR AND VISUAL ANGLE ON HEAD ROTATION SPECTRAL CHARACTERISTICS

By D. K. Shirachi[1]

National Research Council
Resident Research Associate

D. L. Monk and J. H. Black, Jr.

Crew Station Integration Branch
Human Engineering Division
6570 Aerospace Medical Research Laboratory
Wright-Patterson AFB, Ohio 45433

SUMMARY

Dynamic characteristics of the unrestrained human head movement control system are measured as a function of headgear weight and size of the stimulus trajectory envelope. The coherence, gain and phase spectral characteristics are unaffected by variations in the weight of the helmet and associated head line-of-sight measurement hardware; however, a gain amplitude nonlinearity related to stimulus visual field size is shown to exist.

INTRODUCTION

Significant hardware developments during recent years now permit practical, remote measurement of an operator's head line-of-sight with good accuracy and reliability. The advent of this practical capability has stimulated numerous proposed applications of Visually Coupled Systems, control systems which are directed by natural head movements with feedback information displayed in the operator's visual

[1]Present address: Computer Sciences Corporation
1101 San Antonio Road
Mountain View, California 94043

field. The purpose of this investigation of head pursuit tracking was to provide dynamic performance data to aid in the evaluation of the head movement system as an active controller and to identify important design considerations in the future development of head line-of-sight measurement systems.

Several DoD agencies and NASA are seriously considering potential applications of head-aimed control systems for aircraft flight control, head slaved simulator displays, navigation and reconnaissance sensor control, and target designation. Chouet and Young [1] have shown that a head position measurement device can be used as an efficient means of controlling vehicular attitude, especially for three-axis manual control, and other investigations of Visually Coupled Systems [2] have demonstrated the feasibility of head-controlled sensors and weapon systems. Head line-of-sight measurements are also being considered for selection and control of aircraft cockpit information displays and as a means of providing accurate bearing to way points for precision updating of onboard navigation systems.

All these applications of head control take advantage of the operator's proprioceptive feedback and utilize the rapid, precise head movement coordination which is a natural physiological activity in man and is coupled to his perception of and reaction to his environment. The research reported herein describes the characteristics of unrestrained head movement as a function of headgear weight and angular size of the visual field in which the pursuit task occurs.

METHODS

Experimental Apparatus

A Honeywell Helmet-Mounted Sight (HMS) which measures the operator's helmet angular line-of-sight in real-time was used to observe dynamic head movements. The Honeywell HMS [3] computed head line-of-sight coordinates from information generated by scanning infrared light beams transmitted from fixed-coordinate "light fans" mounted beside the experimental subject and received by infrared detectors mounted on a helmet worn by the subject. An electronic computation unit provided analog voltages corresponding to the horizontal and vertical coordinates of the head line-of-sight. The following three helmet configurations weighing 4-1/4, 3 and 2 pounds respectively were used in the experiments: a Navy Model LG1065; a Phase I, lightweight prototype, Model LG1087; and a modified Air Force Model LG1063 with visor, oxygen mask recepticles and associated hardware removed to reduce weight.

The moving target stimuli for the head pursuit tracking were generated by projecting a laser beam directed by an X-Y mirror galvanometer system onto a vertical viewing screen which subtended a visual angle of $\pm 20^{o}$ in both vertical and horizontal axes. The vertical and horizontal inputs to the galvanometer system were

uncorrelated and consisted of band-limited, Gaussian noise with a half-power bandwidth of 3 Hz. The helmet weight experiments used a $\pm 10^{o}$ visual field as the stimulus projection envelope, and the angular field experiments used amplitudes of $\pm 5^{o}$, $\pm 10^{o}$ and $\pm 15^{o}$ for the stimulus field.

The helmet weight experiments were conducted on two experimental subjects; the angular field experiments were performed on three experimental subjects. For all of the experiments, one subject was trained and the other subjects were untrained. The angular field experiments were performed with both the 2 and 4-1/4 pound helmets; however, since the results were identical, only data for the 2 pound helmet is presented here.

DATA ANALYSIS

The data analysis method chosen for investigation of the head movement system dynamics was power spectral analysis [4, 5], and the frequency information of the spectral analysis permitted a comparison of the authors' data with those in the literature. Using power spectral analysis techniques, one may directly compute the system's linear, input-output transfer function and coherence function which is a quantitative measure of the credibility associated with the computed linear transfer function.

It is assumed that the measured output response, $x(t)$, is the sum of an input stimulus, $u(t)$, multiplied by the system transfer function, $h(t)$, plus an additive noise source, $n(t)$, which is uncorrelated with the input.

$$x(t) = h(t)\ u(t) + n(t)$$

$$E[\,n(t)\ u(t)\,] = 0; \quad 0 \leq t \leq T$$

Performing a Fourier transformation of the input and output variables and converting to power spectra

$$G_{ux} = H\, G_{uu} + G_{nx}$$

where G_{uu} = auto-power spectrum of $u(t)$

G_{ux} = cross-power spectrum of $u(t)$ and $x(t)$

G_{nx} = cross-power spectrum of $n(t)$ and $x(t)$

$E[\ ]$ = expected value operator

Assuming that n(t) is uncorrelated with x(t), and n(t) is zero mean, Gaussian noise, then the use of ensemble averaging for the auto- and cross-power spectra for many segments of frequency computations causes G_{nx} to approach zero. Therefore,

$$\bar{G}_{ux} = H \bar{G}_{uu}$$

and

$$H = \frac{\bar{G}_{ux}}{\bar{G}_{uu}}$$

where $\bar{G}$ denotes the ensemble average.

The coherence function, γ^2, is defined as

$$\gamma^2 = \frac{\bar{G}_{ux}^{\ 2}}{\bar{G}_{uu}\,\bar{G}_{xx}}; \qquad 0 \leq \gamma^2 \leq 1.0$$

where G_{xx} = auto-power spectrum of x(t).

The coherence function is the proportion of input power contained by the output power spectrum and is a quantitative measure of the linear causal relationship between the input and output of a system.

Input-output cross-correlations were computed to determine the time delay of the output response relative to a given input stimulus. The lag time corresponding to the maximum value of the cross-correlation function is considered as the time delay of the measured input-output relationship.

The following time responses were recorded: horizontal stimulus, vertical stimulus, horizontal head movement response and vertical head movement response. For each of the stimulus-response pairs, cross-correlation functions, coherence functions and transfer function gain and phase angle spectra were computed so that direct and cross-coupled characteristics of each coordinate axis could be determined.

RESULTS

Helmet Weight

Data recorded from the helmet weight experiments showed no appreciable

differences in the coherence, phase angle or gain characteristics when HMS helmet weight was increased. The spectral characteristics for two subjects are shown on Figures 1 through 6, and these curves show no appreciable differences between helmets of different weight.

Based upon the definition of half-power bandwidth which is the frequency region in which the input-output signal power transfer function remains above 0.5 of maximum signal transmissibility (Bendat and Piersol [4]) and forming an analogous definition for the coherence function where a coherence value of 0.5 is analogous to the half-power point, the bandwidth of the head movement system was found to be approximately 2.0 Hz.

The transfer function gain varied between 0.3 and 0.4 for horizontal movements and 1.0 and 1.5 for vertical movements (figures 3 and 4). One can easily observe that the vertical gain was much greater than the horizontal gain, and these results agree with those of Shirachi and Black [6].

The phase angle curves showed no differences as a function of increasing helmet weight (figures 5 and 6), and the phase angle was a linear function of frequency as determined by a linear least squares fit of the data points with a correlation coefficient greater than 0.98.

Visual Field Size

In contrast with the results for the helmet weight experiments, there was a significant effect of visual field size on the transfer function gain (figures 7, 8 and 9). An increase of visual field size produced sizeable increases of gain throughout the response bandwidth of the head movement system. It should also be noted that the vertical gains were always greater than the horizontal gains, just as in the helmet weight experiments. The $\pm 5^{0}$ stimulus envelope produced quite small gains in the region of 0.07 to 0.15 (horizontal) and 0.2 to 0.7 (vertical) and the $\pm 15^{0}$ envelope produced gains of 0.6 to 1.5 (horizontal) and 1.1 to 3.0 (vertical). These results indicate that an interaction exists between the transfer function gain and size of the stimulus visual field.

The coherence functions for the visual field experiments were similar to those for the helmet weight experiments. Stimulus amplitude appeared to have negligible effect on coherence (figure 10a).

The phase angle curves also showed no amplitude effects (figure 10b), and they were linear with frequency just as in the helmet weight experiments. However, the phase angles in the high frequency region near 1.5 Hz showed less phase lag than the phase curves for the helmet weight experiments.

CONCLUSIONS

The head movement system had previously been thought to exhibit linear behavior which can be modeled by a constant gain term in series with a time delay element (Shirachi and Black [6]). However, new experimental evidence which shows an amplitude-dependent transfer function gain relationship has been presented in this paper which appears to challenge the linear model of Shirachi and Black. The invariance of the coherence and phase angle characteristics with stimulus field size combined with an amplitude-dependent gain characteristic do not conform to the linear system model. It is not readily apparent what mechanism or mechanisms are operating to produce the amplitude-dependent behavior presented here. Transfer function gain may be influenced by head and eye interaction at small stimulus amplitudes. Another probable factor is target angular velocity which varies as a function of stimulus amplitude when the forcing function bandwidth is constant. However, future experimentation is necessary in order to provide sufficient data to explain the transfer function gain behavior.

REFERENCES

1. Chouet, B. A. and L. R. Young. Tracking with head position using an electro-optical monitor. IEEE Trans. Syst., Man and Cybernetics. SMC-4: 192-204, 1974.

2. Birt, J. A. and H. L. Task, ed. Proc. Symp. Visually Coupled Systems: Development and Application. AMD TR-73-1. (AD 916572) 1973.

3. Ferrin, F. J. F4 visual target acquisition system. Proc. Symp. Visually Coupled Systems: Development and Application. AMD TR-73- (AD 916572) 1973.

4. Bendat, J. S. and A. G. Piersol. Random Data: Analysis and Measurement Procedures. Wiley-Interscience, New York. 1971.

5. Roth, P. R. Effective measurement using digital signal analysis. IEEE Spectrum. 8: 62-70, 1971.

6. Shirachi, D. K. and J. H. Black, Jr. Head-eye tracking in two-dimensional pursuit tasks. Proc. Eleventh Annual Conf. Manual Control. NASA TM X-62,464, 1975.

LIST OF FIGURES

Figs. 1 and 2

Coherence functions for two experimental subjects wearing various weight headgear.

Figs. 3 and 4

Transfer function gains for two experimental subjects wearing various weight headgear.

Figs. 5 and 6

Transfer function phase lag for two experimental subjects wearing various weight headgear.

Figs. 7, 8 and 9

Transfer function gains for different stimulus field sizes for three experimental subjects.

Fig. 10a

Coherence functions for different stimulus field sizes.

Fig. 10b

Transfer function phase lag for different stimulus field sizes.

COHERENCE FUNCTION

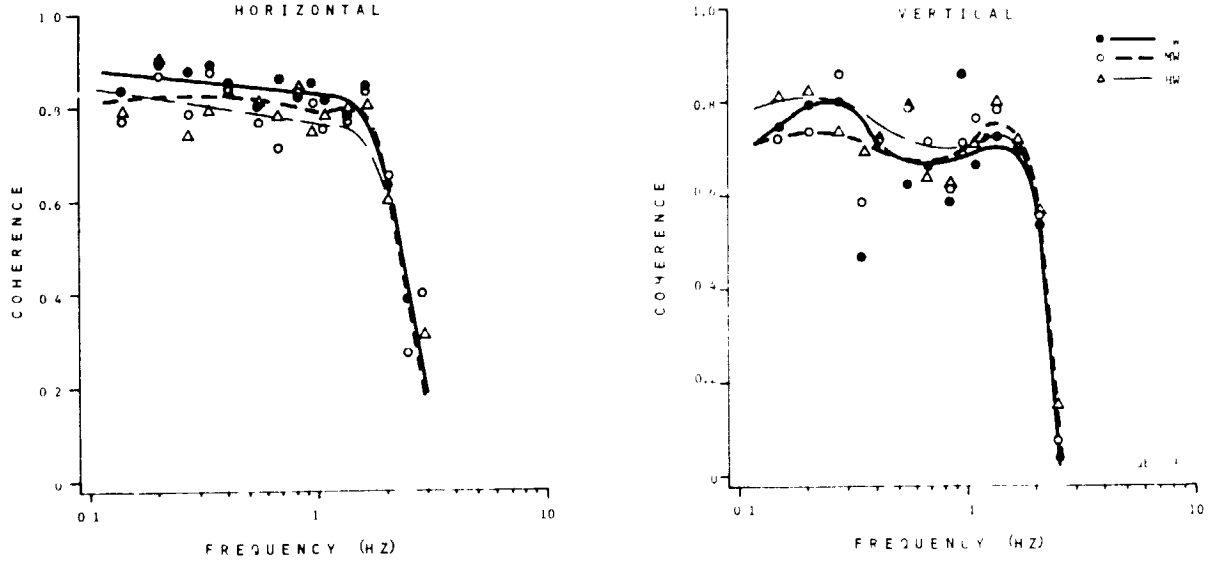

FIGURE 1

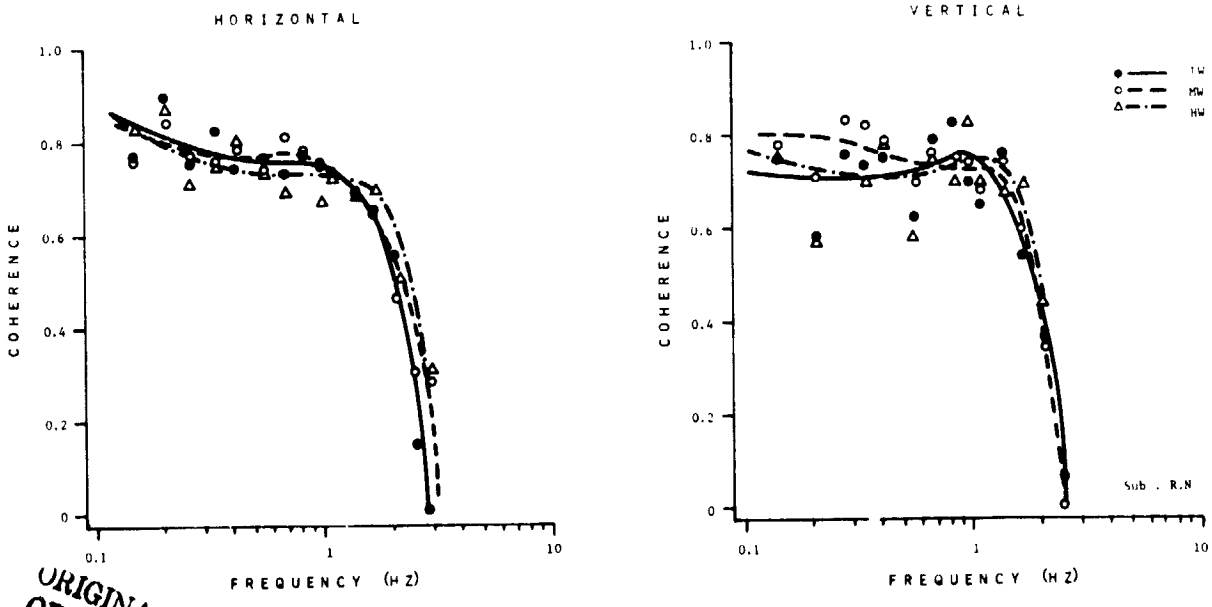

FIGURE 2

TRANSFER FUNCTION GAIN

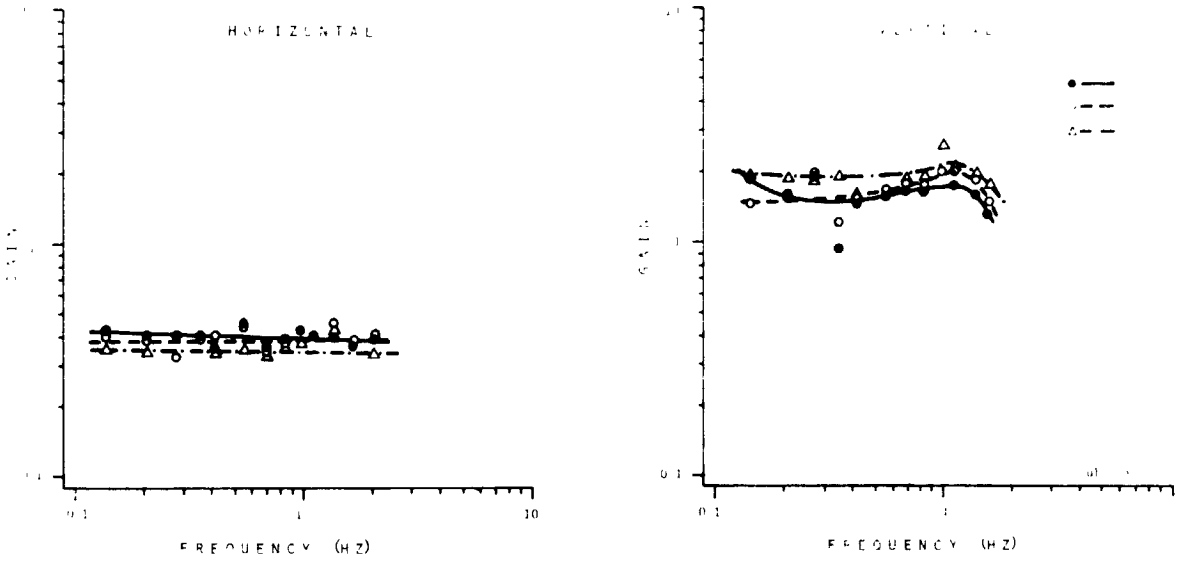

FIGURE 3

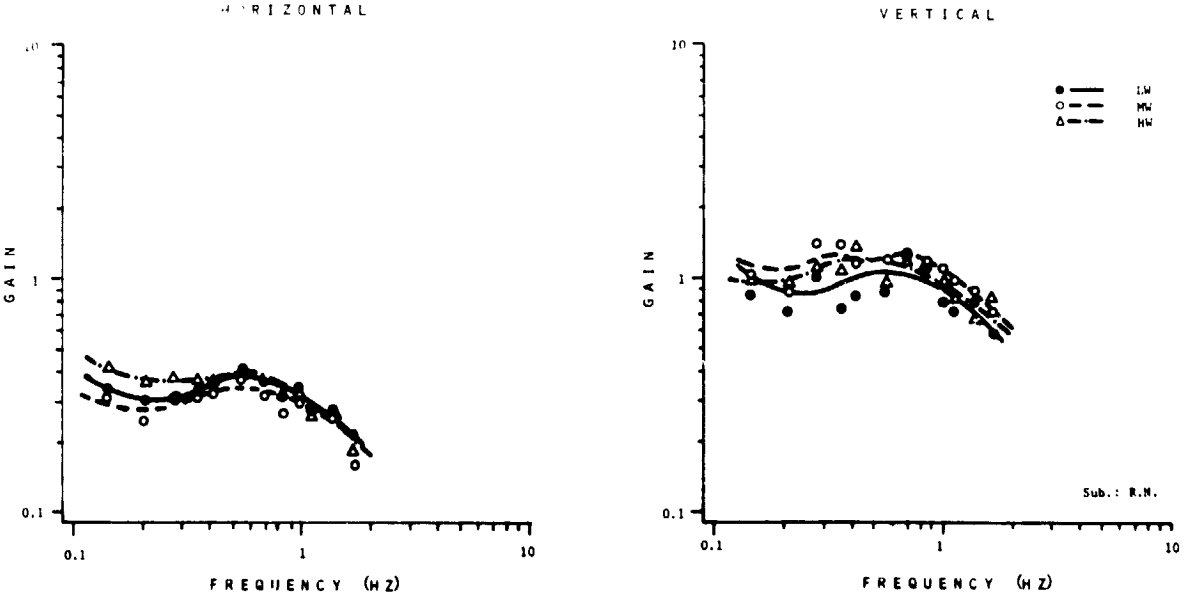

FIGURE 4

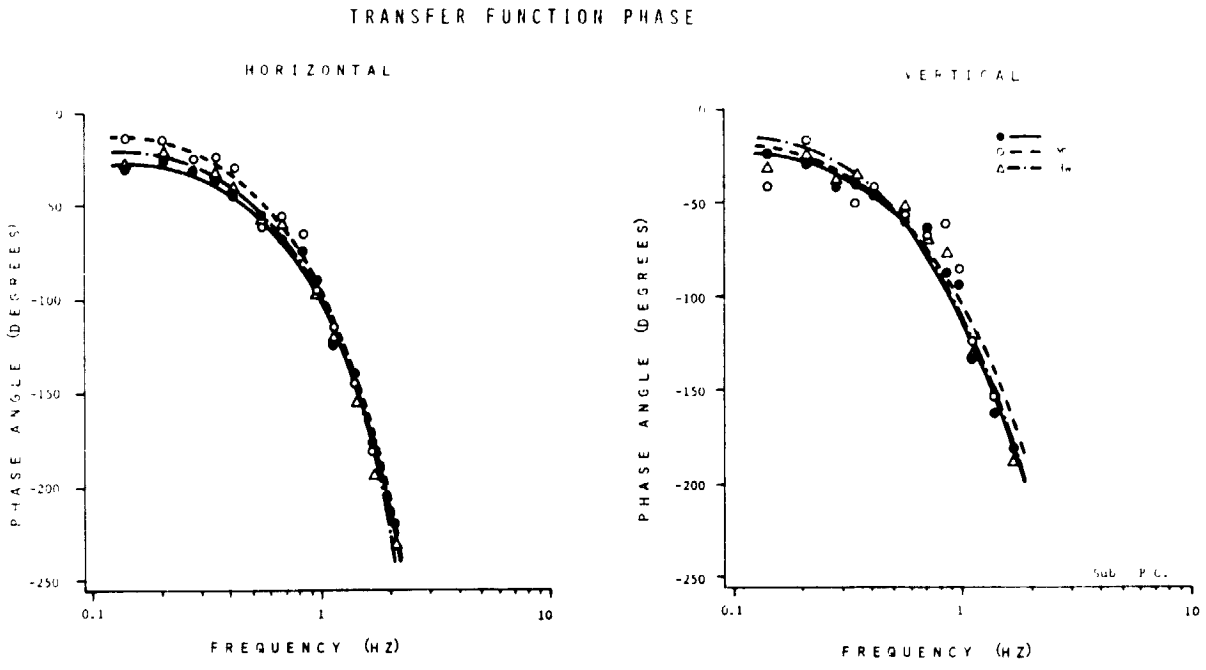

FIGURE 5

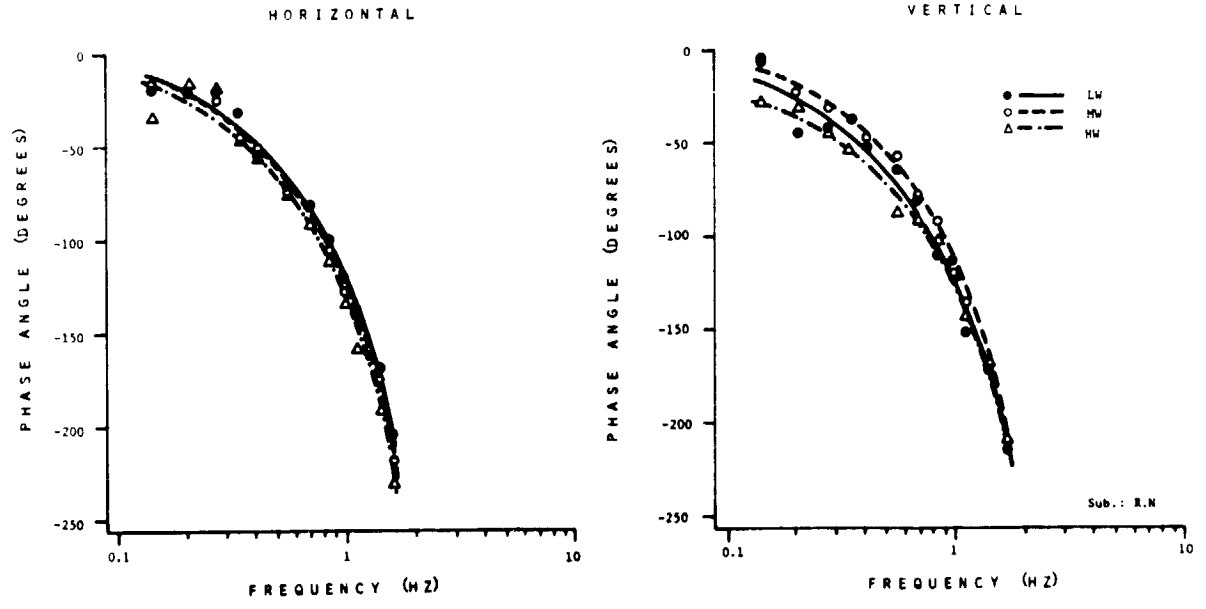

FIGURE 6

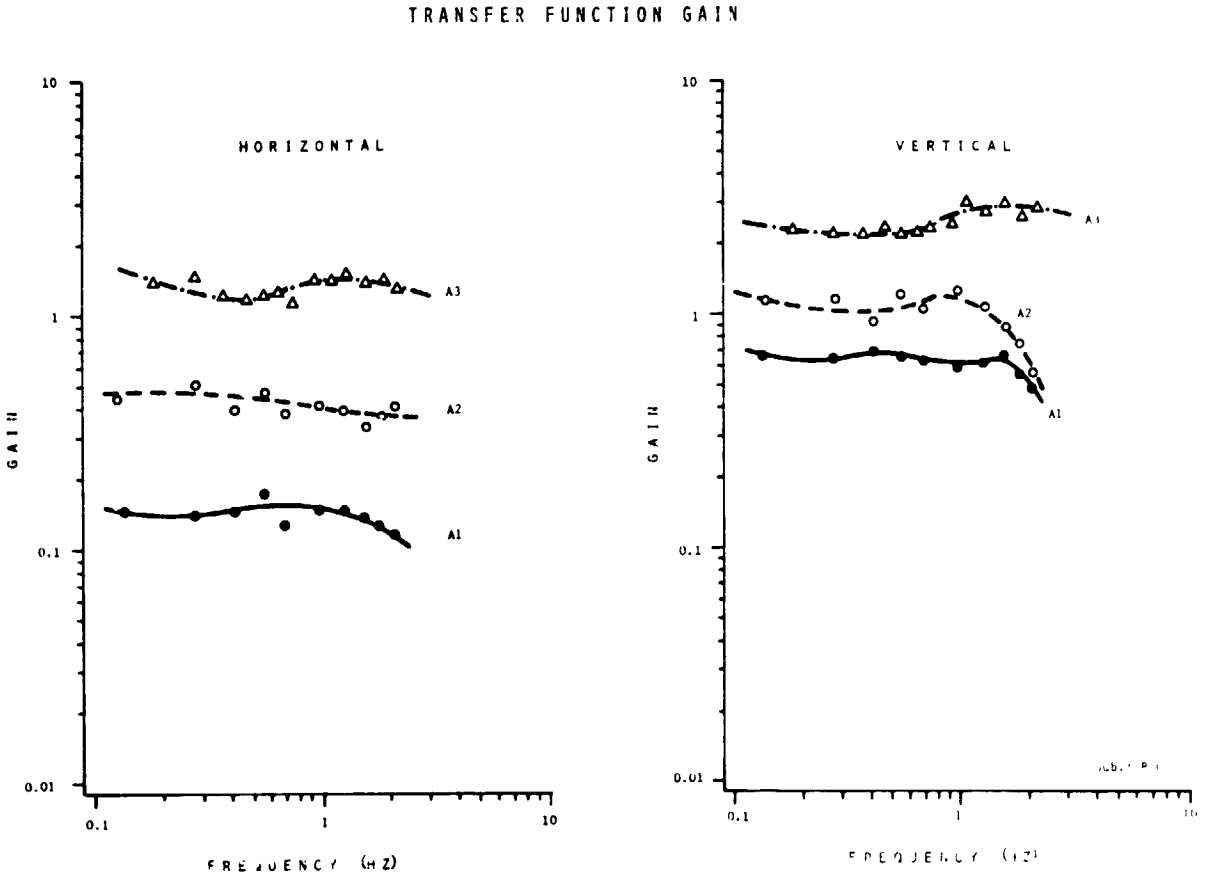
TRANSFER FUNCTION GAIN
HORIZONTAL
VERTICAL
GAIN
10
1
0.1
0.01
A3
A2
A1
0.1
1
10
FREQUENCY (HZ)

FIGURE 7

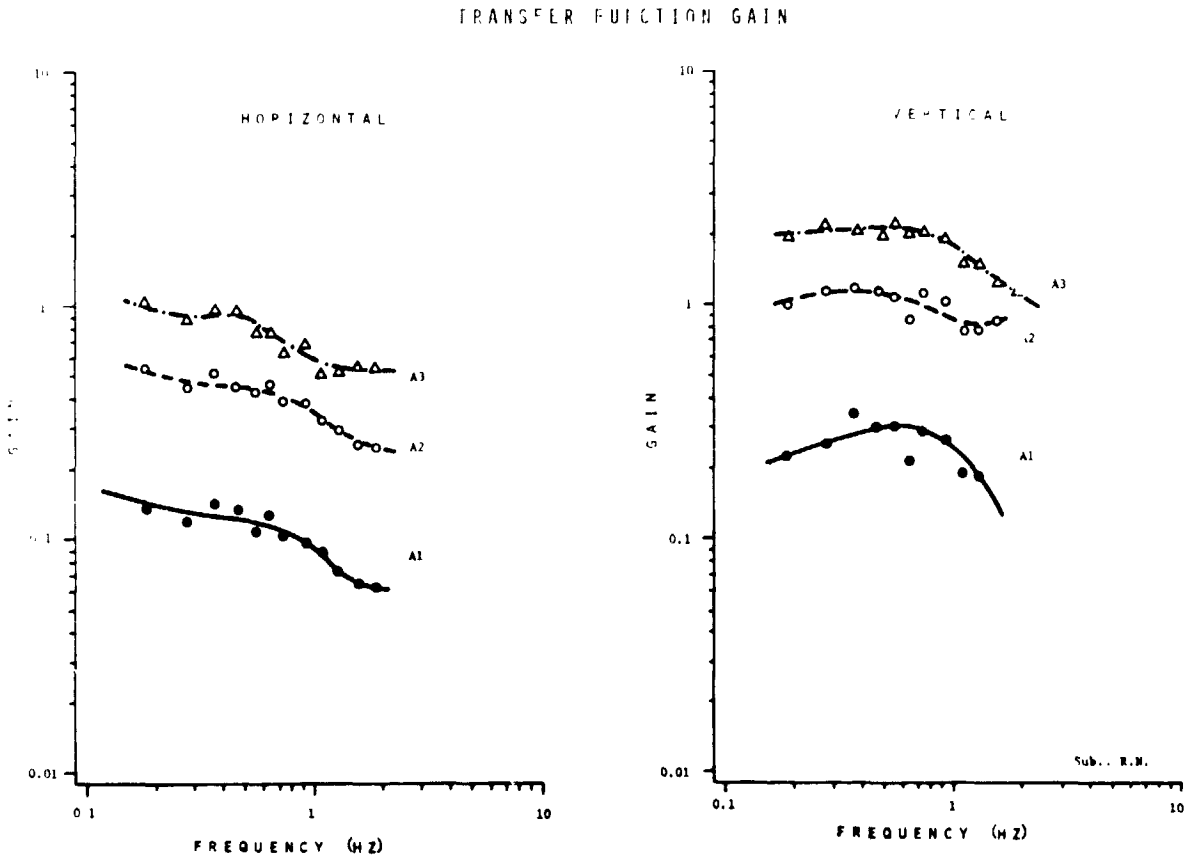

FIGURE 8

TRANSFER FUNCTION GAIN

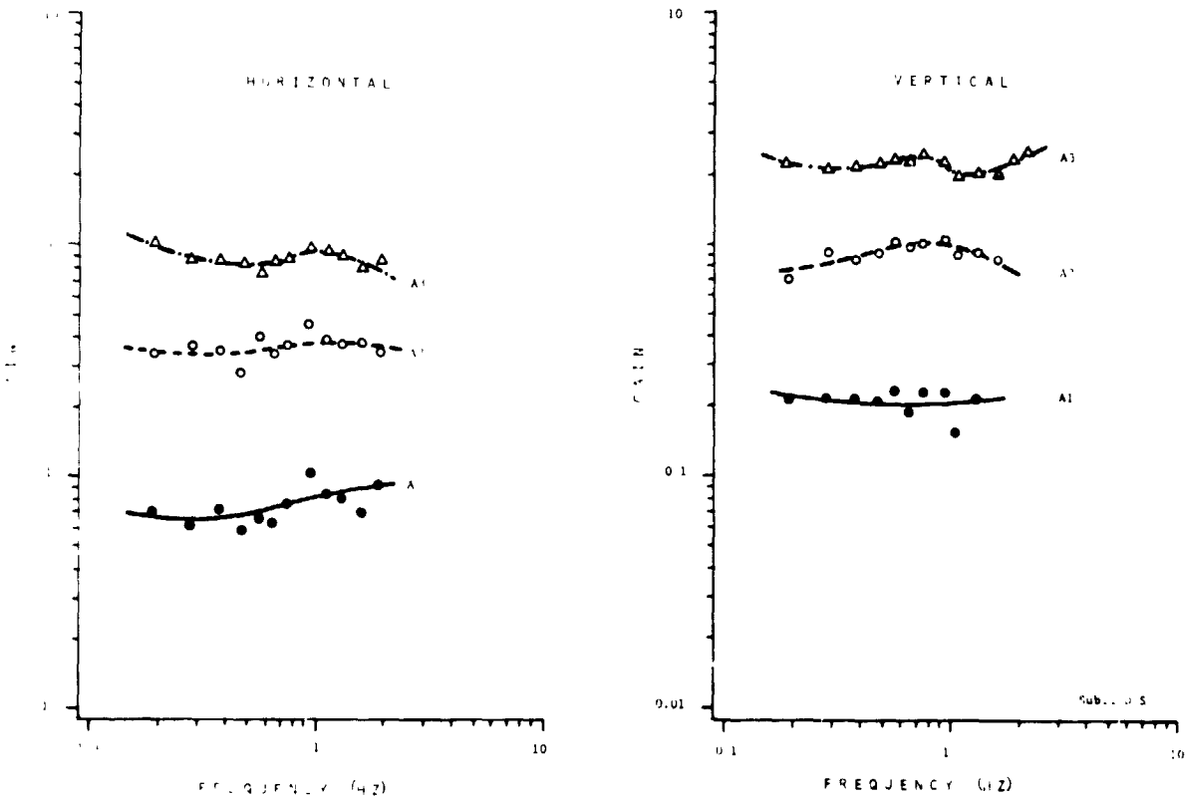

FIGURE 9

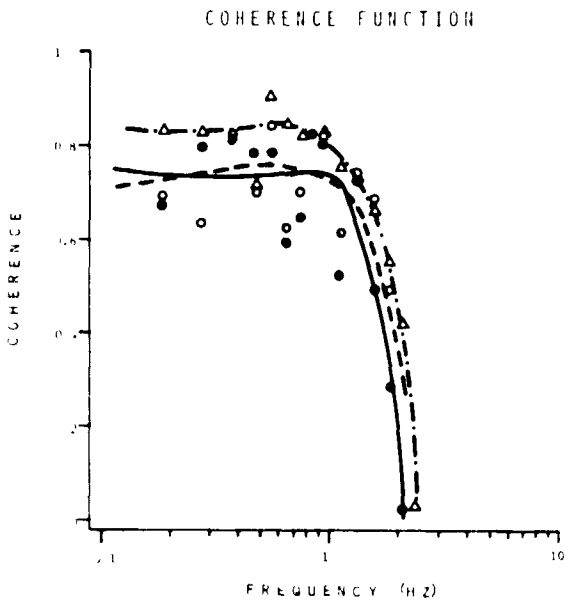

FIGURE 10a

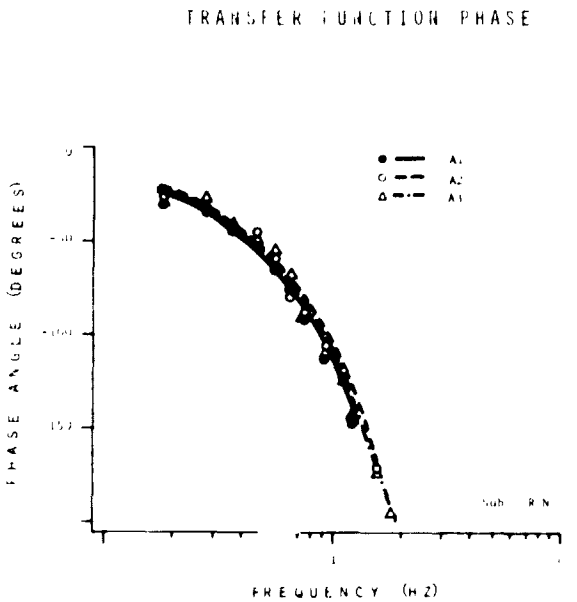

FIGURE 10b

HUMAN ENGINEERING LABORATORY HELICOPTER OBSERVER PERFORMANCE STUDIES

By John A. Barnes

U. S. Army Human Engineering Laboratory
Aberdeen Proving Ground, Maryland

The Systems Performance and Concepts Directorate of the U. S. Army Human Engineering Laboratory has, since 1972, been conducting a series of flight studies relating to some of the typical tasks performed by the U. S. Army helicopter observer. The first series of observer performance studies were called the Human Engineering Laboratory Helicopter Acquisition Tests (HELHAT).

HELHAT I

The initial study, reference 1, was conducted in October 1972 at the Naval Weapons Center, China Lake, California. This study was performed in conjunction with a tri-service target detection/acquisition test. The test was designed to help determine which was the most advantageous location for the observer position in operational helicopters, figure 1. The 68 simulated tactical low level route reconnaissance missions were flown by pilot observers from the 1st Cavalry Division using AH-1 and OH-58 helicopters. The targets were twenty items of 1950-60 era ordnance and three bridges set along a three leg, seven mile flight course over rough terrain with a cover of scrub growth.

The results indicated that although the observers detected a slightly larger number of targets from the left seat of the OH-58, there were no significant differences in the number of detections that could be attributed to the location of the observer in the helicopter.

HELHAT II

The second flight study, reference 2, was conducted in July and August of 1973 at Aberdeen Proving Ground, Maryland. This study was designed to allow us to determine whether a single observer or the pilot and observer team could perform a better job of target detection/acquisition during low level route reconnaissance using the OH-58. The 36 pilots and pilot observers who flew the 24 flights that made up this study were again from the 1st Cavalry Division, and many of them had flown in the previous study at China Lake.

The flight course was set up along a three leg, 15 mile route over the flat wooded area of Aberdeen Proving Ground and nine items of 1950-60 era ordnance and six "Fire Orange" boxes were the targets. The boxes, which measured 4 feet by 8 feet by 1 foot were used as control targets.

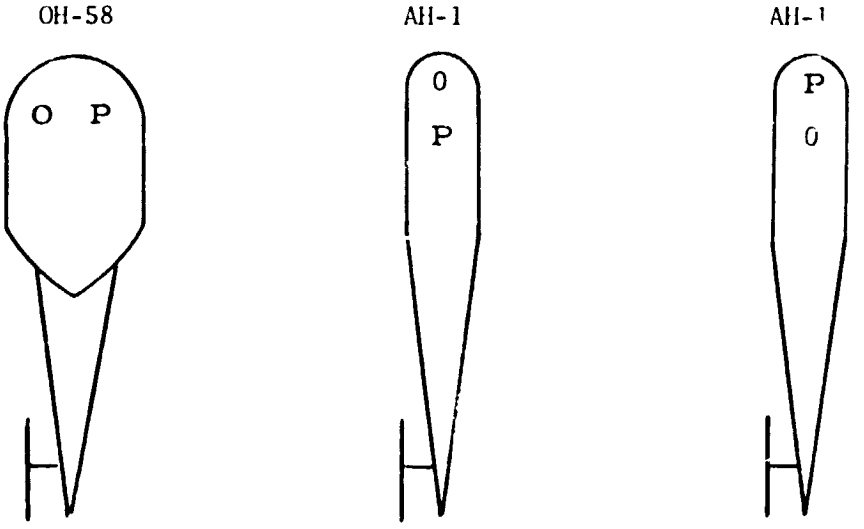

CONFIGURATION

Pilot Right	Observer Front	Pilot Front
Observer Left	Pilot Rear	Observer Rear

1. Experimental Configurations

An ancillary six flight Nap-of-the-Earth (NOE) test was flown after the main study had been completed. This test was flown at the lowest possible altitude depending upon the height of the ground cover; the altitudes varied from three to thirty feet as the crews flew an "S" pattern reconnaissance along the last leg of the low level course in the reverse direction. The NOE crews had great difficulty in maintaining their geographical orientation; crews 4 and 6 became lost and had to be told by the over-flying control aircraft to climb out and return to the base. Crew 5 also became disorientated, but they momentarily went to a higher altitude to reorient themselves and then proceeded to finish the mission NOE. All of these crewmen had combat experience and had had some NOE training.

The results of HELHAT II are shown in Tables 1 and 2.

TABLE 1. TARGETS DETECTED

TARGET TYPE	CREWS	OBSERVERS	NOE
ORDNANCE	40%	42%	44%
ORANGE BOX	76%	42%	67%
OVERALL	55%	42%	55%

TABLE 2. NOE DETECTION RANGE (METERS)

	TARGET					
CREW	15	14	13	12	11	10
1	520	120		470		640
2	160	370	350	770	220	
3				780	400	1110
4	460	200		1470		
5	340	100	90	600		1280
6						

HELHAT

The final portion of this series, reference 3, was published in 1974 and contained the major portions of HELHAT I and II as well as the target detection ranges achieved by the subjects during these two flight studies. The maximum detection ranges and the helicopter altitudes that accompanied them are shown in Table 3. These data, along with other pertinent facts about each detection, were processed using a multiple regression technique to try to determine the significant factors that contribute to successful target detection.

TABLE 3

Low Altitude Target Detection Efforts
(APG and NWC)

Target	Description	Volume (Cubic Feet)	Minimum Detection AGL Minimum AGL (Feet)	Minimum Detection Range (Meters)	Maximum Detection Range Maximum Range (Meters)	Maximum Detection AGL (Feet)
NWC 3	M-211 Trucks (3)	1674 ea	80	1060	1800	280
NWC 6	M-4 Tractor	1273	100	930	1020	210
NWC 10	V-62 Van	1715	80	580	740	320
APG 5	V-62 Van w Antenna[a]	3405	84[b]	570	640	249[c]
NWC 23	Bridge, 2 lane	48,200	100	460	785	150
NWC [illegible]	Supply Dump	69,445	100	420	660	250
NWC 24	Bridge, 1 lane	102,400	90	380	1470	260
NWC 19	M-37 Truck (3)	578 ea	90	280	1130	190
NWC 26	Pickup Truck	665	90	280	890	230
NWC 11	75mm Sky Sweep Gun (3)	1944 ea	90	230	550	270
NWC 16	V-62 Van w Antenna	2910	90	220	1060	340
APG 4	Day-Glo Orange Box	32	80[b]	140	840	214[b]
NWC 15	M-47 Tank	2620	110	250	510	200
NWC 17	Truck, Amphibious	2259	110	580	1290	310
NWC 4	M-535 Van	1678	120	1160	2200	330
APG 1	M-258 Van	2397	120[c]	620	1800	362[b]
NWC 12	Searchlight (3)	307 ea	120	310	441	150
NWC 13	M-38 Jeep (2)	177 ea	120	190	470	300
NWC 14	75mm Sky Sweep Gun	1944	120	190	280	160
NWC 7	Bridge, 1 lane	21,760	140	370	760	280
NWC 27	Tractor and Tanker	3115	160	880	1030	220
APG 2	Day-Glo Orange Box	32	186[b]	230	600	351[c]
NWC 9	V-62 Van	1715	190	670	830	250
APG 3	M-259 Van w Antenna	3394	189[c]	570	1880	251[b]
NWC 2	105mm Howitzer (3)	720 ea	210	1060	1060	210
NWC 1	M-48 Tank	2881	220	610	2320	340
APG 12	Day-Glo Orange Box	64	239[b]	220	400	328[b]
NWC 5	90mm Gun Mount	1637	250	637	1000	330
APG 10	Day-Glo Orange Box	32	268[b]	210	640	361[b]
APG 13	M-21 Rocket Launcher (3)	422 ea	296[b]	950	950	296[b]
APG 15	Day-Glo Orange Box	32	316[b]	400	600	419[b]
APG 14	M-21 Rocket Launcher	422	310[b]	200	500	362[b]
APG 6	M-38 Hard-Top Jeep	434	307[c]	100	500	434[b]
APG 7	Day-Glo Orange Box	64	329[c]	1600	1600	320[c]
APG 9	XM387E1 Missile Truck	1316	370[c]	1240	1290	392[c]
NWC 8	Truck, Amphibious	2259	370	700	700	370

[a]This van had been extended by 3 feet.

[b]Crew score

[c]Observer score

The results of the stepwise multiple regression analysis of the 268 detections in which the desired 29 measures for each detection were available indicated that the significant aspects of target detection were;

Sighting Angle
Terrain Slope/Roughness
Target Background Conspicuity
Target Foreground Conspicuity
Target Distance from Flight Path
Aircraft Heading
Aircraft Altitude Above Ground Level
Aircraft to Target Range
Apparent Target Size
Bearing Estimate Error

When the HELHAT data were analyzed, not considering Conspicuity and Range and Bearing Estimate Errors, there were some changes in the significant variables. These 831 detections added;

Target Difficulty
Relative Bearing to Target
Cloud Cover
Target Length
Target Volume

and caused the deletion of Terrain Slope/Roughness and Apparent Target Size.

POP-UP STUDY

A third flight study, reference 4, investigated the effectiveness of a helicopter using the pop-up tactic and a simulated wire-guided missile against a heavy tank's main gun. This test was flown in August of 1975 at Aberdeen Proving Ground. This was a dynamic encounter rather than a passive one such as HELHAT; the study was primarily to test the ability of the tank crews of two different types of heavy tanks to defend themselves against a helicopter gunship, therefore it was the tank crew that changed rather than the air crew. The test scenario called for the Forward Observer to direct the helicopter to move to one of the eight preselected positions to perform the pop-up tactic. The tank crews had been briefed that they would be liable to encounter helicopter missile fire on certain portions of the extensive tank road course.

The mean Air-to-Ground and Ground-to-Air detection ranges are shown in Table 4. The "LOS Range" entry is the maximum possible range at which either vehicle could have seen the other from that position. The "ND" entry indicates that the tank crew did not detect the helicopter during the attack from that position. A typical engagement plan is shown in figure 2. The Forward Observer located in the area of CP 22G alerts the helicopter to proceed to pop-up position II for the attack as the tank will be in his line-of-sight

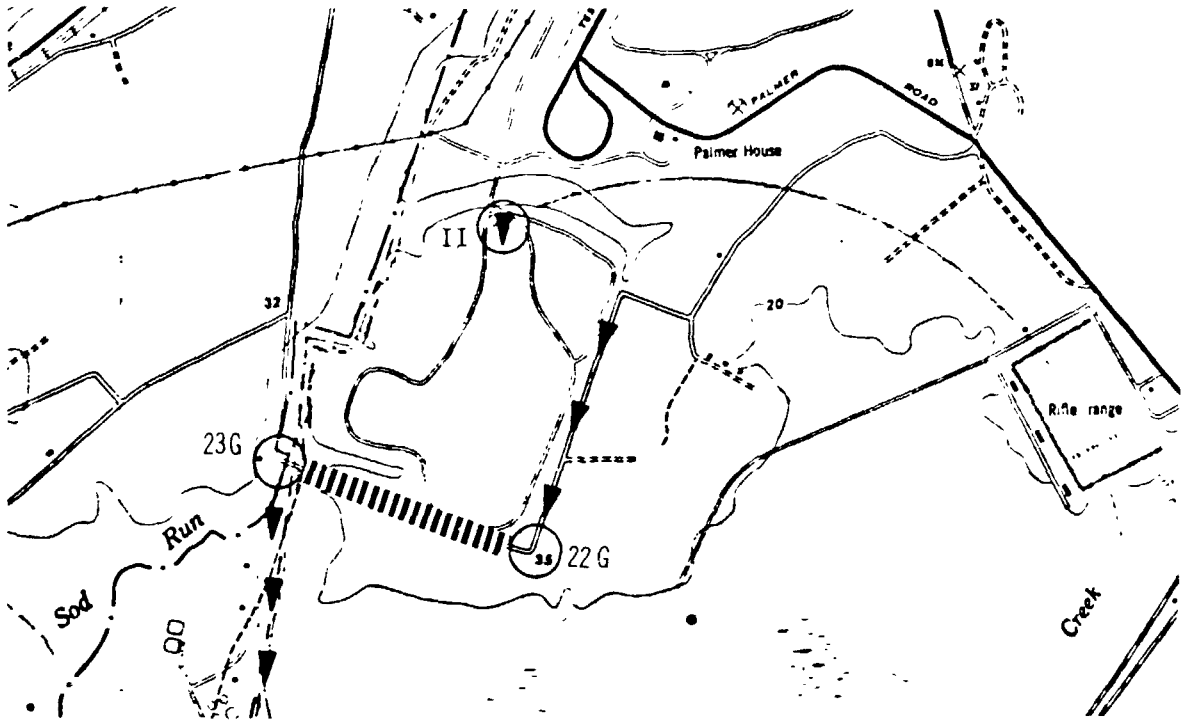

Fig. 2. CP 22G to CP 23G Course Segment, Pop-Up Position II

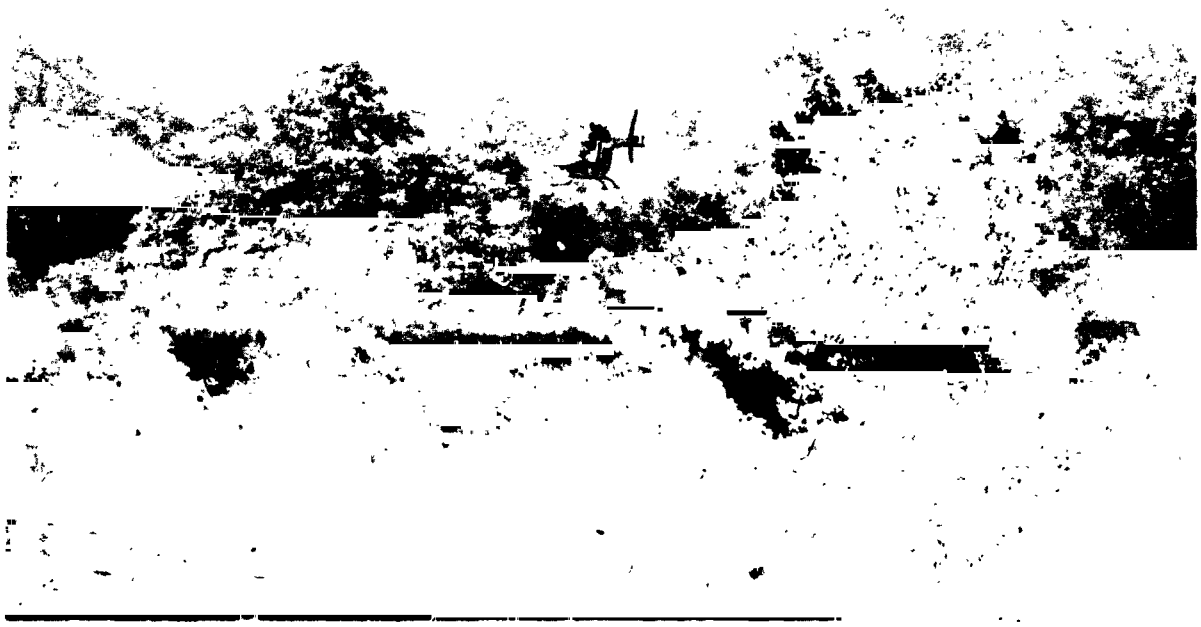

Fig. 3. Helicopter At Pop-Up Position II, Ready For Missile Launch

after it passes CP 22G enroute to CP 23G. Figure 3 shows the helicopter in firing position at position II; an OH-58 was used as a substitute for the AH-1 because of scheduling problems. Figure 4 shows the helicopter on a simulated gunnery run against the tank; this procedure was used to alert the tank crew that they had been under missile attack and that if they had not seen the helicopter before, it was too late!

TABLE 4. POP-UP RESULTS (METERS)

POP-UP POSITION	LOS RANGE	MEAN A-TANK RANGE AIR/GND	MEAN A-TANK RANGE GND/AIR	MEAN F-TANK RANGE AIR/GND	MEAN F-TANK RANGE GND/AIR
1	2250	1640	1511	1631	1070
2	1000	1000	1000	1000	1000
3	3000	1480	1125	1700	1125
4	1400			1100	1120
5	1800	1200	720		
6	1750	1420	485	1303	840
7	2100			2030	ND
8	2950			2100	ND

HELCAT

The current effort, Human Engineering Laboratory Camouflage Application Test (HELCAT), is the air-to-ground portion of a larger, interagency camouflage application test in which the detectability of pattern painted tanks is being compared to that of camouflaged tanks. The day and night airborne phases will be flown in mid-June. During the day phase we will, for the first time, record the observer's actual eye point of regard during an air-to-ground target search. We will measure the single glance dwell time, the total dwell time and the observer field of view for each of the day target detections. The night phase will use the AN/PVS5 Night Vision Device as an observer aid.

The results of the study will compare observer's daytime target detection performance, against pattern painted and camouflaged tanks, with and without the eye movement measurement device. The night portion will compare the observer target detection performance, against the same tanks, with and without the AN/PVS5 Night Vision Device, and the unencumbered day performance with the night AN/PVS5 performance. These results should tell what part of

Fig. 4. Helicopter On Firing Pass From Pop-Up Position II.

the camouflage on the tanks needs to be improved to prevent detection, the amount of detection degradation from day conditions to be expected when the AN/PVS5 devices are used, and the gain in night detection capabil ty to be expected when the AN/PVS5 devices are used.

REFERENCES

1. Barnes, John A.: HELHAT I, The Effect of Observer Position On Target Detection. HEL TM 7-73, 1973.

2. Aviation Team, Systems Performance and Concepts Directorate: HELHAT II, Scout Crew/Observer Target Detection Flight Tests. HEL TN 1-74, 1974.

3. Barnes, John A.: Human Engineering Laboratory Helicopter Acquisition Test (HELHAT). HEL TM 20-74, 1974.

4. Barnes, John A.: Use of the Tank Main Gun for Defense Against Helicopter Attack. HEL TM 14-76, 1976.

INTERACTION BETWEEN WARNING SIGNAL AND FORE-PERIOD IN SIMPLE FOOT REACTION TIME

Nataraj S. Nataraj
Engineering Technologies
Sinclair Community College
Dayton, Ohio 45402

John M. Howard
Dept. of I.E. and O.R.
Wayne State University
Detroit, Michigan 48202

ABSTRACT

This paper reports in part the results of an experiment set up to study the effects of interaction between the fore-period and warning signal on a simple foot reaction time task. The task required the subject to respond with a lateral movement of the right foot from right to left after observing the onset of a temporal visual event. Reaction times were recorded for various combinations of fore-periods and warning signals. Interpretation of results are made with respect to design and operation of foot controls.

INTRODUCTION

In the operation of machine-foot controls the human operator is sometimes required to respond after a varying interval of time which is preceded by a warning signal of variable length. Man/machine interface of this type is most common in an industrial environment. In this setting it is common to find an operator monitoring a set of machine-readiness lights, manipulating material with his hands and operating the machine functions with one or both of his feet. Successful operation of this type of machine is dependent upon many variables, such as working environment, operator experience and motivation, and machine design. In certain situations operator speed of response is crucial to successful and safe machine operation. One factor that may have an observable effect upon the operator's speed of

response is temporal expectancy. Temporal expectancy is defined as an increasing readiness to respond to events (signals) that occur over time. The measurement of simple reaction time can be used as an observation of an increasing readiness to respond. In general, as readiness increases, reaction time decreases.

Naatanen (1970) in a review of the literature points out two diverging tendencies with respect to the relationship between fore-period and simple reaction time: (1) when the fore-period is not varied, a general observation is that the longer the fore-periods, and (2) when fore-periods of different duration are randomly presented, the reaction time--in addition to its being generally longer than in the aforementioned case, is longest after the shortest fore-period in a series. It has also been observed that the longest fore-period in a series yields the shortest reaction time. Naatanen in conclusion proposed that four factors exert an influence on the relationship between fore-period and the reaction time when varying fore-periods with a given range are delivered in a random order. Two of these factors act via the variables called "expectancy": (1) the expectancy-reducing effect of the flow of time after the warning signal, because longer periods are more difficult to estimate than shorter ones; and (2) the expectancy-increasing effects of the flow of time after the warning signal, because the objective probability of the occurence of the stimulus increases.

Several earlier studies used the term expectancy to describe the subject's change in reaction time over a range of time intervals. Deese (1955: 363) hypothesized that "expectancy should be low immediately after a signal, should increase as the mean intersignal interval approaches, and

finally should become quite high as the intersignal interval goes beyond the mean." Baker (1959) offered another hypothesis suggesting that expectancy increases as intersignal interval increases until the mean intersignal interval and then expectancy decreases as fore-period increases further. Both hypotheses have been supported by research. The major difference between the studies supporting one or the other of the hypotheses was in the size of the range of fore-periods.

In experiments that supported the theory of increasing expectancy, ranges of less than 5 sec. were used, while in experiments that supported a U-shaped function the ranges were 18 sec. or greater. In those experiments the varying fore-periods were always preceded by a warning signal of fixed length.

Since the intervals appropriate to the operation of foot-operated industrial machines (such as described previously) are relatively short, and usually include a warning signal (machine ready signal) of varying length, the range of fore-periods and warning signals used in this experiment were short.

Following from those earlier studies it was expected that temporal expectancy and therefore speed of reaction time would vary as a function of the interaction between the duration of both a fore-period (FP) interval within a range of FP and a warning signal (WS) within the range of WS. To test this hypothesis a range of eight common values of WS and FP were paired with itself and with each of the other seven values, producing 64 paired presentations of WS and FP. The eight common values were 250 msec., 500 msec., 1, 2, 3, 4, 5, and 7 sec.

METHOD

Subjects. Forty-eight (30 males, 18 females) volunteer college students served as subjects. All subjects were screened for the absence of visual color defects, corrected 20/20 visual acuity and physical disability with regard to the right leg and foot movement. Twenty-nine male and 15 female subjects were right leg dominant. Table 1 gives the subject characteristic for age, weight and stature.

Apparatus. The foot reaction time measurement apparatus is shown in Figure 1. It consisted of a vertical-horizontal adjustable seat that provided for control of subject knee angle, 30° off vertical. The start and experimental targets were each 6 cm. in diameter and placed 15 cm. apart. The display consisted of a yellow warning signal (WS) and red stimulus light which were mounted vertically (WS below) on a gray panel 15 cm. apart. The gray panel was positioned 266 cm. in front of the subject at seated eye height from the floor. Each light was 6 cm. in diameter. The recording equipment included a sandal sole approximating a 9 1/2 shoe with a brass spike (protruding 2 cm. downward) affixed to the center of the sole. The sandal was attached to the subjects' right foot with straps. The targets were brass plates. An electronic timing measuring device (Beckman Universal Timer) was used to measure response time in 1/1000 sec. Response time was measured from onset of the red stimulus light until the experimental target was contacted.

Experimental Design. Using a table of random numbers, the experimenters assigned a random sequence for the presentation of 64 combinations of WS and FP. The presentation order was counterbalanced to minimize the effects

TABLE I

BIO DATA OF SUBJECTS

	MALE (30)		FEMALE (18)		TOTAL (48)	
	MEAN	STD. DEV.	MEAN	STD. DEV.	MEAN	STD. DEV.
Age (years)	23.45	3.77	23.37	5.08	23.21	4.31
Stature (meters)	1.79	0.07	1.64	0.05	1.73	0.10
Weight (kg.)	75.33	13.91	56.20	10.00	68.70	14.74

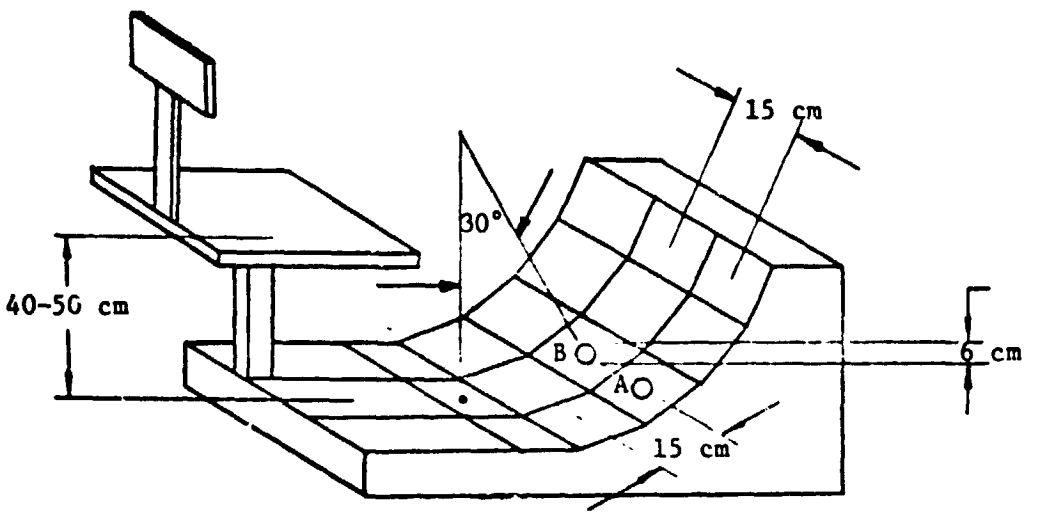

A - Starting Position

B - Experimental Target (6 cm. in diameter)

FIGURE 1 - DIMENSIONS OF THE FOOT REACTION-TIME MEASUREMENT APPARATUS

of subject learning and fatigue. The complete test session took approximately 50 min. All subjects were tested between the hours of 10:00 A.M. and 4:00 P.M. Subjects were not provided with knowledge of results during testing. Subjects were given 5 unscored practice trials (3 sec. WS, 3 sec. FP), during which they became familiar with the foot reaction time measurement apparatus. All subjects were debriefed following testing.

Instruction Given to the Subject. The subject was instructed to sit comfortably but straight, his thighs horizontal, with his right foot over the target. The knee angle was measured 30° off vertical. If necessary, the chair was adjusted to achieve this body posture. The subject was instructed to fixate on the black dot located on the gray panel before them. A yellow light would appear in the circle toward the bottom of the panel and a red light would appear in the circle to the top. The yellow light appeared first, went off and then was followed by the red light. When the red light appeared, the subject was asked to move as rapidly as possible from the start position (right plate) to the experimental target on the left. The speed of this movement was the main objective and therefore the subject was told not to worry about the accuracy of the foot movement, although hitting the target plate was essential to achieving timed scores. After each trial the subjects were free to rest their right leg in any desired position. When the next trial was to begin the subjects were asked to reset their leg to the start position and again fixate on the black dot. Subjects were not permitted to hold onto the apparatus seat during testing.

TABLE II

REACTION TIMES FOR WS OR FP KEPT CONSTANT AT 250 M.SECS.

WARNING SIGNAL OR FORE PERIOD	WARNING SIGNAL KEPT CONSTANT AT 250 M.SEC.			FORE PERIOD KEPT CONSTANT AT 250 M.SEC.		
	N*	MEAN (m.sec.)	STD. DEV. (m.sec.)	N*	MEAN (m.sec.)	STD. DEV. (m.sec.)
250 m.sec.	48	170.93	38.00	48	170.98	46.03
500 m.sec.	47	178.96	40.76	48	173.17	43.58
1 sec.	48	182.27	49.87	48	184.19	45.30
2 sec.	48	190.27	47.88	48	179.58	40.65
3 sec.	48	196.65	61.15	48	181.13	37.38
4 sec.	48	189.08	50.71	47	186.94	36.62
5 sec.	48	189.75	44.68	48	180.58	38.56
7 sec.	48	187.69	48.19	48	184.56	45.13

TABLE III

REACTION TIMES FOR WS OR FP KEPT CONSTANT AT 500 M.SECS.

WARNING SIGNAL OR FORE PERIOD	WARNING SIGNAL KEPT CONSTANT AT 500 M.SEC.			FORE PERIOD KEPT CONSTANT AT 500 M.SEC.		
	N*	MEAN (m.sec.)	STD. DEV. (m.sec.)	N*	MEAN (m.sec.)	STD. DEV. (m.sec.)
250 m.sec.	47	172.04	42.33	47	178.96	40.76
500 m.sec.	48	180.31	39.74	48	179.90	39.12
1 sec.	47	190.72	49.15	48	199.77	60.19
2 sec.	47	187.36	47.45	47	197.13	57.35
3 sec.	47	191.02	38.48	48	179.58	44.94
4 sec.	47	188.36	44.74	48	182.81	43.18
5 sec.	47	193.19	46.99	48	194.35	50.18
7 sec.	48	210.96	49.68	48	189.73	43.70

* NUMBER OF SUBJECTS

TABLE IV

REACTION TIMES FOR WS OR FP KEPT CONSTANT AT 1 SEC.

WARNING SIGNAL OR FORE PERIOD	WARNING SIGNAL KEPT CONSTANT AT 1 SEC.			FORE PERIOD KEPT CONSTANT AT 1 SEC.		
	N*	MEAN (m.sec.)	STD. DEV. (m.sec.)	N*	MEAN (m.sec.)	STD. DEV. (m.sec.)
250 m.sec.	48	184.19	45.31	48	182.06	49.93
500 m.sec.	48	198.21	58.95	47	190.32	50.43
1 sec.	48	204.10	53.08	48	204.15	55.57
2 sec.	48	195.15	50.77	48	189.15	42.42
3 sec.	48	194.13	50.78	48	187.31	51.20
4 sec.	48	194.88	44.22	48	188.73	46.14
5 sec.	48	200.25	45.52	48	193.52	49.51
7 sec.	44	191.41	49.17	43	192.90	53.01

* NUMBER OF SUBJECTS

TABLE V

REACTION TIMES FOR WS OR FP KEPT CONSTANT AT 2 SECS.

WARNING SIGNAL OR FORE PERIOD	WARNING SIGNAL KEPT CONSTANT AT 2 SEC.			FORE PERIOD KEPT CONSTANT AT 2 SEC.		
	N*	MEAN (m.sec.)	STD. DEV. (m.sec.)	N*	MEAN (m.sec.)	STD. DEV. (m.sec.)
250 m.sec.	48	179.63	41.03	48	190.46	48.57
500 m.sec.	48	196.35	57.40	47	187.23	47.51
1 sec.	48	189.15	42.42	48	195.15	50.77
2 sec.	47	194.28	46.79	47	194.06	49.20
3 sec.	48	20 .31	58.75	48	187.96	49.78
4 sec.	48	188.75	41.59	48	189.77	46.90
5 sec.	48	19..25	52.27	48	188.70	45.81
8 sec.	47	190.58	43.09	48	186.88	56.21

*NUMBER OF SUBJECTS

TABLE VI

REACTION TIME FOR WS OR FP KEPT CONSTANT AT 3 SECS.

WARNING SIGNAL OR FORE PERIOD	WARNING SIGNAL KEPT CONSTANT AT 3 SEC.			FORE PERIOD KEPT CONSTANT AT 3 SEC.		
	N*	MEAN (m.sec.)	STD. DEV. (m.sec.)	N*	MEAN (m.sec.)	STD. DEV. (m.sec.)
250 m. sec.	48	181.27	37.35	48	196.02	61.63
500 m.sec.	48	179.60	44.95	48	192.71	38.76
1 sec.	48	188.88	53.16	48	196.48	52.25
2.sec.	48	188.02	46.86	48	203.31	61.12
3 sec.	47	189181.	44.63	48	187.71	43.50
4 sec.	48	192.04	46.52	48	183.10	39.08
5 sec.	48	205.04	49.33	48	204.71	50.47
7 sec.	48	192.81	48.53	48	192.02	46.66

* NUMBER OF SUBJECTS

TABLE VII

REACTION TIMES FOR WS OR FP KEPT CONSTANT AT 4 SECS.

WARNING SIGNAL OR FORE PERIOD	WARNING SIGNAL KEPT CONSTANT AT 4 SEC.			FORE PERIOD KEPT CONSTANT AT 4 SEC.		
	N*	MEAN (m.sec.)	STD. DEV. (m.sec.)	N*	MEAN (m.sec.)	STD. DEV. (m.sec.)
250 m.sec.	47	189.06	39.04	48	188.60	50.63
500 m.sec.	48	182.81	42.81	47	188.40	44.71
1 sec.	48	188.31	48.86	48	190.52	50.01
2 sec.	48	189.81	48.55	48	187.50	43.30
3 sec.	48	183.21	39.03	48	181.94	46.59
4 sec.	48	185.58	39.94	48	185.69	40.04
5 sec.	48	192.23	41.58	48	192.25	50.23
7 sec.	48	192.60	44.76	47	187.66	45.88

* NUMBER OF SUBJECTS

TABLE VIII

REACTION TIMES FOR WS OR FP KEPT CONSTANT AT 5 SECS.

WARNING SIGNAL OR FORE PERIOD	WARNING SIGNAL KEPT CONSTANT AT 5 SEC.			FORE PERIOD KEPT CONSTANT AT 5 SEC.		
	N*	MEAN (m.sec.)	STD. DEV. (m.sec.)	N*	MEAN (m.sec.)	STD. DEV. (m.sec.)
250 m.sec.	48	176.63	44.59	48	189.75	44.68
500 m.sec.	48	193.83	48.33	48	192.63	51.18
1 sec.	48	194.56	50.46	48	200.25	45.27
2 sec.	48	188.79	46.43	48	190.96	51.74
3 sec.	48	204.71	46.11	48	205.04	49.33
4 sec.	48	192.38	48.11	48	192.23	43.93
5 sec.	48	192.46	49.92	48	192.88	53.13
7 sec.	47	196.15	56.17	48	190.92	50.30

* NUMBER OF SUBJECTS

TABLE IX

REACTION TIMES FOR WS OR FP KEPT CONSTANT AT 7 SECS.

WARNING SIGNAL OR FORE PERIOD	WARNING SIGNAL KEPT CONSTANT AT 7 SEC.			FORE PERIOD KEPT CONSTANT AT 7 SEC.		
	N*	MEAN (m.sec.)	STD. DEV. (m.sec.)	N*	MEAN (m.sec.)	STD. DEV. (m.sec.)
250 m.sec.	48	182.48	41.80	48	184.77	51.93
500 m.sec.	47	190.47	51.15	48	210.96	49.68
1 sec.	46	193.72	52.02	44	191.34	48.37
2 sec.	46	187.83	46.27	48	190.19	42.66
3 sec.	46	192.78	47.31	48	192.81	48.53
4 sec.	47	183.59	51.64	48	193.02	44.72
5 sec.	45	191.19	42.10	47	196.38	56.07
7 sec.	47	186.26	39.58	47	186.26	44.85

* NUMBER OF SUBJECTS

TABLE X

REGRESSION VALUES OF REACTION TIMES FOR WS-FP KEPT CONSTANT

WARNING SIGNAL OR FORE PERIOD	WARNING SIGNAL KEPT CONSTANT		FORE-PERIOD KEPT CONSTANT	
	Y-INTERCEPT (m.sec.)	SLOPE	Y-INTERCEPT (m.sec.)	SLOPE
250 m.sec.	180.030	1.996	175.800	1.526
500 m.sec.	177.484	4.118	185.870	0.672
1 sec.	195.307	-0.007	190.140	0.308
2 sec.	190.570	0.376	191.750	-0.601
3 sec.	182.707	2.454	195.467	-0.337
4 sec.	185.660	0.808	189.150	-0.026
5 sec.	188.546	1.368	195.070	-0.260
7 sec.	189.012	-0.166	195.804	-0.910

RESULTS

Results are presented first for the eight common values of FP and WS; these are followed by the regression analysis for each FP and WS kept constant. Data were eliminated from the analysis for trials which subjects failed to respond to stimulus or evidenced unusually long reaction time.

The mean, standard deviation and the number of subjects for each WS-FP combination are shown in Tables II through IX. For 128 combinations of WS-FP, the mean reaction time values ranged from 170.98 m.secs. to 210.96 m.secs. The variability of reaction time varied from 36.62 m.secs. to 61.63 m.secs. The linear regression values for WS-FP kept constant are presented in Table X. The negative regression slope was found when WS was 1 sec. and 7 sec. and for FP values of 2, 3, 4, 5 and 7 secs. In all cases

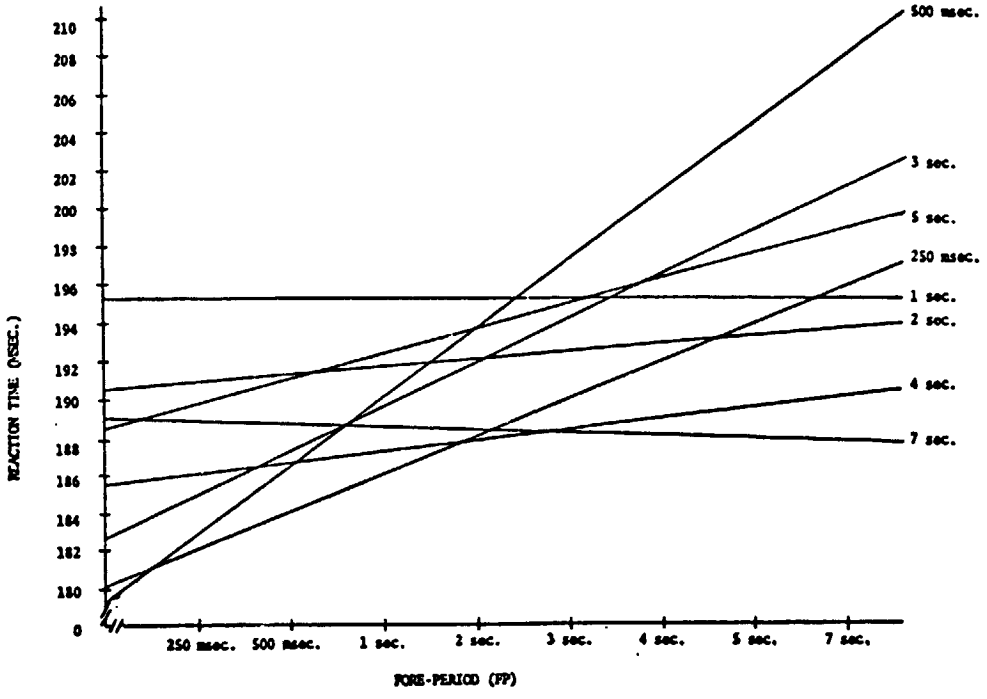

FIGURE 2: REGRESSION PLOT OF REACTION TIME VS. FP (WS KEPT CONSTANT)

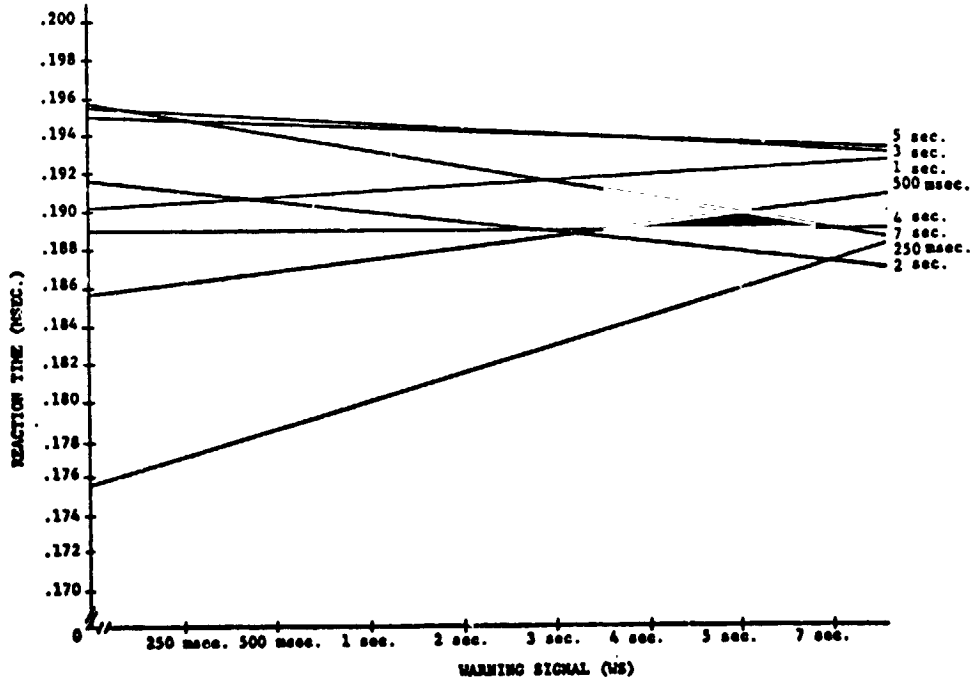

FIGURE 3: REGRESSION PLOT OF REACTION TIME VS. WS (FP KEPT CONSTANT)

except for the 1 sec. WS, the WS regression intercept value was less than the corresponding FP value.

SUMMARY

To study the interactive effects of variable FP and WS on temporal expectancy of foot simple reaction time, forty-eight college students responded to a red visual stimulus by moving the right foot laterally left to a disc target. The WS and FP were paired for 64 combinations with the following common values: 250 m.secs., 500 m.secs., 1, 2, 3, 4, 5 and 7 secs.

Results of the present study suggest that when the FP value is larger than the WS value, the reaction time (temporal expectancy) is usually less than when the WS-FP values are reversed. This finding is indicated mainly for the WS-FP values of 250 m.secs., 500 m.secs., 1 and 2 secs., with the reverse found for the values of 3 through 7 secs. In addition, when a FP value was kept constant at 2 secs. or greater, the reaction time decreased as WS increased. The combination of WS-FP that produced the least variable effect on RT was shown to be a WS kept constant at _ sec. or FP kept constant at 4 secs.

While the results of this study are not conclusive with regard to the interactive effects of variable warning signals and fore-periods, they do indicate that the speed of human operator response (foot reaction time) can be enchanced by controlling the duration of WS-FP intervals. Further analysis of this data and additional studies are in process.

REFERENCES

1. Baker, C. H. Towards a Theory of Vigilance. Canadian Journal of Psychology, 1959, 13, 35-49.

2. Deese, J. Some Problems in the Theory of Vigilance. Psychological Review, 1955, 62, 359-368.

3. Naatanen, R. The Diminishing Time-Uncertainty with the Lapse of Time After the Warning Signal in Reaction-Time Experiments with Varying Fore-Periods. Acta Psychologica, 1970, 34, 399-419.

SESSION VI

AUTOMOBILE DRIVING

Chairman: G. A. Bekey

A SIMULATOR FOR DRIVING RESEARCH[1]

By Rudolph G. Mortimer and Russell L. Adkins

Department of Health and Safety Education
University of Illinois

SUMMARY

A fixed-base simulator is described which is to be used in research on driving skills and the effects of alcohol, as well as other studies of driver-vehicle performance.

INTRODUCTION

In a previous research study by Mortimer and Sturgis (reference 1), a fixed-base simulator was used to evaluate the effects of alcohol on the lateral control cues and motor skills used by drivers. In addition, a preliminary study was carried out of the effect of alcohol on car-following performance. Subsequently, some additional studies were carried out in a vehicle operated on public highways for a comparison with results using the driving simulator. In order to conduct further studies of this type, and having similar objectives, but in addition to assess the effects of stress, incentives and information loading, as well as alcohol on these basic driving skills, a driving simulator is under development at the University of Illinois.

The objective of this report is to provide an overview of the general operating characteristics of the device.

THE DRIVING SIMULATOR

The driving simulator consists of a number of major components, including the following: an automobile in which the driver is seated, a roadway display generation and projection system, a vehicle dynamics simulation, a control console and a data recording and acquisition capability.

---

[1]This research was supported by the National Institute on Alcohol Abuse and Alcoholism, U.S. Dept. of HEW.

The Automobile

A 1969 Simca automobile, cut-off about 0.5 m rear of the front seats is mounted on a supporting structure. The rack has been removed from the rack and pinion steering box and a spring has been attached to the steering column by a nylon cord which winds around the column if the steering wheel is rotated, thereby creating a return force. Steering feel thus achieved was modeled after an American automobile having power steering. A multi-turn rotary potentiometer is attached to the end of the steering column to measure steering wheel displacement. The conventional accelerator and brake pedals are left intact. Depressing the accelerator actuates a linear potentiometer whose output is fed to the analog computer. Similarly, depressing the brake pedal actuates the vehicle's master cylinder which is connected to a hydraulic brake transducer, the electric signal from which is also sent to the analog computer. A position servo which is actuated by a signal proportional to simulated vehicle speed drives the speedometer cable which is directly coupled to the speedometer pointer.

The driver's seat is adjustable in fore and aft position as well as in the rake of the seat back, as is conventional with this vehicle.

Roadway Display Generation and Projection System

At present, a Raytheon 704 digital computer is used to generate a roadway display on a CRT. A television camera views the CRT display and sends the image to an Advent video projector which is mounted above the automobile, in the same longitudinal plane as the driver's position. A curved projection screen 1.8 m wide and 1.3 m high is positioned 2.5 m in front of the driver.

The display consists of a horizon line, the dashed center line and the edge lines of a two-lane road which responds appropriately in lateral translation and yaw to steering inputs and to speed commands originating from the accelerator and brake controls. In addition, the display can show the rear of another vehicle in the right hand lane (presently configured as a straight truck) which will provide the stimulus in car-following studies.

Longitudinal Dynamics Simulation

The automobile dynamics were implemented with the use of an EAI TR-20 analog computer and some additional integrators and multipliers. The extra components were required due to the size of the simulation. The longitudinal dynamics were assumed to be independent of the lateral steering dynamics. Because the car model is to be used in car-following experiments a relatively elaborate model was used for the longitudinal dynamics of the car.

The forces resisting the motion of the car are composed of three parts: a factor proportional to the speed of the car, a factor proportional to the square of the speed, and a constant term. The constant term is

negative and is used to simulate the effects of an automatic transmission. It will accelerate the car from rest without any driver input. The other two factors are positive and may be adjusted to match the coastdown curve of the car to any other desired curve. By eliminating the speed-squared term a linear resistance force may be obtained and the stability derivatives of various cars utilized (see references 2 and 3). Figure 1 shows the coastdown curve for a typical configuration. Note the acceleration of the car from rest due to the negative resistance factor.

The available acceleration force is equal to the rolling radius of the rear tires times the torque applied to them from the driveshaft with the engine at full throttle. For a given car this acceleration force is assumed to be a function of car speed only. This functional relationship is simplified to consist of two linear segments with one breakpoint. By eliminating the breakpoint a linear available acceleration force is obtained and the published stability derivatives may again be used.

The accelerator pedal attenuates the available acceleration force in a linear fashion and thus gives the driver control over the speed of the car. Figure 2 shows the acceleration of the car for various throttle positions.

The driver controls the deceleration of the car by applying a force to the brake pedal. A pressure transducer on the brake line provides an output to the analog computer proportional to the force applied to the brake. To provide the effect of the tires skidding on the road the output of the pressure transducer is diode-limited at a level which provides a deceleration corresponding to the maximum deceleration of a real car. Up to the cutoff level the car will decelerate at a rate proportional to brake pedal force.

Lateral Steering Dynamics Simulation

The lateral steering dynamics are speed dependent and consist of a two-degree-of-freedom model, the roll axis being neglected. For a development of these equations and a comparison to a three-degree-of-freedom model see reference 2. The tire characteristic curves are generated by two diode function generators (one for the front tires and one for the rear tires) which have three positive and three negative breakpoints. The function generators permit a fairly accurate representation of the tire characteristics and also provide a limit on the lateral force provided by the tires. Figure 3 shows the steering response of the car at 30 mph for various step inputs, the input angle being measured at the front tires. Note that the curves are all exponentials. Figure 4 shows the steering response at an increased speed of 50 mph. In this case the response curves are damped oscillations, illustrating the speed dependence of the lateral steering dynamics.

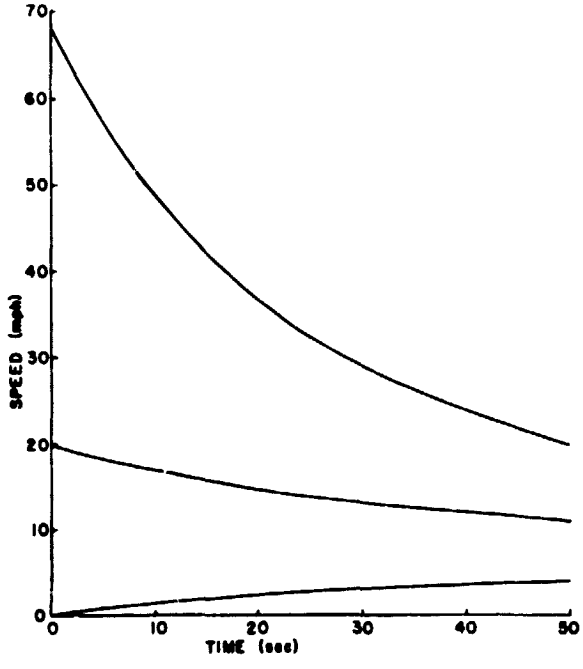

Fig. 1. Coastdown curve for a typical vehicle configuration.

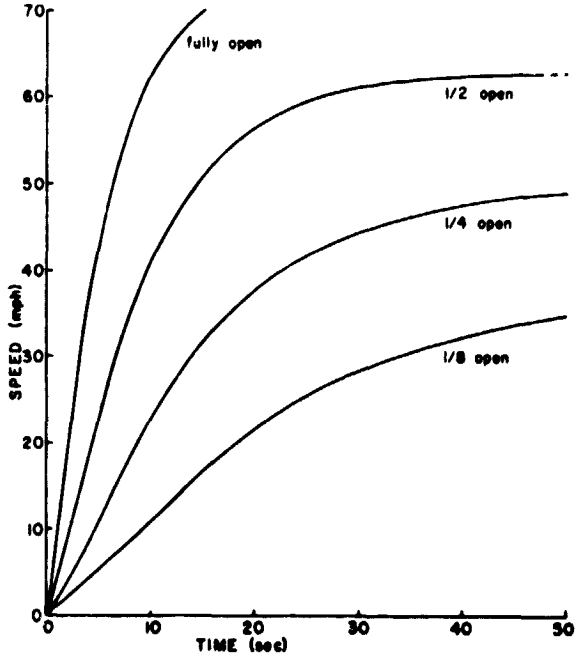

Fig. 2. Acceleration of the car for various throttle positions.

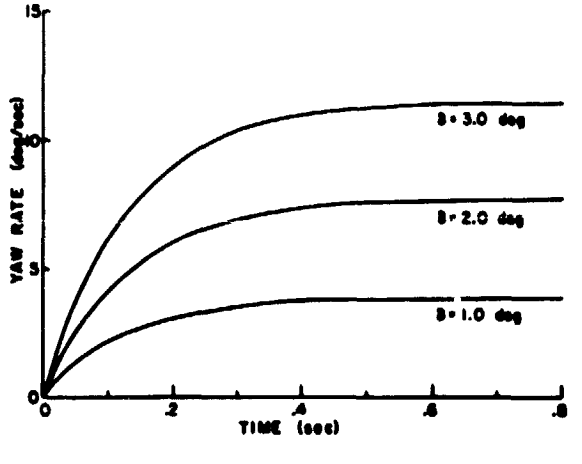

Fig. 3. Steering response of the car at 30 mph for various step inputs to the front wheels.

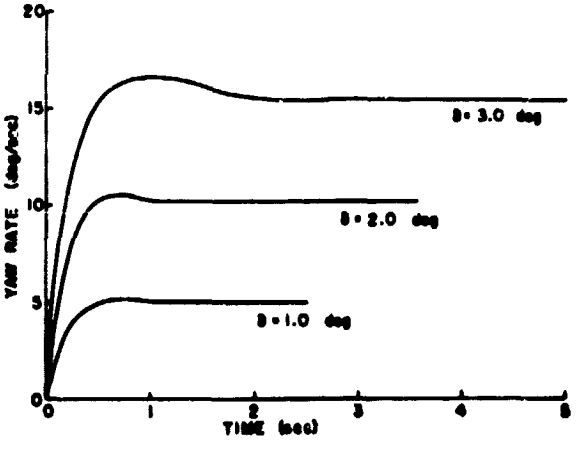

Fig. 4. Steering response of the car at 50 mph for various step inputs to the front wheels.

Control Console

A control console provides the experimenter with status displays, such as the speed and lateral position of the subject's vehicle, as well as a number of control functions, such as to label, initiate and terminate the test trials. Two types of forcing functions will be provided in the lateral control studies, besides road curvature. At all times a low amplitude pseudo-random signal will be added to the subject's steering wheel position output signal to act as a low-level background tracking task, simulating minor inputs from the road, wind or other sources to require continuous vigilance on the part of the driver. Similar signals of higher amplitude will also be used as forcing functions to create a more complex continuous steering task as one type of test input. The second type will consist of a discrete step input signal added to the subject's steering wheel position to simulate a persistent, sudden wind gust.

Additional controls are concerned with setting up initial conditions in car-following studies and for providing both manual or automatic control of the lead-vehicle's speed-time history.

Data Recording and Acquisition

In order to provide continuous monitoring of system operation, including acquisition of data signals, an eight-channel strip chart recorder will be used at all times. This recorder will also be used to monitor physiological recording of heart rate or EMG which will be taken on all subjects. A number of the analog data signals which can be used to describe driver-vehicle performance, such as speed, lateral position, heading angle, yaw rate, etc. in steering and headway, relative velocity, etc. in car-following will be recorded on magnetic tape after digitization at 20 Hz by the same computer used to generate the roadway display. Time series and other analyses will then be carried out on these data.

REFERENCES

1. Mortimer, R.G.; and Sturgis, S.P.: The Effects of Low and Moderate Levels of Alcohol on Steering Performance. Proceedings, 6th International Conference on Alcohol, Drugs and Traffic Safety, The Addiction Research Foundation, Toronto. 329-346. 1975.

2. Weir, D.H.; Shortwell, C.P.; and Johnson, W.A.: Dynamics of the Automobile RElated to Driver Control. Tech. Report, 157-1, Systems Technology, Inc. July, 1966.

3. Wojcik, C.K.; and Allen, R.W.: Studies of the Driver as a Control Element, Phase 3. UCLA Eng. Rept. No. 7148, Inst. of Transportation and Traffic Eng. July, 1971.

SESSION VII

HANDLING QUALITIES AND PILOT RATINGS

Chairman: S. J. Merhav

A STATISTICAL APPROACH TO THE ANALYSIS OF PILOT BEHAVIOR IN MULTILOOP SYSTEMS

By Norihiro Goto*

NASA Ames Research Center

SUMMARY

This work aims at examining the feasibility of a statistical approach to studying the correlation of the pilot rating with pilot behavior in multiloop control situations. Moving-base simulator experiments were conducted at the Ames Research Center with emphasis placed upon the lateral-directional control of an aircraft under gusty air conditions in the landing approach phase. Analyses have been made of the pilot behavior variation with respect to three experimental variables, using the recently developed identification method that utilizes the so-called autoregressive scheme. The effects of one experimental variable, SAS ON or OFF, are particularly discussed in this report to show that the method is quite practical and feasible to obtain unknown pilot dynamics and spectral quantities associated with multiloop control systems and that the correlation can be well understood by this analytical approach.

INTRODUCTION

It would be superfluous to say that the pilot in control of an aircraft is a multivariable processor and controller. He receives more than one feedback cue through visual displays or through his own visual and/or vestibular organs. Then he exerts controls over more than one quantity to offset the gap, if any, between the current states and the desired states of the aircraft, thereby constructing a multiloop feedback system. The evaluation of the aircraft handling qualities made by the pilot in flight tests or simulator tests is considered to be based, except for some particular flight phases, upon the results of the multiloop control. Understanding pilot behavior in multiloop control situations is therefore fundamental to properly interpreting the pilot rating and comments, and also fundamental to setting up the pilot model that might be used as an analytical design tool in making assessments of the handling qualities of aircraft. As pointed out in reference 1, however, there have been instrumental, measurement, and analytical difficulties inherent in identifying the pilot behavior, especially in finding unique pilot describing functions in multiloop systems. This situation may be reflected in the fact that less than half a dozen experimental series pertinent to aircraft multiloop control have been carried out so far to identify pilot behavior (e.g., refs. 2-4). As far as the analytical difficulties are concerned, recent development of identification methods seems to be encouraging us to go

*National Research Council Research Associate.

a step ahead into the area of determining human pilot dynamics for some multiloop situations.

In this work, one of the identification methods, which makes use of the so-called autoregressive scheme, is applied to the analysis of the pilot's lateral-directional control of an airplane in the landing approach phase under gusty air conditions. The simulator experiments, conducted at the NASA Ames Research Center with the use of the FSAA (Flight Simulator for Advanced Aircraft) moving simulator, employed three experimental variables to investigate the variation of the pilot rating and behavior with respect to the variables. This report discusses particularly the correlation of one of the three variables, Roll/Yaw SAS ON or OFF, with the pilot behavior, emphasizing the influence of the aircraft dynamics change. The general objective is directed toward examining the feasibility of the statistical identification approach to understanding and interpreting the pilot rating and behavior. Results may help to define pilot models in realistic multiloop control situations.

SYSTEM MODEL AND THE ANALYTICAL METHOD (AR-MODEL METHOD)

Let us assume the system model to be a typical compensatory control system as shown in figure 1. Although we do not have a definite ground on which the system model like the one shown in the figure is set up by the pilot for aircraft control, we shall proceed with this model for the understanding of the analytical procedure. For the lateral-directional control in the landing approach phase on IFR, however, it will be shown that the model in figure 1 is appropriate.

In figure 1, the vectors $\Pi(n)$ and $\Theta(n)$ ($n = 1, 2, \ldots, N$) may be set for the lateral-directional control of the aircraft as

$$\Pi(n) = [\delta_a(n)\delta_r(n)]' \tag{1}$$

and

$$\Theta(n) = [\phi(n)\psi(n)\beta(n)]' \tag{2}$$

where

$$\left.\begin{aligned} &\delta_a(n) = \text{pilot's wheel movements (rad)},\\ &\delta_r(n) = \text{pilot's pedal movements (cm (in.))},\\ &\phi(n) = \text{roll angle output of the aircraft (rad)},\\ &\psi(n) = \text{yaw angle output of the aircraft (rad)},\\ &\beta(n) = \text{sideslip angle output of the aircraft (rad)}, \end{aligned}\right\} \tag{3}$$

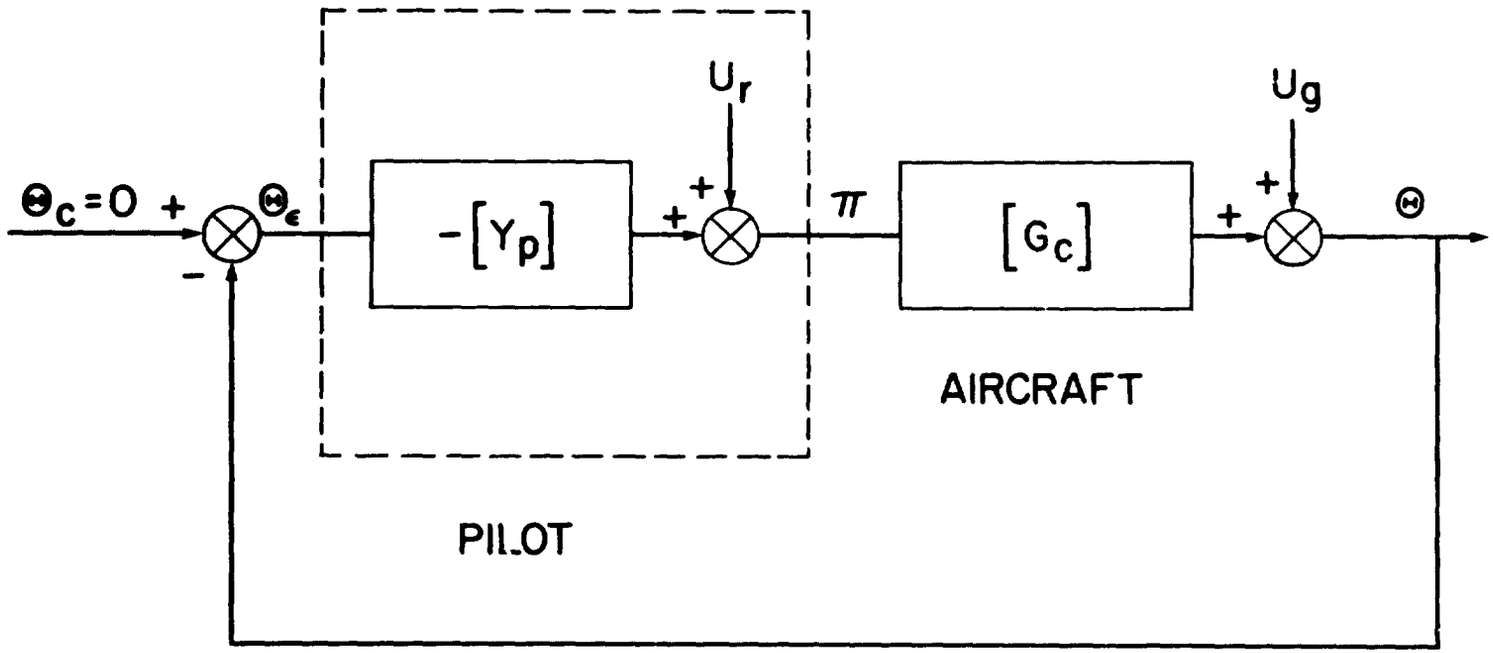

Figure 1.- Block diagram of a compensatory closed system.

and ' denotes the transpose. The matrices $[Y_p(z)]$ and $[G_c(z)]$ represent the pilot dynamics and the aircraft dynamics, respectively. They are defined, if we employ the definitions of equation (3), as

$$[Y_p(z)] = \begin{bmatrix} \frac{\delta_a}{\phi}(z) & \frac{\delta_a}{\psi}(z) & \frac{\delta_a}{\beta}(z) \\ \frac{\delta_r}{\phi}(z) & \frac{\delta_r}{\psi}(z) & \frac{\delta_r}{\beta}(z) \end{bmatrix} \tag{4}$$

and

$$[G_c(z)] = \begin{bmatrix} \frac{\phi}{\delta_a}(z) & \frac{\phi}{\delta_r}(z) \\ \frac{\psi}{\delta_a}(z) & \frac{\psi}{\delta_r}(z) \\ \frac{\beta}{\delta_a}(z) & \frac{\beta}{\delta_r}(z) \end{bmatrix} \tag{5}$$

where z is the backward shift operator, i.e., $z^k y(n) = y(n - k)$. Expand the transfer function matrices $[Y_p(z)]$ and $[G_c(z)]$ into the series in z as

$$[Y_p(z)] = \sum_{m=1}^{\infty} [y_p(m)]z^m \tag{6}[1]$$

$$[G_c(z)] = \sum_{m=1}^{\infty} [g_c(m)]z^m \tag{7}[1]$$

where $[y_p(m)]$ and $[g_c(m)]$ show the impulse response matrices. Then, using the impulse response matrices, we may describe the system of figure 1 by the following equations:

$$\Pi(n) = \sum_{m=1}^{\infty} [y_p(m)]\Theta(n - m) + U_r(n) \tag{8}$$

$$\Theta(n) = \sum_{m=1}^{\infty} [g_c(m)]\Pi(n - m) + U_g(n) \tag{9}$$

---

[1]It is assumed here that $[y_p(0)] = 0$ and $[g_c(0)] = 0$. See reference 5 for the discussion on the inclusion of $[y_p(0)]$ and $[g_c(0)]$.

where $U_r(n)$ is the 2×1 noise vector injected by the pilot, $[u_{\delta_a}(n)u_{\delta_r}(n)]$, and $U_g(n)$ is the 3×1 external noise vector, such as the gust-induced quantities, $[u_\phi(n)u_\psi(n)u_\beta(n)]$. The feedback system model of equations (8) and (9) was first studied by Akaike (refs. 5 and 6).

We set assumptions as follow:

1. $\Pi(n)$, $\Theta(n)$, $U_r(n)$, and $U_g(n)$ are all stationary and zero mean.

2. The feedback system is stable, i.e., all the roots of the determinant of $\{I - [Y_p(z)][G_c(z)]\}$ must lie outside the unit circle.

3. The noise vectors $U_r(n)$ and $U_g(n)$ are uncorrelated with each other, i.e., every element of $U_r(n)$ is uncorrelated with every element of $U_g(n)$.

4. The noise vectors $U_r(n)$ and $U_g(n)$ satisfy the following autoregressive (AR) relationships for a properly selected L:

$$U_r(n) = \sum_{\ell=1}^{L} C_r(\ell)U_r(n - \ell) + W_r(n) \tag{10}$$

$$U_g(n) = \sum_{\ell=1}^{L} C_g(\ell)U_g(n - \ell) + W_g(n) \tag{11}$$

where $W_r(n)$ and $W_g(n)$ are white noise processes, and $C_r(\ell)$ (2×2) and $C_g(\ell)$ (3×3) are coefficient matrices.

Operating the AR filters of equations (10) and (11) conceptually on equations (8) and (9), respectively, we get

$$\Pi(n) = \sum_{\ell=1}^{L} C_r(\ell)\Pi(n - \ell) + \sum_{\ell=1}^{\infty} A_p(\ell)\Theta(n - \ell) + W_r(n) \tag{12}$$

$$\Theta(n) = \sum_{\ell=1}^{L} C_g(\ell)\Theta(n - \ell) + \sum_{\ell=1}^{\infty} A_c(\ell)\Pi(n - \ell) + W_g(n) \tag{13}$$

where

$$A_p(\ell) = [y_p(\ell)] - \sum_{k=1}^{\ell-1} C_r(k)[y_p(\ell - k)] \tag{14}$$

$$A_c(\ell) = [g_c(\ell)] - \sum_{k=1}^{\ell-1} C_g(k)[g_c(\ell - k)] \tag{15}$$

By putting together equations (12) and (13) we arrive at the matrix form

$$X(n) = \sum_{\ell=1}^{\infty} A(\ell)X(n - \ell) + W(n) \tag{16}$$

if we set

$$X(n) = [\Pi(n) \quad \Theta(n)]' \tag{17}$$

$$W(n) = [W_r(n) \; W_g(n)]' \tag{18}$$

$$A(\ell) = \left[\begin{array}{c|c} C_r(\ell) & A_p(\ell) \\ \hline A_c(\ell) & C_g(\ell) \end{array}\right] \tag{19}$$

and $C_r(\ell) = C_g(\ell) = 0$ for $\ell > L$. Equation (16) is the AR model of the vector $X(n)$ of infinite order, which cannot be fitted to the given data.

Instead of having the AR model of infinite order, consider an AR model of finite order M,

$$X(n) = \sum_{\ell=1}^{M} A(\ell)X(n - \ell) + W(n) \tag{20}$$

satisfying the relationships

$$\left.\begin{aligned} E[W(n)] &= 0 \text{ (zero vector)} \\ E[W(n) \cdot X'(n - \ell)] &= 0 \text{ (zero matrix) for } \ell \geq 1 \\ E[W(n) \cdot W'(\ell)] &= \delta_{n,\ell} \, \Sigma_w \end{aligned}\right\} \tag{21}$$

where $\delta_{n,\ell} = 1$ $(n = \ell)$, $= 0$ $(n \neq \ell)$, Σ_w is the covariance matrix of $W(n)$, and E denotes the expectation. In equation (20) it is assumed that

$$A(\ell) = 0 \text{ (zero matrix), for } \ell > M. \tag{22}$$

Suppose we have completed the fitting of the AR model in the form of equation (20). We first partition the estimated AR coefficient matrix $A(\ell)$ as shown by equation (19). Then, the impulse response matrices $[y_p(\ell)]$ and $[g_c(\ell)]$ are calculated from equations (14) and (15) up to any desired ℓ under the assumption of equation (22). The frequency response function matrix of the pilot is obtained by replacing z by $\exp(-j\omega\Delta T)$ in the following equation:

$$[Y_p(z)] = [I - C_r(z)]^{-1}A_p(z) \tag{23}$$

where I is the unit matrix, ΔT the sampling interval, ω the frequency in rad/sec,

$$C_r(z) = \sum_{k=1}^{M} C_r(\ell) z^{\ell}$$

and

$$A_p(z) = \sum_{\ell=1}^{M} A_p(\ell) z^{\ell}$$

The estimation of the AR coefficient matrix $A(\ell)$ is made along the least squares method. From equation (20) we have

$$R_{xx}(n) = \sum_{\ell=1}^{M} A(\ell) R_{xx}(n - \ell), \quad n = 1, 2, \ldots, M \tag{24a}$$

$$= \sum_{\ell=1}^{M} A(\ell) R'_{xx}(\ell) + \Sigma_w, \quad n = 0 \tag{24b}$$

where $R_{xx}(\ell)$ is the covariance matrix of the vector $X(n)$. Equation (24a) is solved for $A(\ell)$ ($\ell = 1, 2, \ldots, M$). Practically, we may use the efficient recursive computational algorithm of the least squares based upon the formulas developed by Whittle (refs. 7 and 8). Note that the estimate of the covariance matrix Σ_w, which is obtained by using the relationship of equation (24b), is important in that it may be used to check assumption 3 stating the uncorrelatedness of U_r and U_g, and thus can be used to check the propriety of the system model.

The determination of the optimal order M in equation (20) is made by the use of an objective judgment criterion MFPE (Multiple Final Prediction Error) proposed by Akaike (ref. 8). This criterion is defined by

$$\text{MFPE} = \left(1 + \frac{Mk + 1}{N}\right)^{k} \left(1 - \frac{Mk + 1}{N}\right)^{-k} \|d_M\| \tag{25}$$[2]

where k = number of the components in the vector X, N = number of the data points, M = order of the AR model, d_M = the estimate of the covariance matrix Σ_w, when the AR model of order M is fitted, and $\|d_M\|$ = determinant of d_M. The criterion MFPE gives the optimal order M that best approximates the possibly infinite-order system such as equation (16) in the sense of the minimization of the mean square error of the one-step-ahead prediction obtained by using the least squares estimates of the AR coefficients.

---

[2]Akaike later generalized the judgment criterion to propose the information criterion called AIC (ref. 9). The use of MFPE and AIC in this work has shown that both give the same order.

The power spectral density matrix $P_X(j\omega)$ of the time series vector $X(n)$ is given by

$$P_X(j\omega) = \Delta T[A(j\omega)]^{-1} \sum_W [\overline{A'(j\omega)}]^{-1} \tag{26}$$

where

$$A(j\omega) = \sum_{\ell=0}^{M} A(\ell)\exp(-j\omega\ell)$$

and $A(0) = -I$ (I: unit matrix), and $\overline{A(j\omega)}$ is the complex conjugate of $A(j\omega)$.

In order to see the effectiveness of our results, given by equation (23) for example, we have to look into the linear coherency, which can be estimated by the use of the spectral density matrix $P_X(j\omega)$. When Σ_W is diagonal, meaning that the components of the vector $W(n)$ are mutually independent, we reach a simple expression which gives the indication of the linear coherency characteristics as

$$r_{ij}(j\omega) = q_{ij}(j\omega)/p_{ii}(j\omega) \tag{27}$$

In equation (27), $p_{ii}(j\omega)$ is the power spectrum of the i-th component of the vector $X(n)$ (e.g., the power spectrum of δ_a if $i = 1$), and $q_{ij}(j\omega) = |[A(j\omega)]^{-1}_{ij}|^2\sigma_{jj}$, where $[A(j\omega)]^{-1}_{ij}$ indicates the (i, j)-th component of $[A(j\omega)]^{-1}$, and σ_{jj} is the (j, j)-th component of Σ_W; r_{ij} shows the contribution in power of the j-th noise source to the power of the i-th component of $X(n)$, and

$$\sum_{j=1}^{k} r_{ij}(j) = 1 \tag{28}$$

This quantity is called the relative power contribution, and it is worth checking even when the off-diagonal elements of Σ_W are not zero but practically small.

EXPERIMENT

Simulator experiments were conducted at the NASA Ames Research Center, using the FSAA 6-degrees-of-freedom moving-base simulator. The simulated flight phase was the final landing approach under gusty air conditions. Thus, the pilot's task was to track the glideslope and the localizer while also keeping the airspeed and the attitude of the aircraft at some desired values. The flight configuration is visualized in figure 2. The flight loading conditions of the STOL transport used are shown in table I, together with the lateral-directional stability dynamics data which were measured prior to the

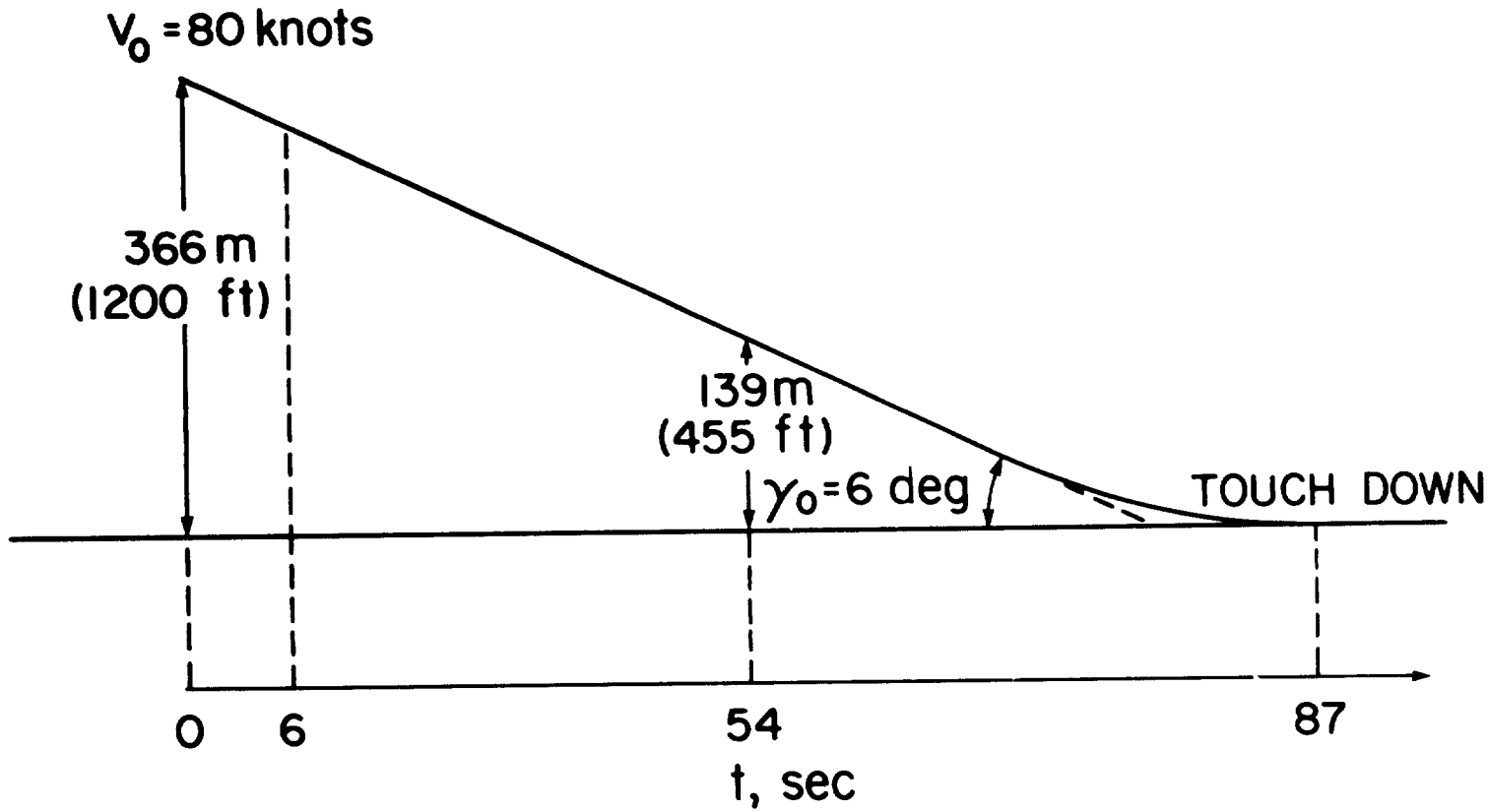

Figure 2.- Landing approach flight configuration.

TABLE I.- FLIGHT LOADING CONDITIONS AND STABILITY DERIVATIVES DATA

Initial conditions	Aircraft dimensions
V_o = 80 knots	W = 68,040 kg (150,000 lb)
H_o = 366.8 m (1203.5 ft)	S = 154.9 m^2 (1667 ft^2)
γ_o = -6.0°	b = 34.0 m (111.6 ft)
α_o = -0.33° deg	I_x = 255,776 kg-m-sec^2 (1,850,000 slug-ft^2)
	I_z = 483,900 kg-m-sec^2 (3,500,000 slug-ft^2)
	I_{xz} = 37,385 kg-m-sec^2 (270,400 slug-ft^2)
Stability derivatives (body axis)[a]	**Response characteristics**
Y_v = -0.1431 1/sec	Roll time constant
L_β = -0.4894 1/sec^2	$1/T_r$ = 0.7778 1/sec
N_β = 0.4397 1/sec^2	Spiral time constant
Y_p = 0.007266 m/sec (0.02384 ft/sec)	$1/T_s$ = -0.09317 1/sec
L_p = -0.5518 1/sec	Dutch-roll mode damping
N_p = -0.08578 1/sec	ζ_D = 0.08798
Y_r = 0.7919 m/sec (2.598 ft/sec)	Dutch-roll mode undamped
L_r = 0.6812 1/sec	natural frequency
N_r = -0.1618 1/sec	ω_D = 0.7938 rad/sec
$Y\delta_a$ = 0.0	
$L\delta_a$ = 0.4428 1/rad-sec^2	
$N\delta_a$ = -0.01632 1/rad-sec^2	
$Y\delta_r$ = 0.1276 m/sec^2/cm (1.063 ft/sec^2/in.)	
$L\delta_r$ = 0.01486 1/sec^2/cm (0.03775 1/sec^2/in.)	
$N\delta_r$ = -0.02341 1/sec^2/cm (-0.05945 1/sec^2/in.)	

[a]To obtain primed stability derivatives, refer to reference 10, p. 257.

experiment. See reference 11, for example, for the details of the FSAA simulator system.

Three experimental variables were selected for this work:

1. Flight rules (VFR or IFR)

2. SAS (Roll/Yaw SAS ON or OFF)

3. Gust intensity σ = 1.2 or 1.8 m/sec (4 or 6 ft/sec)

where σ is the rms value of the vertical gust component. Experimental runs analyzed in this work consisted of six runs with four different configurations as listed in table II. An experienced NASA pilot participated in this experiment, and his rating on each configuration by the Cooper-Harper scale (ref. 12) is also given in table II. It should be mentioned here that seven preliminary runs preceded the six runs for data taking, and the pilot ratings and the greater part of the pilot comments were collected in the preliminary runs. The emphasis of the experiment and of the analysis was placed on the lateral-directional control of the aircraft. Therefore, Pitch-SAS was kept in the ON position so that the influence of the longitudinal control on the lateral-directional control could be made as small as possible. Roll/Yaw SAS utilizes

TABLE II.- SIMULATOR EXPERIMENT FLIGHT CONFIGURATIONS AND PILOT RATING FOR EACH CONFIGURATION

Configuration	Base	Flight rule	Roll/yaw SAS	Gust condition	Pilot rating
A-1	Moving	VFR	OFF	Turbulent[a] σ = 1.2 m/sec (4.0 ft/sec)	5.5 ~ 6.0
A-2	Moving	VFR	OFF	Turbulent σ = 1.2 m/sec (4.0 ft/sec)	5.5 ~ 6.0
B-1	Moving	IFR	OFF	Turbulent σ = 1.2 m/sec (4.0 ft/sec)	6.5
B-2	Moving	IFR	OFF	Turbulent σ = 1.2 m/sec (4.0 ft/sec)	6.5
C-1	Moving	IFR	OFF	Turbulent σ = 1.8 m/sec (6.0 ft/sec)	7.0
D-1	Moving	IFR	ON	Turbulent σ = 1.2 m/sec (4.0 ft/sec)	2.0

[a]Every turbulent condition includes 20 knots headwind. Pitch-SAS is ON for every configuration.

roll angle and roll rate feedback to aileron and roll angle and roll rate in addition to washed-out yaw rate feedback to rudder. The Yaw SAS was also supplemented with an aileron-to-rudder crossfeed, in which the aileron movement signal filtered by a first-order lag was cross-fed to the rudder, principally to remove the effect of aileron yaw. A typical example of the aircraft response to a relay-type wheel input is shown in figure 3 for both SAS-OFF and SAS-ON configurations.

The gust simulated in this experiment was based on the one-dimensional spectral density functions of the Dryden form. References 11 and 13 contain the details of the model and the method to generate it. One point to note is that the gust characteristics are a function of the altitude as the result of employing the assumption of the two-dimensional isotropy near the ground. Setting $t = 0$ at the I.C. ($h = 366$ m (1200 ft)), the time sector used for the analysis was from $t = 6.0$ sec to $t = 54.0$ sec as shown in figure 2. However, the change in altitude may not be so large as to make it necessary to take into account the nonstationary characteristics of the gust (see ref. 14, for example).

Six quantities, δ_a, δ_r, ϕ, ψ, β, y_ε (where y_ε is the deviation angle from the localizer beam and the others are defined by eq. (3)), in addition to some other quantities useful for the analysis, were recorded for each run on RUNDUM tape (ref. 11) and were processed by a TSS/360 computer system at the Ames Research Center. Note that δ_a and δ_r are wheel angle and pedal travel, respectively, instead of forces applied by the pilot to wheel and pedal. So, the pilot dynamics results shown later may contain the wheel and pedal dynamics. The sampling time was 0.06 sec.

Results of the analysis by the AR-model method are shown in figures 4-10 and in table III. The power spectral densities of the pilot control outputs and the aircraft outputs for configuration B-1 (SAS-OFF) and configuration D-1 (SAS-ON), respectively, together with their rms values are shown in figures 4 and 5. Figure 6 is an example of the relative power contribution for configuration B-1. Note that in figures 4, 5, and 6, the abscissa is in the linear scale of the frequency. Figures 7, 8, and 9 are the pilot describing function data (i.e., fig. 7 shows the wheel-related describing functions for configuration B-1; fig. 8 shows the pedal-related describing functions for configuration B-1; and fig. 9 shows the wheel-related describing functions for configuration D-1). The pedal-related describing functions for configuration D-1 are not shown here since the pedal movement of the pilot in this configuration is so small (as indicated by the rms value in fig. 5) that it is not considered to be of any significance. Figure 10 is an example of the comparison of a particular describing function, $\delta_a/\phi(j\omega)$, between configurations B-1 and D-1. Table III gives the normalized d_M's, i.e., the element is given by $d_{ij}/\sqrt{d_{ii}d_{jj}}$, if $d_M = [d_{ij}]$. These data provide a basis for examining the propriety of the system model. Also, the order of the AR model determined by MFPE is shown in table III.

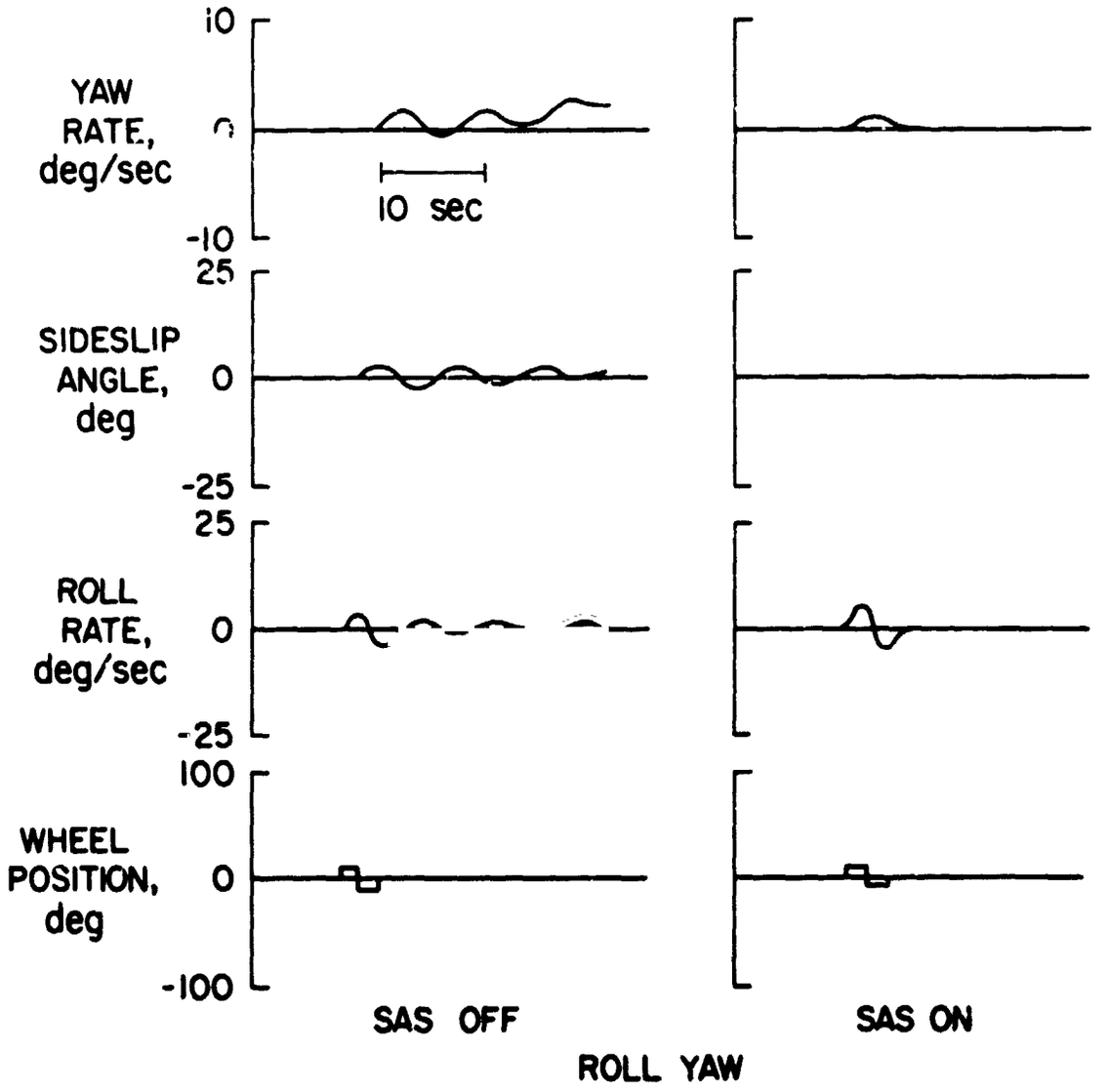

Figure 3.- Effects of Roll/Yaw SAS.

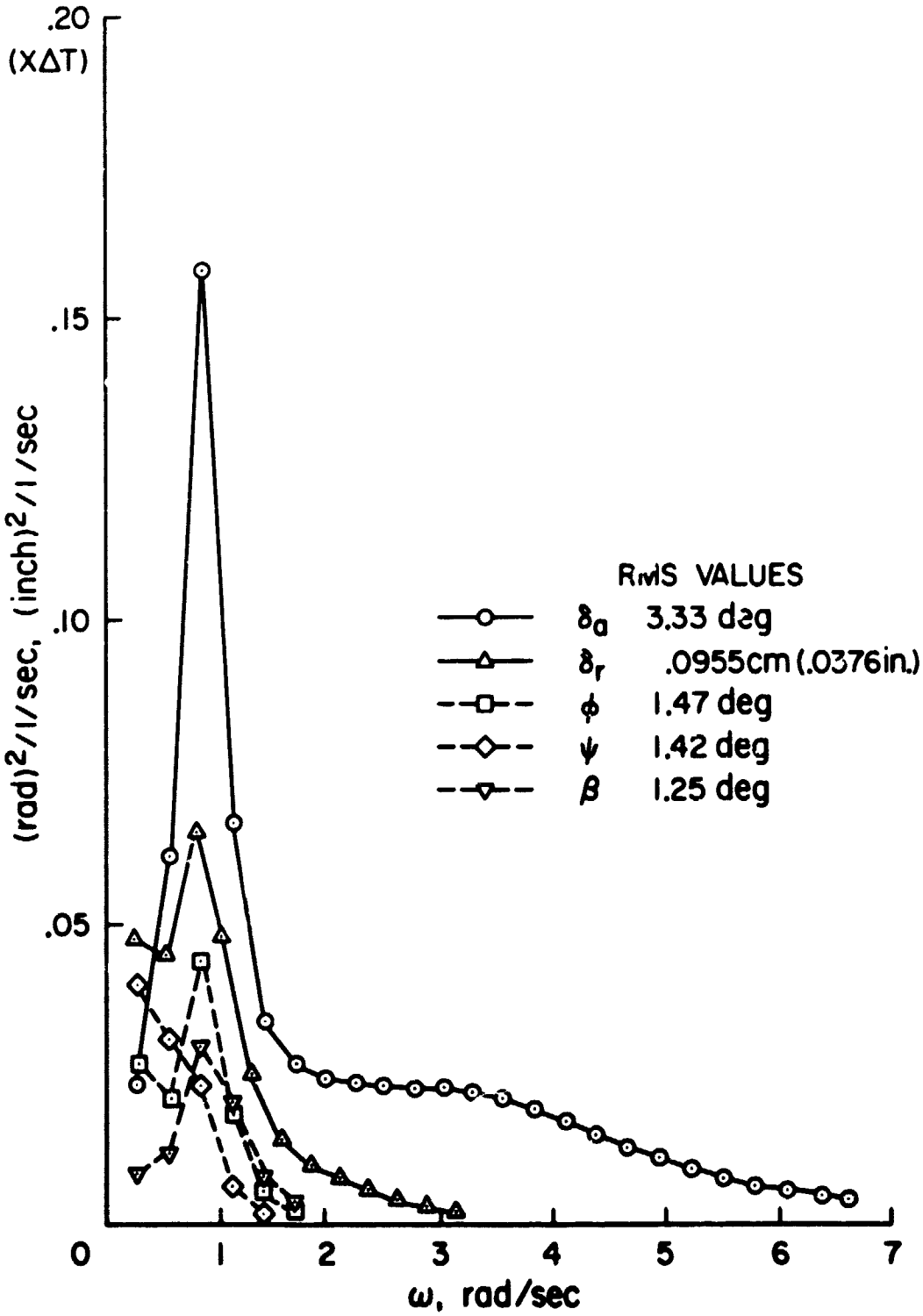

Figure 4.- Power spectra: configuration B-1.

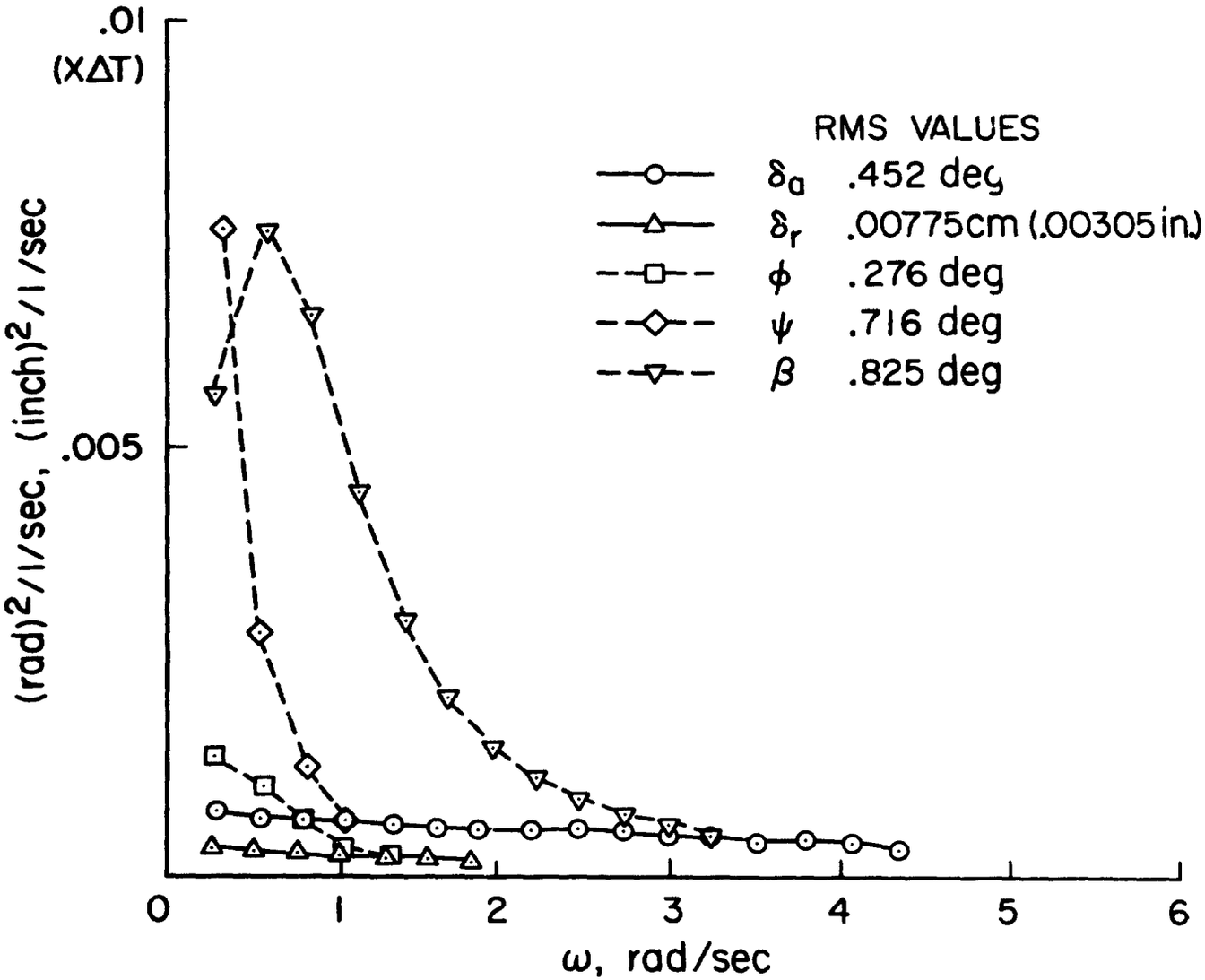

Figure 5.- Power spectra: configuration D-1.

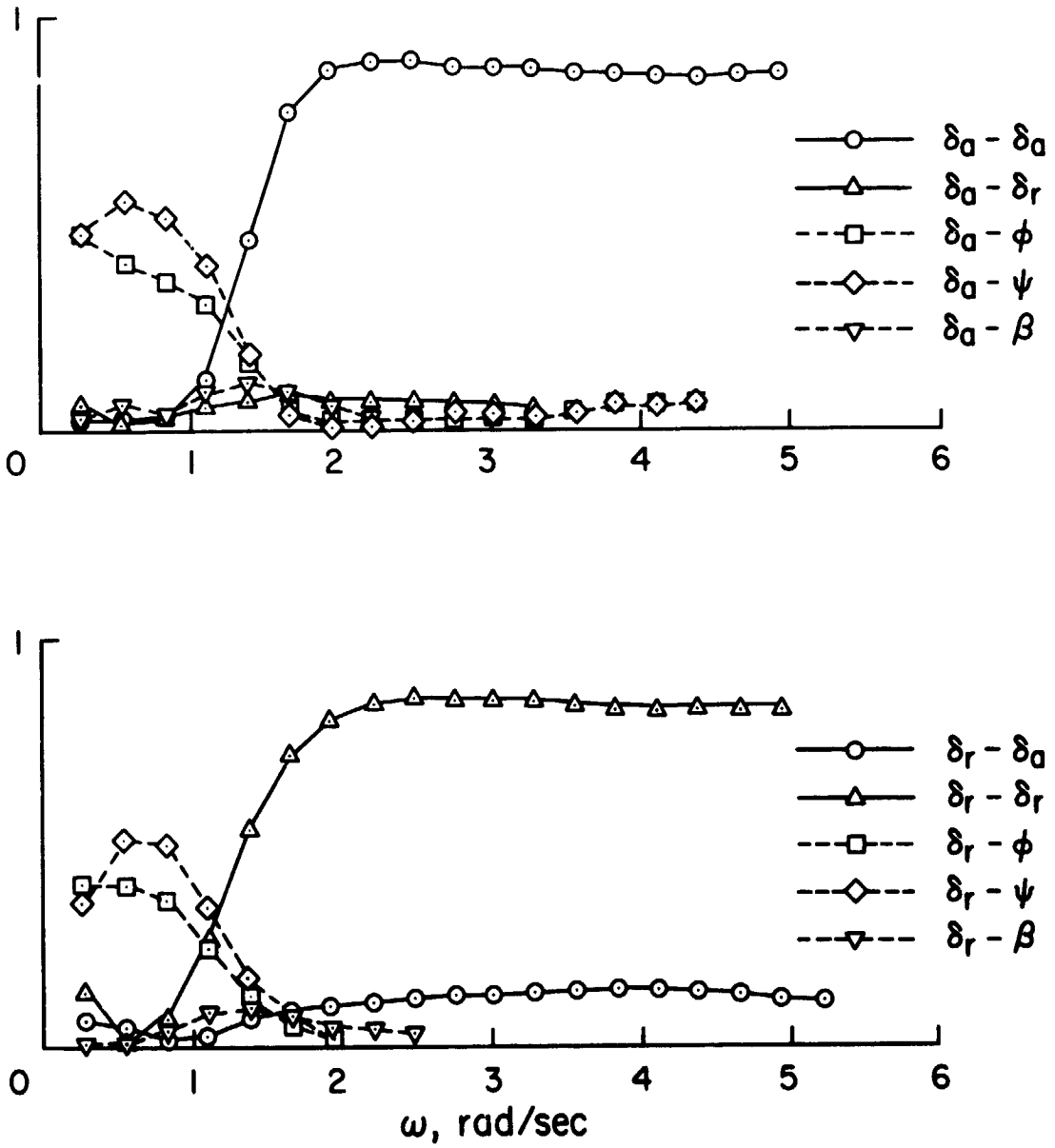

Figure 6.- An example of the relative power contribution: configuration B-1.

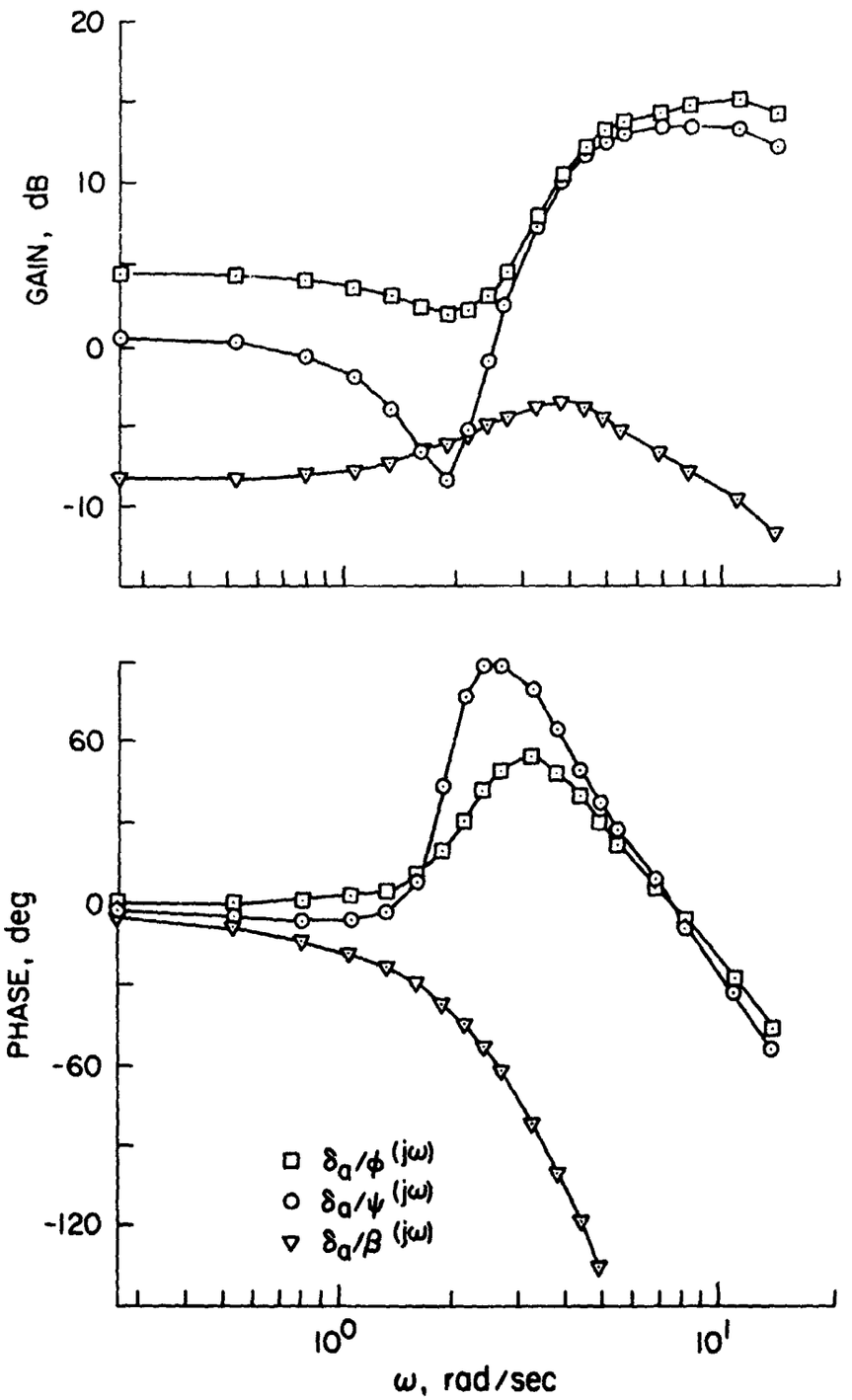

Figure 7.- Wheel-related describing functions of the pilot: configuration B-1.

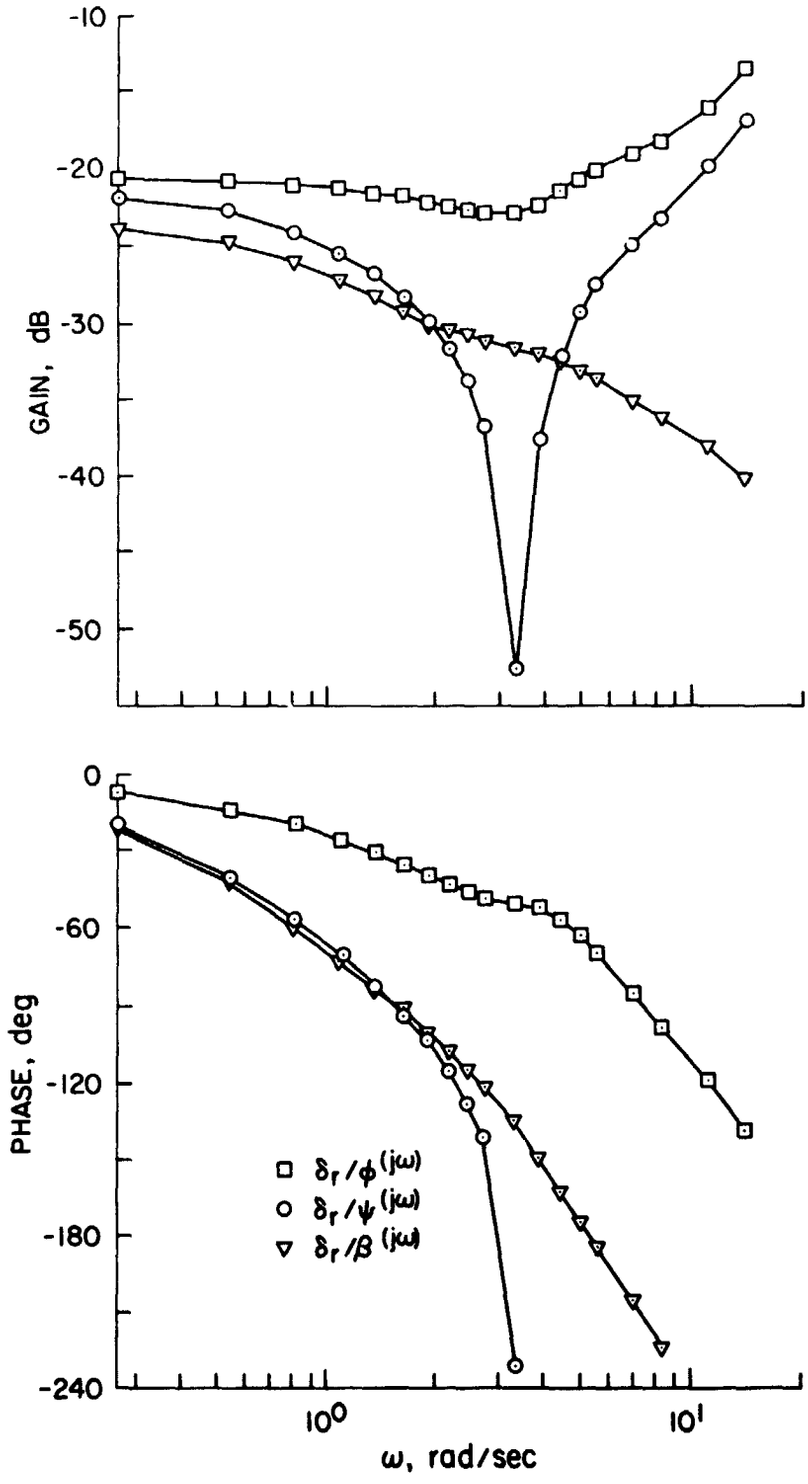

Figure 8.- Pedal-related describing functions of the pilot: configuration B-1.

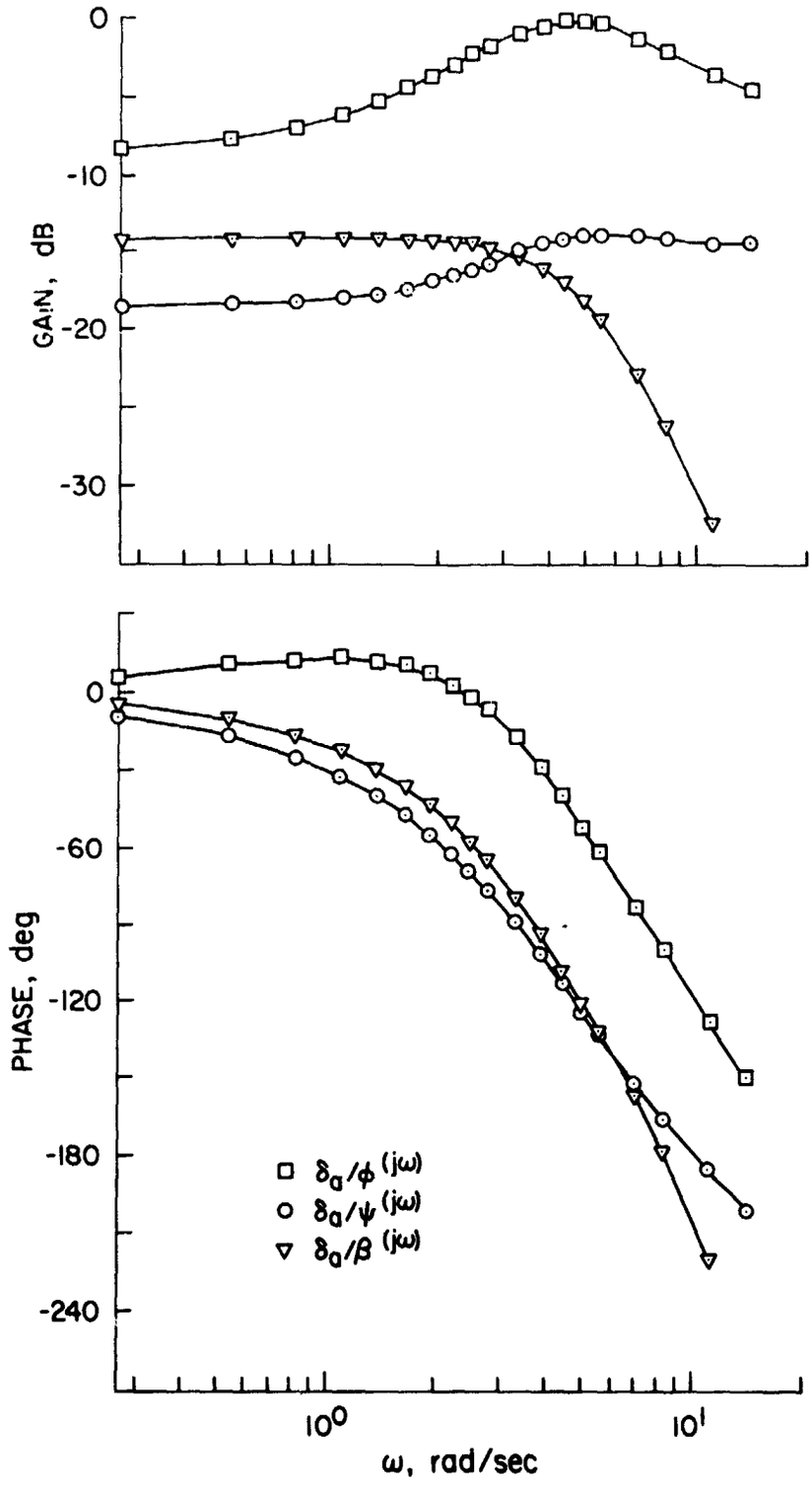

Figure 9.- Wheel-related describing functions of the pilot: configuration D-1.

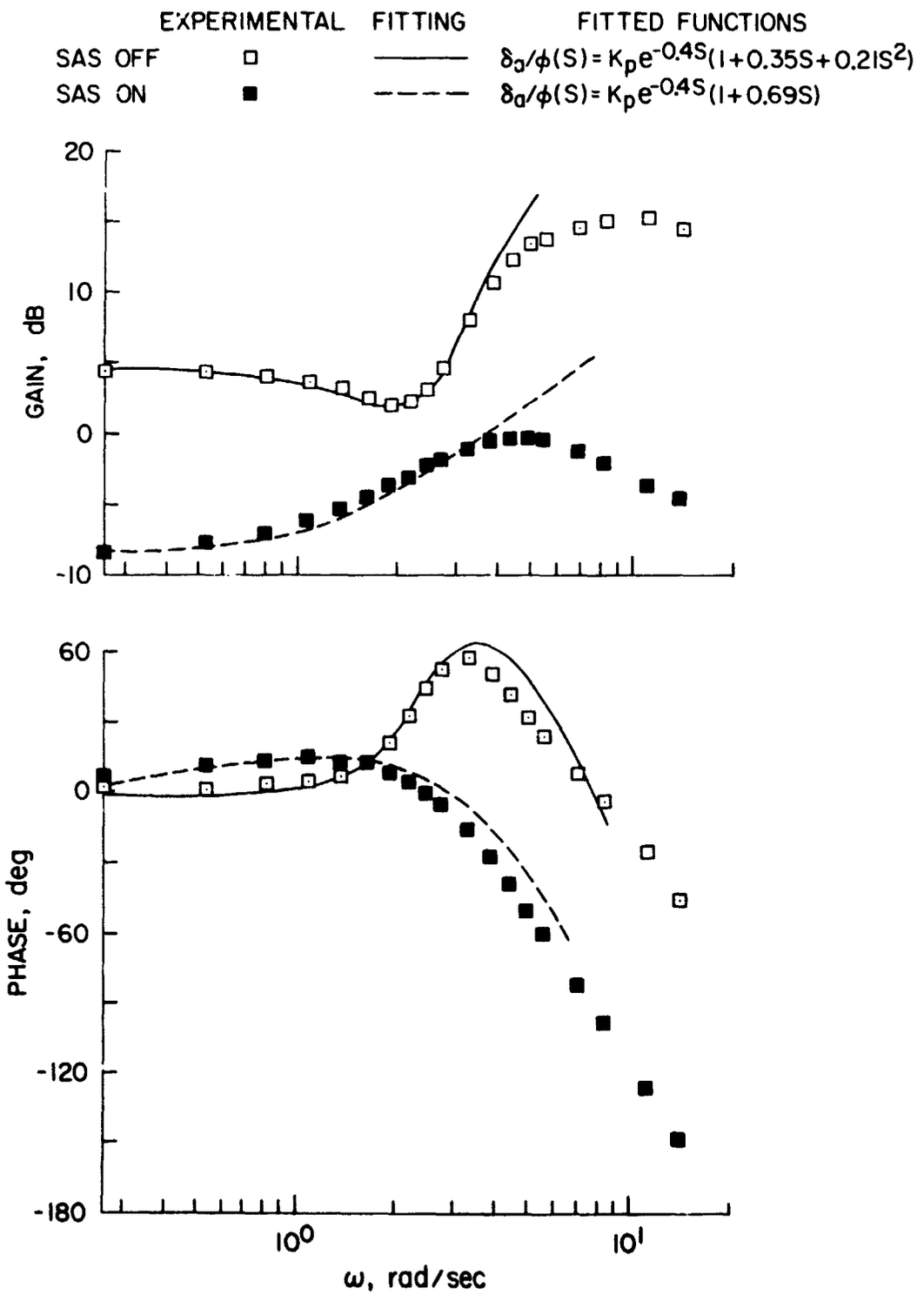

Figure 10.- Comparison of a describing functions, δ_a/ϕ, between configurations B-1 and D-1.

TABLE III.- NORMALIZED COVARIANCE MATRIX d_M AND THE ORDER OF THE AR MODEL

	δ_a	δ_r	ϕ	ψ	β
Configuration B-1 (M = 7)					
δ_a	0.1000000D 01	0.1005529D 00	0.4019349D-02	0.1793190D-01	0.1280636D-01
δ_r	0.1005529D 00	0.1000000D 01	-0.1968628D 00	0.6887329D-02	-0.1113333D 00
ϕ	0.4019349D-02	-0.1968628D 00	0.1000000D 01	-0.9248254D 00	0.3880180D-01
ψ	0.1793190D-01	0.6887329D-02	-0.9248254D 00	0.1000000D 01	0.2108075D-01
β	0.1280636D-01	-0.1113333D 00	0.3880180D-01	0.2108075D-01	0.1000000D 01
Configuration D-1 (M = 4)					
δ_a	0.1000000D 01	0.5945739D-01	0.6133936D-01	-0.1641999D 00	-0.4559047D-01
δ_r	0.5945739D-01	0.1000000D 01	0.1626071D 00	-0.1138606D 00	0.1799904D-01
ϕ	0.6133936D-01	0.1626071D 00	0.1000000D 01	-0.6793050D 00	-0.3196776D-01
ψ	-0.1641999D 00	-0.1138606D 00	-0.6793050D 00	0.1000000D 01	0.2076136D 00
β	-0.4559047D-01	0.1799904D-01	-0.3196776D-01	0.2076136D 00	0.1000000D 01
Digital simulation study (M = 6)					
δ_a	0.1000000D 01	0.6229741D-01	0.1938894D 00	-0.1840873D 00	0.1226025D 00
δ_r	0.6229741D-01	0.1000000D 01	0.1642078D 00	-0.1619289D 00	0.9192547D-01
ϕ	0.1938894D 00	0.1642078D 00	0.1000000D 01	-0.9793968D 00	0.6785351D 00
ψ	-0.1840873D 00	-0.1619289D 00	-0.9793968D 00	0.1000000D 01	-0.7119448D 00
β	0.1226025D 00	0.9192547D-01	0.6785351D 00	-0.7119448D 00	0.1000000D 01

DIGITAL SIMULATION STUDY

Before going into the discussion of the results of the simulator experiment, we now briefly refer to the results of the digital simulation that was made as a credibility study of the AR-model method. The digital simulation made use of the system model of figure 1 with the known pilot dynamics matrix $[Y_p]$ and the aircraft lateral-directional dynamics of table I. For the pilot noise $U_r(n)$, two mutually independent white noises were used. The rms values of these noises were 0.4° for the wheel control and 0.005 cm (0.002 in.) for the pedal control. The gust simulation system was different from that used for the simulator experiment and was based upon the method described in reference 15. The gust intensity was σ = 1.2 m/sec (4 ft/sec). All equations described by the Laplace operator S were reduced to the corresponding difference equations (ref. 16). From the records of the vectors $\Pi(n)$ and $\Theta(n)$, the matrix $[Y_p(j\omega)]$ was identified as unknown.

Results of this simulation study are shown in figures 11 and 12. The normalized estimate of the covariance matrix d_M is seen in table III, by which we may say that the noise correlation is even worse than those in the simulator experiment, possibly because of the different gust generation system; however, the model of figure 1 is appropriate (see the off-diagonal elements in the bracket of the matrix). The estimated $[Y_p(j\omega)]$ appears to be in reasonably good agreement with the theoretical one, at least qualitatively, up

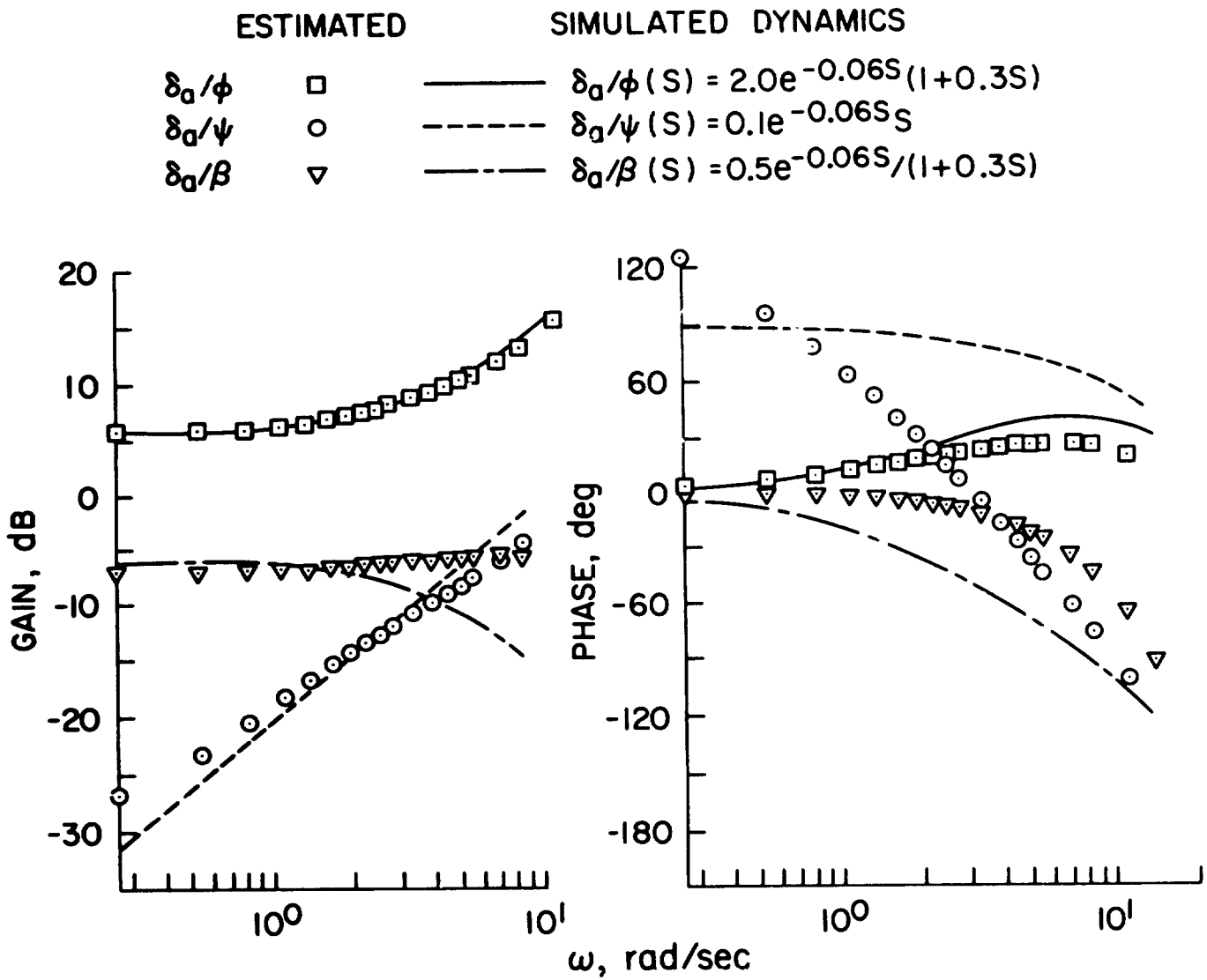

Figure 11.- Results of the digital simulation study: wheel-related frequency response functions.

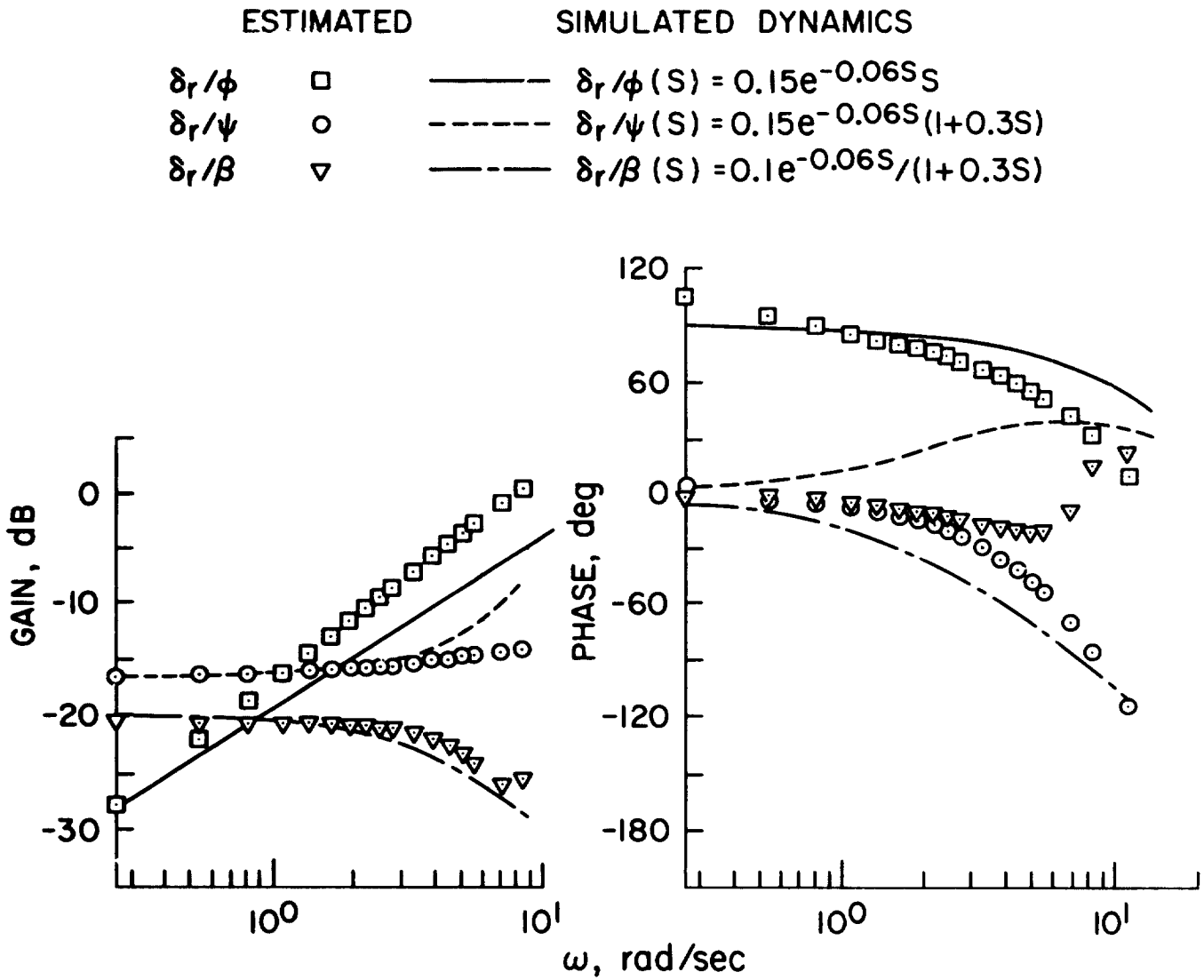

Figure 12.- Results of the digital simulation study: pedal-related frequency response functions.

to a certain frequency. Specifically, the roll-angle-related frequency response functions δ_a/ϕ and δ_r/ϕ are quite good due to the large magnitude of their static gains compared with the others. The discrepancy in δ_a/ψ, especially in its phase, between the simulated dynamics and the estimated dynamics may be due to its relatively small static gain and the computational difficulty to realize a pure differentiator. Since many off-diagonal elements outside the brackets in the normalized d_M shown in table III take on large values compared with 1, it makes little sense to check the relative power contribution. It should be noted that the signal-to-noise ratio deteriorated rapidly from the frequency of 4.0 rad/sec because of the use of white noises as the pilot remnants. Also it should be mentioned that the data are influenced by the computational method of the digital simulation and that the influence of the magnitude and the frequency characteristics of the pilot noises on the estimated results should be studied further in conjunction with the external noise characteristics.

DISCUSSION

With the digital simulation study in mind, we now proceed to the discussion of the results of the simulator experiment, using configurations B-1 and D-1 to see the effects of the Roll/Yaw SAS on pilot behavior. It can be seen that the effects of SAS-ON are very conspicuous. For configuration D-1, pedal movements are zero in actuality, wheel movements are small, and the variation of the aircraft outputs is also small. As seen in table III, most off-diagonal elements in the normalized d_M are small compared with 1 for both configurations, and the correlation between W_r and W_g of equation (18) is small, thereby assuring the propriety of the system model of figure 1. In addition, it is worthwhile to examine the relative power contribution in these configurations for the purpose of looking into the linear coherency characteristics and the effectiveness of the pilot's control in the frequency domain. Figure 6 shows the wheel- and pedal-related relative power contributions only for configuration B-1, but these values are sufficient to find that the pilot's wheel and pedal movements are responding to the variation mainly in roll and yaw angle in the low-frequency region up to about twice the Dutch-roll frequency, beyond which the pilot appears to be just a noise generator. Accordingly, the pilot describing functions are considered to be reliable only in the low-frequency region.

Looking at figure 9 which shows the wheel-related pilot describing functions for configuration D-1, and comparing with figure 7, it can be noticed that the SAS-ON does not require much compensation effort from the pilot; static gains are much lower for configuration D-1 than for B-1, and the first-order lead control is noticeable only for the wheel-to-roll-angle describing function. On the other hand, for configuration B-1, the pilot seems to be employing the second-order lead control for δ_a/ϕ, δ_a/ψ, and δ_r/ψ. This may be suggesting that the pilot is utilizing motion cues for this particular run, or that he is employing a special control technique to cancel out the aircraft's oscillatory Dutch-roll motion (ref. 17).

A comparison of the wheel-to-roll-angle describing function is made in figure 10 between configurations B-1 and D-1. Solid and dotted curves in the figure show an attempt at the function fitting, although there is a great uncertainty in the high-frequency region because of the bad linear coherency. Physically realizable pilot models may have to include the first- or second-order lag terms.

Putting together all the results and the consideration described thus far, details of pilot behavior that may contribute to determining the pilot rating can be understood fairly well. More systematic measurements are necessary in order to develop the multiloop pilot model that can be used as an analytical design tool in making assessments of the aircraft handling qualities.

CONCLUDING REMARKS

The AR-model method has been applied for the first time to the identification of pilot behavior in multiloop tasks. Results show that this is a practical and promising technique for obtaining a general idea of the unknown pilot dynamics in multiloop systems. However, more work is needed to identify pilot describing functions that are reliable over a wide frequency range.

In the experiment described here, three experimental variables were used, and their effects, particularly the effects of the Roll/Yaw SAS, have been made clear to some extent. Pilot behavior and its correlation with the handling quality variable may be further defined by this line of approach.

ACKNOWLEDGMENT

The author thanks Dr. James A. Franklin of the NASA Ames Research Center for his advice and discussion on the experiment and the measurements. The author also wishes to thank Dr. Hirotsugu Akaike of the Institute of Statistical Mathematics, Japan, for his discussion on the analytical method.

REFERENCES

1. McRuer, D. T.: Development of Pilot-in-the-Loop Analysis. J. Aircraft, vol. 10, no. 9, 1973, pp. 515-524.

2. Stapleford, R. L.; McRuer, D. T.; and Magdaleno, R.: Pilot Describing Function Measurements in a Multiloop Task. NASA CR-542, 1966.

3. Weir, D. H.; and McRuer, D. T.: Pilot Dynamics for Instrument Approach Tasks: Full Panel Multiloop and Flight Director Operations. NASA CR-2019, 1972.

4. Beppu, G.: A Study of Pilot Behavior During Controlling the Lateral-Directional Motion of Airplanes in Turbulent Air. NASA TM X-62,464, 1975, pp. 625-644.

5. Akaike, H.: On the Use of a Linear Model for the Identification of Feedback Systems. Ann. Inst. Statist. Math., vol. 20, 1968, pp. 425-439.

6. Akaike, H.: On a Decision Procedure for System Identification. IFAC Kyoto Symposium on System Engineering Approach to Computer Control, 1970, Preprint, pp. 485-590.

7. Whittle, P.: On the Fitting of Multivariate Autoregressions and the Approximate Canonical Factorization of a Spectral Density Matrix. Biometrica, vol. 50, 1963, pp. 129-134.

8. Akaike, H.: Autoregressive Model Fitting for Control. Ann. Inst. Statist. Math., vol. 23, 1971, pp. 163-180.

9. Akaike, H.: A New Look at the Statistical Model Identification. IEEE Trans., vol. 19, no. 6, 1974, pp. 716-723.

10. McRuer, D.; Ashkenas, I.; and Graham, D.: Aircraft Dynamics and Automatic Control. Princeton University Press, Princeton, N.J., 1973.

11. McFarland, R. E.: A Standard Kinematic Model for Flight Simulation at NASA-Ames. NASA CR-2497, 1975.

12. Cooper, G. E.; and Harper, R. P., Jr.: The Use of Pilot Rating in the Evaluation of Aircraft Handling Qualities. NASA TN D-5153, 1969.

13. Parris, B. L.: Modeling Turbulence for Flight Simulations at NASA Ames. CSCR No. 4, prepared by Computer Sciences Corporation for NASA, 1975.

14. Chalk, C. R.; Neal, T. P.; Harris, T. M.; Pritchard, F. E.; and Woodcock, R. J.: Background Information and User Guide for MIL-F-8785B(ASG); Military Specification - Flying Qualities of Piloted Airplanes. AFFDL-TR-68-72, Air Force Flight Dynamics Laboratory, 1969, p. 427.

15. Franklin, J. A.: Turbulence and Lateral-Directional Flying Qualities. NASA CR-1718, 1971, p. 89.

16. Neuman, F.; and Foster, J. D.: Investigation of a Digital Automatic Aircraft Landing System in Turbulence. NASA TN D-6066, 1970.

17. Goto, N.; and Washizu, K.: On the Dynamics of Human Pilots in Marginally Controllable Systems. AIAA J., vol. 12, no. 3, 1974, pp. 310-315.

RIDE QUALITY SENSITIVITY TO SAS CONTROL LAW AND TO HANDLING QUALITY VARIATIONS

Philip A. Roberts, David K. Schmidt, and Robert L. Swaim
School of Aeronautics and Astronautics, Purdue University

SUMMARY

State variable techniques are used to generate the vertical and lateral fuselage loadfactor distributions for the B-52H and B-1 bombers. A comparison of loadfactors resulting from cruise turbulence excitation, reveals that ride quality is not significantly improved by increasing the control law complexity. Control law complexity is meant to imply rate feedback in comparison to full state feedback. Handling quality parameterizations show pronounced effects on the loadfactors. Finally variations under relaxed static stability implementation show that the ride quality is degraded by restoration of handling characteristics to original short period values.

INTRODUCTION

Control Configured Vehicle (CCV) technology is just beginning to affect the design and manufacture of aerospace vehicles. Current technology aircraft like the F-16 fighter and B-1 bomber are utilizing concepts such as ride control, Relaxed Static Stability (RSS), and fatigue reduction. Future vehicles will certainly incorporate active controls, maneuver load control, direct lift, flutter mode control, and gust load alleviation concepts. These future vehicles will be optimized under many manifolds to include Ride Quality (RQ).

The objective of this paper is to discuss the RQ trends which large flexible aircraft exhibit under various parameterizations of control laws and handling qualities. The information was generated as a data base for research supported by NASA Dryden Flight Research Center under grant NSG 4003. The ultimate aim of the project is delineation of handling qualities specifications for highly flexible CCV vehicles. This paper contains a summary of the assumptions and solution technique, a control law parameterization review, a discussion of ride sensitivity to handling qualities, and finally the RQ effects generated by implementing relaxed static stability configurations.

SYMBOLS

A' **Transpose of the A matrix**

$\bar{c}$	Mean aerodynamic chord length
cg	Center of gravity
E{ }	Expected value
HQ	Handling Qualities
ℓ_x	Distance from cg along fuselage centerline, positive forward
$\bar{\ell}_t$	Distance between the tail and wing-body aerodynamic centers
$N_{z,y}$	Loadfactor at a particular body station; z denotes vertical y denotes lateral
rms	Root mean square
RQ	Ride Qualities
RSS	Relaxed static stability
S	Wing planform area
S_t	Tail planform area
U_0	Averaged Steady State Flight Velocity
u	Control(s) vector; elevator, aileron, and/or rudder
$\bar{V}$	Tail volume coefficient
x	State vector; usually associated with physical outputs in this paper
α	Perturbation angle of attack
β	Perturbation side slip angle
ζ	Damping value
η	Scalar unit white noise
θ	Perturbation pitch angle
ξ_i	itn elastic mode generalized displacement
$\phi_i(\ell_x)$	ith orthogonal elastic mode shape value at body station ℓ_x
ϕ	Perturbation roll angle

ψ Perturbation yaw angle

ω Natural frequency

PROBLEM FORMULATION

Equations of Motion for Flexible Vehicles

Time domain representations for the flexible vehicles were decoupled into longitudinal and lateral state variable formats. The Gaussian white noise representation of turbulence was modeled as a state vector system as suggested in reference 1. The gust state vector was appended to the vehicle state equations resulting in the familiar control form (1).

$$\dot{x}(t) = Ax(t) + Bu(t) + G\eta(t) \tag{1}$$

where:
- x (n+p) x 1
- u m x 1
- n number of physical vehicle states
- m number of controls
- p number of gust states
- G (n+p) x 1
- A (n+p) x (n+p)
- B (n+p) x m

Loadfactor Expression

The major contributions to vertical and lateral loadfactors at cruise conditions can be represented by equations (2a) and (2b).

$$N_z(\ell_x,t) = \frac{1}{g}\left[U_0(\dot{\theta}-\dot{\alpha}) + \ell_x\ddot{\theta} - \sum_{i=1}^{K}\phi_i(\ell_x)\ddot{\xi}_i\right] \tag{2a}$$

$$N_y(\ell_x,t) = \frac{1}{g}\left[g\phi - U_0(\dot{\beta}+\dot{\psi}) - \ell_x\ddot{\psi} - \sum_{i=1}^{K}\phi_i(\ell_x)\ddot{\xi}_i\right] \tag{2b}$$

where: K is the number of elastic modes included in the model.

Throughout this paper the standard right hand stability axis system is utilized with the x axis positive forward from the cg as shown in figure 1.

The sign conventions for the vertical and side bending elements are shown in figures 2 and 3.

The loadfactor expressions can be reformulated as functions of the physical state variables by simple substitution.

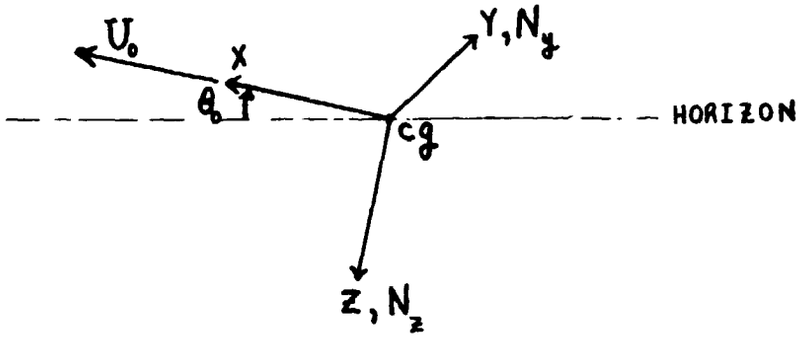

Figure 1: Stability Axis Sign Convention

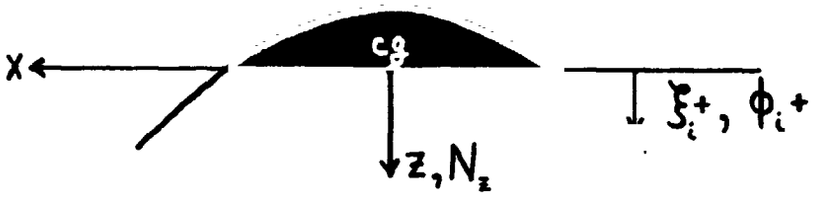

Figure 2: Fuselage Vertical Bending Sign Convention

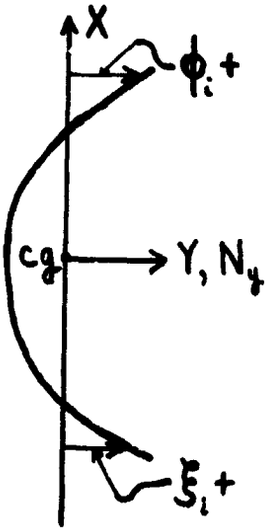

Figure 3: Fuselage Side Bending Sign Convention

$$N_z(\ell_x,t) = P_z\ x_z(t) \tag{3a}$$

$$N_y(\ell_x,t) = P_y\ x_y(t) \tag{3b}$$

The 1x(n+p) row vectors, $P_{z,y}$ are deterministic for a given vehicle equation of motion set, specific control, and specified gain value. Equations (3) can be manipulated into a mean square value expression for the loadfactor.

$$E\{N^2_{z,y}\} = P_{z,y}\ E\{xx'\}_{z,y}\ P'_{z,y} \tag{4}$$

Assuming a stationary, zero mean process for the state differential system (1) leads to an algebraic matrix Riccati equation. This equation can be solved for the symmetric covariance matrix, E{xx'}. Utilizing one algorithm suggested by Gelb in reference 2, convergence can be obtained within 35 seconds on a CDC 6500 for a 16x16 Riccati system. A simple matrix multiplication routine completes the solution utilizing equation (4).

Study Vehicle Descriptions and Flight Conditions

The B-52H and B-1 were chosen for this study because they exemplify the trend toward more elastic structures for future large vehicles. The B-52, and commercial derivatives thereof, was a member of the first generation of elastic vehicles. Since that era, improved structural design techniques and composite materials have made possible vehicles like the highly elastic B-1.

The flight conditions were chosen because they represent cruise conditions which are mission essential and because turbulence encounters at low altitudes must be included in future design considerations.

The B-52H is used by the US Air Force as a long range bomber. It is 47.55 meters long and has a wing span of 56.4 meters. Originally designed as a high altitude bomber, it must now cope with penetration problems by combined high/low altitude profiles. Table 1 describes the flight condition for the B-52H.

Mass = 158,757 kilograms (350,000 lbs.)
Mach = .55
Velocity = 185.56 meters/sec (608.8 fps)
cg at 25% mean aerodynamic chord
Altitude = 609.6 meters (2000 ft)

TABLE 1: B-52H Flight Condition

The B-1 is currently being test flown in a major pre-production effort by Rockwell International and the USAF. It is designed as the replacement vehicle for the aging B-52 fleet. The advanced structures and integrated technology make this vehicle an outstanding example for loadfactor

contributions due to elasticity. The overall length of the B-1 is 46 meters. The reference wing span utilized at the flight condition in Table 2 is 41.8 meters.

Mass = 103,315 kilograms (227,770 lbs)
Mach = .85
Velocity = 289.4 meters/sec (949.45 fps)
cg is at fuselage station 40.67 (meters)
Altitude = 30.48 meters (100 feet)

TABLE 2: B-1 Flight Condition

CONTROL LAW VARIATIONS

Both vehicles were modeled as stable, unaugmented systems in the vertical and lateral cases with the exception of the B-52H which required a small roll subsidence mode stabilization before proceeding. Each vehicle model was theoretically modified utilizing pitch rate, yaw rate, pitch rate/pitch attitude, blended pitch rate with acceleration, and full state feedback control laws. No significant differences in RQ were generated by these variations for identical (or nearly equivalent) handling quality values.

It should be mentioned here that the B-1 Structural Mode Control System was purposely not included or utilized because this study is involved with general control design parameterizations and not the specific RQ optimization of the B-1. For both aircraft studies, only the primary control surfaces (elevator, rudder, and aileron) were used for RQ determinations.

To establish a basis for comparison, the unaugmented vehicle loadfactors were computed for .3048 meter/sec (1 fps) rms (root mean square) gust velocities.

Figure 4 depicts the loadfactor curves for the unaugmented B-52H. The nearly linear loadfactors labeled "rigid body only" include all terms except the summations in equations (2a) and (2b). Hence any interactive rigid body and elastic dynamics from the Riccati solution are included in this output. The second line which has a more pronounced curvature includes all the modes that were utilized in the model. For the B-52H at this flight condition, the maximum elastic contribution to vertical loadfactors is about 15% of the total. (The lateral fuselage modes used in this data were primarily aft-body modes. Hence the rise in elastic effects near the tail.)

Figure 5 shows an impressive increase in the elastic contribution to vertical loadfactors on the unaugmented B-1. The discerning reader will immediately note the changes in vertical scale in figures 4 and 5. The different flight conditions and elastic contributions to ride on the separate vehicles dictated these scale changes.

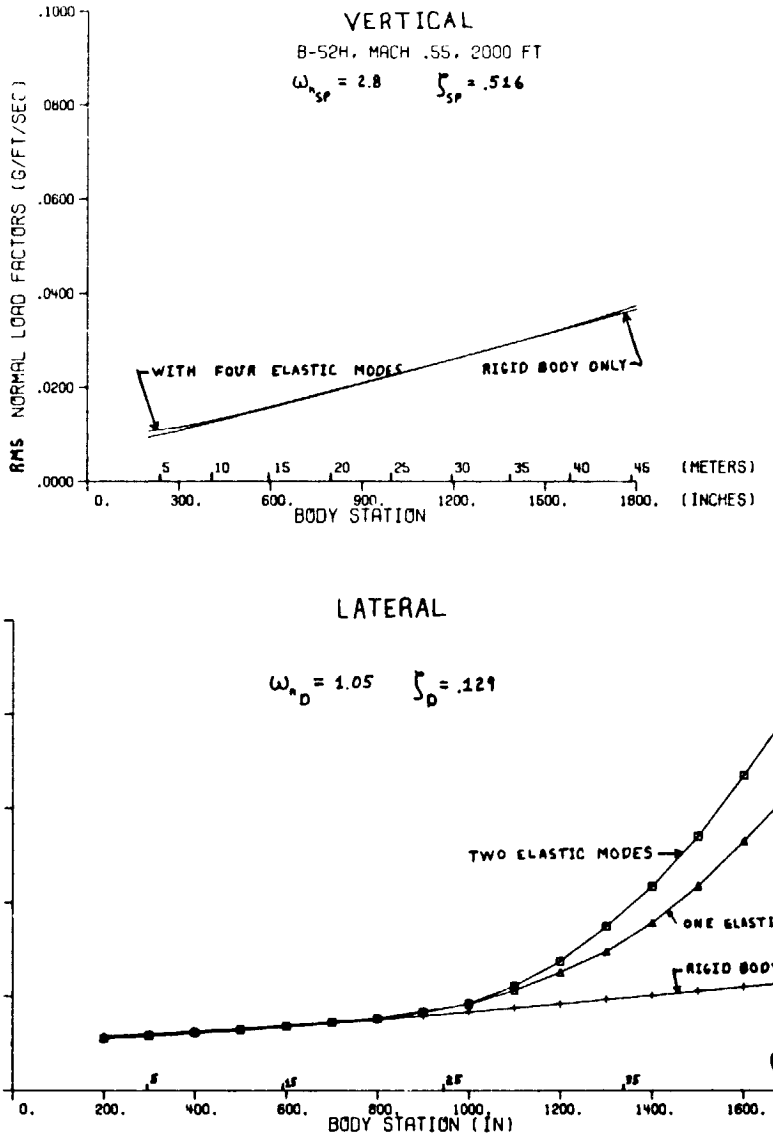

Figure 4: B-52H Unaugmented Loadfactors

RQ SENSITIVITY TO HANDLING CHARACTERISTICS

Under each control law studied, the gains were changed so that a range of handling characteristics and their resulting loadfactors could be cataloged. The values used for the handling characteristics were restricted to the acceptable ranges given in MIL SPEC 8785B. Hence the following boundaries:

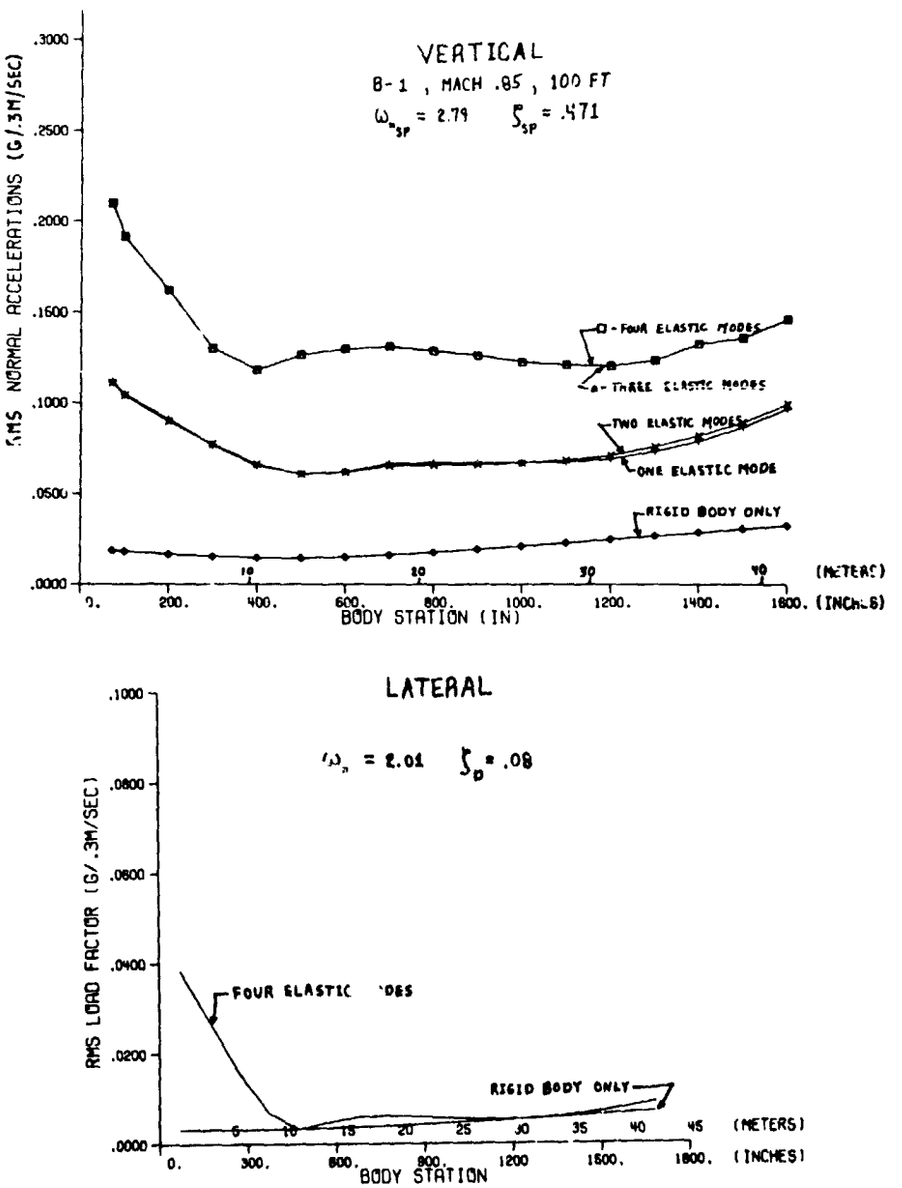

Figure 5: B-1 Unaugmented Load factors

Longitudinal Short Period $\begin{cases} .3 \leq \zeta_{sp} \leq 2.0 \\ 2.0 \leq \omega_n \leq 10.0 \end{cases}$

Lateral Dutch Roll $\begin{cases} .08 \leq \zeta_D \\ .40 \leq \omega_n \end{cases}$

It is important to reiterate at this juncture that the study goal was RQ sensitivity to feasible controls, not the design of an optimal control for either vehicle.

Pitch Rate Feedback (B-52H)

Figure 6 shows the percentage change in loadfactor for various handling characteristics. The baseline in all these cases is the unaugmented vehicle loadfactors from figures 4 or 5, whichever is appropriate. As shown, the increase of damping and frequency for higher stabilizing feedback gains produced better RQ.

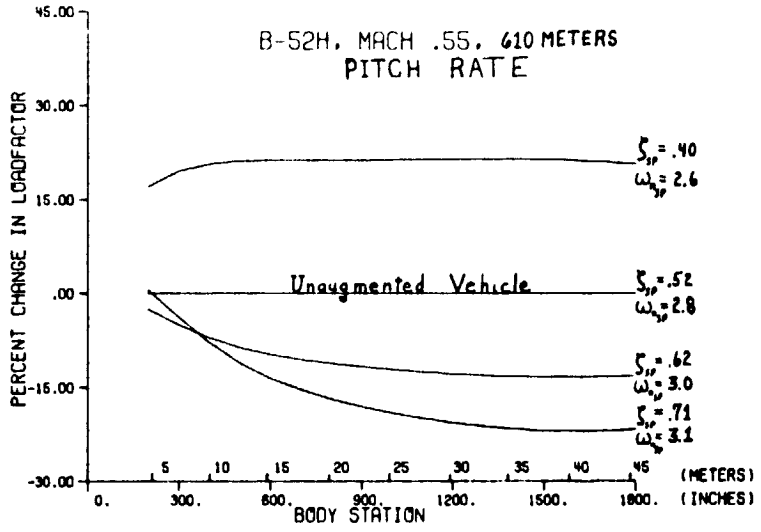

Figure 6: Pitch Rate SAS Changes

Yaw Rate Feedback (B-1)

Figure 7 shows the loadfactor curves for the B-1 lateral dynamics. Notice the effect is similar; increased damping produces better RQ.

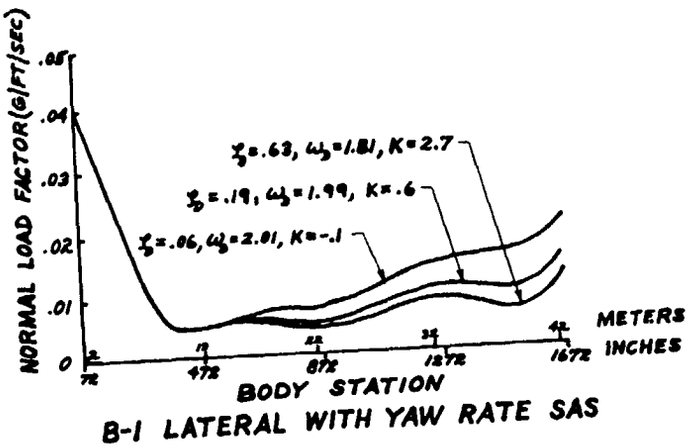

Figure 7: B-1 Yaw Rate SAS Loadfactors

Blended Pitch Rate and Acceleration (C*) (B-1)

Figure 8 shows the percentage changes in loadfactor under the C* control policy with variations in handling characteristics. Again the same general trends appear.

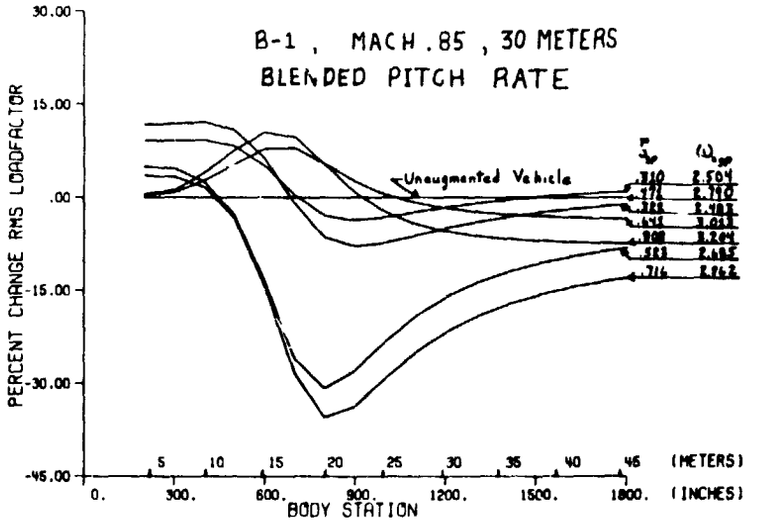

Figure 8: B-1 C* SAS

Full State Feedback (B-52H)

The trend expected by control experts would show that higher frequency and higher damping beget better RQ. This expectation was validated using full state feedback pole placing capacility. Figure 9 shows the results as percentage changes in loadfactor compared to the unaugmented vehicle. The forward fuselage percentage changes were distorted by relatively low baseline loadfactor values. Hence the higher damping/frequency loadfactor curves represent better rides overall. The asterisk cases in figure 9 deserve special mention. In these two cases the elastic mode damping was artificially increased through the elevator feedback control policy. Note that both cases generated appreciably worse RQ. This occurred because of the increased elevator excitation of the rigid body parameters in equations (2). Breakdowns of the elastic contributions to the loadfactors showed the three elastic modes chosen for increased damping actually did contribute less to the rms loadfactor.

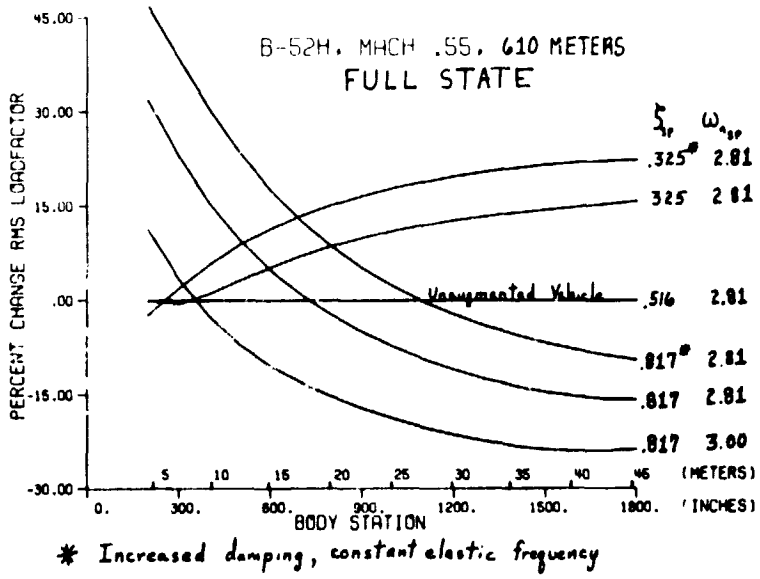

Figure 9: B-52 Full State SAS

This result prompted a theoretical attempt to parametrically plot loadfactor versus frequency and damping. Using a transfer function approach and the Dryden power spectral density for vertical gusts, the loadfactor mean square value was computed as an integral over the frequency domain. The results support the numerical analysis shown in figure 9.

As frequency increases, the RQ gets better. Likewise damping value excursions from the coupled elastic mode eigenvalue at constant frequency will adversely affect the loadfactors. A numerical example was run for the B-52H and is shown in figure 10 for two increased short period frequency cases. The elastic mode increased damping was not included in these cases.

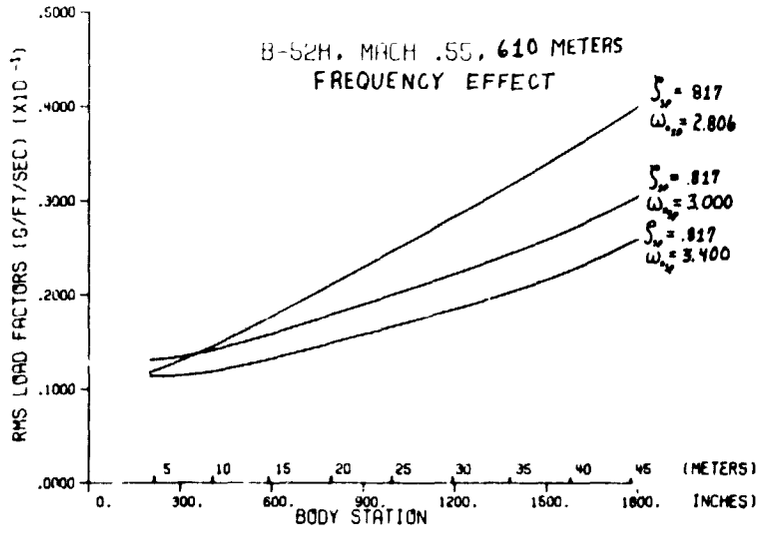

Figure 10: B-52H Increased Short Period Frequency Effect

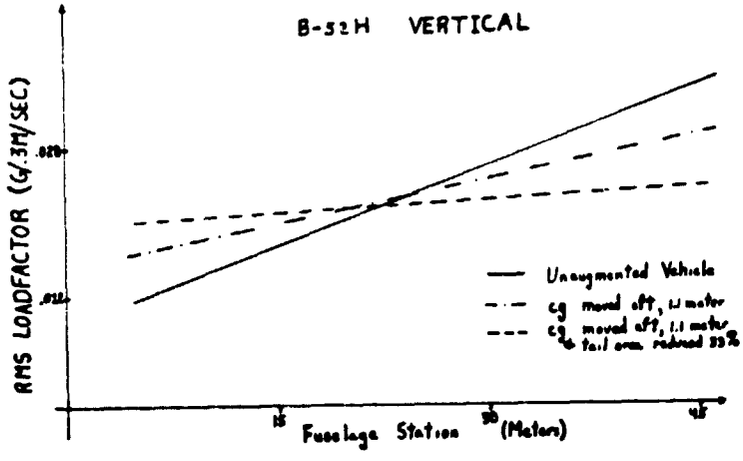

Figure 11: B-52H Rigid Body Relaxed Static Stability

RELAXED STATIC STABILITY (RSS)

Two methods were used to simulate this effect on the study vehicles. First the tail volume coefficient, $\bar{V}$, was reduced.

$$\bar{V} = \frac{\bar{\ell}_t \, S_t}{\bar{c} \, S} \tag{5}$$

This has the effect of shifting the vehicle aerodynamic center toward the center of gravity. Static stability is thereby reduced. The second method involves an artificial cg shift toward the tail. This is the more practical of the two methods, as it has already been incorporated as a fuel transfer or management activity on a test vehicle (CCV B-52).

Figure 11 shows the effect of RSS on vertical ride for the rigid body B-52H vehicle. Essentially pitching moment effects are reduced until at neutral stability the loadfactors are constant and due only to the vertical accelerations. This would logically follow from the definition of the neutral point. The question now arises, what rides are induced by restoring the original handling characteristics of the unaugmented vehicle with an active control system? Figure 12 shows these results in terms of percent loadfactor change. In general the restoration resulted in degraded RQ.

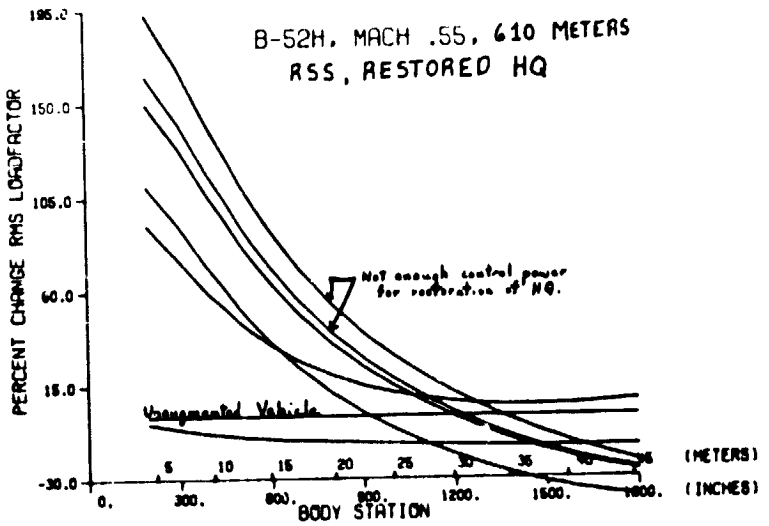

Figure 12: B-52H RSS, Restored Handling Qualities

CONCLUSIONS

1. Ride quality is particularly sensitive to the handling characteristics specifications.

2. Except in optimizing a particular vehicle's control capabilities, ride quality is not dependent on the type of control law chosen.

3. Relaxed Static Stability has a favorable effect on B-1 ride quality in that less pitch acceleration and/or velocity contribute to the loadfactor.

4. Relaxed Static Stability with restored handling qualities generates higher loadfactors on the B-52H and B-1 at the flight conditions studied.

REFERENCES

1. Heath, Robert E., II: State Variable Model of Wind Gusts, Air Force Flight Dynamics Laboratory Technical Memorandum, AFFDL-FGC-TM-72-12, Wright-Patterson AFB, Ohio, July 1972.

2. Gelb, Arthur, et al.: Applied Optimal Estimation, MIT Press, Cambridge, Mass., 1974.

3. Swaim, R. L., et al.: An Analytical Method for Ride Quality of Flexible Airplanes, Proceedings of the 3rd AIAA Atmospheric Flight Mechanics Conference, Arlington, Texas, June 1976.

A UNIFIED THEORY

FOR

PILOT OPINION RATING

By Ralph H. Smith
Vantage Engineering
Frenchtown, NJ

SUMMARY

This paper presents theory for understanding and predicting pilot opinion rating (POR) in closed loop, precision control tasks. The general implementation of the theory requires a unified model for pilot dynamics that is hypothesized to be multiple loop in form with essential nonlinearities. A search for such a model was unsuccessful. However, the apparent self-adaptive nature of the postulated model with respect to controlled element dynamics and system input suggests that, for single axis tracking tasks, a simple POR metric can be estimated using state-of-the-art pilot models. The POR theory was successfully demonstrated using available single axis tracking data. The proposed metric was shown to be a consistent, sensitive measure of POR for these data. Certain of these data were used to calibrate the variation of POR with the POR metric. This calibration, together with a suitable model for pilot-vehicle dynamics, can be used for the prediction of POR. It is suggested, however, that state-of-the-art models for pilot dynamics are generally unsuited for the precision estimation of the postulated POR metric in multiple loop or multiple axis tracking tasks; otherwise the POR theory has no obvious limitations of the sort that bound the validity of available pilot models. A generalized Paper Pilot method is proposed in a form consistent with this theory.

SYMBOLS

J	Cost functional for the optimal pilot model.
K_c	Controlled element gain
K_{D_θ}, K_{D_q}	Describing function approximations for display gains in θ and q loops
K_{F_θ}, K_{F_q}	Equivalent Kalman filter gains in θ and q loops
K_p	Pilot gain in the Servo model representation
K_θ, K_q	Controller gains in the optimal pilot model for the θ and q loops

POR	Pilot Opinion Rating (Cooper-Harper)
q	Pitch attitude rate, deg/sec
q_c	Pitch attitude rate command, deg/sec
q_p	Pitch attitude rate perceived by the human pilot, deg/sec
R	Cost functional weighting on $\sigma^2_{\delta e}$
r	Cost functional weighting on $\sigma^2_{\beta q}$
s	Laplace transform variable, $s = \sigma + j\omega$
T_L	Pilot lead time constant in the servo model representation, secs
t	Time, secs
u	Forward speed, m/sec
W_θ, W_q	Cost functional weightings on σ^2_θ and σ^2_q
Y_c (s)	Controlled element transfer function
Y_p (jω)	Pilot describing function (servo model)
β_q	Central nervous system signal from central processor functions to the neuromuscular system
δ_e	Elevator deflection, deg
$\dot{\delta}_e$	$d\delta e/dt$
θ	Pitch attitude, deg
θ_e	Pitch attitude tracking error, deg
θ_p	Pitch attitude perceived by the human pilot, deg
σ_q	Standard deviation of q, degs/sec
σ_{q_p}	Standard deviation of q_p, degs/sec
$\sigma_{\beta q}$	Standard deviation of βq, degs
σ_{θ_p}	Standard deviation of θ_p, degs

INTRODUCTION

The present state-of-the-art of handling qualities is fundamentally empirical. Available theories for handling qualities are all based upon a network of empirical data, experiences with classical airframe dynamics, servomechanisms analogies, and conjectural hypotheses which attempt to establish a connection between handling qualities and available models for human pilot dynamics. All these have some demonstrated value for the codification of experimental data or for the design of experiments; none has provided significant insight into the physics of handling qualities or has a demonstrated, general capability for a priori prediction of handling qualities. We have no better physical understanding now of the dynamics of human subjective response than we had prior to development of the servomechanisms model for human pilot dynamics.

The elusive, intangible nature of handling qualities has presented a formidible obstacle to the development of a physical theory for the subject. We haven't even successfully defined what we mean by "handling qualities". Attempts to do so are inevitably either personalized and vehicle-centered or general, vague and practically useless. The entire concept of "quality" is involved. Reference 1 is recommended for a discourse on quality and what it can mean to our technology.

The lack of a suitable definition for handling qualities does not prevent us from recognizing degrees of handling qualities in practice. We attempt to systematically code these in terms of airframe and control system parameters as a means for evaluating system design. It is here that the lack of a physical and philosophical understanding of handling qualities has its real impact on research. We arbitrarily invent handling quality metrics and proceed to devote valuable resources to their study. This is all too often done without concern for whether our inventions are capable of bringing unity of understanding to a chaotic subject. This tangential approach has produced no real payoff to research or systems design.

The sad fact is that handling qualities is not entirely credible as a mature design technology; it remains a handbook art. This field differs from other technology areas involved in aircraft design in one fundamental respect: it is without foundation on physical principles such as exist for other fields. Handling qualities has no counterpart to the equations of Navier-Stokes, Maxwell, or Euler-Lagrange. Accordingly, we are unable to quantify the benefits of handling qualities to systems design except on the most primitive level.

The handling qualities discipline originated with the pilot's subjective opinion of ease of aircraft control. Opinion scales were invented to quantify the pilot's subjective response. Pilot opinion rating (POR) is a widely used and poorly understood metric for handling qualities. It has almost become a de facto substitute for handling qualities through familiarity.

POR data often appear to be highly variable and to exhibit unpredictable, systematic biases among the pilot population and random variations for a given pilot. A major tenet of the present work is that anomalies in POR data may be illusory. Without a physical theory for handling qualities (and, therefore, for POR) one should not assume that all the factors parameterizing POR are known for a given experimental configuration. Given the typical handling quality experiment, it is a logical error to classify POR data as inconsistent or variable merely because the same numerical rating was not obtained for multiple runs with the same configurations of vehicle dynamics and system input or because the variation of POR with vehicle response parameters does not obey the analyst's preconceived theory.

As a practical matter we must expect that POR data obtained from a carefully designed, realistic experiment will exhibit a certain amount of variability. What we need to do is develop methods for ensuring that the variability is not the systematic result of applying faulty theory or inadequate metrics for the correlation and assessment of POR data. Unexplained variations in POR would not, in fact, be random if the pilot subjectively responds to a particular system property; in that case POR data might be almost perfectly consistent with a suitable, but unknown, metric--in other words it is conceivable that it is the engineering analyst and not the pilot who establishes the level of variability in POR data!

Of course the pilot is not a machine; run-to-run variability of a genuinely random nature probably must be expected. The Cooper-Harper scale for POR is not perfect and must be selectively interpreted by the evaluation pilot. The present state-of-the-art requires that such effects be minimized by averaging sufficient POR data. We should insist, however, that such data be uncontaminated by effects that are within our capabilities to understand and control. This is not easily accomplished.

The research summarized in this paper is based on the hypothesis that:
(1) a pilot's subjective response originates from a particular point, or area, within his central nervous system, and
(2) POR is directly and uniquely related to the strength of the neural signal at this location. If the validity of this hypothesis can be established, then handling qualities can eventually be quantified by direct measurement; also, handling qualities can be predicted given a satisfactory model for pilot dynamics.

A UNIFIED MODEL FOR PILOT DYNAMICS

There exist only two state-of-the-art models for pilot-vehicle system dynamics and performance that have received general acceptance for analysis of single loop, continuous tracking tasks. The servomechanisms model (reference 3) was developed to parameterize pilot dynamics for a wide range of controlled elements. The Kleinman optimal control model (reference 4) was devised as a formal tool for the prediction of pilot-vehicle system performance. Both models are fundamentally empirical One must depend upon the

existence of baseline data for their parameterization; they are, in a sense, interpolative. Neither model offers real hope for understanding the fine-grain character of pilot dynamics (e.g. the variations of phase margin or crossover frequency with controlled element dynamics, the source of pilot remmant, crossover frequency regression, control stick "pulsing", control stick "pumping", the basis for pilot-generated dynamic equalization, etc.). If we are to develop a general theory for handling qualities, then a more refined and physically oriented model for pilot dynamics is a necessity.

Reference 2 offers two hypotheses which define the scope and nature of the model sought:

HYPOTHESIS 1:

The servo and the optimal control models for human pilot dynamics are linearizations of a more fundamental (and physically acceptable) nonlinear model.

HYPOTHESIS 2:

A model for human pilot dynamics that structurally matches the human physiology in the tracking process will lead to a natural and physical measure for POR.

The pilot model shown in figure 1 was investigated in reference 2 and is proposed to be such a model. It is believed that--when properly parameterized--it will exhibit most of the known response properties of the human pilot. The model of figure 1 is intended to subsume the servo and the optimal control models. Note that figure 1 applies for a pitch attitude tracking task. This is the only case that will be considered in this paper. The model is applicable to any single axis task, however.

The model of figure 1 is nonlinear and multiple loop in form. It has, to this date, not been successfully parameterized in the fashion desired. It is demonstrated in reference 2, however, that the nonlinear model is a very plausible explanation for the parametric variations required by the servo model as a function of controlled element dynamics. This is illustrated in figure 2 for the three familiar controlled element forms: $Y_c(s)=K_c$, K_c/s & K_c/s^2. A highly simplified, linear version of the proposed nonlinear pilot model is shown on figure 2. It may be directly compared with the servo model $Y_p(j\omega)$ following closure of the q-loop; the resulting closed loop model connecting θ_c with δe is then formally the same as $Y_p(j\omega)$ from the servo model representation. The approximate forms for $Y_p(j\omega)$ predicted by the nonlinear model are shown in figure 2 for each of the three elementary controlled elements. The model in figure 2 is assumed to result from combinations of model nonlinearities and closed loop dynamics which create the situation shown where q_c is negligible with respect to q.

The nonlinear model suggests that low frequency approximations to $Y_p(j\omega)$ should resemble

1. a pure gain for $Y_c(s) = K_c/s$
2. a gain and a low frequency lag for $Y_c(s) = K_c$, and
3. a gain with a low frequency lead for $Y_c(s) = K_c/s^2$.

These results are consistent with measured human dynamics as embodied in the servo model. The fact that rate feedback in the nonlinear model (figure 1) can conceivably produce an apparent low frequency lag in measurements of $Y_p(j\omega)$ for pure-gain controlled elements is a remarkable result. When the effects of q_c are not neglibible in comparison with those of q the nonlinear model will predict a gain plus first order lead for $Y_c(s) = K_c/s^2$ rather than the gain with pure lead shown.

Another startling implication of the nonlinear model is that it can exhibit considerable rate feedback without creating an apparent low frequency lead in measurements of $Y_p(j\omega)$--see figure 2 for $Y_c(s) = K_c/s$. In general, the nonlinear model indicates that the level of pilot control of system rate need not be directly reflected in low frequency lead or lag equalization as measured in the describing function $Y_p(j\omega)$--the servo model for pilot dynamics. In contrast, this author's experience with the Kleinman optimal control model indicates that it too can produce a sizable rate feedback gain with a K_c/s-like controlled element. Thus, there is a formal similarity between the Kleinman model and the nonlinear model of figure 1.

A THEORY FOR PILOT OPINION RATING

The qualitative nature of the handling quality tasks posed by each of the three elementary controlled elements is noted on figure 2. It might appear that increasing task difficulty (as reflected in POR) can be associated with an increase in the pilot model's rate gain K_q. This is not entirely true. A more appropriate indication of task difficulty should be expected in measures of closed loop signals since it is these which ultimately determine the linearized forms for the pilot model and its components. It is therefore tempting to speculate that βq, the q-channel response of the nonlinear pilot model, will parameterize POR regardless of system input or controlled element dynamics since βq will depend on both K_q and the closed loop response.

As an illustration of the possible connection between system rate and handling qualities consider that for easily controlled vehicles system rate is seldom large, whereas a vehicle that is difficult to control will demand that the pilot devote considerable effort to the stabilization of rate errors. It should be apparent that if rate cannot be readily controlled then neither can attitude and the handling will suffer. Thus, good rate control is very nearly a necessary and sufficient condition for good handling qualities. The closed loop signal βq would, in the human pilot, consist of a series of neural potentials (or electrical pulses) within a certain region of the central nervous system. These conjectures are formalized in the following

hypothesis.

HYPOTHESIS:

A physiological measure for POR is the rate of nerve impulses (or an equivalent measure) at the point within the central nervous system where all signals originating due to rate control are summed or operated upon by a decision process of some sort. The neuromuscular system is postulated to provide a component to this hypothesized signal junction; this component is dependent upon the feel system characteristics and will affect POR. The relation between POR and the nerve impulse rate is fixed for each pilot. It may depend upon his piloting experiences, training and his personal interpretation of the rating scale. It is independent of controlled element dynamics, input and task.

The postulated output from the human pilot "central processor's" rate channel βq (as depicted in figures 1 & 2) is not directly accessible for measurement. It is internal to the central nervous system. In its simplest form βq probably consists of a series of nerve pulses with the pulse frequency proportional to the neural excitation at the point of impulse generation. For present purposes it is probably sufficient to assume that, in continuous tracking tasks with random inputs, βq can be parameterized by its standard deviation $\sigma_{\beta q}$. Given a high fidelity pilot-vehicle system model, $\sigma_{\beta q}$ can be estimated; perhaps $\beta q(t)$ can eventually be directly monitored given advances in medical technology.

By the above hypothesis and the assumption that βq can be represented by $\sigma_{\beta q}$, we may expect that POR will vary with $\sigma_{\beta q}$ in the manner illustrated in figure 3.

Observe that, by hypothesis, POR is a function of <u>only</u> $\sigma_{\beta q}$ for a given pilot. However, $\sigma_{\beta q}$ is dependent upon anything that affects the signal strength of $\beta q(t)$. This includes controlled element dynamics, input spectrum, display properties (since these affect the signal transmission of rate error) the task and feel system. It may include various vehicle motion cues available to the pilot in a flight test or moving base simulation.

At the present time no model for neuromuscular system dynamics is known to this author which will permit the estimation of feel system effect on $\sigma_{\beta q}$. Many past experiments have confirmed the importance to POR of the feel system. As a result, our present theory for the correlation or prediction of POR appears to be restricted to consideration of only those pilot-vehicle data for which the control system was optimized with respect to POR.

VALIDATION OF THE RATING METRIC IN SINGLE AXIS TRACKING

The hypothesized POR metric $\sigma_{\beta q}$ can be correlated with rating data from

any handling quality experiment provided sufficient data are available to permit the estimation of $\sigma_{\beta q}$ (given a satisfactory model for pilot dynamics), provided that the control feel system was optimized with respect to POR prior to each data run, and given sufficient POR data to permit the estimation of statistically valid POR averages for each tested configuration. Few such data sources exist.

Note that the servo and the optimal control models for pilot dynamics are suitable only for the estimation of <u>average</u> system properties. This will constitute a source for systematic error in any attempts to correlate POR with $\sigma_{\beta q}$ using these pilot models since it is likely that $\sigma_{\beta q}$ will vary from run-to-run with the same configuration due to pilot nonlinearities. It is reasonable to suspect that the run-to-run variance of $\sigma_{\beta q}$ will be greatest for those configurations that are the most difficult to control. Until $\sigma_{\beta q}$ can be directly measured by experiment, there is no way to eliminate this error component from correlations of POR with $\sigma_{\beta q}$; hopefully, its effects will be small relative to the basic trends. If present theory is basically correct, then the run-to-run variation of $\sigma_{\beta q}$ is responsible for much of the so-called pilot variability that pervades the handling qualities data base. It also explains why more data runs are required for the valid estimation of average POR when the vehicle dynamics are poor (reference 5).

It has already been noted that the servo model will not always correctly reflect the level of rate control predicted by the nonlinear or optimal control models for pilot dynamics. When $Y_c(s) \approx K_c/s$ the servo model requires no low frequency equalization (and therefore no rate control) whereas the nonlinear model indicates that considerable rate control may exist. As a rule-of-thumb, when the servo model would require either a lead time constant less than 0.5 seconds or a lag then it should not be used for the estimation of $\sigma_{\beta q}$.

The nonlinear model of figure 1 has not yet been successfully parameterized and therefore cannot be used for the estimation of $\sigma_{\beta q}$. However, there is no objection to use of the optimal control model. A version of this is shown in figure 4 for the pitch attitude control example. This model differs significantly from the conventional Kleinman model. It incorporates describing function representations for the visual threshold nonlinearities in the rate and attitude channels (K_{Dq} & $K_{D\theta}$, respectively); the cost functional is stated in terms of the state variables perceived by the human pilot. A discussion of this model can be found in reference 6 where it was introduced. The cost functional weights shown in figure 4 were selected in reference 6 to optimize the fit between measured and predicted closed loop system performance for Arnold's tracking data (reference 7). Arnold's data are entirely satisfactory for testing the proposed POR metric.

Note that for the Kleinman-Dillow model,

$$\sigma_{\beta q} = K_{Dq} K_{Fq} K_q \sigma_q = K_q \sigma_{q_p}$$

The Kalman filter gain K_{Fq} is describing function approximation to the actual filter operation. The model shown in figure 4 is strictly applicable only after convergence of the optimization routine.

The Kleinman-Dillow model was applied to the Arnold tracking data to estimate $\sigma_{\beta q}$ for each of his dynamic configurations. The Arnold POR measurements were obtained using values of pitch control effectiveness that were approximately optimum with respect to POR, and sufficient data were collected to permit the reasonable determination of average POR for each configuration. Arnold also published measured σ_q; thus the Kleinman-Dillow model was required only for the prediction of rate loop gain $K_{Dq}\ K_{Fq}\ K_q$. The resulting correlation between Arnold's averaged POR data and the model-predicted $\sigma_{\beta q}$ (shown on figure 5) is seen to be quite good; the hash marks represent plus and minus one-half rating unit (Cooper-Harper scale) about the mean curve.

The Arnold-derived correlation shown on figure 5 was obtained from POR data averaged over several pilot subjects. Thus, if present theory is correct the variation of $\sigma_{\beta q}$ with the nominal fit to Arnold's POR data should constitute a model for the <u>prediction</u> of POR, averaged over many pilots, provided only that a satisfactory model for pilot dynamics is available to enable the estimation of $\sigma_{\beta q}$. In other words, the function POR ($\sigma_{\beta q}$) shown in figure 5 should be constant over a wide range of experimental conditions.

The optimal control model of figure 4 was applied <u>without change</u> to McDonnell's data (reference 5). Unfortunately reference 5 did not publish measured σ_q; thus it was necessary that the Kleinman-Dillow model be used for the prediction of the rate loop gains and σ_q. Also, the McDonnell data were very sparse; in order to extend his data base it was necessary to average his POR data for a given configuration without regard for control system gain. The resulting correlation is shown on figure 5; the correlation is supportive of the present theory to a degree that is better than might be expected in view of the data's shortcomings.

Two additional data points were obtained from Johnson (reference 8) who applied the Paper Pilot theory to moving base simulator data published by Onstott, et al (reference 9). The servo model was used to represent pilot dynamics. Of the 35 configurations examine by Johnson only two resulted in non-zero estimates for the pilot lead time constant; thus, these are the only two cases for which the servo model can be used to estimate $\sigma_{\beta q}$. (Time did not permit the application of the Kleinman-Dillow model to these 35 cases). For these two points $\sigma_{\beta q} = K_p\ T_L\ \sigma_q$ where $K_p\ T_L$ are the servo model gain and lead time constant, respectively. Onstott did not publish σ_q and his control system was not optimized relative to POR. Johnson's published values of σ_q, estimated from the Paper Pilot analysis, were used here for the esti-

mation of $\sigma_{\beta q}$. The two Onstott-based data points, shown in figure 5, completely support the present theory.

The three data sets shown on figure 5 represent a wide range of controlled element dynamics, input intensities, manipulator characteristics and piloting backgrounds. The Onstott data were from a motion simualtion. McDonnell's data were for a command input tracking task.

There are no other acceptable data sources known to this author for further testing of the present theory. Based on the correlations obtained, the hypothesis that POR is parameterized by $\sigma_{\beta q}$ is considered as tentatively confirmed under the cited restrictions.

IN-FLIGHT VS. FIXED-BASE POR DIFFERENCES

Arnold compared his fixed-base simulation measurements of POR with those of Neal and Smith obtained from flight test for the same aircraft dynamics (reference 10). This comparison, shown in figure 6, is generally good. Arnold's three best-tested configurations were significantly down-rated in flight, however. He attributed this to task differences between the two experiments.

These three configurations were re-examined using present theory. The Kleinman-Dillow model was modified to simulate the probable display characteristics of the Neal-Smith flight tests. This was done simply by removing the large display threshold present in Arnold's simulation. Predictions were then made of $\sigma_{\beta q}$ for these three cases. The predicted in-flight POR were estimated from the nominal curve fit to Arnold's data shown in figure 5. These revised predictions of in-flight POR are spotted on figure 6.

The good agreement between the predicted and measured in-flight POR for these cases suggests that Arnold's display threshold was a major source for the in-flight vs. fixed-base POR differences. Display threshold effects on the other configurations would be comparatively small. Motion cue effects may be important for explaining the differences between the more poorly rated configurations. These do not appear to be explainable with the Kleinman-Dillow model in the form shown in figure 4.

RATING PREDICTION IN MULTIPLE LOOP TRACKING

Estimates of $\sigma_{\beta q}$ were made for the precision VTOL hover configurations of Miller and Vinje (reference 11) using data supplied to the author by James Dillow of the Air Force Institute of Technology. These were made using the Kleinman model configured to match the measured system performance data. This was the data base used by Anderson in his original Paper Pilot study (reference 12). The Miller-Vinje data were obtained with optimized control

effectiveness. The POR were based on the Cooper scale; these were converted to the Cooper-Harper scale using conversion equations suggested by McDonnell (reference 5).

The Miller-Vinje simulation task was to hover a VTOL aircraft over a ground reference in turbulence. The longitudinal control problem was to create or arrest a forward velocity with pitch attitude control. The pilot was therefore required to control forward position, speed u, pitch attitude θ, and pitch attitude rate q.

The variation of predicted $\sigma_{\beta q}$, with measured POR is shown in figure 7. It appears that $\sigma_{\beta q}$ is not unreasonable as a correlating metric for POR; however, the data do not support the Arnold results except in the region where POR is less than about 3.

Part of the correlation problem is that it isn't clear what we should use as a measure for system rate in a multiple loop system with the Kleinman model. If both u and q are superimposed to form an augmented rate then a somewhat better fit can be obtained as shown in figure 7.

A conclusion of reference 2, however, was that no state-of-the-art pilot model is entirely suited for the estimation of the handling quality metric. It was further concluded that a switching model was a likely candidate for explaining pilot dynamics in multiple loop/axis tracking.

It is interesting that both metrics shown in figure 7 yield POR correlations that are asymptotic to the Arnold data in the region of good handling qualities. This suggests that, in this region, outer loop control of speed or position has little effect on handling qualities.

A GENERALIZED PAPER PILOT METHOD

Dillow and Picha, in reference 6, propose a generalized Paper Pilot method for formalizing the prediction or correlation of POR. They suggest using the Kleinman model for pilot dynamics--incorporating provisions for display or visual thresholds--and a cost functional based on pilot-perceived system states as illustrated in figure 4. By replacing the servo model with the Kleinman model and its attendant cost functional they hoped to eliminate the troublesome Paper Pilot rating functional which has been a principal weakness in the theory. Their rationale for doing this was that it may be easier to select appropriate weights for the Kleinman model cost functional than to find a general rating functional for the Paper Pilot theory.

Their approach to the estimation of POR is empirical. They assume that $POR = \sqrt{J}$, provided that the weights of J (the cost functional) are selected to optimize the model-predicted and measured match of system performance and POR. This rating predictor was totally inaccurate for the McDonnell data when the cost functional was weighted using Arnold's data as a base.

It is suggested in reference 2 that the Dillow-Picha revisions to Paper Pilot have merit provided that J is augmented by a term representing POR (in keeping with the spirit of the original Paper Pilot theory); the POR estimate must then be determined using this component of J and not the total value. For the pitch tracking cases discussed in this paper a suitable cost functional should be

$$J = W_\theta \sigma_p^2 + [W_q + rK_q^2]\, \sigma_{q_p}^2 + R\sigma_{\delta_e}^2$$

$$POR = fcn\ (\sigma_{\beta q})$$

Note that J is now a function of the optimal control gain K_q.

This work was performed under sponsorship of the Air Force Flight Dynamics Laboratory, Wright-Patterson Air Force Base, Ohio; Contract AF 33615-74-C-0035.

REFERENCES

1. Pirsig, Robert M.: Zen and the Art of Motorcycle Maintenance. Bantam Books, April 1975.

2. Smith, Ralph H.: A Theory for Handling Qualities With Applications to MIL-F-8785B. AFFDL-TR-75-119.

3. McRuer, Duane; Dunstan Graham; Ezra Krendel; William Reisener, Jr.: Human Pilot Dynamics in Compensatory Systems: Theory, Models and Experiments With Controlled Elements and Forcing Function Variations. AFFDL-TR-65-15, July 1965.

4. Baron, Sheldon; David L. Kleinman; Duncan C. Miller; William H. Levison; and Jerome I. Elkind: Application of Optimal Control Theory to the Prediction of Human Performance in a Complex Task. AFFDL-TR-69-81, March 1970.

5. McDonnell, John D.: Pilot Rating Techniques for the Estimation and Evaluation of Handling Qualities. AFFDL-TR-68-76, December 1968.

6. Dillow, James D.; Douglas G. Picha: Application of the Optimal Pilot Model to the Analysis of Aircraft Handling Qualities. Air Force Institute of Technology, Wright-Patterson AFB, Ohio, AFIT-TR-75-4, August 1975.

7. Arnold, John D.: An Improved Method for Predicting Aircraft Longitudinal Handling Qualities Based on the Minimum Pilot Rating Concept. Air Force Institute of Technology, Wright-Patterson AFB, Ohio, GGC/MA/73-1, June 1973.

8. Johnson, Robert B.: Predicting Pitch Task Flying Qualities Using Paper Pilot. Air Force Institute of Technology, Wright-Patterson AFB, Ohio, GGC/MA/73-2, June 1973.

9. Onstott, E.D.; E.P. Salmon; R.L. McCormick: Prediction and Evaluation of Flying Qualities in Turbulence. AFFDL-TR-71-162, February 1972.

10. Neal, T.P.; R.E. Smith: An In-Flight Investigation to Develop Control System Design Criteria for Fighter Airplanes. Vol. I and II, AFFDL-TR-70-74, June 1970.

11. Miller, David P.; Edward W. Vinje: Fixed-Base Flight Simulation Studies of VTOL Aircraft Handling Qualities in Hovering and Low Speed Flight. AFFDL-TR-67-152, January 1968.

12. Anderson, R.O.: A New Approach to the Specification and Evaluation of Flying Qualities. AFFDL-TR-69-120, May 1970.

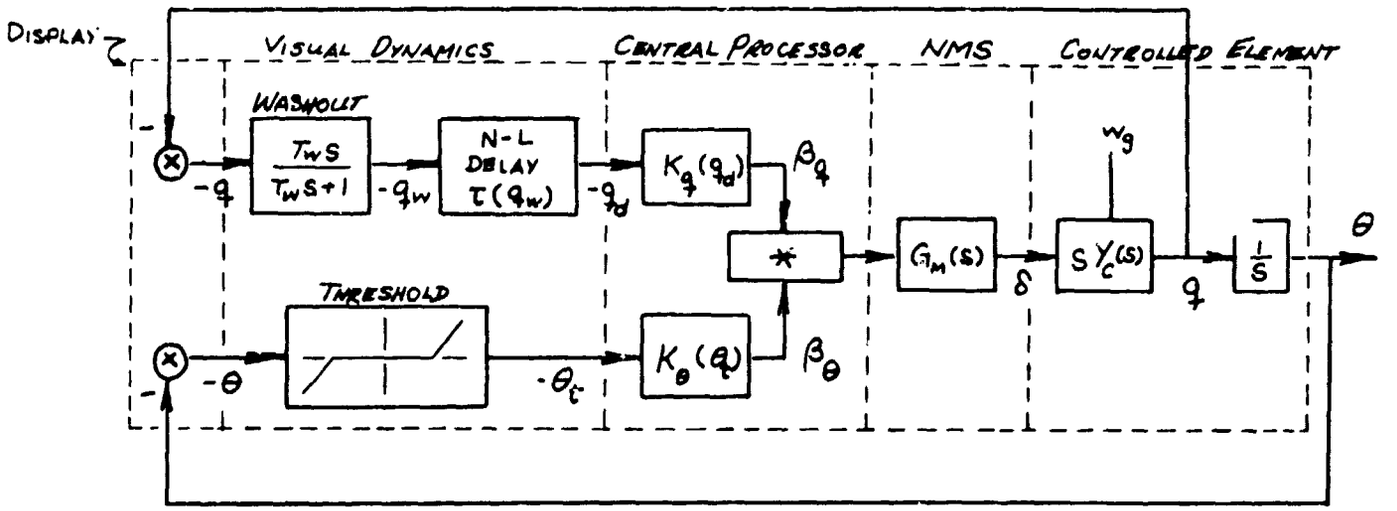

Figure 1....Nonlinear Model for Pilot-Vehicle System

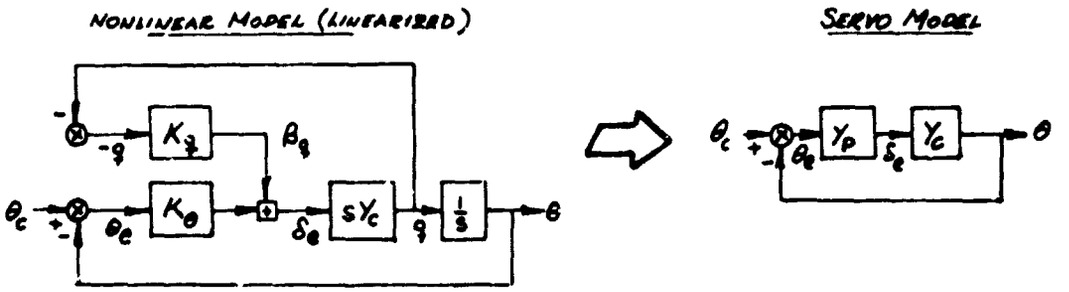

Y_c	$K_c/j\omega$	K_c	$K_c/(j\omega)^2$
$Y_p(j\omega)$	$\frac{K_\theta}{1+K_q K_c}$	$\frac{K_\theta}{K_q K_c j\omega+1}$	$\frac{j\omega\left(K_\theta/K_q K_c\right)}{j\omega/K_q K_c+1}$
TASK DIFFICULTY	EASIEST	NOT DIFFICULT	DIFFICULT

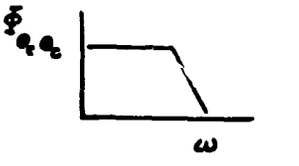

INPUT SPECTRUM

Figure 2....Linear vs. Nonlinear Model Comparisons

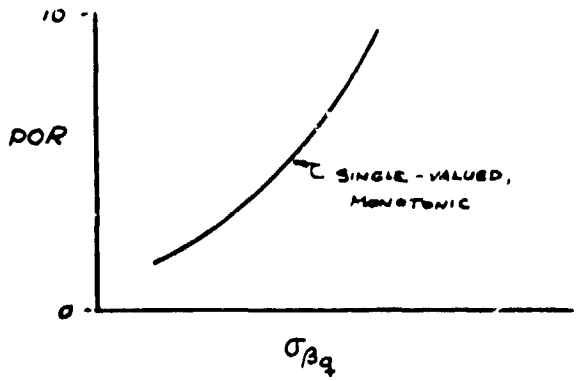

POR= fcn(σ_{β_q} , pilot...experience, background, etc.)

σ_{β_q} = fcn($Y_c(s)$, input, display, task, manipulator)

Figure 3....Hypothetical Variation of σ_{β_q} with POR

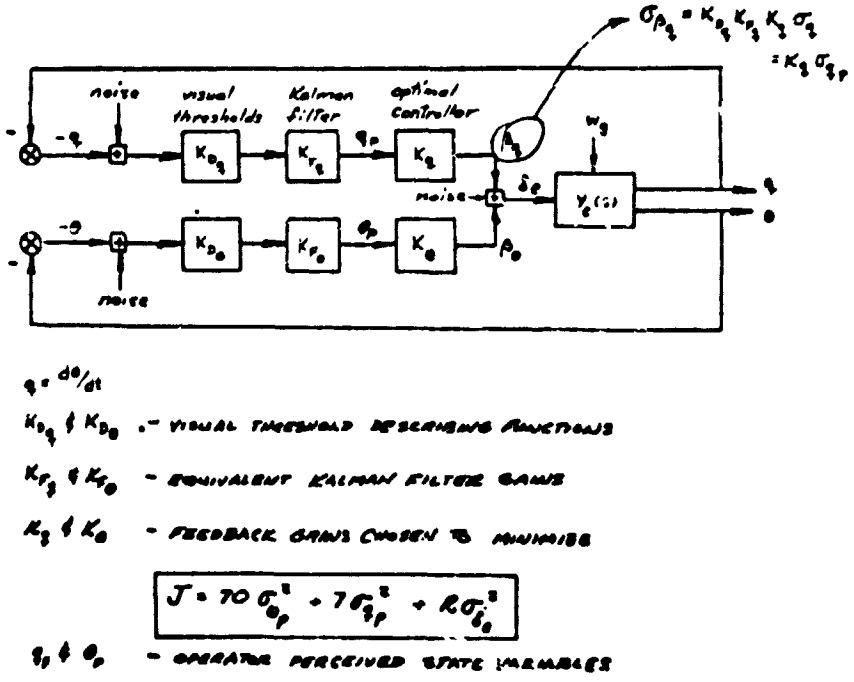

$q = d\theta/dt$

K_{D_q} & K_{D_θ} - VISUAL THRESHOLD DESCRIBING FUNCTIONS

K_{F_q} & K_{F_θ} - EQUIVALENT KALMAN FILTER GAINS

K_q & K_θ - FEEDBACK GAINS CHOSEN TO MINIMIZE

$$J = 70\sigma_{\theta_p}^2 + 7\sigma_{q_p}^2 + R\sigma_{\delta_e}^2$$

q_p & θ_p - OPERATOR PERCEIVED STATE VARIABLES

Figure 4....Equivalent Kleinman-Dillow Model for Pitch Attitude Tracking

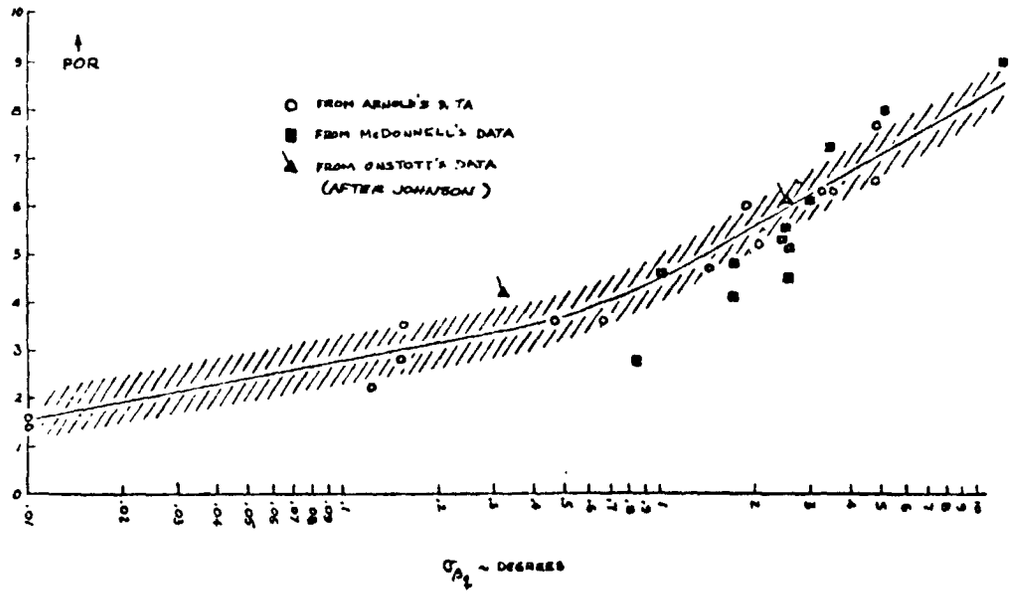

Figure 5....Data Correlations

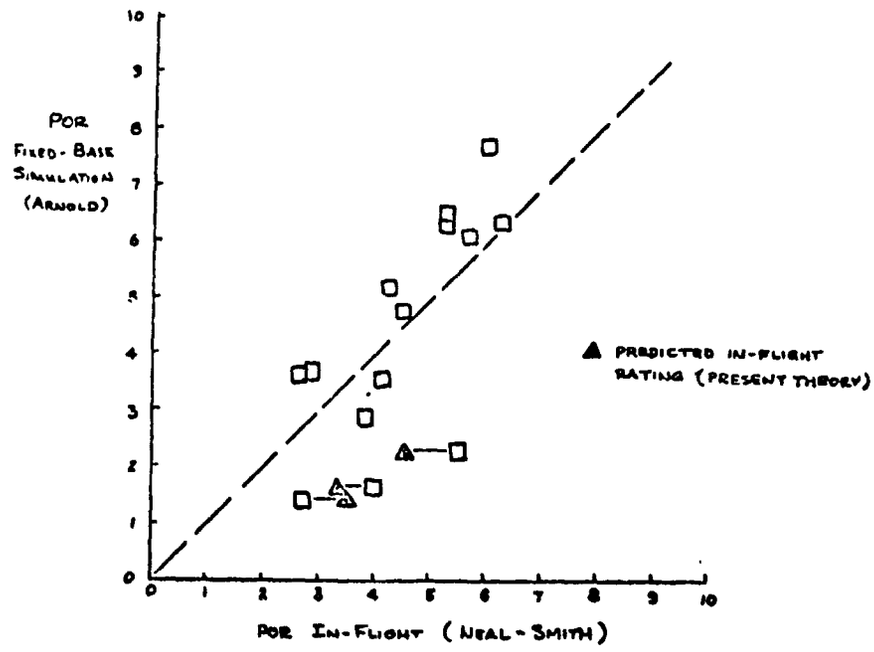

Figure 6....In-Flight vs. Fixed-Base POR Data

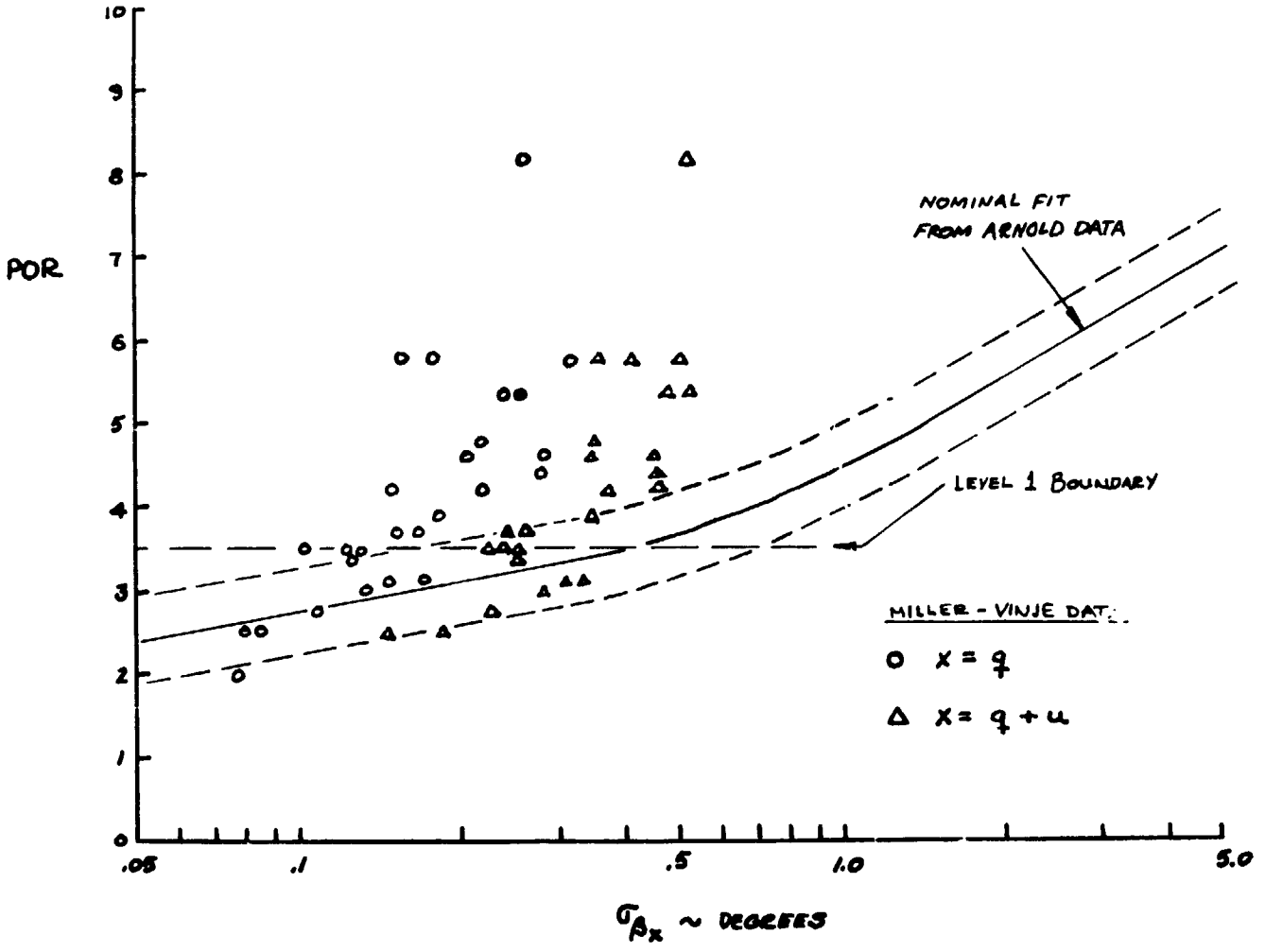

Figure 7....Correlations of Multiple Loop POR Data

LONGITUDINAL FLYING QUALITIES IN THE LANDING APPROACH

By William W. Rickard

McDonnell Douglas Corporation, Douglas Aircraft Company
Long Beach, California 90846

ABSTRACT

An investigation of the longitudinal flying qualities of large transport aircraft in the landing approach was performed as a portion of a long-range flying qualities independent research and development program at the Douglas Aircraft Company. A literature study was performed to gather all criteria which showed promise as estimators[1] of flying qualities. Then a piloted motion base simulator experiment was conducted to produce data which could be used to evaluate the selected criteria. Each criterion was evaluated by comparing the estimated flying qualities it produced for each configuration with the Cooper-Harper ratings given by the pilots. An appraisal was then made of each criterion based on its performance in this study. The criteria evaluated included several from MIL-F-8785B (Reference 1) (flight path stability, short period frequency, short period damping ratio, phugoid stability, and static stability), the short period criterion of SAE ARP 842B (Reference 2), the short period criterion of Reference 3, and a pitch tracking task criterion (References 4,5,6). The best results were obtained by combining the information contained in the flight path stability and pitch tracking task criteria.

INTRODUCTION

The ability to accurately estimate the flying qualities of an airplane which exists only on paper is essential to the aerodynamic, control system, and autopilot design processes. Many criteria exist for estimating flying qualities, of which the best example is the MIL-F-8785B. Unfortunately, this is a military flying qualities specification, containing criteria developed primarily on the basis of research and design experience on military aircraft. The criteria in the MIL-F-8785B can be applied to all types of aircraft, from the smallest trainer to the largest transport. However, there is much less data to support the criteria for large transport (Class III) airplanes than there is for fighter/attack/interceptor (Class IV) airplanes. Designers of civil transport aircraft tend to doubt or even disbelieve the validity of some of the criteria (e.g., the lower limit on short period frequency). Further, civil aircraft tend to have missions which are quite different from those of military aircraft, which suggests that different performance standards would apply. This is not to say that the military criteria are not used; however, they have certain shortcomings when applied to civil transport design.

[1]The term "estimators" is used because the criteria produce quantitative estimate of flying qualities (i.e., pilot ratings or flying qualities levels).

A more serious criticism of most existing criteria is rooted in the fact that they are based on approximations to the response of an airplane. Examples of this are seen in the MIL-F-8785B criteria for the short period. These criteria are based on experimental data for which the short period is well damped and well separated from the phugoid. The current trend toward relaxed static stability airplanes with stability and control augmentation is gradually eroding the ability of such criteria to accurately predict flying qualities, especially for failure cases. There is a trend towards the use of pilot-model-in-the-loop criteria which place performance standards on the pilot plus airplane system, rather than on the airplane alone. At this time, however, no closed loop criteria have been accepted for inclusion in the MIL-F-8785B.

For these reasons, the Douglas Aircraft Company has undertaken a program of research in the area of transport aircraft flying qualities. The goal of this research program is the determination of flying qualities criteria for the design of conventional as well as relaxed static stability airplanes. This paper is a description of the work being done to develop longitudinal flying qualities criteria for large transport aircraft in the landing approach. This description of the research program will be broken down into the following sections: (1) discussion of criteria selected for investigation, (2) design of the experiment, (3) performance of the experiment, and (4) analysis of the results. Each phase will be discussed in detail below.

DISCUSSION OF LONGITUDINAL FLYING QUALITIES CRITERIA SELECTED FOR INVESTIGATION

The first stage of the program of research was a wide-ranging review of the literature for longitudinal flying qualities criteria. There are far too many criteria in existence to be tested in an experimental program or to be discussed in detail here. A relatively small number which showed promise or which are generally accepted, were selected for inclusion in this flying qualities experiment. The criteria of the MIL-F-8785B were included because they are "accepted" criteria. The short period criterion of the ARP 842B was included as an "accepted" criterion in civil aircraft des The short period criterion of Reference 3 was included because it co ins, in a single criterion, the information provided by several other criteria. Finally, a pilot-model-in-the-loop pitch tracking task criterion which had shown promise in earlier studies was included. These criteria will be discussed below for large airplanes (Classes II and III) in the landing approach (Category C phase of flight).

The MIL-F-8785B criteria which were evaluated were: flight path stability ($d\gamma/dV$), short period frequency (ω_{nSP} vs n/α), short period damping (ζ_{SP}), phugoid stability (ζ_{Ph} or T_2), and static stability. All of these criteria, except static stability, are stated in terms of levels of flying qualities. Table 1 shows the relation of the flying qualities levels to pilot ratings and to a set of descriptors. The static stability criterion requires that an airplane exhibit positive static stability at all times. The advent of relaxed static stability airplanes has called this criterion into question, and the question was addressed. The flight path stability criterion limits backside operation by placing limits on the parameter $d\gamma/dV$.

Limiting values are given in Table 2. The short period frequency criterion places upper and lower limits on short period frequency as a function of n/α. Experience with the large transport aircraft (e.g., C-5, DC-10, etc.) indicates that the lower limit is too restrictive. This criterion, when combined with the short period damping ratio criterion, places limits on the short term pitch response. Since n/α is related to T_{θ_2}, all parameters except gain have been specified for the short period pitch transfer function. The short period damping ratio limits are given in Table 3, and the short period frequency requirement in Figure 1. The phugoid stability criterion places limits on long period airspeed oscillations. This criterion, like the static stability criterion, is considered unrealistically restrictive, especially for relaxed static stability airplanes. The phugoid stability limits are given in Table 4.

The ARP 842B short period criterion is based on a presumption that for transport aircraft, the desired ranges of values ω_{nSP} and ζ_{SP} are invariant with flight condition. It is similar to the CAL "thumbprint" which was well accepted in the past, but has lost popularity as it is not in the MIL-F-8785B. The criterion limits are illustrated in Figure 2. The short period criterion of Reference 3 is similar to the MIL-F-8785B short period criterion, combining frequency and damping ratio limits in a single criteria. The parameter n_α was replaced with the closely related variable L_α, as shown in Figure 12.

The pilot-model-in-the-loop pitch tracking task models the pilot task of compensatory tracking of pitch attitude in the presence of random disturbances. It is in some respects similar to the Crossover Model (References 7,8) and to the Paper Pilot (References 9,10). The criterion places the following performance requirements on the closed loop system: (1) no more than 3db droop in the decade below the bandwidth frequency, (2) bandwidth of 1.2 radians per second, (3) closed loop phase angle of -90° at the bandwidth frequency, and (4) minimum closed loop resonance at any frequency greater than the bandwidth frequency divided by 10. The pilot model has a gain, a transport delay (generally taken to be 0.3 seconds), a lead, and a lag. Inclusion of a low frequency lag ($e^{-\alpha/s}$) was found to have at best no positive effect on the criterion, though the theory indicates that a low frequency lag should be included for very slow controlled elements (see, e.g., Reference 8). The pilot lead, lag, and gain must be adjusted to satisfy the performance requirements, as the pilot transport delay and the airplane model are fixed. The flying qualities are then estimated as a function of pilot phase compensation (exclusive of the transport delay) and system resonance. The phase compensation is represented by the phase angle of the pilot model lead-lag network at the bandwidth frequency. Figure 3 illustrates the boundaries for this criterion. This criterion will be referred to as the Bandwidth Model.

DESIGN OF THE EXPERIMENT

A flying qualities experiment was designed to provide data for evaluation of the selected flying qualities criteria. The proper approach to designing such an experiment is first to collect all the parameters involved in the criteria to be evaluated. They are as follows: static stability, $d\gamma/dV$, ω_{nSP}, ζ_{SP}, n/α, ω_{nPH}, ζ_{PH}, phase compensation, and resonance. A set of configurations should then be designed which vary each parameter independently,

so that the effects of each parameter may be isolated. Assuming that four values of each parameter will cover the region of interest, and that static stability is not independent, there will be 4^8 or 65536 configurations. The pilots would probably get bored evaluating so many configurations, so a balanced fractional factorial design could be used to reduce the matrix by a factor of perhaps eight, leaving only 8192 configurations.

Since this proper approach yields impractical results, two other approaches were used to design two groups of configurations. The twenty-six configurations of the first group are either typical wide-body airplanes with cg location varied from far forward to far aft of the neutral point, or such airplanes with a single stability derivative varied to change the flying qualities. The characteristics of these configurations are given in Table 5. The configurations of Group II, on the other hand, were obtained by specifying the characteristics given in Table 6, and solving for the equations of motion coefficients. The solution to this transformation is not unique, as there are more than twice as many unknowns as there are conditions. A computer program was written to solve this transformation on the basis of minimizing a weighted sum of squared errors between the specified values of the parameters and the values calculated for a trial set of equations of motion constants. The algorithm exhibited poor convergence properties in general, and in particular for $|\zeta_{Ph}| < 0.04$. However, several hundred configurations were calculated for which the algorithm converged. The sixteen configurations of Group II were selected from these.

PERFORMANCE OF THE EXPERIMENT

The configurations were rated by pilots flying the McDonnell Douglas six-axis motion base simulator located at Long Beach. The simulator, shown in Figure 4, is supported by six hydraulic jacks arranged in a configuration developed by the Franklin Institute. The limits of linear and rotary motion of this system are given in Table 7. Interior and exterior views of the simulator cockpit are shown in Figures 4 and 5. The airplane equations of motion are programmed on a hybrid computer system, of which the major elements are a Xerox Sigma Five digital computer and a Comcor Astrodata Ci-5000 analog computer. Cockpit motion commands are generated in the hybrid system and transmitted to a DEC PDP 11/40 minicomputer. The minicomputer computes the geometric transformations and controls the hydraulic jacks in a closed loop fashion, using LVDT transducer feedback from the jacks. Figure 6 is a schematic of the elements of the motion base simulator facility. The visual display is generated by a Redifon II system, using a detailed terrain model for landing approaches. Figure 7 is a layout of the System Simulation Laboratory, of which the motion base simulator is a part.

Five Douglas Aircraft Company test pilots performed 154 evaluations of the forty-two configurations over a period of two weeks. Each evaluation consisted of one to three ILS approaches, at the pilot's discretion, after which the pilot gave the configuration a pilot rating on the Cooper-Harper scale. The ILS approach began at a range of 13.7 kilometers (7.4 n.mi.) from the threshold, at an altitude of 457 meters (1500 feet), and on the extended runway centerline. The three-degree glide slope was intercepted at a range of about 8.7 kilometers (4.7 n.mi.). The pilot then flew down the

glide slope in a turbulent atmosphere. Lateral-directional dynamics typical of a wide-body transport were simulated but held constant throughout the experiment. After breakout at an altitude of 213 meters (700 feet), the pilot transitioned to the visual display for flare and touchdown. The simulation permitted the pilot to stop, turn, and taxi the airplane on the ground, but this was not part of the evaluation task. The test engineer, who rode in the copilot seat, recorded the pilot rating and pilot comments. Figure 8 is a typical evaluation record. Every variable of interest (and many of no interest) was recorded on half-inch-wide nine-track tape on 760 meter (2500 feet) reels at a rate of four hertz, while the simulation computer cycle rate was twenty hertz. The configurations were presented to the pilots in random order, with a different random order for each pilot.

RESULTS AND ANALYSIS

The evaluation of the flying qualities criteria was performed by comparing the level of flying qualities predicted for a given configuration with the actual, or true, level of flying qualities for that configuration. The true level of flying qualities for each configuration was assumed to be represented by the average of the ratings that the pilots gave that configuration. The Cooper-Harper pilot rating scale used in this experiment is repeated here as Figure 9. The results of this experiment are given in Tables 8 and 9 for the Group I and Group II configurations, respectively. The first column in each of these tables lists the configurations by number. The next column gives the mean pilot rating for each configuration. The third column, labeled R_o, is the actual, or true, level of flying qualities for each configuration, based on the mean pilot rating. Every configuration in Group I was rated by at least three different pilots, some by four, and some by all five pilots. In Group II, one configuration was rated by one pilot, one by two pilots, and the rest by three, four, or five pilots. The average number of ratings per configuration was 3-2/3 for both groups.

While the criteria generally do not have half levels, a configuration that falls near a level boundary probably is indistinguishable from a configuration just across the boundary. Therefore, half levels were created for most of the criteria by the rules given in Table 10. Some of the criteria do not have a boundary for every level. The MIL-F-8785B short period frequency criterion, for example, has a common lower boundary for levels 2 and 3. A level 2 boundary was added midway between the level 1 and level 3 boundaries, as shown in Figure 10, to facilitate evaluation of this criterion. The ARP 842B short period criterion is stated, not in terms of levels, but by the terms "acceptable augmented," "acceptable unaugmented," and "unacceptable." These terms bear a similarity to the definitions of the flying qualities levels, so were equated to levels 1, 2, and 3, respectively, as shown on Figure 11.

The fourth column, labeled R_1, is the level of flying qualities predicted for each configuration using the Bandwidth Model criterion. The name Bandwidth Model is used to refer to the pilot-model-in-the-loop pitch tracking task criterion. The number at the bottom of the column (23 for Group I and 23 for Group II) is the total error (in half levels) of these predictions.

Inspection of the totals for all criteria reveals that the Bandwidth Model criterion is the best performer for the Group I configurations and is second to $d\gamma/dV$ for Group II.

The flight path stability criterion (R_2) is the second best performer for the forty-two configurations. This is an indication that pilots are more sensitive to bad flight path response than they are to bad pitch response. The MIL-F-8785B short-period-frequency criterion (R_3) was the poorest performer overall and also for Group II, but was slightly better than the worst for Group I. The short-period-damping-ratio criterion (R_4) performed better than R_3, though pilot opinion should be insensitive to it over a wide range. Even the phugoid stability criterion (R_5) outperformed R_3. The static stability criterion (R_6) was evaluated, but not on the basis of levels. The positive answer was considered an estimate of level 1 to 2-1/2, and a negative answer as level 3 to 4. On this basis, R_6 was wrong for eight of the twenty-six configurations of Group I. A more meaningful observation is that only half of the statically unstable configurations are level 3 or worse. This means that in half the cases, a requirement for positive static stability was not needed to achieve level 2 flying qualities. The performance of R_6 with Group II is not mentioned because it was not varied in Group II.

There is not any methodology in the MIL-F-8785B for combining the estimates for several criteria to get an overall airplane level of flying qualities. One can only guess that the overall flying qualities will be as bad as the worst rating or perhaps worse. Criterion R_{10} is an overall predicted level of flying qualities based on the MIL-F-8785B criteria. It is equal to the worst of R_2 to R_6, and turns out to be a poorer performer than any other criteria except R_3 and R_5. The prediction of R_{10} was better than actual in six cases, and worse than actual in twenty-eight cases. While it is better to err on the conservative side, this performance is too conservative.

The last two criteria evaluated, the short period criteria of ARP 842B (R_8) and of Reference 3 (R_9) performed well, being third and fourth best out of eight when both groups are considered. They both performed better than the MIL-F-8785B short-period criteria.

Inspection of the data for R_1 and R_2 shows that when R_1 is better than R_0, R_2 is worse than R_1, and thus probably closer to R_0, in 85% of the cases. When R_1 is worse than R_0, R_2 is better than R_1 in 78% of the cases. But, when R_1 is the same as R_0, R_2 is better than R_1 in 77% of the cases. Thus, when R_2 is worse than R_1, R_0 is generally worse than R_1. But when R_2 is better than R_1, the odds are even that R_0 is the same as R_1 or better than R_1. This suggests a combination criterion, R_{13}, which is defined by the equations:

$$R_{13} = R_1 \qquad \text{when} \quad R_1 > R_2$$

$$= \frac{1}{2}(R_1 + R_2) \qquad \text{when} \quad R_1 < R_2$$

The results show that this combination criterion is better than any of the other criteria evaluated. The sum of the errors is thirty half-levels for forty-two configurations. Further, when the characteristics covered by the various criteria are taken into account, such a criterion makes more

sense. The Bandwidth Model criterion is sensitive to all parameters varied in this experiment, except $d\gamma/dV$. Thus, a criterion which takes both the Bandwidth Model and $d\gamma/dV$ criteria into account, is sensitive to all the parameters varied in this experiment.

RECOMMENDATIONS FOR FURTHER WORK

1. Since there was enough data collected in the simulator experiment to permit the evaluation of virtually any longitudinal criterion, it is recommended that some additional criteria be evaluated. Obvious candidates are the Crossover Model (Reference 8) and the Pitch Paper Pilot (Reference 10). The Crossover Model will be difficult to evaluate on two counts. First, one must decide how to model the task. The performance of a landing approach appears to be a two-input, two-output task longitudinally, which the Crossover Model cannot handle. Second, assuming that a suitable system model can be determined, and the required pilot model adjustments made, one must then have a rule for estimating flying qualities. The information available in the literature indicates that the estimated flying qualities depend on the amount of pilot compensation required and on the nature of the controlled system. Further candidates for evaluation include the following: (a) McPilot (Reference 11), (b) c* (Reference 12), (c) $\dot{\theta}/\dot{\theta}_{SS}$ and $n_Z/n_{Z_{SS}}$ (Reference 13), (d) c_N^* (Reference 14), and (5) maneuvering stability (F_S/n_Z) (Reference 1).

2. Another line of further work would be identification of the parameters of a model of the human pilots. This was attempted briefly, but abandoned when the algorithm failed to converge. The computer program used was Program Newton, a modified Newton-Raphson technique documented in Reference 15.

3. While the combined criterion, R_{13}, performed quite well for the present study, it should be tested against other longitudinal flying qualities data for large transport aircraft in the landing approach. A source of such data is Reference 6, an in-flight simulation of a large delta wing transport in the landing approach.

SUMMARY AND CONCLUSIONS

A number of longitudinal flying qualities criteria were evaluated against the results of a motion base simulation of large transport aircraft in the landing approach. The criteria of MIL-F-8785B performed poorly overall. Two short-period criteria, from ARP 842B and Reference 3, performed adequately. The best performance was exhibited by a criterion combining the results of a pitch tracking task and the flight-path-stability criterion.

REFERENCES

1. Anon.: Flying Qualities of Piloted Airplanes. MIL-F-8785B(ASG), Aeronautical Systems Division, 1969.

2. Anon.: Design Objectives for Flying Qualities of Civil Transport Aircraft. ARP 842B, Society of Automotive Engineers, 1970.

3. Shomber, H.A., and Gertsen, W.M.: Longitudinal Handling Qualities Criteria: An Evaluation. AIAA Paper 65-78, 1965.

4. Neal, T.P., and Smith, R.E.: An In-Flight Investigation to Develop Control System Design Criteria for Fighter Airplanes. AFFDL-TR-70-74, Volumes I and II, 1970.

5. Wasserman, R., Mitchell, J.F., Rickard, W.W., Huber, R.W., and Schelhorn, A.E.: In-Flight Investigation of Minimum Longitudinal Stability for Large Delta-Wing Transports in Landing Approach and Touchdown. AFFDL-TR-72-143, Volume 2, 1973.

6. Rickard, W.W.: A Review of Flying Qualities Estimation and Flying Qualities Estimators. Douglas Memorandum C1-250-Aero-75-399, 10 July 1975.

7. McRuer, D., Graham, D., Krendel, E., and Reisener, W., Jr.: Human Pilot Dynamics in Compensatory Systems. AFFDL-TR-65-15, 1965.

8. McRuer, D.T., et al.: New Approaches to Human-Pilot/Vehicle Dynamic Analysis. AFFDL-TR-67-150, 1968.

9. Anderson, R.O.: A New Approach to the Specification and Evaluation of Flying Qualities. AFFDL-TR-69-120, 1970.

10. Anderson, R.O., Connors, A.J., and Dillow, J.D.: Paper Pilot Ponders Pitch. AFFDL/FGC-TM-70-1, 1970.

11. Bruelle, R.V., and Anderson, D.C.: Design Methods for Specifying Handling Qualities for Control Configured Vehicles. AFFDL-TR-73-142, 1973.

12. Tobie, H.N., Elliot, E.M., and Malcolm, L.B.: A New Longitudinal Handling Qualities Criterion. National Aerospace Electronics Conference, Dayton, Ohio, 16-18 May 1966.

13. Sudderth, R.W., Bohn, J.G., Caniff, M.A., and Bennett, G.R.: Development Of Longitudinal Handling Qualities Criteria for Large Advanced Supersonic Aircraft. NASA CR-137635, 1975.

14. Kisslinger, R.L., and Wendl, M.J.: Survivable Flight Control System Interim Report No. 1, AFFDL-TR-71-20 Supplement 1, 1971.

15. Taylor, L.W., Jr., and Iliff, K.W.: Systems Identification Using a Modified Newton-Raphson Method — A Fortran Program. NASA TN D-6734, 1972.

TABLE 1. FLYING QUALITIES LEVELS

Level	Cooper-Harper Pilot Rating	Description of Flying Qualities
1	1 - 3.5	Clearly adequate for mission.
2	3.5 - 6.5	Adequate to accomplish mission but with reduced performance or increased pilot workload.
3	$6.5 - 9^{+}$	Safely controllable but excessive workload or inadequate performance.
>3	$9^{+} - 10$	Loss of control probable.

TABLE 2. FLIGHT PATH STABILITY CRITERION (MIL-F-8785B)

Level	$d\gamma/dV$ Less Than
1	0.06 deg/kt
2	0.15 deg/kt
3	0.24 deg/kt

TABLE 3. SHORT PERIOD DAMPING RATIO LIMITS (MIL-F-8785B)

Level	ζ_{SP} Min	Max
1	0.35	1.3
2	0.25	2.0
3	0.15	- -

TABLE 4. PHUGOID STABILITY LIMITS (MIL-F-8785B)

Level	ζ_{Ph} or T_2 (sec)
1	0.04
2	0
3	55 (sec)

TABLE 5. GROUP I CONFIGURATION CHARACTERISTICS

V = 140 kts γ = -3° W = 350,000 lb

	ω_{nSP}	ζ_{SP}	ω_{nPh}	ζ_{Ph}	n/α	dγ/dV	$1/T_{\theta 1}$	$1/T_{\theta 2}$
1	0.846	0.628	0.186	0.072	3.80	-0.0399	-0.084	-0.506
2	0.732	0.708	0.169	0.063	3.94	-0.0432	-0.083	-0.528
3	(-0.633)	(-0.307)[1]	0.086	0.318	4.14	-0.0491	-0.082	-0.556
4	(-0.811)	(+0.090)[2]*	0.200†	0.636†	4.20	-0.0511	-0.082	-0.564
5	(-0.909)	(+0.158)[3]*	0.184†	0.210†	4.24	-0.0530	-0.082	-0.568
6	0.828	0.645	0.190	0.057	3.80	0.148	-0.083	-0.577
7	0.819	0.653	0.192	0.049	3.80	0.236	+0.015	-0.605
8	0.811	0.662	0.194	0.041	3.80	0.324	+0.041	-0.631
9	0.804	0.565	0.188	0.084	2.75	0.0054	-0.102	-0.339
10	0.795	0.502	0.191	0.089	1.78	0.095	[0.166]	[0.917]
11	0.723	0.431	0.194	0.117	0.82	0.400	[0.143]	[0.587]
12	0.853	0.888	0.184	0.080	3.80	-0.0399	-0.084	-0.531
13	0.836	0.337	0.188	0.066	3.80	-0.0399	-0.084	-0.481
14	0.829	0.149	0.189	0.064	3.80	-0.0399	-0.084	-0.466
15	(-0.991)	(+0.225)[4]*	0.211†	0.388†	4.29	-0.0551	-0.082	-0.575
16	(-1.061)	(+0.291)[5]*	0.210†	0.331†	4.35	-0.0572	-0.082	-0.583
17	(-1.125)	(+0.358)[6]*	0.209†	0.295†	4.43	-0.0593	-0.081	-0.595
18	0.953	0.570	0.165	0.107	3.65	-0.0360	-0.087	-0.484
19	0.596	0.841	0.141	0.073	4.06	-0.0465	-0.082	-0.544
20	0.843	0.395	0.187	0.106	0.71	0.498	[0.141]	[0.545]
21	0.441	0.665	0.170	0.043	1.05	0.285	[0.149]	[0.676]
22	(-0.577)	(+0.152)[7]*	0.190†	0.347†	1.22	0.222	[0.154]	[0.731]
23	(-0.767)	(+0.341)[8]*	0.196†	0.240†	1.37	0.173	[0.158]	[0.776]
24	(-0.904)	(+0.499)[9]*	0.196†	0.207†	1.54	0.133	[0.163]	[0.828]
25	0.833	0.263	0.188	0.065	3.80	-0.0340	-0.084	-0.475
26	0.831	0.197	0.189	0.064	3.80	-0.0340	-0.084	-0.470

( ) First-order factor [ω] [ζ]

[1] ω = 0.441, ζ = 1.07 [4] T_2 = 3.08 [7] T_2 = 4.56

[2] T_2 = 7.70 [5] T_2 = 2.38 [8] T_2 = 2.03

[3] T_2 = 4.39 [6] T_2 = 1.94 [9] T_2 = 1.39

*Tested against phugoid criterion

†Tested against short period criterion

TABLE 6. GROUP II CONFIGURATION CHARACTERISTICS

V = 140 kts $\quad \gamma = -3°$ $\quad$ W = 350,000 lb

Config	ω_{SP}	ζ_{SP}	ω_{Ph}	ζ_{Ph}	n/α (g/rad)	$d\gamma/dV$ (deg/kt)	$1/T_{\theta_1}$	$1/T_{\theta_2}$
27	1.39	0.50	0.16	0.12	3.5	0.1	-0.0607	-0.325
30	1.05	0.85	0.16	0.12	2.0	0.1	-0.334	-0.179
39	(-0.744)[1]	(-2.585)[1]	0.16	0.28	3.5	0.1	-0.0372	-0.484
40	1.05	0.85	0.16	0.12	2.0	0.1	-0.119	0.0435
43	1.39	0.5	0.08	0.12	3.5	-0.05	-0.0534	-0.293
49	1.05	0.5	0.08	0.12	2.0	0.1	-0.0397	-0.221
1	1.39	0.85	0.08	0.28	3.5	0.1	-0.0428	-0.555
52	1.05	0.85	0.08	0.12	2.0	0.1	-0.0408	-0.218
70	0.592	0.85	0.08	0.12	3.5	0.1	-0.0681	-0.380
75	(-0.318)[2]	(-1.10)[2]	0.16	0.28	3.5	0.1	-0.0471	-0.608
76	0.592	0.85	0.08	0.28	3.5	-0.05	-0.0767	-0.430
84	0.447	0.85	0.16	0.12	2.0	-0.05	-0.171	0.0295
85	0.447	0.5	0.16	0.12	2.0	0.1	-0.0494	-0.272
90	0.592	0.5	0.08	0.12	3.5	-0.05	-0.0761	-0.400
91	0.447	0.5	0.08	0.12	2.0	-0.05	-0.0860	-0.458
96	1.05	0.5	0.08	0.12	2.0	0.1	-0.186	0.0667

[1]Equivalent $\omega_{n_{SP}} = 1.39, \quad \zeta = 1.2$

[2]Equivalent $\omega_{n_{SP}} = 0.592, \quad \zeta = 1.2$

TABLE 7. MOTION LIMITS FOR THE MOTION BASE

Motion	Excursion	Velocity	Acceleration
Heave	±116 cm (±46 in.)	(±81 cm/sec (±32 in./sec)	±1.75 G
Sway	±147 cm (±58 in.)	±98 cm/sec (±38.5 in./sec)	±1.45 G
Surge	±152 cm (±60 in.)	±98 cm/sec (±38.5 in./sec)	±1.45 G
Roll	±30°	±23°/sec	6.9 rad/sec^2
Pitch	±30°	±23°/sec	6.9 rad/sec^2
Yaw	±30°	±30°/sec	8.1 rad/sec^2

TABLE 8. GROUP I — COMPARISON OF CRITERIA

		R_0	R_1	R_2	R_3	R_4	R_5	R_6	R_8	R_9	R_{10}	R_{13}
				MIL-F-8785B								
Config	PR	PR Level	Bandwidth Model	dγ/dV Level	ω_{nSP} vs α Level	ζ_{SP} Level	ζ_{Ph} or T_2 Level	Static Stab.	ARP-842 ω_{nSP} vs ζ_{SP}	L_α/ω_{nSP} vs ζ_{SP} Level	Worst of R_2-R_6	
1	2.50	1	1	1	1	1	1	Yes	1	1½	1	1
2	2.20	1	1½	1	2	1	1	Yes	2	2	2	1
3	3.30	2	2	1	4	1	2	Yes	3	3	4	1½
4	3.93	1½	2	1	4	1	4	No	3	3	4	2
5	5.17	2	2½	1	4	3	4	No	3	3	4	2
6	5.00	2	1	2½	1	1	1	Yes	1	2	2½	2½
7	4.25	2	1	3½	1	1	1	Yes	1	2	3½	2
8	8.33	3	1½	4	1	1	1	Yes	1	2	4	2½
9	5.00	2	1	1½	1	1	1	Yes	1	1	1½	1½
10	5.67	2	1	2	1	1	1	Yes	2	1	2	1½
11	7.33	3	2½	4	3	1	1	Yes	2	1	4	3½
12	4.00	2	1	1	1	1	1	Yes	3	2	1	1
13	4.00	2	1½	1	1	2	1	Yes	2	2	2	1½
14	7.00	3	3	1	1	3½	1	Yes	3	3	3½	3
15	6.67	2½	2½	1	4	1	4	No	3	3	4	2½
16	7.67	3	3	1	4	2	4	No	3	3	4	3
17	9.00	3	3	1	4	2	4	No	3	3	4	3
18	3.75	1½	1	1	1	1	1	Yes	1	1	1	1
19	4.00	2	2	1	4	1	1	Yes	2	3	4	2
20	8.00	3	3½	4	3	1	1	Yes	2	3	4	4
21	6.17	2½	2	4	2	1	1	Yes	2	1	4	3
22	6.33	2½	2	3	4	1½	4	No	3	3	4	2½
23	9.33	3½	3	3	4	3	4	No	3	3	4	3
24	9.33	3½	3	2	4	3	4	No	3	3	4	2½
25	5.00	2	2	1	1	2	1	Yes	2½	3	2	1½
26	5.67	2	2½	1	1	3	1	Yes	3	3	3	2
			25	50	57	47	59		34	34	51	18

TABLE 9. GROUP II — COMPARISON OF CRITERIA

		R_0	R_1	R_2	R_3	R_4	R_5	R_6	R_8	R_9	R_{10}	R_{13}
						MIL F-8785B						
Config	PR	PR Level	Bandwidth Model	$d\gamma/dV$ Level	ω_{nSP} vs n/α	ζ_{SP} Level	ζ_{Ph} or T_2 Level	Static Stab.	ARP-842B	L_α/ω_{nSP} vs ζ_{SP} Level	Worst of R_2-R_6	
27	7.00	3	1½	2	1	1	1	Yes	1	3	2	2
30	4.75	2	1	2	1	1	1	Yes	2½	3	2	1½
39	5.75	2	1	2	1	1	1	Yes	3	3	2	1½
40	4.63	2	1	2	1	1	1	Yes	2½	3	2	1
43	3.75	1½	2	1	1	1	1	Yes	1	3	1	2
49	3.50	1½	2	2	1	1	1	Yes	1	3	2	2
61	5.00	2	1	2	1	1	1	Yes	2½	3	2	1½
62	3.63	1½	1	2	1	1	1	Yes	2	3	2	1½
66	4.00	2	1½	2	3	1	1	Yes	2½	3	3	2
75	4.50	2	1½	2	3	1	1	Yes	3	3	3	2
76	3.33	1½	1½	1	3	1	1	Yes	2½	3	3	1½
84	3.25	1½	2	1	3	1	1	Yes	2½	3	3	2
85	5.50	2	2	2	3	1	1	Yes	3	3	3	2
90	3.00	1	2	1	3	1	1	Yes	2	3	3	2
91	5.60	2	2	1	3	1	1	Yes	3	3	3	2
96	7.25	3	1	2	1	1	1	Yes	1	3	2	1½
			23	11	37	29	29		30	35	25	14
			48	61	94	76	88		64	69	76	32

TABLE 10. SOME NOTES ON THE APPLICATION OF THE FLYING QUALITIES CRITERIA

1. PR Levels:

PR	1-3	3.01-3.99	4-6	6.01-6.99	7-9	9.01-9.49	9.50-10
Level	1	1½	2	2½	3	3½	4

2. Bandwidth Model: Half levels were created by saying that any configuration within 0.7 dB or 3.5° of a boundary would be rated as an average of the adjacent levels.

dγ/dV:

Level	1	1½	2	2½	3	3½	4
dγ/dV	+0.045	0.0451-0.0749	0.075-0.135	0.1351-0.1649	0.165-0.225	0.2251-0.2549	0.255 & Up

4. $\omega_{n_{SP}}$ vs n/α: See Figure 10 — No half levels for lower boundaries.

5. Half Levels for Other Criteria: When parameter falls on or very close to boundary, it is considered half way between levels.

6. R_{10}: The standard way of applying MIL-F-8785B is to compute flying qualities of an airplane for a number of criteria. The only way to estimate the overall flying qualities of the airplane is the let it be the same as the worst estimate.

7. R_{13}: This criterion is a combination of the Droop-Bandwidth criterion and the dγ/dV criterion. If the level for dγ/dV is worse than the level for bandwidth, the two are averaged. If not, the bandwidth level is taken.

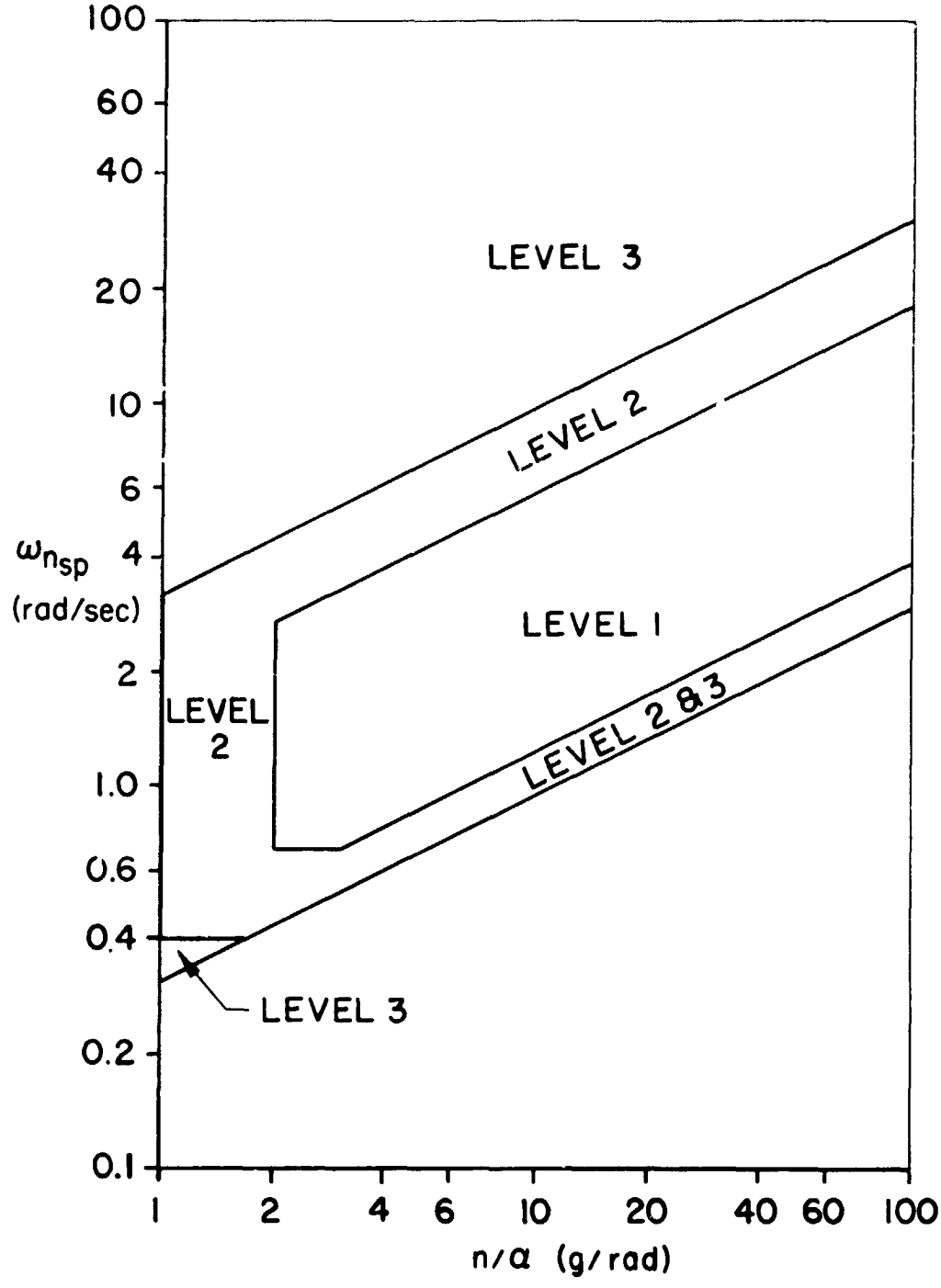

FIGURE 1. MIL-F-8785B SHORT PERIOD FREQUENCY CRITERION

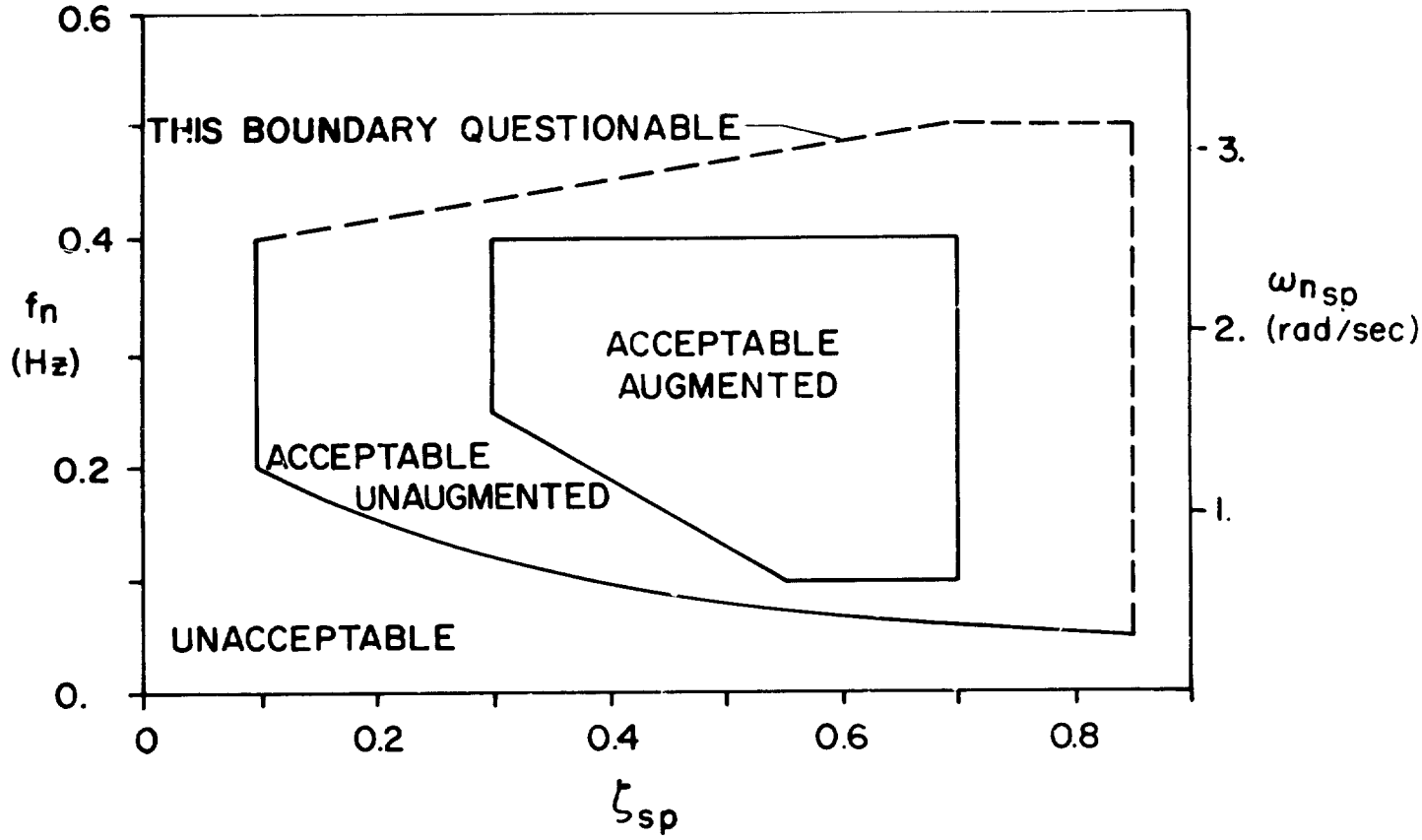

FIGURE 2. ARP 842B SHORT PERIOD CRITERION

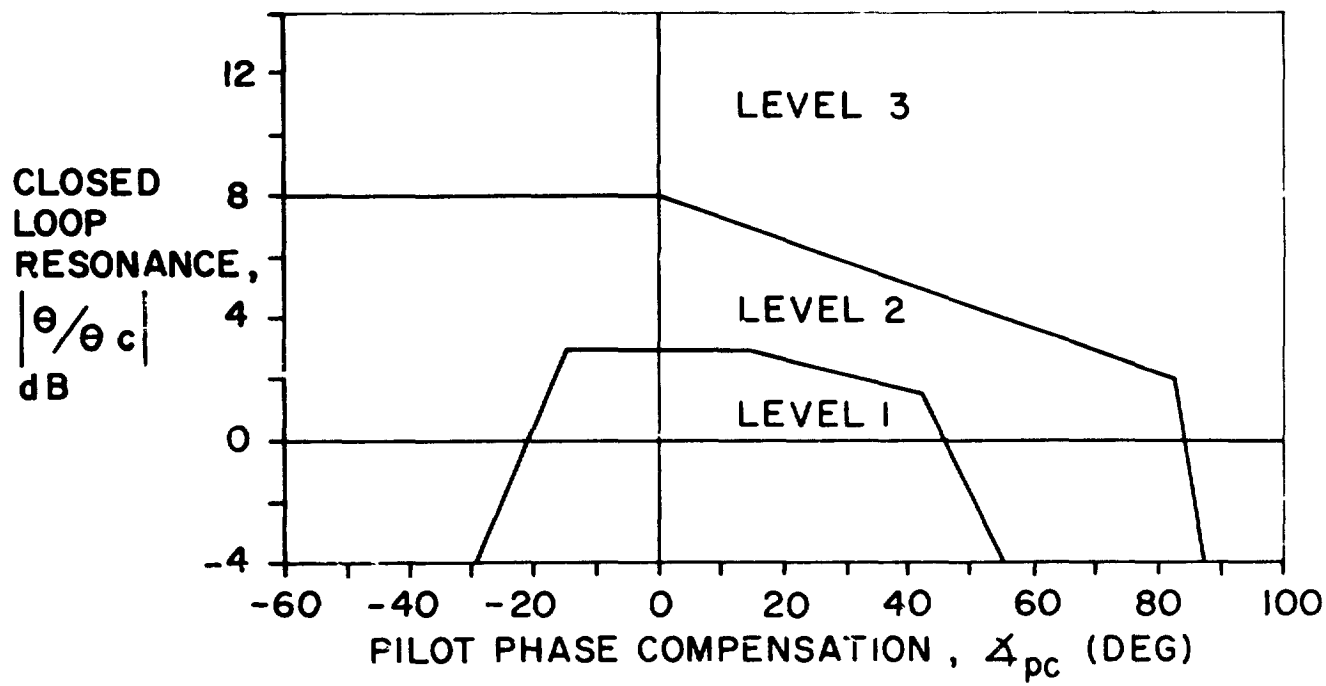

FIGURE 3. BANDWIDTH MODEL CRITERION

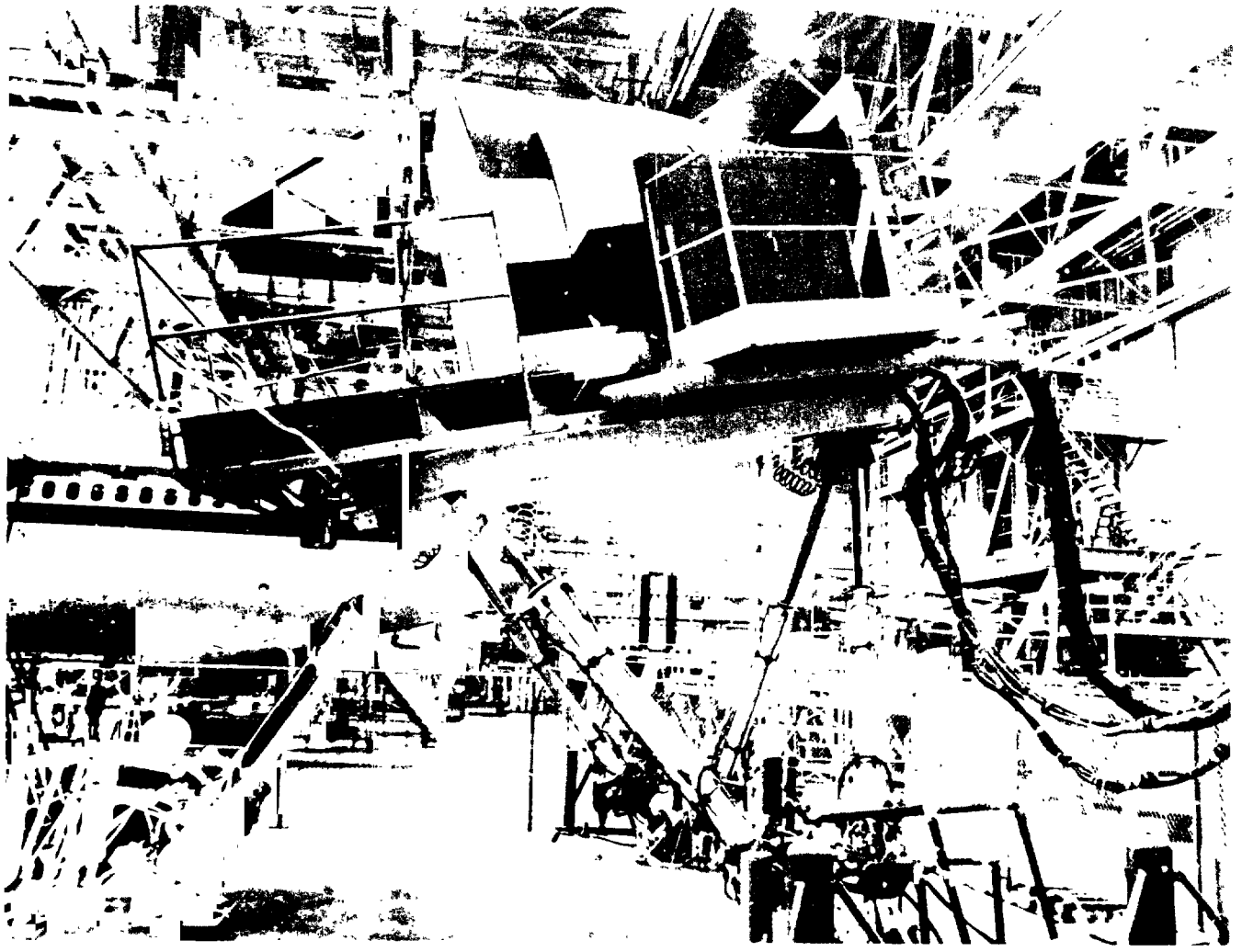

FIGURE 4. MOTION BASE SIMULATOR.

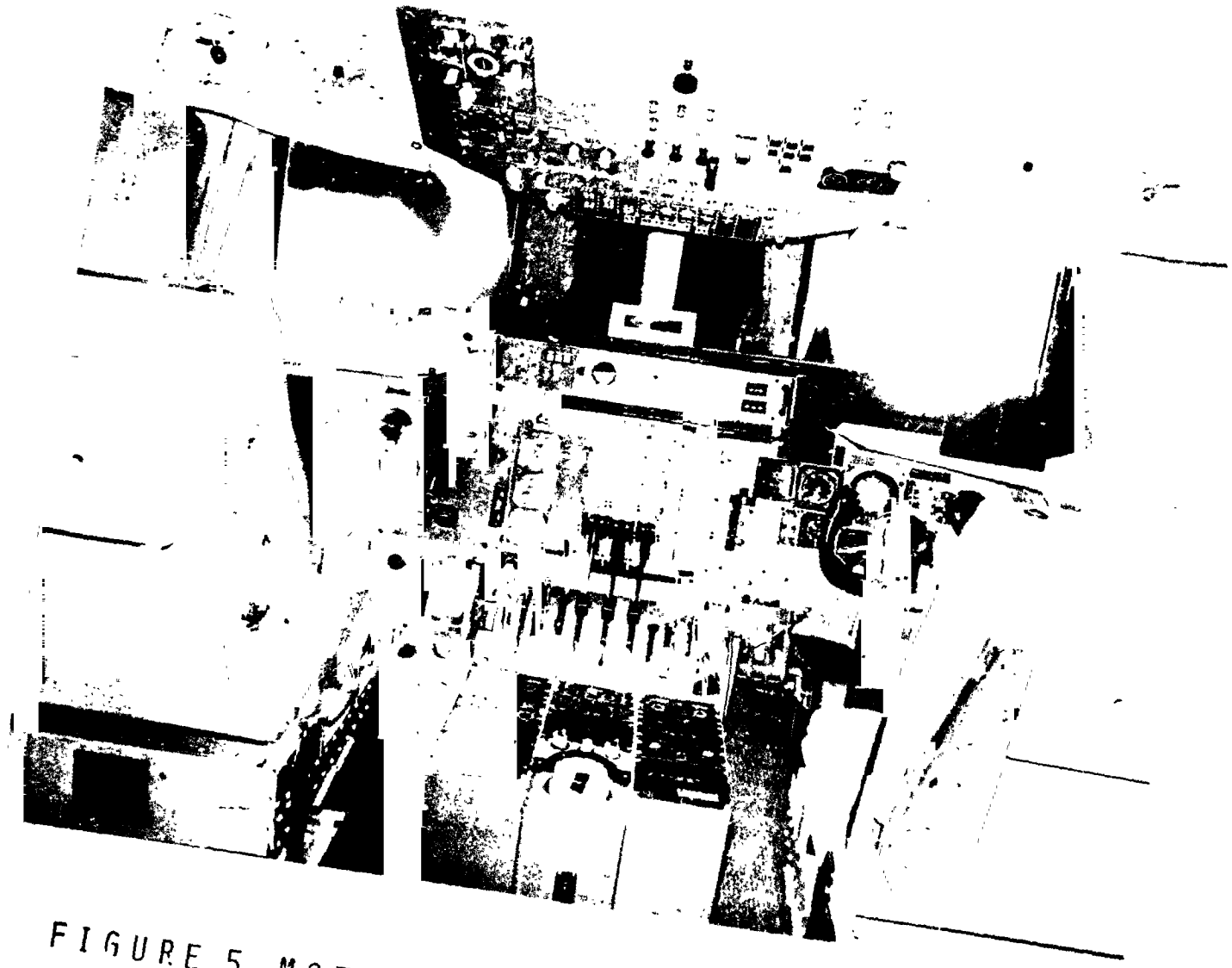

FIGURE 5. MOTION BASE SIMULATOR COCKPIT.

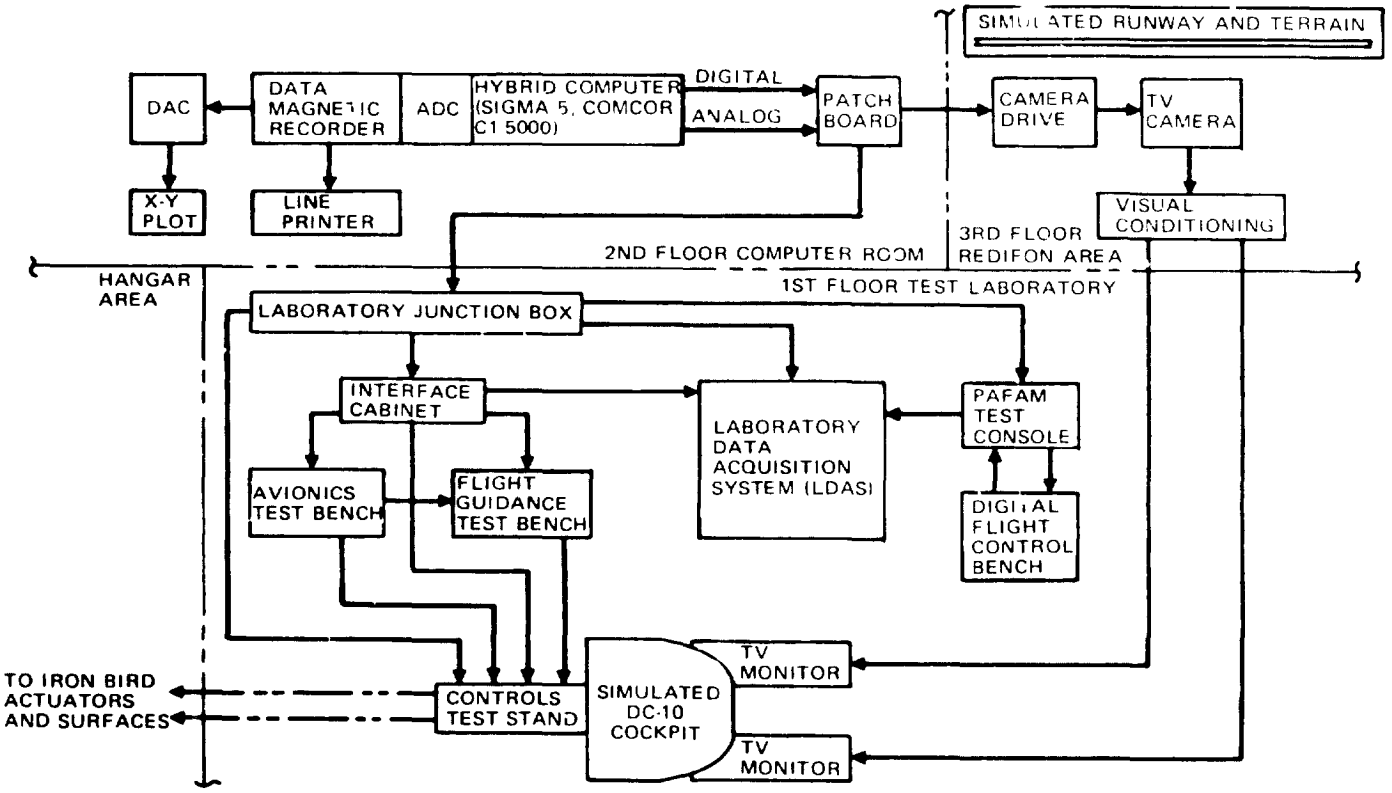

FIGURE 6. FIXED BASE SIMULATOR.

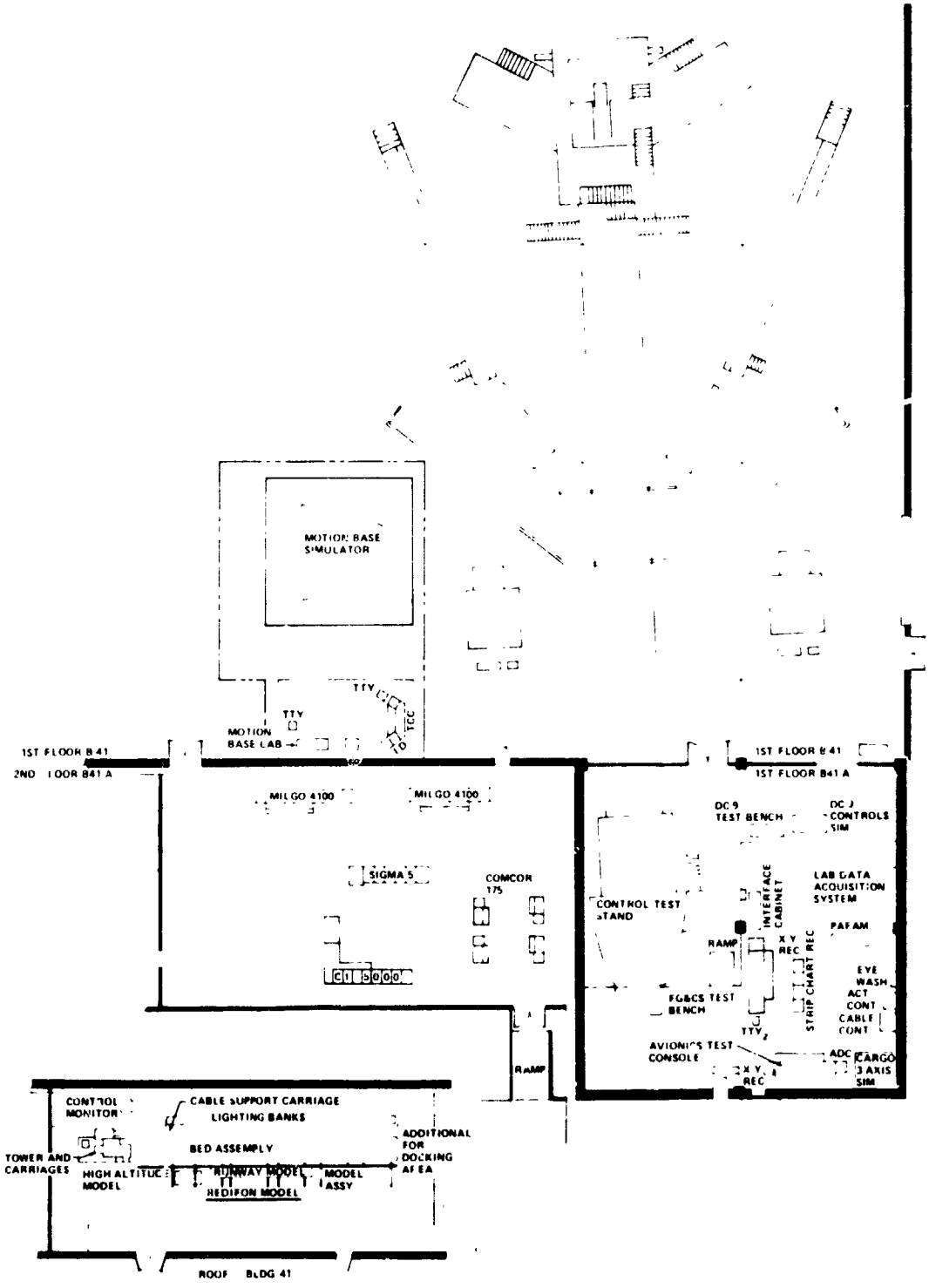

FIGURE 7. SYSTEM SIMULATION LABORATORY.

PILOT DEBRIEFING FORM

Date: 12-3-75

Name: Pilot A

Run No. 1

Configuration No. 5

Turbulence Level Moderate

Time of Day (Start): a) 11:55:32
b) 11:57:46

Ability to control flight path:

Good

Ability to control airspeed:

Satisfactory - good

Pitch response:

Damping on weak side

Other:

Requires considerable attention because of weak pitch damping. Tends to oscillate slightly in pitch.

Pilot Rating: 4

Main reason for rating, if adverse:

FIGURE 8. TYPICAL EVALUATION RECORD.

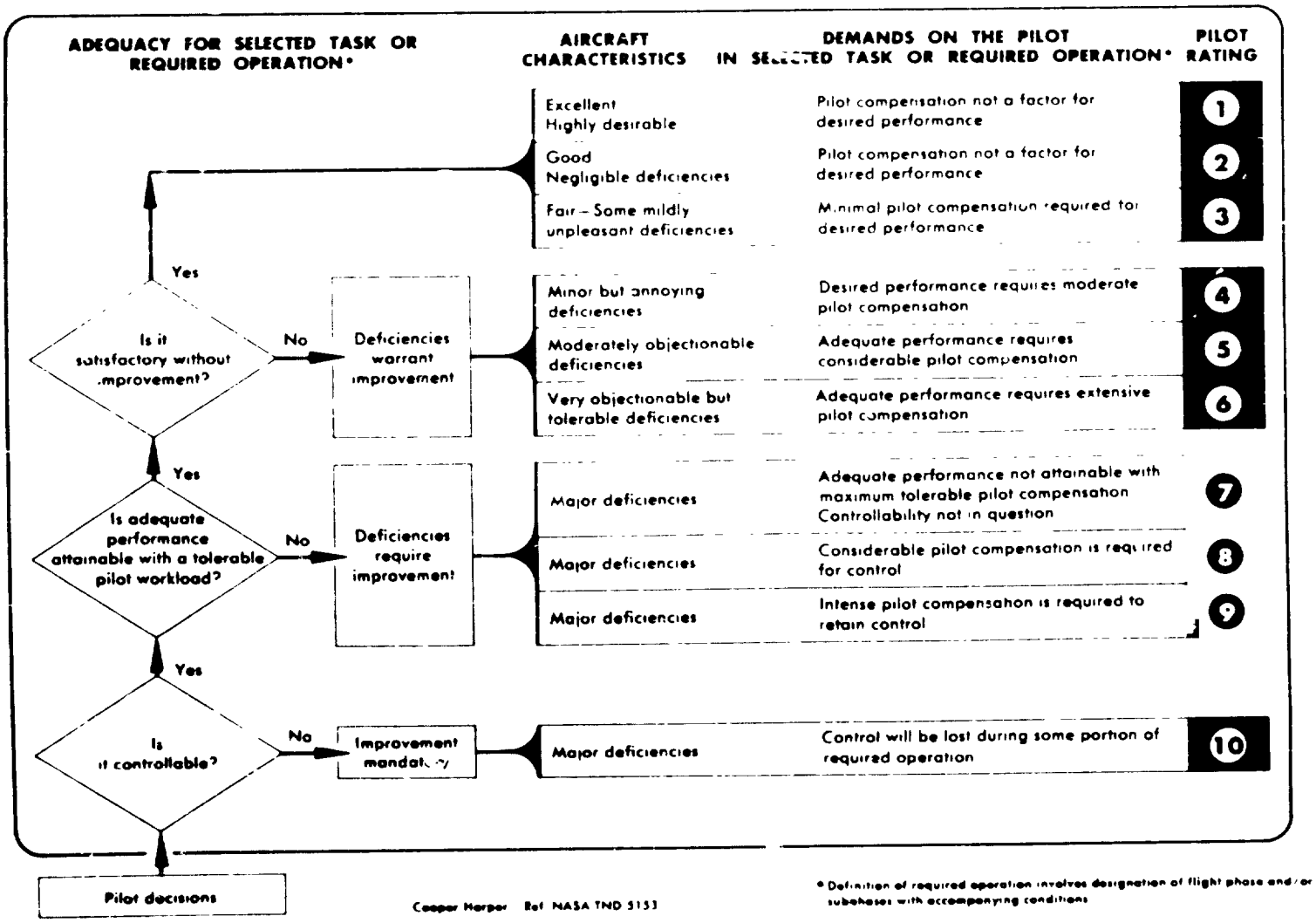

FIGURE 9. COOPER-HARPER PILOT RATING SCALE.

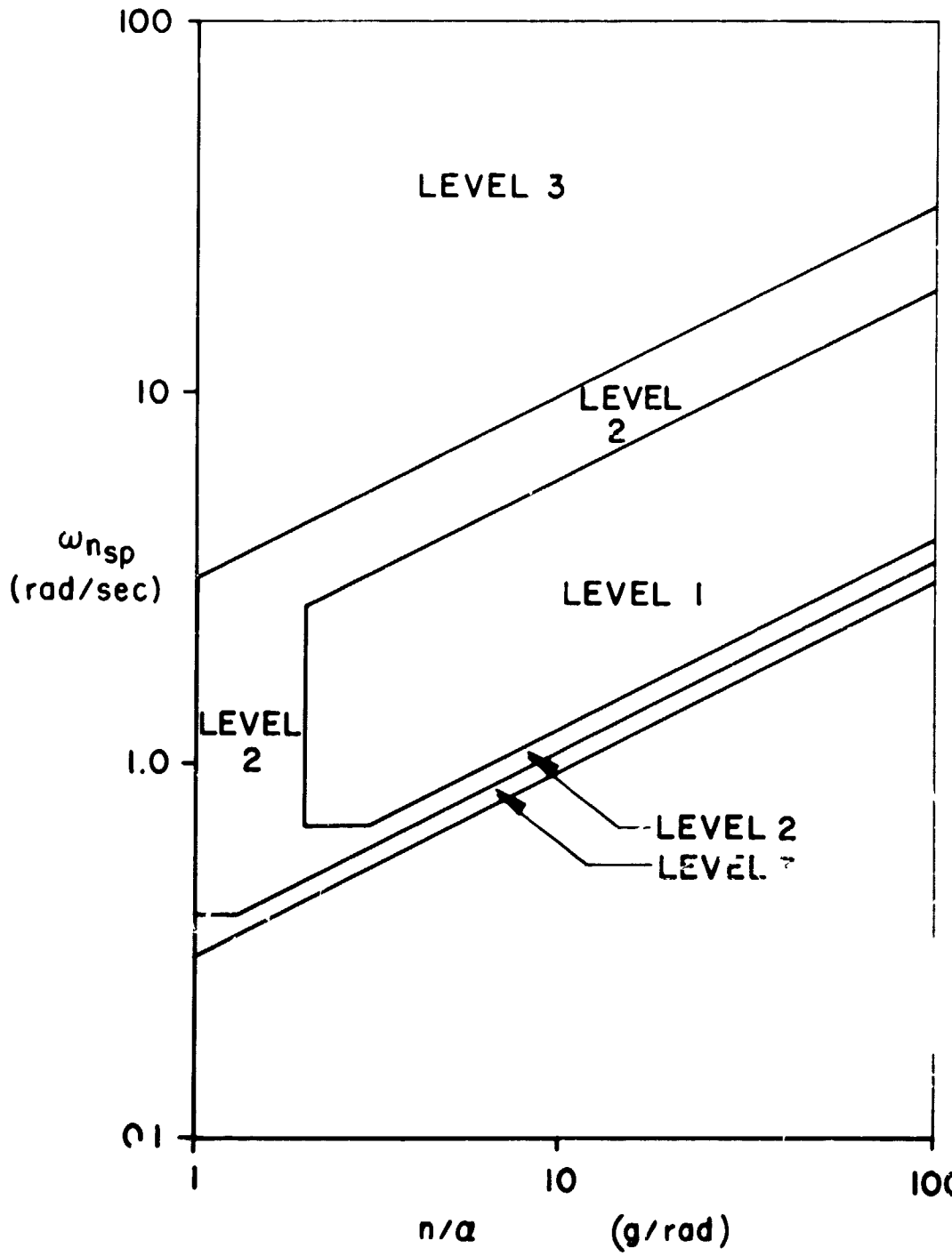

FIGURE 10. MIL-F-8785B SHORT PERIOD FREQUENCY CRITERION

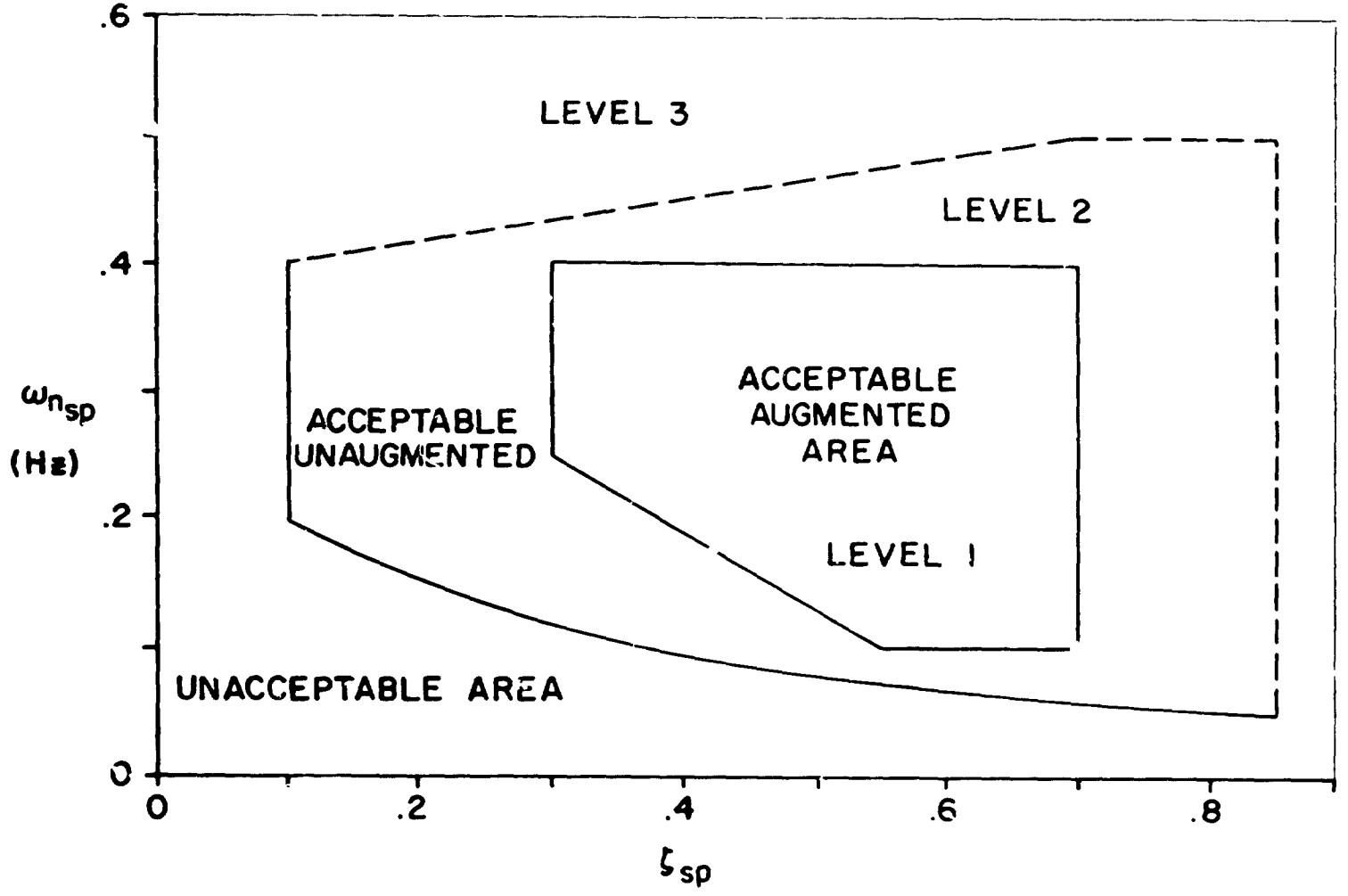

FIGURE 11 ARP 842B SHORT PERIOD CRITERION

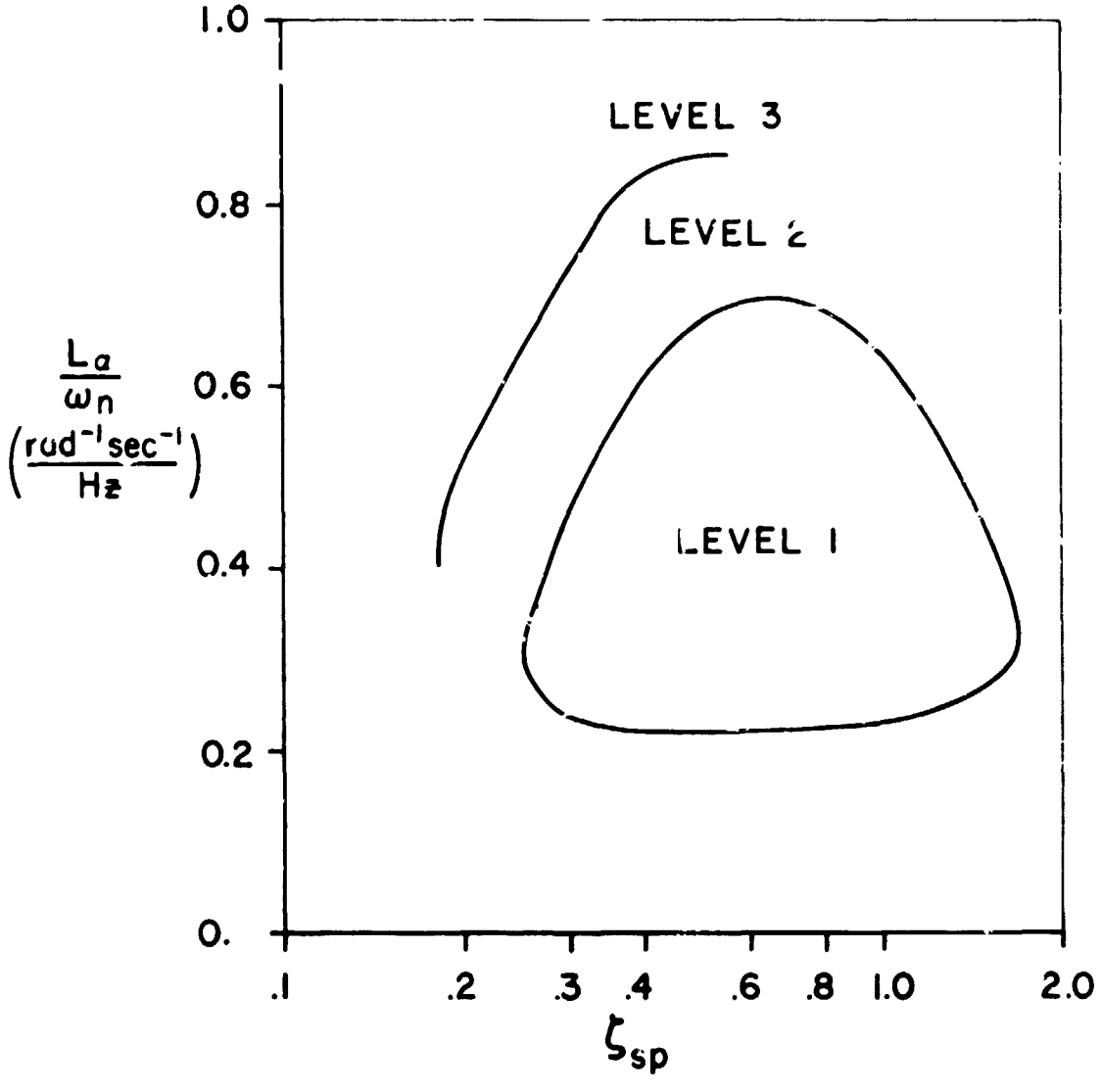

FIGURE 12. SHORT PERIOD CRITERION OF REFERENCE 3

WORTH ASSESSMENTS OF APPROACH TO LANDING

Renwick E. Curry

Man Vehicle Laboratory
Massachusetts Institute of Technology
Cambridge, Mass. 02139

ABSTRACT

The objective of worth assessment is to determine the relative importance of attrib tes in the overall preference of objects, i.e., to determine the functional relationship between preference and the known, physical attr butes of a set of objects. This technique is described below and is applied to the assessment of worth functions in approach to landing for general aviation and air carrier pilots.

INTRODUCTION

The objective of the worth assessment technique is to determine a functional relationship between preference in a set of objects and their known attributes (say) x_1, x_2, x_3... . In other words, we wish to be able to create a function $W(x_1, x_2, ...)$ which can be used to determine the relative importance of the attributes as well as determining the preference between any pair of objects with those attributes. As we will show, the technique is identical to the regression point of view in the analysis variance, and we will further show how one can obtain essentially interval scale data from ordinal, ranked preference for objects.

Applications of this technique have been used primarily in marketing research (Green and Wind, 1973). There are many possibile applications within the man-machine systems area as well; for example , in display evaluation (with attributes of displayed variables, resolution, etc.) and in handling qualities, where the Cooper rating is known to depend on the dynamic element being controlled, the disturbance level, the RMS error, etc.

WORTH MODELS

Suppose we have a set of objects or stimuli (S_i) with attributes limited to, for illustrative purposes, three variables x_1, x_2, x_3. In this section we will discuss the techniques for obtaining a worth function for this set of objects under two conditions: in the first case magnitude estimates of worth are available from the subject, i.e., numerical values for preference; in the

second case, a rank ordering of all objects in a set is used to obtain the worth function.

Magnitude Estimation

There are many situations where the only feasible way of measuring preferences is by numerical estimate provided by the subject. This is the well-known magnitude estimation technique, known to have many pitfalls (Poulton, 1968), but is a useful way to gather data when treated with caution. If, in the example above, we have three attributes with various levels along each, we can assume various forms for the worth function. Perhaps the most common form is the additive worth function given by

$$W(X_1, X_2, X_3) = W_1(X_1) + W_2(X_2) + W_3(X_3)$$

Denoting the numerical responses to the stimuli by y_{ijk}, we may express these responses in the traditional main-effects analysis of variance format.

$$y_{ijk} = \mu + A_i + B_j + C_k + e_{ijk}$$

There are many analysis of variance programs, for example, BMD10V (from the UCLA Biomedical Package), which treat analysis of variances as regression problems. In this case, the vector of the responses can be expressed in terms of the design matrix and of unknown parameters in the form

$$y \simeq \hat{y} = Z\beta$$

Treating the numerical representations for preference in this way, one is able to reconstruct the additive partial worth functions W_1, W_2, W_3 from the coefficients β.

Assuming additive worth functions of the type described above allows for complete freedom in the shape of the individual or partial worth functions. For example, we may still have a non-monotonic worth function as would be true of someone who prefers one teaspoon of sugar in coffee: cups with one teaspoon of sugar are preferred to cups with zero teaspoons or two teaspoons of sugar, leading to an inverted U-shaped partial worth function for sugar.

On the other hand, there are many worth functions where it is known a priori that the worth functions are monotonic with the attribute, e.g., money. For such worth functions, it is not unreasonable to assume a linear/interaction (LINT) form for the worth functions as given by equation

$$W(X_1, X_2, X_3) = \beta_1X_1 + \beta_2X_2 + \beta_3X_3 + \beta_4X_1X_2 + \beta_5X_1X_3 + \beta_6X_2X_3$$

Whether the additive worth functions or the LINT worth function models are used, the number of objects to be evaluated, i.e., cases to be evaluated, will depend on the requirement for the regression to be non-singular. Certainly the factorial presentation will suffice in both of the above cases.

Rank Ordering of Preferences

In many cases it is feasible, and, from a psychological scaling point of view, more desirable to obtain the rank order preferences of the objects within the set. To obtain the worth functions from these rankings, we assumed that these rankings are related to the (internal) worth by the following

$$r_{ijk} = M(A_i + B_j + C_k)$$

where $M(\cdot)$ is any monotonic function of the apparent worth provided by the model, i.e., $A_i + B_j + C_k$. This worth can be formulated in the same form as equation 3, with the coefficients β adjusted to minimize some suitable statistical criterion. In our work, we have used the Spearman rank-order correlation coefficient, which is equivalent to minimizing the RMS rank error between the ranks provided by the model and the ranks provided by the subject. A reasonable initial value for these β is to do a least squares fit, assuming that the ranks are in fact the scale values. That is, we assume all objects are at equal distances along the interval scale, an assumption which is no doubt untrue. However, this is a reasonable starting point for the βs to be further iterated to minimize the RMS rank error. In all of the cases we have tried to date, we have not found any coefficients β that could improve the RMS rank error below that obtained by the least square procedure. Thus it seems reasonable, although it should always be checked, that the assumption of equal-intervals along the interval scale is in practice a good one.

WORTH OF APPROACH TO LANDING

We have applied the worth assessment techniques to evaluation of different landing conditions by general aviation and air carrier pilots. In the first experiment, we placed all possible combinations of a limited set of wind direction, wind strength, runway surface conditions, and turbulence level on 36 computer cards. These computer cards were rank ordered by a general aviation pilot and a DC-9 first officer. The two wind directions (340° and 090°) were symmetrical about the runway heading of 035°. The additive worth functions obtained from these two pilots are shown in Figure 1, where it can be seen that both pilots had no preference for wind direction, and essentially the same preference to the effect of turbulence. The major differences occur in the attributes of wind strength and runway surface conditions, where it can be seen that the general aviation pilot is more sensitive to wind strength, whereas the DC-9 first officer is much more sensitive to the runway surface conditions. Presumably these results reflect the concerns of both of these pilots of the relative importance of these attributes during the landing operation.

We continued this experiment by providing 36 computer cards containing the factorial combinations of attributes shown in Figure 2 to seven air carrier pilots; the results for six of these are shown in Figure 2. It can be seen that there is a wide variety in individual responses to the day/night condition, the wind strength condition, and the braking conditions. Most pilots had essentially the same response to the visibility condition (RVR), the dominant attribute.

After these pilots had ranked the approaches, the instructions continued as follows:

> "You have just finished ranking the approaches in the order of preference of which you would like to make them. Some are good, some are bad, so bad, in fact, that you would never attempt an

approach under those conditions. Assume the following situation holds. You have had a good night's sleep and now you are about to make the first landing of the day. Your alternate is 200 miles away. Place the colored card between those approaches you would attempt (the top group) and those approaches you would not attempt (the bottom group)."

The results of this are shown in Figure 3 which displays the number of approaches that the pilots would attempt as a function of age and total flight time. Besides showing correlation between age and total flight time, there is a surprising consistency across all pilots with one exception. It cannot be inferred from this procedure that this one pilot really would attempt 24 of the approaches because of possible misinterpretation of instructions, nonetheless it appears that this might be a reasonable way to assess risk taking tendencies.

THE WORTH OF WORTH ASSESSMENT

The approaches of worth assessment outlined here appear to be a convenient method to determine the relative importance of various attributes from object preferences, whether these preferences be expressed in numerical terms (magnitude estimates) or in terms of rank ordering various objects in a set. These techniques have the advantage that standard ANOVA programs can be used to process the data if they provide regression coefficients as part of the output. We have found in our experience that ranks seem to be a good approximation to the actual scale value when processing the rank-order data. This is particularly useful since it allows one to obtain essentially interval scales from ordinal responses. We suggest using models incorporating both additive worth functions and those with interactions, since the latter may be important under some conditions. (For six out of the seven air carrier pilots in the evaluation of landing approaches, additive worth functions gave better agreement to the actual responses than any of the LINT models.)

We have also found that the card sorting procedure may yield artifacts, since subjects seem to sort the cards based on the one or two most important attributes, and then sort cards within the major attributes according to some algorithm which does not truly reflect preference. It also may be an indication that the attributes beyond the first two are ignored (Shepard, 1964) and perhaps may not be important relative to other attributes.

All in all, the worth assessment techniques outlined here should prove to be a very useful analytical tool in man-machine system studies.

REFERENCES

1. Green, P.; Wind, Y.: Multiattribute Decisions in Marketing, Hinsdale, Ill.: The Dryden Press, 1973.

2. Poulton, C.: The New Psychophysics: Six Models for Magnitude Estimation, Psychol. Bull., *64*, 1-18, 1968.

3. Shepard, R.: On Subjectively Optimum Selection Among Multiattribute Alternatives, in Shelly and Bryan (Eds.), Human Judgements of Optimality, New York: Wiley, 1964.

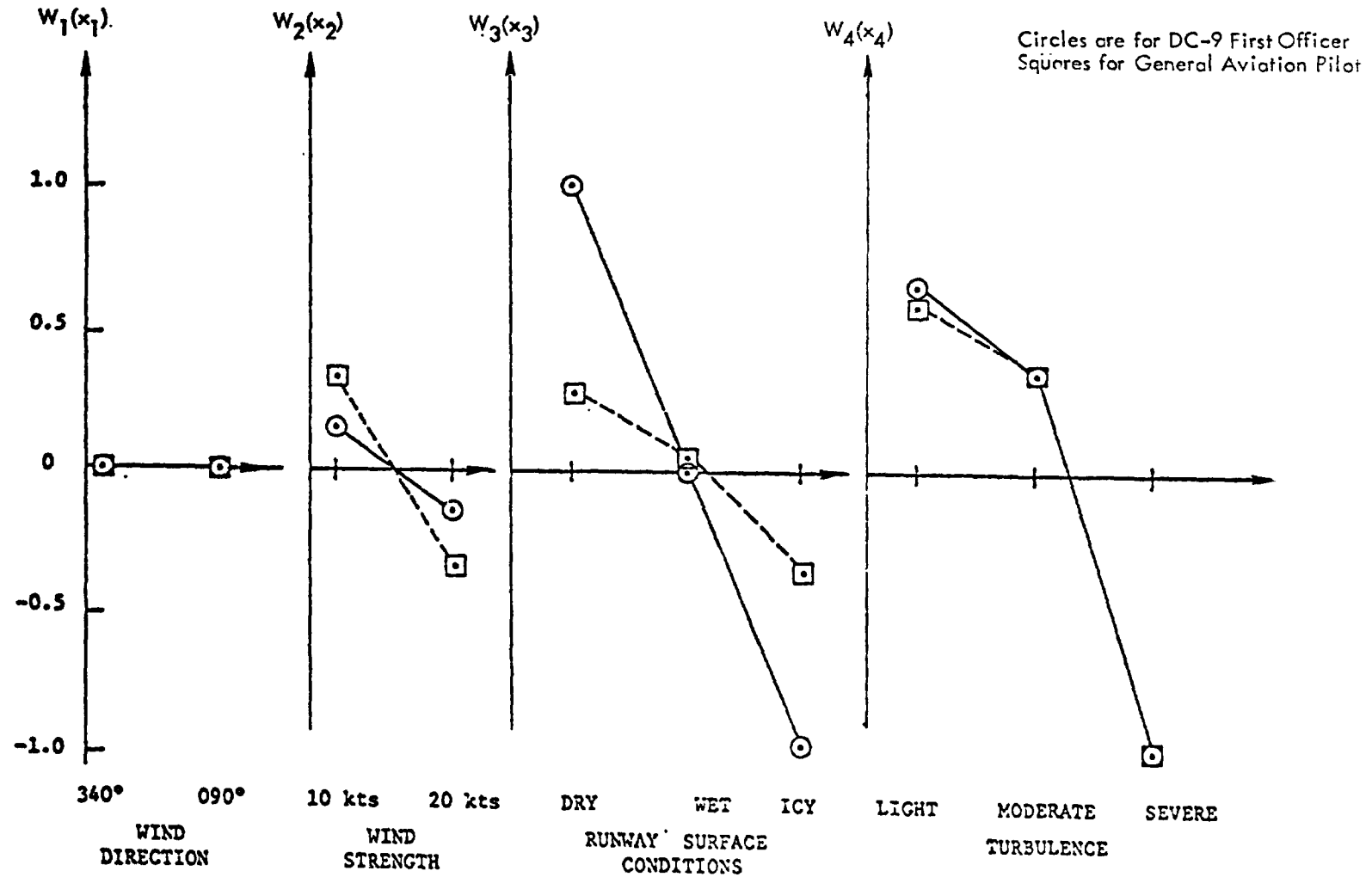

Figure 1: Partial Worth Functions for Approach to Landing - General Aviation Pilot and DC-9 First Officer

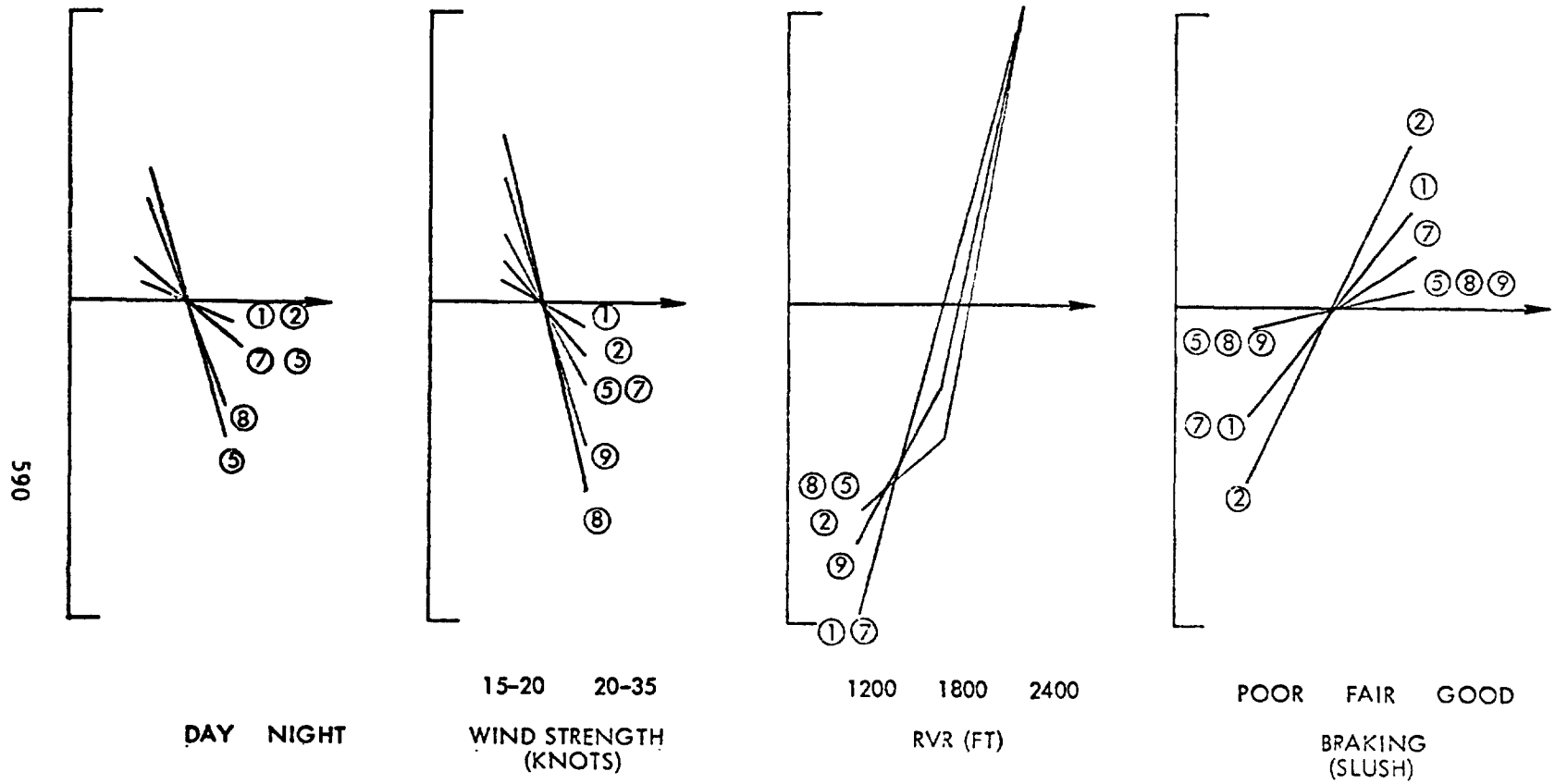

Figure 2: Partial Worth Functions for 6 Air Carrier Pilots

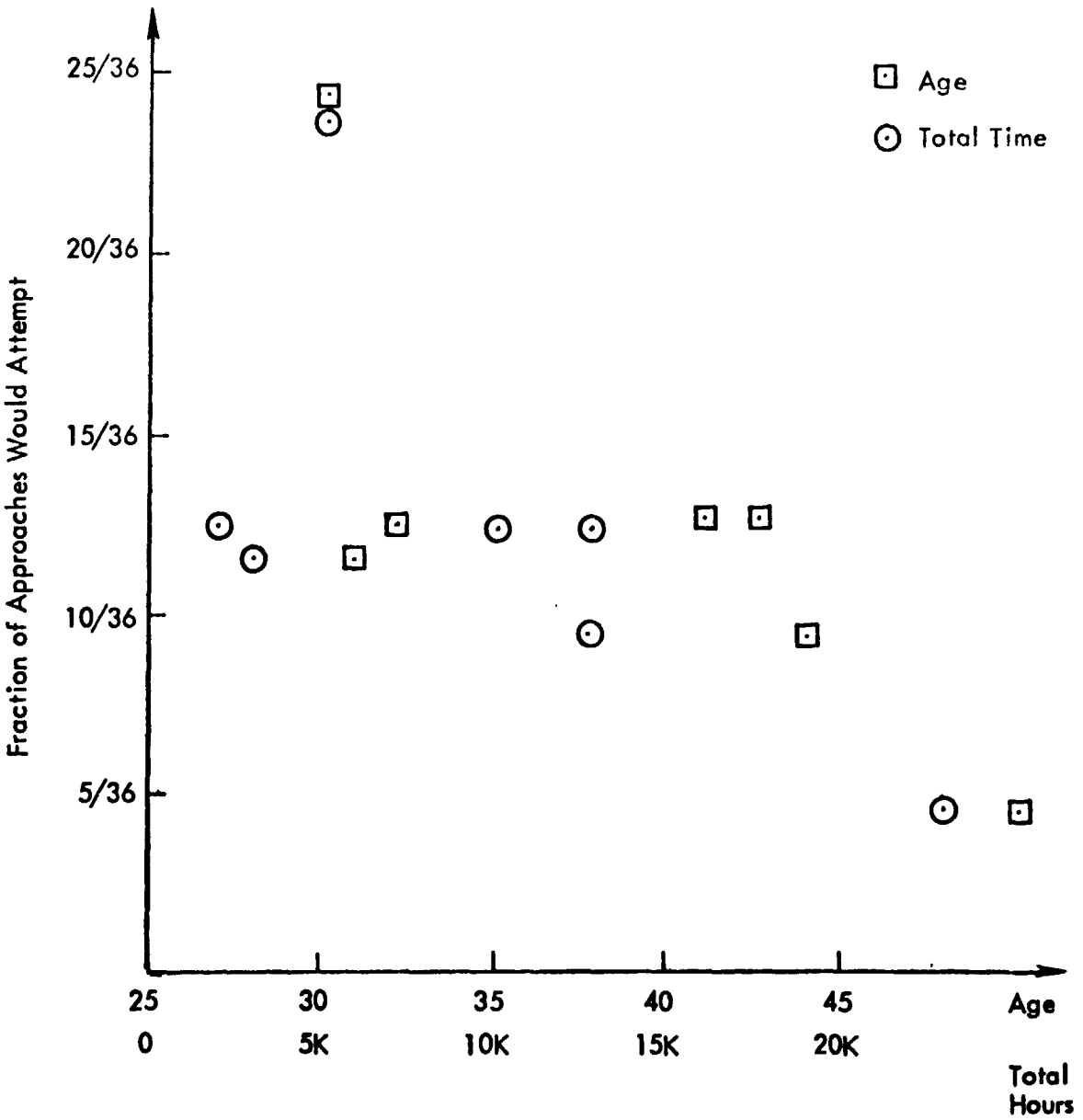

Figure 3: Fraction of Approaches Pilots Would Attempt vs. Total Time and Age.

SESSION VIII

REMOTE MANIPULATION

Chairman: T. B. Sheridan

A COMPUTER-CONTROLLED MACHINING AND MANIPULATING DEVICE

By Tony C. Woo and John M. Paul

Coordinated Science Laboratory

University of Illinois

Urbana, Illinois

SUMMARY

This paper concerns the control of a laboratory scale machining and manipulating device for automatic fabrication of three-dimensional mechanical parts. The device performs the function of pickup of stock, setup and clamping of stock, cutting, and transfer under the control of a time-sharing DEC-10 system.

INTRODUCTION

As part of the Advanced Automation Research Group in the Coordinated Science Laboratory, the manufacturing automation project has embarked on the goal of automatic fabrication of discreet mechanical components from designs. There have been three tasks defined within the present scope--the design and description of parts, automatic interpretation of designs, and automatic fabrication. This paper describes the hardware and control aspects of a device for fabrication.

Three-dimensional parts are designed with volumetric primitives [1, 6]. The primitives are unit solids such as cubes, cylinders, and fillets. In addition to such conventional operations as translation, rotation, and scaling, the primitives can be glued together graphically via an ADD command or negated and then intersected with other volumes via a REMOVE command. The logic involved in ADD and REMOVE of solids is quite different than the conventional Boolean logic.

Before a design can be realized by cutting a piece of stock, certain procedural information must be obtained from the design. Among the information to be derived are the cutting tools required, the cutter paths, stock size, and manipulation and clamping information. The difficulty in arriving at these information lies in the fact that the geometry of the volumetric designs are locally simple yet globally complex. To combat this difficulty, the concept of a cavity is employed as an intermediate description between design and fabrication. The automatic interpretation process is reported elsewhere[7].

One way of creating three-dimensional objects from derived data is via cutting. Though paper tape driven numerical controlled machines have long been available, the idea of treating a milling machine as a computer peripheral device in conjunction with computer graphics has only been explored recently [3]. One of the advantages of having a three-dimensional model made from graphical data is the enhancement of visualization. A user, for example, does not need to integrate multiple views in order to appreciate the subtleties often not detectable in graphical form.

The device reported in this paper has a modest manipulating capability as well as cutting capability. Our interest in the manipulation aspect relates strongly to productivity in manufacturing and programmable automation. According to one recent study [4], over 95 percent of the time a part spends in a factory is in transfer, positioning, loading, etc. This motivates our implementation of programmable transfer and fixture capabilities as an integral part of the reported device.

The combined machining and manipulating capabilities enable us to automate the fabrication process without human assistance. A typical scenario involving our device is as follows. After initialization, a piece of stock is picked up and placed on a worktable. Pneumatic clamps are positioned around the stock and are tightened to the worktable. A cutter is then selected and the cutting proceeds. The entire process is reversed after cutting is finished.

The computer controlled machining and manipulating device is interfaced to a DEC-10 KI processor via a 7 megabaud I/O bus . The device was originally designed as a robot for hand-eye coordination studies [2]. It has a gantry configuration, capable of reaching anywhere in a five

by five by five foot volume. The arm can be moved in the x,y and z directions. The arm contains a shaft with an 11/16 chuck which can be rotated in the theta direction by means of either a high or low speed motor.

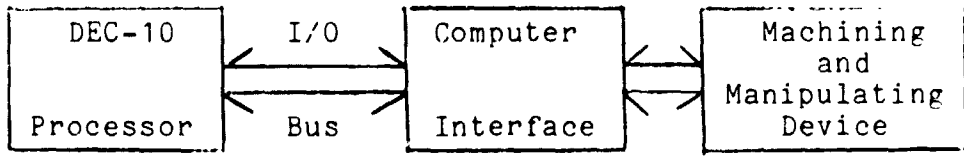

A work table in the form of a raised platform in the work space is constructed so as to minimize the bending moment of the z-axis under cutting force. The table top is an aluminum plate with an array of half inch threaded holes spaced two inches apart. The holes serve a dual purpose. Small chips can be vacuumed through the holes to a vacuum cleaner under the work table. Blocks can also be fastened to the worktable for automatic clamping and set up. A tool rack rests on one side of the worktable. The tools include cutters for drilling, milling, facing, and a socket for tightening the bolts on the programmable blocks.

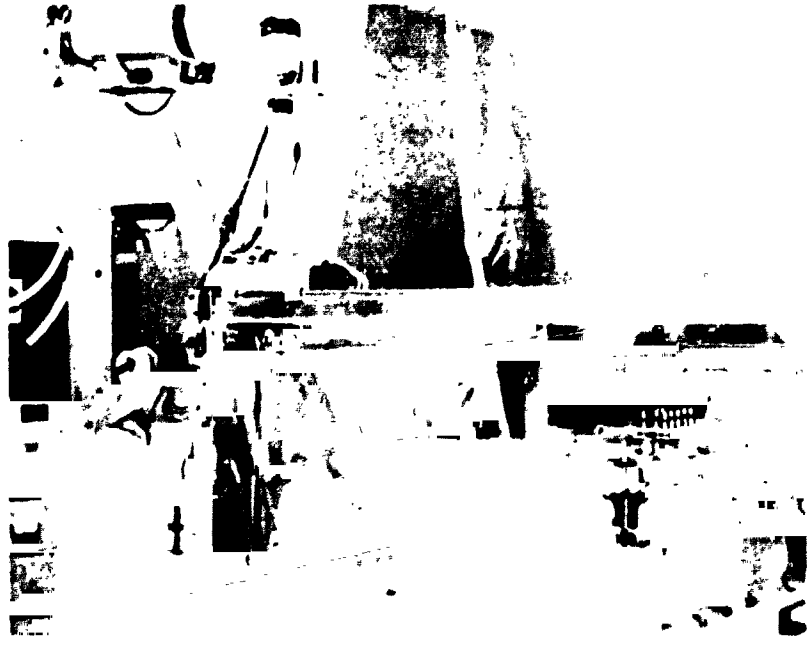

Machining and Manipulating Device

FEATURES

X,Y and Z Movement

Movement of the arm in the three translational directions is accomplished with computer controlled stepping motors. The X and Y axis have 120 steps per inch and the Z direction has 96.4 steps per inch. Scaling can be done with software and will be discussed later. The control of the stepping motors is open loop, therefore if a stepping motor stalls for any reason the arm will have to be reset. The speed of movement in any direction is under computer control with a maximum rate of 1 inch per second.

Quick Change

For computer controlled changing of tools on the wrist shaft a solenoid actuated quick change mechanism with a 11/16 inch chuck is used. All the tools, including cutters, sockets and the hand can be placed on the rotary shaft of the arm under computer control. Then either the low speed stepping motor or the high speed cutting motor can be used to rotate the arms shaft.

Pneumatic Clamp

Automatic clamping of materials to be machined is accomplished with an air vise. Two blocks are positioned with the hand and bolted down with the socket tool. Then through computer control one of the blocks slides under air pressure to clamp the work piece in place. The pressure created by the vise is also under computer control.

Hand with fingers

As mentioned earlier a hand may be placed on the rotary shaft of the arm. Then by means of the low speed stepping motor the hand may be rotated in the + and - theta direction. The hand has two fingers which can be used to grasp objects and can also apply varying amounts of pressure through the fingers. The hand can be attached and detached from the arm completely under computer control.

High Speed Shaft Rotation

The shaft may be rotated at high speeds (70-25,000 RPM) with an AC motor. There are 256 increments in the speed control and this motor can only engaged if the low speed stepping motor is disengaged.

Low speed shaft rotation

The low speed stepping motor can be used to rotate the shaft in increments of 4 degrees. The maximum rotational velocity with this motor is approximately 120 RPM. However torque is greater at a low speed.

HARDWARE CONTROLLER

The DEC-10 has a 36 bit word format. All hardware is interfaced to the I/O bus through a 36 bit parallel word. Three different I/O instructions can be used to communicate with the device:

DATAO <address>, <accumulator>

CONO <address>, <accumulator>

CONI <address>, <accumulator>

where <address> is the devices address on the I/O bus (424) and <accumulator> contains the appropriate 36 bit word or in the case of CONI will contain the 36 bit word read. The DATAO instruction writes the contents of the accumulator to the device as data. The CONO instruction writes the contents of the accumulator to the device as condition information. The CONI reads a 36 bit word from the sensors of the device. Appendix A contains the bit assignments for each of the 3 different instructions. For example by executing a DATAO instruction with bit 35 of the accumulator a "1" the arm will move one step in the +x direction. Executing 10 consecutive DATAO'S will step the arm 10 steps in the +x direction. It can be seen that speed and feed control is strictly done with software. A CONI instruction that returns a "1" in bit 35 will indicate that the +x limit switch has been depressed. It can be seen that the majority

of the actual hardware is just 36 bit data latches, along with a high speed motor controller, AC solenoid drivers, an air pressure controller, stepping motor drivers, and interrupt handling hardware. Software is responsible for the majority of control.

SOFTWARE CONTROL

The control program for the device is called Robhnd.exe[5,736] and can be run interactively with the DEC-10 monitor command:

```
.ru robhnd[5,736]
```

After typing the above monitor command the program will respond with:

```
ROBOT READY, GIVE RESET FIRST
OR DETACH
```

If DETACH is typed, the robot-handler program is ready to accept calls from programs written in higher level languages. If RESET is typed, the device is ready to accept commands. The following commands are valid:

RESET

Used to initialize the device or to recover from "HARD" errors. A reset leaves the arm at the absolute position, X=-3240 Y=-3240 Z=1400 and W=0, where W represents the wrist. All pressure registers are cleared.

SENSE

Returns current status of the arm which includes X position, Y position, Z position, and W position.

XREL N

Move N steps in the x direction relative to its current location. -3241 < N < 3241.

XABS N

Moves to location N on the X axis. Again, -3241 < N < 3241.

YREL N

Moves N steps in the y direction.

YABS N

Moves to the y coordinate position N.

ZREL N

Moves N steps in the z direction (N may be negative).

ZABS N

Moves to the z coordinate position N.

SETVEL N

where N is a number between 0 and 1, and is used as a scale factor for velocity (feed) when moving in the X,Y,Z, or W direction.

SETVC N

this set the hand pressure control power source.

0 for current

1 for voltage

It should be set to 0 with the hand attached.

SETPR N

where N is between 0 and 1777. A number greater than 1777 is loaded as 1777 and any number less than 0 is loaded as 0. This controls the D/A controlled power supply to either current magnitude of 0-5 amps, or voltage magnitude of 0-15 volts.

HAND N

if N equals 1 the hand opens

N equals -1 the hand closes

N equals 0 no power will be delivered to the hand.

SETHS N

where N is between 0 and 255. This sets the speed for the high speed motor controller between 0 and 25,000 RPM with 100 RPM increments.

SETAP N

where N is between 0 and 255. This set the air pressure for the air vise to between 0 and 60 PSI.

HIGHS N

a 0 turns off the high speed motor, a 1 turns on the motor. This is interlocked with engaging the low speed motor by hardware.

LOWSP N

a 0 disengages the low speed motor, a 1 engages the low speed motor. This is interlocked with the high speed motor in hardware.

AIR N

a 0 turns off the pneumatic clamp, and a 1 turns it on.

QUICK N

a 0 disengages the quick change, and a 1 engages the quick change.

ACKNOWLEDGEMENT

This work was supported by the Joint Services Electronics Program (U. S. Army, U. S. Navy and U. S. Air Force) under Contract DAAB07-72-c-0259.

REFERENCES

[1] Briad, I. C. Designing with Volumes, Cantab Press, Cambridge, England, 1975.

[2] Jones, V. C. A simple robot arm, CSL AI Technical Note 1, University of Illinois, 1973.

[3] Lang, C. A. A three-dimensional model making machine, in Computer Languages for Numerical Control (J. Hatvany, ed.), pp.109-119, North Holland Publishing Company, 1973.

[4] Merchant, M. E. The future of CAM systems, Proceedings of 1975 National Computer Conference, pp.793-799.

[5] Snyder, W. E. and Jones, V. C. A user's guide to the CSL vision system, CSL Report R-714, University of Illinois, 1976.

[6] Voelcker, H. B. et. al. Part and assembly description language, Report TM-20a, University of Rochester, 1974.

[7] Woo, T. C. Computer understanding of designs, CSL Report R-695, University of Illinois, 1975.

APPENDIX A

bit	meaning	notes
DATO bits		
0-2	3 bit field for Priority Interrupt Channel	i
3-6	4 bit field for AC solenoid control 0000 not used 0001 quick change on 0010 quick change off 0011 not used 0100 not used 0101 high speed motor on 0110 high speed motor off 0111 low speed motor engaged 1000 low speed motor disengaged 1001 air pressure off 1010 air pressure on 1011 not used 1100 not used 1101 not used 1110 not used 1111 set all functions off	s
7-8	2 bit field to determine which register is loaded with bits 21-29 00 not used 01 set air pressure 10 set high speed motor register 11 clear all above register	s
9	load hand pressure register flag	j
10	set slow wrist if wrist busy	j
11	start timer	s
12	move -z	s
13	move -y	s
14	turn off hand solenoid	s
15	open jaw	s
16	move -w if not slow wrist	s
17	move -x	s
21-29	8 bit data field for air pressure register	

	high speed motor register hand pressure register depending on bits 7,8 or 9	
30	move +z	s
31	move +y	s
32	turn on hand solenoid	s
33	close jaw	s
34	move +w if not slow wrist	s
35	move +x	s

CONO control bits

18-26	load "page register" (these bits specify the upper 9 bits of the address to which interrupts will vector)	c
27	clear "change interrupt"	s
28	clear "slow wrist and wrist busy	s
29	clear "time interrupt"	s
30	clear "time enable" (enable timer interrupts)	c
31	set "time enable"	c
32	set "time interrupt" if "time enable and timer not running	
33-35	load PI channel	c

CONO bits

0	slow wrist flip flop	a
1	jaw open	b
2	finger 1 touching	b
3	finger 2 touching	b
4	not used	
5	jaw closed	b
6	hand down (soft)	c
7	hand down (hard)	d
8	extra switch	-
9	hand code	e
10	-z limit switch	d
11	-y limit switch	d
12	hand locked	e
15	hand energized	e
16	wrist home	e
17	-x limit switch	d

27	change interrupt	
28	wrist busy	e
29	time interrupt	
30	+z limit switch	d
31	+y limit switch	d
35	+x limit switch	d

notes:

a: set by DATAO bit 10, if wrist busy
"change interrupt" is also set
b: the first jaw switch "on" sets interrupt
c: this switch sets "interrupt" when it changes state
d: this group of seven switches sets "interrupt"
when the first switch turns "on"
e: no interrupt
i: occurs during interrupt sequence
j: occurs during CONO CLR or DATAO CLR time
s: occurs during CONO SET or DATAO SET time

MECHANICAL DESIGN AND COMPUTER CONFIGURATION IN THE COMPUTER-AIDED MANIPULATOR CONTROL PROBLEM

By Philippe Coiffet[1], Jean Vertut[2], and Etienne Dombre[3]

SUMMARY

Use of a computer-aided manipulator for performing a given task implies that the computer keeps in memory a mathematical model of the manipulator in order to periodically generate control signals. Interesting dynamical performances may be obtained if the computer works very rapidly or the model is simple enough.

The algorithms necessary for control of an articulated system depend on the complexity of its dynamic equations. A study of the French AMC-MA23 manipulator considers the effects of changes in the mechanical design on this relationship.

For a given control algorithm, methods which allow one to propose computer configurations able to generate this algorithm are also presented. Time minimization, memory size and eventual cost are taken into account.

These previous elements are of most interest in the design of new manipulators since they would lead to a suboptimal control system from the standpoint of performance-cost relationship.

INTRODUCTION

In the design of robots which are not provided with refined algorithms of an artificial intelligence type, manual control is necessary since man has to interact with them at different levels. However, the purpose is to decrease the psychological and muscular cost to the human operator who is required until the robot can be driven without the help of man.

Since the end of World War II, the evolution of manipulators corroborates this previous trend: since Goertz' sophisticated mechanical grasping device, manipulators are now provided with electrical servo-systems and are coupled with computers. The physical duty of the operator has then been removed and now becomes more psychological.

---

[1]Laboratoire d'Automatique de Montpellier, USTL, Place E. Bataillon, 34060 Montpellier, Cedex, France.
[2]Centre d'Etudes Nucléaires de Saclay, France.
[3]Laboratoire d'Automatique de Montpellier, France. Currently at Rancho Los Amigos Hospital, Downey, California.

However, these improvements have been done in an empirical manner and it appears that a general theory of robot synthesis, manipulators especially, is still lacking.

Our purpose in what follows is to make propositions regarding some aspects of the synthesis of manipulators, mainly to point out the linkages between the mechanical structures and different methods of control, as well as a means to define these controls according to a cost-performance criterion. A French manipulator, the MA-23, designed by the CEA-Saclay, will be put forward as an example when required.

DIFFICULTIES OF THE SYNTHESIS PROBLEM

A manipulator is no more than a kind of sophisticated tool. Therefore, it is an interface between man and tasks to be performed. In order to support man, this interface has to be provided with helpful characteristics such as:

- versatility; i.e., the ability to perform various tasks
- adaptability; i.e., the ability to execute a given task despite environmental modifications

The major problem encountered in the synthesis of a manipulator is the definition of an interface when the two systems to be coupled are not fully defined (systems which are evolutionary and interactive with the interface).

For this reason the synthesis is generally done taking into account specifications required by the customer (or by the builder who has made a survey of some specific application). There are three steps:

a) Generation of a mechanical structure which will execute the specified tasks

b) Setting up of control algorithms. There are two classes:

   (1) Elementary task type algorithms; i.e., those which link the control variables to the variations of the manipulator variables (degrees of freedom, applied forces, etc.)

   (2) Algorithms of strategy; i.e., the arrangement of the elementary task sequence according to a goal and/or to a determined criterion.

c) Implementation of the control methods which makes the execution of those algorithms possible.

The result, that is to say, the final realization is intended to satisfy several requirements such as:

- the actual execution of the desired tasks under the desired conditions.

- the minimization of the cost of realization in order that the manipulator can be actually used.

This cost-performance criterion is present in all the steps of the synthesis as well as in all their interconnections.

INFLUENCE OF THE MECHANICAL STRUCTURE ON THE CONTROL COST IN ELEMENTARY TASK TYPE ALGORITHMS

The specifications give the necessary conditions but usually, they are not sufficient to provide a unique mechanical structure. Indeed, the predicted tasks have to be executed, but they must be executed under certain constraints and the simplification of the control algorithms must be facilitated. (As a matter of fact, the simplification is connected with the cost of the implementation and, therefore, with the cost of the manipulator.)

The MA-23 will help us to show the connection between structure and complexity of the algorithms. The MA-23 (references 1 and 2) is the most recent of a series of telemanipulators which have been designed by the "Centre d'Etudes Nucléaires" in Saclay (France). Manipulation of radioactive elements and operations in hot environments were the first goal. The MA-23 possesses 6 degrees of freedom (θ_i) shown in figure 1, plus the closing up of the terminal device. It is activated by electrical torque-motors secured on the fixed frame of the manipulator (fig. 2). The transmissions and reductions are performed by cable systems and metallic tape systems. Gears are used only for the wrist. The benefit of metallic tapes with respect to gear transmission systems is to reduce markedly static friction and backlash. Moving counterweights enables one to obtain a neutral equilibrium, whatever the configuration of the unloaded manipulator. Three patterns of load are available, 60, 100 and 250 Newtons respectively.

Kinematic Model and Position Control Coupling

The kinematic modeling consists in relating the generalized variables Θ_i (or degrees of freedom of the manipulator) to the coordinates of the different lever extremities, especially the coordinates of the terminal device X_j. These coordinates are located in a fixed tridimensional reference system, related to the manipulator holding frame. Therefore, the motor control voltage is related to the previous coordinates. This can be described as below:

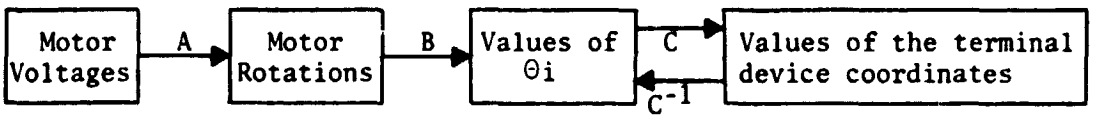

The system can be position-controlled if the terminal device coordinates can be predicted from the command θ_i and vice versa (since generally, the displacements are fixed and the corresponding command is generated).

Therefore, the complexity of the control depends on:

a) The complexity of A, B and C

b) The fact that it may happen that A, B and C are not reversible.

The connections A and B concern the means of control to implement in order to enable the transformation C and C^{-1}. Those are nothing more than the kinematic model of the manipulator, which by the way, has to be simplified in an important manner.

The complexity of the kinematic control is due to many characteristics such as:

a) The number of degrees of freedom (however, the minimal number depends on the type of tasks to be performed.)

b) The geometrical complexity of the manipulator which affects the nature of the transformation formulas between the fixed reference system and the generalized variables.

c) The minimal number of variables which have to be known about the terminal device in order to elicit clearly the actual values of the generalized variables. This is the problem of the manipulator <u>realizability</u>.

The MA-23 does not exhibit any translational degree of freedom. Therefore, the transformations from one coordinate system to another may be represented by rotation matrices. Their product becomes more complex when the fixed reference system is transformed into a terminal device coordinate system.

The realizability of the MA-23, that is to say the analytical description of C^{-1}, is possible only if the points C and E and the angle Θ_6 (fig. 1) are known, or if the coordinates of C and the terminal device orientation are known.

In other words, for a given manipulator, the structure interacts with the position control in the kinematic mode. The complexity of the control depends on the solution to the realizability problem.

Kinematic Model and Rate Control Coupling

The kinematic model for rate control consists of relating the generalized variables (Θ) to variations $\Delta\Theta$ and ΔX of the terminal device rather than to its coordinates (X).

The new connection is established from C by appropriate derivation. Therefore, the existence of the command depends on the issue of realizability. The complexity of this rate control is consequently directly related to the complexity of the position control but the problem becomes more serious considering the existence of singularities.

A singular point corresponds to a specific configuration where it is impossible to get a given ΔX from any $\Delta\Theta$. (This problem occurs usually when a determinant is zero.) If these singularities occur in configurations which are used often during the execution of tasks, the implementation of the control is made more difficult since the singularities must be detected and the algorithm must be consequently modified. Therefore, the cost increases.

For the MA-23, the main singularities happen when a lever axis (for instance, the axis Z_7 of the terminal device in fig. 1) goes through another joint. Thus, the ranges of each degree of freedom have been computed in order to avoid those configurations during actual motion. It can be noticed, in Table 1, that despite this constraint, the amplitudes of motion remain significant.

Dynamic Model and Dynamic Control Coupling

The equations describing the manipulator dynamics have to account for inertia and acceleration of each generalized variable. They are then generally very complicated. For the MA-23, the set of equations can be written as follows:

$$(1)\quad \left\{ \sum_{j=1}^{6} \left\{ A(i,j)\,\ddot{\theta}_j + C(i,j)\,\dot{\theta}_j^{\,2} + \sum_{k=j+1}^{6} B(i,j,k)\,\dot{\theta}_j\,\dot{\theta}_k \right\} = Q(i) + \Gamma_{\theta_i} \right.$$
$$\left. i = 1,6 \right.$$

The A(i,j), B(i,j,k) and C(i,j) coefficients are, for the most part, functions of the generalized variables θ_i of the inertias and the masses of the manipulator and of its geometry. They are not explicitly dependent upon time. The terms Q(i) represent the torques due to gravity and are functions of the configuration and of the masses of the system. The terms Γ_{θ_i} are the motor-torques which act about the different degrees of freedom.

Looking for a command consists in searching the Γ_{θ_i} to be applied in order that the manipulator be driven with the required characteristics and following equations (1). Any control algorithm refers to equations (1) which are then to be simplified to a great extent.

In the case of the MA-23, provided with 4 levers and 6 degrees of freedom (not accounting for the closing of the terminal device) there are 36, 90 and 36 terms for A(i,j), B(i,j,k) and C(i,j) which means a total of 162 terms. Most of them need several lines of writing.

To decrease the cost of the control, the expression of Γ_{θ_i} has to be simplified. The solution is to void or make negligible as many terms of A, B or C as possible.

Three possibilities are available:

a) The general theorems of the theory of mechanics with which it may be written for instance:

$$A(i,j) = A(j,i)$$

$$C(i,i) = 0 \qquad \text{etc . . .}$$

b) The mechanical structure design as for instance the cutting out of θ_6 with respect to the other angles, the parallelism between certain axis of rotation, etc. . .

c) The maximal rates admissible, which leads one to neglect some centrifugal force terms or Corriolis' force terms. This point can only be verified by simulation.

Table 2 gives the number of coefficients which can be neglected by simplifications specific to the MA-23 (reference 1). Those simplifications can be done if the maximal rate of the terminal device and the maximal load do not go beyond 1 m./s. and 50N respectively. Equations (1) are written as:

$$\begin{cases} \sum_{j=1}^{6} A(i,j)\,\ddot{\theta}_j = Q(i) + \Gamma_{\theta_i} \\ i = 1,6 \end{cases}$$

(The A(i,j) coefficients represent a symmetrical matrix with ' zeros. There are only 15 <u>different</u> terms left.)

Therefore, the connection between control cost and mechanical structure has been established. However, it must be noticed that in order to define a structure on which the previous simplifications are possible, it is necessary to write the overall equations of the system. Furthermore, the behavior must be simulated for several structures, the outcomes of mechanical modifications on the behavior must be forecast, etc. . . It is then obvious that the writing of the equations by hand is not only tedious but difficult to get through without any mistake.

This is the reason why a computer program has been prepared (reference 3), using the PL1 language. From heuristic data on a tree-like network, such as number of levers, number of degrees of freedom, relation order, etc., the program yields <u>literally</u>:

* the different coordinate transformation matrices
* the coordinates of each lever end point in a fixed reference system
* the gravity torques
* the dynamic coefficients A(i,j), B(i,j,k) and C(i,j)

To date, this program is restricted to systems with only rotational degrees of freedom (the extension to translational motions is in progress). It needs 2 minutes (CPU) on an IBM 360-65 to give the results corresponding to the MA-23. Another computer program, making use of the standard Runge-Kutta method, simulates the manipulator behavior from the results of the first program.

These results form an interesting and efficient tool for the determination of a structure which decreases the control cost.

INFLUENCE OF THE MECHANICAL STRUCTURE ON THE CONTROL COST IN THE STRATEGY TYPE ALGORITHMS

Since the strategy type algorithms use a sequence of elementary task type algorithms according to a given criterion of execution (reference 4), it can be said that the connection between mechanical structure and strategy type algorithms is relatively flexible. The connection operates only if the transducers which are necessary to the criterion elaboration introduce a modification of the structure by means of their physical presence. For instance, if visual information is desired, the TV camera which could be put on a light lever of the manipulator would modify the masses and inertias in an important manner. Likewise, changes in the shape of the terminal device would be necessary if a sonar was supposed to be set up.

Usually, mechanical structure and algorithm are supposed to be completely unrelated. With this hypothesis, researchers have been able to propose complex artificial intelligence type algorithms but they are not concerned with the mechanical structure to be controlled. Likewise, the computer which is supposed to generate the algorithms is seldom specified. This, then, is another problem from the standpoint of cost-performance criterion.

IMPLEMENTATION OF A CONTROL ALGORITHM

So far, we have discussed the specifications required for a mechanical structure to minimize the complexity of the elementary task type algorithm in order to decrease the system cost (references 5 and 6). Those algorithms being established, as well as the strategy type algorithms, we are now concerned with the implementation in order that their efficiency and their cost be optimized.

Practically this means that the motions of the manipulators must be fast enough (usually with a rate near that the man uses to carry over a load) but that the "computer" and the manipulator must cost about the same.

The hypotheses of references 7, 8 and 9 are recalled below:

a) The algorithm is assumed to be given with a fixed mathematical formulation

b) The mathematical methods used in the processing (for instance, to get the inverse matrix) are given

c) The computer structure is given as well. It is, at the present time, a multiprocessor structure with unique memory (figure 3)

The problem is to define the number of processors to be used and the respective minimal memory size in order to execute the algorithm in a given time (this time is imposed by the expected performances of the manipulator).

For this purpose, the execution of the algorithm is described by a state transition graph with nodes and arcs. The arcs represent the crossing conditions from one node to another. Computation times and memory sizes are associated with nodes (figure 4).

The application of the "critical path method" (references 10, 11, 12 and 13) to the state transition graph gives the minimal time of execution for the algorithm if sufficient resources (number of processors and memory size) are allocated to it. In this way, it is possible to determine an upper limit for these resources. The purpose is to minimize the resources accounting for the time constraint.

Two algorithms have been studied, with which it is possible to minimize the memory size when the number of processors is given.

- The first one is of an heuristic type and the distance between its solution and the optimum is unknown.

- The second one gives the optimum but all the possible configurations of the task have to be specified.

Finally, a method allowing one to obtain the configuration which minimizes the cost of the hardware (the cost is defined as a linear function of the number of processors and of the memory size) and avoiding the specification of all the possible configurations has been developed with a progressive evaluation and separation procedure (PSEP) (reference 14).

Research is currently in progress in order to extend the hypothesis. The possibility of conflict between several processors, from the standpoint of memory access, is taken into account. Besides, it is assumed that an addition of large but slow access memories, such as disks, is provided.

Currently in progress as well, is the realization of the control of the MA-23 with microprocessors. (To date, this control is made with a T-1600 type of computer from "Télémécanique" (France) with a memory size extended by a disk unit.)

CONCLUSION

The present robots or manipulators used in industry are all controlled in a kinematic mode and without adaptive characteristics (in other words, without closed loop strategy type of algorithms). It might be thought that the implementation of control algorithms in the dynamic mode and of adaptive algorithms costs too much if the efficiency of open loop controlled robots is considered. However, the robots are supposed to perform tasks which are mainly those bringing out the versatility and the adaptability of the human operator (assembly tasks, transfers of load, etc. . .).

The research presented in this paper is a contribution to the synthesis of modern manipulators. The criteria of realistic cost and of performance of the system are emphasized.

REFERENCES

1. Vertut, J.; and Coiffet, P.: Bilateral Servo Manipulator in Direct Mode and Via Computer Optimized Control. Second Conference on Remotely Manned Systems, Los Angeles, June 1975.

2. Vertut, J.; Charles, J.; Coiffet, P.; and Petit, M.: Advance of the New MA-23 Force Reflexive Manipulator System. 2nd Int. Symp. on Ro. Man. Sy., Warsaw (Poland), Sept. 1976.

3. Liegeois, A.; and Coiffet, P.: Le Projet Pilote SPARTACUS. Institut de Recherche en Informatique et Automatique, Rocquencourt (France) March 1976.

4. Liegeois, A.; and Renaud, M.: A Method for the Dynamic Control of Redundant Manipulators. Proc. of 5th Int. Symp. on External Control of Human Extremities. Dubrovnik, August, 1975.

5. Coiffet, P.; Liegeois, A.; Fournier, A.; Khalil, W.; Molinier, P.; and Vertut, J.: Computer Aided Control of Force Reflective Manipulators. Symposium IFAC, Automatic Control in Space, Rottach-Egern, May 1976.

6. Liegeois, A.; Khalil, W.; Dumas, J. M.; and Renaud, M.: Mathematical and Computer Models of Interconnected Mechanical Systems. 2nd Int. Symp. on Theory and Practice of Robots and Manipulators, (Ro. Man. Sy.) Warsaw (Poland), Sept. 1976.

7. Dumas, J.M.; and Prunet, F.: A Method for Local and Reduced Studies in Parallel and Processes Models. Digital Processes, 1976.

8. Prunet, F.; Floutier, D. and Dumas, J.M.: Computer Aided Design of Industrial Control Systems. 12th Design Automation Conference, Boston, 1975.

9. Dumas, J.M.; and Prunet, F.: Searching for Properties on a Parallel Processes Model. Proceedings of the Int. Workshop of Real Time Processes, Boston, August, 1975.

10. Cerf, V.G.: Multiprocessors, Semaphores and a Graph Model of Computation. Ph.D. Thesis, University of California (1972).

11. Parent, M.R.: The Control Graph Models: A Unified Approach to Performance Evaluation. Case Western Reserve University, June, 1974.

12. Fernandez, E., et al.: Bounds on the Number of Processors and Time for Multiprocessor Optimal Schedules. IEEE Tran. on Computers, C-22, 8, August 1973.

13. Serlin, O.: Scheduling of Time Critical Processes. Spring Joint Computer Conference, 1972.

14. Roy, B.: Algebre moderne et theorie des graphes. 2 tomes, Dunod, Paris, 1969.

15. Proceedings of the 3e CIRT, Nottingham, March, 1976.

Ranges of motion and lengths of the different levers for the MA-23 (see Figure 1)

OA = 320 mm

AB = 400 mm

BD = 650 mm

$-60^{\circ} < \theta_1 < +60^{\circ}$

$-70^{\circ} < \theta_2 < +57^{\circ}$

$-135^{\circ} < \theta_3 < -30^{\circ}$

$-179^{\circ} < \theta_4 < 179^{\circ}$

$-81^{\circ} < \theta_5 < +57^{\circ}$

$-180^{\circ} < \theta_6 < 180^{\circ}$

$BCD = 128^{\circ}$

Table 1

Table of simplifications to calculate the dynamic coefficients of the MA-23 type of manipulator

Dynamic Coefficients	Number to be evaluated	Decrease in the number to be evaluated		Number of Coefficients Remaining
		Due to	Number	
A_{ij}	$n^2 = 36$	General Theorems of the Theory of Mechanics	$\frac{n(n-1)}{2} = 15$	21
		Mechanical Design	6	15
		Maximal Rates Admissible	0	15
B_{ijk}	$\frac{n^2(n-1)}{2}$	General Theorems of the Theory of Mechanics	$\frac{n(n-1)}{2} = 15$	75
		Mechanical Design	Disjunction of $\theta_6 = 35$	40
			Parallel Axis = 11	29
		Minimal Rates Admissible	29	0
C_{ij}	$n^2 = 36$	General Theorems of the Theory of Mechanics	n = 6	30
		Mechanical Design	15	15
		Maximal Rates Admissible	15	0
Total	$\frac{n^3 + 3n^2}{2} = 162$		147	15

Table 2

Captions

Figure 1: Skeletal of the MA-23

θ_1 and θ_4 are zero when O.A.B,C and D are in the OYZ plane

θ_6 is zero when the terminal device is in an orthogonal plane with respect to OYZ

Figure 2: A view of the MA-23

(1) Motors
(2) Servo - Systems
(3) Cable Reducers
(4) Counterweights

Figure 3: General architecture of the computer

MC = central memory
P_i = processors

Figure 4: Example of graph associated to the calculation of two commands V_1 and V_2

$V_1 = \sqrt{\sin S_1} + \sin S_2$

$V_2 = \cos S_1 + \sqrt{\cos S_2}$

A computation time and a memory size are associated to each mode

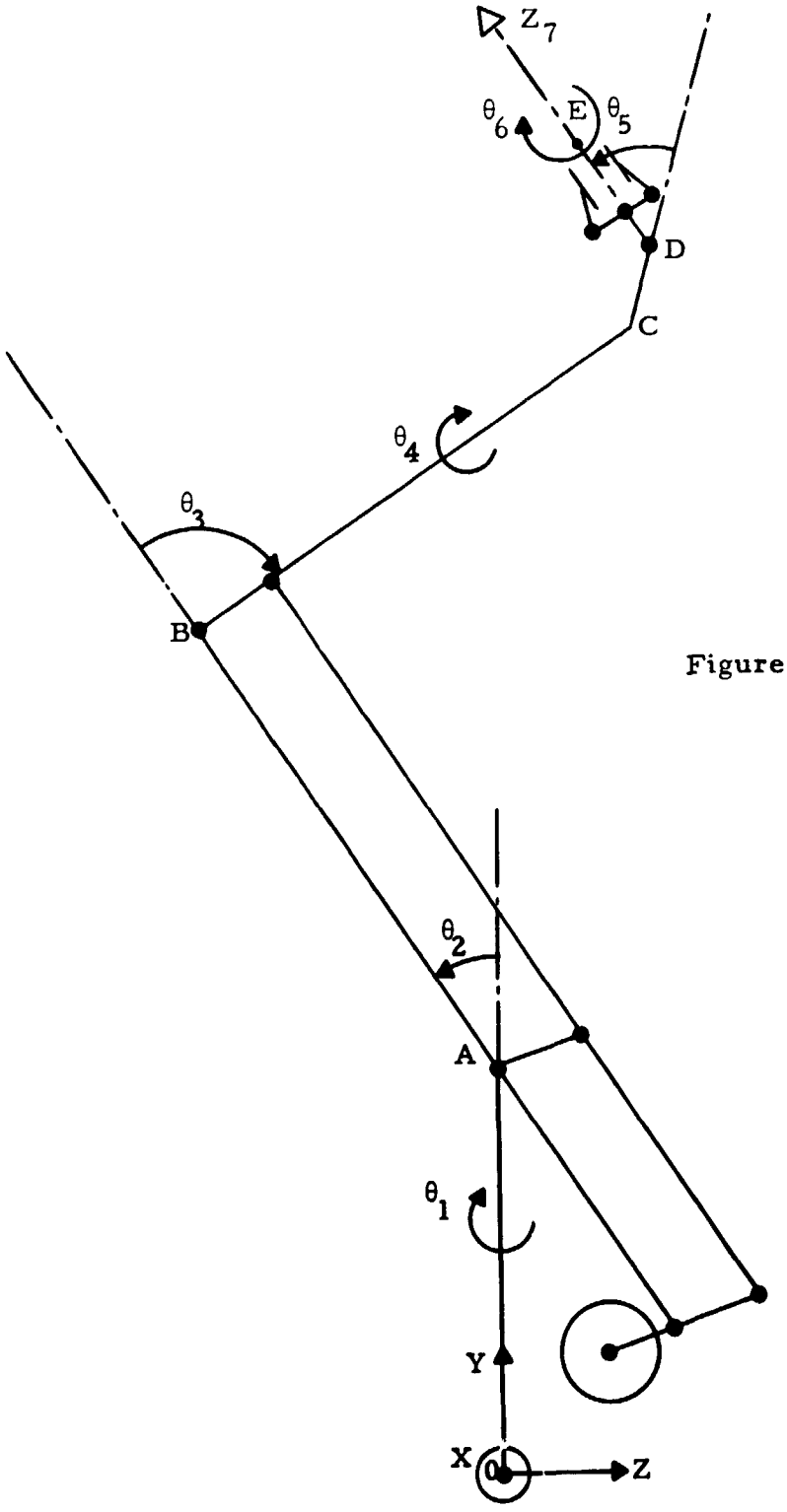

Figure 1

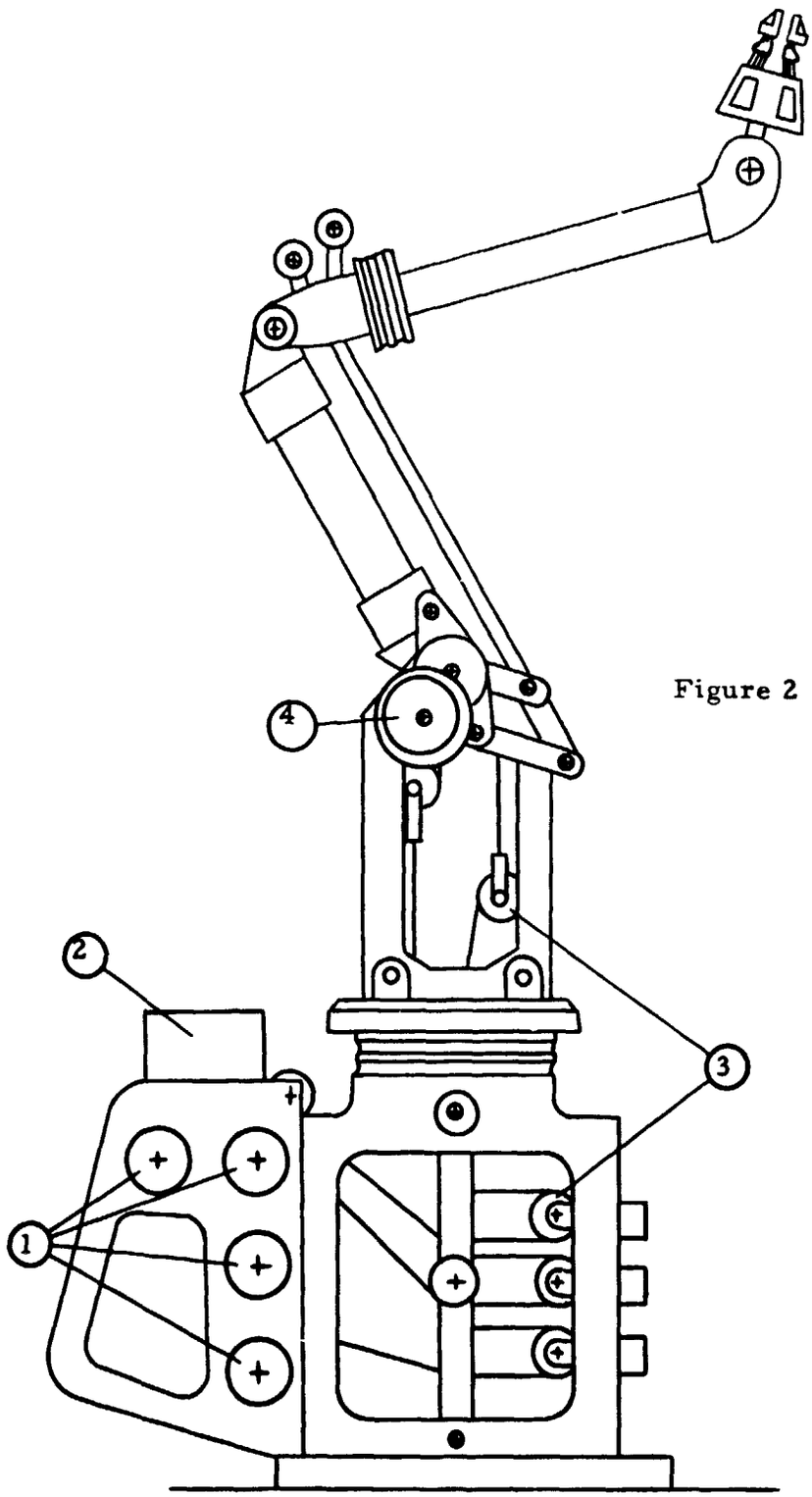

Figure 2

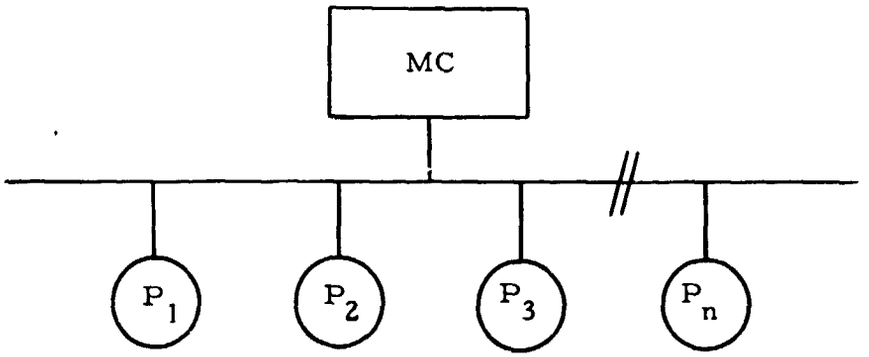

Figure 3

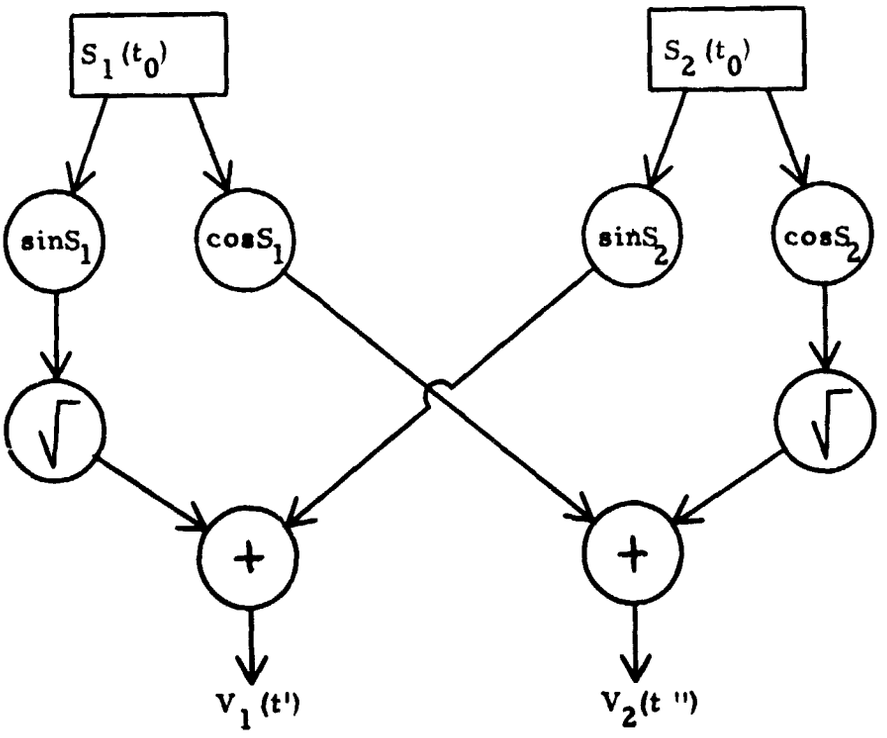

Figure 4

A PRELIMINARY EVALUATION OF MANUAL CONTROL TASKS ASSOCIATED WITH THE SPACE SHUTTLE REMOTE MANIPULATOR SYSTEM*

Lloyd D. Reid

University of Toronto
Institute for Aerospace Studies

SUMMARY

A major hardware component in the Space Shuttle cargo handling system is a large (50' long) remote manipulator arm. This arm is employed in the zero-g space environment to load and unload cargo while in orbit. Due to weight restrictions this arm must be of light construction and consequently care must be taken to ensure that flexibility induced problems do not arise while it is under the control of human operators.

The purpose of the present project was to perform a preliminary investigation of the ability of human operators to control the arm. In particular attention was focused on the human's ability to damp out structural oscillations of the system. This was achieved by implementing the system equations of motion on an analog computer and employing a pictorial display on a CRT driven by a digital computer. The simulation was based on a single-degree-of-freedom model.

Both arm stiffness and display update were varied in order to assess their impact on system performance. Phase plane plots and tracking precision measures were obtained as part of the study. It was found that the system was best controlled by a form of open loop response and that the structural oscillations could be successfully damped out.

INTRODUCTION

At the present time a group of Canadian firms is developing a Remote Manipulator System (RMS) for the space shuttle. This arm will be used to move payloads into and out of the cargo hold. It is approximately 15.2m (50 ft.) in length with a shoulder joint, elbow joint, wrist joint, and end effector. One mode of operation involves three axes rate control by a human operator while viewing the arm either directly out a window or on a closed-circuit TV monitor.

In order to minimize the system weight design trade-offs must be made against arm rigidity. This in turn can lead to significant structural

*Work awarded to SPAR Aerospace Products Ltd. by the National Research Council of Canada, contract file 31053-5-385.

oscillations when the system is operated. The present study was intended to investigate the ability of human operators to damp out structural oscillations in the arm when a massive payload is held by the end effector. A secondary goal was the evaluation of the influence of computer induced time delays and display update lags in order to assess their importance in future RMS simulations.

OVERALL SYSTEM DESCRIPTION

The task to be simulated was a simplified single-degree-of-freedom version of the real task (see Fig. 1). Our laboratory was provided with the appropriate equations of motion at the start of the project. These described a single joint arm system. The human operator's task was to damp out vertical oscillations (relative to the space shuttle body axes) of a 29,030 kg (32 ton) payload at the end of a 15.2m (50 ft.) flexible arm.

Working in from the payload, the simulated system consists of:

(1) The 15.2m (50 ft.) arm, described by its first mode of oscillation (the cantilever mode). Arm stiffness values employed ranged from 0.57 to 13.7 mm deflection per Newton force applied at the tip. Structural damping ratios employed ranged from 1% to 2.4%.

(2) The shoulder joint servo generates a relative angle γ between the root of the arm and the space shuttle horizontal body axis. This servo system is rate limited and torque limited such that the nominal maximum arm tip vertical speed is less than 7.6 cm/s (neglecting structural oscillations) and the nominal maximum tip force that can be applied to a payload by the shoulder joint servo system is 129 N.

(3) The space shuttle was free to roll and translate in the transverse body axes plane. An automatic roll attitude control system was employed to attempt to maintain $\theta = 0$ referenced to an inertial frame. This involved a rather limited pulsing rocket thruster.

VISUAL DISPLAY

The visual display employed was a mini-computer generated simulation of a closed circuit television monitor. It depicted a 3 x 3 x 6m rectangular payload on the end of a 15.2m arm (see Fig. 2). For the simple task studied here a close-up picture of the payload was employed. The inverted V is a screen fixed reference mark (see Fig. 3). The display is generated by a high-speed digital-to-analog converter and is based on a 256 x 256 dot matrix presentation on a 20 x 28 cm screen.

HARDWARE

The system equations of motion were programmed on a TR-48 analog computer and the visual display generated by an HP 2100 mini-computer. The work station contained the display and the controller. The latter was hand held and finger operated and does not represent anticipated flight hardware.

TASK DETAILS

In the present study the payload was assumed to be already attached to the end of the arm with the arm flexed and at rest. The task begins with the release of the system from these initial conditions.

The primary recording device employed was an X-Y plotter. This was used to generate phase plane plots of payload vertical speed vs. payload vertical position (positive upwards) (see Fig. 4). This figure depicts the nature of these phase plane plots when no human control is present. It is seen that the overall system behaves much like a second order system despite the presence of nonlinearities. In this plot the time in seconds following system release is indicated by the flagged numbers located at the horizontal axis crossings.

The overall system period and damping ratio as measured from phase plane plots have been used to identify the various cases in Fig. 5. Four different systems have been studied and two different display update rates employed. The subjects were selected from a group of 6 volunteers on the basis of good performance on the present task. A total of 272 final runs were analyzed.

As can be seen in Fig. 5, the system's period of oscillation was quite long and the damping modest. As a result it was found that in order for the subjects to damp out the oscillation an intermittent form of control activity was required. Attempts at continuous closed-loop control on the part of the subjects almost always led to an instability.

Figure 6 can be used to illustrate the problem. Here all the elastic properties of the arm are concentrated in a spring at its root. The human operator is assumed to control the angle γ through the integrated effects of his rate command inputs. Structural damping is absent.

In order to damp out the structural oscillation of this system the energy contained in the elastic deflection of the spring and the motion of the payload must be dissipated. When the system is released from position (1) all the energy is contained in the spring. By the time the payload passes through $Z = 0$ (provided that γ still is zero) all the energy resides in the kinetic energy of the payload. Attempting to oppose this motion is not very effective because this tends to simply shift the energy of the oscillation from kinetic energy to strain energy of the spring. The simplest

way to dissipate the energy is to rapidly release the spring by appropriate control over γ at some point where $\dot{Z} = 0$.

In addition, since we wish to bring the payload to rest at $Z = 0$ the net change in γ during these operations must also be zero. A possible sequence to achieve this is to release half the strain energy at (1) by commanding down γ and half at (2) by commanding up γ. Note that in order to release strain energy from the spring up control is applied when the deflection is upward, etc.

This approach can be applied to the present system. Typical results are shown in the plot of the elastic deflection of the arm tip in Fig. 7. The upper trace shows the response following the release from an initial downward deflection when no control is applied. The middle trace shows the effect of up command when the deflection is still downward. The bottom trace shows the influence of applying up command at the upward deflection peak in the cycle.

HUMAN OPERATOR CONTROL

The actual control technique adopted by the subjects was similar to that outlined above. They were instructed to damp out the structural oscillation which resulted when the arm plus payload was released from an initial deflection and to bring the payload to rest at the centre of the display (marked by the inverted V symbol). The latter corresponds to $\gamma = 0$. The task was allowed to run for 2 min.

Figure 8 illustrates the control activity of our best subject. He employed strain energy relieving commands at the peak deflections and generally followed an up command by a down in order to maintain γ near zero. The latter technique was necessary because the simulated system gives the operator no indication of the arm root angle γ. Thus with a rate command system he must keep track of the integrated effect of his inputs to the system in order to bring the payload to rest at $\gamma = 0$.

Figure 9 illustrates an actual phase plane plot for the system under human control. It was found that quite effective control could be exercised over the system after a reasonable period of training (8 hrs). The rectangle drawn around the origin represents an artificial target zone used to assess the time taken to achieve effective control over the system. Its dimensions are $Z = \pm 14$ cm and $\dot{Z} = \pm 1$ cm per sec. The time taken to enter this zone of the phase plane was termed "time to capture". (Note that the display resolution represents 6 cm full scale with the present configuration.)

EXPERIMENTAL MEASUREMENTS

Performance was judged by the residual energy in the structural oscilla-

tion at the end of 2 min. of human control and by the final value of γ (see Fig. 10). The residual energy was indicated by the peak-to-peak amplitude of the structural oscillation and the final value of γ by $|Z|$ steady state. The time to capture was also recorded. Only the detailed results for the runs performed by the group of 4 subjects are presented here.

An analysis of variance performed on the data indicated that subject and stiffness effects were significant at the 5% level while update interval effects were not. This applied to all three sets of data.

CONCLUSIONS

The following conclusions are based on the results for the systems with periods of oscillation of 27 and 51 sec.

(1) Flexibility is more important than display update rate in determining system performance. Stiffer arms result in better performance.

(2) Update rates (along with system time delays) of up to 2 sec. have no significant influence on the performance measures employed in this study.

(3) Performance in some cases approached the resolution limit of the display.

(4) The tasks performed were quite complex in nature and the individual subjects showed significant interaction effects with flexibility.

(5) An indication to the human operator of shoulder joint position would probably have simplified the tasks considerably.

The results for the systems with periods of oscillation of 11 and 22 sec. were too limited to allow the formation of firm conclusions. However, it appeared that the stiffer arm was marginally better and that increased display update intervals tended to cause poorer performance.

JOINT SERVO
- RATE COMMAND
- SATURATION
- RATE LIMITER

GEAR BOX
- BACKLASH

ATTITUDE CONTROLLER
- DEAD BAND
- SATURATION
- PULSE RATE

ARM DYNAMICS
- FIRST MODE

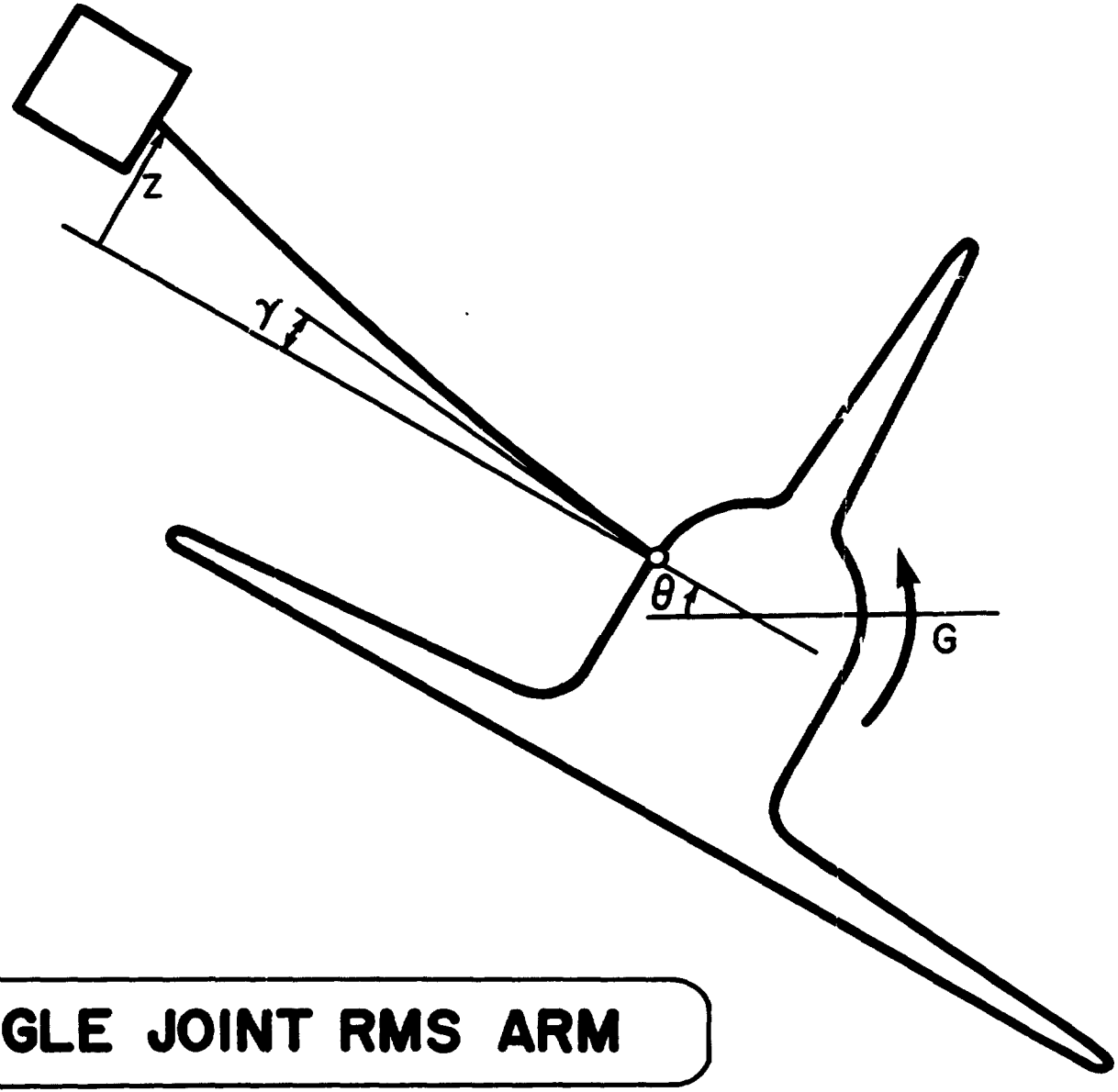

SINGLE JOINT RMS ARM

FIGURE 1

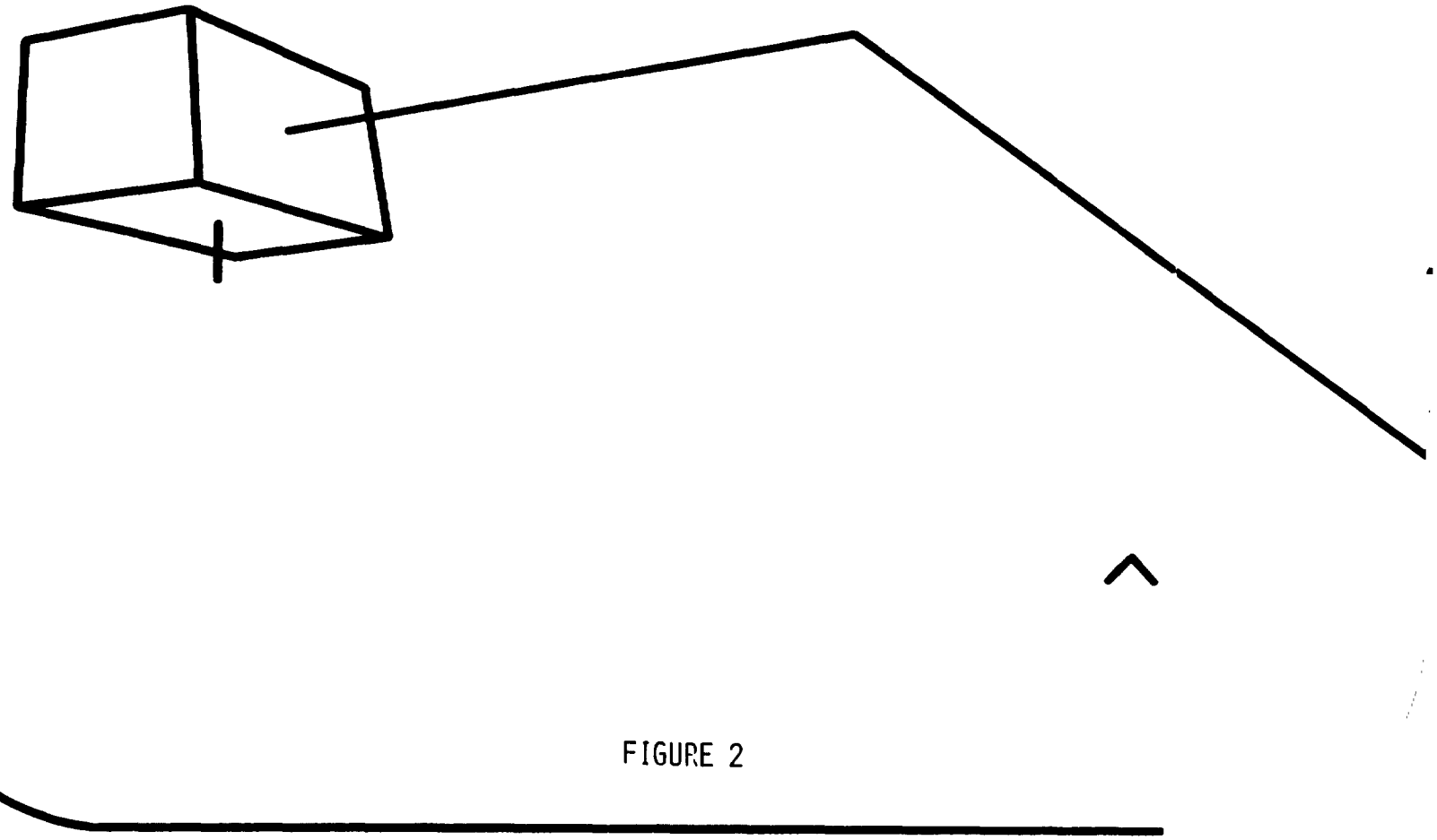

FIGURE 2

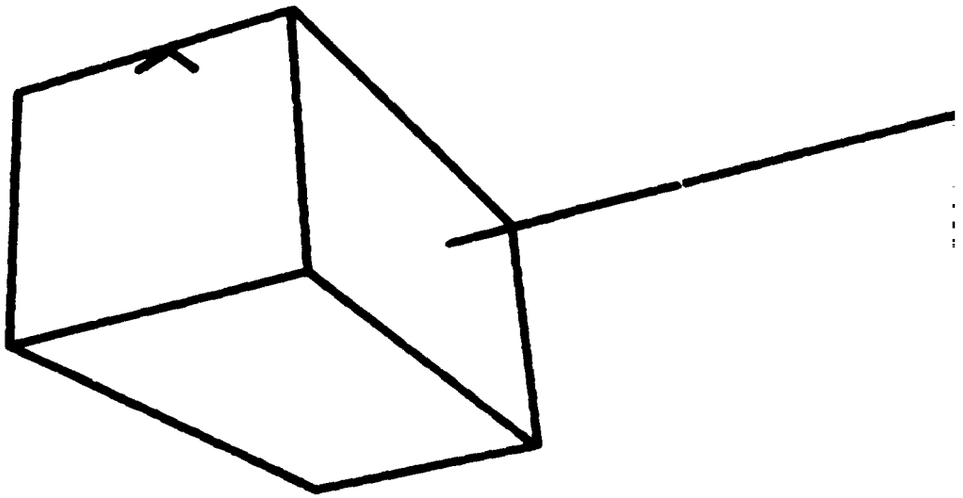

FIGURE 3

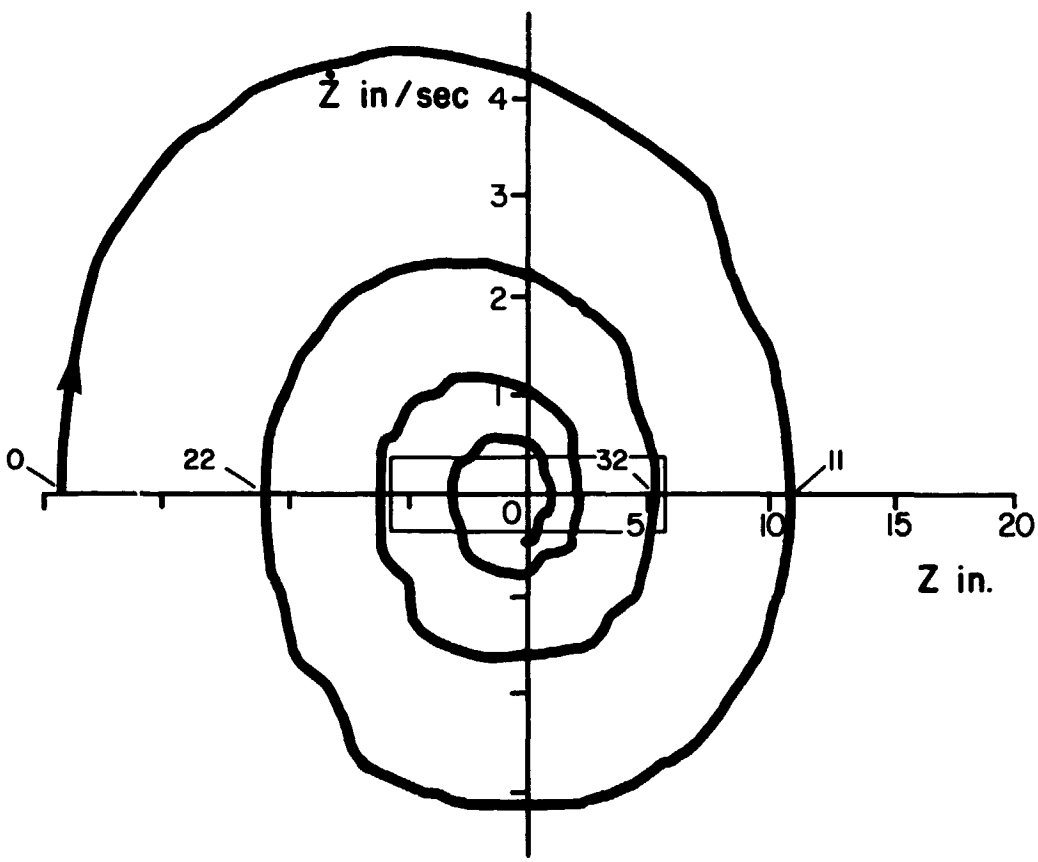

PHASE PLANE PLOT
PAYLOAD DISPLACEMENT

PERIOD = 22 SEC., ζ = 0.08

FIGURE 4

TASK	PERIOD	ζ	UPDATE INTERVAL	INITIAL DEFLECTION	NUMBER OF SUBJECTS	NUMBER OF FINAL RUNS
	SEC		MS	FT		
1	51	.019	50	2.67	4	48
2	27	.018	50	2.67	4	48
3	51	.019	2000	2.67	4	48
4	27	.018	2000	2.67	4	48
C	22	.080	50	1.60	2	20
D	11	.146	50	1.60	2	20
E	22	.080	2000	1.60	2	20
F	11	.146	2000	1.60	2	20

FIGURE 5

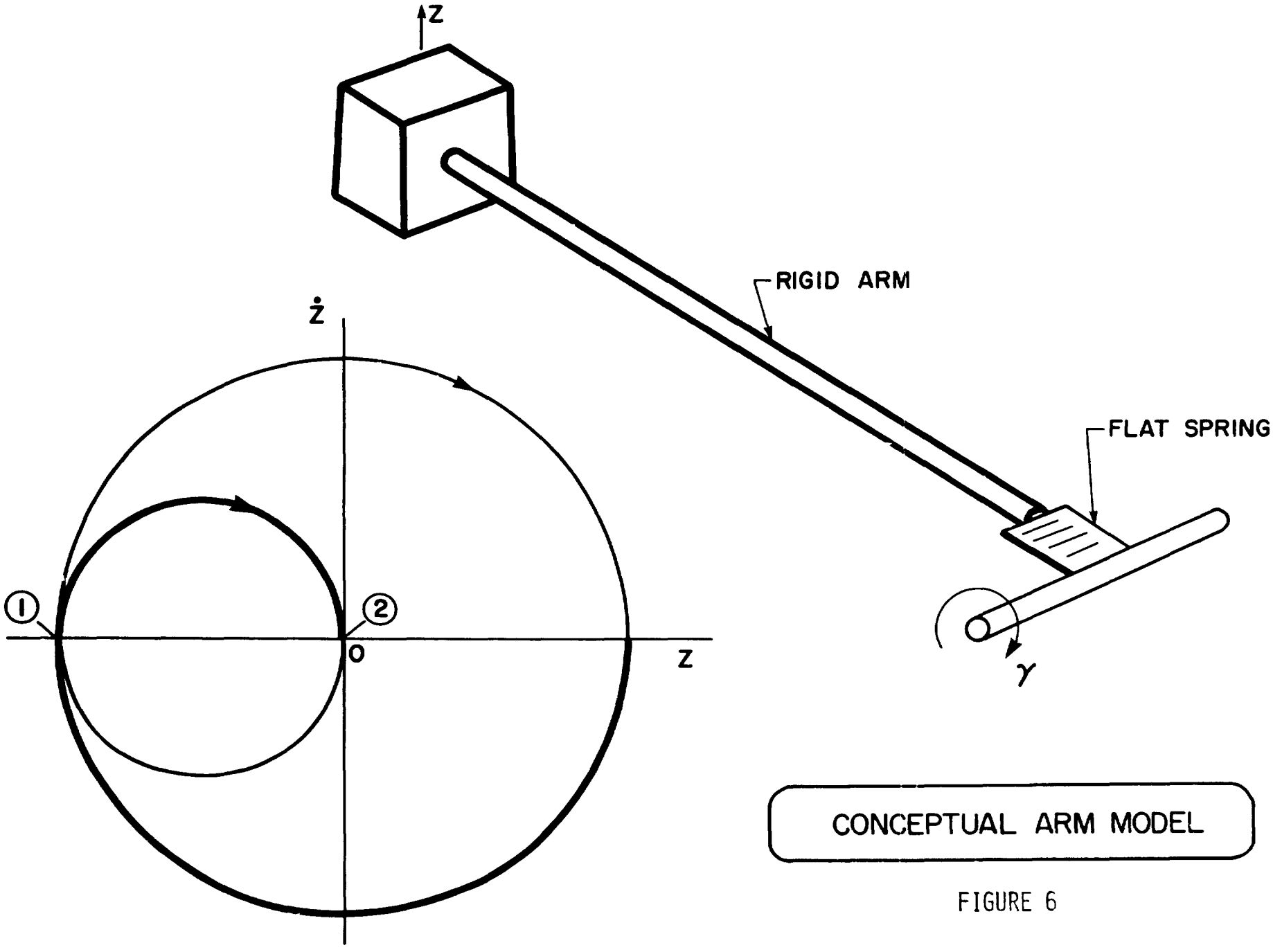

CONCEPTUAL ARM MODEL

FIGURE 6

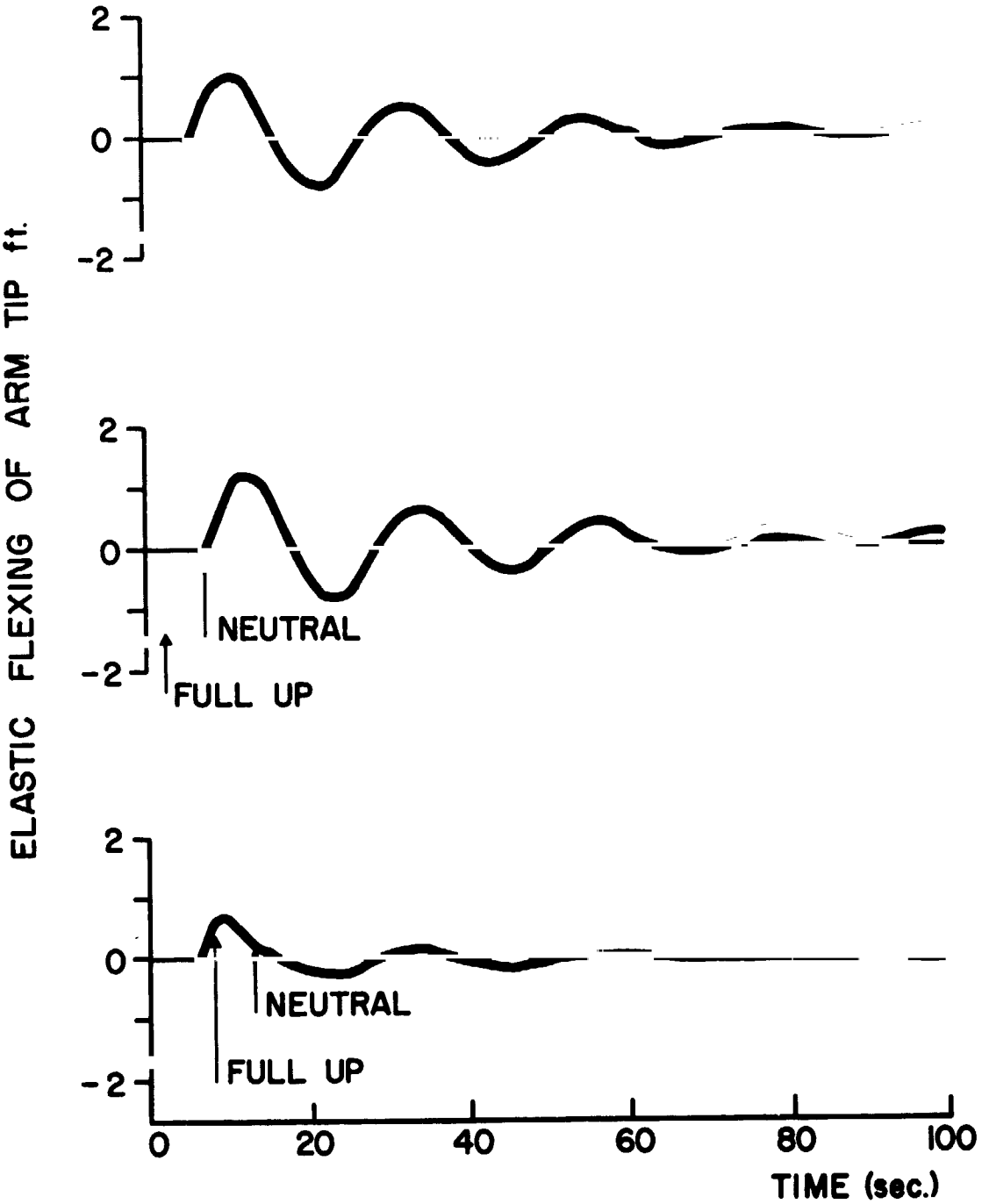

CONTROL EFFECT ON FLEXING OF ARM

PERIOD = 22 SEC., ζ = .08

FIGURE 7

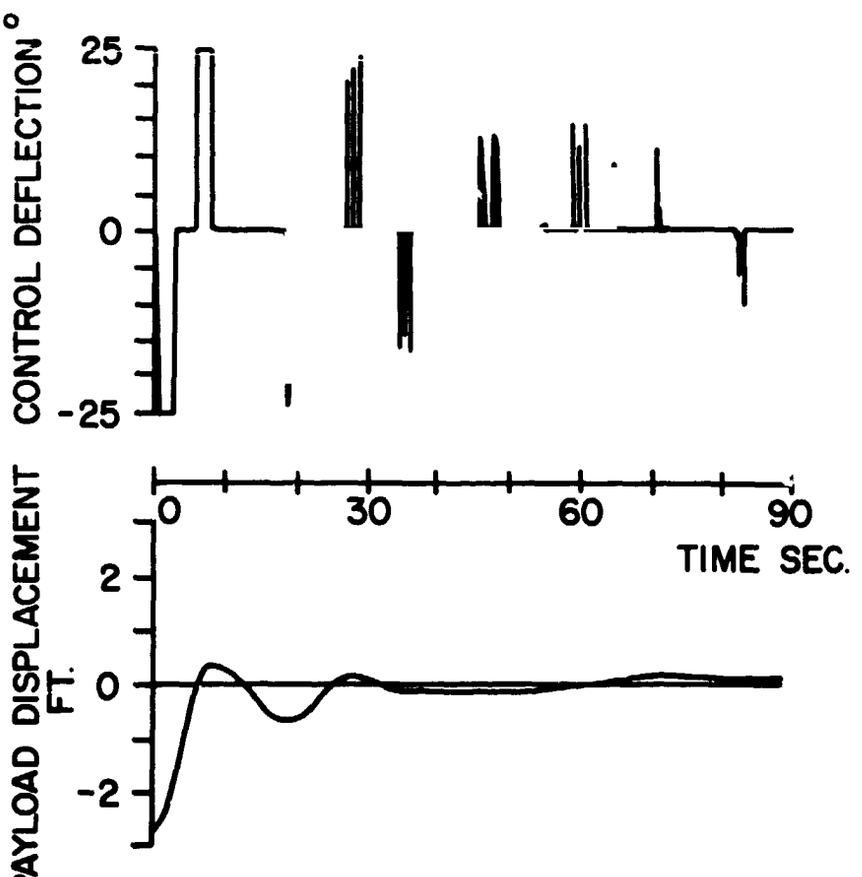

TYPICAL HUMAN CONTROL RESPONSE

PERIOD = 27 SEC., ζ = .018

UPDATE INTERVAL = 50 ms

FIGURE 8

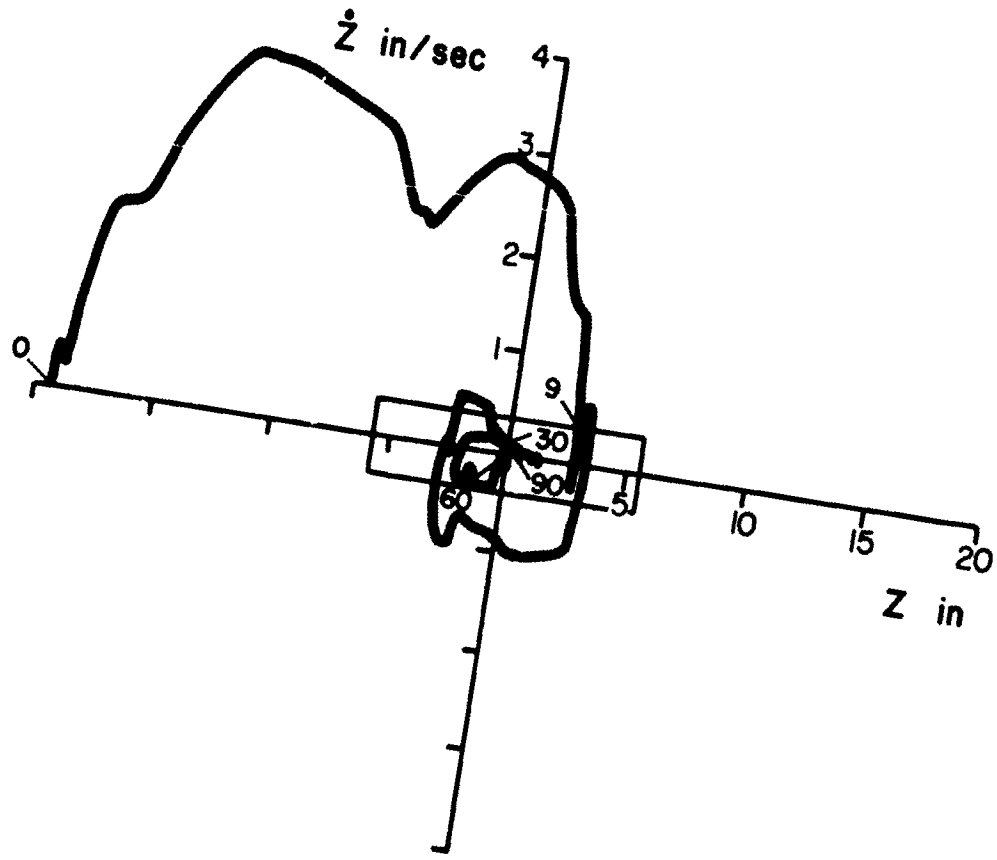

PHASE PLANE PLOT
PAYLOAD DISPLACEMENT
UNDER HUMAN CONTROL

PERIOD = 22 SEC., ζ = 0.08
DISPLAY UPDATE INTERVAL = 50 ms

FIGURE 9

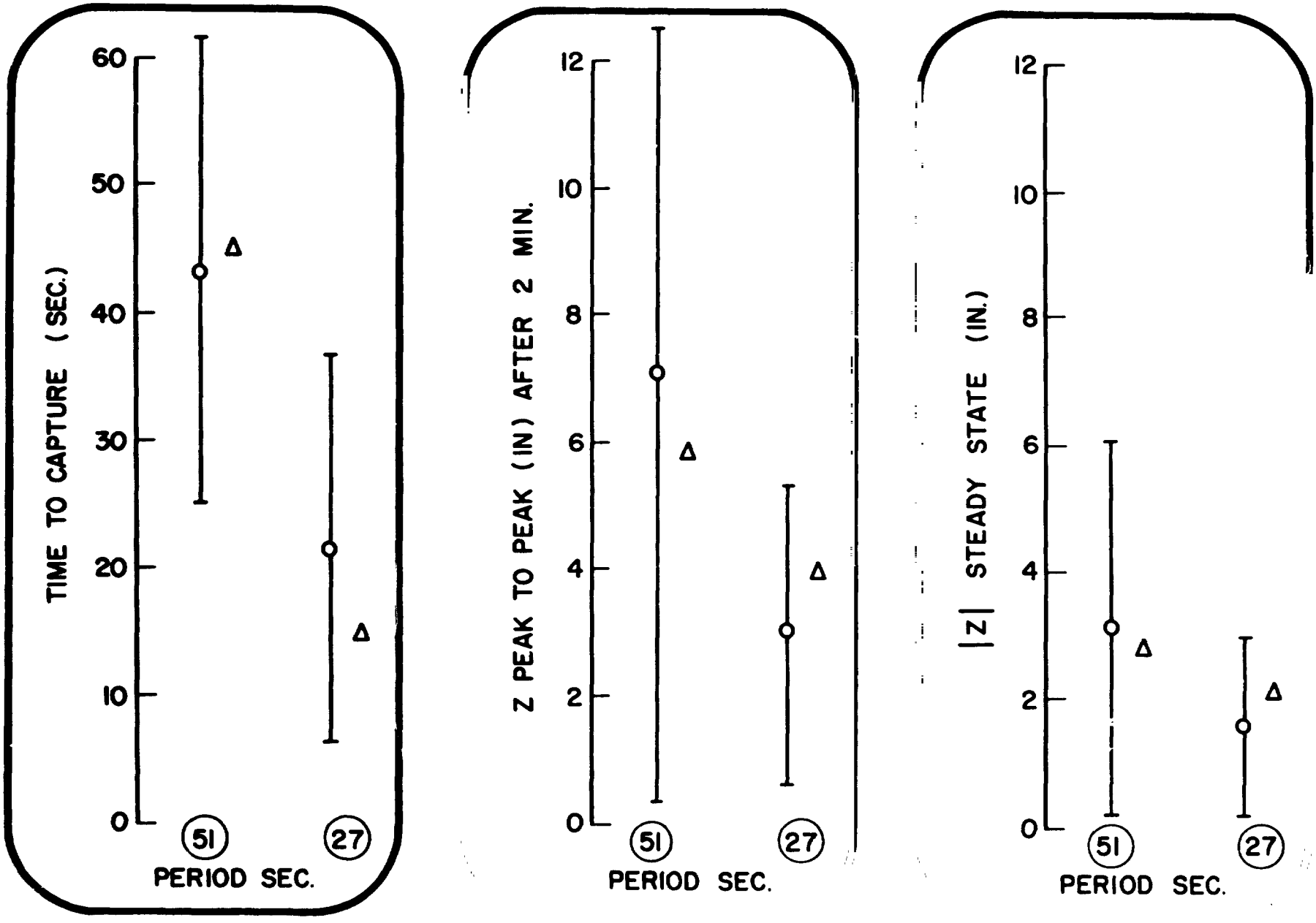

FIGURE 10

UPDATE INTERVAL 50 ms o ; 2000 ms Δ
40 REPLICATES

MODELING A MANIPULATION TASK OF VARIABLE DIFFICULTY

John W. Hill
Stephen J. Matthews

Stanford Research Institute

SUMMARY

In this paper we describe a manipulation experiment of variable difficulty carried out with an Ames manipulator, Rancho manipulator, and the unencumbered human hand. The difficulty of the task is changed not by varying the precision in the usual manner but by varying the number of degrees of freedom (or constraints) of a fitting operation. The goal of this work is to model human performance with real-world tasks.

The preliminary model developed to describe the experimental results requires that the tasks be broken down into consecutive phases or therbligs similar to the units used in industrial time and motion analyses. This model has several advantages over the information-theory model (Fitts' law) proposed in reference 1. For example, the index of difficulty for nonprecise tasks is zero. In Fitts' approach, the index of difficulty for such tasks remains large, and his original model cannot be easily extended to predict the manipulator results from the hand results as can the consecutive-phases model. We also develop an explanation for the failure of Fitts' law in high-precision tasks where the task time increases abruptly as the precision exceeds a certain limit.

INTRODUCTION

Previous experiments have examined manipulation tasks such as placing a peg in a hole where the difficulty was controlled by the precision of fit (references 1 through 6). In this study, we describe a manipulation task where the difficulty is controlled by varying the degrees of freedom; the translational and rotational degrees of freedom of the task are constrained one by one, and the real-time trajectories are recorded and analyzed. The constraints will be measured as degrees of constraint (DOC) after the system introduced in reference 7. As the number of degrees of freedom are reduced, the DOCs increase from 0 to 6. This approach allows us to extend the results of the previous laboratory studies to real-world tasks which seldom fit the positioning and peg-in-hole tasks often used.

Fitts has shown that the completion time for a number of different tasks is proportional to the task difficulty expressed in bits,

$$\text{movement time} = a + b\ (\text{index of difficulty}). \tag{1}$$

This relation is commonly referred to as Fitts' law. Neither intercept a nor slope b are the same, however, for a complex task, such as placing a peg in a hole, or for a simple task, such as touching the inside of a rectangular bar with a pencil point. These constants also change by a large amount (10 to 1) with different manipulators.

The usefulness of Fitts' law in describing actual manipulation data is limited to a moderate range of difficulties, between 5 and 10 bits. When difficulties are less than 5 bits, time is required for the trajectory and does not go to 0 with zero difficulty. An offset, proposed in reference 3, assumes that the subject is aiming for the far side of the target rather than at the center. Another failure is with very precise tasks having difficulties greater than 10 bits; here, time increases disproportionately as the difficulty is increased. After a point, such tasks take so long that they effectively cannot be done.

Another problem with Fitts' law is in calculating the index of difficulty (I_d) of the task. For example, consider Task A in figure 1. The difficulty in touching the inside of a rectangle of height H and width W, from distance d, with a pointed tool is (reference 1)

$$I_d = \log_2\left(\frac{2d}{W}\right) . \tag{2}$$

The question is to determine how the difficulty changes as the height of the rectangle is decreased (Task B in figure 1). If movements on the two axes are independent, the difficulties could be summed on the two axes. In Task B, this leads to the solution,

$$I_d = \log_2\left(\frac{2d}{W}\right) + \log_2\left(\frac{0}{H}\right) . \tag{3}$$

The 0 in the numerator of the second term is the distance on the vertical axis corresponding to d on the horizontal axis of the task. The second term

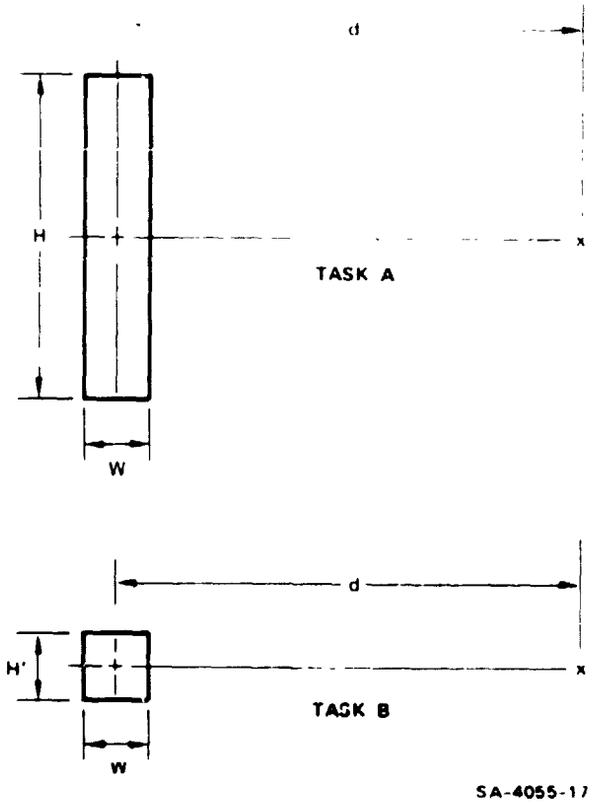

FIGURE 1 TWO SIMPLIFIED TASKS

evaluates to minus infinity, and it is impossible to assign a physical meaning to this result.

This example is just a simple case showing the difficulties that arise when we try to apply Fitts' approach to fitting real objects together. If the tool in the above example were not a point but a rectangular bar (figure 2), the task would be even more difficult to quantize. To enter the hole, not only must the tolerances on the x- and y-axes be within the tolerances (W-w) and (H-h), but the rotational orientation around the z-axis must be within certain limits. These limits are described by the three-dimensional volume illustrated in figure 3. Outside these limits, the block will not enter.

Furthermore, if the block is to descend into the hole, tolerances on the two additional angles (θ_x and θ_y defined in figure 2) must also be within certain limits. If the receptacle or the manipulator have adequate compliance, the object need only be inserted into the hole; the full insertion will be no more difficult than the entry. If, however, the receptacle and manipulator are rigid, the θ_x and θ_y tolerances will increase the difficulty of the insertion task.

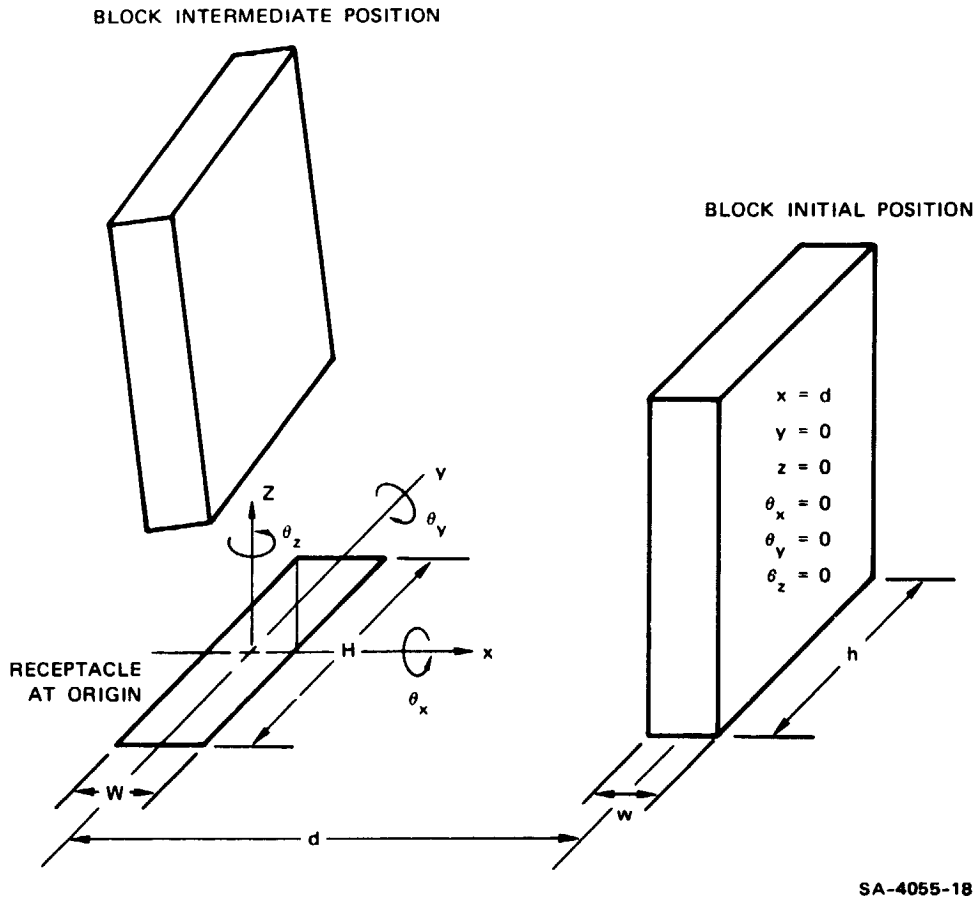

FIGURE 2 REALISTIC TASK TO BE ANALYZED

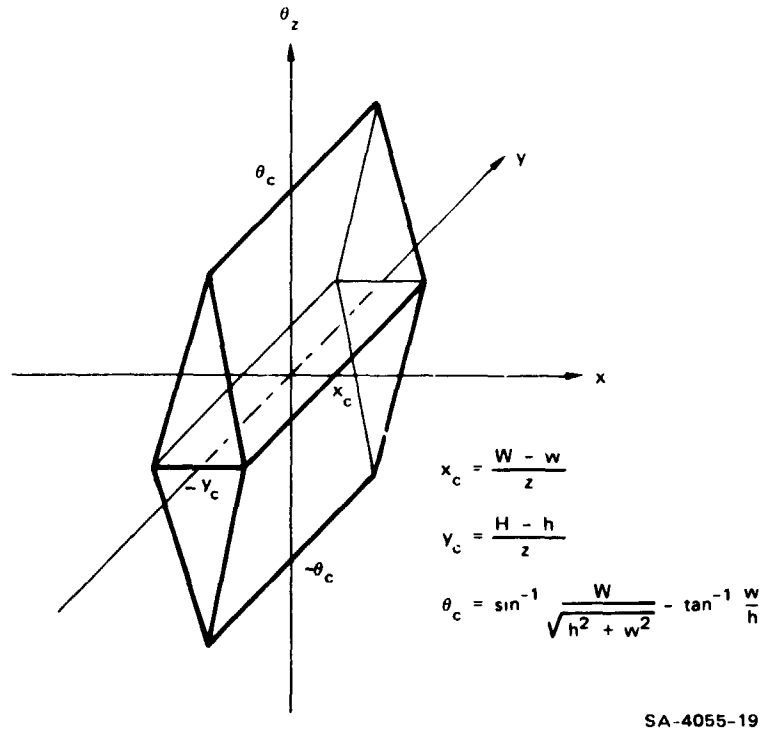

FIGURE 3 ENTRANCE VOLUME

The parallelopiped describes the coordinates of the base of a rectangular block permitting entrance into a rectangular hole.

We know intuitively that, even when the tolerances are the same, inserting a bar into a hole will be more difficult than inserting a pencil point, but it is not easy to extend the formulation used in reference 1 to such a realistic case. In figure 2, only motion along the x-axis contributes a finite difficulty; alignments on the other four axes require no motion and all evaluate to minus infinity. We could begin immediately to speculate about different means for measuring the difficulty of such real-life tasks; however, we have decided to conduct a practical experiment to obtain a data base to test such hypotheses. The experiment requires the fitting of a tool into a receptacle where the DOCs of the task are increased one by one.

MULTIPLE DEGREES OF CONSTRAINT EXPERIMENT

Our experiment was performed with a multiple-DOC task board. The task consisted of moving a previously grasped tool to a given receptacle and inserting it into the receptacle. Tool trajectories were recorded on magnetic tapes as a function of time, using the minicomputer-based data-acquisition system described in reference 8. The variables of interest were generated by off-line computer analysis of these data tapes.

Apparatus

The multiple-DOC task board is shown in figure 4. Initially, a tool was held over the liftoff switch so that the switch was depressed until the experimenter signaled "go." The tool was then moved to the specified receptacle on the left portion of the task board and was inserted. The matching of receptacles and tools for the six tasks is illustrated in figure 5. In the 0-DOC and 1-DOC tasks, a microswitch signaled the completion of the task by lighting a lamp. In the other tasks, a linear potentiometer measured progress into the hole and triggered the lamp after a certain distance (38.1 mm) was reached.

Based on the dimensions of the tools and receptacles, the tolerances for each of the six placement tasks (0-DOC to 5-DOC) are listed in table 1. Tolerances are the total translational or rotational motion on each axis, as indicated by the dimension (W-w) in figure 2 or twice the critical distances in figure 3. In table 2, the total distances moved are those traversed by the end point of the manipulator, not the end point of the tool. When the Rancho arm was used, the initial angles (θ_{xi} and θ_{zi} in figure 4) were -20° and 0°, respectively; for the Ames arm, they were 10° and -30°. These angles were chosen for convenience in holding the tools over the liftoff switch.

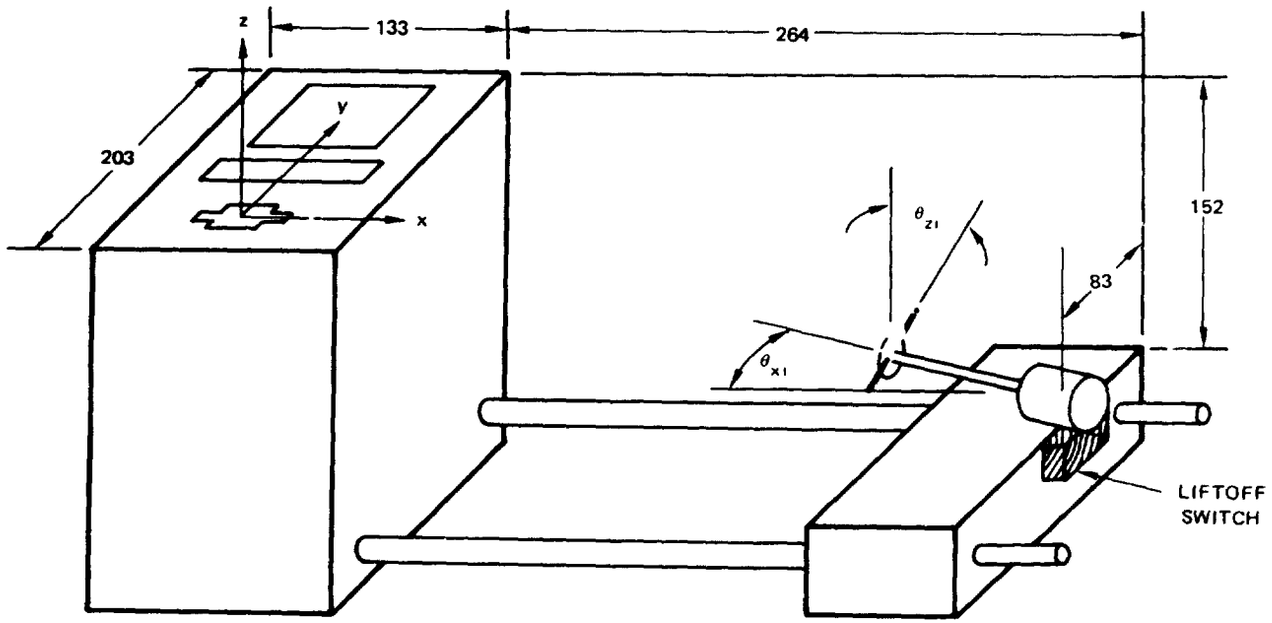

NOTE: Dimensions in millimeters.

SA-4055-20

FIGURE 4 6 DOC TASK BOARD

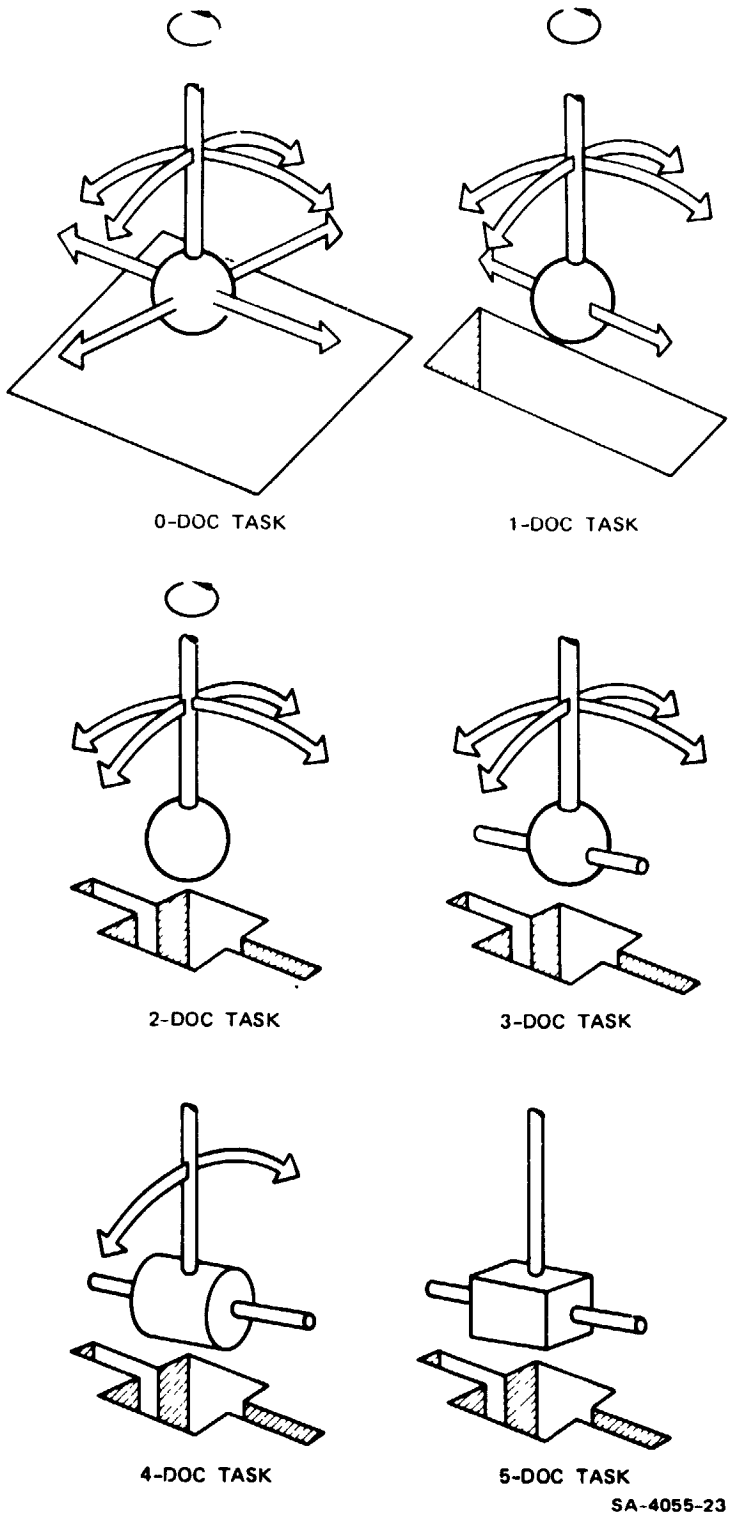

FIGURE 5 FITTING TOOLS INTO SPECIAL HOLE
Arrows indicate free angular alignments.

Table 1

TOLERANCES OF THE MULTIPLE
DEGREES OF CONSTRAINT TASK BOARD

Task	ΔX (mm)	ΔY (mm)	$\Delta\theta_x$ (degrees)	$\Delta\theta_y$ (degrees)	$\Delta\theta_z$ (degrees)
0-DOC	71.4	76.2	180	180	360
1-DOC	76.2	3.2	76	150	360
2-DOC	3.2	3.2	42	47	360
3-DOC	2.4	3.2	42	47	3.0
4-DOC	2.4	3.2	42	18	3.0
5-DOC	3.2	3.2	18	20	3.0

Table 2

BASIC DISTANCES AND ANGLES MOVED IN THE DOC TASKS
(distances in mm; angles in degrees)

Task	X	Y	Z	Straight-Line Distance	θ_x	θ_y	θ_z
0-DOC	322	48	-373	495	0	90	0
1-DOC	319	-10	-373	490	0	90	0
2-DOC	319	-59	-373	494	0	90	0
3-DOC	319	-59	-373	494	0	90	0
4-DOC	319	-59	-373	494	0	90	0
5-DOC	319	-59	-373	494	0	90	0

Procedure

The three manipulating means used in this experiment were the Rancho arm, Ames arm, and an unencumbered hand. Two male subjects participated in all three parts of the experiment.

Each experimental run consisted of one trial with each of the DOC tasks. Runs were repeated ten times for each subject. The order of presentation of

the different DOC tasks was randomized for each run. Several practice trials were performed prior to data collection. The subject and experimenter exchanged roles to provide rest periods. Continuous operation was limited to less than 30 minutes without rest.

Contour pads fitted to the manipulator jaws (on both the Rancho and Ames arms) ensured proper tool location in the jaws. The pads also served to eliminate any possible slipping of the tools in the jaws during final positioning.

Results

The mean times for the two subjects during ten repetitions of the tasks are plotted in figure 6. The results obtained from the two manipulators and the hand indicate a general increase in the task time as the constraints of the task are increased. The task times with the human hand and Ames manipulator were particularly linear with the number of DOCs; the linear trend accounted for at least 95 percent of the variance, and the nonlinear components were not statistically significant. The task times with the Rancho manipulator was not linear, and the cubic or S-shaped component was statistically significant [$F(1,90) = 5.25$, $p < 0.05$]. Completion times for the tasks varied greatly among the manipulators; the Ames was approximately four times slower and the Rancho was approximately 20 times slower than the hand.

The normalized task times plotted in figure 7 were obtained by dividing each time by the time for the 0-DOC task. The resulting spread between the three manipulators indicates that this simple scaling does not account for the differences observed; in particular, as the rotational constraints of the 3-DOC and 4-DOC tasks are added, a disproportionately longer time is required compared to the simpler tasks. In other words, the DOC measure does not produce an index of difficulty that satisfactorily unifies the human and manipulation results.

BREAKDOWN INTO SUBTASKS

We wish to determine whether there is a natural breakdown of the manipulation tasks into the therbligs traditionally used in time and motion studies (reference 8). The therbligs for this task are transport loaded and position. The first therblig describes the motion between the liftoff switch and a close proximity to the hold, and the second indicates the alignment or orientation of the tool to the receptacle.

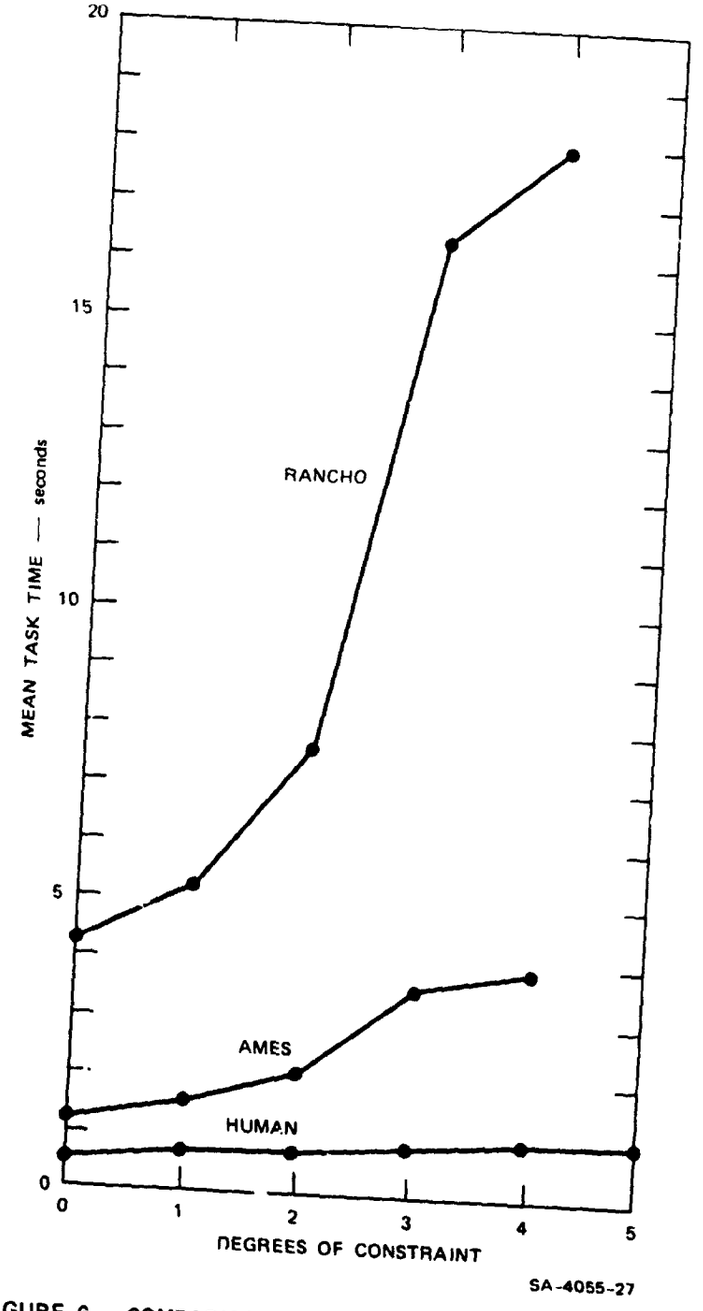

FIGURE 6 COMPARISON OF THE THREE MANIPULATORS

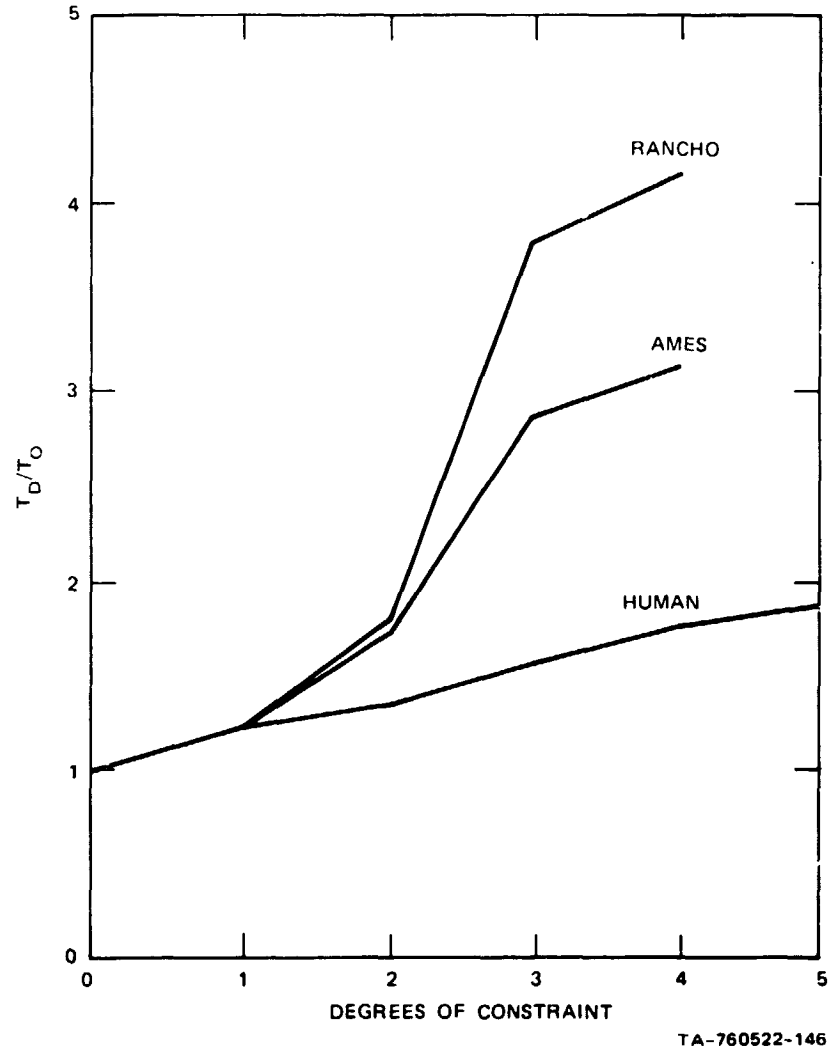

FIGURE 7 NORMALIZED RESULTS OF THE THREE MANIPULATORS

Using the digitized trajectories recorded on magnetic tape, the x, y, and z coordinates of the tool at the first contact with the hole were obtained. By comparing x, y, and z coordinates measured at previous points on the trajectory, the times to a given distance from the contact position were obtained. Times from two intermediate distances from the receptacle to the end of the trajectory are plotted in figure 8 for the three manipulators of the experiment.

Time for the first part of the trajectories from liftoff to a distance of 25 or 50 mm from the hole (corresponding to the transport therblig) is relatively independent of the DOCs. This is evidenced by the nearly

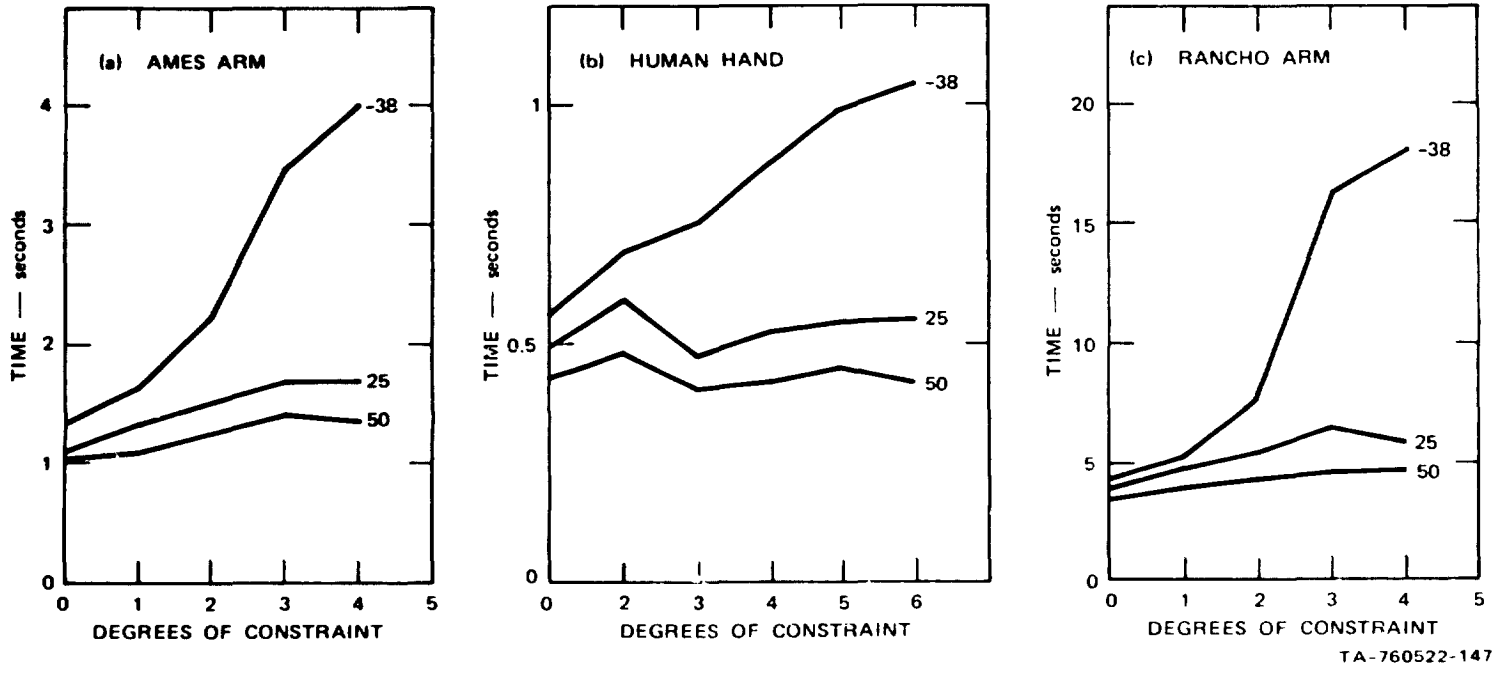

FIGURE 8 COMPARISON OF THE THREE DIFFERENT MANIPULATIONS. Task times are shown as a function of distance in millimeters from first contact with the hole: -38 mm corresponds to full insertion, 0 to first contact, and 25 mm and 50 mm to the first time those distances were obtained from the contact point.

horizontal lines in the lower part of the figure. For the human hand, these results are horizontal; however, for the two manipulators, there is a slight upward slope which indicates a more conservative strategy as the DOCs increase. These results are similar to those described in references 2 and 5 where the transport times were found to be independent of task difficulty. The second phase of the trajectories, between 25 to 50 mm of the receptacle to full insertion (corresponding to the position therblig), depends greatly on the DOCs.

There are several major differences between the unencumbered-hand and manipulator therbligs. For both manipulators, the transport time (time to 25 mm of first contact) increases approximately 10 percent per DOC instead of remaining constant as it does for the human hand. The position therblig for the manipulators is more time-consuming than that for the hand.

MODELING EXPERIMENTAL RESULTS

The DOC measure does not take into account the tolerance of the task. In a task with a fixed number of DOCs, time is proportional to an index of difficulty. In many tasks, this takes the logarithmic form previously given in equation 2. The problem here is to extend the approach originated in reference 1 and subsequently used by others to realistic tasks with constraints on several axes.

Using an information-theory approach, Fitts proposed that the decrease in uncertainty of the task be calculated by subtracting the uncertainty of the final position from the uncertainty of the initial position. For these uncertainties, he used

$$H_{final} = \log_2 \Delta x \tag{4}$$

$$H_{initial} = \log_2 2x, \tag{5}$$

and the resulting difficulty index is

$$I_d = H_{initial} - H_{final} = \log_2 \left(\frac{2x}{\Delta x}\right) . \tag{6}$$

In this case, the initial uncertainty of the object is twice the reach distance, and Fitts' formulation inherently assumes that the initial position of the object is uniformly distributed between +x and -x from the final position. This approach is incorrect because, in most cases, the initial position is well known. For example, if the object is held in a fixture, all its coordinates and angles are known exactly and its initial uncertainty is zero.

A new approach to the analysis of the task combines the results of the time and motion studies and the information-theory approach. We assume that the motion is composed of two parts, an initial but uncertain open-loop trajectory between the initial and final positions, followed by a corrective-positioning motion. This approach is supported by references 2 and 6 in which it was observed that, in the first part of the manipulation tasks, the trajectory time from initial to final position is independent of task difficulty. All variability in the task time with difficulty must occur in the final positioning phase.

To determine the feasibility of this two-phase model, we conducted a simple experiment, using the same unencumbered hand and the Ames and Rancho manipulators. The standard deviation of the open-loop positioning error was measured by having two subjects make 20 moves each from a fixed initial point toward a final point separated by 500 mm. They were instructed to shut their eyes as the move began and not to open them until after the move was finished. For the translation measurements, a string tensioner was attached to the tip of a pencil-like tool to measure the position after each move. Angular motions were measured by having the subjects turn a potentiometer fitted with a pointer and graduated scale between two fixed angles. The results of these experiments are listed in table 3.

Table 3

STANDARD DEVIATIONS FOR SINGLE-AXIS MOVES

Manipulator	σ_x (mm)	σ_θ (degrees)
Human hand	7.5	5.4
Ames	28	3.7
Rancho	29	4.7

In this two-phase approach, the initial uncertainty is zero because the position of the tool is known. The intermediate uncertainty of the normal distribution of errors after the open-loop move is

$$H_{intermediate} = \log_2 \sqrt{2\pi e}\ \sigma \doteq 2.05 + \log_2 \sigma, \qquad (7)$$

where σ is the standard deviation of the normal distribution. We assume that the shape of the distribution after final positioning is the clipped distribution shown in figure 9. Its uncertainty is approximately that of a rectangular distribution if Δx is small,

$$H_{final} \doteq \log_2 \Delta_x \qquad \Delta_x < 2\sigma, \qquad (8)$$

and is approximately that of the original distribution if Δx is large,

$$H_{final} \doteq H_{initial}, \qquad \Delta x > 5\sigma.$$

The reduction in uncertainty ($H_{initial} - H_{final}$) for intermediate values of Δx obtained by numerical integration are plotted in figure 10.

If the translational and rotational errors given in table 3, which are measured on only one axis, are assumed valid for all axes, then the uncertainty after the open-loop move can be calculated. Using the dimensional tolerances for the task board in table 1, the standard deviations in table 3, and the formulation in figure 10, we obtained the indices of difficulty for each manipulator, as plotted in figure 11.

One of the surprising results of this analysis is that there is very little difference in difficulty between the 2-, 3-, and 4-DOC tasks. The orientational constraints introduced by these tasks are much less than the open-loop positioning ability of the subjects. The round-bottomed tools employed in the first four tasks may also have less than the calculated difficulty because of their self-guiding behavior when inserted into the hole.

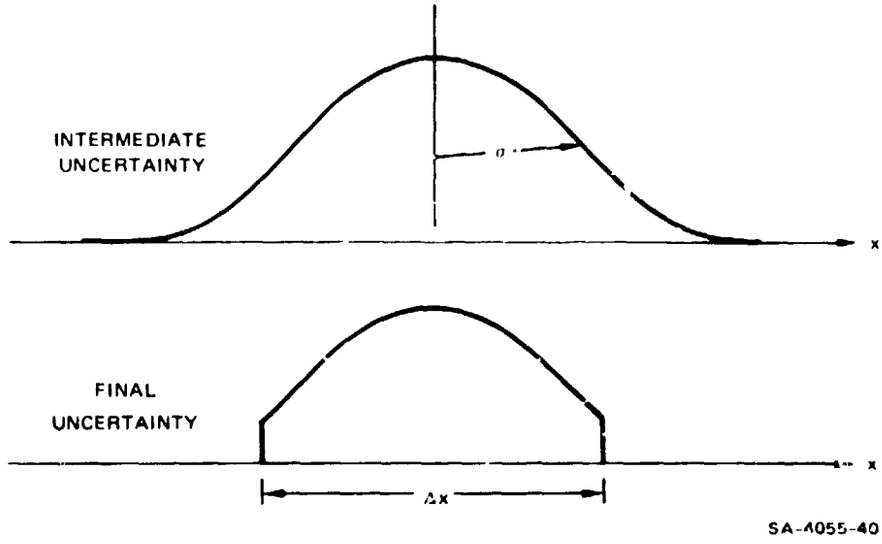

FIGURE 9 CLIPPING OF NORMAL DISTRIBUTION

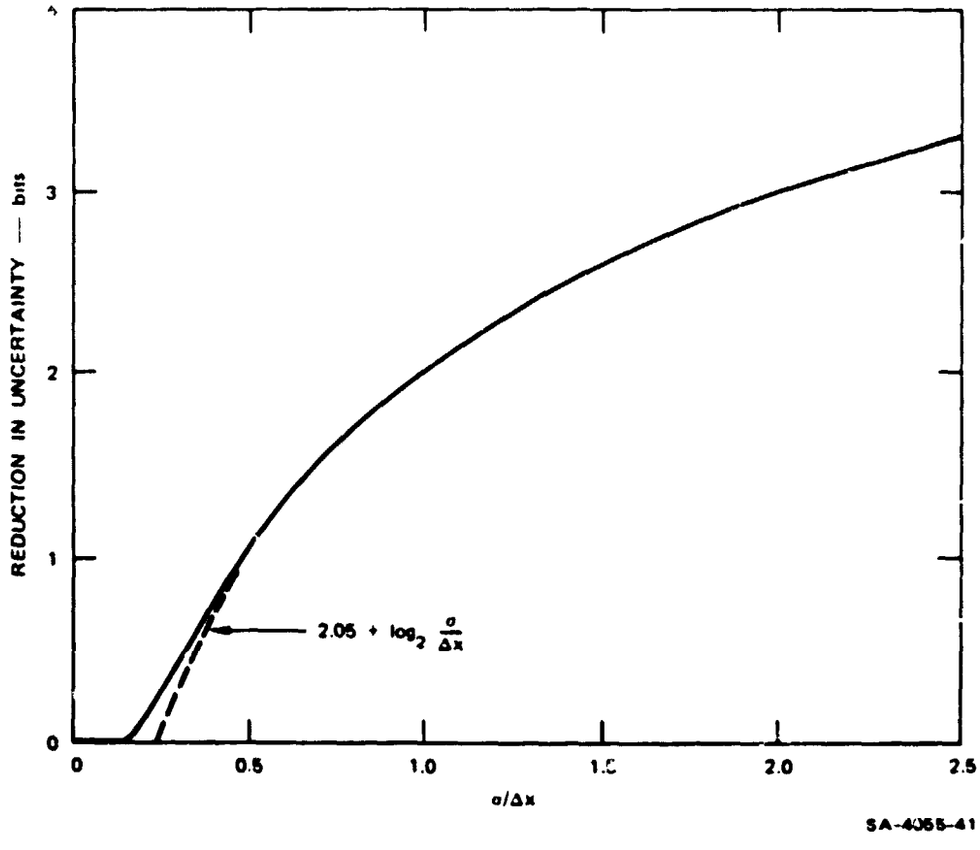

FIGURE 10 NUMERICAL INTEGRATION RESULTS

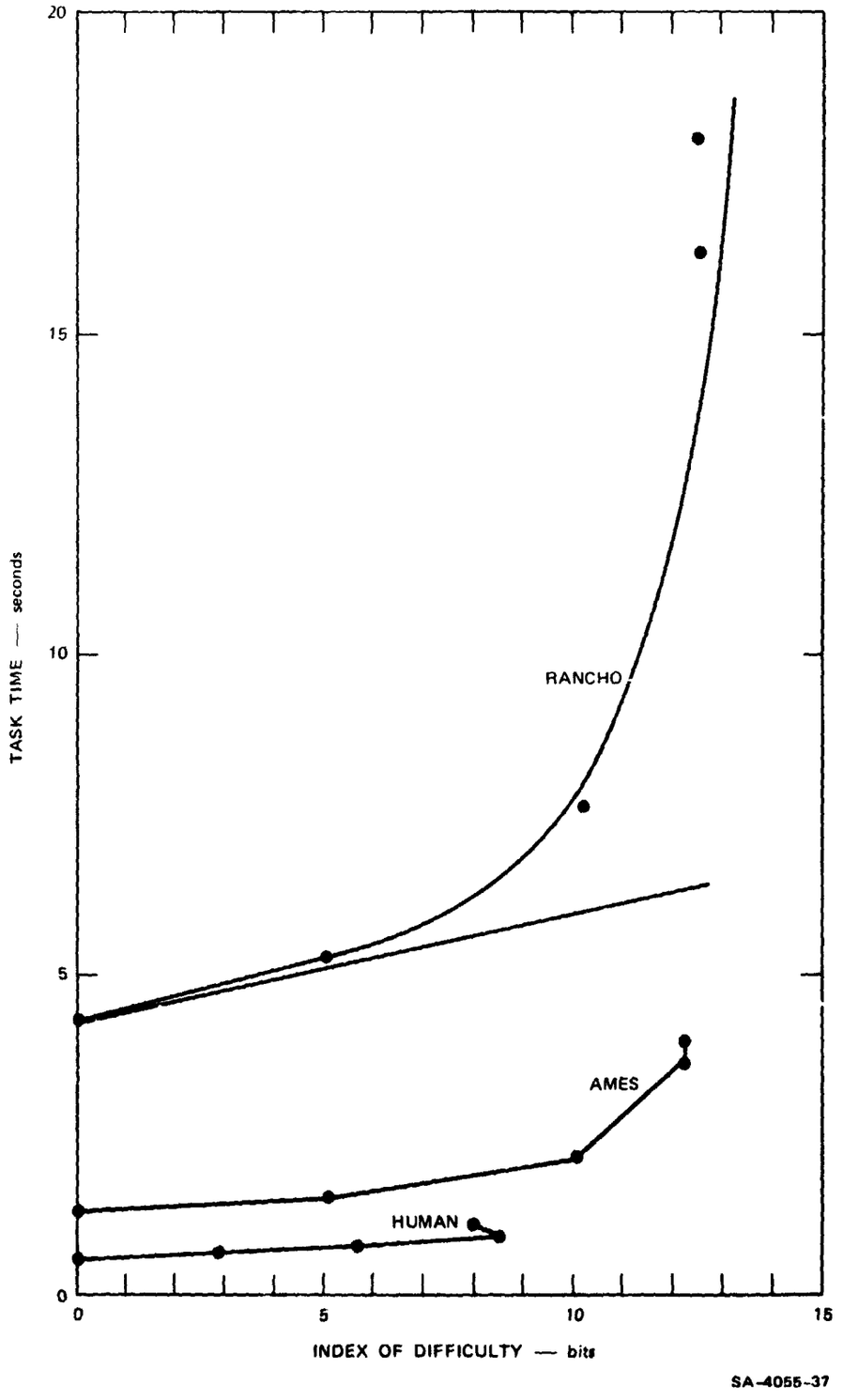

FIGURE 11 EXPERIMENTAL RESULTS WITH NEW INDEX OF DIFFICULTY

One advantage of the task model is that the 0-DOC task has practically zero difficulty because the receptacle is large enough for the tool to be inserted with the eyes closed. In contrast, Fitts' formulation [equation (2)] yields a task difficulty of 3.8 bits. The time we measure for the 0-DOC task is then the time for the transport therblig which is assumed constant for all the tasks. A second advantage of the model is that the difference between manipulators may be largely resolved into different time factors. When the task times of each manipulator are normalized by dividing by the 0-DOC task time, the curves superimpose as shown in figure 12. This attributes one portion of the time to the task--the part that changes with the index of difficulty--and a second that multiplies the first--a constant for each manipulator.

The disadvantage of the model is that the results are not linear at high difficulties. This may be caused by underestimating the difficulties on the 3-, 4-, and 5-DOC tasks. For example, the 4- and 5-DOC tasks have the same difficulty, but the 5-DOC task always takes a longer time. A possible explanation for the upward curving lines of figure 11 may be the limited accuracy of even the smallest moves. The small moves of the Rancho manipulator approach a limit cycle with a standard deviation of 3 mm and 1.2°. In this limit cycling, there is only a fixed probability of entering the receptacle within the correct positions and angles for each move. With each added bit of difficulty, the probability of being in the correct positions and angles reduces by one-half. For example, consider the probability of being inside the parallelopiped in figure 3 when the uncertainty of the tool is described as a sphere around it. With each added bit of difficulty (or uncertainty), the probability of entering the parallelopiped decreases by half and the number of moves or time to enter doubles. The curve in figure 11 describes this phenomenon for the Rancho results. The mathematical form of the curve is

$$T = 0.20\, I_d + 2^{(I_d - 10.0)}, \qquad (10)$$

where the first term denotes a slope (the portion where Fitts' law applies), and the second term represents the limited positioning ability of the arm.

A real-time explanation of this behavior is plotted in figure 13. The first phase of motion is the open-loop move toward the target. The accuracy at the termination of this phase is roughly that required by the 0-DOC task. This is followed by an exponential decrease in position error, the exponential-alignment phase in which the accuracy increases by a factor of 2 every 0.20 seconds (for the Rancho arm, see equation 10). The 1- and 2-DOC tasks fall in this region for the Rancho. After the uncertainty has been reduced by

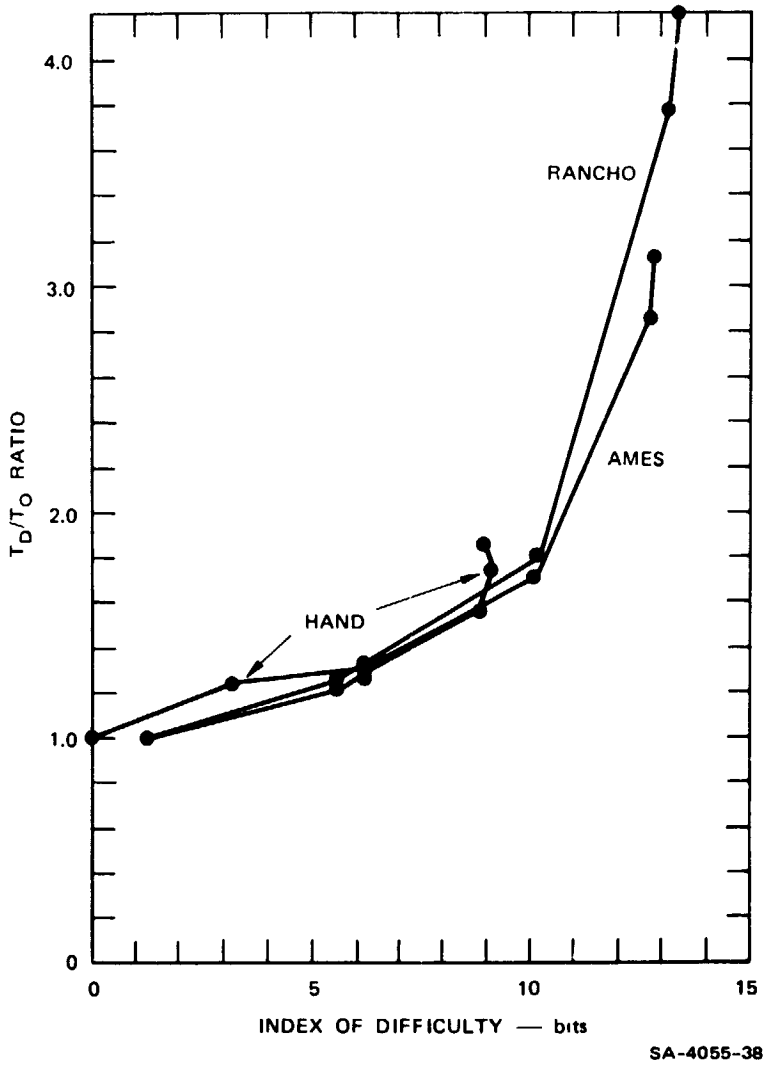

FIGURE 12 NORMALIZED EXPERIMENTAL RESULTS

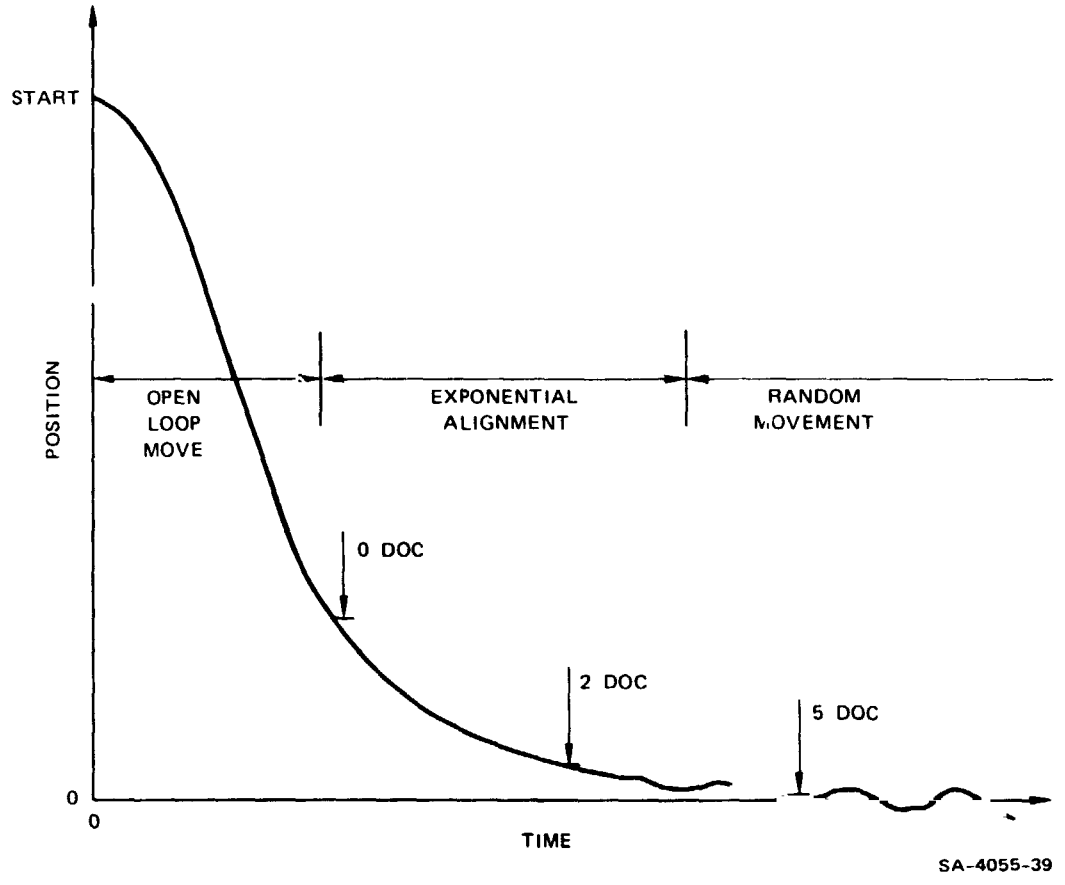

FIGURE 13 PHASES OF MANIPULATION ACTIVITY

10.0 bits (again for the Rancho arm), the random-movement phase begins, corresponding to the 4- and 5-DOC tasks. During this last phase, there is only a fixed probability of completing the task per unit time.

REFERENCES

1. Fitts, P. M.: The Information Capacity of the Human Motor System in Controlling Amplitude of Movement. J. Exp. Psychol., Vol. 47, (1954) pp. 381-391.

2. Annett, J.; Golby, C. W.; and Kay, H.: The Measurement of Elements in an Assembly Task - The Information Output of the Human Motor System. Q. J. Exp. Psychol., Vol. 10 (1958), pp. 1-11.

3. Welford, A. T.: The Measurement of Sensory Motor Performance: Survey and Reappraisal of Twelve Years Progress. Ergonomics, Vol. 3, 1960, pp. 189-230.

4. Fitts, P. M.; and Pet son, J. R.: Information Capacity of Discrete Motor Responses. J. Exp. Psychol., Vol. 67, No. 2, 1964, pp. 103-111.

5. McGovern, D. E.: Factors Affecting Control Allocation for Augmented Remote Manipulation. Ph.D. dissertation, Stanford University, Stanford, California, November 1954.

6. McGovern, D. E.: Comparison of Two Manipulators Using a Standard Task of Varying Difficulty. Paper 74-WA/Bio-4, presented at the Annual Meeting of the ASME, New York, November 1974.

7. Mundel, M. E.; and Lazarus, I. P.: Predetermined Time Standards in the Army Ordinance Corps. J. Ind. Eng., November 1954, pp. 13-20.

8. Hill, J. W.: McGovern, D. E; and Sword, A. J: Study To Design and Develop Remote Manipulator System. Final Report, NAS 2-7507, Stanford Research Institute, Menlo Park, California, May 1974.

9. Niebel, B. W.: Motion and Time Study. 5th edition, R. D. Irwin, Inc., Homewood, Illinois, 1972.

NOTES

The work reported it this paper was supported by National Aeronautics and Space Administration under contract NAS2-8652 with Stanford Research Institute. The authors wish to acknowledge the contribution of Douglas E. McGovern in carrying out the dof-experiment and developing much of the data processing software.

A COMPARISON OF MASTER-SLAVE AND RATE CONTROL IN THE PRESENCE OF A TRANSMISSION TIME DELAY

By Gregory P. Starr

Stanford University

SUMMARY

When a time delay is inserted into the feedback loop of a manual control system, in this case a remote manipulator system, certain characteristics of the control system may change in importance. We conducted a one-dimensional discrete tracking experiment to simulate manipulation and compared three controllers. Performance using a joystick rate controller degraded less with increasing time delay than that using the same joystick as a position controller. The results indicate the need for a comparison using a manipulator system.

INTRODUCTION

When a time delay is inserted into the feedback loop of a man-manipulator system as occurs when the manipulator is very distant, the normal temporal organization of stimulus and response is disrupted. This disruption has been shown (references 1, 2, 3) to be very detrimental to performance.

Ferrell (reference 1) found that his subjects used one of two strategies to deal with the time delay. The first strategy, that of moving slowly, requires the operator to keep track of his movements for one full delay period in the past to predict the position of the manipulator. This is very difficult to do with delays of several seconds and operator frustration often occurs.

The second strategy, which was called "move-and-wait" by Ferrell, was spontaneously adopted by seven of his eight subjects. In the move-and-wait strategy, moves are made open-loop, i.e. without visual feedback, then the control is held stationary until the manipulator "catches up." Ferrell's results were obtained using a simple two degree-of-freedom manipulator. In subsequent experiments Blackmer (reference 2) and Black (reference 3) both observed the move-and-wait strategy being followed using a six degree-of-freedom manipulator. Although all of these studies were carried out using master-slave position control, Ferrell believed that the move-and-wait strategy would be used with rate control as well.

Both Blackmer and Black noted a problem in using the move-and-wait

strategy: the subjects often had trouble holding the master control motionless while waiting for the manipulator to respond. Undesired "drifting" of the control made it more difficult for them to use the move-and-wait strategy.

A master controller with an operator-actuated brake which would provide positive locking of the master, a completely counterbalanced master, or a spring-centered rate controller are controllers which would make it easier for the operator to hold the manipulator motionless while waiting for feedback.

Tracking and Manipulation

Some aspects of manipulation resemble pursuit or compensatory tracking. Many of the motions involved in manipulation have as their goal the minimization of a visually perceived error, which is the definition of tracking.

The manipulation task differs from continuous tracking tasks in that all of its elements except the manipulator are usually motionless, and therefore the manipulation task is a self-paced task. In contrast, a continuous tracking task requires the operator to follow a constantly moving target. Discrete tracking provides a situation similar to manipulation, since the target is not moving during the positioning task.

Perhaps the main difference between tracking and manipulation is the number of degrees of freedom of the controlled element. Tracking usually involves one or occasionally two degrees of freedom, while manipulation ordinarily requires control of six.

Taking into account the differences between tracking and manipulation, we feel that a sufficient degree of commonality exists between them to justify the use of a discrete tracking task as a preliminary experiment in an investigation of position versus rate control of a manipulator.

EXPERIMENT

We performed a discrete tracking experiment with controller, target distance, and time delay as the variables. The task was to bring a dot, the controlled element, into the target as quickly as possible. The target was represented by two vertical lines. The dot and target were both displayed on a closed circuit TV monitor. The target lines were three cm. in length and were 0.88 cm. apart. The dot was one mm. in diameter. The task was completed when the subject kept the dot continuously inside the target for two seconds. After the completion of the task, the target then appeared at a new location on the TV monitor, signifying the beginning of another task.

Generation of the target lines and dot as well as data acquisition was done by an IBM 1800 digital computer. The computer program which generated the display used a sampling rate of 120 samples per second to insure a flicker-free image. The positions of the dot and target were recorded on magnetic tape during each sample frame. This provided an accurate recording of the subjects' performance. These tapes were the data base from which all

of the results were extracted.

The dynamics of the dot were either zeroth order, corresponding to position control, or first order, corresponding to rate control. In neither case were effects such as inertia, damping, or static friction simulated.

Controllers

Three controllers were used in the experiment; two for position control and one for rate control. The controllers were a joystick for position control, the same joystick for rate control, and a linear displacement position control. These controllers were respectively analogous to the following manipulator controllers: master-slave control, spring-centered rate control, and counterbalanced or lockable master-slave control.

The joystick position controller was originally a three-axis joystick. We physically locked out the yaw axis and used the roll axis as the command axis. Position of the dot was proportional to stick deflection about this axis. The joystick was spring centered but there was no detent at the center position. The torque/deflection ratio of the joystick was 1.16 newton-meter/radian.

The second position controller is termed a linear displacement control. The position of the dot was proportional to the position of the controller handle along its axis. The primary reason this controller was included for study is that no force need be applied to the controller to hold it stationary at an arbitrary position. This was true of the joystick. A subject could remove his hand from the linear position control and the control would remain in position. We felt that this would prove advantageous when using the move-and-wait strategy.

The third controller was the same joystick previously described, but this time used as a rate controller. The characteristics of the joystick were the same as before, with one important difference, which was the use of a centering detent. This provided a positive indication of the center position. The velocity of the dot was proportional to the deflection from center of the joystick. When the operator removed his hand from the joystick, the center detent insured that the velocity of the dot would be zero.

Controller Gains

One characteristic of the tracking system which has not been mentioned is the controller gain, i.e. the amount of dot motion produced by a unit displacement of each controller. The gain for both position controllers was dictated partially by hardware considerations. The optimal rate gain was determined experimentally.

Gibbs (reference 4) investigated the choice of gain in a position control tracking system using thumb, hand, and forearm controlled joysticks. He found that best results were obtained with the lowest controller gains. We decided on the basis of Gibbs' findings to set the position controller

gains as low as possible. Considering the range of motion of the joystick position controller and the necessary range of motion of the dot, the resulting gain for this controller was 33.8 cm. of dot motion per radian of stick rotation. In terms of stick tip translation the gain of the joystick was 2.65 cm. of dot motion per one cm. of joystick tip translation. We wished to set the gain of both position controllers at the same value, so dissimilar gains would not be the cause of differences between them. The gain for the linear position control was therefore also set at 2.65 cm. of dot motion per one cm. of handle motion.

We conducted an experiment to determine the optimum gain for our rate controller. Two subjects, both right-handed and with good vision, participated in the experiment. We investigated six rate gains. The gains, expressed as ratios of dot velocity in radians/second at the subject's eye divided by joystick deflection in radians, were 0.20, 0.30, 0.40, 0.50, 0.60, and 0.70 seconds^{-1}. The corresponding maximum dot velocities were 9.86, 14.72, 19.73, 24.66, 29.89, and 34.01 cm/second measured at the display. Data were taken at no delay and with a 1.5 second time delay.

Each subject made one run at each of the twelve conditions of rate gain and time delay. One run consisted of a sequence of 100 tasks. When the subject completed one task, the target jumped to a new position, and the next task was begun. The distance from one target to the next was randomized by using a computer subroutine to generate random numbers. The "seed" number for the subroutine was the same on each run, so the resulting random sequences were identical for all of the runs.

We obtained two performance measures: the sum of completion times for the 100 tasks and the sum of the distances moved by the dot for the 100 tasks. The completion time was defined as the time interval from the beginning of the subject's first move to the time when the dot entered the target for the last time, plus one delay time. This last delay time was added because the task cannot be considered as completed until the operator knows it is completed.

With no time delay, increasing the gain beyond 0.30 seconds^{-1} did not improve performance in terms of completion time or distance moved. With the 1.5 second time delay, the 0.30 seconds^{-1} gain was the best in terms of both measures. Therefore the 0.30 seconds^{-1} gain was selected as the optimum gain for the rate controller.

Method

We used a factorial experimental design. The factors were controller (C), time delay (T), target distance (D), and subjects (S). The controllers were the joystick position control, linear position control, and joystick rate control. The time delays were 0, 0.33, 1.0, and 3.0 seconds. Five target distances were used, 1.766 cm., 5.297 cm., 8.828 cm., 12.359 cm., and 15.890 cm., all distances measured on the screen of the display. Four subjects participated in the experiment, all were right-handed with good vision.

Each subject performed in two sessions, held on separate days. A session consisted of 12 runs, one at every condition of controller and time

delay. One run consisted of the sequential presentation of 50 targets. The course of 50 targets was pseudo-randomized over the five task distances. Constraints on the course were:

1) 10 tasks at each of the 5 distances must be presented

2) Of these 10 tasks, 5 must require dot motion from right to left and 5 from left to right.

These constraints, when combined with the magnitudes of the target distances and the width of the display, ruled out a true randomized course. The width of the display, about 25 cm., prevented certain distances and directions of the tasks from following one another. For example, a left-to-right task of 15.890 cm. could not follow a left-to-right task of 12.359 cm. In all, 4800 individual positioning tasks were completed.

RESULTS

Analysis of Variance

We perfomed an analysis of variance on the completion times and found all of the main effects (C, D, T, S) to be significant at the .01 level, as were all but one of the interactions. Since the CxDxT interaction was significant, it is not valid to test any of the lower order terms containing the C, D, or T factors against the residual. We will therefore examine the results at each condition of C, D, and T.

Figure 1 shows mean completion time vs. target distance for each controller at each time delay. Breakdown analyses of variance were done at each condition of C, D, and T, and the results are shown in Table 1. As time delay increased, performance with the joystick rate controller degraded less than with the joystick position controller at the 5.297 cm. and 8.828 cm. target distances. At the 12.359 cm. and 15.890 cm. distances the rate control system's maximum attainable velocity of 14.72 cm/second became a limitation, and at these distances the rate controller did not compare as favorably with the joystick position controller. The linear position controller, however, became the most effective controller of the three as time delay increased. These results indicate that the suitability of the controller to the move-and-wait strategy becomes increasingly important as the time delay increases.

Move Analysis

To examine the accuracy of individual moves, as well as to determine if the move-and-wait strategy was being employed by the subjects, we broke down the position vs. time record into periods of moving and waiting. The first step was development of move criteria, i.e. the conditions under which the subject would be considered to be moving. We wanted to distinguish between moves which were separated by at least one delay time and those which were not. The former were called "move-and-wait" moves, since the subject had seen the results of the previous move before making the current move, while

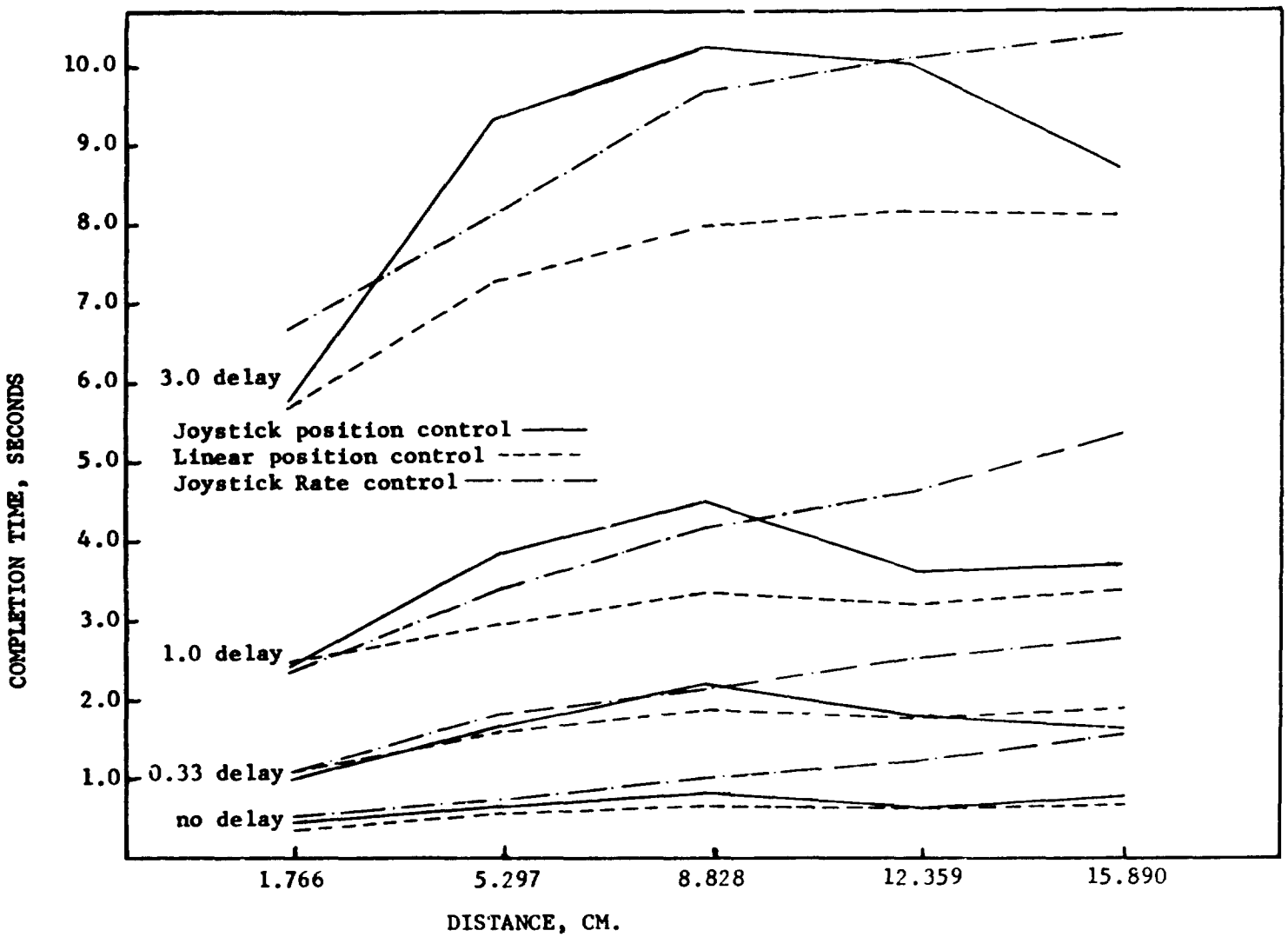

Figure 1. Completion time vs. distance at all time delays

P denotes joystick position control
L denotes linear position control
R denotes joystick rate control

Time Delay	Distance	F	sig. level %	Means			Least Significant Difference
				P	L	R	
0.0	1.766	3.96	2.5	0.297	0.283	0.405	L P R
	5.297	4.61	1	0.558	0.497	0.654	L P R
	8.828	17.15	1	0.775	0.591	0.941	L P R
	12.359	125.9	1	0.576	0.594	1.178	P L R
	15.890	139.3	1	0.730	0.635	1.548	L P R
0.33	1.766	.491	-	0.955	1.056	1.023	P R L
	5.297	.786	-	1.683	1.580	1.759	L P R
	8.828	2.40	-	2.203	1.883	2.113	L R P
	12.359	19.42	1	1.768	1.737	2.531	L P R
	15.890	30.75	1	1.601	1.840	2.746	P L R
1.0	1.766	.043	-	2.386	2.439	2.377	R P L
	5.297	5.34	1	3.769	2.912	3.346	L R P
	8.828	6.84	1	4.436	3.255	4.137	L R P
	12.359	15.83	1	3.590	3.115	4.570	L P R
	15.890	20.43	1	3.688	3.352	5.282	L P R
3.0	1.766	2.234	-	5.657	5.603	6.538	L P R
	5.297	5.431	1	9.123	7.132	8.004	L R P
	8.828	6.218	1	10.019	7.798	9.464	L R P
	12.359	5.042	1	9.829	8.032	9.881	L P R
	15.890	6.596	1	8.489	7.972	10.198	L P R

Table 1. Results of breakdown analyses of variance at each condition of distance and time delay.

the latter were designated "non move-and-wait" moves, since the results of the last move had not yet been seen when the current move was initiated. The move criteria in their final form consist of two velocity-time thresholds plus a time criterion and a distance criterion. They were the following (all distances were measured on the display):

(1) Beginning of move: velocity greater than 1.24 cm/second continuously for 0.042 seconds.

(2) End of move: velocity less than 0.52 cm/second continuously for 0.042 seconds.

(3) Moves shorter than 0.172 cm. were disregarded.

(4) If the elapsed time between the end of the previous move and the beginning of the current move were equal to or greater than the delay time, the current move was classified as a "move-and-wait" move; if not, then it was classified as a "non move-and-wait" move.

The normalized task completion time, broken down into periods of time spend executing "move-and-wait" moves, "non move-and-wait" moves, and time spend waiting, is shown in Figure 2. The percentage of time spent waiting increases with time delay, as expected from the move-and-wait strategy. The most interesting aspect of Figure 2 is the comparatively large percentage of time spent in the execution of "non move-and-wait" moves with the joystick position control. At the 3.0 second time delay, the time spent executing "non move-and-wait" moves is one-fourth the time spent executing "move-and-wait" moves. This indicates a substantial departure from the pure move-and-wait strategy with the joystick position control. The linear position control exhibits less time spent in "non move-and-wait" moving and the joystick rate controller shows the least time spent executing "non move-and-wait" moves.

It appears that the move-and-wait strategy was adhered to most rigidly by subjects when they were using the joystick rate control, and least when they were using the joystick position control. Greater adherence to the move-and-wait strategy does not necessarily correspond to better performance, but in this experiment they were correlated.

FUTURE RESEARCH

The next step is comparison of position control and rate control in controlling a multi-degree-of-freedom manipulator. The manipulator control situation is obviously much more complex than the one-dimensional task we have considered here. The difficulty of coordinating manipulator joint motions using a rate control system may more than compensate for the ease in holding the manipulator stationary during waiting periods. We are currently comparing master-slave position control and resolved motion rate control (reference 5) using the seven degree-of-freedom Ames manipulator (reference 6).

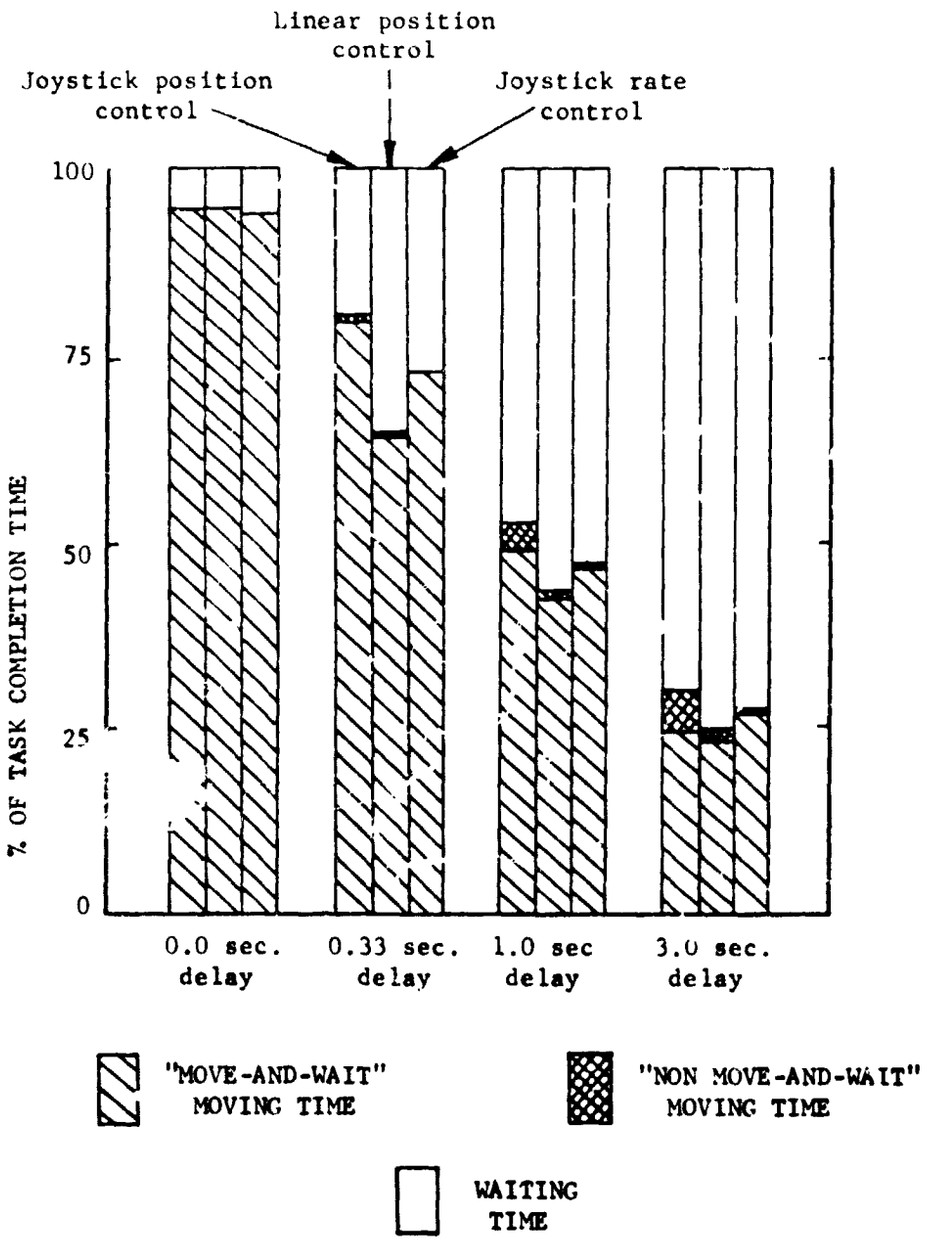

Figure 2. Breakdown of normalized completion time into periods of moving and waiting.

CONCLUDING REMARKS

In this one-dimensional discrete tracking experiment with a transmission time delay we have shown that the level of performance was correlated with the subjects' adherence to the move-and-wait strategy. Since manipulation bears substantial similarity to discrete tracking, controllers for manipulator systems in which there is a time delay should be chosen with this in mind. The particular characteristic of the controller which determines its suitability is the extent to which human operator input is required to maintain a stationary position of the controlled element, or manipulator. By this criterion, center-off rate controllers and fully counterbalanced (or equivalent system) position controllers are the best choice.

REFERENCES

1. Ferrell, W. R.: Remote Manipulation with Transmission Delay, NASA TN D-2665, 1965.

2. Blackmer, R. H.: Remote Manipulators and Mass Transfer Study, AFAPL-TR-68-75, Wright-Patterson AFB, 1968.

3. Black, J. H., Jr.: Factorial Study of Remote Manipulation with Transmission Time Delay, M.S. Thesis, Mech. Engr. Dept., MIT, 1970.

4. Gibbs, C. B.: Controller Design: Interaction of Controlling Limbs, Time Lags, and Gains, in Positional and Velocity Systems, Ergonomics, v. 5, n.2, 385-402, 1962.

5. Whitney, D. E.: Resolved Motion Rate Control of Manipulators and Human Prostheses, IEEE Trans. on Man-Machine Systems, MMS-10, n.2, 47-53, 1969.

6. Vykukal, H. C. et al: An Anthropomorphic Master-Slave Manipulator System, Proc. of the First National Conf. on Remotely Manned Systems, E. Heer, ed., 189-198, Sept. 1972.

SESSION IX

SYSTEM IDENTIFICATION

Chairman: L. Reid

A COMPARISON OF TECHNIQUES FOR IDENTIFYING HUMAN OPERATOR DYNAMICS UTILIZING TIME SERIES ANALYSIS

by

Keiji Tanaka*, Norihiro Goto**, Kyuichiro Washizu***

*Instrumentation and Control Division, National Aerospace Laboratory, Tokyo, **Department of Aeronautical Engineering, Kyushu University, Fukuoka, ***Department of Aeronautics, University of Tokyo, Tokyo

ABSTRACT

Several human operator models were identified utilizing the current spectral analysis technique and the time domain analysis techniques based on the Akaike's Minimum Final Prediction Error (MFPE) method. Evaluation of the time domain techniques is aimed at in this report. Analyses were made of the data obtained from compensatory tracking tasks involving a human operator and from digital simulations using a human model.

The results of the time domain techniques are generally in good accordance with each other. Moreover one of the techniques can offer the remnant shaping filter, the controlled element dynamics and the impulse response of the human operator.

Some preliminary consideration of the correlation between the human lead operation and the human function to forecast the system output has been made through the analysis of the human operator dynamics in control of unstable second order systems.

SYMBOLS

$\underline{A}_M(m)$	m-th autoregressive coefficient matrix when the order is M
B	backward shift operator
c(t),c(n)	human operator output
dB	decibel
$\underline{d}_M$	estimated variance matrix of noise source when the order is M

e(t), e(n)	displayed error
F{x(t)}	Fourier-transform of x(t)
j	$\sqrt{-1}$
MFPE(M)	Multiple Final Prediction Error when the order is M
m(t), m(n)	controlled element output
N	data length
n	sampling time (= nΔ)
r(t), r(n)	remnant
s	Laplace operator
t	time, seconds
$Y_c(j\omega)$	controlled element
$Y_p(j\omega)$	describing function of a human operator
$y_p(B)$, $y_p(\tau)$	impulse response of a human operator
Δ	sampling interval, seconds
τ	time shift, seconds
$\Phi_{xy}(j\omega)$	cross power spectrum between x(t) and y(t)
ω	frequency, rad/sec

INTRODUCTION

Recent progress in aircraft size, variety, and automation of flight control has greatly changed the role of the human pilot in aircraft control. The change causes more complex man-machine system problems than ever, and to solve them requires essential knowledges about the human operator dynamic characteristics. In most cases human operator dynamics have been investigated on the basis of the describing functions, such as the crossover model, in tracking tasks. The obtained human operator dynamics, however, usually show a large variety according to the objects or circumstances of the experiments. This is mainly because of his inherent adaptive dynamics, which include threshold, memory, and learning characteristics. For this reason precise and general techniques for identifying the human operator dynamics have been

required.

Confining ourselves to the approaches to identify the human operator dynamics, we may say that there are several techniques which have been fully discussed and put in order in literatures. In this paper, existing techniques are briefly summerized in the next section, followed by the introduction of several new techniques utilizing Akaike's MFPE method, which takes advantage of the recent development of the time series analysis and the statistical system identification. Results of the new techniques are compared with those obtained by the existing well-developed closed-loop spectral method. They indicate that the structure of the human operator dynamics can be distinctly expressed by employing the techniques of the MFPE method, and elucidate the superiority of the new techniques to the existing ones.

REVIEW OF EXISTING IDENTIFICATION TECHNIQUES

The man-machine system treated in this paper is confined to the simple compensatory tracking system as Fig.1, where the human operator output, $c(t)$, is the sum of the linear response to the displayed error, $e(t)$, and the remnant, $r(t)$. The objective of the identification is to determine the linear portion of the operator model, Y_p; namely the describing function of the human operator. Also, the term "identification" is sometimes used to mean the determination of the model structure and the parameters in that linear model.

The existing techniques for identifying the human operator dynamics may be calssified roughly into the following five kinds; the first three are in the frequency domain, while the last two are in the time domain:

(A) Closed-Loop Spectral Method [Refs.1 ∿ 4]

Let the portion irrelevant to the input in the human operator output $c(t)$ be $p(t)$. Then, $p(t)$ can be

$$p(t) = c(t) - \int_0^\infty g(\tau) i(t-\tau) d\tau \ , \qquad (1)$$

where $g(\tau)$ is the closed-loop impulse response function from $i(t)$ to $c(t)$. The impulse response function $g(\tau)$ may be determined in such a way that it minimizes the variance of $p(t)$. By using a few other relationships and the Fourier-transform, we obtain the well known result as to the estimate of the unknown human operator dynamics, as;

$$\hat{Y}_{pa}(j\omega) = \frac{\Phi_{ic}(j\omega)}{\Phi_{ie}(j\omega)} \ . \qquad (2)$$

It is generally admitted that this method can offer less fluctuant estimate than the following two methods.

(B) Open-Loop Spectral Method [Ref.3]
If we minimize the variance of

$$r(t) = c(t) - \int_0^\infty y_p(\tau)e(t-\tau)d\tau \ ,$$

we obtain the second estimate of the describing function as follows;

$$\hat{Y}_{pb}(j\omega) = \frac{\Phi_{ec}(j\omega)}{\Phi_{ee}(j\omega)} \quad . \tag{3}$$

It is generally admitted that cares should be taken of the fact that if

$$\Phi_{ii}(\omega) << \Phi_{rr}(\omega)$$

then

$$\hat{Y}_{pb}(j\omega) = -\frac{1}{Y_c(j\omega)} \quad . \tag{4}$$

(C) Direct Fourier-Transform Method [Ref.3]
Direct Fourier-transform of the signals, e(t) and c(t), can offer the estimate;

$$\hat{Y}_{pc}(j\omega) = \frac{F\{c(t)\}}{F\{e(t)\}} \quad . \tag{5}$$

The describing functions obtained from the three methods mentioned above have inevitable fluctuations in the frequency domain; therefore it is a common practice to derive from these describing functions a human operator model with a small number of parameters by the use of additional criteria.

(D) Impulse Response Function Method [Refs.2,5,6]
The human impulse response function can be estimated by applying the least squares algorithm, the criterion of which is the same as that of the method B. In the sampled data form the estimate $\hat{\underline{y}}_{pd}$ is given by

$$\hat{\underline{y}}_{pd} = [\ \underline{E}^T\underline{E}\ ]^{-1}\underline{E}^T\underline{c} \tag{6}$$

where

$$\hat{\underline{y}}_{pd} = [\hat{y}_{pd}(1),\hat{y}_{pd}(2),\cdots,\hat{y}_{pd}(M)]^T$$

$$\underline{c} = [c(M),c(M+1),\cdots,c(N)]^T$$

$$\underline{E} = \begin{bmatrix} e(M) & e(M-1)\cdots & e(2) & e(1) \\ \vdots & & & \vdots \\ e(N) & \cdots\cdots\cdots & & e(N-M+1) \end{bmatrix} \ ,$$

and hereafter any $x(n)$ $(n=1,2,\cdots)$ denotes the time series which is assumed to be sampled from the corresponding continuous signal $x(t)$ with the sampling interval Δ. M is the length of the human operator impulse response, and N is the data length. A describing function can easily be estimated by carrying out the Fourier-transform of $\hat{y}_{pd}$. This method has an advantage of the physical realizability of the estimate, but it should be noted that the same caution as in Y_{pb} must be paid to this method. It has also been pointed out that in the case of estimating an element in a feedback loop, it is not possible to obtain an unbiased estimate unless the remnant is white [Ref.7]. Also note that the orthogonal filter method uses the basically same criterion as this method [Ref.5].

(E) Improved Impulse Response Function Method

The second named author has succeeded in obviating the difficulty existing in the preceding method by pre-whitening the remnant [Ref.8]. He assumes the remnant to be a shaped output of a white noise and to be given in a discrete autoregressive form by

$$r(n) = \sum_{\ell=1}^{L} h(\ell) r(n-\ell) + \varepsilon(n) \quad , \tag{7}$$

where $\varepsilon(n)$ $(n=1,2,\cdots,N)$ is a white noise process, and $h(\ell)$ $(\ell=1,2,\cdots,L)$ are autoregressive coefficients of $r(n)$. Then, $h(\ell)$ $(\ell=1,2,\cdots,L)$, and $y_p(m)$ $(m=1,2,\cdots,M)$ are estimated by applying the least squares algorithm, the criterion of which is the minimization of the variance of $\varepsilon(n)$. This procedure gives a good estimate regardless of the existence of feedback links.

AKAIKE'S MFPE METHOD

The method E in the preceding section is essentially different from the others, A to D, in that it estimates the remnant parameters and the system (human operator) parameters. It, however, has a difficulty in determining the number of parameters to be estimated. Namely, though the model may improve the fidelity to reproduce the experimental data with an increase of the number of parameters, the value of each estimated parameter possibly loses its accuracy. Recently a very practical criterion to determine the order of the model has been proposed by Akaike [Ref.7], and a brief account of the method is introduced here.

We consider the case of model identification when the data are of k-dimensions. According to a properly selected regression order L, the following k-dimensional autoregressive model can be fitted to the data vector $\underline{x}(n)$, which is assumed stationary and zero-mean:

$$\underline{x}(n) = \sum_{m=1}^{L} \underline{A}_L(m) \underline{x}(n-m) + \underline{\varepsilon}(n) \quad , \tag{8}$$

where

$$\underline{x}(n) = [x_1(n), x_2(n), \cdots, x_k(n)]^T \quad ,$$

and $\underline{\varepsilon}(n)$ is a k-dimensional white noise vector given by

$$\underline{\varepsilon}(n) = [\varepsilon_1(n), \varepsilon_2(n), \cdots, \varepsilon_k(n)]^T \quad ,$$

the elements of which are assumed to be mutually independent. Also, in Eq.(8)

$$\underline{A}_L(m) = \begin{bmatrix} a_{L11}(m) & a_{L12}(m) & \cdots & a_{L1k}(m) \\ a_{L21}(m) & a_{L22}(m) & & \vdots \\ \vdots & & & \vdots \\ a_{Lk1}(m) & \cdots\cdots\cdots & & a_{Lkk}(m) \end{bmatrix} \quad , \quad (m=1,2,\cdots,L)$$

denoting the m-th k×k-dimensional autoregressive coefficient matrix when the order of regression is selected to be L. Values of $\underline{A}_L(m)$ and the estimated variance matrix of $\underline{\varepsilon}(n)$, denoted by $\underline{d}_L$, are determined by making use of the estimated variance matrix of $\underline{x}(n)$, denoted by $\underline{C}(\ell)$ $(\ell=1,2,\cdots,L)$ as follows: where

$$\underline{d}_L = \begin{bmatrix} \sigma_{11}^2 & \sigma_{12}^2 & \cdots & \sigma_{1k}^2 \\ \sigma_{21}^2 & \sigma_{22}^2 & & \vdots \\ \cdot & & & \vdots \\ \sigma_{k1}^2 & \cdots\cdots & & \sigma_{kk}^2 \end{bmatrix}$$

and

$$\underline{C}(\ell) = \begin{bmatrix} c_{11}(\ell) & c_{12}(\ell) & \cdots & c_{1k}(\ell) \\ c_{21}(\ell) & c_{22}(\ell) & & \vdots \\ \vdots & & & \vdots \\ c_{k1}(\ell) & \cdots\cdots\cdots & & c_{kk}(\ell) \end{bmatrix} \quad , \quad (\ell=1,2,\cdots,L),$$

also

$$c_{ij}(\ell) = \frac{1}{N} \sum_{n=1}^{N-\ell} x_i(n+\ell)x_j(n) \quad , \quad (\ell=1,2,\cdots,L) \quad . \qquad (9)$$

Upon multiplying the i-th equation of Eq.(8) by $x_h(n-\ell)$, we obtain

$$x_i(n)x_h(n-\ell) = \sum_{m=1}^{L} \sum_{j=1}^{k} a_{Lij}(m)x_j(n-m)x_h(n-\ell) + \varepsilon_i(n)x_h(n-\ell) \quad . \qquad (10)$$

On taking the expectation of the both sides of Eq.(10), we obtain the following k-dimensional Yule-Walker equations;

$$\gamma_{ih}(\ell) = \sum_{m=1}^{L} \sum_{j=1}^{k} a_{Lij}(m)\gamma_{jh}(\ell-m) \quad , \quad (h=1,2,\cdots,k;\ell=1,2,\cdots,L) \quad , \quad (11)$$

where $\gamma_{in}(\ell)$ denotes the covariance between x_i and x_h. Note that the expectation $E[\varepsilon_i(n), x_h(n-\ell)]$ vanishes when $\ell > 0$. By substituting the estimate $c_{ij}(\ell)$ for $\gamma_{ij}(\ell)$, we can solve Eq.(11) for $\underline{A}_L(m)$ $(m=1,2,\cdots,L)$. At the same time, from Eq.(8), $\underline{d}_L$ is obtained by using $\underline{A}_L(m)$ as;

$$\underline{d}_L = \underline{C}(0) - \sum_{m=1}^{L} \underline{A}_L(m)\underline{C}^T(m) \quad . \tag{12}$$

The calculation can be performed by an iterative procedure, where it is to be noted that the lower order coefficients $\underline{A}_{L-1}(m)$ $(m=1,2,\cdots,L-1)$, $\underline{A}_{L-2}(m)$ $(m=1,2,\cdots,L-2),\cdots$, $\underline{A}_1(m)$ $(m=1)$ are also obtained during the iterative process of determining $\underline{A}_L(m)$ $(m=1,2,\cdots,L)$. Then, the Akaike's method proposes to determine the order M as the value of L which minimizes the following criterion

$$\text{MFPE}(L) = \left(1 + \frac{Lk+1}{N}\right)^k \left(1 - \frac{Lk+1}{N}\right)^{-k} |\underline{d}_L| \quad . \tag{13}$$

This is called the multiple final prediction error, which means the mean-square error of the one-step-ahead prediction obtained by using the estimated coefficients $\underline{A}_L(m)$ $(m=1,2,\cdots,L)$. In Eq.(13), $|\underline{d}_L|$ denotes the determinant of $\underline{d}_L$, and N is the number of data points.

The present method, which will be called Akaike's MFPE method hereafter, has been applied by the first named author to identifying the human operator dynamics in the control system shown in Fig.1. By the use of the MFPE method, the following techniques have been developed:

(1) The MFPE Method Utilizing Data of e(t) and c(t)

A two-dimensional autoregressive model by the use of e(t) and c(t) is determined first. Then, after checking the model appropriateness by the values of the off-diagonal elements of $\underline{d}_M$, (namely, the estimated cross-covariance of the white noises be very small compared with the diagonal elements,) we obtain from Eq.(8) the autoregressive equations of e(n) and c(n) in a matrix form as

$$\begin{vmatrix} c(n) \\ e(n) \end{vmatrix} = \begin{vmatrix} A_{11}(B) & A_{12}(B) \\ A_{21}(B) & A_{22}(B) \end{vmatrix} \begin{vmatrix} c(n) \\ e(n) \end{vmatrix} + \begin{vmatrix} \sigma_{11} & 0 \\ 0 & \sigma_{22} \end{vmatrix} \begin{vmatrix} \xi_1(n) \\ \xi_2(n) \end{vmatrix}, \tag{14}$$

where

$$A_{ij}(B) = a_{ij}(1)B + a_{ij}(2)B^2 + \cdots + a_{ij}(M)B^M, \quad (i,j=1,2)$$

$$Bx(n) = x(n-1) \quad \text{[Refs.9 and 10]} \; .$$

M is the order of the model determined by MFPE, and $\xi_i(n)$ $(i=1,2)$ denote white noise process of unit variance, which are independent of each other. It should be noted that $\varepsilon_1(n)$ $[= \sigma_{11}\xi_1(n)]$ and $\varepsilon_2(n)$ $[= \sigma_{22}\xi_2(n)]$ are the estimated noise sources of the remnant r(n) and the external forcing function i(n), respectively, as shown in Fig.2.

Then, we obtain from the first equation of Eq.(14),

$$\{1 - A_{11}(B)\}c(n) = A_{12}(B)e(n) + \sigma_{11}\xi_1(n)$$

and consequently

$$c(n) = \frac{A_{12}(B)}{1 - A_{11}(B)}\, e(n) + \frac{\sigma_{11}}{1 - A_{11}(B)}\, \xi_1(n) \quad . \qquad (15)$$

Therefore an estimate of the human impulse response function is given by

$$\hat{y}_{p1}(B) = \frac{A_{12}(B)}{1 - A_{11}(B)} \quad . \qquad (16)$$

The operator B can be replaced by $\exp(-j\omega\Delta m)$ to get the frequency response function as;

$$\hat{Y}_{p1}(j\omega) = \frac{A_{12}(j\omega)}{1 - A_{11}(j\omega)} \qquad (17)$$

where

$$A_{ij}(j\omega) = \sum_{m=1}^{M} a_{ij}(m)\, e^{-j\omega\Delta m} \quad .$$

Eq.(17) will be called the first estimate of the describing function. Moreover, an estimated shaping filter of the remnant is given by

$$\hat{F}_r(j\omega) = \frac{\sigma_{11}}{1 - A_{11}(j\omega)} \quad . \qquad (18)$$

From the second equation in Eq.(14), an estimate of the controlled element frequency response and the shaping filter of the forcing function are also given by

$$-\hat{Y}_c(j\omega) = \frac{A_{21}(j\omega)}{1 - A_{22}(j\omega)} \quad , \qquad (19)$$

and

$$\hat{F}_i(j\omega) = \frac{\sigma_{22}}{1 - A_{22}(j\omega)} \quad , \qquad (20)$$

respectively.

(2) The MFPE Method Utilizing i(t) and c(t)

An estimate of the closed-loop frequency response, $\hat{Y}_{ic}(j\omega)$ is calculated as before. Making use of $Y_{ic}(j\omega)$ and the known $Y_c(j\omega)$ gives the second estimate of the describing function as;

$$\hat{Y}_{p2}(j\omega) = \frac{\hat{Y}_{ic}(j\omega)}{1 - Y_c(j\omega)\hat{Y}_{ic}(j\omega)} \quad . \qquad (21)$$

(3) The MFPE Method Utilizing e(t) and m(t)

An estimate of the open-loop frequency response from e(t) to m(t), $\hat{Y}_{em}(j\omega)$ is calculated. By making use of $\hat{Y}_{em}(j\omega)$ and the known $Y_c(j\omega)$, the third estimate is given by

$$\hat{Y}_{p3}(j\omega) = \frac{\hat{Y}_{em}(j\omega)}{Y_c(j\omega)} \quad . \tag{22}$$

DIGITAL SIMULATIONS

Before proceeding to the identification of a human operator dynamics, digital simulations were carried out to check the validity of the MFPE method. The block diagram of the simulations is shown in Fig.1, where the controlled element dynamics and the known filter corresponding to the human operator dynamics were

$$Y_c(s) = \frac{9}{s^2 + 2s + 9} e^{-0.05s} \tag{23}$$

and

$$Y_p(s) = \frac{0.5}{1 + 0.2s} e^{-0.25s} \quad , \tag{24}$$

respectively. The simulated system was driven by two random number series: one was for the simulated input and the other for the simulated remnant.

Data analyses were carried out to obtain $\hat{Y}_{pa}$, $\hat{Y}_{p1}$, $\hat{Y}_{p2}$ and $\hat{Y}_{p3}$. These were compared with the theoretical results. Examples are shown in Figs.3 ~ 6. It is found that:

(1) $\hat{Y}_{pa}$, $\hat{Y}_{p1}$ and $\hat{Y}_{p2}$ prove to be correct, while $\hat{Y}_{p3}$ to be nearly correct.

(2) The order of the extent of independency from the influence of the remnant is, from small to large, $\hat{Y}_{p1}$, $\hat{Y}_{p2}$ and $\hat{Y}_{pa}$.

HUMAN TRACKING DATA AND THEIR REDUCTIONS

Next, single-loop compensatory tracking experiments involving a human operator as shown in Fig.7 were carried out. Three male subjects participated in the experiments, and the following twelve kinds of controlled elements were mechanized by an analogue computer:

$$Y_c(s) = 1, \frac{1}{s}, \frac{2}{s \pm 2} \tag{25}$$

and

$$Y_c(s) = \frac{\omega_n^2}{s^2 + 2\zeta\omega_n s + \omega_n^2} \qquad (26)$$

with ω_n = 3, 5 [rad/sec], and ζ = 0.167, 0, -0.167, -0.333.
The forcing function was generated by shaping a white noise by the filter,

$$F_i(s) = \frac{22.5}{(s + 1.5)^2} + - \frac{100}{(s + 10)^2} \quad . \qquad (27)$$

Data reductions were implemented on NAL magnetic-tape-data reduction system and FACOM 230-75 computer.

RESULTS OF HUMAN TRACKING DATA ANALYSIS

The techniques investigated were $\hat{Y}_{pa}$, $\hat{Y}_{p1}$, $\hat{Y}_{p2}$ and $\hat{Y}_{p3}$. It was chosen that Δ = 0.1 [sec]. The number of the data points, N, was 1200 (ten minutes), and the number of variance functions used was 100 (ten seconds). Also for $\hat{Y}_{pa}$, Hamming-window was used.

Examples of the human operator describing functions of $\hat{Y}_{p1}$, $\hat{Y}_{p2}$ and $\hat{Y}_{p3}$ are shown in Fig.8 ∿ 11 for Y_c = 1, 1/s, $9/(s^2-s+9)$ and $9/(s^2-2s+9)$, respectively. They show good accordance with each other. In order to compare the identified models with the describing function based on the spectral analysis, $\hat{Y}_{p1}$ and $\hat{Y}_{pa}$ are plotted one over the other. Examples are shown in Figs.12 and 13, where it can be observed that $\hat{Y}_{p1}$ and $\hat{Y}_{pa}$ are in good agreement.

It is noted, however, that the off-diagonal element of $\underline{d}_N$ of the auto-regressive model of $\hat{Y}_{p3}$ takes a relatively high value; therefore the modeling of $\hat{Y}_{p3}$ is not always successful. Also caution has to be paid to the values of the relative noise contribution to confirm the effectiveness of the identified models: the relative noise contribution $R_{ij}(\omega)$ is defined under the assumption of the mutual independence of $\varepsilon_i(n)$'s in Eq.(8 ∿

$$R_{ij}(\omega) = \frac{q_{ij}(\omega)}{p_{ii}(\omega)} \qquad (28)$$

where $p_{ii}(\omega)$ is the power spectrum of $x_i(n)$, and $q_{ij}(\omega) = |[\underline{A}^{-1}(\omega)]_{ij}|^2 \sigma_{jj}^2$, the contribution from each noise source to the total power of $x_i(n)$. $[\underline{A}(\omega)]_{ij}^{-1}$ is the (i,j)-element of $[\underline{A}(\omega)]^{-1}$,

$$\underline{A}(\omega) = \sum_{m=0}^{M} \underline{A}_M(m)\exp(-j\omega\Delta m)$$

where $\underline{A}_M(0) = -\underline{I}$, and σ_{jj}^2 is the variance of $\varepsilon_j(n)$. The relative noise contribution of the noise source of i(n) to c(n) is often in low level when Y_c is unstable; this may suggest that in this case the human operator is in Pilot-Induced-Oscillation.

An example of the comparison between the model output c*(n), which is

computed through the convolution of $\hat{y}_{pl}(s)$ and $e(n)$ of the data, and the human operator actual output data, $c(n)$, is shown in Fig.14. It is indicated that the linear model of $\hat{y}_{pl}$ accounts for a considerable portion of the human output.

SOME OBSERVATIONS OBTAINED FROM IDENTIFIED HUMAN OPERATOR MODELS

Several observations obtained from the identified human operator models may be summarized as follows:

(1) It is fairly clear that the describing functions of the human operators in controlling the elements;

$$Y_c(s) = 1, \frac{1}{s}, \frac{2}{s+2} \quad ,$$

can be expressed by the crossover model, whereas those in controlling an unstable second-order system can be approximated by

$$Y_p(s) = K_p \frac{1 + T_L s + T_L' s^2}{1 + T_N s} e^{-\tau_e s} \quad . \qquad (29)$$

(2) Examples of $\hat{y}_{pl}(\tau)$, shown for $Y_c = 1$ and $9/(s^2-s+9)$ in Figs.15 and 16 respectively, indicate that the net time delay, which is the dead time in the impulse response of the human operator, τ_0, seems to be about 0.1 ~ 0.2 [sec] and is relatively smaller than the effective time delay, τ_e in Eq.(29).

(3) It is often observed that when the controlled element is unstable, there exists a human lead operation which is expressed by the lead terms in the human operator describing function. It is quite natural to presume that when a human operator becomes familiar with the system dynamics, he can grasp the characteristics of the controlled element and predict the output of the controlled element [Ref.3]. This leads us to consider that the first- and the second-order lead terms in human models may indicate the human operator's function to forecast the output of the controlled element.

(4) The describing functions $-\hat{Y}_c$ and $\hat{F}_i$ have proved to be nearly correct in the frequency range between 0 and 10 [rad/sec]. Also, the describing function F_r seems to be correct. However, it has no tendency of depending on Y_c.

FINAL REMARKS

The linear models of a human operator controlling unstable systems, which have been considered so far to be hard to estimate, have been precisely identified by the MFPE method. These models have proved to be successful in

expressing a considerable part of the human operation.

The identification techniques utilizing the recently developed time series analysis can offer very evident results. It may be concluded that these techniques are effective tools to analyze the man-machine systems with, and that $\hat{Y}_{pl}$ offers the most information among the three. Yet, it should be noted that in order to validate the model, full attention must be paid to the variance matrix of noise sources, the coherency and the relative noise contribution. As this MFPE method is primarily quite effective when applied to multi-variable systems, it is expected to become one of indispensable tools for multi-variable system analyses.

ACKNOWLEDGMENT

The authors wish to express their thanks to Dr. H.Akaike, and Mr. G.Kitagawa of the Institute of Statistical Mathematics of Japan for valuable discussions, and to Mr. S.Arai of Fujitsu Co. for his support in applying TAT.

REFERENCES

1. McRuer,D.T.; and Krendel,E.S.: The Human Operator as a Servo System Element. Rept. from Journal of Franklin Institute, Vol.267, No.5 and No.6, 1959.

2. Shirley,R.S.: A Comparison of Techniques for Measuring Human Operator Frequency Response. Sixth Annual Conference on Manual Control, 1970, pp.803-869.

3. Frostell,C.E.: A Comparison of Pilot Describing Function Measurement Techniques. UTIAS TN No.167, 1971

4. McRuer,D.T.; and Krendel,E.S.: Mathemetical Models of Human Pilot Behavior. AGARD-AG-188, 1974.

5. Wingrove,R.C.: Comparison of Methods for Identifying Pilot Describing Functions from Close -Loop Operating Records. NASA TN D-6235, 1971.

6. Taylor,L.W.Jr.: A Comparison of Human Response Modeling in the Time and Frequency Domain. Third NASA-University Conference on Manual Control, NASA SP-144, 1967, pp.137-153.

7. Akaike,H.; and Nakagawa,T.: Statistical Analysis and Control of Dynamic Systems. 1972, Science Co., (in Japanese).

8. Goto,N.; and Washizu,K.: On the Dynamics of Human Pilots in Marginally Controllable Systems. AIAA Journal, Vol.12, No.3, 1974.

9. Shinners,S.M.: Modeling of Human Operator Performance Utilizing Time Series Analysis. IEEE Trans. on Systems, Man and Cybernetics, Vol. SMC-4, No.5, 1974.

10. Box,G.E.P.; and Jenkins,G.M.: Time Series Analysis Forecasting and Control. 1970, Holden Day.

11. FACOM 230 TAFT [Time series Analysis in Frequency and Time Domain] Manual. 1974, Fujitsu Co., (in Japanese).

12. Akaike,H.: Autoregressive Model Fitting for Control. Ann. Inst. Statist. Math., Vol.23, 1971, pp.163-180.

C.8

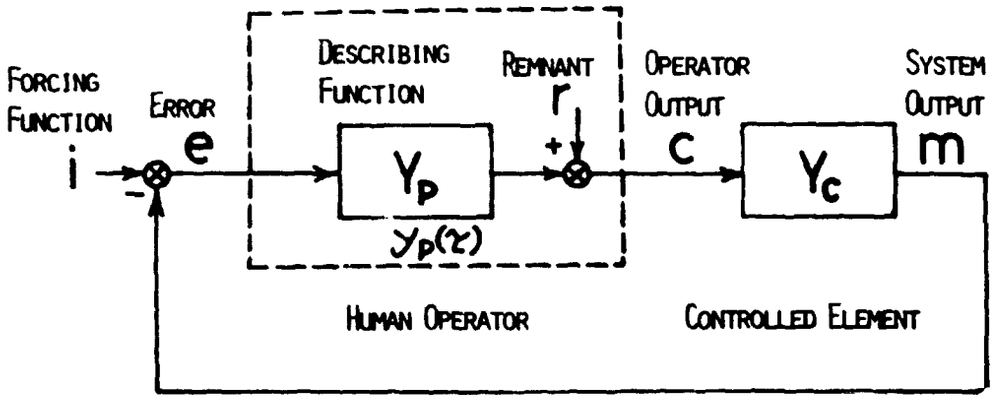

Figure 1. Equivalent Block Diagram of Compensatory System

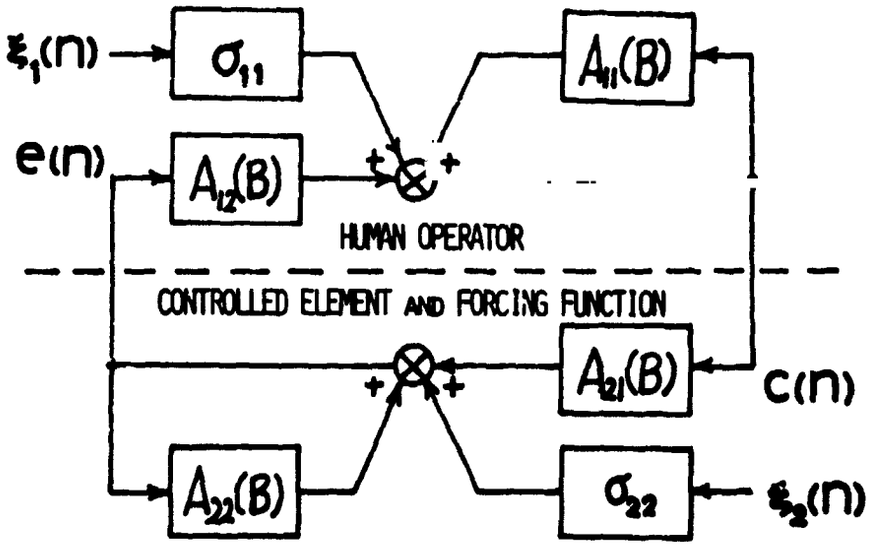

Figure 2. Block Diagram of Compensatory System by MFPE Method

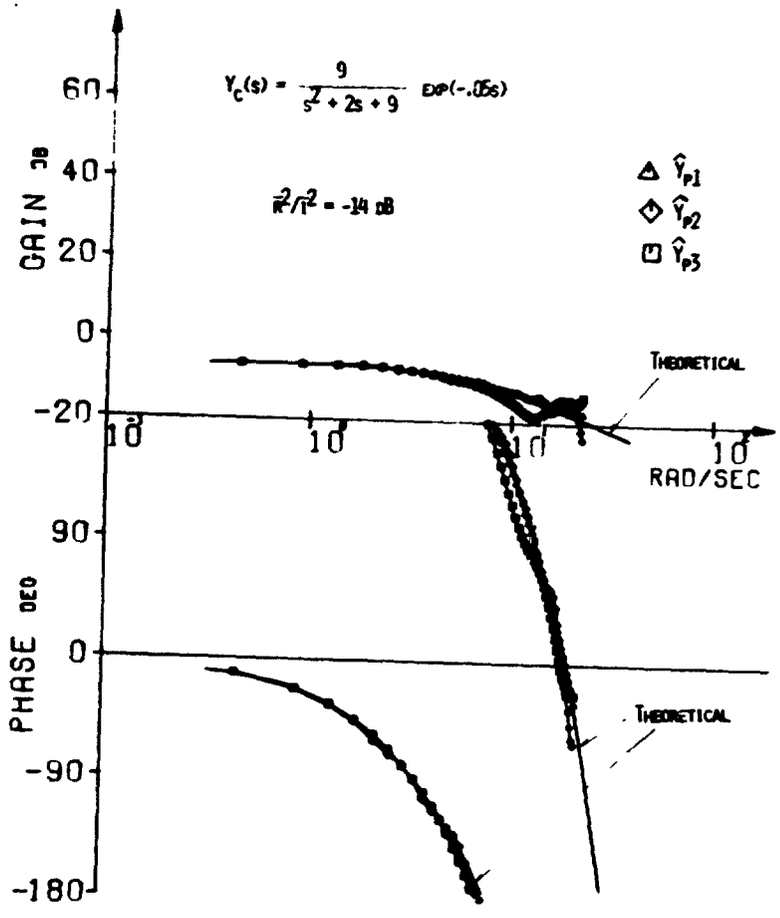

Figure 3. Estimated Frequency Responses of a Known Filter by MFPE Method

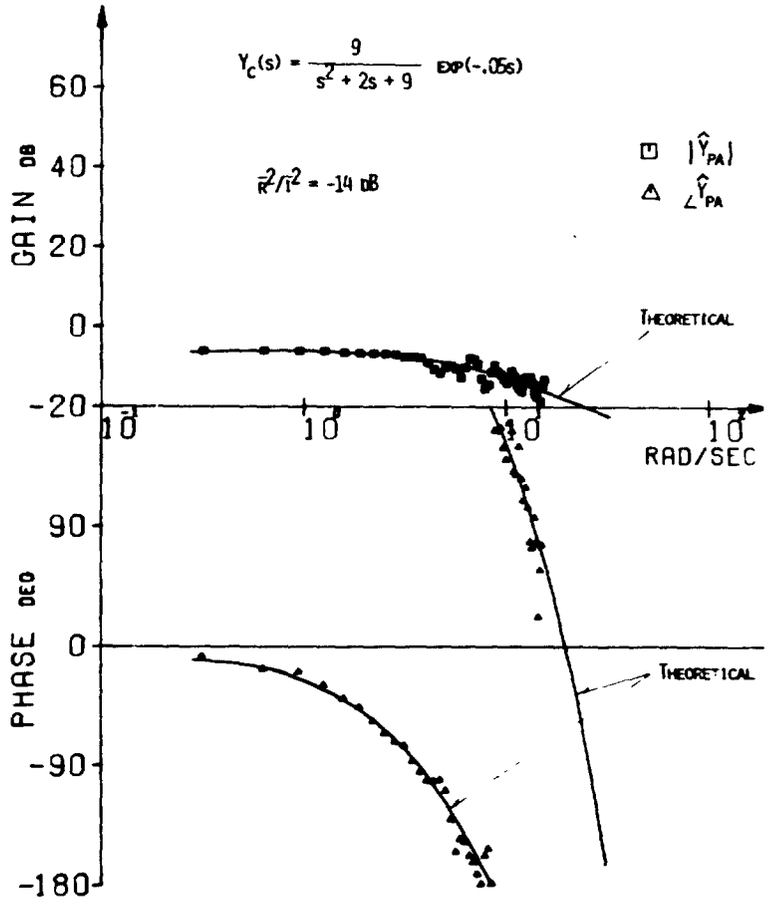

Figure 4. Estimated Frequency Response of a Known Filter by Spectral Analysis

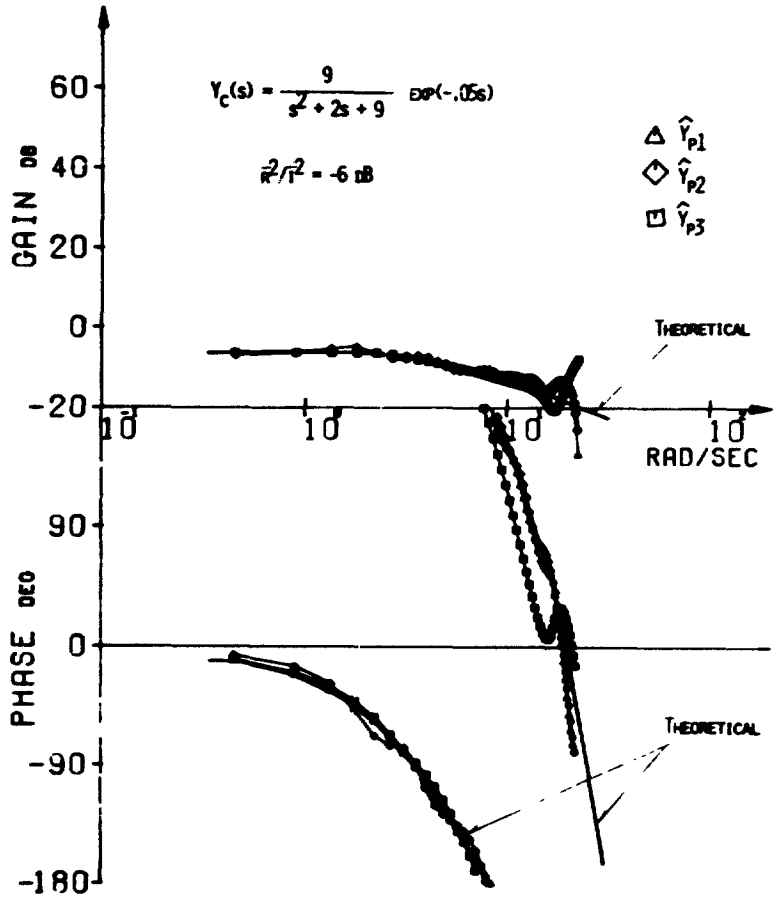

Figure 5. Estimated Frequency Responses of a Known Filter by MFPE Method

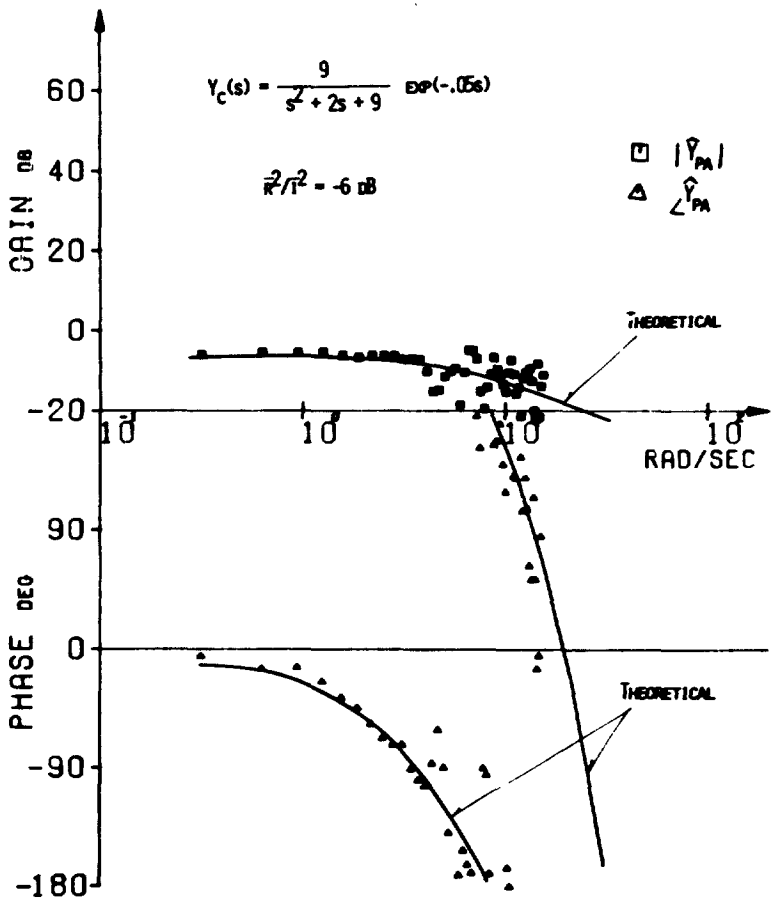

Figure 6. Estimated Frequency Response of a Known Filter by Spectral Analysis

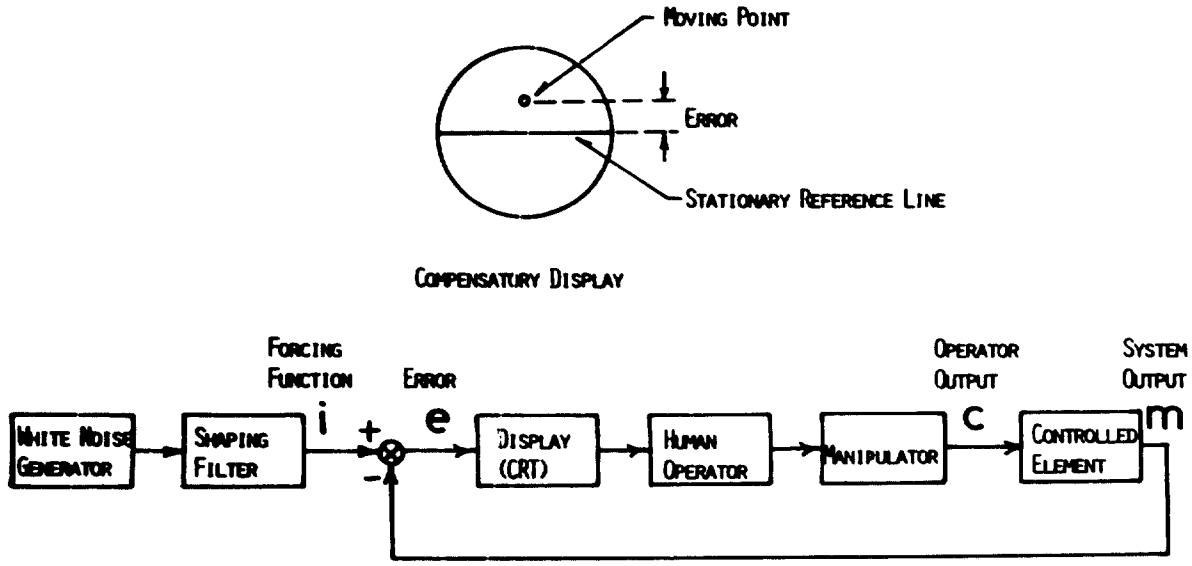

Figure 7. Block Diagram of Simple Compensatory Manual Control System

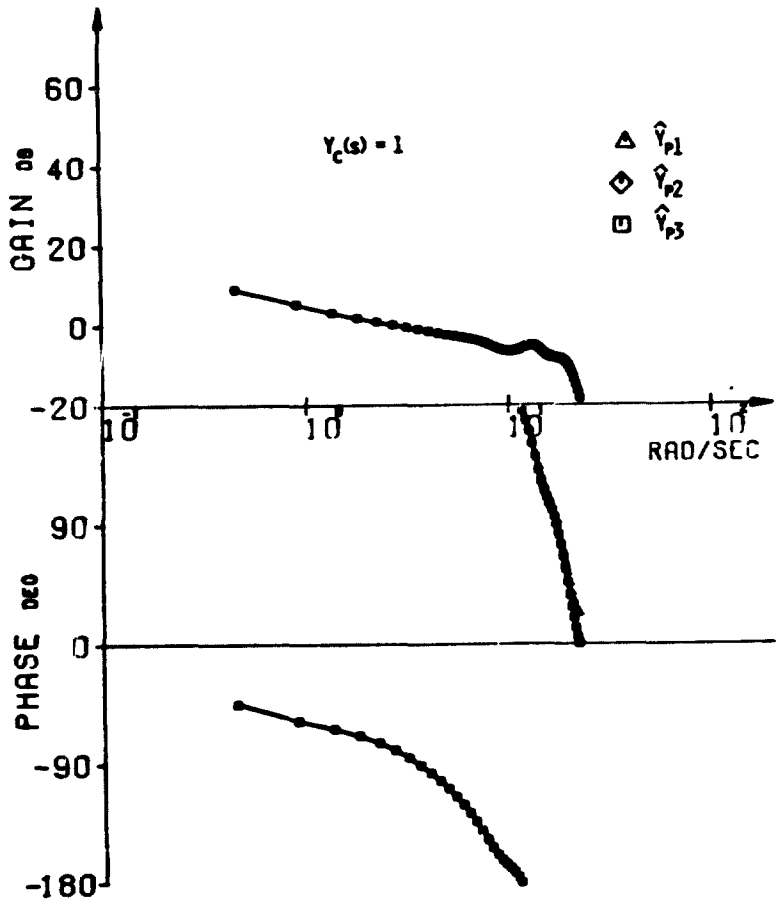

Figure 8. $\hat{Y}_p(j\omega)$

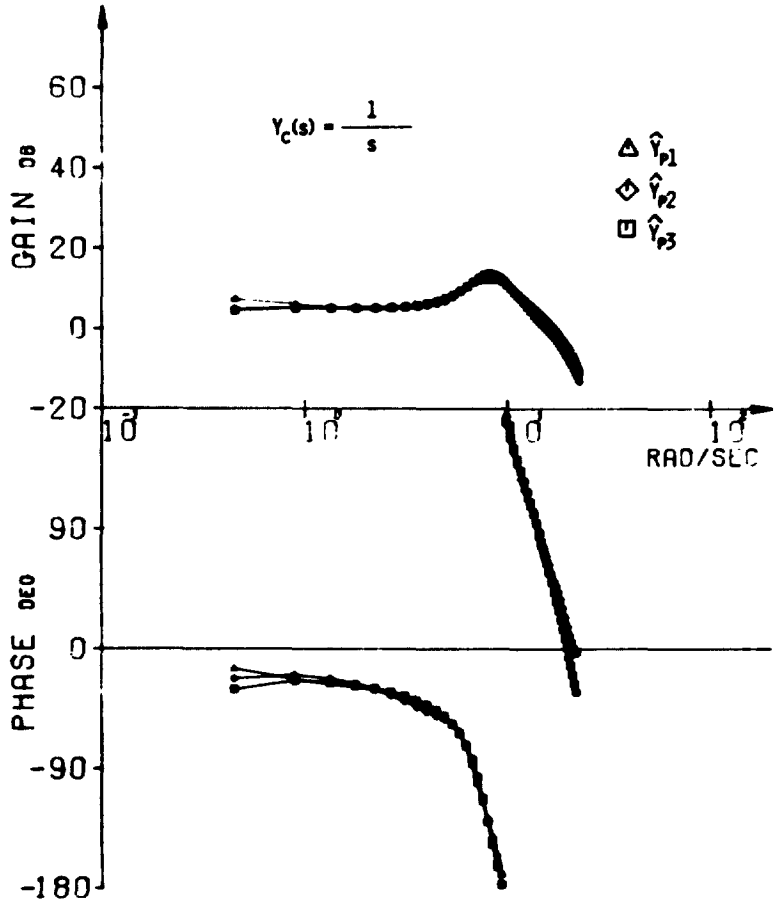

Figure 9. $\hat{Y}_p(j\omega)$

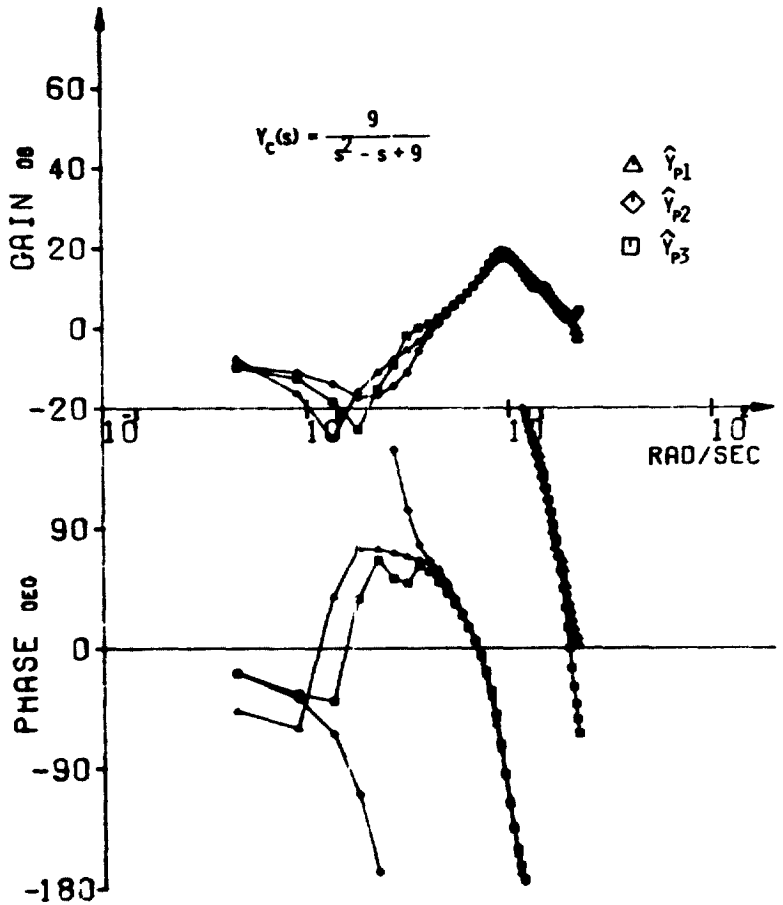

Figure 10. $\hat{Y}_p(j\omega)$

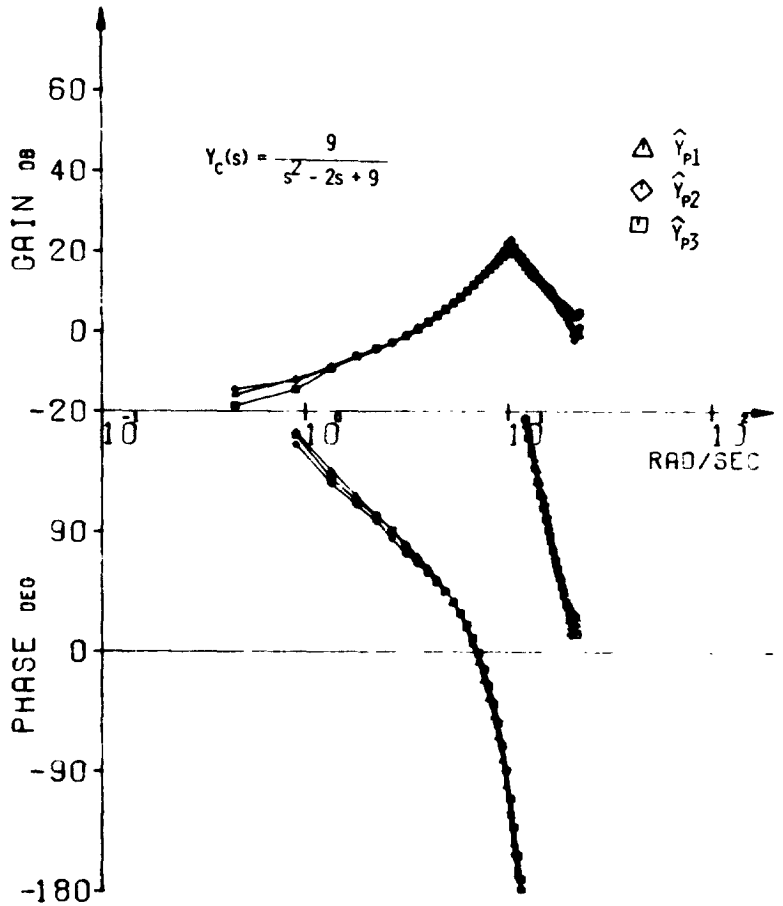

Figure 11. $\hat{Y}_p(j\omega)$

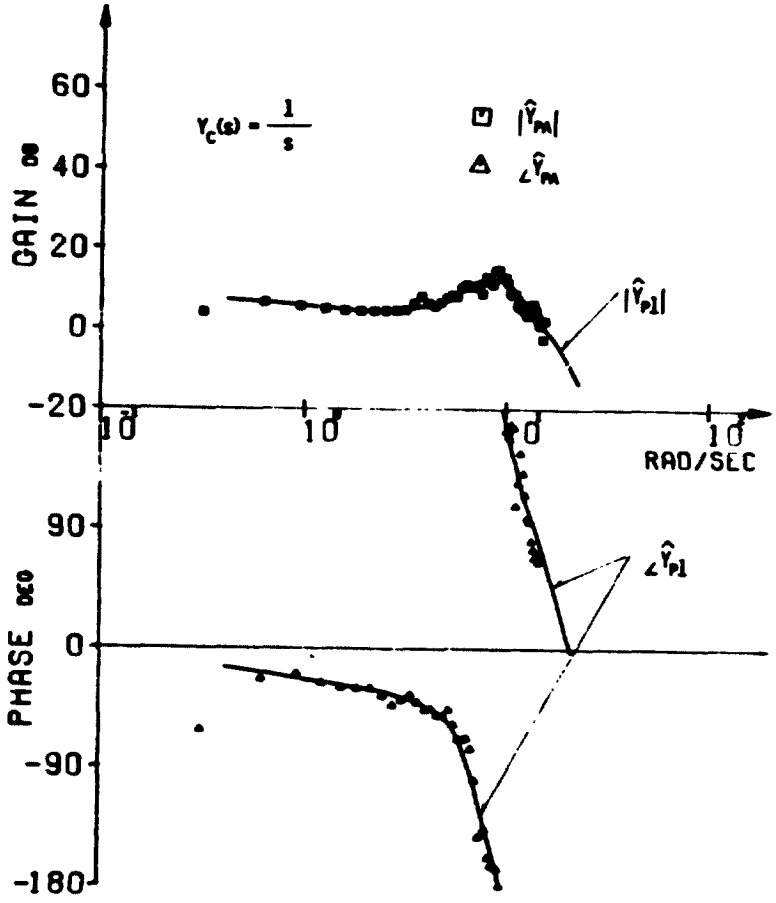

Figure 12. $\hat{Y}_{pa}(j\omega)$ and $\hat{Y}_{pl}(j\omega)$

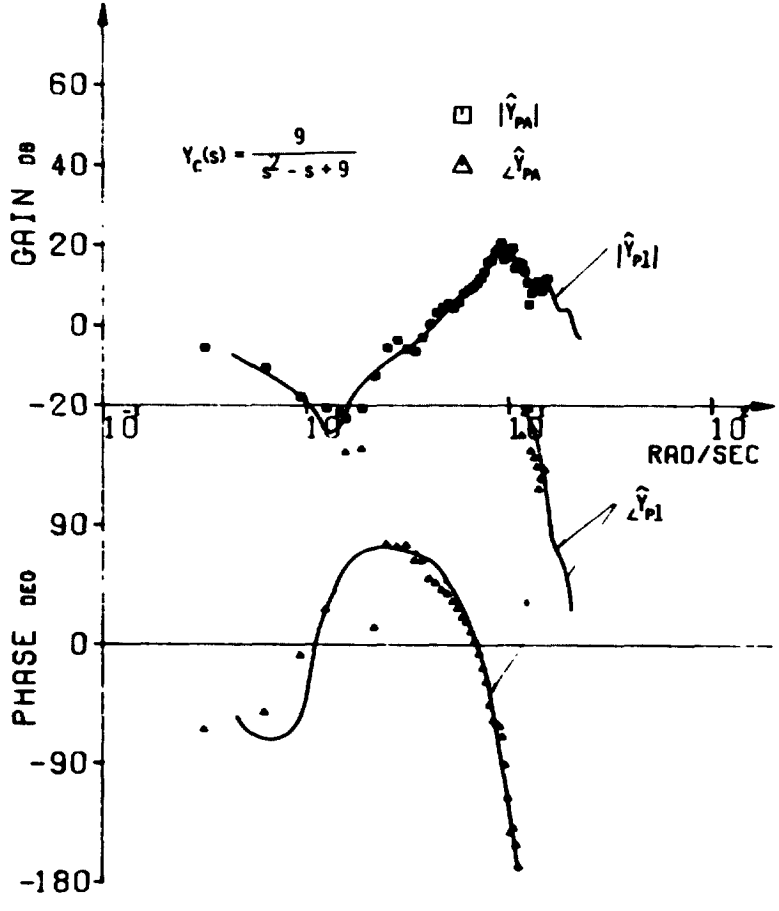

Figure 13. $\hat{Y}_{pa}(j\omega)$ and $\hat{Y}_{pl}(j\omega)$

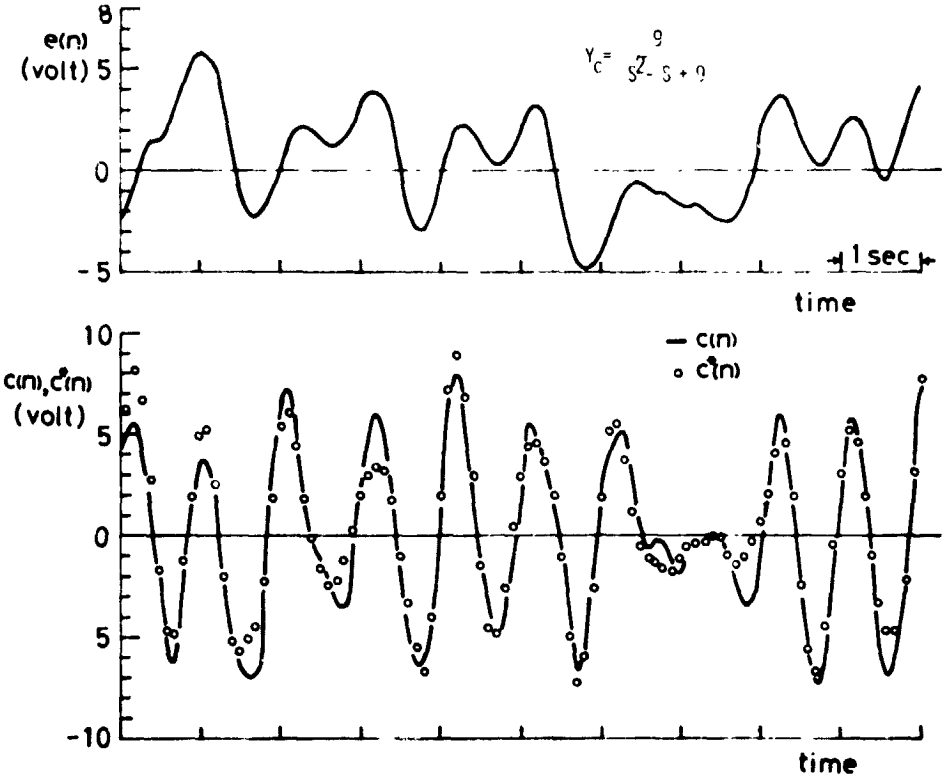

Figure 14. A Comparison between Human Output (c(n)) and Model Output (c*(n)) Computed through Error (e(n)) and Identified Human Impulse Response ($\hat{y}_{pl}$)

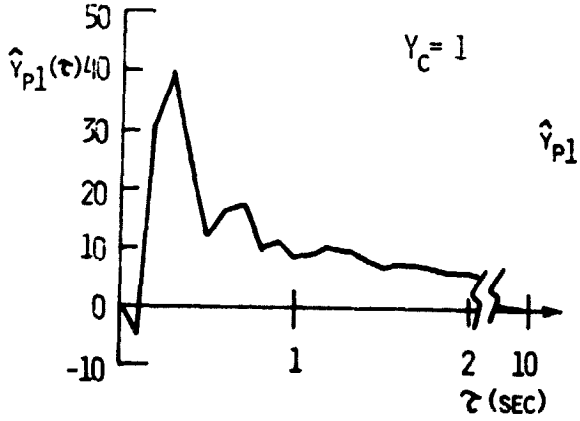

Figure 15. $\hat{y}_{pl}(\tau)$

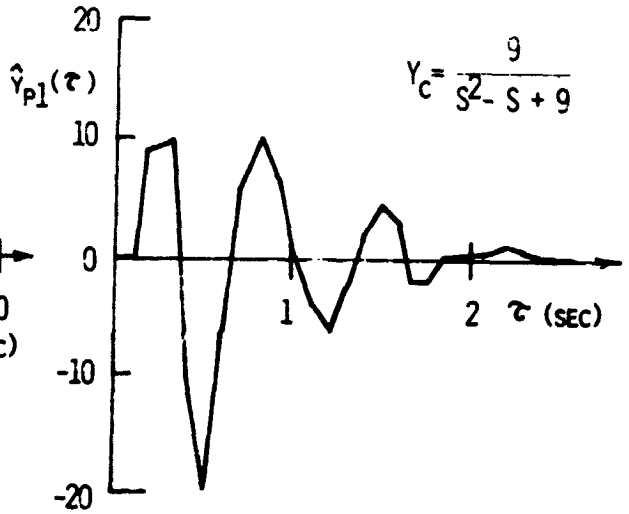

Figure 16. $\hat{y}_{pl}(\tau)$

SYSTEM IDENTIFICATION VIA A MICROCOMPUTER

Ralph Mekel and Avtar Singh

The City College of The City University of New York
New York, N. Y. 10031

SUMMARY

The purpose of this paper is twofold. The first part describes an adaptive identification technique for updating the parameters of a mathematical model and in the second part it is shown how the identification process may be implemented through a microcomputer system consisting of a microprocessor (CPU unit), RAMs, ROMs, I/O devices, a clock generator and other interfaces.

INTRODUCTION

The identification technique is formulated using a model-reference system approach in conjunction with Liapunov's direct method to insure the convergence of the identification process. An appropriate Liapunov function is chosen whose time derivative provides the identification law equations. An important feature is the simplicity of the system adaptive laws which are decomposed into primitive forms for easier implementation on the microcomputer. These adaptive laws depend explicitly on the model-reference system state variables and input. Therefore, in this identification technique it is assumed that the entire state vector is known or accessible for measurement.

The dotted block in Fig. 1. shows the part of the identification process which is to be realized by the microcomputer. Figure 2. describes the sequence of operations performed by the microcomputer in the process of identification. The identification process is a program on 8 ROMs each serving a specific purpose. The RAMs contain the initial, intermediate and final identified model as well as the system input, state vectors and various matrices used in the process of identification. The RAMs are also used for intermediate steps of calculations which need to be stored.

DERIVATION OF THE IDENTIFICATION LAW EQUATIONS

A block diagram depicting the identification process is given in Fig. 1. Let the reference system be described by

$$\dot{\underline{z}} = A\underline{z} + H\underline{r} \qquad (1)$$

This research is supported by NASA Langley Research Center, Grant No. NSG1169

and the model to be identified by

$$\dot{\underline{x}} = K\underline{x} + (B - K)\ \underline{z} + C\underline{r} \tag{2}$$

where $\underline{z}$, $\underline{x}$ are the state vectors each of order n, K is a stable n x n matrix, $\underline{r}$ is the input vector of order m. Matrices A, B, C and H are initially different. The objective of the identification process is to generate a scheme that dynamically adjusts the elements of matrices B and C so that

$$\lim_{t\to\infty} B = A \tag{3}$$

$$\lim_{t\to\infty} C = H \tag{4}$$

$$\lim_{t\to\infty} (\underline{x} - \underline{z}) = \lim_{t\to\infty} \underline{e} = 0 \tag{5}$$

Define the misalignment of the matrices as

$$(B - A) = \sum_{i=1}^{n} \underline{b}_i\, \underline{u}_i^T \tag{6}$$

and

$$(C - H) = \sum_{i=1}^{n} \underline{d}_i\, \underline{w}_i^T \tag{7}$$

where $\underline{b}_i$ and $\underline{d}_i$ are constant column vectors with i-th row as 1 and all other rows being zero and $\underline{u}_i$ and $\underline{w}_i$ are the misalignment vectors. Next, define the model-reference system error as

$$\underline{e} = (\underline{x} - \underline{z}) \tag{8}$$

The time derivative of (8) yields

$$\dot{\underline{e}} = \dot{\underline{x}} - \dot{\underline{z}} \tag{9}$$

Substitution of (1) and (2) into (9) yields the following differential equation for the error

$$\dot{\underline{e}} = K(\underline{x} - \underline{z}) + (B - A)\ \underline{z} + (C - H)\ \underline{r} \tag{10}$$

Using (6), (7) and (8), Eq. (10) can be rewritten as

$$\dot{\underline{e}} = K\underline{e} + \left[\sum_{i=1}^{n} \underline{b}_i \underline{u}_i^T\right] \underline{z} + \left[\sum_{i=1}^{n} \underline{d}_i \underline{w}_i^T\right] \underline{r} \tag{11}$$

Equation (11) may be viewed as consisting of (2n + 1) pertubations $\underline{u}_i$, $\underline{w}_i$ and $\underline{e}$. An appropriate Liapunov function should be positive definite in error as well as other perturbations. Therefore, one may choose a Liapunov function of the form

$$V = \underline{e}^T M \underline{e} + \sum_{i=1}^{n} \underline{u}_i^T N_i \underline{u}_i + \sum_{i=1}^{n} \underline{w}_i^T Q_i \underline{w}_i \tag{12}$$

where M, N_i and Q_i are positive definite symmetric matrices. For simplicity Q_i and N_i may be selected as diagonal matrices with positive elements, i.e.

$$N_i = \text{diagonal } \left[n_{ij}\right] \qquad 1 \leq j \leq n \tag{13}$$

and

$$Q_i = \text{diagonal } \left[q_{ij}\right] \qquad 1 \leq j \leq n \tag{14}$$

The time derivative of V yields

$$\dot{V} = \underline{e}^T (K^T M + MK) \underline{e} + 2 \sum_{i=1}^{n} \left[\underline{\dot{u}}_i^T N_i + \underline{z}^T (\underline{b}_i^T M \underline{e}) \right] \underline{u}_i + 2 \sum_{i=1}^{n} \left[\underline{\dot{w}}_i^T Q_i + \underline{r}^T (\underline{d}_i^T M \underline{e}) \right] \underline{w}_i \tag{15}$$

Liapunov's criterion for stability calls for $V > 0$ and $\dot{V} \leq 0$. One way to comply with Liapunov's criterion for stability and to generate the controller equations is to let

$$K^T M + MK = -D \tag{16}$$

$$\underline{\dot{u}}_i^T = -\underline{z}^T (\underline{b}_i^T M \underline{e}) N_i^{-1} \tag{17}$$

$$\underline{\dot{w}}_i^T = -\underline{r}^T (\underline{d}_i^T M \underline{e}) Q_i^{-1} \tag{18}$$

where $D = D^T (> 0) = \text{diagonal } \left[d_{ii}\right] \quad 1 \leq i \leq n$ (19)

Differentiating Eqs. (6) and (7) and assuming that the system matrices A and H can be considered time invariant during the identification interval, one obtains

$$\dot{B} = \sum_{i=1}^{n} \underline{b}_i \underline{\dot{u}}_i^T \tag{20}$$

and $$\dot{C} = \sum_{i=1}^{n} \underline{d}_i \underline{\dot{w}}_i^T \tag{21}$$

Substitution of (17) and (18) into (20) and (21) respectively yields

$$\dot{B} = -\sum_{i=1}^{n} \underline{b}_i \underline{z}^T (\underline{b}_i^T \underline{M} \underline{e}) N_i^{-1} \tag{22}$$

$$\dot{C} = -\sum_{i=1}^{n} \underline{d}_i \underline{r}^T (\underline{b}_i^T \underline{M} \underline{e}) Q_i^{-1} \tag{23}$$

Integrating (22) and (23) yields

$$B = B_o - \int_0^t \left[\sum_{i=1}^{n} \underline{b}_i \underline{z}^T (\underline{b}_i^T \underline{M} \underline{e}) N_i^{-1} \right] dt \tag{24}$$

and $$C = C_o - \int_0^t \left[\sum_{i=1}^{n} \underline{d}_i \underline{r}^T (\underline{d}_i^T \underline{M} \underline{e}) Q_i^{-1} \right] dt \tag{25}$$

where B_o and C_o are initially assumed model matrices. Substitution of (24) and (25) into Eq. (2) gives the final model representation

$$\dot{\underline{x}} = K\underline{x} + \left\{ B_o - \int_0^t \left[\sum_{i=1}^{n} \underline{b}_i \underline{z}^T (\underline{b}_i^T \underline{M} \underline{e}) N_i^{-1} \right] dt - K \right\} \underline{z} +$$

$$+ \left\{ C_o - \int_0^t \left[\sum_{i=1}^{n} \underline{d}_i \underline{r}^T (\underline{d}_i^T \underline{M} \underline{e}) Q_i^{-1} \right] dt \right\} \underline{r} \tag{26}$$

The dotted block in Fig. 1. shows the part of the identification process to be realized by the microcomputer system and the next section describes the microcomputer hardware needed for implementing the identification process.

MICROCOMPUTER HARDWARE FOR IDENTIFICATION PROCESS

The identification process based upon the adaptive laws described in the previous section can be implemented on a microcomputer system shown in Fig. 3. The microcomputer system accepts the reference system input and states as

analog inputs and initial model and identification matrices as digital inputs. The analog signals are converted to digital equivalents by A/D converters such as Datel's DAS-16-L8B which takes in an analog signal and puts out an 8-bit digital signal. For entering the initial model and identification matrices, a teletype may be used along with proper interface to the microcomputer. One such interface is Intel's 8251 - programmable, synchronous/asynchronous communication interface, which accepts serial information from the teletype, constructs 8-bit words and presents to the computer. The same interface can be used to print out the identified model parameters. In transmitting mode, it accepts 8-bit words and converts to serial information to drive the teletype.

The initial and intermediate model parameters along with the identification matrices and signals from the reference system are stored in 256 byte RAM memory which can be constructed from a pair of 256x4 RAM chips. Input and output buffering for the RAM memory can be constructed using Intel's 8212 data buffers.

The identification algorithm is stored in 8 different ROM chips such as Intel's 8308 ROM which is 1024x8 bit and stores up to 1024 bytes. The total programming memory will be 8K, which is quite sufficient for the identification of a second order system. ROM memory chip selection unit can be constructed using Intel's 8205 - one out of eight decoder. For a higher order reference system it may be necessary to expand the ROM memory.

The program execution takes place in the CPU such as Intel's 8080 microprocessor. The CPU is run by a two phase clock generator and driver such as Intel's 8224. The total system consisting of ROMs, RAMs, A/D converters, teletype and CPU is coordinated by the system controller unit such as Intel's 8228. To service interrupts from various I/O devices, Intel's 8214 priority interrupt control unit may be used.

CONCLUDING REMARKS

We have described an identification technique based upon Liapunov's direct method in conjunction with a model-reference system configuration. The adaptive laws are partitioned so that they can be implemented on a microcomputer system. The later part of the paper shows directions for implementing the identification technique on a microcomputer system. Faster implementation can be achieved by using the microprocessor in conjunction with hardware multipliers and linear circuits (such as integrators).

REFERENCES

1. Graupe, D.: Identification of Systems. Van Nostrand Reinhold Co. 1972

2. Kalman, R. E.; and Bertram, J. E.: Control System Analysis and Design Via the Second Method of Lyapunov. Trans. of ASME, June 1960.

3. Mekel, R.: Nonlinear and Digital Man-Machine Control Systems Modeling. NASA Langley Research Center, Report No. 72-447-01, Nov. 1972.

4. Mekel, R.; Montgomery, R. C.; and Dunn, H. J.: An Adaptive Learning Control System for Aircraft. Eighth Asilomar Conference on Circuits, Systems and Computers, Dec. 3-5, 1974.

5. Datel Systems, Inc.: Engineering Products Handbook, A/D and D/A Converters, 1974.

6. Intel Corporation: 8080 Microcomputer Systems User's Manual, Sept. 1975.

7. Graupe, D.: Multifunctional Control of Artificial Upper Limbs Based on Parameter Identification of Myoelectric Signals. Decision and Control Conference, 1975.

8. Torrero, E. A.: Microprocessors, New Directions for Designers. Hayden Book Company Inc., July 1975.

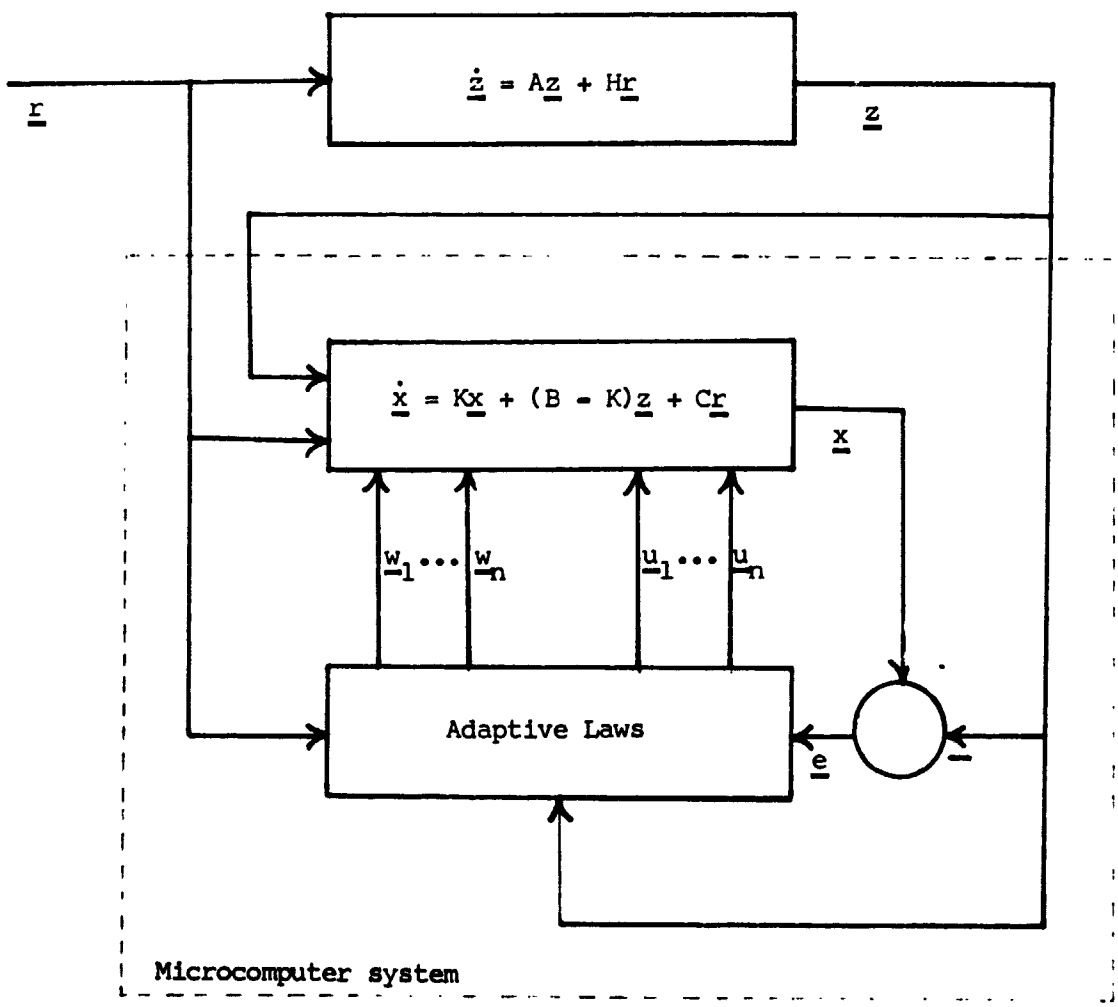

Fig. 1. Identification Process.

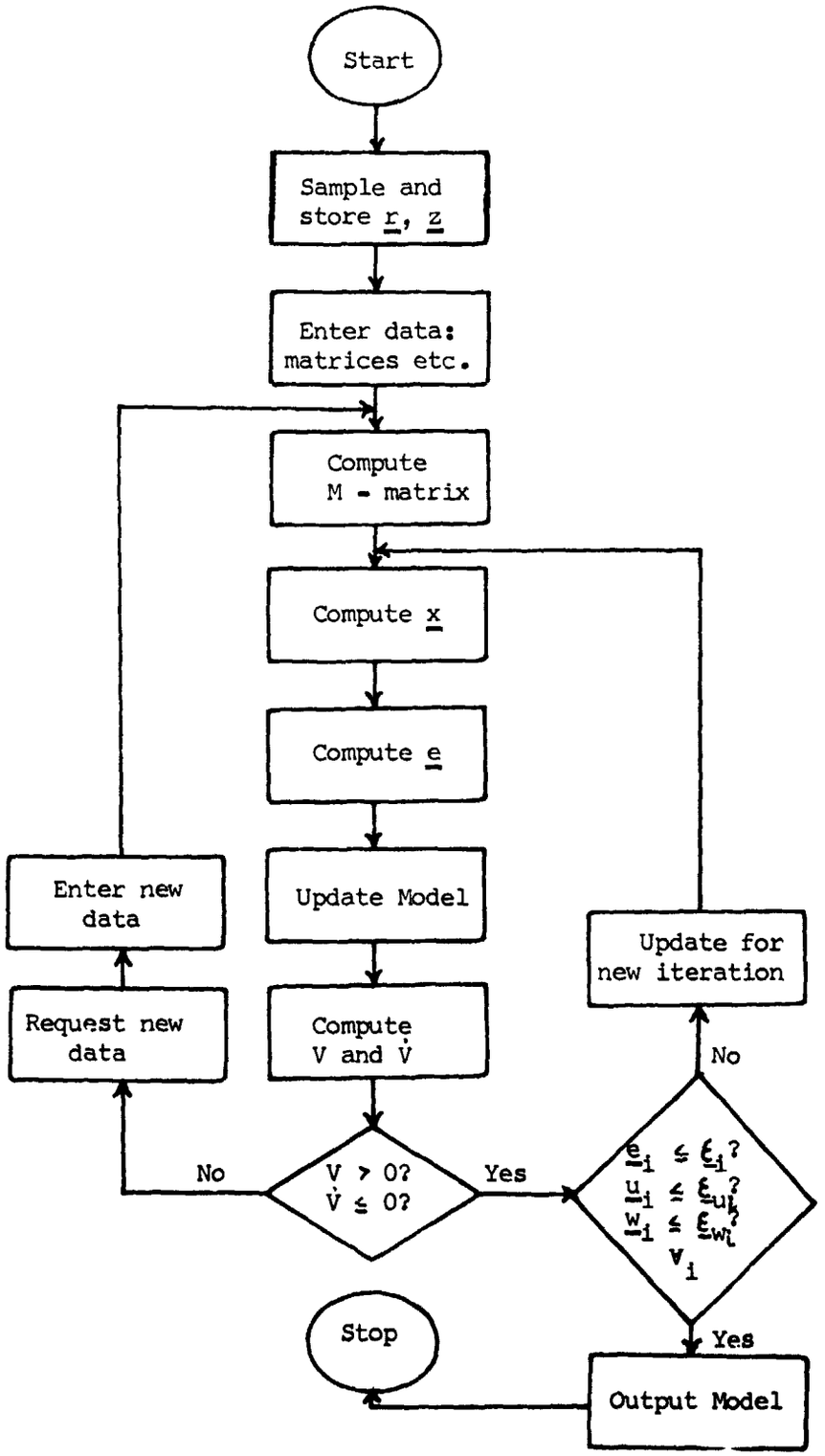

Fig. 2. Logic Flow Chart.

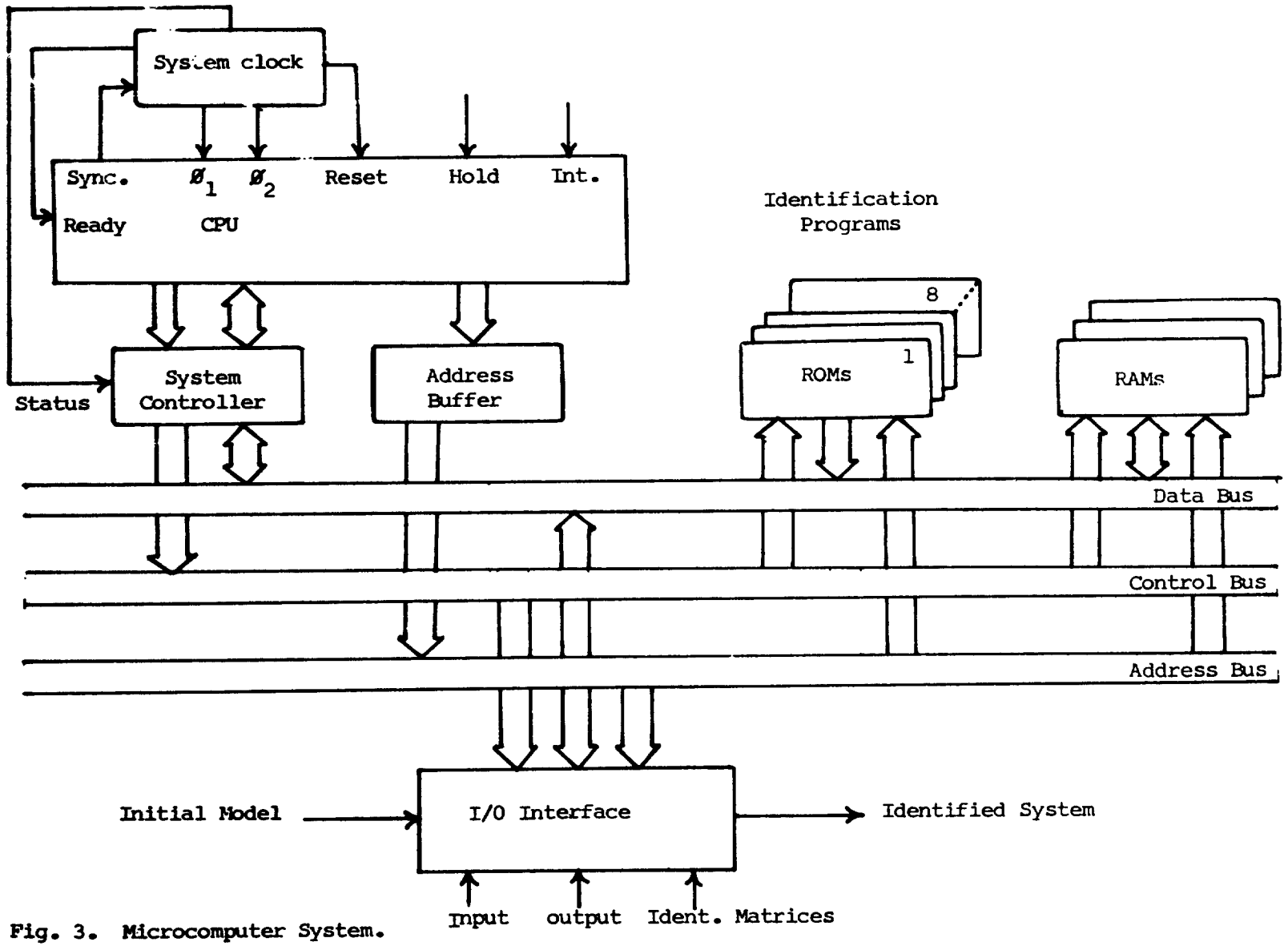

Fig. 3. Microcomputer System.

PID (PROPORTIONAL INTEGRAL DERIVATIVE) MODELING TECHNIQUES APPLIED TO STUDIES OF MOTION AND PERIPHERAL DISPLAY EFFECTS ON HUMAN OPERATOR PERFORMANCE*

By Daniel W. Repperger and Andrew M. Junker

Aerospace Medical Research Laboratory
Wright-Patterson Air Force Base, Ohio 45433

SUMMARY

A preliminary approach to system identification is introduced in which a man in a closed loop tracking task is modeled in a Proportional Integral Derivative (PID) manner. In order to obtain a PID type model for man's transfer function, a choice of state variables had to be selected in a proper manner. The PID type model presented here is an approximation and is accurate within the linear representation of man's transfer function. Closed loop remnant signals may also influence PID parameters. Therefore, an investigation of human remnant (remnant reflected at the human's observation point) was also studied. This type of modeling approach yields interesting results on the manner in which man uses the displayed error signal to generate his stick response. The data base for this study includes motion cues of a roll axis tracking task and also a peripheral display experiment, both of which studied effects on tracking performance.

INTRODUCTION

The term PID (Proportional Integral Derivative) controller is well known from process control and other applications as indicated by Athans, reference (1). Recently in the area of manual control, PID type optimal control models have been considered by Phatak and Kessler, reference (2). The approach presented here is not an optimal control technique but is a method to identify particular structures of man when he is involved in a closed loop tracking task. The optimal control models can be considered as methods to predict performance in the future (this may be termed "A Priori" modeling). The approach presented in this paper is to investigate what happened in the past from an experiment when all the data has been collected (this may be termed "A Posteriori" modeling.) The modeling technique presented here can be used only after the data has been collected; this technique cannot be used to pre-

*The research reported in this paper was sponsored by Aerospace Medical Research Laboratory, Aerospace Medical Division, Air Force Systems Command, Wright-Patterson Air Force Base, Ohio 45433. Further reproduction is authorized to satisfy needs of the U.S. Government.

dict performance ahead of time as compared to the optimal (A Priori) control type models. The approach presented here combines modern control theory techniques (a least squares identification algorithm) with describing function techniques. A study of human remnant effects must be considered and a rudimentary statistical analysis is done. It is emphasized here that the results obtained are only preliminary because of some approximations which must be made in the sequel of this paper. It will take a more complete study to consider this problem without the approximations.

Description of the Data Base Used

The study of motion effects on man and peripheral displays is extensive as indicated in the work of Shirley, reference (3), Young, reference (4), Stapleford, reference (5), Ringland, reference (6), and others. The data base from the roll axis tracking study used here differs from the data used in the above references by the following:

(1) The roll motion in the Aerospace Medical Research Laboratory (AMRL) study was strictly in the roll axis with no washout circuits built in to aline the g-vector with the spine of the subject.

(2) In the AMRL motion study, the input was purely a command signal; i.e. the plant was driven only by the subject's control inputs. In the earlier studies, the input disturbance was applied in such a manner that both the visual display and the motion simulation were driven by the input (i.e. the input was applied essentially in parallel with the pilot's control).

(3) The plant dynamics in the AMRL study were higher order than those in the previous studies.

Reasons (2) and (3) were pointed out by W. Levison, reference (7) and in the report by Levison and Baron, reference (8). In the report, reference (8), phase droop was identified as one of the important factors which is a consequence of motion effects and also they were able to predict (in an A Priori manner) when motion would help performance for simplier plant dynamics as a function of attention allocation. The data base discussed in this paper has been discussed by Junker and Price, reference (9), Moriarty, reference (10), and Price, reference (11), and details of the particular experiment can be found in any of these references. It is noted that some of the analytic results presented here for this motion study may not be in complete agreement with the analytic results of previous studies, references (3,4,5,6). The primary reason for this fact is that different simulators were used. Since the study of motion effects is a very deep and complex area, the analytic results from different simulators should be considered separately. Perhaps if the analytic techniques presented here were applied to the earlier data, the same conclusions would have been obtained.

The Tracking Problem of Interest

With reference to Figure (1a), the typical man-in-the-loop problem is illustrated. The input forcing function is a sum of sine waves with

randomized initial phase angles. e(t) denotes the displayed error signal and st(t) denotes the stick output signal of man (rate command). The machine denotes all non-human elements appearing in the closed loop which includes the effects of the display and other non-human factors. For the data presented here, the plant had dynamics characterized by:

$$H(s) = \frac{14.0}{s^2(1+s/.5)(1+s/6.)} \qquad (1)$$

Although this plant appears very difficult to control, the input forcing function to the closed loop had a 1/2 power point at 0.5 radians; hence this plant is actually between second and third order (with respect to the input forcing function).

Three modes of operation were considered in this study, they were

(1) Static

(2) Motion

(3) Peripheral

where the motion mode of operation was in the roll axis and the peripheral mode consisted of TV monitors mounted on the side of the simulator in a fixed base situation. Details of different aspects of this experiment can be found in references (8,9,10,11).

It is interesting to observe how performance in the closed loop changed during the three possible modes of operation. Of the five subjects involved in this experiment, Table 1 illustrates the performance results averaged over the subjects after a sufficient training period for the same plant and input.

From Table 1, it is observed that the peripheral (fixed base) mode of operation was apparently as helpful in improving performance (using the static case as a reference point) as compared to the motion case (which is a moving base simulation). These results made the data base very attractive to study and also to apply some new analysis techniques.

The PID Modeling Approach

With reference to Figure (1b), an internal loop approach will be considered. This can only be done if the measured time series e(t) and st(t) are available to do the modeling. For this study, e(t) and st(t) were stored on magnetic tape and represent the input (displayed error) and output(force stick response) of the man. By taking this internal loop approach, certain advantages exist for purposes of modeling. With reference to Figure (1b), $\hat{st}(t)$ denotes the estimate of st(t) from the computer model. The output modeling error in Figure (1b) represented the difference between the true data st(t) and the estimate $\hat{st}(t)$ from the computer model. Ideally we would like to have the output modeling error identically zero; in this manner the model and the man would agree exactly. In the true application, however, the output

modeling error is never zero due to many sources of uncertainty (including human remnant). There are two reasons why this internal loop approach has advantages for modeling. First, when remnant is modeled in a closed loop, it is best represented by a point injected (vector) noise source at the point e(t). This has been discussed by Jex, Allen, and Magdaleno, reference (12). The variance of the remnant injected noise source when normalized with respect to the magnitude of the closed loop error signal is down to almost -20db as a colored noise source for most practical plants. Using the number .01π as a magnitude relationship, one can expect by going internal to the loop that a 3% input to a linear system will only affect the output by 3% when normalized. Thus remnant will not distort the modeling answers by that much of a factor. It is true for this particular plant that the remnant spectrum was higher on a db scale (a high lead case) when normalized but the above argument still holds. A second advantage in this internal loop approach is that modeling is a correlation between the input and the output time series. A white injected noise at the point e(t) does not influence correlation because the noise source is white. Hence the remnant will only bias the variance of the output modeling error and not directly affect the linear model obtained.

Motivation (For Physiological Studies) For a PID Structure

With reference to Figure (2), it is desired to replace the man in the closed loop by a PID type structure. This approach to modeling is not limited to just man-in-the-loop problems but can be applied to any two measured time series (for this case e(t) and st(t)) which may result from any biological process. The representation transfer function of the man-in-the-loop is specified by:

$$\text{Man} = G(s) = a_o + a_1 s + a_2 s^2 + \frac{a_3}{s} + \frac{a_4}{s^2} \qquad (2)$$

where s indicates the Laplace transform operator. The advantages of this simple type structure to investigate how the input-output time series are related can be seen by rewriting equation (2) as follows:

$$\text{Man} = a_o\left[1. + c_1 s + c_2 s^2 + c_3/s + \frac{c_4}{s^2}\right] \qquad (3)$$

where the terms c_1 and c_2 indicate the ability of the man to differentiate and c_3, c_4 indicate how memory (or integration) is being used. The term a_o depends on the display gain, stick gain, scaling and other factors. With reference to equation (3), and recalling the classical definition of pilot lead (displayed in Figure (3)), one can relate pilot lead to the bracketed terms of equation (3). The terms c_1 and c_2 may be dominant with respect to 1 if they are non zero. Also, the memory terms c_3 and c_4 may or may not be zero. The question of the existence of the coefficients (being non zero) can only be answered in a statistical manner. The choice of the form of equation (3) including the terms c_3 and c_4 was chosen for tracking tasks which may not be compensatory. In the well known book of Sheridan and Ferrell, reference (13), it is mentioned that the three hierarchies of tasks (precognitive, pursuit,

and compensatory) are of interest in the study of man-machine systems. The choice of the structure given in equation (3) was motivated by the need to have a modeling approach applicable for all types of tasks (precognitive, pursuit, and compensatory).

It is now necessary to consider two basic problems that arise. First, we must determine a_i ($i = o,---4$) given in equation (2) and secondly it is necessary to implement this modeling approach.

The Technical Approach to Determine the PID Coefficients

Laplace transforming equation (2) yields:

$$\frac{ST(s)}{E(s)} = \frac{a_2s^4+a_1s^3+a_os^2+a_3s+a_4}{s^2} \tag{4}$$

in order to apply state variables to such an expression as equation (4), certain difficulties arise. Taking the reciprocal of both sides of equation (4) yields:

$$\frac{E(s)}{ST(s)} = \frac{s^2}{a_2s^4+a_1s^3+a_os^2+a_3s+a_4} \tag{5}$$

In the time domain, this can be written

$$a_2\dddot{e}+a_1\ddot{e}+a_o\dot{e}+a_3\dot{e}+a_4e = \ddot{st} \tag{6}$$

For simplicity, equation (6) will be written:

$$\dddot{e}+b_1\ddot{e}+b_2\dot{e}+b_3\dot{e}+b_4e = b_5\ddot{st} \tag{7}$$

It is necessary to now discuss what physically occurred in the transition from equation (4) to equation (5). In order to determine the coefficients $b_1,---b_5$, an input error identification procedure must be used. This is a consequence of going from equation (4) to (5).

With reference to Figure (4), a comparison between output error identification and input error identification is illustrated. For input error identification, st(t) is the input into the computer model and $\hat{e}(t)$ is the best estimate of e(t) generated by the computer model. Input error identification has been used by Shinners (14), and is used commonly in Europe as discussed by Astrom, reference (15). In order to implement this type of identification, the input-output data channels have to be switched in order and the time lag (approximately .2 seconds) is accounted for in the input-output data by a shift of an integral multiple of the sampling rate (25 hz). The time lag is actually positive with this type of shift on the data channels. It is noted that input error identification has advantages over output error identifi-

cation if e(t) is known with more certainty (i.e., less noise) than st(t). The choice of the modeling approach may depend on the type of data available.

Implementation of the PID Model

In order to implement equation (7), the following state variables are chosen:

$$x_1(t) = e(t) \tag{8a}$$

$$\dot{x}_1(t) = x_2 \tag{8b}$$

$$\dot{x}_2(t) = x_3 + b_5\, st(t) \tag{8c}$$

$$\dot{x}_3(t) = x_4 + (-b_1 b_5)\, st(t) \tag{8d}$$

and $\dot{x}_4$ satisfies equation (7).

Differentiating the state vector yields the following state equations:

$$\dot{\bar{x}} = A\bar{x} + B\, st(t) \tag{9a}$$

$$y(t) = H\bar{x} = [1, 0, 0, 0]\,\bar{x} = e(t) \tag{9b}$$

Where:

$$A = \begin{bmatrix} 0, & 1, & 0, & 0 \\ 0, & 0, & 1, & 0 \\ 0, & 0, & 0, & 1 \\ -b_4, & -b_3, & -b_2, & -b_1 \end{bmatrix}, \quad B = \begin{bmatrix} 0 \\ b_5 \\ -b_1 b_5 \\ (b_1^2 - b_2)\, b_5 \end{bmatrix} \tag{10}$$

It is noted that the [A,H] matrix is observable but A may not be stable (for $b_1 > 0$). The [A,B] matrix is in a form in which it cannot be determined if it is controllable due to the non-linear relationships which appear in the third and fourth elements of B. It would be necessary to now implement a constrained (with these non-linear constraints) least squares algorithm on the unknowns $b_1, \ldots, b_5$. For reasons to be mentioned in the sequel, the following approach is chosen to implement this method. Choose:

$$B = \begin{bmatrix} 0 \\ b_5 \\ b_6 \\ b_7 \end{bmatrix} \tag{11}$$

where b_6 and b_7 are free. There are three practical engineering reasons for doing this: (1) After allowing b_6 and b_7 to be identified, the average values of $b_1,---b_7$ are checked by the following non-linear constraint relationship:

$$b_6 = - b_1 b_5 \tag{12a}$$

$$b_7 = (b_1^2 - b_2)\, b_5 \tag{12b}$$

since b_6 and b_7 are identified independently of $b_1,---b_5$, the non-linear constraint relationship seems to check within the same order of magnitude. Hence, even with the constrained least squares algorithm, the results are probably not different. (2) Let us now examine the third and fourth state variable of equation (9a):

$$\dot{x}_3 = x_4 + (-b_1 b_5)\, st(t) \tag{13a}$$

$$\dot{x}_4 = -b_4 x_1 - b_3 x_2 - b_2 x_3 - b_1 x_4 + (b_1^2 b_5 - b_2 b_5)\, st(t) \tag{13b}$$

with reference to Table 1, and recalling that $b_1,---b_5$ were identified independently of the remaining parameters, the terms $\ddot{e}$ and $\dddot{e}$ were compared to the non-linear terms multiplying st(t). In all cases the non-linear product terms were significantly below 1% of $\ddot{e}$ and $\dddot{e}$. In other words, the non-linearities were well below the noise level in the time series measurement e(t). This technique is typical of control theory problems such as in the area of digital filtering. State variables which are two derivatives below the measured time series are generally only approximated. (3) If we were to omit the memory terms (c_3 and c_4) of equation (3), the non-linear constraints disappear. Since this experiment was a compensatory tracking task, we would expect c_3 andc_4 to not exist but the method is presented here for completeness in hope of its possible application in a precognitive or pursuit type tracking task.

Statistical Analysis of the PID Coefficients

The statistical analysis section of this paper will answer two important questions concerning the coefficients c_1, c_2, c_3 and c_4 of equation (3):

(1) The question of existence (non-difference from zero).
(2) The question of change (from the static mode, the motion mode, and the peripheral mode of operation).

One method to study the question of existence of the coefficients c_1, c_2, c_3 and c_4 is to test whether they are statistically non-different from zero (using their means and variances). A two-tailed t-test versus zero was performed using a pooled variance. Three subjects were chosen based on the plots of their respective time series (although Pouldon, reference (16), recommends a minimum of six subjects for any intra or between subject variability) and

six replications were used (averaged over subjects) with the results presented in Table 2. It is noted that these averages contained outlying points (outliers) and in some cases points were rejected using outlier tests in the same manner as is done in FFT studies. In FFT studies, a frequency measurement will be rejected if it differs significantly from adjacent measurements.

In all cases (static, motion, and peripheral), the coefficients c_3 and c_4 were not statistically non-different from zero. Hence they did not exist in a statistical sense. This is to be expected since this was a compensatory tracking task and c_3 and c_4 were representative of memory terms. The following interesting statistical relationships arise from Table 2:

$$c_{3_{p,m,s}} = 0 \tag{14a}$$

$$c_{4_{p,m,s}} = 0 \tag{14b}$$

The subscripts p, m, and s, of course, correspond to the peripheral, motion, and static modes of operation.

From the results of Table 2. we can conclude that the transfer function of man can be written in the following manner:

$$\text{Man} = a_o\,[1+c_1 s+c_2 s^2] \tag{15}$$

In other words, his transfer function was of a second order nature.

The second question the statistical analysis must answer is the question of changes between coefficients. To answer this question, a two-tailed t-test of the means of the coefficients (with a pooled variance) was computed. The results are presented in Table 3.

The three permutations of static-motion, static-peripheral, and motion-peripheral are displayed. At a .05 α level the following statistical results can be determined:

$$c_{1_m} \approx c_{1_p}\,,\; c_{2_m} \approx c_{2_p}\,,\; c_{2_m} > c_{2_s}$$

At a .1 α level it can be said that:

$$c_{2_p} > c_{2_s}$$

But it cannot be said that:

$$c_{1_m} > c_{1_s}\,,\text{ or } c_{1_p} > c_{1_s}$$

even though the means of these variables indicate this fact. Also it is interesting to note that in the motion mode of operation the α level distin-

guishing $c_{2_m} > c_{2_s}$ is much sharper than the α level distinguishing $c_{2_p} > c_{2_s}$. This indicates that in the motion mode of operation the double lead term c_2 is the most important factor. In the peripheral case, however, the double lead term c_2 may not be that important. The results on the motion study agree (for this simulator) with those results presented by Junker, Repperger, and Neff, reference (17). What is perhaps most interesting about this analysis is that if we were to look at Table 1 for the error scores, it would be concluded the motion and peripheral modes of operation had similar effects on the closed loop error and one mode of operation could not be distinguished from another based on the error scores. Looking at Table 3, however, it is easily seen that there exists changes in the means of these coefficients (although statistically they cannot be distinguished) and in addition, sharper changes in the α levels for c_{2_m} versus c_{2_s} compared to c_{2_p} versus c_{2_s}. Hence the statistical test gives us some incite into some model parameter changes which cannot be seen by looking directly at the error scores.

CONCLUSIONS

An A Posteriori approach to modeling a man involved in a static, motion, peripheral experiment was considered. The PID coefficients were identified (based on an engineering approximation) and a statistical analysis was performed. For the data base of the simulation used here, the man was found to be of a second order nature, and he used second order lead information in the motion mode, less second order lead information in the peripheral mode, and the smallest second lead information in the static mode of operation.

REFERENCES

1. Athans, M., "On the Design of PID Controllers Using Optimal Linear Regular Theory", Automatica, Vol. 7, 1971, pp 643-647.

2. Phatak, A.V., and Kessler, K.M., "Evaluation of Optimal Control Type Models for the Human Gunner in an Antiaircraft Artillery (AAA) System", The Eleventh Annual Conference on Manual Control, Ames Research Center, Moffett Field, California, NASA TM X-62,464.

3. Shirley, R.S., "Motion Cues in Man-Vehicle Control", M.I.T., Cambridge, Mass., Sc.D. Thesis, January, 1968.

4. Young, L.R., "The Current Status of Vestibular System Models", Automatica, Vol. 5, pp 369-383, 1969.

5. Stapleford, R.L., Peters, R.A., and Alex, F., "Experiments and a Model for Pilot Dynamics with Visual and Motion Inputs", NASA CR-1325, May, 1969.

6. Ringland, R.F. and Stapleford, R.L., "Experimental Measurements of Motion Cue Effects on STOL Approach Tasks", NASA CR-114458, April, 1972.

7. Levison, W.H., "A Model for the Pilots Use of Motion Cues", The Twelfth Annual Conference on Manual Control, University of Illinois at Urbana-Champaign, May 25-27, 1976.

8. Levison, W.H. and Baron, S., "Modeling the Effects of Environmental Factors on Human Control and Information Processing", Bolt, Beranek and Newman, Report No. 3258, March, 1976.

9. Junker, A.M. and Price, D., "Comparison Between a Peripheral Display and Motion Information on Human Tracking About the Roll Axis", AIAA Visual and Motion Simulation Conference, Dayton, Ohio, April, 1976.

10. Moriarty, T.E., Junker, A.M., and Price, D.R., "Roll Axis Tracking Improvement Resulting from Peripheral Vision Motion Cues", The Twelfth Annual Conference on Manual Control, University of Illinois at Urbana-Champaign, May 25-27, 1976.

11. Price, D.R., "A Study of the Effect of Peripheral Vision Motion Cues on Roll Axis Tracking", Master of Science Thesis, Air Force Institute of Technology, December, 1975.

12. Jex, H.R., Allen, R.W., and Magdaleno, R.E., "Display Format Effects on Precision Tracking Performance, Describing Functions, and Remnant", AMRL-TR-71-63, Systems Technology, Inc., August, 1971.

13. Sheridan, T.B. and Ferrell, W.R., "Man-Machine Systems: Information, Control, and Decision Models of Human Performance", The M.I.T. Press, 1974.

14. Shinners, S., "Modeling of Human Operator Performance Utilizing Time Series Analysis", IEEE Transactions on Systems, Man, and Cybernetics, September, 1974, pp 446-458.

15. Astrom, K.J. and Eykhoff, P., "System Identification - A Survey", Automatica, Vol. 7, pp 123-162.

16. Poulton, E.C., "Tracking Skill and Manual Control", Academic Press, 1974.

17. Junker, A.M., Repperger, D.W., Neff, J.A., "A Multiloop Approach to Modeling Motion Sensor Responses", Eleventh Annual Conference on Manual Control, NASA TM X-62, 464, May, 1975.

TABLE 1

e_{RMS} SCORES IN DEGREES

	STATIC	MOTION	PERIPHERAL
e_{RMS} ERROR	33.714	18.73	19.21
RATE VARIANCE FOR ERROR	22206.	1031.2	1211.3

TABLE 2

RESULTS OF THE T-TEST VERSUS ZERO (EXISTENCE OF COEFFICIENTS):

	COEFFICIENTS	MEAN	VARIANCE	N_1	MEAN	VAR.	N_1	t STATISTIC	α
STATIC	C_1	.3912	.2343	6	0	0	6	4.0898	.0022
	C_2	.5571	.3559	6	0	0	6	3.8343	.0033
	C_3	.8479	1.5913	6	0	0	6	1.3052	.2211
	C_4	1.49	2.5952	6	0	0	6	1.4063	.1899
MOTION	C_1	.426	.297	6	0	0	6	3.5134	.0056
	C_2	1.327	.58	6	0	0	6	5.6043	.0002
	C_3	.4187	1.3905	6	0	0	6	.7376	.4777
	C_4	1.1294	1.6201	6	0	0	6	1.7076	.1185
PERIPHERAL	C_1	.4401	.2851	6	0	0	6	3.7812	.0036
	C_2	1.132	.6721	6	0	0	6	4.1256	.0021
	C_3	1.0813	1.7482	6	0	0	6	1.5151	.1607
	C_4	1.1893	1.8751	6	0	0	6	1.5536	.1513

TABLE 3

T-TESTS VERSUS MEANS (CHANGES IN COEFFICIENTS):

	COEFFICIENT	MEAN	VAR	N_1	MEAN	VAR	N_2	t STATISTIC	α
		Static			Motion				
STATIC VERSUS MOTION	C_1	.3912	.2343	6	.426	.297	6	-.2253	.8263
	C_2	.5571	.3559	6	1.327	.58	6	-2.7713	.0197
		Static			Peripheral				
STATIC VERSUS PERIPHERAL	C_1	.3912	.2343	6	.4401	.2851	6	-.3246	0.7522
	C_2	.5571	.3559	6	1.132	.6721	6	-1.8517	.0938
		Motion			Peripheral				
MOTION VERSUS PERIPHERAL	C_1	.426	.297	6	.4401	.2851	6	-.0839	.9348
	C_2	1.327	.58	6	1.132	.6721	6	.538	.6023

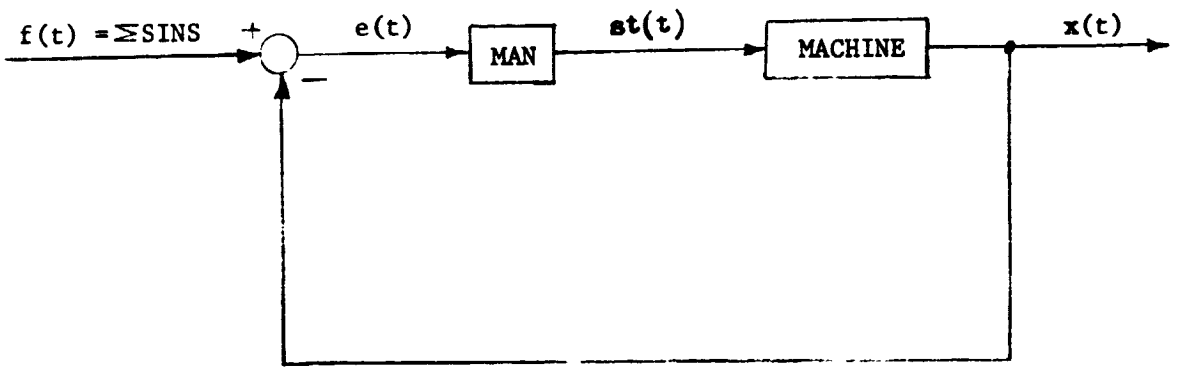

Figure (1a) - The Closed Loop Tracking Task

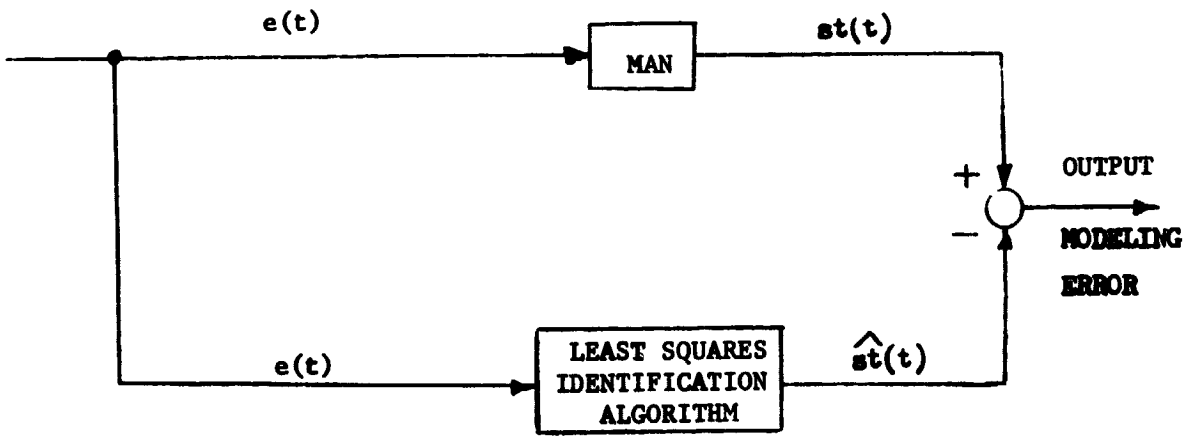

Figure (1b) - The Internal Loop Approach

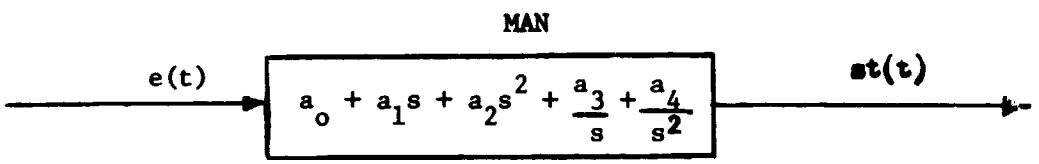

Figure (2) - Replacing Man By His PID Parameters

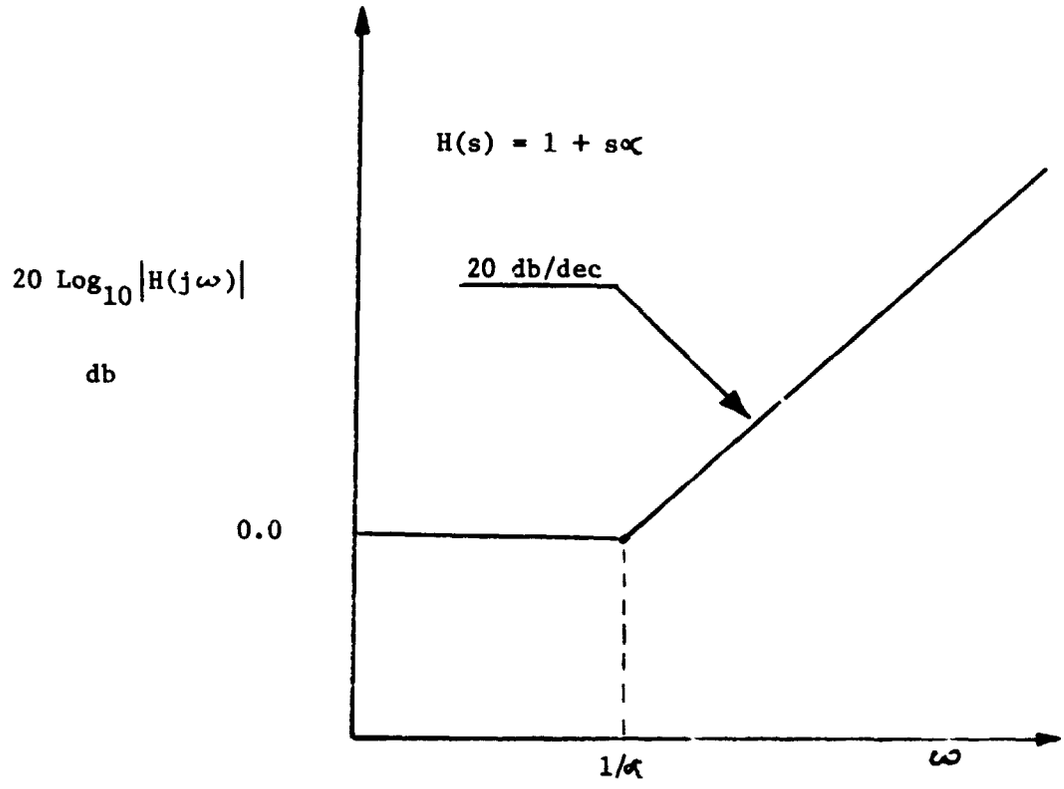

Figure (3) - The Definition of Pilot Lead

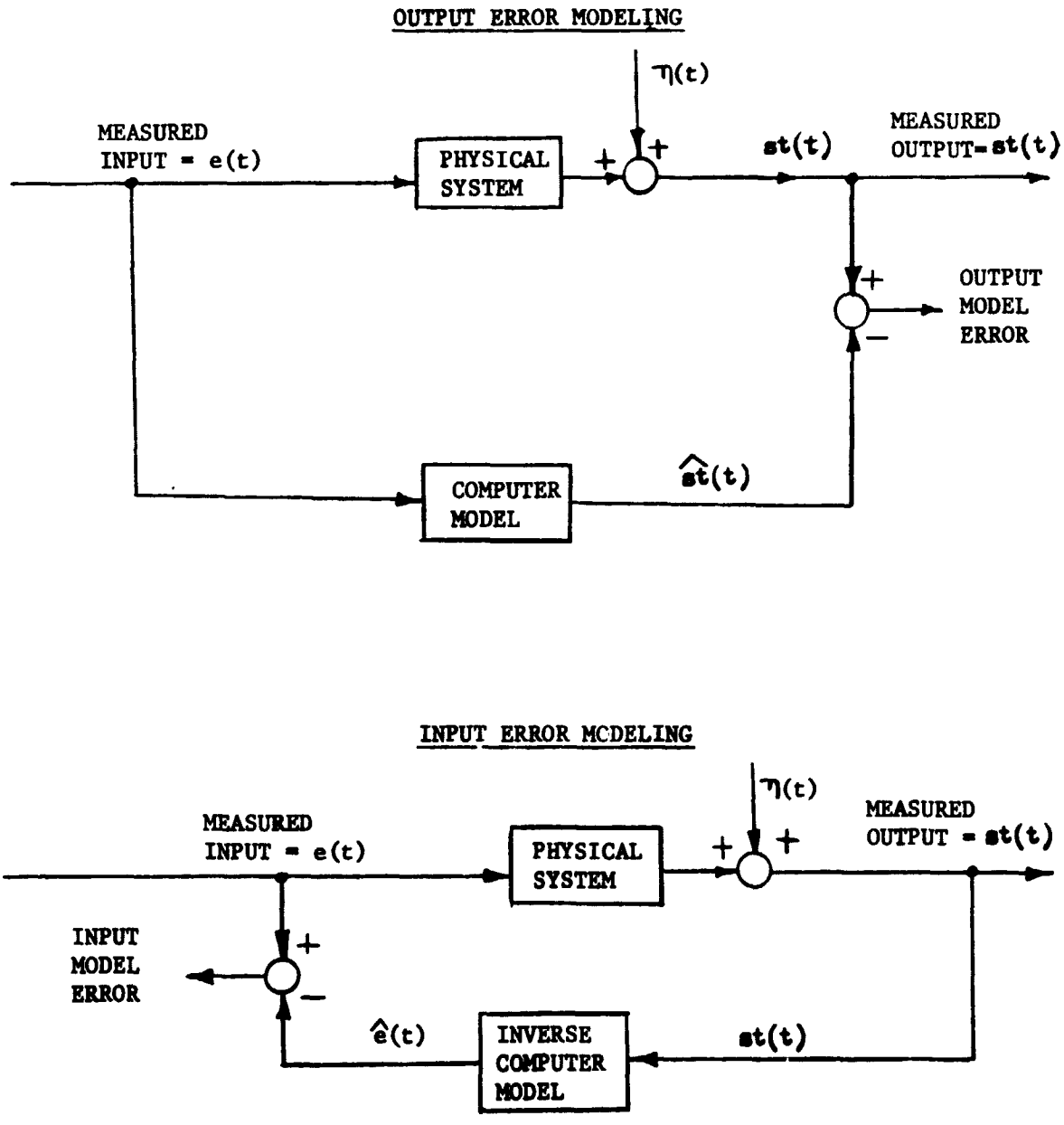

Figure (4) - Output Error Modeling Compared To Input Error Modeling

SENSITIVITY ANALYSIS OF MOTION AND PERIPHERAL DISPLAY EFFECTS ON TRACKING PERFORMANCE*

By Daniel W. Repperger and Andrew M. Junker

Aerospace Medical Research Laboratory
Wright-Patterson Air Force Base, Ohio 45433

SUMMARY

A study of sensitivity was initiated in an effort to determine what variables effect the decision making processes of a human as he performs a tracking task. If the sensitivity of the closed loop tracking error can be determined with respect to data variables such as displayed error and its respective derivatives, then some knowledge can be obtained about the decision making aspects of the human. In addition, if some other data is useful for the human in his tracking, sensitivity analysis will indicate this pertinent data. A Proportional Integral Derivative (PID) type modeling approach was used with a sum of sins input tracking task to enable sensitivity coefficients to be calculated. Coefficients of sensitivity were computed at each frequency and comparisons of these coefficients were determined over a wide frequency range for different experimental conditions. Data from a motion experiment and a peripheral display experiment were used in this study.

INTRODUCTION

The study of sensitivity in control theory has its origin from the classical paper of Cruz and Perkins reference(1). More recently Boniveto reference(2) has defined the term sensitivity in a manner which is related to identifiability. What is meant by this statement is that in a modeling approach in which data has already been collected (A Posteriori modeling), it is important to ascertain which parameters are important or sensitive and thus determine the proper model structure. If a parameter in a modeling approach is a sensitive parameter, then this parameter is important in the chosen model structure. Conversely, if a parameter is not sensitive in the modeling approach, then it should probably not be considered for the model

*The research reported in this paper was sponsored by Aerospace Medical Research Laboratory, Aerospace Medical Division, Air Force Systems Command, Wright-Patterson Air Force Base, Ohio 45433. Further reproduction is authorized to satisfy needs of the U.S. Government.

structure. From the sensitivity analysis, it is possible to determine the influential parameters and thus to concentrate our effort and attention on these parameters.

In this paper a conjecture is made on how to guess cost function weightings on optimal control models based on calculated sensitivities. Since most optimal control models require weighting of the closed loop error (and its derivatives), a method will be explored to choose these weightings based on the sensitivity (or gradients) of the closed loop error with respect to parameters.

Since error in the closed loop is a measure of performance for the closed loop tracking task, it is of interest to observe how this error changes or how its sensitivity varies as a function of the parameters in the closed loop system. In this manner it is possible to see how performance in the closed loop is influenced by certain relevant or sensitive parameters.

Using the (A Posteriori) PID model presented in reference (3), the sensitivity of the closed loop error was calculated with respect to the PID parameters already obtained. The data base and experiments used here are the same as in reference (3).

Closed Loop Error Sensitivity

With reference to Figure 1, the transfer function of man (using the PID model) is denoted as:

$$\text{Man} = G(s) = a_o + a_1 s + a_2 s^2 \tag{1}$$

using the fact that

$$\frac{X(s)}{F(s)} = \frac{GH}{1+GH} \tag{2}$$

and

$$\frac{X(s)}{E(s)} = GH \tag{3}$$

yields

$$\frac{E(s)}{F(s)} = \frac{X(s)}{F(s)} \cdot \frac{1}{\left(\frac{X(s)}{E(s)}\right)} = \frac{1}{1+GH} \tag{4}$$

or

$$E(s) = \frac{F(s)}{1+G(s)H(s)} \tag{5}$$

therefore

$$E(s) = \frac{F(s)}{1+(a_o+a_1 s+a_2 s^2)\,H(s)} \tag{6}$$

Equation (6) is in an ideal form. On the right hand side of the equation is all the loop variables which influence the closed loop error. This includes the external forcing function, the plant, and the man represented by PID parameters. On the left hand side of equation (6) is the isolated expression for the closed loop error as a Laplace transform. The simplicity of equation (6) is that the performance in the loop is isolated on the left hand side of the equation and all the possible variables that effect this performance are isolated on the right hand of this expression.

Since a sum of sins input was used in these experiments, it is possible to set $s = j\omega_i$ ($i = 1,2,\ldots,12$ frequencies used) and for each value of ωi, the error and (as it will be shown in the sequel) the partial derivatives of E(s) with respect to the parameters a_o, a_1, and a_2 can also be obtained.

In order to obtain the partial derivatives of the closed loop error with respect to the PID parameters, it is noted that at each fixed value of frequency ωi, the partial derivatives of the closed loop error with respect to the parameters a_o, a_1, and a_2 can be obtained quite easily. Simple differentiation (for a fixed ωi) of equation (6) with respect to a_o, a_1, and a_2 yields:

$$\frac{\partial E}{\partial a_o} = \frac{-F(s)H(s)}{[1+(a_o+a_1s+a_2s^2)H(s)]^2} = \frac{A_1e^{j\theta_1}}{A_2e^{j\theta_2}} \tag{7a}$$

$$\frac{\partial E}{\partial a_1} = \frac{-sF(s)H(s)}{[1+(a_o+a_1s+a_2s^2)H(s)]^2} = \frac{A_3e^{j\theta_3}}{A_2e^{j\theta_2}} \tag{7b}$$

$$\frac{\partial E}{\partial a_2} = \frac{-s^2F(s)H(s)}{[1+(a_o+a_1s+a_2s^2)H(s)]^2} = \frac{A_4e^{j\theta_4}}{A_2e^{j\theta_2}} \tag{7c}$$

Equations (7a-c) are written in phasor notation since both the numerator and denominator have different magnitude and phase angle shifts respectively at each value of frequency. The following relationship can easily be shown:

$$\frac{\partial E}{\partial a_2} = s\frac{\partial E}{\partial a_1} = s^2\frac{\partial E}{\partial a_o} \tag{8}$$

Using equations (7a-c), the gradients (or sensitivities) of E with respect to a_o, a_1, and a_2 were calculated. The results were given in Table 1.

The plots of the (averaged) sensitivities are displayed in Figure (2) for the static case. In this plot it is noted that the sensitivity functions peak near the crossover frequency which was approximately 1.35 radians for the static mode of operation. The frequency at which peaks of all three curves occurred did not differ by more than 1 radian.

In Figure (3) the sensitivity functions are plotted for the motion case. In Figure (3) the curves of $\partial E/\partial a_o$ and $\partial E/\partial a_1$ were not radically different. The curve for $\partial E/\partial a_2$, however, had an unusually different peak three times as large as the other two peaks and shifted to the right (beyond the crossover frequency) by almost 2 radians. Since these results are averaged over subjects and replications, it appears that in the motion mode of operation, the closed loop error has its greatest sensitivity to the double lead parameter a_2. This is in concurrence with reference (3) where the statistical analysis was performed and also with some previous work done in reference (4).

In Figure (4), the sensitivity curves are plotted for the peripheral case (ensemble averaged) and they appear similar to the static case. The peaks are only 0.5 radians apart and are located near the crossover frequency.

When comparing the peripheral case to the static case, however, the peripheral peaks are much higher than the static case. Comparing the $\partial E/\partial a_2$ curves (the second lead term), for the peripheral mode of operation versus the motion mode, the motion case has the greatest shift to the right (and beyond the crossover frequency) but not as great a magnitude as in the peripheral case. Hence it appears that the second lead term a_2 is more dominant in the motion case, less dominant in the peripheral case, and much less dominant in the static case. These results agree with the statistical analysis obtained in reference (3). A method of choosing cost function weightings based on the inverse variances of the sensitivity functions will now be conjectured.

Conjecture: How To Pick Cost Function Weightings in An A Posteriori Sense

Figure (5) illustrates a close up view of the static mode of operation of Figure (2) near the crossover frequency. Also illustrated on this plot is one standard deviation (at the frequency 1.572 radians) of the averages obtained for the three curves. Since a greater variance in the estimate of this sensitivity indicates less effect of this parameter on the closed loop error, the following conjecture arises:

Conjecture: Given a cost function of the form

$$J = \frac{1}{T}\int_0^T ||e(t)||^2_{K_1} + ||\dot{e}(t)||^2_{K_2} + ||\dot{e}^*(t)||^2_{K_3}\, dt \qquad (9)$$

where T may become infinite. One may attempt to pick the unknown cost functions K_1, K_2, and K_3 in the following manner:

$$K_1 = \alpha\, [\text{VAR}\ \partial E/\partial a_o]^{-1} \qquad (10a)$$

$$K_2 = \alpha\, [\text{VAR}\ \partial E/\partial a_1]^{-1} \qquad (10b)$$

$$K_3 = \alpha\, [\text{VAR}\ \partial E/\partial a_2]^{-1} \qquad (10c)$$

where α = A constant of proportionality. If cost function weightings are chosen in this manner, then for parameters with a large variance in the sensitivity values the corresponding weighting matrices should have the smallest values in the cost function. In other words if the closed loop error is not sensitive to a particular parameter (which is indicated by a large variance), then the weighting for this parameter should be small. Conversely if the closed loop error has a large sensitivity with respect to a given parameter

(as indicated by a small variance in the estimate of the sensitivity function), then the cost function should be weighted more. In Figure (5), we would weight K_1 and K_2 (corresponding to e(t) and $\dot{e}(t)$) more than we would weight K_3 (corresponding to $\ddot{e}^{\circ}(t)$). This approach is consistent with the inverse of the standard deviations shown in Figure (5) and also has agreement with the statistical analysis demonstrated in reference (3). It is hoped that with additional work, this conjecture can be more carefully quantified and perhaps more rigorously shown.

CONCLUSIONS

A study of closed loop error sensitivity is introduced for a PID type model structure. The closed loop error sensitivity is computed for the three PID parameters across three tasks denoted as the Static, Motion, and Peripheral mode of operation. The peak sensitivities show quite a bit of difference between the three modes of operation. For this simulator the second lead term seems to have the greatest sensitivity of the closed loop error in the motion (roll axis) task. A method of guessing at cost function weightings based on the inverses of the variances of the sensitivities is hypothesized. Further work needs to be done on this topic.

REFERENCES

1. Cruz, J.B. and Perkins, W.R., "A New Approach to the Sensitivity Problem in Multivariable Feedback System Design", IEEE Transactions on Automatic Control, Vol. AC-9, No. 3, 1964, pp 216-223.

2. Boniveto, C., "Structural Insensitivity Versus Identifiability", IEEE Transactions on Automatic Control, April, 1973, pp 190-192.

3. Repperger, D.W. and Junker, A.M., "PID Modeling Techniques Applied to Studies of Motion and Peripheral Display Effects on Human Operator Performance", The Twelfth Annual Conference on Manual Control, May, 1976.

4. Junker, A.M., Repperger, D.W., Neff, J.A., "A Multiloop Approach to Modeling Motion Sensor Responses", Eleventh Annual Conference on Manual Control, NASA TM X-62, 464, May, 1975.

TABLE 1

TABLE OF CALCULATED GRADIENTS

FREQUENCY s	STATIC			MOTION			PERIPHERAL		
	$\frac{\partial E}{\partial a_o}$	$\frac{\partial E}{\partial a_1}$	$\frac{\partial E}{\partial a_2}$	$\frac{\partial E}{\partial a_o}$	$\frac{\partial E}{\partial a_1}$	$\frac{\partial E}{\partial a_2}$	$\frac{\partial E}{\partial a_o}$	$\frac{\partial E}{\partial a_1}$	$\frac{\partial E}{\partial a_2}$
.077	.0313	.00241	1.855×10^{-4}	3.155×10^{-2}	2.43×10^{-3}	1.87×10^{-4}	3.15×10^{-2}	2.43×10^{-3}	1.86×10^{-4}
.192	.3825	.0394	7.565×10^{-3}	2.175×10^{-1}	4.17×10^{-2}	8.005×10^{-3}	.214	4.11×10^{-2}	7.89×10^{-3}
.307	.68	.1175	3.61×10^{-2}	.4465	.137	4.21×10^{-2}	.4295	.132	4.045×10^{-2}
.460	1.339	.313	.144	1.008	.463	.213	.9215	.423	.1945
.690	1.339	.9205	.6365	2.79	1.925	1.328	2.39	1.649	1.1345
1.035	5.26	5.445	5.635	39.76	41.13	42.6	4.655	4.815	4.9805
1.572	4.795	7.565	11.855	1.3592	2.1365	3.3585	12.185	19.1335	30.11
2.378	1.2505	2.9665	7.05	.2988	.6635	1.5845	.67	1.593	3.788
3.567	.1825	.651	2.32	7.68×10^{-2}	.2744	.9765	.1179	.4196	1.497
5.369	.04845	.260	1.398	.002101	.1127	.6065	3.325×10^{-2}	.1783	.958
8.053	.0115	.0429	.748	.000704	.05685	.4575	$.85\times10^{-2}$	.0685	.5525
12.08	5.09×10^{-4}	6.125×10^{-3}	7.425×10^{-2}	.0007	.003965	.137	6.87×10^{-4}	8.28×10^{-3}	1.003×10^{-2}

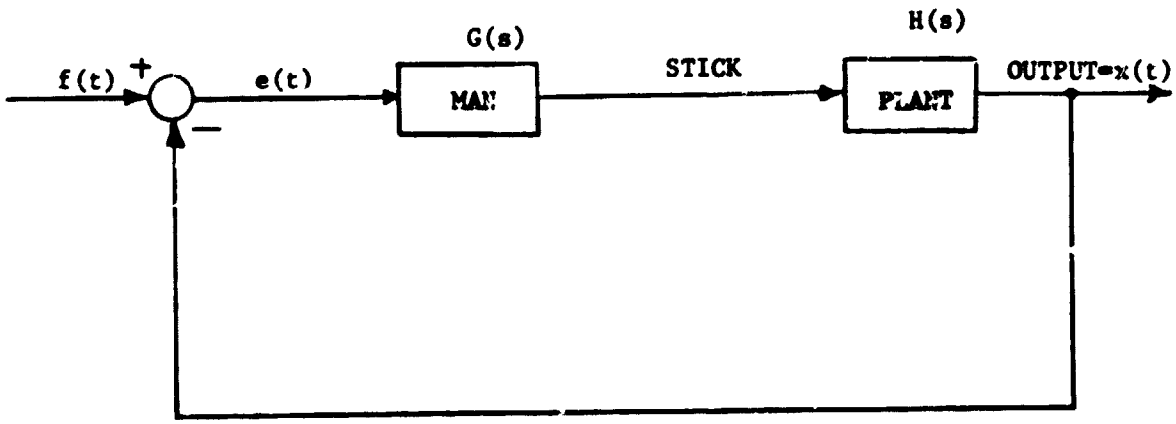

FIGURE 1 - CLOSED LOOP ERROR SENSITIVITY

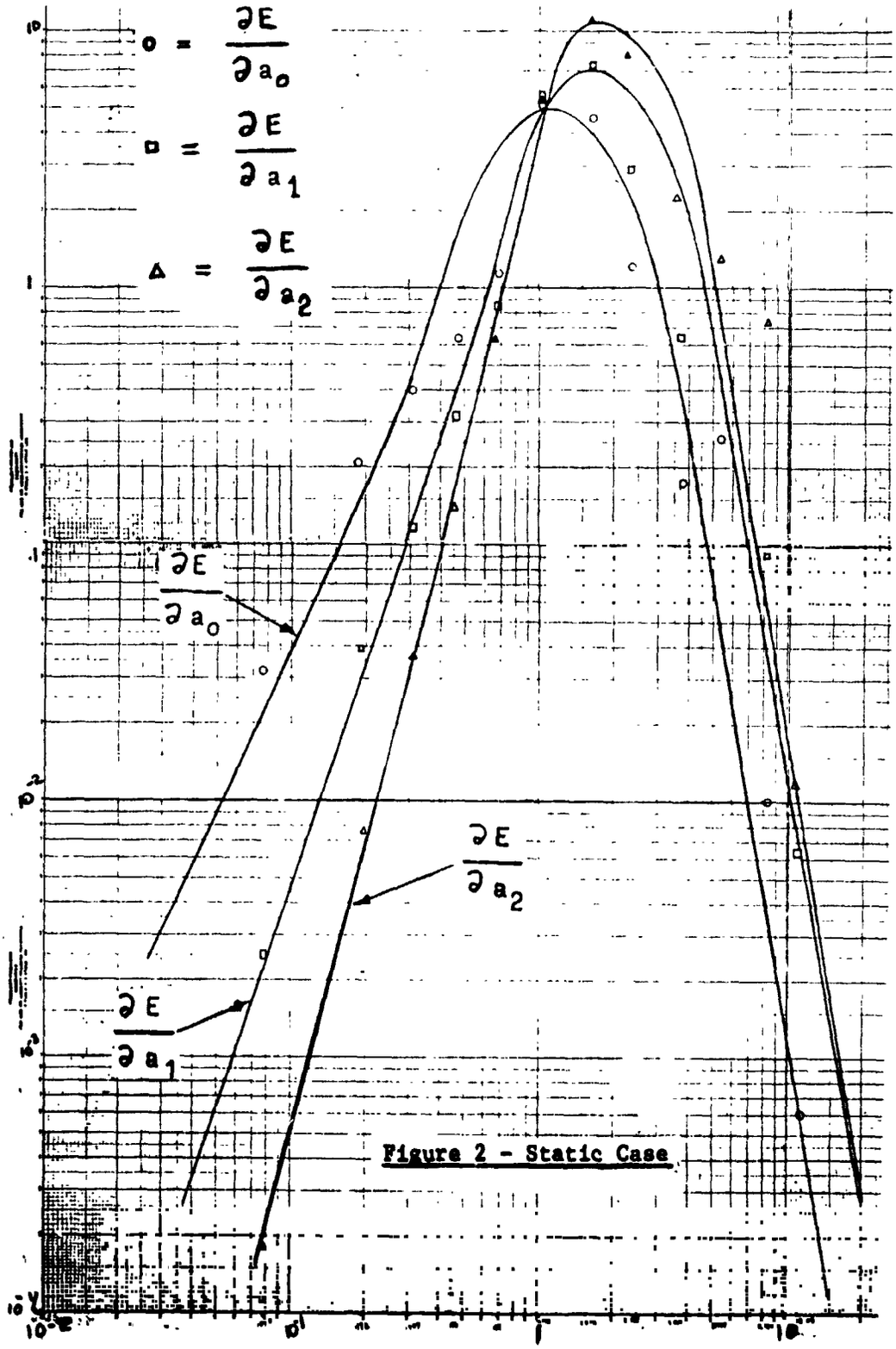

Figure 2 - Static Case

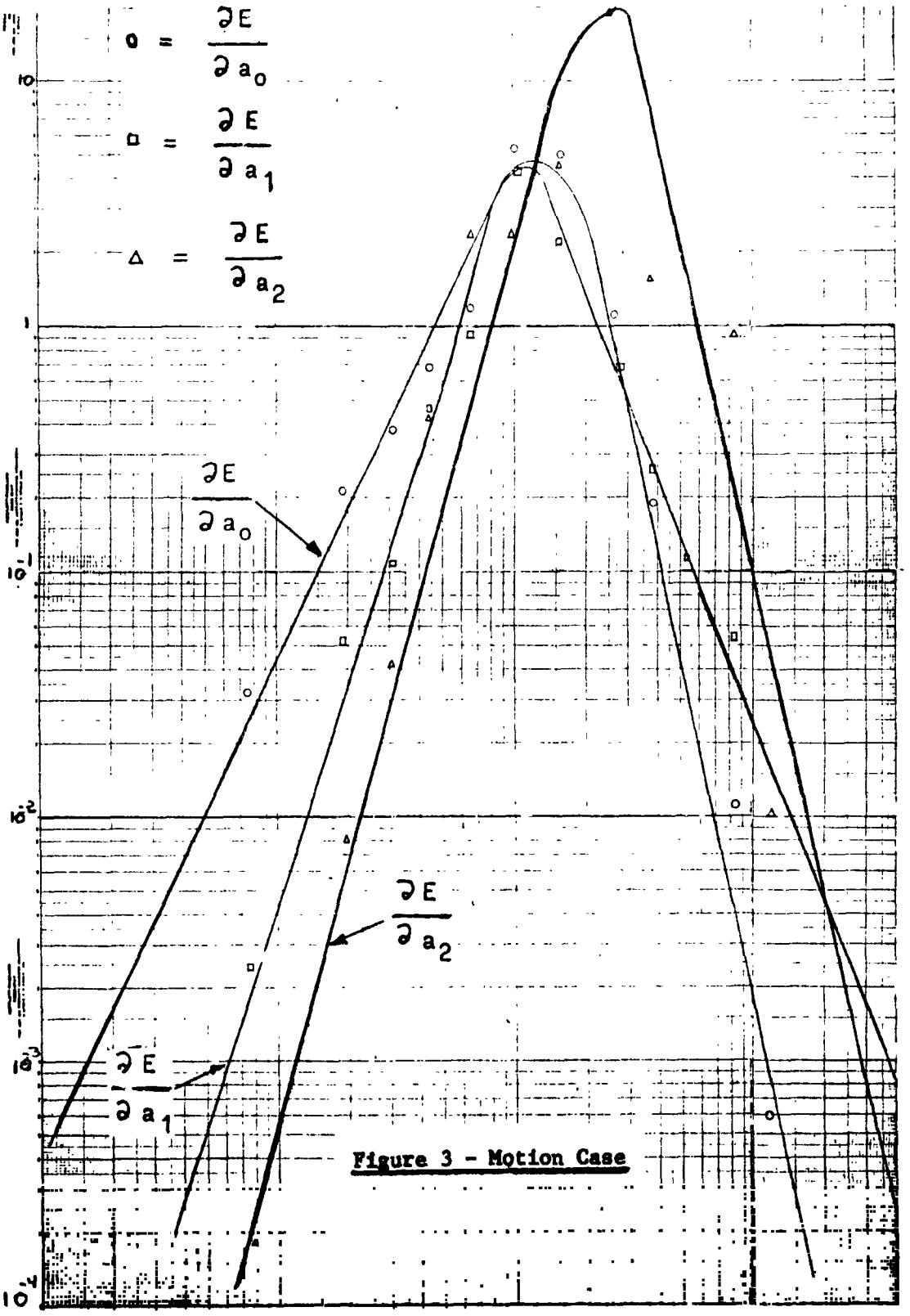

Figure 3 - Motion Case

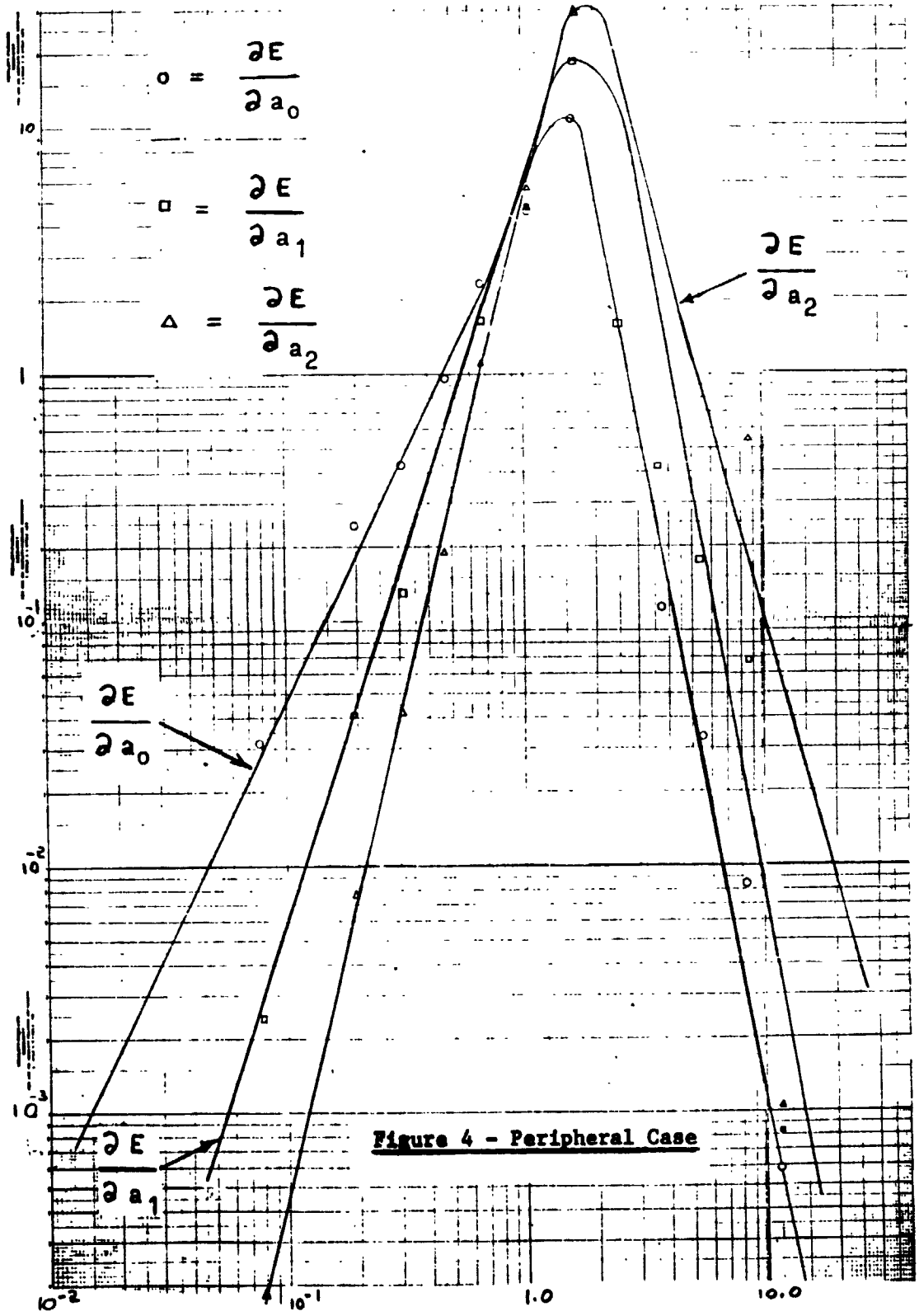

Figure 4 - Peripheral Case

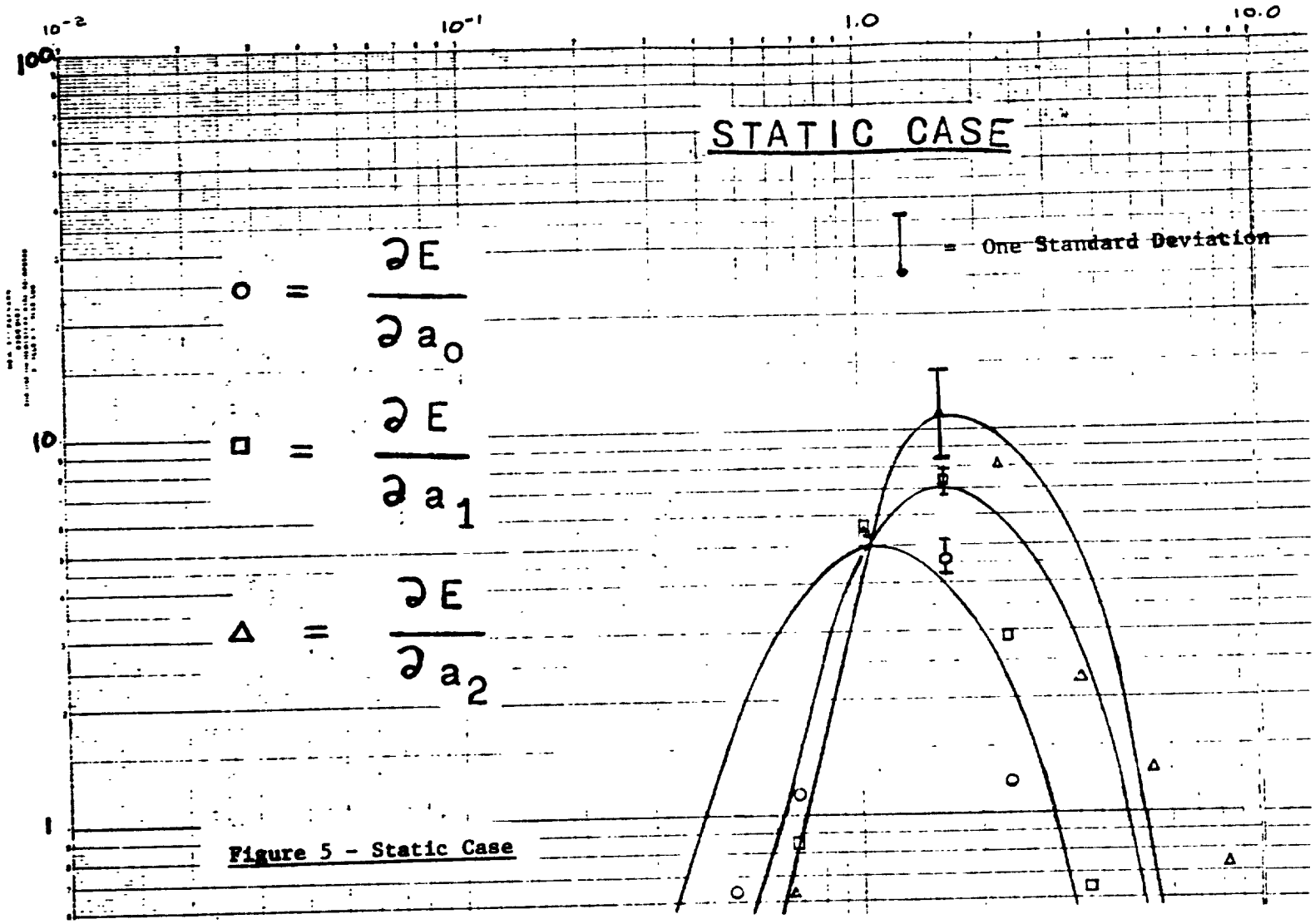

Figure 5 - Static Case

SESSION X

CONTROL MODELS

Chairman: S. Baron

LOW VISIBILITY LANDING SIMULATION EXPERIMENTS

Capt R.V. Gressang, Capt J.J. Pollard and Mr. D.L. Kugel
Air Force Flight Dynamics Laboratory

SUMMARY

The paper describes two experiments which simulated a transport aircraft landing in reduced visibility. The experiments were conducted as part of a low visibility landing simulation program sponsored at the Air Force Flight Dynamics Laboratory by the Federal Aviation Administration. Data during the experiments were collected in a form suitable for use in an optimal control pilot model.

For the experiments, a C-135B was simulated using six degree of freedom nonlinear equations on a hybrid simulator. Visual, motion, and sound cues and a gust disturbance were provided. The effects of reduced visibility were simulated by driving a sky plate in the TV lense system focal plane.

The first experiment used two subjects, and considered four visibility conditions. The second experiment used one subject, and considered three visibility conditions. The experiment results included statistics on glide slope and localizer tracking and on touchdown conditions. Pilot comments were recorded, and limited data are available from the second experiment on pilot eye scanning.

I. INTRODUCTION

This paper describes two experiments conducted to collect data suitable for developing a pilot model of low visibility landing. A sampling of the results is presented in this paper, and the complete results can be found in References 1 and 2.

These experiments were conducted as part of a low visibility landing simulation program conducted for the Federal Aviation Administration (FAA) by the Air Force Flight Dynamics Laboratory (AFFDL). The program was to investigate low visibility landing operations while minimizing new equipment costs by making maximum use of AFFDL flight simulators. The overall program aims were as follows: to develop a capability to evaluate and validate pilot workload and performance in Category II and III weather conditions; to determine the utility of visual cues in Category II and III landing operations; and to identify simulator improvements required for adequate and realistic engineering simulation of low visibility landing operations.

As part of the low visibility landing program, the Flight Dynamics Laboratory undertook to develop a pilot model. The rationale for developing a low visibility landing pilot model was that a pilot model would permit analytical studies of low visibility landing to be made for a relatively large number of aircraft configurations, visibilities, and disturbances.

These analytical studies would then be used in planning to effectively allocate use of the engineering flight simulator.

The pilot model being developed (and described in another paper given at this conference) is of the optimal control type, and is adapted to tasks which are time varying. A model capable of treating time varying tasks was chosen because of the variations in task dynamics as a function of range and due to the flare maneuver. To develop this model, ensemble statistics of the landing task state variables are required as a function of range. Thus the data base for the pilot model must be established using experiments containing sufficient replications for ensemble statistics to be meaningful.

The data base for the pilot model was established through two experiments using the multicrew cab simulator. The first experiment was conducted and the data from it analyzed, which revealed some limitations of the simulation. Efforts were made to reduce these limitations, and the second experiment was then conducted.

II. DESCRIPTION OF THE SIMULATION

The aircraft used for this manned simulation was the military C-135B transport, which is similar to the commercial Boeing 707. The aircraft configuration had a weight of 160,000 pounds, the center of gravity located at 28.2 percent of the mean aerodynamic chord, a flap setting of 50 degrees, and the landing gear down. The aircraft mathematical model used was a six degree of freedom nonlinear model, and was programmed on a hybrid computer. Each experimental run began from trimmed flight conditions at 956 feet altitude on a three degree glide slope.

A conventional C-135B flight control system was used in the simulation. The controls included wheel (aileron), column (elevator), and rudder pedals. Thumb buttons for pitch and roll trim were located on the wheel; a crank for rudder trim was on the center console. Throttle, flap, gear, and speed brake handles were fully operational.

The cockpit instruments were those typical of the C-135B. The instruments driven during the simulation were the attitude director indicator (ADI), horizontal situation indicator (HSI), airspeed indicator, rate of climb indicator, barometric altimeter, radar altimeter, angle of attack indicator, G meter, Mach meter, clock, compass indicator (RMI), engine pressure ratio gauges, tachometers, exhaust gas temperature gauges, fuel flow meters, and oil pressure gauges. Annunciators for the outer, middle, and inner markers were driven. Flight director pitch and roll steering command bars were driven in accordance with the glide slope tracking mode of the Collins FD-109 flight director.

The aircraft simulated during the first experiment did not have a yaw damper. Between the two experiments, a yaw damper was added to the aircraft model. This yaw damper was used throughout the second experiment.

The cockpit used was an actual C-135 cockpit modified for use as a research and development simulator. It was mounted upon a three degree of freedom motion base, and capable of limited pitch, roll, and heave motion. Sound cues duplicating the sound of four turbojet engines were produced. These cues were proportional to throttle position and airspeed.

Visual cues simulating real world changes in size and perspective with respect to aircraft movements were produced using an illuminated three dimensional terrain model and television camera-screen projection system. The field of view of the screen was 60 degrees diagonally with appropriate cockpit cutoff angles for the C-135. The view was large enough to present a realistic scene through the front windows, but there were no peripheral cues. The pilot saw a daylight rural terrain with an airport complex including strobe, approach, and VASI lights. The visual display was automatically controlled by computer to simulate homogeneous fog with the following initial visual contact altitude/runway visual range conditions:

a. Unlimited/unlimited

b. 400 feet/1600 feet

c. 300 feet/1200 feet

d. 100 feet/1200 feet

The reduced visibility conditions were generated by driving a knife edge in the focal plane of the TV camera. The visibility conditions were settled upon in consultation with the first experiment's subject pilots so as to appear realistic.

During the simulation runs, light turbulence was added as a disturbance to the aircraft. This turbulence had the Dryden spectra of MIL-F-8785B corresponding to an average altitude of 500 feet[3].

During the simulation, the pilot's task was to conduct an instrument flight rules (IFR) landing. The pilots had no auxiliary tasks, such as communication, to perform. The pilot was assisted by a copilot, but this assistance was limited to the copilot calling the initial appearance of cues in the visual scene and the copilot monitoring such quantities as airspeed and altitude.

During the course of the experiments, certain limitations of the simulation became apparent. The most serious limitations were difficulty in obtaining a satisfactory representation of the lateral directional dynamics of the C-135 on the simulator, too high sink rates at touchdown in the simulator, and an overly sensitive flight director command bar. Between the two experiments, the simulation was modified to improve the lateral dynamics data match, the flight director gains were modified, a yaw damper was added, a landing gear simulation was added, the ground effects model was modified, the instrument drive signals were refined, and new plumbicon tubes were installed to improve the visual display. The simulation fidelity was improved in the second experiment. The main limitation remaining in

the second experiment was a mean touchdown sink rate which was still higher than that obtained in actual aircraft.

The subject pilots used in the experiments were USAF Rated Officers with C-135 experience. The pilots in the first experiment had 2930 and 2686 total flying hours. The pilot in the second experiment had 970 total flying hours.

Further information about the simulation can be obtained in References 1 and 4.

III. DESCRIPTION OF THE EXPERIMENTS

The main objective of the experiments was to obtain ensemble statistics for developing the pilot model. Subsidiary objectives were to determine the effect of reduced visibility upon the pilot's landing performance, and in the second experiment to measure the pilot's inside/outside cockpit scan behavior.

The first experiment used a complete factorial experiment plan, with the factors being pilot (two levels) and visibility (four levels). The experiment was replicated 10 times, resulting in a total of 80 simulation runs. The order of presentation of the visibility conditions to the pilots was random. Each pilot had a training session of about one hour duration before data were collected.

The second experiment used a randomized block plan, with three different visibilities (∞/∞, 400/1600, 100/1200). The order of presentation of the visibility conditions to the pilot was random, and he had had about four hours of experience on the simulator before the experiment was conducted.

Each simulation run was initiated with the aircraft trimmed, on the glide slope and localizer, at a range of 15,000 feet from the glide path intercept point (GPIP). The pilot did not know in advance what the visibility conditions would be, and he was instructed to fly the simulator as if it were a real aircraft. He was also instructed not to execute a missed approach, but to land regardless of circumstances, and comment later if he thought he should have gone around. He was briefed that there would be light to moderate turbulence, but no crosswinds.

The simulation run was ended after touchdown, and pilot comments were then collected via a questionnaire. During the simulation runs, the variables listed in Table 1 were recorded at a rate of 10 samples per second. During the second experiment, whether the pilot was looking inside or outside the cockpit was determined using electro-oculography. The electro-oculographic method used is described in Reference 2, where are also presented the results of a pre-experiment which established that wearing the electrode assembly did not affect the pilot's performance.

TABLE 1. VARIABLES RECORDED DURING THE EXPERIMENTS

1. R - Range, ft.
2. Y - Cross track error, ft.
3. h_{cg} - c.g. height, ft.
4. h_{eye} - Eye height, ft.
5. $\dot{x}$, $\dot{y}$, $\dot{h}$ - Earth referenced velocities, ft/sec.
6. u, v, w - Body axis referenced velocities, ft/sec.
7. a_x - Longitudinal acceleration, ft/sec^2.
8. n_z - Normal acceleration, g.
9. ψ, θ, ϕ - Euler angles, degrees
10. γ- Flight path angle, degrees.
11. p, q, r - Body axis angular velocities, deg/sec.
12. $\dot{\psi}$- Yaw rate, deg/sec.
13. $\dot{h}_{ind}$ - Indicated sink rate, ft/min.
14. V_e - East velocity, knots.
15. PSB - Pitch steering bar.
16. RSB - Roll steering bar
17. G/S $Error_{ind}$ - Indicated glide slope error.
18. Loc $error_{ind}$ - Indicated localizer error.
19. RPM 1, 2, 3, 4 - Engine RPM, for 4 engines, percent.
20. δ_{e_c} - Elevator deflection, degrees.
21. δ_{a_c} - Aileron deflection, degrees.
22. δ_{r_c} - Rudder deflection, degrees.
23. T_{δ_1}, T_{δ_2}, T_{δ_3}, T_{δ_4} - Throttle positions, for 4 engines, degrees.
24. V_{wind} - Wind velocity.

25. Event

26. u_g, v_g, w_g, p_g, q_g, r_g - Gust disturbances.

27. SVR - Slant visual range, ft.

28. ΔX, ΔY - Aim point coordinates, ft.

29. Run number

30. Time, sec.

IV. RESULTS OF THE EXPERIMENTS

Ensemble statistics were computed for each combination of pilot and visibility existing in both experiments. Using the data from the ten simulation runs for each combination of pilot and fog condition, a mean value and a standard deviation were calculated as a function of range (equivalent to time) for localizer error, glide slope error, roll, pitch, aileron deflection, and elevator deflection. In addition, for experiment two calculations were also made for displayed glide slope error, displayed localizer error, x, u, y, v, h, w, p, q, ψ, r, and δ_r. These quantities were then plotted as a function of range, in the form of a mean trajectory and plus or minus one standard deviation about the mean. The glide slope error and localizer error plots for the ∞/∞, 400/1600, and 100/1200 cases of experiment two are given as Figures 1 through 6. References 1 and 2 present the complete set of plots.

Overall, the ensemble statistics indicate that all three pilots improved their tracking of the glide slope as out of the cockpit visibility deteriorated. Based upon pilot comments and the in/out scanning data, this improvement in glide-slope tracking was caused by increased attention being paid to the flight instruments. Localizer tracking also tended to improve as visibility decreased. In the first experiment, difficulties with the flight director mechanization resulted both pilots exhibiting an "s" curve phenomena in tracking the localizer.

In the first experiment the pilots were unable to execute a proper flare and touchdown. Pilot comments indicated that this was due to difficulty in judging height and sink rate from the visual display, due to lack of peripheral vision cues. Therefore statistics were not computed for touchdown position and sink rate for experiment one. In the second experiment, however, the pilot was able to execute a flare and the touchdown sink rates, while high, were not unrealistic. The touchdown statistics for experiment two are given in Table 2. The only statistically significant effects due to visibility in the touchdown data were the mean and standard deviation of the longitudinal touchdown point were larger for the 100/1200 visibility case.

In addition to the ensemble statistics, means and standard deviations of h, y, ψ, θ, ϕ, p, q, r, δ_e, δ_a, and δ_r were computed for all of the data

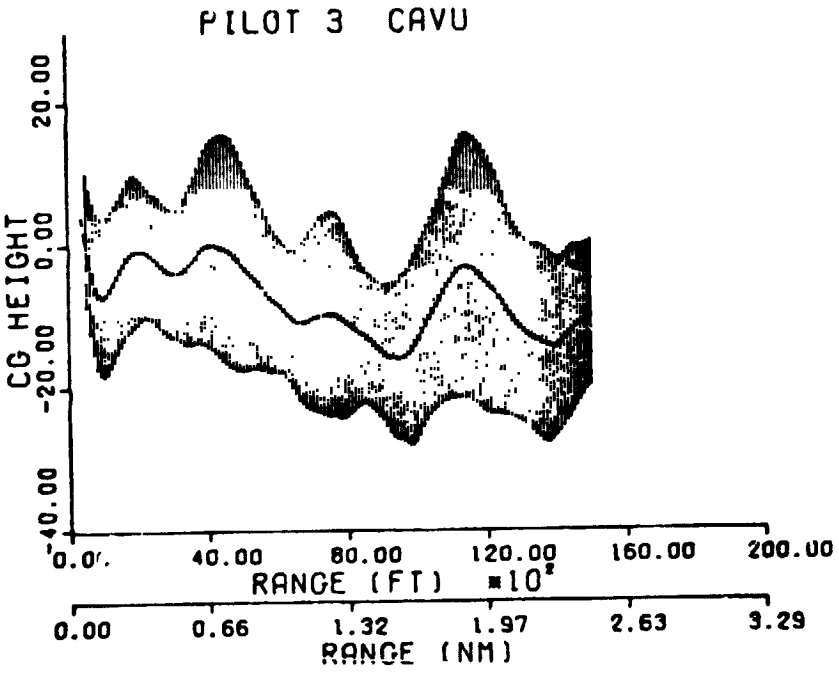

FIGURE 1. GLIDE SLOPE ERROR ENSEMBLE STATISTICS, ∞/∞

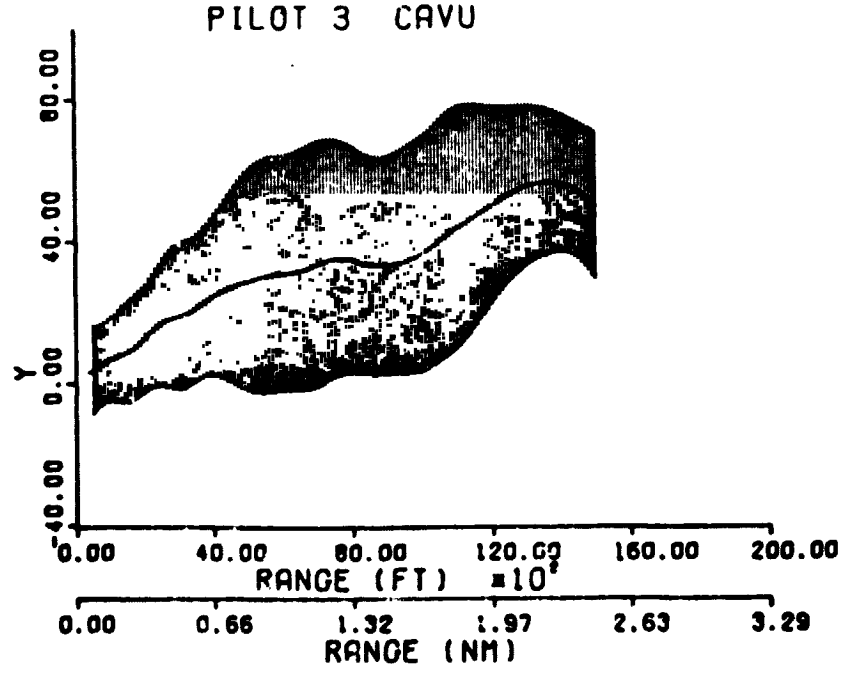

FIGURE 2. LOCALIZER ERROR ENSEMBLE STATISTICS, ∞/∞

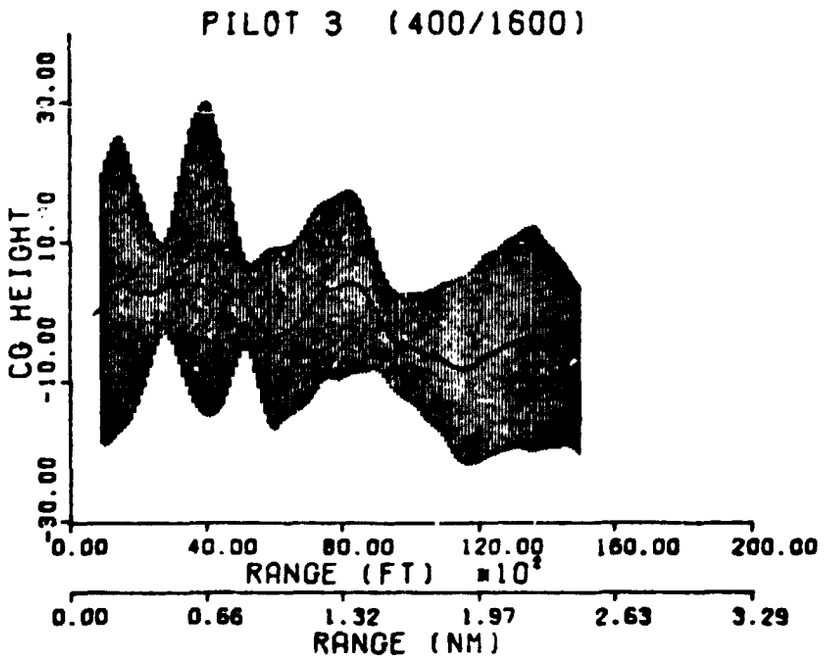

FIGURE 3. GLIDE SLOPE ERROR ENSEMBLE STATISTICS, 400/1600

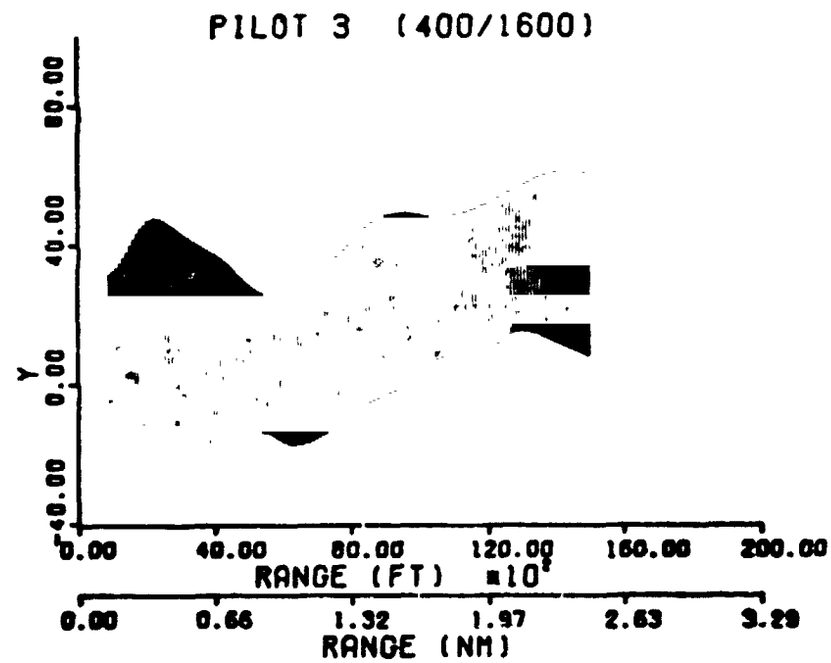

FIGURE 4. LOCALIZER ERROR ENSEMBLE STATISTICS, 400/1600

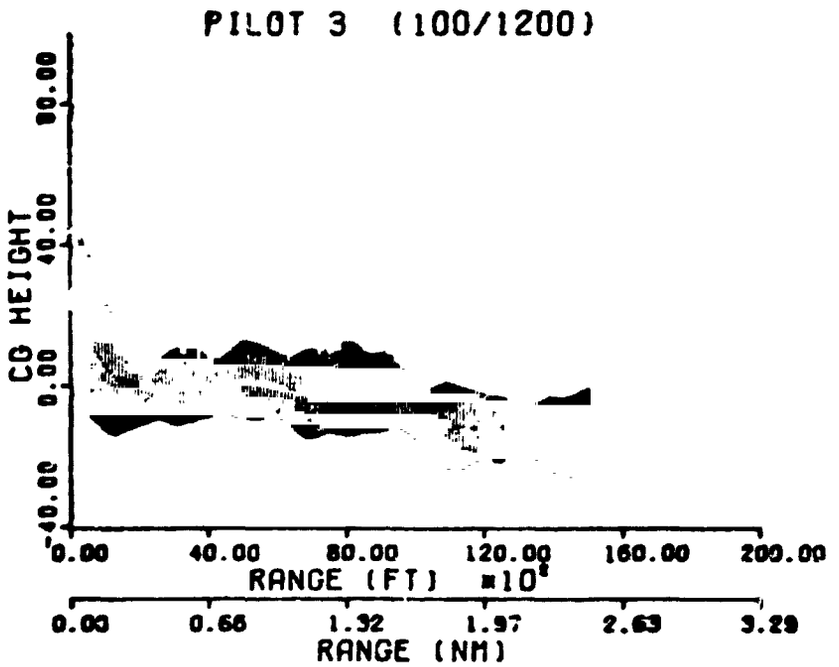

FIGURE 5. GLIDE SLOPE ERROR ENSEMBLE STATISTICS, 100/1200

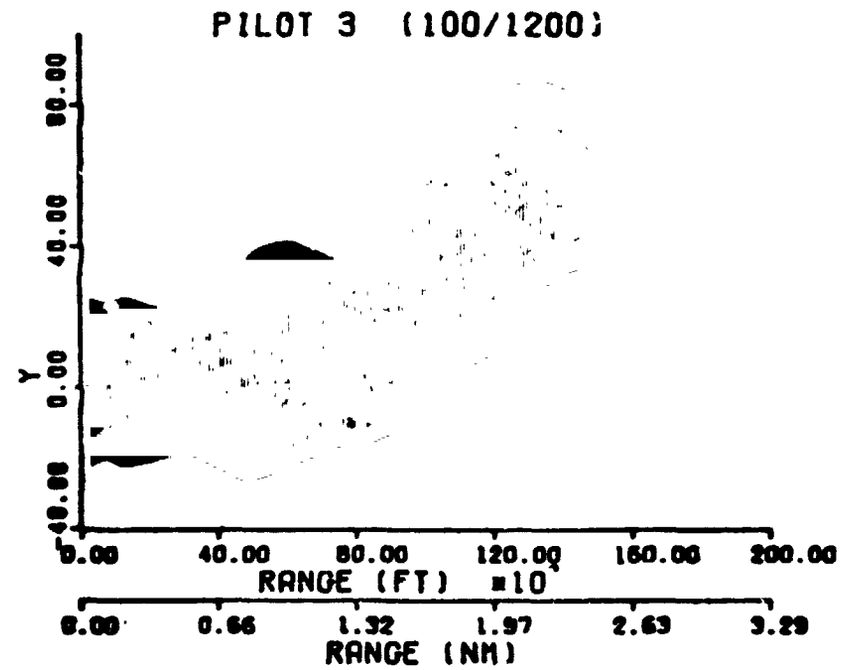

FIGURE 6. LOCALIZER ERROR ENSEMBLE STATISTICS, 100/1200

collected on each run for ranges to the GPIP of from 5000 ft to 1500 ft. The standard deviations of all the runs that each pilot made in each visibility condition were then averaged, and used as a measure of the pilot's glide slope and localizer tracking performance. These average standard deviations are presented in Table 3 for all three pilots. The third pilot seemed to use more control in the longitudinal axis, which resulted in somewhat larger standard deviations when compared with the first two pilots. He used smaller control inputs in the lateral axes than the first two pilots, and achieved better performance there. This might be due to the yaw damper improving the handling qualities of the aircraft. Visibility did not seem to strongly influence the pilot's performance for any of the three pilots. Most differences in the data between pilots and visibilities can be related to differences in the control inputs δ_e, δ_a, and δ_r, and the probable cause of these differences is the difference between pilots.

TABLE 2: TOUCHDOWN STATISTICS, EXPERIMENT TWO

	VISIBILITY	
STATISTIC	∞/∞ AND 400/1600	100/1200
x mean	125 ft	743 ft
x standard deviation	474 ft	1031 ft
y mean	6.3 ft	.9 ft
y standard deviation	19 ft	31 ft
correlation coefficient	-.14	-.015
$\dot{h}$ mean	-6.5 ft/sec	
$\dot{h}$ standard deviation	2.4 ft/sec	
probability ellipse parameters		
semi major axis	559 ft	1214 ft
semi minor axis	22 ft	37 ft
eccentricity	.999	1.000

TABLE 3: AVERAGE STANDARD DEVIATIONS

PILOT	VISIBILITY		
	∞/∞	400/1600	100/1200
	Glide Slope Error - h - ft		
1	6.78	5.40	5.77
2	6.17	7.64	3.65
3	5.26	11.63	8.95
	Localizer Error - y - ft		
1	13.66	16.44	27.18
2	12.10	21.40	18.90
3	11.79	11.93	11.33
	Yaw - ψ - degrees		
1	1.24	1.19	.91
2	.73	1.00	1.05
3	.95	.73	.81
	Pitch - θ - degrees		
1	.56	.51	.70
2	.66	.64	.54
3	.72	.95	.80
	Roll - ϕ - degrees		
1	1.56	1.45	1.57
2	1.73	2.17	1.20
3	2.08	2.59	1.28
	Yaw Rate - p - deg/sec		
1	.79	.87	.80
2	.96	1.24	.97
3	.58	.90	.75
	Pitch Rate - q - deg/sec		
1	.51	.49	.57
2	.59	.55	.55
3	.67	.73	.70

TABLE 3: CONTINUED

PILOT	VISIBILITY		
	∞/∞	400/1600	100/1200
	Roll Rate - r - deg/sec		
1	.64	.52	.67
2	.53	.77	.57
3	.84	.78	.55
	Elevator Deflection - δ_e - degrees		
1	.84	.78	.87
2	1.04	.95	.95
3	1.07	1.72	1.47
	Aileron Deflection - δ_a - degrees		
1	3.54	3.67	2.57
2	4.20	5.60	3.82
3	4.07	4.27	4.11
	Rudder Deflection - δ_r - degrees		
1	.14	.04	.00
2	.12	.84	.00
3	.84	.78	.55

During the second experiment, data were collected on whether the pilot was looking inside or outside the cockpit during the approach. These data were collected using an electro-oculargraphic technique, which is fully described in Reference 2. The data as to whether the pilot was looking inside the cockpit at the instruments or outside the cockpit at the visual display were used to determine the number of in/out/in scans made on each run, the duration of each scan, the time intervals between scans, the duration of the interval immediately before touchdown during which the pilot was completely visual, and the wheel height at which the pilot went completely visual. For each visibility condition, medians and ranges of the quantities were determined, and are presented in Table 4. Medians and ranges were used instead of means and standard deviations becuase the data were obviously distributed in a nongaussian manner.

The pilot was always flying visually at touchdown, and never referred to the instruments below a wheel height of 40 feet. Since the copilot called initial visual contact, the pilot never scanned outside the cockpit before initial visual contact.

For 100 feet initial visual contact, the pilot did not scan on the majority of runs, and commented that there was not enough time. He stated

that any references back to the instruments were for the purpose of checking aircraft attitude.

On those runs where the pilot always had visual ground contact, he scanned back and forth between the instruments and the visual display throughout the run, finally transitioning to only the visual display around 150 feet altitude. While scanning between the instruments and visual display, the pilot apportioned his time so that an average of 61 percent was spent on the instruments. Kolmogorov-Smirnov tests accepted the hypothesis that the duration of the intervals of time spent inside the cockpit and outside the cockpit had exponential distributions. This implies that the probability that the pilot will scan outside the cockpit is not affected by the time since his last scan[5].

TABLE 4: PILOT SCANNING STATISTICS

VARIABLE	STATISTICS	VISIBILITY		
		∞/∞	400/1600	1(1200
Duration of Final	Median	18.5 sec	16.25 sec	14.3 sec
Fully Visual Period	Range	23.2 sec	14.4 sec	22.8 sec
Wheel Height at	Median	147.5 ft	105 ft	60 ft
start of final fully	Range	285 ft	115 ft	40 ft
visual period				
Number of scans outside	Median	7	1.5	0
cockpit during approach	Range	5	3	1
Duration of outside	Median	1.8 sec	.9 sec	1.2 sec
cockpit scans	Range	29.6 sec	.9 sec	8.6 sec
Duration of intervals	Median	4.0 sec	4.5 sec	.6 sec
between outside cockpit	Range	22.2 sec	20.9 sec	.4 sec
scans				

When the initial visual contact altitude was 400 feet, the pilot's scanning behavior was intermediate between the 100 feet case and the ∞ case. Scanning from the instruments to the visual scene and back was present on the majority of these runs, only now the pilot apportioned 83% of his time to the instruments, and transitioned to the visual display at about 100 feet altitude. The histogram of the scan times outside the cockpit indicated that this time was almost constant at .6 to .8 seconds, while the times between scans were nearly uniformly distributed over the interval of 1 to 8 seconds.

These results indicated that the pilot's scanning behavior changed radically as the visibility conditions changed. The approach and touchdown statistics for the aircraft trajectory are not strongly affected by changes in visibility, indicating that the pilot increases his reliance on the instruments as visibility degrades, and thus successfully maintains a consistent landing performance.

Pilot comments were obtained during the course of both experiments as to what instruments the pilot referred to after he considered that he had transitioned to visual flight, what if any special conditions occurred when he transitioned to visual flight, and he was asked to give a rating of the difficulty of the landing task in that visibility. The rating scale used was a modification of the Cooper Harper scale used for handling qualities. Further development is required to adapt it to rating low visibility approaches, as all three pilots tended to rate the aircraft rather than the task, thus the rating differences were very small. The modification of the rating scale used in the second experiment did exhibit constant sensitivity, a characteristic of the psychological continuum[6].

The instruments most often referred to after transitioning to visual flight were the ADI (for aircraft attitude), the airspeed indicator, and the vertical velocity indicator. All three pilots were unable to correctly estimate what the visibility conditions were, usually giving the initial visual contact altitude as being lower than it actually was, and thinking that the runway visual range was greater than it was. For the 100 foot initial visual contact runs, all three pilots stated that there was insufficient time to refer back to the instruments after transitioning out of the cockpit. The special circumstances surrounding transition all occurred in the 100/1200 visibility condition. They involved either initially interpreting the aircraft as being in a severe nose down attitude, or the aircraft appeared to be lower than it was, or the pilot could not detect cross runway drifts early enough.

V. CONCLUSIONS

The three pilots involved in these two experiments were able to compensate for reduced visibility and achieve performance comparable to their clear air performance in the situations considered in these simulations. The main factor involved in the compensation appears to be increasing the amount of attention devoted to the instruments and modifying the pilot's

inside/outside scan pattern as visibility is degraded. The variation in performance between pilots was as great as any variation in a single pilot's performance due to visibility changes. The data collected has been usable for developing an optimal control type pilot model for glide slope and localizer tracking.

REFERENCES

1. Gressang, Stone, Kugel, and Pollard. Low Visibility Landing Pilot Modeling Experiment and Data. AFFDL TR 75-41, December 1975.

2. Gressang. Low Visibility Landing Pilot Modeling Experiment and Data, Phase II. AFFDL TR 75-57, August 1975.

3. Chalk, Neal, Harris, Pritchard, and Woodcock. Background Information and User Guide for MIL-F-8785B(ASG), "Military Specification -- Flying Qualities of Piloted Airplanes." AFFDL TR 69-72, August 1969.

4. Bunnell and Eicher. C-135B Low Visibility Landing Simulation. AFFDL TM 75-60 FGD, June 1975.

5. Parzen. Modern Probability Theory and Its Applications. John Wiley, New York, 1960.

6. McDonnell. Pilot Rating Techniques for the Estimation and Evaluation of Handling Qualities. AFFDL TR 68-76, December 1968.

THE APPLICATION OF PILOT MODELING TO THE STUDY OF LOW VISIBILITY LANDING

By Captain Walter W. Harrington

AFFDL/FGD
Wright-Patterson AFB

SUMMARY

The optimal pilot model is developed for the analysis of simulation experiments conducted by AFFDL/FGD for the FAA to investigate the effects of low visibility conditions on approach and landing. To adequately model the experiments, the complete aircraft system is considered. Thus, the aircraft system model contains both longitudinal and lateral dynamics in the form of linearized equations for the control feel system, aerodynamics, gusts, and instruments, including Collins FD-109 flight director dynamics for this application. To provide effective analysis of the experiments, developments are made to the optimal human response model. Areas of development include the control law, i.e., state penalties, control rate and amplitude penalties, and control bandwidth, and the information processing model, i.e., observed quantities, indifference thresholds, and degradation of performance due to work load. The resulting model is designed for confident analysis of the low visibility experiments and easy extension to other aircraft systems and tasks.

INTRODUCTION

Low visibility conditions create a hazardous environment for aircraft approach and landing. The Air Force Flight Dynamics Laboratory (AFFDL) conducted a simulation program, in support of the FAA/USAF Inter-Agency Agreement DOT-FA7ØWAI-173, Modification No. 12, to investigate pilot interaction with this environment. Specific objectives included the evaluation and validation of visual clues, pilot work load, and flight performance in Category II and III landing operations. As one possible method of approaching the objectives, an effort was undertaken to develop a mathematical model of the pilot's control activity. Experiments were conducted under two phases of simulation to collect data for pilot modeling [1, 2]. This paper presents the pilot model developed from this data base and the analysis of the Phase II experiments.

SYMBOLS

a_1, a_2 Control feel system coefficients

A	Open loop dynamics matrix (n_s x n_s)
A_{cl}	Closed loop dynamics matrix (n_s x n_s)
A_p	Open loop dynamics matrix containing neuromuscular filter (n_s x n_s)
A_0, A_1	Second order system response coefficients
B	Control distribution matrix (n_s x n_c)
C	Measurement distribution matrix (n_m x n_s)
C_m	Motor noise coefficient
C_y	Measurement noise coefficient
D	Vertical deviation
E	Expected value
E	Disturbance distribution matrix (n_s x n_d)
F	Feedback matrix (n_c x n_s)
G	Control amplitude penalty matrix (n_c x n_c)
i	Index
I	Moment of inertia
j	Complex coefficient, $\sqrt{-1}$
J	Control cost
$\underline{m}$	Pilot's commanded control ($\underline{u}$) a vector of dimension n_c
n_c	Number of controls
n_d	Number of disturbances
n_m	Number of measurements
n_s	Number of states
P	Riccati control gain matrix (n_s x n_s)
P_m	Motor noise to signal ratio
P_y	Measurement noise to signal ratio
Q	Measurement penalty matrix (n_m x n_m)

R	Control rate penalty matrix (n_c x n_c)
t	Time
T	Gaussian input describing function for measurement indifference threshold
$\underline{u}$	Pilot's control input, a vector of dimension n_c
$\underline{V}_m$	Autocovariance of motor noise, a vector of dimension n_c
$\underline{V}_y$	Autocovariance of measurement noise, a vector of dimension n_m
$\underline{w}$	A disturbance vector of Gaussian white noise of dimension n_d
$\underline{x}$	State of the system, a vector of dimension n_s
X	State covariance matrix
$\underline{y}$	A vector of observations, or measurements, available to the pilot, of dimension n_m
Y	Lateral tracking deviation
δ_c	Controller deviation, a vector of dimension n_c
ζ	Damping ratio
π	Pi
σ	Root-mean-square of subscripted parameter
$\sum$	Riccati filter covariance matrix (m_j x n_j)
τ	Pure time delay
ϕ	Phase angle
ω_c	Control cutoff frequency
ω_d	Damped natural frequency
ω_n	Natural frequency
ω_N	Neuromuscular frequency

Subscript:

a	Augmented
p	Perceived

Superscripts:

T	Transpose
*	Optimal
^	Estimated parameter

Abbreviations:

BH	Breakout Height
CAVU	Ceiling and Visibility Unlimited
RVR	Runway Visual Range

SYSTEM TO BE MODELED

This modeling effort is directed to the synthesis and analysis of low visibility piloted approach as simulated by AFFDL. The Phase II pilot modeling simulation visual test matrix contained Category I through Category III linear for structures.

FOG STRUCTURE SPECIFICATION (BH/RVR)	PHASE II SIMULATION (PILOT 3)
CAVU	10 Runs
122m/488m (400 ft/1600 ft)	10 Runs
30.5m/366m (100 ft/1200 ft)	10 Runs

Figure 1. Phase II Pilot Modeling Test Matrix

The particular aircraft used in the simulation is the Boeing C-135B. The C-135B (a military version of the Boeing 707) is a large swept wing four engine jet transport. It has fan jet engines, and conventional arrangement of control surfaces. It falls within Category III of MIL-F-8785B, and is representative of its class.

The AFFDL multicrew cab (C-135 cockpit) was used for the simulation. Cockpit support systems include a three degree-of-freedom motion base system (pitch, roll, and heave), instrument, visual display, control force loading, communication, and sound effect systems. Instrumentation for the simulation included a Collins FD-109 flight director system.

The approach task required tracking of a .05 radian (3. degree) glide slope from a range of 4,572 meters (15,000 feet) to flare. The pilot was instructed to follow the flight director and use raw data and visual cues as required.

OPTIMAL PILOT MODEL

The optimal pilot model concept, developed by Kleinman, Baron, and Levison [3 - 20], was selected for this application due to its apparent success in modeling similar [12] and complex, time varying [13] control tasks. The optimal pilot model is a mathematical construct designed to synthesize pilot control performance and behavior. The model is based on the assumption that the human operator will control a dynamic, stoichastic system optimally subject to his inherent limitations. These limitations are considered to be

1. A time delay, representing cognitive, visual central processing, and neuromotor delays.

2. "Remnant" signals, divided into an observation noise to represent signal degradation due to work load, scanning effects, and signal thresholds, and a motor noise to represent random errors in executing the intended control.

3. A "neuromuscular lag" to represent neuromuscular dynamics.

The control commands are synthesized by a continuous linear equalization network which contains a full state optimal filter (Kalman filter), a full state optimal predictor, and a full state optimal feedback control law. The control law is derived for an augmented state system which results from introducing the neuromuscular lag by means of a control rate penalty. The structure of the model results from a suboptimal solution to a control problem involving a time delay and observation noise. The model is shown in Figure 2.

The mathematical algorithm of the optimal pilot model is developed from the following control problem:

Given the quadratic cost functional of the form

$$J = 1/2 \int_0^\infty E \{\underline{y}^T(t)\ Q\ \underline{y}(t) + \underline{u}_a{}^T(t)\ R\ \underline{u}_a(t)\}\ dt$$

Subject to the constraints

$$\dot{\underline{x}}_a(t) = A_a\ \underline{x}_a(t) + B_a\ \underline{u}_a(t) + E_a\ w_a(t)$$

$$\underline{y}(t) = C_a\ \underline{x}_a(t - \tau) + \underline{V}_y(t - \tau),$$

determine the non-anticipation feedback control $\underline{u}_a^*(t)$ which minimizes the cost functional.

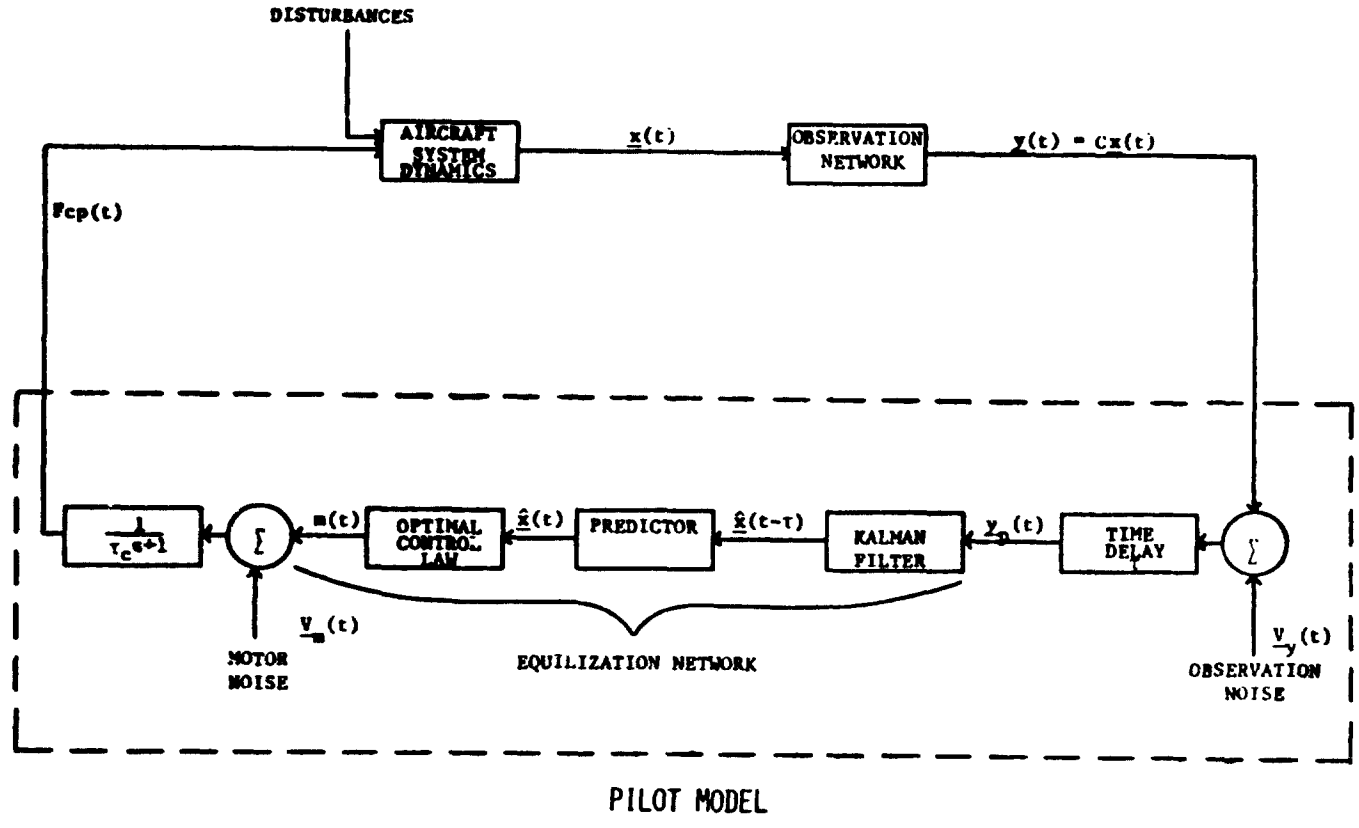

Figure 2 Structure of Optimal Pilot Model

The mathematical algorithm, including developments, of the optimal pilot model is presented in the following sections.

Optimal Pilot Model Computer Program

The optimal pilot model algorithm is executed by the digital computer program FGD PILOT. FGD PILOT is a "batch run" Fortran computer program designed for the Cyber 74 computer. The program uses subroutines from a version of Kleinman's pilot model program [16] except for the solution of the steady state Riccati equations and the filter estimate covariance equation. The program originally used a Newton Raphson method of solving steady state Riccati equations developed by Kleinman [17, 18]. However, the subroutines proved to be unsuitable for the C-135B lateral equations [21]. The program now uses a diagonalization of the canonical equations method [22, 18] from the program OPTSYS, which was furnished to AFFDL by Dr. Earl Hall of Systems Control, Inc.

The program FGD PILOT is designed for easy, confident analysis. Developments to the programming algorithm are presented in the following sections.

Application of the Optimal Pilot Model to the AFFDL Low Visibility Simulatio

The flight simulation which is to be modeled contained a nonlinear, time varying, six degree-of-freedom, hybrid aircraft system model. Some considerations and assumptions allow the hybrid simulation to be modeled within the constraints of the optimal pilot model structure.

The optimal pilot model provides steady state optimal control and state estimation. The flight simulation dynamics were time varying. But, they can be considered slowly time varying for the approach task. It is then assumed that the steady state solution of control and filter gains at each point in time represents the adaptive abilities of the pilot in a physically realizable manner. The model is thus applied to a slowly time varying system with the calculations repeated with updated parameters as the system varies.

The optimal pilot model requires a linear representation of the aircraft system dynamics. It is therefore required that the components of the simulated aircraft system be represented by sets of first order, linear, piecewise constant coefficient, differential equations. The development of a system model of this form is discussed below.

The mathematical model of the aircraft system is augmented to allow the introduction of a first order, closed loop, pilot lag. This lag is first order and linear by definition. But, since it results from the solution of the nonlinear control Riccati equation, iteration is required to obtain the desired filter coefficient.

The filtered control signal is the force the pilot applies to the aircraft controllers. The C-135B contains a conventional wheel and rudder controller configuration. These devices can be modeled as nonlinear, second order systems. Controller deflection is given by

$$\ddot{\delta c}(t) = \frac{1}{I} F_{cp}(t) - a_1 (\sigma_{\dot{\delta c}})\, \dot{\delta c}(t) - a_0 (\sigma_{\delta c})\, \delta c(t)$$

$$\dot{\delta c}(t) = \int \ddot{\delta c}(t)\, dt$$

where a_0 and a_1 are nonlinear coefficients. Statistical linearization techniques [9] can be applied to linearize these coefficients. Iteration is required, then, to adapt the coefficients to the resulting system performance.

The controller deflection to surface deflection transfer functions can be modeled by pure gains for the C-135B dynamics. These are easily incorporated into the linearized dynamics.

The surface deflections provide inputs to the airframe dynamics. Airframe equations are derived by linearizing the nonlinear six degree-of-freedom equations for rigid body motion about a trim condition. The trim condition used corresponds to the aircraft being in the nominal landing configuration with .93 radian (50 degree) flaps and a flight path angle of -.05 radians (-3. degrees). The differential equations are written in the stability axis coordinate system [23]. Aerodynamic forces and moments are represented by dimensional, primed stability derivatives obtained from a link data package used for C-135B simulators [24]. The stability derivatives need not be varied with state or time since they vary only slightly throughout the range of conditions corresponding to approach. Instead, they are maintained constant at the values of a typical trim condition, thus resulting in a linear constant coefficient system.

The Phase II simulation C-135B lateral airframe dynamics were augmented by a first order, linear yaw damper. The yaw damper equation satisfies the model constraints without modification.

In addition to stability dynamics, positional dynamics were generated in the flight simulation. Glide slope and localizer error are considered important for modeling the instrumented approach task. Both can be synthesized by linear, piecewise constant coefficient, differential equations.

Turbulence disturbances to the aircraft were provided in the simulation by implementation of the state variable model derived by Heath [25] of the Dryden spectrum of wind gusts described in MIL SPEC 8785B. Constant model scales were used corresponding to an altitude of 152 meters (500 feet) as specified by MIL SPEC 8785B for powered approach. The intensity of the turbulence was nominally to be 1/4 of the 152 meter (500 feet) moderate turbulence level. The state variable model is a linear system driven by white noise. For a constant turbulence level, the result is a linear constant coefficient system.

Control command cues were presented to the pilot by a Collins FD-109 flight director. The flight director contains dynamic, nonlinear, and time varying elements. Statistical linearization techniques [9] can be applied to the nonlinear elements. Iteration is then required to adapt the linearized coefficients to the current flight director performance. The time varying elements can be considered slowly time varying. Thus, the flight director is modeled as a linearized, piecewise constant coefficient system.

Raw aircraft data were presented to the pilot through instrument, visual, and motion cues. The dynamics of instruments providing raw data are neglected for this model. Then raw data instrument cues and visual cues can be modeled by the same information channels. Discrimination between instrument cues and visual cues is thus left to the human operator model Motion cues are assumed negligible considering the C-135B dynamics, the low turbulence levels, and the limited response of the C-135 cockpit motion drive system.

The aircraft system model presented above satisfies the constraints of the optimal pilot model. In addition, the model is separable into two single control input, linearized, piecewise constant coefficient systems.

Optimal Pilot Model Control Law

The optimal pilot model equalization network contains a full state optimal feedback control law. The pilot model determines the feedback control $\underline{u}_a^*(t)$ which minimizes the cost functional

$$J = 1/2 \int_0^{\infty} E \{\underline{y}^T(t)\ Q\ \underline{y}(t) + \underline{u}_a^T(t)\ R\ \underline{u}_a(t)\}\ dt$$

subject to the constraints

$$\dot{\underline{x}}_a(t) = A_a\ \underline{x}_a(t) + Ba\ \underline{u}_a(t)$$

$$\underline{y}(t) = C_a\ \underline{x}_a(t)$$

by the solution of the steady state Riccati control matrix equation

$$A_a^T P_a + P_a A_a + C_a^T Q\ C_a - P_a B_a R^{-1} B_a^T P_a = 0$$

where

$$\underline{u}_a^*(t) = R^{-1} B_a^T P_a\ \underline{x}_a(t).$$

The control law therefore requires the specification of the measurement penalty matrix Q and the control rate penalty matrix R.

If the pilot does not intentionally couple the longitudinal and lateral axis systems, i.e., Q and R are block diagonal in a manner similar to the decoupling of the system equations, the control problem formed by seeking the

feedback control $\underline{u}_a^*(t)$ which minimizes J decouples into two separate control problems. Each control problem can be addressed separately, reducing the dimension of the system, and subsequently the time and core requirements for computer implementation of the pilot model. Also, only a single control input pilot model is required for this application. Thus the matrix R reduces to a scalar.

The measurement penalty matrix Q is then specified to provide rms minimization of measured quantities in each axis system. The matrix Q is normally specified as a diagonal matrix. Therefore, to simplify and clarify the specification of this matrix, the vector TASK is defined such that:

$$\text{TASK} = \text{Diagonal } (Q).$$

The vector, of dimension n_m xl, provides one-to-one correspondence of measurement penalties to the measurements given by the vector $\underline{y}(t)$. The vector is named TASK so that it will be thought of as a numerical presentation of the flight task.

For the low visibility approach task, the pilot was instructed to follow the flight director and use raw data and visual cues as required. The flight director task required the minimization of pitch steering bar and roll steering bar deviations. Due to the flight director task, the C-135B dynamics, and the low turbulence levels, it is assumed that the measured raw data quantities were not controlled in an rms sense. Instead, the information was used to evaluate the safety of the aircraft and the performance of the flight director, i.e., to detect adverse flight conditions or flight director failures. The measurement of raw data and visual cues is therefore considered a side task. The primary flight task is simply the minimization of pitch steering bar and roll steering bar amplitude deviations.

The minimization of flight director steering bar deviations is a simple, well defined task. The TASK vector is specified as a numerical representation of this task by:

$$\text{TASK}(i: y(i) = \text{steering bar amplitude}) > 0$$

otherwise

$$\text{TASK}(i) = 0.$$

The amplitude of the TASK vector is related to the control rate penalty R in the following section. For complex tasks, the elements of the TASK vector can be estimated based upon expected maximum errors [11] or upon the weightings of similar tasks.

Control Frequency Response

Pilot control frequency response is regulated in the optimal pilot

model by a first order filter which processes the commanded control signal. The filter cutoff frequency, ω_c, is an output of the control solution and is determined by the relative amplitude of control penalties to measurement penalties (TASK vector). It is required by the closed loop dynamics matrix,

$$A_{cl} = A_a - B_a R^{-1} B_a^T P_a,$$

that, for a single control input system,

$$\omega_c = \frac{P_c}{R}$$

where P_c is the Riccati gain matrix element associated with the control filter. The control law therefore requires iteration to adjust R or P_c until the control frequency ω_c attains a desired value.

Consider the more general cost functional for a single control input system:

$$J = \frac{1}{2} \int_0^\infty E\{\underline{y}^T(t) Q \underline{y}(t) + R\, u_a^2(t) + G\, u^2(t)\}\, dt$$

where u(t) is the control amplitude and G is a control amplitude penalty. Then, for a given TASK vector, G and R can be adjusted to regulate P_c/R to attain the desired control frequency. It is then required to specify ω_c, R, and G uniquely for a given control problem.

The model has assumed that the pilot is highly motivated and controls the system to his neuromuscular frequency limit. Neurological data [23, 26, 27] indicate that the neuromuscular time constant is given by

$$\tau_N \simeq .1 \text{ seconds.}$$

Thus, the model has assumed that

$$\omega_c = \omega_N = \frac{1}{\tau_N} \simeq 10 \text{ radians/second.}$$

It has also been assumed that G = 0, thus requiring adjustment of only the control rate penalty R. This, incidentally, results in a unique solution to the control law for a given task specification. The control rate penalty R adapts to the TASK vector to attain the desired frequency response. This results in a unique control solution which is independent of the actual numerical value of the TASK vector. However, this algorithm has been found to predict "optimistic" performance for the control of real aircraft systems.

To account for the degradation of pilot control performance encountered in real aircraft systems, the estimation of control rate and amplitude penalties based upon expected maximum control performance [11] has been considered. Thus,

$$R \propto \frac{1}{(u_a^2(t))_{max}}$$

and

$$C \propto \frac{1}{(u^2(t))_{max}}$$

But, the maximum values of control rate and amplitude can be difficult to predict, i.e., control force rate and amplitude to a controlled.

It is therefore desired to create a control law algorithm which can be used predictively yet account for the controller configuration, the aircraft dynamics, and the pilot's workload. Consider the following approach. We make the following assumption:

Assumption: A pilot's control activity is limited to that required by the system dynamics under the condition of a normal aircraft workload. Thus, the pilot can control the aircraft system with a bandwidth less than that of the neuromuscular system. The control frequency, ω_c, is then a "commanded control frequency." Furthermore, ω_c is limited by the pilot's neuronuscular response for the particular controller configuration, i.e.,:

$\omega_c \leq$ 10 radians/sec for a side stick controller

$\omega_c \leq$ 3.3 radians/sec for a center stick or wheel controller.

The 3.3 radians/sec figure for the center stick and wheel controllers is a first order estimate of the frequency response of the extended arm system these controllers require and is consistent with the force gradients allowed for these controllers. [28].

The control law is handled as follows. The control rate penalty R appears to determine the control $u^*(t)$. The control amplitude penalty G merely allows the increase of ω_c by the reduction of the augmented control $u_a^*(t)$. The control law is apparently overspecified by the introduction of the control amplitude penalty G. We, therefore, let G = 0 so that ω_c directly reflects the control activity of the pilot. Note that the control solution is then unique if ω_c is specified.

The control frequency ω_c must reflect the system dynamics as well as the pilot's workload. Consider "normal" aircraft dynamics, i.e., damped

short period, phugoid, and Dutch roll modes, a stable roll mode, and a stable or slightly dirvegent spiral mode. System oscillations occur at damped natural frequencies, ω_d, and decay or diverge at a rate determined by the product of the damping ratio, ζ, and the natural frequency, ω_n. Given the aircraft dynamics described above and a normal aircraft work load, let

$\omega_c = (\omega_d)_{max}$, the maximum damped natural frequency of the closed loop system

where

$$\omega_c \leq \omega_N \text{ (controller)}.$$

The closed loop damped natural frequencies can be determined by an eigenvalue analysis of the closed loop dynamics. We thus require that the control solution outputs ω_c and $(\omega_d)_{max}$ be equal. This can be accomplished by adjusting the control rate penalty R in a manner similar to previous control law algorithms until ω_c is satisfactorily close to $(\omega_d)_{max}$. This iteration is done automatically in the computer program FGD PILOT with the algorithm

$$R(k+1) = \frac{P_c(k)}{(\omega_d)_{max}(k)}$$

with the convergence criteria

$$|| \omega_c(k) - (\omega_d)_{max}(k) || \leq \varepsilon$$

where

$$\omega_c(k) = \frac{P_c(k)}{R(k)} .$$

The control law is therefore uniquely determined, based on the controller configuration, the aircraft dynamics, and the pilot's work load. The only entries required by the computer program for the control law are the nonzero elements of the vector TASK and the pilot's neuromuscular frequency limit for the particular controller configuration.

The control law entries required for this application are therefore

TASK (i:$\underline{y}$(i) = steering bar amplitude) > 0

and

ω_N = 3.3 radians/second.

As an example, consider the longitudinal dynamics of the C-135B. The pole plot is shown in Figure 3. The system dynamics require that

ω_c = .94 radians/second

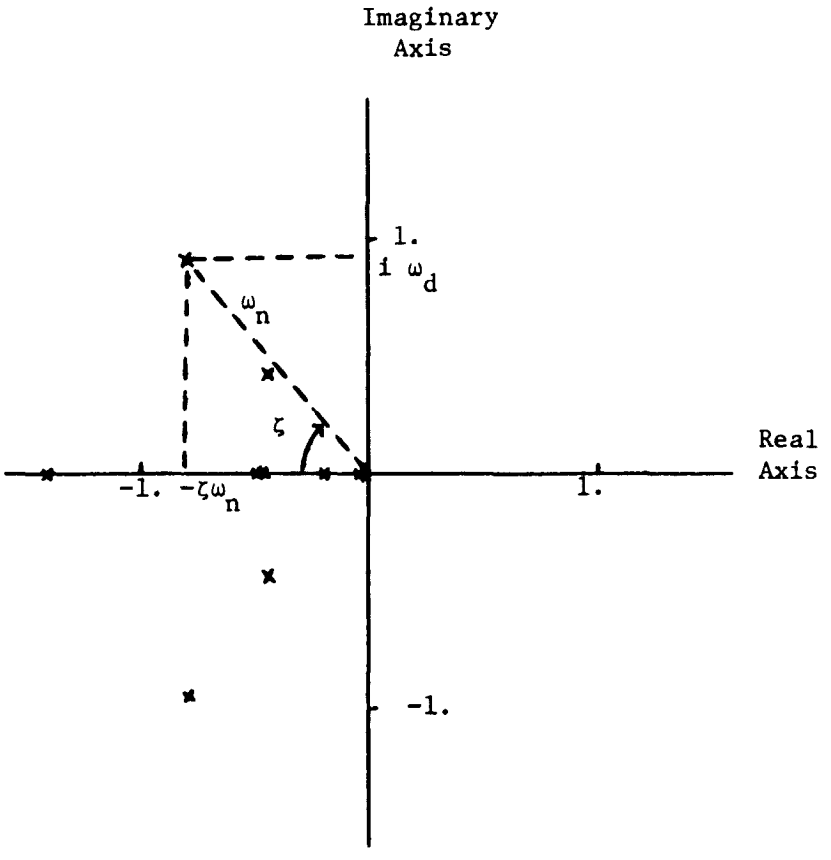

Real Pole Response:

$$C(t) = A_0 + A_1 e^{st}$$

Complex Pair Response:

$$C(t) = A_0 + A_1 e^{-\zeta\omega_n t} \sin(\omega_d + \phi)$$

Figure 3 Closed Loop Poles of C-135B Longitudinal Dynamics

which is considerably less than the neuromuscular frequency response of 3.3 radians/second for a control wheel. The predicted ω_c corresponds reasonably well with the measured half power point of the power spectral density of elevator deflection obtained from simulation data reduction, as shown in Figure 4. Furthermore, the resulting performance predictions are very good, as shown for vertical tracking error in Figure 6. The predicted control frequency is further supported by control frequency sensitivity curves, which are presented in Figure 5 for selected turbulence conditions. A similar analysis applies to the C-135B lateral dynamics.

Full State Estimation

The optimal pilot model equalization network generates a full state estimate of the aircraft system based on noisy, delayed observations of the system. This estimate is the output of a Kalman filter. The Kalman filter gains are determined from the covariance matrix Σ which is the solution to the steady state Riccati filter equation

$$A_p\Sigma + \Sigma A_p^T + W - \Sigma C_a^T V_y^{-1} C_a \Sigma = 0$$

where A_p is a modified open loop dynamics matrix containing the pilot control filter generated by the control law,

$$W = EV_dE^T$$

where E is the state disturbance distribution matrix and V_d is the variance matrix of state disturbances of which the autocovariance of the motor noise $\underline{V}_m$ is an element, and

$$\underline{V}_y = \text{Diagonal } (V_y)$$

where $\underline{V}_y$ is the autocovariance of the measurement noise. The filter therefore requires specification of the autocovariance of the measurement noise $\underline{V}_y$ associated with the measurements $\underline{y}(t)$ and the autocovariance of the motor noise $\underline{V}_m$ associated with the control $u(t)$. A prerequisite to this is the specification of the pilot model measurements $\underline{y}(t)$.

Pilot Model Measurements

The optimal pilot model is well suited for realistic synthesis of human operator information processing. The pilot model can observe those instruments or quantities which the pilot would observe to perform the flight task. Furthermore, the pilot model can contain algorithms for amplitude and rate information processing, instrument scanning, and signal perception. These concepts are discussed below.

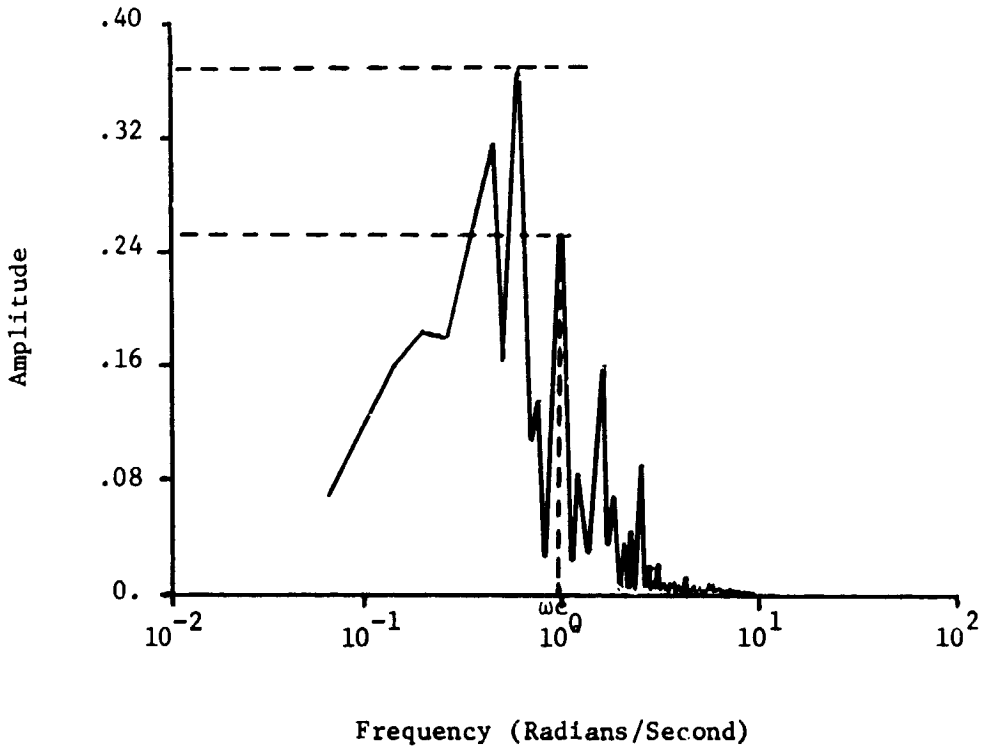

Figure 4 Power Spectral Density of C-135B Elevator Deflection From Simulated Power Approach

Turbulence Amplitude
meters/second (feet/second)

Curve	$\sigma_{u\ gust}$	$\sigma_{w\ gust}$
A	1.5 (5.)	1. (3.3)
B	.76 (2.5)	.5 (1.65)
C	.38 (1.25)	.25 (.825)
D	.19 (.625)	.125 (.4125)

NOTE: perceptual threshold = .008 radians

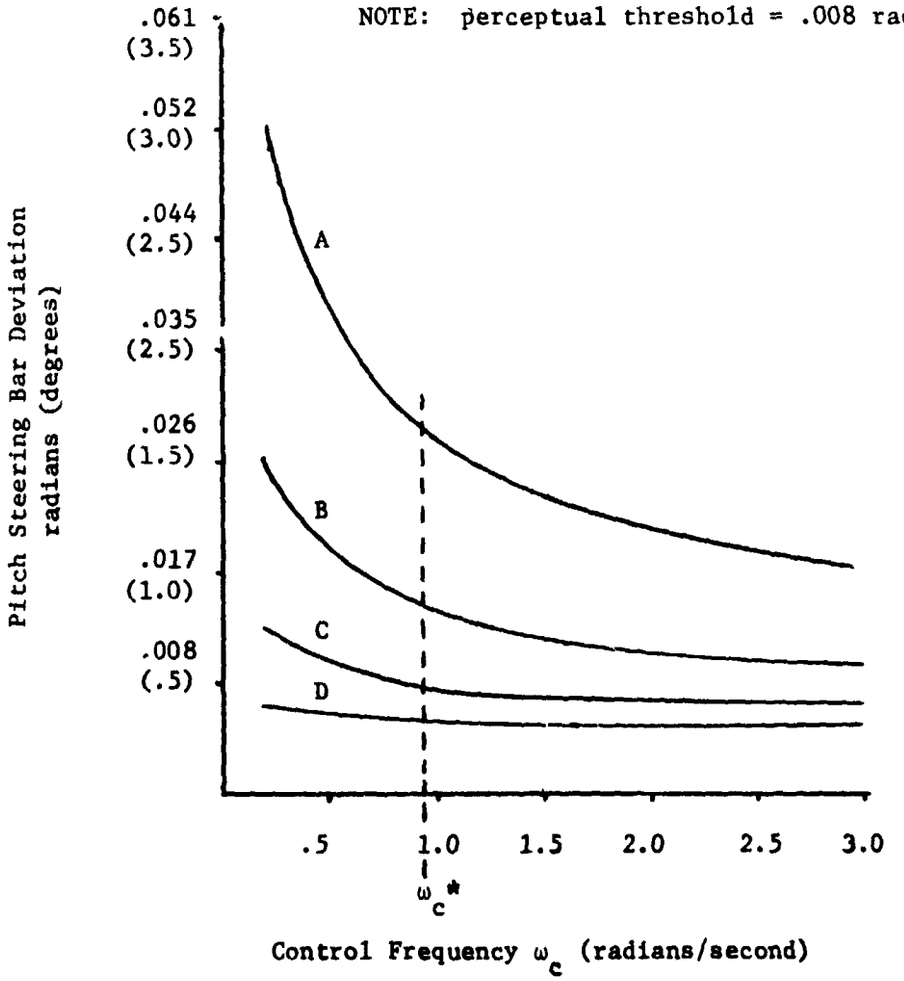

Figure 5 Pitch Steering Bar Sensitivity Curves for Selected Turbulence Conditions

The observations available to the pilot are given by the vector $\underline{y}(t)$. To specify those instruments or quantities selected by the pilot to perform the flight task, the vector SCAN, of dimension n_m, is defined such that

SCAN(i:$\underline{y}$(i) is observed) = 1.

SCAN(i:$\underline{y}$(i) is not observed) = 0.

This vector is used to activate observation of the specified instruments or quantities in the computer program FGD PILOT. For this application, the only observation required to perform the primary flight task is of the flight director. The required entry is then

SCAN(i:$\underline{y}$(i) = steering ear amplitude) = 1.

The model has assumed that both the amplitude and first derivative of an observed quantity are available to the pilot. But, the pilot must estimate the rate of an explicity displayed quantity by observing its time rate of change. This rate estimation process is a function of the Kalman filter in the pilot model. Therefore, let the pilot model observe only those quantities explicitly displayed to the pilot; and, let the rate estimation process be a part of the state estimation process performed by the Kalman filter.

Although only one observation is required in each axis system for the main flight task, a scanning algorithm is required to synthesize the degradation of information quality due to the multi-axis control task and the side task. Scanning can be described by the qualities of pattern, frequency, and dwell time. These qualities have two basic effects on information processing:

1. The effective perceptual threshold of an observed quantity is increased as the frequency at which it is observed is decreased.

2. The quality of the perceived information is decreased as the dwell time for which the quantity if observed is decreased.

Scanning algorithms [29] have addressed information degradation as a function of total attention to an observed quantity. However, this approach does not account for the dynamics of an observed quantity, nor the frequency or dwell time with which it is scanned. Thus, it is desired to create a scanning algorithm which realistically accounts for the effects of scanning.

Consider the following approach. Three types of thresholds are defined:

1. Perceptual threshold: The minimum deviation of an observed quantity which the pilot can detect.

2. Scanning threshold: The effective perceptual threshold which results from the superposition of scanning on the dynamics of an observed quantity.

3. Indifference threshold: The deviation of an observed quantity below which the pilot will not take control action.

The perceptual threshold can be calculated [12] from the pilot's minimum arc of resolution (typically .00087 radians (.05 degrees)), the distance to the display, and the display scale. The scanning threshold arises from the dynamics of an observed quantity and the pattern and frequency with which it is observed. The following assumption is made:

Assumption: For a well designed scanning pattern of displays in a real aircraft system and normal pilot work load, the scanning threshold of an observed quantity will be approximately half the standard deviation of that quantity.

This assumption allows the pilot model to adapt to the dynamics of the displayed quantities as well as a changing aircraft environment. The indifference threshold is subjective and represents the deviations of an observed quantity which the pilot will tolerate. The observation threshold used in the pilot model is defined to be the maximum of the three thresholds discussed above:

$$\text{Threshold} = \text{Maximum (perceptual threshold, scanning threshold, indifference threshold)}$$

Due to the hazardous flight conditions of low visibility approach, it is assumed that the indifference threshold will not exceed the scanning threshold. The observation thresholds are then given by

$$\text{Threshold } (\underline{y}(i) = \text{Maximum (perceptual threshold } (\underline{y}(i), 1/2\ \sigma_{\underline{y}(i)})$$

The quality of information perceived by the pilot when observing a quantity will depend upon the dwell time, the scanning frequency, and also upon the correlation of the quantity with other observed quantities. In the optimal pilot model, information quality is given by the noise to signal ratio of the observation noise. For the scanning of displays for a two axis control task, across which information is uncorrelated, it has been found that the noise to signal ratio of observations should be increased by 3 dB or a factor of two. Correlated observations should not require as much signal degradation. Thus, the following measurement noise coefficient is proposed:

$$C_y = 2 \times \text{number of observations.}$$

This form results in a 3 dB increase in noise to signal ratio of the observation noise for the two axis control task, and proportionately smaller increases for additional observations in the same axis system.

This scanning algorithm is incorporated into the observation noise algorithm of the optimal pilot model. The observation noise algorithm is presented in the following section.

Pilot Model Observation Noise

The optimal pilot model contains observation noise to represent signal degradation due to work load, scanning effects, and signal thresholds. The autocovariance of the observation noise $\underline{V}_y$ is given by

$$\underline{V}_y(i) = \frac{C_y \pi P_y}{T(\underline{y}(i))} E\{\underline{y}^2(i)\}$$

where P_y is the noise to signal ratio given by

$$P_y = .01,$$

C_y is the measurement noise coefficient given by

$$C_y = 2 \times \text{number of observations},$$

and $T(\underline{y}(i))$ is a Gaussian input describing function for the threshold nonlinearity [9]

$$T(\underline{y}(i)) = \text{cerf} \quad \frac{\text{threshold } (\underline{y}(i))}{\sqrt{2}\,(E\{\underline{y}^2(i)\}^{1/2})}$$

Iteration of the covariance calculations is required since the threshold gain is a function of system performance. This iteration is done automatically in the computer program FGD PILOT.

Pilot Model Motor Noise

The optimal pilot model contains motor noise to represent random errors in the execution of the intended control. The autocovariance of the motor noise V_m is given by

$$V_m = C_m \pi P_m E\{u^2(t)\}$$

where P_m is the noise to signal ratio given by

$$P_m = .003$$

and C_m is a motor noise coefficient to give a 3 dB increase for the two axis control task, given by

$$C_m = 2.$$

The autocovariance of the motor noise completes the specification of quantities required by the Kalman filter.

Full State Prediction

The optimal pilot model equalization network contains an optimal, full state predictor which updates the delayed full state estimate generated by the Kalman filter. It is required by the predictor to specify the pure time delay τ by which the observations $\underline{y}(t)$ are delayed. The typical value of .2 seconds [3 - 12] is selected for the pilot model algorithm.

Pilot Model Performance Prediction

The optimal pilot model synthesizes pilot control performance by the generation of piecewise constant aircraft system statistics. The state covariance matrix X arises from the sum of the covariance of the filter estimate, the covariance of the estimation error, and the covariance of the predictor error [8]. Thus,

$$X = E\{\underline{x}_a(t)\underline{x}_a^T(t)\}$$

$$= \int_0^{\infty} e^{A_{cl}\sigma} e^{A_p\tau} \sum C_a^T V_y^{-1} C_a \sum e^{A_p^T\tau} e^{A_{cl}^T\sigma} d\sigma$$

$$+ e^{A_p\tau} \sum e^{A_p^T\tau} + \int_0^{\tau} e^{A_p\sigma} W e^{A_p^T\sigma} d\sigma .$$

The standard deviation of the aircraft states is then given by

$$E\{\underline{x}_i(t)\} = \sqrt{(X)_{ii}} \quad .$$

Pilot model analysis can then be performed by the evaluation of the performance statistics. Evaluation is typically based on the subjective criterion of whether or not the pilot model predictions exhibit sufficent correlation with the experimental results. The additional criterion that the pilot model performance be within the 95% confidence interval [3C] of the experimental results is imposed. This gives a firm, but realistic, measure of the correlation between the pilot model performance and experimental results.

Analysis of Phase II Simulation

Both ensemble statistics and stationary statistics were calculated for the three visibility conditions from the recorded simulation data. The stationary statistics were found to be consistently smaller than the ensemble statistics, indicating insufficient run length to obtain a stationary system. Therefore, pilot model analysis can be applied only to the ensemble statistics. Furthermore, only ten data runs were made for each visibility condition, resulting in a relatively low confidence data set. Therefore,

statistically significant trends are evaluated relative to the 95% confidence intervals.

The mean and standard deviation of the ensemble statistics were plotted as a function of range from the glide slope intercept point. The plots for the vertical and lateral tracking error for the three visibility conditions are presented in Figures 6 through 8. The lateral tracking error is initially displaced to the right, in all three cases, indicating an erroneous initial trim condition. The time varying means are indicative of the nonstationarity of the system. The deviations of the mean error from the nominal were found to be reasonably correlated with the nonstationary gust statistics. Therefore, the gust model in the pilot model program is scaled to piecewise constant gust statistics measured from the simulation.

ANALYSIS OF PHASE II PROGRAM OBJECTIVES

Pilot model performance predictions were made at 30.5 meter (100 feet) altitude increments. To provide comparison by visual inspection, the pilot model standard deviation predictions are plotted about the experimental mean in Figures 5 through 10. By visual inspection, the pilot model predictions and simulation performance appears to be well correlated, with the exception of the performance at 30.5 meters (100 feet) altitude. Analysis of the pilot model indicates that due to large gust statistics at that altitude, limiters in the flight director had become saturated. Therefore, insufficient control information is provided to the pilot with just the flight director. In the flight simulation, the pilot must have changed his control strategy, based on raw data scanning, to compensate for the poor flight director performance. Motion cues may also have assisted the pilot in performing the tracking task.

To evaluate the effect of the visibility conditions on the pilots performance, scatter diagrams of the predicted versus measured performance were plotted. The 95% confidence intervals for the measured data were included for the evaluation. The scatter diagrams for the vertical and lateral tracking error are presented in Figures 9 and 10. Except for a few data points, particularly those from the 30.5 meter (100 feet) altitude cases, all the predicted data points are within the 95% confidence intervals of the measured data. Therefore, no statistically significant trends occur between visibility conditions.

SUMMARY OF OPTIMAL PILOT MODEL

An optimal pilot model algorithm has been developed for the analysis of the complete aircraft system. The aircraft system model contains both longitudinal and lateral dynamics in the form of linearized, piecewise constant coefficient equations for the control feel system, aerodynamics, stability augmentation, gusts, and instruments. Statistical linearization is applied as required. Developments to the human response model include (1) an optimal

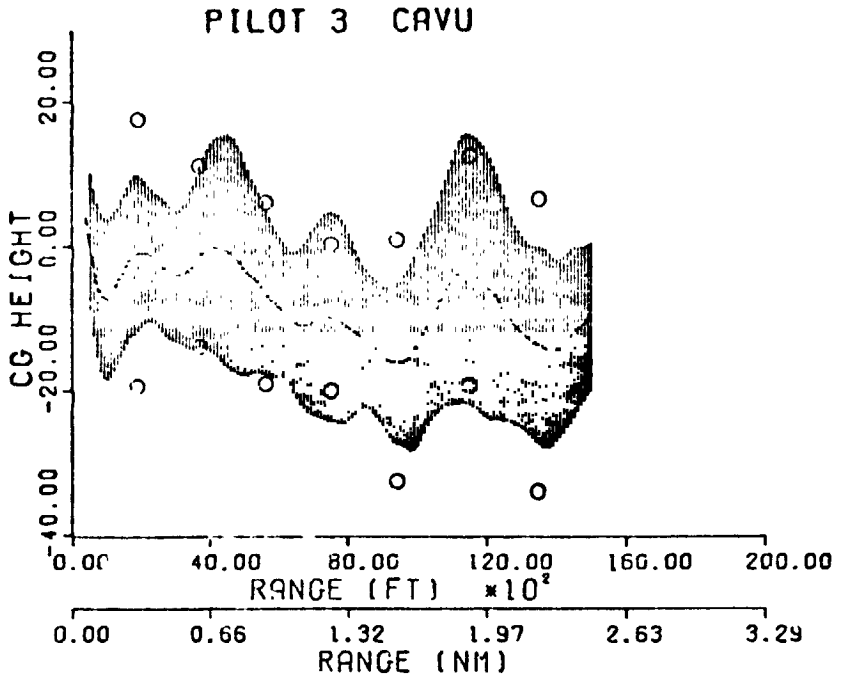

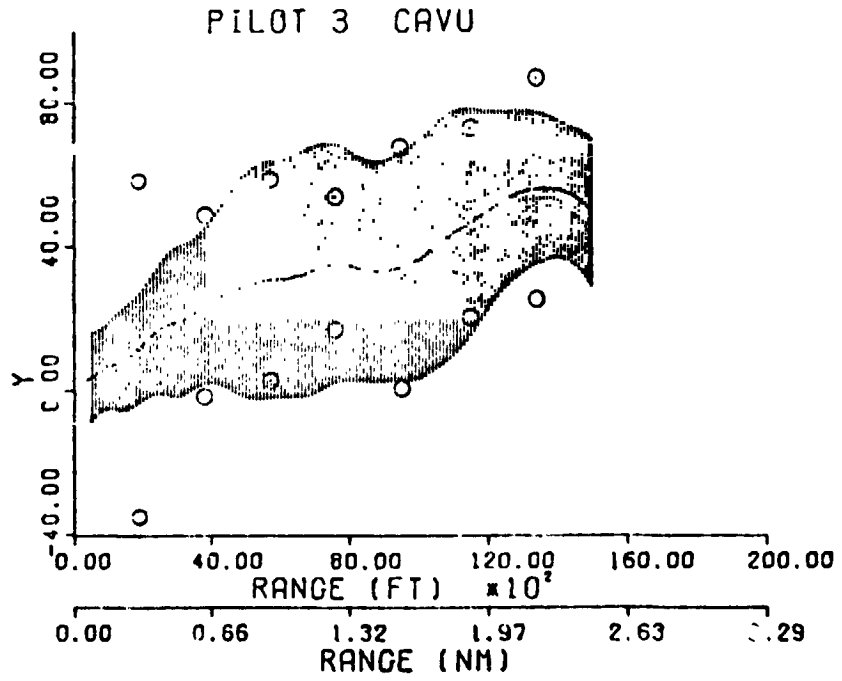

Figure 6 Ensemble Tracking Statistics, Phase II Simulation, CAVU Weather Conditions

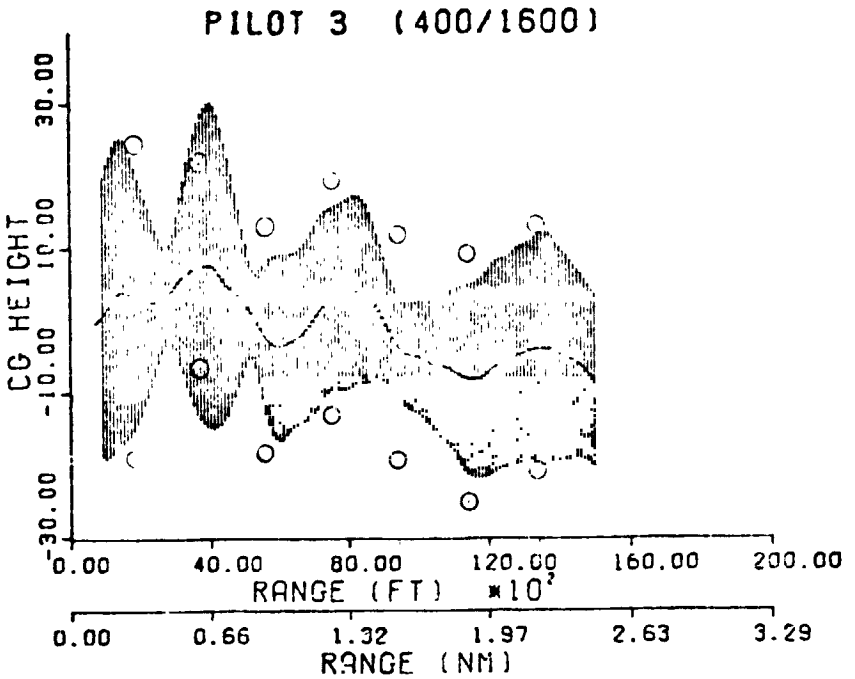

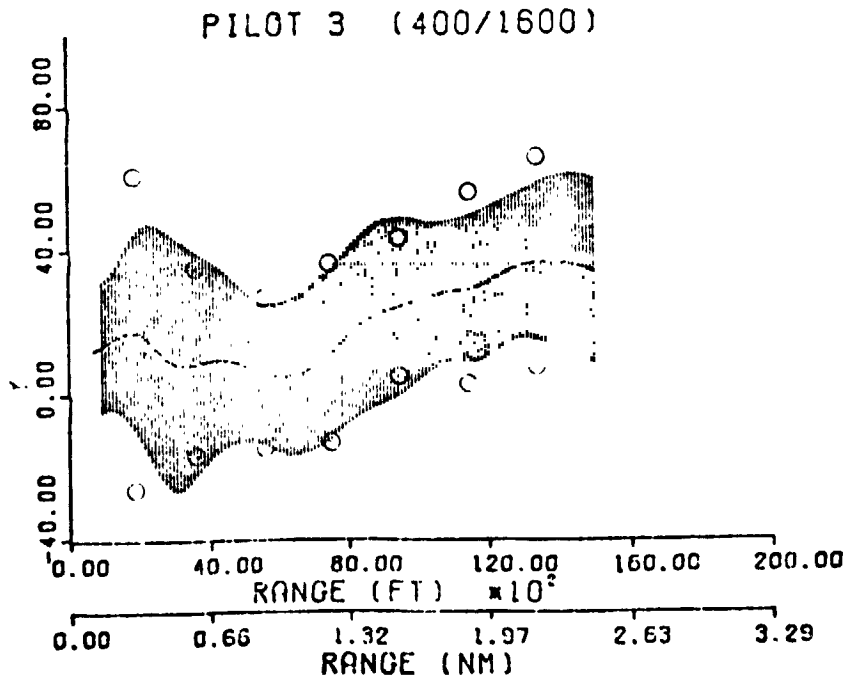

Figure 7 Ensemble Tracking Statisti ., Phase II Simulation, 400/1600 Weather Conditions

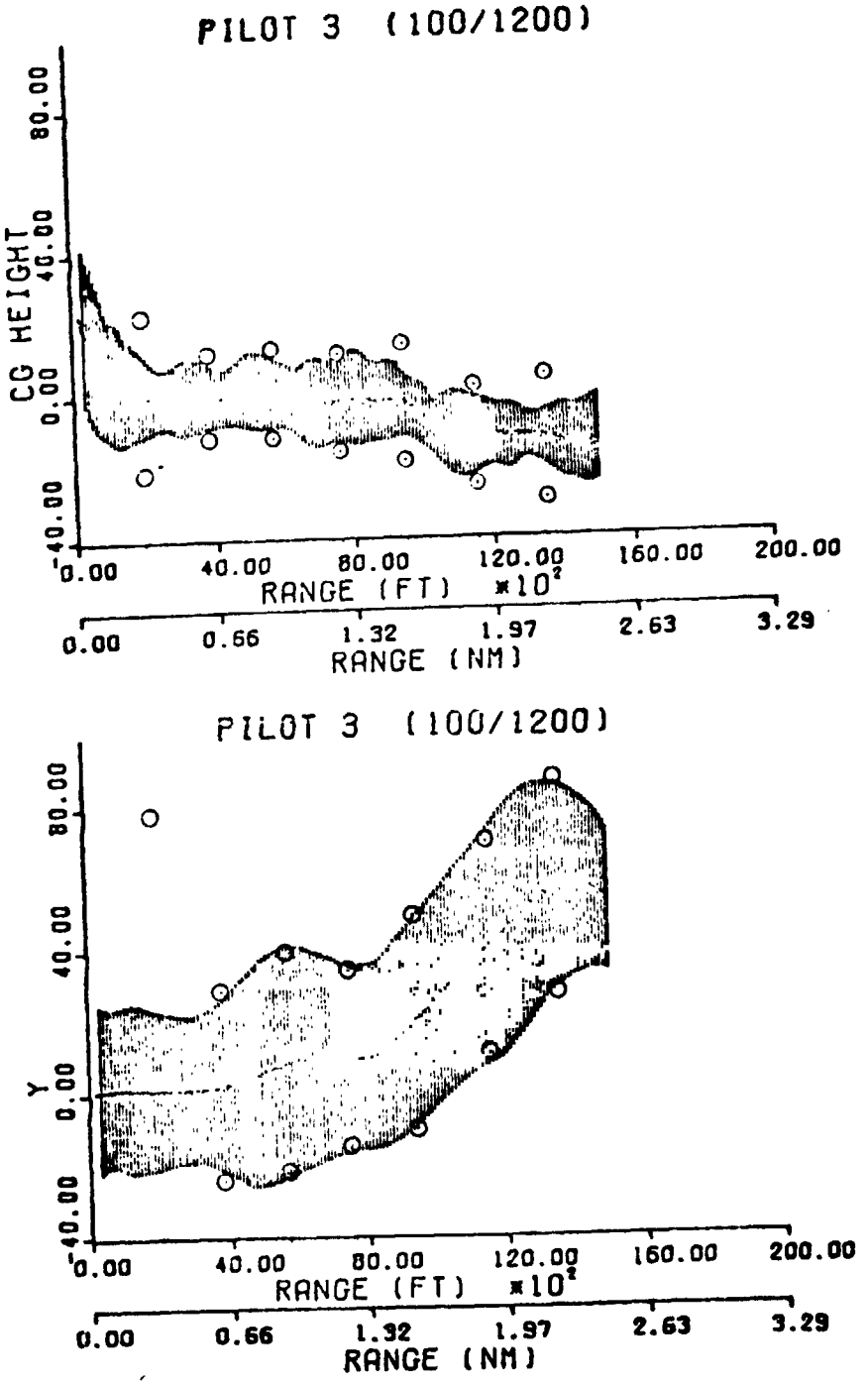

Figure 8 Ensemble Tracking Statistics, Phase II Simulation. 100/1200 Weather Conditions

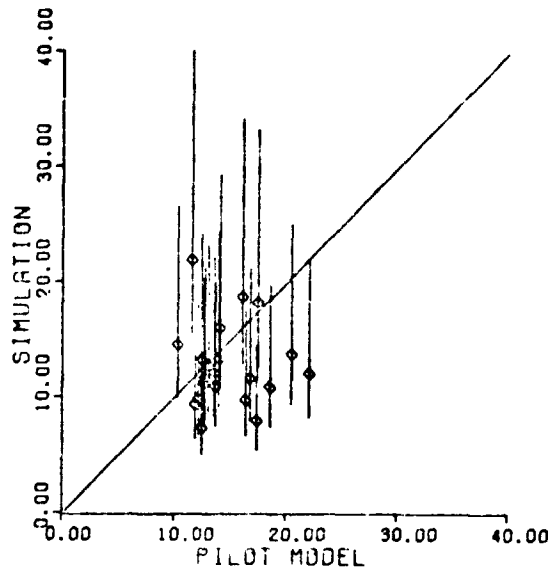

Figure 9 Scatter Diagram for Vertical Tracking Error, Phase II Simulation

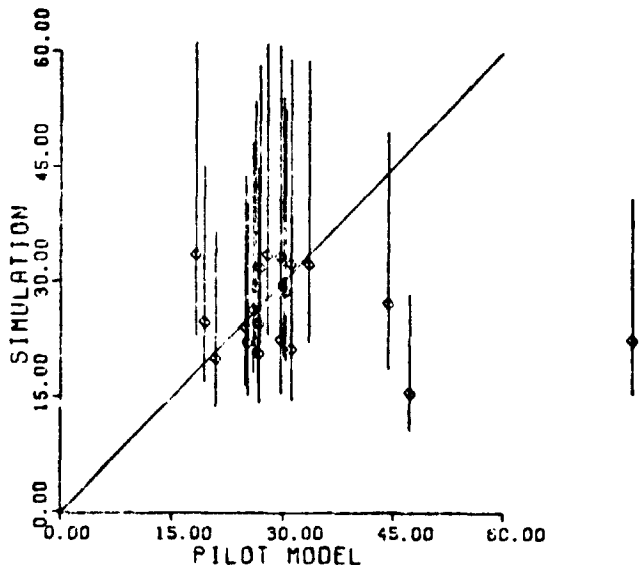

Figure 10 Scatter Diagram for Lateral Tracking Error, Phase II Simulation

control law which represents the task, is related to the closed loop system frequency response, and is unique, (2) a full state estimator which observes those instruments or quantities available to perform the flight task, and (3) a scanning algorithm which accounts for the scanning pattern, frequency, and dwell time, as well as the dynamics of the observed quantities.

The optimal pilot model is executed by the digital computer program FGD PILOT. The program requires specification of the aircraft configuration, the appropriate stability derivatives and aircraft model gains, and the gust parameters. The program requires minimal inputs for the pilot model to perform the control task: (1) the TASK vector to define the flight task, (2) the neuromuscular frequency limit for the controller configuration, (3) the SCAN vector to define the instruments or quantities available to perform the flight task, and (4) the perceptual thresholds of those instruments or quantities. Otherwise, the program is self-contained and executes the control frequency analysis, the scanning algorithm, and all iterations required to satisfy the control law and statistical approximations made in the aircraft model. Thus, the program is designed for easy use and extension to other aircraft systems and tasks.

SUMMARY OF THE ANALYSIS OF THE PHASE II LOW VISIBILITY SIMULATION

The following conclusions are drawn about the data base:

1. The data base from the simulation is nonstationary, precluding optimal pilot analysis of the stationary statistics.

2. Initial trim condition problems resulted in non-zero mean lateral tracking error.

The following conclusions are drawn from or supported by the pilot model analysis:

1. The glide slope and localizer tracking errors depend significantly upon the current gust statistics.

2. Under the conditions of approach with a flight director through linear fogs in a gusty environment with no cross wind, glide slope and localizer tracking performance does not depend upon the fog structure.

3. The Collins FD-109 flight director can saturate at low altitude, requiring the pilot to change his control strategy. Although the saturation property can aid in aircraft safety by reducing control activity at low altitude, the resulting degradation of information quality can produce a dangerous control situation during a critical phase of low visibility approach.

CONCLUDING REMARKS

The optimal pilot model has demonstrated effective synthesis of a complete piloted aircraft system. The pilot model algorithm should be extended and verified for aircraft systems with other stability characteristics, controller configurations, displays, and for other control tasks. This development process will result in a pilot model which can be used confidently for performance prediction and analysis of aircraft systems.

REFERENCES

1. Gressang, Stone, Pollard, and Kugel: Low Visibility Landing Pilot Modeling Experiment and Data, Phase I. AFFDL TR 75-41, April 1976.

2. Gressang: Low Visibility Landing Pilot Modeling Experiments and Data, Phase II. AFFDL TR 75-57, August 1975.

3. McRuer and Krendel: Mathematical Models of Human Pilot Behavior. AGARDograph No. 188, January 1974.

4. Baron and Kleinman: The Human As An Optimal Controller and Information Processor. IEEE Trans. Man-Machine Systems, Vol. MMS-10, March 1969, pp 9 - 17.

5. Baron et al: Application of Optimal Control Theory to the Prediction of Human Performance In A Complex Task. AFFDL TR 69-81, March 1970.

6. Kleinman, Baron, and Levison: A Control Theoretic Approach to Manned-Vehicle Systems Analysis. IEEE Trans. Auto. Control, Vol. AC-16, December 1971, pp 824 - 832.

7. Kleinman, Baron, and Levison: An Optimal-Control Model of Human Response, Part I: Theory and Validation. Automatica, Vol. 6, 1970, pp 357 - 369.

8. Kleinman: Optimal Control of Linear Systems With Time-Delay and Observation Noise. IEEE Trans. Auto. Control, Vol. AC-14, October 1969, pp 524 - 527.

9. Graham and McRuer: Analysis of Nonlinear Control Systems. Dover Publications, New York, 1971, Chapter 6.

10. Baron and Levison: An Optimal Control Methodology for Analyzing the Effects of Display Parameters On Performance and Work Load in Manual Flight Control. IEEE Trans. on Systems, Man, and Cybernetics, Vol. SMC-5, July 1975, pp 423 - 430.

11. Bryson and Ho: Applied Optimal Control. Ginn and Co., Waltham, Mass., 1969, Chapter 5.

12. Kleinman and Baron: Analytic Evaluation of Display Requirements for Approach to Landing. NASA CR-1952, October 1971.

13. Kleinman and Perkins: Modeling Human Performance in a Time-Varying Anti-Aircraft Tracking Loop. IEEE Trans. Auto. Control, Vol. AC-19, August 1974, pp 297 - 306.

14. Harvey: Application of An Optimal Control Pilot Model to Air-to-Air Combat. AFIT Thesis GA/MA/74M-1, March 1974.

15. Zillow, Picha and Anderson: Slushy Weightings for the Optimal Pilot Model. 11th Annual Conference on Manual Control, May 1975.

16. Kleinman: Computer Programs Useful in Linear Systems Studies. Systems Control, Inc., Technical Memorandum, December 1971.

17. Kleinman: On An Iterative Technique for Riccati Equation Computation. IEEE Trans. Auto. Control, Vol. AC-13, February 1968, pp 114 - 115.

18. Kwakernaak and Sivan: Linear Optimal Control Systems. John Wiley, New York, 1972, Chapter 3.

19. McRuer, Ashkenas, and Graham: Aircraft Dynamics and Automatic Control. Princeton University Press, 1973, Chapters 5 and 6.

20. Kleinman and Killingsworth: A Predictive Pilot Model for STOL Aircraft Landing. NASA CR-2374, March 1974.

21. Gressang: A Note on Solving Riccati Equations Associated with Optimal Pilot Models. AFIT/AIAA Mini Symposium on Recent Advances in Aeronautical Research Development, and Systems, WPAFB, 26 March 1975.

22. Bryson and Hall: Optimal Control and Filter Synthesis by Eio-envector Decomposition. Report, Dept. of Aero. and Astr., Stanford University, December 1971.

23. McRuer and Graham: Human Pilot Dynamics in Compensatory Systems. AFFDL TR 69-72, July 1965.

24. C-135B Aerodynamic, Flight, Ground, and Engine Equations. Report ER-459, Link Division, General Precision, Inc., Binghamton, NY, 11 January 1963.

25. Heath: State Variable Model of Wind Gusts. AFFDL/FGC TM-72-12, July 1972.

26. Stark: Neurological Control Systems, Studies in Bioengineering. Plenum Press, New York, 1968.

27. Milsum: Biological Control Systems Analysis. McGraw-Hill Book Company, New York, 1966.

28. Chalk, Neal, Harris, Pritchard, and Woodcock: Background Information and User Guide for MIL-F-8785B(ASG), "Military Specification -- Flying Qualities of Piloted Airplanes". AFFDL TR 69-72, August 1969.

29. Curry, Young, Hoffman, and Kugel: A Pilot Model with Visual and Motion Cues. AIAA Visual and Motion Simulation Conference, Dayton, Ohio, April 1976.

30. Crow, Davis, and Maxwell: Statistics Manual, Dover Publications, New York, 1947.

STABILITY OF THE PILOT-AIRCRAFT SYSTEM IN MANEUVERING FLIGHT*

by

John R. Broussard and Robert F. Stengel
The Analytic Sciences Corporation
Six Jacob Way
Reading, Massachusetts 01867

ABSTRACT

A control-theoretic pilot model is incorporated in the analysis of pilot-aircraft motions during maneuvers. The pilot model is found to be of value for the definition of maneuvering flight stability boundaries, and it simulates pilot control actions during a representative task with reasonable fidelity. It is concluded that the pilot model developed here, which is synthesized rapidly using new algorithms for solution of matrix Riccati equations, provides important capabilities for evaluation of flying qualities and for identifying proper piloting procedures during difficult maneuvers.

INTRODUCTION

High-performance aircraft are susceptible to degraded flying qualities during maneuvering flight, and the effects of piloting actions play a significant role in determining overall system stability. The pilot's task is made difficult by the need to adapt control strategies to varying aircraft dynamics, by potentially high work load, and by the physical and mental stresses associated with maintaining safe flight. Under such circumstances, improper piloting procedures can lead to inadvertent loss of control. This paper presents results from a study of pilot-aircraft interactions during high angle-of-attack flight. A multi-input/multi-output, control-theoretic human operator model is developed

*Contract No. N00014-75-C-0432 for the Office of Naval Research, Department of the Navy.

Presented at the 12th Annual Conference on Manual Control, Urbana, Illinois, May 25-27, 1976

and applied to the stability problem. Effects of control mechanisms (e.g., conventional stick-surface linkages and aileron-rudder interconnect), and pilot adaptation to flight condition are described. Proper (i.e., stabilizing) control actions for maneuvering flight are illustrated, and an example of pilot-induced oscillation (PIO) due to pilot non-adaptivity is demonstrated.

CONTROL THEORETIC PILOT MODEL

The optimal control pilot model (Fig. 1) used for this analysis contains the following elements: an estimator, which processes the pilot's observations to provide an estimate of the aircraft state; a controller, which mechanizes the pilot's regulating functions and transmits the results to the neuromuscular dynamics; and a neuromuscular model, which represents

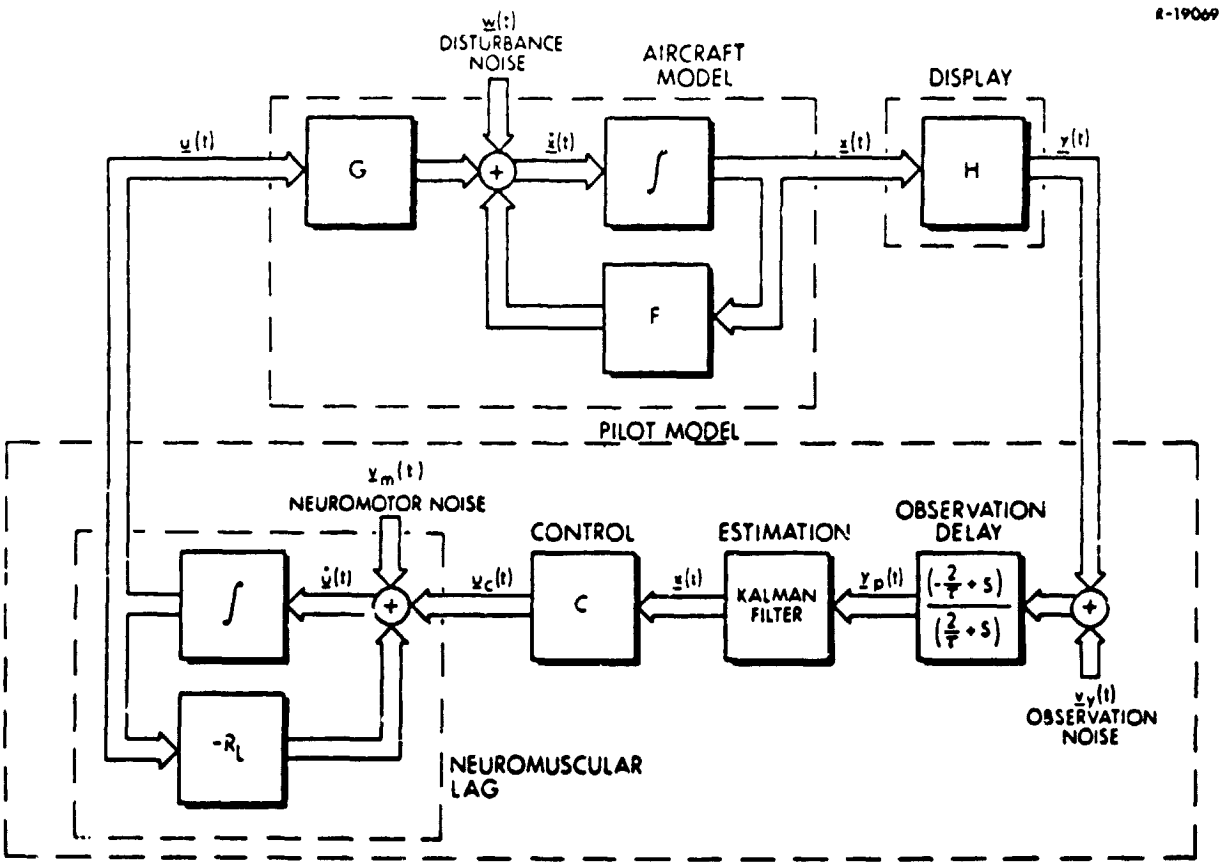

Figure 1. Block Diagram of the Pilot Model Containing the Pade approximation to Pure Time Delay

the dynamics of the pilot's limbs. A block diagram of the model depicting the three elements is shown in Fig. 1. The model replaces the pure time delay that is commonly modeled in human observations (Ref. 1) by a first-order Padé approximation, a substitution frequently made in analysis of human response using quasi-linear human models (Ref. 2) The substitution is useful, because it allows the predictor quations in the pure-time-delay optimal-control model to be eliminated. The aircraft and pilot model then can be combined in a single linear, time-invariant equation, shown by Eq. 6 in the appendix. This form is easier to simulate, and its stability and response characteristics are readily defined by eigenvalues and eigenvectors. From the separation principle for linear-optimal stochastic regulators (Ref. 3), the stability of the pilot model's estimation and control dynamics can be defined independently, i.e., the eigenvalues (or poles) of the pilot estimator are uncoupled from the closed-loop poles of the pilot controller-aircraft system. Similarities between the pure-time-delay model and the model in Fig. 1 include identical numerical values for the pilot control strategy matrix, C, the observation covariance matrix associated with $\Delta v_y(t)$, and the neuromotor noise covariance matrix associated with $\Delta v_u(t)$.

Two new algorithms have been derived for generating the coefficients of the pilot model. One solves the regulator Riccati equation and the other solves the estimator Riccati equation. These algorithms, are self starting and completely automated for computer implementation. The regulator algorithm is shown in the appendix, and the estimator algorithm can be found in Ref. 4. A unique feature of these algorithms is that any number of controls can be used, and current results have been obtained with up to three concurrent pilot outputs (longitudinal stick, lateral stick, and rudder pedals). The pilot model for this analysis is supported by a fully coupled, linear, six degree-of-freedom, aircraft simulation, (Ref. 5). The pilot model longitudinal/lateral-directional modes are coupled or uncoupled depending on the coupling in the aircraft model.

Investigations of pilot-aircraft instability using the control-theoretic pilot model fall into two categories: those in which the pilot fails to stabilize an unstable aircraft, and those in which the pilot destabilizes a stable aircraft. In the first case, the pilot's time delay, observation noise, neuromuscular time constants, and scanning factors are important parameters. Assuming that the aircraft's linearized dynamics have one or more unstable eigenvalues, the analysis determines pilot parameters for which the optimal control model fails to exist. The optimal control model fails to exist when one of the model algorithms diverges, i.e., when it is not possible to obtain a steady-state solution to one of the Riccati equations.

The second category is related to the pilot's ability to adapt to changing flight conditions. Straight-and-level flight at low angles of attack is a typical operating condition. In

many situations, such as air combat and tracking, the pilot must maneuver the aircraft through widely varying flight conditions at high angles of attack, resulting in rapidly changing aircraft dynamics. These include such changes as the onset of adverse yaw due to ailerons, the migration of roll and spiral roots to unstable positions, and large variations in the natural frequency and damping of short period and Dutch roll modes. With the mean angle of attack, α_o, changing in some instances faster than a degree per second, the pilot may not have the time to update his control strategy fast enough, and local instabilities can result. For example, pilot-induced oscillations (PIO) and departures can occur because a control strategy which is appropriate to one flight condition is destabilizing in another.

The control-theoretic pilot model can be used to analyze nonadapting pilot behavior in a straightforward manner. In the examples considered here, the pilot model's control strategy matrix, C, is first determined at a low-α_o flight condition. This gain matrix is frozen and the aircraft's dynamics are allowed to change. The stability of the pilot-aircraft system is determined by its eigenvalues. The Kalman filter dynamics are always assumed to be adapted and stable; thus, the Kalman filter only affects the simulation transient of the non-adapted pilot model and does not affect its stability.

EFFECTS OF FLIGHT CONDITIONS ON PILOT-AIRCRAFT STABILITY

The open-loop stability limits of the reference aircraft are shown in Fig. 2. The primary instabilities are an unstable Dutch roll mode in a band centered near α_o = 20 deg and an unstable roll/spiral combination in a band near α_o = 3[illegible]

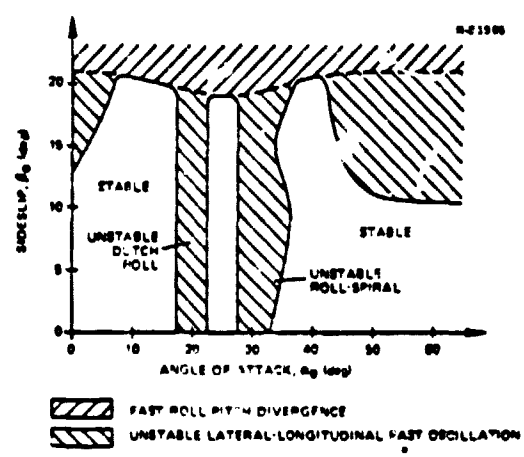

Figure 2. Open-Loop Stability Limits of the Reference Aircraft

The pilot's control outputs can include lateral stick for roll control, longitudinal stick for pitch control, and pedals for yaw control. When the aileron-rudder interconnect system (ARI) is engaged, the lateral stick commands to aileron are phased out as α_0 increases beyond 10 deg, and lateral stick-to-rudder commands are phased in. Above α_0 = 30 deg, the lateral stick controls rudder only. The purpose of the ARI is to reduce adverse yaw effects due to aileron at high α_0, allowing the pilot to use low-α_0 strategies at high angle of attack. This will be verified with the nonadapted pilot model.

The next three figures show simulations of the adapted linear-time-invariant control-theoretic model. In all cases, the noise terms are set to zero, and the model starts with a 10-deg heading error, which is to be nulled by the pilot model. Figure 3 shows piloting procedure at low-α_0 flight conditions using lateral stick alone and lateral stick plus rudder pedal. The figures illustrate that the modeled control patterns are very similar to the normal operating procedures of a human pilot. Initially, negative lateral stick movement rolls the aircraft and starts the heading change; this is followed by positive stick deflection to null roll rate and to zero roll angle at the new heading. The figure also demonstrates how the pilot can quicken lateral response by coordinated control of stick and pedals.

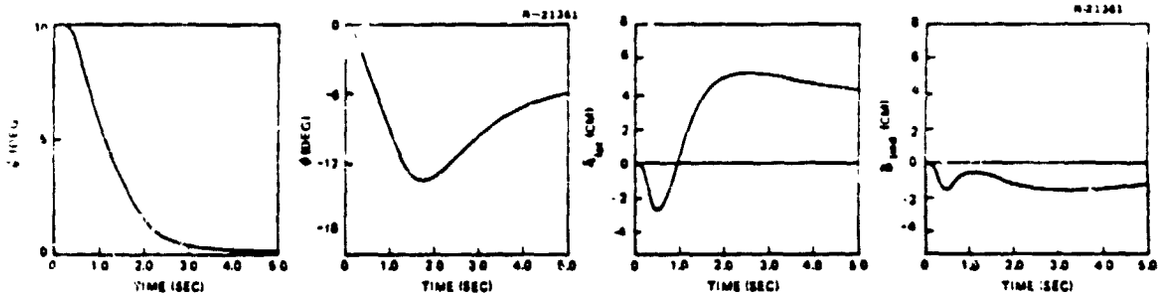

a) Lateral Stick Plus Rudder Pedal

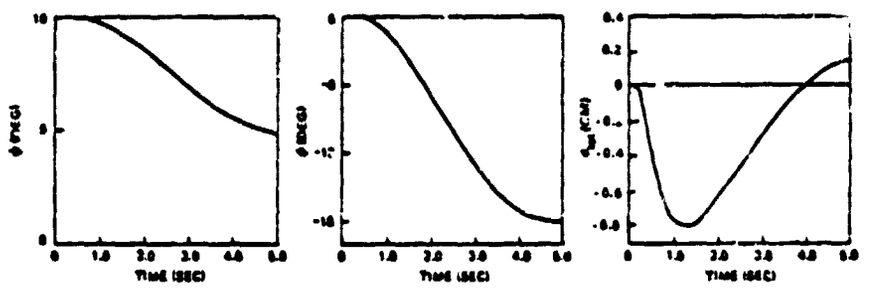

b) Lateral Stick Alone

Figure 3. Adapted Piloting Procedures at α_0 = 10 deg

At higher angles of attack, adapted pilot model behavior with and without the ARI can be determined. Figure 4 shows such behavior at α_o = 30 deg, β_o = 0 deg for control with lateral stick alone. When the ARI is off, as in Fig. 4b, the pilot model must use a stick deflection which is opposite to the normal movement to null the yaw angle. When the ARI is on, as in Fig. 4a, the pilot model uses normal low-α_o procedure to null the yaw angle, i.e., negative lateral stick to roll negatively. From Fig. 4, it can be seen that the ARI achieves its purpose, in terms of maintaining the same piloting procedure at high and low-α_o for lateral stick control.

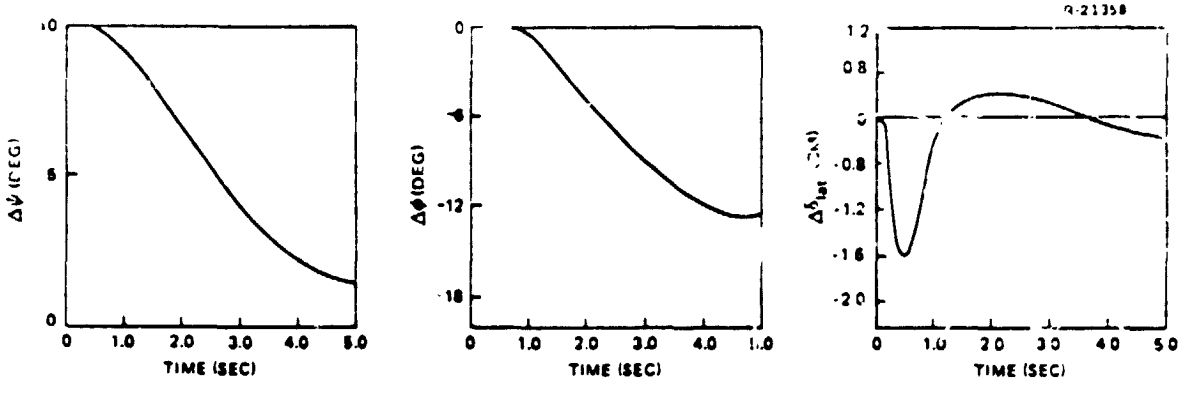

a) ARI On

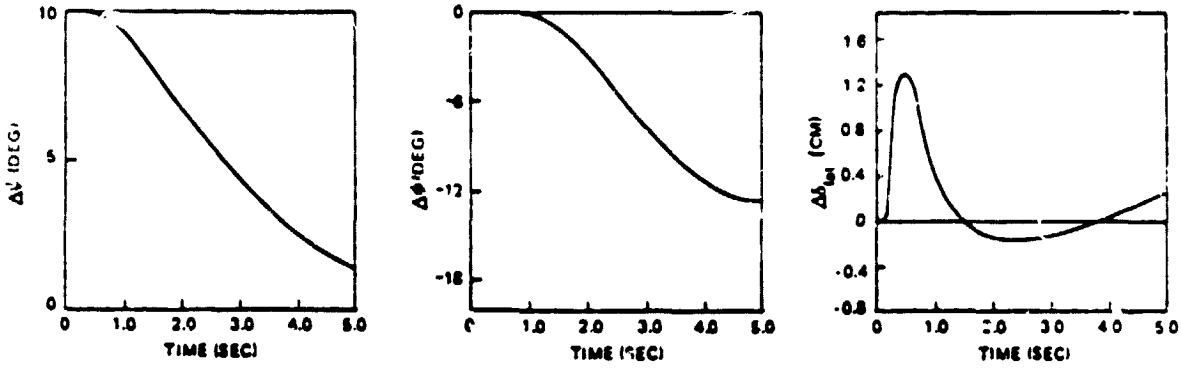

b) ARI Off

Figure 4. Adapted Lateral Stick Alone Piloting Procedure at α_o=30 deg

Figure 5 shows adapted pilot model behavior at high-α_o for combined control with lateral stick and pedals. A comparison of Fig. 5b with Fig. 3a shows that the lateral stick movements are similar, as are the initial pedal movements; however, the final pedal positions are opposite in sign. The positive pedal position in Fig. 5b is counteracting the adverse yaw caused by

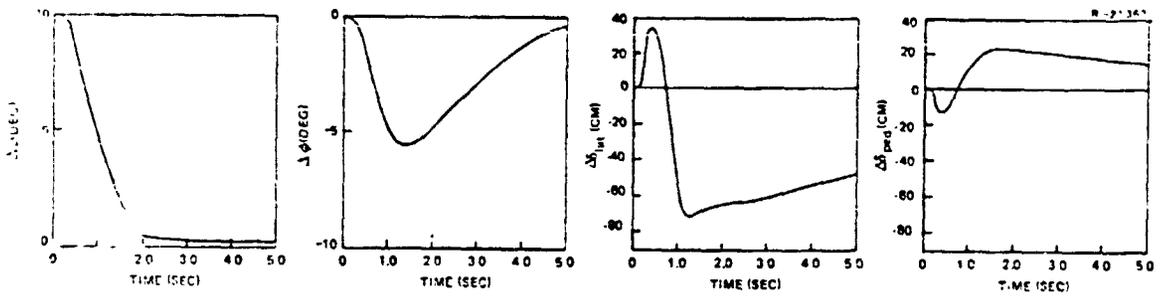

a) ARI On

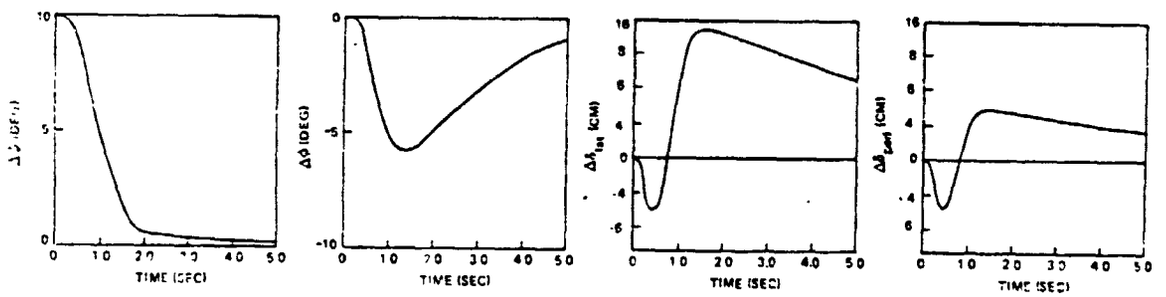

b) ARI Off

Figure 5. Adapted Lateral Stick and Pedal Piloting Procedure at α_o = 30 deg

positive lateral stick at high α_o. Figure 5a shows stick/pedal control procedure at high α_o with the ARI on. The large control movements are not unexpected. At α_o = 30 deg, lateral stick and pedal both control only rudder and their movements conflict. It would be possible to incorporate this known conflict by increasing the appropriate penalty weights in the design equation. In the present examples, the weighting matrices are held constant to illustrate the effects of the pilot maintaining constant tradeoffs between allowed state errors and control usage.

Nonadapted piloting effects on pilot-aircraft stability regions can be presented in the aircraft's α_o-β_o plane. The regions of instability are determined, as previously mentioned, by fixing pilot control strategy, C, and determining eigenvalues of the closed-loop system (Eq. 6). Figure 6 shows the stability regions for three-control piloting procedures, and Fig. 7 shows stability regions under the assumption that the pilot does not use pedal control. In all cases the pilot model is adapted to α_o = 10 deg and β_o = 0 deg (denoted by ⊗ in the figures). The instabilities of the longitudinal modes (phugoid and short period) are the same in both cases, since the ARI does not affect longitudinal control. From Fig. 3a and 4b, it is evident that if the pilot model does not adapt, at some point low-α_o piloting

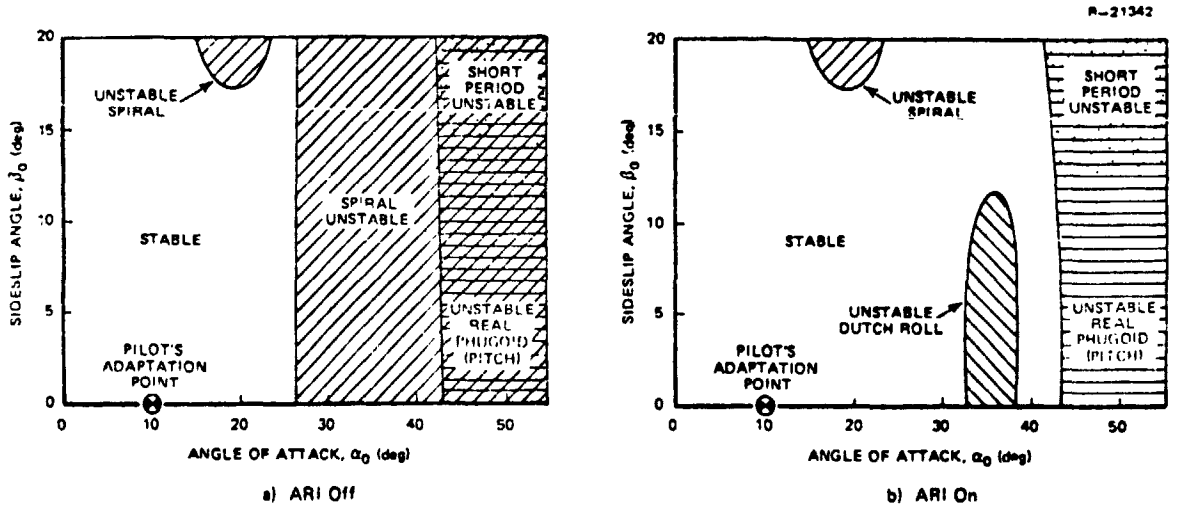

Figure 6. Stability Boundaries for 3-Control Piloting Procedures

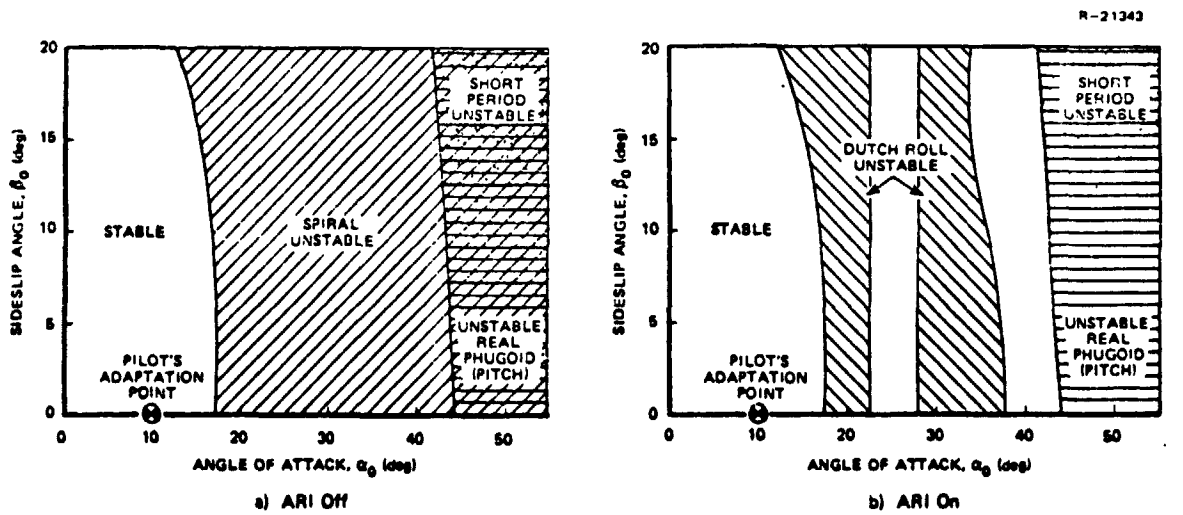

Figure 7. Stability Boundaries for 2-Control Piloting Procedures

procedure will cause an instability because of adverse yaw. In Fig. 7a this occurs at $\alpha_0 \approx 17$ deg, and the incorrect procedure is characterized by an unstable (closed-loop) spiral mode. When three controls are used with the ARI off, the instability due to incorrect procedure does not occur until $\alpha_0 \approx 26$ deg, as shown in Fig. 6a. Figures 6b and 7b indicate that the ARI eliminates the spiral instability seen in Figs. 6a and 7a, but it introduces an unstable Dutch roll mode. In the stick-alone case, the instability occurs in bands centered on 20 deg and 32 deg angle of attack.

Simulations of nonadapted procedure are readily obtained using the control-theoretic model, and these are shown in Figs. 8 and 9. Figure 8b shows the unstable spiral mode response with ARI off where negative lateral stick yaws the aircraft positively. Figure 8a shows the unstable Dutch roll mode with ARI engaged, of which only one cycle is evident. Note that negative lateral stick deflection causes the correct initial yaw response, but the pilot model's stick movement does not compensate fast enough. Figure 9b shows the unstable spiral mode for three controls with the ARI off. The initial direction in yaw angle is correct, but sluggishness in control movement, particularly in pedal, causes the instability. The simulation in Fig. 9a is stable for three controls with the ARI on. A comparison of Fig. 9a with Fig. 3a shows that the pilot model successfully uses the same strategy in both cases, but the 10-deg strategy provides too little damping at α_o = 30 deg.

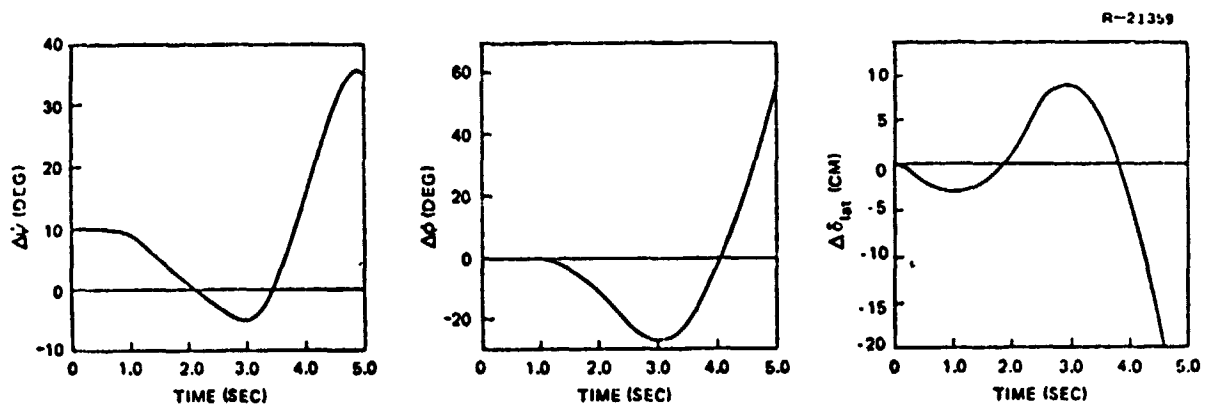

a) ARI On

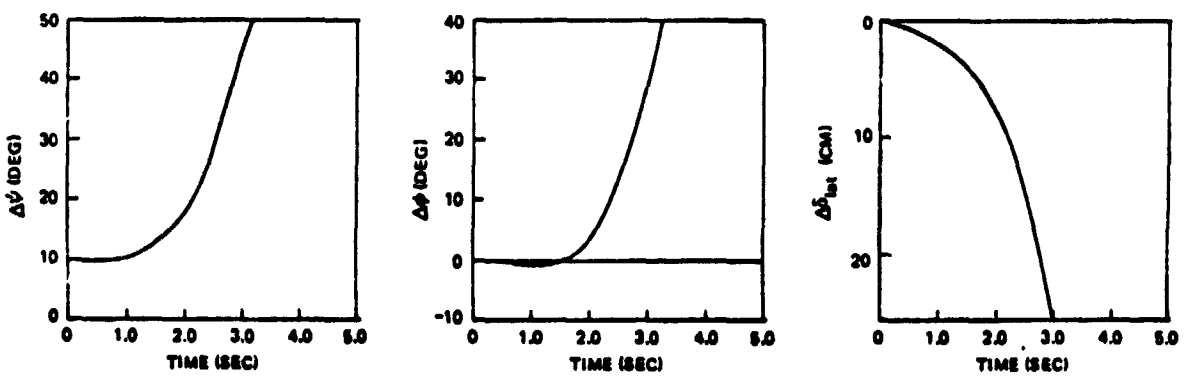

b) ARI Off

Figure 8. Use of Low-α_o Piloting Procedure in High-α_o Flight With Lateral Stick Alone. Pilot is Adapted to α_o = 10 deg; aircraft is at α_o = 30 deg.

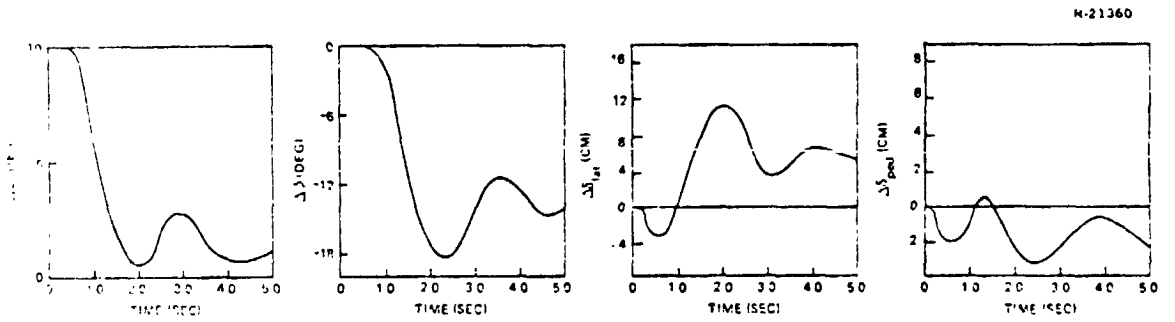

a) ARI On

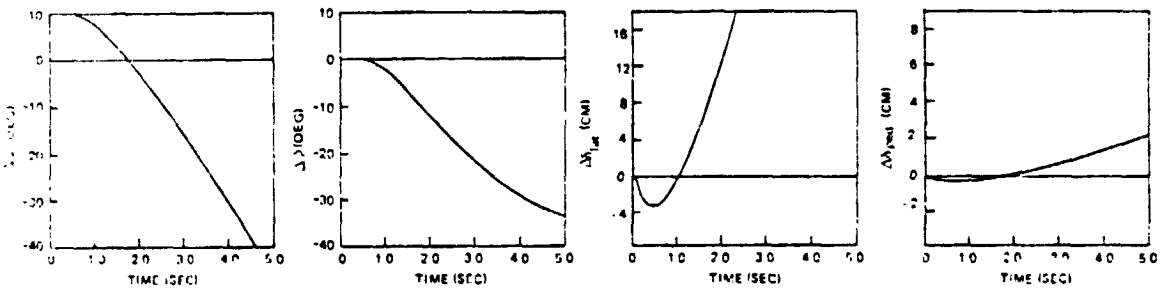

b) ARI Off

Figure 9. Use of Low-α_o Piloting Procedure in High-α_o Flight with Lateral Stick Plus Rudder Pedals

A direct indication of the destabilizing influence which a nonadapted pilot could have and which could lead to pilot induced oscillations is illustrated in Fig. 10. Figure 10a shows the natural rolling motion of this aircraft at α_o = 20 deg, which is a consequence of a slightly unstable Dutch roll mode. In Fig. 10b, the ARI is on, the pilot model is adapted to α_o = 10 deg flight, and there is an initial sideslip perturbation ($\Delta\beta$) of one deg. If the pilot uses the low-α_o learned response to attempt to null $\Delta\beta$ and Δp, he may inadvertently "pump" energy into the growing $\Delta\beta$ oscillation through the aileron's adverse yaw. The result is a pilot-induced diverging oscillation whose characteristics would normally be associated with wing rock. The highly oscillatory nature of the control actions presumably is the result of limitations on the control rates which the pilot model is able to use.

LIMITS OF CONTROLLABILITY

For the reference aircraft and flight conditions, no pilot model algorithm instabilities are encountered in this

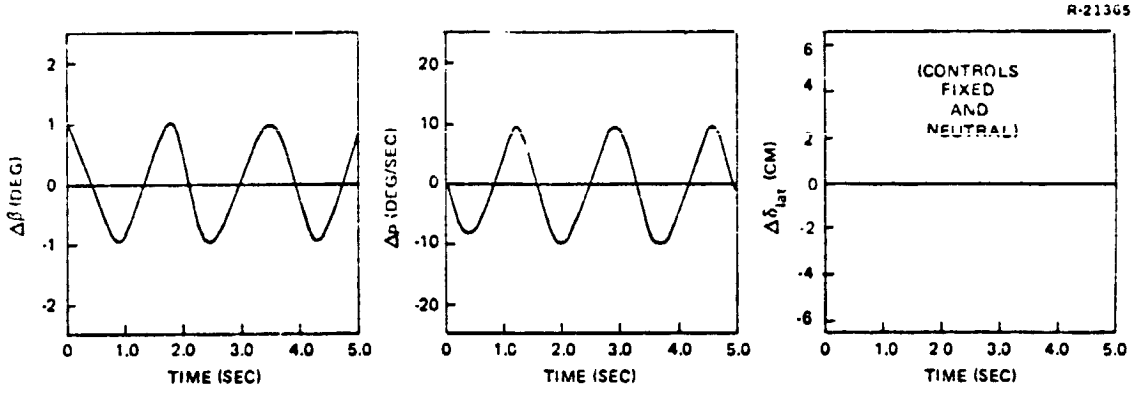

a) Open Loop Response

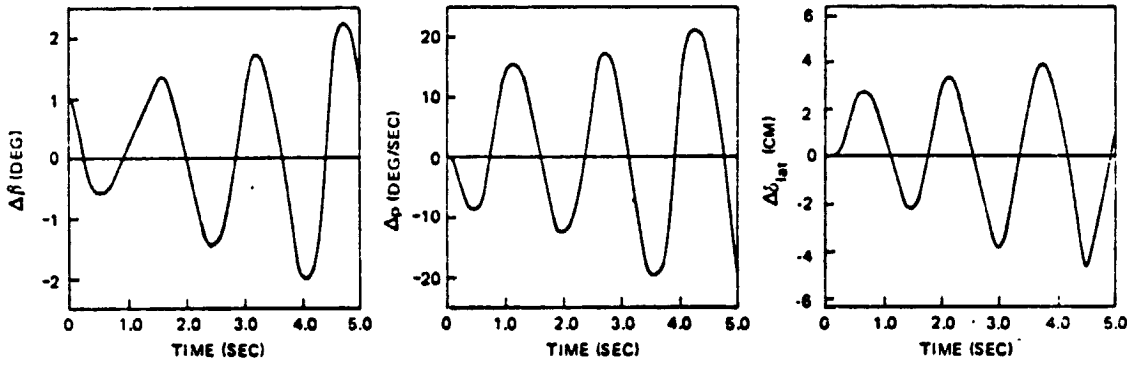

b) Piloted Response

Figure 10. Sideslip Response at α_o = 20 deg with Lateral Stick Alone, ARI On, and the Pilot Model Adapted to α_o = 10 deg

analysis, even when parameters of the pilot model are varied within accepted limits of neurophysiological capability. In other words, the model indicates that the pilot is capable of adapting his control strategy to stabilize the aircraft throughout the flight regine investigated here. Nevertheless, for other aircraft or flight conditions, the model could fail to exist, and this would be a direct indication that a human pilot could not provide effective control in a similar situation.

The lack of an optimal control pilot model for certain conditions has been shown indirectly in Refs. 6 and 7, and examples of the nonexistence of optimal control pilot models are shown explicitly in Ref. 4 for a scalar system with time constant, τ_s. Reference 4 indicates that the pilot model regulator Riccati equation does not have a solution if $2\tau_n \leq -\tau_s$, where τ_n is the neuromotor time constant. A comparison of this result with actual experimental results contained in Ref. 8 can be made. In Ref. 8,

values of τ_s which first resulted in unstable conditions are determined. Values of τ_n can be predicted as $\tau_n = -\tau_s/2$, since this is the stability boundary for the control-theoretic pilot model. Table 1 summarizes the results of the comparison. There is good agreement between values of τ_n shown in Table 1 and known values of τ_n(0.08 to 0.12 sec). The control-theoretic model has existence difficulties for the regulator if the system's unstable eigenvalues are greater than 5.0 ($\tau_n \geq .10$). Experience with the pilot model estimator algorithm in Ref. 4 has shown that estimator existance difficulties can be encountered with system open-loop eigenvalues as low as 1.0. In this case, the pilot's attention allocation becomes the deciding factor for instability.

Table 1

Experimental Stability Boundaries

Subject	Value of τ_s at Stability Boundary in Ref. 8, sec	Corresponding Optimal Control Model Predicted τ_n, where $\tau_n = -\tau_s/2$, sec
ETP	-0.152	0.076
EWV	-0.169	0.085
MHS	-0.182	0.091
KED	-0.222	0.111

CONCLUSION

This paper has illustrated several ways in which a control-theoretic pilot model can be useful for examining the stability of the pilot-aircraft system. It is shown that this system can be unstable for one of two reasons: either the aircraft itself is unstable and the pilot is incapable of providing stabilizing control actions or the pilot can destabilize an otherwise stable aircraft by inapproproate control actions. The latter case can result when the pilot does not adapt to changing flight conditions, applying control strategies which are suitable for one flight condition in a dynamically dissimilar situation. Although not detailed in this paper, the stability boundaries and simulated time histories established with the nonadapted pilot model are compatible with experimental results obtained from manned simulation and flight test.

An inverse interpretation of the results obtained with the adapted pilot model is that they specify what the pilot must do in a given dynamic condition to achieve well-behaved, stable aircraft response. Given the accepted physiological parameters contained in the design equations, the model illustrates what the well-motivated pilot can do to null flight path errors with available control effectors; hence, it identifies logical cues for compensatory control, and it graphically depicts control deflection histories which can be learned as adjuncts to precognitive control. It is concluded that the control-theoretic pilot model is a valuable tool for further analysis of aircraft handling qualities and for understanding the piloting skills which are necessary for maneuvering flight.

REFERENCES

1. Kleinman, D.L., Baron, S., and Levison, W.H., "A Control Theoretic Approach to Manned-Vehicle Systems Analysis," IEEE Trans. on Automatic Control, Vol. AC-16, No. 6, December 1971.

2. Kugel, D.L., "Determination of In-Flight Pilot Parameters Using a Newton-Raphson Minimization Technique," Proceedings of the Tenth Annual Conference on Manual Control," April 9-11, 1974.

3. Tse, E., "On the Optimal Control of Stochastic Linear Systems," IEEE Trans. on Automatic Control, Vol. AC-16, No. 6, December 1971.

4. Taylor, J.H., Broussard, J.R., Berry, P.W., and Stengel, R.F., "Analytical Techniques for High Angle-of-Attack Stability and Control," The Analytic Sciences Corp., TR-612-1 (to appear as an ONR Contractor Report).

5. Stengel, R.F. and Berry, P.W., "Stability and Control of Maneuvering High Performance Aircraft," The Analytic Sciences Corp., TR-587-1 (to appear as a NASA Contractor Report), January 1976.

6. Curry, R.E., Kleinman, D.L., and Hoffman, W.C., "A Model for Simultaneous Monitoring and Control," Proceedings of the Eleventh Annual Conference on Manual Control, May 21-23, 1975.

7. Kleinman, D.L., "Optimal Stationary Control of Linear Systems with Control Dependent Noise," IEEE Trans. Automatic Control, Vol. AC-14, No. 6, December 1969.

8. Pitkin, E.T. and Vinje, E.W., "Evaluation of Human Operator Aural and Visual Delays with the Critical Tracking Task," Proceedings of the Eighth Annual Conference on Manual Control, May 17-19, 1972.

9. Kleinman, D.L., "On an Iterative Technique for Riccati Equation Computations," IEEE Trans. Automatic Control (Correspondence), Vol. AC-13, February 1968.

10. Kleinman, D.L., "Numerical Solution of the State Dependent Noise Problem," IEEE Trans. Automatic Control (Correspondence), Vol. AC-21, June 1976.

APPENDIX

Mathematical Equations

Small perturbations in aircraft motion are approximated by the linear-time-invariant system

$$\Delta\dot{\underline{x}}(t) = F\Delta\underline{x}(t) + G\Delta\underline{u}(t) + \Delta\underline{w}(t) \qquad (1)$$

where $\Delta\underline{x}(t)$ represents the perturbation motion, $\Delta\underline{w}(t)$ represents disturbance noise, and $\Delta\underline{u}(t)$ is the pilot's compensatory control. The observations of the pilot are assumed to be

$$\Delta\underline{y}(t) = H\Delta\underline{x}(t-\tau) + D\Delta\underline{u}(t-\tau) + \Delta\underline{v}_y(t-\tau) \qquad (2)$$

where τ is the pilot time delay and $\Delta\underline{v}_y(t)$ represents pilot observation noise. The pilot is assumed to choose $\Delta\underline{u}(t)$, when behaving optimally, by minimizing an infinite-time quadratic cost functional. This produces the control law

$$\Delta\dot{\underline{u}}(t) = -R_L\Delta\underline{u}(t) + C\Delta\hat{\underline{x}}(t) + \Delta\underline{v}_u(t) \qquad (3)$$

where $\Delta\underline{v}_u(t)$ represents pilot neuromotor noise. The matrix, C, is the pilot's feedback control strategy and the matrix, R_L, has the form

$$R_L = \begin{bmatrix} \frac{1}{\tau_{n_1}} & 0 & 0 \\ 0 & \frac{1}{\tau_{n_2}} & 0 \\ 0 & 0 & \frac{1}{\tau_{n_3}} \end{bmatrix} \qquad (4)$$

where the scalars, τ_{ni}, are neuromotor time constants of human limbs. The vector, $\Delta\hat{\underline{x}}(t)$, represents the pilot's estimate of the aircraft states based on observing $\Delta\underline{y}(t)$. The pilot model observations can be restructed by using the Padé approximation to $e^{-\tau s}$ in Eq. (2) as follows:

$$\Delta\underline{y}(s) = \frac{2-\tau s}{2+\tau s}\left((H\Delta\underline{x}(s) + D\Delta\underline{u}(s) + \Delta\underline{v}_y(s)\right) \qquad (5)$$

Using Eq. (1), (3), and (5), the closed-loop pilot aircraft system can be shown to be

$$\begin{bmatrix} \Delta\dot{\underline{x}}(t) \\ \Delta\dot{\underline{u}}(t) \\ \Delta\dot{\underline{z}}(t) \\ \hline \Delta\dot{\tilde{\underline{x}}}(t) \\ \Delta\dot{\tilde{\underline{u}}}(t) \\ \Delta\dot{\tilde{\underline{z}}}(t) \end{bmatrix} = \left[\begin{array}{ccc:ccc} F & G & 0 & 0 & 0 & 0 \\ C & -R_L & 0 & C & 0 & 0 \\ H & D & \left[\frac{2}{\tau} I\right] & 0 & 0 & 0 \\ \hline & & & & & \\ & 0 & & & F_f & \end{array}\right] \begin{bmatrix} \Delta\underline{x}(t) \\ \Delta\underline{u}(t) \\ \Delta\underline{z}(t) \\ \hline \Delta\tilde{\underline{x}}(t) \\ \Delta\tilde{\underline{u}}(t) \\ \Delta\tilde{\underline{z}}(t) \end{bmatrix} + \left[\begin{array}{c:c} & \\ I & 0 \\ & \\ \hline & \\ -I & K \\ & \end{array}\right] \begin{bmatrix} \Delta\underline{w}(t) \\ \Delta\underline{v}_u(t) \\ \Delta\underline{v}_y(t) \\ \hline \\ -\Delta\underline{v}_y(t) \\ \end{bmatrix} \qquad (6)$$

In Eq. (6), F_f is the closed-loop filter matrix and K is the Kalman filter gain. The states $\Delta\tilde{\underline{x}}(t)$, $\Delta\tilde{\underline{u}}(t)$, and $\Delta\tilde{\underline{z}}(t)$ are the estimation errors. The states $\Delta\underline{z}(t)$ are used to represent the delay after the Padé approximation. The matrix C does not change.

Assumptions

The pilot model outputs drive the aircraft through the matrix, G, which is adjusted to account for the ARI being on or off. The pilot is assumed to observe only the perturbation angles and angular rates of the aircraft. The pilot's observation noise-to-signal ratio is set at 0.025π to account for scanning. The neuromotor noise-to-signal ratio is set at 0.003π. The pilot is assumed to have a time delay of 0.2 sec and a neuromuscular time constant of 0.1 sec for each limb.

The state and control weighting matrix, Q, is adjusted until a reasonable set of mean-square covariance values of the aircraft states are obtained (Ref. 4). Present results indicate that closed-loop eigenvalues of the pilot model regulator may be relatively insensitive to Q. The adjustment of the control-rate weighting to maintain R_L in the optimal control pilot model appears to have a strong effect on relative weightings of states and controls. The control-rate weighting matrix, R, is found using the following new algorithm.

Pilot Model Regulator Algorithm

The pilot model regulator Riccati equation is given by

$$0 = SF' + F'^{T}S + Q - SG'R^{-1}G'^{T}S \tag{7}$$

where R weights the control rate and Q weights the states and controls in a quadratic cost functional. The following substitutions are made:

$$F' = \left[\begin{array}{c|c} F & G \\ \hline 0 & 0 \end{array}\right] \tag{8}$$

$$G' = \begin{bmatrix} 0 \\ \hline I \end{bmatrix} \tag{9}$$

$$S' = \left[\begin{array}{c|c} S_{11} & S_{12} \\ \hline S_{21} & S_{22} \end{array}\right] \tag{10}$$

$$R_L = R^{-1}S_{22} \tag{11}$$

Solving for R in Eq. (11) and using Eq. (9), Eq. (7) can be restated as follows:

$$0 = SF' + F'^{T}S + Q - SG'(G'^{T}SG'R_L^{-1})^{-1}G'^{T}S \tag{12}$$

Using a procedure similar to that of Ref. 9, if an initial S_o can be found in the contraction mapping convergence sphere of Eq. (12), repeated substitution converges to the solution of Eq. (12). The following iterative scheme strives to achieve the solution:

(1) Choose a positive definite R_o and solve for S_o in

$$0 = S_oF' + F'S_o + Q - S_oG'R_o^{-1}G'^{T}S_o$$

(2) Continue with the following until some convergence criterion is satisfied (unless R_1 does not become greater than R_2):

$$R_K = G'^{T}S_{K-1}G'R_L^{-1}$$

$$C_K = R_K^{-1}G'^{T}S_{K-1} \qquad K = 1, 2, \ldots$$

$$F_K' = F' - G'C_K$$

$$0 = S_K F_K' + F_K' S_K + Q + C_K^T R_K C_K$$

(3) If R_1 does not become greater than R_2, increase R_o and go back to (1).

(4) If R_o exceeds a maximum acceptable value, either R_o is larger than the stopping value or no solution exists.

The philosophy is to choose a stabilizing S_o that is greater than the solution S. Reference 10 provides a similar algorithm in which $R_L = \sigma I$, where σ is a scalar; R is therefore symmetric (Eq. (11)). The algorithm devcloped here requires only that R_L be an appropriate positive definite matrix; hence, R may be asymmetric.

ANALYSIS OF A MANNED ANTI-AIRCRAFT ARTILLERY (AAA) SYSTEM USING A PROPORTIONAL-INTEGRAL-DERIVATIVE (P-I-D) STRUCTURE OPTIMAL CONTROL GUNNER MODEL*

By Anil V. Phatak and Kenneth M. Kessler

Systems Control, Inc. (Vt)
Palo Alto, California

INTRODUCTION

An important problem in threat analysis is the evaluation and prediction of system performance of a manned anti-aircraft artillery (AAA) system. A systematic approach to manned threat quantification requires the development and integration of models for the weapon system, the target trajectory and the human gunner into a composite analysis algorithm that can be used for analytical and predictive purposes. The accuracy and, hence, the confidence in the analysis algorithm is clearly dependent on the fidelity of the models used to describe the individual subcomponents of the weapon system and most importantly the human gunner.** There exist several computer simulation programs [1] for predicting aircraft attrition when exposed to various air defense systems. However, a serious weakness of existing anti-aircraft artillery attrition algorithms is in the submodels they utilize to describe human target tracking performance. Typically, fixed empirical models for the human gunner are used without adequate theoretical justification or systematic validation.

This paper describes the formulation and validation of a human gunner model suitable for inclusion into a general anti-aircraft artillery attrition algorithm. An optimal control theoretic model with a proportional-integral-derivative (P-I-D) controller structure is shown to describe the human gunner's input-output characteristics in the most effective manner. Experimental data from manned AAA simulations is used in formulating and validating the P-I-D optimal control gunner model. The gunner model includes target trajectory dependent parameters to account for the adaptive characteristics of the human controller, and allows for lower order internal (to the human) representations of the system dynamics (weapon system and target trajectory) to reflect realistic human psychophysical limitations. The model formulation is in terms of the tracking error and a sufficient number of its higher order derivatives. This output vector model formulation represents a significant

* This work was supported by the 6570th Aerospace Medical Research Laboratory, Wright-Patterson Air Force Base, Ohio, under Contract No. F33615-76-C-5001.

** In practice, as in the case described in this paper, there may be two gunners involved in the AAA task. However, the singular form is used here to indicate one or more gunners.

departure from the standard optimal control model [2] which requires explicit state vector representation of the plant/noise (weapon system/target trajectory in this case) dynamics. The P-I-D formulation in terms of the display output (tracking error) in the AAA task has improved mathematical properties over the standard representation (e.g., complete controllability with respect to the control input) and, in addition, has the advantage of being intuitively appealing and easily reconcilable with classical control theory methodology.

The human gunner response data used for developing and validating the gunner model was obtained from experiments conducted at the Aerospace Medical Research Laboratory (AMRL/EMT), WPAFB, Ohio. A brief description of the anti-aircraft artillery (AAA) simulation is given below to provide the reader with the necessary background to interpret the results presented in this paper.

THE ANTI-AIRCRAFT ARTILLERY TASK

The general configuration of the manned AAA simulation is shown in Figure 1. Two gunners, one each for the azimuth and elevation axes, observe the target aircraft through a gunsight with approximately a 5° field of view. The size of the displayed aircraft subtends approximately a constant 0.5° visual angle with respect to the gunner. Consequently, no range information can be obtained from the visual display. The gunsight dynamics were selected to be representative of an actual AAA weapon system. Rate-aided sight dynamics given by

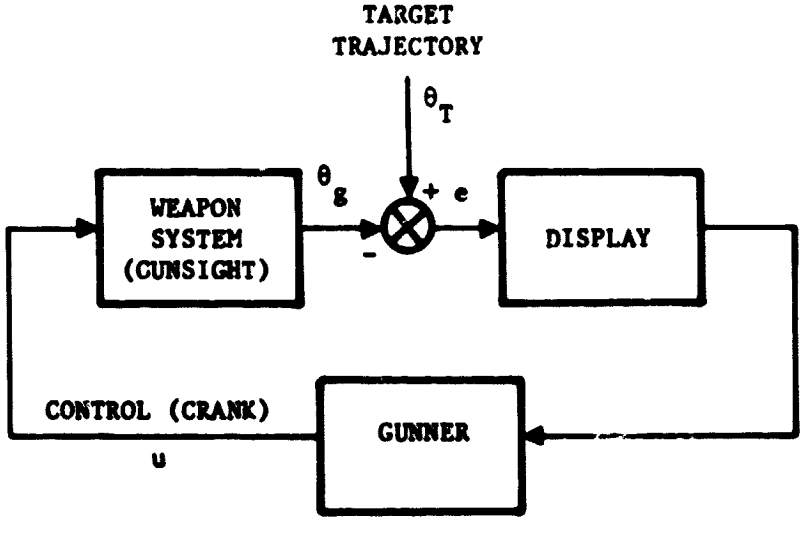

Figure 1. Configuration of the Manned AAA Simulation Experiments (Conducted at the AMRL, WPAFB, Ohio)

$$G(s) = \frac{\theta_g(s)}{u(s)} = \frac{64(s+1)}{s(s^2 + 12s + 64)} \qquad (1)$$

were used for both the azimuth and elevation axes. The two axes are uncoupled and have two independent hand cranks for use by the human gunners. Target aircraft fly-bys of 45 s duration corresponding to various levels of difficulty were selected in a randomized fashion from a set of 4 trajectories as shown in Figure 2. The operators were sufficiently trained before tracking data was collected. Specifically, 15 runs per target trajectory were conducted. Time histories corresponding to the azimuth and elevation axes were recorded for target trajectory, gunsight position, gunsight rate and crank position and digitized at 25 Hz. These data were ensemble averaged across the 15 runs per team to yield the ensemble statistics of the recorded variables. Any representation for the human gunner must be capable of duplicating these response patterns according to some consistent functional model. The following paragraphs describe the development and validation of a human gunner model that is consistent with the AMRL experimental data and known human psychophysical characteristics and limitations.

HUMAN GUNNER MODEL DEVELOPMENT

Several different approaches toward human operator modeling have been proposed over the past thirty years. The human has been characterized as a digital controller, a finite-state machine, a describing function, and an optimal feedback controller. However, since its formulation about seven years ago, the standard optimal control model [2] has emerged as one of the most promising models for the study of complex man-in-the-loop control systems. The primary reason for the success of the optimal control theoretic model lies in the flexibility of the modeling technique in handling multivariable, multiaxes, multicue, nonlinear and nonstationary stochastic control situations within a well developed and general state variable optimal control (Linear-Quadratic-Gaussian) framework. The details of the standard optimal control model are documented extensively in the literature and, therefore, are not discussed in this paper. However, recent efforts have shown the utility of using a simplified version of the standard optimal control model [3-5].

The modified optimal control model [4] retains the basic hypothesis that a trained human operator in a precision control task behaves like an optimal estimator and controller in achieving the task objectives subject to his inherent psychophysical limitations or constraints. Specifically, the model assumes that: (1) the trained human operator has an internal state variable model relating the displayed variables to his controls, (2) the operator has a noisy perceptual channel and perceives the displayed variables (not rates) contaminated by observation noise, (3) the operator is a full state (internal model state) estimator and controller, and (4) the operator chooses a control law that minimizes a quadratic cost functional in terms

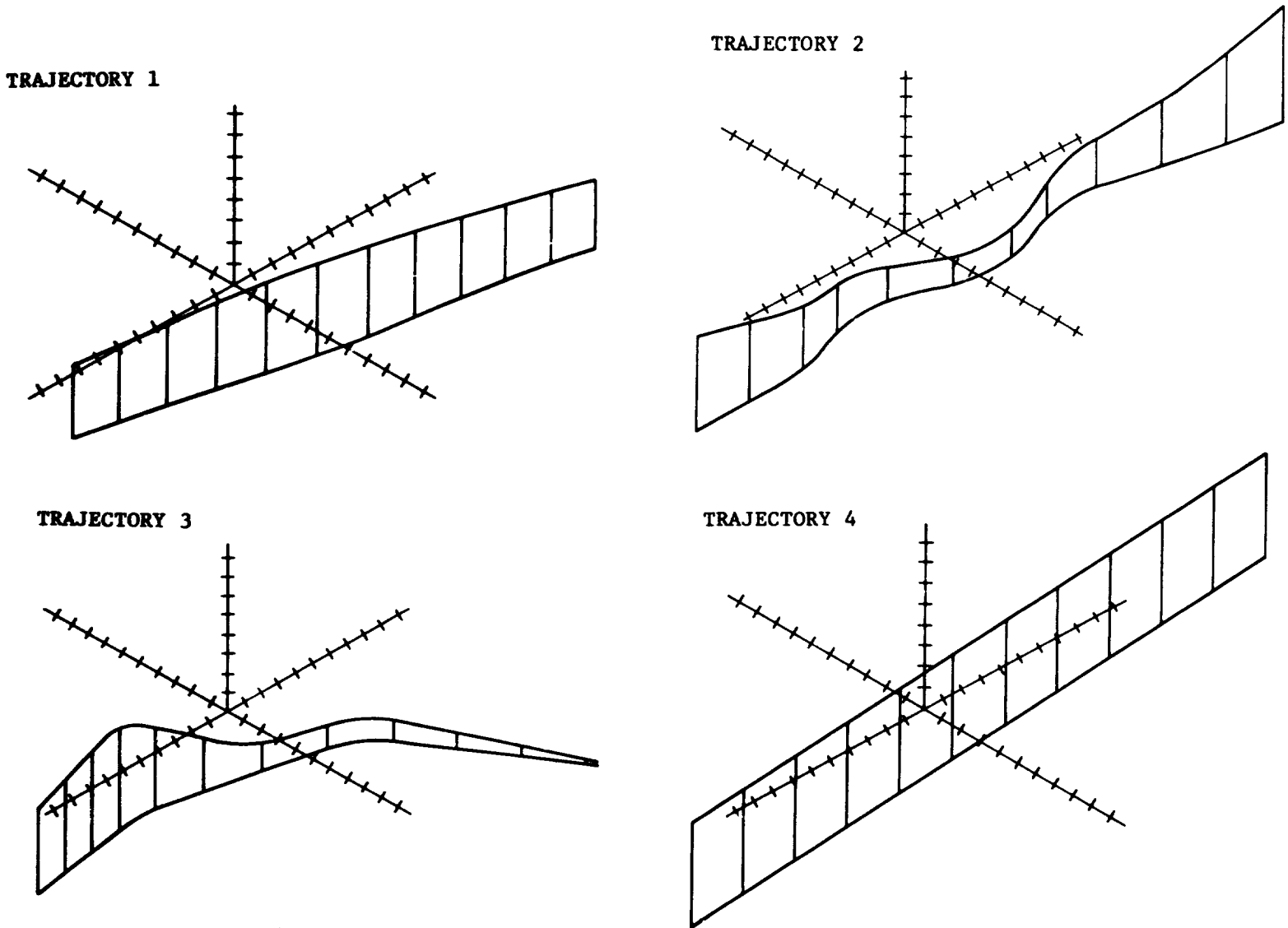

Figure 2. Perspective View of Four Target Trajectories

of the internal state vector, the control vector, and in some cases, higher order control derivatives (k^{th} derivative formulation). The resulting modified optimal control model [4] is as shown in Figure 3. The displayed state $y(t)$ is corrupted by observation noise $v_y(t)$ and the operator is assumed to perceive their sum. The Kalman filter utilizes the internal state variable model adopted by the human operator in estimating the internal states. The controller subsequently operates on this state estimate according to an optimal control law to yield the operator's control actions (inputs to the controlled system).

Inherent to this approach is the central assumption that the human has learned or developed an internal state variable model for the system from knowledge of his control (efferent) and perceived (afferent) variables. The standard approach is to assume that the human has explicit internal state variable models for the controlled system dynamics (gunsight), noise disturbances and command inputs (target trajectories). An alternative formulation is to assume that the human learns an input-output type of internal model relating the human's control variables to the displayed variables alone, requiring no explicit representation of the actual system dynamics or disturbance/command inputs. Such a model is feasible and preferable from an analytic as well as intuitive viewpoint for describing human gunner behavior in an AAA tracking task [5]. Under these assumptions, the resultant modified optimal control model (shown in Figure 3) has the familiar proportional-integral-derivative (P-I-D) controller structure which has improved mathematical properties over the standard representation and is easily reconcilable with classical control theory methods.

The objective of this paper is to show the applicability and utility of the P-I-D controller modified optimal control model [5] in describing and predicting human gunner response in AAA tracking tasks. The next few paragraphs give the details of the model structure formulation for the AAA task.

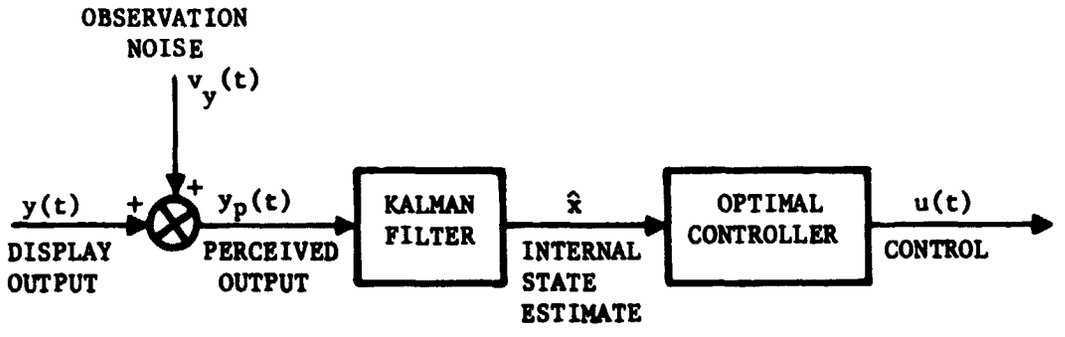

Figure 3. Modified Optimal Control Model for the Human Operator

P-I-D Controller Formulation

The P-I-D controller formulation assumes that the human operator has an internal model for the AAA task in terms of the tracking error and its higher derivatives. However, before such a model can be formulated it is first necessary to have reasonable representations of the internal models for the target trajectories and gunsight dynamics implicitly assumed by the human operator. The following development assumes decoupled azimuth and elevation axes and is consistent with the AMRL experimental design. Extension to coupled multivariable situations should be feasible, although, with increased difficulty and complexity.

Internal model for target trajectory.- The actual target trajectories in azimuth and elevation coordinates are characterized by deterministic functions of time that are not finite polynomial representations. However, a reasonable internal model for the target motion that may be assumed by the human gunner is

$$\theta_T^{(k)}(t) = w(t); \quad W(t) = \mathrm{Var}[w(t)] \tag{2}$$

where $w(t)$ is colored noise with variance $W(t)$ representing internal model uncertainty. For $k = 2$, this model represents a constant velocity target assumption; for $k = 3$ a constant acceleration assumption, and so on. A piecewise constant velocity ($k = 2$) internal model for the target motion is shown to be adequate for this application.

Internal model for gunsight dynamics.- The actual sight dynamics as given by Eq. (1) have a zero at $s = -1$, a real pole at $s = 0$ and a pair of complex poles with a damping coefficient of 0.75 and a natural frequency of 8 rad/s. An appropriate internal model of the sight dynamics is

$$\frac{\theta_g}{u} = \frac{s+1}{s}$$

or

$$\dot{\theta}_g = u + \dot{u} \tag{3}$$

The complex poles can be neglected in the internal model in view of their high natural frequency (8 rad/s) and near critical damping ($\zeta = 0.75$).

Internal model in terms of tracking error.- The tracking error is given by

$$e(t) = \theta_T(t) - \theta_g(t) \tag{4}$$

Then

$$\ddot{e} = \ddot{\theta}_T - \ddot{\theta}_g$$

$$= w - \ddot{u} - \dot{u}$$

or

$$\ddot{e} = -\tilde{u} + w \quad \text{where} \quad \tilde{u} = \dot{u} + \ddot{u} \tag{5}$$

In state vector form

$$\dot{x} = Fx + G\tilde{u} + \Gamma w \tag{6}$$

$$y = Hx$$

where

$$x' = [e \quad \dot{e}]$$

$$F = \begin{bmatrix} 0 & 1 \\ 0 & 0 \end{bmatrix} \; ; \quad G' = [0, \quad -1]$$

$$\Gamma' = [0 \quad 1] \; ; \quad H = [1 \quad 0] \tag{7}$$

represents the internal model used by the human operator for estimation and control.

Task cost functional.- The human gunner is assumed to behave as an optimal controller with respect to the cost functional

$$J(u) = E\left\{\frac{1}{T_f}\int_0^{T_f} (e^2 + g\tilde{u}^2)\, dt\right\} \tag{8}$$

Optimal controller and Kalman filter.- The optimal control law is given by

$$\tilde{u}(t) = \ddot{u}(t) + \dot{u}(t) = -\lambda'\hat{x}(t) \tag{9}$$

where $\hat{x}(t)$ is the output of a Kalman filter

$$\dot{\hat{x}} = (F - G\lambda' - KH)\hat{x} + Ky_p = F^{\dagger}\hat{x} + Ky_p \tag{10}$$

where

$$y_p = Hx + v_y = e + v_y \quad ; \quad V_y(t) = \text{var}[v_y(t)] \tag{11}$$

λ and K are obtained by solving the appropriate control and filter Riccati equations [6].

Human gunner transfer function.- For stationary assumptions, Eqs. (9)-(11) give the transfer function for the gunner model as

$$\frac{u(s)}{y_p(s)} = \frac{u}{\tilde{u}}(s)\,\frac{\tilde{u}}{y_p}(s) \tag{12}$$

$$= \frac{1}{s(s+1)}\,[-\lambda'(sI - F^{\dagger})^{-1}K]$$

$$= \frac{1}{s(s+1)}\;\frac{2\,\frac{\psi^2}{\omega_n^2}\left(\frac{\omega_n}{\psi}s+1\right)}{\left\{\frac{s^2}{\omega_n^2}+\frac{2(.707)s}{\omega_n}+1\right\}} \tag{13}$$

where

$$\psi = \frac{1}{\sqrt{2}}\left(\frac{\gamma}{g}\right)^{1/4}$$

$$\omega_n = \gamma^{1/4} + \frac{1}{g^{1/4}}$$

$$\gamma = \frac{W}{V_y} \tag{14}$$

The block diagram for the stationary closed-loop manned AAA system is given in Figure 4.

The overall time-varying closed-loop manned AAA system can be simulated digitally by solving the vector-matrix differential equation

$$\dot{z} = \Lambda_1 z + \Lambda_2(\theta_T + v_y) \tag{15}$$

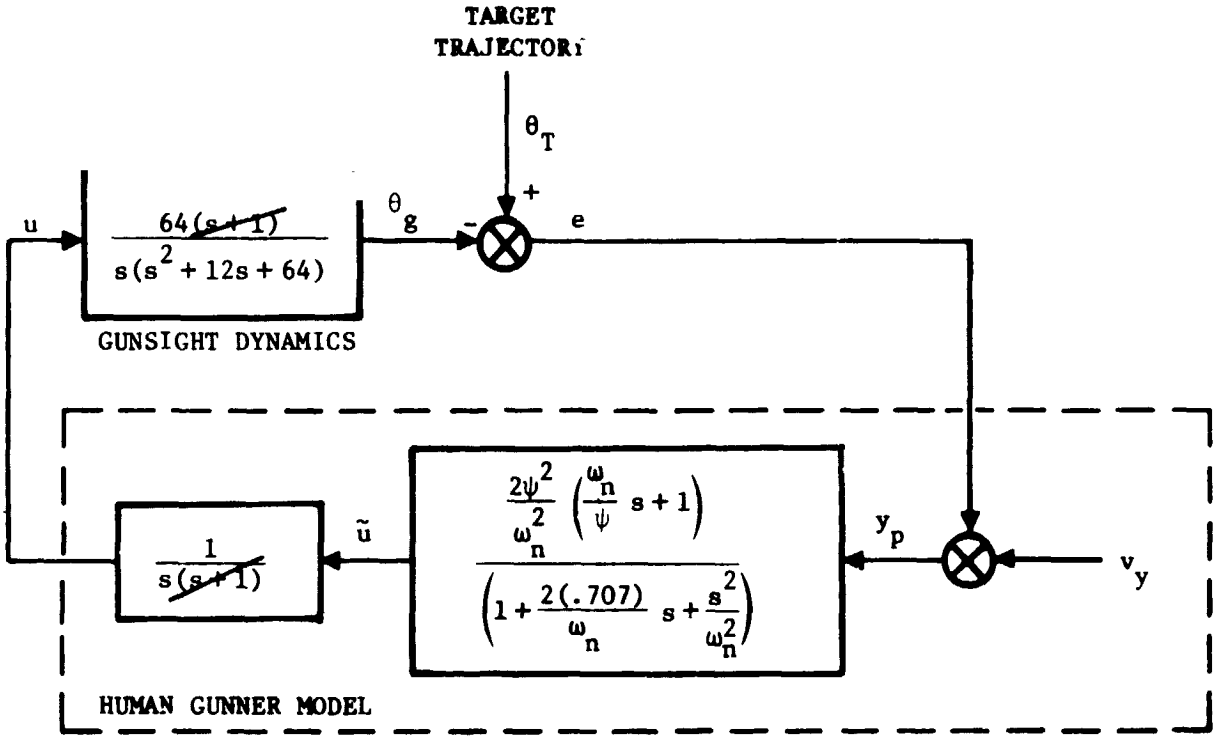

Figure 4. Stationary Closed-Loop Manned AAA System Block Diagram (Azimuth and Elevation)

where

$$z' = [\hat{x}, x_g, x_u]$$

where $\hat{x}$ is obtained from Eqs. (10) and (11).

$$\dot{x}_g = F_g x_g + G_g x_{1u}$$

$$x_g' = [\theta_g, \dot{\theta}_g] \tag{16}$$

corresponds to the transfer function

$$\frac{\theta_g}{x_{1u}} = \frac{64}{s^2+12s+64}$$

and

$$\dot{x}_u = F_u x_u + G_u \tilde{u}$$

$$x_u' = [x_{1u}, x_{2u}] \tag{17}$$

corresponds to the transfer function

$$\frac{x_{1u}}{\tilde{u}} = \frac{1}{s^2}$$

Thus, Eqs. (16) and (17) represent the equivalent transfer function between θ_g and $\tilde{u}$, namely

$$\frac{\theta_g}{\tilde{u}} = \frac{\theta_g}{x_{1u}} \frac{x_{1u}}{\tilde{u}} = \frac{64}{s^2 + 12s + 64} \frac{1}{s^2} \tag{18}$$

The matrices Λ_1 and Λ_2 in Eq. (15) can be derived by appropriate augmentation of Eqs. (4), (10), (11), (16) and (17).

The human gunner model $\left(\frac{u}{y_p}\right)$ has some interesting structural properties. The transfer function has a zero and four poles (two real poles at $s = 0$ and -1 and a pair of complex poles with a damping coefficient of 0.707 and a natural frequency of ω_n). Note that the invariant pole at -1 exactly cancels the zero in the gunsight dynamics. The values of ψ and ω_n depend only upon the ratio W/V_y. Since the noise variances W and V_y are in general time dependent, the low frequency gain $2\psi^2/\omega_n^2$, the zero ψ/ω_n and the complex pole natural frequency ω_n are not expected to remain constant throughout the course of the tracking engagement. The migration of these varying parameters as well as their operating range is considered in greater detail in the next section. The most important property in this transfer function is the existence of a pole at $s = 0$ which guarantees zero steady state tracking error if the target trajectory maintains constant velocity. The open-loop man/gunsight dynamics have a type 2 structure for a constant velocity model for the target motion. Similarly, a type "k" open-loop man/gunsight transfer function is obtained for a constant $(k-1)^{th}$ derivative assumption on the target motion. Such a model structure implies integral feedback compensation--hence, the name proportional-integral-derivative (P-I-D) controller. The P-I-D controller structure, by definition, gives zero steady state tracking error for exact model assumptions on target dynamics. However, the tracking error deviates from zero whenever the internal target model assumptions do not match actual data.

While the transfer function representation is convenient from a structural point of view, Eq. (15) must be used to compute the (time-varying) mean, covariance, and perhaps a sample solution for the augmented state, z. This formulation of the P-I-D structure was used in a computer program called HOGUM (Human Operator Gunner Model) to match input-output human gunner tracking data in response to four target trajectories for both azimuth and elevation axes. Results of this validation process are discussed next.

MODEL VALIDATION RESULTS

The key parameters of the P-I-D modified optimal control gunner model are: (1) k - the order of the human gunner's internal model of the target motion, (2) W(t) - the variance of the human gunner's uncertainty in the internal model for the target motion, (3) $V_y(t)$ - the observation noise variance corresponding to the displayed tracking errors, and (4) g(t) - the control weighting in the human's cost functional. The values of these parameters over the tracking period are determined using HOGUM in an iterative fashion until model predictions of the ensemble means and standard deviations of the tracking errors match actual human gunner tracking error ensemble statistics obtained from data. The resulting functional model for the parameters that consistently describes the data for the four target trajectories (azimuth and elevation) is as follows:

$$k = 2$$

$$W = \left[\frac{1}{T_f}\int_0^{T_f} \{\ddot{\theta}_T(t)\}^2 dt\right]^{1/2}$$

$$V_y(t) = .000375\ (10)^{|\ddot{\theta}_T(t)|} \qquad (19)$$

$$g \leq 10^{-4}$$

The parameter functional model is extremely simple and is easily reconcilable with known human psychophysical limitations and constraints. Moreover, the "tuning" process is only a function of the target trajectory. This mechanization allows for predicting tracking performance while performing a sensitivity analysis on various target trajectories and weapon systems parameters. Model predictions of the tracking errors and control inputs in azimuth and elevation coordinates are compared with data in Figures 5-8. Both the tracking error and control crank predictions using HOGUM compare very favorably with actual gunner response data. (The crank predictions match almost identically. Only trajectories 2 and 3 in elevation show any discernible deviation.)

Trajectory 3 (elevation) indicates a sharp spike in tracking error near 28.5 seconds. This is a direct result of a sudden slope change in the trajectory caused inadvertently in the mechanization of the AAA simulation. It is interesting, however, that HOGUM predicts the same type of discontinuity in the error. This is because the actual target motion is directly utilized as input to HOGUM instead of a numerical approximation of this function.

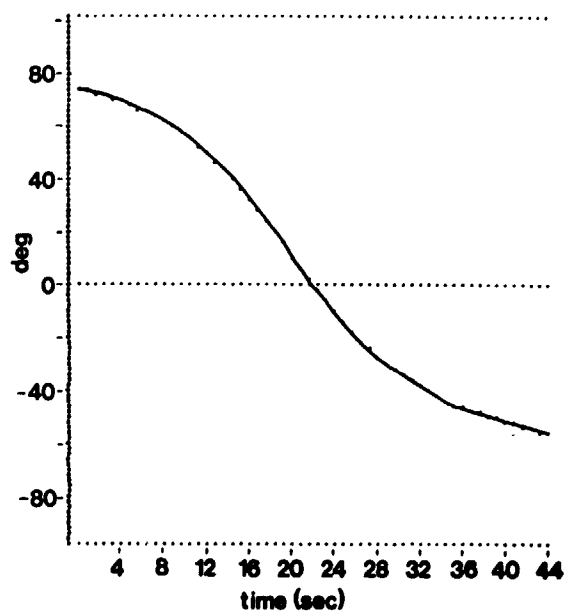

(a) Target Trajectory

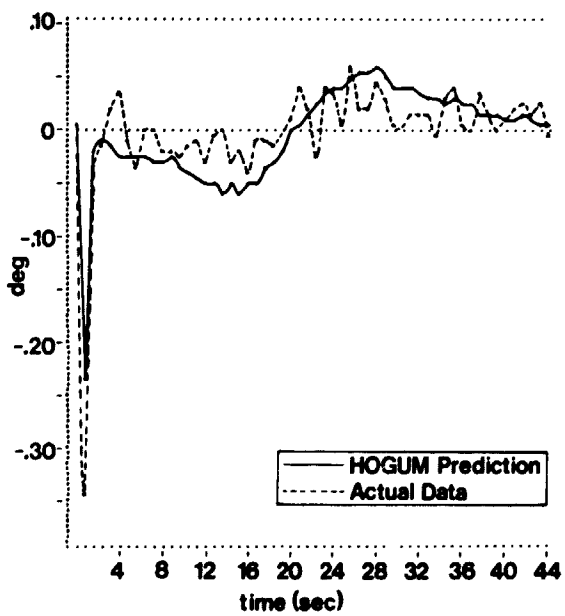

(c) Mean Tracking Error

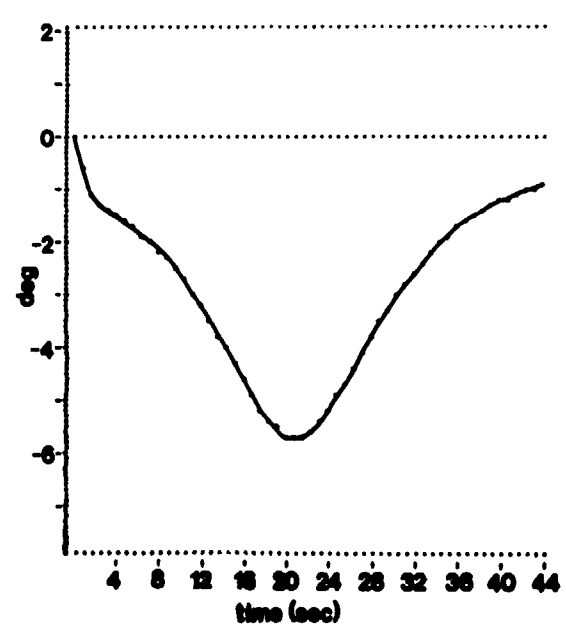

(b) Crank Position

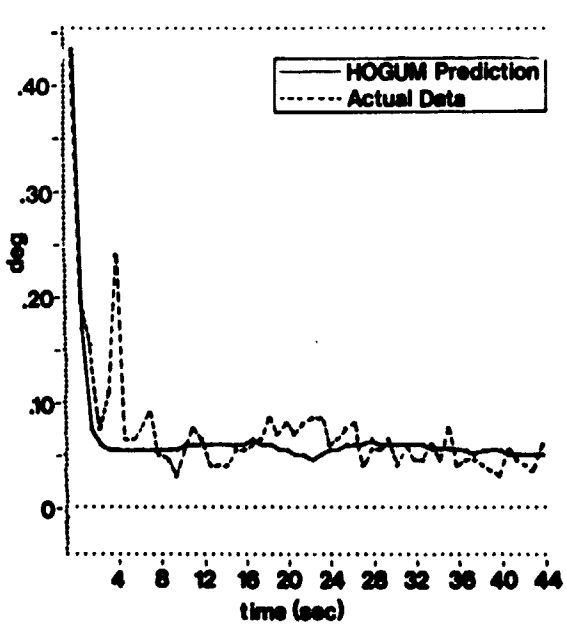

(d) Standard Deviation of Error

Figure 5a. Trajectory 1 - Azimuth (HOGUM Predictions and Data)

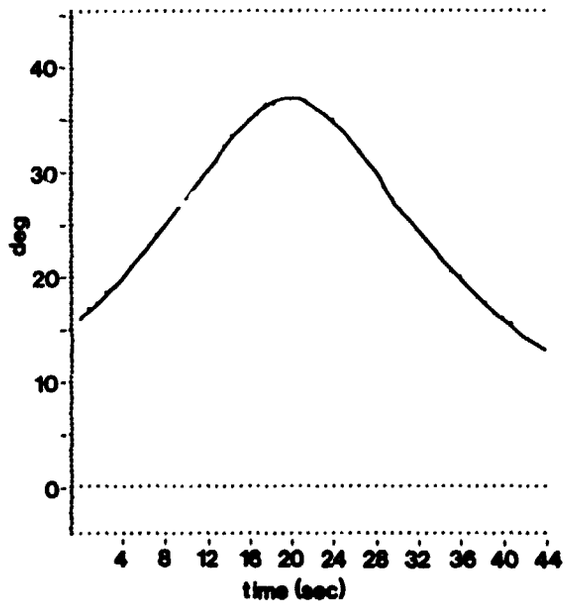

(a) Target Trajectory

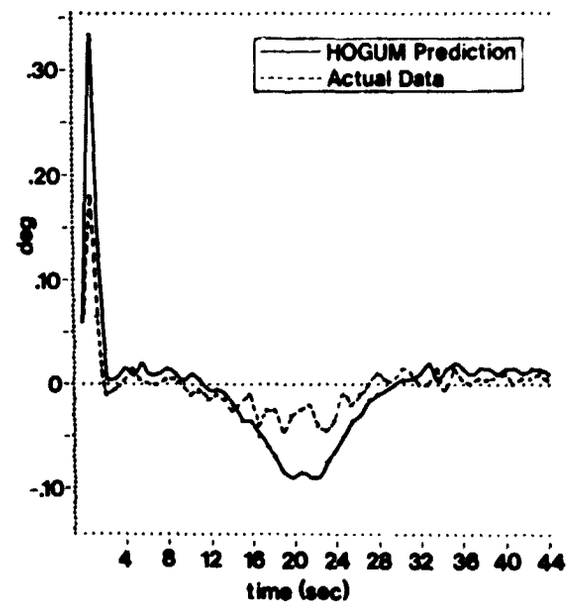

(c) Mean Tracking Error

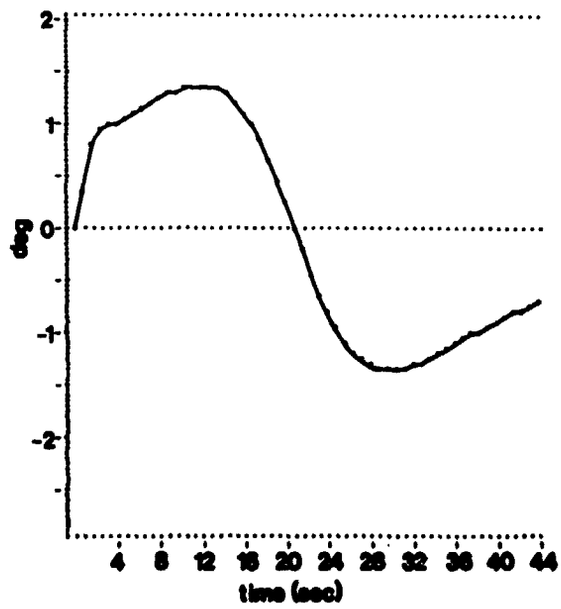

(b) Crank Position

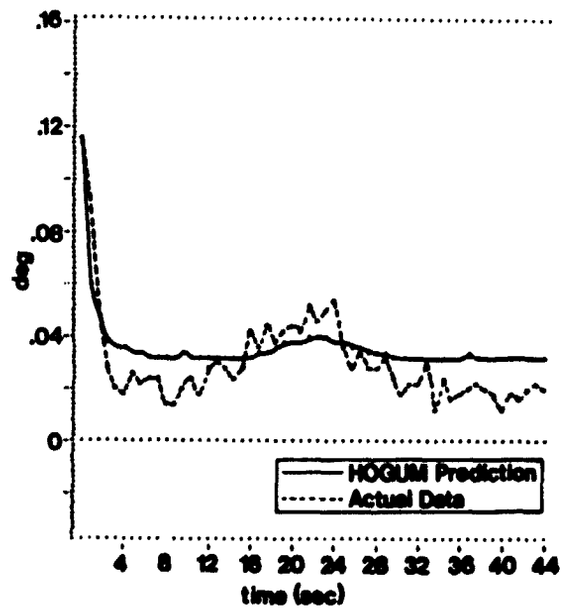

(d) Standard Deviation of Error

Figure 5b. Trajectory 1 - Elevation (HOGUM Predictions and Data)

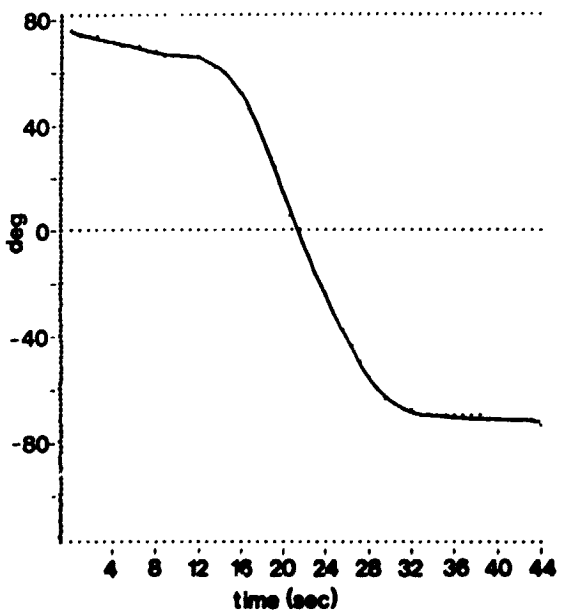

(a) Target Trajectory

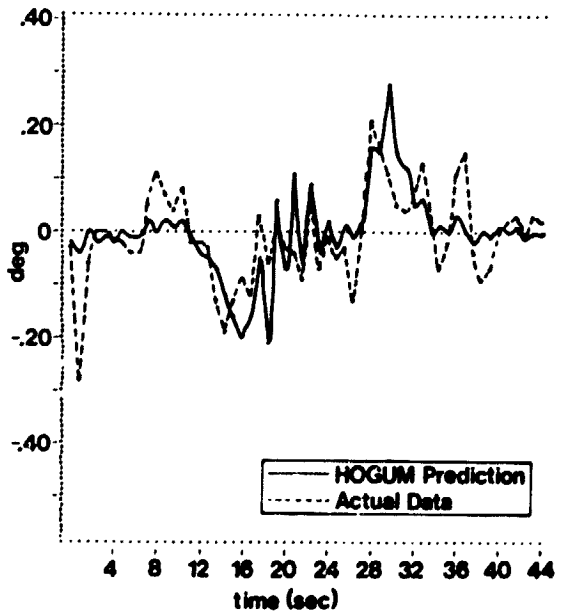

(c) Mean Tracking Error

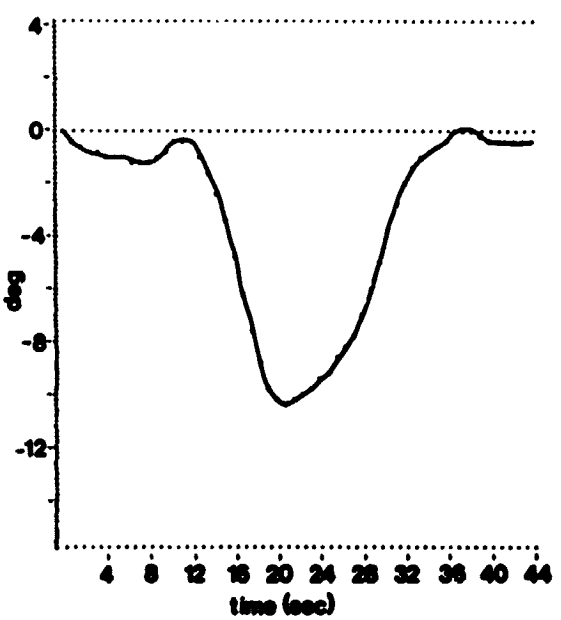

(b) Crank Position

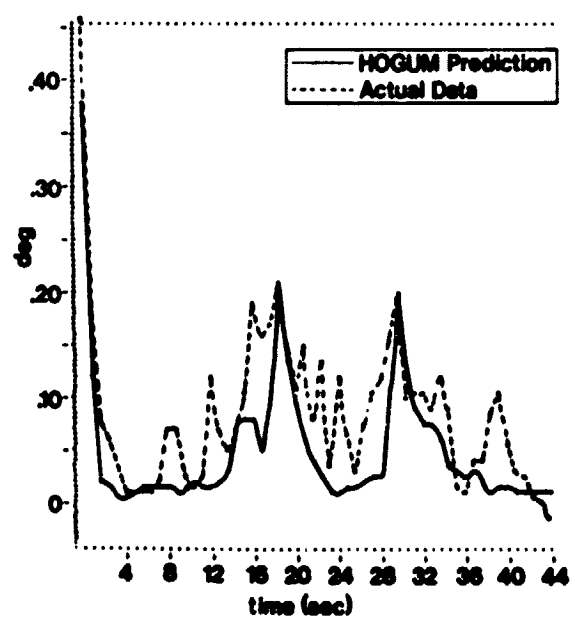

(d) Standard Deviation of Error

Figure 6a. Trajectory 2 - Azimuth (HOGUM Predictions and Data)

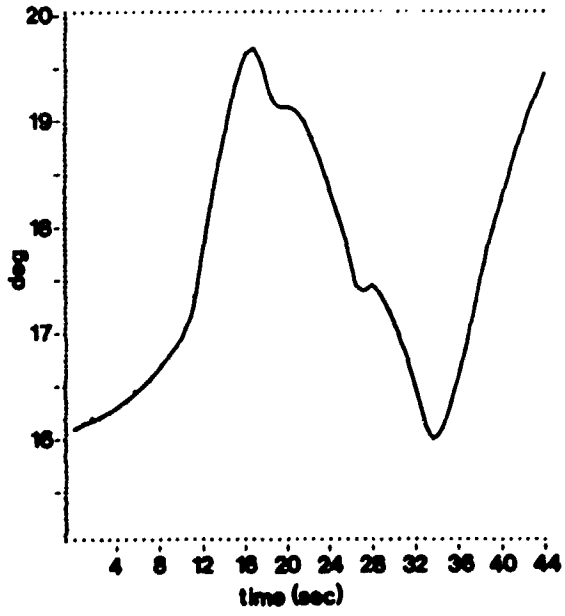

(a) Target Trajectory

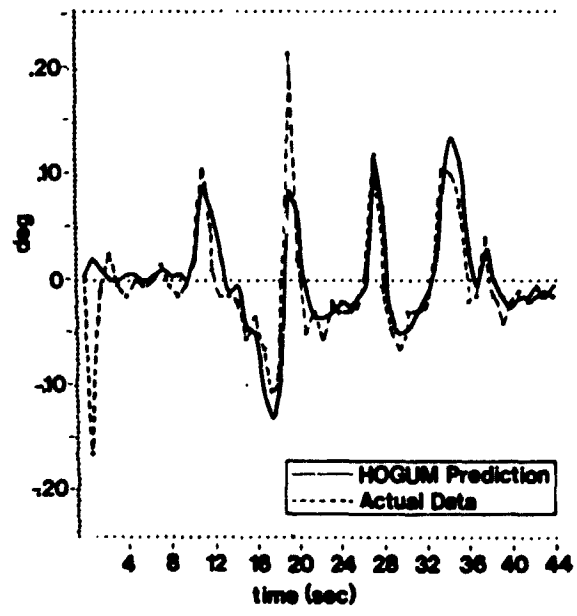

(c) Mean Tracking Error

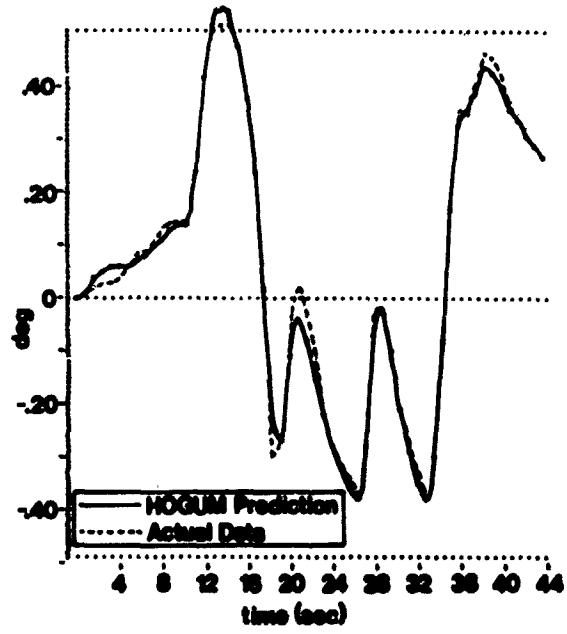

(b) Crank Position

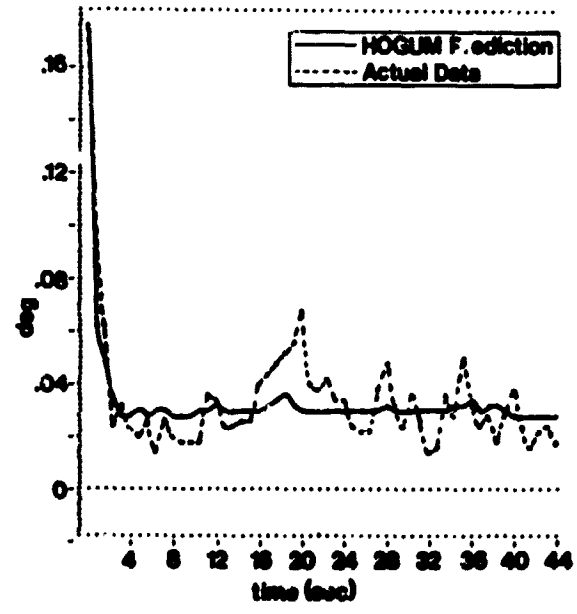

(d) Standard Deviation of Error

Figure 6b. Trajectory 2 - Elevation (HOGUM Predictions and Data)

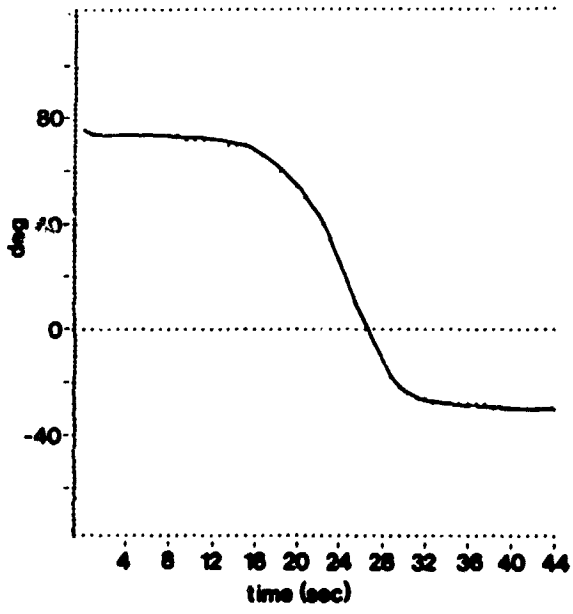

(a) Target Trajectory

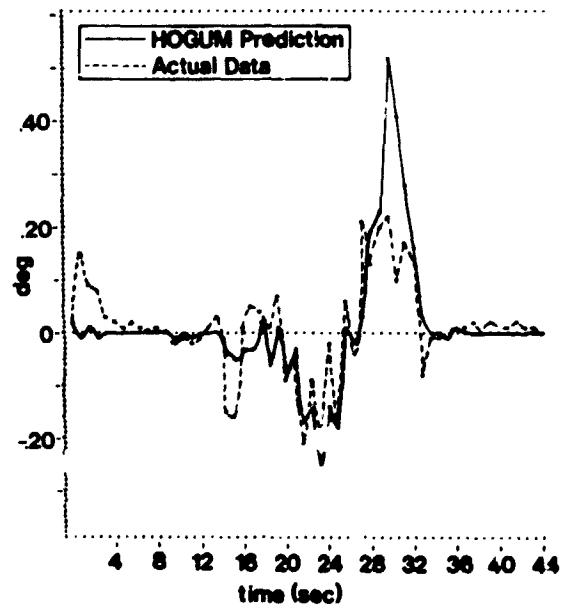

(c) Mean Tracking Error

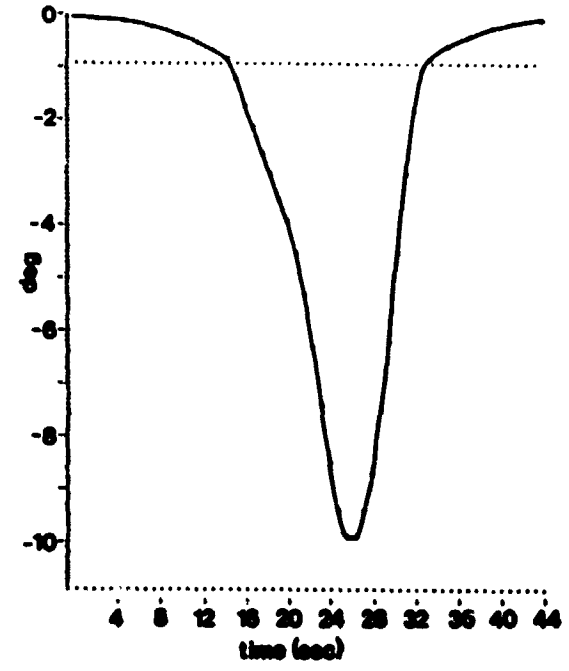

(b) Crank Position

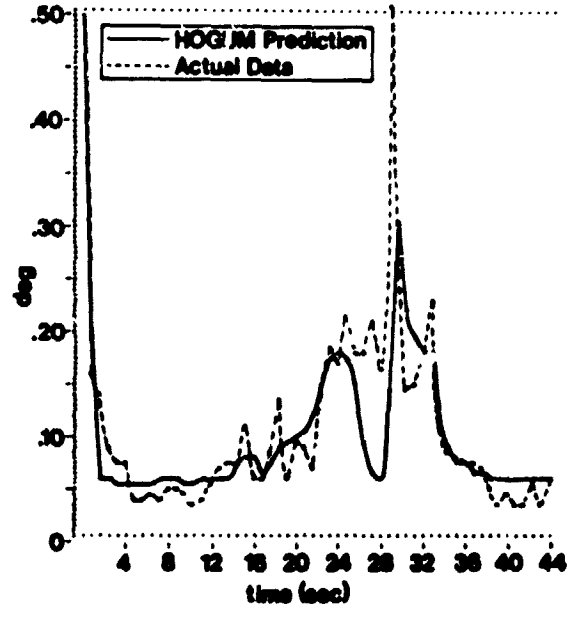

(d) Standard Deviation of Error

Figure 7a. Trajectory 3 - Azimuth (HOGUM Predictions and Data)

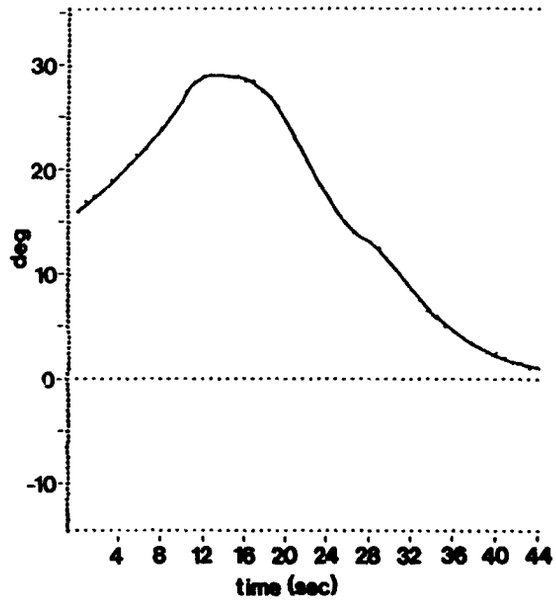

(a) Target Trajectory

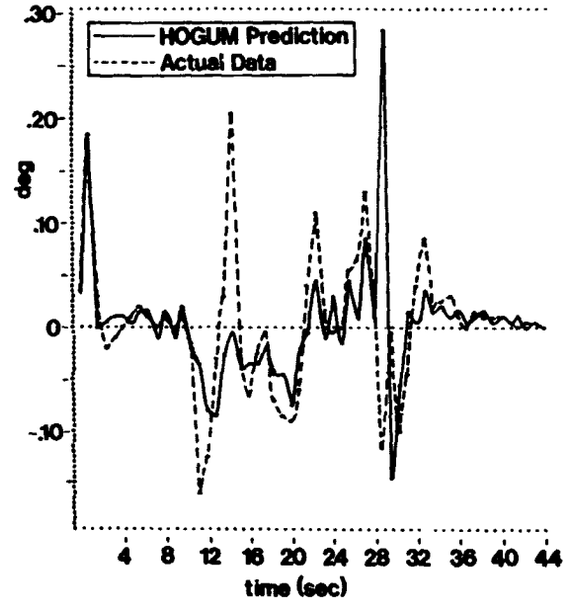

(c) Mean Tracking Error

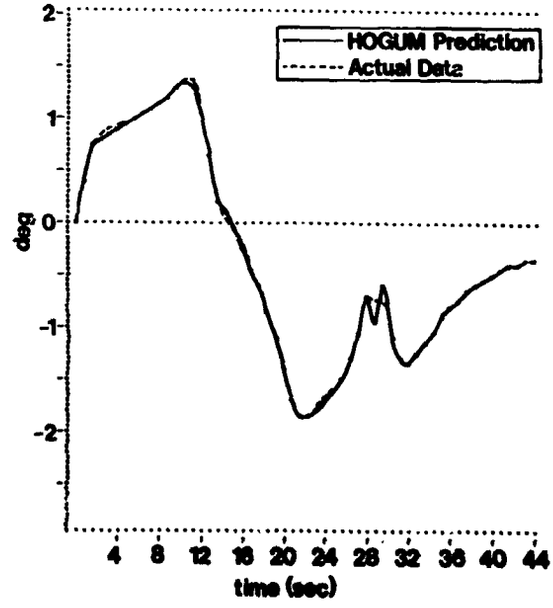

(b) Crank Position

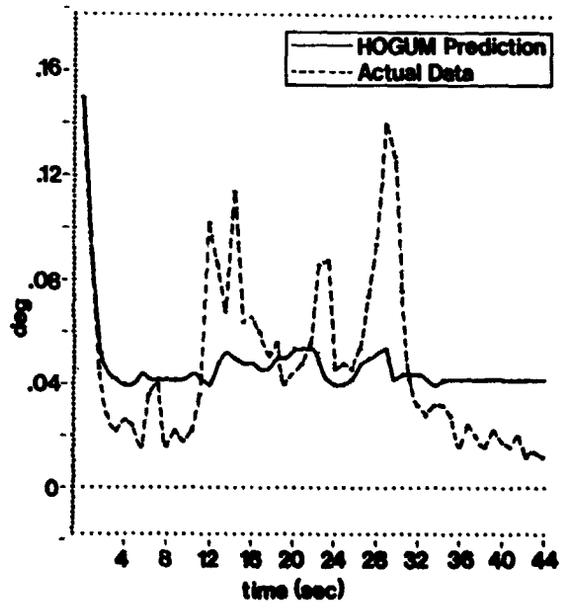

(d) Standard Deviation of Error

Figure 7b. Trajectory 3 - Elevation (HOGUM Predictions and Data)

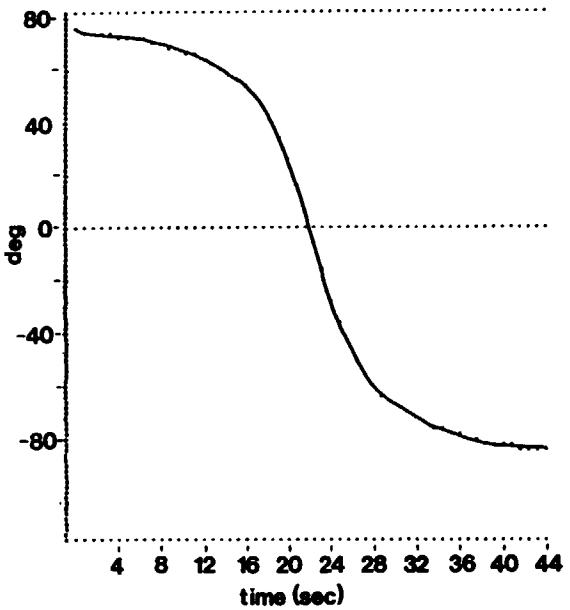

(a) Target Trajectory

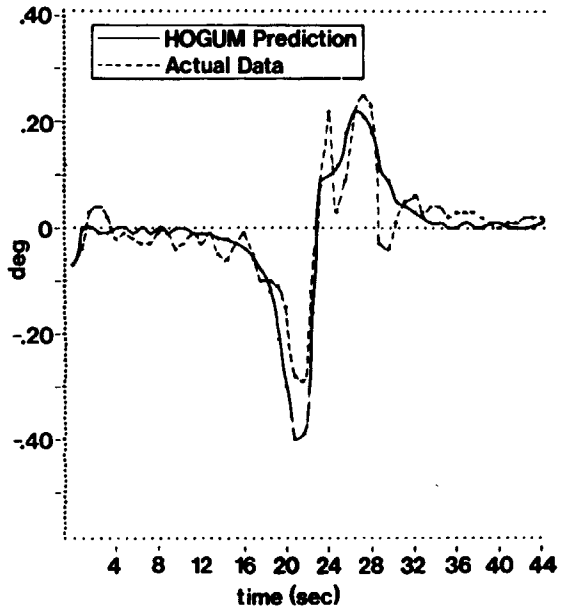

(c) Mean Tracking Error

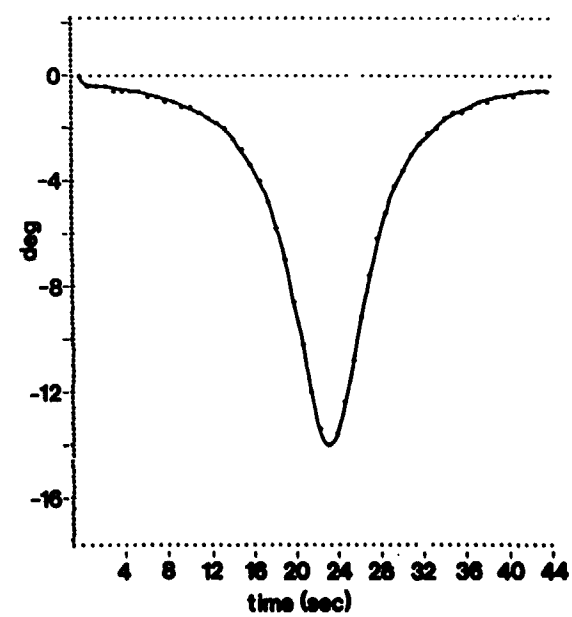

(b) Crank Position

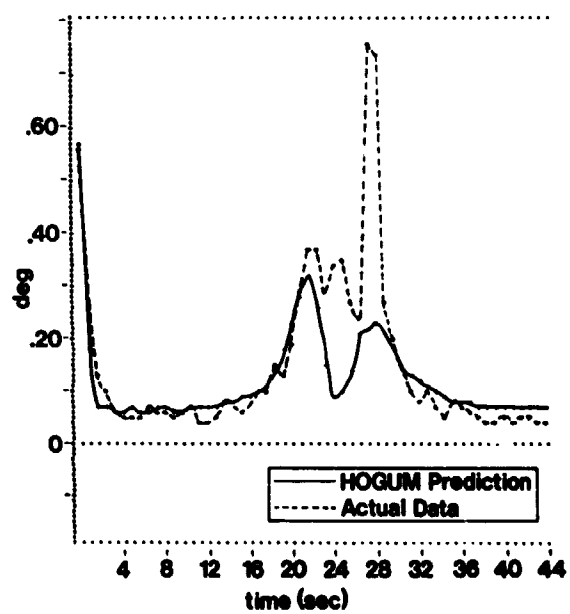

(d) Standard Deviation of Error

Figure 8a. Trajectory 4 - Azimuth (HOGUM Predictions and Data)

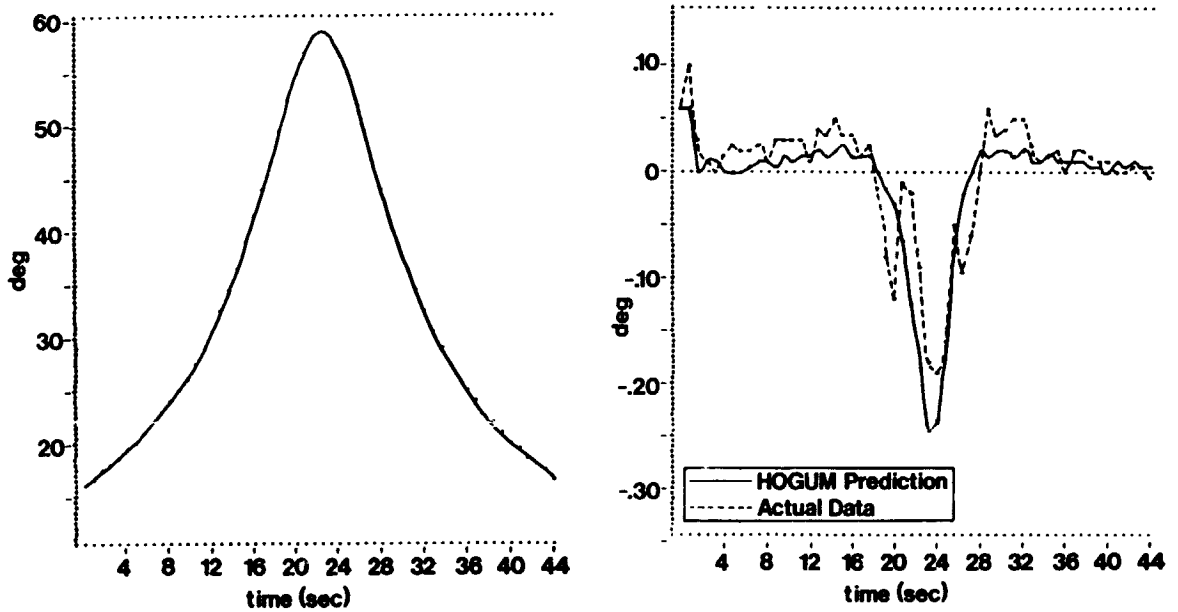

(a) Target Trajectory

(c) Mean Tracking Error

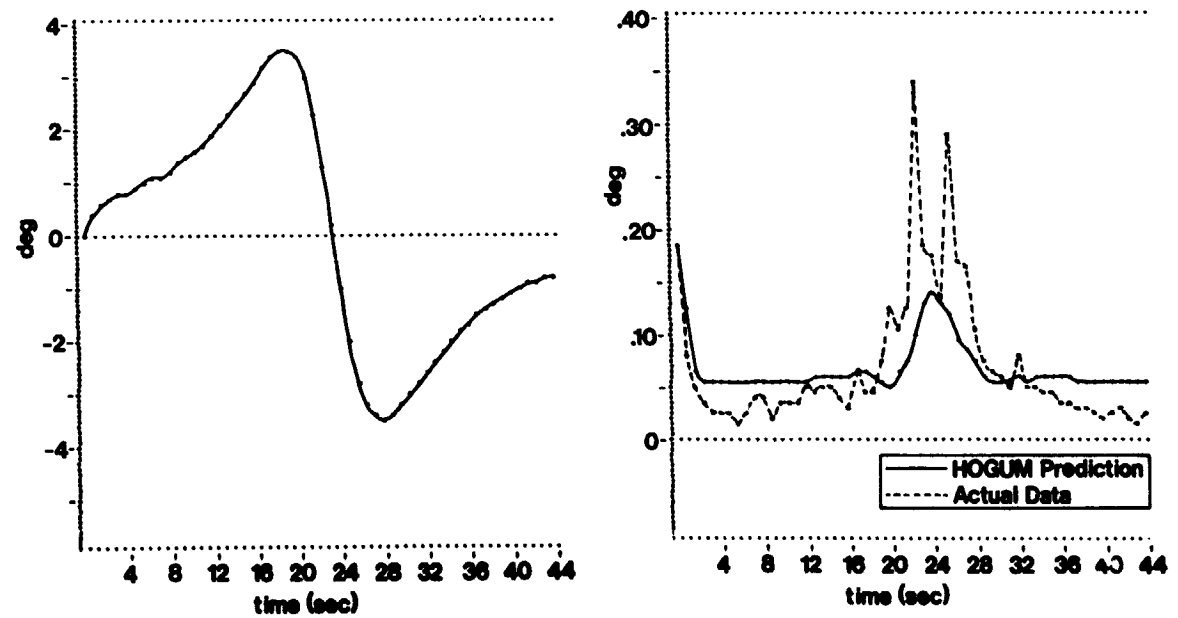

(b) Crank Position

(d) Standard Deviation of Error

Figure 8b. Trajectory 4 - Elevation (HOGUM Predictions and Data)

The general methodology used in this model tuning process is presented in the following paragraphs. It results in the identification of a functional model for the selection of HOGUM parameters for the four different target trajectories. Note that the analysis here is limited to independent or uncoupled azimuth and elevation axes. Extension to coupled gunsight dynamics should follow, although, with greater complexity.

Selection of k: The value of k assigns a structure to the internal model of the target motion adopted by the human gunner. For example, $k = 2$ implies a constant velocity target motion, $k = 3$ a constant acceleration assumption and so on. Under steady-state conditions, the value of k also defines the "type" of the gunner transfer function model given by Eq. (12). A value of $k = 2$ gives a type 1 gunner transfer function (i.e., one pole at $s = 0$) as given by Eq. (13); $k = 3$ gives a type 2 gunner model, and in general for a rate-aided gun, $k = m$ implies a type $(m-1)$ gunner transfer function. A human operator in a closed-loop tracking task is able to track a constant velocity (within reasonable limits) target motion with zero steady-state mean error (reasonably short setting time). On the other hand, it is not always possible for a human to track an accelerating target with zero mean tracking error. These observations indicate a value of $k = 2$ as being consistent with known human psychophysical limitations and, therefore, is used as the standard value in the gunner model.

Selection of W(t): $W(t)$ reflects the uncertainty in the human gunner's mind about the accuracy of his internal model for the assumed target motion. Target trajectories in an AAA task do not satisfy the constant velocity assumption at all times. Thus $W(t)$ should be approximately proportional to $\{\ddot{\theta}_T(t)\}^2$, the square of the target acceleration. However, it seems unreasonable to assume that the human gunner learns a time-varying internal representation for the target model uncertainty $W(t)$. A sensitivity analysis of $W(t)$ using the HOGUM program indicates that a constant value of $W(t) = W$ throughout the tracking period is reasonable in describing gunner response data. A value of

$$W = \left[\frac{1}{T_f}\int_0^{T_f} \ddot{\theta}_T^2(t)dt\right]^{1/2}$$

is chosen (RMS value of $\ddot{\theta}_T(t)$).

Selection of $V_y(t)$ and $g(t)$: Given $k = 2$ and fixed W as above, there remain only two free parameters with which to tune the HOGUM program outputs--$g(t)$ and $V_y(t)$. The gunner model transfer function in Eq. (13) indicates that the model parameters--namely the low frequency gain, the zero and the pair of complex poles--depend only upon g and (W/V_y). Note that it is not mathematically proper to entertain the concept of transfer functions for time-varying systems. However, it is still possible to get considerable

insight into the gunner model characteristics using quasi-stationary or frozen-point analysis arguments. Figure 9 shows the migration of the low frequency gain, zero and the natural frequency ω_n of the complex poles with respect to g and the ratio (W/V_y). As previously mentioned, the pair of complex poles with a damping coefficient of 0.707 and a natural frequency ω_n could be considered to be analogous to the "so-called" neuromotor time constant $[1/(T_N s+1)]$ referred to in human modeling literature [2]. A value of $\omega_n \geq 10$ rad/s would be adequate from the neuromuscular system viewpoint. Figure 9 shows that ω_n is quite insensitive to variations in (W/V_y) and depends primarily on the value of g. A value of $g \leq 0.0001$ results in $\omega_n \geq 10$ rad/s. Hence $g = 0.0001$ is adopted as the constant control term weighting in the cost functional given by Eq. (8).

The only remaining parameter to be tuned is $V_y(t)$ - the observation noise covariance. Tracking error data in Figures 5-8 reveals some interesting characteristics. The mean error is nearly zero and the standard deviation constant for segments of the target trajectories which agree with the human's internal model assumption of constant velocity motion. This is equivalent to constant g, W and V_y. However, both the mean and the standard deviation of the error deviate from their nominal values between target trajectory segments satisfying the constant velocity assumptions. Data in Figures 5-8 show that both the mean and the standard deviation of the tracking error $e(t)$ relate monotonically with $|\ddot{\theta}_T|$. A similar relationship holds with respect to V_y in steady state. Thus $V_y(t)$ should vary monotonically with $|\ddot{\theta}_T(t)|$. The functional model

$$V_y(t) = .000375\ (10)^{|\ddot{\theta}_T(t)|}$$

gives the best fit of the model predictions to ensemble data as seen in Figures 5-8. The functional model for $V_y(t)$ takes on an intuitive meaning if one observes that

$$10 \log V_y(t) \left(= V_y(t)\Big|_{dB} \right)$$

is proportional to $|\ddot{\theta}_T(t)|$, which indicates that the observation noise in decibels is proportional to $|\ddot{\theta}_T|$. The changing value of $V_y(t)$ in conjunction with the actual target trajectory (input to HOGUM) deviating from constant velocity motion, causes error transients in both the mean and standard deviation.

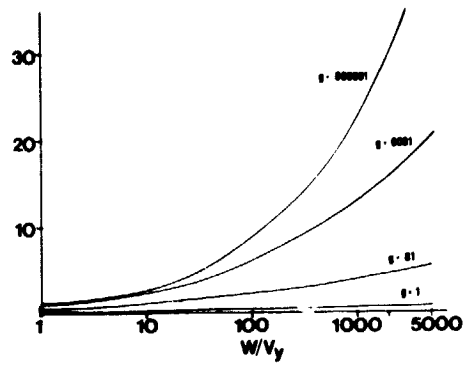

(a) Low Frequency Gain, $\frac{2\psi^2}{\omega_n^2}$

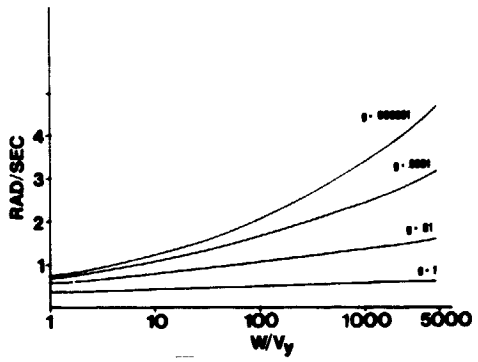

(b) Zero Location, $\frac{\omega_n}{\psi}$

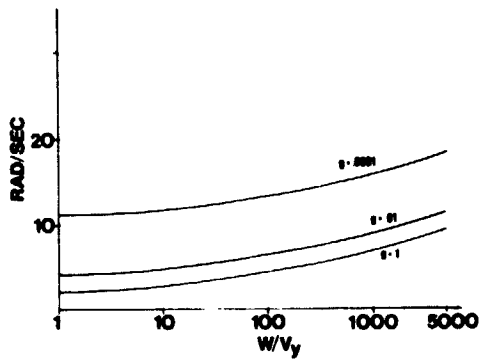

(c) Natural Frequency, ω_n

Figure 9. Characteristics of $\left(\frac{\tilde{u}}{y_p}\right)$; Human Gunner Model Transfer Function (Stationary Assumptions)

Table 1 indicates the range of γ values $\left(\gamma = \frac{W}{V_y}\right)$ corresponding to each of the four trajectories for both azimuth and elevation. Typically, the smaller values of γ occur near crossover (when $\ddot{\theta}_T(t)$ obtains maximum values). From Figure 9, it is possible to determine the corresponding range of values for the low frequency gain, the zero location and the natural frequency of the transfer function representing the human operator.

The functional model discussed above is not claimed to be unique. However, it does reflect reasonable assumptions on the known psychophysical characteristics of the human operator.

Table 1

Range of γ Values $\left(\frac{W}{V_y}\right)$

TRAJECTORY	AZIMUTH	ELEVATION
1	250-50	27-15
2	2700-175	13-8
3	2100-350	160-100
4	4000-200	960-275

CONCLUDING REMARKS

The P-I-D controller model has been shown to accurately predict human tracking behavior. This model can be used as a baseline to determine the effects on human performance due to differing environmental conditions, target motions, countermeasure tactics as well as sight system parameters. In addition, various system configurations can be incorporated into this model with only minimal modification. The computer program, HOGUM, is fast, efficient and modular, and, as such, can be effectively used to determine performance sensitivity to various system parameters.

It is to be noted that these functional relationships have been validated using four target trajectories. Due to the highly adaptive nature of the human operator, these relationships might require modification for extreme values of $\ddot{\theta}_T(t)$. Additional trajectories would be required to validate the model in such cases.

The P-I-D gunner model as represented by HOGUM can be used to describe human gunner performance in general purpose air defense evaluation programs such as the AFATL P001 [1]. Extensions of this model to include coupled gunsight dynamics, two-axis control cross coupling and task interference effects, and on-carriage tracking (using some form of fire control system) is recommended to generalize the capability of HOGUM for evaluating different AAA weapon systems.

ACKNOWLEDGEMENTS

The authors wish to thank Dr. C.N. Day, Capt. J. Hull, Dr. D. Repperger and Mr. W. Summer of the 6570th Aerospace Medical Research Laboratory, WPAFB, Ohio, for their continued support throughout the entire project effort. The assistance of Mr. R. Ducot of SCI (Vt) was invaluable in developing and implementing HOGUM, and is gratefully acknowledged.

REFERENCES

1. J. Severson and T. McMurchie, "Antiaircraft Artillery Simulation Computer Program - AFATL Program P001 - Vol. I, User Manual," Developed by Air Force Armament Laboratory, Eglin AFB, Florida; Published under the Auspices of the Joint Aircraft Attrition Program, Advanced Planning Group.

2. D. Kleinman, S. Baron, and W.H. Levison, "A Control Theoretic Approach to Manned-Vehicle Systems Analysis," IEEE Trans. Automatic Control, AC-16, pp. 824-832, 1971.

3. S. Baron and W.H. Levison, "A Manual Control Theory Analysis of Vertical Situation Displays for STOL Aircraft," NASA CR-114620, April 1973.

4. A. Phatak, H. Weinert, I. Segall and C. Day, "Identification of a Modified Optimal Control Model for the Human Operator," Automatica, Vol. 12, pp. 31-41, 1976.

5. A.V. Phatak and K.M. Kessler, "Evaluation of Optimal Control Type Models for the Human Gunner in an Anti-Aircraft Artillery (AAA) System," Eleventh Annual NASA Conf. on Manual Control, NASA/Ames Research Center, Moffett Field, CA 94035, May 1975.

6. A.E. Bryson, Jr., and Y.C. Ho, Applied Optimal Control, John Wiley and Sons, 1975.

Analysis of Controls and Displays for a Terminal Controlled Vehicle

by

William H. Levison and Sheldon Baron
Bolt Beranek and Newman Inc.
Cambridge, Massachusetts

The optimal-control pilot/vehicle model was applied to the analysis of a Terminal Controlled Vehicle in approach and landing. Approach tracking errors and landing statistics were predicted for two control configurations (attitude control wheel steering and velocity control wheel steering) and for two display conditions (with and without electronic presentation of a perspective runway). Steady-state analysis was performed to explore performance-workload tradeoffs for these control/display combinations, and time-varying analysis was performed to obtain approach and landing statistics in the presence of zero-mean turbulence. The results of this analysis were compared with experimental data obtained in fixed-base simulations performed at NASA Langley Research Center.

A MODEL OF THE EMG-TORQUE-MOVEMENT RELATIONSHIPS FOR KNEE EXTENSION**

By

Etienne Dombre
Laboratoire d'Automatique de Montpellier
U.S.T.L., Place E. Bataillon,
34060 MONTPELLIER CEDEX, France*

George A. Bekey, Ph.D.
Department of Biomedical Engineering
University of Southern California*

Jacquelin Perry, M.D.
Chief, Pathokinesiology Service
Rancho Los Amigos Hospital, Downey, California

ABSTRACT

This paper describes work currently in process at Rancho Los Amigos Hospital on further clarification of the quantitative relationship between the electrical activity of a muscle and the movement it produces. The usefulness of such a relationship is obvious for rehabilitation purposes.

This research is based on the use of intramuscular wire electrodes to provide specific signals from each muscle at a given joint. The output of the system is the angular position of the moving limb. This input-output relationship is represented by a dynamic mathematical model which includes the length-tension and velocity-tension relationships of the actuating muscles as well as a mechanical model of the knee joint. Methods for quantifying and validating the model are described.

Our objective is to build a model which is valid even near the limits of the range of motion when various conditions of external constraints are applied and when different modes of contraction are considered.

**This work was supported in part by the Rehabilitation Services Administration, DHEW, under Grant #RD-23-P-55442.

*Currently at Rancho Los Amigos Hospital, Downey, California

INTRODUCTION

Since the work of LIPPOLD (1952), (reference #9) it is known that the EMG - tension relationship in isometric situations is linear (although, some disagreement exists concerning the precise value of the constant of proportionality, as shown by LINDSTROM et al., 1974)(reference #8). But, problems arise when the same relationship has to be described in the presence of movement. Generally, these studies are performed with constraints of constant velocity or of constant loading as in past studies at the kinesiology laboratory at Rancho Los Amigos Hospital (PERRY et al., 1974)(reference #11). Such limitations lessen the clinical usefulness of the results since no one knows exactly how to handle the information content of the EMG signal produced by the muscle during free motion.

Among the large number of muscle models which have been proposed since HILL's classical work (1938)(reference #6) only a few attempts have been made to build mathematical models of the EMG-muscle force relationship in the presence of movement.

GOTTLIEB and AGARWAL (1971), (reference #5) published a model which relates EMG and force for the anterior tibialis muscle during isometric effort. Basically, the model consists of series and parallel elastic elements, a parallel dissipative element and an active contractile element. The contractile element was represented by a first order filter acting on the raw EMG signal picked up by the surface electrodes. The model responses match measured forces very well during repeated isometric plantar flexions. A similar model was used to simulate the EMG-force relation in the human triceps brachii by COGGSHALL (1968), (reference #4) and in the human gastrocnemius and soleus muscles by AGARWAL et al., (1971), (reference #1). Apparently, these models have not yet been applied successfully to non-isometric situations.

An alternative approach to relating EMG and force has been based on summing the electrical activity and twitch produced by single motor units using an appropriate recruitment hypothesis. OSTROY et al., (1970) (reference #10) then BRODY et al., (1974) (reference #3) synthesized such a model from an isometric study of the cat flexor hallucis longus muscle and of the human biceps brachii respectively. More recently, WANI and GUHA (1975), (reference #14) obtained EMG-motion characteristics for elbow flexion by a similar approach. As far as we know, this is the only dynamic model which is not limited to isometric cases. However, models based on motor-unit recruitment incorporate so many assumptions that their validity is questionable.

This paper deals with a model of the EMG-tension-position relationships in the knee joint without restriction to isometric or isokinetic movements. Eccentric and concentric contractions are modeled as well. The validity of the model will be shown by a

tridimensional representation of the length-velocity-tension relationships. The performance of the process will be described with a simple example. Finally, methods for quantifying and validating the model will be outlined.

In what follows, we call EMG the electrical activity of the muscle after it has been rectified and integrated. The raw EMG is picked up by dual intramuscular wire electrodes to provide specific signals from each muscle at the knee joint. The recording and processing techniques have been described by PERRY et al.,(1974)(reference #11).

MODEL OF THE EMG-FORCE-POSITION RELATIONSHIP IN PRESENCE OF MOVEMENT

The fundamental assumption of this model is that the EMG is proportional to the neural input of the muscle. In other words, the actual representation of the process by a single input and two parallel outputs can be described using a series representation as shown in figure 1.

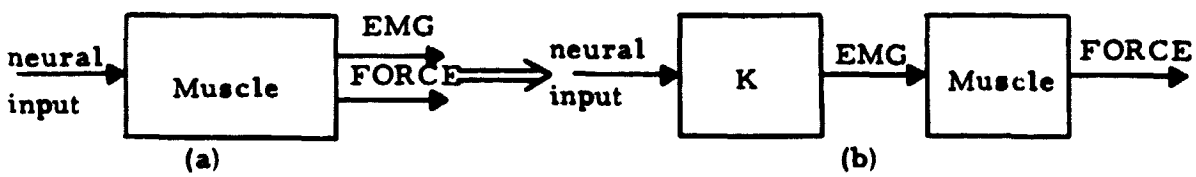

Figure 1: Neural input- EMG- muscular force relationships (a) actual parallel representation,(b) assumed model using two series elements.

The EMG signal is then considered as an input of the process rather than as a parallel output. Furthermore, it is assumed that the EMG-neural input relationship is static and time invariant so that the EMG signal is representative of the actual muscle input whatever the movement.

In isometric contractions, the EMG-tension relationship is linear. Taking into account the foregoing hypotheses, a simple EMG-tension relationship in presence of movement should also exist. If this is not so, the variables which do not appear in the static mode must be more carefully described. It is then necessary to concentrate on the muscle dynamics and on the joint dynamics.

Muscle Model

Let us consider for instance the input-output model of GOTTLIEB and AGARWAL (1971)(reference 5),(figure 2a). It relates the raw EMG to the isometric tension produced by the muscle for a fixed muscle length. If changes in length occur, the model is no longer valid unless its parameters are fitted again. The proposed model,(figure 2b) allows one to get rid of this constraint.

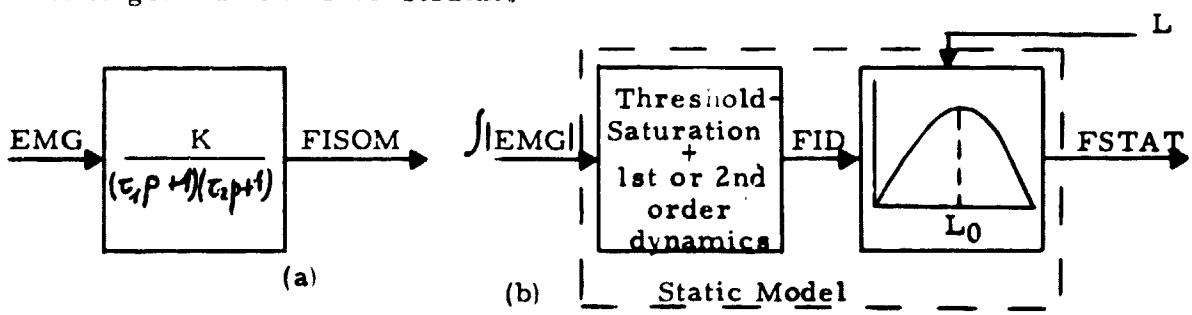

Figure 2: (a) GOTTLIEB and AGARWAL (1971)(reference#5)model
(b) Static model for the muscle

The changes in the muscle length L are automatically accounted for, using the length-tension characteristic as a filter on the output of and "ideal" black box. This black box would be sufficient to model the muscle if its force output were not dependent on length. Actually, the first block yields an ideal force FID which is the isometric force at rest length (L_0) whatever the muscle state. The static force FSTAT is the filtered ideal-force which represents the muscle behavior in isometric mode at any length. Therefore, FSTAT is equal to FID when the muscle is at rest length.

The first box of figure 2b is similar** to GOTTLIEB's model. A threshold-saturation type of non-linearity, followed by a first or second order filter will be used.

In order to generalize the static model to non-isometric situations, the muscle velocity has to be included. The tension-velocity characteristic is used for this purpose and used similarly to the length-tension filter: the static force FSTAT is filtered by it to yield the actual dynamic force FDYN produced by the muscle during movement (figure 3). In isometric situations, this filter behaves as a gain whose value is one.

** It might be identical if the experimental conditions (type of electrode, electrode location...) and the signal processing techniques used were the same.

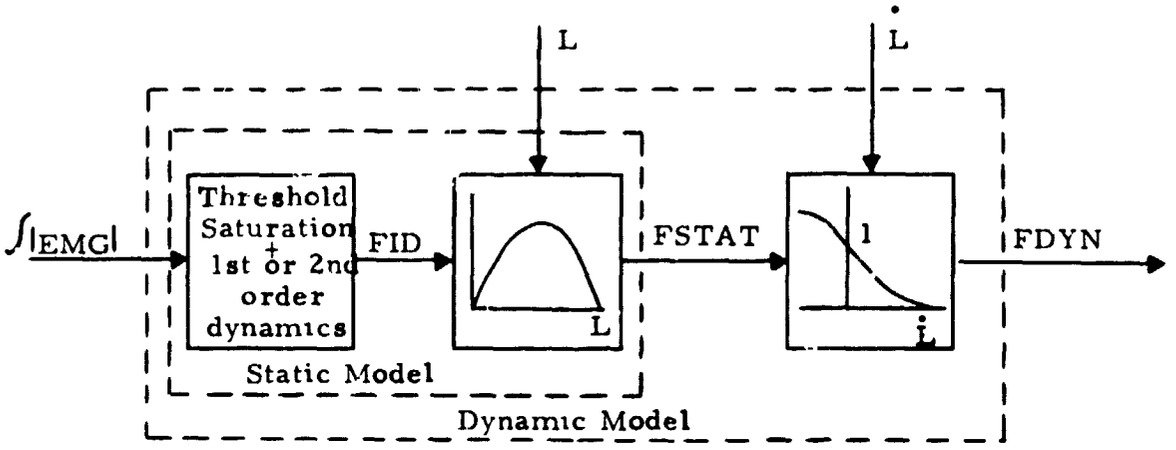

Figure 3: Overall muscle model

The muscle is then represented by the overlapping of a static and a dynamic model. The first one can represent isometric contraction by itself. Since the dynamic force is not observable, a model of the joint is necessary in order to relate FDYN to the limb position θ.

Model of the Knee Joint

Let us consider the joint shown in figure 4. In what follows, the study is restricted to the knee joint and the extensor muscle group of the leg (quadriceps). For sake of simplicity, it will be assumed that the five muscles in the quadriceps group may be represented by a single muscle whose dynamic properties are equivalent to the whole extensor muscle group dynamics. The thigh is assumed to be firmly secured in a horizontal position and at right angles with the trunk.

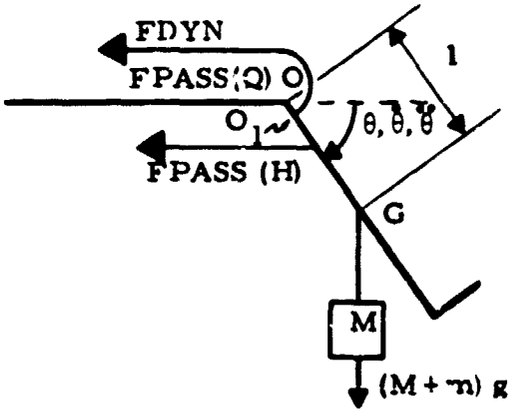

Figure 4: Forces applied to the leg.

The meaning of the parameters and variables of figure 4 is as follows:

- g is the mass acceleration due to gravity.
- m is the mass of leg.
- M is an external load assumed to be hung at the center of gravity G of the lower leg.
- l is the distance from the center of gravity of the leg to the center of rotation O of the knee. The foot is assumed to keep a constant angle with respect to the tibia. Furthermore, it is assumed that the changes in the center of rotation O of the knee are not significant with respect to l.
- FDYN is the dynamic force produced by the quadriceps and is equal to the output of the muscle model.
- FPASS (H) is the passive force developed by the antagonist muscle group when it is lengthened beyond its rest length.
- FPASS(Q) is the passive force developed by the quadriceps under the same conditions as FPASS (H).

The directions of FDYN, FPASS (H) & FPASS (Q) are assumed to be parallel to the femur.

Note that FPASS(Q) corresponds to the passive force of the length-tension diagram. It is necessary to represent it in this part of the model since the length-tension filter of the muscle model deals only with the active force (figure 5):

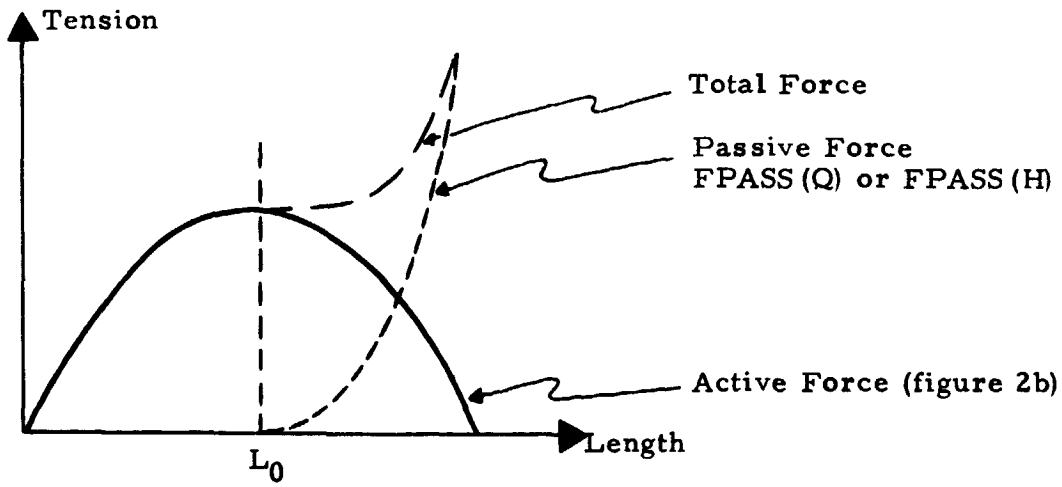

Figure 5: Length-Tension diagram

This representation of the length-tension relationship by two separate elements may be justified by the fact that the passive force is a mechanical characteristic of the muscle group which does not produce any electrical activity. Likewise, FPASS(H) which is the passive force developed by the antagonist group, acts upon the agonist dynamics through the joint and is not related to the electrical activity of the quadriceps.

The dynamic equation of motion for the system shown in figure 4 is given by:

$$J\ddot{\theta} = TDYN + TPASS(Q) - TPASS(H) - C\dot{\theta} - gl(M + m)\cos\theta$$

where:

- J is the moment of inertia of the lower leg.
- C is the damping coefficient in the knee joint and its surrounding soft tissue.
- $\theta, \dot{\theta}, \ddot{\theta}$ are the position, velocity and acceleration of the leg respectively.
- TDYN is the torque corresponding to FDYN.
- TPASS(H) and TPASS(Q) are the torques corresponding to FPASS(H) and FPASS(Q). They include stretching of tendon and ligaments and are significant beyond the rest position θ_o.

The complete input-output model of the extensor muscle group and knee joint is now described by the block diagram of figure 6.

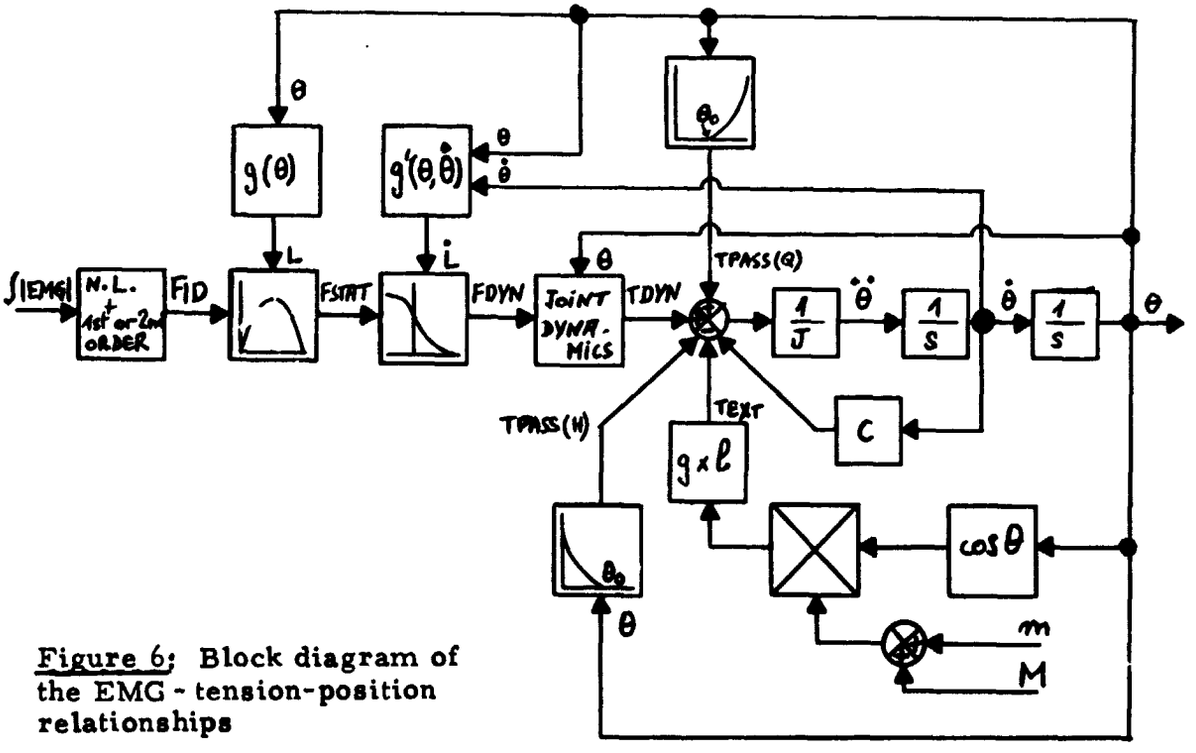

Figure 6: Block diagram of the EMG - tension-position relationships

In this diagram:

- s is the Laplace transform variable.
- L and $\dot{L}$ are the muscle length and velocity respectively, corresponding to θ and $\dot{\theta}$. The functions g and g' realize these transformations. Since the L - θ relationship is non linear, it may be written:

$$L = g(\theta)$$

yielding:

$$\dot{L} \frac{\partial g}{\partial \theta} \dot{\theta} = g'(\theta, \dot{\theta})$$

g' is then a function of the position and velocity of the joint.

- The joint dynamics box transforms FDYN into TDYN accounting for the changes in the center of rotation of the knee which imply a non linear variation of the moment arm OO_1 of figure 4 with respect to the knee position θ.

INTERPRETATION OF THE MUSCLE MODEL

The effects of the L.T. and V.T. filters may be explained by a tridimensional diagram where the axes are length (L), velocity (V) and tension (T). SONNENBLICK (1965)(reference #12) and BAHLER (1968) (reference #2) used this representation to study the interconnections between L., T. and V. . .

Let us follow what happens to the ideal force FID when the muscle contraction is anisotonic at non-constant velocity (figure 7a). The ideal force FID is first transformed into a static force FSTAT in the L.T. plane. FSTAT belongs to a surface which would contain the dynamic force if the muscle behavior were not dependent on velocity. If this hypothesis is true, the so-called FDYN-IDEAL would be the anisotonic muscle force. Actually, the dynamic force FDYN belongs to a surface which is elicited from the previous theoretical one by the V.T. filter.

Different modes of contraction may be described with this representation, (as shown by curves b and c in figure 7) as well as the dependence of the V.T. relationship on the initial muscle length.

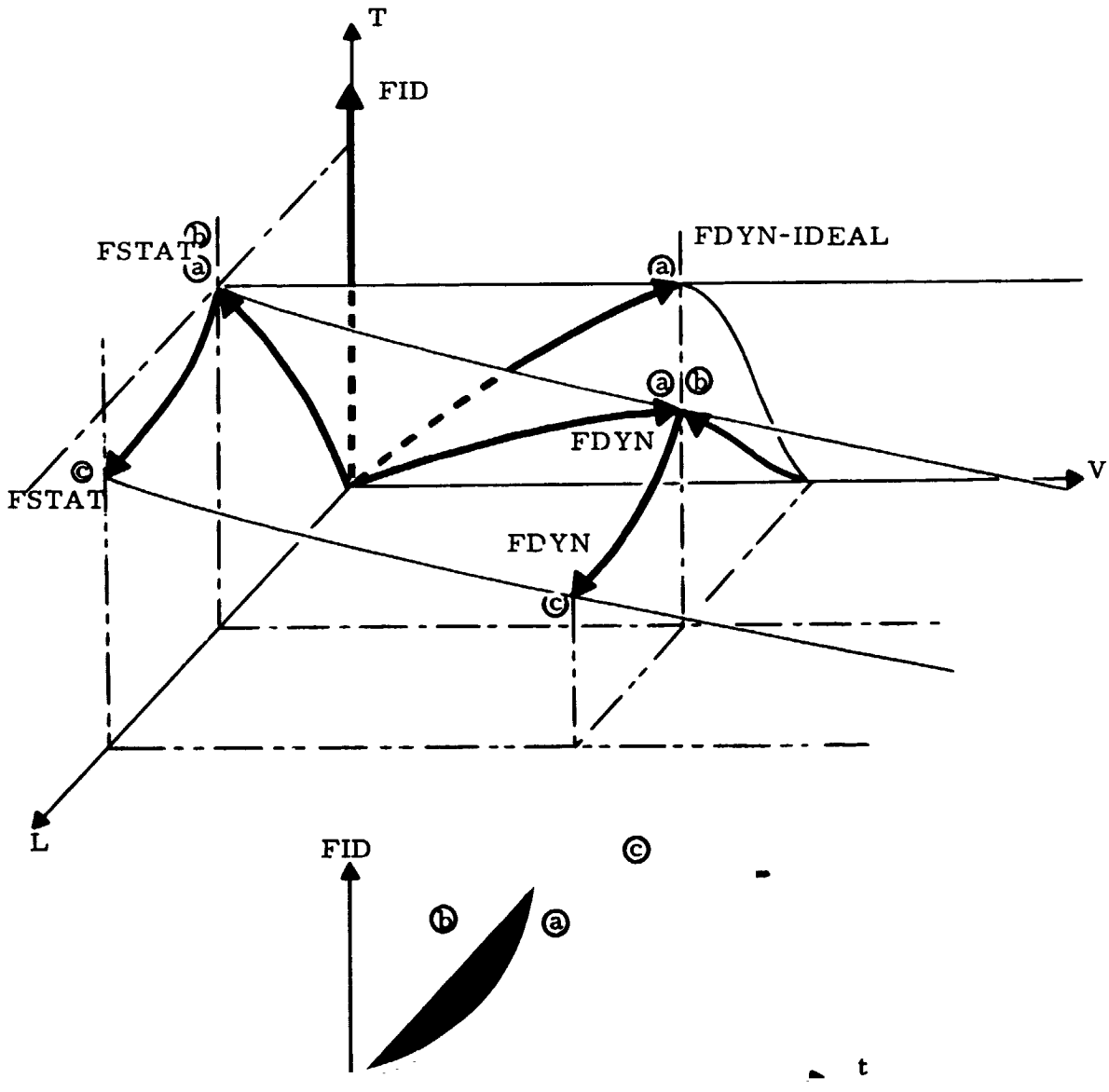

Figure 7 Tridimensional representation of the L.T. and V.T. filter effects on the ideal force FID during concentric contractions.

ⓐ. anisotonic contraction at non-constant velocity
ⓑ. anisotonic - isokinetic contraction
ⓒ. isotonic - isokinetic contraction
Situations a, b and c are sketched in the FID (t) diagram

Let us show now the behavior of the L.T. and V.T. filters when submaximal forces are developed during eccentric or concentric contractions.

A linearized form is chosen for the L.T. characteristic as shown in figure 8. Each point of the solid lines represents the maximal force produced at a given muscle length within the range [LMIN - LMAX]. LMIN and LMAX represent the minimum and maximum lengths the muscular group can have during a functional movement.

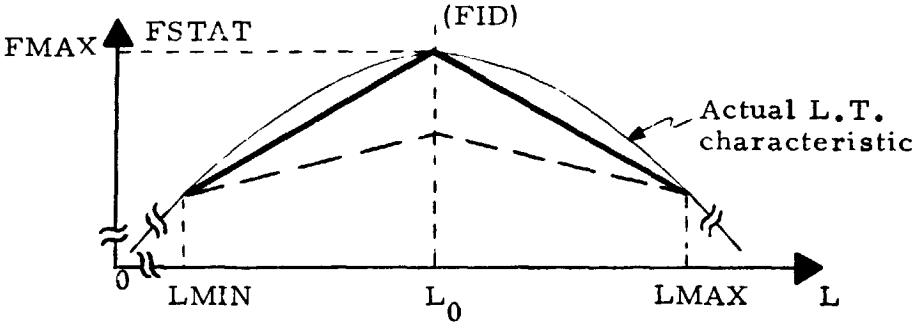

Figure 8: Structure of the L.T. filter

We shall assume that the level of activation of a muscle is directly related to its cross section rather than its length: when a muscle is fully activated, it develops its maximum force and the whole cross-section is involved. If its activation is half the maximum, the maximal force is halved at any length and the slopes of the lines in figure 8 are halved.

The ideal force FID represents the level of activation of the muscle but is independent of its length. Therefore, a variation of FID (t) is equivalent on the figure 8 to a variation on the FSTAT ($L = L_0$) axis, whatever the changes in length. The actual value of the static force, taking into account the changes in length at a given time, is the ordinate of a point belonging to the straight line:

$$FSTAT(L) = \begin{cases} \dfrac{L - LMIN}{L_0 - LMIN} \times FID & \text{If } L \leq L_0 \\ \dfrac{L - LMAX}{L_0 - LMAX} \times FID & \text{If } L \geq L_0 \end{cases}$$

The slope of the line is determined by the instantaneous ideal-force. When FID is equal to FMAX, FSTAT(L) is given by the solid lines of figure 8. If FID (t) is equal to FMAX/k, the slope is divided by k (broken lines). The L.T. filter process is illustrated by an example in figure 9.

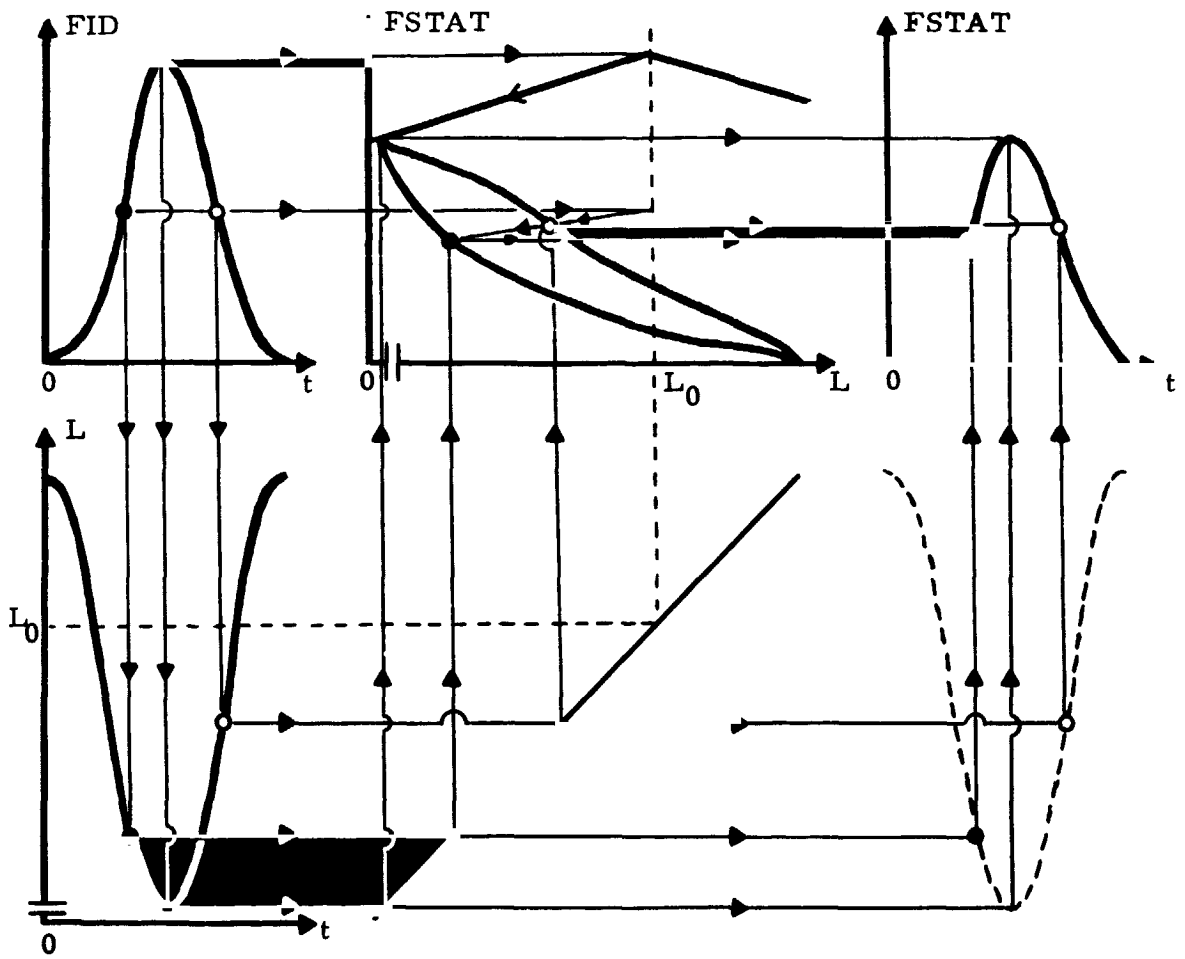

Figure 9 Effect of the L.T. filter on the ideal force FID. FID (t) (top left) is arbitrary for free movement. The muscle length L is assumed to be time varying in a sinusoidal manner (bottom left). The contraction of the quadriceps is concentric when L decreases and eccentric when L increases. The antagonist muscular group is passive during the movement. The FSTAT (L) curve (top center) is elicited by construction from FID (t) and L (t) as shown with dots ● and o . These two dots belong to the same L.T. characteristic but are related to different muscle lengths. The FSTAT (t) curve (top right) represents the L.T. filter output.

The representation of STARK et al., (1962)(reference #13) has been adopted to characterize the V.T. filter. It is a linearized model of HILL's curve (1938) which has been generalized by KATZ (1939)(reference #7) for eccentric contractions (figure 10). STARK used this diagram for simulation of the agonist-antagonist muscle system behavior during hand motion.

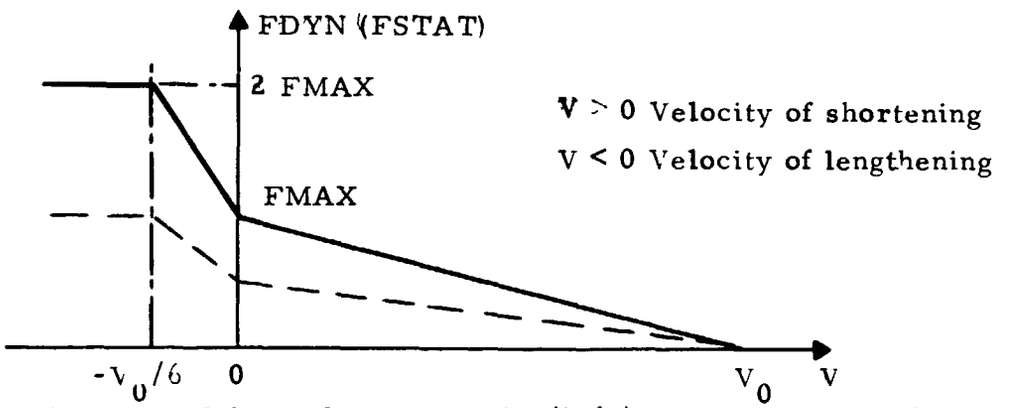

Figure 10. L.T. filter of STARK et al. (1962). V_0 is the maximal velocity of shortening.

As mentioned above, the muscle force depends on its cross-section. Furthermore, its maximal velocity Vo is a function of the muscular fiber length and hence, is a constant of the process. Then, as for the L.T. characteristic, when the muscular force is reduced, the slope of the relation is lessened proportionally (broken lines of figure 10).

The static force FSTAT appears on the FDYN (V=0) axis (figure 10). Each value of FSTAT corresponds, then, to a value of FDYN resulting in the association of the instantaneous muscle velocity and the force FSTAT produced at the same time. FDYN can be written as:

$$\text{FDYN}(V) = \begin{cases} 2 \times \text{FSTAT} & \text{If } V \leq -Vo/6 \\ \dfrac{|V| + Vo/6}{Vo/6} \times \text{FSTAT} & \text{If } -\dfrac{Vo}{6} \leq V \leq 0 \\ \dfrac{Vo - V}{Vo} \times \text{FSTAT} & \text{If } V \geq 0 \end{cases}$$

The V.T. filter works as the L.T. filter does. Its effect is shown in figure 11 with the same example used in figure 9.

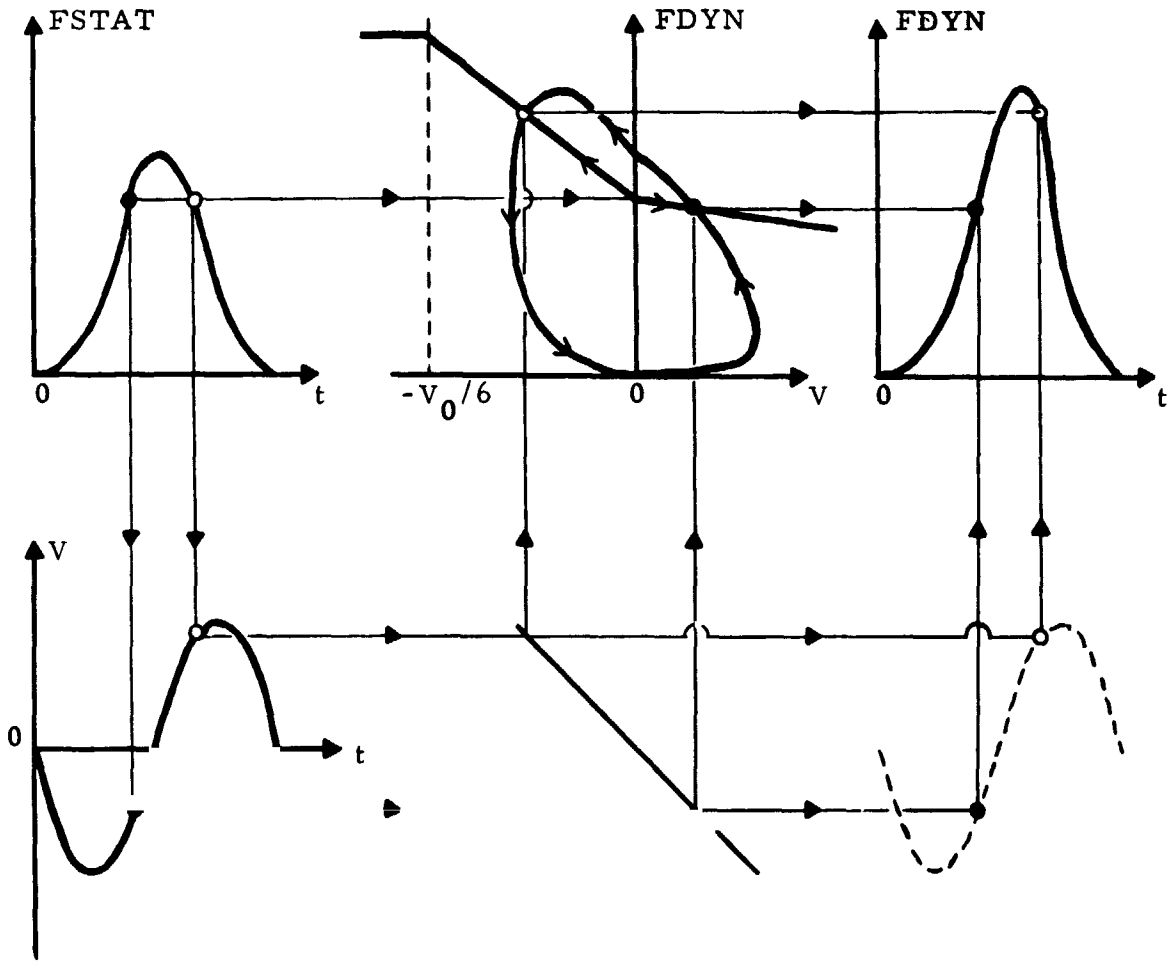

Figure 11 Effect of the V.T. filter on the static force FSTAT. The FSTAT(t) curve (top left) is the L.T. filter output of figure 9. The V(t) curve (bottom left) is the first derivative with respect to time of the previous L(t) curve. For this example, concentric contraction occurs when $V < 0$. The sign of V must then be reversed (bottom center) in order to keep the same V.T. diagram as figure 10. The FDYN curve (top center) is elicited by construction from FSTAT(t) and V(t) as shown with the dots ● and o . These two dots belong to the same V.T. characteristic : the first is related to a velocity of shortening, the second is related to a velocity of lengthening. The FDYN(t) curve (top right) represents the overall muscle model output.

DATA ANALYSIS

Quantification and validation of the model will be performed in the following sequence of steps:

a. First, the basic parameters of the model will be obtained by experiments. These parameters include the mass of the leg segments, the damping of the knee, the inertia of the lower leg, the passive tensions of the agonist and antagonist muscular group, the maximum isometric force with respect to limb position, etc.
b. The second step is the calculation of the ideal force produced by the muscle from the knee position data, by simulation. While in figure 6, the force appears as the input and the position as the output, the recorded knee position will be used as the input to a computer simulation and FID will be calculated.
c. Then, a parameter identification procedure will be performed to determine the parameters of the relationship between the integrated EMG and the ideal force. It is expected that a non-linearity which includes threshold and saturation and a first or second order model would be adequate to represent the process.
d. Finally, the aggregate model of both muscle and joint will be verified. For a given integrated EMG and taking into account the experimental conditions, the model must give the same knee position as the corresponding recorded actual position.

CONCLUSION

The model of the EMG-force-position relationships we propose includes:

- a muscle model using the length-tension and velocity-tension relationships as basic elements. The series filter representation makes it possible to relate EMG to force during isometric contractions as well as during more general movements without constraints on velocity, length or force.
- a model of the knee joint accounting for its mechanical characteristics (damping, changes in the center of rotation...) and the passive torques produced by muscles.

The tridimensional representation shows the validity of the model for various types of contraction. The velocity-tension diagram used

enables concentric and eccentric movements to be modeled. Submaximal forces may be described as well, as pointed out by the example.

Therefore, the proposed model is a general model of the joint and its actuators, relating the electrical activity of the muscles to the angular displacement of the moving limb and providing a prediction of internal muscle force.

REFERENCES

1. Agarwal, G.C.; Cecchini, L.R.; and Gottlieb, G.L.: Further Observations on the Relationship of EMG and Muscle Force. Proc. of the 7th Annual Conference on Manual Control, pp.115-118, 1971.

2. Bahler, A.S.: Modeling of Mammalian Skeletal Muscle. IEEE Trans. Biomed. Engng., BME-15: 249-257, 1968.

3. Brody, G.; Scott, R.N.; and Balasubramanian, R.: A Model for Myoelectric Signal Generation. Med. and Biomed. Engng., 12: 29-41, 1974.

4. Coggshall, J.C.: Mathematical Models of Muscle. Ph.D. Thesis, Technical Report, USCEE Report 303, U.S.C., 1968.

5. Gottlieb, G.L.; and Agarwal, G.C.: Dynamic Relationship Between Isometric Muscle Tension and the Electromyogram in Man. J. App. Physiol., 30: 345-351, 1971.

6. Hill, A.V.: The Heat of Shortening and the Dynamic Constants of Muscle. Proc. Roy. Soc.(London), B126: 136-195, 1938.

7. Katz, B.: The Relation Between Force and Speed in Muscular Contraction. J. Physiol., 96: 45-64, 1939.

8. Lindström, L.; Magnusson, R.; and Petersén, I.: Muscle Load Influence on Myo-Electric Signal Characteristics. Scand.J. Rehab. Med., Suppl.3: 127-148, 1974.

9. Lippold, O.C.J.: The Relation Between Integrated Action Potentials in Human Muscle and its Isometric Tension. J. Physiol. 117: 492-499, 1952.

10. Ostroy, L.; Phatak, A.V.; and Bekey, G.A.: On the Grading of Tension during Voluntary Contraction of Skeletal Muscle. Proc. of the 6th Annual Conf. on Manual Control, 1970.

11. Perry, J.; Antonelli, D.; and House, K.: Eléctromyography as a Force Measurement. N.I.H. Grant AM-13466, Dec., 1974.

12. Sonnenblick, E.H.: Determinants of Active State in Heart Muscle: Force, Velocity, Instantaneous Muscle Length, Time. Fed. Proc., 26: 1396-1409, 1965.

13. Stark, L.; Houk, J.C.; Willis, P.A.; and Elkind, J.L.: The Dynamic Characteristics of a Muscle Model Used in Digital Computer Simulation of an Agonist-Antagonist Muscle System in Man. Quart. Prog. Rept., Research Lab. of Electronics, M.I.T., 64: 309-315, 1962.

14. Wani, A.M.; and Guha, S.K.: Summation of Fibre Potentials and the EMG-Force Relationship during the Voluntary Movement of a Forearm. Med. and Biol. Engng., 12: 174-181, 1974.

A MODEL OF THE REFLEX ARC AND ANALYSIS OF THE BEHAVIOR OF THE PERIPHERAL RECEPTORS DURING CLONUS

Joseph E. Dollman
The University of Toledo
Toledo, Ohio 43606

Anthony M. Iannone
Medical College of Ohio
Toledo, Ohio 43614

Lee T. Andrews
Medical College of Ohio
Toledo, Ohio 43614

INTRODUCTION

At the present time, our knowledge of the physiology of peripheral receptors, the reflex arc and skeletal muscle has progressed to the point, where reasonable models of each of these individual elements is now described. It was the purpose of this project to combine these elements into a model of the entire skeletal muscle system. The system model was then thoroughly tested to insure its accuracy. Upon verification, the model provided a facility which allowed a prediction of the behavior of each element of the system, during rapid and reflex movement, to be made and compared with physiological observations. Of primary interest were the changes in system specifically related to rythmic oscillation of skeletal muscle referred to as clonus.

The ability of the model to portray rapid and reflex movement was of primary importance, as the mechanisms of these movements were believed to be directly involved in the tremorous instabilities, which were of interest in this study. Each peripheral receptor was, therefore, thoroughly analyzed to determine its role in the regulation of reflex contraction. The complexity of the model was minimized by assuming a simple monosynatic reflex. This assumption allowed us to omit those elements which are primarily involved in higher level controls of posture and deliberate movement. Thus, the joint receptor, the renshaw cell and secondary spindle endings do not appear in our model. The elements included in the model appear in Figure 1.

FORMULATION OF THE MODEL

Selection Criteria

In the process of reviewing publications, to select information necessary for the formulation of any of the elements of this model, certain selection criteria must be established. A comparison to these criteria will provide a method, by which information may be evaluated and the most feasible representation of the individual elements selected. Primary consideration, of course, should be given to the accuracy with which a given model portrays the characteristics of the system. In formulating such an accurate model care must be taken not to lose track of the physiological meaning of the parameters in the

model. That is to say, it is possible to very accurately fit the response curve of a particular organ with a high order equation. What is lost, though, is the physiological explanation for the coefficients of that equation. This makes implementation of changes, representing physiological phenomenon, very difficult. Thus, the task of relating the behavior of such a model to that of the physiological system becomes unduly complicated.

Another desirable trait of the model is simplicity. This will allow for efficient use of the facilities plus greatly enhance the ease with which the model can be operated. It was also deemed to be more representative, if when programmed, each model would have a single input and single output as this not only facilitated response studies of individual organs but also was considered more realistic. Therefore, the criteria or choosing a particular model were finalized as:

1) the accurate portrayal of the characteristics of the organ,
2) the physiological realizability of the model,
3) the minimum of complexity.

Muscle Fiber

The section of the model representing muscle tissue was the first subsystem concentrated on. The literature presently contains a very large number of applicable models. The complexity of these models vary from the simple viscoelastic representation to models based on the nonlinear Hill force velocity equation.

The final representation, shown in Figure 2, was chosen to be a contractile force generator in parallel with the passive tissue representation used by Houk [4] in his Golgi Tendon Organ experiments.

The parallel elements K_m and K_c represent the elasticity of the muscle tissue and the connective tissue, respectively. Using this representation also allows the Golgi Tendon Organ to be positioned in such a way that the entire tension developed by the contractile force generator is transmitted through the tendon organ. Tension developed by passive loading, however, is distributed between the tendon organ and the connective tissue which will enhance the representation of the Golgi Tendon Organ.

The parameters suggested by Houk for this model were

$K_1 = K_c + K_m = 346$ g/mm
$K_2 = 420$ g/mm
$K_c = 233$ g/mm
$K_m = 113$ g/mm
$B = 18$ g/mm/sec

When tested the parameters proved very satisfactory.

The step response of the fiber with an appropriate mass attached is shown in Figure 3. Increasing the damping caused increased oscillation involving the K_2 term, the elasticity of the tendon, as it effectively stiffened the contractile unit. Decreasing the damping was seen to increase oscillation related to the series combination of the springs K_1 and K_2. It was decided, therefore, to use these parameters as they provided what appeared to be an adequate response.

The limb dynamics involved in motion play an important part in causing inertial effects in the muscle response. Without these inertial effects the overshoot seen in the figure would not be present. Therefore the limb dynamics were assumed to be the movement of a mass, M, representing the mass of the limb and the mass of the muscle. Limb motion was assumed to be directly proportional to the muscle length for the magnitude of movements to be involved in the study.

The transfer function for the model can then be derived in terms of the input force. If we let G represent the total force, that is the acceleration due to gravity plus the disturbance, F_1, then the displacement, E_p, is given by

$$E_p(s) = \frac{M(K_m + K_c + K_2 + BS)}{MB\left(s^3 + \frac{K_m + K_c + K_2}{B}s^2 + \frac{K_2}{m}s + K_2\frac{(K_m + K_c)}{MB}\right)} G(s)$$

Golgi Tendon Organ

The Golgi Tendon Organ is the source of inhibitory signals in the reflex arc. These signals serve as a load detector and overload protection mechansim in the muscle control system. A great deal of work has been published by J. C. Houk [4,5,6] and his associate on the function and modelling of these organs. The tendon, in these works, is modelled with a linear equation. The nonlinearities known to be present in the system were defined as adaptation and threshold functions preceding and following the linear dynamics, respectively. The saturation curve precedes the linear dynamics so as not to decrease the overshoot in response to rapid movements. Conversely, the threshold was seen to follow the linear dynamics, as it was Houk's conviction that this phenomenon was the product of conversion of receptor potentials to I_b potentials.

By fitting recorded data to exponential responses Houk originally derived a second order transfer function, h(s).

$$h(s) = K\frac{(s + .95)(s + 13.65)}{(s + 1.8)(s + 25.0)}$$

Further work indicated that a third order term representing the low frequency "mechanical filtering" of the muscle tissue was needed. However, Houk stated his transfer function as a response to a force input at the end of the tendon. The input to the tendon organ in the proposed model has been chosen to be the tension, TIN, at the point previously indicated, Figure 2, between

the contractile element and the tendon. In calculating the tension at this point from displacement, load and contractile force information, the low frequency "mechanical" filtering required by Houk has already taken place. Thus, the second order system will accurately model the dynamics of system in question.

The nonlinearity related to threshold proved to have a very significant effect when studying instabilities in the motor system. The inhibitory effects of the tendon signals, which exceeded the threshold, were responsible for limiting otherwise growing oscillations. Increased sensitivity to these signals and/or lowered thresholds could also be seen to have a significant effect on the damping of what would otherwise be sustained oscillation. The adaptation function, however, did not appear to have extraordinary effects on the system. The movements being studied were caused by forces of a magnitude such that they fell below levels which would be thought to cause significant adaptation. Leaving this term out would also help compensate for the different response to active force by not saturating during the high tension conditions which those forces cause.

Another control must be considered before accepting this model for the system. The degree to which the α motor neuron responds to the inhibitory signals, propagated along the I_b neuron, is in some way controlled by the central nervous system. A suggestion for this is that the nervous system controls the excitability of the interstitial neurons forming the polysynaptic connection between the I_b and the α motor neuron. This can be represented as gain, ranging from 0 to 1, which is controlled by a central nervous system input. The final form of the model is described in Figure 4, where h(s) is the second order representation stated above.

Muscle Spindle

The muscle spindle provides excitatory feedback to the contractile force generator. These signals are essential in the proprioceptive network, necessary for rapid movement and reflex activity. The secondary endings located in the nuclear chain fibers of the spindle are slow responding and more adapted to postural control. Therefore, only a model of the rapidly responding nuclear bag fiber of the spindle was deemed necessary for this model.

The works of Rudjord [10] and of Andrews [1,2] both strongly suggest that a second order model would be accurate for this case. A number of second order Bode plots were given to demonstrate how well these models would fit the actual data.

The Bode plots suggest a pole near 100 which caused the decrease in phase and the leveling off of the gain as it approached that frequency. A zero, z_1, is seen to be in the neighborhood of 1 hz. The second pole was chosen to be around 200 hz. so as to represent the great attenuation in response which is seen at frequencies near 500-1000 hz. The second zero, z_2, was chosen so as to cancel the phase lag effects the pole at 200 has on high frequency response. The value was also chosen high enough so as to eliminate any effects it would have on the low frequency response. Thus z_2 was set to 600. The

asymptotic approximation of the Bode plot is shown in Figure 5. The transfer function is then:

$$h(s) = K_\gamma \frac{(s + z_1)(s + z_2)}{(s + 100)(s + 200)}$$

where z_2 has been chosen to have a value of 600. The choice of an exact value for z_1 requires that consideration be given to the effects of γ innervation on the low frequency response of the system. If the elastic stiffness in the bag fiber were to increase with innervation, the position of z_1 would change, moving farther into the left half plane. Green [11] has suggested neural control of stiffness and damping was responsible for control of the contractile element of muscle so why not the same effect for the control of the contractile sections of the spindle fibers. Rudjord, however, had indicated doubt that this change in stiffness was an accurate portrayal of the effects of innervation on the spindle and suggested the effects were similar to those of a force generator in parallel with elements of fixed value. The idea of a force generator seemed a more logical representation of gamma control of muscle length. However, it did not seem sufficient to explain the ease with which the system could be driven unstable under conditions of high γ innervation. An examination of a typical plot of extension versus tension for muscle fiber shows a significant increase in stiffness as tension increases. Thus, even if γ does not directly control the stiffness of the fiber, increased activation of the contractile force generator will increase tension in the fiber thereby increasing the stiffness.

It was decided, therefore, to make the position of z_1 a function of γ while also including a γ controlled force generator. The force generator was to be represented in a manner similar to Dijkstra's [3]. That is, the stretch sensed by the spindle is measured with respect to some reference length, $Ep_{reference}$. The force generator is, therefore, a control of that reference length and can be represented merely as a level to be added or subtracted from the actual displacement. The input to the system, Ep_{in}, becomes then:

$$Ep_{in} = Ep + Ep\ (\gamma)_{reference}$$

with the transfer function of the spindle being:

$$H(s) = \frac{(s + z_1(\gamma))(s + 600)}{(s + 100)(s + 200)}$$

Similar to the I_b activity, the signals transmitted along the I_a neuron do not have a constant effect on the α motor neuron. Even in the case of a monosynaptic connection with the α motor neuron, sensitivity to excitation is controlled by the central nervous system. The physiological explanation for this is that inhibitory signals from the central nervous system can reduce the sensitivity of the anterior horn cell to I_a inputs. To account for this a sensitivity term, having a value between 0 and 1, is multiplied by the I_a at its input to the contractile force generator. The only other addition to the model is a diode in the feedback path which limits the excitation to the di-

rection of contraction only.

Contractile Force Generator

The contractile forces generated by muscle fibers are known to be functions of spindle, tendon organ and central nervous system activity. Effects from renshaw cells and from the linkage with antagonist muscles were neglected due to their absence from the model. The contractile force was then defined as f_c where:

$$f_c = K(CNS + k_1 I_a - k_2 I_b)$$

The gain, K, represents the conversion from frequency of firing in the α motor neuron to actual contractile force. The gains, k_1 and k_2, represent the sensitivity term of the anterior horn cell and the interstitial neurons discussed in the spindle and tendon organ models.

The inhibitory effect of the I_b, modeled by subtracting it from the summation of excitatory inputs, could, in an extreme case, cause a sign change in the contractile force. Since this would be analogous to the muscle pushing the limb, a physiological impossibility, a diode was used to rectify the generated contractile force thus assuring that it always maintains a positive value.

Initial Analysis

The above elements were assembled in the proper order. A root locus analysis was carried out under two conditions:

1) the Golgi Tendon Organ sensitivity set to zero, and
2) the Golgi Tendon Organ inputs predominant.

The characteristics predicted by the model were very closely related to those which would be expected of a skeletal muscle system. That is:

1) The open loop response shows less than critical damping, $\zeta=1$, for physical parameters of the system.
2) Feedback from the spindle, at moderate levels, increases damping in the systems step response.
3) Excessive sensitivity to spindle output can cause oscillation.
4) Significant changes in the position of the gamma controlled zero, $z_1(\gamma)$, will induce oscillation.
5) Feedback from the Golgi Tendon Organ is the limiting factor in the magnitude of the oscillation and affects the sensitivity to I_a needed to sustain oscillation.

Verification of the Model

The initial analysis of the system showed the model to be very promising. Therefore, the model was wired on the analog computer. Before attempting to model clonus, however, more tests were made to verify the model.

To check the reflex loop, steps in stretch were applied under open loop, normal and high tendon organ activity situations. A step response run during high tension conditions was run to check the function of the diodes in the feedback paths.

Satisfied that the reflex loop was operating properly, simulations of activated movements were made to insure that the model adhered to currently accepted theory of α,γ and α-γ linked innervation of movement. The model performed very well in these tests adding support to the assumption that spindle innervation includes a control of a γ dependent zero in the bag fiber.

The satisfactory completion of these tests indicated that the model was very representative of a skeletal muscle control system. A study of clonus using this model, therefore, could be expected to produce accurate results.

CLONUS

Explanation and Analysis

Mountcastle [9] defines clonus as "the tendency to oscillate at approximately 8 to 12 hz., a behavior that is believed to be caused by excessive feedback from spindle receptors". Generating a 10 hz. sinusoid, however, is not the major point behind the model. The model should not only display the sinusoidal movement but also the proper phase relationship between the excitatory signals and movement. To determine what the relationship should be data, recorded by Iannone, Angle et. al. [8], on ankle clonus was examined. A plate taken from Iannone's notes is shown in Figure 6. In the photograph down is the direction of stretch with the spindle output being the upper trace, the EMG activity the center and displacement the lower trace. It can be seen in the recording that spindle activity begins increasing significantly with movement in the direction of stretch. The EMG activity is seen to reach its maximum approximately 20 msec before the muscle reaches maximum stretch. The frequency of the oscillation, being approximately 10 hz., means the excitatory signal leads the displacement by approximately 72°. In his notes Iannone mentions the results of recording the afferent activity of Golgi Tendon Organs. It is his finding that the activity of the Golgi Tendon Organ occurs just after the EMG has ended. It is his contention that the purpose of the Golgi Tendon Organ during clonus is more one of inhibiting excitation during the returning phase of the oscillation than one of ending the excitation itself.

The implications of this statement about the function of the Golgi Tendon Organ are that the I_b response should be almost in phase with the displacement itself. If one assumes the spindle output to be primarily proportional to the rate of stretch, the time delay involved in the 100 m/sec. propagation rate of the I_a fiber will shift the phase of the excitatory signal to a neighborhood of 72° of lead, quite easily. Likewise, the small velocity component of the tendon organ transfer function can cause the tendon output to lead the displacement by only a small amount. The time delay involved in propagating these signals along the I_b fiber, whose propagation rate is similar to that

of the I_a, could then easily compensate for this, putting the inhibitory effects in phase with the displacement. Another comment made by Iannone was that large Golgi Tendon Organ events took place occasionally during clonus. This would seem to indicate that clonus generates tensions which only occasionally exceed the threshold necessary to generate effective inhibitory signals from the tendon organ. Thus, the I_b threshold of the model can be set at a level just above that which would inhibit small magnitude oscillations and still be representative of the actual circumstances.

This assumption, about the threshold of the I_b, was tested on the model by simulating a condition with very large position sensitivity in the feedback loop. Such a condition will, unless inhibited, cause an oscillation which will grow in magnitude continuously until reaching the limits of the simulation. With the Golgi Tendon Organ threshold set at a specific level the oscillations were noted to grow until the tension required to excite them exceeded the tendon organ threshold. The magnitude of the oscillation ceased to grow at this point with the I_b activity taking place at peak tension and inhibiting the excitation. Similarly, the level of such an oscillation could be lowered by further lowering the I_b threshold. For marginally stable systems, the excitatory signals were seen to produce subthreshold tensions only large enough to sustain the oscillation. Lowering the I_b threshold in such a case was seen to damp out these oscillations. Since Mountcastle had commented on the small magnitude of clonic oscillation and a marginally stable system would allow the largest amount of phase lead in the excitatory signal, it was justifiable to set the I_b threshold high enough that inhibitory signals would not effect the oscillation of the system under marginally stable conditions. In doing this it is felt that the model of clonus would be able to give the maximum phase lead possible and still represent the tendon organ effects seen by Iannone.

Model Results

The phase relationship, established above, was readily duplicated by the model. The phenomenon of clonus was initiated by allowing the system to reach steady state, then adjusting the position of the zero for marginal stability. After the zero had been adjusted a disturbance was added to the load to initiate a movement.

Figures 7 and 8 display the phase relationships produced by the model. The spindle activity was seen to lead the displacement by 19 to 20 msec., that is 68° to 72° of lead. The Golgi Tendon Organ activity leads displacement by less than .01 seconds. This timing of the tendon organ activity reinforces the suggestion by Iannone that they are primarily responsible for suppression of ill-timed signals. Since the properly timed excitatory signals are already rapidly decaying when the tendon organ activity is building, the role of tendon organ in terminating these excitations is not shown to be significant.

Conclusions

The proposed model has been tested with respect to step response, α, γ and α-γ linked activations. The results being outputs which can be explained

by current theory and compare adequately with published data. This being the case, the changes made in the model in order to cause clonus can be assumed to be analogous to those which take place in the physiological system itself. Those changes being primarily excess γ activity represented in two forms. This activity causes increased tension, analogous to reference length changes in the contractile regions of the spindle. Due to this change in tension, changes in the elasticity of the fiber also take place, which when represented in the model greatly enhance the ability of the model to portray clonus.

Comments

To understand motor behavior it is imperative to have a thorough understanding of each of the peripheral elements. We feel that knowledge of the individual elements is extensive and there is a need to integrate this knowledge into model of the motor system. Thus, allowing a study of the interaction of these elements in generating control commands from the feedback loops of the motor system. We believe the model presented here has accomplished a first step in this direction and can now be extended to include the higher level influences of the central nervous system.

REFERENCES

1. Andrews, L. T., Ewing, D. J., and Iannone, A. M., "An Anatomically Based Mathematical Model of Mammalian Muscle Spindle," Modeling and Simulation, Vol. 4, Proc. of the 4th Annual Pittsburgh Conference, April 1973, pp. 386-390.

2. Andrews, L. T., Iannone, A. M., and Ewing, D. J., "The Muscle Spindle as a Feedback Element in Muscle Control," 9th Annual Conference on Manual Control, May 1973.

3. Dijkstra, S. J., and Denier VanderGon, J. J., "An Analog Computer Study of Fast, Isolated Movements," Kybernetik 12, 102-110, 1973.

4. Houk, James, "A Viscoelastic Interaction Which Produces One Component of Adaptation in Responses of Golgi Tendon Organs," J. Neurophysiol., 1967, Vol. 30, pp. 1482-1493.

5. Houk, James and Henneman, Elwood, "Response of Golgi Tendon Organs to Active Contraction of the Soleus Muscle of the Cat," J. of Neurophysiology, Vol. 30, 1967, pp. 466-481.

6. Houk, James and Simon, William, "Responses of Golgi Tendon Organs to Forces Applied to Muscle Tendon," J. of Neurophysiology, Vol. 30, 1967, pp. 1466-1481.

7. Houk, J. C., Singer, J. J., and Goldman, M. R., "An Evaluation of Length and Force Feedback to Soleus Muscles of Decerebrate Cats," J. of Neurophysiology, Vol. 33, 1970, pp. 784-811.

8. Iannone, A. M., Angel, R., and Zajac, F. E., "Laboratory Notebook, Subject: Clonus," Stanford University, 1967.

9. Mountcastle, Vernon, Medical Physiology, 12th Ed., C. V. Mosby Co., St. Louis, 1968.

10. Rudjord, T., "A Second Order Mechanical Model of Muscle Spindle Primary Endings," Kybernetik, February 1970, Vol. 6, pp. 205-213.

11. Green, D. G., "A Note on Modeling Muscle in Physiological Regulators," Med. Biol. Eng., Vol. 7, 1969, pp. 41-48.

Figure 1

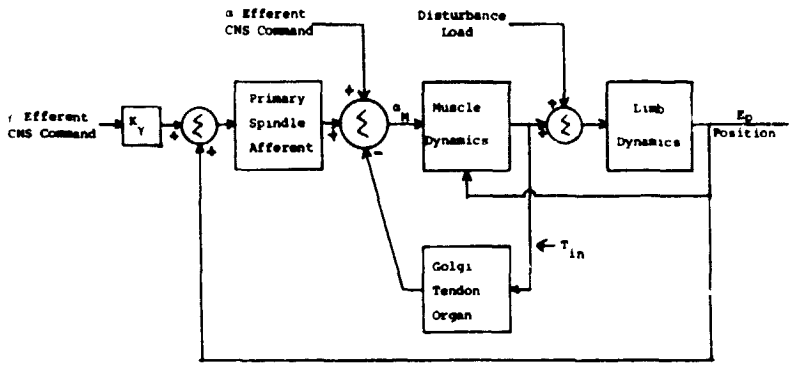

Figure 2

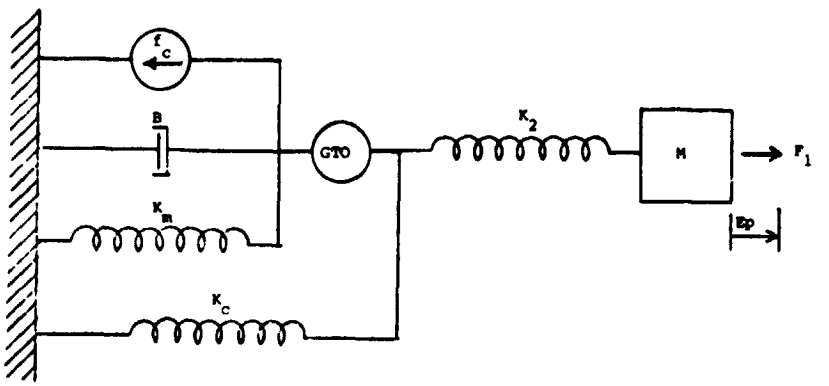

Figure 3

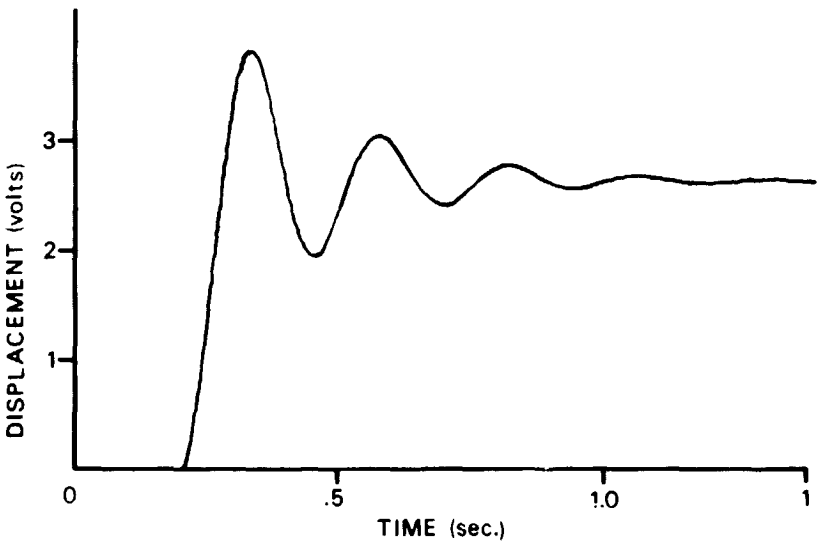

Figure 4

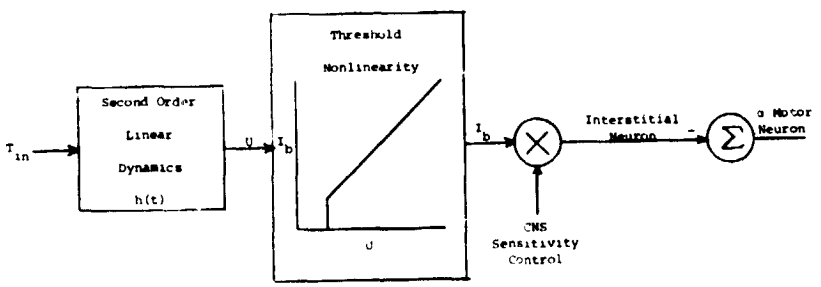

Figure 5

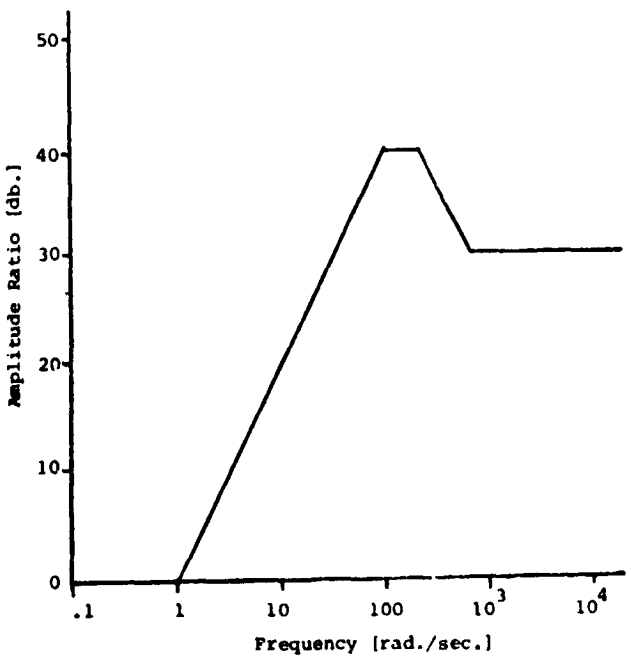

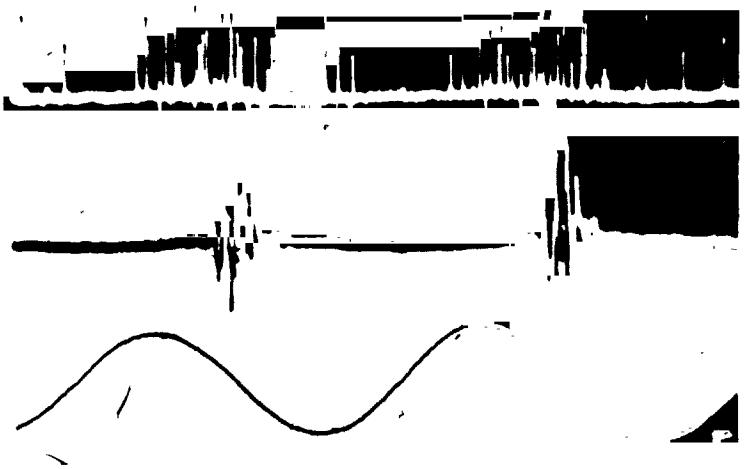

Figure 6

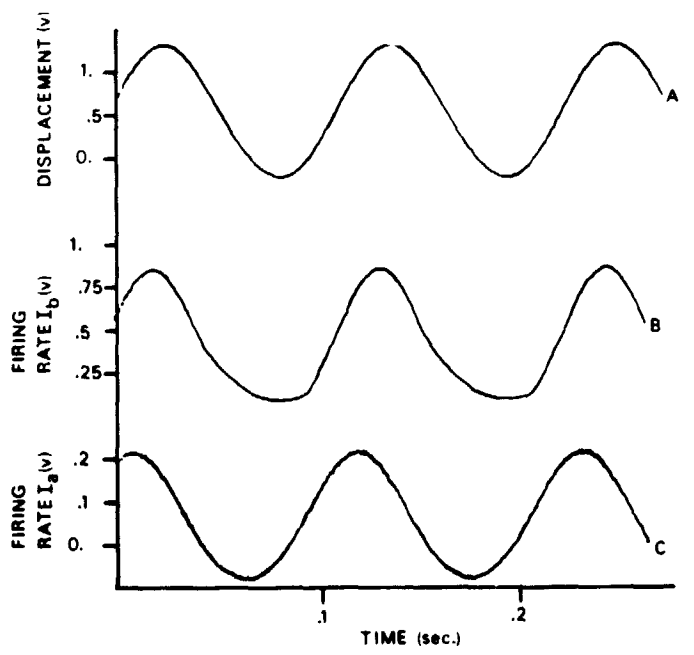

Figure 7

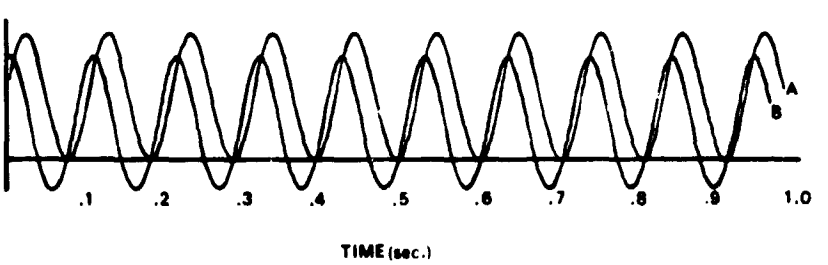

Figure 8

SESSION XI

MOTION AND VISUAL CUES

Chairman: R. C. Williges

A PILOT MODEL WITH VISUAL AND MOTION CUES*

Renwick E. Curry
Massachusetts Institute of Technology
Cambridge, Massachusetts

Lawrence R. Young
Massachusetts Institute of Technology
Cambridge, Massachusetts

William C. Hoffman
Aerospace Systems, Inc.
Burlington, Massachusetts

Daniel L. Kugel
Flight Dynamics Lab
Wright Patterson AFB, Ohio

Abstract

A model of pilot control performance is developed to account for the effects of motion cues and external visual (VMC) cues. The starting point for the model is the optimal control model of the human operator, which has been well validated in fixed-base IMC (e.g., instrument cues) situations. The first goal was to incorporate motion cues by augmenting the controlled-state vector with the dynamic description of the vestibular sensory organs (semi-circular canal and otolith). Comparison of the model predictions with experimental results of motion-only tracking indicates that the noise/signal ratio for the vestibular measurements can be modeled as approximately -18 dB. This new model was applied to a VTOL hovering task and did an excellent job of describing the control performance with and without motion cues, both on an absolute and relative basis. The difference between IMC and VMC visual cues was accounted for in the model by decreasing the quadratic penalty on roll rate (i.e., higher roll rates are allowed). The model provides a good description of control performance with and without motion and VMC cues, and predicts the change in scanning behavior observed under these conditions.

I. Introduction

Many successful attempts have been made to model the rms performance and equalization strategies of the human operator in the control loop. The two basic approaches are the frequency domain approach (Reference 1) and the optimal control formulation (Reference 2). These two approaches have stressed the fixed-base condition with visual cues being derived from instrument displays. The extensions of these models to include motion cues and VMC cues has been based on experimental data generated before the advent of the modeling effort. Reference 5 has compiled experimental data for a roll tracking task covering a wide range of controlled elements for three experimental conditions: motion only, visual only (IMC), and visual and motion combined. Reference 6 compared the pilot performance in the fixed-base configuration and moving-base with angular-only motion cues and linear and angular cues. Reference 7 reports roll control data taken in fixed-base IMC conditions, fixed-base VMC (large contact-analog display), in-flight IMC, and in-flight VMC.

Two attempts at combining these and other data into a model are described in References 3 and 4. Reference 3 concludes that the otolith provides low frequency orientation information, whereas the equalization and improvement in tracking ability comes primarily through the semi-circular canal contribution. Reference 4 used the data of Reference 5 to provide some interesting ideas concerning the weighting of perceived variables rather than absolute variables.

The objective in this effort is to provide a model which describes the important aspects of motion and VMC cues with the eventual intent of determining simulator requirements. Specifically, the goals are to show the differences in control performance between moving-base and fixed-base conditions as well as IMC and VMC conditions. The approach has been to modify the optimal control model of the human operator from those conditions in which it has already been validated (i.e., fixed-base IMC cues). To this end, the model was first applied to the roll tracking data of Reference 5 to determine those components in the model which describe the data. This portion of the model was next validated with the VTOL hovering task reported in Reference 6. The effects of VMC cues on the model parameters were evaluated using the data of Reference 7, and were then compared with both VMC and motion cues in other data reported in Reference 7.

II. Modeling Motion Cues

A block diagram of the optimal control model of the pilot is presented in Figure 1, which shows the information flow and the interaction of the pilot with the controlled element. The displayed information, $y(t)$, passes through the threshold element (either a psychophysical threshold or an indifference threshold). Perceptual observation noise, $V_y(t)$, is added to this quantity, which then passes through the perceptual time delay, τ. The perceived displays, $y_p(t)$, are the inputs to the core of the model, which consists of a Kalman filter and predictor to compensate for the observation noise and time delay. The current state estimate, $\hat{x}$, is combined linearly to provide a commanded control signal, to which is added motor noise, v_u, with the result passing through a neuromuscular/manipulator first order lag. The covariance of each observation noise depends on several important parameters and has the form

$$V_{yi} = \frac{\rho_i}{f_i}\left[\frac{n_{yi}}{N(\sigma_{yi}, \alpha_i)}\right]^2 \qquad (1)$$

where in the above expression V_{yi} is the covariance of the

* Research sponsored by USAF Flight Dynamics Laboratory, under Contract No. F33615-75-C-3069.

Paper also presented at the AIAA Visual Motion and Simulation Conference, 1976.

white observation noise; f_i is the fraction of attention devoted to the i^{th} display; σ_{yi} is the standard deviation of the i^{th} displayed quantity; N is the describing function for the dead zone element of width $2\alpha_i$, and ρ_i is the multiplicative noise/signal ratio which has been found to describe human performance under full-attention, fixed-base, visual IMC tracking. It has been found that a value of $V_{yi} \triangleq -20$ dB (or .01 π) provides a good description of the observed results.

One element of the model which is not shown in the block diagram is the quadratic functional which is minimized by the choice of the control gains, L. In its most general form this is

$$J = E\left\{\int_0^\infty (y'Q_y y + x'Q_x x + \dot{u}'Q_{\dot{u}}\dot{u} + u'Q_u u)\,dt\right\}^2 \quad (2)$$

where Q_y, Q_x, $Q_{\dot{u}}$, and Q_u are weightings on the displays, state, control rate, and control, respectively. In practice, it has usually been sufficient to weight the display deviations from nominal and ignore weights on the state x and control displacement, u. The weights on control rate are chosen to provide a neuromuscular time constant (T_N in Figure 1) consistent with the manipulator, with a value of $T_N = .1$ second being typical.

In spite of its seeming complexity, there are few free parameters in the model: for fixed-base IMC control tasks, these parameters are the display weights and display thresholds. A good prediction of control performance under these conditions can be obtained be weighting the display deviations inversely proportional to the square of their maximum values, and choosing thresholds consistent with an indifference value, i.e., a value a pilot is likely to accept without taking corrective action.

To extend the use of this model to incorporate motion cues, we first assume that the semi-circular canal and otolith signals can be represented by an equivalent set of vestibular organs aligned with the body axes, i.e., the coordinate transformations required would all be performed internally. Following Reference 8, we use the following transfer functions between the physical stimulus and the efferent firing rate (expressed in terms of the stimulus units):

Semi-circular canal

$$Y_{scc}/\phi = \frac{.0069 s^3 (s + 50)}{(s + .0555)(s + .0333)} \quad (3)$$

$$(deg/sec^2)/(deg/sec^2)$$

Otolith

$$Y_{oto}/f = \frac{2.024 (s + .0988)}{(s + .20)} \quad (4)$$

These transfer functions represent the effects of the vestibular "displays" shown in the block diagram in Figure 1, with the dynamics of the vestibular sensors incorporated in the equations of the system dynamics.

To examine the effects of the noise to signal ratio for vestibular only measurements, the rms predictions of the model were compared with the experimental data described in Reference 5 for five typical plants. The shelf spectrum used in Reference 5 was approximated by a fourth-order filter as described in Reference 4. Figure 2 compares the rms model predictions with the experimental data for noise to signal ratios. For all of these data, the motor noise was set at the recommended noise/signal ratio of -25 dB. At the present time the only explanation for the somewhat deviant behavior of the control plants k/s and $k/(s^2 + 10)$ is the interaction of the motion with the manipulator, which might be accounted for by decreasing the motor noise for k/s and increasing it for $k/(s^2 + 10)$. Based on these comparisons, however, a representative noise to signal ratio for vestibular measurements appears to be approximately -18 dB, compared to the -20 dB typically used for visual inputs.

To test the model with these motion cues incorporated, it was used to predict the performance in a VTOL hovering task. This hovering task was run under three motion conditions: fixed base; angular cues only; and angular and linear cues. The dynamics were programmed in accordance with the simulation description (Reference 6). The weighting coefficients and indifference thresholds for the visual and vestibular inputs are shown in Table 1. No weights were applied on the vestibular outputs, i.e., the vestibular outputs were used as measurements only and were not to be nulled. The vestibular threshold levels were taken as three times the typical laboratory-determined thresholds, to account for masking and effects of the simulator. Using these parameters in the model resulted in the rms performance predictions shown in Figure 3, which also indicates the range of means of the three subjects. Figure 3 clearly demonstrates that there is good agreement, both qualitatively and quantitatively, between the model predictions and the results for the three subjects (a small population). Both the model and the experimental data show little difference between fixed-base and moving-base conditions because the simulator seemed to be operating near the vestibular thresholds much of the time (Reference 6).

Table 1. Weighting Coefficients and Indifference Thresholds, VTOL Hovering Task

Display Variables	Display Gain	Weighting Coefficient	Indifference Threshold
x,y	1 in/9.1 ft	$1/(1\,in)^2$	.2 in
u,v	(1 in/sec)/(9.1 fps)	$(5\,sec/1\,in)^2$	.2 in/5 sec
θ,ϕ	$5(180/\pi)$ deg/rad	$1/(10\,deg)^2$	2 deg
$\dot{\theta},\dot{\phi}$	$5(180/\pi)\frac{deg/sec}{deg/sec}$	$(1\,sec/10\,deg)^2$	2 deg/1 sec
z	1.0	$1/(10\,ft)^2$	2 ft
w	1.0	$(5\,sec/10\,ft)^2$	2 ft/5 sec
SCC	1.0	0	$.57\,deg/sec^2$
OTO	1.0	0	.015 g

III. VMC Cues

The primary difference between IMC and VMC cues (as reported anecdotedly) seems to be that the pilot is willing to tolerate larger excursions of attitude angle to more closely control position (Reference 6) or to use higher bank angle rates to null position error (Reference 7). There are several places in the model where this might be accounted for: decreased noise or threshold on angular rate because of increased peripheral stimulation, or by decreased weighting on attitude rate to reflect different pilot strategy. Both of

these parameter changes were explored in comparing pilot describing function data reported in Reference 7 for two fixed-base roll tracking tasks: one with IMC cues (conventional roll attitude display), and one with VMC cues (wide-field contact analog display). The results of varying the perceived rate threshold on the calculated pilot describing function are shown in Figure 4. The effects of varying the maximum roll rate are shown in Figure 5. These figures indicate that the describing function is far more sensitive to changes in the maximum roll rate than to its threshold, because this particular tracking task was being performed above the assumed threshold values. This leads to the conclusion that for the increased pilot gain observed in VMC attitude control tasks, VMC cues can be incorporated in the model by decreasing the penalty on attitude rate, or increasing the maximum value of attitude rate.

To determine the effects of these VMC cues in a more complicated condition, the model was used to predict the pilot describing function determined from in-flight experiments in a VMC roll control task as described in Reference 7. In comparing the predicted describing function and the measured values, we found good agreement except at low frequencies (a not uncommon characteristic of the model). The primary discrepancy between the predictions and the data lies in a low frequency fall off in gain and a corresponding increase in phase lead, whereas the pilots maintained the gain with no phase lead at frequencies below .3 radians per second. At the present time there is no adequate explanation for the difference between the model predictions and the data, since changing the weights on canals and otolith measurements in comparison to the visual display has only minor effect on the pilot describing functions shown here. The primary difference in the complete forward loop transfer function is that the model looks like a high gain first-order system at low frequencies, whereas the data imply that the forward transfer function behaves more like an integrator at these low frequencies.

IV. Conclusions

The optimal control of the pilot has been extended to incorporate motion and visual cues outside the cockpit. The vestibular measurements appear to be adequately accounted for by incorporating their dynamic properties in the controlled element dynamics, and including their afferent signals as measurements with noise to signal ratios of approximately -17 to -18 dB. Using this approach we have accurately predicted the difference between fixed-base and differing moving-base cues in a VTOL hovering task both on an absolute and a relative basis. The incorporation of VMC cues in attitude control tasks appears to be modeled by a change in the weighting coefficients of the quadratic cost functional, which are equivalent to raising the maximum value of attitude rate. Using this technique to predict pilot describing function data for both motion and VMC cues provides excellent agreement at the mid- to high-frequency range, but as yet there is no adequate explanation for the discrepancy between the model and reported data at low frequencies (.1 - .3 radians per second). In spite of this, it appears as though the model as it currently stands is capable of providing an excellent prediction of changes in pilot performance with the addition of motion and VMC cues.

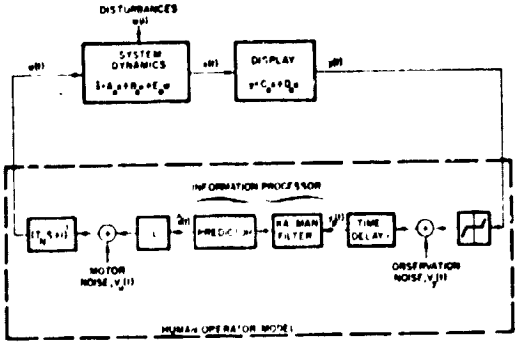

Figure 1. Optimal Control Model of Human Response.

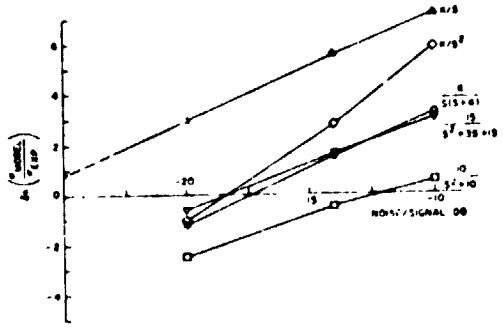

Figure 2. Comparison of Model and Experimental Data Versus Noise/Signal Ratio - Motion Only.

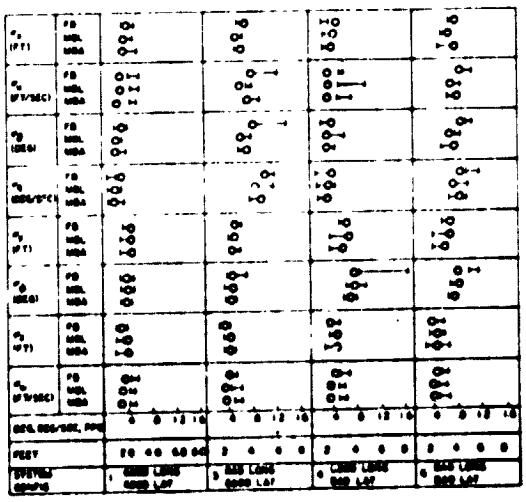

Figure 3. Predictions of Control Task Performance Compared to Range of Means of Three Subjects.

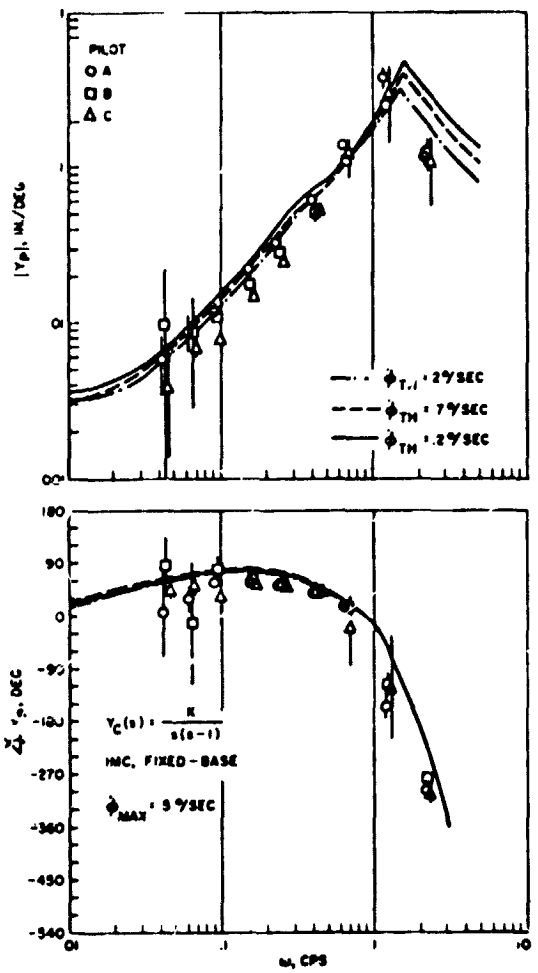

Figure 4. Effect of Attitude Rate Threshold on Pilot Describing Function (Reference 7).

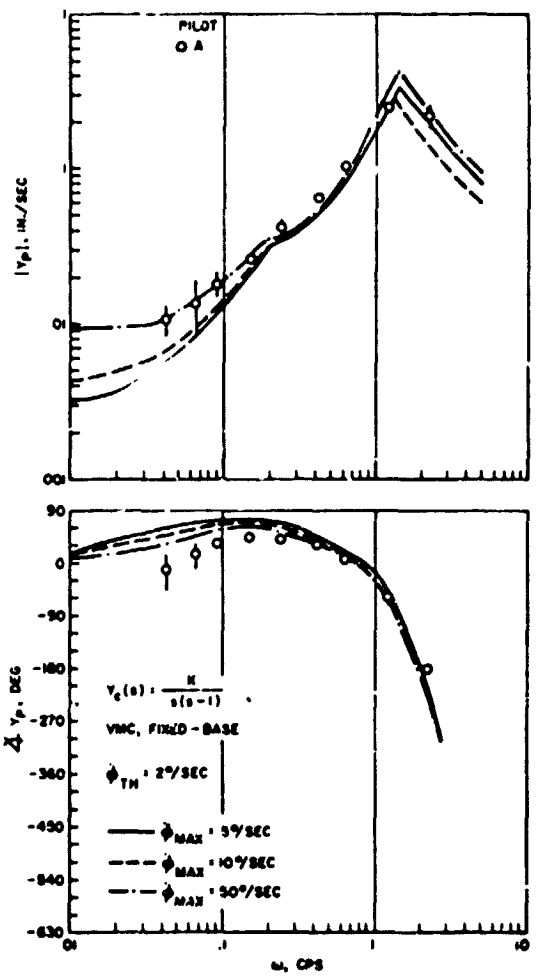

Figure 5. Effect of Attitude Rate Cost Weighting on Pilot Describing Function (Reference 7).

References

1. McRuer, D. T.; and Krendell, E. S.: Mathematical Models of Human Pilot Behavior. AGARDograph No. AG-188, January 1974.

2. Kleinman, D. L.; Baron, S.; and Levison, W. H.: A Control Theoretic Approach to Manual Vehicle Systems Analysis. IEEE Transactions on Automatic Control, AC-16, December 1971.

3. Stapleford, R. L.; Peters, R. A.; and Alex, F. R.: Experiments and a Model for Pilot Dynamics with Visual and Motion Inputs. NASA CR-1325, May 1969.

4. Dillow, J. D.; Picha, D. G.; and Anderson, R. O.: Study Weightings for the Optimal Pilot Model. Proceedings of the Eleventh Annual Conference on Manual Control, NASA TM X-62,464, May 1975.

5. Shirley, R. S.: Motion Cues in Man-Vehicle Control. Ph.D. Dissertation, Massachusetts Institute of Technology, Department of Aeronautics and Astronautics, January 1967.

6. Ringland, R. F.; Stapleford, R. L.; and Magdaleno, R. E.: Motion Effects on an IFR Hovering Task - Analytical Predictions and Experimental Results. NASA CR-1933, November 1971.

7. Newell, F. D.; and Smith, H. J.: Human Transfer Characteristics in Flight and Ground Simulation for a Roll Tracking Task. NASA TN D-3007, February 1969.

8. Ormsby, C. C.: Model of Human Dynamics Orientation. NASA CR-132537, January 1974.

THE EVALUATION OF PERIPHERAL DISPLAY UNITS IN A FIXED BASE SIMULATOR

by Lloyd D. Reid and Andrew J. Fraser

University of Toronto
Institute for Aerospace Studies

SUMMARY

As part of the design of a fixed base hovercraft simulator a peripheral display unit has been constructed. This unit operates in conjunction with a central computer generated perspective view of a roadway lined with poles and a horizon line. The peripheral display is controlled by the computer in such a manner as to duplicate the passage of the poles through the pilot's peripheral field of view.

In order to assess the effectiveness of the peripheral display, an automobile simulation was implemented and a tracking task carried out. The observed improvement in tracking performance with the displays operating was found to be statistically significant. In addition, subjective comments from those involved in the test program indicated that the peripheral displays added much to the realism of the simulation.

INTRODUCTION

The present display development has been undertaken as part of a program at our Institute to study air cushion vehicle technology. My interest is in putting together a fixed base simulator capable of performing useful air cushion vehicle control studies. In particular we intend to investigate the control of air cushion vehicles of modest size during cruise conditions when operated over restricted pathways. Such situations arise in river or overland applications in the Canadian North.

GENERAL SYSTEM DETAILS

In order to achieve a suitable simulation of this task it is necessary to develop a display incorporating the essential visual cues. Based on a limited budget it was felt that this could best be achieved by using our mini-computer to generate a CRT display. The system is based on an HP 2100 driving an electronic X-Y plotter with an 20 x 28 cm CRT through a high speed 8 bit digital-to-analog converter. This results in a 256 x 256 dot matrix display. A TR-48 analog computer is used to simulate the vehicle

equations of motion.

The work station was configured with suitable vehicle controls. It was decided to augment the central display with a peripheral display in order to provide additional velocity cues and added realism.

CENTRAL DISPLAY

The format of the central display was selected to represent a straight pathway lined with marker poles. See Figure 1. This is a view, in perspective, of the scene as observed out the front cab window. The sides of the pathway provide lateral position cues, the poles provide velocity cues, and the vanishing point heading cues. A horizon line completes the picture and provides pitch and roll attitude cues. The amount of detail must be restricted to allow the mini-computer to maintain a display update rate sufficient to achieve smooth display motion. The present system is updated with a newly computed picture at a rate of 25 per second.

Figure 2 represents the display with non-zero vehicle attitude variables.

PERIPHERAL DISPLAY

The peripheral display units are located on either side of the central display. See Figure 3. As a pole leaves the central display it is picked up on the peripheral display at the appropriate time and, under mini-computer control, traverses the display screen. The correct angular position of the pole in the field of view is achieved through suitable software. The total field of view of the display is 170 when the viewer's eyes are 18 in. from the central display.

The mechanical features of the peripheral display units are shown in Figure 4. The front face of the unit is a translucent plexiglass screen. A single pole is projected on to the rear of the screen by using a vertical line light source. Motion of the pole is achieved by employing a galvanometer mounted mirror. The galvanometer deflection is controlled by a 12 bit high speed digital-to-analog converter that is part of the mini-computer system. The left and right hand units are under independent computer control. The poles can move, if required, either forward or backward since the system is based on position information. Each unit, however, is restricted to the display of a single pole. If a situation arises where two poles lie in the field of view represented by a single peripheral display unit then only the pole closest to the central CRT is displayed.

When a pole leaves the peripheral display the light beam is parked out of sight at the front end of the unit by driving the galvanometer at its maximum rate to this position. No detectable light beam motion results from this flyback operation. An alternative to this approach, namely the use of a shutter to blank the light source, was deemed to be too complex and unnecessary.

DISPLAY EVALUATION

In order to evaluate the display it was first necessary to simulate some vehicle on the analog computer. Because the equations of motion for the air cushion vehicle were not yet available it was decided to simulate a car driving task. See Figure 5. This also simplified the job of finding qualified operators at this stage in the program. The equations of motion employed represent a standard North American sedan travelling at 30 mph (reference 1). A steering ratio of 20:1 was employed along with a 3° steering wheel deadband.

A task distrubance signal was incorporated in the form of a road wheel angle perturbation. This signal was made up of a sum of 4 sine waves with frequencies between 0.5 and 6.28 rad./sec. The dc level was zero and the rms corresponded to 3.25° of steering wheel angle. The diagram of Figure 6 represents the analog computer implementation of this system. (Note that Yr has been dropped from the equations because V >> Yr.)

During the tests 3 display configurations were evaluated:

Mode A: full central display and peripheral units.
Mode B: full central display without peripheral units.
Mode C: partial central display (poles absent) without peripheral units.

In the case of the latter (Mode C) no forward motion cues are present.

Over a period of several days, 3 subjects underwent a series of sessions in the simulator lasting about 45 min. each. The first few sessions were used for training, while the last three formed the data base for the experimental test results. The number of training sessions per subject was adjusted to ensure that each individual's learning curve had flattened out.

TEST RESULTS

Typical tracking records are shown in Figure 7. Here δ_d is the road wheel disturbance signal, α_s is the steering wheel position, ψ is the

heading angle and T_y is lateral displacement from the center of the road. The task was to drive down a straight road in the presence of the disturbance signal. The car's speed was maintained at 30 mph by the computer. Tracking score was measured as the standard deviation of lateral position. After the training period and after the last test session, the subjects were questioned about their impressions of the simulator, and suggestions for improvements were invited.

Figure 8 gives the tracking scores achieved by the subjects based on 6 replicates per data point. The average of the scores achieved by all 3 subjects shows a 9% improvement in going from Mode B to A and a 14% improvement in going from Mode C to A. An analysis of variance performed on these data indicated that display mode effects were significant at the 5% level.

The following observations were made concerning the present simulation: An initial tendency to fixate on the motion of the vanishing point to the exclusion of road side line cues resulted in inadvertent control reversal, which was most pronounced (and persistent) in the Mode C display with its lack of forward motion cues. With training, subjects found they used an aiming point 60 to 90m down the road and were then better able to utilize the display. During Mode C tests subjects stated that they lost all realism, and felt they were merely controlling an instrument. In general they felt that the motion cues provided by the poles on the central display were essential to the simulation and that the peripheral displays enhanced their ability to interpret the display as a real world situation.

CONCLUSION

Use of peripheral displays to complement the motion depicted on a small two dimensional screen creates a more compelling simulation of the real world. Human operator performance improves under [illegible] conditions and they are more easily able to project into the task. [illegible] effect, the use of peripheral displays can generate a larger simulator display without greatly increasing system complexity.

(Further details concerning this project are contained in reference 2).

REFERENCES

1. Allen, R.W.; Jex, H.R.; McRuer, D.T.; and Di Marco, R.J.: Alcohol Effects on Driving Behaviour and Performance in a Car Simulator. IEEE Transactions on Systems, Man, and Cybernetics, Vol. SMC-5, No. 5, September 1975, pp. 498-505.

2. Fraser, A.J.: Development and Testing of a Fixed-Base Hovercraft Simulator. UTIAS Tech. Note. No. 197, December 1975.

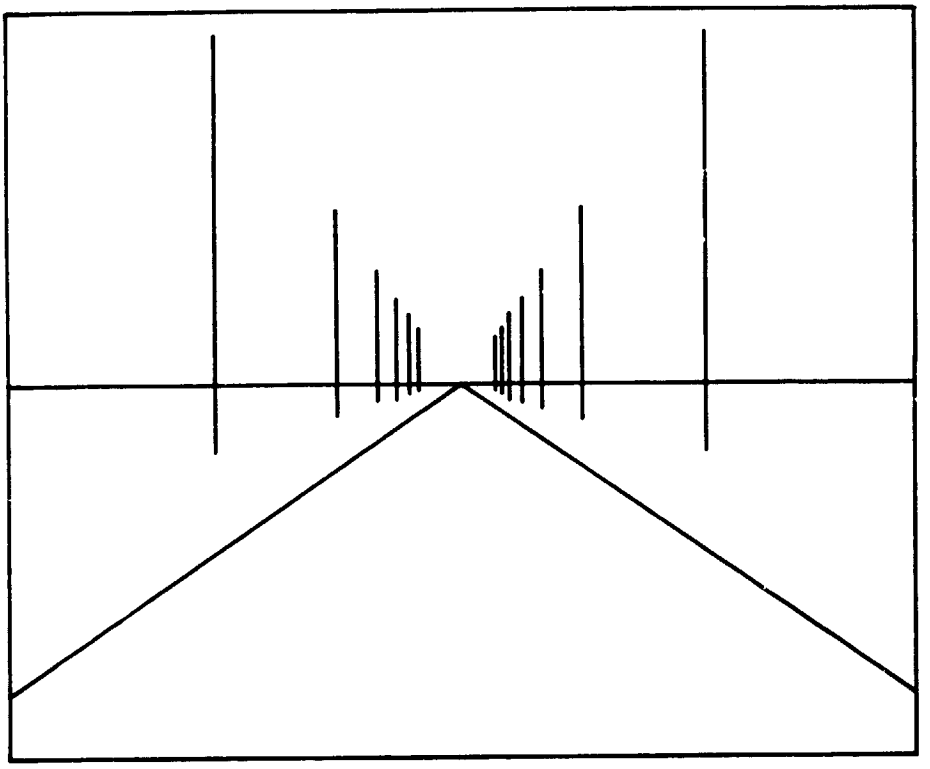

$\phi = 0$
$\theta = 0$
$\psi = 0$
$T_y = 0$

SIMULATION CONSTANTS

Pathway width	12 ft.
Distance-edge of road to pole	9 ft.
Distance to furthest pole	700 ft.
Distance between poles	100 ft.
Height of poles	25 ft.
Eye level	4 ft.

FIGURE 1

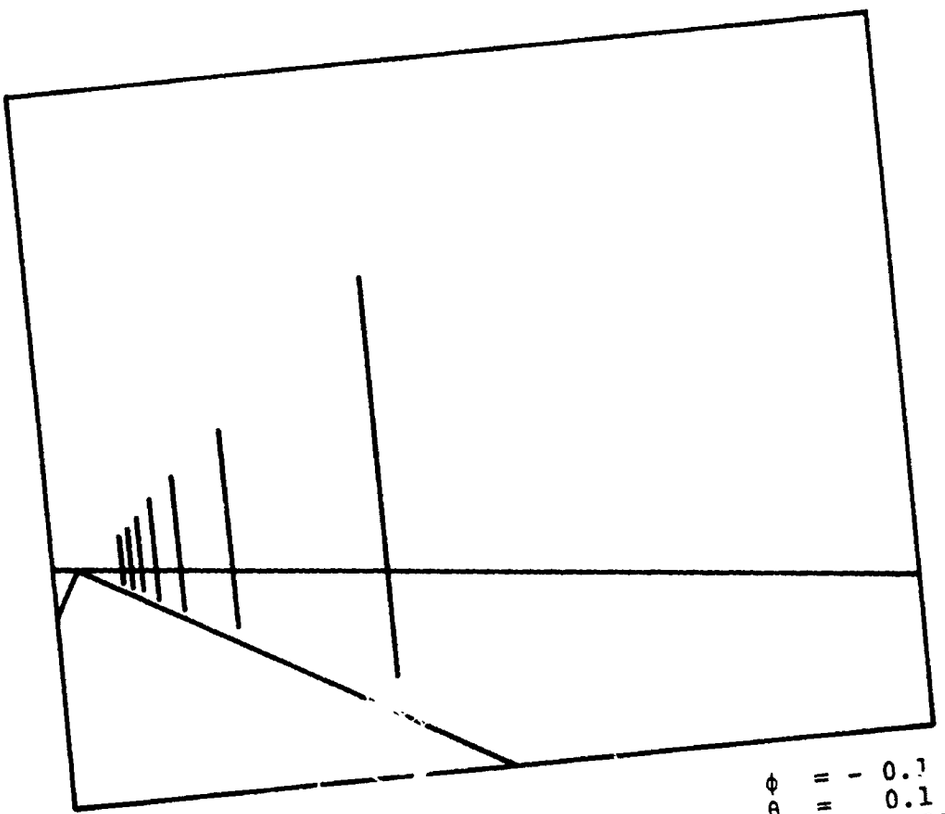

ϕ = - 0.1 rad.
θ = 0.1 rad
ψ = 0.25 rad.
T_y = - 4.0 ft.

SIMULATION CONSTANTS

Pathway width	12 ft.
Distance-edge of road to pole	9 ft.
Distance to furthest pole	700 ft.
Distance between poles	100 ft.
Height of poles	25 ft.
Eye level	4 ft.

FIGURE 2

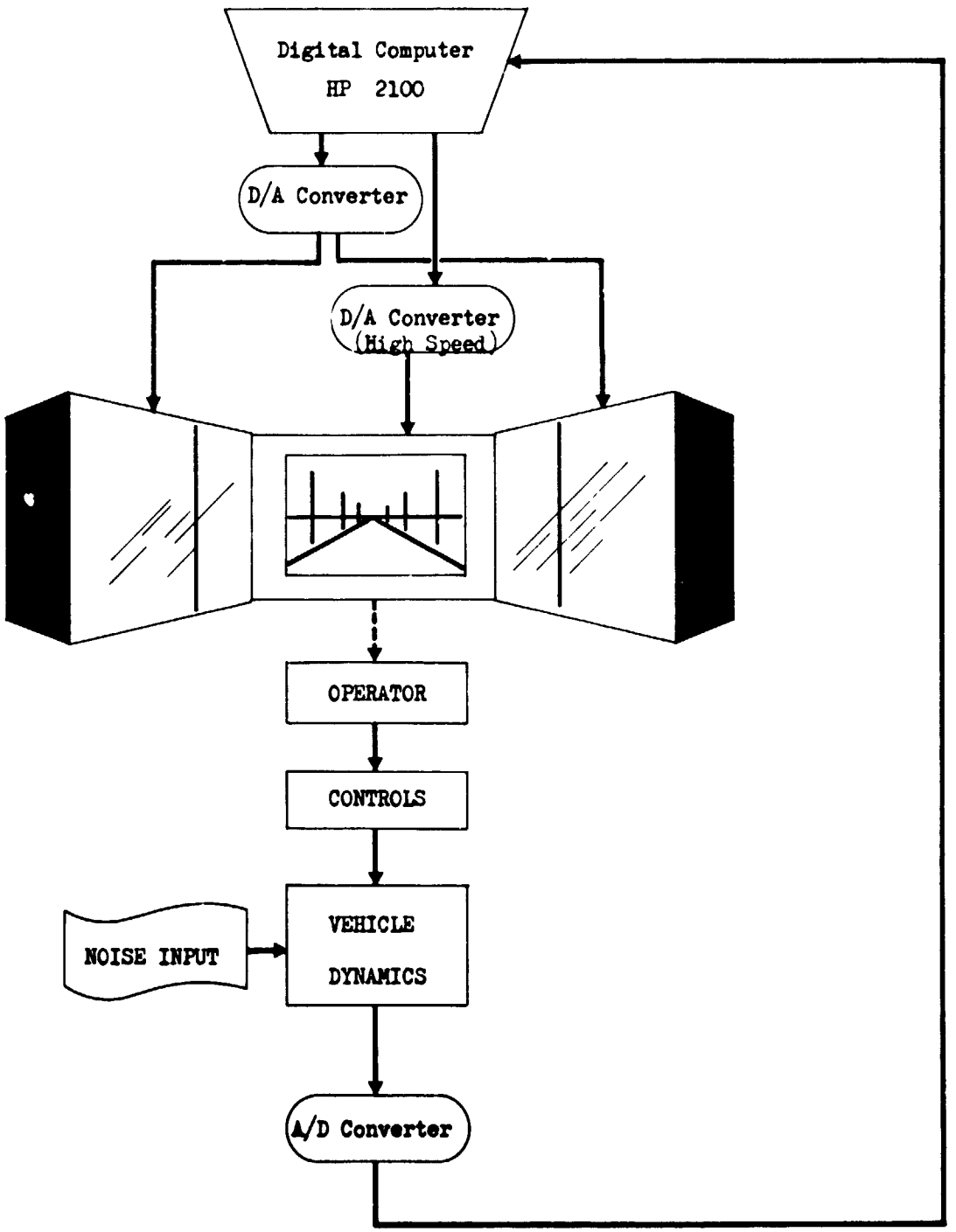

Simulation Control Flow

FIGURE 3

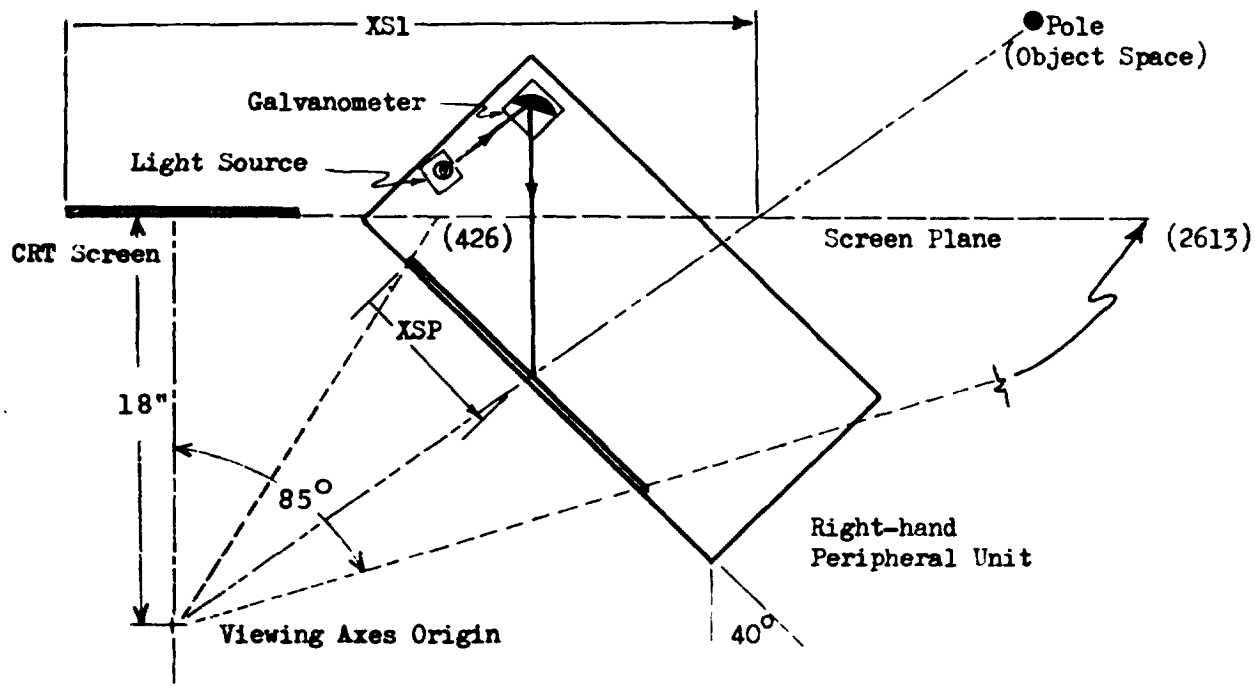
XS1
Pole
(Object Space)
Galvanometer
Light Source
CRT Screen
(426)
Screen Plane
(2613)
XSP
18"
85°
Right-hand
Peripheral Unit
Viewing Axes Origin
40°

FIGURE 4

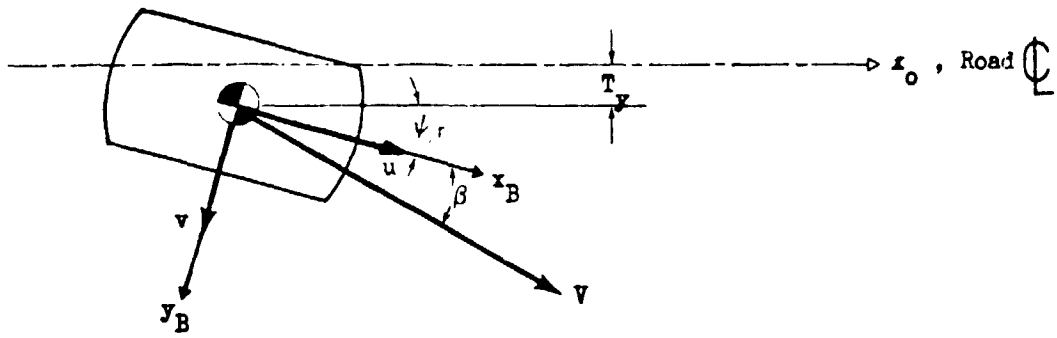

Automobile Motion Vectors

$$\begin{bmatrix} s - Y_v & V - Y_r \\ -N_v & s - N_r \end{bmatrix} \begin{bmatrix} v \\ r \end{bmatrix} = \begin{bmatrix} Y_\delta \\ N_\delta \end{bmatrix} \delta$$

Automobile Lateral-Directional Matrix

$$G_\delta^{T_y} = \frac{90.9(s^2 + 2(.36)(7.6)s + 7.6^2)}{s^2(s^2 + 2(.94)(5.6)s + 5.6^2)}$$

$$G_\delta^{\psi} = \frac{19.5(s + 6.1)}{s\,(s^2 + 2(.94)(5.6)s + 5.6^2)}$$

Automobile Transfer Functions

Vehicle:	North American Sedan
Speed	44 fps
Y_δ	90.9 ft/sec^2 - rad
Y_v	-5.6 sec^{-1}
Y_r	2.87 ft/sec - rad
N_δ	19.5 sec^{-2}
N_v	0.094 rad/ft - sec
N_r	-4.86 sec^{-1}

Automobile Dynamic Parameters

FIGURE 5

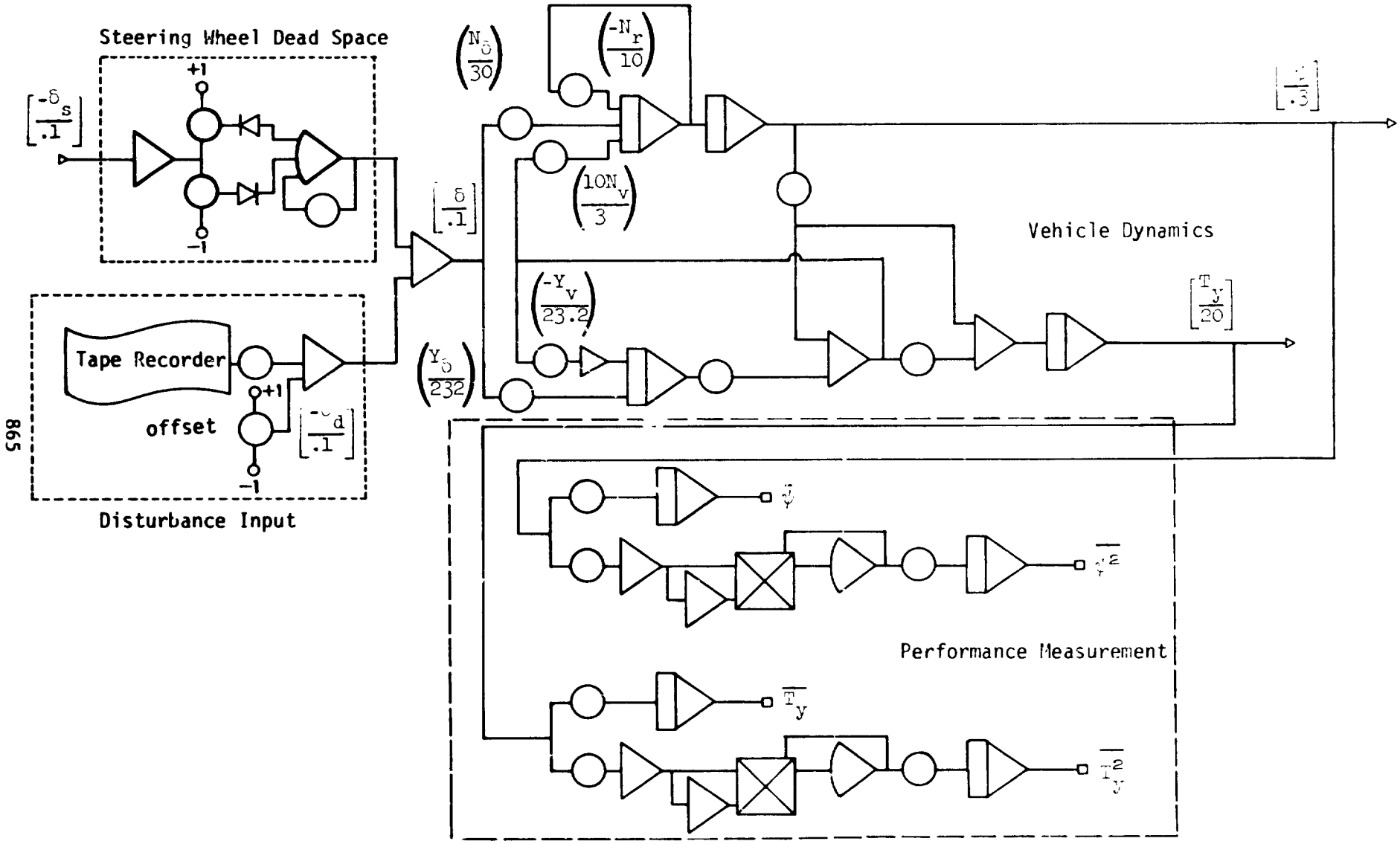

AUTOMOBILE SIMULATION ANALOGUE PROGRAMMING

FIGURE 6

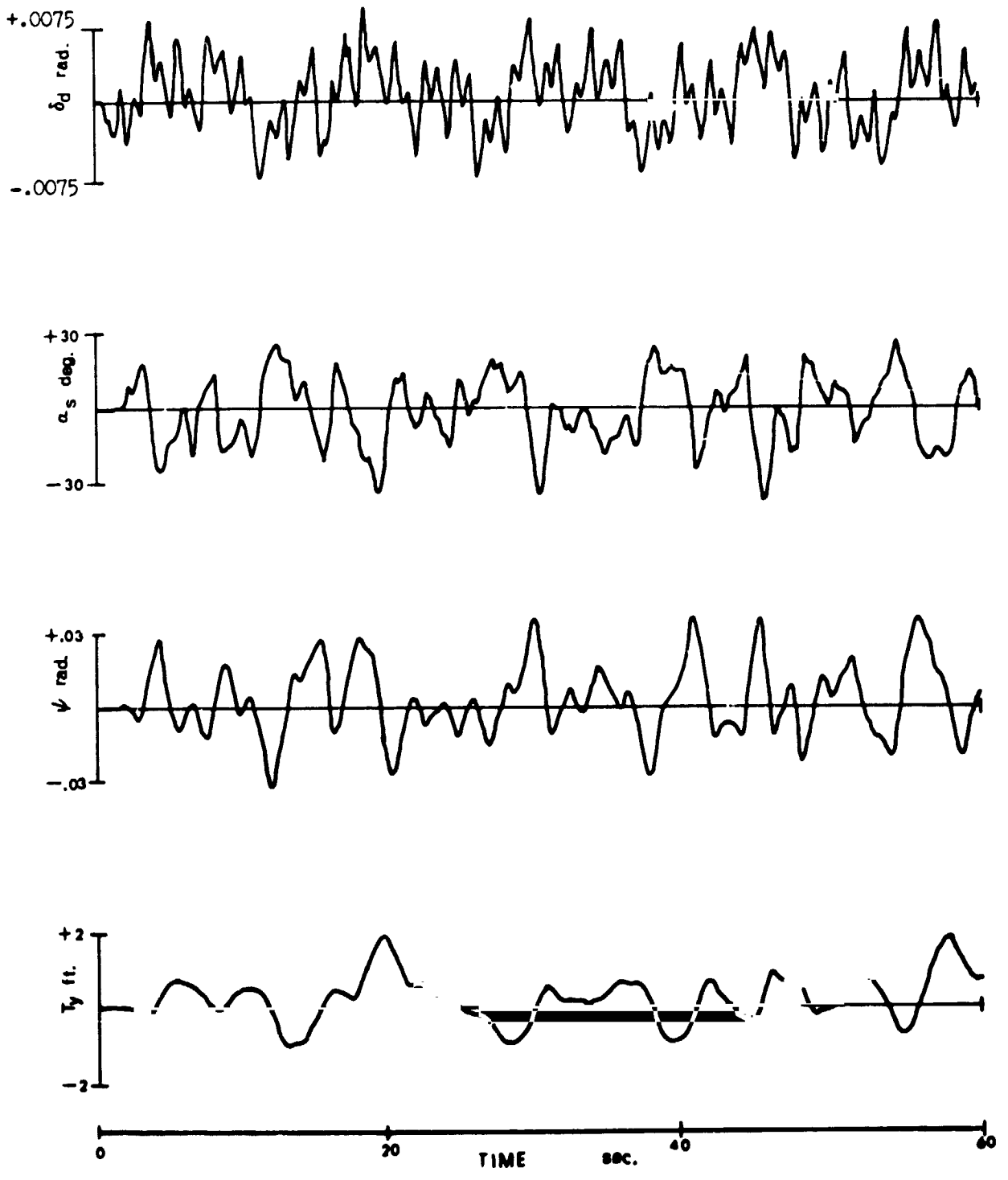

Time Trace of Subject Performance

FIGURE 7

□ MODE A: FULL CENTRAL DISPLAY AND PERIPHERAL UNITS.
○ MODE B: FULL CENTRAL DISPLAY WITHOUT PERIPHERAL UNITS.
▽ MODE C: PARTIAL CENTRAL DISPLAY (POLES ABSENT) WITHOUT PERIPHERAL UNITS.

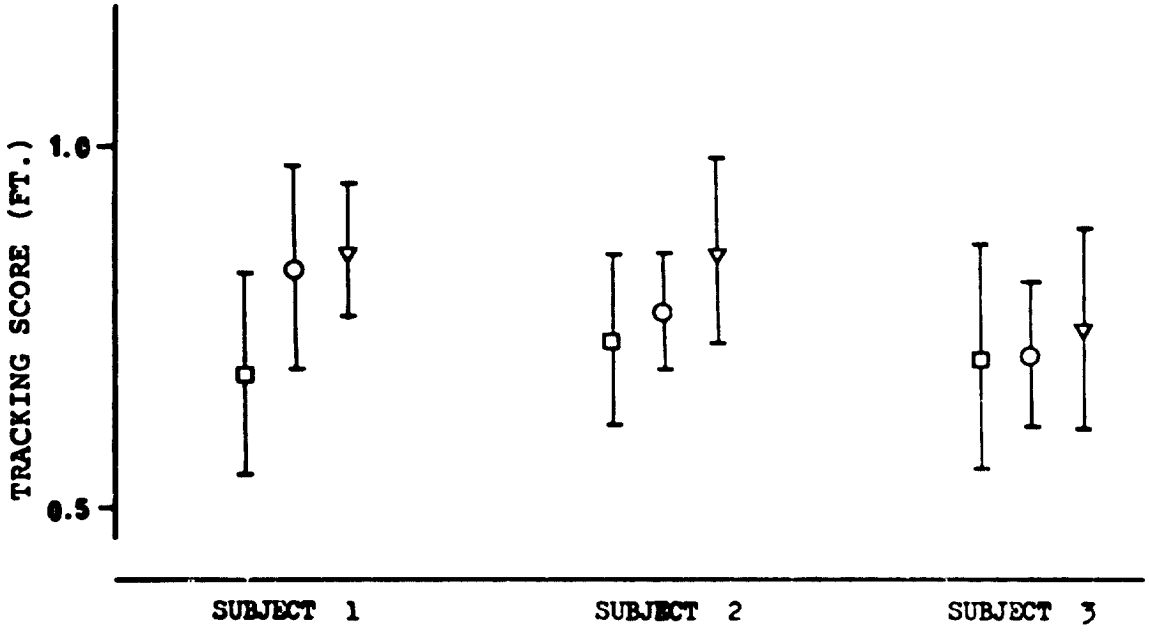

Mean Performance Scores by Subject & Mode
(Bars Indicate Standard Deviation)

FIGURE 8

ROLL AXIS TRACKING IMPROVEMENT RESULTING FROM PERIPHERAL VISION MOTION CUES

Thomas E. Moriarty, Air Force Institute of Technology
Andrew M. Junker, Aerospace Medical Research Laboratory
Don R. Price, Aeronautical Systems Division

SUMMARY

Subjects performed a compensatory roll-axis tracking task, with and without peripheral vision motion cues. Controlled vehicle dynamics, of the general forms K/S^2 and K/S^3, were simulated on an analog computer. Control was commanded via a force stick in a stationary cockpit mockup. Plant roll rate, in the form of vertically moving black and white grid lines, was displayed on television screens positioned on either side of the cockpit. The target aircraft's motion was simulated by a sum-of-sines input forcing function.

Roll axis tracking performance is shown to improve marginally stable plants of the general form K/S^3, when peripheral plant roll rate information is provided. Subject-controlled plant describing functions are compared for both plants, with and without the peripheral motion cues. Subject describing functions are also compared. The tracking error spectra are broken into correlated and remnant contributions, and are compared for all four conditions.

INTRODUCTION

In the last ten years, research has been performed which indicates that peripheral vision cues might be used to assist in accomplishing manual control tasks (Ref 1, 2, 3). This is particularly attractive from the viewpoint of allowing the human controller to have additional information without increasing the complexity of his foveal display. Another motivating factor for research into peripheral vision cues is the possibility of substituting, at least in part, peripheral vision displays for actual moving base capabilities in simulation.

The Aerospace Medical Research Laboratory at Wright-Patterson AFB, Ohio is presently engaged in a long term study of the effects of motion on the human operator, including the effects of both peripheral vision motion cues and actual moving base cues for roll-axis tracking tasks. This experimental study, performed by personnel at the Air Force Institute of Technology at Wright-Patterson AFB, is in support of the laboratory's overall effort and addresses the specific question of whether a stationary operator's performance of roll-axis compensatory tracking is improved when controlled plant roll

rate, in the form of vertically moving black and white grid lines, is displayed in the human operator's field of vision. Implicit in this study is an analysis of the operator's control strategy and performance characteristics.

LIST OF SYMBOLS

Y_c - controlled plant transfer function
Y_s - subject describing function
Φ_m - phase margin
Φ_{ee_c} - correlated error power spectrum
Φ_{ee_r} - remnant error power spectrum
ω_c - system gain crossover frequency

EXPERIMENT DESCRIPTIONS

Subjects were given a roll axis tracking task in a fixed-base simulation shown schematically in Figure 1. In particular, the subjects were asked to follow a target aircraft in the roll axis by minimizing the centrally displayed angular error. The task was accomplished both with and without peripheral display units which provided the subject with the plant roll rate.

Controlled Plant Dynamics. Two different controlled plants were used in the experiment. The choice of plant dynamics permitted a comparison of peripheral vision motion cue effects on human operator control strategy for different levels of task difficulty. The "easy" plant had a transfer function of

$$G(s) = \frac{135}{s(s+1)(s+10)}$$

and was considered to be an easy plant to control ($\sim \frac{K}{s^2}$). The "difficult" plant was designed to be more difficult to control ($\sim \frac{K}{s^3}$) and consisted of

$$G(s) = \frac{63.75}{s^2(s+0.5)(s+10)}$$

Figures 2 and 3 show the frequency responses of the easy and difficult plants respectively. The characteristics were similar to two of the plants used in a motion effects study performed by Junker and Replogle (Ref 4:819-822).

Sum-of-Sines Tracking Input. A different sum-of-sines input signal was used with each of the two controlled plants. The input for the easy plant was the sum of 12 sinusoidal components with a bandwidth of 1.25 radians/sec and a 20 degree RMS amplitude, and is shown on Figure 2. For the difficult

plant, the 12 components had a bandwidth of 0.5 radians/sec and an RMS amplitude of 40 degrees. Figure 3 shows the input power spectrum for the difficult plant. Table 1 contains a list of the twelve input frequencies.

Table 1

Input Forcing Function Frequencies (rad/sec)

$\omega_1 = 0.077$	$\omega_7 = 1.572$
$\omega_2 = 0.192$	$\omega_8 = 2.378$
$\omega_3 = 0.307$	$\omega_9 = 3.567$
$\omega_4 = 0.460$	$\omega_{10} = 5.369$
$\omega_5 = 0.690$	$\omega_{11} = 8.053$
$\omega_6 = 1.035$	$\omega_{12} = 12.080$

EQUIPMENT & FACILITIES

The controlled plant dynamics were simulated on analog computers which accepted inputs from a side-mounted force stick and produced output signals to drive the central and peripheral display units. A digital computer was used to generate the sum-of-sines input forcing function, and was also used for data collection and frequency analysis computations. The subject was seated in a stationary fighter-type cockpit mockup which was, in turn, in an isolated room with a low light level. The central and peripheral displays were positioned as shown in Figure 4.

Central (Foveal) Display. The foveal display was presented on a 12½ in by 12½ in square area of a television monitor. The inside-out display consisted of a 1 7/8 in long rotating line whose center was superimposed upon a stationary horizontal line, as shown in Figure 5. Upright orientation was provided by a 1/8 in perpendicular line at the center of the rotating line. The angle between the rotating and stationary lines, Φ_e, depicted the difference between the controlled plant roll angle and the forcing function roll angle.

Peripheral Display. The peripheral display was presented on two 21 inch televisions placed on opposite sides of the cockpit mockup as shown in Figure 4. The two television screens were vertically located such that their midpoints were within 1½ degrees of subject eye level. The horizontal position of the screens was such that the peripheral viewing field went from 40 degrees nasal to 90 degrees nasal.

The peripheral display presented plant roll rate in the form of vertically moving alternate black and white bars 2 3/4 in wide. The bar motion was scaled such that

$$V_p = 16.5\ \omega$$

where V_p was the display pattern vertical velocity in in/sec and ω is the instantaneous plant roll rate in rad/sec. The distance between the centerline of the foveal display and each peripheral display is 16.5 in. Polarity was such that the motion of the lines represented the apparent background motion that would result from cockpit motion.

EXPERIMENTAL PROCEDURE

Four experimental conditions were experienced by each subject. The subjects were divided into two groups, denoted as "morning" and "afternoon" and then briefed on the experimental task. The three subjects in the morning group first experienced the "easy" plant without peripheral display; and daily replications were accomplished until the RMS error scores indicated that the subjects had reached a sustained level of task proficiency. After the subjects had "learned" the task, signals were recorded for subsequent analysis. The peripheral display was then added and the morning subjects performed the task until learning had been achieved and data could be recorded. The afternoon group of three subjects performed the same tasks but were exposed first to the easy plant with peripheral display and then to the task without the peripheral units.

The experimental procedure for the "difficult" plant was changed somewhat due to subject limitations. The number of subjects was reduced by one and they were combined into one group. In an attempt to insure that separate control strategies could be developed without biasing, each subject experienced alternating tasks of one run with peripheral followed by one run without the peripheral display.

Data Recording

RMS error scores were computed from digitized data for each subject and each run. Once the RMS error scores indicated that the subjects of an experimental group had "learned" the tracking task for a given experimental condition, time histories were digitized and recorded for use in analyzing subject control strategy. The time histories from the last 4 replicates for each subject in each condition consisted of input forcing function, error, stick, and controlled plant output signals.

DATA ANALYSIS

A Fast Fourier Transform (FFT) technique was used to convert the raw digital data into useful performance measures. Power spectral densities were generated for both correlated and remnant components of the input, error, stick (subject) and plant signals. Transfer characteristics (describing functions) were calculated for the subject and the subject-plant combination.

The analysis methods used in this study are based upon those presented in Ref 5, and will be briefly summarized here.

For a 12 component sum-of-sines input, correlated power can only exist at the twelve nominal input frequencies. Thus, any power observed at non-input frequencies is directly identifiable as remnant under the usual definition (Ref 6, 7, 8). For each recorded experiment run, the remnant power was calculated at the FFT frequencies (base frequency ω_o = 0.038 rad/sec) over a frequency band encompassing 0.125 octaves on either side of, but not including, each nominal frequency. Correlated power at the nominal frequency was then computed as the difference between the total power at the nominal and the average remnant in the corresponding band.

The experimental results were combined by groups for presentation and the statistical significance of apparent group mean data was determined by means of a small sample t-test (Ref 9). The group means along with an indication of plus-or-minus one standard deviation were used for graphical presentation.

RESULTS AND CONCLUSIONS

The results and conclusions are presented with emphasis upon determining if the peripheral motion cues improved subject performance in the compensatory tracking task and, when performance was improved, determining how the peripheral cues were used. Overall subject performance is presented first, using RMS error scores of the tracking task as the performance metric Analysis of subject control strategy follows and is performed in the frequency domain.

RMS Tracking Error

Figures 6 and 7 show the group RMS tracking error scores for the "easy" and "difficult" tasks respectively. The means (indicated by circles) and standard deviations are plotted by day for each of the two experimental conditions encountered for each plant.

The morning groups performance for the easy plant is not shown because a circuit malfunction in the analog computer plant simulation made it difficult to validly compare the peripheral to nonperipheral condition tracking

error scores.

The afternoon group "easy" plant tracking error, shown in Figure 6, indicates that after learning has occured there is little improvement to be obtained by providing peripheral roll rate information. Applying a t-test to the last four runs with peripheral and the last four runs without peripheral resulted in no significant difference between the population samples (< 0.6 level).

The "difficult" plant results, shown in Figure 6, show that the use of the peripheral plant roll rate display yields a significant (> 0.001 level) reduction in the RMS tracking error.

It can thus be concluded that for more difficult plants (K/s^2-type controlled plant dynamics) roll-axis tracking performance of a static human controller is significantly improved when plant roll rate information, in the form of vertically moving black and white horizontal grid lines, is displayed in the peripheral field of vision. Tracking performance is not significantly improved by displaying plant roll rate in the human operator's peripheral field of vision when the controlled plant is stable with control dynamics of the form K/s^2.

Frequency Domain Analysis

Frequency domain data and analysis of the tracking task results are presented separately for the two controlled plants with the "easy" plant results treated first. In order to assess the effect of the peripheral display upon the correlated portion of the subject's response, the group mean subject-controlled plant describing functions ($Y_s Y_c$) are compared for the two conditions of with and without peripheral displays. The group mean subject describing functions (Y_s) are then compared and finally the associated error signal power spectra (Φ_{ee_c} and Φ_{ee_r}) are examined. All data plots depict group mean values in circles with an indication of plus or minus one standard deviation.

"Easy" Plant. Figures 8 and 9 show the $Y_s Y_c$ describing function for the two conditions of with peripheral display and without peripheral display respectively. A visual comparison of the two describing functions yields little noticeable difference and since Y_c is constant over the two conditions, the subject describing function Y_s should yield a more direct indication of different control strategies. Figures 10 and 11 are plots of the group mean describing functions without and with the peripheral roll rate display. The Y_s data agrees with the Y_s characteristics implied by the $Y_s Y_c$ describing functions. The Y_s data points which differ the greatest in value fo the two experimental conditions were at $\omega = 1.035$ rad/sec, the

difference was not significant at the 0.1 level. Both group Y_s describing functions exhibit similar adjustment characteristics. First order lead was applied over the measurement range through the crossover frequency, but the accompanying phase angles indicate lag/time-delay effects below the measurement range. Additional lead was applied at frequencies beyond crossover prior to the well known high frequency neuromuscular lag effects appearing between ω=5 and ω=10 rad/sec.

Easy plant group error power spectra averages are presented in Figures 12 and 13. Included on the figures are the average percentages of total error power, and one standard deviation, calculated for correlated and remnant error contributions. In both cases, the remnant error power was less than 25 percent of the total error power. Correlated error power magnitudes were relatively constant at nominal input frequencies up to slightly beyond the system crossover frequency and fell off sharply thereafter. The two correlated error spectra show no appreciably different characteristics.

The two continuous remnant power spectra were similar in waveform shape with the greatest values of remnant power occuring at the lower frequencies of the measurement band. In each case, a lower magnitude plateau is evident for a frequency band that includes the system crossover frequency, and a high frequency roll-off is observed similar to that noted for the correlated error signal.

"Difficult" Plant. Subject - controlled plant describing functions with the difficult plant as the controlled element are presented in Figures 14 and 15. The Y_sY_c describing functions differ in amplitude slope and phase angle at the lower frequencies but are strikingly similar at the higher nominal input frequencies. The crossover frequency is about ω=1.4 rad/sec in each case but the phase margin (Φ_m) is about 38 degrees with the display and about 22 degrees without the display.

Group averaged subject describing functions, Y_s, are shown in Figures 16 and 17. The Y_s describing functions indicate that considerably more low frequency lead was generated with the peripheral display present. The phase angle differences were significant at less than the .001 level for measurement frequencies $\leq$ 1.572. The describing functions both reflect a 40 db/decade slope at and somewhat above the crossover frequency with higher frequency lag effects above ω=5 rad/sec.

Figures 18 and 19 show the error power spectra without and with the peripheral display respectively. The spectra present the same general characteristics for the two conditions but they do differ in magnitude. Annotations on the figures indicate the significantly higher percentage of correlated error present when the peripheral information was available. Error correlated power is comparable for both conditions except at the frequencies near crossover where error levels for the peripheral display condition is somewhat less. Both remnant spectra are relatively flat through ω_c and roll off sharply at higher frequencies, similar to the corre-

lated power high frequency decrease. Remnant power with the peripheral display present is consistently 4 to 6 db less at frequencies below gain crossover.

CONCLUSIONS

The $Y_s Y_c$ and Y_s describing functions did not indicate any appreciable differences in subject control strategy due to peripheral display effects for the easy plant. Minor differences can be observed, but since there was no apparent improvement in tracking performance or changes in error spectra, the overall conclusion is that peripheral rate display has little effect upon the subject's roll axis tracking performance for the easy ($\sim \frac{K}{s^2}$) plant.

For the more difficult plant, the presence of peripheral rate information allowed the subjects to insert more low frequency lead. Above crossover, there were essentially no difference between the describing functions for the two conditions. The correlated error power spectra showed minor differences but the remnant contribution to total power was appreciable reduced in the peripheral display condition. The remnant power was reduced mostly in the frequency range below crossover. Thus, it can be concluded that for the difficult ($\sim \frac{K}{s}$) controlled plant, the roll-axis tracking performance of a static human controller is significantly improved when plant roll rate information, in the form of vertically moving black and white horizontal grid lines, is displayed in the peripheral field of vision.

REFERENCES

1. Vallerie, L. L. Peripheral Vision Displays. NASA CR-808. Washington: National Aeronautics and Space Administration, June 1967.

2. Rogers, J. G. "Peripheral Contrast Thresholds for Moving Images." Human Factors, 14:199-205, (June 1972).

3. Ener, E. L. A Study of Pilot Performance During a Glide-Slope Approach When Rate Information is Supplied Via the Peripheral Vision. AFIT Thesis GE/MA/74D-2, W-PAFB, Ohio: Air Force Institute of Technology, December 1974. AD A005284

4. Junker, A. and C. Replogle. "Motion Effects on the Human Operator in a Roll Axis Tracking Task." Aviation, Space, and Environmental Medicine, 46:819-822 (June 1975).

5. Levison, W. H. Techniques for Data Analysis and Input Waveform Generation for Manual Control Research. BBN Technical Memorandum CSD-75-2. Cambridge: Bolt, Beranek, and Newman, Inc., January 1975.

6. McRuer, D. T., et al. Human Pilot Dynamics in Compensatory Systems, Theory, Models, and Experiments with Controlled Elements and Forcing Function Variations. AFFDL-TR-65-15. W-PAFB, Ohio: Air Force Flight Dynamics Laboratory, July 1965.

7. Levison, W. H. and D. L. Kleinman. "A Model for Human Controller Remnant." Fourth Annual NASA-University Conference on Manual Control. 3-14, NASA SP-192. Washington: National Aeronautics and Space Administration, 1969.

8. Jex, H. R., et al. Display Format Effects on Precision Tracking Performance, Describing Functions, and Remnant. AMRL-TR-71-[illegible]. W-PAFB, Ohio: Aerospace Medical Research Laboratory, August 1972.

9. Chapanis, A. Research Techniques in Humar Engineering. Baltimore: The John Hopkins Press, 1959.

SIGNAL DEFINITIONS

Φ_i = INPUT FORCING FUNCTION (TARGET ROLL ANGLE)

Φ_e = ROLL ANGLE ERROR

$\dot{\Phi}_c$ = CONTROL STICK OUTPUT

Φ_p = PLANT ROLL ANGLE

$\dot{\Phi}_p$ = PLANT ROLL RATE

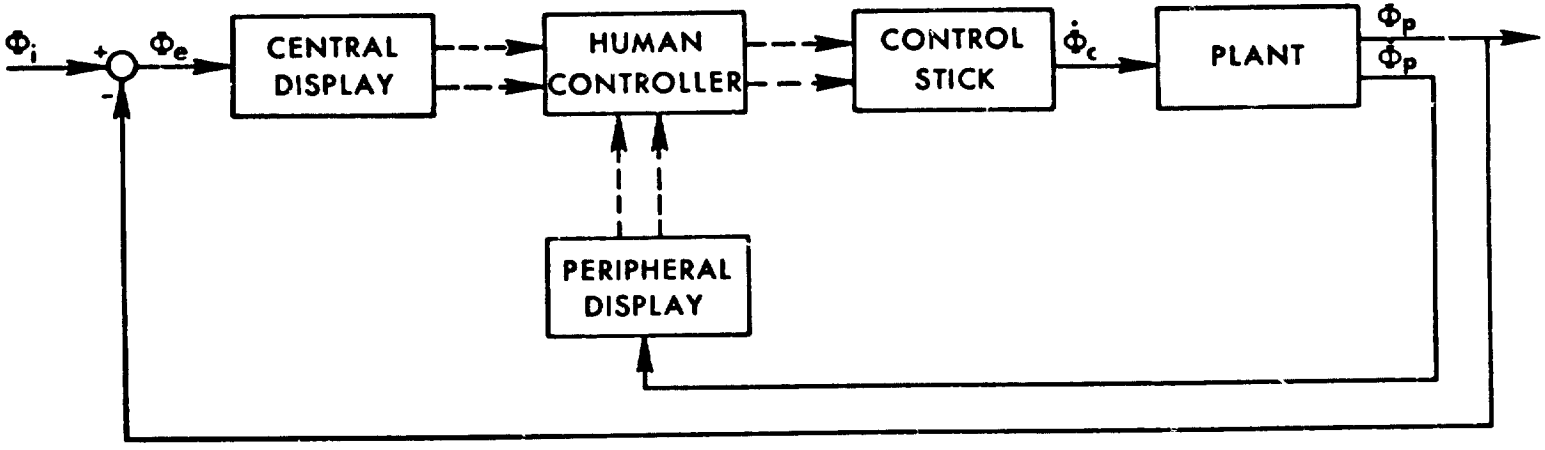

Figure 1. Simulation Block Diagram for Roll Axis Tracking Task

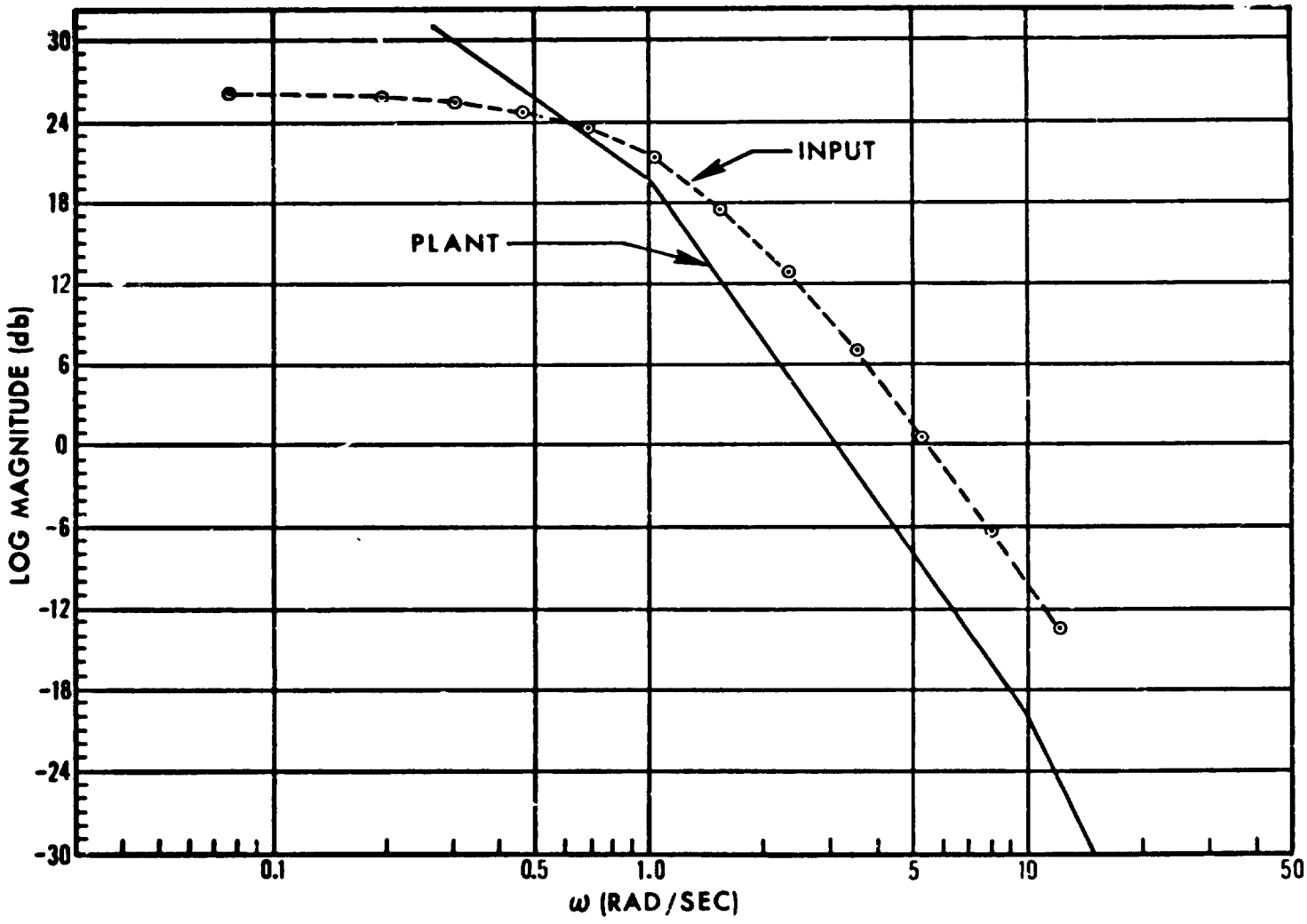

Figure 2. Easy Plant Frequency Response and Input Power Spectrum (Frequency Components Denoted by Circles)

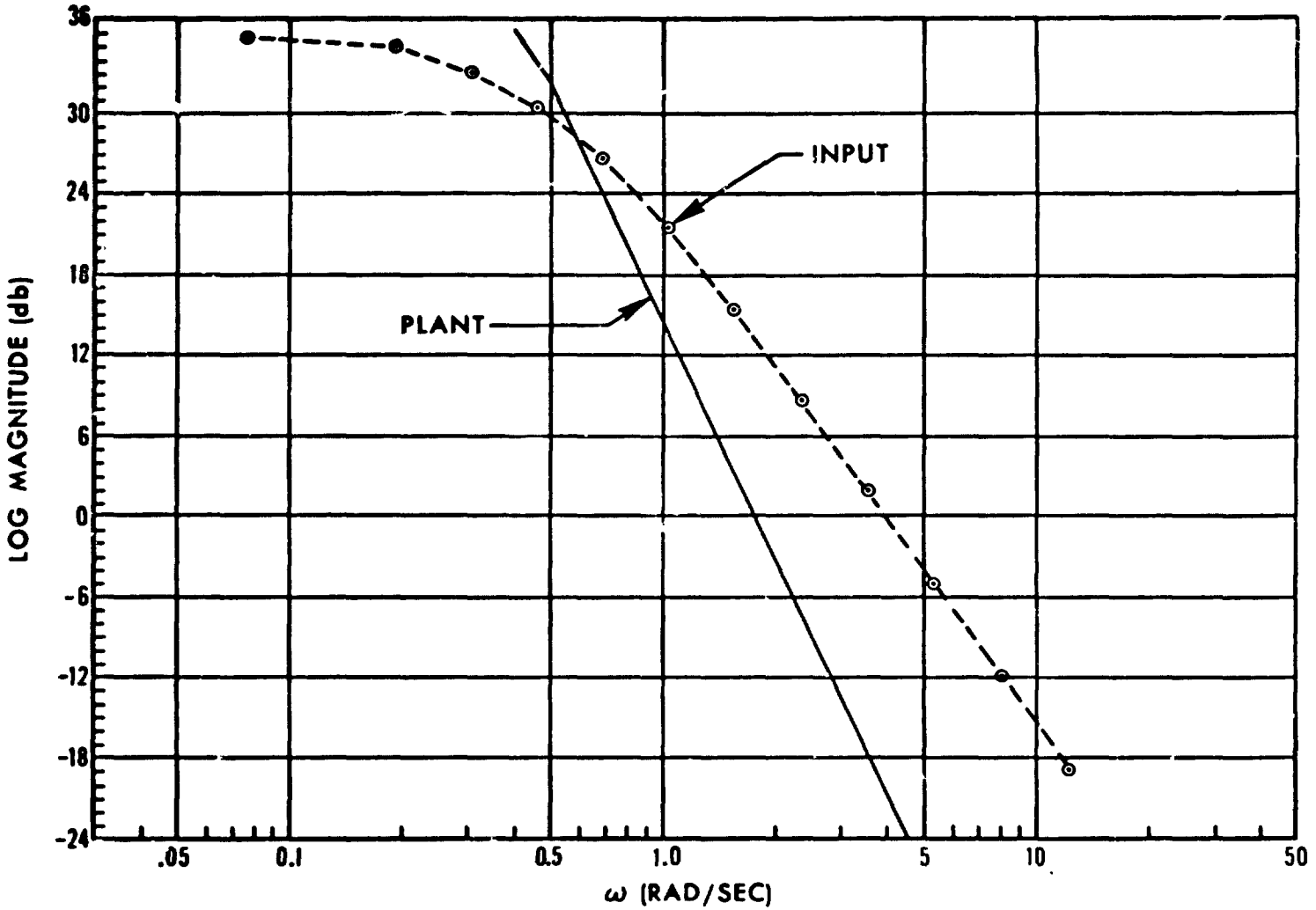

Figure 3. Difficult Plant Frequency Response and Input Power Spectrum (Frequency Components Denoted by Circles)

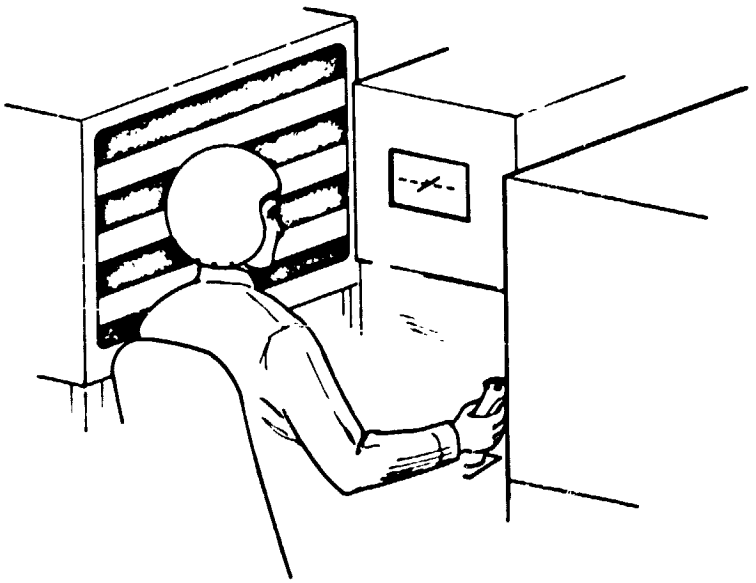

Figure 4. Display Layout

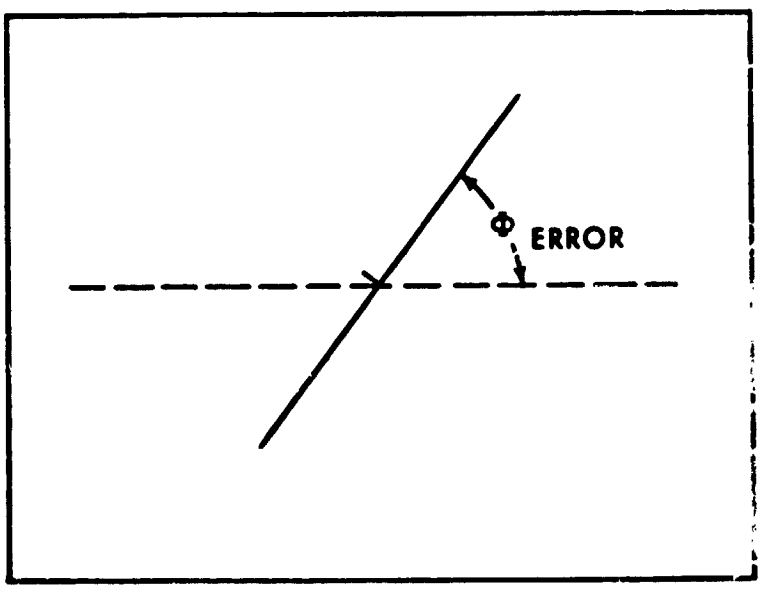

Figure 5. Central Display

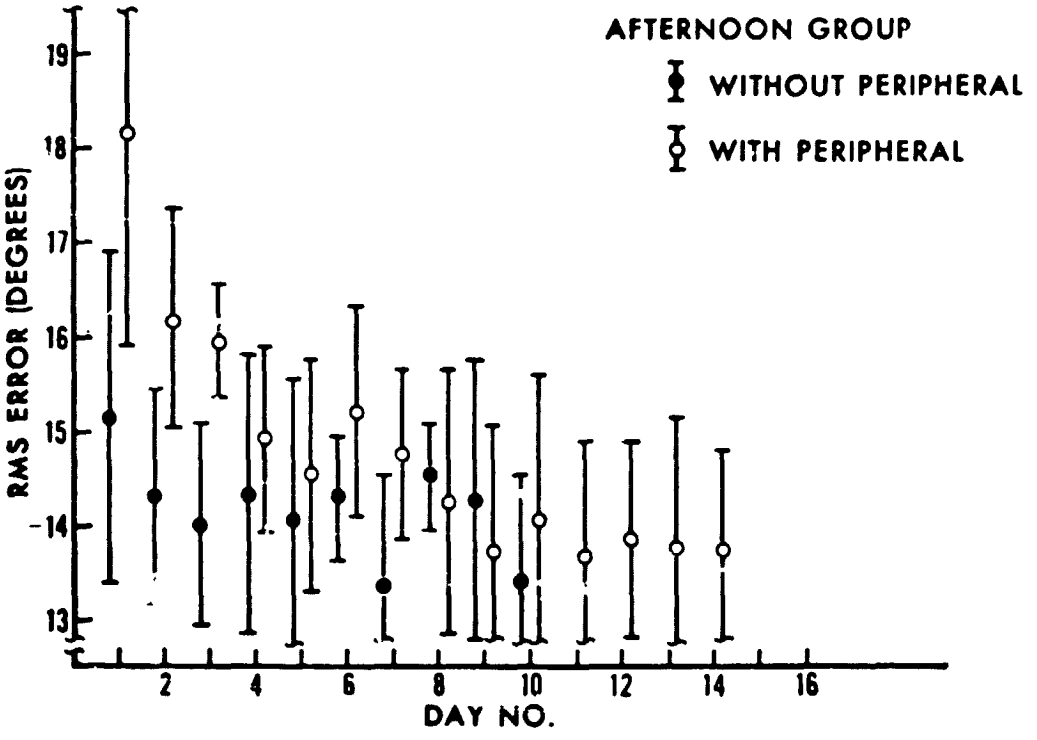

Figure 6. RMS Error Scores for Easy Plan

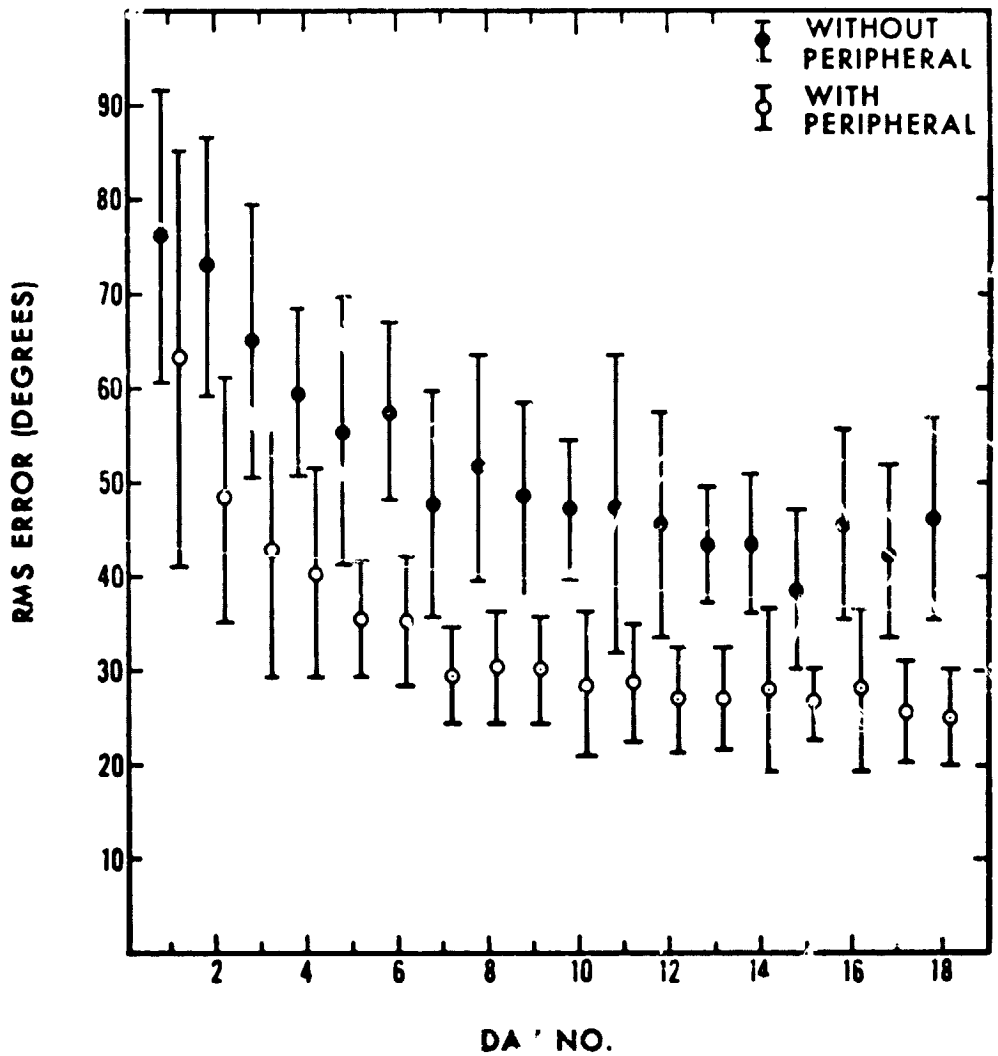

Figure 7. RMS Error Scores for Difficult Plant

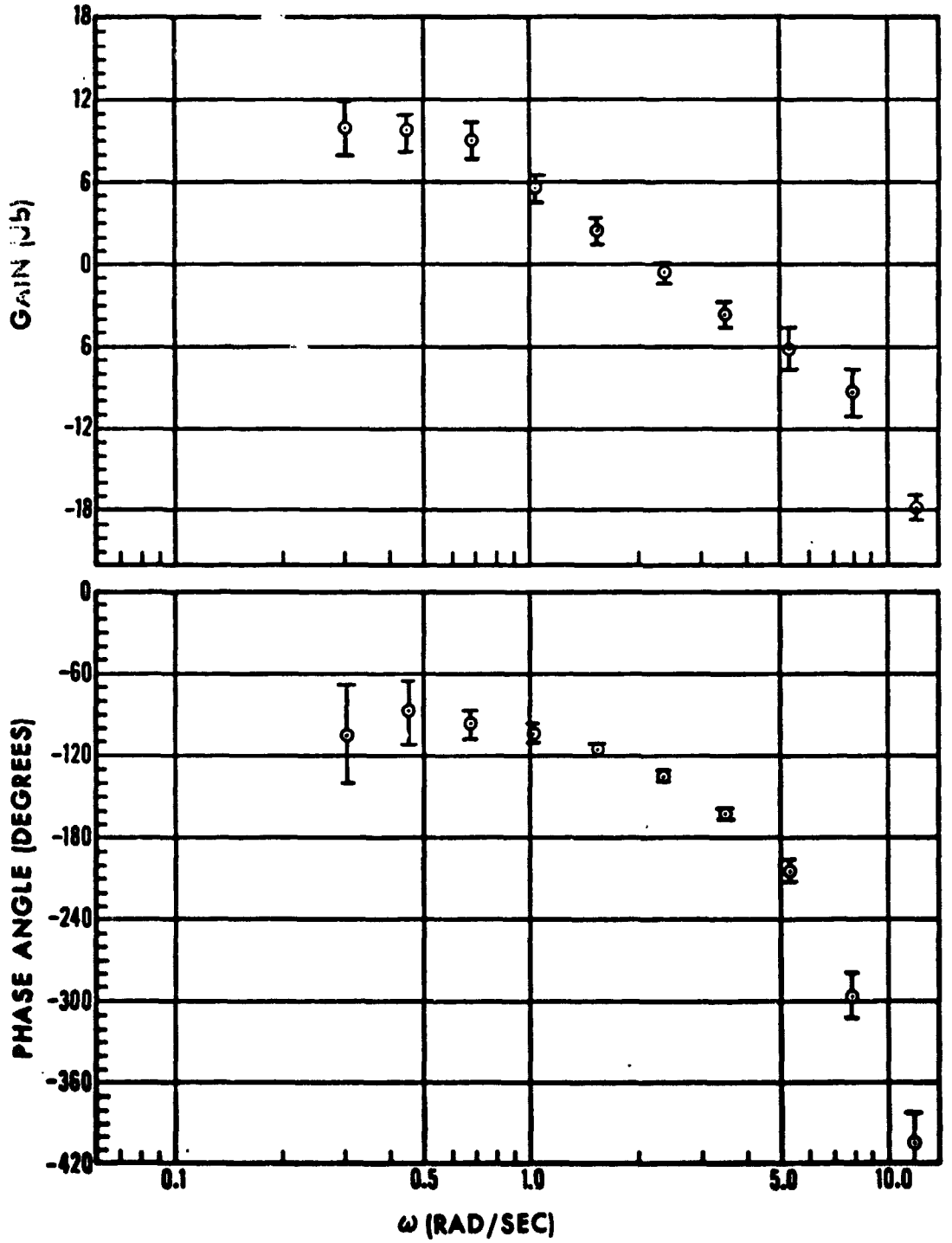

Figure 8. Group Mean Subject-Controlled Plant Describing Function for Afternoon Group and Easy Plant - Without Peripheral Display

C-10

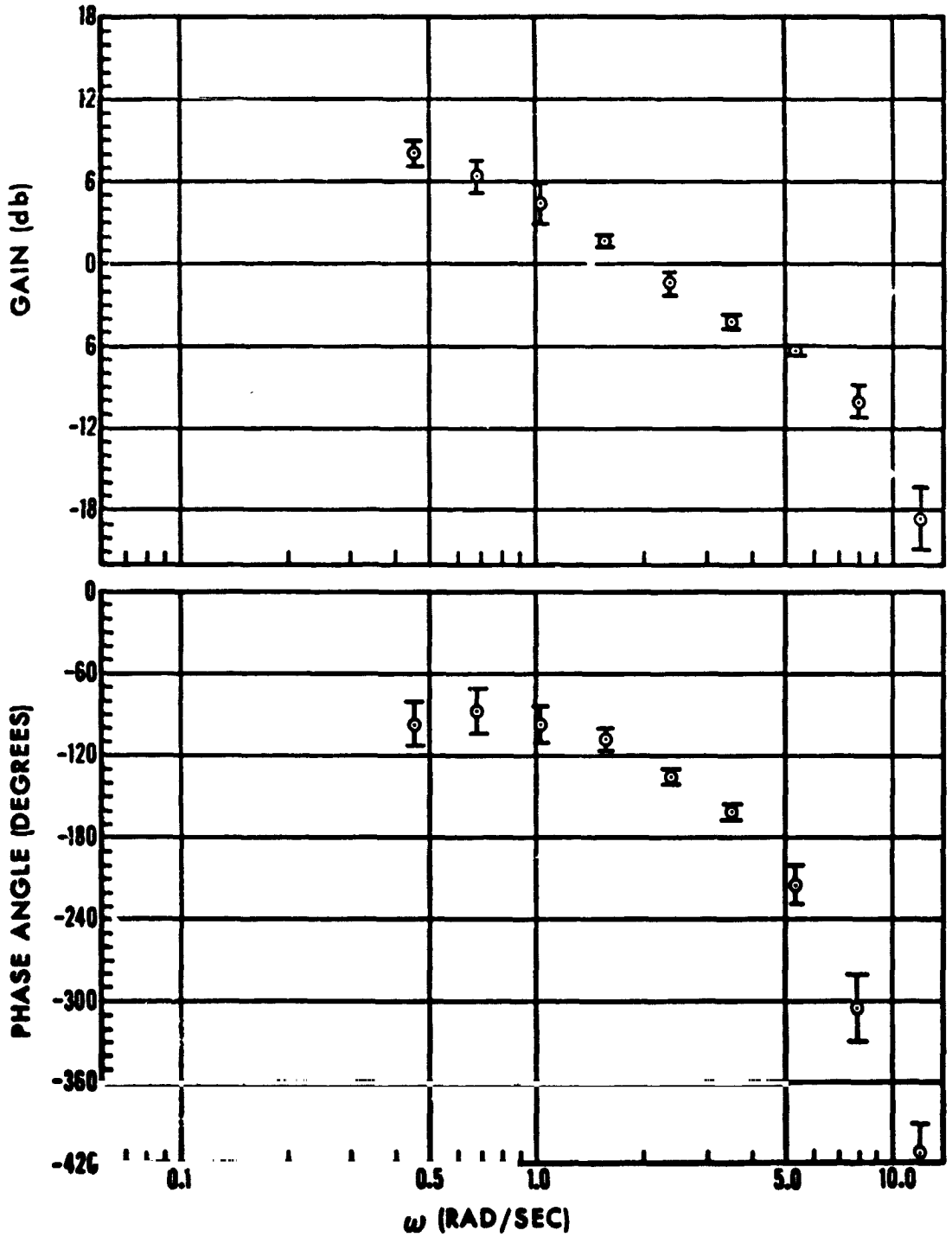

Figure 9. Group Mean Subject-Controlled Plant Describing Function for Afternoon Group and Easy Plant - Peripheral Display Present

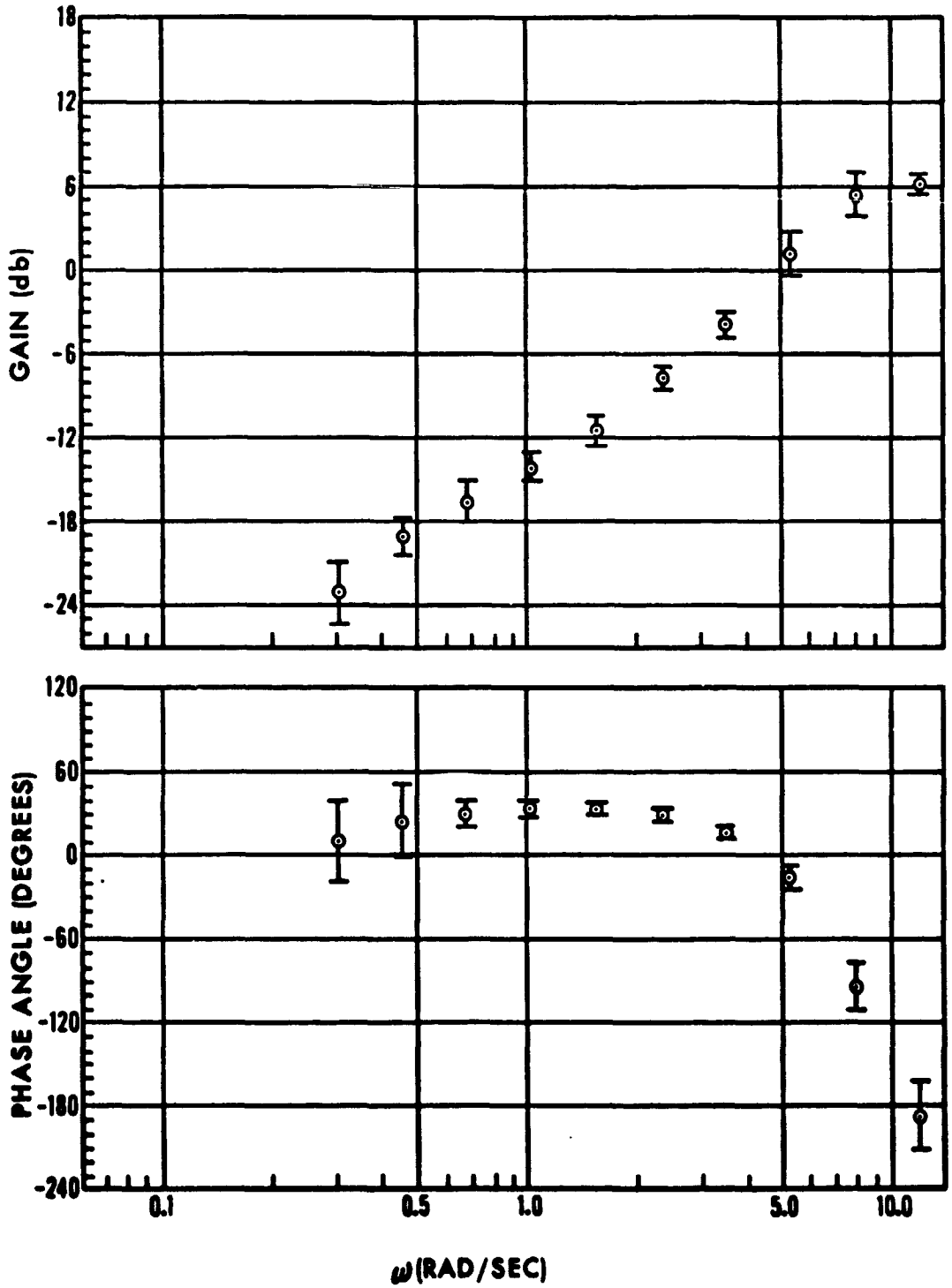

Figure 10. Afternoon Group Mean Subject Describing Function - Without Peripheral Display (Easy Plant)

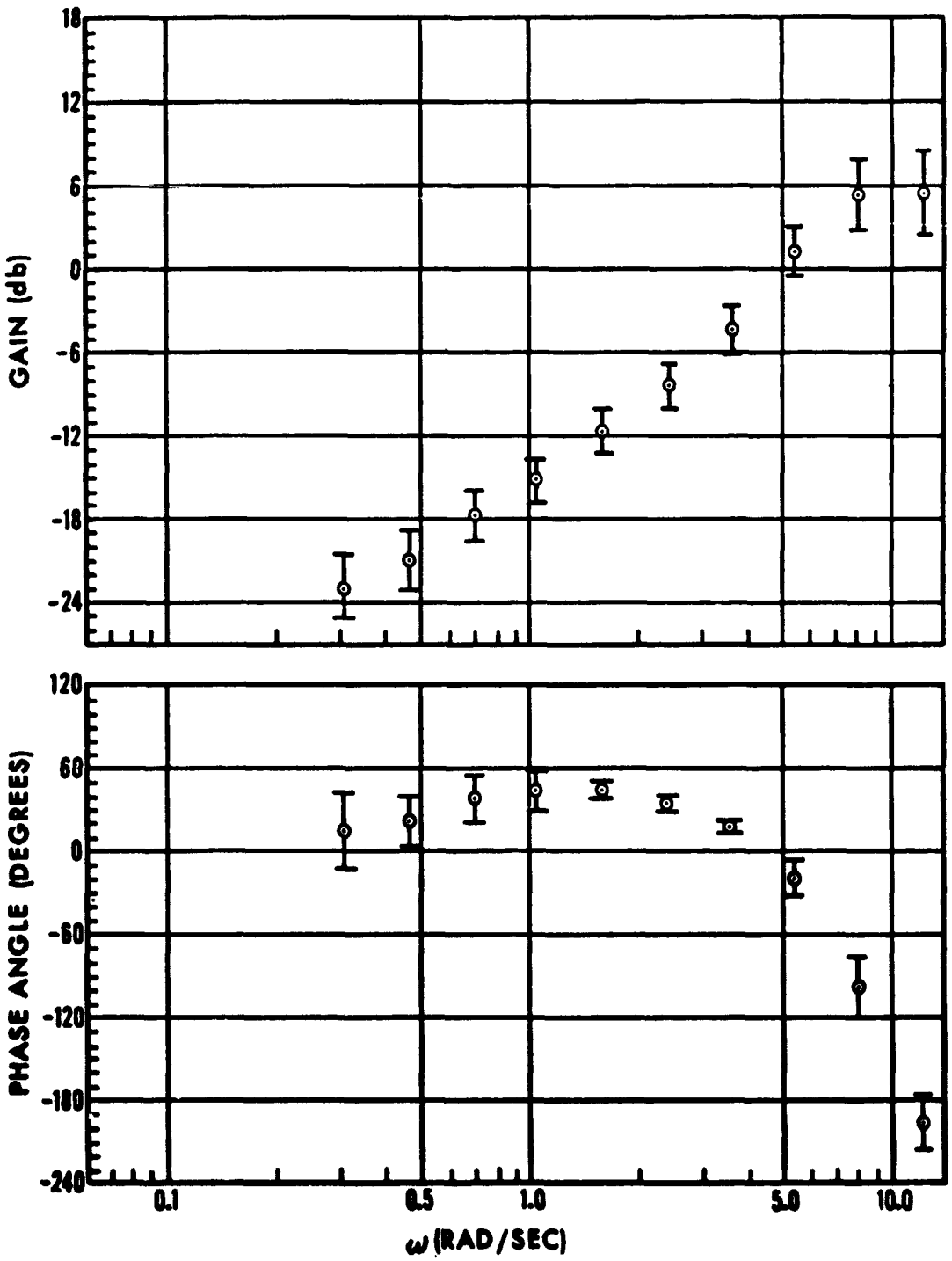

Figure 11. Afternoon Group Mean Subject Describing Function - Peripheral Display Present (Easy Plant)

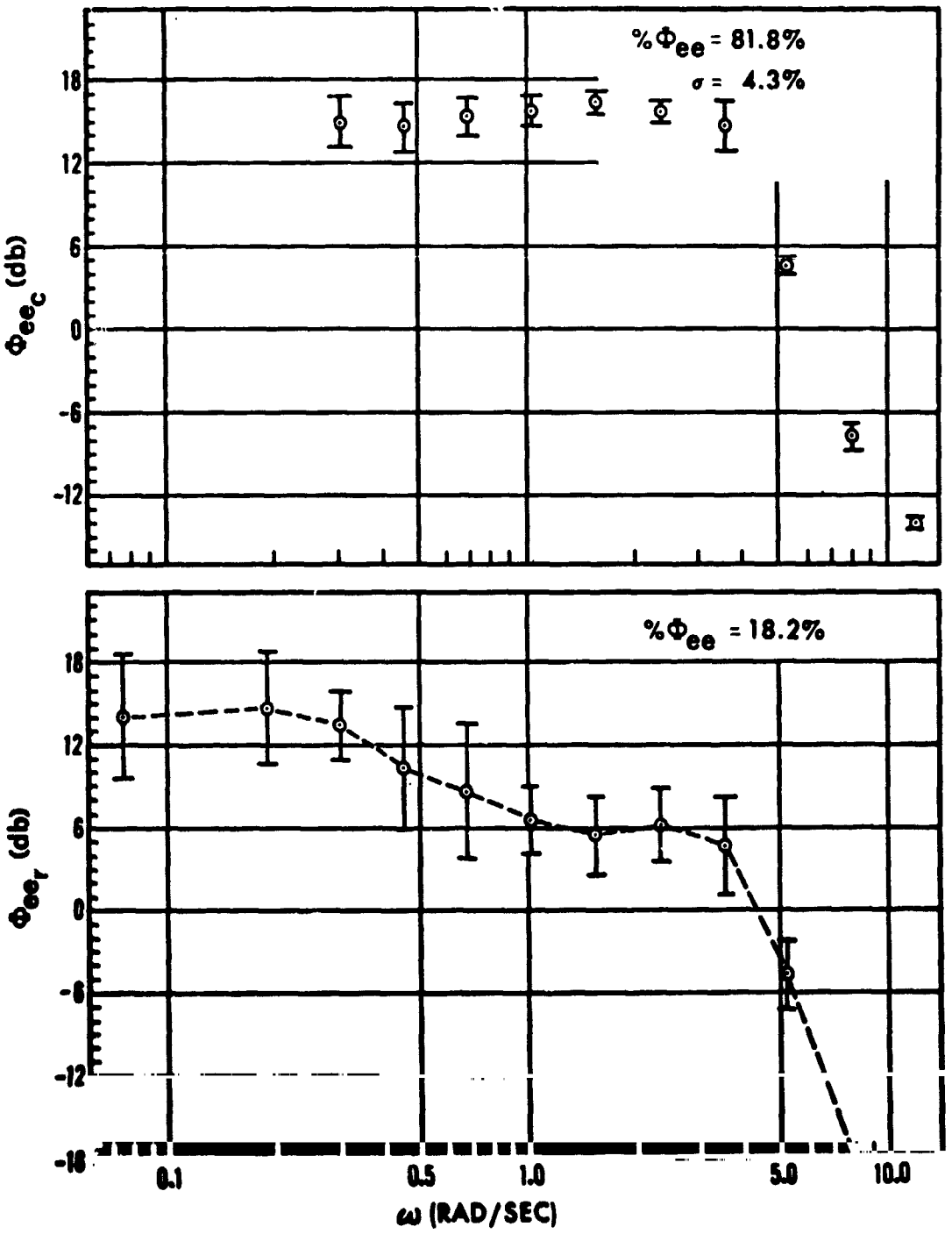

Figure 12. Averaged Afternoon Group Error Power Spectra - Without Peripheral Display (Easy Plant)

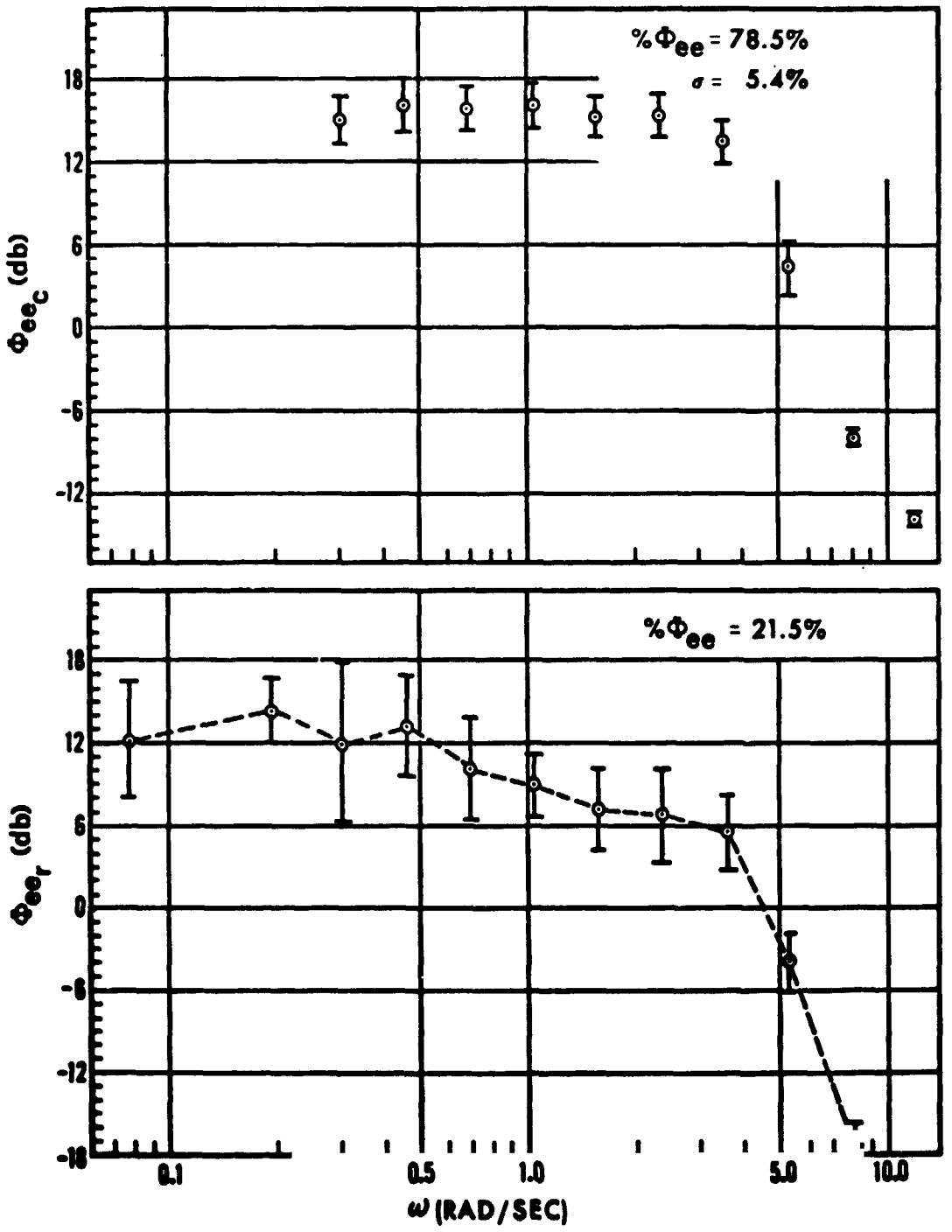

Figure 13. Averaged Afternoon Group Error Power Spectra-Peripheral Display Present (Easy Plant)

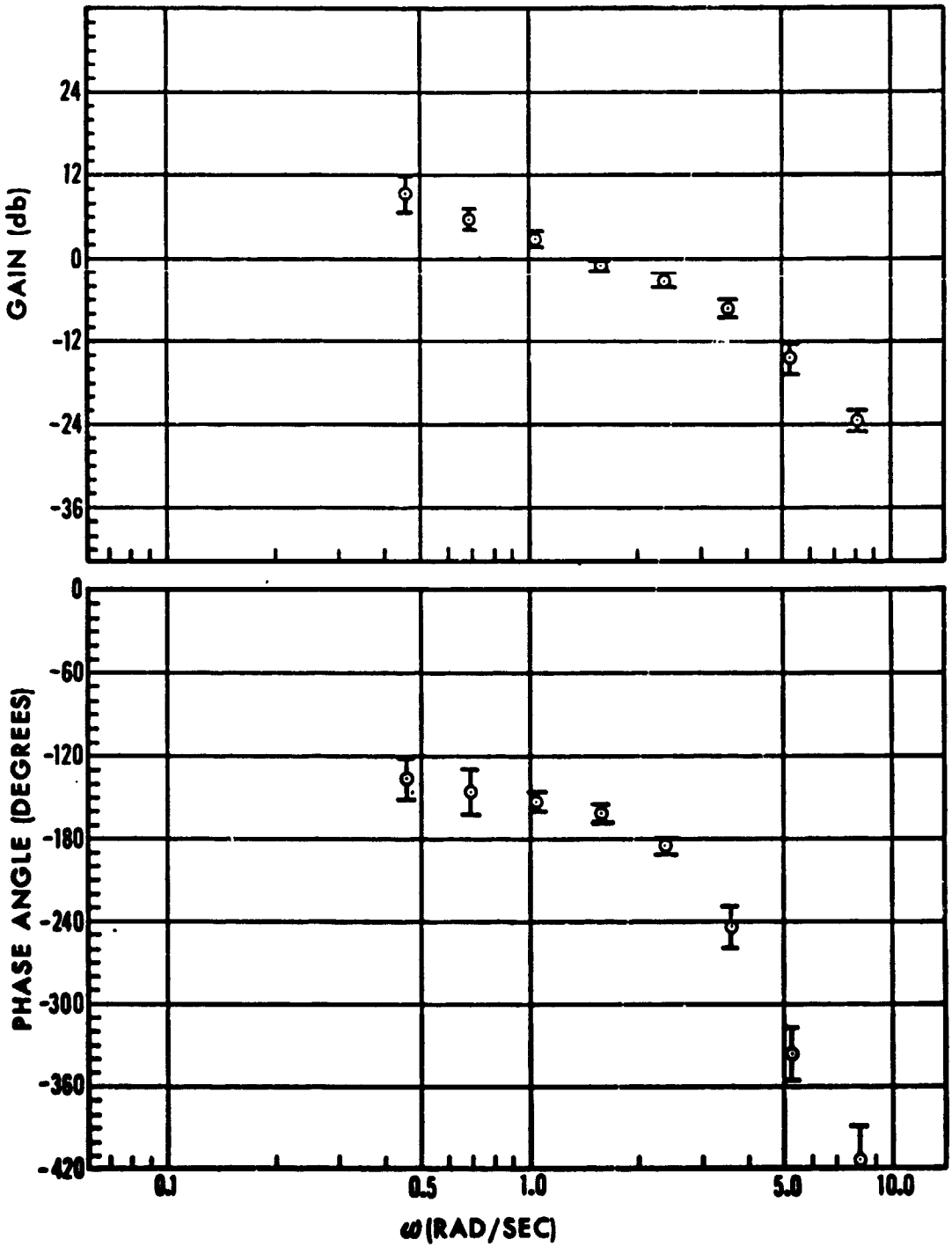

Figure 14. Group Mean Subject-Controlled Plant Describing Function with Difficult Plant - Without Peripheral Display

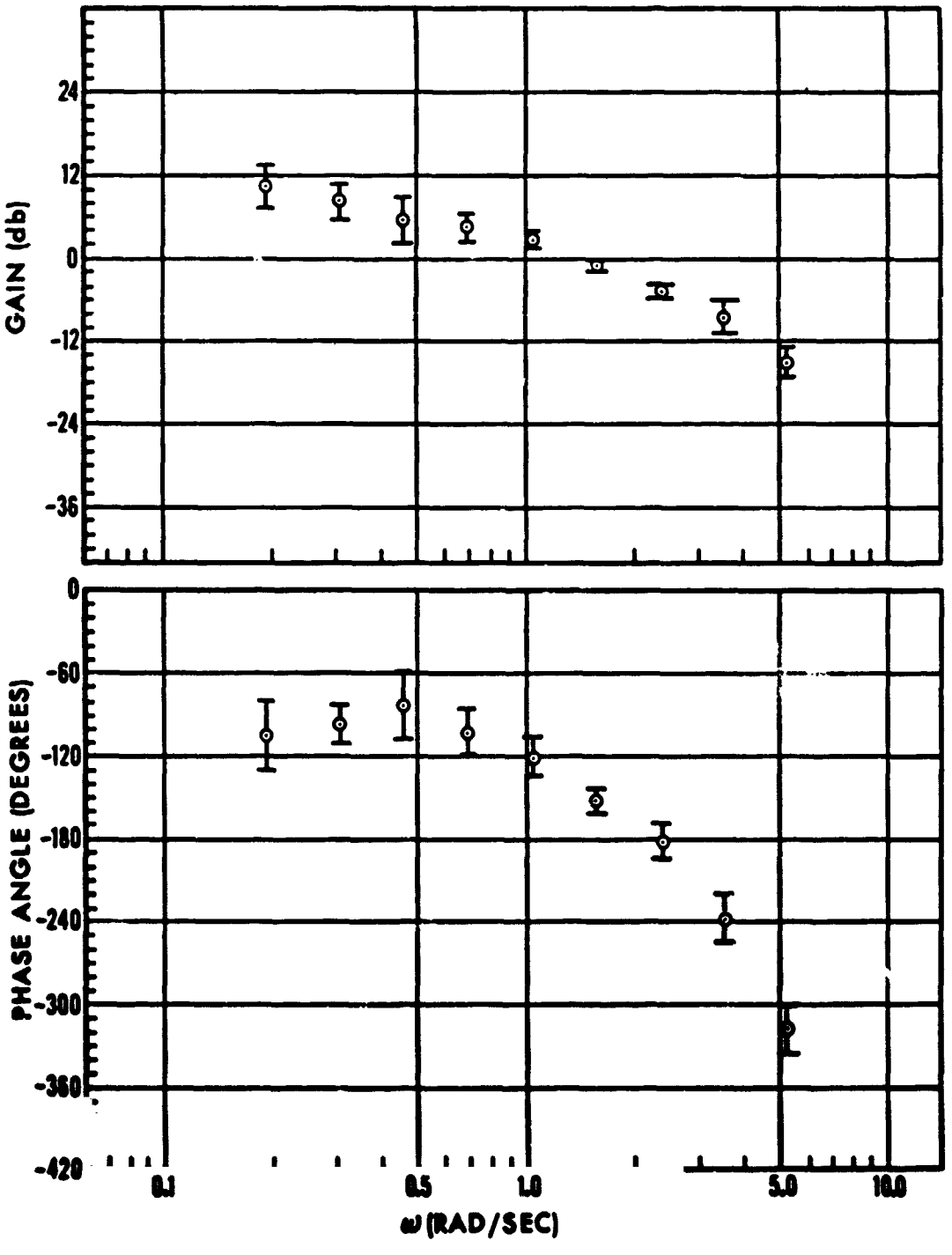

Figure 15. Group Mean Subject-Controlled Plant Describing Function with Difficult Plant - Peripheral Display Present

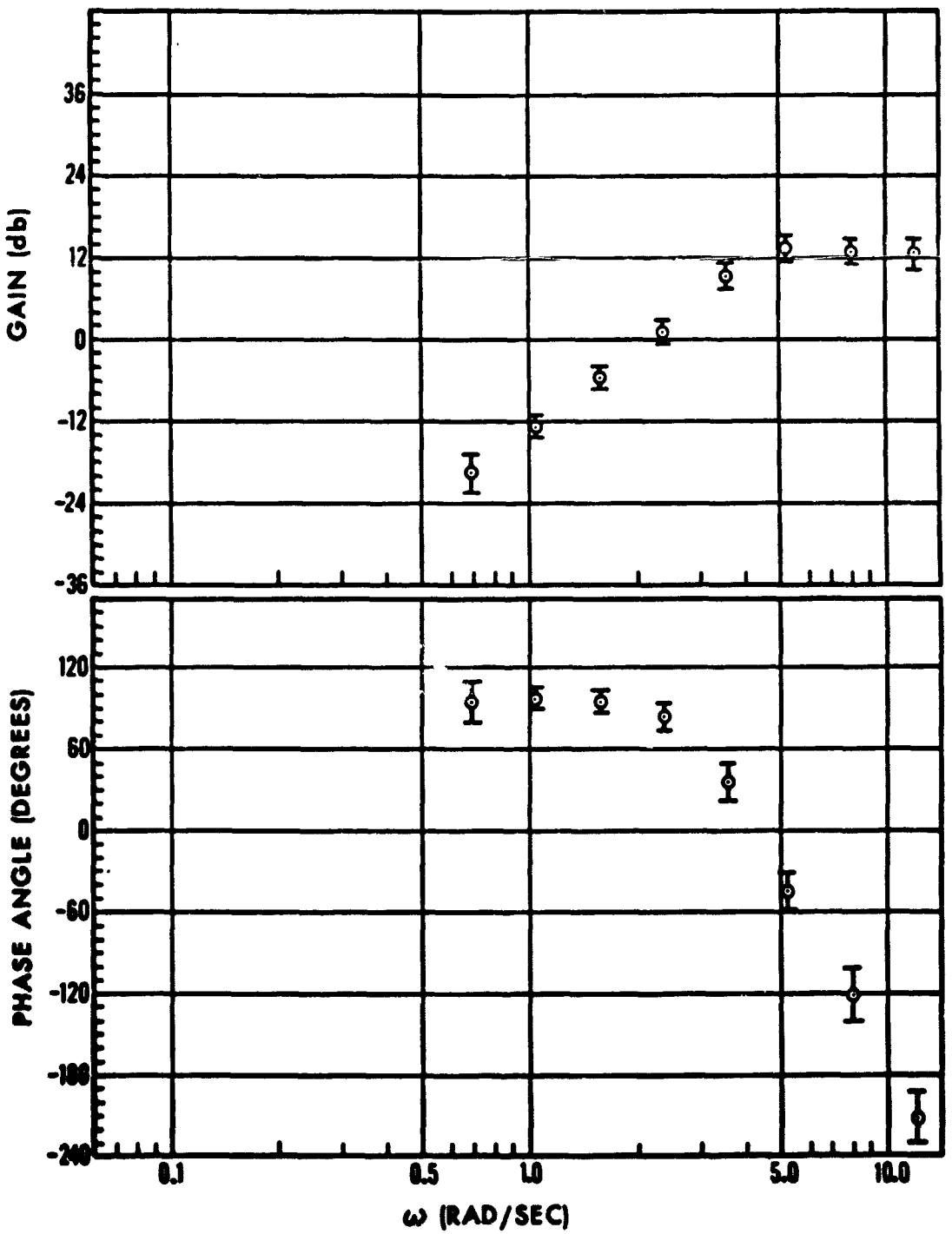

Figure 16. Group Mean Subject Describing Function, Difficult Plant - Without Peripheral Display

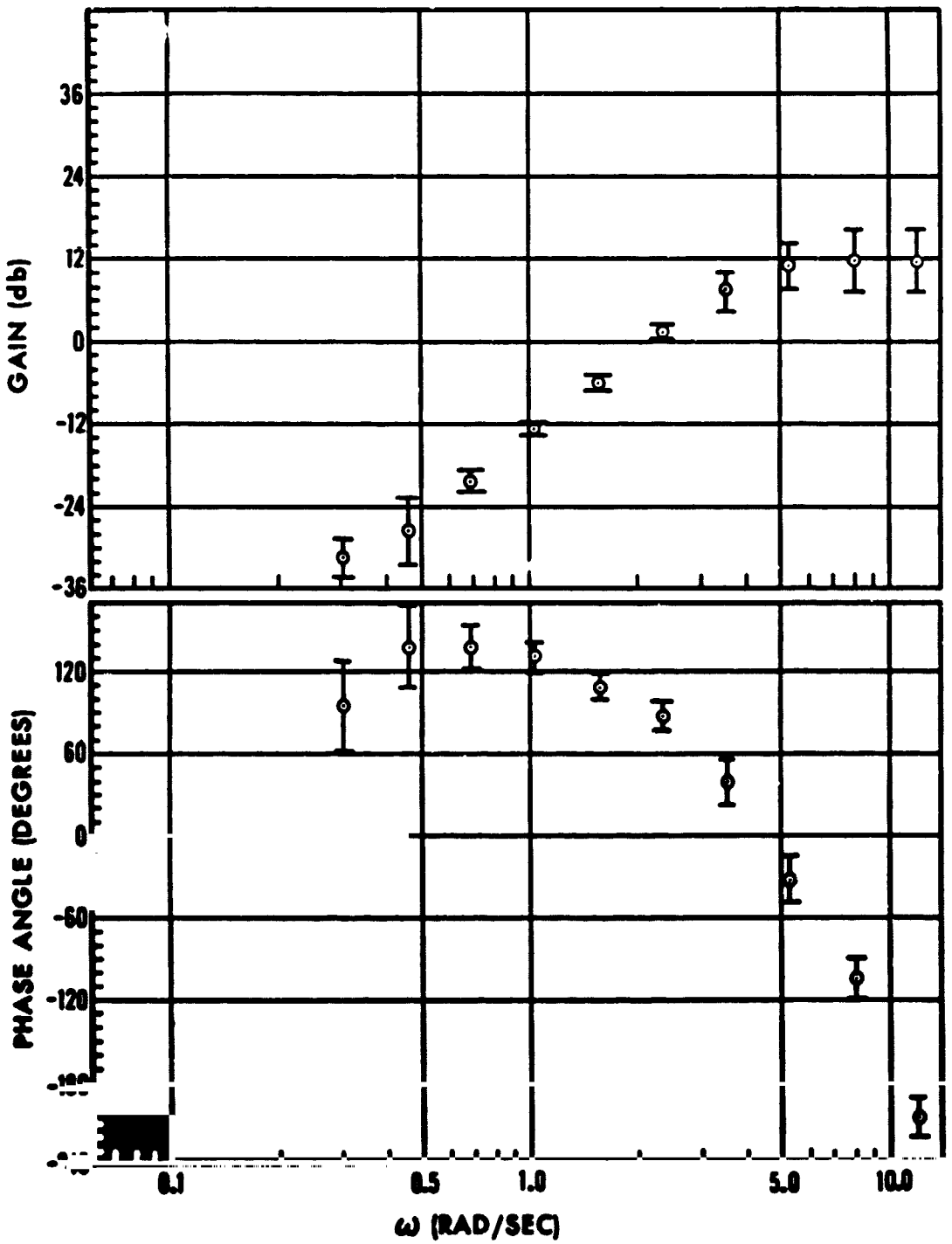

Figure 17. Group Mean Subject Describing Function, Difficult Plant - Peripheral Display Present

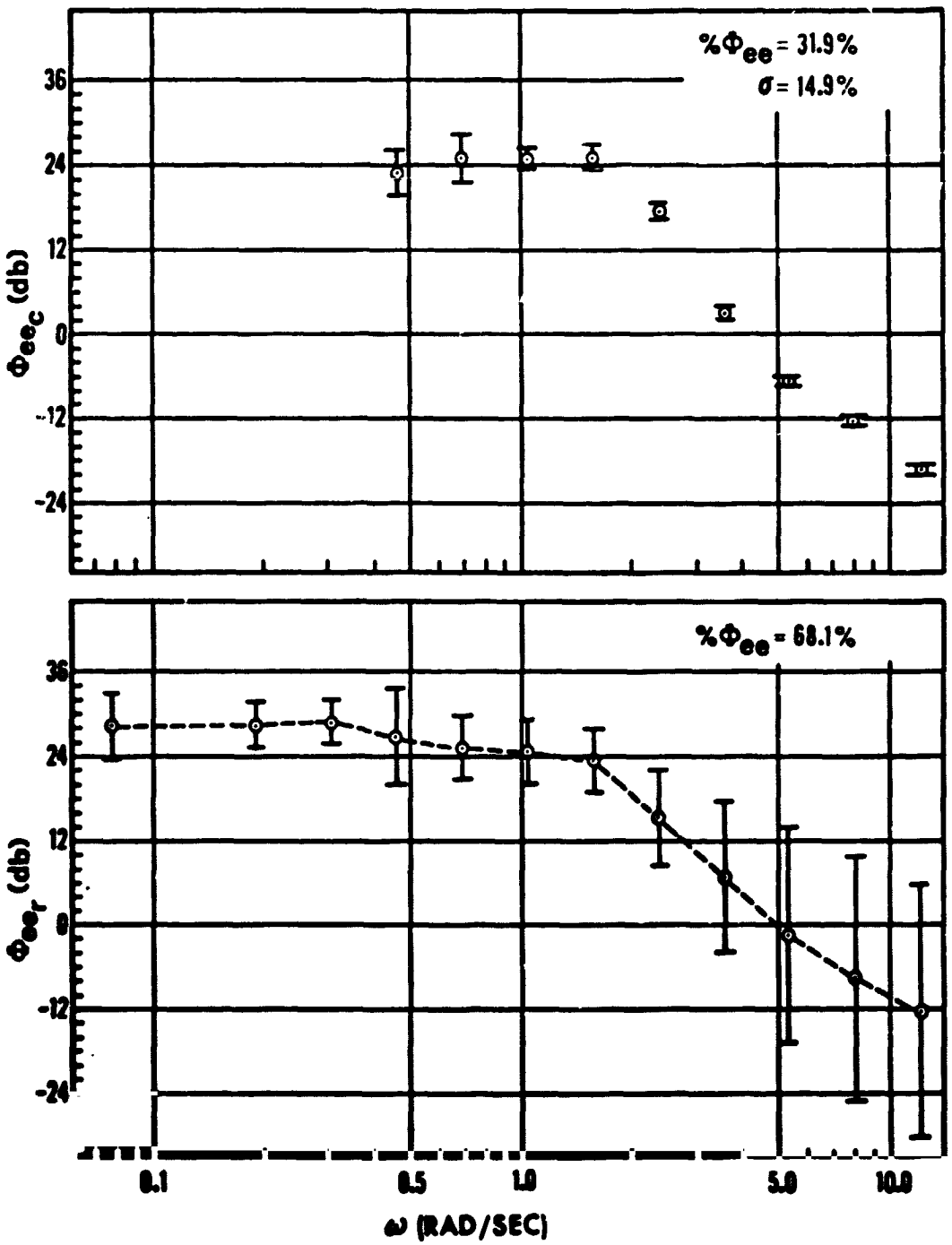

Figure 18. Averaged Group Error Power Spectra, Difficult Plant - Without Peripheral Display

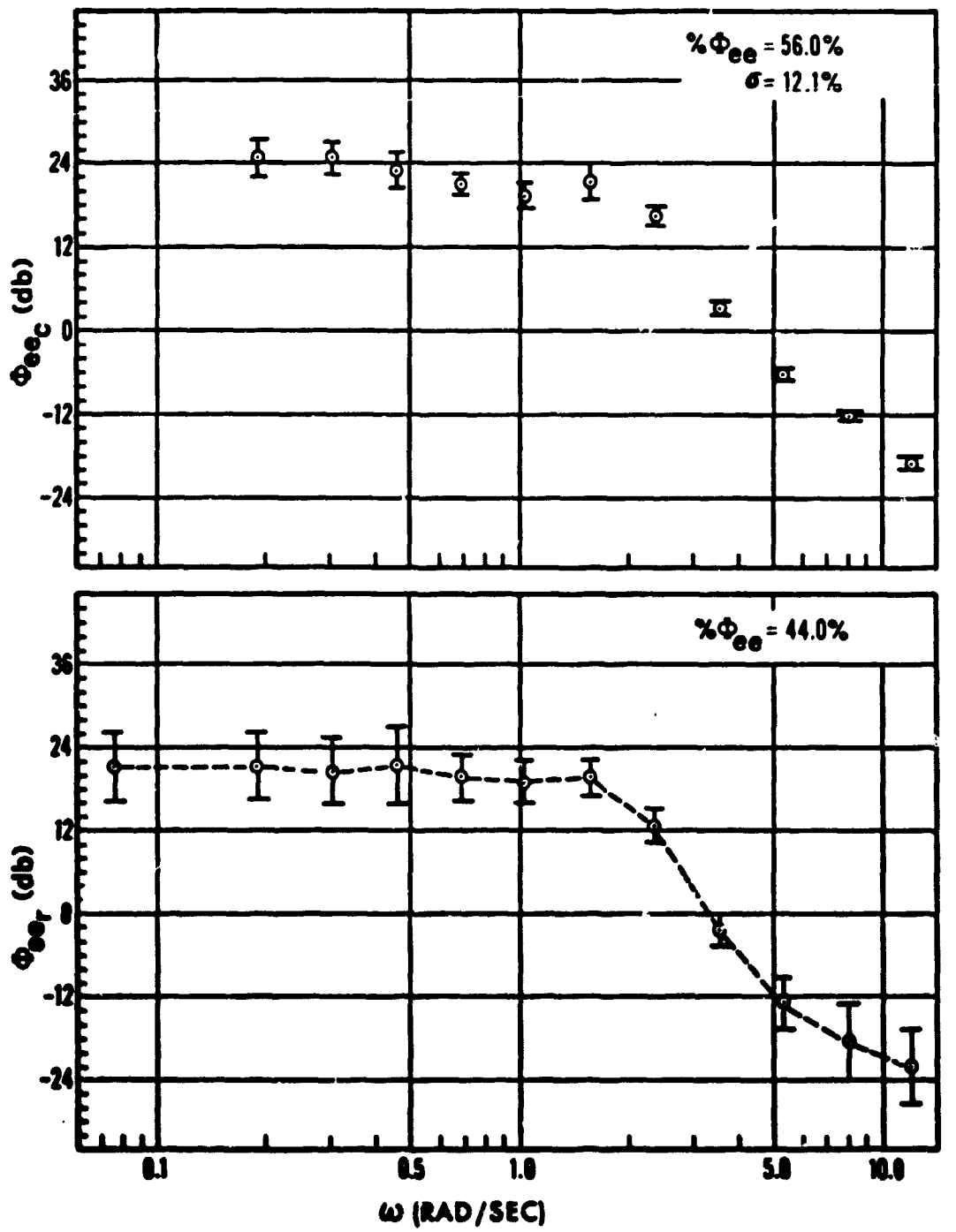

Figure 19. Averaged Group Error Power Spectra, Difficult Plant - Peripheral Display Present

USE OF MOTION CUES IN STEADY-STATE TRACKING*

by

William H. Levison
Bolt Beranek and Newman Inc
Cambridge, Massachusetts

Presented at the Twelth Annual Conference on
Manual Control, May 25-27, 1971 University of
Illinois at Urbana-Champaign

ABSTRACT

Data obtained in an experimental study of roll-axis tracking are analyzed. The effects of motion cues on tracking performance are modeled by (a) an increment of 0.05 seconds to the pilot time delay, and (b) inclusion of sensory variables that are likely to be provided by motion cues (position, rate, and acceleration of the vehicle roll angle in these experiments). The model replicates the important experimental results; namely, that motion cues cause (a) an increase in low-frequency phase lead, (b) an increase in high-frequency phase lag, (c) no change in man-machine gain-crossover frequency, (d) a reduction in rms tracking error only for the more difficult plant. Modeling of motion-sensor dynamics is not required.

INTRODUCTION

This paper reviews the results of an analytical and experimental study to explore the use of motion cues in a simulated roll-axis tracking task. The experiments were performed at the Aerospace Medical Research Laboratory (AMRL), Wright-Patterson Air Force Base. Primary data reduction was performed by the Air Force; statistical analysis and modeling were performed by Bolt Beranek and Newman Inc (BBN). The results of this study are documented in greater detail in Levison, Baron, and Junker (1).

This paper is concerned with the use of motion-related sensory information for continuous flight control. Other potential effects of motion, such as providing alerting cues to the pilot or providing "realism" to aircraft simulations, are not considered here.

Analysis of the AMRL experimental results was directed towards developing a generalized description of the manner in which the pilot uses motion

*This work was performed in part under AFOSR Contract No. F44620-75-C-0600. Lt. Col. William Wisecup of the Air Force Office of Scientific Research was contract monitor. Mr. Andrew Junker of the Aerospace Medical Research Laboratory directed the experimental study of which some of the results are summarized in this paper.

cues, with the ultimate goal of providing a model that can predict the effects of motion cues on system performance in a variety of control situations. Such a model would have a number of important applications; for example, one might use the model to:

(1) determine whether or not motion cues are used by the pilot in a particular control situation;
(2) extrapolate the results of fixed-base simulation to a motion environment;
(3) facilitate the design of ground-based simulators;
(4) identify situations where misinterpretation of motion cues is likely to cause a pilot response that seriously degrades system performance.

Although a number of experimental studies have been conducted to determine the effect of motion cues on pilot response behavior (2-5), a generalized model has not been developed and tested. Rather, the conclusions reached in these studies have been restricted to the context of the experiments yielding the data.

Perhaps the most comprehensive study of the effects of motion cues on tracking performance was conducted by Shirley (4). He explored overall system performance and pilot response behavior in a series of tasks that included a wide range of vehicle dynamics. Most of his results conformed to the following set of rules:

1. The human operator uses motion to generate additional lead at high frequencies, which permits an increase in pilot gain and therefore an increase in the gain crossover frequency of the man-machine system.

2. Greatest percentage reduction in rms error scores with motion is achieved for systems that respond to inputs above 3 rad/sec. That is, improvement is greater for low-order than for high-order systems.

3. Motion is used to greatest advantage in marginally stable or unstable systems.

Stapleford et al (3) also found that high-frequency phase lag decreased and gain crossover frequency increased when motion cues were present; furthermore, these effects generally decreased as the vehicle dynamics increased in difficulty. In contradiction to Shirley they found that, on the average, the effects of motion cues on error score increased for increasing vehicle difficulty.

Because the effect of motion simulation on tracking performance is highly dependent on the details of the tracking task, generalizations of the type reviewed above cannot be reliably extended beyond situations similar to those studied experimentally. Therefore, an alternative philosophy has been suggested and partially explored: namely, to account for the pilot's use of motion cues by including additional sensory feedback paths in the pilot model (2). Given a model structure that allows one to predict the influence of these feedbacks on pilot response as a function of task parameters, one may then extend

experimental results to a variety of control situations. The "optimal-control" pilot model developed by BBN appears to contain the desired structure, and application of this model to the AMRL roll-axis study is reviewed in this paper.

EXPERIMENTAL PROCEDURES

The experimental data analyzed by BBN were only a portion of the data obtained in a larger study of the pilot's use of visual and motion cues in manual control tasks; we review below those aspects of the experimental program that pertain to the analysis performed by BBN.

Description of the Tracking Task

The tracking task was mechanized similarly to that used in a previous study (6). Briefly, the closed-loop roll-axis motion simulator consisted of a drive system, aircraft seat, central visual display, and motion controls. The rotating system dynamics were identified and simulated on a hybrid computer. A block diagram of the resulting system is shown in Figure 1. The task was to follow a target aircraft in the roll axis. The difference between the target roll angle and the controlled plant position was provided to the human operator on a television monitor in the format shown in Figure 2. The angle between the rotating and stationary lines, e, depicted the difference between the controlled plant roll angle and the target roll angle.

Plant Dyanmics

Data were obtained for two sets of plant dynamics. "Task 1" used a plant that had approximate second-order response characteristics over much of the measurement bandwidth, whereas "Task 2" employed dynamics that were approximately third-order. Previous experimental results indicated that performance on Task 1 would be relatively unaffected by the presence of motion cues, while the presence of motion cues would appreciably enhance performance on Task 2. These two tasks were explored to provide a check on the consistency of the model developed to account for the pilot's use of motion cues.

Because of the complex dynamics and nonlinearities of the rotating machinery, the plant dynamics did not conform exactly to the desired theoretical response behavior. In order to minimize difference in plant dynamics between the motion and static (i.e., fixed-base) conditions, an effort was made to simulate the rotating dynamics in the static cases.

Figure 3 shows the transfer functions of the two plants as derived from the experimental data,along with analytic ("model") fits to these transfers. Plant dynamics for corresponding static and motion conditions are nearly identical over most of the measurement range, but differences appear at the highest frequencies. As these frequencies are well above the gain crossover frequency of the combined man-machine system, differences between static and motion plant dynamics were expected to have little effect on pilot behavior and system performance.

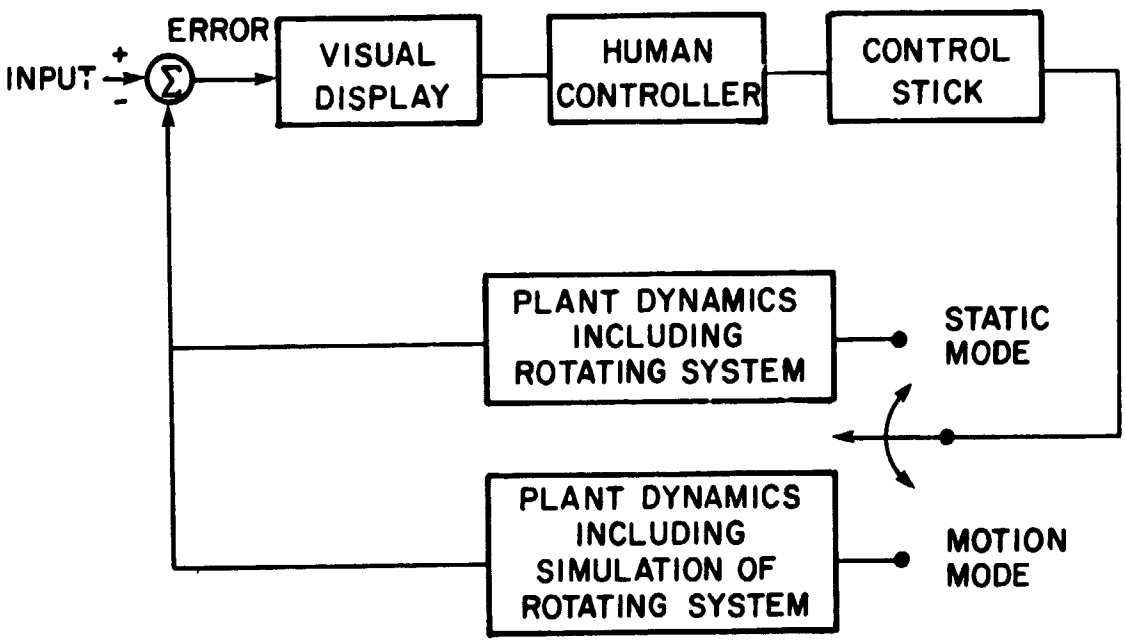

Figure 1. Block Diagram of Tracking Task.

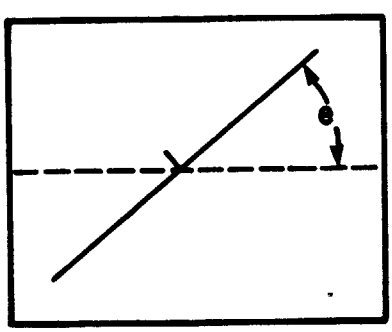

WHL-327

Figure 2. Sketch of Tracking Display.

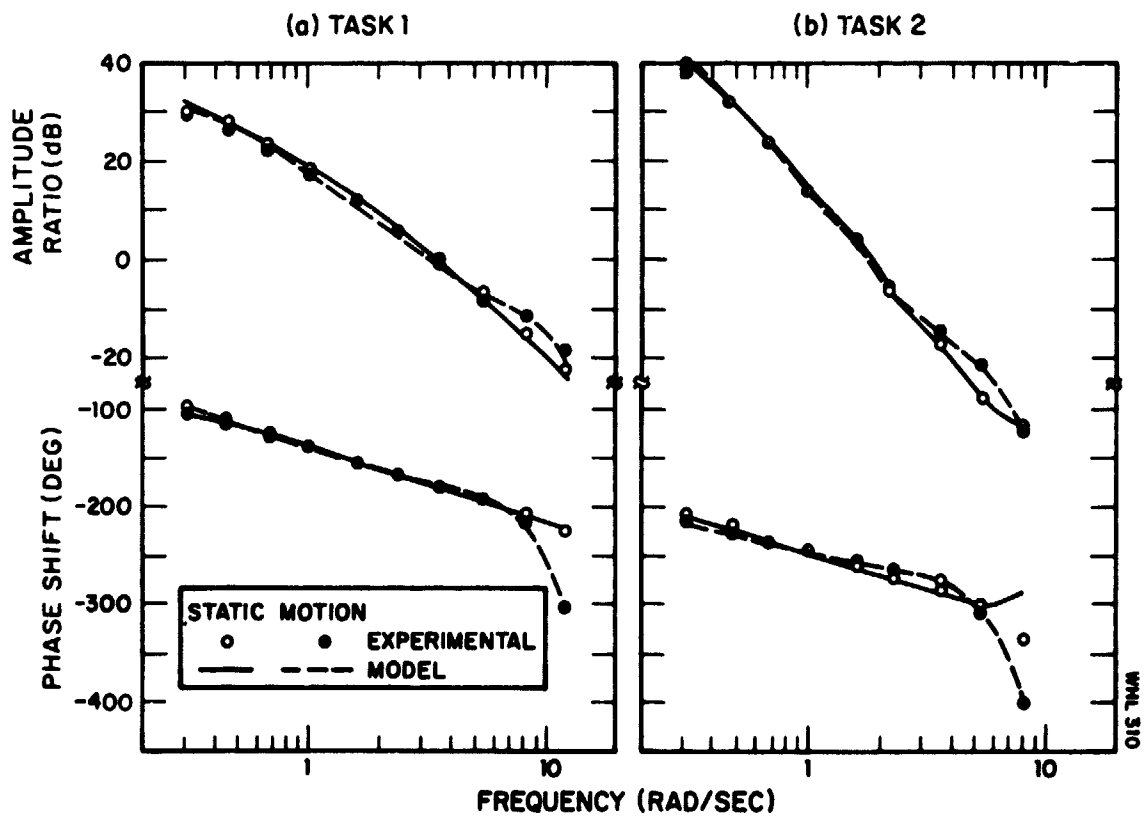

Figure 3. Frequency Response of the Controlled Plants. 0 dB represents 1 degree of roll angle per in-lb of control torque

A side-mounted force stick was used for all tracking runs. A comfortable stick gain was selected at the beginning of the experiment and maintained throughout so that the same stick gain was used for all subjects for all runs.

Input Forcing Function

The target roll angle was driven by a random-appearing input signal that consisted of 12 sine waves with frequencies and amplitudes chosen to approximate the power density spectrum of Gaussian white noise passed through a second-order low-pass filter having a double pole. The properties of the input signal were varied from one controlled plant to the next so that the subjects were always provided with a challenging tracking task, but one that did not severely restrict the bandwidth of the pilot's response. Rms amplitudes and (simulated) critical frequencies for the input signals were 20 degrees roll angle and 1.25 rad/sec for Task 1, and 40 degrees and 0.5 rad/sec for Task 2.

Training and Data-Collection Procedures

The same three subjects provided data for both Tasks 1 and 2; data from a fourth subject was analyzed for Task 2. All subjects were young, healthy adults between the ages of 18 and 21 with previous tracking experience on the simulator in both the static and motion modes. Since this tracking experience was not for the plants explored in this study, additional training was required.

Training and data collection were completed first for Task 1; tracking performance on Task 2 was then studied. In both phases of the experimental study, the training procedure consisted of tracking in the static and motion modes until the rms error scores appeared to reach asymptotic levels. The subjects were provided their rms error scores after each tracking trial. To maintain subject motivation, subjects were also informed of each other's performance scores.

During both training and data collection, each subject performed four tracking runs per day. These consisted of two static and two motion runs of about 164 seconds duration. Each subject experienced two consecutive runs at a time - one static and one motion - with the order randomized. After the final subject in the group accomplished his second run, the subjects completed the session by experiencing two additional replicates of the tracking task in the same subject sequence as before. In order to prevent the subjects from learning the input waveforms, a random number generator was used to vary the phase relationships of the input sinusoids from one experimental trial to the next.

EXPERIMENTAL RESULTS

Analysis Procedures

Variance scores were computed for each experimental trial for the tracking error, tracking error rate, plant position, plant rate, control, and control rate. These variance scores were averaged across the four replications of

a given experimental condition within each subject. The square root was taken of each subject mean to yield an rms performance measure*, and the mean and standard deviation of the subject means pertaining to the same experimental condition were then computed. In order to test for significant differences between motion and static conditions, paired differences were formed from corresponding subject means; these differences were subjected to a two-tailed t-test. Difference scores significant at the 0.05 confidence level or smaller were considered "significant".

Analysis procedures were similar to those used in previous studies of manual control (7-10). Fast-Fourier transform techniques allowed computation of pilot describing functions and signal spectra, with the spectra being partitioned into input-correlated and remnant-related components (where "remnant" is defined as signal power not linearly correlated with the input forcing function). The pilot describing function was computed by dividing the Fourier transform of the control response by the transform of the tracking error. This response measure, therefore, included response to both visual and motion cues.

Means and standard deviations were computed for the describing function amplitude ratio (in dB), for the describing function phase shift (in degrees), and for spectral quantities (in dB). Statistics were computed at each input frequency; in the case of spectra, statistics were computed separately for input-correlated and remnant-related components. T-tests were performed on paired differences of selected frequency-response measures to determine the significance of motion cues on these quantities.

The input-correlated spectral components, which were discrete spectra because of the sum-of-sines inputs, were converted to equivalent continuous-frequency spectral density functions to be compatible with the spectral densities generated by the pilot/vehicle model. The conversion scheme is described in (1). For notational conciseness, all power spectral density functions, whether theoretical or derived from experimental data, are referred to in this paper simply as "spectra".

RMS Performance Scores

Variables for which rms performance scores were computed, their units, and their symbolic notation are shown in Table 1. Average rms performance scores are shown in Figure 4, with significant static-motion differences indicated by the arrows.

*More precisely, the resulting scores should be termed "standard deviation scores", since the contributions of mean components, if any, were removed. However, to avoid confusion we restrict the usage of the term "standard deviation" to indicate subject-to-subject variability.

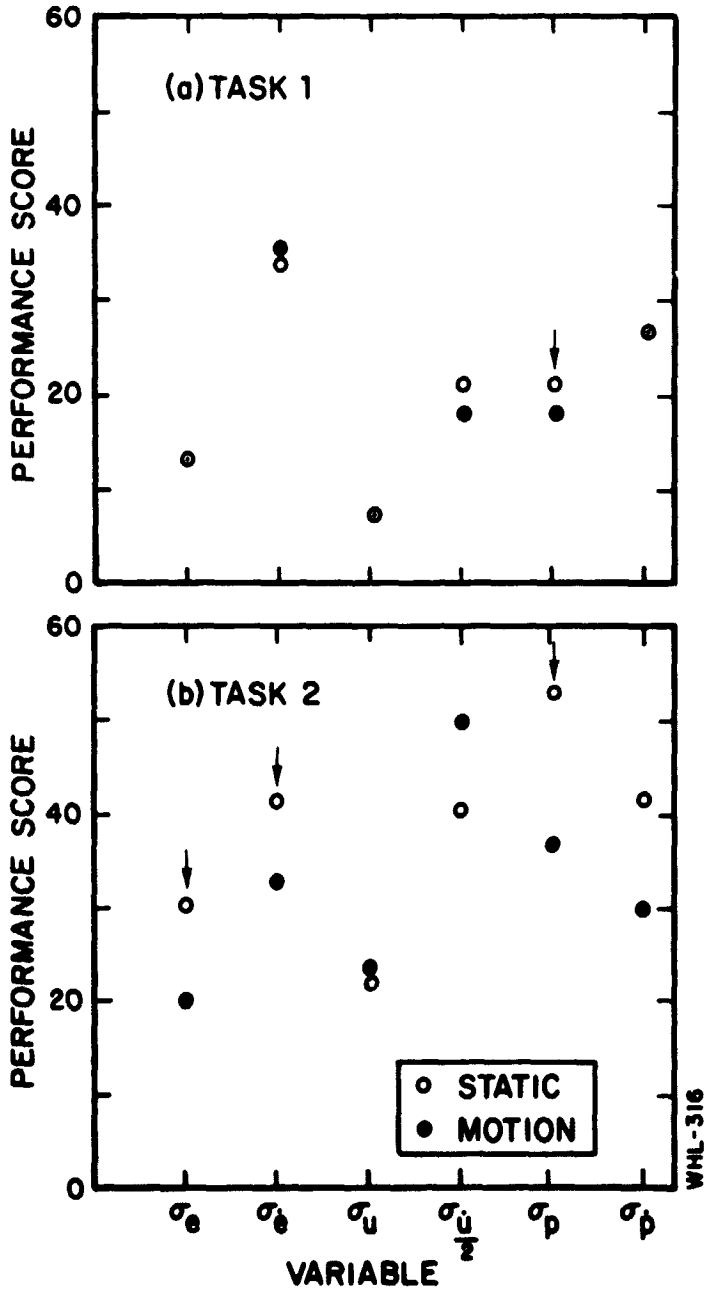

Figure 4. Effect of Motion Cues on Average RMS Performance Scores.

Table 1

Tracking Variables Analyzed

Variable	Symbol	Units
Tracking Error	e	degrees
Tracking Error Rate	$\dot{e}$	degrees/sec
Plant Position	p	degrees
Plant Rate	$\dot{p}$	degrees/sec
Control	u	in-lb
Control Rate	$\dot{u}$	in-lb/sec

Error and control variables were virtually unchanged by the presence of motion cues in Task 1. Only rms plant position was significantly influenced by motion cues and was about 12% less when motion was present. When the third-order plant (Task 2) was controlled, however, motion simulation allowed large and significant reductions in rms tracking error, error rate, plant position, and plant rate. Rms control torque was essentially unaffected by motion. Although rms control rate increased by about 23% on the average when motion was simulated, this change was not statistically significant.

Frequency Response

Figure 5 shows average pilot frequency-response behavior. The four sets of curves shown for each tracking task are, from top to bottom, the amplitude ratio of the pilot describing function, the phase shift of the pilot describing function, the input-correlated component of the spectrum of the pilot's control response, and the remnant-related component of the control spectrum. The presence of apparent "system noise" associated with the motion simulation in Task 2 prevented reliable estimates of pilot remnant at the lowest three measurement frequencies shown in Figure 5. Therefore, estimates of remnant at these frequencies are not plotted for the Task 2 motion simulation.

The effect of motion cues on performance in both tasks was to increase low-frequency phase *lead* while also increasing high-frequency phase *lag*. In addition, motion simulation in Task 2 significantly modified the control spectrum. Input-correlated and remnant-related components were reduced at frequencies corresponding to gain-crossover and lower. No significant changes occurred in the correlated power at high frequencies, whereas remnant increased. No motion-related changes in amplitude ratio were observed in the region of gain-crossover for either task.

The "open-loop" describing functions shown in Figure 6 give a more direct

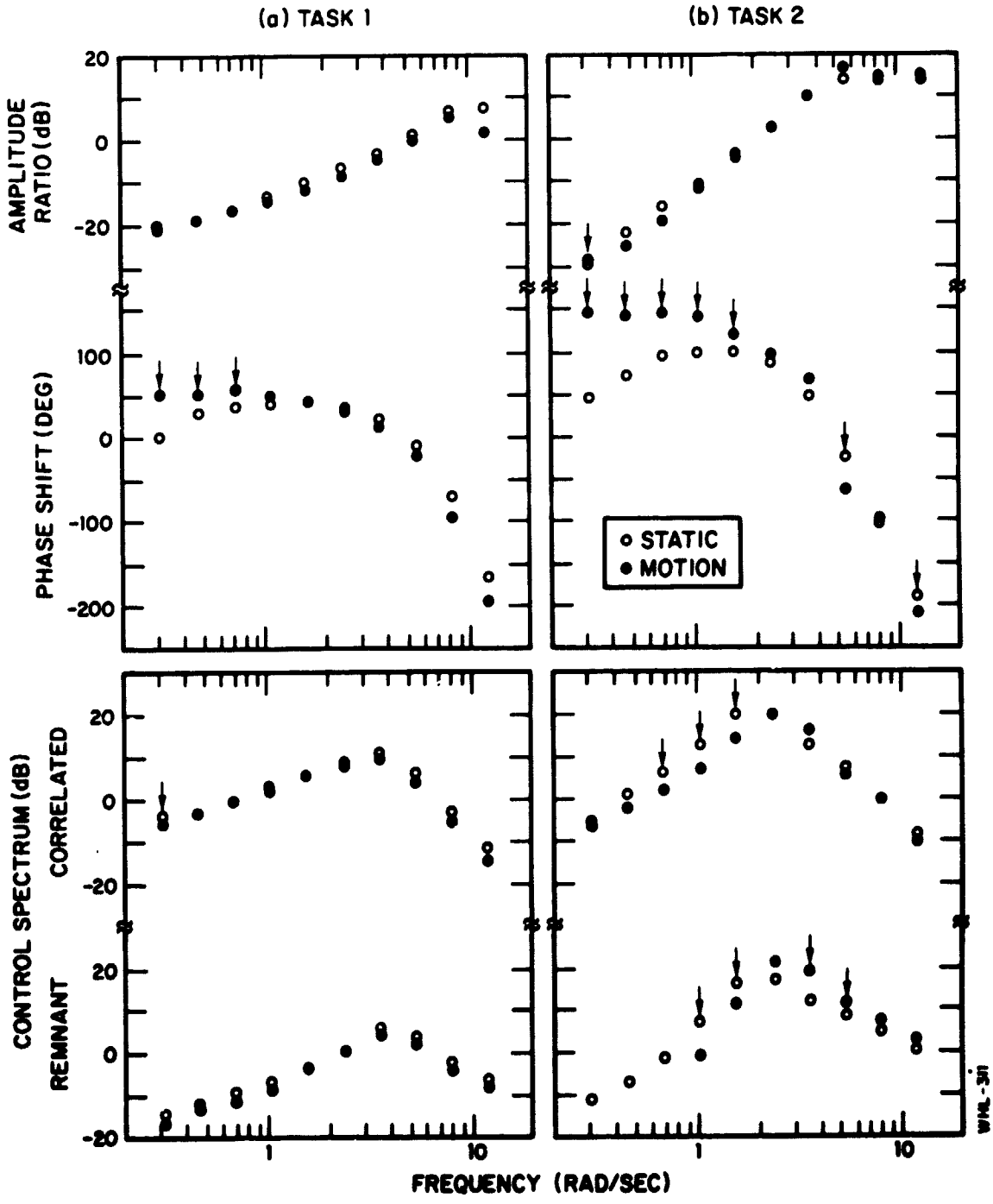

Figure 5. Effect of Motion Cues on Average Pilot Frequency Response
0 dB represents 1 in-lb control torque per degree roll for the amplitude ratio and 1 $(\text{in-lb})^2/(\text{rad/sec})$ for control power

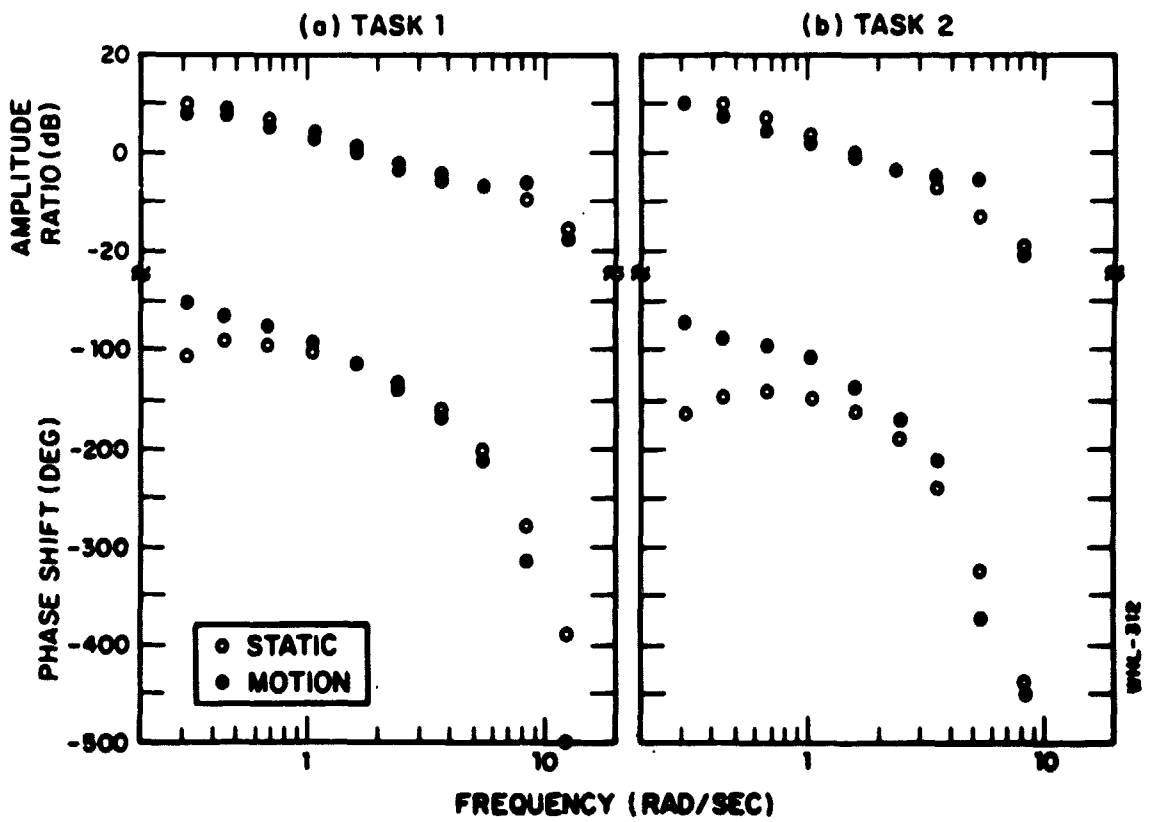

Figure 6. Effect of Motion Cues on Open-Loop Describing Function.
0 dB = 1 (dimensionless)

indication of combined man-machine response capabilities. The gain-crossover frequency is in the range of 1.5-1.8 rad/sec and is little affected by either plant dynamics or by the presence of motion cues. The phase margin, on the other hand, is quite variable. Phase margin is about 60-70 degrees for Task 1. Phase margin is reduced to about 40 degrees for Task 2 with motion simulation and to about 20 degrees for Task 2 in the static mode. Apparently, the increase in phase margin, combined with the reduction in controller remnant at frequencies below crossover, account for the reduced error score in the Task 2 motion simulation.

Comparison with Previous Experimental Results

The experimental results presented here appear to conflict with the findings of others regarding the effects of motion cues on tracking performance. Both Shirley (4) and Stapleford et al (3) concluded that the addition of motion cues allows the pilot to generate greater lead at high frequencies, thereby permitting an increase in gain-crossover frequency. Furthermore, Shirley concluded that motion cues were relatively more beneficial for tracking tasks involving low-order plants than for those involving high-order dynamics. On the contrary, the results presented above show that motion cues result in more high-frequency phase lag (rather than lead), no appreciable change in gain crossover, and greater relative improvement with the higher-order plant.

These apparent contradictions do not necessarily indicate that the AMRL experimental subjects used motion cues in a manner different from the subjects who participated in the studies of Shirley and of Stapleford et al. There were some important differences between the AMRL experiments and the earlier studies. Both Shirley and Stapleford et al applied the input disturbance in such a manner that both the visual display and the motion simulator were driven by the input. (That is, the input was applied essentially in parallel with the pilot's control.) In the AMRL/BBN study, the input was purely a command signal; the plant was driven only by the subject's control input. Thus, in the latter study, motion cues provided direct perceptions of vehicle response behavior; this was not the case in the earlier studies. In addition, the dynamics used in Task 2 of the AMRL/BBN study were higher order than those explored in the previous studies.

Because of the strong interaction between pilot response behavior and task parameters, we cannot tell from experimental data alone whether or not subjects participating in two different experiments obeyed the same set of rules with regard to the use of motion cues. A model is needed to account both for the limitations inherent in the human's use of perceptual information and for the interaction between task parameters and human response. Given this model, we can then try to find a consistent set of rules for selecting pilot-related parameters that accounts for the use of motion cues across a variety of task conditions.

The results of model analysis applied to the AMRL experimental data are described below.

MODEL ANALYSIS

Model Structure

The model applied to the foregoing experimental results was a modified version of the "optimal-control" pilot/vehicle model that has been applied in numerous previous studies of manual control (11-18). The modification to the model described in the literature consisted of the following revised treatment of motor-related sources of pilot remnant: (1) "motor noise" was treated as a wide-band noise process added to control rate, rather than to commanded control, and (2) the concept of "pseudo" motor noise was introduced to allow a differentiation between the actual noise driving the system ("driving" motor noise) and the pilot's internal model of this noise (the "pseudo" noise). No modifications were made to the model structure specifically to treat the pilot's use of motion cues.

Injecting motor noise to control rate allowed the model to reproduce the low-frequency "phase droop" exhibited by most pilot describing functions. Although tracking performance is generally little affected by low-frequency phase response, it was necessary to obtain an accurate model of this aspect of controller behavior because of the importance of low-frequency phase characteristics on performance in the AMRL/BBN roll-axis tracking study. By introducing the concept of pseudo motor noise, we gained added flexibility in representing pilot uncertainties about his own control behavior and about vehicle response. The mathematical implications of this model revision, as well as applications of the revised model to previous laboratory tracking results, are documented in Levison, Baron, and Junker (1).

The focus of the modeling effort was to represent the effects of motion primarily by appropriate definition of the sensory variables assumed to be available to the pilot. Thus, static-mode tracking was modeled with a two-element "display" vector consisting of tracking error and error rate. In the case of motion tracking, the display vector was augmented to include quantities that would be provided by the pilot's motion-sensing capabilities; specifically, plant position (i.e., roll angle), plant rate, and plant acceleration. These motion-related variables were considered individually and in combination.

Because we were dealing with steady-state tracking signals of moderate bandwidth, we did not expect motion-sensor dynamics to have an important effect on tracking performance. Therefore, sensor dynamics were not included in the pilot model: informational quantities included in the display vector were assumed to be corrupted only by observation noise and not by bandwidth limitations.

Identification Procedure

The primary goal of the model analysis was to seek a consistent set of rules for selecting pilot-related model parameters that would allow reliable predictions of the effects of motion cues in a variety of control tasks. A second (and related) goal was to determine the specific motion-related cues that the subjects had used in the AMRL/BBN experimental study.

The identification scheme employed in this study was similar to that used by BBN in previous studies (7, 9) and was applied to reduced data rather than to time histories. Parameter values were sought that would simultaneously provide a good match to performance scores, describing functions, and control spectra. A quantitative "matching error" was defined as described in (1), and pilot-related model parameters were selected to minimize this error.

A number of iterations were required to arrive at a set of pilot-related parameter values that would explain the maximum amount of data with minimum variations in parameters. The logical (if not entirely chronological) steps in the identification procedure were as follows: (1) analysis of previous laboratory tracking experiments provided an initial set of values for pilot-related paramters; (2) the Task 1, static-mode data were matched to determine modifications, if any, to these parameter values for the roll-axis tracking results; (3) the data of Task 2, both static and motion, were matched to test specific hypotheses concerning the use of motion cues; (4) the results of Step 3 were then applied to the static and motion data from Task 1 to verify the consistency of the treatment of motion cues, and (5) iterations on Steps 3 and 4 led to the final selection of model parameters.

Primary Results of the Model Analysis

Parameter values identified from the roll-axis tracking data are given in Table 2. The following considerations were involved in arriving at this set of parameter values:

Control-rate Cost Coefficient: We initially attempted to match experimental results with control-rate cost coefficients corresponding to a motor time constant of 0.1 seconds, in keeping with previous model applications. We found, however, that weightings so chosen yielded rms control-rate scores that were much greater than those observed experimentally; accordingly, weightings were re-adjusted to provide a better overall match to the data. (Predicted rms error scores were relatively insensitive to the choice of control-rate cost coefficient.)

Time Delay: A time delay of 0.2 seconds was selected on the basis of previous studies and provided a good match to the static results. It was necessary to increase the delay to around 0.25 seconds, however, to account for the greater high-frequency phase shift observed in the motion experiments.

Motor Noise: Motor noise was neglected as a source of direct input to the control system. Pseudo-motor noise, reflecting the subject's uncertainties about the system as well as uncertainty about his own control action, was adjusted to match the low-frequency portion of the pilot's phase characteristics.

Observation Noise: An observation noise/signal ratio of -20 dB was adopted as the noise level corresponding to nominal "full attention".*

* On the basis of previous studies, the observation noise/signal ratio was assumed to vary inversely with "attention" (7, 17, 18).

Table 2

Identified Model Parameter Values

Model Paramter	Task 1 Static	Task 1 Motion	Task 2 Static	Task 2 Motion
Control-Rate Cost Coefficient	0.02	0.02	0.08	.01
Motor Time Constant (sec)	0.126	0.130	.193	.145
Time Delay (sec)	0.20	0.25	0.20	0.25
Driving Motor Noise/Signal Ratio (dB)	Negl.	Negl.	Negl.	Negl.
Pseudo Motor Noise/Signal Ratio (dB)	-35	-35	-35	-35
Observation Noise/Signal Ratio (dB)	-20	-20	-20	-20
Attention to Error Displacement	0.1	0.095	0.1	0.07
Attention to Error Rate	1.0	0.95	1.0	0.70
Attention to Motion Variables	-	0.05	-	0 30

On the basis of the re-examination of previous K/s^2 tracking results, attention to error displacement was assumed to be only one tenth the attention to error rate (1). Thus, "full attention" to visual display variables was modeled by observation noise/signal ratios of -10 dB on error displacement and -20 dB on error rate. The model parameters relating to attentional allocation in Table 2 reflect the hypothesis that attention must be shared between visual variables as a group and motion variables as a group. All motion cues (plant position, rate, and acceleration) were assumed available, and there was assumed to be no interference among these informational quantities.

Model-generated rms performance scores were compared with experimental results in Figure 7. The left-hand graphs show the results for "displacement" (i.e., zero derivative) variables, whereas rate variables are diagrammed in the right-hand graphs. With one exception, model results show a near-perfect match to experimental scores for displacement variables. The match is less good for rate variables, but (again with one exception) the model correctly predicts the influence of motion cues on the trends of the performance measures.

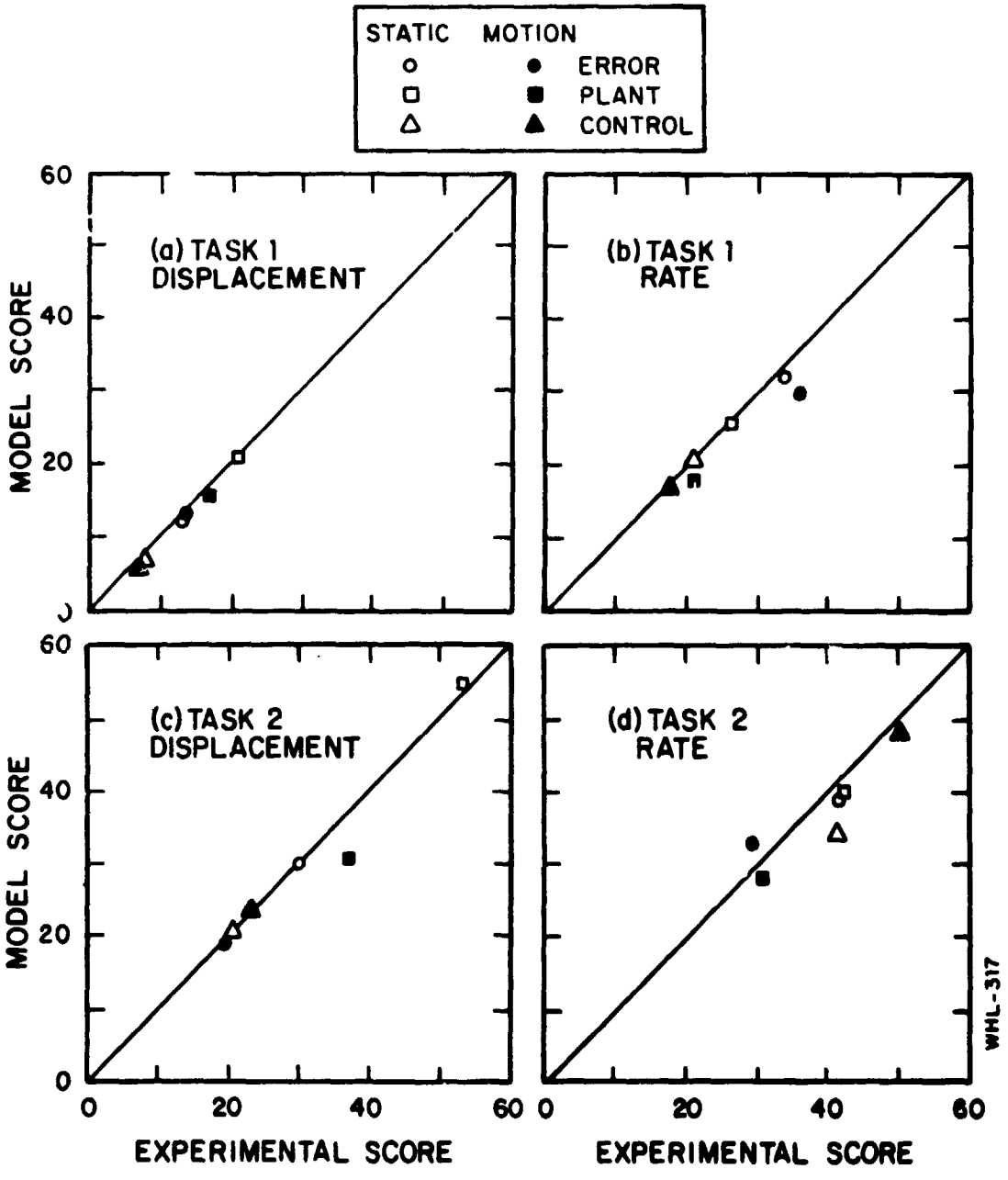

Figure 7. Comparison of Model and Experimental RMS Performance Scores.

Comparisons of model and experimental frequency-response curves are provided in Figure 8. In general, model response curves closely match experimental measures. Most importantly, the major effects of motion cues--the increase in low-frequency phase lead and the reduction in pilot remnant at low frequencies--are mimicked by the model, as is the constancy of the gain-crossover frequency between static and motion conditions.

Having quantified the effect of motion cues on pilot-related model parameters, we can now use the model to extrapolate the experimental results to situations beyond those studied in the laboratory. A particularly useful application of the pilot/vehicle model is to predict performance-workload tradeoffs (17, 18), especially as it is very difficult to obtain objective measures of workload experimentally.

Figure 9 shows predicted rms tracking error as a function of attention to the tracking task, where "attention" is related to the observation noise/signal ratio as described in Section 2. A relative attention of unity corresponded to -20 dB in this analysis.

Although not apparent from Figure 9, attentional allocation between visual and motion perceptual variables was readjusted to achieve minimum performance cost at different levels of overall attention. For both Task 1 and Task 2, decreasing overall attention required that an increasing fraction of available attention be devoted to motion variables.

Motion cues affect the predicted tradeoff curves differently for the two experimental tasks explored in the AMRL/BBN study. The dependency of rms error on attention is similar for Task 2 static and motion conditions, with error being consistently lower for the motion case. The effect of motion cues for Task 1 is basically to reduce the sensitivity of performance to workload at low levels of workload. That is, perofmrance is about the same for moderate to high workload levels; at low workload, motion cues apparently provide stabilizing information that prevents severe deterioration of performance.

Discussion of Model Results

As we noted in the discussion of experimental results, the AMRL roll-axis experiments produced results different from those observed in previous studies. Specifically, gain-crossover frequency remained virtually constant, high-frequency phase shift changed in the direction of more lag, low-frequency phase lead increased, and the benefits of motion cues were greater for the high-order (i.e., low-bandwidth) plant; most of the Stapleford et al and Shirley data showed opposite trends.

Except for the greater high-frequency phase lag, the effects of motion in the AMRL/BBN study are accounted for by a straightforward information analyses. The increase in high-frequency phase lag is modeled best by an increase in effective pilot time delay. One possible cause of the apparent increase in delay is the lag introduced by the dynamics associated with information processing by the semi-circular canals (19, 20).

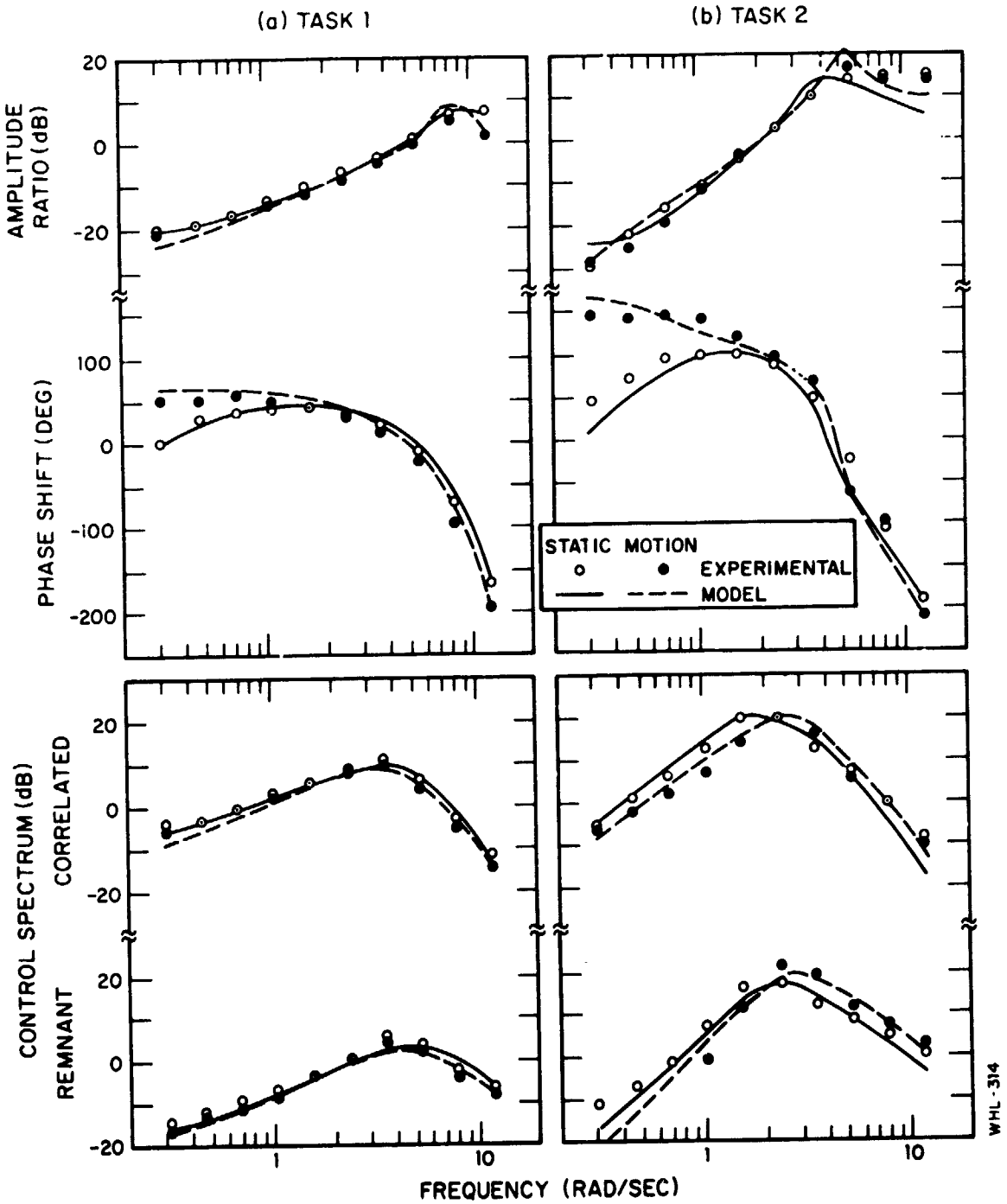

Figure 8. Comparison of Model and Experimental Frequency Response.

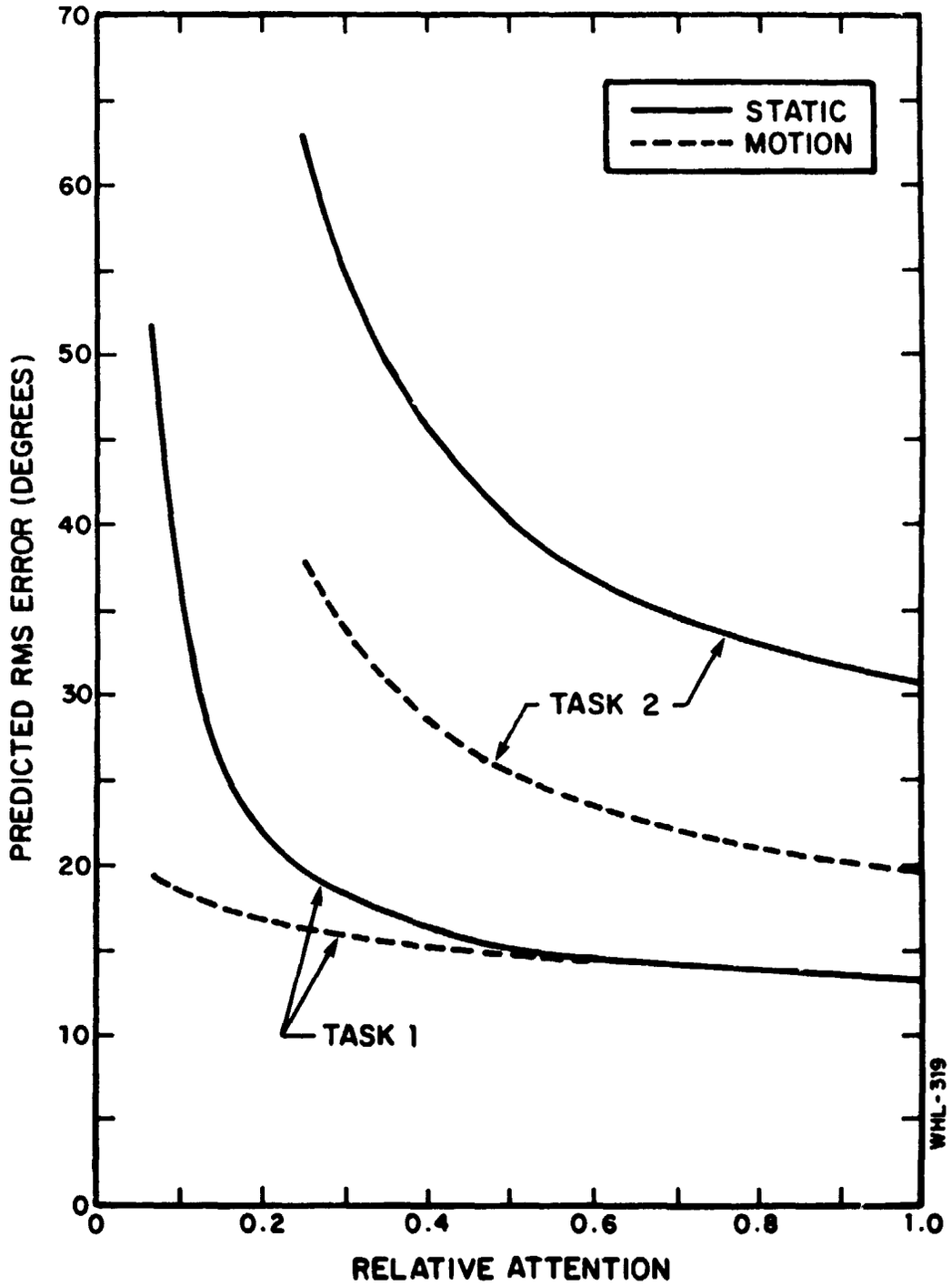

Figure 9. Effect of Motion Cues on Predicted Performance - Workload Tradeoff.

The time delay increase may also be related to limb motion induced by simulator motion. Recent studies of tracing in vibration environments have shown that effective pilot delay increases under vibration conditions (8, 9). Large increases in motor diving noise were also associated with vibration, however; similar effects were not observed in the AMRL/BBN study.

The model results shown in Figures 7 and 8 are consistent with the hypothesis that (a) the pilot obtains position, rate, and acceleration cues from the motion simulation, and (b) visual and motion-related sensory information mutually interfere. Other hypotheses were also tested; in particular, that (a) only rate information is obtained, and (b) there is no interference between visual and motion information..

As documented in (1), these various hypotheses yielded similar matching error scores. Thus, analysis did not provide a clear-cut choice of hypotheses concerning the use of motion cues in the roll-axis experiments, and some subjective judgement was required to select a modeling philosphy. Since there is a physiological basis for assuming that postion, rate, and acceleration information will be provided in a moving environment (at least in combination, if not as distinctly separate sensations), we adopt the more general hypothesis that all these cues are obtained; we let the model then determine the extent to which the available cues will be used in a specific tracking situation.

There is some supporting evidence to indicate that attention is shared between motion and visual cues. The attentions shown in Table 2 were derived on the basis of providing the best quantitative match to the experimental data. The model was also used in a purely predictive manner to find the allocation of attention (assuming interference) that would provide the lowest cost, where "cost" was defined as a weighted sum of error and control-rate variances. The attentional allocation that yielded least cost was very close to the allocation that best matched experimental data.

As documented in Levison, Baron, and Junker (1), additional model analysis was performed to search for a consistent set of rules for selecting control-related cost weightings. In the case of the roll-axis tasks discussed in this paper, the subjects appeared to operate at a point where the slope of the error-vs-control-rate curve reaches a minimum. This finding suggests a notion of physical workload that is similar to the ideas of attentional workload offered various researchers (7, 21); namely that the pilot will operate in a region in which additional improvement in overall system performance is offset by the additional cost of the effort required (where "cost" is defined in terms of pilot noise/signal ratios in the case of attentional workload and control or control rate activity in terms of physical workload).

CONCLUSIONS

The principal results of this study may be summarized as follows:

1. The effects of motion cues on roll-axis tracking performance obtained by AMRL can be modeled by (a) an increment of 0.05 seconds to the pilot time delay, and (b) inclusion of sensory variables that are likely to be provided by motion sensors (position, rate, and accel-

eration of the plant roll angle in these experiments). Modeling of dynamics associated with motion sensing is not required.

2. The experimental results do not allow us to determine whether motion and visual cues are processed in parallel, or whether the pilot must "share attention" between modalities. Furthermore, we are unable to determine whether the pilot obtains only rate cues from his motion sensors, or whether he uses a combination of position, rate, and acceleration cues.

3. If we assume that attention is shared between modalities, tracking performance is consistent with the notion that attention is shared optimally. Moreover, optimal allocation of attention between motion and visual sensory variables is different for the two control systems explored in the AMRL study.

4. Although tracking error is not greatly affected by the selection of a relative "cost coefficient" on control-rate activity, a good match to control scores requires that this weighting be readjusted for the two plants explored in this study; furthermore, different weightings are found for motion and static tracking for the more difficult plant.

5. The results of the AMRL experiment are different in certain respects from earlier studies of motion-based tracking. The AMRL study shows that motion cues result in an increase in low-frequency phase lead, an increase in high-frequency phase lag, and no important change in gain-crossover frequency; whereas other studies have shown that motion has little effect on low-frequency phase lead, reduces high-frequency phase lag, and allows an increase in gain-crossover frequency.

6. Although motion cues did not enhance tracking performance for the less difficult plant explored in the AMRL study, model analysis predicts that motion will enhance performance on this task if the pilot is required to allocate a substantial fraction of his attention to another task. That is, the less attention paid to the tracking task, the greater the relative benefit of motion cues.

The results of this study suggest a number of areas for future research, some of which are likely to be the subject of a follow-on to the study described herein. Recommended areas include:

1. application of the model to tracking situations explored in preceding studies of motion cues to determine whether or not a consistent modeling philosophy accounts for the use of motion cues in a variety of steady-state tracking situations;

2. consideration of vestibular dynamics in the pilot model, specifically to determine whether or not the apparent increase in time delay can be accounted for by the lags associated with vestibular dynamics;

3. effects of motion cues on performance in a high workload environment;

4. effects of motion cues in tracking tasks with transient inputs, especially in situations where visual/motion conflicts may be important; and

5. a controlled study of the effects of control gain and system bandwidth to help refine the motor aspects of the pilot/vehicle model.

REFERENCES

1. Levison, William H., S. Baron and A. M. Junker, "Modeling the Effects of Enviornmental Factors on Human Control and Information Processing," BBN Report No. 3258, May 1976.

2. Ringland, R. F., R. L. Stapleford, and R. E. Magdaleno, "Motion Effects on an IFR Hovering Task--Analytical Predictions and Experimental Results," NASA CR-1973, November 1971.

3. Stapleford, R. L., R. A. Peters, and F. Alex, "Experiments and a Model for Pilot Dynamics with Visual and Motion Inputs", NASA CR-1325, May 1969.

4. Shirley, R. S., "Motion Cues in Man-Vehicle Control", M.I.T., Cambridge, Mass., Sc.D. Thesis, January 1968.

5. Ringland, R. F. and R. L. Stapleford, "Experimental Measurements of Motion Cue Effects on STOL Approach Tasks", NASA CR-114458, April 1972.

6. Junker, A. and C. Replogle, "Motion Effects on the Human Operator in a Roll-Axis Tracking Task", Aviation, Space and Environmental Medicine, Vol. 46, pp. 819-822, June 1975.

7. Levison, W. H., J. I. Elkind and J. L. Ward, "Studies of Multivariable Manual Control Systems: A Model for Task Interference", NASA CR-1746, May 1971.

8. Levison, W. H. and P. D. Houck, "Guide for the Design of Control Sticks in Vibration Environments", Aerospace Medical Division, Wright-Patterson Air Force Base, Ohio, AMRL-TR-74-127, February 1975.

9. Levison, W.H., "Biomechanical Response and Manual Tracking Performance in Sinusoidal, Sum-of-Sines, and Random Vibration Environments", AMRL-TR-75-94, Aerospace Medical Division, Wright-Patterson Air Force Base, Ohio, April 1976.

10. Levison, W. H., "The Effects of Display Gain and Signal Bandwidth on Human Controller Remnant", Wright-Patterson Air Force Base, Ohio, AMRL-TR-70-93, March 1971.

11. Baron, S., D. L. Kleinman, et al., "Application of Optimal Control Theory to the Prediction of Human Performance in a Complex Task", AFFDL-TR-69-81, March 1970.

12. Kleinman, D. L., S. Baron and W. H. Levison, "An Optimal-Control Model of Human Response, Part 1: Theory and Validation", Automatica, Vol. 6, pp. 357-369, 1970.

13. Kleinman, D. L. and S. Baron, "Manned Vehicle Systems Analysis by Means of Modern Control Theory", ASA CR-1753, June 1971.

14. Kleinman, D. L., S. Baron and W. H. Levison, "A Control Theoretic Approach to Manned-Vehicle Systems Analysis", IEEE Trans. on Auto. Control, Vol. AC-16, No. 6, December 1971.

15. Baron, S. and D. L. Kleinman, et al., "An Optimal Control Model of Human Response - Part II: Prediction of Human Performance in a Complex Task", Automatica, Vol. 6, pp. 371-383, Pergamon Press, London, England, May 1970.

16. Baron S. and W. H. Levison, "Analysis and Modelling Human Performance in AAA Tracking", BBN Report No. 2557, Bolt Beranek and Newman Inc., Cambridge, Mass., March 1974.

17. Baron, S. and W. H. Levison, "A Manual Control Theory Analysis of Vertical Situation Displays for STOL Aircraft", NASA CR-114620, April 1973.

18. Baron, S. and W. H. Levison, "An Optimal Control Methodology for Analyzing the Effects of Display Parameters on Performance and Workload in Manual Flight Control", IEEE Trans. on Systems, Man, and Cybernetics, Vol. SMC-5, No. 4, July 1975.

19. Young, L. R., "The Current Status of Vestibular System Models", Automatica, Vol. 5, pp. 369-383, 1969.

20. Peters, R. A., "Dynamics of the Vestibular System and Their Relation to Motion Perception, Spatial Disorientation, and Illusions", NASA CR-1309, April 1969.

21. Wewerinke, P. H., "Human Operator Workload for Various Control Situations", Proceedings of the Xth Annual Conference on Manual Control," Wright-Patterson Air Force Base, Ohio, April 1974.

THE INFLUENCE OF LOSS OF VISUAL CUES ON PILOT PERFORMANCE DURING THE FINAL APPROACH AND LANDING PHASE OF A REMOTELY PILOTED VEHICLE MISSION

James C. Howard

NASA-Ames Research Center
Moffett Field, California 94035

SUMMARY

Remotely piloted research vehicles (RPRVs) are currently being flown from fixed-base control centers, and visual information is supplied to the remote pilot by a TV camera mounted in the vehicle. In these circumstances, the possibility of a TV failure or an interruption in the downlink to the pilot must be considered. To determine the influence of loss of TV information on pilot performance during the final approach and landing phase of a mission, an experiment was conducted in which pilots were asked to fly a fixed-base simulation of a Piper PA-30 aircraft with loss of TV information occurring at altitudes of 15.24, 30.48, and 45.72 m (50, 100, and 150 ft). For this experiment, a specially designed display configuration was presented to four pilots in accordance with a Latin square design. Initial results indicate that pilots could not ensure successful landings from altitudes exceeding 15.24 m (50 ft) without the visual cues supplied by the TV picture.

INTRODUCTION

To facilitate control of remotely piloted research vehicles (RPRVs), visual information is supplied to the remote pilot by a TV camera mounted in the vehicle as shown in figures 1 and 2. Because of the possibility of TV failure, an experiment was conducted to determine the influence of loss of visual cues on pilot performance during the final approach and landing phase of a mission. A recent study (ref. 1) established that the display of state variables shown in figure 3, was an effective configuration for RPRV pilots. In the configuration used, the basic display consisted of a TV picture of the terrain and runway, a horizon bar, and an aircraft symbol. Pilot opinion and experimental evidence indicated that pitch attitude, glide slope information, and a chevron combined with digital readouts of airspeed, altitude, and vertical velocity were the most useful additions to the basic display. The chevron, which is a sensitive indicator of altitude and sink rate, is shown separately in figure 4. It enables the RPRV pilot to control these variables with the precision necessary for successful landings. In all simulated landings, the chevron appeared on a head-up display at an altitude of 30.48 m (100 ft). In the present experiment, the TV picture was blacked out at altitudes of 15.24, 30.48, 45.72 m (50, 100, and 150 ft), and pilot performance was measured as a function of loss of visual information.

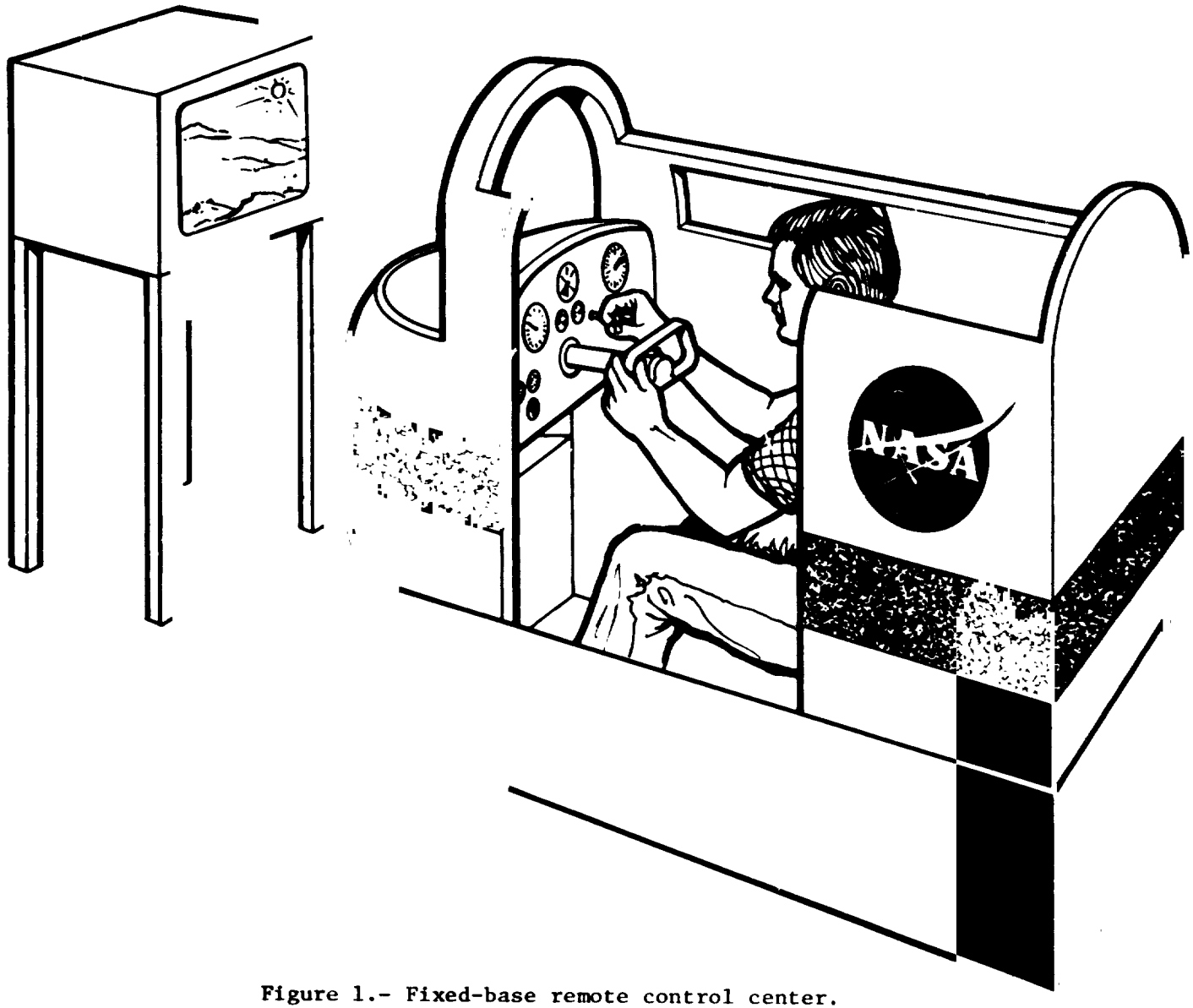

Figure 1.- Fixed-base remote control center.

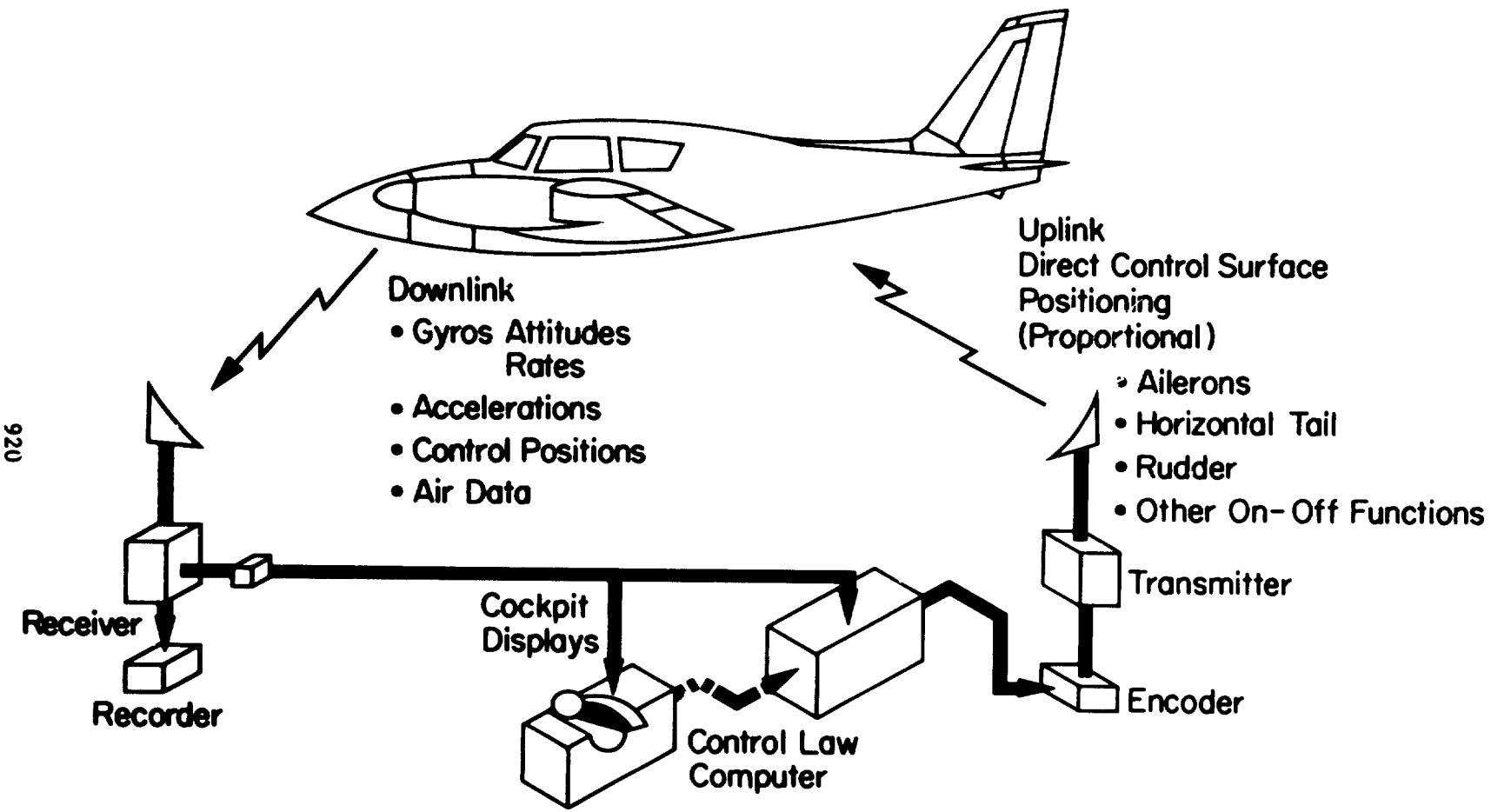

Figure 2.- Avionics link used in the NASA remotely piloted research vehicle.

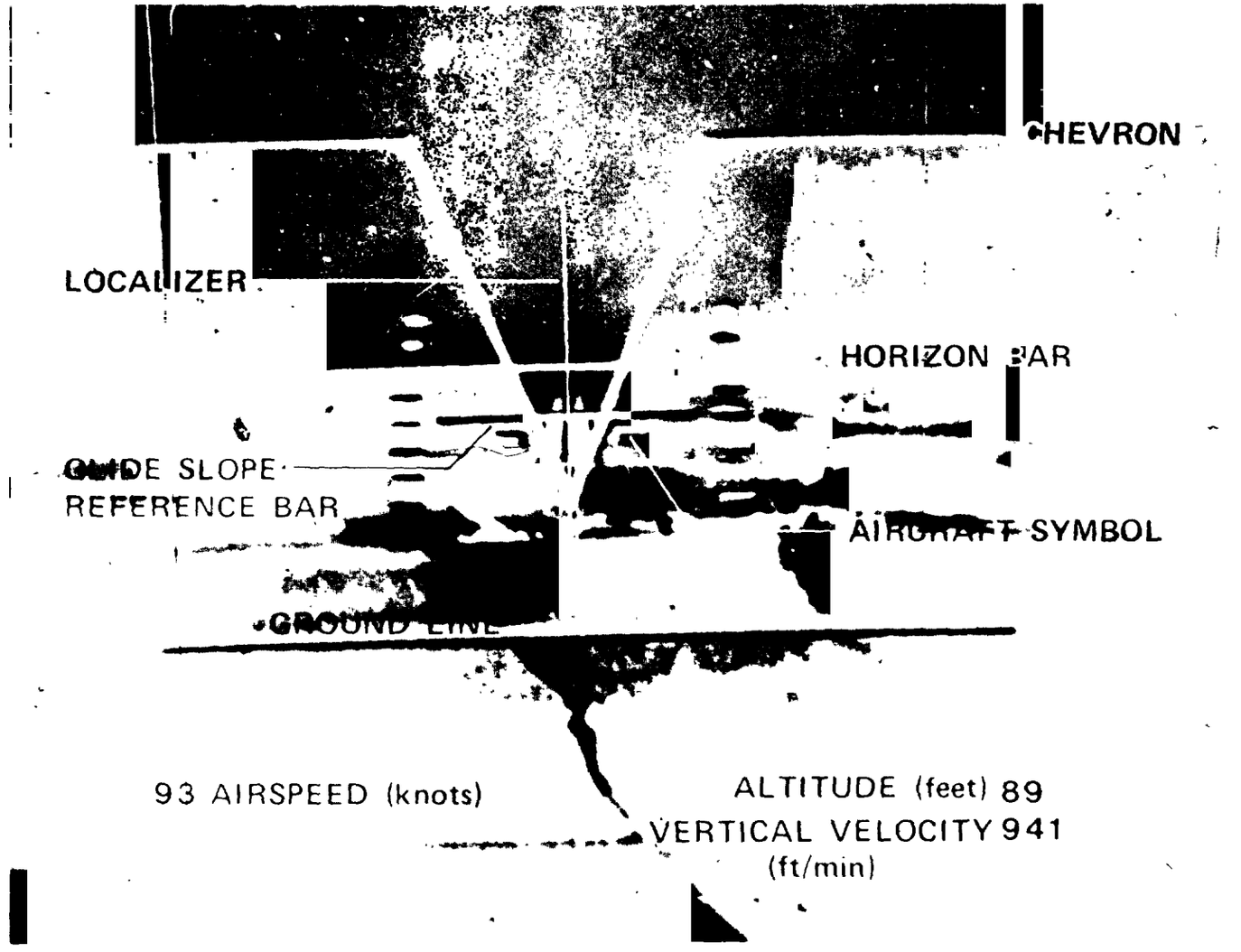

Figure 3.- Display configuration.

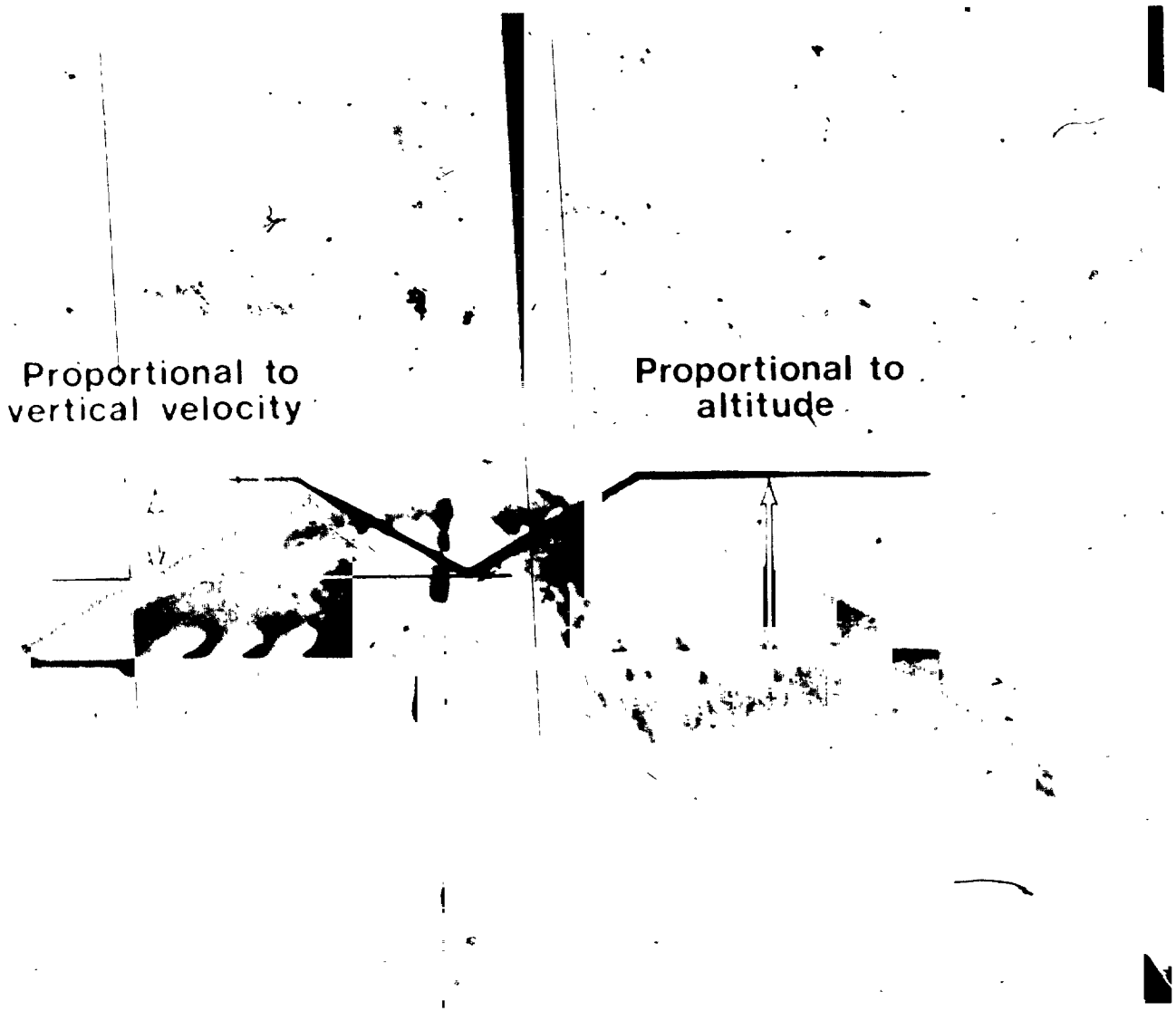

Figure 4.- Chevron characteristics.

EQUIPMENT AND METHOD

Aircraft Description

A Piper PA-30 aircraft was simulated for this experiment. This aircraft was chosen because it is currently being used at NASA's Flight Research Center for RPRV flight test experimentation. It is a low-wing monoplane, powered by two Lycoming, four cylinder, aircooled engines, each capable of delivering 160 rated horsepower. Figure 5 gives the principal dimensions. The airplane has a wing span of 10.97 m (35.98 ft), a wing area of 16.54 m^2 (178 ft^2), an aspect ratio of 7.3, and a mean aerodynamic chord of 1.52 m (5 ft) (ref. 2). The airplane has the standard three-control system. The horizontal tail is the all-movable type with a control deflection range of 4° to -14°. The tail has a trailing-edge tab which moves in the same direction as the tail, with a deflection ratio (tab deflection to tail deflection) of 1.5. The control deflection on each aileron is from 14° to -18°. The rudder control deflection range is ±27° (ref. 2).

Simulator and Vehicle Model

The Piper PA-30 aircraft was simulated on a Systems Engineering Laboratory (SEL) 840 digital computer. The final-approach model was based on available data from FRC's simulation model and references 2 and 3. The model consisted of the rigid body, six-degrees-of-freedom equations of motion that are perturbation equations in the stability axis system (ref. 3). After passage through a digital to analog converter (DAC), the output from the SEL 840 computer was used to drive a visual-flight attachment via an Applied Dynamics, Inc. (ADI) 256 analog computer. The output from the SEL 840 computer was also used to drive an Evans and Sutherland (E and S) LDS-2 display generator, which was mounted in parallel with the visual-flight attachment. The E and S display generator was used to superimpose geometric representations of state variables on the pictorial scene of terrain and runway generated by the visual-flight attachment. The visual-flight attachment used in this experiment was a General Precision Systems (GPS) model. The essential components of this attachment are a servo-driven television camera, an optical probe, and a TV monitor (ref. 4). A fixed-base simulator, consisting of a pilot's cab equipped with a conventional cockpit display and augmented with the GPS visual scene, was used to assess the importance of the E and S generated displays in assisting RPRV pilots to execute the final approach and landing phase of a mission without a TV picture of the terrain.

EXPERIMENTAL DESIGN

The configuration shown in figure 3 was used as a head-up display superimposed on a picture of the terrain. The picture of the terrain represents the visual information supplied to the RPRV pilot by the TV camera mounted in the vehicle. Four landing conditions were devised, three with loss of TV information at different altitudes and one with no loss of TV information. The

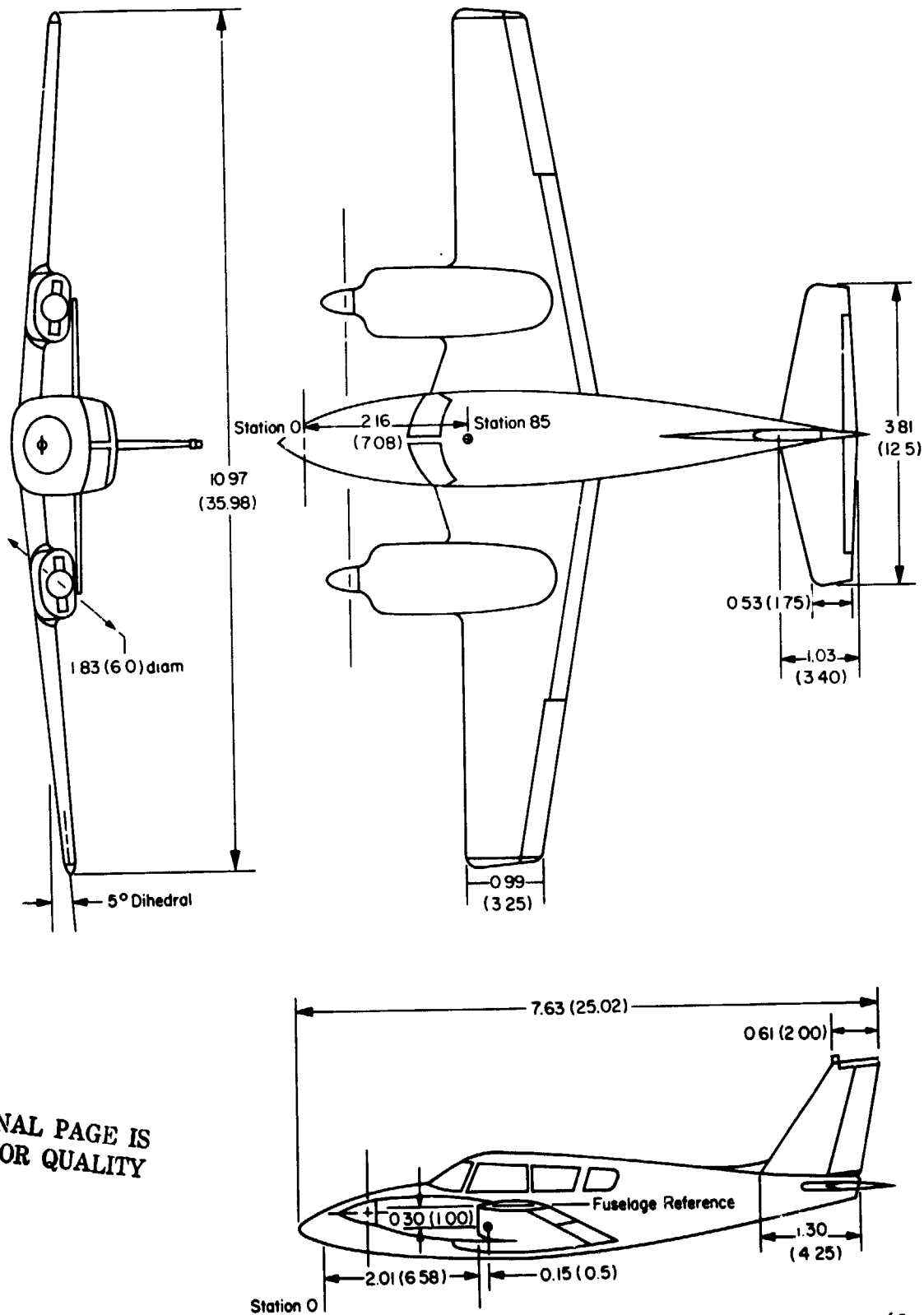

Figure 5.- Three-view drawing of airplane. All dimensions are in meters (feet).

resulting tasks were given to four pilot subjects in accordance with a Latin square design. If a Latin square with four displays is used, the error mean square will have only six degrees of freedom. To obtain an estimate of error with a larger number of degrees of freedom, the experiment was replicated using eight Latin squares. Each Latin square was then treated as a block in a randomized block design, with the square X display sum of squares corresponding to the block X treatment sum of squares in a randomized block design.

In the applications to which the Latin square has been typically applied in the fields of psychology, physiology, and drug research, each row of a square corresponds to a single subject, with the columns corresponding to successive periods or tests. This procedure was followed in the present design, where the element in a given Latin square gives the performance measure obtained during a test run with the corresponding display.

Each pilot was instructed to execute final approaches and landings starting from an initial distance of 2743 m (9000 ft) from the runway threshold, and an initial altitude of 152 m (500 ft). For each series of runs, the Latin square design assures that a subject never encounters the same order of presentation more than once, and that the order effect, whether it be practice, fatigue, boredom, etc., is independent of particular displays.

During each run the following performance measures were taken for subsequent statistical evaluation: sink rate at touchdown, root mean square (rms) of sink rate, rms of stick activity during the final 30.48 m (100 ft), and rms of distance from runway centerline.

RESULTS AND DISCUSSION

Sink Rate at Touchdown

The influence of loss of visual information on pilot performance may be seen by tabulating the sink rate at touchdown for each condition. In the following matrices of performance measures, S denotes subject, L the Latin square, and C the condition. Condition 1 is the condition without loss of TV visual information. Conditions 2, 3, and 4 represent loss of visual information at altitudes of 15.24, 30.48, and 45.72 m (50, 100, and 150 ft), respectively. The elements of the matrices are measures of sink rate at touchdown in ft/sec.

S = 1				
C =	1	2	3	4
L = 1	-2.53000	-1.66400	-3.07900	-0.60400
2	-1.79900	-0.78000	-0.90300	-0.59100
3	-1.95200	-1.04600	-1.46200	-1.76100
4	-1.84200	-0.77900	-1.21000	-1.48900
5	-1.76500	-1.82300	-1.72300	-1.42900
6	-1.86600	-1.31700	-0.76700	-0.95100
7	-1.87800	-1.15200	-1.24300	-1.26000
8	-1.62200	-1.12800	-1.11700	-1.77700

S = 2				
C =	1	2	3	4
L = 1	-4.88000	-3.35400	-2.18200	-1.91900
2	-3.50800	-5.20800	-7.84600	-3.66900
3	-4.12400	-0.83700	-6.55600	-3.64200
4	-4.33100	-2.65200	-2.32100	-2.03900
5	-4.00300	-2.82300	-1.48300	-4.64600
6	-4.06800	-1.15800	-0.79800	-3.17200
7	-2.59000	-6.17300	-1.62100	-4.66800
8	-2.93900	-0.63400	-0.94100	-1.78200

S = 3				
C =	1	2	3	4
L = 1	-0.93200	-2.91900	-4.09000	-2.10800
2	-3.30600	-1.63500	-2.52300	-1.86800
3	-2.82900	-3.10100	-1.47900	-2.75400
4	-1.60300	-2.23200	-4.27900	-4.22900
5	-1.51800	-1.40300	-8.47300	-1.28400
6	-1.20400	-2.29900	-1.86800	-2.54900
7	-1.75900	-0.80800	-2.06900	-7.27100
8	-1.73000	-1.15500	-0.91400	-0.74700

S = 4				
C =	1	2	3	4
L = 1	-1.41100	-3.06000	-1.01800	-6.52400
2	-3.20000	-1.19300	-2.05300	-3.62200
3	-1.52300	-0.68100	-5.54500	-1.67500
4	-1.42300	-1.33100	-1.14000	-1.40000
5	-0.69000	-0.69100	-1.62500	-2.05400
6	-0.37500	-0.91400	-3.82400	-0.71000
7	-0.86000	-1.10300	-3.87600	-0.84500
8	-1.22400	-0.83300	-1.84700	-0.77100

The computed value of the variance for the four conditions was 3.24. An error variance of 2.08 gave rise to an F ratio of 1.6. For a significance level of 0.05, the critical value of F for a condition variance with three degrees of freedom and an error variance with nine degrees of freedom is 3.86, and it is evident that the experimental value is not statistically significant.

rms Values of Sink Rate

To assess the influence of loss of visual information on pilot performance, as measured by rms values of sink rate, this parameter was computed during the final 30.48 m (100 ft) of altitude. The mean rms value of sink rate for all subjects and all error conditions was 1.9 m/s (6.24 ft/sec). As in the case of sink rate at touchdown, the rms values of sink rate were tabulated for each landing condition and are presented in the matrices below. The elements of the following matrices are rms values of sink rate, calculated during the final 30.48 m (100 ft) of altitude.

S = 1				
C =	1	2	3	4
L = 1	5.52900	6.32900	4.66000	5.02100
2	5.56400	4.65300	5.61100	5.42800
3	5.52200	4.85200	5.14200	5.20800
4	5.85000	6.25700	5.50800	5.07500
5	6.30900	5.75800	5.00800	5.81200
6	5.89200	5.90300	5.73000	5.88900
7	6.10300	6.32100	6.02800	5.81700
8	6.71100	5.73100	6.58100	5.92200

S = 2				
C =	1	2	3	4
L = 1	5.38800	5.90100	7.59300	6.86600
2	5.26900	7.20300	27.47600	6.28000
3	7.38000	7.14700	8.69200	7.33400
4	7.09000	6.57400	8.50800	6.22200
5	6.77900	8.47500	6.92600	7.48000
6	7.33600	5.90700	9.12400	7.02900
7	6.17800	9.79200	7.37500	7.66600
8	6.96200	6.48700	7.98700	8.24400

S = 3				
C =	1	2	3	4
L = 1	6.51300	5.82200	5.65900	6.41800
2	4.60200	6.44900	3.76000	4.04800
3	5.70600	4.20300	4.45500	5.57700
4	4.87800	4.55400	3.93900	5.33500
5	4.92600	5.88200	5.28100	5.54900
6	4.78600	5.30900	4.77500	4.51300
7	5.31400	5.06000	4.47300	4.56700
8	4.58700	5.03800	6.20800	4.09100

S = 4				
C =	1	2	3	4
L = 1	5.25900	6.20000	7.01000	9.07200
2	5.32100	6.21400	6.41900	7.65600
3	5.43000	6.67900	8.15900	6.30600
4	5.05000	5.47300	5.74400	5.41900
5	5.59300	5.31500	6.37900	6.59300
6	6.14500	7.49800	8.18100	6.68200
7	5.13300	6.03400	7.37300	6.67900
8	5.11000	6.18800	7.69200	5.84000

The computed value of the variance for the four landing conditions was 8.71. An error variance of 7.2 gave rise to an F ratio of 1.21. For a significance level of 0.05, the critical value of F for a condition variance with three degrees of freedom and an error variance with nine degrees of freedom is 3.86. It is evident that the experimental value obtained on the basis of rms values of sink rate measures is not statistically significant.

rms Values of Stick Activity

In order to determine the influence of loss of visual cues on pilot work load, as measured by rms values of stick activity, this parameter was measured during the final 30.48 m (100 ft) of altitude. The mean rms value of stick activity for all subjects and all conditions was 0.39 in.

As in the case of sink rates, the rms values of stick activity were tabulated for each condition. In the matrices of performance measures, the same notation applies here as in the preceding two cases, and the range of conditions is the same. The elements of the following matrices are rms values of stick activity measured during the final 30.48 m (100 ft) of altitude.

S = 1				
C =	1	2	3	4
1	0.14900	0.14800	0.29300	0.19400
2	0.15600	0.26600	0.18800	0.14900
3	0.13800	0.19400	0.18100	0.15600
4	0.13100	0.14300	0.16300	0.18400
5	0.12000	0.14900	0.17600	0.16600
6	0.11500	0.16100	0.13100	0.12500
7	0.12700	0.12200	0.12500	0.13100
8	0.10500	0.14200	0.12600	0.15300

S = 2				
C =	1	2	3	4
1	0.31300	0.21000	0.15400	0.36600
2	0.21100	0.40200	0.10100	0.21800
3	0.21400	0.17100	0.34700	0.24700
4	0.19900	0.17400	0.33300	0.12800
5	0.20500	0.14100	0.18800	0.13700
6	0.17700	0.11800	0.20200	0.21400
7	0.15400	0.12600	0.19300	0.18500
8	0.14300	0.25200	0.14000	0.12000

S = 3				
C =	1	2	3	4
1	0.77900	0.85000	1.30300	1.42800
2	0.54900	1.51500	1.02500	1.13900
3	0.24500	1.56500	0.49000	0.89100
4	0.57600	1.52000	1.98700	0.56300
5	0.73900	1.90900	1.92800	0.42200
6	0.52000	0.49300	0.58400	1.37900
7	0.52200	0.72300	0.32500	2.25800
8	0.72600	0.63500	0.71600	1.41000

S = 4				
C =	1	2	3	4
1	0.23300	0.21600	0.17700	0.21200
2	0.23400	0.17100	0.15400	0.15400
3	0.20700	0.25500	0.11800	0.21500
4	0.23200	0.20200	0.17200	0.20700
5	0.18900	0.22500	0.29300	0.15600
6	0.19600	0.14500	0.11300	0.14900
7	0.25400	0.23000	0.10700	0.13500
8	0.21300	0.17000	0.10400	0.18700

The computed value of the variance of stick activity for all conditions was 0.15. An error variance of 0.16 gave rise to an F ratio of 0.97. As in the preceding two cases, the critical value of F for a significance level of 0.05 is 3.86. It is evident that the variation of workload with loss of visual cues, is not statistically significant.

Lateral Offset from Runway Centerline

The data obtained indicate that with the head-up display configuration used, the absence of a TV picture of the terrain made no significant difference to the pilot's ability to control sink rate. Moreover, landing under these conditions imposed no additional workload on the pilots. However, the disappearance of the visual scene provided by the TV camera impaired the pilot's ability to land on the runway. In terms of distances from the runway centerline, the performance data assumed the following form:

	S = 1			
	C = 1	2	3	4
L = 1	-16.19398	39.46399	-90.33099	13.10200
2	-15.98100	-60.21599	30.13300	6.74900
3	-11.48700	-33.71100	26.88399	14.50500
4	0.81300	-18.58699	-12.41300	-99.40199
5	2.48700	5.56700	-62.53600	-83.81200
6	-9.32900	-20.62399	-157.37900	-65.90500
7	-8.54200	21.83099	-139.63100	17.70599
8	-0.42100	-0.24400	-123.98499	-108.51999

	S = 2			
	C = 1	2	3	4
L = 1	1.49000	28.60500	-136.31799	-143.21199
2	-1.18900	-121.96199	-19.43799	4.77600
3	12.89300	-35.34799	-83.18599	46.59299
4	22.04599	2.92600	-67.99300	76.88899
5	2.95300	-6.29400	-43.64899	81.21599
6	5.96100	31.53699	-69.62900	52.13899
7	5.27100	-9.15000	-133.36800	-69.99599
8	-6.56800	2.72700	-149.36899	-219.23499

S = 3				
C =	1	2	3	4
L = 1	-13.77200	7.39100	-32.41599	158.53600
2	14.23500	-3.22000	64.41699	-77.44899
3	8.16900	-234.73499	-19.11499	-10.81500
4	10.01300	24.25000	-237.16800	-15.80800
5	4.97700	57.75000	115.48999	-22.53899
6	14.15400	13.89200	-0.06200	-45.82999
7	6.12600	4.43200	20.12399	-62.76299
8	-10.66700	0.91000	13.35600	-46.70200

S = 4				
C =	1	2	3	4
L = 1	-26.34999	52.68100	16.80499	-29.35300
2	-33.31799	51.51299	-3.57100	24.44398
3	-10.27100	39.03400	-11.63700	19.67899
4	-8.64900	24.05399	45.72299	-4.87100
5	-13.30500	25.73199	75.36400	19.04199
6	-11.76900	1.32400	-2.29400	23.49399
7	8.50900	-27.18500	-22.34698	-26.70599
8	-19.03799	-14.80900	-15.26000	18.64999

Since these data clearly indicate the influence of TV information on the pilot's ability to land on the runway, there is no need to perform an analysis of variance. However, to facilitate the interpretation of these data, the rms values of lateral offset from runway centerline in feet are shown in the following table for each pilot and each condition.

Subject	Condition			
	1	2	3	4
1	3.08 m (10.10 ft)	9.39 m (30.82 ft)	29.22 m (95.85 ft)	19.80 m (64.97 ft)
2	3.00 m (9.83 ft)	14.49 m (47.53 ft)	29.97 m (98.33 ft)	32.49 m (106.59 ft)
3	3.30 m (10.82 ft)	26.24 m (86.10 ft)	29.66 m (97.30 ft)	21.61 m (70.91 ft)
4	5.64 m (18.49 ft)	10.31 m (33.82 ft)	10.19 m (33.42 ft)	6.68 m (21.92 ft)

The number of times each pilot failed to land on the runway, for each condition, is shown in the following table.

Subject	Condition			
	1	2	3	4
1	0	0	4	3
2	0	1	4	4
3	0	1	2	2
4	0	0	1	0

CONCLUSIONS

Statistical evaluation of the data obtained indicates that for the range of conditions considered, there is no significant difference in landing performance, as measured by sink rate, that can be attributed to the absence of a TV picture of the terrain. Workload, as measured by stick activity, did not increase significantly when the pilot was deprived of visual cues. However, there appeared to be increased rudder activity as the pilot attempted to control heading without the visual scene. The sudden transition from visual to instrument reference conditions was disconcerting to the pilots, and when this occurred at 30.48 m (100 ft) or more, the probability of drifting off the runway increased, particularly if the transition occurred when the localizer error was large.

REFERENCES

1. Howard, James C.: Display Requirements for the Final Approach and Landing Phase of an RPV Mission. NASA TM X-62,346, 1974.

2. Funk, Marvin P.; and Freeman, Delma C., Jr.: Full Scale Wind-Tunnel Investigation of Static Longitudinal and Lateral Characteristics of a Light Twin-Engine Airplane. NASA TN D-4983, 1969.

3. Koziol, Joseph S., Jr.: Simulation Model for the Piper PA-30 Light Maneuverable Aircraft in the Final Approach. Transportation Systems Center Technical Memorandum, July 1971.

4. Chase, Wendell D.: Evaluation of Several TV Display Systems for Visual Simulation of the Landing Approach. NASA TN D-6274, 1971.

SIMULATION OF CONVENTIONAL AIRCRAFT APPROACH AND LANDING: THE EFFECT OF WITHHOLDING MOTION OR INSTRUMENT CUES

By R.V. Gressang, Capt, USAF

AF Flight Dynamics Laboratory

SUMMARY

The results of two experiments conducted using the multicrew cab simulator of the Flight Control Division, Air Force Flight Dynamics Laboratory are presented. The first experiment was concerned with the effect upon approach and landing performance of fixed base versus moving base operation. The second experiment was concerned with the effect of denying instrument information upon approach and landing performance in a simulator. For this experiment, the instruments were frozen at their initial trim values, and the pilot had to land the simulator using only visual, motion, and sound cues.

The aircraft simulated was a four engine jet transport of about 180,000 pounds. During the experiments, the aircraft was simulated both with and without its stability and control augmentation system (SCAS).

The first experiment established that performance changes due to fixed base versus moving base operation were slight, and were much smaller than changes induced by turning off the SCAS system. In this simulator, the pilot could achieve a credible landing without using the instruments, but he had more difficulty if the SCAS was off. If instrument information were denied, he flew a lower, slower approach.

INTRODUCTION

The simulation of aircraft approaches and landings has recently become important because of the low cost, safe, flexible opportunities it presents for aircrew training, pilot/aircraft system research and engineering, investigation of potential flight hazards, and accident investigations[1], [2], [3]. For these applications to be feasible, it is necessary to know how simulation results and performance compare with actual results and performance for the appropriate task. It is also necessary to know that the pilot does not significantly change his behavior in going from an actual aircraft to a simulation of that aircraft, and to know what cues must be provided in the simulator to allow the pilot to fly the simulator without changing his basic behavior pattern for the task being simulated.

Experience to date indicates that it is difficult to simulate landing an aircraft in such a way that the touchdown performance is comparable to the performance achieved by a pilot in a real aircraft[2-8]. The statistic most commonly reported about landing simulations is the mean sink rate at

touchdown, which is generally significantly higher in the simulation than it would be for an actual aircraft. This has been observed in over fourteen different simulations, involving at least four different aircraft, both fixed base and three degree of freedom moving base, and at least five different types of visual display.[2-8]

Experimental investigations of the differences between simulator landing performance and aircraft landing performance have not determined any specific single factor which contributes most of the difference between simulator and aircraft performance. Since no single specific factor has been related to the difference between simulator and aircraft performance, and since attaining maximum realism of cues in a simulator is limited by necessary physical limitations (such as the amount of travel allowed in motion drive systems) and the economic law of diminishing returns, the objective of attaining realistic pilot behavior in landing simulations must be obtained by carefully determining the sensitivity of the pilot's performance to the various cues.

One approach to attaining realistic performance has been to thoroughly familiarize the pilot with the simulation, giving him several hours of simulation time before the experiment is started and data collected. However, it has been objected that this results in training the pilot to fly the simulator as a simulator rather than as an aircraft. An alternate approach is to analyze what cues are used by the pilot to accomplish the landing task, and then concentrate on providing accurately only the minimum cues necessary. The difficulty with this approach is that no clear concensus exists as to what cues are used during landing, and what their relative importance is.

The experiments reported on in this paper provide information useful to either of the above approaches. Information was obtained on how many simulation runs would result in stabilized touchdown sink rates, while the effect of freezing the instruments (thus preventing the pilot from flying the simulator using only the instruments) was studied. Similarly, the effect of the limited motion cues available upon touchdown performance was studied. When the instruments were frozen, it was determined that visual and limited motion cues were sufficient to land the simulator. The pilot did succeed in landing the simulator with sink rates representative of real aircraft, but his behavior was slightly modified from what it would have been in a real aircraft.

DESCRIPTION OF THE SIMULATION

The objectives of the experiments reported on in this paper were to investigate the effects of visual and motion cues upon simulated aircraft landings. The pilot's task was to execute a conventional Visual Flight Rules (VFR) approach and landing, depending mainly upon the visual display for flight path guidance. All approaches were conducted under simulated clear air daylight conditions. Each experimental run began from trim conditions at 750 feet on a three degree glide slope. The pilot used visual path information to fly a nominally three degree glide slope approach to the runway, flare, and touch the aircraft down. The run was terminated after touchdown.

The aircraft used for this simulation was modeled by six degree of freedom nonlinear equations of motion on a hybrid computer[9]. The aircraft was a four engine jet transport of approximately 180,000 pounds gross weight. The aircraft had conventional aileron, elevator, rudder, and throttle controls. It also had a direct lift control obtained by using spoilers, and blown flaps. The blown flaps resulted in considerable powered lift. Longitudinal control was accomplished through the direct lift control and pitch trim button, while lateral control was accomplished using the ailerons. In normal configuration, the aircraft had an extensive stability and control augmentation system (SCAS). Certain runs were made with the SCAS on, and other runs made with the unaugmented aircraft.

The instrument panel was organized in a conventional manner. No flight director was used. The cockpit was a C-135 cockpit that had been modified for research and development use. It was mounted upon a three degree of freedom (roll, pitch, heave) motion base[10]. Sound cues duplicating four turbojet engines were generated.

Visual cues simulating real world changes in size and perspective with respect to aircraft motion were produced using a three dimensional illuminated terrain model and television camera-screen projection system. The field of view of the screen was 60 degrees diagonally. The view was large enough to present a realistic scene through the front windows, but there were no peripheral cues. During an approach, the pilot saw a daylight rural terrain with an airport complex.

Turbulence inputs were inserted into the simulation. These inputs corresponded to light turbulence of the Dryden spectra of MIL-F-8785B[1].

DESCRIPTION OF THE EXPERIMENTS

Two experiments were conducted, with the following objectives:

1. Does the motion system affect landing performance?
2. Can the simulator be landed as a conventional aircraft without the use of the cockpit instruments?
3. Can the simulator be landed as a conventional aircraft with realistic values of sink rate at touchdown?

The first experiment was to answer objective 1, and was a 2x2x10 factorial experiment. The factors were motion system on or off, SCAS on or off, and replication (10 replications). Before the experiment began, the pilot executed 10 practice runs. During the experiment, the various conditions were presented to the pilot randomly.

The second experiment consisted of 20 simulated approaches and landings, made with the cockpit instruments frozen at their initial trim values. Half of these runs were made with the SCAS on, and half with the SCAS off. SCAS on or off was presented randomly to the pilot.

The third objective was satisfied by recording the touchdown sink rates of all the approach and landing runs that the subject pilot made. On each simulation run, data were collected both at the instant of touchdown and during the approach. The data collected at touchdown consisted of the instantaneous values of x, $\dot{x}$, z, θ, q, y, $\dot{y}$, ϕ, ψ, p, and v. During the approach the means and standard deviations of θ, q, h (glide slope deviation in feet), α, ϕ, p, ψ, r, y (localizer deviation in feet) and β were computed in real time for all points on the approach lying between 500 feet altitude and 50 feet altitude.

The subject pilot for these experiments was an Air Force pilot with 1700 hours total flying time. He was briefed on the purpose of the experiments, and conducted the simulated approaches and landings alone, without the assistance of a copilot. He had no tasks to perform in addition to landing the aircraft.

RESULTS OF THE EXPERIMENTS

The data collected during the experiments are presented in Tables 1 through 4. Table 1 presents the longitudinal touchdown data, Table 2 presents the lateral touchdown data, Table 3 presents the longitudinal approach data, and Table 4 presents the lateral approach data. The classification scheme used for the data denotes the (SCAS, motion) combination as A, (SCAS, no motion) as B, (No SCAS, motion) as C, (No SCAS, no motion) as D, (SCAS, no instruments) as E, and (No SCAS, no instruments) as F.

A complete statistical analysis of the data, using t tests, F tests, M tests for homogenous variances, and analysis of variance can be found in reference 12. The results of this analysis are summarized in the following paragraphs.

The largest effects observed during the experiments were due to the control system (SCAS). The aircraft was more difficult to fly when the control system was off, and this was reflected in more scatter in the aircraft variables during the approach and at touchdown.

The only effects observed due to motion cues were a lesser tendency to "duck under" the nominal glide slope when the motion was off combined with a tendency to land further down the runway. However, the tendency to land further down the runway was in conjunction with a similar but more prominent tendency associated with the control system being off.

When the pilot was forced to fly the simulator using only the visual display, he flew more slowly and had more difficulty in controlling airspeed. He "ducked under" the nominal glide slope to a greater extent, and the control system being off increased the scatter in the aircraft variables, especially the lateral variables. Despite these differences, the pilot was able to fly and land the simulator as an aircraft.

The lack of an appreciable effect due to the motion system being on or

off is not unexpected for the landing task. The standard deviations of p, q, and r are all of the same magnitude or smaller than the thresholds for human sensing of these angular velocities, so motion cues would not be expected to be important in the task simulated.

The data available for studying whether the simulator can be landed as a conventional aircraft with realistic values of sink rate at touchdown consisted of values of the sink rate at touchdown on 128 simulated landings by the same pilot. These 128 sink rate values were listed chronologically, examined for learning behavior and the effects of changing experiments, and classified as to the various landing strategies used by the pilot. The data most readily available concerning landing sink rates of actual aircraft is in the form of a nominal sink rate, and sometimes a standard deviation. Typical values are -2 ft/sec mean and a standard deviation of .5 ft/sec.

The mean and standard deviation of the simulation touchdown sink rates were computed for groups of 10 runs, with the division into groups being on a chronological basis. The exceptions to this were the last two groups, which were of 7 and 11 runs respectively, and so divided because of a change in pilot strategy. The means and standard deviations for each group are given in Table 5.

Examining the data in Table 5, a learning effect is present throughout the first 40 runs, and terminates in a sudden step improvement in performance about run 40. The duration of the learning period agrees well with the data in references 8 and 13. The pilot's performance then plateaued until about run 80, when either a three-week layoff or changing experiment conditions resulted in the pilot having to relearn to his previous level of proficiency. The sink rate performance then approaches the previous level until run 118.

The most interesting part of the data is the sudden decrease in sink rate starting at Run 118, as it is associated with the pilot saying he changed his landing strategy. The first strategy used by the pilot involved trading off longitudinal touchdown position for sink rate. During the flare, the pilot would retard the throttles as would be normal in an aircraft. The change that resulted in the second strategy was that the pilot waited until after touchdown to chop the throttles. This change resulted in a mean and standard deviation of touchdown sink rate which compares very well with the values for actual aircraft. Since the only change in the pilot's behavior which occurred and resulted in the agreement with actual aircraft sink rates was in the timing of the throttle chop, the possibility is raised that simulator sink rate problems during landing may be due to either pilot difficulty in judging height, or due to poor models of engine thrust dynamics.

CONCLUSIONS

The overall conclusions of these experiments are that:

1. The limited motion system used in these experiments had minimal effect upon the pilot's landing performance.

2. The simulator can be landed as a conventional aircraft without instrument cues.

3. The simulator can be landed as a conventional aircraft with realistic values of sink rate at touchdown provided the pilot cuts the throttles after touchdown.

4. Changing the aircraft dynamic response has a much greater effect upon the pilot's landing performance than turning off the motion system.

REFERENCES

1. Laynor and Roberts. A Wind Shear Accident as Evidenced by Information from the Digital Flight Data Recorder. SASI International Seminar, Ottawa, Canada, 7-10 October 1975.

2. Gressang, Stone, Kugel, and Pollard. Low Visibility Landing Pilot Modeling Experiment and Data. AFFDL TR 75-41, December 1975.

3. Gressang. Low Visibility Landing Pilot Modeling Experiment and Data, Phase II. AFFDL TR 75-57, August 1975.

4. Armstrong. Difficulties with the Simulation of Aircraft Landings. RAE TR 68116, May 1968.

5. Brown. A Preliminary Simulator Investigation of the Problems of Category II Operation. RAE Tech Memo, BLEU 135, May 1968.

6. Brown. An Examination of Simulator Landing Problems. RAE Tech Memo Avionics 49, March 1970.

7. Armstrong and Musker. Training for Low Visibility Landings. RAE TR 70225, November 1970.

8. Palmer and Cronn. Touchdown Performance with a Computer Graphics Night Visual Attachment. Unpublished paper, NASA Ames Research Center.

9. Bankovskis. Equations of Motion and Constants for the AFFDL Hybrid Simulator. AFFDL TM 75-98-FGD, June 1975.

10. Naylor. Proposed Methods of Driving AFFDL Engineering Flight Simulator Motion Systems. AFFDL TM 75-22-FGD, February 1975.

11. Chalk, Neal, Harris, Pritchard, and Woodcock. Background Information and User Guide for MIL-F-8785B(ASG), "Military Specification--Flying Qualities of Piloted Airplanes". AFFDL TR 69-72, August 1969.

12. Gressang. Landing Simulation Experiments: Fixed Versus Moving Base and Purely Visual Approach. AFFDL Draft Technical Report.

13. Parrish, Rollins, and Martin. Visual-Motion Simulation of CTOL Flare and Touchdown Comparing Data Obtained from Two Model Board Display Systems. AIAA Visual and Motion Simulation Conference, Dayton, Ohio, 26-28 April 1976.

TABLE 1: LONGITUDINAL TOUCHDOWN PARAMETERS

VARIABLE		CONFIGURATION					
		A	B	C	D	E	F
x	Mean	83.02	191.87	450.86	902.13	27.5	679.2
	Std. Dev.	556.5	457.42	679.92	999.02	919.21	869.44
$\dot{x}$	Mean	185.44	187.07	182.61	179.79	169.93	166.93
	Std. Dev.	3.37	6.33	5.27	6.36	19.91	8.19
$\dot{z}$	Mean	-4.64	-4.30	-5.47	-5.96	-5.86	-5.29
	Std. Dev.	2.15	1.90	2.51	2.48	3.99	1.59
θ	Mean	4.27	4.72	5.88	5.30	8.07	9.10
	Std. Dev.	.67	2.39	2.50	2.40	3.89	1.98
q	Mean	.45	.50	1.56	.79	.34	1.58
	Std. Dev.	.76	.58	.84	2.07	.82	1.36

Table 1: Units are ft., ft/sec., deg., deg/sec.

TABLE 2: LATERAL TOUCHDOWN PARAMETERS

VARIABLE		CONFIGURATION					
		A	B	C	D	E	F
y	Mean	15.11	14.77	-4.31	1.94	15.87	1.87
	Std. Dev.	16.22	21.07	13.50	25.08	26.59	27.52
$\dot{y}$	Mean	-.63	.20	.85	1.07	-.10	-1.19
	Std. Dev.	2.86	4.75	3.53	2.99	1.27	3.58
ϕ	Mean	.45	.80	.47	1.04	-.29	.68
	Std. Dev.	1.18	1.62	3.73	6.05	.77	3.12

TABLE 2 (Continued)

VARIABLE		CONFIGURATION					
		A	B	C	D	E	F
ψ	Mean	89.49	89.36	88.94	88.19	90.19	90.06
	Std. Dev.	.60	1.16	1.59	2.39	.95	1.62
p	Mean	-.43	1.29	.78	-.95	-.01	-.30
	Std. Dev.	2.15	1.88	2.13	3.25	1.14	2.19
r	Mean	0.57	-.27	.29	-.05	.30	-.38
	Std. Dev.	1.08	1.00	1.43	1.72	1.47	.93

Table 2: Units are ft., ft/sec., deg., deg/sec.

TABLE 3: LONGITUDINAL APPROACH STATISTICS

VARIABLE		CONFIGURATION					
		A	B	C	D	E	F
θ	Mean	1.622	1.948	1.555	2.102	3.408	2.652
	Std. Dev.	.478	.502	.993	1.077	1.156	1.011
q	Mean	-.0035	-.004	-.002	.007	.039	-.013
	Std. Dev.	.309	.348	.866	.888	.375	.727
h	Mean	-24.6	-14.6	-27.6	-13.7	-34.07	-29.67
	Std. Dev.	9.36	11.38	11.77	13.67	14.75	12.95
α	Mean	4.716	4.880	4.442	5.131	6.581	5.652
	Std. Dev.	.628	.653	.936	.964	.989	.819

Table 3: Units are ft., deg., deg/sec.

TABLE 4: LATERAL APPROACH STATISTICS

VARIABLE		CONFIGURATION					
		A	B	C	D	E	F
ϕ	Mean	.449	.597	1.074	1.096	.097	.513
	Std. Dev.	1.185	1.747	3.387	3.281	.830	4.555
p	Mean	-.031	.035	.032	.018	-.035	-.033
	Std. Dev.	1.598	1.814	2.375	2.478	.887	2.472
ψ	Mean	89.525	88.921	88.434	88.392	90.095	89.315
	Std. Dev.	.992	1.098	1.315	1.527	.900	1.381
r	Mean	.044	.002	.069	.013	.018	-.005
	Std Dev.	.827	.862	1.193	1.243	.507	1.042
y	Mean	-4.4	22.8	-4.5	-3.3	17.9	17.4
	Std. Dev.	27.0	31.9	25.4	19.6	21.3	38.1
β	Mean	.394	.921	1.476	1.598	-.147	.392
	Std. Dev.	1.033	1.285	1.846	1.933	.686	2.069

Table 4: Units are ft., deg., deg/sec.

TABLE 5: TOUCHDOWN SINK RATE MEANS AND STANDARD DEVIATIONS

RUNS	MEAN $\dot{z}$	$\dot{z}$ STANDARD DEVIATION
1 to 10	-7.81	3.18
11 to 20	-6.63	2.16
21 to 30	-6.34	2.37
31 to 40	-6.00	2.31
41 to 50	-4.04	1.37
51 to 60	-4.09	1.97
61 to 70	-4.38	1.59
71 to 80	-4.76	1.75
81 to 90	-6.58	3.67
91 to 100	-6.37	2.59
101 to 110	-4.71	2.39
111 to 117	-4.51	1.15
118 to 128	-1.94	.57

Table 5: Units are ft/sec.

EFFECTS OF DIFFERING MOTION SYSTEM DRIVES ON SIMULATION OF APPROACH AND LANDING

Capt Joseph Pollard
Air Force Flight Dynamics Laboratory

SUMMARY

A discussion of simulator testing for motion response is coupled with a scientific experiment to determine the effects of differing motion drive equations on approach and landing of a heavy aircraft. The conditions of no motion, motion driven by linear combinations of rate and attitude, and motion driven by linear accelerations are tested to determine if significant statistical differences exist between systems. All other factors were held constant. The simulation was performed at the Flight Control Development Laboratory utilizing the Multicrew Cab. The results of the simulation analysis are clearly shown to be affected by the required choice of motion drive equations in simulation design. Specific performance variables are indicated as most seriously affected.

INTRODUCTION

One of the tasks most often investigated at the Flight Control Development Laboratory is that of landing including power approach flare, and touchdown. A simple experiment was designed to investigate the sensitivity of pilot performance to changes in the drive equations applied to the limited motion base simulator. The tracking performance of the pilot during power approach was found to be relatively insensitive; however, the variations in many of the aircraft states at touchdown were found to be statistically significant. [1]

SYMBOLS

The following symbols are used throughout this paper. The most commonly used units are given for presentation with this paper.

a_x, a_y, a_z	Aircraft inertial earth axis accelerations, ft/sec^2
$\dot{u}$, $\dot{v}$, $\dot{w}$	Aircraft body axis linear accelerations, ft/sec^2
$\dot{p}$, $\dot{q}$, $\dot{r}$	Aircraft body axis rotational accelerations, deg/sec^2
θ	Aircraft pitch angle, deg

ϕ	Aircraft roll angle, deg
ψ	Aircraft heading angle, deg
p	Aircraft roll rate, deg/sec
q	Aircraft pitch rate, deg/sec
r	Aircraft yaw rate, deg/sec
θ_o	Aircraft nominal pitch angle, trim, deg
ℓ_x, ℓ_y, ℓ_z	Offsets from aircraft center of gravity to the pilot's station, ft
g	Acceleration due to gravity, 32.2 ft/sec^2
s	Laplace operator
α	Confidence level assigned to statistical testing
F	A ratio of variances used in statistical tests

THE SIMULATOR

A three degree of freedom motion base simulator with a multicrew cab instrumented as an AMST aircraft was used for the experiment. The motion system is a scissors configuration utilizing two forward hydraulic cylinders and one aft. The forward cylinders are identical and have a stroke of $\pm$ 12 inches while the rear cylinder has a travel of $\pm$ 18 inches. Hydraulic power was supplied by a 60 gpm pumping system at 3000 psi. Each actuator was flow limited to 10 gpm. The motion base was programmed so that all three cylinders provided heave while the two forward cylinders were operated asymetrically to produce roll. The rear cylinder was operated alone to produce pitch. Figure 1 shows an exterior view of the simulator. Each of the three cylinders was also electrically and mechanically safety limited.

The motion base was instrumented with three accelerometers located at the pilot's station to measure a_x, a_y, and a_z. The pitch rate and roll rate were detected using gyros.

A Redifon terrain board projection visual system was used to provide visual cues to the pilot. The full color projection is 48° x 36°. Landing lights were provided to the pilot.

THE AIRCRAFT SYSTEM AND TASK

An AMST similar aircraft was utilized as the system airframe. These dynamics were heavily and nonlinearly augmented. The pilot was asked to land the aircraft in a conventional manner utilizing a 3° ILS. A matrix of 30 runs was then accomplished with each of two motion drive systems and no motion drive being the experimental factor tested. This matrix provided ten replications of each motion condition. No other factors were willfully changed. Light turbulence (4 ft/sec rms) was applied to the aircraft dynamics for each run. Each approach took about 90 seconds at 120 knots. Initial altitude was 750' AGL.

THE MOTION DRIVES

Drive system A is depicted graphically in Figure 2. This system was a blend intended to present angular and angular rate information to the pilot. The heave axis was driven by a blend of q and $\dot{h}$. All signals were passed through washout circuits. For each system component the time constants used are shown in Table 1.

Washout Time Constants Drive A

Pitch	$\tau = 4$
Roll	$\tau = 2.86$
Heave	$\tau = 4$

Table 1

Motion fade and cab leveling circuits are also included to provide a means of initializing the simulator.

Drive System B was designed to present linear acceleration data to the pilot. Linearized equations expressing these accelerations are given by:

$$a_x = \dot{u} - \ell_y \dot{r} + \ell_z \dot{q} + \sin\theta \qquad (1)$$

$$a_y = \dot{v} - g\phi \cos\theta_o - \ell_x \dot{r} - \ell_z \dot{p} \qquad (2)$$

$$a_z = \dot{w} + g\theta \sin\theta_o - \ell_x \ddot{q} \qquad (3)$$

For purposes of implementation, these were simplified to:

$$a_x = \dot{u} + \ell_z \dot{q} \tag{4}$$

$$a_y = \dot{v} - g\phi + \ell_x \dot{r} - \ell_z \dot{p} \tag{5}$$

$$a_z = \dot{w} - \ell_x \dot{q} \tag{6}$$

For washout circuits, a model similar to that representing the otoliths of the ear was used since it is assumed that they are the primary means of motion perception. A typical model is

$$G(s) = \frac{k(t_3 s+1)}{(t_1 s+1)} \quad \frac{1}{t_2 s+1} \tag{7}$$

where t_3 is large compared to t_2 and t_1.

Thus the model is simplified to the washout plus filter given by:

$$G_1(s) = \frac{1.5s}{(s+1.5)(s+.19)} \tag{8}$$

Due to inherent 400 Hz noise in the hybrid simulator the acceleration rate terms were filtered before use by

$$G_2(s) = \frac{10}{s+10} \tag{9}$$

Further each actuator was determined to be accurately modeled by

$$G_3(s) = \frac{2\pi(.4)}{s+.4(2\pi)} \simeq \frac{2.51}{s+2.51} \tag{10}$$

Therefore a compensator of the form

$$G_4(s) = \frac{10(s+.251)}{(s+2.51)} \tag{11}$$

was inserted to pre-emphasize each drive signal. Figure 3 shows a block diagram of the system called Drive B.

DATA COLLECTED

The data collected can be divided into two types: statistical and discrete point. Time average statistics (mean and standard deviation) were computed from 500' to 50' altitude on each run for w_g, v_g, θ, ϕ, ψ, a_x a_y, a_z, p, q, r and glide slope error. These same data were collected at discrete points along the trajectory including the touchdown point. Tables 2, 3, 4 and 5 present the mean and rms data for the time average statistics. As can be seen there is no statistical difference among these parameters.

The touchdown parameters, however, are statistically significantly different. Tables 6 and 7 show the raw and average data. Figure 4 shows scatter plots for a_y and ϕ. Differences are clearly illustrated. The parameters a_y, ϕ, a_z, θ, p, q, and r are statistically different between Drive A and Drive B. No significant difference exists between Drive A and no motion but Drive B differs from no motion in a_y, a_z, ϕ, and r. The smaller dispersions of the data occur for Drive B. All testing was done for $\alpha = .05$ level of significance.

CONCLUSIONS AND RECOMMENDATIONS

Differing drive equations have been shown to cause a statistically significant change in touchdown parameters in the landing of an AMST similar aircraft utilizing a conventional approach. No significant difference was seen in the power approach phase.

Extreme caution should therefore be exercised in the choice of drive equations for use with a limited motion base simulator.

BIBLIOGRAPHY

Pollard, J.J. and C. Jackson, "An Investigation of the Multicrew Motion System Capabilities and Drive Signal Effects," AFFDL TM 76-25-FGD, November 1975.

TABLE 2 - RAW MEAN APPROACH DATA

MEAN 500' - 50' Motion System Test

Run #		w_g	v_g	θ	ϕ	ψ	a_x	a_y	a_z	p	q	r	GS Err
	Drive B												
3		4.81	3.26	1.84	.17	90.93	-.28	-.13	-.04	.01	.10	.02	-25.6
4		7.30	3.02	1.51	-.04	90.72	-.26	-.08	.07	.01	.10	.04	-17.4
12		6.25	.50	1.52	.37	90.03	-.18	-.08	.20	-.02	-.06	.03	-13.3
15		7.19	1.95	1.63	.28	90.02	-.11	-.07	.29	-.02	.03	.02	-51.8
16		8.01	1.31	1.20	.53	89.53	-.07	-.04	-.04	.02	.04	.02	-17.2
19		4.34	1.65	1.94	.26	90.47	-.37	-.11	.16	-.02	.15	.01	-26.6
21		3.30	.69	1.55	.05	89.91	.10	.10	.41	-.02	-.08	.00	-14.6
23		3.32	.68	1.43	-.12	89.80	-.03	.04	-.31	-.04	.13	.02	-50.0
31		4.43	-.15	1.32	.39	90.54	-.30	-.14	.17	.00	.00	.06	-32.0
32		1.13	.51	3.63	-.20	90.52	-.28	.06	.22	-.04	.04	-.02	-117.9
	Drive A												
1		2.13	.67	1.46	.63	90.11	.07	-.17	-.29	.04	-.01	.05	-39.4
2		7.33	2.14	1.57	.43	90.23	-.32	-.06	-.08	.02	.12	-.02	-18.2
7		5.64	1.28	1.50	.23	89.69	-.11	.10	-.04	-.01	.00	-.05	-21.3
8		6.96	2.65	2.17	-.08	90.67	-.27	-.08	.19	.02	-.03	.04	-29.4
10		4.17	1.14	1.80	.30	90.20	-.03	-.15	.09	.02	-.01	.03	-45.6
11		8.14	2.96	2.39	-.03	90.61	-.16	-.11	-.07	.03	.10	.03	-40.8
14		6.46	-.20	.72	.24	90.17	-.08	-.06	-.37	-.01	.05	.00	00.9
17		3.84	2.00	1.30	.33	90.01	-.16	.00	.12	-.03	.06	-.01	6.05
20		5.11	.61	1.67	.15	89.88	-.03	.01	.07	-.03	.00	.01	11.3
25		2.66	.61	.22	.38	90.10	-.18	-.01	.07	-.03	.05	-.06	-23.7
	No Motion												
5		8.86	3.16	1.85	.05	90.51	-.13	-.05	-.24	.00	.09	.01	-12.1
9		5.00	2.36	1.81	.28	89.00	-.32	.16	.07	-.07	.04	.02	-22.0
13		5.92	1.36	1.43	.70	90.08	-.09	-.22	.32	.06	-.09	.05	-16.0
22		2.11	.82	2.31	1.24	90.32	-.21	-.62	-.01	-.14	.01	.00	-35.3
24		5.05	-.11	.93	.02	89.84	.01	.00	.30	.03	-.02	.01	-10.6
26		2.89	.33	1.39	.22	90.14	-.21	.02	.11	.01	.03	-.01	-29.6
27		.88	-.40	1.79	.18	89.61	-.09	.11	.21	.08	.02	.01	-45.9
28		2.63	+.02	2.08	-.01	90.04	.03	.03	.02	.00	-.02	-.01	-43.1
29		1.65	.65	1.12	.10	90.48	.03	-.08	-.14	.01	.06	.02	-34.6
30		3.24	.42	2.32	.21	90.18	-.18	-.10	.20	.00	.06	.01	-72.1

TABLE 3 -- AVERAGE MEAN AND DISPERSION OF MEAN APPROACH DATA

Mean 500' - 50' Motion System Test

	v_g	v_g	θ	ϕ	ψ	a_x	a_y	a_z	p	q	r	GS Err
Drive B												
Mean	5.01	1.34	1.75	.17	90.25	-.18	-.04	.11	-.01	.04	.02	-36.5
Std Dev	2.16	1.12	.69	.24	.45	.15	.08	.20	.02	.07	.02	31.4
Drive A												
Mean	5.24	1.34	1.48	.26	90.18	-.13	-.05	-.02	.00	.03	.00	-17.7
Std Dev	2.02	1.02	.64	.21	.29	.15	.08	.18	.03	.05	.04	16.5
No Drive												
Mean	4.02	.86	1.70	.30	90.02	-.12	-.08	.08	.00	.02	.01	-32.13
Std Dev	2.20	1.13	.48	.39	.45	.12	.22	.18	.06	.05	.02	18.7

TABLE 4 -RAW RMS APPROACH DATA

RMS 500' - 50' MOTION SYSTEM TEST

Run #	w_g	v_g	θ	φ	ψ	a_x	a_y	a_z	p	q	r	GS Err
Drive B												
3	6.02	4.62	.72	.67	.90	.46	.48	2.08	.79	.67	.24	8.8
4	6.40	4.29	.74	.65	.51	.46	.45	2.16	.83	.70	.36	8.5
12	4.52	4.82	.74	.89	.47	.52	.55	2.31	.74	.68	.27	13.3
15	5.52	4.20	.69	.84	.61	.47	.57	1.99	.62	.72	.22	14.4
16	4.64	4.25	.27	.99	.88	.41	.71	1.85	.90	.61	.32	15.7
19	4.42	4.96	.78	.85	.70	.57	.59	2.26	.79	.72	.30	13.5
21	5.55	4.79	.86	.99	1.16	.54	.67	2.56	.74	.67	.33	39.2
23	6.39	2.06	.42	.79	.90	.31	.62	1.28	.71	.71	.39	19.1
31	4.92	2.08	1.26	.87	.55	.44	.59	1.50	.81	.48	.31	15.0
32	4.98	2.08	1.10	.84	.84	.46	.63	1.24	.70	.50	.34	27.5
Drive A												
1	6.47	4.46	.93	1.10	1.22	.60	.76	2.22	1.09	.67	.41	21.0
2	4.88	4.65	.95	.98	1.18	.64	.77	2.56	.94	.72	.43	8.5
7	4.80	4.00	.57	.58	.58	.45	.41	1.93	.53	.57	.24	12.6
8	4.31	3.98	.74	.37	.96	.46	.36	2.19	.37	.67	.33	15.4
10	5.20	4.24	.59	1.02	.62	.47	.64	2.12	.90	.65	.34	29.3
11	6.85	3.98	.72	.68	.93	.46	.50	2.36	.51	.73	.27	10.4
14	6.25	5.31	.54	.75	.42	.51	.49	2.15	.61	.56	.24	12.2
17	5.52	4.59	.72	1.16	.90	.54	.78	2.62	1.02	.73	.40	15.9
20	5.17	5.15	.56	1.07	1.03	.55	.77	2.53	.94	.68	.42	25.2
25	6.10	2.04	.47	1.00	1.03	.42	.73	1.22	1.14	.44	.35	7.0
No Motion Dr												
5	7.12	3.78	.30	.43	.63	.39	.42	2.02	.40	.63	.29	6.6
9	4.50	4.31	.99	1.57	1.95	.56	1.17	2.06	1.27	.75	.52	23.1
13	4.83	4.42	.76	1.08	.85	.46	.65	2.02	1.00	.65	.35	20.0
22	4.28	4.31	1.13	2.00	2.53	.77	1.82	2.83	3.43	1.15	1.97	27.4
24	5.41	2.27	.33	.58	.60	.32	.43	1.32	.64	.36	.31	10.0
26	5.81	2.33	.64	.69	.46	.34	.44	1.46	.59	.45	.19	4.5
27	5.74	2.11	.51	.76	.77	.35	.56	1.19	.70	.45	.36	16.4
28	5.64	1.96	.30	.54	.56	.31	.37	1.14	.40	.29	.26	18.2
29	5.80	2.25	.20	.35	.32	.31	.32	1.13	.29	.38	.21	7.0
30	5.52	2.32	.59	.98	1.07	.35	.69	1.12	.89	.36	.36	21.2

TABLE 5 - AVERAGE MEAN AND DISPERSION OF RMS APPROACH DATA

RMS 500' - 50' Motion System Test

	w_g	v_g	θ	ϕ	ψ	a_x	a_y	a_z	p	q	r	GS Err
Drive B												
Mean RMS	5.24	3.81	.76	.87	.75	.46	.58	1.92	.76	.64	.31	17.5
Std Dev RMS	.84	1.22	.29	.11	.22	.07	.08	.45	.08	.09	.05	9.3
Drive A												
Mean RMS	5.55	4.24	.68	.87	.89	.51	.62	2.19	.81	.64	.34	15.8
Std Dev	.82	.90	.16	.26	.26	.07	.16	.41	.27	.09	.07	7.3
No Drive												
Mean RMS	5.50	3.00	.57	.89	.97	.42	.69	1.62	.96	.55	.48	15.4
Std Dev RMS	.82	1.05	.31	.53	.71	.14	.46	.57	.92	.26	.53	7.9

TABLE 6 - RAW TOUCHDOWN PARAMETERS

RUN #		w_g	v_g	a_x	a_y	a_z	θ	ϕ	ψ	p	q	r	y	$\dot{h}$	$\dot{y}$
	Drive B														
3		1.22	-1.22	-1.31	.53	.46	8.08	-1.05	89.14	.56	.06	.72	60.6	-7.69	-.36
4		1.34	.85	-.46	.07	-.46	8.23	.17	89.63	.31	.84	.13	34.9	-3.54	-.37
12		7.32	7.20	-1.90	.12	-3.73	8.08	.22	90.41	-.41	-.13	-.33	13.3	-5.00	-3.54
15		.61	1.46	-1.63	-.36	1.34	9.54	.65	91.09	-.22	+1.52	.01	9.1	-5.24	-3.29
16		9.76	5.49	-1.73	.02	-.07	8.81	.26	88.99	.17	1.20	.06	-15.1	-6.47	+1.83
19		.85	3.78	-1.85	-.31	.61	10.52	.51	89.92	-.17	.01	-.03	4.4	-3.78	1.34
21		-.12	3.66	-1.02	-.36	-.95	9.30	.70	91.00	.61	.94	.20	-50.3	-7.93	.12
23		15.38	-2.07	-.41	.12	-1.00	7.25	-.02	90.41	-.56	.30	-.37	24.1	-1.34	-4.76
31		-1.09	2.07	-1.46	-.07	1.00	7.78	.26	89.48	.46	1.23	.52	24.0	-4.51	-1.09
32		-5.37	-1.34	-1.97	-.09	-2.12	9.59	.17	91.29	.61	.33	-.25	2.8	-3.78	-2.56
	Drive A														
1		11.1	-.12	-1.63	-.49	3.10	5.78	1.09	90.75	-.32	1.18	.13	-5.7	-3 29	-3.78
2		-4.0	5.98	-2.22	.22	3.34	8.17	-.17	89.09	-.02	1.13	-.03	18.2	-7.20	1.09
7		.48	2.80	-2.37	.39	3.58	8.91	-.56	91.00	-.46	.52	-.54	3.6	-3.05	-3.29
8		10.62	4.02	-.85	-1.49	.56	7.30	1.78	91.34	+.22	3.31	.94	4.2	-10.62	-.61
10		4.51	2.84	-1.61	-.71	.12	7.44	1.68	90.17	1.29	1.72	.59	18.6	-7.20	-3.29
11		7.56	-3.54	.24	.80	3.44	6.81	-.75	88.65	1.39	2.08	.67	30.1	-4.27	3.54
14		4.76	9.76	-2.39	-.85	-4.71	6.76	1.68	89.92	.51	2.50	.52	-11.5	-9.39	.61
17		1.95	5.61	-2.02	.02	-4.41	11.64	-.22	88.75	-.75	-.50	-.06	-21.5	-5.00	2.80
20		1.83	7.56	-2.0.	-.07	-2.86	10.32	.41	90.85	-.22	+1.16	.37	-30.0	-5.73	-1.58
25		3.78	2.19	-1.65	-.95	-1.44	5.83	.26	91.00	.56	1.64	-.23	12.2	-7.69	1.83
	No Motion														
5		6.22	-2.56	-0.24	-.31	7.10	5.34	.41	90.32	.02	2.82	.11	26.38	-8.91	-1.09
9		5.73	-3.17	-1.39	-1.07	-.61	8.81	1.19	92.22	.07	1.77	.28	21.89	-5.98	-.61
13		3.78	-4.76	-.32	-.26	+2.80	7.83	.75	90.51	-.02	.52	-.01	50.9	-5.73	-3.78
22		10.62	-3.66	-.61	1.05	.65	9.69	-1.68	89.09	.22	.20	.11	17.3	-2.31	4.02
24		-1.95	3.66	-2.58	-.51	-.80	6.27	1.09	91.44	-.65	.64	-.11	-1.8	-1.58	-3.29
26		10.62	.48	-1.24	.70	.41	7.69	-.36	90.02	.17	2.23	.79	23.04	-6.71	-.61
27		-.85	.85	-1.39	-.56	-.80	7.64	.51	92.66	.17	.91	.11	-23.81	-4.27	-3.05
28		.24	1.88	-.73	.22	1.78	6.71	-.41	89.97	-.51	1.94	-.09	15.74	-5.24	.12
29		.12	-1.09	-1.22	.26	-.65	6.71	-.31	90.17	.80	1.45	-.11	45.31	-3.78	-1.58
30		7.20	.85	-1.02	-.02	.26	7.49	-0.12	90.17	-1.34	.25	.11	40.39	-3.29	-3.05

TABLE 7 - AVERAGE TOUCHDOWN PARAMETERS

	w_g	v_g	a_x	a_y^*	a_z^*	θ^*	ϕ^*	ψ	p	q^*	r	y	$\dot{h}$	$\dot{y}$
Drive B														
Mean	2.73	1.99	-1.38	-.03	-.49	8.72	.19	90.14	.14	.63	.07	10.8	-4.93	-1.27
S.D.	6.19	3.07	.58	.27	1.54	1.00	.49	.83	.44	.59	.35	29.6	2.02	2.19
Drive A														
Mean	4.68	3.71	-1.67	-.31	.09	7.89	.54	90.15	.22	1.47	.25	1.82	-6.34	-.27
S.D.	4.14	3.82	.81	.70	3.27	1.90	.99	1.01	.72	1.05	.45	19.02	2.52	2.65
No Drive														
Mean	4.17	-.75	-1.05	-.05	1.01	7.42	.11	90.66	-.11	1.27	.12	17.16	-4.78	-1 29
S.D.	4.64	2.72	.71	.62	2.44	1.25	.86	1.11	.59	.90	.27	26.15	2.19	2.30

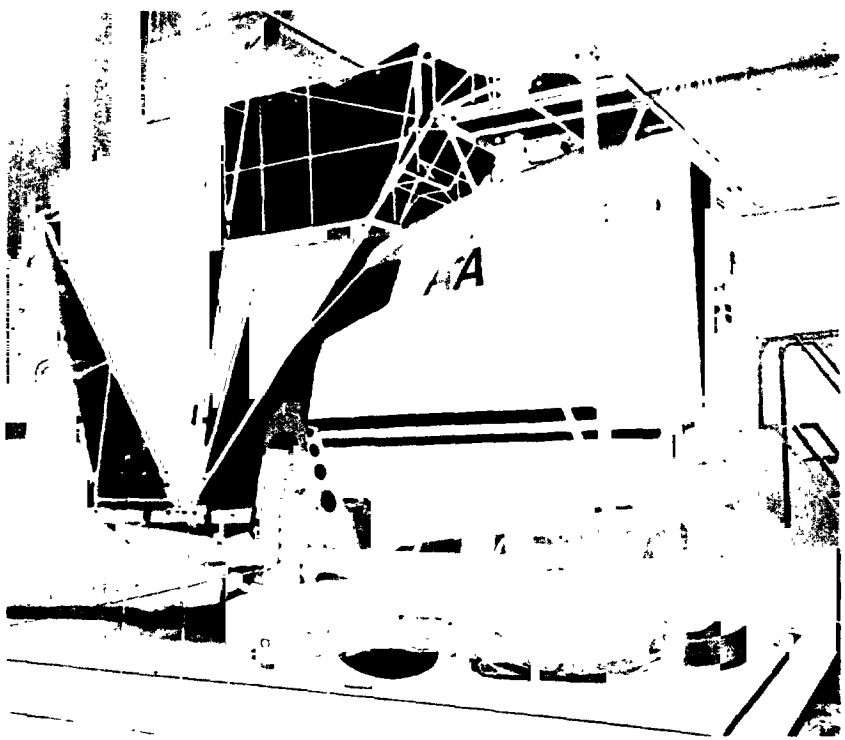

MULTICREW SIMULATOR

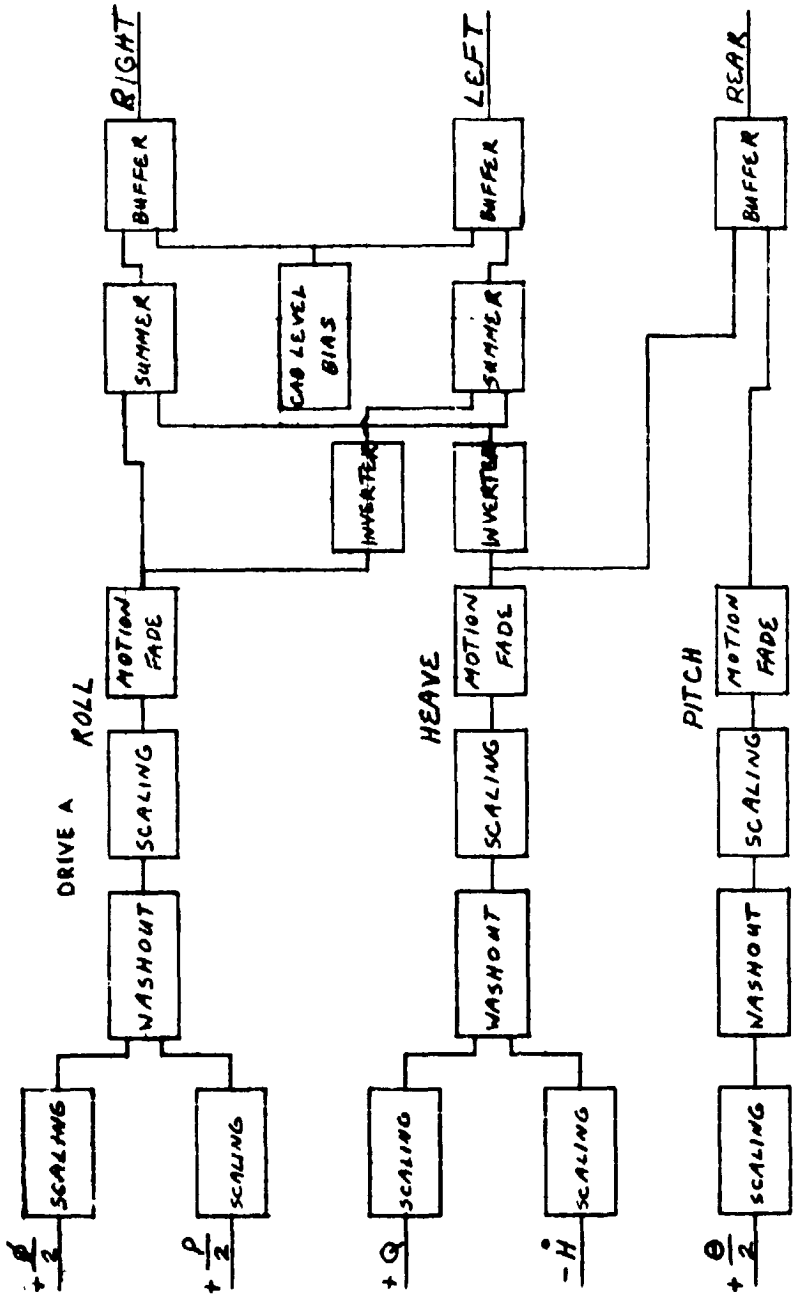

FIGURE 2--DRIVE A BLOCK DIAGRAM

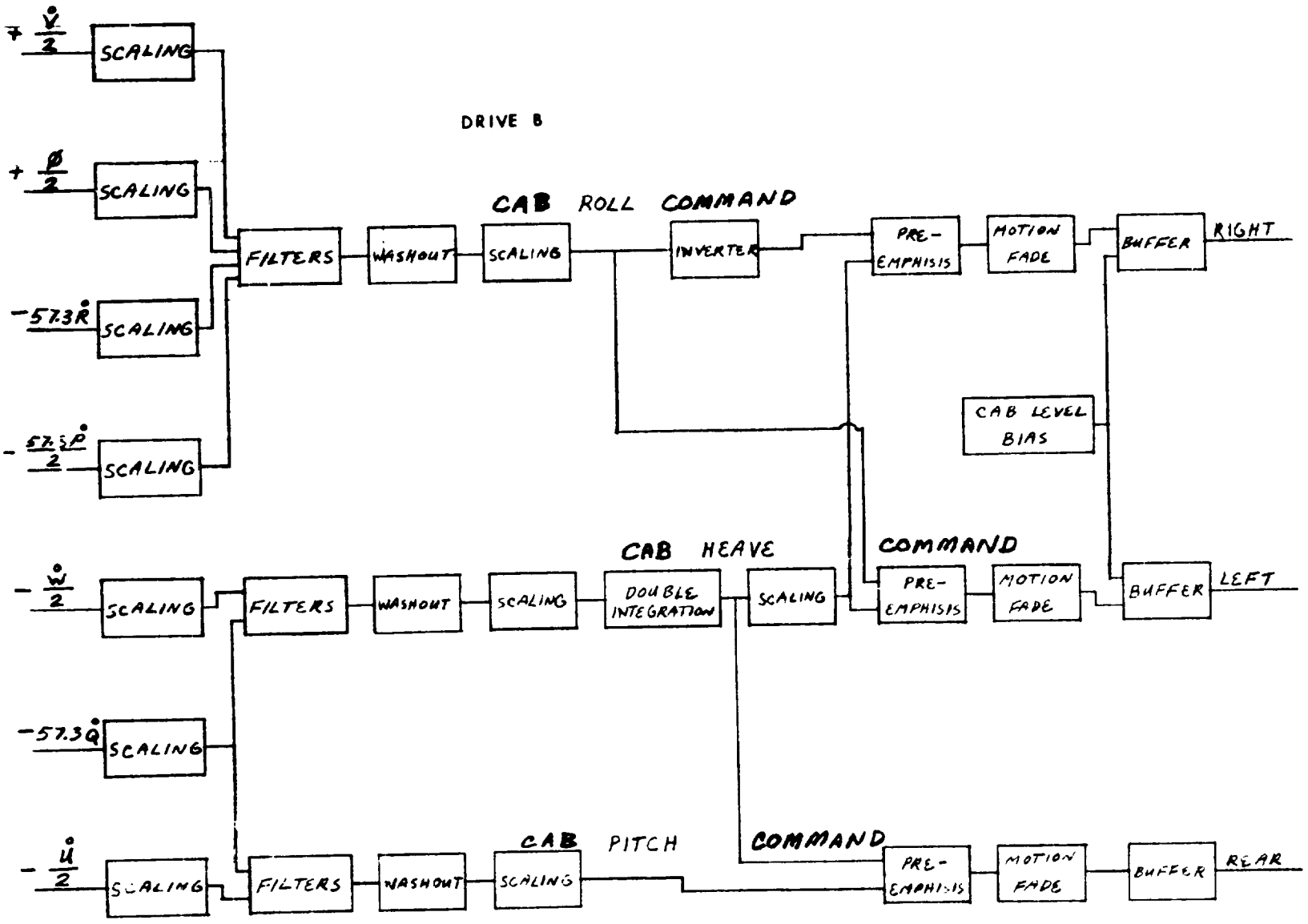

FIGURE 3 --DRIVE B BLOCK DIAGRAM

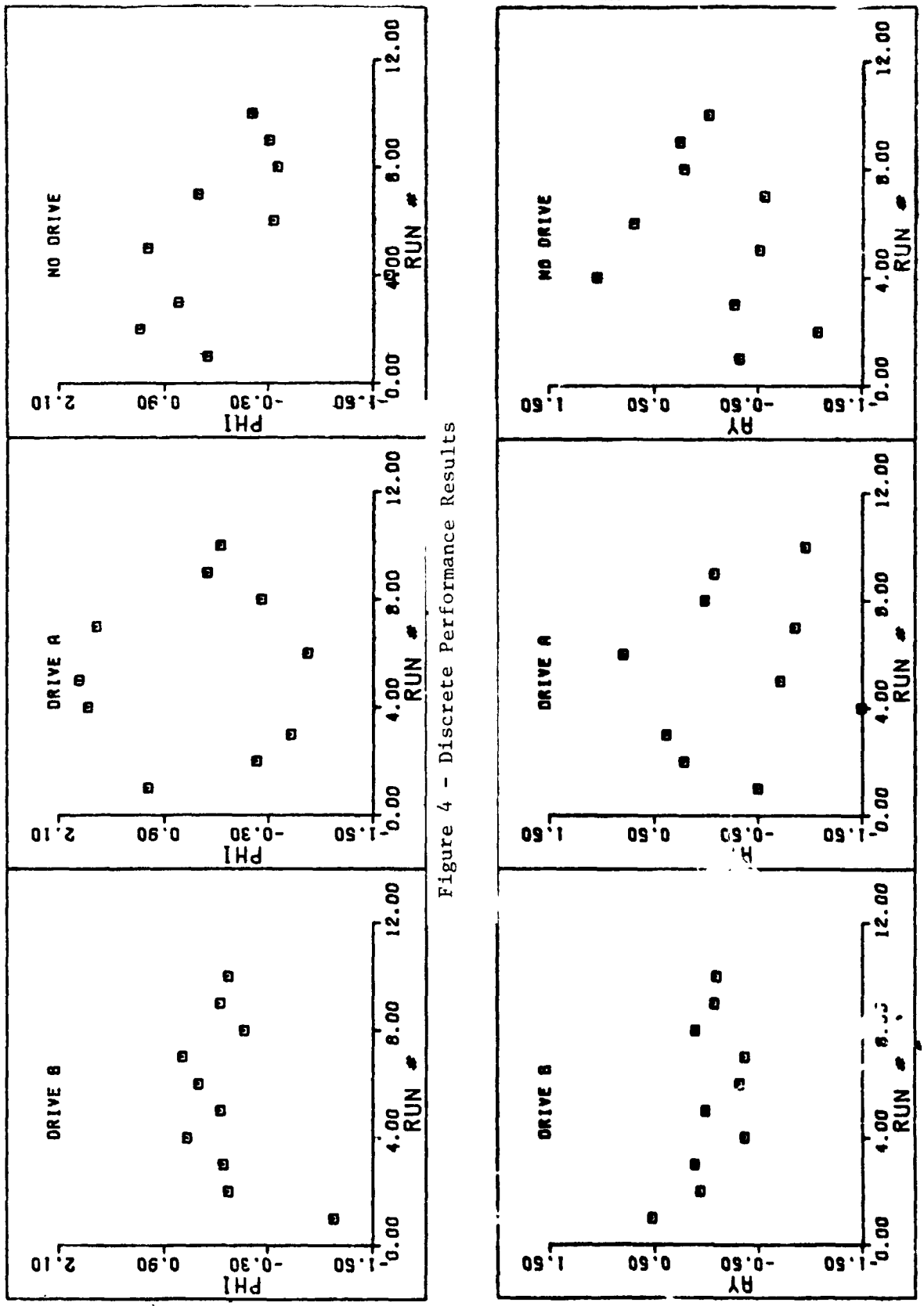

Figure 4 - Discrete Performance Results

THRESHOLDS OF MOTION PERCEPTION

MEASURED IN A FLIGHT SIMULATOR

R.J.A.W. Hosman and J.C. van der Vaart

Delft University of Technology
Department of Aerospace Engineering

SUMMARY

Thresholds for the perception of angular acceleration and specific forces were experimentally determined in a moving base flight simulator.

The thresholds were determined by using sinusoidally changing test signals at a number of frequencies. It was shown that the thresholds of the semicircular canals of the vestibular system are directly related to a minimum cupula displacement, if the latter is calculated in accordance with the well known overdamped torsion pendulum model.

When using the available otolith models, a similar direct relation for thresholds for specific forces and otolith displacement could not be established.

The experimentally determined thresholds for angular accelerations were significantly lower than those commonly found in the literature.

It was further shown that mentally "loading" subjects with additional tasks considerably increased the thresholds for motion perception.

INTRODUCTION

For a number of years research has been performed at the Department of Aerospace Engineering of the Delft University of Technology in the field of manual control.
The investigations are primarily related to pilot behaviour, handling qualities of aircraft and flight simulation. See Refs. 1 and 2.

Theoretical work on pilot behaviour and handling qualities is aimed at the development of a self adaptive pilot model, experimental reseach is done to support this work on the pilot modelling and flight simulation, especially motion simulation.

The lack of detailed knowledge of motion perception necessary for its implementation in pilot models and the availability of a simulator with a three degree of freedom motion system with high fidelity characteristics, inspired the start of the experimental work on motion perception.

The motion system was developed at the Department of Mechanical Engineering under the responsibility of Viersma. The application of hydrostatic bearing in the hydraulic servo actuators results in almost rumble free simulator motions. In fact under normal conditions motion noise is below the thresholds of motion perception.
The simulator's three degrees of motion freedom allow five degrees

of freedom to be simulated: pitching and rolling rotations and heave translations in the normal frequency range of aircraft simulation and specific forces in the X- and Y-directions by tilting the simulator at very low frequencies. A general impression of the simulator is given in Fig. 1. Details of the motion system are summarized in the Appendix. In this paper the usual aircraft frame of reference OXYZ is used to define motions of the simulator as well as of the subjects.

It was decided to first determine the thresholds of motion perception using this particular simulator. Thereby the suitability of the simulator motion system for research on motion perception was to be evaluated. If the apparatus indeed showed to be an efficient tool for this purpose, a more extensive research program related to motion perception and the problems of pilot modelling and motion simulation, could be started.

Further, some answers might be found to questions concerning the applicability of the available vestibular models as well as of the related threshold values in the rather special case of pilot modelling and flight simulation. In particular effects due to the differences in laboratory environment and the working environment of the flightdeck, where a pilot controls the aircraft, are to be expected.

Finally it has to be considered that till now most research on the vestibular system was directed at passive motion perception in contrast to the pilot controlled situation where the motion perception plays part in the control of aircraft.

In the design of the experiments and in the interpretation of the results use has been made of a rather important and general concept of control by a human operator, namely that of the "internal model". This concept implies that for perception as well as for control a human operator uses an internal - or mental - model of the system to be controlled. At any moment this internal model is based on all the preceding information processed up to that moment. Thus the internal model can be seen as the result of a learning process.

When implementing motion perception in pilot models based on the internal model of the aircraft, the following should be borne in mind. The perception of motion does not originate from the vestibular system alone but is also based on the sensory information of pressure, touch and kinesthesia receptors on the one hand and visual cues on the other hand. It is of great importance to investigate the influence of these sensors on motion perception and to incorporate all relevant motion related information in pilot models and in flight simulation.

Based on the above considerations some experiments were performed to evaluate the simulator motion system and to investigate the influence of the information processing on motion perception.

MOTION PERCEPTION, MODELS OF THE VESTIBULAR ORGANS AND PILOT BEHAVIOUR

Motion and the flight environment

The effect of motion perception on the behaviour of a pilot controlling an aircraft is generally accepted as favourable. It has been experimentally demonstrated, see Ref. 3, that the presence of "motion" increases the control performance in the case of simulated systems with noted "difficult" control characteristics. The use of moving base simulators is therefor not only justified for improving simulation realism, motion provides the pilot with cues that appear to be as essential as visual inputs for the manual control of a given system.

Whereas this effect of motion cues on the control task is generally recognized, little appears to be exactly known about the motion a human pilot is able to feel (thresholds of perception), nor is it clear whether certain motion cues may be more essential than others, see Ref. 4. The work of many researchers is presently aimed at improving the knowledge in this particular field.

The research on motion perception has a long history. It has, from the beginning, been based on the function of the vestibular system, consisting of the semi-circular canals and the otoliths, man's sensors of angular acceleration and specific force respectively. Most investigations carried out have been related to laboratory situations where the experimental conditions were such that results are not readily extrapolated to the flight environment. In laboratory experiments subjects are usually strapped to maintain a fixed position of head and body. In contrast, a pilot in a flight environment is free to adjust his chair and [illegible]ety belts mostly do not restrict head and trunk movements. Apart from this difference in physical limitations an enormous difference may be observed in the psychological conditions of a laboratory subject and a pilot controlling an aircraft.

When studying the applicability of the models of the vestibular system, see Refs. 5 and 6, and the associated thresholds of motion perception in relation to pilot modelling and aircraft simulation, the above considerations should be taken into account.

A good starting point appears to consider the pilot as a multi-input multi-output system with certain (as yet unknown) information processing of all sensory input signals. Using this black box concept, one can try to evaluate the influence of the pilot's information processing of these signals. Of course the influence of the vestibular inputs should not be rejected or underestimated but should be considered as an integral part of the information processing of all sensory inputs.

Mathematical models of motion perception

Presently only models for perception of motion by the vestibular system are available. These models, in which motion sensing by other organs such as

proprioceptors, etc. is not included, are briefly discussed below. For a complete description of the vestibular system and its characteristics, the reader is referred to a number of excellent reviews, Refs. 5, 7, 8, 9 and 10. A schematic drawing of a semi-circular canal is given in Fig. 2a.

According to the overdamped torsion pendulum analogy of the semi-circular canals of the vestibular organs as formulated by van Egmond, Jongkees and Groen, the transfer function, relating the Laplace transforms of input and output signals, is:

$$\frac{\xi(S)}{\alpha(S)} = \frac{1}{(S + a)\ (S + b)} \qquad (1)$$

where:

ξ = the cupula deflection
α = the input angular acceleration
$a \approx 0{,}1$ rad/sec
$b \approx 10$ rad/sec

In Fig. 3 the modulus and phase angle of the above transfer function are plotted.

In eq. (1) the constants a and b are dependent on the mechanical characteristics of the organ such as the moment of inertia of the endolymph, the spring stiffness of the cupula and the viscous damping of the endolymph in the canals. From experiments described in Refs. 6 and 8 it is clear that the coefficients a and b differ from subject to subject. As a consequence the above values have to be considered as averages.

Investigations into the perception of specific force have by far not been as succesfull as those into the perception of angular acceleration. The structure of the otoliths suggests the dynamics of an overdamped mass-spring-dashpot accelerometer, or, more exactly, a specific force sensor. A schematic drawing of an otolith is given in Fig. 2b.
An attempt to measure and describe the dynamic properties has been made by Meiry, Ref. 10, resulting in the revised otolith model of Young and Meiry, Ref. 11, the transfer function of which is:

$$\frac{A_p(S)}{A_i(S)} = \frac{1.5}{(S + c)\ (S + e)} \cdot (S + 0.076) \qquad (2)$$

where:

A_p = perceived specific force
A_i = input specific force
$c \approx 1.5$ rad/sec
$e \approx 0.19$ rad/sec

Eq. (2) may be devided into a part relating otolith displacement d and specific force A_i:

$$\frac{d(S)}{A_i(S)} = \frac{1.5}{(S + c)\ (S + e)} \tag{3}$$

and a neural processing term, relating perceived specific force A_p and otolith displacement d:

$$\frac{A_p(S)}{d(S)} = (S + 0.076)$$

The numerical values of the constants c and e, dependent on the mass of the otoconia, the viscous damping due to the endolymph and the supporting structure of the otolith and the restraining spring forces of the hair cells, are again to be taken as averages.

In Ref. 11 a reasonable fit of experimental data to the model according to eq. (2) is shown. Other researchers, however, give experimental results that are not in agreement with this model, see Refs. 6, 8, 12 and 13.

The ability of labyrinthine defective (L.D.) subjects to perceive tilt, though with decreased accuracy with respect to normal subjects, shows that touch, pressure and kinesthesia receptors also provide information on specific forces acting on the human body.

An indication that motion is possibly also perceived by the motion of internal organs is to be found when considering the transfer function of the human body for vibrations, see Ref. 14. There is a prominent resonance peak at about 2 c.p.s. for vertical vibration of the erect body, a reasonance which is due to the mass, stiffness and damping of the internal organs within the trunk.

A slightly different otolith model is suggested by Mayne in Ref. 12. It is argued there that in the vestibular system the sensory cells can be devided into three groups, sensitive to otolith displacement, rate of displacement or both. The proposed transfer function becomes:

$$\frac{x_o(S)}{\ddot{u}(S)} = K_1 - \frac{K_2\omega_1\omega_2}{(S + \omega_1)\ (S + \omega_2)} \tag{4}$$

This expression can be visualized as describing both the characteristics of a conventional accelerometer (first right hand term of the equation) and of a differentiating accelerometer (second right hand term). Neglecting ω_2, representing the upper break frequency, Mayne suggests the following transfer function:

$$\frac{x_o(S)}{\ddot{u}(S)} = K_1 - K_2 \cdot \frac{\omega_1}{S + \omega_1} \tag{5}$$

where:

x_o = otolith displacement
$\ddot{u}$ = input specific force
$K_1 = 24.25\ sec^2$

$K_2 = 15.26\ sec^2$
$\omega_1 = 0.232$ rad/sec

The difference between the above presented models, see Fig. 4, according to eqs. (2) and (5), is that the latter has a constant gain at high frequencies.

Whether the mechanical properties of the otoliths (mass, restraining force and damping) are also supposed to be accounted for in this model, is not quite clear.

Thresholds of motion perception, pilot models and the conception of an "internal model"

As already mentioned in the introduction the results of measuring the thresholds of motion perception in a three degree of freedom aircraft simulator will be discussed in this paper. As will be clear from the preceding discussion the semi-circular canals and the otolith organs behave as dynamic systems, usually described by relatively simple mathematical equations.

It stands to reason that neural signals from the cells in the cupula and the otolith are, in some way, proportional to cupula deflection and otolith displacement. These displacements are not only dependent of the input signals but also, of course, of the dynamics of the vestibular organs as described by eqs, (1) and (3). Therefore, the procedure used by van Egmond, Jongkees and Groen, Refs. 8 and 15, to correct the experimentally determined threshold values in the case of angular oscillatory accelerations by reducing the threshold values to a normalized frequency, is essentially correct. A similar procedure is followed in this paper by relating the threshold of motion perception to the cupula or otolith displacements.

The techniques described in Refs. 6, 8, and 10 to determine the constants in the models according to eqs. (1) and (3) are partly based on the determination of the threshold values. In this way there is a danger, however, that the importance if the thresholds is being over-emphasized and that numerical values of thresholds are considered as absolute.

It appears more appropriate to accept that all neural signals and in particular those resulting from cupula deflections or otolith displacements, are noisy signals, representing motion related measurements, see Fig. 7. Using the concept of an "internal model" as mentioned in the Introduction, these measurements can be thought as serving to update the estimate of the internal model of the state of the system to be controlled. Stated in terms of modern control theory, all sensory motion related signals (vestibular, visual, proprioceptive etc.) can thus be considered as being used by the human operator to improve the estimate of the state of the system to be controlled.

Returning now more specifically to the role of the vestibular organs, the above proposed concept firstly enables the thresholds of perception to be stated in terms of measurement noise: if the sensory signal is weak, it cannot be recognized from the background of measurement noise, see Fig. 5. This concept of thresholds in terms of unfavourable signal to noise ratio has already been stated elsewhere (Ref. 6).

Secondly, if the concept of the internal model is accepted it should be concluded that an influence of the internal model and the information processing on the thresholds measured is to be expected.

There is evidence that the state of the internal model indeed affects the thresholds of motion perception. It is well known that in vestibular sensing, as well as in hearing and vision, man is able to feel (or hear or see) a slowly increasing signal at a very low level, but is not able to definitely recognize it until it has exceeded a certain level (threshold). When next the signal is decreased, however, he can still recognize its characteristics far below this threshold: the internal model built during the preceding period helps to recognize the signal from a background of measurement noise.

Based on the foregoing, two experiments using the motion simulator, were designed. A first experiment was designed to measure thresholds in terms of cupula and otolith deflections. A second experiment was set up to demonstrate the influence of mental load of the pilot on the processing of the vestibular information.

The next Chapter described these experiments and the results obtained.

EXPERIMENTS

Experiment I. The effect of input signal frequency on thresholds of motion perception

Based on the models of the vestibular system as described in the preceding Chapter, a dependency of the threshold value on the frequency of sinusoidal input motions to be perceived should be expected and an experiment was designed to demonstrate this. Due to the limitations of the three degrees of freedom motion system, only pitch, roll and heave oscillations could be generated. The range of frequencies for these modes of motion were limited in a number of ways, as will become clear in the following.

Firstly the noise characteristics of the servo system set the minimum frequency of the heave motion at 1 rad/sec. The maximum frequency for heave was chosen equal to the maximum frequency for roll and pitch, i.e. 14 rad/sec.

Further the lower limit input signal frequency for roll and pitch was set by the fact that the pitch and roll angles necessary to produce pitch and roll accelerations at low frequencies become so large as to be recognized by the perception of change in specific force due to the change in gravity component. Given the simple relation, in the case of sinusoidal oscillations, between angular acceleration and angle of tilt and the threshold values for both angular acceleration and specific forces, the minimum frequency for pitch and roll was determined at 0.6 rad/sec.

Finally the maximum frequency for rotations was determined by the fact that the subject's head was not situated on the rotation axes of the simulator (see the Appendix). The specific forces acting at the position of the subject's head due to angular accelerations set the maximum frequency at 14 rad/sec.

For the heave mode 8 frequencies betweem 1 and 14 rad/sec and for the pitch and roll modes 10 frequencies between 0.6 and 14 rad/sec were chosen.

Two threshold values were obtained at each input frequency. The first

one when the amplitude was increasing and where the subject had to correctly identify both the mode (pitch, roll or heave) and the frequency of oscillation. This threshold value will be called the upper threshold in this paper. The second, lower threshold, was defined as the value measured when, with the amplitude of the test signal decreasing, the subject was no longer able to follow the oscillation. The subjects reported their observations verbally. An example of a time history of the test signal is given in Fig. 6.
Two preliminary experiments were performed to establish the technique used in the final experiment. Especially the rates of increasing and decreasing the amplitude of the input signal showed to have a significant influence and consequently these rates had to be chosen as low as possible. In Fig. 6 an example of the time history of the input signal used to determine both the threshold values is shown.

Three subjects, general aviation pilots, participated in the experiment and three replications were taken. The 28 combinations of modes of motion and frequencies were presented to the subjects in random order in three sessions of approximately 30 minutes each for each replication. The preliminary experiments were also used to train the subjects. For the final experiment 504 threshold value measurements were made.

Experiment II. The effect of mental load on the thresholds of motion perception

One of the questions raised very often, see Refs. 6 and 16, is whether the thresholds for motion perception, as described in the previous Chapter, are applicable in the case of a pilot when performing a task in the aircraft. As this question is very important when designing washout filters for simulation and when developing pilot models, an experiment was designed to investigate the influence of mental load on threshold values. To mentally load the subjects two additional tasks were used. One was a control task, incorporating either the symmetric or asymmetric control characteristics of a simulated twinjet airliner, the other was an auditory binary choice task.

Five theshold values under different additional mental load conditions were determined using an oscillatory input signal for either pitch, roll or heave with increasing amplitude or a ramp function for specific force in X- or Y-directions by tilting the simulator.

During such a test the subject was asked to control the symmetric or the asymmetric motions of the simulated aircraft and to further observe and verbally report any disturbance caused by a test signal in the degrees of freedom not involved in the control task. The symmetric control task consisted of maintaining constant altitude by controlling the pitch attitude. In the asymmetric control task constant heading was to be maintained by controlling the roll angle. The simulated aircraft was disturbed by atmospheric turbulence in both cases.

The binary choice task was used at three levels, 0, 40 and 80% of the maximum the subjects could perform. This maximum was defined by the number of tones the subject could answer in one minute making not more than one error.

In Table 1 the experimental combinations used are summarized. In this experiment four subjects participated, three of them were general aviation pilots, two of whom also participated in Experiment I. The fourth was a student

pilot. As each experimental combination was repeated 4 times, the total number of threshold values determined was 6 x 5 x 4 x 4 = 480.
These thresholds were determined during 288 runs of the additional tasks lasting 150 seconds each. As a rule two threshold values were obtained during one run, but in a limited number of runs no test signal was presented. This was done to avoid the subjects concentrating too much on the determination of the thresholds. The subjects were instructed and trained to do their best on the additional tasks and their performance in these tasks was monitored. In the case of poor performance test runs were rejected, thus improving the subject's motivation.

Results of Experiment I

In Figs. 9 and 10 the input related threshold values for pitch and roll accelerations are plotted as a function of frequency. Both the values obtained with increasing and decreasing amplitudes, i.e. the upper and the lower thresholds respectively, are given with their standard deviations. The thresholds can be seen to increase with frequency while the slope of the upper threshold is nearly equal to one, thus approximating the slope of the inverse of the modulus of the transfer function of the cupula model (eq. (1)). The slope of the lower threshold is slightly smaller.

The pertaining results of the analysis of variance are summarized in Tabel 2. The difference in thresholds for pitch and roll appears to be negligable. This could be expected as both pairs of vertical semi-circular canals are activated by pitch as well as by roll accelerations, see Fig. 2c. The analysis of variance confirms this equality.

The difference between upper and lower thresholds is probably significant. The differences between subjects and the interactions of the subjects with the other main effects are significant. This is not amazing bearing in mind that, as stated in the preceding Chapter, each subject will have different vestibular characteristics.

The interaction between frequency and upper and lower threshold and hence the difference in slope of the upper and lower threshold is significant.

The threshold values for specific forces along the vertical axis are presented in Fig. 9. It will be clear that here a dependency of the input related threshold of frequency cannot be concluded, see also the results of the analysis of variance in Table 2.

The difference of the upper and lower thresholds, however, is probably significant. The treshold values again demonstrate significant differences for the subjects and the interaction between subjects and frequency. Just as for the angular accelerations a significant difference in slope of the upper and lower threshold was found.

Results of Experiment II

In Table 3 the average input related threshold values of all experimental conditions are given. A review of the results of the analyses of variance is

presented in Table 4. The specific forces A_X, A_Y and A_Z show a difference in input signal. For the specific forces A_X and A_Y a ramp signal had to be used, whereas in the Z-direction a sinusoidal signal (ω = 1.88 rad/sec) was used. The input related threshold for specific force in the Z-direction is equal to the value found in Experiment I, see Fig. 9.

The higher values for the X- and Y-directions are in accordance with the otolith models (eqs. (2) and (4)) if it is assumed that the otolith displacement is a measure for the threshold value. The difference between the X- and Y-directions can, among others, have the following reasons.

Firstly the subjects were much more firmly fixed by the pilot's chair in the Y-direction than in the X-direction. The subjects often remarked that they observed changes in touch on their back due to roll angles of the simulator, thus influencing their perception.

Secondly the orientation of the macula relative to the X-axis for a normal seated subject could also be of importance.

The maximum increase of the threshold values due to the mental loading tasks is roughly 25, 50 and 100% for A_X, A_Y and A_Z respectively. Analysis of variance, see Table 4. shows a possible significant increase for the thresholds in the Y- and Z-directions only. From the data it appears that the control task produced a larger increase in thresholds than the binary choice task. More research is necessary to elucidate the ways in which different sources of mental load influence the subjective threshold values.

The input related thresholds for angular acceleration show a significant increase due to the additional tasks. Differences for pitch and roll are small. The maximum increase of the threshold value is 40 and 80% for pitch and roll respectively.

It may be noticed that the threshold values presented here for the case of no additional task do not correspond with the values found in Experiment I. This is due to the fact that Experiment II was actually performed before Experiment I at a time when the strong dependency of thresholds on the rate of increase of amplitude was not yet fully appreciated, and the rates of increase had not yet been set at more appropriate lower values. With the original rate of increase, however, these threshold values can easily be reproduced.

Summarizing this paragraph it can be concluded that the threshold values for motion perception can indeed be influenced by the mental load of the pilot.

DISCUSSION

Some conclusions to be drawn from the experiments described, hold for the perception of specific forces as well as for the angular accelerations. Therefor these more general conclusions will be discussed first, to be followed by a seperate treatment of the findings that are more specifically related to either the perception of angular accelerations or to the perception of specific forces.

Differences among subjects, the internal model and the influence of additional tasks

From Experiment I, see Figs. 7, 8 and 9 it appears that the spread of the threshold values measured is rather large. The analyses of variance show that this is mainly a result of differences among subjects as well as interactions between subjects and the other main effects. After subtraction of these significant effects the remaining standard deviations, independent of subject, of the mean values for Experiment I as given in Figs. 7, 8 and 9 are $0{,}103^{o}/sec^2$ and $0{,}006$ m/sec^2.

These values cannot be ascribed to experiment related measurement noise alone but should also be interpreted as being caused by the noise present in the ouput signals of the vestibular systems themselves. Especially at threshold deflections of the cupula and at threshold deviations of the otolith the unfavourable signal to noise ratio seriously affects the motion perception as discussed earlier in this Report, see Fig. 5.

Apart from differences between subjects as far as physical characteristics of the vestibular systems are concerned, differences in judgment may also be present. Already during the evaluating experiment it appeared that some subjects were more inclined to guessing while others refrained from reporting on perceived motions until they were quite certain. This effect was diminished as much as possible by training but it nevertheless was still present in the final experiments.

Finally it should be remarked that the subjects usually reported that they were moving long before they were able to identify the mode (pitch, roll or heave) and the frequency of the test signal, which confirms the findings of Ref. 6.

The results of Experiment I demonstrate that the threshold value is considerably decreased if the motion is known and expected by the subject. This is in agreement with the idea that the human operator is able, by using an internal model of the system to be controlled, to predict the state of the system. In the case of a known sinusoidal motion cue the subject, using this internal model, only needs a relatively weak vestibular signal to observe the motion. Hence it is not amazing that the upper threshold values measured for angular accelerations are approximately two and a half times the lower threshold values and the upper thresholds for specific forces along the Z-axis are twice the lower threshold values.

The results of Experiment II show a significant influence of the additional tasks on the threshold values and this influence was strongest in the case of rotations, see Table 4. The conclusion from these findings is that threshold values for motion perception are determined partly by the physical characteristics of the semi-circular canals and the otoliths and partly by the processing of the vestibular information: the more attention the subject can share to motion perception, the lower the threshold values will be.

The above can be summarized by concluding that using an internal model gives the pilot a tool to improve the prediction of future motion cues and to improve the ability to perceive these cues. A mental loading of the pilot, however, oppresses the information processing of the vestibular signals. Hence threshold values will depend on the total workload and on the amount of necessary information the pilot can derive from the motion cues in order to

estimate the state of the aircraft with sufficient accuracy.

The thresholds for angular accelerations expressed in terms of minimum perceived cupula deflections

As already shown in the preceding Chapter the input related threshold value for angular accelerations increases with frequency in such a way that multiplying the input by the modulus of the transfer function according to eq. (1) should yield a nearly constant cupula deflection at the threshold. The modulus as a function of frequency, however, is only known if the parameters of the transfer function of each subject were known, which was not the case in the present experiments. Therefore an approximation suggested by Jongkees and Groen, see Ref. 15, was used. Between the break frequencies of the transfer function the modulus is approximated by:

$$M = \frac{1}{a.\omega} \qquad (6)$$

see Fig. 3.

For Experiment I the maximum input frequency was 14 rad/sec which is only slightly above the generally used break frequency of $\frac{1}{b}$ = 10 rad/sec (see Fig. 3), allowing the approximation according to eq. (6) still to be used to compute the cupula deflections for pitch and roll. The results are plotted in Fig. 10. It can be seen that the cupula deflection is not quite constant with frequency, which could be expected from Figs. 7 and 8. This may be caused by the experimental technique used to determine the threshold values. As stated before the rate of increase of the input signal has a strong influence on the thresholds determined.

Finally it is of course interesting to see how the threshold values determined experimentally compare with results of other experiments. For this purpose the threshold values have been corrected for the modulus of the transfer function (according to eq. (6)). The threshold values of angular acceleration thus derived are in fact those found at very low frequencies where the modulus is constant, see Fig. 3, and could be termed "cupula related thresholds". Theoretically these values should be equal to those found by experiments using step input accelerations. The following cupula related thresholds for pitch and roll accelerations are found.

Input acceleration	Upper threshold ($^o/sec^2$)	Lower threshold ($^o/sec^2$)
roll	0.023 - 0.035	0.0069 - 0.015
pitch	0.022 - 0.053	0.0082 - 0.026

These values are remarkably below those found by other researchers:

Input acceleration	Authors	Threshold ($^o/sec^2$)
yaw, sinusoidal, corrected	Jongkees, Groen, 1948, Ref. 13	0,18 - 2,0
yaw, step input	Meiry, 1965, Ref. 8	0,1 - 0,2
yaw, pitch, ro l, step input	Clark, Stewart, 1968, Ref. 15	0,06 - 2,24

The thresholds for specific forces

As shown in the preceding paragraph a certain minimum cupula deflection can be considered to determine the lower bound of the thresholds for angular acceleration perception. However, nor from the literature nor from the results of the present experiments such a similar conclusion can be drawn with respect to otolith displacement. If, based on the input related thresholds in Experiment I and the revised otolith model of Meiry and Young (eq. (3)), the otolith displacement is computed, then the threshold appears to decrease with frequency. According to Mayne's model (eq. (5)) the otolith displacement would be independent of frequency. Mayne (Ref. 12), however, does not specify the upper break frequency ω_2 of his complete model (eq. (4)) and, as shown in Fig. 4, the modulus of the simplified model is constant at frequencies larger than 1 rad/sec. This can not actually be the case and the use of Mayne's model would only be justified if a reliable estimate of ω_2 were available.

At low frequencies both models have the same modulus, see Fig. 4, and are in correspondence with the higher threshold values found in Experiment II for the specific forces in the X- and Y-directions.

From Refs. 8 and 13 it can be concluded that the perception of specific forces is much more complicated than would be expected from the simple otolith models mentioned. As stated before, specific force perception by pressure, touch and kinesthesia receptors should not be excluded. As mentioned earlier labyrinthene defective subjects have thresholds for specific force perception that are only slightly higher than those of normal subjects (0,2 and 0,1 m/sec^2 respectively).

Another possible explanation of the fact that the threshold values determined do not fit the models could be that the subjects were seated in a normal pilot's chair without fixation of head and trunk. As already mentioned due to mass and stiffness of the internal organs of the body a resonance frequency is found at about 12 rad/sec (Ref. 14). Therefore the specific forces acting on the subject's head could in fact have been larger than the specific forces acting on the simulator.

At this moment only a provisional conclusion can be drawn. For oscillatory specific forces the threshold value is approximately 0.085 m/sec^2 fitting very well with the threshold values reviewed in Ref. 4.

Mach	1875	0.10 - 0.12 m/sec^2
Jongkees and Groen	1946	0.06 - 0.13 m/sec^2
Meiry	1965	0.10 m/sec^2
Present experiment		
Upper threshold		0.07 - 0.03 m/sec^2
Lower threshold		0.04 - 0.06 m/sec^2

For very low frequencies as for instance a specific force due to sustained tilt, the threshold value is higher ranging from 0.35 - 0.50 m/sec^2 depending on the direction of the specific force.

CONCLUSIONS

In this paper two experiments to investigate the motion perception of the pilot in the aircraft environment were described. The first experiment was carried out to measure threshold values for motion perception as a function of frequency. A second experiment was designed to demonstrate the effect of mental load on motion perception, especially on threshold values. Based on the results and the discussion in the preceding chapter, the following conclusions can be drawn.

1. Threshold levels for motion perception depend on the physical characteristics of the vestibular system as well as on the information processing of the motion related sensory signals.
2. As a consequence of the signal to noise ratio of the output signals of the vestibular system, physically determined thresholds are not to be considered as descrete values but rather as transition ranges from not perceivable to fully perceivable motions.
3. A considerable improvement of motion perception can be achieved and consequently lower thresholds are obtained if a human operator is able to identify an internal model of the motion to be perceived.
4. Threshold values for angular acceleration are directly related to a minimum perceivable cupula deflection.
5. Thresholds for specific forces cannot definitely be ascribed to otolith displacement alone. For oscillating specific forces a constant value independent of frequency is a good approximation for a pilot in an aircraft environment.

REFERENCES

1. Hosman, R.J.A.W.: Pilot Vehicle analysis. AGARD Conference Proceedings,

No. 106, AGARD, 1971.

2. Hosman, R.J.A.W.: Pilot tracking behaviour under additional workload, Delft University of Technology, Department of Aerospace Engineering, Report VTH-199, 1975.

3. Bergeron, H.P., Adams, J.J., and Hurt, G.J.: The effects of motion cues and motion scaling on one- and two-axis compensatory control tasks. NASA-TN D 6110, 1971.

4. Davies, P.: Approval of flight simulator flying qualities. Aeronautical Journal, July 1975.

5. Young, L.R.: The current status of vestibular models. Automatica, Vol. 5, pp. 368-383, 1969.

6. Guedry, F.E.: Psychophysics of vestibular sensation. In: Kornhuber, H.H. (ed.): Handbook of Sensory Physiology. Volume VI/2, Springer Verlag, Berlin, Heidelberg, New York, 1974.

7. Kornhuber. H.H. (ed.): Handbook of Sensory Physiology. Volume VI/2. Vestibular system: Psychophysics, applied aspects and general interpretations. Springer Verlag, Berlin, Heidelberg, New York, 1974.

8. van Egmond, A.A.J., Groen, J.J. and Jongkees, L.B.W.: The function of the vestibular organ. Practica-Oto-Rhino-Laryngologica, Vol. XIV, Supplement 2, 1952.

9. Peters, R.A.: Dynamics of the vestibular system and their relation to motion perception, spatial disorientation and illusions, NASA CR-1303, 1969.

10. Meiry, J.L.: The vestibular system and human dynamic space orientation. NASA CR-628, 1966.

11. Young, L.R. and Meiry, J.L.: A revised dynamic otolith model. Proceedings of the third symposium on the role of the vestibular organs in space exploration. NASA SP-152, 1968.

12. Mayne, R.: A systems concept of the vestibular organs. In: Kornhuber, H.H. (ed.): Handbook of Sensory Psychiology. Vol. VI/2, Springer Verlag, Berlin, Heidelberg, New York, 1974.

13. Graybiel, A.: Measurement of otolith function in man. In: Kornhuber, H.H. (ed.): Handbook of Sensory Psychiology. Vol. VI/2, Springer Verlag, Berlin, Heidelberg, New York, 1974.

14. Garg, D.P. and Ross, M.A.: Vertical mode human body vibration transmissibility. I.E.E.E. Transactions on Systems, Man and Cybernetics. Vol. SMC-6, No. 2, February 1976.

15. Groen, J.J. and Jongkees, L.W.B.: The threshold of angular acceleration perception. J. Physiology, 107, 1-7, 1948

16. Gundry, J.: Man and motion cues. Proceedings of the Royal Aeronautical Society Third Flight Simulation Symposium on "Theory and Practice in Flight Simulation", 1976.

17. Clark, B. and Stewart, J.D.: Thresholds for the perception of angular acceleration about the three major body axes. In: Fourth Symposium on The Role of the vestibular organs in Space Exploration, NASA SP-187, 1968.

APPENDIX

THE CHRACTERISTICS OF THE SIMULATOR MOTION SYSTEM

The three degree of freedom motion system of the simulator has three hydraulic servo actuators. These actuators, having hydrostatic bearings, produce a nearly rumble free motion of the simulator. The maximum attainable single degree of freedom performance is presented in Table 5.

The angular accelerations and the specific forces applied during the experiments are small in relation to the maximum performance of the motion system. As this puts high demands on the motion system with respect to the motion noise, a calibration program to determine the transfer functions between motion system input and output angular accelerations or specific forces and to evaluate the motion noise, was carried out.

For all input signals of Experiment I the modulus and phase shift of the transfer function was measured. In addition the power spectral density of the motion noise was computed. It turned out that due to small differences in the dynamic characteristics and due to slightly different loading of the servo actuators the input signals also excite the other two degrees of freedom.

As an example, the data for the heave motion are presented in Table 6. The amplitudes of the angular accelerations linearly related with the input heave signal are roughly one tenth of the thresholds for angular acceleration and increase with frequency.

The angular acceleration noise decreases with frequency hence increases with the amplitude of servo actuator speed.

Although the standard deviation may appear rather large, it should be borne in mind that the noise measured has a large bandwidth and moreover could not be perceived by the subjects.
The noise of the vertical acceleration is small.

In Fig. 11 the position of the test subject relative to the rotational axes of the simulator is given.

Binary Choice Task	Control task	Symmetric			Asymmetric	
		Specific force A_x	Specific force A_z	Angular Acc $\dot{q}$	Specific force A_y	Angular Acc $\dot{p}$
0 %	-	1	1	1	1	1
40 %	-	2	2	2	2	2
80 %	-	3	3	3	3	3
0 %	asymmetric	4	4	4		
40 %	control	5	5	5		
80 %	task	6	6	6		
0 %	symmetric				4	4
40 %	control				5	5
80 %	task				6	6

Table 1a. Survey of the experimental conditions for which the thresholds are determined in Experiment II. Numbers are related to Table 4.

	Specific force A_x	Specific force A_z	Angular Acc $\dot{q}$	Specific force A_y	Angular Acc $\dot{p}$
motion test signal	ramp-function	sinusoidal ω = 1.88 rad/sec	sinusoidal ω = 0.94 rad/sec	ramp-function	sinusoidal ω = 0.94 rad/sec

Table 1b. Survey of test signals used in Experiment II.

Main effects and interactions	Input related thresholds		
	Specific force	Angular Acc.	
	A_z	$\dot{q}$	$\dot{p}$
Frequency		*****	*****
K Upper - Lower	**	**	***
Subjects	*****		****
FS	*****	*****	*****
KS		****	*
FK	*****	*****	*****
FKS			
Replicates			

$\alpha < 0.05$ *
$\alpha < 0.025$ **
$\alpha < 0.01$ ***
$\alpha < 0.005$ ****
$\alpha < 0.001$ *****

Table 2. Survey of the results of the analyses of variance on the results of Experiment I.

No	Input related threshold				
	Specific force			Angular Acc.	
	A_x m/sec^2	A_y m/sec^2	A_z m/sec^2	$\dot{q}$ ^{o}/sec^2	$\dot{p}$ ^{o}/sec^2
1	0.57	0.31	0.08	0.85	0.81
2	0.65	0.36	0.08	0.94	1.00
3	0.67	0.37	0.09	1.05	1.15
4	0.71	0.48	0.15	1.07	1.13
5	0.69	0.44	0.15	1.07	1.16
6	0.71	0.47	0.16	1.20	1.45

Table 3. The threshold values resulting from Experiment II.
Numbers are related to table 1a.

Main effects and interactions	Input related thresholds				
	Specific forces			Angular Acceleration	
	A_x	A_y	A_z	$\dot{q}$	$\dot{p}$
Additional tasks	-	*	*****	*****	****
Subjects	*****	*****	*****	*****	*****
AS	-	****	*	-	-
Replicates	-	-	-	-	-

$\alpha < 0.05$ *
$\alpha < 0.025$ **
$\alpha < 0.01$ ***
$\alpha < 0.005$ ****
$\alpha < 0.001$ *****

Table 4. Survey of the results of the analyses of variance on the results of Experiment II.

	Travel	Speed	Acceleration
Heave	$\pm$ 0.3 m	$\pm$ 1 m/sec	+ 15 m/sec^2 - 28 m/sec^2
Roll	$\pm$ 16°	$\pm$ 73°/sec	$\pm$ 1090°/sec^2
Pitch	$\pm$ 15.5°	$\pm$ 50°/sec	+ 315°/sec^2 - 460°/sec^2

Table 5. Single degree of freedom performance of the three degree of freedom motion system of the flight simulator. September 1975.

Input frequency rad/sec	Modulus M	Phase angle (degrees)	Noise σ_{A_z} m/sec^2	Pitch		Roll	
				Amplitude ^{o}/sec^2	Noise $\sigma_{\dot{q}}$ ^{o}/sec^2	Amplitude ^{o}/sec^2	Noise $\sigma_{\dot{p}}$ ^{o}/sec^2
14	0.675	-89	0.016	0.165	0.501	0.418	0.546
12	0.745	-77	0.017	0.114	0.615	0.343	0.675
10	0.834	-64	0.017	0.093	0.672	0.257	0.782
8	0.907	-50	0.018	0.129	0.734	0.133	0.803
6	0.968	-37	0.017	0.067	0.760	0.118	0.889
4	1.00	-24	0.018	0.031	0.817	0.086	0.953
2	1.01	-11	0.017	0.021	0.853	0.032	1.006
1	1.00	- 5	0.018	0.031	0.894	0.021	1.071

Table 6. The transfer- and noise characteristics of the motion system for a sinusoidal input signal producing a heave acceleration amplitude of 0.085 m/sec^2.

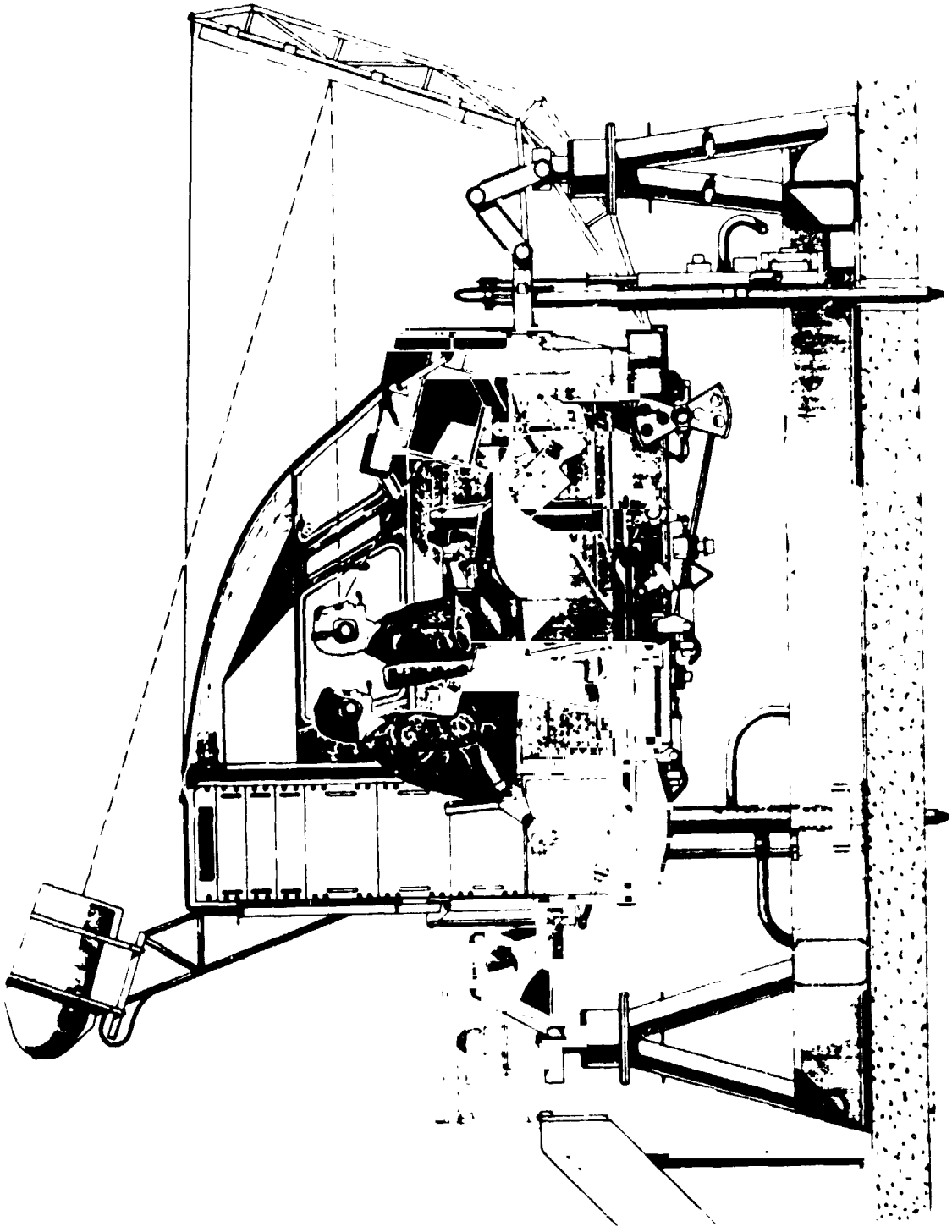

Fig. 1. Layout of the flight simulator.

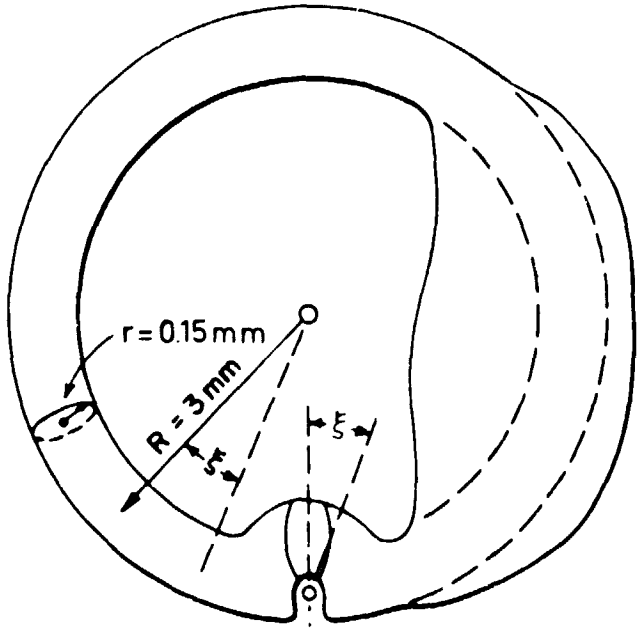

Fig. 2a. Schematic Diagram of the Semicircular Canal (Ref. 10).

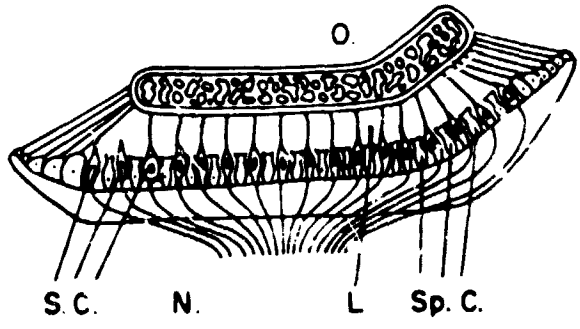

Fig. 2b. Schematic drawing of a cross section of an otolith and its macula. O is the otolith, suspended by strands which run from the margins to the macula, consisting of supporting cells (Sp.C.) and sensory cells (S.C.). Between the otolith and the macula there is a thin Layer (L) to allow the otolith to slide over the macula. N is the nerve (Ref. 10).

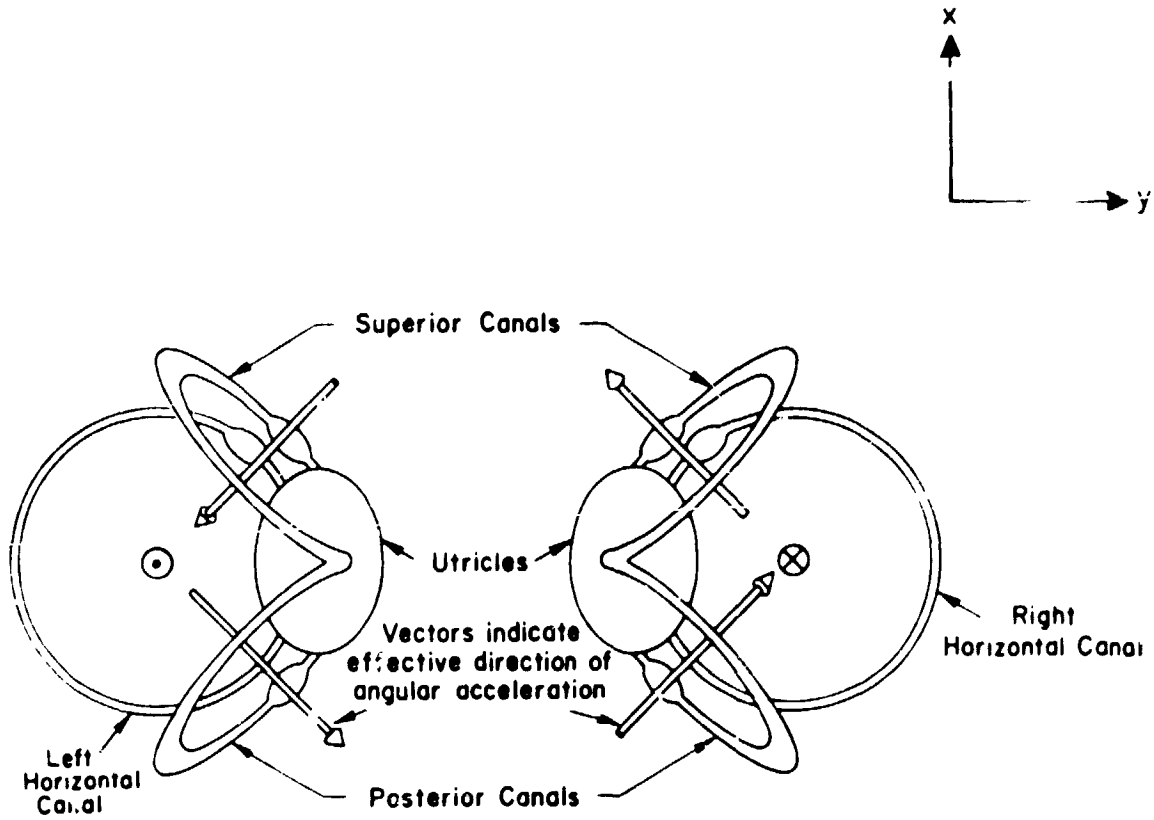

Fig. 2c. The approximate orientation of the sime-circular canals (Ref. 9).

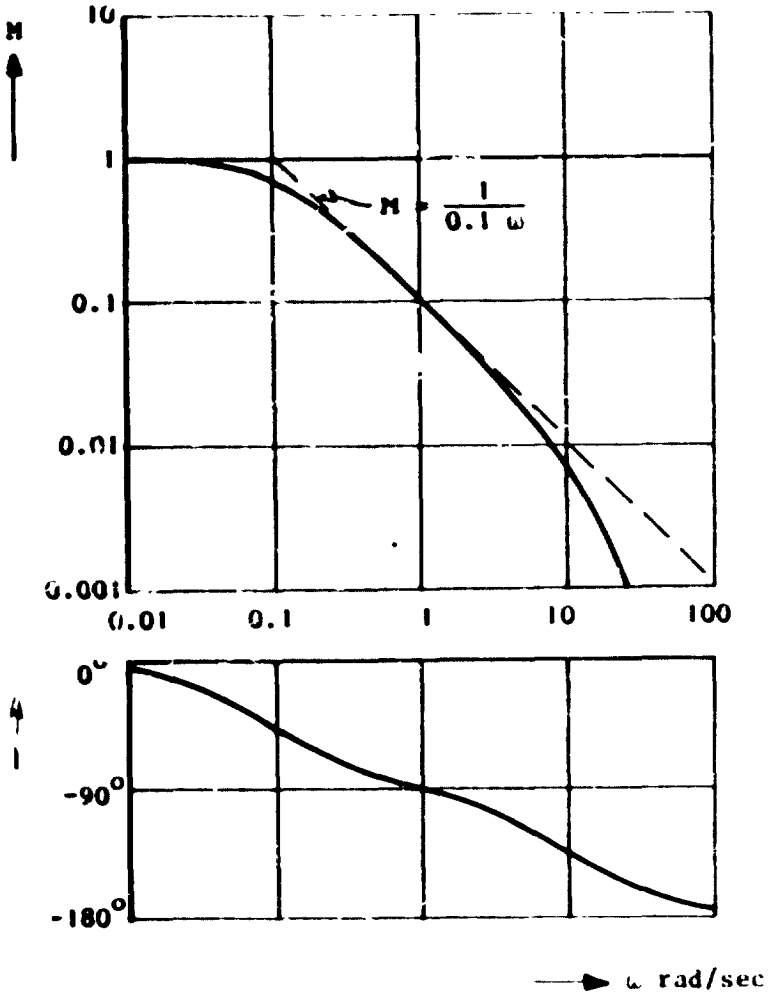

Fig. 3. Modulus and phase angle of the semicircular canals according to eq. (1).

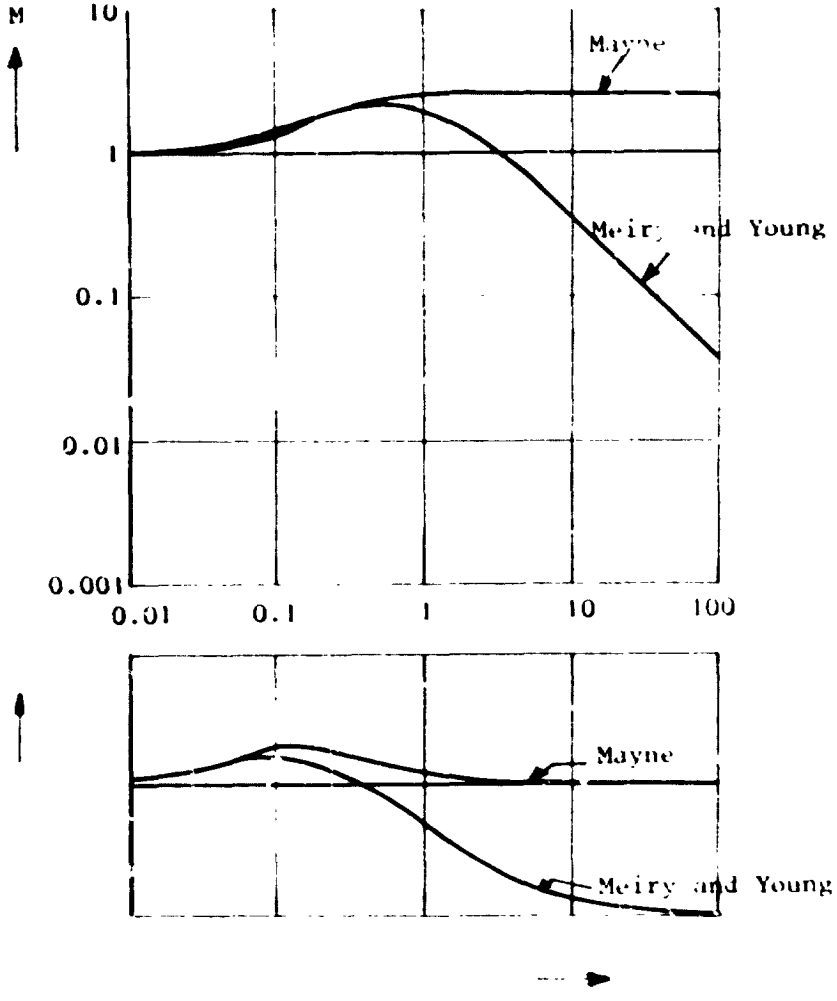

Fig. 4. Modulus and phase angle of the otolith according to eqs. (2) and (5).

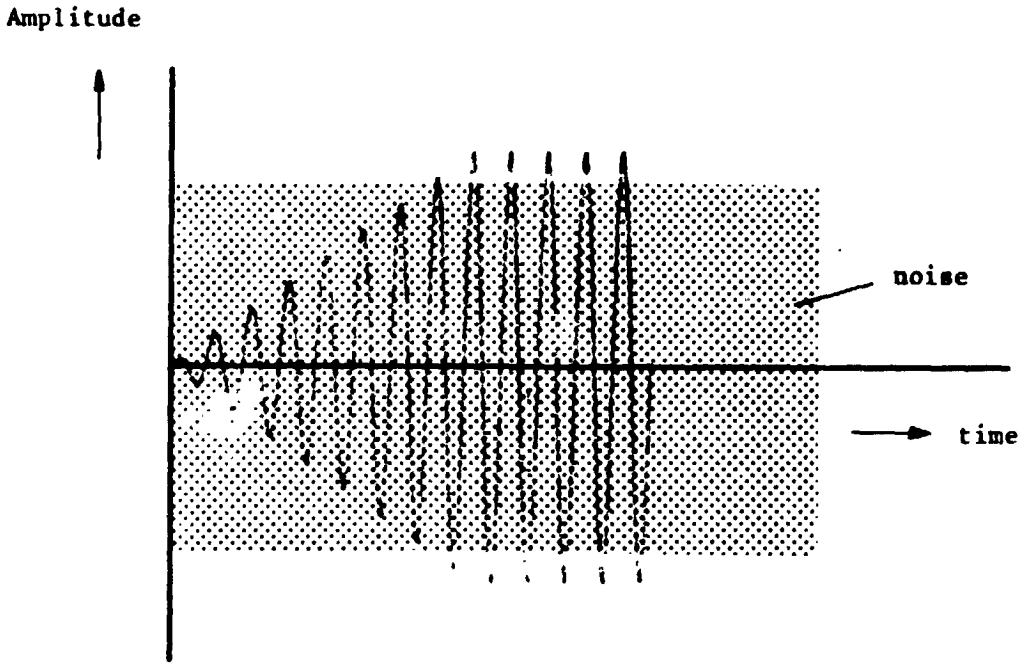

Fig. 5. Schematic diagram showing the change in signal to noise ratio of the vestibular output due to an increasing sinusoidal input motion cue.

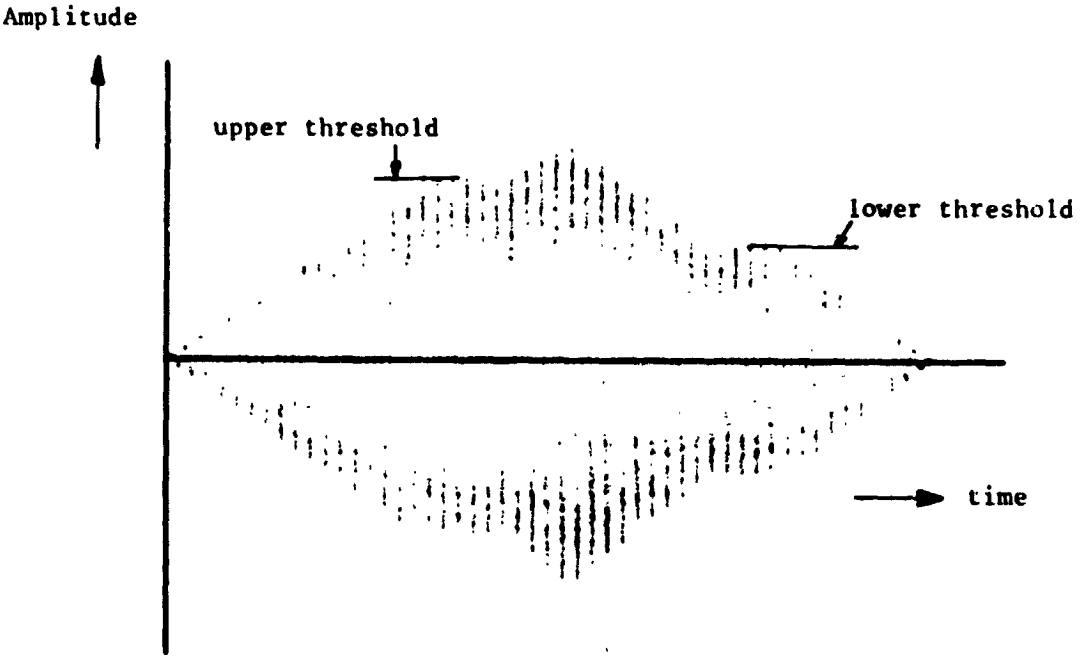

Fig. 6. Examples of the time history of the test signal to determine upper and lower thresholds.

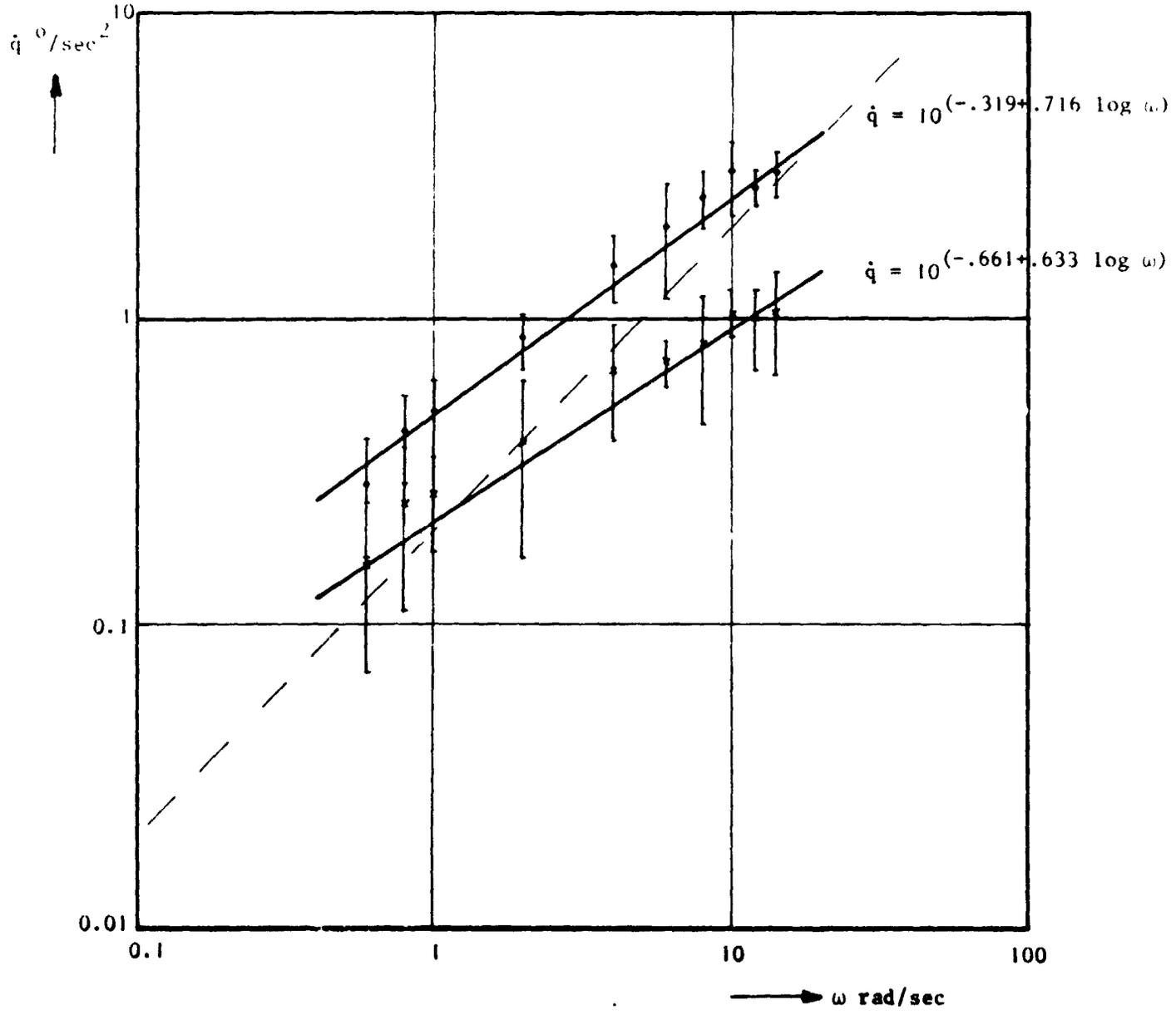

Fig. 7. Input related threshold values for pitch angular acceleration.

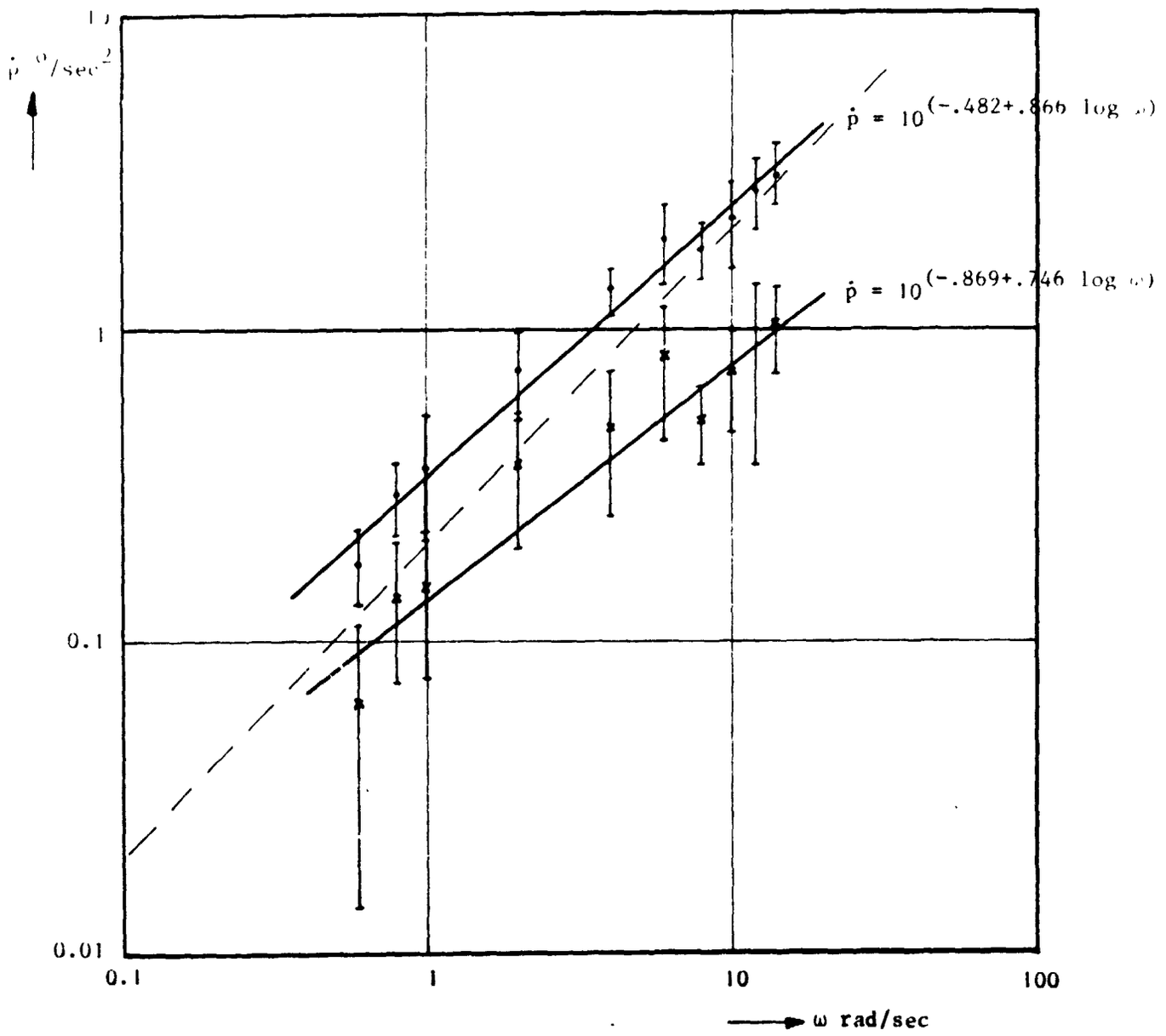

Fig. 8. Input related threshold values for roll angular acceleration.

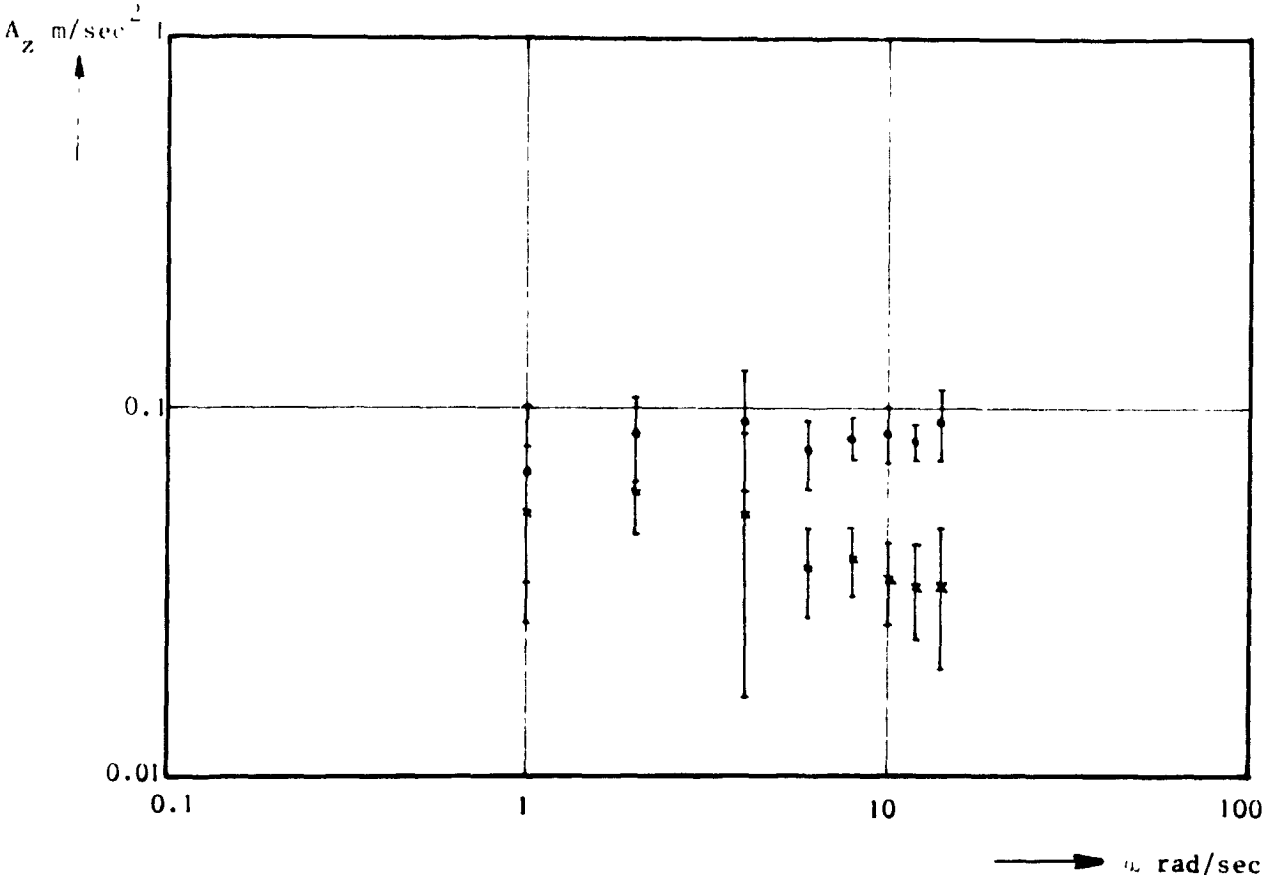

Fig. 9. Input related threshold values for specific force along the Z-axis.

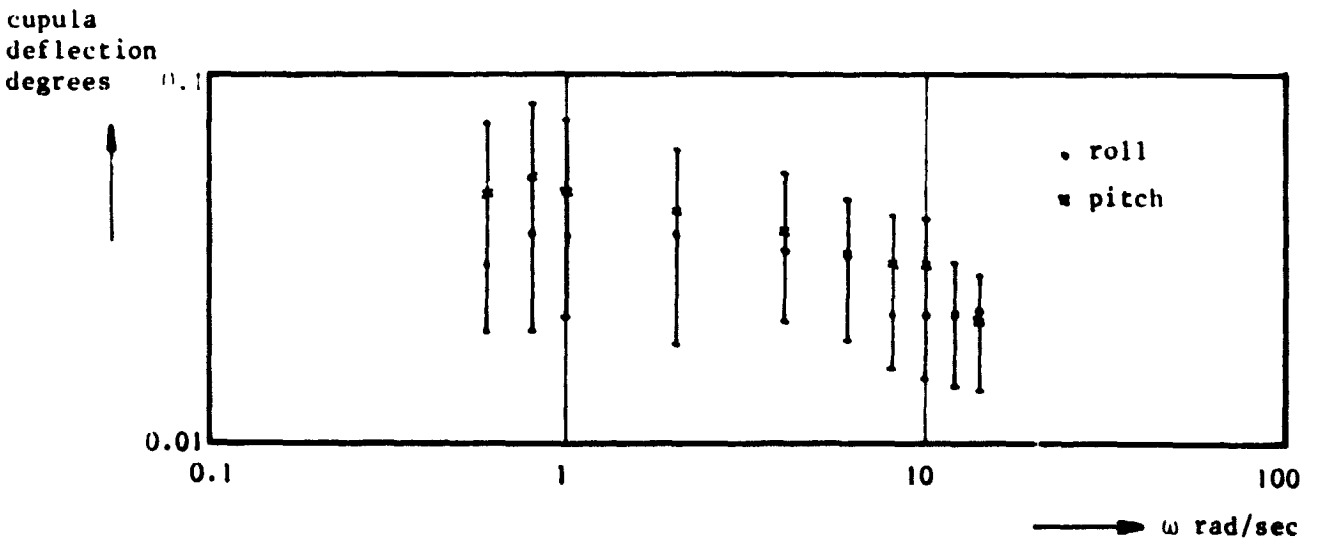

Fig. 10. Cupula deflection at threshold value for pitch and roll.

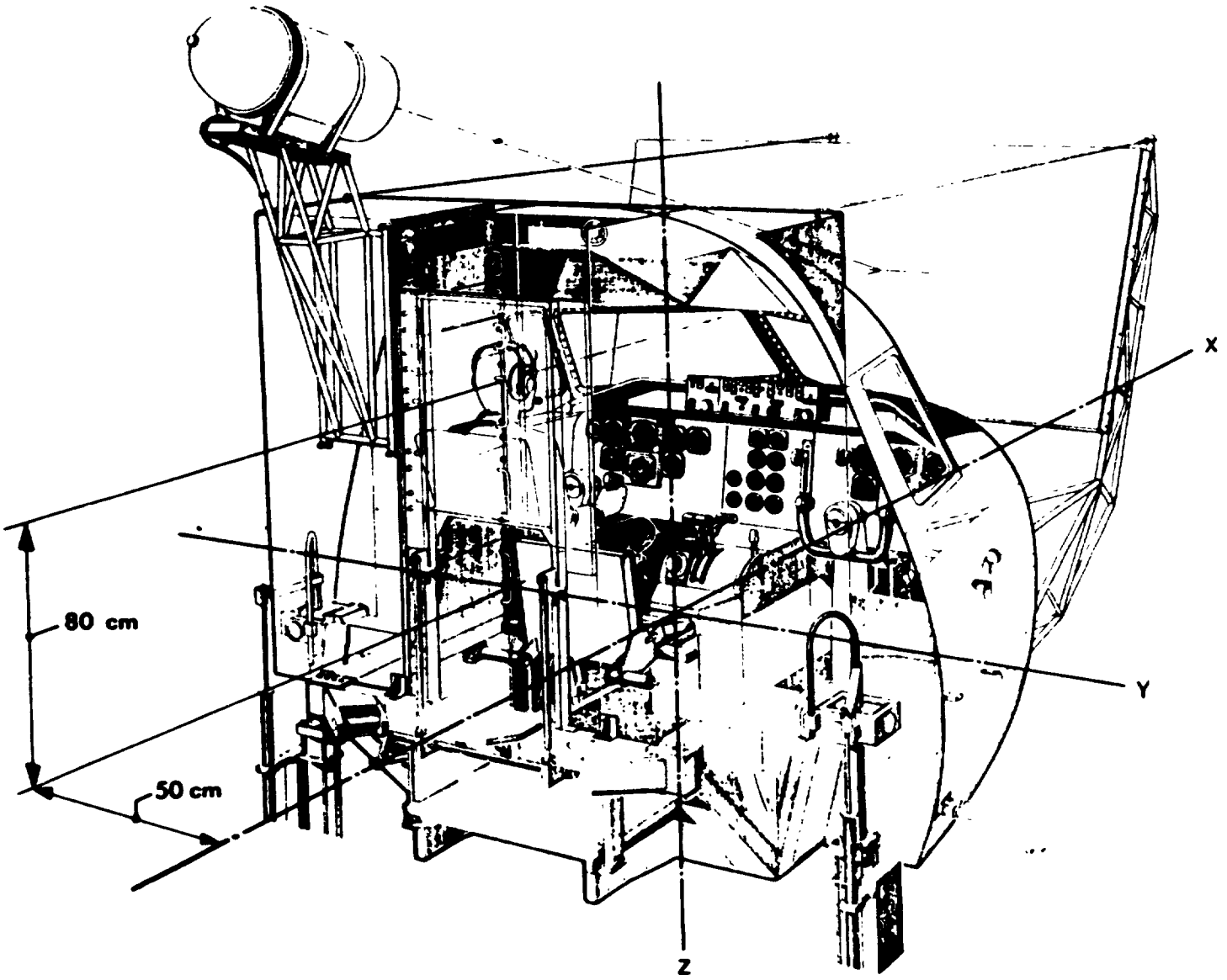

Fig. 11. Position of the subject relative to the axes of rotation.

BIOMECHANICAL RESPONSE AND MANUAL TRACKING PERFORMANCE IN SINUSOIDAL, SUM-OF-SINES, AND RANDOM VIBRATION ENVIRONMENTS*

By William H. Levison

Bolt Beranek and Newman Inc.

Cambridge, Massachusetts

ABSTRACT

A set of manual control experiments was conducted to explore biodynamic response and tracking performance in sinusoidal, sum-of-sines, and random z-axis vibration environments. Primary experimental variables were vibration spectrum, vibration amplitude, and stick spring gradient. Biomechanical response mechanisms were approximately linear for the vibration environments explored in this study and, with the exception of stick feedthrough, were independent of stick parameters. As seen in previous studies, stick feedthrough was considerably greater for the control stick with the higher spring gradient. Tracking performance was degraded by vibration primarily through an increase in effective pilot time delay and through increased motor-related pilot remnant. Good model results were obtained by assuming that motor noise/signal ratio and time delay varied linearly with rms shoulder acceleration. A model-based mapping procedure was defined and validated for extrapolating the results of single-sine vibration/tracking experiments to complex vibration environments. Mapping in the reverse direction was also validated.

INTRODUCTION

As technology continues to expand the performance envelope of military aircraft, pilots will have to function in increasingly severe physical environments. Vibration, either alone or in combination with other stressors, may be an important part of this environment. In order to better understand and predict the effects of vibration on pilot performance, the Aerospace

---

*This work was sponsored by the Aerospace Medical Research Laboratory, Wright-Patterson Air Force Base, under Contract No. 33615-75-C-5043. Lt. Philip D. Houck was the Technical Monitor for this contract and Project Engineer for the AMRL experimental program.

Medical Research Laboratory has undertaken a long-term study of manual tracking in vibration environments. Recent programs have explored the nature of biomechanical response and the interactions between tracking, vibration and control-stick parameters [1-4].

This paper summarizes the results of a joint AMRL/BBN study that builds upon the results of these programs. This study had two major objectives: (1) to further define the interaction between vibration parameters and tracking performance, and (2) to develop a mapping procedure to extrapolate among single-sine, sum-of-sines, and random vibration environments. More details may be found in [5].

One of the difficulties of vibration research is that the vibration environments of ultimate interest are not the environments that are most amenable to laboratory exploration. A vibration environment encountered in flight may well consist of a component that is continuous in frequency over some band plus one or more sinusoidal (or near-sinusoidal) components. Laboratory shake tables, however, are often constrained to generating sinusoidal vibration inputs. Even when random vibration is possible, sum-of-sine (rather than continuous-frequency) inputs may be desired so as to maximize signal/noise ratios and thereby maximize the measurement bandwidth. Thus, an extrapolation (or "mapping") procedure is needed so that measurements obtained in one type of vibration environment can be used to predict the effects on performance of some other environment.

Because of the ways in which vibration influences tracking behavior, a simple weighting function will generally not be sufficient to extrapolate results from discrete sinusoid vibration environments to more complex environments. First of all, a number of biodynamic response mechanisms may be involved in determining the effects of vibration on tracking performance, with the various mechanisms having different response characteristics. Secondly, vibration-related performance degradation is largely not traceable to simple additive effects. Except for stick feedthrough (which typically accounts for a small fraction of the tracking error variance), the effects of vibration are manifested as increases in pilot remnant and in other adverse changes to basic information-processing capability. Finally, the pilot partially compensates for this unfavorable environment by re-adjusting the adaptable elements of his response behavior. Thus, in general, a rather comprehensive set of models will be required in order to allow the results of one set of experiments to be extrapolated to different experimental situations.

The "optimal-control" pilot/vehicle model appears to have a structure that allows one to predict adaptive changes in tracking response strategy that accompany whole-body vibration. This model has been applied successfully in previous studies of vibration/tracking [2-4] and forms the basis for the mapping procedure outlined in this paper.

The strategy adopted for this research study was basically as follows: (1) verify the linearity of biodynamic response mechanisms, (2) determine

the relation between biodynamic response and pilot-related model parameters, and (3) demonstrate a method for using the optimal-control model to predict tracking performance as a function of vibration parameters.

DESCRIPTION OF EXPERIMENTS

Experimental appara us and procedures were similar to those employed in the previous study. Therefore, only a brief description of experiments is given here. Readers desiring additional details on mechanization of the tracking task and vibration inputs are referred to [3].

The tracking task consisted of a single-axis compensatory task with K/s controlled-element dynamics. The tracking input was constructed by summing five sinusoids of random phase relations with amplitudes selected to approximate a first-order noise process having a break frequency at 2 rad/sec. This disturbance input was added to the pilot's control input to simulate a vehicle distrubance. Fore-aft motions of the control stick resulted in vertical motion of the tracking error, which was displayed on a CRT.

The test subject, control device, and display were located on the vibration table. Tracking response in the following vibration environments was explored: (1) single sinusoid vibration at 2, 3.3, 5, 7, and 10 Hz; (2) sum-of-sines vibration having equal acceleration components at 2, 3.3, 5, 7, and 10 Hz; (3) random continuous-frequency vibration, with the driving noise filtered in such a way as to approximate a flat acceleration spectrum over the range 2-10 Hz.

Nominal rms vibration amplitudes of 0.15 g and 0.3 g were explored for all environments; in addition, 0.2 g rms was explored for random vibration. All vibration was vertical (i.e., z-axis).

Two control sticks were used in this study, a "spring stick" having a spring constant of 7.5 lbs/inch and a "stiff stick" having a spring constant of 130 lbs/inch. The control stick was always located in the center position.

Seven subjects participated in all of the experimental conditions and provided the data base summarized in this report. An accelerometer mounted on the subject's shoulder permitted measurement of vibration transmitted to the body. Accelerometers mounted on a bitebar held between the teeth provided measurements from which head translational and rotational accelerations could be computed.

Each data-taking session consisted of a series of six trials lasting approximately 2 minutes each. Rest periods were provided between successive trials as desired by the subject. (A 30-second rest period was typical.) Each session consisted of one static trial and five trials under different vibration conditions. Presentation of experimental conditions was balanced across subjects to minimize bias in the results due to learning effects. By

the completion of the experimental program, each subject tracked in the static condition three times and under each vibration condition once for each of the two control stick configurations.

EXPERIMENTAL RESULTS

Biodynamic Response

Rms acceleration scores for shoulder and head response were averaged across the seven test subjects and analyzed to explore the effects of stick configuration (i.e., stiff or spring) on biodynamic response. No statistically significant differences with regard to stick configuration were found for these variables. Measures of vibration-induced control response, on the other hand, were strongly influenced by control stick parameters.

Figure 1 illustrates the basic linearity of the relevant biodynamic response mechanisms. Mean rms shoulder and head translation accelerations obtained in the complex-vibration experiments are shown versus rms platform acceleration. Data from the two control stick configurations are lumped in this presentation. The dashed lines (found through least-squares regression) indicate the best straight-line fits to the data that pass through the origin. In general, these fits lie within one standard deviation of the experimental measures. The linear fit is especially good for the rms shoulder acceleration, which seems to be the most critical biodynamic variable with regard to predicting tracking performance.

Describing functions relating control response to platform acceleration are shown in Figure 2 for the spring and stiff stick configurations. Measurements from the three types of vibration spectra (random, sum-of-sines and single-sine) are compared for the 0.3 g input. The single-sine describing function is a composite of the frequency-response measures obtained individually at each of the five vibration frequencies.

Except possibly for a greater phase lag associated with the random vibration input, there were no consistent differences in response behavior across the three vibration spectra. With regard to predicting input-correlated response power (which depends only on amplitude ratio), we can consider this response mechanism to be independent of the shape of the platform vibration spectrum. There were important differences between spring-stick and stiff-stick measurements, however, since feedthrough is determined by the interaction between the biomechanical configuration and control-stick characteristics such as mechanical impedance and electrical gain.

We conclude, therefore, that coupling between platform and control input can be treated as linear over the range of vibration amplitudes considered in this study. Accordingly, we can expect to predict response to complex vibration inputs on the basis of experiments made with single-sinusoid

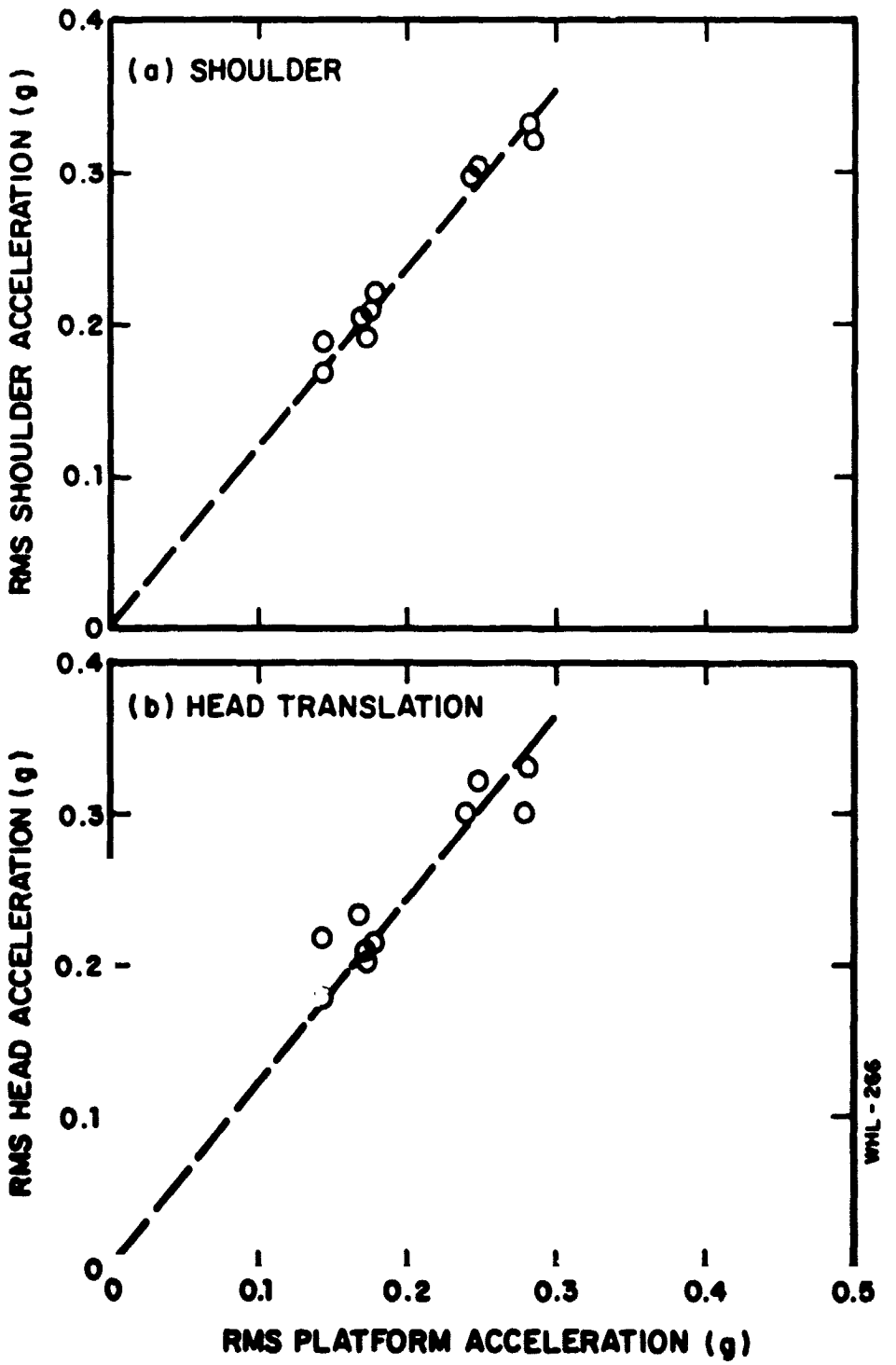

Figure 1. Relation Between Biodynamic Response Scores and Platform Acceleration

Complex vibration spectra.

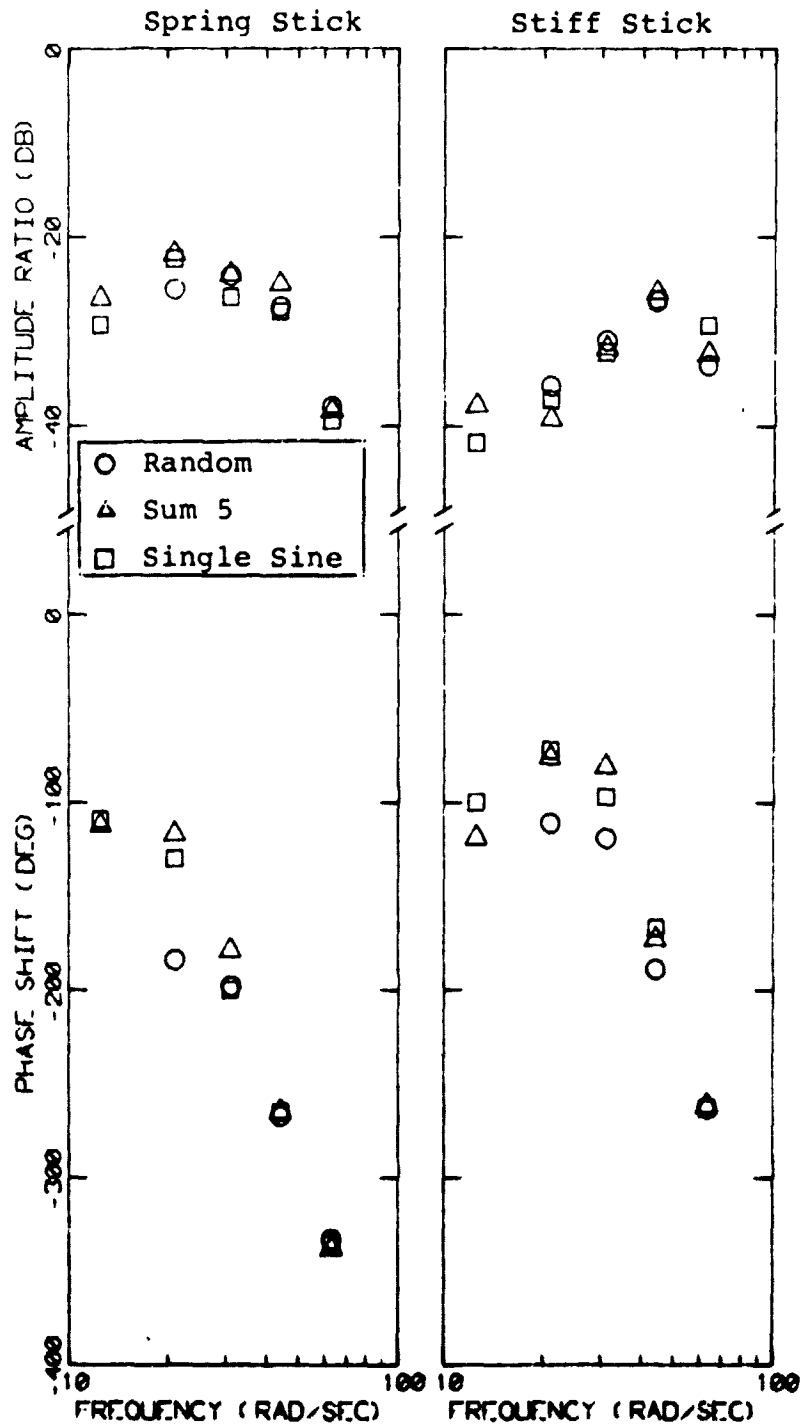

Figure 2. Effect of Vibration Spectrum on Control/Platform Describing Functions

0.3 g platform acceleration, average of 7 subjects. 0 dB = 1 inch/g.

vibration (and vice versa).*

Figure 3 shows that the spectral content of the platform vibration had no consistent effect on the shoulder/platform describing function. Vibration amplitude also had negligible effect, indicating that this biodynamic response mechanisms is basically linear.

Describing functions relating head translational response to platform acceleration showed a similar degree of invariance across vibration parameters. The relationship between head rotation and platform was also largely invariant to vibration parameters, except for the amplitude ratio at the lowest vibration frequency (2 Hz). Figure 4 shows that the amplitude ratio increases as spectral complexity increases from single-sine to random. The total increase is relatively large (12 dB) and statistically significant. Analysis of variance shows that the differences between single-sine and sum-of-sine measures, and between sum-of-sine and random measures, are significant at the 0.05 level. (Differences in phase shift at 2 Hz were not significant.) Apparently, the subjects "predicted" the 2 Hz vibration input and thereby partially compensated for head motion response. As expected, predictive capability diminished with increasing spectral complexity.

If the biodynamic response mechanisms described above are linear, it should be possible to use the frequency-response curves obtained with any vibration spectrum and predict rms response motion for any other vibration spectrum (within the range of amplitudes and frequencies for which the data are valid). Of greatest practical interest is the ability to extrapolate from measurements obtained in single-sine vibration environments to predictions of response in complex vibration environments.

Rms biodynamic response scores were predicted for (a) vibration-correlated control input, (b) shoulder acceleration, and (c) head translation for each of the five (three random, two sum-of-sines) complex platform spectra explored in this study.

Extrapolation of single-sinusoid measurements was performed as follows. Biodynamic transer functions obtained from single-sine experiments (averaged over vibration amplitude) were cascaded with the complex platform vibration spectra to yield predicted response spectra. For sum-of-sines vibration, estimates of response power predicted at each measurement frequency were summed to yield predicted mean-squared response power. For random platform vibration, the predicted response power spectral density was integrated over the frequency range 2-10 Hz to predict mean-squared

---

*Until further data are obtained, predictions are restricted to steady-state vibration inputs. One is not justified in extrapolating these results to pulse-like acceleration inputs, for example.

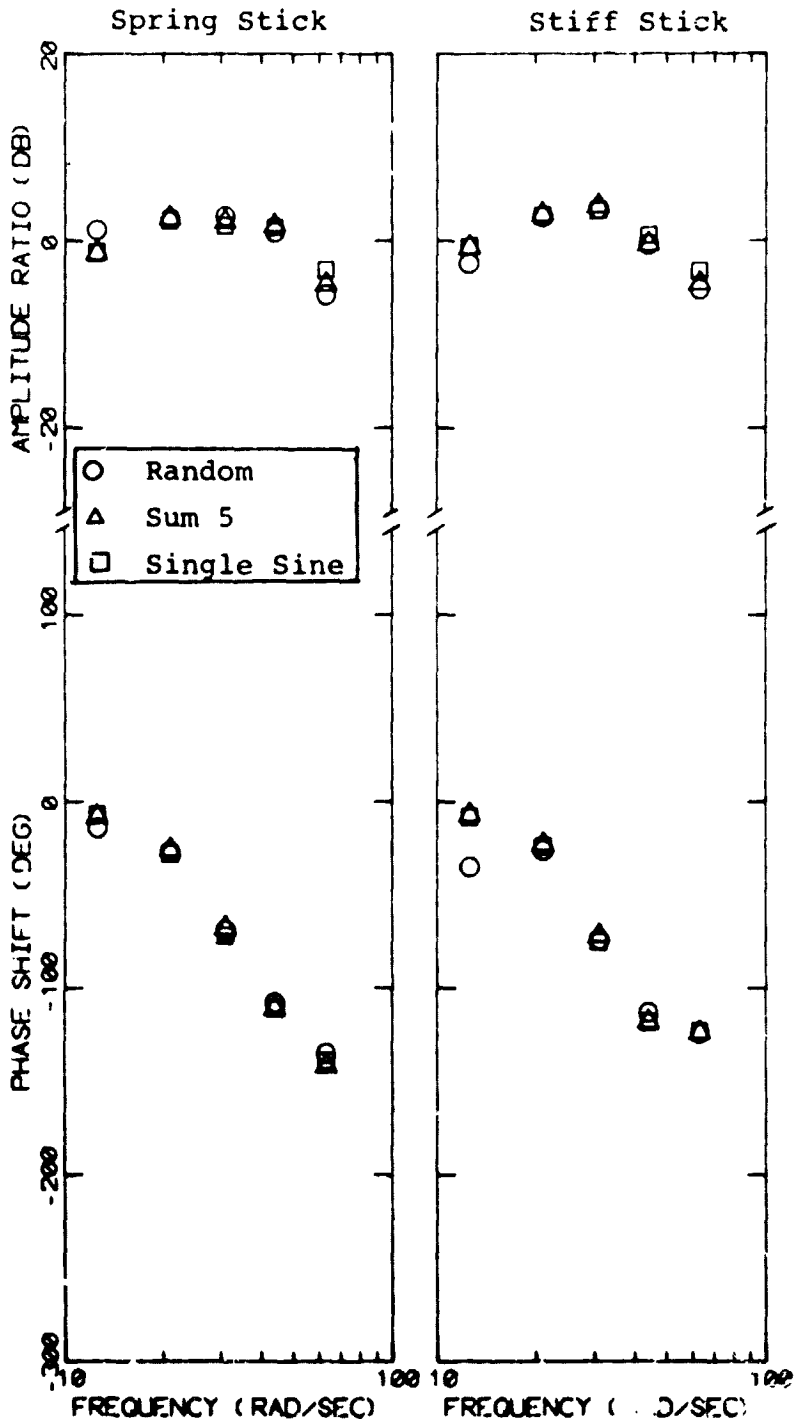

HL-273

Figure 3. Effect of Vibration Spectrum on Shoulder/Platform Describing Function

Average of 7 subjects. 0.3 g rms platform acceleration. 0 dB = 1 g/g.

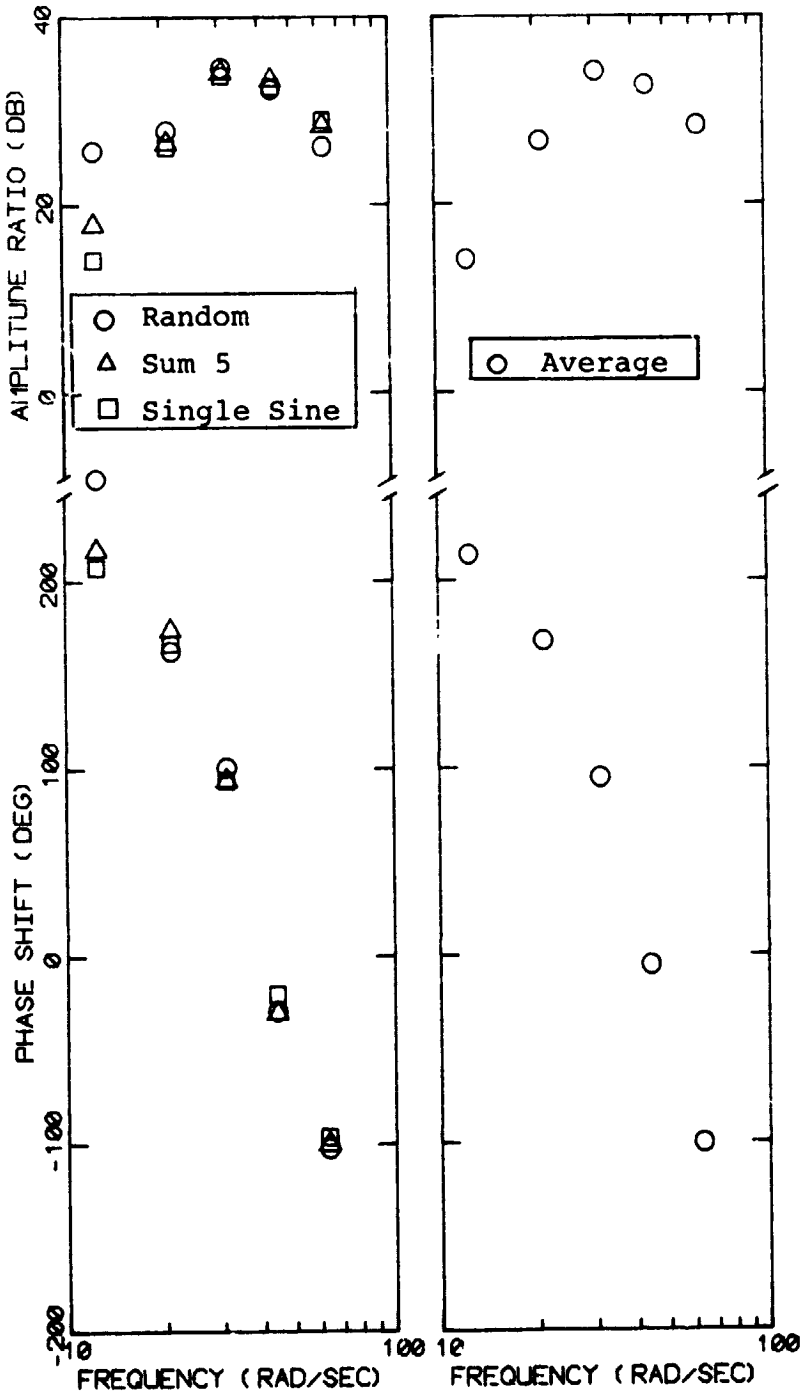

UHL-277

Figure 4. Effect of Vibration Spectrum on Describing Functions Relating Head Rotation to Platform Acceleration

Average of 7 subjects. 0 dB = 1 (radian/sec^2)/g.

response power.* Square roots of these predictions were performed to obtain estimates of rms response.

Predicted and measured rms response scores are compared in Figure 5. Head and shoulder response scores have been averaged across the two stick configurations. On the whole, predictions agree reasonably well with measured quantities; average fractional difference is about 20%.

Tracking Performance

Error and control scores for the complex vibration conditions are plotted versus vibration amplitude in Figure 6 and exhibit the following trends: (1) error and control scores increase monotonically with increasing vibration amplitude; (2) the increase in control score is more severe for the stiff stick; and (3) tracking error is less for the stiff stick than for the spring stick in the static case, but these differences become less as vibration amplitude is increased. These results are not surprising and generally reflect the findings of the earlier study of Levison and Houck [3].

The error scores associated with single-sine vibration were generally larger than scores associated with complex vibration. However, actual rms platform vibration levels were somewhat larger for single-sine experiments than for complex-vibration experiments for the same nominal vibration level [4]. Therefore, one cannot properly conclude from these results that single-sine vibration inputs are inherently more disruptive than complex vibration inputs.

Rms error and control scores were compared against various biodynamic response measures to determine the response variable (excluding stick feedthrough) most likely responsible for the degradation of tracking performance in vibration environments. Comparisons were made with (a) rms shoulder acceleration, (b) rms shoulder velocity, (c) rms rate-of-change of shoulder acceleration, and (d) estimated rms relative motion between eye point-of-regard and display. Data obtained from single-sine vibration trials were used in this test. Visual inspection of these comparisons revealed that the relation between error (or control) and biodynamic response variable was most nearly monotonic when shoulder acceleration was considered.

Relationships between tracking variables and rms shoulder acceleration are shown in Figure 7. The contribution of stick feedthrough has been removed from the control scores shown in this figure, since we are interested

---

*Straight-line interpolation was performed between estimates of response power density at adjacent measurement frequencies on a log-log basis. Piecewise integration over the entire range of measurement frequencies was then performed.

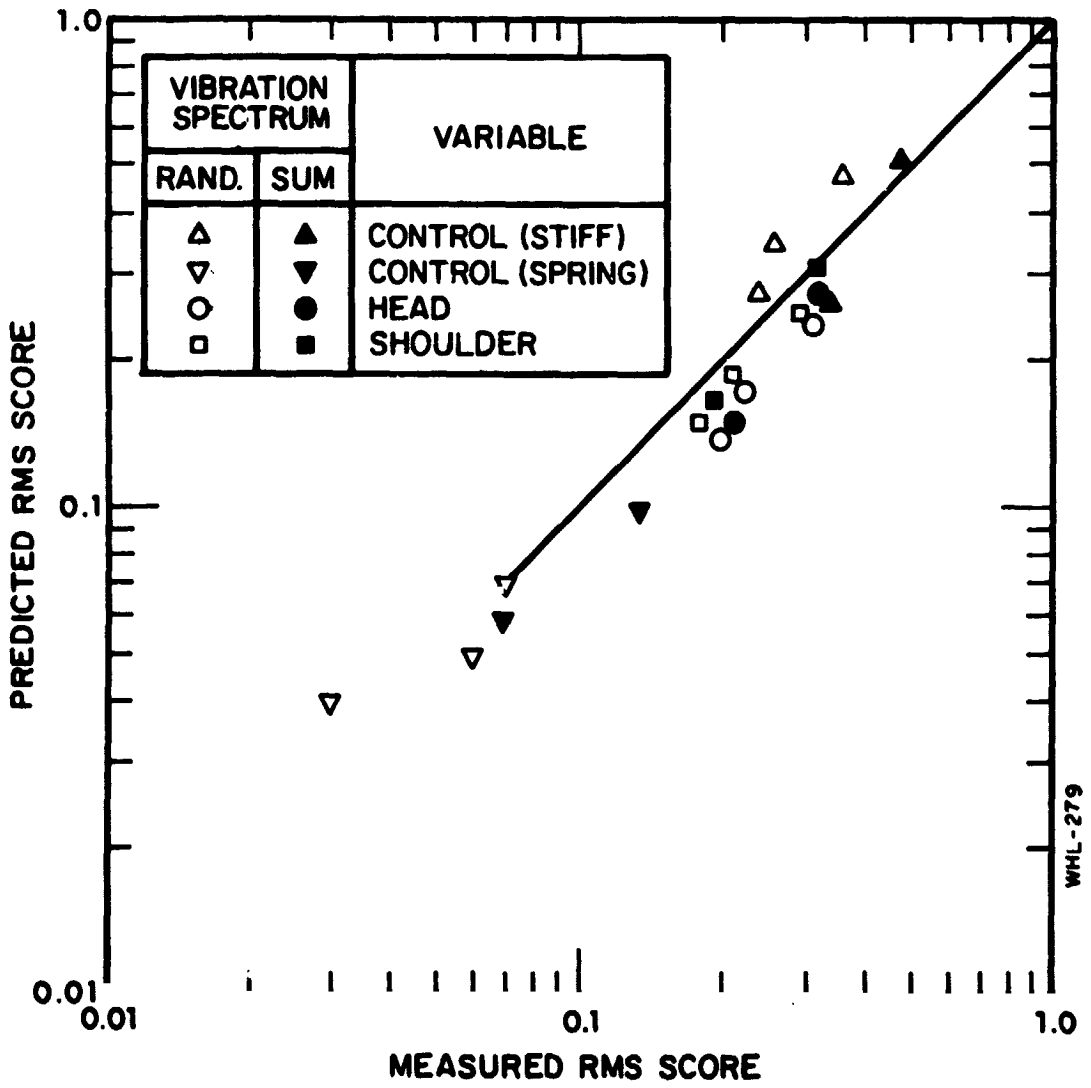

Figure 5. Comparison of Predicted and Measured Rms Scores

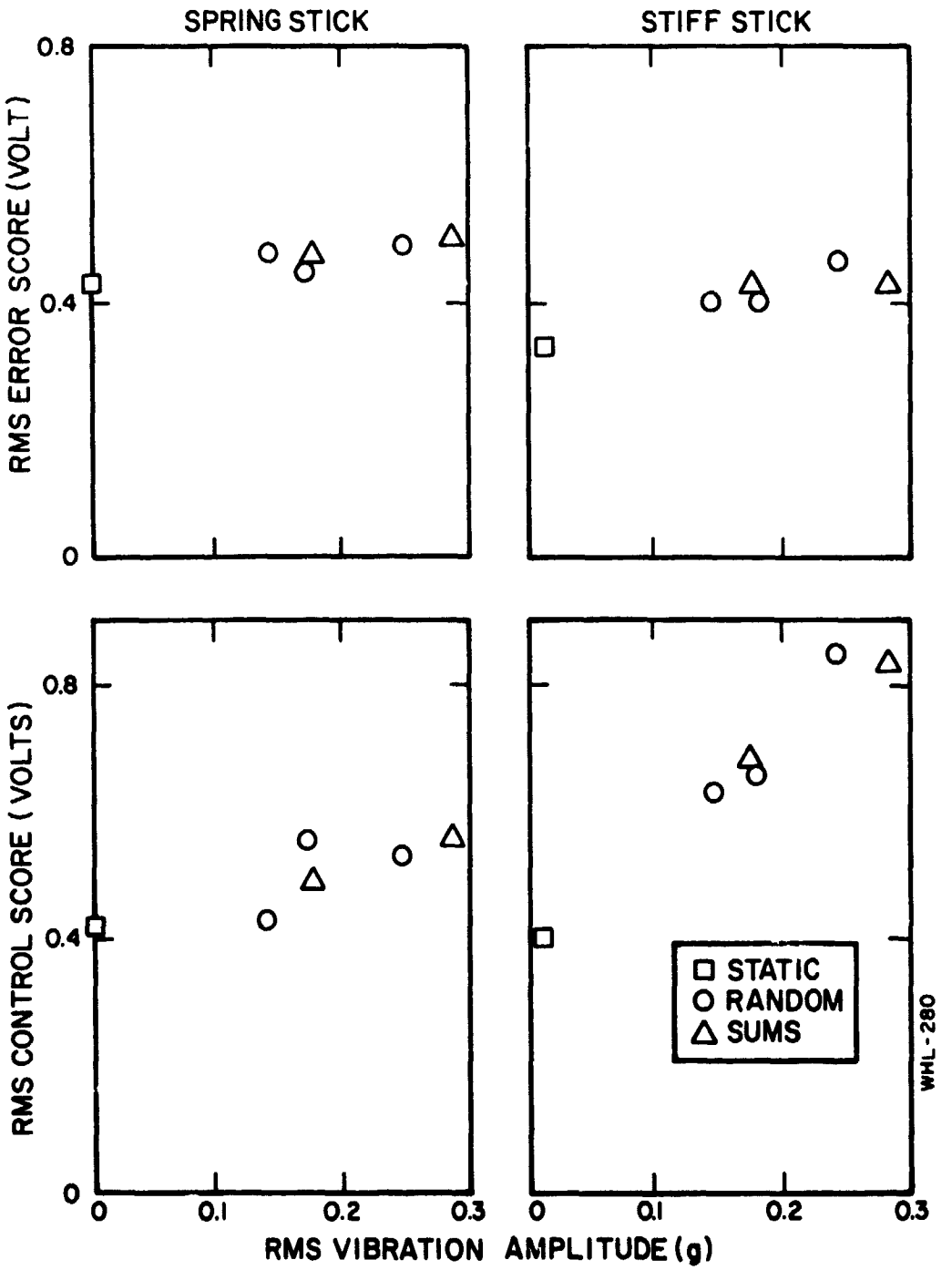

Figure 6. Effect of Vibration Amplitude on Rms Performance
Average of 7 subjects.

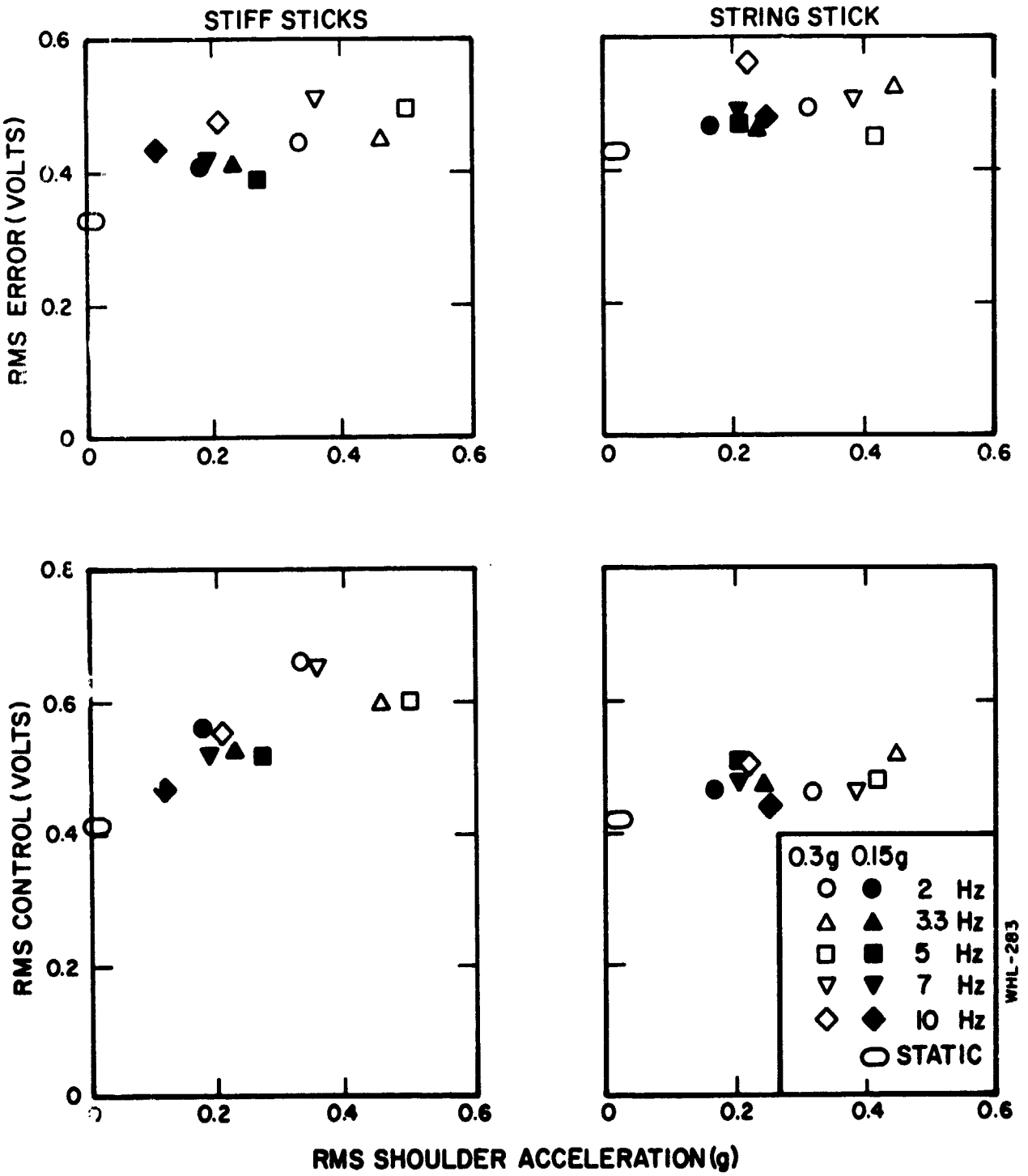

Figure 7. Tracking Variables Versus Shoulder Acceleration

Single-sine vibration environments.
Average of 7 subjects.

here primarily in the effect of vibration on tracking response behavior. Relationships between tracking variables and the other biodynamic variables considered (not shown here) tended to show less structure than the relationships shown in Figure 7. Therefore, we have tentatively concluded that motor-related interference with tracking performance is associated primarily with shoulder acceleration. There may, of course, be other response variables not explored in this study (say, elbow acceleration) that correlate equally well or better. Nevertheless, as we show later, reliable predictions of tracking performance can be made on the assumption that motor-related pilot model parameters vary linearly with rms shoulder acceleration.

The effects of vibration on frequency-response measures are typified by Figure 8, which compares static performance with performance in the 0.3 g, sum-of-sines vibration environment. Results are for the spring stick configuration. Amplitude ratio and phase shift refer to the pilot describing function and relate control activity (in volts) to tracking error (volts); "rem/cor" is the ratio of remnant-related stick power to input-correlated stick power at each input frequency.*

Increasing the rms platform acceleration from 0 (static) to 0.3 g produced the following general trends: (1) amplitude ratio decreased at frequencies below 6.3 rad/sec, remained nearly constant at 6.3 rad/sec, and increased at 10.5 rad/sec;** (2) phase lag increased at 6.3 and 10.5 rad/sec; (3) remnant ratio generally increased at all frequencies. On the whole, deviations from static measurements were greater for the 0.3 g platform acceleration than for the 0.15 environment, and vibration effects were greater for stiff-stick tracking than for spring-stick tracking. The single-sine vibration environments showed similar influence on frequency-response measurements, with 7 Hz vibration having a somewhat greater effect than 2 Hz vibration. Overall, the frequency-response measures are similar to those found by Levison and Houck [3].

Model analysis using the optimal-control model [5-8] was performed so that vibration-induced performance changes could be interpreted in terms of changes in the pilot's basic information-processing capabilities. A second-order model of the pilot/stick interface was included in the description of system dynamics as described in [5].

Static tracking results were first matched to provide a baseline set

---

*The ratio is based on what the input-correlated and remnant-related spectra would be if the tracking input spectrum were continuous rather than sum-of sines. Details of this computation are given in [3].

**Changes in frequency response are referred to input frequencies. Other than having been included in the set of input frequencies, the frequencies of 6.3 and 10.5 rad/sec have no special significance.

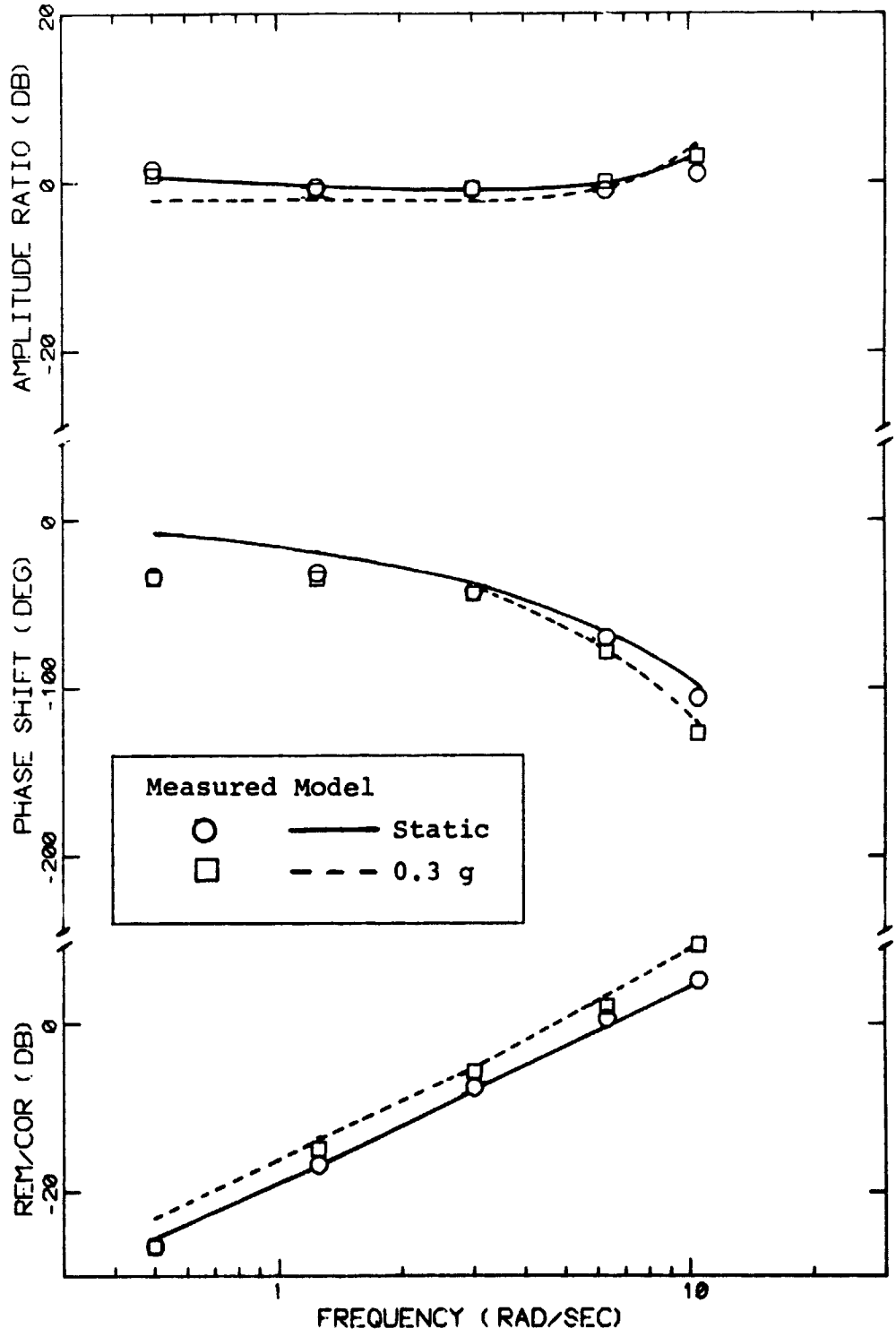

WL-290

Figure 8. Comparison of Measured and Model Frequency-Response Measures, Spring Stick

Sum-of-sines vibration.

of pilot-related model parameters. The following values--used also to match static results in the preceding study [3]--provided a good match to static results: 0.15 second time delay, a "motor time constant" of 0.1 seconds, an observation noise/signal ratio of -21 dB, and a motor noise/signal ratio of 0.004 (about -30 dB).

The sum-of-sines 0.3g vibration data were then matched to determine the effects of vibration on pilot-related model parameters. As in the preceding study, two vibration-dependent parameters were identified: time delay and motor noise/signal ratio. Time delay was increased to 0.2 seconds, and motor noise/signal ratio was increased to 0.02. As shown by the solid curves in Figure 7, these parameter changes allow the pilot/vehicle model to reproduce the trend of the frequency-domain results, and both error and control scores (shown further on) are reproduced to within an accuracy of about 5%.

Once the 0.3g data were matched, the 0.15g sum-of-sines results were analyzed to determine the appropriate relationships between pilot parameters and rms shoulder acceleration. A linear variation of both time delay and noise/signal ratio with rms shoulder acceleration provided a good match to the data and was adopted for the mapping procedure outlined in the following section of this paper.

The increment in time delay for 0.3 g vibration was the same as that found by Levison and Houck for a similar vibration environment [3]. However, the motor signal/noise ratio was only half that found in the earlier study, and no visual effects were found in this study. These differences may well reflect a higher level of subject familiarity with the vibration environment in this study. First of all, the experimental program was completed in a shorter period of time than in the Levison and Houck study; thus, there was greater opportunity for the subjects to optimize the tracking strategy for the vibration environments. Secondly, the subjects had participated in a tracking study exploring the same plant dynamics and similar vibration environment for the three months prior to this study, which allowed them to begin this experimental program in a high state of training.

MAPPING AMONG VIBRATION ENVIRONMENTS

A general model structure is described below which is intended for predicting tracking performance in a variety of control situations. In addition to predicting the effects of vibration amplitude and spectral shape (which are given primary emphasis in this report), the model can predict performance as a function of (a) vehicle dynamics, (b) tracking input characteristics, (c) control-stick characteristics, (d) display gain, (e) performance requirements, and (f) attention to the task. Numerical relationships between pilot-related tracking parameters and biodynamic response parameters are based on the experimental results documented in [5]; until further data are available, these relationships must be considered valid only for z-axis vibration and for the specific biodynamic configuration explored in this study.

This model is used as the basis of a "mapping" procedure for extrapolating results obtained in a given vibration environment to other vibration environments. A definition and demonstration of the mapping procedure follows the discussion of the basic model.

Model Structure

An outline of the model structure is diagrammed in Figure 9. This model consists of the optimal-control pilot/vehicle model referred to above, plus an element (labeled "vibration feedthrough") to account for control inputs linearly related to platform vibration. For simplicity of exposition we consider a single-variable tracking task; extension of the model to multi-input, multi-control systems is straightforward.

Input variables shown in Figure 9 are the tracking input, i, assumed to be a zero-mean Gaussian random process; the platform vibration, α_p; the pilot's observation noise process, $\underline{v}_e$; and the pilot's motor noise process, v_u. Response variables include tracking error, $\underline{e}$, the pilot's control force, u, the electrical control input provided by the control device, δ_t, the control input due to vibration feedthrough, δ_v, and the total control input, δ, given as the sum of the tracking and feedthrough control components. (We assume that platform vibration is at frequencies beyond the bandpass of the man/machine system so that the pilot cannot effectively track out the feedthrough-related inputs.) Error and observation noise are shown as vector quantities, since the pilot will generally obtain and use both displacement and velocity information from a single error indicator [10, 11].

The reader is directed to the literature for detailed mathematical discussion of the basic optimal-control model [6, 7]. Pilot-related model parameters and relevant biodynamic response properties are reviewed below.

Time delay. The following empirical relationship was found in this study: $T=0.15+0.15\alpha_s$, where T is the pilot's effective time delay in seconds, and α_s is the rms shoulder acceleration in g's.
Observation Noise. In the ideal display situation, each component of the observation noise vector $\underline{v}_e$ scales with the corresponding rms variance of the corresponding display quantity. In non-ideal situations, threshold and residual noise components must also be considered, as described in [5, 8, 9]. There is some evidence -- albeit inconsistent -- that degradation of visual information due to vibration can be represented as an increment in the residual noise variance. Levison and Houck obtained a good match to experimental data by setting the residual noise variance (associated with perception of indicator displacement) equal to the estimated variance of the relative displacement between eye point-of-regard and display [3]. On the other hand, best results were obtained in this study by ignoring visual effects altogether. Clearly, additional study is needed to determine how head and/or eye movements interfere with acquisition of visually-presented information in a tracking task.

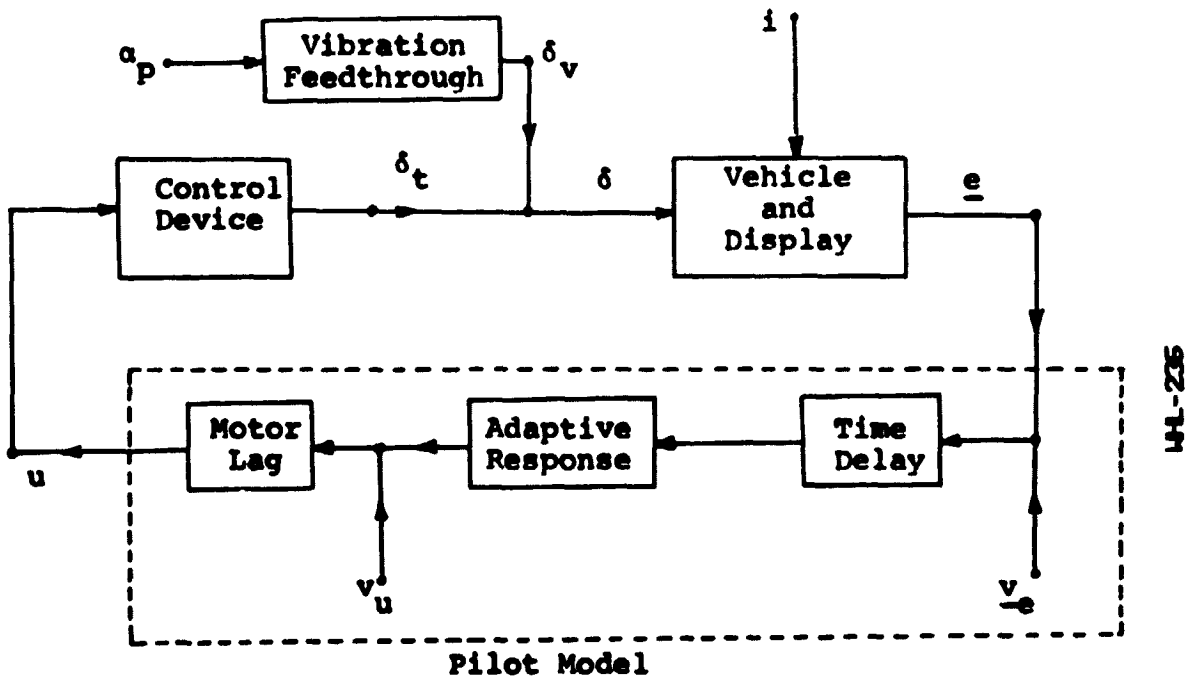

Figure 9. Outline of the Model Structure

Motor Noise. The following empirical relation was found in this study: $V_u=(0.004+0.05\alpha_s)\ \sigma_u^2$, where V_u is the variance of the motor noise and σ_u^2 the variance of the pilot's control input.
Motor Time Constant. For most single-variable tracking tasks in which excessive control forces are not required, the pilot will adopt a control strategy appropriate to minimizing a weighted sum of error and control-rate variances. The relative weighting on control-rate variance is chosen to yield a motor time constant (i.e., first-order lag) of about 0.1 seconds. Results of this study, as well as of the study of Levison and Houck [3], indicate that motor time constant is not effected by Z-axis platform vibration.
Stick Feedthrough. "Stick feedthrough" is defined as the portion of control motion that is linearly related to the platform vibration due to biomechanical coupling. Once the relationship between platform vibration and control response has been determined, the contribution of feedthrough to error and control variances can be predicted for a given platform vibration spectrum as described in the literature [3-5].

The Mapping Procedure

Because of the limited data base available for validation, the generality of the mapping procedure is restricted to the following situations: (1) the tracking task is single-input, single output; (2) vibration occurs at frequencies beyond the effective man/machine response bandwidth; (3) vibration is applied in a single linear axis. All of these assumptions simplify the mapping procedure. In particular, if the second assumption holds, the pilot will not effectively track out the unwanted inputs produced by vibration feedthrough. Thus, we can compute variance scores due to feedthrough separately from variance scores related to the tracking input and combine the results.

For purposes of demonstration, assume that a series of single-sine vibration experiments have been performed and that we wish to extrapolate these results to a specific complex vibration environment. (The procedure for extrapolating from complex to single-sine environments is virtually identical.) The mapping procedure is outlined in Figure 10.

Tracking performance in sum-of-sines and random vibration environments was predicted on the basis of the single-sine vibration results obtained in the AMRL experimental program described above. The following procedure, which generally parallels the mapping scheme defined in Figure 10, was employed:

1. Static tracking results were first analyzed to determine pilot-related model parameters. Parameter values obtained in the Levison and Houck study [3] provided a good match to static performance in this study.

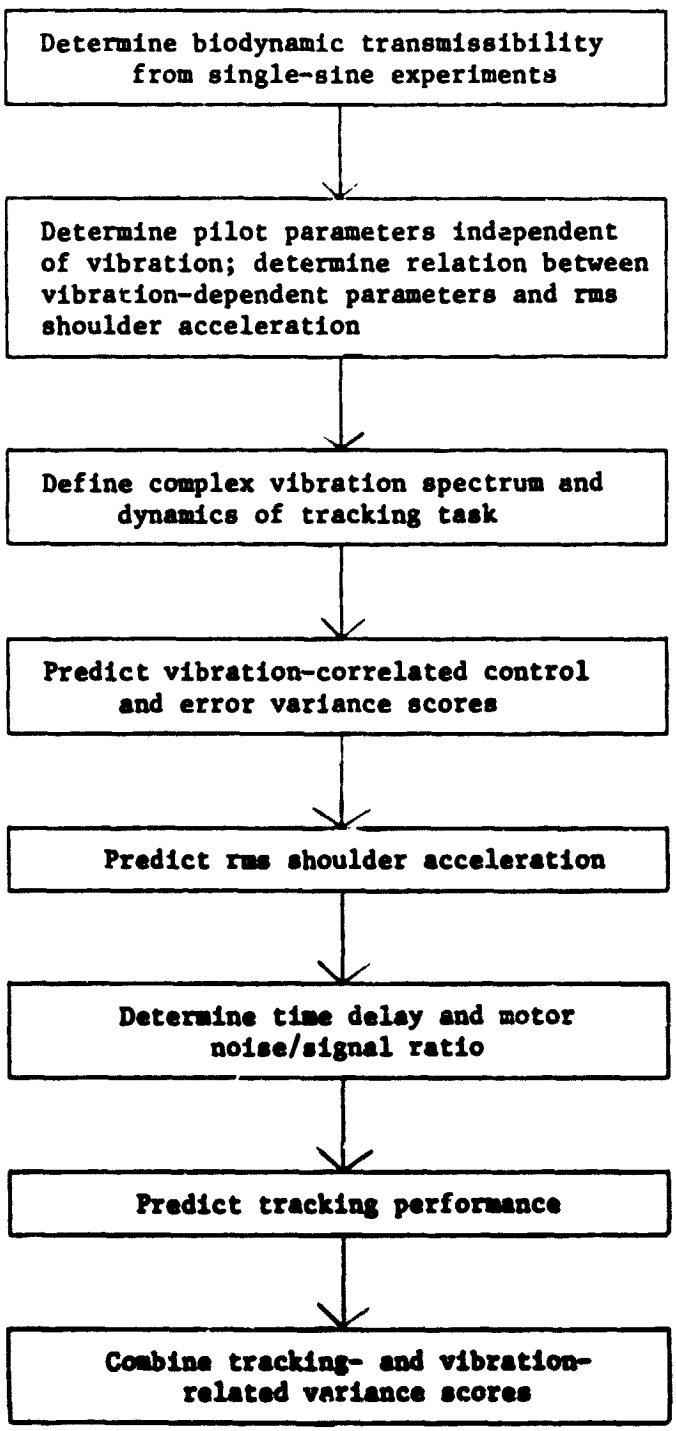

Figure 10. Mapping Single-Sine to Complex Vibration Environments

2. The sum-of-sines results were matched to determine the relation between vibration-dependent pilot parameters (time delay and motor noise) and biodynamic response parameters.*

3. Biodynamic describing functions obtained with single-sine vibration (averaged across g levels as well as across subjects) were used to predict rms shoulder vibration and vibration-correlated control variance for the sum-of-sines and random vibration spectra. Variance scores for the sum-of-sines environments were predicted by simply adding the platform spectrum (in dB) to the appropriate transfer magnitude (in dB), transforming to absolute units, and summing across frequencies. A curve-fitting procedure was needed, however, to perform frequency-domain integrations required for random vibration inputs. The single-sine transfer magnitudes were cascaded with the power density levels of the platform acceleration at the five measurement frequencies; piecewise-linear approximations to the resulting power density spectrum were made on a log-output versus log-frequency basis; each straight-line segment was integrated analytically; and the results were combined to yield the variance (and rms) of the biodynamic response variable.

4. The remainder of the mapping procedure defined in Figure 10 was carried out, except that the computation of vibration-correlated error was omitted because of its small contribution (generally less than 2%) to total error variance.

Rms error and control scores predicted in this manner are compared with experimental results in Figures 11 and 12 for the spring and stiff stick configurations, respectively. Also shown in this figure are the standard errors for each of the experimental measures. Model predictions reproduced the trends of the data quite well, generally falling within one standard error of the mean.

The reverse mapping is also demonstrated in [5], in which results of the sum-of-sines vibration conditions are extrapolated to single-sine vibration inputs. Again, predicted rms error and control scores were within one standard deviation of the experimental means.

---

*One of the objectives of this analysis was to determine as reliably as possible in the empirical relation between pilot parameters and biodynamic response in a complex vibration environment. Therefore, the sum-of-sines data were used, rather than the single-sine data that would have been used in a pure demonstration of the mapping procedure.

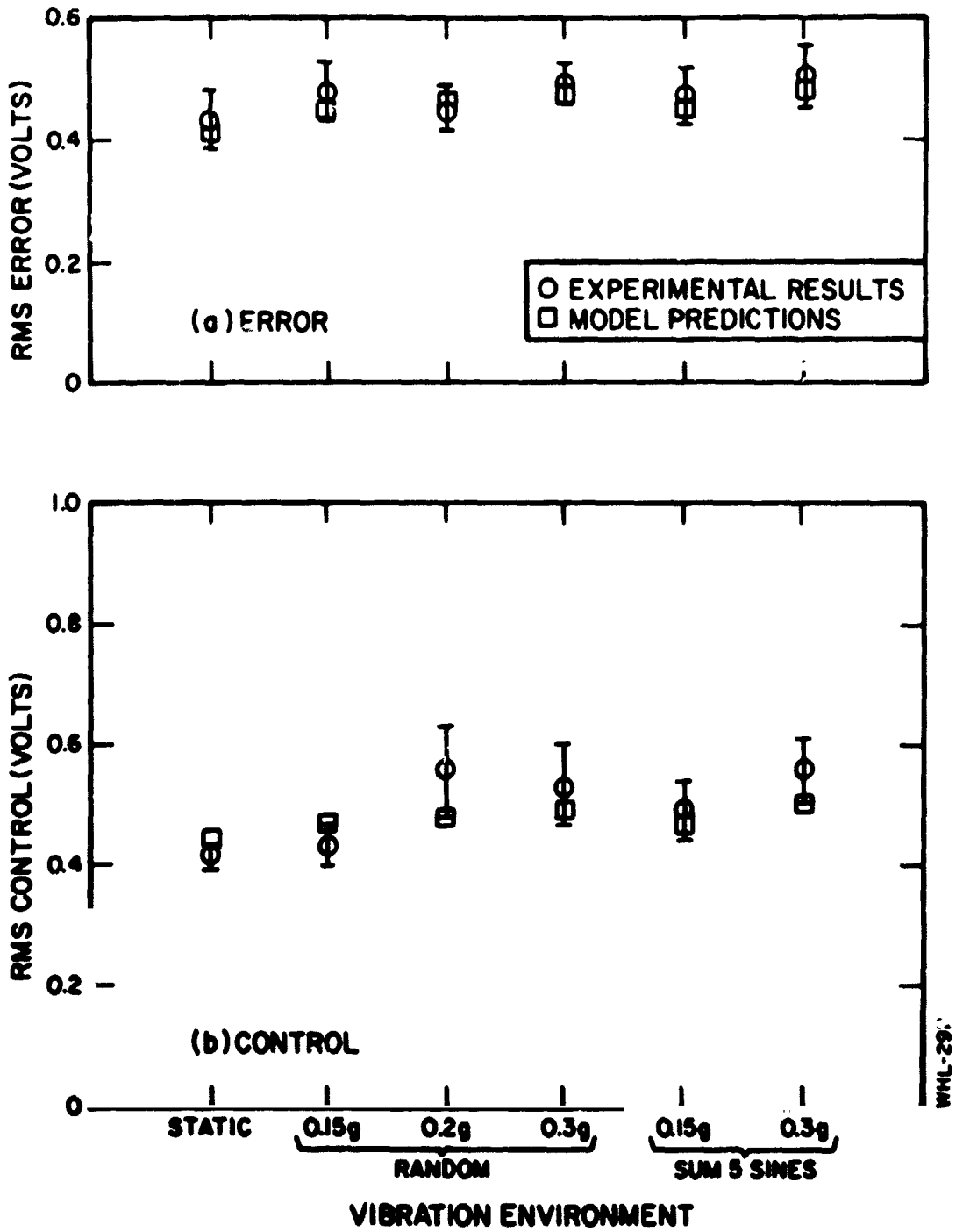

Figure 11. **Measured and Predicted Performance Scores for Spring-Stick Configuration**

Average of 7 subjects

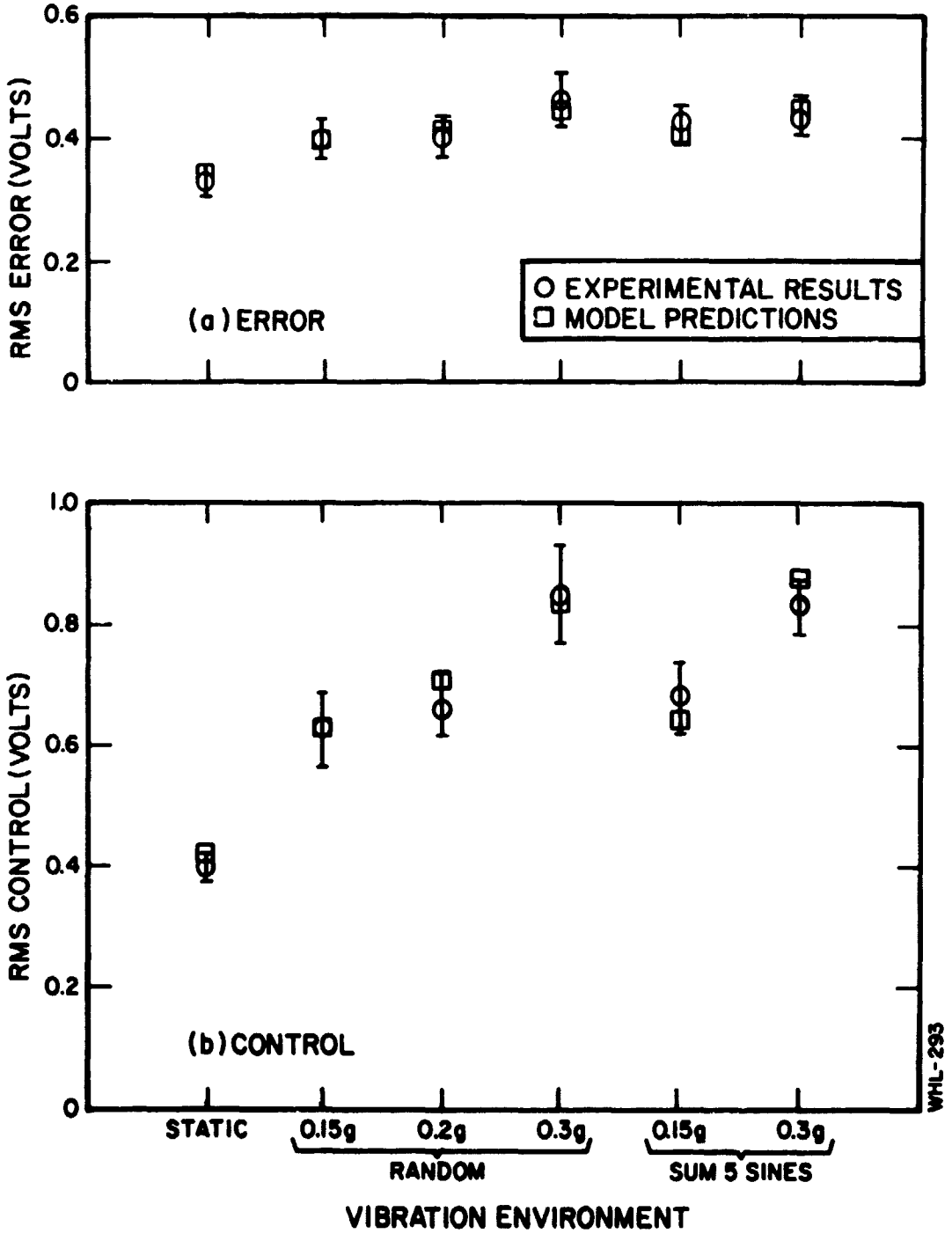

Figure 12. Measured and Predicted Performance Scores for Stiff-Stick Configuration

Average of 7 subjects.

SUMMARY

The results of the study documented in [5] may be summarized as follows:

Biomechanical Response. Biomechanical response mechanisms were essentially linear for the range of vibration amplitudes and spectra explored in this study. Rms shoulder and head acceleration scores varied linearly with rms platform acceleration. In addition, describing functions relating control input, shoulder acceleration, and head translational and rotational accelerations to platform acceleration were largely independent of the parameters of the platform vibration.

Effects of Stick Parameters. Shoulder and head response to platform vibration was independent of stick parameters, whereas feedthrough was considerably more severe for the stiff stick than for the spring stick. Although static error scores were less for the stiff stick, vibration induced a relatively greater increase in error for the stiff-stick than for the spring-stick tracking tasks.

Stick Feedthrough. Stick feedthrough for the stiff stick was similar to that obtained in a similar experimental situation by Levison and Houck [3]; feedthrough for the spring stick; however, was considerably less than that in the prior study.

Vibration Interference Effects. Feedthrough accounted for a negligible fraction (2% or less) of the tracking error variance. In terms of the pilot/vehicle model employed in the analysis, the important effects appeared to be an increase in motor-related remnant and time delay. Both the motor noise/signal ratio and time delay appeared to vary linearly with rms shoulder acceleration. No interference with visual processes was identified.

Mapping Procedure. A model-based mapping procedure was defined and verified for extrapolating the results of single-sine vibration/tracking experiments to complex vibration environments. Mapping in the reverse direction was also verified.

Because we lack models for extrapolating existing results to other axes of vibration or other biomechanical configurations, the mapping procedure defined in this paper is intended to apply only to z-axis vibration and to the biomechanical configuration employed in recent AMRL studies. We can, however, extrapolate results to other steady-state z-axis vibration patterns, provided that rms platform vibration is on the order of 0.3 g or less. Furthermore, because of the demonstrated capability of the underlying pilot/vehicle model to predict tracking performance in a variety of

control situations, we expect the mapping procedure to be useful in exploring tracking tasks beyond those studied in the laboratory.

REFERENCES

1. Allen, R. W.; Jex, Henry R.; and Magdaleno, R. E.: Manual Control Performance and Dynamic Response During Sinusoidal Vibration. AMRL-TR-73-78, Aerospace Medical Research Laboratory, Wright-Patterson Air Force Base, Ohio, October 1973.

2. Levison, William H.: Analysis of Vibration-Induced Pilot Remnant. BBN Report No. 2608, Final Report, Bolt Beranek and Newman Inc., Cambridge, Mass., under Contract No. F33615-71-C-1207, August 1973.

3. Levison, William H.; and Houck, Philip D.: Guide for the Design of Control Sticks in Vibration Environments. AMRL-TR-74-127, Aerospace Medical Research Laboratory, Wright-Patterson Air Force Base, Ohio, February 1975.

4. Levison, William H.: Effects of Control-Stick Parameters on Tracking Performance in a Vibration Environment. Proc. of the Eleventh Annual Conference on Manual Control, Ames Research Center, Moffett Field, California, May 1975.

5. Levison, William H.: Biomechanical Response and Manual Tracking Performance in Sinusoidal, Sum-of-Sines, and Random Vibration Environments, AMRL-TR-75-94, Aerospace Medical Research Laboratory, Wright-Patterson Air Force Base, Ohio, April 1976.

6. Kleinman, D.L.; Baron, S.; and Levison, W. D.: An Optimal-Control Model of Human Response, Part 1: Theory and Validation. Automatica, Vol. 6, pp. 357-369, 1970.

7. Kleinman, D. L.; Baron, S.; and Levison, W. H.: A Control Theoretic Approach to Manned-Vehicle Systems Analysis. IEEE Trans. on Auto. Control, Vol. AC-16, No. 6, December 1971.

8. Kleinman, D. L.; and Baron, S.: Analytic Evaluation of Display Requirements for Approach to Landing. NASA CR-1952, November 1971.

9. Baron, S.; and Levison, W. H.: A Manual Control Theory Analysis of Vertical Situation Displays for STOL Aircraft. NASA CR-114620, April 1973.

10. Levison, W. H.; Baron, S.; and Kleinman, D. L.: A Model for Human Controller Remnant. IEEE Trans. Man-Machine Systems, Vol. MMS-10, No. 4, December 1969.

11. Levison, W. H.: The Effects of Display Gain and Signal Bandwidth on Human Controller Remnant. Wright-Patterson Air Force Base, Ohio, AMRL-TR-70-93, March 1971.

☆ US GOVERNMENT PRINTING OFFICE: 1976-789-745/38